# INAUGURAL DISSERTATION

for obtaining the

**Doctoral Degree**

of the

**Combined Faculty of Mathematics,**

**Engineering and Natural Sciences**

of the

**Ruprecht – Karls – University**

**Heidelberg**

presented by

**Raphael René Steimbach, M. Sc.**

born in Pforzheim, Germany

Oral examination on 23rd March 2023

# SELECTIVE INHIBITORS AND TARGETED DEGRADERS OF HISTONE DEACETYLASE 10

**Referees:** Prof. Dr. Christian D. Klein

Prof. Dr. Andres Jäschke

# Acknowledgements/Danksagung

I am deeply grateful to my Doktorvater Dr. Aubry K. Miller for his mentorship and for providing me with this project. It was a privilege to work under his guidance and with his constant support and unconditional trust in my ability to bring the project to where it is now. The opportunities and leadership he provided formed me as a scientist and are the foundation of this work.

I sincerely thank Prof. Christian Klein for agreeing to be my first referee and for ensuring the project stays on track. I highly appreciate Prof. Andres Jäschke for being my second referee and chairperson of the examination commission. I also thank Prof. Tobias Dick und Dr. Christiane Opitz for being on my examination commission and Dr. Ina Oehme for the scientific input in my TAC meetings.

I want to thank the students and interns who contributed to this thesis: Hannah Steffke for her diligent and excellent PROTAC work, Taddäus Strunden for working at night during the pandemic in search for new zinc binders and Gergely Tihanyi for his productive work early in my PhD. I also want to explicitly thank all the collaborators that are mentioned in this dissertation. Their scientific contributions allowed for the impact of this work and my compounds would be worthless without them. I want to thank Dr. Peter Sehr for his help with establishing the FRET assay in the Miller Lab.

Thanks a lot to the current and former members of the Drug Discovery Group, especially Andi, Jasmin, Elena, Michael, Daniel, Nick, Sven, Roman and Teresa. I had a great time with you! Special thanks go to Johanna, who taught me everything in the biology lab and made all the Western blots in this work. I thank Dr. Karel Klika for the NMR support and his interest in my compounds.

Nicole, dir bin ich unendlich dankbar für die liebevolle Unterstützung über die Jahre und ganz besonders in den letzten Wochen der Doktorarbeit. Danke für dein Verständnis, deine Korrekturen der Arbeit, den seelischen Beistand, einfach danke für alles!

Mein besonderer Dank gilt meinen Eltern, die so viel in meine Bildung investiert haben, und die gemeinsam mit Isabel immer an mich geglaubt haben. Ihretwegen habe ich es so weit geschafft und ihnen widme ich diese Doktorarbeit.

# Abstract

Histone deacetylase 10 (HDAC10) stands out among the eleven zinc-dependent hydrolases of the histone deacetylase family as the only polyamine deacetylase. It exhibits remarkable substrate specificity for *N*-acetylputrescine and $N^8$-acetylspermidine over $N^1$-acetylspermidine and shows no activity on acetyllysine residues. Although the role of selective polyamine deacetylation in health and disease is enigmatic, HDAC10 received little attention from medicinal chemists and no selective inhibitors suitable as chemical probes were available prior to this study.

To address this deficiency, I developed the first well-characterized selective chemical probes for HDAC10 with unprecedented selectivity over other HDAC isozymes. The inhibitors were designed to imitate HDAC10's polyamine substrates without also binding HDAC6, its closest relative. Insertion of an amino group into the hexyl linker moiety of the approved drug Vorinostat (SAHA) at the γ-position to the hydroxamic acid transformed SAHA from an unselective pan-inhibitor into a selective HDAC10 inhibitor. I further optimized the aza-SAHA scaffold in a medicinal chemistry campaign, which yielded **DKFZ-748**, a chemical probe for HDAC10 with a 22 nM $IC_{50}$ against HDAC10 in cells and >500-fold selectivity over HDAC6, as well as Class I enzymes (HDAC1, 2, 3, 8). Selectivity and potency were validated by biochemical and cellular target engagement assays. Furthermore, cells treated with **DKFZ-748** showed only accumulation of the polyamine substrates, but not hyperacetylation of HDAC6 or Class I substrates. Potency of the aza-SAHA derivatives could be rationalized with HDAC10 co-crystal structures and selectivity within the entire target landscape of HDAC drugs was demonstrated. Moreover, **DKFZ-748** was successfully applied in a polyamine-limited in vitro tumor model, where it enabled HeLa cell growth inhibition, but showed no toxicity under other circumstances.

With potent and selective HDAC10 binders at hand, I transitioned from occupancy-driven pharmacology of inhibitors to the event-driven pharmacology of targeted degraders that can remove HDAC10 in cells via induced proteasomal degradation, including potential scaffolding functions of the HDAC10 protein. I demonstrated targeted degradation of HDAC10 using pan-inhibitor-based compounds as a proof of principle, and established a solid-phase synthesis of aza-SAHA-based degraders. These are promising candidates for the selective degradation of HDAC10, based on the excellent selectivity profile of the aza-SAHA derivatives.

Furthermore, in a separate approach, I investigated new scaffolds for selective HDAC10 inhibition based on a compound library screen. This part of the project aimed to develop selective HDAC10 inhibitors without the use of amino hydroxamic acids, which opens new therapeutic applications for HDAC10 inhibition beyond cancer therapy.

# Kurzfassung

Die Histondeacetylase 10 (HDAC10) sticht unter den elf zinkabhängigen Hydrolasen der Histondeacetylase-Familie als einzige Polyamin-Deacetylase hervor, die eine bemerkenswerte Substratspezifität für *N*-Acetylputrescin und $N^8$-Acetylspermidin gegenüber dem $N^1$-Acetylspermidin, sowie keine Aktivität für Acetyllysine in Proteinen, aufweist. Obwohl die Rolle der selektiven Polyamin-Deacetylierung in Physiologie und Pathophysiologie bisher ungeklärt ist, wurde HDAC10 von medizinischen Chemikern nur wenig untersucht, und zu Beginn der vorliegenden Arbeit waren keine selektiven Hemmstoffe verfügbar, die sich als chemische Sonden eignen.

Um diese Lücke zu schließen, habe ich die ersten gut charakterisierten selektiven chemischen Sonden für HDAC10 entwickelt, die eine noch nie dagewesene Selektivität gegenüber anderen HDAC-Isoenzymen aufweisen. Die Hemmstoffe wurden so konzipiert, dass sie die HDAC10 Polyaminsubstrate imitieren, ohne auch HDAC6, ihren nächsten Verwandten, zu binden. Durch Einbau einer Aminogruppe in die Hexyl-Linkergruppe des zugelassenen Medikaments Vorinostat (SAHA) in der γ-Position zur Hydroxamsäure wurde SAHA von einem unselektiven Pan-Inhibitor zu einem selektiven HDAC10-Hemmstoff. Ich habe das Aza-SAHA-Gerüst durch systematische Derivatisierung weiter optimiert, was **DKFZ-748** hervorbrachte, eine chemische Sonde für HDAC10 mit einer $IC_{50}$ von 22 nM in Zellen und einer >500-fachen Selektivität gegenüber HDAC6 sowie Enzymen der HDAC Klasse I (HDAC1, 2, 3, 8). Selektivität und Wirksamkeit wurden durch biochemische und zelluläre Bindungsassays validiert. Darüber hinaus zeigten Zellen, die mit **DKFZ-748** behandelt wurden, nur Akkumulation der Polyaminsubstrate, nicht aber Hyperacetylierung von HDAC6- oder Klasse-I-Substraten. Die Potenz der Aza-SAHA-Derivate konnte mit HDAC10-Kokristallstrukturen verstanden werden, und die Selektivität innerhalb der möglichen Wirkziele von HDAC-Hemmern wurde nachgewiesen. Darüber hinaus wurde **DKFZ-748** erfolgreich in einem polyaminlimitierten In-vitro-Tumormodell eingesetzt, wo es ermöglichte das Wachstum von HeLa-Zellen zu hemmen, aber unter anderen Umständen keine Toxizität zeigte.

Mit den potenten und selektiven HDAC10-Bindern als Grundlage wechselte ich von der bindegesteuerten Pharmakologie der Inhibitoren zur ereignisgesteuerten Pharmakologie des gezielten Proteinabbaus, womit sich HDAC10 in Zellen durch induzierten proteasomalen Abbau gezielt entfernen lässt. Dies schließt auch potenzielle Interaktionen des HDAC10-Proteins mit anderen Biomolekülen ein. Den gezielten Abbau von HDAC10 konnte ich mithilfe von Verbindungen auf der Basis von Pan-Inhibitoren nachweisen und ich habe zudem eine Festphasensynthese von Aza-SAHA-basierten Derivaten entwickelt. Diese sind aufgrund des hervorragenden Selektivitätsprofils der Aza-SAHA-Verbindungen vielversprechende Kandidaten für den spezifischen, ausschließlichen Abbau von HDAC10.

Darüber hinaus untersuchte ich in einem separaten Ansatz neue Strukturmotive für die selektive Hemmung von HDAC10 auf der Grundlage eines Substanzbibliotheks-Screens. Dies zielte darauf ab, selektive HDAC10-Inhibitoren ohne den Einsatz von Aminohydroxamsäuren zu entwickeln, was neue therapeutische Anwendungen für die HDAC10-Hemmung über die Krebstherapie hinaus eröffnet.

# Publications and presentations

The work presented in this dissertation was conducted under the supervision of Dr. Aubry K. Miller at the Cancer Drug Development Group of the German Cancer Research Center (DKFZ) from June 2018 till December 2022. Funding was provided by the Helmholtz International Graduate School for Cancer Research.

Parts of this work are published in

Steimbach, R. R.; Herbst-Gervasoni, C. J.; Lechner, S.; Stewart, T. M.; Klinke, G.; Ridinger, J.; Géraldy, M. N. E.; Tihanyi, G.; Foley, J. R.; Uhrig, U.*; et al.* Aza-SAHA Derivatives Are Selective Histone Deacetylase 10 Chemical Probes That Inhibit Polyamine Deacetylation and Phenocopy HDAC10 Knockout. *J. Am. Chem. Soc.* **2022**, *144*, 18861–18875

and reproduced with permission from *J. Am. Chem. Soc.* 2022, 144, 41, 18861–18875. Copyright 2022 American Chemical Society. Full text is available at http://pubs.acs.org/articlesonrequest/AOR-3FNDPMXUJSG7D4TNB9KD.

Parts of this work are also contained in the following patent:

Miller, A. K.; Steimbach, R. R.; Géraldy, M. NOVEL INHIBITORS OF HISTONE DEACETYLASE 10. Patent WO2020193431A1; Mar 20, **2020**.

Besides the work presented in this dissertation, I participated in other HDAC-related projects in the Miller Group and with collaborators. I contributed HDAC activity data and became co-author on the following publications:

Lechner, S.; Malgapo, M. I. P.; Grätz, C.; Steimbach, R. R.; Baron, A.; Rüther, P.; Nadal, S.; Stumpf, C.; Loos, C.; Ku, X.*; et al.* Target deconvolution of HDAC pharmacopoeia reveals MBLAC2 as common off-target. *Nat. Chem. Biol.* **2022**, *18*, 812–820.

Herp, D.; Ridinger, J.; Robaa, D.; Shinsky, S. A.; Schmidtkunz, K.; Yesiloglu, T. Z.; Bayer, T.; Steimbach, R. R.; Herbst-Gervasoni, C. J.; Merz, A.*; et al.* First Fluorescent Acetylspermidine Deacetylation Assay for HDAC10 Identifies Selective Inhibitors with Cellular Target Engagement. *ChemBioChem* **2022**, *23*, e202200180.

Herbst-Gervasoni, C. J.; Steimbach, R. R.; Morgen, M.; Miller, A. K.; Christianson, D. W. Structural Basis for the Selective Inhibition of HDAC10, the Cytosolic Polyamine Deacetylase. *ACS Chem. Biol.* **2020**, *15*, 2154–2163.

Morgen, M.; Steimbach, R. R.; Géraldy, M.; Hellweg, L.; Sehr, P.; Ridinger, J.; Witt, O.; Oehme, I.; Herbst-Gervasoni, C. J.; Osko, J. D.*; et al.* Design and Synthesis of Dihydroxamic Acids as HDAC6/8/10 Inhibitors. *ChemMedChem* **2020**, *15*, 1163–1174.

Chen, X.; Chen, X.; Steimbach, R. R.; Wu, T.; Li, H.; Dan, W.; Shi, P.; Cao, C.; Li, D.; Miller, A. K.*; et al.* Novel 2, 5-diketopiperazine derivatives as potent selective histone deacetylase 6 inhibitors: Rational design, synthesis and antiproliferative activity. *Eur. J. Med. Chem.* **2020**, *187*, 111950.

Géraldy, M.; Morgen, M.; Sehr, P.; Steimbach, R. R.; Moi, D.; Ridinger, J.; Oehme, I.; Witt, O.; Malz, M.; Nogueira, M. S.; Koch, O.; Gunkel, N.; Miller, A. K. Selective Inhibition of Histone Deacetylase 10: Hydrogen Bonding to the Gatekeeper Residue is Implicated. *J. Med. Chem.* **2019**, *62*, 4426–4443.

My compounds were the basis for the following publications:

Stewart, T. M.; Foley, J. R.; Holbert, C. E.; Klinke, G.; Poschet, G.; Steimbach, R. R.; Miller, A. K.; Casero, R. A. Histone deacetylase-10 liberates spermidine to support polyamine homeostasis and tumor cell growth. *J. Biol. Chem.* **2022**, *298*, 102407.

Steimbach R. R.; Tihanyi G.; Géraldy M.; Wzorek A.; Miller A. K.; Klika K. D. Can an Intermediate Rate of Nitrogen Inversion Affect Drug Efficacy? *Symmetry* **2021**, *13*, 1753.

I presented this work at the following international conferences and summer schools:

| | | |
|---|---|---|
| 03/2019 | Frontiers in Medicinal Chemistry | poster presentation |
| 01/2021 | DECHEMA Advances in Chemical Biology* | poster presentation |
| 03/2021 | Frontiers in Medicinal Chemistry* | poster presentation |
| 06/2021 | European School of Medicinal Chemistry* | poster presentation |
| 08/2021 | EFMC International Symposium on MedChem* | poster presentation |
| 06/2022 | NUVISAN 1st Berlin MedChem Workshop | poster presentation |
| 08/2022 | ACS Fall 2022 in Chicago | oral presentation |

*online event with virtual poster session

Unrelated to the HDAC project, I contributed to the following publication during my PhD:

Schilling, D.*; Barayeu, U.*; Steimbach, R. R.; Talwar, D.; Miller, A. K.; Dick, T. P. Commonly Used Alkylating Agents Limit Persulfide Detection by Converting Protein Persulfides into Thioethers. *Angew. Chem. Int. Ed. Engl.* **2022**, *61*, e202203684. *: These authors contributed equally.

# Contents

# 1 Introduction and state of the art

## 1.1 Histone deacetylases

Histone deacetylases (HDACs) are a diverse family, named after the first identified member: HDAC1 – a mammalian histone deacetylase.[2] Today they are comprised of 18 members categorized in four classes based on homology with yeast proteins and similarity in functional domains.[3] Classes I, II and IV are $Zn^{2+}$-dependent hydrolases, while the seven Class III enzymes are called sirtuins (SIRTs), require $NAD^{+}$ and are structurally as well as mechanistically distinct.[4,5] The term HDAC is herein after only used for the $Zn^{2+}$-dependent classes. Class I HDACs are HDAC1, 2, 3 and 8, Class IIA consists of HDAC4, 5, 7 and 9, and Class IIB members are HDAC6 and 10, while the only member of Class IV is HDAC11. A schematic overview on their structure, subcellular localization and major substrates is provided in **Figure 1**.

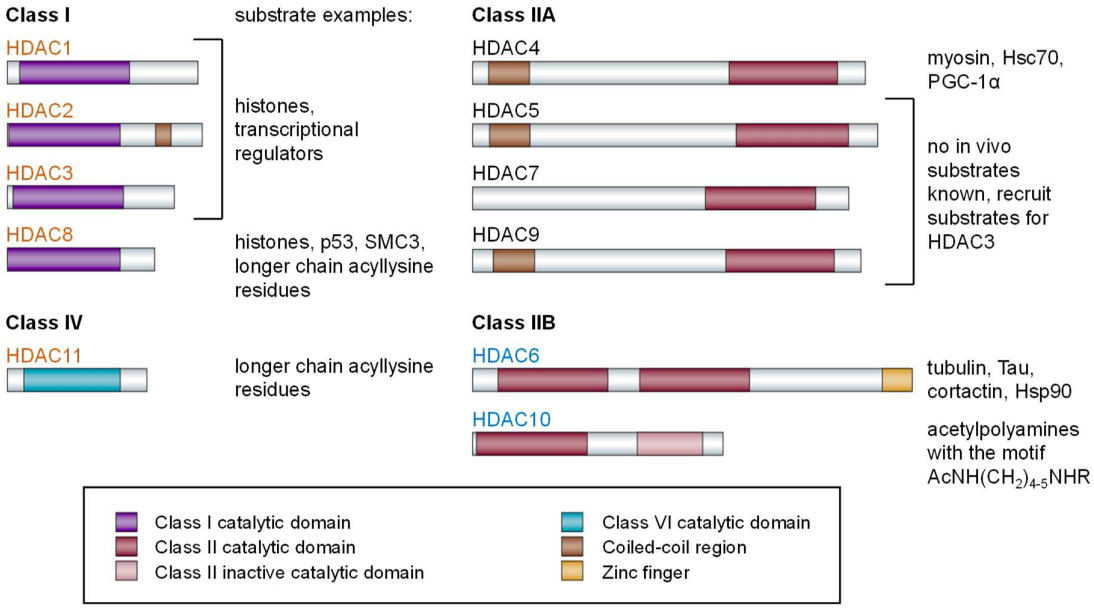


**Figure 1.** Schematic structural overview, classification and substrate examples of zinc-dependent histone deacetylases. HDAC labels are color coded according to major subcellular localization: orange: nucleus; blue: cytoplasm; black: both. Based on Bolden et al.[6] and Ho et al.[7]

The HDAC family covers a wide range of substrates beyond histones. In fact, only Class I enzymes, especially HDAC1–3, show a clear preference for acetyl groups on histone tails.[8,9] This "classical" HDAC activity is found ubiquitously in eukaryotes[3] and regulates gene expression, as discussed in more detail below. Genetic knock-out of Class I HDACs in mice causes embryonic or early post-natal lethality, which indicates essential physiological roles.[10] The Class I enzymes are mainly localized in the nucleus, where HDAC3 is only active in complex with nuclear receptor co-repressor (NCoR) and silencing mediator of retinoic and thyroid

receptors (SMRT).[9] HDAC8 is distinct from the other Class I members as it appears to have diverged from other Class I enzymes early in evolution and therefore developed a separate function and broader substrate scope beyond histones. This includes non-histone nuclear proteins like p53 and structural maintenance of chromosomes protein 3 (SMC3).[11] The deacetylase activity of HDAC8 is lower than for the other Class I enzymes, but the substrates are not limited to acetamides. In fact, the catalytic efficiency of HDAC8 on octanoyl-, dodecanoyl-, and myristoyl-modified lysines of histone H3 peptides was better than on acetyllysines.[12]

Another HDAC with activity on long chain acyllysine peptides is HDAC11. It is with 39 kDa the smallest currently described HDAC, also mainly located in the nucleus, but phylogenetically separate from other HDACs and therefore the only Class IV member. It exhibits negligible intrinsic deacetylation activity, but was later identified as an effective fatty acid deacylase.[13,14]

Unlike the other HDACs, Class IIA members HDAC4, 5, 7 and 9 are not found in all cell types but are expressed in a tissue-specific manner. They are shuttled between the nucleus and cytoplasm based on their phosphorylation state. Due to their weak catalytic activity and enigmatic physiological function, they are often regarded as pseudoenzymes, scaffolding proteins or acetyllysine readers.[15] However, HDAC4 was eventually found to be an active deacetylase of the myosin heavy chain, peroxisome proliferator-activated receptor gamma co-activator 1alpha (PGC-1α), and heat shock cognate 71 kDa protein (Hsc70).[16]

The Class IIB enzymes are mainly located in the cytoplasm and are characterized by two catalytic domains. However, the second (C-terminal) domain of HDAC10 is inactive, since it lacks the residues required for deacetylation. HDAC10 is with 71 kDa also much smaller than HDAC6. HDAC10's active catalytic domain has a distinct substrate specificity for certain acetylated polyamines. A glutamic acid gatekeeper (E274 in zebrafish HDAC10, E272 in human HDAC10) is the main determinant for this specificity. The structure and function of HDAC10 is covered in detail in sections 1.1.4 and 1.2.

HDAC6, the closest relative of HDAC10, is a lysine deacetylase (KDAC) acting on a broad range of non-histone protein substrates, most importantly tubulin.[17] Both catalytic domains of HDAC6 are active and exhibit different substrate requirements.[18] HDAC6 is with 131 kDa the largest isozyme and the only one with a zinc finger domain. The structure and separate functions of the two closely related Class IIB isozymes are outlined in section 1.1.2.

### 1.1.1 The physiological role of "classical" HDACs

Deacetylation of histones promoted by the first described histone deacetylase enzymes gave rise to the name for the entire family of HDACs, although this is only fully applicable to Class I HDACs. Histones are small, basic proteins that are involved in the condensation of DNA in the nucleus by wrapping 146-147 base pairs of DNA around an octamer of histone proteins in a structure called a nucleosome (**Figure 2**). Nucleosomes are further compacted through coiling into chromatin, which can be either more transcriptionally active and loose (euchromatin) or denser and more tightly packed (heterochromatin). Gene regulation and chromatin

remodeling are highly complex processes. They are influenced by acetylation of lysine residues on the N-terminal tails of histones by histone acetyltransferases (HATs), which loosens the chromatin structure and leads to higher levels of gene expression of affected regions in the genome. Class I HDACs are "eraser" enzymes[19] of this epigenetic code that revert this process by cleaving acetate from acetylated ε-amino groups of lysines in histones. This leads to stronger interactions between the positively charged lysine and the negatively charged phosphate esters of DNA, promoting the denser heterochromatin (**Figure 2**).[20,21]

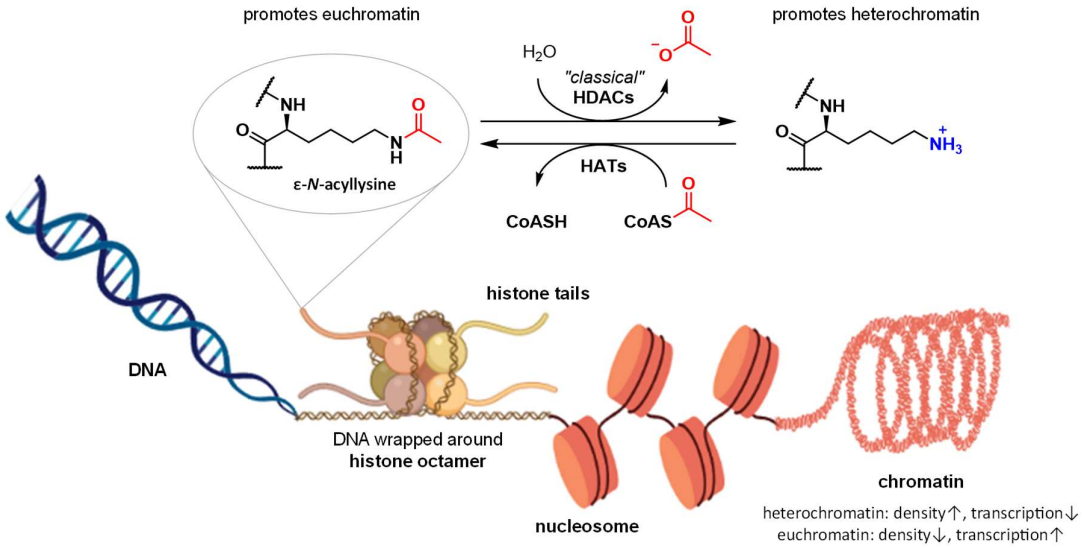


**Figure 2.** Schematic representation of classical histone deacetylase (HDAC) and histone acetyltransferase (HAT) activity influencing chromatin structure and therefore gene expression. Partly created with BioRender.com.

This "classical" HDAC activity sparked immense scientific interest in the HDAC family, as aberrant changes in gene expression that are modulated by epigenetic codes are thought to be linked to the development of diseases, particularly cancer.[6,22] This ignited an arms race in both the pharmaceutical industry and academia; consequently, more than 700 clinical trials have targeted HDACs.[7] Nevertheless, only five HDAC inhibitors[7] have been approved worldwide to date, a disappointing clinical conclusion considering the initial optimism surrounding epigenetic approaches in cancer therapy.[23] Since dose-limiting toxicity may result from targeting multiple HDAC isoforms simultaneously with pan-inhibitors, isoform selective compounds are becoming more widely explored, also beyond cancer chemotherapy.[10,24,25] HDAC inhibitors are covered in more detail in section 1.3.

### 1.1.2 HDAC Class IIB

HDAC Class IIB is composed of the lysine deacetylase (KDAC) HDAC6 and the polyamine deacetylase (PDAC) HDAC10. Both are mainly localized in the cytoplasm and they share over 50% sequence identity. Despite their distinct physiological functions and substrate specificities (for more details see sections 1.1.3 and 1.1.4), it has been challenging to target the

two closely related isozymes separately with selective inhibitors. HDAC6 is the only HDAC family member with two catalytic domains, designated CD1 and CD2. The latter catalytic domain accepts a broad scope of acetyllysine substrates.[18,26] Crystal structures are available for both Class IIB isozymes, which allow a structurally informed rational design approach to selective inhibitors and a better understanding of substrate recognition. **Figure 3** shows an aligned comparison of the HDAC6-CD2 (A) and HDAC10 (B) protein surfaces surrounding the substrate binding tunnel entrances. It is obvious that the HDAC10 active site evolved to occupy cationic substrates, since the binding tunnel is flanked by the negatively charged glutamate residues E24 and E274, which make the binding tunnel also much narrower than in HDAC6. Instead of the HDAC10 gatekeeper residue E274, HDAC6 harbors L749 at roughly the same location, and instead of a negative charge, positive H651 is exposed to the surface of HDAC6 at the tunnel entrance. Another important difference in the structures of the two substrate binding tunnels is F680 in HDAC6, which corresponds to W205 in HDAC10. Those hydrophobic residues form the tunnel surface and are in direct contact with the substrate or inhibitor linker moieties.

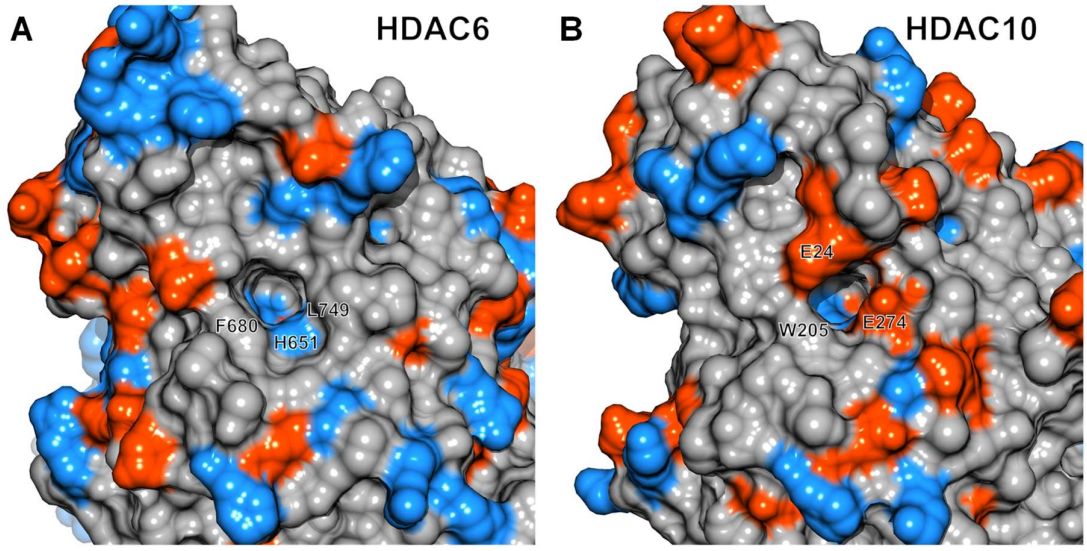


**Figure 3.** Surface comparison of human HDAC6-CD2 and humanized zebrafish HDAC10 active site entrances. Surface colors: red: residues with negative charge; blue: with positive charge. Figure is own work based on PDB 5EDU[18] and 7KUQ.[27]

### 1.1.3 HDAC6

HDAC6 is unique among the HDAC family since it is the only isozyme that has two active catalytic domains with different substrate specificities and functions. Both domains show KDAC activity: catalytic domain 1 (CD1) was proven to be highly selective towards peptides acetylated at C-terminal lysine residues,[18,28] while CD2 exhibits broad substrate specificity,[18,26] most importantly towards α-tubulin[17] and cortactin.[29] The physiological role of reversible acetylation at C-terminal lysine residues remains enigmatic, but the KDAC activity of CD2 is implicated in a number of physiological processes. This makes HDAC6 the most important cytosolic KDAC and a potential therapeutic target.[30,31]

HDAC6-mediated deacetylation of α-tubulin regulates microtubule stability and cell motility.[17] It was also shown that HDAC6 deacetylates cortactin, an actin-remodeling protein, which regulates the migration of endothelial cells and plays a role in angiogenesis.[29] Furthermore, HDAC6 might also be implicated in protein folding by regulating the activity of the Hsp90 chaperone via its deacetylation.[32,33] Another major therapeutic area with HDAC6 involvement is neurodegeneration, where it was shown to deacetylate the microtubule-associated protein Tau.[34,35]

It is noteworthy that HDAC6-depleted knock-out mice are viable and do not show an obvious phenotype or signs of impairment although they have drastically increased tubulin acetylation.[36] This confirms the KDAC activity of HDAC6 on tubulin, but also implies that the HDAC6-mediated regulation of the cytoskeleton is not essential, or perhaps redundant. The same applies to the other reported physiological functions of HDAC6. Nevertheless, this also suggests that selective HDAC6 inhibitors could be well tolerated and have therapeutic potential beyond oncology.

### 1.1.4 HDAC10

HDAC10 was isolated, characterized and named in 2002 by four groups independently.[37–40] It was categorized as the second member of Class IIB based on its over 50% sequence identity with HDAC6. The predicted amino acid sequence suggested that both isozymes have undergone a partial duplication event leading to a second catalytic domain that is inactive in the case of HDAC10. The active N-terminal deacetylase domain of HDAC10 was assumed to have catalytic activity on acetylhistone substrates and all four initial descriptions of HDAC10 report activity on $^{3}$H-Ac-labeled histones. However, the activity was much lower than for Class I enzymes and more comparable to the activity of HDAC6 and Class IIA enzymes on the same substrates. It is now known that histones are not the in vivo substrates of Class II HDACs[15,17,18,41] and the activity likely stemmed from contamination with highly active Class I enzymes present in the eukaryotic expression systems used.

HDAC10 was found to be expressed ubiquitously in all cell types, localized in the nucleus[37] and both, nucleus and cytoplasm,[38–40] with enrichment in the cytoplasm.[40] The amino acid sequence indicated a nuclear receptor-interacting motif, but also an unusually leucine-rich region that promotes a cytoplasmatic localization. HDAC10's main physiological role was suggested as a transcriptional regulator, but remained elusive due to the lack of deacetylate activity on acetyllysine substrates.[41–43] This changed upon discovering its enzymatic activity as a polyamine deacetylase (PDAC) by Christianson and co-workers.[41] This was a major breakthrough in our understanding of HDAC10, which I summarized in the following section.

#### 1.1.4.1 Enzymatic activity and substrate specificity

In 2017, Christianson and co-workers[41] reported the polyamine deacetylase (PDAC) activity of human HDAC10 (hHDAC10) with a distinct substrate specificity and solved the crystal structure of zebrafish HDAC10 (zHDAC10). Notably, this PDAC activity had been observed in rat liver extracts nearly four decades prior by Blankenship and Libby independently.[44,45] At

that time, the involved enzymes could not be isolated and identified; however, the biochemical characterizations of that period accurately describe the enzymatic activity and substrate specificity of HDAC10, as later determined in the Christianson Lab.

They expressed hHDAC10 in *E. coli*, mitigating the risk of contamination with other eukaryotic deacetylases, and used highly purified enzymes in a LC/MS-based discontinuous assay to test a variety of acetylpolyamine and acetyllysine substrates. Only linear polyamines with an amine four or five carbons distanced from an *N*-acetyl group, such as $N^8$-acetylspermidine ($N^8$-AcSpd), $N^{1,8}$-diacetylspermidine ($N^{1,8}$-$Ac_2$Spd), *N*-acetylputrescine (AcPut) and *N*-acetylcadaverine (AcCad) were deacetylated by HDAC10 (**Figure 4**, left). Polyamines with a shorter three carbon amine–acetamide separation like **1** or the regioisomer of $N^8$-AcSpd, $N^1$-acetylspermidine ($N^1$-AcSpd), are not accepted (**Figure 4**, right). Non-basic substrates like simple acetamide BuNHAc and peptides containing an acetylated lysine (**2**) are also poor substrates for HDAC10. Notably, this remarkable substrate specificity was already described for the cytosolic PDAC[46,47] before it was identified as HDAC10. It is also noteworthy that the good HDAC10 substrates are not accepted by HDAC6.

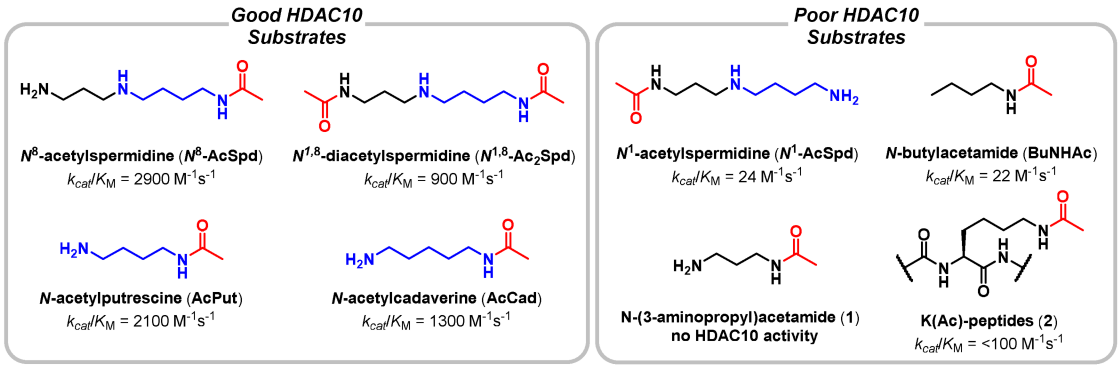


**Figure 4.** Acetamides that are good and poor substrates of HDAC10. The four or five carbon diamine separation, which is the recognition motif for HDAC10 acetylpolyamine substrates, is highlighted in blue. $k_{cat}/K_M$ values are reported for hHDAC10 and taken from Hai et al.[41]

### 1.1.4.2 Protein structure

The remarkable substrate specificity of HDAC10 described in the previous section could be rationalized by X-ray crystallography, initially with zHDAC10 in complex with a transition-state analogue inhibitor.[41] Later, Herbst-Gervasoni et al. reported an improved, "humanized" zHDAC10 with the substitutions A24E and D94A that provide an active site contour more similar to that of human HDAC10;[48] hence I refer to the humanized zHDAC10 mutant as just "HDAC10". Further crystallographic work subsequently yielded cocrystal structures of natural substrates and even snapshots of the acetamide hydrolysis tetrahedral intermediate.[27] These crystal structures provided solid proof for the catalytic mechanism discussed in section 1.1.4.3.

Christianson and co-workers revealed an overall butterfly-like structure of HDAC10 with two domains, an N-terminal, active PDAC domain (blue in **Figure 5**) and a C-terminal, inactive pseudo-deacetylase (ΨDAC) domain (pink). The ΨDAC domain lacks residues required for

zinc-binding and hydrolase activity, although it adopts the characteristic α/β arginase-deacetylase fold of catalytic HDAC centers. Multiple α-helices define the symmetry interface between the two domains. The PDAC domain is similar to canonical HDAC active sites, but possesses a narrower and longer substrate binding tunnel than other HDACs due to a constriction formed by the $P^{23}ECE^{26}$ ($P^{23}ACE$ in zHDAC10) $3_{10}$ helix (red in **Figure 5**) on one side and the gatekeeper residue E274 (yellow) on the opposing side. Such a constricted and elongated binding site, together with the negative electrostatic surface potential provided by the glutamate residues, results in specificity for the slender polyamine substrates over acetyllysine residues, as confirmed by mutagenesis studies.[41] Removal of the constricting $P^{23}(E,A)CE$ $3_{10}$ helix resulted in over 10-fold decreased PDAC activity and at the same time similarly increased HDAC activity. The significance of the E274 gatekeeper (E272 in hHDAC10) was demonstrated by the E274L mutant, which reduced the activity on $N^8$-AcSpd by 20-fold and increased activity for acetyllysine by 100-fold. The single residue point mutation effectively turned HDAC10 from a PDAC into a KDAC.

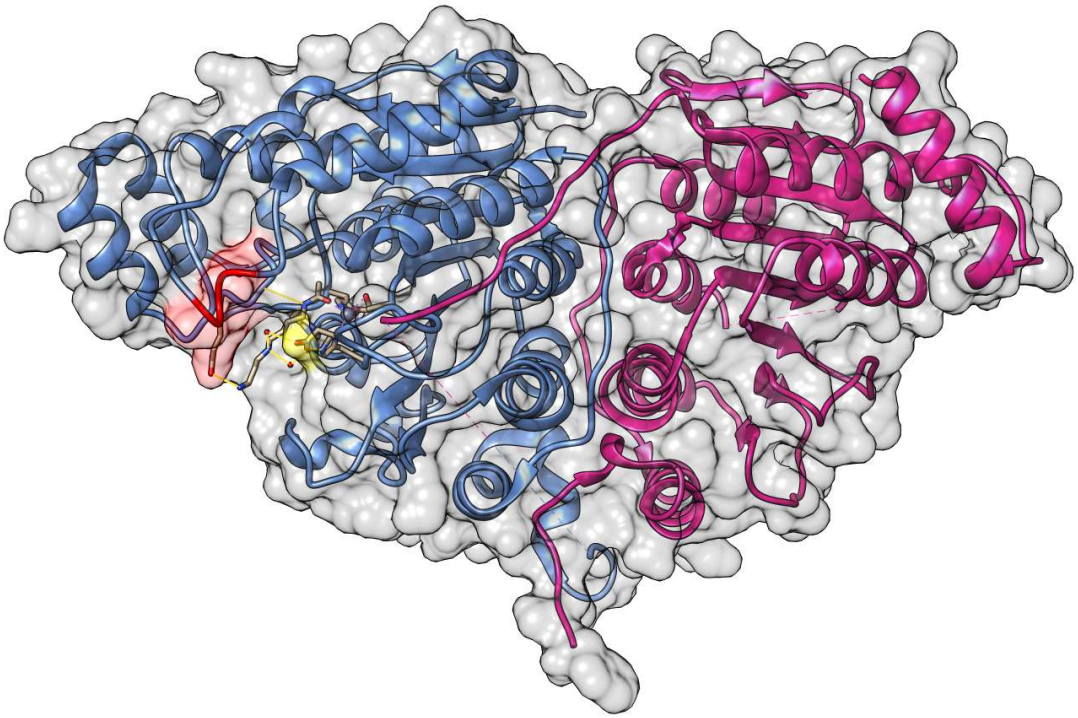

**Figure 5.** Ribbon with surface representation of the $HDAC10^{Y307F}$ crystal structure. Catalytic active site residues and the bound $N^8$-AcSpd substrate are highlighted. Predicted hydrogen bonding interactions of the substrate with the protein are depicted as yellow lines. The surface defined by the gatekeeper residue E274 is highlighted in yellow, the $P^{23}ECE^{26}$ helix is shown in red. Ribbon colors: blue: PDAC domain; pink: inactive ΨDAC domain. Figure is own work based on PDB 7KUQ.[27]

As detailed in section 1.1.4.1, HDAC10 is not active on all types of basic acetylpolyamine substrates but exhibits a remarkable substrate specificity for acetylated polyamines with an amine four or five carbons distanced from the *N*-acetyl group, such as in $N^8$-AcSpd. This

substrate specificity can be rationalized by the distinct features of the HDAC10 active site and its interactions with the $N^8$-AcSpd substrate, which have been elucidated by a cocrystal structure (**Figure 6**). The substrate's amide is coordinated by the zinc ion and forms a hydrogen bond with the backbone amide of G145 and presumably also with Y307. However, the latter residue is absent in **Figure 6**, since a crystal structure with the intact substrate could only be obtained from the Y307F mutant. E24 and E274 provide a negative electrostatic surface potential that is complementary to cationic substrates. However, only E24 forms a direct hydrogen bond to the primary amine of $N^8$-AcSpd, but gatekeeper E274 is the residue driving selectivity for $N^8$-AcSpd over its regioisomer $N^1$-AcSpd. The crystal structure suggests that the differentiation between the three and four carbon amine–acetamide separation is achieved by indirect hydrogen bonding of E274 with the secondary amine of $N^8$-AcSpd through two water molecules (**Figure 6**). Active site constraints likely cause $N^1$-AcSpd, like $N^8$-AcSpd, to bind in an extended conformation, but the secondary amino group of $N^1$-AcSpd would be oriented away from E274, unable to participate in the water-mediated hydrogen bond network.

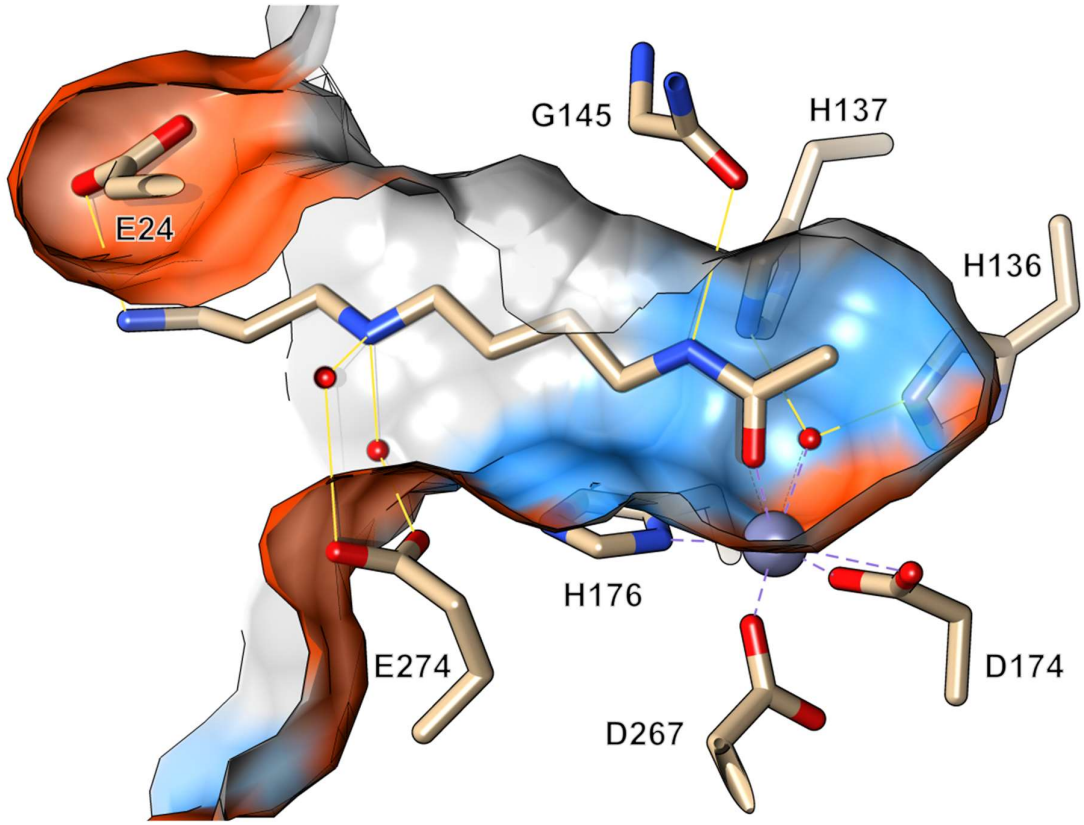


**Figure 6.** Cut-off view of the HDAC10$^{Y307F}$ active site binding substrate $N^8$-AcSpd. Selected residues and water molecules are depicted with calculated hydrogen bonds (yellow) and coordination to the zinc ion (purple). Surface colors: red: residues with negative charge; blue: with positive charge. Figure is own work based on PDB 7KUQ.[27]

#### 1.1.4.3 Catalytic mechanism

Adding to the first zHDAC10 crystal structure of Hai et al.,[41] Corey Herbst-Gervasoni solved five additional crystal structures of humanized zHDAC10 bound to the substrates $N^8$-AcSpd and AcPut, as well as their hydrolysis product acetate. Utilizing active site point mutations, he even managed to crystallize HDAC10 bound to tetrahedral intermediates of the acetylpolyamine hydrolysis. This provided X-ray crystallographic snapshots of the substrate binding and hydrolysis from start to finish. Supported by these structural insights, Herbst-Gervasoni and Christianson formulated a detailed catalytic mechanism (**Scheme 1**) highlighting the interactions responsible for transition state stabilization and product formation.[27]

The $Zn^{2+}$ ion at the end of the HDAC10 substrate binding tunnel is coordinated by protein residues D267, D174 and H176 and a water molecule, which in turn accepts a hydrogen bond from protonated H137 and donates a hydrogen bond to H136 (**Scheme 1,** top left). Only slender polyamine substrates fit into the narrow binding tunnel, which is constricted by the $P^{23}ECE^{26}$ helix. E24, together with the gatekeeper E274, provide a negative electrostatic surface potential that is complementary to cationic substrates (see **Figure 6** for a 3D model). While E24 forms a direct hydrogen bond to the primary amine of $N^8$-AcSpd in the substrate-bound state, for E274 the hydrogen bonding interaction with the secondary amine is mediated through two water molecules. Although not via direct hydrogen bonding, the interaction of E274 with the secondary amine of $N^8$-AcSpd is the critical determinant of the observed substrate specificity.[41] Additionally, $N^8$-AcSpd is positioned and oriented for nucleophilic attack in the active site by the backbone amide of G145, which accepts a hydrogen bond from the substrate amide bond. The substrate carbonyl oxygen is coordinated by the zinc ion and presumably also accepts a hydrogen bond from Y307. Both interactions are essential to activate the amide carbonyl group for nucleophilic attack by the water molecule at the active site. This water molecule is in hydrogen bonding distance to the catalytic histidine dyad, general base H136 and general acid H137, and coordinates to the zinc ion, which directs the nucleophilic attack of the amide (**Scheme 1,** top right and **Figure 6**).

**Scheme 1. Mechanism of HDAC10-catalyzed hydrolysis of $N^8$-AcSpd as proposed by Herbst-Gervasoni and Christianson[27] based on their structural investigations**

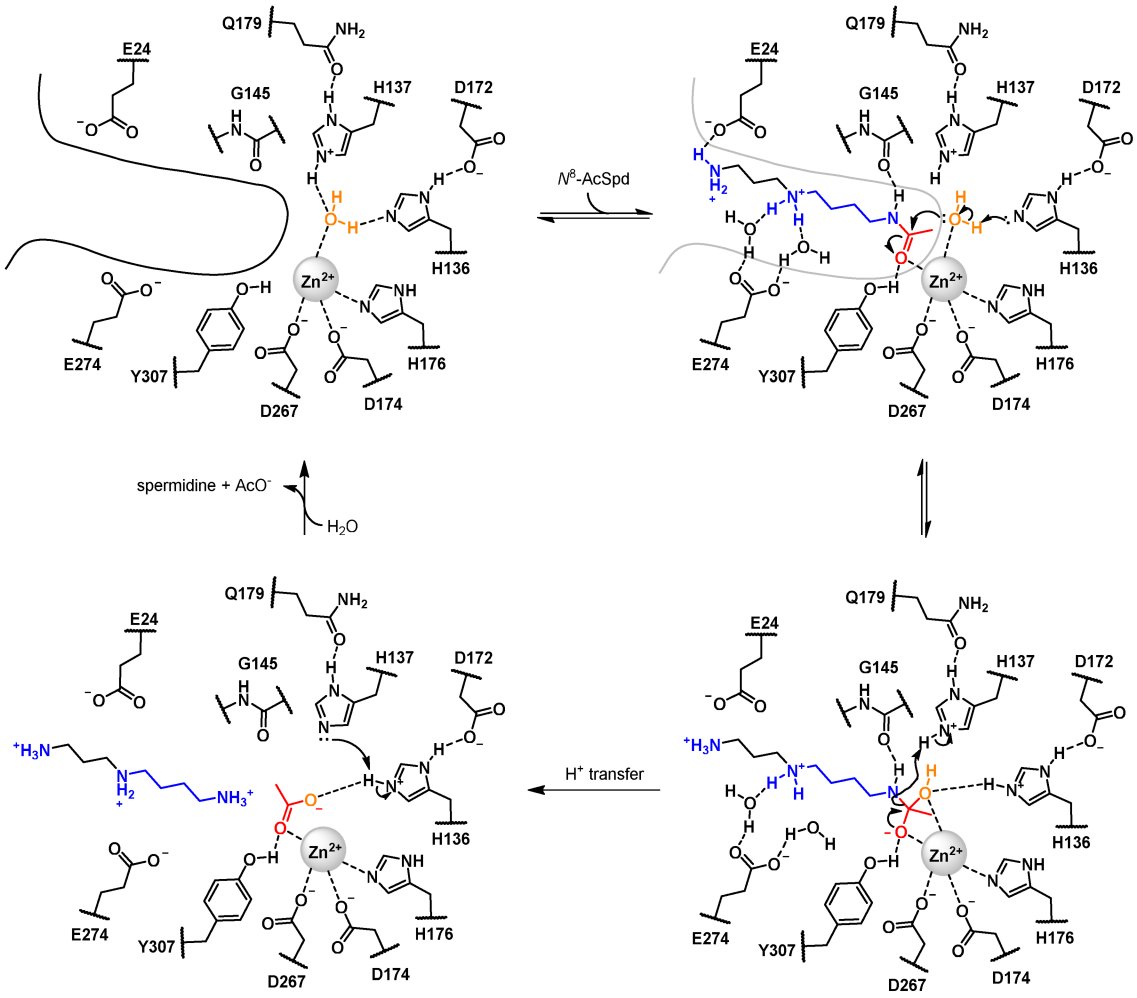


This leads to the formation of a stabilized tetrahedral intermediate, which was successfully captured in a crystal structure (bottom right). As expected, the active site structure is perfectly suited to bind and stabilize the reaction intermediate, with the interactions that orient the substrate also aiding in the binding of the reaction intermediate – a fundamental principle of enzyme catalysis.[49] Only the substrate specificity guiding interactions of E24 and E274 appear weaker than in the previous state, as they were not all re-confirmed in the crystal structure of the intermediate. Still, the newly formed hydroxyl group in the intermediate retains the hydrogen bond to H136 that was already present prior to the formation of the C–O bond. Binding and bond forming events along the reaction coordinate so far are in principle reversible. The essential step towards the ultimately irreversible formation of the hydrolysis products is the acid-catalyzed collapse of the tetrahedral intermediate. Herbst-Gervasoni and Christianson demonstrated that H137, acting as a proton donor, is required for the collapse of the tetrahedral intermediate into the primary amino group and acetic acid. This includes a proton exchange, likely in a concerted fashion. The resulting protonated spermidine and acetate then diffuse out of the active site. Acetate was also cocrystallized with HDAC10

(**Scheme 1,** bottom left), coordinated to the zinc ion and hydrogen bonding to Y307 and the properly still protonated general base H136, which transfers the proton back to H137 to act as an acid in the next catalytic cycle.

#### 1.1.4.4 Involvement in disease and therapeutic potential

The physiological significance of HDAC10 remains somewhat enigmatic. However, it is reported to be involved in various diseases and potentially implicated in multiple physiological functions. It may be involved in the regulation of autophagy as demonstrated by HDAC10-mediated chemotherapy resistance in neuroblastoma, presumably via its PDAC activity.[50–52] HDAC10 was shown to potentially restrict cell proliferation,[53] and furthermore has been implicated in important physiological processes such as homologous recombination,[54] DNA mismatch repair[55] and angiogenesis.[56] However, HDAC10 knock-out mice have been found to develop normally and remain viable without signs of disease.[57] HDAC10 has been implicated in various diseases, particularly cancer,[50,58,59] but with contradicting prospects regarding the benefit of HDAC10 inhibition. Its role in these diseases is not fully understood, but some studies have suggested that decreased HDAC10 expression is correlated with a poor prognosis in various cancer types, including colon carcinoma,[60] renal cell carcinoma,[61] gastric cancer[62] and lung cancer.[63] HDAC10 has also been recently implicated in inflammatory disorders[64] and transplant rejection.[57] Hancock and coworkers demonstrated that HDAC10 deletion in mice allows long-term allograft survival of fully MHC-mismatched cardiac transplants,[57] suggesting that HDAC10 plays an important role in immunomodulation and inflammation. In another study, HDAC10 was demonstrated to restore polyamine levels and provide growth rescue of cancer cells under polyamine-limiting conditions utilizing exogenous $N^8$-AcSpd.[65] This opens perspectives in polyamine blocking cancer therapy.[66]

Therefore, HDAC10 inhibitors have been suggested as potential therapeutic agents in cancer[50,58,65] or as immunomodulators.[57] In particular, HDAC10 has been found to be a marker for poor overall survival in neuroblastoma, and inhibition of HDAC10 has been shown to sensitize neuroblastoma cells to treatment with doxorubicin.[50] However, more research is needed to fully understand the role of HDAC10 in these diseases. Chemical probes for HDAC10 can serve as valuable tools to further understand the role of HDAC10 in physiology and disease, and to validate HDAC10 as a therapeutic target.

## 1.2 Metabolism of acetylated polyamines – the substrates of HDAC10

Polyamines are small, aliphatic and mostly linear molecules containing two or more amino groups. They are positively charged at physiological pH, therefore they are considered important counter ions for the negative charges in other biomolecules such as the acidic residues in proteins, phospholipids and nucleic acids.[67] Polyamines occur in millimolar concentrations in the cell and are conserved throughout all three domains of life,[68,69] because they are involved in numerous essential physiological processes and required for cell

proliferation and survival.[67,70] These include but are not limited to regulation of gene expression,[71,72] packaging and modulation of DNA[73,74] and RNA structure,[75,76] apoptosis[77] and cell cycle progression.[78,79]

Polyamine metabolism is a complex interconnected system of uptake, export, biosynthesis, modification and catabolism.[71,80,81] These pathways are conserved, with some variations, from bacteria to eukaryotes.[67] Selected major pathways of the eukaryotic polyamine metabolism are depicted in **Scheme 2**. Putrescine (Put) is the central four-carbon diamine building block in polyamine biosynthesis. It is synthesized from L-arginine via arginase that forms urea and the non-proteinogenic amino acid L-ornithine (Orn), which is decarboxylated by ornithine decarboxylase (ODC) to Put. This makes ODC the first rate-limiting enzyme in polyamine biosynthesis.[71] Plants, prokaryotes,[67] but also certain mammalian cell types[82,83] have access to an alternative synthesis of Put from arginine (Arg) via agmatine (Agm). In this pathway, Arg is directly decarboxylated to Agm by arginine decarboxylase (ADC), which is then hydrolyzed by agmatinase to Put and urea. Put is extended by spermidine synthase (SRM) with an aminopropyl group from *S*-adenosylmethioninamine (**3**) to form the triamine spermidine (Spd). Catalyzed by spermine synthase (SMS), Spd can be further extended by an aminopropyl group to form spermine (Spm), which in turn can be catabolized back to Spd by spermine oxidase (SMO).

Acetylation is an important chemical modification of polyamines to regulate their function, transport and catabolism.[71,84] **Scheme 2** contains the most important (de)acetylation pathways. The acetyl source for all polyamine acetylation reactions is acetyl-CoA. The primary polyamine acetyltransferase is spermidine/spermine $N^1$-acetyltransferase (SSAT), which is considered the rate-limiting essential catabolic enzyme of the polyamine metabolism.[80,85] That is because the alkylation of Put to Spd is irreversible and the transformation back to Put first requires acetylation of Spd to $N^1$-acetylspermidine ($N^1$-AcSpd). While Spd is not a substrate of $N^1$-acetylpolyamine oxidase (APAO), $N^1$-AcSpd – formed by SSAT – is effectively converted back to Put by the constitutively expressed APAO.[86] SSAT is highly inducible by elevated levels of free polyamines and can also form $N^1$-acetylspermine ($N^1$-AcSpm).[85] Both acetylated polyamines, $N^1$-AcSpd and $N^1$-AcSpm, are subjected to cellular export or oxidative catabolism by APAO to regulate the intracellular polyamine balance.[87] The SSAT substrate scope is limited to polyamines with the general structure $H_2N(CH_2)_3NH–R$. It can acetylate Spd only at the $N^1$-position, but $N^1$-AcSpd and Put are not substrates of SSAT.[88]

**Scheme 2. Selected pathways of the eukaryotic polyamine metabolism**

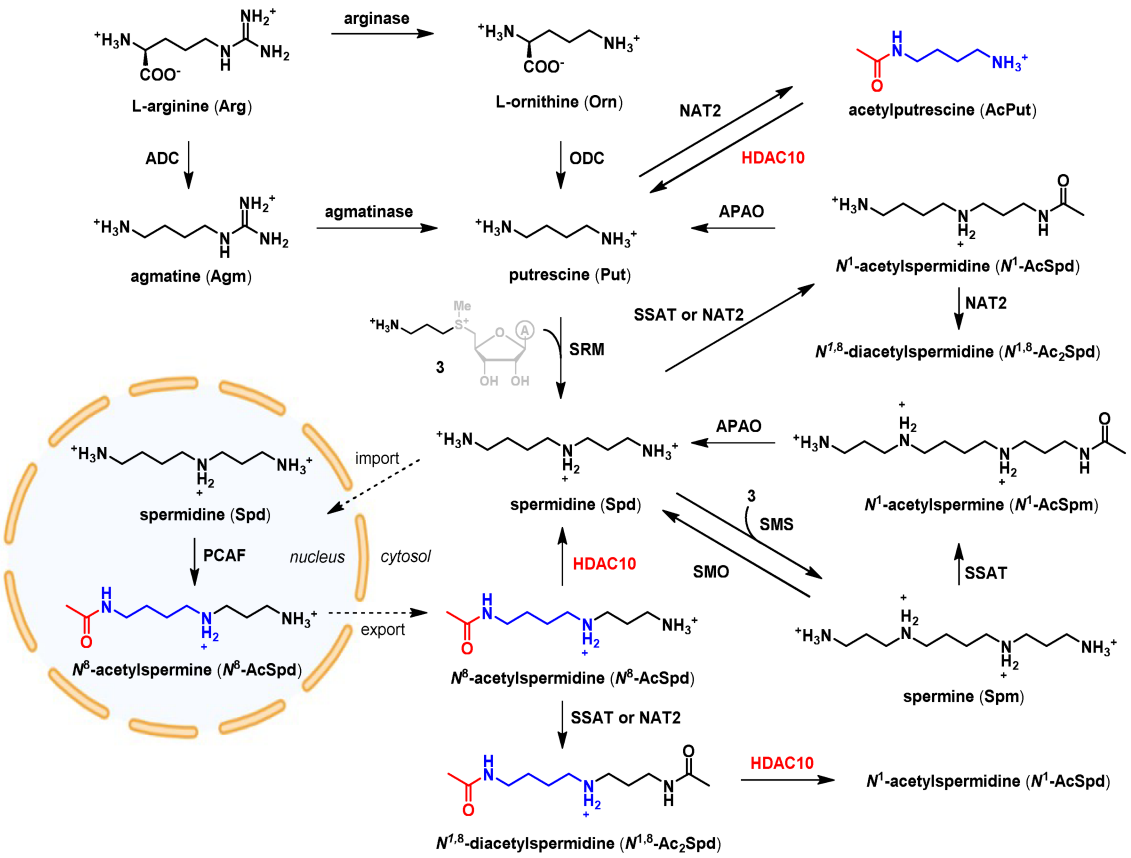


ADC: arginine decarboxylase; ODC: ornithine decarboxylase; SSAT: spermidine/spermine $N^1$-acetyltransferase; NAT2: arylamine *N*-acetyltransferase 2; APAO: $N^1$-acetylpolyamine oxidase; SRM: spermidine synthase; SMS: spermine synthase; SMO: spermine oxidase; PCAF: p300/CBP-associated factor. Acetamide moieties which can be hydrolyzed by HDAC10 are highlighted in red, the $AcNH(CH_2)_4NH_2^+$–R recognition motif of HDAC10 substrates is highlighted in blue. Figure based on Shinsky and Christianson[51] and Conway et al.[89]

Despite their low concentration, acetylated polyamines that cannot be formed by SSAT have been known for decades.[90–92] However, the acetyl transferases responsible for their biosynthesis and the deacetylase to reverse this process remained unknown for a long time. One example of such an acetylation reaction with a previously unknown acetyl transferase is the $N^8$-acetylation of $N^1$-AcSpd by arylamine *N*-acetyltransferase 2 (NAT2) to $N^{1,8}$-diacetylspermidine ($N^{1,8}$-$Ac_2$Spd),[89] a common constituent of human urine.[90] In 2020, NAT2 was reported to exhibit a broad substrate scope beyond its originally described acetylation of aromatic xenobiotics and includes a diverse set of aliphatic amines, including endogenous metabolites with three or four carbons between the amino groups.[89] While polyamines with three carbons between the amino groups are also substrates of SSAT, polyamines with a four carbon spacer seem to rely on NAT2 for acetylation. An alternative path for the formation of $N^{1,8}$-$Ac_2$Spd via the SSAT catalyzed acetylation of $N^8$-acetylspermidine ($N^8$-AcSpd) was also hypothesized.[80] The acetylation of Put to acetylputrescine (AcPut) by a 1,4-diaminobutane *N*-acetyltransferase first described in 1974[93] can now be attributed to NAT2 as well.[89] AcPut could be a source of GABA in the brain, since high-affinity uptake of AcPut, but not of Put, was

observed with rat brain synaptosomes.[94] AcPut can then be oxidized to GABA[95] by monoamine oxidase B.[96]

In 2017, the polyamine deacetylase responsible for the hydrolysis of terminal *N*-acetyl groups (highlighted red in **Scheme 2**) attached to 1,4-diaminobutyl moieties of polyamines (highlighted in blue) was finally identified as HDAC10.[41] It catalyzes the direct deacetylation of AcPut back to Put and can also act on the $N^8$-acetyl group of $N^{1,8}$-$Ac_2$Spd to form $N^1$-AcSpd, which is then broken down to Put by APAO. A substrate unique to HDAC10 is $N^8$-AcSpd, which is formed from imported Spd in the nucleus through the acetyl transferase p300/CBP-associated factor (PCAF). PCAF is a histone acetyltransferase (HAT) with spermidine $N^8$-acetyltransferase activity as well. Formed $N^8$-AcSpd increases PCAF HAT activity, which can be rationalized by the binding of $N^8$-AcSpd to the PCAF bromodomain. Conversely, high Spd concentrations have been observed to inhibit histone acetylation. This is likely due to spermidine competing with histones as an alternative substrate.[97] Thus, this process could be a polyamine acetylation-mediated epigenetic regulation mechanism. Once $N^8$-AcSpd is formed in the nucleus, it is exported to the cytoplasm,[80,84] where it is deacetylated back to Spd by HDAC10.[41]

There are many open questions regarding the role of polyamine acetylation in the complex metabolism and the significance of HDAC10 within it. Even after decades of intense research, polyamines remain a mystery of molecular biology.[76,98] At an abstract level, polyamine acetylation is a molecular marker that reduces the charge of a polyamine and thereby significantly alters its structure for molecular recognition, while polyamine deacetylation by HDAC10 reverses this process. The change of charges can be a signal for catabolism[86,87] as detailed above and allows the selective transport of polyamines within cellular compartments or out of the cell.[84] Furthermore, the function of polyamines as counter ions, especially for nucleic acids, is greatly altered by (de)acetylation. Acetylspermidines bind only weakly to DNA[99,100] compared to Spd and do not stabilize DNA to the same extent. The HDAC10 substrate $N^8$-AcSpd might have a regulatory function for gene expression by modulating PCAF as outlined above.

Implications of polyamine (de)acetylation in diseases are currently equally enigmatic. Acetylated polyamines are suggested as biomarkers, for example $N^{1,8}$-$Ac_2$Spd serum levels were observed to correlate with the severity of Parkinson's disease.[101] Elevated $N^8$-AcSpd plasma levels were reported as metabolome biomarkers for ischemic cardiomyopathy[102] and the extremely rare Snyder-Robinson syndrome.[103] However, these reports are mainly based on clinical metabolomics and statistics, but do not provide mechanistic explanations for their findings.

The polyamine metabolism and its regulation have long been connected to cancer.[66,104,105] Since polyamines are essential for cell proliferation, targeting their biosynthesis by inhibiting ODC with α-difluoromethylornithine (DFMO) was an early approach with little success in cytotoxic cancer therapy.[106] This may be due to the compensatory increase of polyamine uptake when polyamines are depleted in the cell. This can be overcome by reducing the dietary polyamine supply or by combination therapy with a polyamine transport inhibitor.[66] My contributions to

the field helped to identify $N^8$-AcSpd as an alternative source of spermidine in cancer cells under polyamine-limiting conditions. HDAC10 activity restored polyamine levels and provided growth rescue from DFMO treatment utilizing exogenous $N^8$-AcSpd.[65] This fits with reports of HDAC10 as a mediator of autophagy[50,107] which can promote chemotherapy resistance in neuroblastoma, supported by findings that increased spermidine levels induce autophagy and extend the life span of a variety of model organisms.[108]

## 1.3 HDAC inhibitors

The history of histone deacetylase inhibitors (HDACis) is a beautiful example of how chemical probes and natural product synthesis can enable biomedical research, significantly advance our understanding of cellular processes, and ultimately open the doors to an entirely new class of therapeutic agents. HDACis were initially investigated and developed in separate fields without any knowledge of their cellular targets. These approaches eventually converged when their common target was identified as Class I HDAC enzymes.[2,109]

The development of the first FDA-approved HDACi (**Figure 7**), suberoylanilide hydroxamic acid (SAHA, **4**; Vorinostat, Zolinza), began with the observation that DMSO induces murine erythroleukemia cells (MELC) to differentiate and synthesize hemoglobin, indicative of becoming nonmalignant cells.[110] This finding prompted Marks and Breslow's team to test many polar solvent-like species and later also tether two amide groups with a linear alkyl linker in order to exploit chelating effects and entropy advantages towards more potent differentiation inducers.[111] SAHA, which was patented in 1992,[112] was among the second generation of these so-called "hybrid polar compounds" (HPCs). At that point, SAHA's cytotoxic potential and ability to cause cell cycle arrest in tumor cells was known;[113] however, the cellular target remained elusive. Still, the interesting structure-activity relationship (SAR) of these HPCs led medicinal chemists to believe that a particular cellular receptor must be responsible for the observed effects, rather than a chelation or solvation effect. It is worth mentioning that many of these HPCs are in fact not HDACis, although they led to the design of SAHA. In hindsight, the targets were changed serendipitously to HDACs late in the medicinal chemistry campaign.[111]

In parallel, trichostatin A (TSA, **5**), a hydroxamic acid containing natural product from *Streptomyces*, was identified by Yoshida et al. to have the same effect on MELC as the DMSO-derived HPCs.[114] Three years later, in 1990, the same group discovered that TSA is a potent and specific inhibitor of histone deacetylation, making it the first identified natural product HDACi (**Figure 7**).[115] They also identified cyclic tetrapeptide trapoxin A (**6**), bearing an α-keto-epoxide as a naturally occurring inducer of histone hyperacetylation and cell cycle arrest with an irreversible mode of action. This discovery demonstrated that different chemotypes and mechanisms can provide HDAC inhibition. Later, many more naturally occurring HDACis were identified, including thiol-based examples like largazole (**7**) and romidepsin (**8**).[116]

The cellular targets of these histone hyperacetylation inducing natural products were finally uncovered by Schreiber and co-workers[2] in 1996 using a trapoxin affinity matrix. With the identification of epigenetic regulation by HDACs as the mechanism of action, HDACis became a

hot topic in medicinal chemistry for over a decade. The field was optimistic to have found a major cause of diseases, especially cancer,[6,22,117] in the regulation of gene expression by HDACs (see section 1.1.1), and there were plenty of chemical tools to target them. Based on the common structural features of TSA and trapoxin, in 1997, Jung et al.[118] suggested a simple three component HDACi pharmacophore consisting of a hydrophobic cap group, a linker and a zinc binding group (ZBG) (see **Figure 7**), which holds up until today. The following year, SAHA was also finally recognized as an HDACi and can be seen as the archetype of HDACis as it perfectly represents the HDACi pharmacophore.

The HDACi field quickly developed into a massive area of research and caught the interest of many medicinal chemists. As of now, Web of Science lists nearly 18 000 publications on the topic of HDACis with around a thousand new publications every year, which remained steady since 2010.[119] There are currently over 700 clinical trials listed on ClinicalTrials.gov using HDACis, and over 100 of them are still ongoing, which illustrates the significance and magnitude of the HDACi field and their therapeutic potential. However, only five HDACis achieved clinical approval so far (**Figure 7**, compounds on the left). As mentioned before, SAHA (**4**) was the first HDACi to be approved by the FDA in 2006.[120] It is used in the treatment of cutaneous T-cell lymphoma. The natural product romidepsin[121] (**8**) and the hydroxamic acid Belinostat[122] (**9**) were later approved for the same indication. Panobinostat (**10**), developed at Novartis, is currently the latest addition to the list of FDA-approved HDACis and is used against multiple myeloma.[123] Tucidinostat (chidamide, **11**) is the first orphan drug that was developed entirely in China and is approved there against peripheral T-cell lymphoma and as part of a combination therapy with exemestane against breast cancer.[124]

Overall, it is fair to say that the HDACis did not live up to their high expectations.[23] Although they are responsible for a significant research output in medicinal chemistry, the vast majority of clinical trials failed to meet their efficacy and safety goals. The five approved drugs are only used against two cancer types in monotherapy and none of them is a first-line therapy against these indications.[7] Clinical success is mainly limited by the safety and tolerability of HDACis, since toxic side-effects like myelosuppression, cardiac effects including QTc interval prolongation, and hepatic and gastrointestinal effects require dose-reduction or even discontinuation of therapy.[125] Clinical effects are mainly driven by inhibition of HDAC1–3, but all approved HDACis are pan-inhibitors with a broad isozyme target spectrum. Therefore, even if the correct isozyme in a patient is hit by an HDACi drug, side-effects from inhibition of other isozymes may overshadow the benefit and limit the treatment success. Considering the many distinct physiological functions of different HDAC isozymes, it is perhaps not surprising that the clinical phenotype of HDACi is more reminiscent of traditional cytotoxic agents used in chemotherapy than of a targeted therapy.[7]

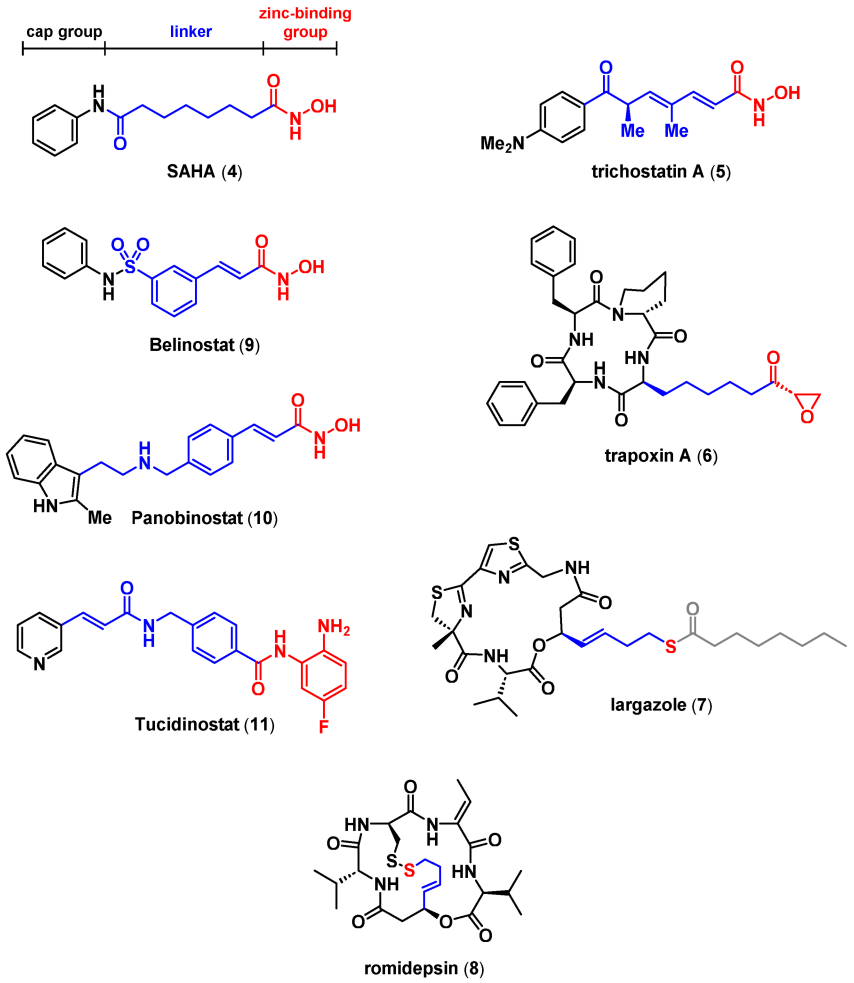


**Figure 7.** Clinically approved (left) and natural product (right) HDACis.

The next generation of HDACi drugs must therefore be isozyme-selective.[25,126] To develop isozyme-selective HDACis, the field needs suitable in vitro assay systems to evaluate drug candidates and establish selectivity profiles. I summarized these assay systems in section 1.4. Since the HDAC family covers a diverse substrate scope, specialized assay systems are required for at least some isozymes. There are also indications for misclassification of HDAC inhibition, potentially due to contamination with highly active Class I enzymes present in the preparation of Class II enzymes.[42,43,127] As a result, it is difficult to compare selectivity profiles of HDACis in the literature, since $IC_{50}$-values also depend strongly on the assay conditions and enzyme preparation used.

A recent report by Lechner et al.[128] with my involvement developed a powerful quantitative chemical proteomics approach to establish global selectivity profiles of commonly used HDACis. We were able to cover nine of the eleven HDAC isozymes and identified previously unknown non-HDAC off-targets. The approach allows the determination of apparent $pK_D$ values by dose-dependent competition of inhibitors against the HDAC affinity matrix followed by mass spectrometric quantification of captured proteins. Since this is the largest consistent HDACi selectivity profile dataset, I selected examples out of the 53 tested compounds to

illustrate the relationship between inhibitor structure and target profile. This serves to provide representative examples of the HDACi pharmacopeia. The inhibitors were clustered according to their selectivity profile. **Figure 8** depicts the structures and apparent p$K_D$ values from the chemical proteomics approach.

Cluster 1 contains SAHA (**4**) and other closely related hydroxamic acids, such as M344 (**12**) and ricolinostat (**13**) with the same hexyl linker but different cap groups. Compounds in this cluster are HDAC pan-inhibitors that share pronounced off-target activity, especially on isochorismatase domain-containing protein 2 (ISOC2). All HDAC isozymes are engaged, except for Class IIA enzymes and HDAC8. This reveals a potential blind spot in the approach, as it is well established that SAHA binds HDAC8, although to a lower extend than HDAC6, which is also strongly inhibited by SAHA-derivatives **12** and **13**. The cap groups in **12** and **13** reduce HDAC3 binding significantly compared to SAHA; **13** is a notably better HDAC10i.

Cluster 2 is the largest one, also mainly composed of hydroxamic acids including TSA (**5**), but also the naturally occurring disulfide romidepsin (**8**) and the two remaining FDA-approved inhibitors Belinostat (**9**) and Panobinostat (**10**). While the compounds in this cluster are not particularly selective, since they engage Class I, Class IIB and some even Class IIA, they are the most potent. Romidepsin (**8**) stands out with the highest affinity for all Class I enzymes and also excellent potency against all other isozymes, except HDAC10. Quisinostat (**14**) has a similar profile to Panobinostat (**10**) but surprisingly does not bind HDAC6 in this method. Abexinostat (**15**) is like **10** and **14** an extremely potent but unselective HDAC10 binder, which was confirmed by my FRET and BRET assay. Notably, all three compounds bear a sterically unhindered basic amine at the end of the linker region in roughly the same distance to the hydroxamic acid. Dacinostat (**16**) is closely related to **10** but features a hydroxyethyl substituted amine, which could be responsible for the reduced activity against HDAC10 and other isozymes.

Cluster 3 consists solely of o*rtho*-aminoanilides, which are selective for HDAC1–3. Clinically approved Tucidinostat (**11**) and Entinostat (**17**) have higher target affinity than "cap-less" inhibitor BG45 (**18**). These examples together with romidepsin (**8**) show that potent HDAC inhibition is feasible without hydroxamic acids and that the ZBG can provide selectivity, at least for certain classes.

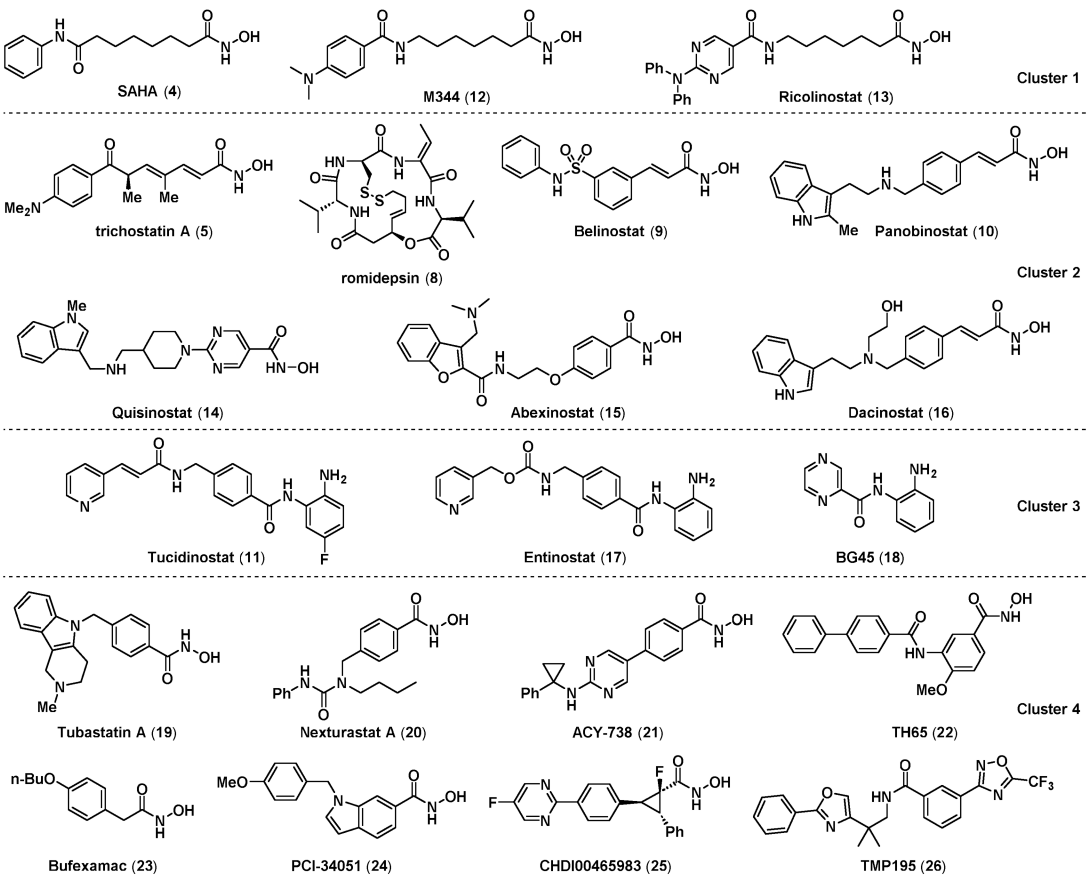


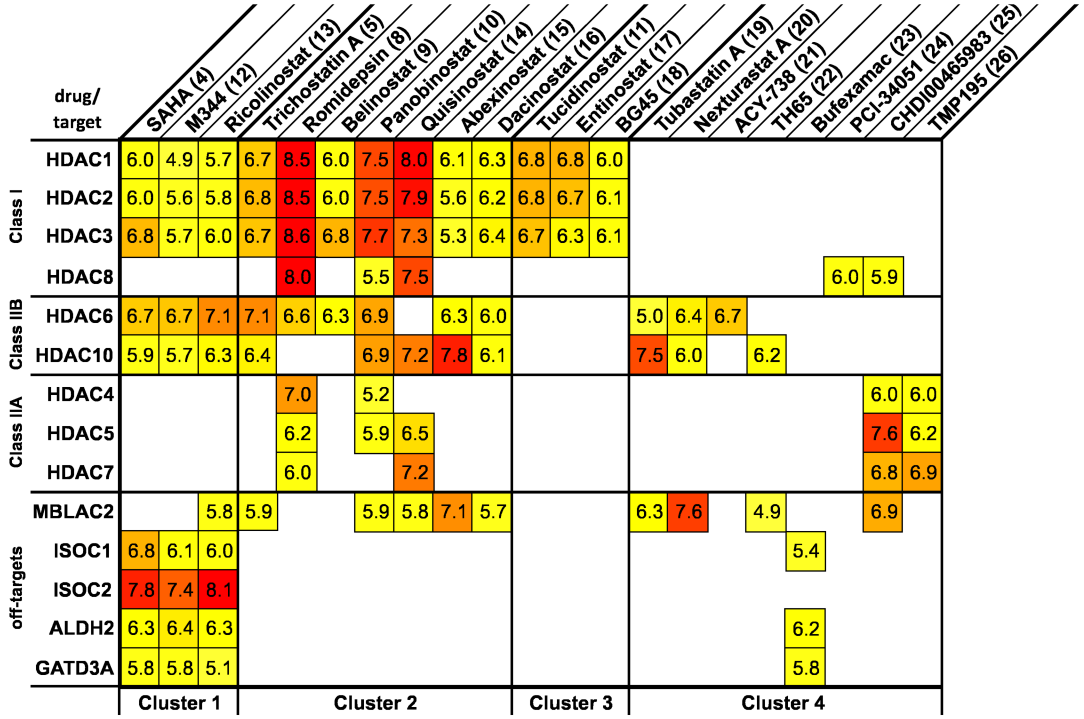


**Figure 8.** Target landscape of selected HDACis by Lechner et al.[128] Shown are apparent p$K_D$ values determined by chemical proteomics profiling. Empty fields indicate p$K_D$ < 4.5.

The remaining Cluster 4 is the most interesting for my goal of selective HDAC10 inhibition, as it contains the Class IIB-selective compounds. This Class is also dominated by hydroxamic acids, which is representative of the overall chemical space of HDACis. In Cluster 4 we find the well-known chemical probes that were developed as selective HDAC6 inhibitors, like Tubastatin A (**19**),[129] Nexturastat A (**20**) and ACY-738 (**21**). However, only the latter is actually HDAC6 selective, while the other two also bind HDAC10. In the case of Tubastatin A (**19**), HDAC10 binding is significantly stronger than HDAC6 activity, which confirms earlier findings of the Miller Lab.[43] The SAR indicates that *para*-substituted benzhydroxamic acids are a good starting points for Class IIB selective compounds, but an aromatic linker or basic cap group is not sufficient for HDAC10 selectivity. TH65 (**22**) looks like a reasonably potent selective HDAC10i, but the promising selectivity profile could not be confirmed in the cellular BRET assay or biochemical assays against HDAC10 and 6, as TH65 (**22**) showed below 10-fold selectivity for HDAC10 in these assay systems. A possible explanation for these inconsistencies with other assays is the high detection limit for binding, since only $pK_D^{app} > 4.5$ can be quantified. Therefore, modest binders often appear more selective than they actually are. Potentially another example for this effect is the now withdrawn topically used anti-inflammatory drug Bufexamac (**23**). In a prior, similar chemical proteomics approach, it was identified as a selective Class IIB HDACi with moderate (micromolar) potency.[130] Phenyl acetohydroxamic acids like **23** are only rarely used and may have potential for Class IIB and ultimately HDAC10 selectivity.

Further highly selective chemical probes that were confirmed in the study by Lechner et al. are the indole-linked hydroxamic acid PCI-34051 (**24**), which only binds HDAC8, and CHDI00465983[131] (**25**) and trifluoromethyloxadiazole TMP195[132] (**26**), which are Class IIA selective. The structures of these compounds clearly differ from pan-inhibitors by a more rigid and bend shape, which is responsible for their selectivity. Inhibitor **26** is noteworthy, since it exemplifies that potent HDAC7 binding can be achieved without a hydroxamic acid ZBG.

**Figure 8** illustrates that isozyme selective HDAC inhibition is challenging, especially in combination with high potency. There are many more promising and selective HDAC probes in the literature that were not included in this study.[25,126] Nevertheless, the fact that compounds like Tubastatin A (**19**) are still used as chemical tools to draw conclusions about one isozyme shows the need for more selective compounds and increased awareness about the selectivity profiles, especially for neglected isozymes like HDAC10. Selective chemical probes can also provide a starting point for better therapeutic agents to help overcome the clinical drawbacks of pan-inhibitors.

### 1.3.1 Previous work on selective HDAC10 inhibitors

While the HDACi field is vast and the previous section did just scratch the surface of the gigantic body of literature available, only few contributions dedicated to selective HDAC10is were made prior to my work, and no selective HDAC10is were discovered serendipitously as far as I know. Although there is increasing awareness for HDAC10 as a potential target, especially in oncology and immunology (see section 1.1.4.4, page 17), the first report of a medicinal chemistry

campaign dedicated to the development of selective HDAC10is came out of the Miller Lab as recently as 2019 with my involvement.[43] A reason for the comparatively late development of HDAC10is is the fact that their enzymatic activity as polyamine deacetylases was also discovered rather recently in 2017.

In this first study towards selective HDAC10is, we identified Tubastatin A (**19**), which was previously regarded as HDAC6 selective, to be an even better HDAC10 binder. This was later confirmed independently by quantitative chemical proteomics.[128] We could identify the tertiary amine of the tetrahydro-γ-carboline ring as the structural feature responsible for HDAC10 activity, presumably via electrostatic interaction with the HDAC10 glutamate gatekeeper residue, which was later confirmed by X-ray crystallography.[133] HDAC10 activity could be well modulated and increased down to the single-digit nanomolar range in the HDAC10 BRET assay for carboline ring-opened derivatives (**27**–**30**), with $pIC_{50}$ values of 8.4 for pyrrolidine **27** and gramine **29**. When the basic amine was removed (compounds **31** and **32**), acetylated in **33**, or replaced with an oxygen in **34**, the HDAC10 activity dropped and the compounds became HDAC6 selective. However, the limit for HDAC10 selectivity in this study was around 40-fold since the HDAC6 activity could not be abolished in the Tubastatin scaffold.

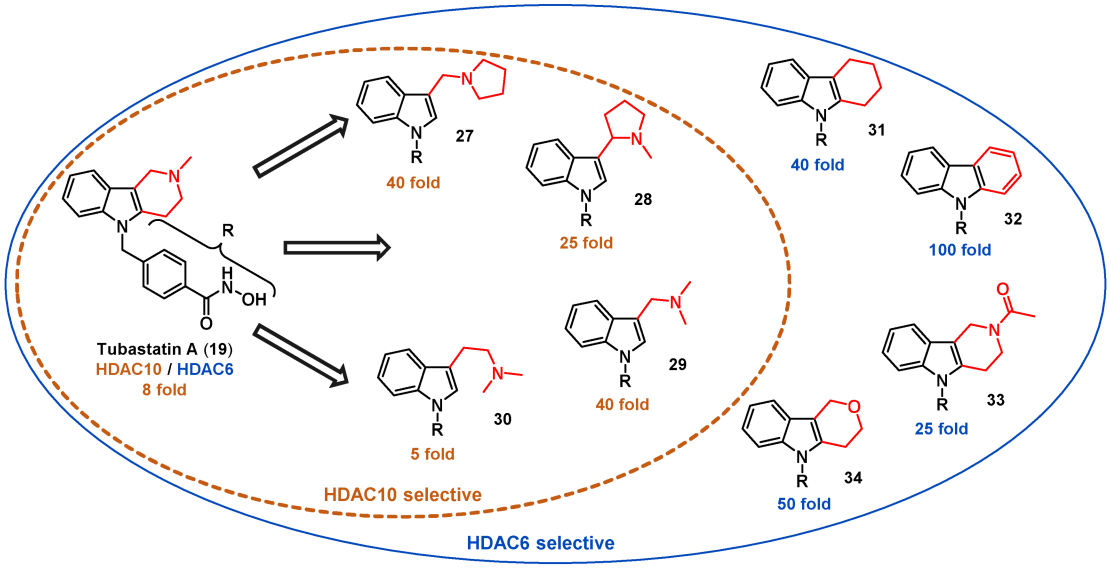


**Figure 9.** Structure-activity relationship study of Géraldy et al.[43] towards selective HDAC10is based on Tubastatin A. The tertiary amine of the tetrahydro-γ-carboline ring was identified as the driver of HDAC10 activity.

However, there were attempts towards selective HDAC10is before HDACs were even discovered. Fries and Blankenship developed inhibitors[134,135] against the cytoplasmic $N^8$-AcSpd deacetylase, extracted from rat liver,[44] which we now know must have been HDAC10. Their inhibitors were inspired by the structure of the known polyamine substrate and the first generation of inhibitors utilized a ketone like **35** (**Figure 10**) for zinc binding.[134] Based on a deacetylation assay that measures radiolabeled acetic acid released from $N^8$-[$^3$H]acetylspermidine, they report an apparent inhibition constant ($K_i$) of 0.18 µM for **35**.

Notably, they correctly predicted key aspects of the HDAC10 active site by postulating two anionic sites for substrate recognition and a zinc ion at the acetamide binding pocket. They also demonstrated that inhibitor **35** leads to the accumulation of $N^8$-AcSpd in mice and HeLa cells, but does not affect histone acetylation, which indicates that they were targeting HDAC10.[47] Later, they employed ε-aminohydroxamic acid **36**, which increased the potency by 160-fold compared to ketone **35** in their deacetylation assay.[135]

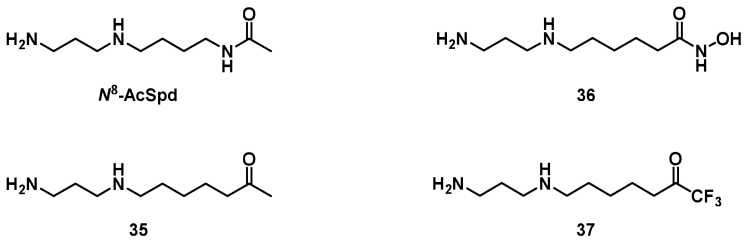


**Figure 10.** Early polyamine-mimicking $N^8$-AcSpd deacetylase (HDAC10) inhibitors and the enzyme substrate $N^8$-AcSpd for comparison.

Inhibitors **35** and **36** were revisited nearly 20 years later by the Christianson Lab and augmented with additional derivatives bearing different zinc binding groups (see section 1.3.1.1), such as trifluoromethyl ketone **37**, which exists in aqueous solution predominantly as gem-diol hydrate.[136] In this form, it closely resembles the tetrahedral transition state of acetamide hydrolysis by HDAC10 and is able to effectively coordinate the active site zinc. These compounds were first targeted against the bacterial acetylpolyamine amidohydrolase, the bacterial equivalent of HDAC10, but inhibitor **37** later became the transition state mimicking ligand in the first crystal structure of zHDAC10 that identified it as a PDAC.[41] Herbst-Gervasoni and Christianson crystallized inhibitors **35** and **36** with zHDAC10 as well and found that inactivated ketone **35** bound in the gem-diol hydrate form, like electron deficient ketone **37**. ε-Aminohydroxamic acid **36** donates a bifurcated hydrogen-bond to gatekeeper E274, which helps to rationalize the high binding affinity ($IC_{50}$ = 120 nM) measured by HPLC $N^8$-AcSpd deacetylation assay with purified zHDAC10.[133]

Parallel to my investigations, Daniel Herp (Jung Group, University of Freiburg) was working on HDAC10is with a focus on novel enzymatic assays for HDAC10. His NDA fluorescence quenching assay system is briefly summarized in section 1.4.5. He also developed a class of potent piperidine-4-hydroxamic acid HDAC10is (**Figure 11**, compounds **38–41**).[137] The best compounds, diamines **40** and **41**, are comparable in selectivity and potency to my inhibitors of the aza-SAHA series (section 3.2). A cocrystal structure of inhibitor **40** with HDAC10 indicates the piperidine amine forms a water-mediated hydrogen bond to the gatekeeper E274 and potentially a cation-π interaction with W205, while E24 engages the secondary amine.

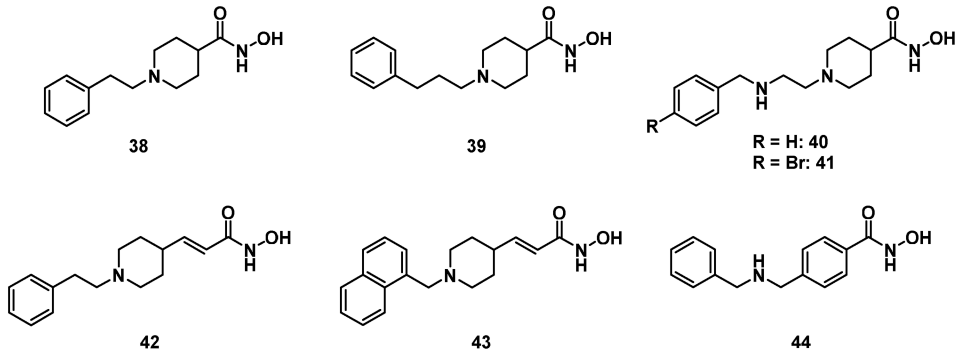


**Figure 11.** HDAC10is developed in parallel to my investigations.[137,138]

Zeyen et al. also reported an independent approach towards HDAC10is using amino hydroxamic acid inhibitors like **42–44** that exploit the HDAC10 gatekeeper residue, which was also confirmed by X-ray crystallography.[138] Their inhibitors were evaluated with Herp's NDA fluorescence quenching assay with zHDAC10 and an AMC-based assay for other isozymes. The best inhibitors showed 50 to 80% less selectivity over HDAC6 compared to Herp's or my compounds. α,β-unsaturated hydroxamic acid **42** was found to be the best binder of HDAC10; however, it is limited by only 23-fold selectivity over HDAC8.

#### 1.3.1.1 Alternative zinc binding groups for HDAC10 inhibition

Hydroxamic acids currently dominate the HDACi field as a potent and reliable zinc binding group (ZBG) (see section 1.3, page 21), although they suffer from poor ADMET properties and can be mutagenic, which severely limits their clinical use, especially beyond oncology.[139] Nevertheless, selective Class IIB inhibition suggests promising clinical applications in neuroprotection[129] for treating neural disorders[140] such as Alzheimer's disease[141–143] and Charcot–Marie–Tooth disease.[144] Furthermore, HDAC10 and HDAC6 have been reported to be involved in inflammation,[64] T-regulatory cell function[145–147] and transplant rejection.[57] Non-hydroxamate inhibitors are especially interesting as neuroprotective agents[148] and immunomodulators, since they can avoid the aforementioned drawbacks such as dose-limiting toxicity. Additionally, isozyme selectivity can be modulated by using less promiscuous ZBGs.

There was little prior work on selective HDAC10is with reliable HDAC10 data when I started the project and only a few non-hydroxamate compounds were evaluated. The early work by Fries and Blankenship[134,135] on the at that time unidentified $N^8$-AcSpd PDAC from rat liver[44] started out with sulfonamides, ketones, carboxylic acids and an α-chloroacetamide in an attempt for a covalent, irreversible inhibitor. However, of these ZBGs, only methyl ketones yielded inhibitors with sub-micromolar apparent $K_i$ values, which were quickly replaced by the much more potent hydroxamic acid-based inhibitors we use today. Only one additional report by Herbst-Gervasoni and Christianson[133] using alternative ZBGs on polyamine analogues specifically for HDAC10 inhibition became available thus far. They tested the previously reported PDAC inhibitors **35** and **36** against zHDAC10 and compared their activity with a series of analogues that bear alternative ZBGs (**Figure 12**, compounds **45–49**). Furthermore,

they described X-ray crystal structures of zHDAC10 complexed to the inhibitors in **Figure 12**, which illuminates the binding geometries of the different ZBGs.

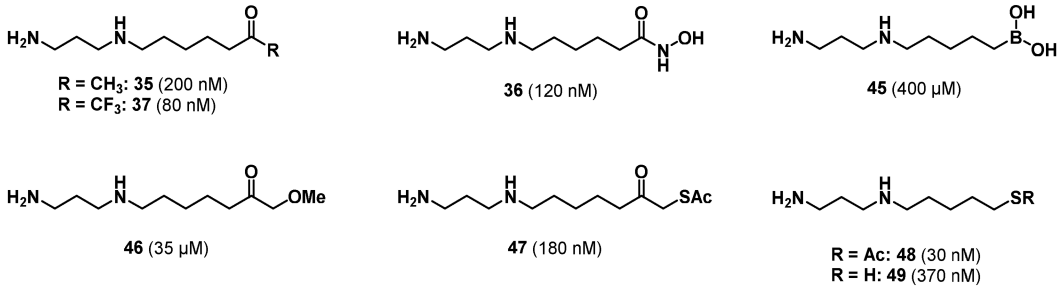


**Figure 12.** Polyamine analogue HDAC10is utilizing different ZBGs. $IC_{50}$ values for zHDAC10 determined by HPLC $N^8$-AcSpd deacetylation assay in parenthesis.

Since different ZBGs were employed with the same inhibitor scaffold, I can compare the HDAC10 activity and attribute it to the ZBG; however, they did not report HDAC6 activity or data for other isozymes, so only HDAC10 potency, but not selectivity can be compared. Ketones **35**, **46** and **47**, as well as boronic acid **45** are weak HDAC10 binders despite their polyamine structure, which makes these zinc binding groups uninteresting. The only ketone that was superior to hydroxamic acid **36** was trifluoromethyl ketone **37**. Although this ZBG provides good binding affinity in biochemical assays, electron deficient ketones are metabolically even less stable than hydroxamic acids due to their fast reduction by carbonyl reductases to the corresponding inactive alcohols.[149,150] The poor pharmacokinetic properties of ketone ZBGs are unacceptable, even for use as chemical probes.[151] Therefore, only thiols are left as alternative zinc-binders with available HDAC10 inhibition data. Indeed, they were the most potent HDAC10 binders, even significantly better than hydroxamic acid **36**. Interestingly, thioacetate **48** was the best binder in this study, surpassing its corresponding free thiol **49** by over 10-fold. However, the HDAC10–inhibitor complexes of thiol/thioacetate compounds **47**–**49** all show binding of a thiolate to the active site zinc, so thioacetates **47** and **48** hydrolyzed during the crystallization process. For **47**, we found only the resulting thiol, but not the ketone to coordinate the zinc. This makes the assay data hard to interpret, as the active binders are clearly thiols like **49** and the thioesters are acting as prodrugs. The higher $IC_{50}$ of **49** compared to **48** is likely due to instability of the free thiol in solution, which readily oxidizes to the disulfide, while prodrug **48** provides "fresh" active thiol **49** in situ. It was also speculated that HDAC10 catalyzes the hydrolysis of the thioester to form the active inhibitor depending on the residual activity. This was not further investigated so far, but may be an interesting prodrug approach for HDAC10 inhibition.

Overall, thiol ZBGs are quite well established and nature already took the prodrug approach to compensate for the poor stability of free thiols as exemplified in thioester largazole (**7**, page 23) and disulfide romidepsin (**8**), which is even FDA-approved for cancer therapy against T-cell lymphoma. There are no other literature reports on HDAC10 inhibition using alternative ZBGs, and Lechner et al.[128] did not find any of the few non-hydroxamate HDACis in their broad study on the targets of the HDAC pharmacopoeia to bind HDAC10. Still, this could be due to the

elongated binding tunnel of HDAC10, so compounds with good ZBGs but a too short linker moiety would not bind HDAC10. However, I can speculate on potentially successful zinc binders, based on available data for the closest relative – HDAC6.

For selective HDAC6 inhibition, there are a few reports that successfully employ alternative ZBGs beyond simple thiols, which could potentially also work for HDAC10 and already provide selectivity over Class I. Selectivity for HDAC10 within Class IIB could then be provided by the linker moiety or the cap group. The best described alternative ZBGs for HDAC6 are SAHA-like mercaptoacetamides (**50**), which were pioneered by the Kozikowski Lab.[152,153] Christianson later elucidated the binding geometry of these inhibitors with HDAC6.[154] The mercaptoacetamide ZBG was recently also employed in the Tubastatin scaffold, where it is attached to a benzyl linker (**51**).[155] A medicinal chemistry campaign at Nycomed investigated trithiocarbonates with a wide range of S → N, O, $CH_2$ substituted analogues.[156] Structural motifs **52**–**54** provided sub-micromolar HDAC6 inhibition. However, they did not investigate whether at least some of their ZBGs were actually prodrugs of α-thio acetophenones. A patent from 2016 describes difluoromethyl-1,3,4-oxadiazoles (**55**) as potent HDAC6 inhibitors[157] and the Hansen Lab has recently developed targeted degraders using this ZBG as the warhead.[158]

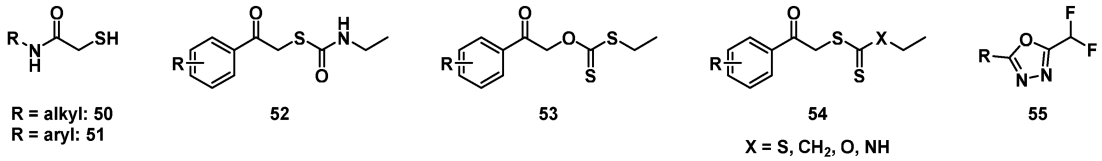


**Figure 13.** ZBGs successfully used for selective HDAC6 inhibition. These could potentially also bind HDAC10.

## 1.4 Assays for the evaluation of HDAC inhibitors

Biological activity assays are crucial for medicinal chemistry to evaluate prepared compounds and to establish structure-activity relationships (SAR), which guide the design of new compounds. The ideal assay has high throughput, is fast and inexpensive to conduct and provides robust and reproducible activity data. An additional requirement is effective assay data analysis and handling capabilities with increasing assay throughput. Target-based screening in early drug discovery utilizes cell-free, purely biochemical assays and cellular in-vitro assays. Both types can either measure only target binding of a test substance or generate a readout based on inhibition of the target's enzymatic activity.[159]

A wide variety of assay systems for histone deacetylases have been developed in the past decades with readouts including LC/MS,[41] differential scanning fluorimetry,[160] direct fluorescence,[161] fluorescence resonance energy transfer (FRET),[162] luminescence[163] and bioluminescence resonance energy transfer (BRET).[164] However, not all assay systems provide the throughput required for a medicinal chemistry campaign and SAR-studies. Also, not all assay systems are applicable to all HDAC isozymes. Especially HDAC10 activity cannot be evaluated using conventional enzymatic HDAC assays due to its specificity for only certain

polyamine substrates and poor activity on peptidic substrates.[41–43] This section describes the most important HDAC assay systems and the ones I used for the evaluation and selectivity profiling of my HDAC10 inhibitors.

### 1.4.1 Acetyllysine-AMC-based enzymatic assays

Enzymatic cell-free assay systems that utilize the fluorescence of 4-amino-7-methylcoumarin (AMC) are commonly used to measure HDAC activity and to evaluate HDAC inhibitors.[42,161] The operational principle of acetyllysine-AMC-based assays and underlying chemistry is detailed in **Scheme 3.** These assays utilize an artificial, often peptidic substrate (**56**) with an acylated lysine bound C-terminal to AMC as the reporter moiety. If R in **56** is a methyl group, then it is a good substrate of Class I enzymes. AMC-based assays are also available for HDAC11 with R = long alkyl ($\sim C_{13}$)[14] and Class IIA with R = $CF_3$.[42] AMC (**57**) can only be released from the substrate once the acetyllysine side chain is deacylated by HDAC activity. The resulting free amine is recognized by trypsin, which can then cleave AMC from the substrate. This results in a 30-fold increase in fluorescence emission at 460 nm compared to the lysine-bound AMC moiety.[161] The HDAC enzymatic activity on the substrate is highly dependent on the substrate structure (acyl moiety, peptide sequence and C-terminal protecting group) and isozyme.[42,165] It is by now well established that HDAC10 shows poor activity on acetyllysine-AMC substrates.[41,42] Therefore, HDAC10 activity data that is sometimes found in the literature using such assays has to be interpreted with caution.

**Scheme 3. Chemistry of acetyllysine-AMC-based enzymatic assays**

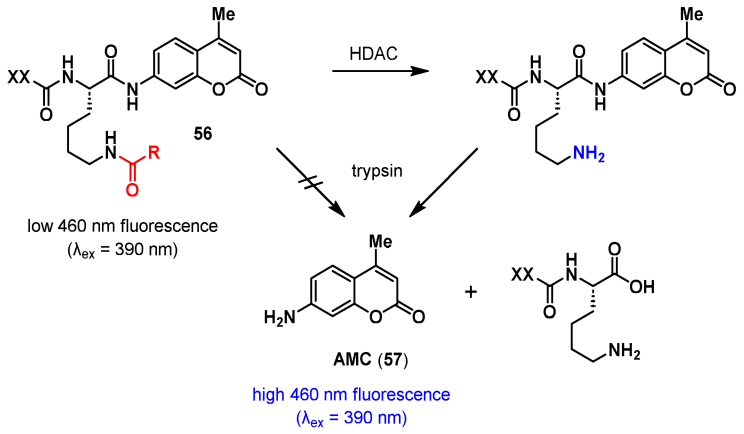


The C-terminal acyllysine in the peptidic substrate is deacylated by HDAC activity, R = Me for substrates of Class I HDACs, R = long alkyl ($\sim C_{13}$) for HDAC11, R = $CF_3$ for Class IIA. Only then can the trypsin liberate AMC, which exhibits enhanced fluorescence and provides a signal proportional to the HDAC activity. Figure based on Wegener et al.[161]

### 1.4.2 HDAC-Glo I/II assay

To evaluate Class I and HDAC6 activity, I used the cell-free HDAC-Glo assay, which is based on the commercial HDAC-Glo I/II assay and screening system kit by Promega. It operates similarly to AMC-based assays, but instead of using fluorescence, it provides a luminescence readout proportional to the HDAC enzymatic activity. The Glo assay operational principle and

underlying chemistry is detailed in **Scheme 4**. The signal is generated in a coupled three-enzyme reaction cascade using a proprietary proluminogenic peptidic substrate (**58**). This substrate is a three amino acid peptide based on an optimized consensus sequence derived from histone 4 with the N-terminus Boc-protected and a C-terminal amide bond to 6-aminoluciferin.[166] Although the exact peptide sequence is not disclosed, Halley et al.[163] provide BocHN-GAK$^{Ac}$-C-aminoluciferin as an example for a suitable HDAC Class I and II substrate. The peptide-bound 6-aminoluciferin is not a substrate of the luciferase in the assay mix and no luminescence signal is produced in the absence of HDAC activity. Only when the Glo substrate (**58**) is deacetylated, it becomes the substrate for a proteolytic trypsin-like developer enzyme, liberating free 6-aminoluciferin (**59**), which in turn is processed by a proprietary firefly luciferase to produce a strong luminescence readout even in a miniaturized assay format. All three coupled enzymatic reactions occur simultaneously once the developer reagent (containing trypsin and luciferase) has been added. The luminescence intensity depends only on the HDAC activity, as this becomes the rate limiting step of the enzyme cascade once a steady state has been reached, typically after 15–45 min.

**Scheme 4. Chemistry of the HDAC-Glo I/II assay**

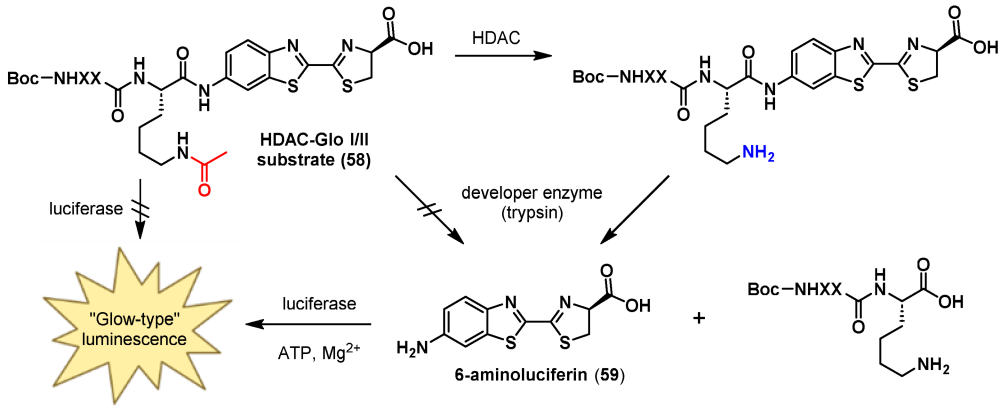


The C-terminal acetyllysine in the peptidic HDAC-Glo I/II substrate is deacetylated by HDAC activity. Only then can the proteolytic developer enzyme liberate 6-aminoluciferin, which is the substrate for a luciferase that provides a strong luminescence signal proportional to the HDAC activity once the three coupled enzyme reactions reach a steady state. Figure based on the technical manual of the Promega HDAC-Glo I/II assay and screening system.[166]

The advantages of the Glo assay over AMC-based assays are a better signal-to-noise ratio as well as robustness towards assay interference, e.g. by autofluorescence of test compounds. Therefore, I could perform the Glo assay in 384-well plates at an assay volume of 15 µL, which provided high throughput and was also required due to reagent costs. According to the manufacturer, it can be used on HDAC1–11; however, enzymatic activity on the Glo substrate varies by three orders of magnitude, with the highest activity seen with HDAC1 and 2, and poor activity described with Class IIA, HDAC10 and 11.[166] By now, it is well established that HDAC10 has poor activity on peptidic substrates.[41–43] Due to this, enzymatic assays – like the Glo assay – are highly susceptible to contamination from Class I enzymes when evaluating the less active isozymes like HDAC10 or Class IIA. Assay data reported for HDAC10 using peptidic substrates is likely measuring the activity of contaminant Class I HDACs and should be interpreted with

caution. Therefore, I used the Glo assay only with Class I enzymes and HDAC6, and employed the FRET assay for HDAC10 (see next section and section 3.1.2).

### 1.4.3 TR-FRET ligand displacement assay

While reliable high-throughput assays to measure the enzymatic activity of Class I enzymes and HDAC6 were developed nearly two decades ago, no suitable enzymatic assays for HDAC10 were available when I started the project in 2018. This is rooted in HDAC10's specificity for certain polyamine substrates and its poor activity on conventionally used peptidic substrates.[41–43] To determine this substrate specificity, the Christianson Lab used an LC/MS-based discontinuous assay, which would be unsuited for a medicinal chemistry campaign due to the low throughput.

Contract research organizations and the HDAC-Glo I/II assay and screening system offer profiling of HDAC10 despite the low activity on the employed substrates in these enzymatic assay systems. This is problematic, since other isozymes have several orders of magnitude higher activity on the employed substrates.[42,165,166] Therefore, minute contaminations of other, more active HDACs result in wrong selectivity profiles despite satisfactory assay performance metrics. Such observations were made with Class IIA HDAC activity in an AMC-based assay that depended on the expression system of the tested enzyme preparation. Contamination with Class I HDACs was proposed as the main source of assay signal for certain AMC-based substrates.[127] In light of these findings, it is likely that HDAC10 assay data obtained with enzymatic assays are the result of such cross-contaminations. Notably, commercially available HDAC10 enzyme preparations are often expressed in Sf9 insect cells, which are known for hypoacetylated histones caused by high basal HDAC Class I activity.[167] This hypothesis is further supported by an analysis of HDACi selectivity literature data subjected to hierarchical clustering.[43] The analysis revealed a correlation between HDAC Class I and HDAC10 activities, while HDAC6 gave a completely distinct target profile despite the fact that HDAC6 and 10 are often targeted by the same inhibitors due to their close structural similarity. Therefore, it was essential for my project to establish a non-enzymatic high-throughput HDAC10 binding assay in the Miller group.

To develop selective HDAC10is, I utilized a cell-free time-resolved fluorescence resonance energy transfer (TR-FRET) binding assay for HDAC10, which was described previously.[162] The TR-FRET assay operational principle is depicted in **Figure 14**. In the absence of an HDAC10 binder, the fluorescent tracer binds to the active site and upon irradiation with 340 nm flashes, fluorescence resonance energy transfer (FRET) from the 615 nm europium emission to the tracer Cy5-dye results in 665 nm fluorescence, which is detected time-resolved. FRET can only occur over nanoscale distances (typically 1–10 nm) due to an inherent inverse-sixth-power distance dependence,[168] which requires the $Eu^{3+}$-labelled Streptactin and the tracer bound to the same HDAC10 protein for FRET to occur. When another HDAC10 binder (the test substance) is present, the FRET tracer is displaced from the active site and the 665 nm FRET signal is disrupted depending on the dose and binding affinity of the test substance.

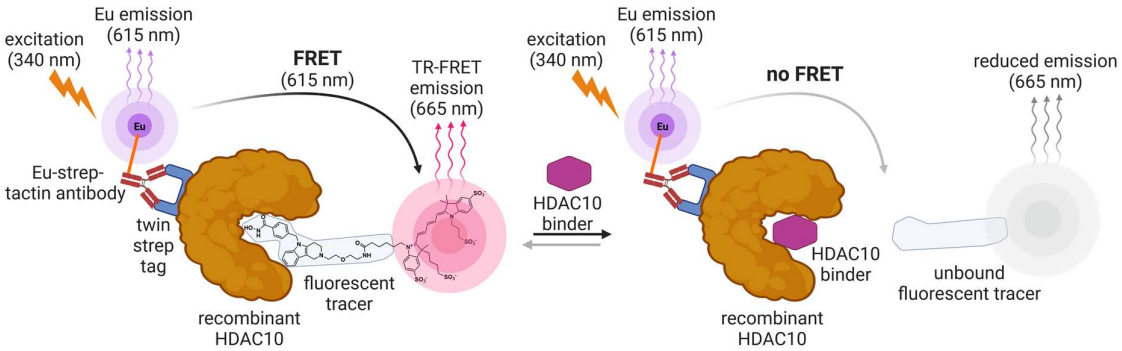


**Figure 14.** Schematic representation of the HDAC10 TR-FRET assay. When a Europium-labeled Streptactin antibody and a fluorescent tracer bind the TwinStrep–tagged HDAC10 protein simultaneously, FRET occurs upon irradiation with 340 nm flashes resulting in 665 nm emission. In the presence of an HDAC10 binder, which competes with the tracer, FRET is disrupted and a change in the time-resolved signal is observed. Created in BioRender.com based on Géraldy et al.[43]

The advantage of the TR-FRET HDAC10 binding affinity assay is that it is insensitive to contamination with other, structurally related enzymes, since only proteins with the genetically encoded TwinStrep-tag can elicit a FRET signal upon binding of the tracer. Furthermore, the assay requires only one addition step and can be performed in a miniaturized 15 µL/well format at high throughput due to a good and persistent signal-to-background ratio. This makes it ideal for evaluating inhibitors in SAR-studies.

### 1.4.4 Cellular BRET target engagement assay

The BRET cellular target engagement assay was developed by scientists at Promega[164] and operates similarly to the FRET assay. The BRET assay operational principle is depicted in **Figure 15**. It is also a ligand displacement assay with the main difference that the donor for the resonance energy transfer is not a fluorophore, but a genetically encoded nanoLuciferase (nLuc). Therefore, the assay system requires the expression of an HDAC-nLuc fusion protein. The advantage is that using a cell permeable fluorescent tracer as BRET acceptor and a cell permeable nLuc substrate allows the quantification of target binding events and compound residence times in live cells. In the absence of an HDAC binder, the SAHA-NCT-dye conjugate tracer is bound to the fusion protein and upon addition of the nLuc substrate, BRET occurs from the nLuc emission ($\lambda_{max} \approx 450$ nm) to the fluorescent tracer. This induces tracer fluorescence at 610 nm with a low background. When another HDAC10 binder (the test substance) enters the cell, the BRET tracer is displaced from the active site and the 610 nm emission is greatly reduced depending on the dose and binding affinity of the test substance, because BRET is highly distance-dependent.

Due to its cellular nature, the BRET assay can provide ADME data to some extent, since cell permeability, potential efflux and intracellular stability for several hours incubation time is represented in the assay results. The drawbacks of the BRET assay are longer preparation times and a lower throughput, since at least in my hands, a 96-well plate format was required. Although BRET signals can be strong, they depend on the expression levels of the HDAC-nLuc

fusion protein, so BRET assays can perform poorly if the nLuc construct is insufficiently expressed. For the development of my selective HDAC10i, I utilized the BRET assay with HDAC10 and its closest relative HDAC6 to obtain cellular target engagement and selectivity data.

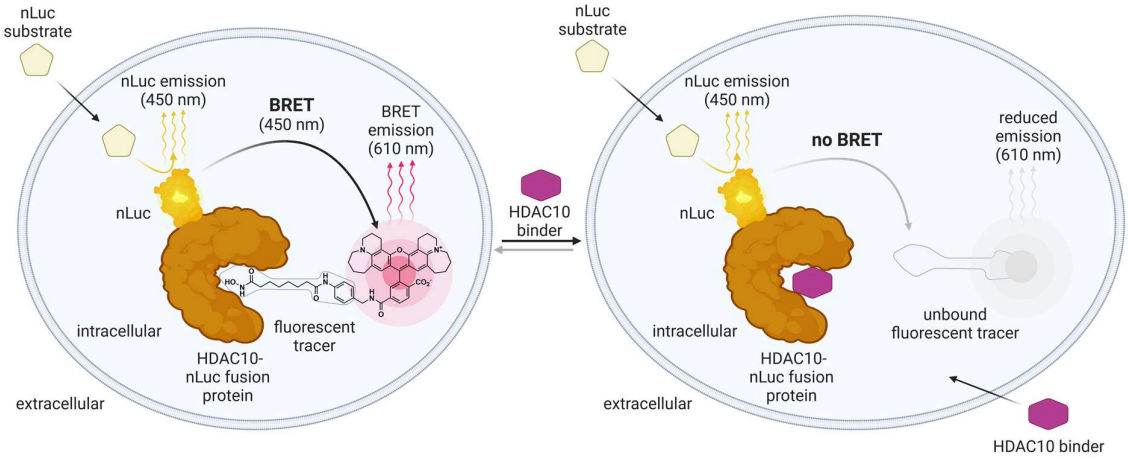


**Figure 15.** Schematic representation of the BRET assay. When cells expressing an HDAC10-nLuc fusion protein are treated with the fluorescent BRET tracer and nLuc substrate, BRET from the nLuc emission to the tracer dye induces tracer fluorescence. In the presence of an HDAC10 binder, BRET is disrupted. nLuc: nano Luciferase. Created in BioRender.com based on Géraldy et al.[43] and Robers et al.[164]

### 1.4.5 Enzymatic HDAC10 NDA fluorescence quenching assay

The development of selective HDAC10is was hampered by the unavailability of high-throughput enzymatic assays for HDAC10 due to its specificity for polyamine substrates and inactivity on peptidic HDAC substrates used in conventional AMC- or luciferase-based assays. This changed in 2020, when Herp et al.[169] reported the first fluorescent acetylspermidine deacetylation assay for HDAC10. The operational principle and underlying chemistry are detailed in **Scheme 5**. The assay uses an $N^8$-acetylspermidine-derived fluorescent substrate (**60**), which is deacetylated to **61** by HDAC10. Upon addition of a stop solution that contains naphthalene-2,3-dialdehyde (NDA, **62**), only deacetylated substrate **61** with the free primary amine can undergo benzisoindole formation with NDA and Mesna (**63**) present in the assay buffer. Benzisoindole-modified **64** shows reduced fluorescence at 390 nm compared to the unconverted HDAC10 substrate (**60**) due to fluorescence quenching of the AMC fluorophore by the newly formed benzisoindole moiety.

The main advantage of this assay system is its specificity for HDAC10 over other isozymes and the fact that it is currently the only enzymatic HDAC10 assay suitable for high-throughput microplate formats. It may not be as sensitive and robust as FRET/BRET or luminescence-based assay systems due to its direct fluorescence readout. This is represented in the comparably lower z'-values, which are reported in the range of 0.50–0.55. The NDA assay has so far only been validated with zebrafish HDAC10. By the time the NDA fluorescence quenching assay was published, I had already established the FRET and BRET assays as reliable methods

to evaluate human HDAC10 binding and confirmed enzymatic inhibition in cells using a metabolomics workflow. Therefore, I did not employ this assay thus far.

**Scheme 5. Chemistry of the HDAC10 NDA fluorescence quenching assay**

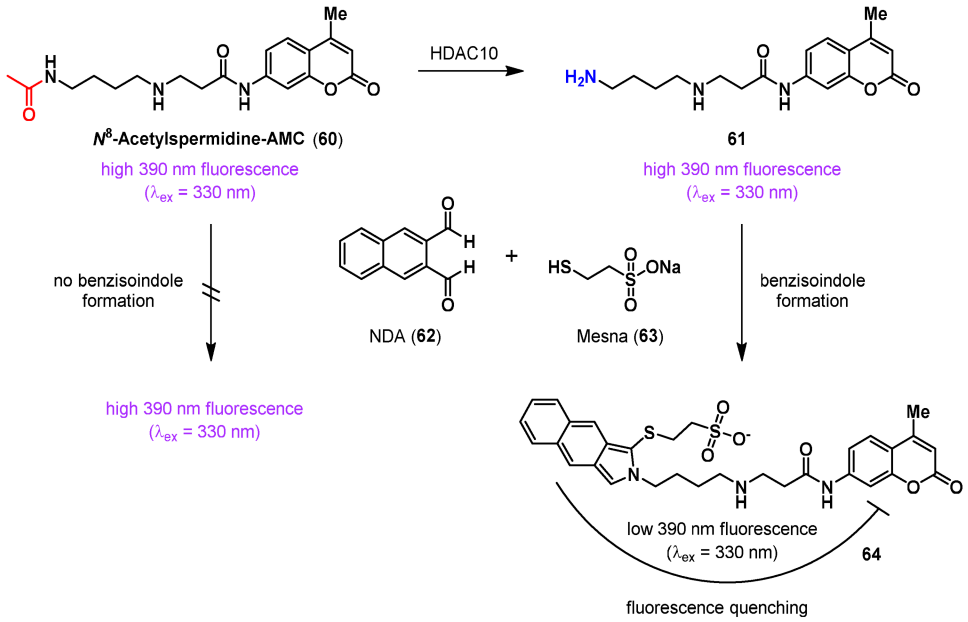


Substrate (**60**) is deacetylated by HDAC10. Upon addition of the stop solution containing NDA (**62**), the deacetylated substrate (**61**) can form a benzisoindole with Mesna (**63**) in the assay buffer. This leads to a reduction in fluorescence dependent on the HDAC10 enzymatic activity due to fluorescence quenching of the AMC-moiety in (**64**). Scheme based on Herp et al.[137]

## 1.5 Targeted degraders for histone deacetylases

Targeted protein degraders, such as proteolysis-targeting chimeras (PROTACs), have attracted an immense interest as chemical tools and as a new generation of therapeutics.[170] PROTACs are a small molecule technology to remove a protein of interest (POI) from live cells by inducing its degradation via the ubiquitin proteasome system. A PROTAC molecule is composed of two protein binders, joined together by a linker: a POI-binder (called warhead) and a ubiquitin E3 ligase ligand (E3 ligase recruiter). The mechanism of action (**Figure 16**) is not purely based on target occupancy like classical pharmacology, but requires simultaneous binding of the POI and an E3 ligase to form a ternary complex. This induces proximity of the POI with the E3 ligase, making it a (neo-)substrate of the E3 ligase, which leads to (poly)ubiquitination and ultimately proteasomal degradation of the POI. Once the ternary complex is dissociated, the PROTAC is again available to repeat the process. This event-driven mechanism of action is therefore catalytic with respect to the PROTAC molecule and only limited by the formation of a productive ternary complex and the capability of the ubiquitin–proteasome system. Another advantage of the PROTAC technology is that it allows us to target previously "undruggable" protein targets, since the warhead is not required to produce a change in activity or function when engaging the POI. Moderate affinity for an arbitrary binding site can be sufficient, as long as a suitable ubiquitination site for the E3 ligase is available in the ternary complex.[171]

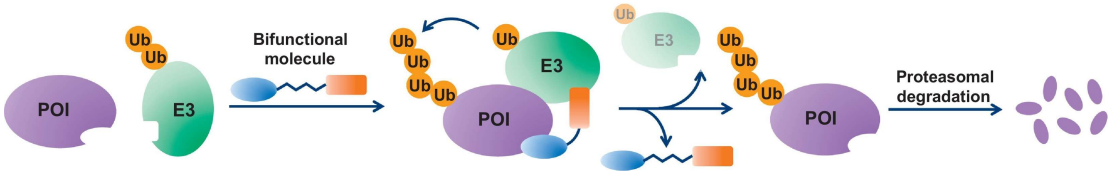


**Figure 16.** PROTAC mechanism of action. Blue part of the bifunctional molecule (PROTAC): POI-binder (warhead); orange part: E3 ligase recruiter. Taken from Scheepstra et al.[172]

HDACs with their defined substrate binding pockets are far from "undruggable", but targeted degraders against them are still interesting since they allow us to target scaffolding functions of the HDAC proteins that are independent of their enzymatic activity. PROTACs provide a "chemical knock-down" of the POI, which is valuable for example in target validation studies, and can be the starting points for small molecule therapeutics beyond occupancy-driven pharmacology.[173]

The first PROTAC against a zinc-dependent HDAC was reported in 2018 by the group of Weiping Tang.[174] They showed that their PROTAC **65** (**Figure 17**) degraded HDAC6, but not HDAC1 or 2, despite employing a pan-inhibitor warhead. Such selectivity in PROTACs from promiscuous binders is now well established and was observed in many protein families.[175] Importantly, this first study demonstrated that degradation of HDAC family members is possible by recruiting cereblon (CRBN) using the commonly used immunomodulatory imide drugs (IMiDs) such as Thalidomide, or in the case of degrader **65**, Pomalidomide. Further reports demonstrated that HDAC6 could also be degraded using other warheads, like the Class IIB selective HDACi Nexturastat A in degrader **66**[176] and **67**.[177] PROTAC **67** is noteworthy, since it demonstrated that not only CRBN is a suitable E3 ligase for HDAC degradation, but that HDAC6 can also be marked for proteasomal degradation by recruiting the von Hippel–Lindau E3 ligase (VHL). Another SAHA-based HDAC6 degrader is PROTAC **68**, which is interesting since it was synthesized from amino acid building blocks on solid support using an Fmoc peptide synthesis strategy.[178]

The HDAC PROTAC reports discussed so far suggest that HDAC6 is readily degradable by E3 ligase recruitment. However, HDAC10 degradation was not evaluated in any of the aforementioned reports and its degradability remained unknown until Eric Fischer and co-workers reported a large scale chemo-proteomics exploration of the HDAC degradability using a library of 48 PROTACs.[179] The library employed SAHA and Dacinostat warheads to bind HDAC Class I and IIB and two other warheads to cover Class IIA. Four different E3 ubiquitin ligase recruiters were utilized in the library to bind CRBN, VHL and inhibitor of apoptosis proteins (IAP). With a small selection of linker lengths and compositions, they were able to target HDAC1–8 and 10 in the neuroblastoma KELLY cell line or multiple myeloma MM.1S cells. HDAC11 was the only zinc-dependent isozyme which they could not reliably quantify with their tandem mass tag (TMT) LC-MS3-based global quantification and HDAC9 was the only isozyme that could not be degraded by one of the PROTAC library members.

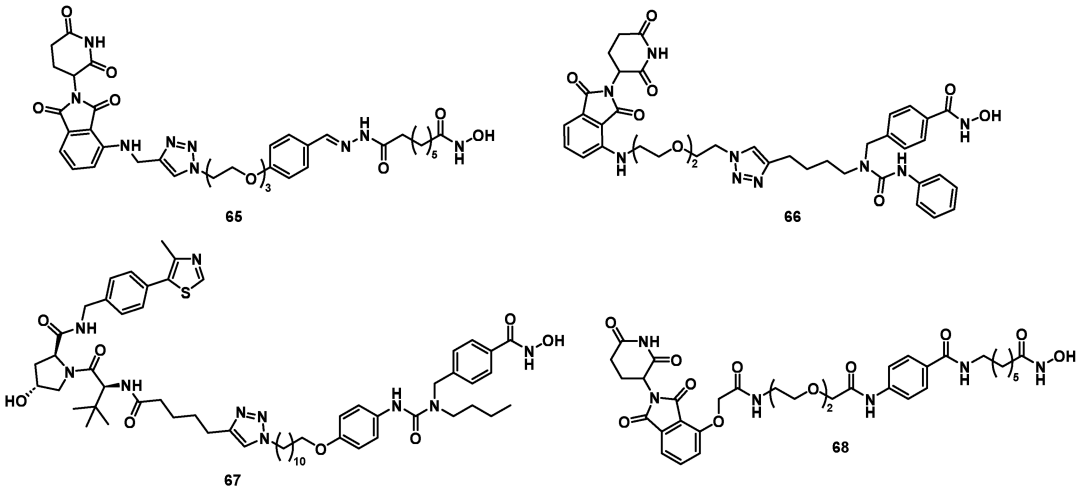

**Figure 17.** Reported HDAC6 PROTACs that potentially also degrade HDAC10.

Their HDAC degradability study justified the literature bias for HDAC6 degraders, since 20 compounds out of the 48 in the library could degrade HDAC6, making it the most frequently targeted isozyme. Furthermore, they demonstrated that HDAC10 can also be degraded in MM.1S cells using pan-HDAC inhibitor SAHA (PROTAC **69**) or Dacinostat (PROTACs **70** and **71**). CRBN and VHL recruitment was successful in degrading HDAC10. Selected examples of their HDAC10 degraders are shown in **Figure 18**. PROTAC **72** is noteworthy, as it employs a non-hydroxamate zinc binder with a warhead that has not been previously reported to engage HDAC10. While the study did not identify a selective HDAC10 degrader from pan-HDAC inhibitor warheads and most HDAC10 degraders show only poor efficacy, it provides a degradability roadmap for the development of isozyme selective PROTACs. Their valuable dataset also confirms prior lore in the PROTAC field regarding cell-line dependent degradability and isozyme preferences of E3 ligases.

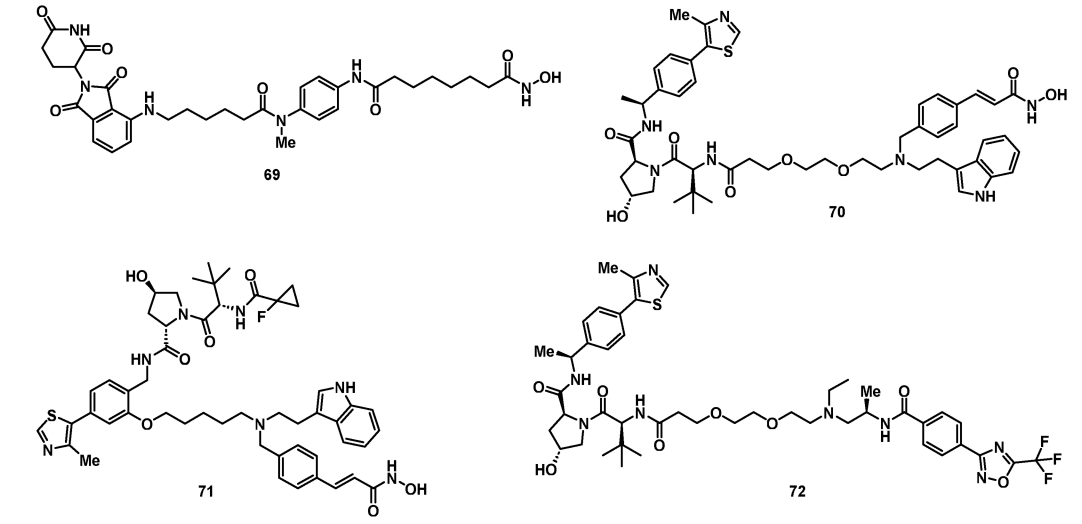

**Figure 18.** Examples of unselective HDAC10 degraders reported by Xiong et al. using global quantitative chemo-proteomics.[179]

# 2 Aims

The aim of this project was to develop selective HDAC10 inhibitors (HDAC10is) as chemical probes to provide pharmacological tools for the further investigation of HDAC10 biology and to validate HDAC10 as a drug target. Chemical probes can serve as a starting point for drug candidates to ultimately evaluate the therapeutic potential of selective HDAC10 inhibition. For this purpose, my HDAC10 chemical probes should fulfill the following criteria:

- >100-fold selectivity, ideally confirmed by multiple independent assays/methods
- <100 nM $IC_{50}$ in a biochemical binding assay
- <1 μM $IC_{50}$ in a cellular binding assay
- demonstrated intracellular target engagement
- availability of multiple active scaffolds and inactive controls based on a SAR-study
- structural confirmation of active site binding in alignment with SAR
- inhibition of the target's enzymatic activity/biological function in cells
- functional pharmacology connected with a relevant cellular phenotype
- no effect on relevant off-target biomarkers

The main obstacle in achieving HDAC10 selectivity lies in the structural similarity with its closest relative HDAC6, as both enzymes are often targeted simultaneously, even when selectivity for only one isozyme is desired.[43,128,180] Therefore, I took inspiration from the crystal structure of zebrafish HDAC10[41] and my first objective was the synthesis of inhibitors which exploit the HDAC10 gatekeeper residue (E274 in zHDAC10, E272 in hHDAC10) for higher binding affinity compared to HDAC6. Candidates for synthesis were initially designed by adding basic groups to the linker region of the known HDAC inhibitor SAHA. The initial idea was to form a salt bridge with the HDAC10 gatekeeper residue to obtain a strong ligand–target interaction that would be unique to HDAC10. To demonstrate cellular target engagement and to establish selectivity profiles in the context of an SAR-study, I aimed to establish the following assays in our lab for reliable and high-throughput compound testing:

- biochemical, cell-free HDAC-Glo I/II assay (Promega) for HDAC1, 2, 3, 6, and 8
- biochemical, cell-free FRET assay for HDAC10
- cellular BRET assay using monoclonal nLuc fusion proteins with HDAC6 and 10

Once SAHA-based selective HDAC10is were developed, the next aim was the development of selective HDAC10is using alternative zinc binders without relying on hydroxamic acids. The starting point for this project was a compound library screen with the aim to discover novel HDAC10 selective inhibitor chemotypes.

Lastly, I aimed to transfer the knowledge from the occupancy-driven pharmacology of selective HDAC10 binders to the emerging field of event-driven pharmacology by converting my selective HDAC10is into selective targeted degraders of HDAC10. This would allow us not only to target the enzymatic activity of HDAC10 but to also provide pharmacological tools for chemical knock-down, including potential scaffolding functions of the HDAC10 protein.

# 3 Results and discussion

## 3.1 HDAC activity assays

For the development of HDAC10 selective chemical probes, I first established and optimized three different HDAC assay systems in the group, which are further discussed in the following sections.

### 3.1.1 HDAC-Glo assay

Before I joined the project, the Glo assay was only used with HDAC2 and was attempted with HDAC6 by students in the group. To be able to characterize my inhibitors with a more complete HDAC selectivity profile, I extended the assay to be performed in our group with HDAC1, 2, 3, 6 and 8. I systematically optimized the assay for each isozyme, since the HDAC-Glo kit does not provide active HDAC enzymes. Based on the literature, I decided to use human recombinant HDACs from BPS Bioscience and performed an enzyme titration series with each isozyme to identify the optimal enzyme concentration in the assay. For each enzyme concentration, I tested uninhibited positive controls and fully inhibited negative controls (50 µM SAHA), with six replicates for each to determine the assay window (luminescence intensity of pos. controls/neg. controls) and sample variance. This allows the calculation of z'-values (equation 1)[181] for each enzyme concentration.

$$\mathbf{z' = 1 - \frac{3\sigma_{pos.\ controls} + 3\sigma_{neg.\ controls}}{|\mu_{pos.\ controls} - \mu_{neg.\ controls}|}} \qquad (\mathbf{1})$$

σ: standard deviation, µ: mean

**Figure 19** shows the data for assay performance depending on the isozyme and concentration. Based on the z'-values, I chose the optimal concentration for each enzyme. The subsequently used enzyme concentrations are listed in **Table 1**. The differences in enzymatic activity on the Glo substrate are apparent from the assay window, which is several hundred-fold for HDAC1 and 2 at enzyme concentrations below 1 nM. This is also reflected in the excellent z'-values for these isozymes. It is desirable to keep the enzyme concentration as low as possible, while maintaining good assay performance. Enzyme concentrations above 1 nanomolar resulted in a reduced assay window for HDAC1 and 2, due to increased background signal. The HDAC3 enzyme was used as the active NcoR2 complex and showed a comparatively low activity in the assay. Concentrations over 1 nanomolar were required for the assay window to be reliably >4. Pleasingly, the sample variance was low and therefore z'-values >0.8 could be achieved. HDAC6 and 8 provided assay windows of around 30-fold at 1 nM, with good z'-values. Since HDAC8 activity appeared slightly lower in later trials, I had to increase the enzyme concentration to 4.7 nM to achieve high z'-values reliably. Excellent z'-values were achieved with HDAC6 below 1 nM enzyme concentration. Especially for enzymes with low enzymatic activity, it was

essential to include 0.1% (1 mg/ml) BSA in the enzyme dilution, otherwise most activity was lost when intermediate dilutions were prepared from the master stock.

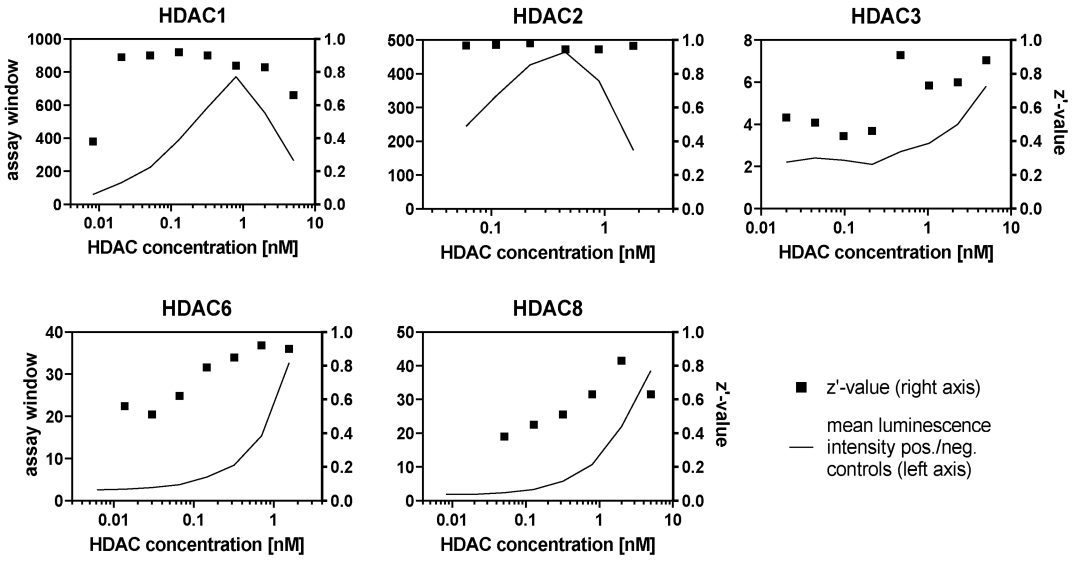


**Figure 19**. Evaluation of HDAC-Glo assay performance at different enzyme concentrations after 30 min incubation time. The required enzyme amount for good assay performance is highly isozyme dependent. The assay window (mean luminescence intensity of pos./neg. controls) provides information on the signal intensity (signal-to-background ratio). The z'-value[181] (see equation 1) is a characteristic parameter for the assay quality taking sample variability into account. An ideal assay approaches z' = 1.

**Table 1. Optimized HDAC enzyme concentrations used in the Glo assay**

| HDAC | concentration [nM] | concentration [ng/mL] | purity by supplier |
|---|---|---|---|
| **1** | 0.123 | 7.00 | 79% |
| **2** | 0.446 | 25.0 | 84% |
| **3/NcoR2 complex** | 4.02 | 200 | 80% |
| **6** | 0.621 | 100 | 75% |
| **8** | 4.65 | 200 | 90% |

The next assay parameter I optimized was the substrate incubation time. The kit manufacturer claims a signal half-life >3 h once the steady state of the three-enzyme cascade has been reached. To determine the minimal incubation time to reach the steady state with my enzyme dilutions, I recorded luminescence of uninhibited positive controls and fully inhibited negative controls (50 µM SAHA), with six replicates for each, and calculated the z'-value for each time point (see **Figure 20**). Some isozymes showed a lag period of 30 min until they reached the maximum assay signal, z'-values remained excellent over the tested time period, although the signal slowly declined over time as expected. I decided to allow for 30 min substrate incubation time in this assay system for all isozymes. Furthermore, I also tested the DMSO-tolerance of the

Glo assay and could confirm little to no effect on all isozymes with up to 1–2.5% DMSO (**Figure 21A**). Therefore, I allowed DMSO-levels up to 1% in the assay and omitted DMSO normalization.

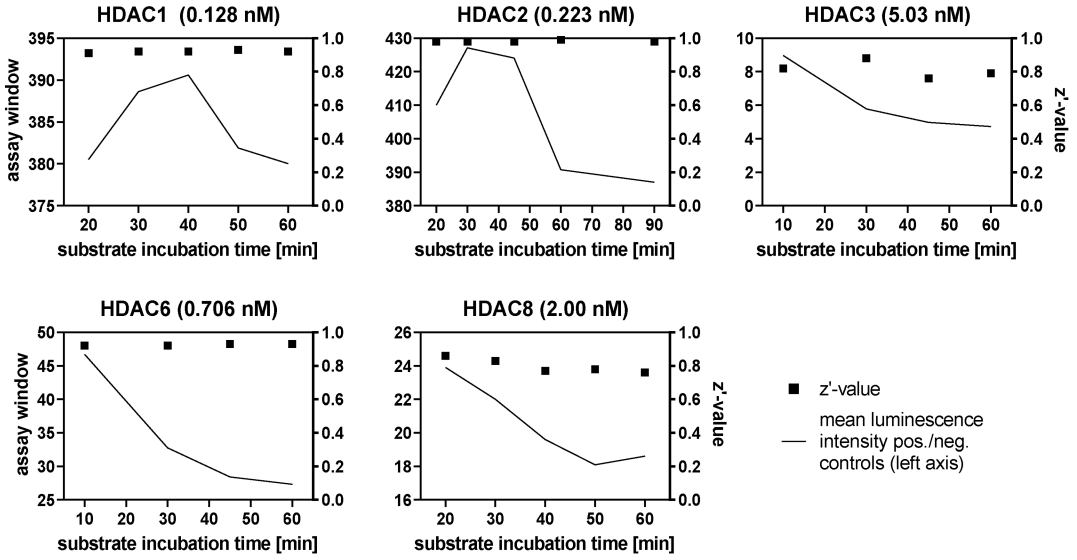


**Figure 20.** Evaluation of HDAC-Glo assay performance after different incubation times. The assay window (mean luminescence intensity of pos./neg. controls) provides information on the signal intensity (signal-to-background ratio). The z'-value[181] (see equation 1) is a characteristic parameter for the assay quality taking sample variability into account. An ideal assay approaches z' = 1.

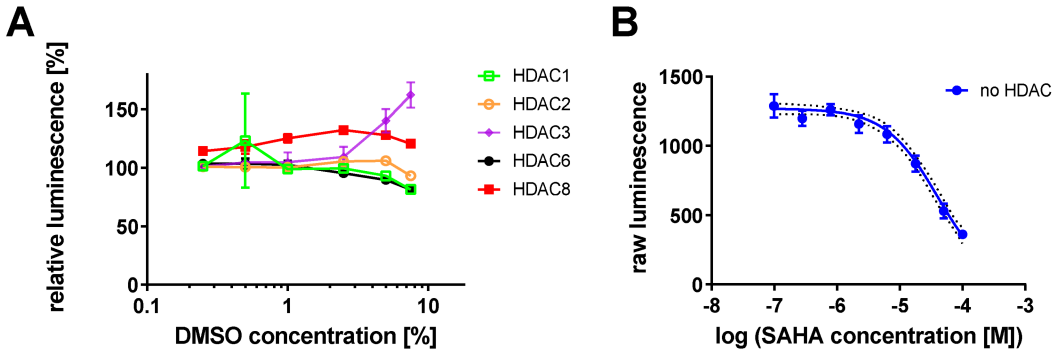


**Figure 21.** A: DMSO tolerance of the Glo assay. Little effect was observed until 1% DMSO for all isozymes. B: Investigation of potential assay interference caused by inhibition of non-HDAC assay components. SAHA reduced the luminescence signal dose-dependently in the absence of an HDAC enzyme. This effect becomes negligible when an uninhibited HDAC is present, as raw luminescence values are typically in the range of $10^4$–$10^5$.

I typically normalize each assay plate with uninhibited samples defining 100% signal and fully inhibited negative controls (50 µM SAHA) defining 0% signal. However, I also tried negative

control samples without any HDAC enzyme and noticed slightly higher background signal than with SAHA inhibited samples containing enzyme. This could be due to SAHA inhibiting the developer enzyme or the luciferase to some extent. Indeed, I observed a dose-response relationship between SAHA and the luminescence intensity, starting at 1 µM SAHA, even without HDAC enzyme present **Figure 21B**. However, I could confirm that this effect does not influence the compound evaluation, since the luminescence signal with active HDAC present is by orders of magnitude higher and the obtained dose-response curved are highly isozyme-depended. That way, I can exclude assay interface by inhibition non-HDAC assay components, like the luciferase or developer protease. Nevertheless, this demonstrates that all wells should contain the enzyme of interest and negative controls are better defined by full inhibition of the enzyme with an appropriate control compound instead of by the absence of enzyme and inhibitor. An alternative hypothesis for the SAHA dose-dependent signal in the absence of an HDAC enzyme could be a contamination of the assay developer reagent (containing luciferase and trypsin) with a hydrolase enzyme that is also inhibited by SAHA. This contamination could also be responsible for the weak HDAC Class IIA and HDAC10 activity that is claimed with the Glo substrate. However, it is unlikely that this hypothetic contamination is a Class I HDAC, since the SAHA binding affinity for them is considerably higher than what I observed in the experiment.

### 3.1.2 HDAC10 TR-FRET assay

Before I joined the project, Dr. Peter Sehr had already established a previously described[162] time-resolved fluorescence resonance energy transfer (TR-FRET) binding assay for HDAC10 and had optimized it using a commercial FRET tracer and their EnVision plate reader (PerkinElmer) equipped with a TR-FRET laser module. He had prepared $Eu^{3+}$-labelled Streptactin and used recombinant TwinStrep-GST-tagged human HDAC10, produced at the EMBL Protein Expression and Purification Core Facility.[182]

With his help, I optimized the assay so it can also be carried out in the Miller Lab using our CLARIOstar (BMG Labtech) plate reader equipped with a xenon flash lamp and TR-FRET filters using a "home-made" Tubastatin–AF647 tracer. Since the enzyme and Eu–Streptactin concentrations were already optimized, I only had to perform a tracer titration experiment (**Figure 22A**) to identify the optimal tracer concentration. I tested uninhibited positive controls and fully inhibited negative controls (30 µM SAHA), with six replicates for each tracer concentration to determine the assay window (FRET ratio) and sample variance. This allows the calculation of z'-values (see equation 1)[181] for each tracer concentration and the tracer dissociation constant ($K_d$), see **Figure 22A**. A $K_d$ of 11.5 nM indicates strong binding of the Tubastatin–AF647 tracer and excellent z'-values were already achieved at low nM tracer concentrations, with the optimal concentration at 10–50 nM. Therefore, I used the tracer at 25 nM and the HDAC enzyme at the previously determined 5 nM. I also tested the FRET signal persistence and equilibrium binding kinetics of the FRET assay. At least 60 min were required until the assay signal stabilized, then it remained stable for hours, as long as solvent evaporation was prevented. Therefore, I used 90 min incubation time in the FRET assay.

Furthermore, I also tested the DMSO-tolerance of the FRET assay and could confirm no effect up to 1% DMSO (**Figure 22B**). At higher DMSO-levels, the assay signal (FRET ratio) of uninhibited control samples diminishes and becomes similar to partially inhibited (150 nM SAHA) samples, reducing the assay window or even causing false positives if not corrected for DMSO inhibition. Therefore, I allowed DMSO-levels up to 1% in the assay and omitted DMSO normalization.

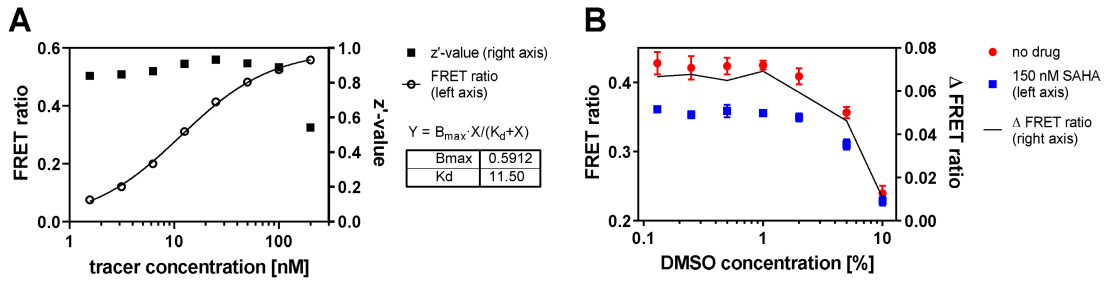


**Figure 22.** A: Evaluation of FRET assay performance at different tracer concentrations. The optimal tracer concentration is 10–50 nM. The assay window (FRET ratio) provides information on the signal intensity and allows the calculation of the tracer dissociation constant ($K_d$). The z'-value[181] (see equation 1) is a characteristic parameter for the assay quality taking sample variability into account. An ideal assay approaches z' = 1. B: DMSO tolerance of the FRET assay, no effect was observed until 1% DMSO.

### 3.1.3 HDAC10 and HDAC6 cellular BRET assay

The BRET assay was previously established and performed in the group by Johanna Hummel-Eisenbeiß[43] with commercially available plasmids expressing an HDAC6-CD2- (only the catalytic domain 2 of HDAC6) or HDAC10-nLuc fusion protein as part of the Promega NanoBRET Target Engagement Intracellular HDAC Assay kit. Johanna transfected HeLa cells with the plasmids and selected a stably transfected clone for HDAC10. I then optimized the assay performance and selected a stable clone for HDAC6-CD2 as well. In my hands, the BRET assay achieved typically z'-values (see equation 1)[181] around 0.6. The BRET assay showed higher variance than the biochemical assays due to the cellular nature and varying expression levels of the nLuc fusion proteins. Therefore, I tested all compounds in two biological replicates. I also noticed that the stably transfected cells, showed reduced expression of the nLuc fusion protein with increasing passage number, which I identified as the major source for decline in assay performance over time. Since the BRET assay was performed on intact, live cells, the final concentration of the DMSO vehicle in the medium was limited and normalized to 0.5% in all wells to avoid cytotoxicity and to control for DMSO-dependent membrane permeation of test compounds.

## 3.2 Selective HDAC10 inhibitors based on amino hydroxamic acids

This section describes the development of highly selective HDAC10 chemical probes using amino hydroxamic compounds that are inspired by HDAC10 substrates. Results of this study were published in Steimbach et al.;[1] therefore, data here is mostly repeated and augmented with unpublished results. Some descriptive, data-related texts, as well as figures, schemes and tables are reused and were originally written and prepared by me.

### 3.2.1 SAHA aza-scan

Even before HDAC10 was recognized as a polyamine deacetylase in 2017,[41] our group had uncovered that many commonly used HDAC6 "selective" inhibitors also have high affinity for HDAC10.[43] Among the HDAC10/6 inhibitors is Tubastatin A (**19**)[129] (**Figure 23**, left box), for which a SAR-study revealed that the tertiary amine in the tetrahydro-γ carboline is driving strong HDAC10 binding. However, we were unable to modulate HDAC6 activity independent of HDAC10 affinity in the Tubastatin A scaffold with the benzoic hydroxamate linker and ZBG. Gramine-capped **DKFZ-480** was the most selective HDAC10 binder (40-fold selectivity) in this compound series due to increased HDAC10 binding, but still unaltered HDAC6 affinity. These results encouraged us to move away from the Tubastatin A scaffold and by that time, the remarkable polyamine substrate specificity of HDAC10 had recently been discovered[41] and demonstrated biochemically. Classical peptidic HDAC substrates containing acetylated lysines or simple, unfunctionalized acetamides like *N*-butylacetamide are not accepted by HDAC10. Only acetylated polyamines with four or five carbon atoms distance between the *N*-acetyl and the basic amine are deacetylated (for details see **Figure 4** in section 1.1.4.1, page 11). In particular, between the two acetylation isomers of spermidine, $N^8$-acetylspermidine with a four atom amine–acetamide separation is an excellent HDAC10 substrate, while regioisomer $N^1$-acetylspermidine is a poor substrate due to its three atom amine–acetamide distance (**Figure 23**, middle box). Another essential aspect of substrate specificity lies in HDAC6: it does not accept the acetylated polyamine substrates of HDAC10.

Integrating the substrate landscape of HDAC10 and HDAC6, our group hypothesized that polyamine substrate mimicry could allow for the development of HDAC10 selective inhibitors following a rational design approach. The slender, linear scaffold of FDA-approved pan-HDAC inhibitor SAHA was chosen as a starting point for polyamine mimicry (**Figure 23**, middle box). While linear diamine PDAC inhibitors like **36** were reported decades ago,[134,135] amino hydroxamic acids with amine–hydroxamate separations shorter than five carbons were barely explored. Additionally, the SAHA scaffold includes a cap-group, which renders the chemical probes much more drug-like than previously reported direct polyamine analogues.[134–136,183] This structural feature also opens chemical space for optimization towards cellular efficacy – an essential aspect of chemical probes.

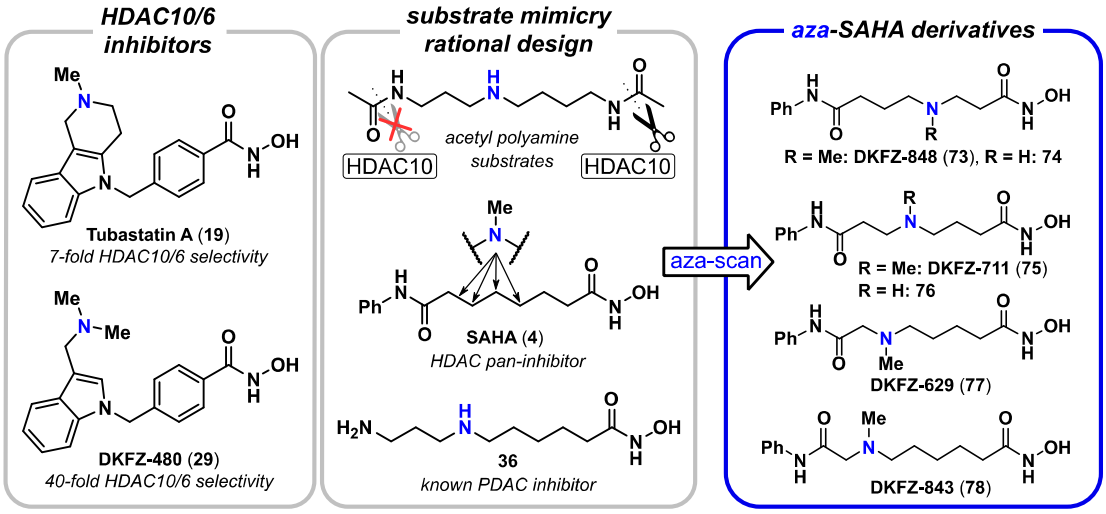


**Figure 23.** Previous work towards selective HDAC10is on the Tubastatin A scaffold and rational inhibitor design using substrate mimicry by aza-scan on the SAHA scaffold.

Former post-doctoral researcher Magalie Géraldy started the synthesis of aza-SAHA derivatives with the goal to systematically replace the methylene groups in the SAHA hexyl linker with a secondary amine to closely resemble a linear acetylpolyamine. She isolated the secondary β- and γ-amino hydroxamic acids (**74** and **76**), but the δ-amine required methylation to the tertiary amine to prevent lactamization with the hydroxamic acid during synthesis (see equation 2, page 51). Dr. Géraldy isolated the pure secondary γ-amine **76** as confirmed by analytical data and an HDAC6 and 10 BRET assay performed shortly after the isolation of the compound suggested high HDAC10 selectivity and good potency. However, I could not reproduce these results from the same DMSO stock, as the compound had decomposed by the time I performed the HDAC activity assays of the secondary γ-aminohydroxamic acid **76**. I could confirm cyclization to the corresponding pyrrolidinone by LC/MS analysis, despite the compound being stored as TFA-salt in DMSO at –20°C.

Therefore, I performed the SAHA aza-scan (**Figure 23**, right box) by synthesis of the tertiary methyl amines **DKFZ-848** (**73**) and **DKFZ-711** (**75**) for direct comparison with **DKFZ-629** (**77**), as prepared by Dr. Géraldy. Additionally, I also prepared ε-amine **DKFZ-843** (**78**), which required extension of the SAHA hexyl linker by a conceptual amine insertion, as the methylene replacement would have resulted in a non-basic urea.

### 3.2.1.1 Inhibitor evaluation

To evaluate the selectivity profiles of the four aza-SAHA derivatives **73**, **75**, **77**–**78**, I tested them together with SAHA for comparison against HDAC1, 2, 3, 6 and 8 using the biochemical, enzymatic HDAC-Glo assay (see sections 1.4.2 and 3.1.1). For quantification of HDAC10 binding affinity, I used the HDAC10 FRET assay (see sections 1.4.3 and 3.1.2).

The selectivity profiles are depicted as a heatmap with $pIC_{50}$s in **Figure 24**. As expected, my assays confirm pan-HDAC inhibition for SAHA with the lowest activity on HDAC8 ($pIC_{50}$ = 6.16)

and the highest activity on HDAC6 ($pIC_{50}$ = 7.72). Importantly, SAHA also shows good affinity for HDAC10 ($pIC_{50}$ = 6.93). The introduction of an amino functionality in the β-position of the SAHA hexyl linker with **DKFZ-848** abolished nearly all HDAC activity, only HDAC10 binding remained in the single digit µM range ($pIC_{50}$ = 5.65). γ-Aminohydroxamic acid **DKFZ-711** features a distinctive selectivity profile with stark reduction in HDAC6 and 8 activity accompanied by complete loss of HDAC1–3 binding, but at the same time 3.5-fold higher HDAC10 activity ($pIC_{50}$ = 7.48) compared to SAHA. As a result, **DKFZ-711** shows unprecedented simultaneous selectivity over HDAC6 (110-fold) and Class I (620-fold selectivity over HDAC1). Moving the amino group one atom further away from the hydroxamic acid to the δ-position in **DKFZ-629** results in HDAC10 activity that is again similar to SAHA, while affinity for the other isozymes is on average reduced by around 1 log unit. Therefore, **DKFZ-629** has only a slight HDAC10 preference. ε-Aminohydroxamic acid **DKFZ-843**, with the elongated linker and the five carbon amine-hydroxamate separation as in previously reported PDAC inhibitor **36**, is 63 times more active on HDAC10 than SAHA. However, affinity for the other isozymes is reduced to only a small extent. Therefore, despite **DKFZ-843** being far ahead of the other compounds in this series regarding HDAC10 potency, the moderate selectivity for HDAC10 over HDAC1 (44-fold) and especially the low HDAC10/6 selectivity (26-fold) makes **DKFZ-843** inferior to γ-amine **DKFZ-711.** Higher selectivities have been achieved with previous approaches[43] towards selective HDAC10 inhibition by compounds like Tubastatin A derivative **DKFZ-480**.

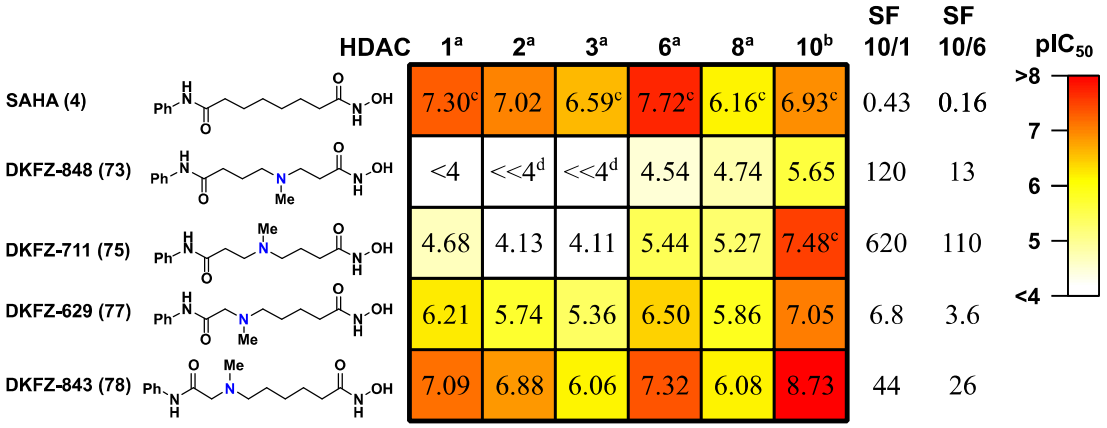


**Figure 24.** HDAC isozyme selectivity heatmap and $pIC_{50}$ values of aza-SAHA derivatives reveal diverse inhibitory profiles depending on the nitrogen position. $pIC_{50}$ values are the mean of two replicates, each determined by four-parameter non-linear regression analysis with eight dose levels in triplicate with HDAC Glo assay[a] or FRET assay[b]. [c] Mean of three individual experiments. [d] Curve fit was not convergent at 100 µM. SF (selectivity factor) = $10^{(pIC50(HDAC10) - pIC50(HDAC6 \text{ or } HDAC1))}$ rounded to two significant figures. For 95% confidence intervals, see Table S1. Modified from Steimbach et al.[1]

In order to complement the ligand displacement HDAC10 FRET assay, we collaborated with the Chemical Biology Core Facility and the Protein Expression and Purification Core Facility at EMBL Heidelberg, where Dr. Karine Lapouge performed a differential scanning fluorimetry thermal shift assay with recombinant HDAC10. Although this assay does not directly provide $IC_{50}$ values for tested inhibitors, it serves as an independent semi-quantitative biophysical

confirmation of HDAC10 binding. Protein melting curves annotated with melting temperatures are depicted in **Figure 25**. The vehicle control treated enzyme denatured at 69.6 °C, while SAHA-bound HDAC10 is stabilized by an additional 5.0 °C under the assay conditions. β-Amine **DKFZ-848**, a weak HDAC10 binder, stabilized the enzyme only by 2.2 °C. HDAC10 selective γ-amine **DKFZ-711** induced a thermal shift of 8.2 °C, which confirms strong HDAC10 binding. δ-Amine **DKFZ-629** with a lower $pIC_{50}$ in the FRET assay also gave a smaller shift of 7.1 °C. The most potent HDAC10 binder in this series, ε-amine **DKFZ-843**, was confirmed by the largest thermal shift of 11.7 °C.

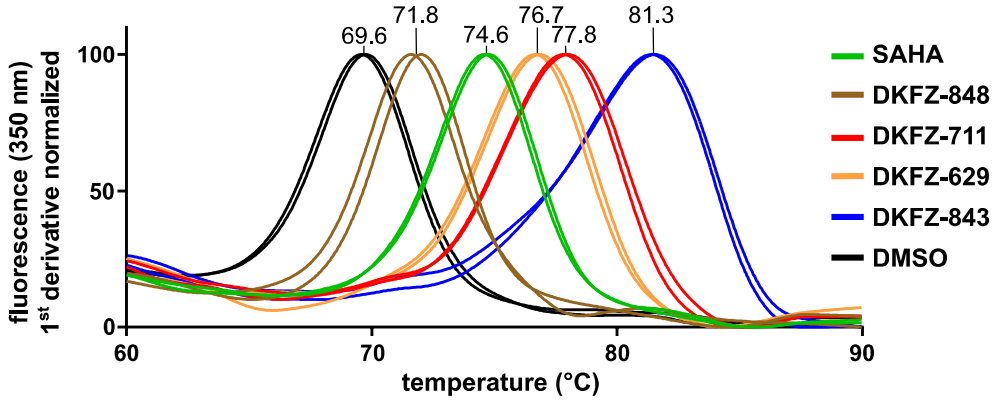


**Figure 25.** Differential scanning fluorimetry thermal shift assay of aza-SAHA derivatives (500 µM) performed in duplicate with recombinant HDAC10 (4 µM) by Dr. Karine Lapouge (EMBL Heidelberg). Maximal turning points represent HDAC10 melting temperatures, annotated as means in °C. For method description see Steimbach et al.[1]

HDAC10 binding and selectivity profiles of aza-SAHA derivatives are well supported by biochemical and biophysical evidence, but cellular target engagement must be demonstrated for chemical probes and drug candidates. Therefore, I optimized a cellular target engagement BRET assay for HDAC6 and 10 together with Johanna Hummel-Eisenbeiß. This allows me to evaluate HDAC10/6 binding and selectivity in cells.

**Figure 26** shows dose-response curves of aza-SAHA derivatives tested with the BRET assay against HDAC10 (red) and HDAC6 (blue). Since the BRET assay was not established for Class I enzymes, HDAC2 curves (black) from the Glo Assay are included for comparison. Pleasingly, when HDAC6 and 10 were measured in the same cellular BRET assay system, the selectivity profile from the biochemical assays was successfully validated. This is important since the biochemical selectivity profiling uses an assay for HDAC10 that is mechanistically different from those used for the other tested isozymes due to its distinctive substrate requirements.

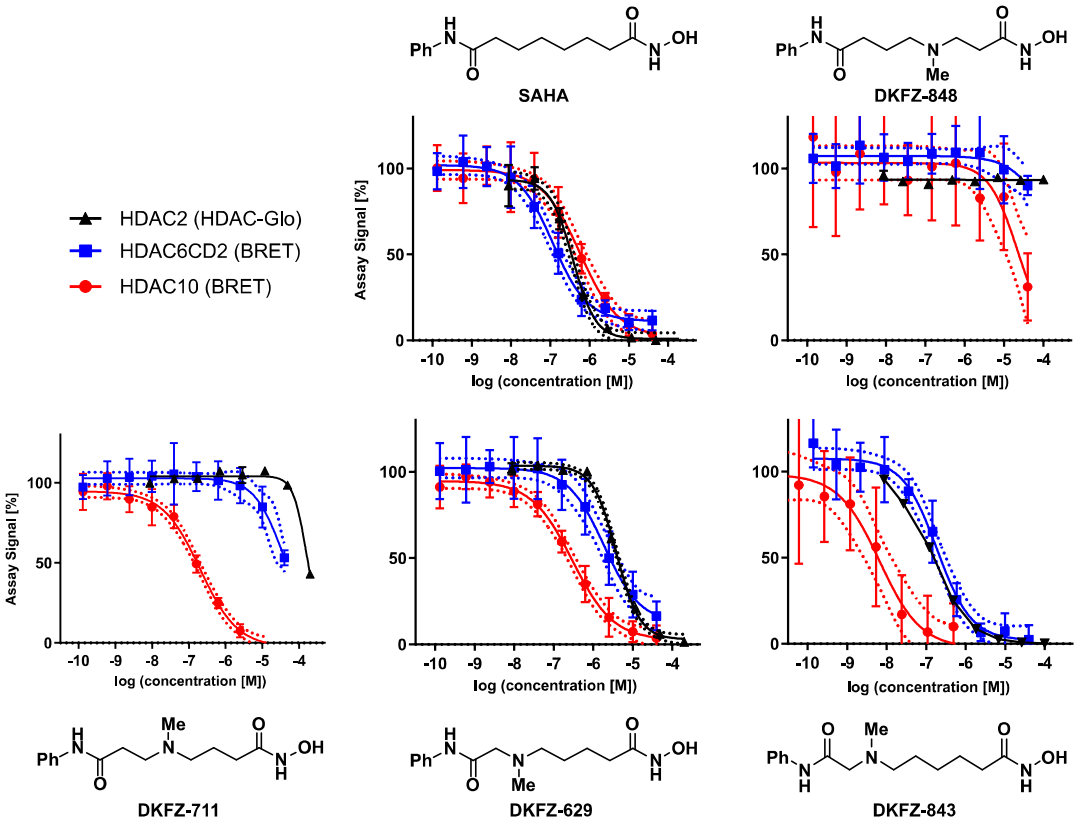


**Figure 26.** Cellular selectivity and target engagement of aza-SAHA derivatives is confirmed with BRET assay on HDAC10 (red) and HDAC6 (blue). Dose-response curves are calculated from four-parameter non-linear regression analysis of two separate experiments, each performed in triplicates. Whiskers show standard deviation and dotted lines indicate 95% confidence intervals of the curve fit. HDAC2 curves (black) from one biochemical HDAC-Glo assay performed in triplicates are representative of Class I activity. For tabulated BRET data with 95% confidence intervals, see Table S3.

When comparing the $pIC_{50}$s of the biochemical assay with the BRET experiments, a trend can be observed. Compounds in the aza-SAHA series show 11–40% of their biochemical HDAC10 activity in the BRET assay (see HDAC10 BRET/FRET activity, Table S3), but the ratio appears to be related to the amine position. Compounds **DKFZ-848** and **DKFZ-711** with the amino group closer to the hydroxamic acid show a smaller proportion of their FRET activity in the BRET assay (11% and 18%), while amine-free SAHA and **DKFZ-629** and **DKFZ-843** with the amino group closer to the hydrophobic cap, and therefore shielded, tend to show higher BRET/FRET activities (30–40%). This is in line with observations from the Tubastatin A scaffold, where the basic amine is also close to the indole cap and 58% of the FRET activity is retained in the BRET assay with Tubastatin A.

#### 3.2.1.1 Synthesis strategy

Generally, I synthesized aza-SAHA derivatives by amine alkylation of amino acid derivatives, followed by in situ esterification with methanol, and then, as the final step, hydroxamic acid formation by KCN catalysis. This proceeded best with high catalyst loading (0.6 equiv KCN) and

pre-activation of amino esters in dioxane before adding $NH_2OH$ (50 wt% in $H_2O$) as reagent and co-solvent (1:1 with dioxane). When choosing the alkylation reaction partners to build the aza-SAHA linker, I was limited by competing intramolecular cyclization to pyrolidones or piperidones (equation 2) for γ- and δ-amines. Therefore, secondary amino hydroxamic acids were avoided and γ- and δ- amino acids were esterified at the tertiary amine stage of the synthesis, since the corresponding secondary amino esters lactamized readily under basic conditions.

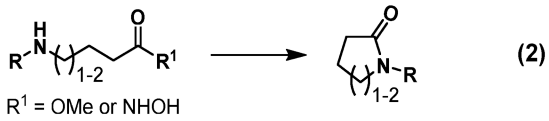


(2)

Synthesis routes of aza-SAHA derivatives **73**, **75**, **77–78** are shown in **Scheme 6**. For the preparation of β-amino hydroxamic acid **73**, I Boc-deprotected **79**, then added methyl acrylate to the liberated amine, followed by conversion to the hydroxamic acid. The synthesis of γ-amino hydroxamic acid **DKFZ-711** (**75**) began with aza–Michael addition of **81** to **80**, followed by in situ esterification to give **82**, which upon treatment with hydroxylamine provided **DKFZ-711**. δ-Amino hydroxamic **77** was first prepared by Dr. Magalie Géraldy using base-mediated alkylation of amino acid **84** with bromide **83** to give the corresponding tertiary amino acid, which was converted in situ to the corresponding methyl ester, and, in a second step, to the desired hydroxamic acid **77**. To prepare ε-amino hydroxamic acid **78**, I inverted the reactivity polarities using methyl amine (**85**) and methyl 6-bromohexanoic acid (**86**). Conversion of the resulting carboxylic acid to a hydroxamic acid proceeded as before.

**Scheme 6. Synthesis[a] of aza-scan compounds 73, 75, 77–78**

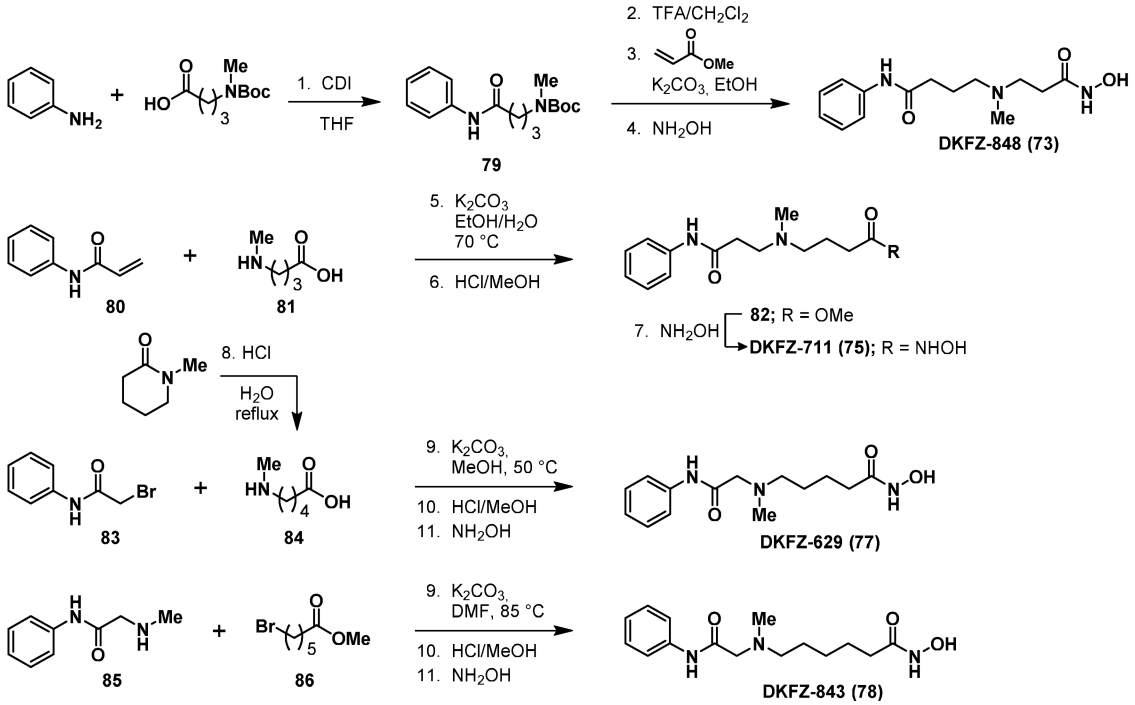


[a] Reagents and conditions 1. CDI, THF, rt, 8 h, 86%; 2. 30% TFA in $CH_2Cl_2$, rt, 1 h; 3. methyl acrylate, $K_2CO_3$, EtOH, rt, 66 h; 4. KCN, dioxane, rt, 1 h, then $NH_2OH$ (50 wt% in $H_2O$), 24 h, rt, 8% over three steps; 5. $K_2CO_3$, EtOH/$H_2O$, 70 °C, 7 h; 6. HCl/MeOH, rt, 72 h, 82% (2 steps); 7. KCN, dioxane, rt, 1 h, then $NH_2OH$ (50 wt% in $H_2O$), rt, 24 h, 66%; 8. 6.4 M HCl, reflux, quant; 9. $K_2CO_3$, MeOH, 50 °C, 45 h or DMF, 85 °C, 40 h; 10. HCl/MeOH, rt, 18 h; 11. KCN, dioxane, rt, 1 h, then $NH_2OH$ (50 wt% in $H_2O$), rt, 24 h, 62% for **77** (3 steps), 14% for **78** (3 steps). Taken from Steimbach et al.[1]

### 3.2.2 Structure-activity relationship study of γ-amino hydroxamic acids

With the promising HDAC10 selective lead **DKFZ-711** in hand, I initiated a medicinal chemistry campaign to investigate the structure-activity relationship around the γ-amino hydroxamic acid scaffold. Every structural element of **DKFZ-711** was put under scrutiny to determine its influence on HDAC10 activity and selectivity. The SAR-study is outlined in **Figure 27** and HDAC activity profiles are discussed in section 3.2.2.1. Alternative approaches towards selective HDAC10 inhibition without the use of hydroxamic acids are presented in section 3.2.4.

I investigated cyclic derivatives of the γ-amino hydroxamic acid scaffold (**Figure 27**, green box) in order to find a conformationally restricted, less flexible γ-amine with an ideal fit and charge location in the active site. Prepared compounds include four-membered rings with an exocyclic basic amine (amino cyclobutanes) or with the amine as part of the ring as azetidine. Aziridines were avoided for stability reasons but could be interesting in further studies towards covalent HDAC10 inhibitors and affinity-based probes. Pyrrolidines were avoided since they would introduce a bend to the linker structure, which I expect to be ill-fitted in the deep narrow HDAC10 binding tunnel. The disubstituted pyrrolidines would also be chiral, a complicating feature in an unpromising scaffold. However, an 1,4-substituted piperidine, similar to the

inhibitors by Herp et al.[137] (**Figure 11**, page 29) was prepared by Fulbright intern Hannah Steffke under my supervision.

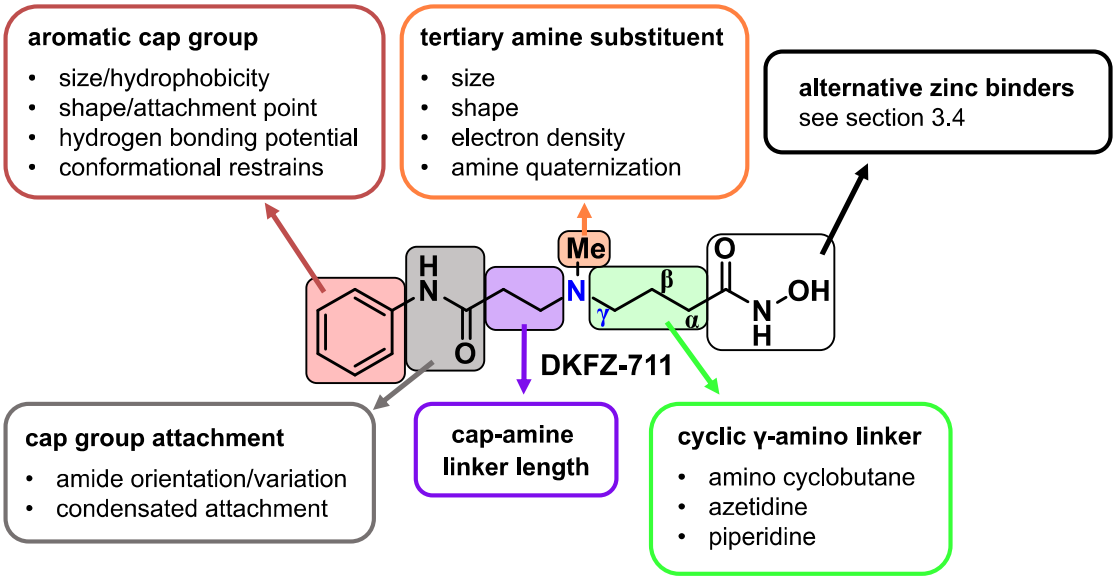


**Figure 27.** Design and SAR concepts of γ-amino hydroxamic acids on **DKFZ-711**. For structures of synthesized derivatives see **Figure 28**.

**DKFZ-711** became a tertiary amine out of necessity to avoid lactamization with the hydroxamic acid (see equation 2, page 51), but a strictly linear secondary amine linker would have been the closer polyamine mimic. To better understand the influence of the required amine substituent (**Figure 27**, orange box), a series of alkyl-substituted tertiary amines was synthesized by Gergely Tihanyi, a master student who joined us for a lab rotation under my supervision. Additionally, I investigated the influence of the positive charge introduced by a basic amine in the linker: I prepared an electron-deficient non-basic tertiary amine, and I also quaternized the amine to the permanently charged ammonium salt.

The cap–amine linker length was also varied (**Figure 27**, purple box), which moves the cap group and the attachment amide in or out the binding tunnel. I also varied the structure and orientation of the cap attaching anilide in **DKFZ-711** (**Figure 27**, grey box) to examine potential hydrogen bonding interactions with the enzyme. This includes the synthesis of 2-substituted benzimidazole-capped compounds, which represent a condensated/dehydrated *ortho*-aminoanilide cap derivative of **DKFZ-711**.

Lastly, I studied the SAR of the hydrophobic cap group (**Figure 27**, red box), which includes differently sized and shaped aromatic systems, such as naphthalenes, anthracene and biphenyl. The three aromatic substitution vectors of **DKFZ-711** were also probed for favorable polar interactions with the protein surface, using phenol and aniline functionalities among others. Due to the large number of possible and reasonable cap groups, I sampled this SAR-aspect with more derivatives than the other ones. A complete overview on all derivatives is shown in **Figure 28**, page 60.

#### 3.2.2.1 Biochemical inhibitor evaluation

The structure-activity relationship around the linker region in lead compound **DKFZ-711** is presented in the form of tabulated $pIC_{50}$ values for HDAC1, 2, 3, 6, 8 and 10 in **Table 2** with Tubastatin A (**19**) as a reference. First, looking at larger substituents of the tertiary amine than methyl (**Table 2**, orange box), no increase in potency or selectivity can be observed. In fact, HDAC10 potency and steric bulk of the amine substituent show a negative correlation (**89–92**), which is consistent with the narrow binding tunnel of HDAC10 that is best suited for slender, secondary amines as found in the polyamine substrates. While the steric bulk is detrimental for HDAC10 activity, Class I enzymes and HDAC6 are only mildly affected. Benzylamine **92** even shows increased HDAC6 and 8 activity resulting in a slight preference for HDAC6 over HDAC10.

Electron-poor 2,2,2-trifluoroethylamine **DKFZ-888** (**93**) demonstrates that the basic amine is only important for HDAC10 binding. Amine **93** is expected to be three orders of magnitude less basic (by calculated $pK_a$) than ethylamine **87** and with the $pIC_{50}$ = 5.84, **93** is over 10 times less active on HDAC10 than the non-fluorinated ethyl derivative **87** ($pIC_{50}$ = 6.93). In contrast, HDAC6 and Class I activity did not diminish, but slightly increased with the introduction of the fluorine atoms. Since the positive charge of a protonated amine seems crucial for potent HDAC10 binding, I also tested the quaternary ammonium hydroxamate **DKFZ-777** (**94**) with a permanent positive charge at the linker nitrogen and still minimal steric bulk around the quaternary center. Obviously, such a compound is expected to have poor cell permeability and therefore an unacceptable DMPK profile, even for a chemical probe. However, even in cell-free assay systems, **DKFZ-777** exhibits one order of magnitude lower HDAC binding across all tested enzymes. This brings Class I and HDAC6 activity below the detection limit of the assay and yields an HDAC10 $pIC_{50}$ of 6.41. I suspect that the poor solubility of the internal salt, even in aqueous buffers, could be responsible for the overall poor activity. Furthermore, **DKFZ-777** could act as a methylation agent for nucleophiles in the assay, e.g. cysteins or lysines in proteins, which would liberate the excellent inhibitor **DKFZ-728** and mask the activity profile of the quaternary ammonium salt.

**Table 2. $pIC_{50}$ values[a] of γ-amino hydroxamic acids with linker modifications**

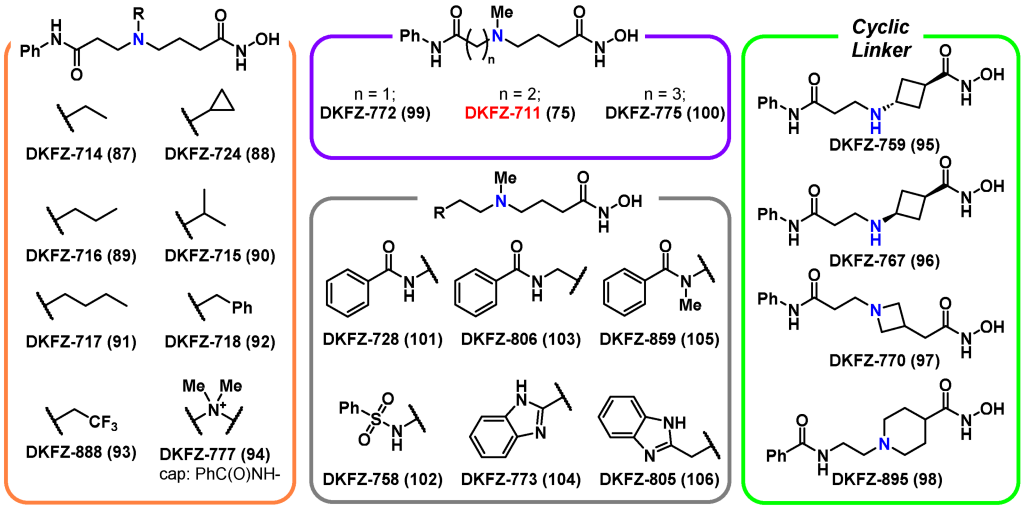


| compound | HDAC1[b] | HDAC2[b] | HDAC3[b] | HDAC6[b] | HDAC8[b] | HDAC10[c] | SF 10/1 | SF 10/6 |
|---|---|---|---|---|---|---|---|---|
| DKFZ-711 (75) | 4.68 | 4.13 | 4.11 | 5.44 | 5.27 | 7.48[d] | 620 | 110 |
| DKFZ-714 (87) | 4.30 | 4.13 | <4 | 5.26 | 5.07 | 6.93 | 430 | 47 |
| DKFZ-724 (88) | 4.41 | <4 | <4 | 5.38 | 5.58 | 6.69 | 190 | 20 |
| DKFZ-716 (89) | 4.09 | <4 | <4 | 5.11 | 5.00 | 6.56 | 290 | 29 |
| DKFZ-715 (90) | <4 | <4 | <<4[e] | 4.68 | 5.14 | 6.44 | 650 | 57 |
| DKFZ-717 (91) | 4.09 | <4 | <4 | 5.29 | 5.05 | 6.37 | 190 | 12 |
| DKFZ-718 (92) | 4.63 | 4.21 | <4 | 5.98 | 5.65 | 5.85 | 16 | 0.74 |
| DKFZ-888 (93) | 4.64 | 4.46 | <4 | 5.36 | 5.20 | 5.84 | 16 | 3.0 |
| DKFZ-777 (94)[f] | <<4[e] | <<4[e] | <<4[e] | <<4[e] | <<4[e] | 6.41 | >>260 | >>260 |
| DKFZ-759 (95) | 4.69 | 4.25 | <4 | 5.60 | 4.84 | 6.25 | 36 | 4.4 |
| DKFZ-767 (96) | 4.78 | 4.57 | <4 | 5.68 | 5.05 | 6.89 | 130 | 16 |
| DKFZ-770 (97) | 4.24 | 4.05 | <<4[e] | 5.05 | 4.67 | 6.87 | 420 | 66 |
| DKFZ-895 (98) | <4 | <4 | <<4[e] | 5.04 | 5.08 | 7.06 | 2000 | 110 |
| DKFZ-772 (99) | 4.70 | 4.55 | <4 | 6.05 | 5.48 | 7.39 | 480 | 21 |
| DKFZ-775 (100) | **4.29** | **<4** | **<<4[e]** | **4.65** | **4.61** | **8.08** | **6200** | **2700** |
| DKFZ-728 (101)[d] | **4.50** | **4.07** | **<<4[e]** | **5.02** | **4.96** | **7.97** | **2900** | **890** |
| DKFZ-758 (102) | 4.50 | 4.06 | <<4[e] | 5.30 | 5.14 | 7.44 | 870 | 140 |
| DKFZ-806 (103)[f] | **4.28** | **4.10** | **<<4[e]** | **4.58** | **4.58** | **7.72** | **2800** | **1400** |
| DKFZ-773 (104) | **4.92** | **4.67** | **<4** | **5.74** | **5.23** | **8.08** | **1500** | **220** |
| DKFZ-859 (105) | 4.19 | 4.00 | <<4[e] | 5.03 | 4.80 | 6.86 | 460 | 66 |
| DKFZ-805 (106) | **4.39** | **4.26** | **<<4[e]** | **4.79** | **4.79** | **8.09** | **5000** | **1800** |
| **Tubastatin A (19)** | 5.66 | 4.78 | <<4[e] | 7.88 | 5.75 | 8.28[d] | 416 | 2.5 |

[a] $pIC_{50}$ values are the mean from two separate experiments, each determined by four-parameter non-linear regression analysis with eight dose levels in triplicate with HDAC Glo assay[b] or FRET assay[c]. [d] Mean of at least three individual experiments. [e] Curve fit analysis not convergent at 100 µM. [f] $pIC_{50}$ values from one experiment in triplicates. SF (selectivity factor) = $10^{(pIC50(HDAC10) - pIC50(HDAC6 \text{ or } 1))}$ rounded to two significant figures. Activity profiles for the best HDAC10 inhibitors are highlighted in bold. Tubastatin A is listed as a reference. For an extended version of this table with 95% confidence intervals, see Table S2. Taken from Steimbach et al.[1] and extended.

Variation of the cap–amine linker length (**Table 2**, purple box) had a substantial impact on HDAC10 selectivity. Shortening the cap–amine linker of **DKFZ-711** from two to only one methylene in **DKFZ-772** resulted in a 5-fold drop in HDAC10/6 selectivity, mainly due to increased HDAC6 activity of **DKFZ-772**, while its HDAC10 affinity remained nearly unchanged. Inhibitor **DKFZ-775** with the one carbon longer propyl linker exhibited a promising gain in

selectivity. HDAC6 activity is reduced to the double digit µM range ($pIC_{50}$ = 4.65); at the same time, HDAC10 activity increased to single digit nM ($pIC_{50}$ = 8.08). This results in HDAC10/6 and 10/1-selectivities of 2700 and 6200, respectively. Unfortunately, this excellent profile did not fully continue in the cellular BRET assay (see **Figure 29**, page 62).

Cyclized variants of the γ-amino linker (**Table 2**, green box), with four-membered rings as *trans*- or *cis*-cyclobutanes in **DKFZ-759** and **DKFZ-767**, respectively, as well as azetidine **DKFZ-770**, seem to lock the γ-amine in an unfavorable confirmation. Class I activity was again only slightly affected and HDAC6 binding was only reduced in azetidine **DKFZ-770**. HDAC10 binding, on the other hand, was inferior to lead **DKFZ-711** in all compounds bearing a four-membered linker. As a consequence, HDAC10 selectivity factors are low for the two amino cyclobutanes, especially *cis*-cyclobutanes **DKFZ-759.** The selectivity profile of azetidine **DKFZ-770** is comparable to the best Tubastatin derivatives but with one order of magnitude lower HDAC10 affinity. Piperidine **DKFZ-895** is the only cyclic linker compound to provide selectivity similar to **DKFZ-711**, but HDAC10 affinity dropped by 0.4 log units. Therefore, I decided to not further develop the cyclic linker scaffolds.

Most advantageous and insightful were modifications of the amide that joins the cap group with the linker in lead **DKFZ-711**. Inverting this amide from the anilide to the benzamide orientation in **DKFZ-728** provided a considerable gain in HDAC10 potency ($pIC_{50}$ = 7.97) and simultaneously increased selectivity with about 890- and 2900-fold selectivity for HDAC10 over HDAC6 and 1, respectively. A similar advance was compound **DKFZ-806**, which I synthesized and tested at a later point in time. **DKFZ-806** is a second-generation inhibitor that combines the beneficial SAR observed in propyl-linked **DKFZ-775** with the benefit from inverting the amide to the benzamide orientation as in **DKFZ-728.** The SAR is at least partially additive and **DKFZ-806** could retain the increased HDAC10/6 selectivity from the additional carbon in the amine–cap linker. However, HDAC10/6 selectivity is not improved over **DKFZ-728** and the affinity for HDAC10 is even lowered in **DKFZ-806** ($pIC_{50}$ = 7.72), compared to two carbon linked benzamide **DKFZ-728.**

Since both inverting and moving the cap-linker bridging amide by varying linker length influenced HDAC10 potency and selectivity, I wanted to test the hypothesis that the amide provides a beneficial hydrogen bonding interaction at the HDAC10 active site tunnel entrance. Therefore, I synthesized and tested **DKFZ-859** with an *N*-methylated linker benzamide. Indeed, a methyl group replacing the polar amide hydrogen is responsible for over 10-fold reduction in HDAC10 potency without influence on HDAC6 affinity and therefore causes a sharp drop in HDAC10/6 selectivity compared to **DKFZ-728**. This SAR heavily suggests potential for a hydrogen bonding interaction only with HDAC10, but not other isozymes. Interestingly, when the benzamide is substituted with a benzenesulfonamide as in **DKFZ-758**, the benefits of the apparent hydrogen bonding interaction are lost and the potency/selectivity becomes again similar to anilide **DKFZ-711**.

Inspired by the importance of a suitable hydrogen bond donor/acceptor system between the cap group and the linker in aza-SAHA derivatives, I explored alternatives to simple amides. Therefore, I employed benzimidazoles **DKFZ-773** and **DKFZ-805**, which can be seen as *ortho*-

aminoanilide caps that are dehydrated and consequently cyclized into a bicyclic aromatic cap group with excellent hydrogen bonding capacities next to the linker attachment. Benzimidazole **DKFZ-773** shows double the selectivity of **DKFZ-711**, driven by a 0.6 log units increase in HDAC10 binding, even surpassing the HDAC10 affinity of **DKFZ-728**. When the benzimidazole cap group is combined with the extended propyl linker in **DKFZ-805**, no change in HDAC10 activity occurred ($pIC_{50}$ = 8.09) compared to ethyl-linked **DKFZ-773**, but Class I and HDAC6 activity dropped significantly. This provides **DKFZ-805** with excellent selectivities of 5000 and 1800 for HDAC10/1 and 10/6, respectively, which are only outperformed by propyl-linked anilide **DKFZ-775**.

In summary, the γ-amino hydroxamic acid scaffold of **DKFZ-711** could be further optimized with changes to the linker amide, providing an improvement in HDAC10 selectivity and potency. The best HDAC10 inhibitor selectivity profiles are highlighted in bold in **Table 2**. A graphical overview of biochemical assay data in the form of a potency versus selectivity plot is presented in **Figure 28** on page 60. The extension of the linker by one carbon to propyl as in anilide-capped **DKFZ-775** and benzimidazole **DKFZ-805** provided the highest HDAC10 potency in this series with a $pIC_{50}$ around 8.1 and at the same time the highest HDAC10/6 selectivity (>1800). Also bearing the propyl linker, benzamide **DKFZ-806** showed the third-highest selectivity over HDAC6 but with reduced potency. However, the promising selectivity profiles of those three propyl-linked compounds did not fully translate into the cellular BRET assay and I wanted to keep the linker as short as possible to optimize ligand efficiency. Ethyl-linked benzamide **DKFZ-728** has the best combination of potency, selectivity and ligand efficiency, both in biochemical assays and in the cellular BRET assay (see **Figure 29**, page 62), where **DKFZ-728** is the best compound discussed so far. Furthermore, diversification of the cap group in order to optimize this part of the inhibitor is more efficient with benzamides than with anilides or benzimidazoles. Different benzamide-capped inhibitors can be made by simple amide coupling of the same diamine precursor to a plethora of commercially available benzoic acid derivatives. Therefore, the SAR of the cap group was investigated with derivatives of ethyl-linked benzamide **DKFZ-728.**

Structures and biochemical assay data of inhibitors for investigating the SAR around the cap group are shown in **Table 3.** All cap group derivatives of **DKFZ-728** have reduced selectivity, in particular 2-methyl indole compounds **DKFZ-749** and **DKFZ-756**, where HDAC10/6 selectivity dropped below 100-fold and 10/1 selectivity to 170 and 350, respectively. Potency, however, could be well modulated by different aromatic cap groups, although often at the price of reduced selectivity. Fused bicyclic (hetero)aromatic ring systems provide the highest potency, while mostly retaining selectivity. This is seen with indazoles **DKFZ-754** and **DKFZ-757**, which are more potent than any compound in **Table 2**, and still remain among the most selective. The highest HDAC10/6 selectivity, close to the 890-fold of **DKFZ-728,** was achieved by 1-naphthamide **DKFZ-748** with 640-fold. It is also among the most potent compounds ($pIC_{50}$ = 8.29). Only its 4-methoxy derivative **DKFZ-774** and anthraceneamide **DKFZ-771** ($pIC_{50}$ = 8.34 and 8.47) show higher HDAC10 affinity, albeit with substantial loss of selectivity over HDAC6. Interestingly, **DKFZ-748** is only slightly more potent on HDAC10 than its regioisomer 2-naphthamide **DKFZ-769**, but superior since **DKFZ-769** is a better HDAC6

inhibitor ($pIC_{50}$ = 5.81) and shows even 13-fold increased activity on HDAC1 ($pIC_{50}$ = 5.63) compared to its regioisomer. The increased potency of larger aromatic cap groups can be rationalized by unspecific hydrophobic interactions with the protein surface, but the poor performance of biphenyl capped **DKFZ-746** illustrates that increased hydrophobicity does not automatically yield better HDAC10 binders, especially when adjusted for the number of heavy atoms in the ligand efficiency metric (see Table S2 for ligand efficiencies).

**Table 3. $pIC_{50}$ values[a] of DKFZ-728–derivatives**

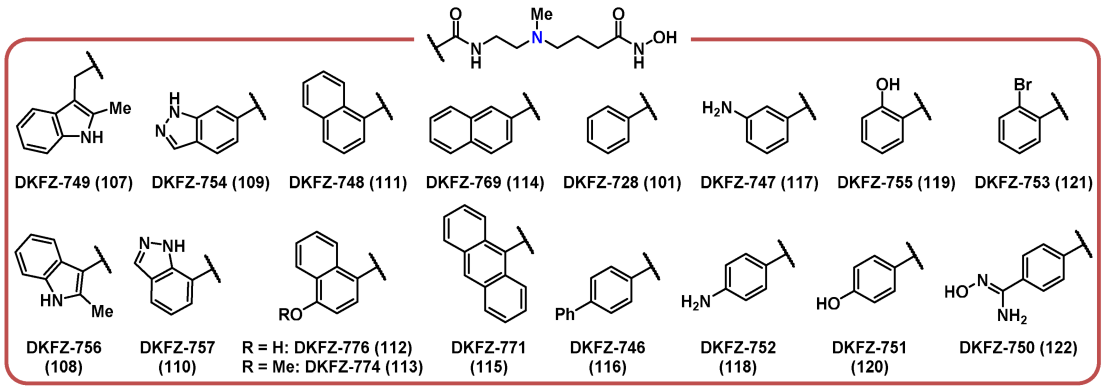


| compound | HDAC1[b] | HDAC2[b] | HDAC3[b] | HDAC6[b] | HDAC8[b] | HDAC10[c] | SF 10/1 | SF 10/6 |
|---|---|---|---|---|---|---|---|---|
| **DKFZ-728 (101)**[d] | 4.50 | 4.07 | <<4[e] | 5.02 | 4.96 | 7.97 | 2900 | 890 |
| **DKFZ-749 (107)** | 4.98 | 4.35 | <<4[e] | 5.43 | 5.53 | 7.22 | 170 | 63 |
| **DKFZ-756 (108)** | 5.13 | 4.52 | 4.05 | 5.82 | 5.32 | 7.68 | 350 | 72 |
| **DKFZ-754 (109)** | 5.00 | 4.43 | <4 | 5.44 | 4.95 | 8.12 | 1300 | 480 |
| **DKFZ-757 (110)** | 4.91 | 4.34 | <4 | 5.44 | 5.08 | 8.17 | 1800 | 530 |
| **DKFZ-748 (111)** | 4.89 | 4.29 | <4 | 5.49 | 5.87 | 8.29 | 2500 | 640 |
| **DKFZ-776 (112)** | 5.02 | 4.82 | <4 | 5.88 | 5.98 | 8.19 | 1500 | 200 |
| **DKFZ-774 (113)** | 5.22 | 5.01 | <4 | 5.71 | 5.64 | 8.34 | 1300 | 430 |
| **DKFZ-769 (114)** | 5.63 | 5.39 | 4.38 | 5.81 | 5.70 | 8.22 | 390 | 260 |
| **DKFZ-771 (115)** | 5.70 | 5.58 | 4.60 | 6.05 | 5.93 | 8.47 | 600 | 260 |
| **DKFZ-746 (116)** | 5.58 | 4.95 | 4.44 | 5.52 | 5.15 | 7.90 | 210 | 240 |
| **DKFZ-747 (117)** | 4.50 | <4 | <<4 | 5.23 | 4.77 | 7.62 | 1300 | 250 |
| **DKFZ-752 (118)** | 4.78 | 4.26 | <4 | 5.47 | 4.63 | 7.81 | 1100 | 220 |
| **DKFZ-755 (119)** | 4.12 | <4 | <<4[e] | 4.92 | 4.19 | 7.41 | 2000 | 310 |
| **DKFZ-751 (120)** | 4.75 | 4.23 | <4 | 5.84 | 4.65 | 8.05 | 2000 | 160 |
| **DKFZ-753 (121)** | 4.50 | <4 | <<4[e] | 5.26 | 5.03 | 7.76 | 1800 | 310 |
| **DKFZ-750 (122)**[f] | 4.82 | <4 | <<4 | 5.24 | 4.60 | 7.75 | 860 | 330 |

[a] $pIC_{50}$ values are the mean from two separate experiments, each determined by four-parameter non-linear regression analysis with eight dose levels in triplicate with HDAC Glo assay[b] or FRET assay[c]. [d] Mean of at least three individual experiments. [e] Curve fit analysis not convergent at 100 µM. [f] $pIC_{50}$ values from one experiment in triplicates. SF (selectivity factor) = $10^{(pIC50(HDAC10) - pIC50(HDAC6 \text{ or } 1))}$ rounded to two significant figures. Activity profile for the best HDAC10 inhibitors are highlighted in bold. For an extended version of this table with 95% confidence intervals, see Table S2. Based on Steimbach et al.[1]

I also explored the three aromatic substitution vectors of **DKFZ-728**, with anilines in the *meta*-(**DKFZ-747**) and *para*-position (**DKFZ-752**), as well as phenol functionalities in salicylamide **DKFZ-755** and in *para*-hydroxybenzamide **DKFZ-751**. Taken together, no beneficial vector for factorable polar interactions was identified; inhibitors **117-120** gave poor potency and selectivity compared to the parent compound **DKFZ-728**. *Ortho*-bromide **DKFZ-753** together

with salicylamide **DKFZ-755** were designed to limit rotation of the aryl cap, which did not prove advantageous in the tested examples.

Amidoxime containing inhibitor **DKFZ-750** was initially conceived as an aryl nitrile, but it reacted with hydroxylamine in the last synthesis step. Despite the unintended incorporation of this rare functionality, the amidoxime compound provides insightful data. Amidoximes are potential O→N bioisosteres of hydroxamic acids and were also used to bind various divalent pollution metal cations from wastewater, including $Zn^{2+}$.[184] *Para*-anilide and urea substituted benzamidoximes similar to **DKFZ-750** are reported as sub-micromolar HDAC inhibitors in HeLa nuclear extract, but the HDAC selectivity profile was not established.[185] My activity data of amidoxime **DKFZ-750** indicates no binding in "reverse orientation" with the benzamidoxime as the ZBG. No increase in affinity for any isozyme can be observed and all HDAC binding is in concordance with other amino hydroxamic acids.

The entire structure-activity relationship of amino hydroxamic acid inhibitors is summarized in a double-logarithmic biochemical potency versus selectivity plot in **Figure 28**, including structures of all tested γ-amino hydroxamic acid inhibitors. To conclude, the compounds in the aza-SAHA series (**Figure 28**, blue dots) have the most diverse selectivity profiles depending on the position of the amine in the linker, with only γ-amino hydroxamic acid **DKFZ-711** combining HDAC10 potency with selectivity over HDAC6 and Class I enzymes. Similarly, the distance between the basic amine and a hydrogen bond donor/acceptor system connecting to the hydrophobic cap group has an enormous influence on HDAC10 potency and selectivity and so does the orientation and composition of the linker-cap group bridge. The influence of these factors is represented by the spread – mainly along the selectivity axis – of the purple and grey dots in **Figure 28.** Only when the hydrogen bond donor is removed entirely, as in methylated benzamide **DKFZ-859**, are potency and selectivity subverted. Restraining the γ-amino hydroxamic acid with cyclic linkers (green dots in **Figure 28**) was universally inferior to the flexible, linear SAHA linker in all tested examples. Substituents of the tertiary amine other than methyl reduced HDAC10 potency and selectivity as a function of their steric bulk (orange dots). The quaternization (as in **DKFZ-777**) of the amine or an electron-withdrawing substituent (as in **DKFZ-888**) is detrimental for HDAC10 binding in the otherwise excellent HDAC10 inhibitor scaffold.

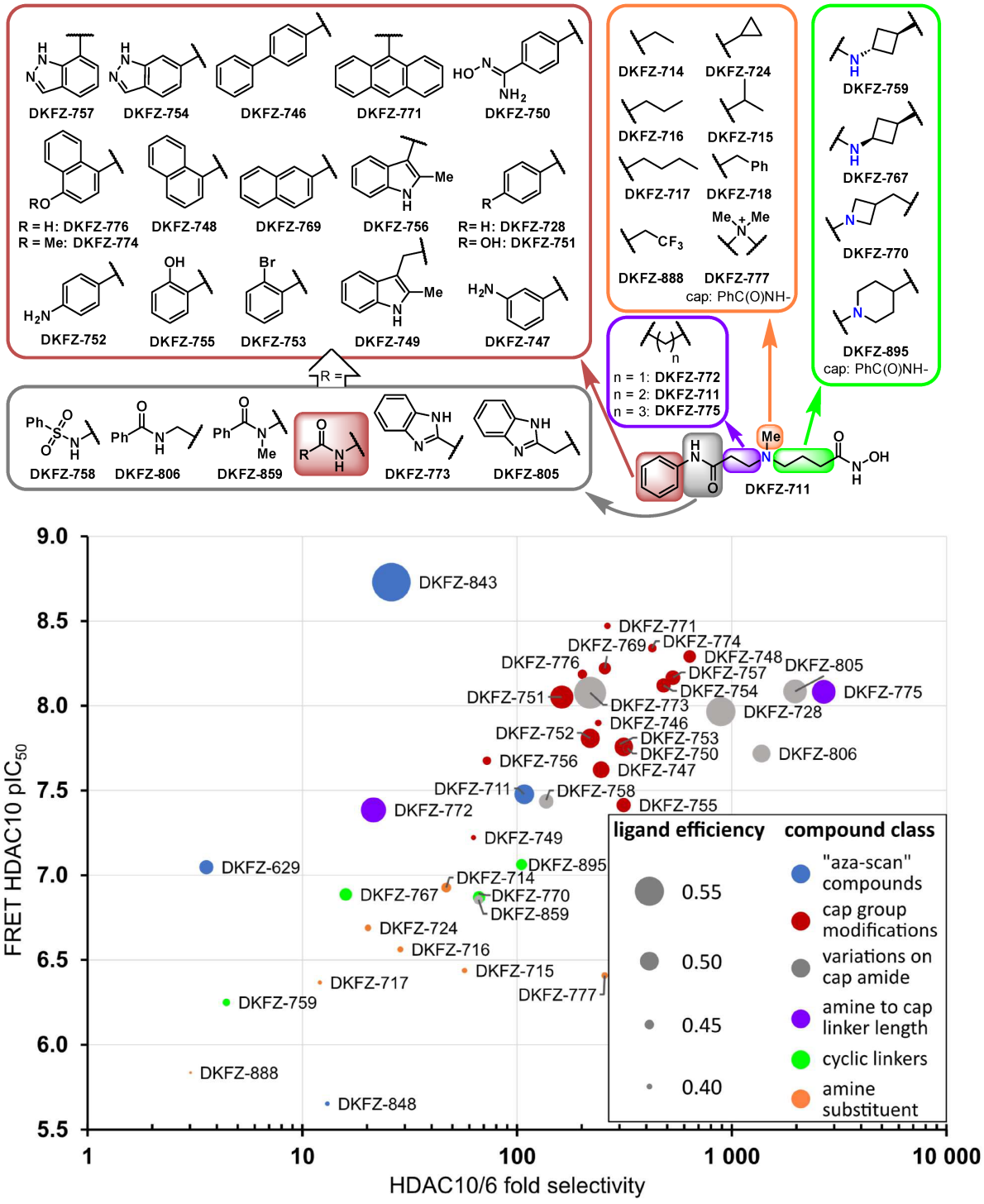


**Figure 28.** Biochemical HDAC10 potency versus selectivity logarithmic plot of amino hydroxamic acid inhibitors. Dot size represents ligand efficiency (LE = 1.37 x $pIC_{50}$(HDAC10) / number of heavy atoms)[186]. Dot colors represent which part of DKFZ-711 was investigated with the respective set of compounds depicted above. For a tabulated and extended version of this plot with 95% confidence intervals, see Table S2. Based on Steimbach et al.[1]

Finally, the cap group can be used to modify physicochemical properties and modulate potency, as the HDAC10 binding site seems remarkably tolerant of differently sized and shaped cap groups as well as polar functionalities. Cap-modified inhibitors (red dots in **Figure 28**) all cluster above and below, but always to the left of their parent **DKFZ-728.** This conveys that only HDAC10 potency, but not selectivity, can be improved by the cap group.

#### 3.2.2.2 Evaluation of cellular target engagement and selectivity

So far, compound evaluation and SAR studies in this chapter were mainly driven by the biochemical Glo- and FRET assay due to the high throughput of these assay systems and the broad isozyme spectrum of the HDAC Glo assay. However, demonstrating cellular target engagement is essential for chemical probes. Furthermore, HDAC10/6 selectivity estimations using two mechanistically different assay systems are prone to compound (class)-dependent biases, for example caused by differences in assay buffer composition.

Therefore, I tested a selection of compounds in the cellular BRET assay against HDAC6 and 10. **Figure 29** visualizes the assay data in a double-logarithmic cellular potency versus selectivity plot. All four aza-SAHA derivatives were tested in the BRET assay (for dose-response curves see **Figure 26**, page 50), but only **DKFZ-843** and **DKFZ-711** (blue dots in **Figure 29**) achieved an HDAC10 $pIC_{50}$ > 5.5 and an HDAC10/6 selectivity >10, with only **DKFZ-711** being a selective HDAC10i. The BRET assay confirms the poor performance of inhibitors bearing a tertiary amine substituted with groups other than methyl (orange dots). The same observation can be made with the cyclic linkers (green dots). In terms of selectivity, the best compounds come from variations of the cap amide (grey dots) and amine to cap linker length (purple dots) of **DKFZ-711**. This is where the biochemical and cellular assay data slightly diverge. Biochemically, the best compounds seem to be propyl-linked anilide **DKFZ-775** followed by propyl-linked benzimidazole **DKFZ-805** and propyl-linked benzamide **DKFZ-806** (see **Figure 28**). However, the BRET data highlights ethyl-linked benzamide **DKFZ-728** as the superior compound of this series, equipotent with benzimidazole **DKFZ-773**, but more selective. Anilide **DKFZ-775** has a similar BRET profile as **DKFZ-728,** but lower ligand efficiency due to the longer linker. The anilide attachment would have made cap group diversification more laborious and therefore less efficient, and the same applies to benzimidazole **DKFZ-773**. Based on this BRET data, I decided to diversify the cap group with the ethyl-linked benzamide **DKFZ-728**.

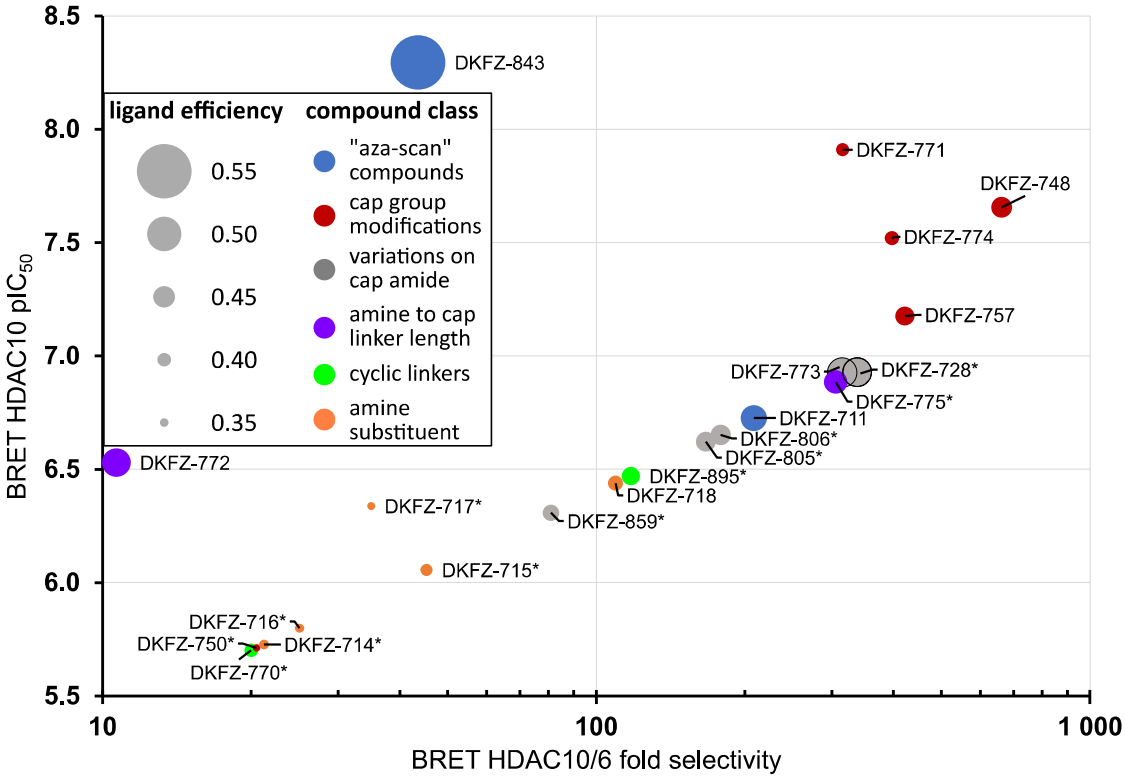


**Figure 29.** Cellular logarithmic HDAC10 potency versus selectivity plot of selected HDAC10 inhibitors. Dot size represents ligand efficiency (LE = 1.37 x $pIC_{50}$(HDAC10) / number of heavy atoms).[186] Dot colors represent which part of DKFZ-711 was investigated with the respective set of compounds depicted in Figure 28. *: HDAC6 $pIC_{50}$ could not be accurately determined due to lack of activity. Selectivity was calculated using the HDAC6 assay limit ($pIC_{50}$ of 4.4), actual selectivity may be higher. For a tabulated and extended version of this plot with 95% confidence intervals, see Table S3. Based on Steimbach et al.[1]

One limitation of the selectivity determination using the BRET assay is that, for technical reasons, the highest dose level used in the assay is 40 µM. This effectively limits accurate $pIC_{50}$ determination to ~4.4 for inhibitors with poor activity, usually on HDAC6. The maximum detectable fold selectivity is therefore dependent on HDAC10 potency, and selectivity for less potent compounds may be underestimated. Compounds that hit this limitation are marked with an asterisk (*) in **Figure 29** and tend to cluster along a diagonal line in the potency versus selectivity plot. While the biochemical assays, in principle, have the same limitation, the effect does not occur in **Figure 28**, since HDAC6 and 10 potencies are generally higher in the biochemical assays than in the cellular BRET assay, but also depend on the compound. The ratio of HDAC10 BRET/FRET activity is provided in **Table S3**. BRET data is, to some extent, reflecting cell permeability and uptake/efflux rates, and therefore depends on physicochemical properties and DMPK characteristics much more than biochemical assays. Indeed, more polar compounds like benzimidazoles **DKFZ-773** and **DKFZ-805** show a lower BRET/FRET ratio (6 and 4%) than **DKFZ-728** (9%). Less polar compounds tend to show a higher proportion of their FRET activity in the BRET assay, for example SAHA (30%), naphtamide **DKFZ-748** (23%), piperidine **DKFZ-895** (27%) or **DKFZ-859** (22%), which has been deprived of a hydrogen

bond donor by *N*-methylation of **DKFZ-728**. Linker length seems to play a role as well, since the propyl-linked compounds tend to have a lower BRET/FRET ratio than their ethyl counterparts. This drop in potency, together with the aforementioned limits in measuring the HDAC10/6 selectivity of weak HDAC6 binders, could be an explanation for the reduced performance of **DKFZ-805** and **DKFZ-806** in the BRET assay, compared to their promising biochemical profile.

Inhibitors with large hydrophobic cap groups performed well in the BRET assay and their biochemical potency and selectivity was confirmed. Only amidoxime **DKFZ-750** did not retain its biochemical potency and selectivity, most likely due to the added polar functionality for the reasons outlined above. One HDAC10 selective inhibitor stands out in the BRET assay: naphtamide **DKFZ-748**. It was already biochemically the most selective compound and among the most potent cap-optimized inhibitors. **DKFZ-748** retained its excellent selectivity in the BRET assay and is, with a 660–fold cellular HDAC10/6 selectivity and a cellular $IC_{50}$ of 22 nM (FRET $IC_{50}$ = 5.1 nM), my best selective HDAC10 inhibitor.

### 3.2.2.3 Synthesis strategy

Preparation of the tertiary amine substitution series (**87–93**) is described in **Scheme 7**. I started with the synthesis of secondary amino acid **123** by aza–Michael addition of GABA to *N*-phenylacrylamide in gram-scale, since **123** could be crystallized as its HCl-salt. This provided Masters intern Gergely Tihanyi with facile access to alkyl-substituted derivatives **87–92** by reductive amination, following esterification and conversion to the hydroxamic acid at the tertiary amine stage.

I prepared inhibitor **DKFZ-888** (**93**) bearing an electron-deficient 2,2,2-trifluoroethyl substituted amine using catalyst-free trifluoroethylation[187] with TFA. The trifluoroethylation method failed on amino acid substrate **123**, therefore I used amino alcohol **124**, prepared by aza–Michael addition of 1,4-aminobutanol to *N*-phenylacrylamide to access trifluoroethyl amino alcohol **125.** This alcohol was then oxidized to the amino acid by Jones oxidation followed by in situ esterification to **126**, which I converted to hydroxamic acid **DKFZ-888**.

**Scheme 7. Synthesis[a] of tertiary amine substitution series 87–93**

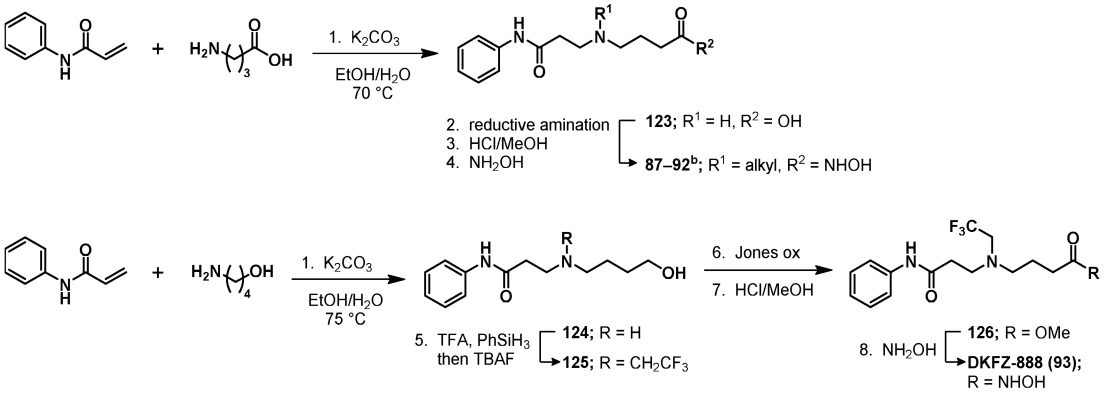

[a] Reagents and conditions 1. $K_2CO_3$, EtOH/$H_2O$, 70 °C, 3.5 h, 32% for **123** or 75 °C, 2 h, 83% for **124**; 2. aldehyde or ketone, $Et_3N$, $Na(OAc)_3BH$, THF, 0 °C–rt, 2–3 h or cyclopropanone ethyl trimethylsilyl acetal, HCl, $NaCNBH_3$, $H_2O$, rt, 7 d; 3. HCl/MeOH, rt, 18 h; 4. KCN, dioxane, rt, 1 h, then $NH_2OH$ (50 wt% in $H_2O$), rt, 24 h, 15–56% (3 steps); 5. TFA, $PhSiH_3$, THF, reflux, 4 h, then $CH_2Cl_2$, 1 M aq. NaOH, TBAF, 76%; 6. Jones reagent, acetone, 0 °C; 7. HCl/MeOH, rt, 16 h, 63% (2 steps); 8. KCN, dioxane, rt, 1 h, then $NH_2OH$ (50 wt% in $H_2O$), rt, 24 h, 39%. [b] Compounds prepared by Gergely Tihanyi during his lab rotation under my supervision. Taken from Steimbach et al.[1]

Preparation of cyclic linker compounds **95–98** is described in **Scheme 8**. To prepare inhibitors **95** and **96** with amino cyclobutane linkers, I started with aza–Michael addition of methyl 3-amino cyclobutane carboxylate (**127**) or carboxylic acid **128** to *N*-phenylacrylamide**,** followed by in situ esterification to amino esters **129** and **130,** and lastly hydroxamic acid formation. Azetidine containing inhibitor **DKFZ-770** could be accessed in a similar fashion starting from amino acid **131**. Hannah Steffke prepared piperidine compound **DKFZ-895** by alkylation of methyl piperidine-4-carboxylate with bromide **132**, followed by Boc deprotection to diamino ester **133**. Amidation of the primary amine with benzoyl chloride to **134** following hydroxamic acid formation provided **DKFZ-895**.

**Scheme 8. Synthesis[a] of cyclic linker compounds 95–98**

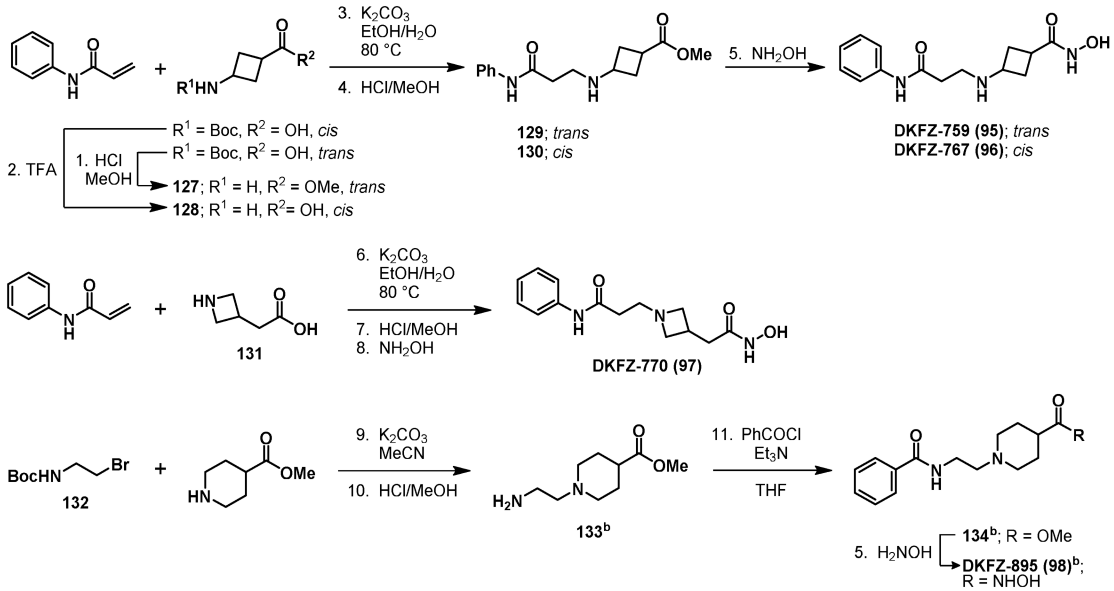


[a] Reagents and conditions 1. 2 M in HCl in MeOH, quant.; 2. 20% TFA in $CH_2Cl_2$, quant.; 3. $K_2CO_3$, EtOH/$H_2O$, 80 °C, 24–38 h; 4. HCl/MeOH, rt, 4 h, 58% for **129** (2 steps), 38% for **130** (2 steps); 5. KCN, dioxane, rt, 1 h, then $NH_2OH$ (50 wt% in $H_2O$), 24 h, rt, 43% for **95**, 72% for **96**, 36% for **98**; 6. $K_2CO_3$, EtOH/$H_2O$, 80 °C, 5 h; 7. HCl/MeOH, rt, 3 h; 8. KCN, dioxane, rt, 1 h, then $NH_2OH$ (50 wt% in $H_2O$), 24 h, rt, 6% (3 steps); 9. $K_2CO_3$, MeCN, reflux, 3 h; 10. HCl/MeOH, rt, 1.5 h, 65% (2 steps); 11. PhCOCl, $Et_3N$, THF, rt, 2.5 h, 28%. [b] Compound prepared by Hannah Steffke during her Fulbright internship under my supervision. Taken from Steimbach et al.[1]

**Scheme 9. Synthesis of compounds 99 and 100**[a]

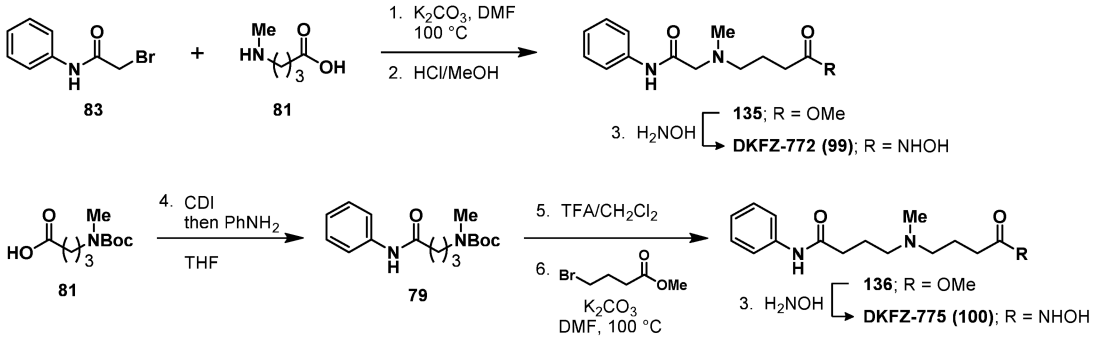


[a] Reagents and conditions 1. $K_2CO_3$, DMF, 100 °C, 1 h; 2. HCl/MeOH, rt, 18 h, 26% (2 steps); 3. KCN, dioxane, rt, 1 h, then $NH_2OH$ (50 wt% in $H_2O$), 24 h, rt, 73% for **99**, 82% for **100**; 4. CDI, THF, rt, 3 h, then aniline, rt, 5 h, 86%; 5. 20% TFA in $CH_2Cl_2$, rt, 1 h; 6. methyl 4-bromobutyrate, $K_2CO_3$, DMF 100 °C, 4.5 h, 66% (2 steps). Modified from Steimbach et al.[1]

Synthesis of cap–amine linker length varying compounds **99** and **100** is summarized in **Scheme 9**. **DKFZ-772** (**99**) was prepared by base-mediated alkylation of amino acid **81** with bromide **83** to give the corresponding tertiary amino acid, which I converted to amino ester **135**, and then to the desired hydroxamic acid **99**. The preparation of **DKFZ-775** (**100**) began with amidation of **81** with aniline to **79,** following Boc deprotection, and alkylation with methyl 4-bromobutyrate to amino ester **136**, which I converted to hydroxamic acid **100** in the last step.

Inhibitors with the *N*-ethylpropyl amine linker and a benzamide-type cap group, like **DKFZ-728** (**101**) (**Scheme 10**), were prepared from diamino ester **141,** which I, in turn, prepared by alkylation of mono Boc-protected diamine **137** with ethyl 4-bromobutyrate**,** followed by acid-catalyzed transesterification and simultaneous Boc deprotection. I prepared diamino esters **141** in gram scale, which enabled me to diversify the capping moiety for this linker scaffold (including the synthesis of **DKFZ-748**) by amidation of the primary amine with a plethora of benzoic acid derivatives. To access *N*-dipropyl amine compound **DKFZ-806** (**103**), I used the same route starting with the respective propyl diamine **138** to make Boc-protected diamino ester **140**, proceeding to deprotected diamine **142** and hydroxamic acid precursor **145**.

Quaternary ammonium salt **DKFZ-777** (**94**) was prepared by Menshutkin reaction of **DKFZ-728** using methyl iodide (**Scheme 10**). I purified the product by ion exchange chromatography following preparative HPLC under basic conditions, which yielded the internal ammonium hydroxamate salt as is evident from NMR analysis.

*N*-methylated **DKFZ-728** derivative **DKFZ-859** (**105**) could not be made by direct methylation of **DKFZ-728** or its ester precursor using amide alkylation reactions via deprotonation. Therefore, I prepared **105** starting with the 9-BBN-assisted mono-acylation of DMEDA to benzamide **146**,[188] which was then alkylated with methyl 4-bromobutyrate to amino ester **147** and subsequently converted to the hydroxamic acid **105**.

**Scheme 10. Synthesis of compounds 94, 101–103, 105, 107–122**[a]

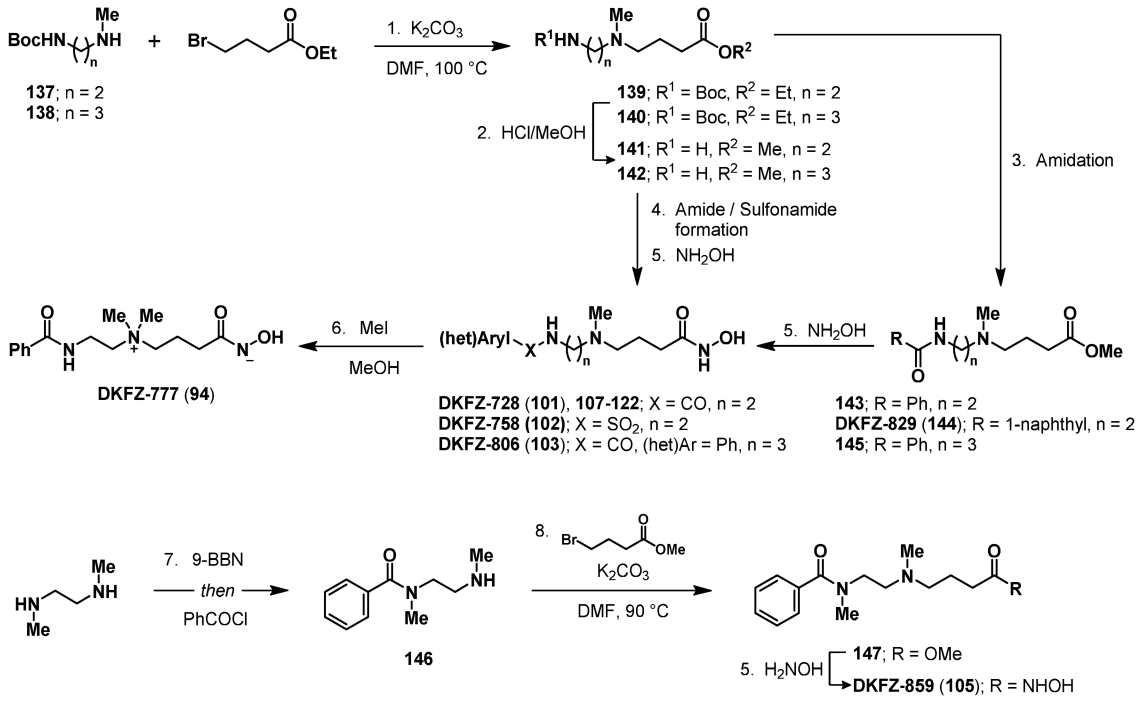


[a] Reagents and conditions 1. $K_2CO_3$, DMF, 100 °C, 16 h, 81 or 88%; 2. HCl/MeOH, rt, 26 h, quant; 3. PhCOCl, $Et_3N$, dioxane, rt, 2 h, 88% for **S18** or 1-naphthoic acid, *i*-$Pr_2NEt$, HOBt, EDC, $CH_2Cl_2$, rt, 18 h, 83% for **49** or BzCl, $NaHCO_3$, EtOAc/$H_2O$, rt, 90 min, 86% for **145**; 4. ArCOCl, $NaHCO_3$, EtOAc/$H_2O$, rt, 10–90 min or $PhSO_2Cl$, $K_2CO_3$, $H_2O$/MeCN, rt, 5 h or (het)aryl carboxylic acid, *i*-$Pr_2NEt$, HOBt, EDC or DCC, $CH_2Cl_2$, rt, 12–48 h; 5. KCN, dioxane, rt, 1 h, then $NH_2OH$ (50 wt% in $H_2O$), 24 h, rt, 22–80% (for individual yields see specific procedures[1]); 6. only with **DKFZ-728**: MeI, MeOH, rt, 7 h, 42%, 7. 9-BBN, hexane/THF, rt, 1 h, then BzCl, rt, 2.5 h, 31%; 8. methyl 4-bromobutyrate, $K_2CO_3$, DMF, 90 °C, 4 h, 59%. Based on Steimbach et al.[1]

Benzimidazole-containing inhibitors **DKFZ-773** (**104**) and **DKFZ-805** (**106**) were synthesized (**Scheme 11**) from the corresponding methyl esters **150** and **153**, starting with the amidation of aniline **148** with acryloyl chloride or with acid **151.** Towards ethyl-linked benzimidazole **104**, I performed an aza–Michael addition of **81** to acrylamide **149.** In the synthesis of propyl-linked **106**, the γ-amino ester was formed by removal of the Boc protecting groups of **152** and alkylation of the aliphatic amine with ethyl 4-bromobutyrate. In both cases, the benzimidazole and methyl ester were formed simultaneously by refluxing the alkylation/addition product in acidified methanol.

**Scheme 11. Synthesis of benzimidazole-capped inhibitors 104 and 106**[a]

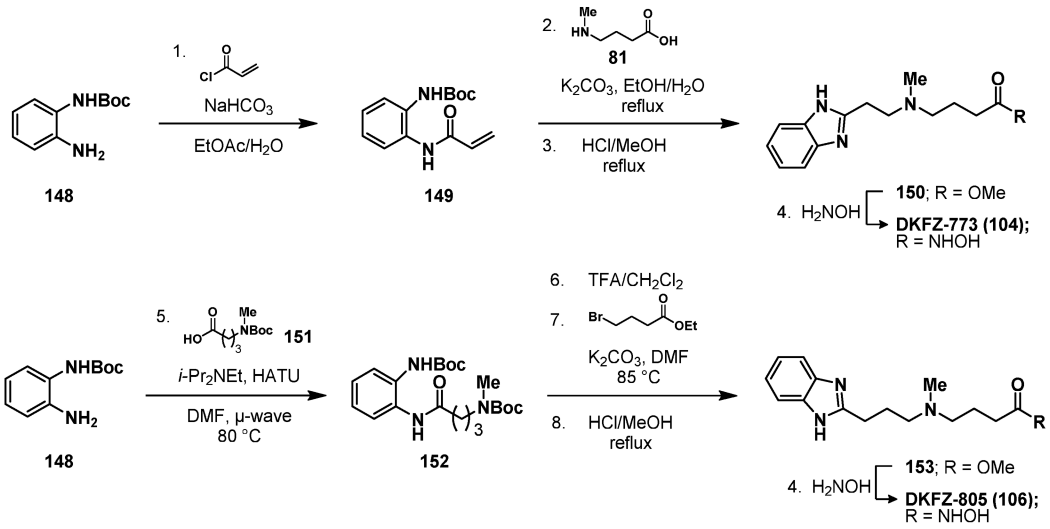


[a] Reagents and conditions 1. acryloyl chloride, $NaHCO_3$, $EtOAc/H_2O$, rt, 10 min, 98%; 2. **81**, $K_2CO_3$, $EtOH/H_2O$, reflux, 16 h; 3. HCl/MeOH, reflux, 18 h, 49% (2 steps); 4. KCN, dioxane, rt, 1 h, then $NH_2OH$ (50 wt% in $H_2O$), 24 h, rt, 66–68%; 5. **151**, *i*-$Pr_2NEt$, HATU, DMF, 80 °C, μ-wave, 20 min, 91%; 6. 25% TFA in $CH_2Cl_2$, rt, 90 min; 7. ethyl 4-bromobutyrate, $K_2CO_3$, DMF, 85 °C, 18 h; 8. HCl/MeOH, reflux, 21 h, 53% (3 steps). Adapted from Steimbach et al.[1]

## 3.2.3 Structural confirmation of selective HDAC10 binding

This project was propelled by a fruitful collaboration with the Christianson Lab at the University of Pennsylvania, where HDAC10 was originally recognized as a polyamine deacetylase and the crystal structure of zebrafish (*Danio rerio*) HDAC10 was determined.[41] Post-doctoral researcher Corey Herbst-Gervasoni later optimized the crystallization procedure and "humanized" zebrafish HDAC10 by introducing two substitutions in the substrate binding region. These substitutions, A24E and D94A, were made to more closely approximate the active site of human HDAC10 and to facilitate cocrystallization with inhibitors.[182] Hence, I hereafter refer to the humanized zebrafish HDAC10 mutant as just "HDAC10". Dr. Herbst-Gervasoni solved the crystal structures of SAHA and three of my aza-SAHA inhibitors bound to HDAC10 at 2.10–2.25 Å resolution.[1] **Figure 30** depicts cartoon representations of HDAC10 with simulated annealing omit maps of SAHA (A), δ-amine **DKFZ-629** (B), and γ-amines **DKFZ-711** (C) and **DKFZ-728** (D) residing in the active site. Except for **DKFZ-711**, whose hydroxamate group coordinates to the $Zn^{2+}$ ion with monodentate geometry, as indicated by a relatively large C=O---$Zn^{2+}$ separation of 2.8 Å, all other inhibitors' hydroxamate groups coordinate to the $Zn^{2+}$ ion with bidentate geometry. Another feature shared by all four (aza-)SAHA structures is a hydrogen bonding network that involves H136 donating to the $Zn^{2+}$-bound hydroxamate N–O– groups and H137 accepting a hydrogen bond from the hydroxamate NH groups. Additionally, each hydroxamate carbonyl oxygen accepts a hydrogen bond from Y307.

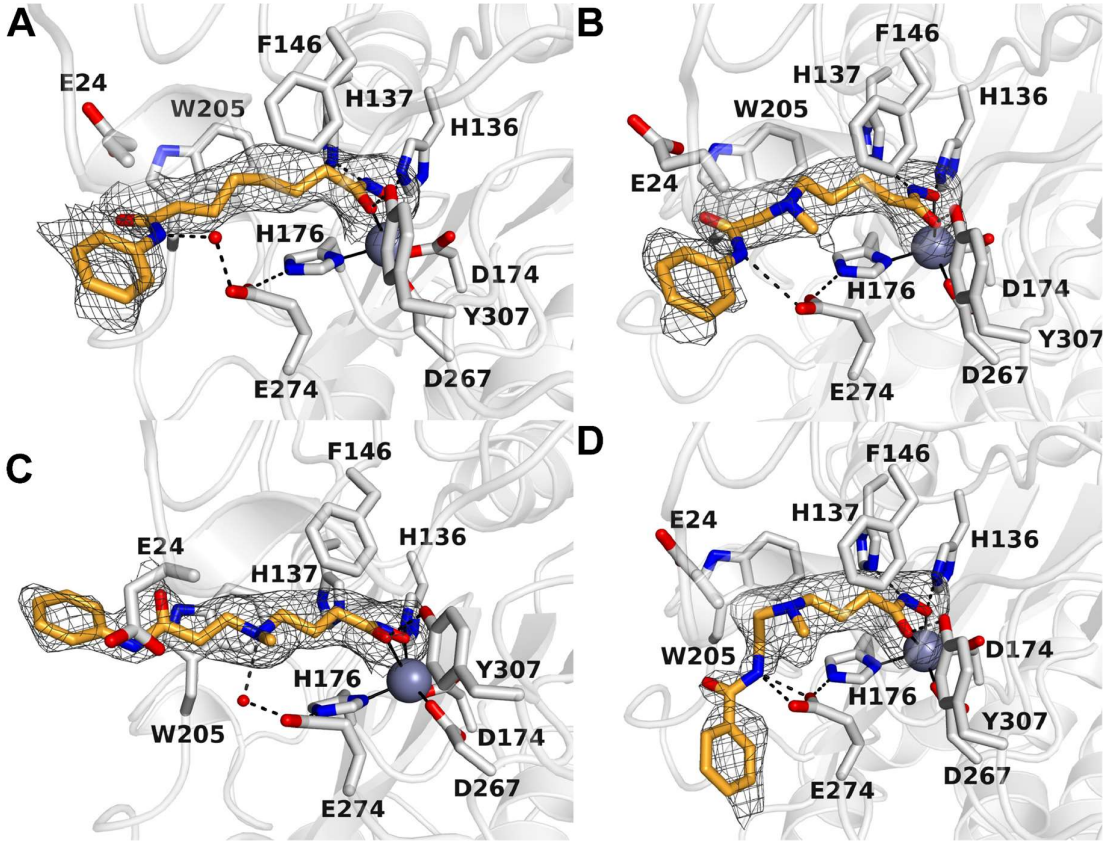


**Figure 30.** X-ray crystal structures of inhibitors bound to HDAC10. Simulated annealing omit maps of inhibitors in the active site of HDAC10: A. SAHA (contoured at 1.7σ), PDB: 7SGG; B. DKFZ-629 (contoured at 2.3σ), PDB: 7SGI; C. **DKFZ-711** (contoured at 2.4σ), PDB: 7SGJ; D. **DKFZ-728** (contoured at 2.2σ), PDB: 7SGK. Atoms are color-coded as follows: C = light gray (HDAC10) or orange (inhibitors), N = blue, O = red, and $Zn^{2+}$ = gray sphere. Metal coordination interactions are shown as solid black lines and hydrogen bonds are represented as dashed black lines. Figure prepared by Dr. Corey J. Herbst-Gervasoni and taken from Steimbach et al.[1]; see publication for method descriptions.

While interactions involving the hydroxamic acid zinc binder are mostly identical among the four inhibitors, the interactions with the cap group–linker bridging amide differ between the inhibitors. In the HDAC10–SAHA complex (**Figure 30A**), the NH of the anilide capping group provides a hydrogen bond to a water molecule. This water then donates a hydrogen bond to the E274 gatekeeper residue, which itself is located within H-bonding distance to H176, a residue coordinating the zinc ion. Such water-mediated hydrogen bond networks involving H176 and E274 – sometimes also directly interacting with each other – have also been observed in other HDAC10 complexes,[137,138] including HDAC10 substrates[27] and ring-opened Tubastatin A derivatives, like in **DKFZ-480.**[48]

In contrast to SAHA, its direct C→ $N_{\delta}$-Me analog, **DKFZ-629** (**Figure 30B**), has no water spanning a hydrogen bonding network from the anilide NH via E274 to zinc ligand H176. The γ-amine isomer **DKFZ-711** complex (**Figure 30C**) adopts a different binding mode compared to the complex with δ-amine **DKFZ-629**, even though the two inhibitors only differ by the

amine position in the linker. There are no hydrogen bond interactions between HDAC10 and the anilide capping group, but a water-mediated hydrogen bond between the tertiary γ-amine and gatekeeper E247, which is again interacting with H176.

The complex with γ-amine **DKFZ-728** (**Figure 30D**) is distinct, as it is the only one with an inhibitor that has the cap amide inverted relative to SAHA. This change from an anilide to a benzamide cap increased HDAC10 binding and selectivity significantly (see **Table 2**, page 55). Furthermore, by preparing and testing appropriate derivatives, I demonstrated that a correctly located hydrogen bond donor is responsible for the improved HDAC10 binding. In the case of **DKFZ-728**, I removed the amide N-H hydrogen bond donor by methylation of the amide in **DKFZ-859**. This led to a nearly 10-fold drop in HDAC10 activity compared to the non-methylated amide in **DKFZ-728**. The HDAC10–**DKFZ-728** complex now offers a structural explanation for this SAR: gatekeeper E274 forms a strong bifurcated hydrogen bond with the benzamide N-H directly, while still involved in binding zinc ligand H176. These interactions are advantageous because they enable the HDAC10 active site to adopt a favorable conformation and release a water molecule compared to the HDAC10–**DKFZ-711** complex.

We were surprised to see that the γ-amino group does not directly bind the gatekeeper residue E274, since we originally incorporated the amine to mimic the polyamine substrates. I expected that the ammonium cations of strong binders would directly interact with E274, based on previous crystal structures of HDAC10 bound to ε-amino hydroxamic acid **36**[133] and Tubastatin A.[48] Unexpectedly, the three newly solved aza-SAHA structures share the feature that each ammonium forms a cation-π interaction with W205. In each complex, the ammonium cations are positioned similarly close to W205 despite being differently distanced (γ- or δ-positions) to the hydroxamic acid, indicating that the cation-π interaction is strong and anchors the amine in the binding tunnel so that the rest of the molecule adopts a conformation around it and the fixed position of the zinc-binder. **Figure 31** illustrates this feature by superimposing the three HDAC10–aza-SAHA complexes.

The key cation-π interaction could be the reason why cyclic and therefore conformationally restricted γ-amino hydroxamic acid inhibitors like amino cyclobutanes **DKFZ-759** and **DKFZ-767** and azetidine **DKFZ-770** show reduced HDAC10 activity. They likely do not allow for a conformation in which the ammonium cation is ideally placed to interact with W205. A slightly better but still suboptimal placement of the ammonium is possibly the case in piperidine **DKFZ-895**. Similarly, when the amine is located too close to the hydroxamic acid, as in β-amine **DKFZ-848**, W205 and the zinc ion cannot be engaged correctly at the same time. Furthermore, the assay data indicates that a protonated amine too close to the catalytic zinc is universally detrimental for Class I, as well as Class IIB binding, but a closer proximity is tolerated by HDAC10.

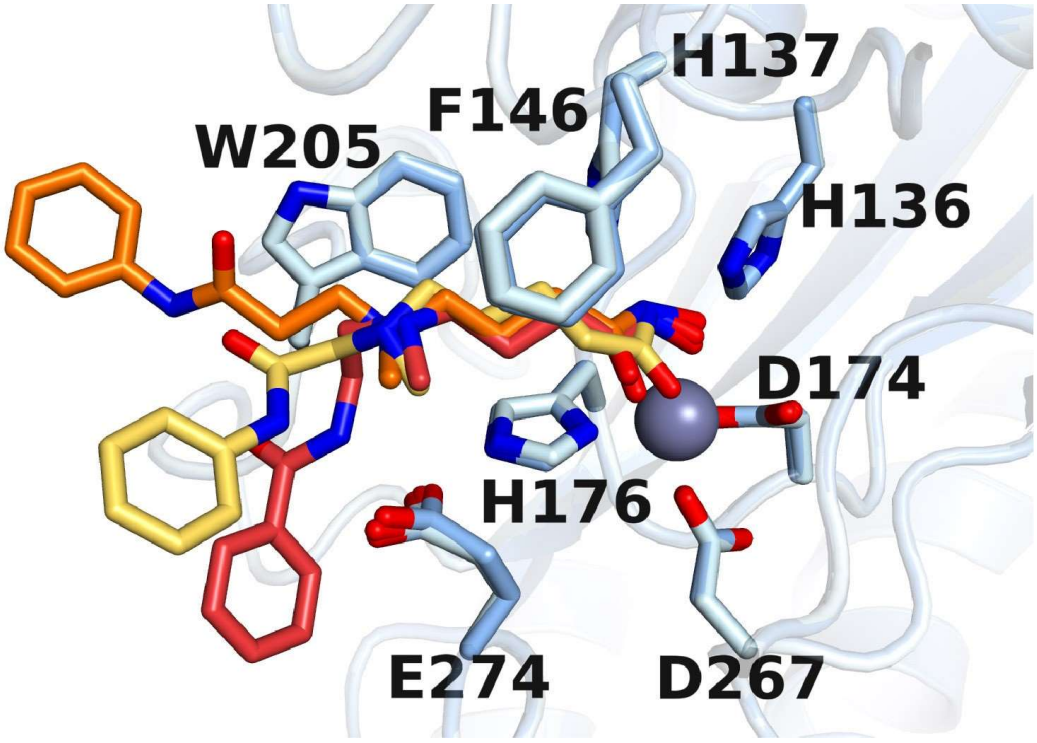


**Figure 31.** Overlay of HDAC10–inhibitor structures of aza-SAHA derivatives from Figure 30. Blue: HDAC10 residues; yellow: DKFZ-629; orange: DKFZ-711; red: DKFZ-728. Figure prepared by Dr. Corey J. Herbst-Gervasoni and taken from Steimbach et al.[1]; see publication for method descriptions.

When I compare the previous crystal structure of ε-amino hydroxamic acid **36** bound to HDAC10[133] with my γ- or δ-amines in light of the HDAC10 activity data of the aza-scan compounds (**Figure 24**, page 48), it becomes clear that there are two favorable locations for a protonated amine in an HDAC10 ligand. One location is quite close to the zinc binder and well occupied by a linear γ-amine as in **DKFZ-711**, **DKFZ-728** and most likely their derivatives. The binding interaction here is a cation-π interaction with W205, which requires a positive charge in the narrow binding tunnel. The second favorable location is towards the binding tunnel entrance and is well filled with an ε-amine in linear inhibitors (such as **36**[133] or presumably **DKFZ-843**) or a gramine cap group as in Tubastatin A derivative **DKFZ-480**[48]. This interaction is more flexible regarding the chemotype of the ligand. Protonated amines can form a strong polarized H-bond to the gatekeeper residue E274, but amides, such as the benzamide in **DKFZ-728**, can also benefit from E274 by regular hydrogen bonding. Both interactions can be strong and are the reason why potent HDAC10 binders either can be linear γ- or ε-amines or can have a basic group as part of the capping region.

Although interactions with both residues (W205 and E274) increase HDAC10 affinity, they are not equally associated with HDAC10 selectivity. Engaging the gatekeeper residue E274 alone is apparently insufficient to provide HDAC10 selectivity, as these inhibitors do not experience unfavorable interactions in other HDAC isozymes. I suspect this is the reason why the HDAC10 selectivity of Tubastatin A derivatives was limited to around 40-fold and also why ε-amine

**DKFZ-843** only shows 26-fold HDAC10/6 selectivity despite its excellent potency and likely interaction with E274, as does related ε-amino hydroxamic acid **36**[133]. Instead, the common feature in the crystal structures of HDAC10 binders with simultaneously reduced HDAC6 affinity is the cation-π interaction with W205. Still, when the gatekeeper E274 is engaged in addition to that, a selective HDAC10 binder receives additional potency, as observed with the amide inversion in **DKFZ-711** to **DKFZ-728**.

While the structural data with HDAC10 helps to rationalize the SAR regarding improved HDAC10 affinity and resulting selectivity, it does not provide definitive answers on why my γ-amino hydroxamic acids essentially lost all Class I activity and most of their affinity for HDAC6. Perhaps the reason lies in the favorable cation-π interaction with W205, which is unique to HDAC10. Class I HDACs and HDAC6 bear a phenylalanine instead of a tryptophan in this location, which is perhaps not suited for a comparable cation-π interaction. To help us better understand what drives HDAC10 selectivity of my γ-amino inhibitors over the closest relative HDAC6, Dr. Ulrike Uhrig (Chemical Biology Core Facility, EMBL Heidelberg) performed a docking study on HDAC6. She docked **DKFZ-711** (**Figure 32A**) and SAHA (**Figure 32B**) into HDAC6 based on the HDAC6–trichostatin A complex[18] (PDB 5EDU), since no SAHA cocrystal structure with HDAC6 is available and trichostatin A is also a linear, slender hydroxamic acid based pan-inhibitor. To emphasize changes in the water network caused by the incorporation of an amine to the SAHA linker region, she modeled the hydrogen locations into the crystal structures of HDAC10 with DKFZ-711 and SAHA (**Figure 32C** and **D**). This serves as a comparison to the HDAC6 docking models with the same inhibitors.

Assessing the representative docking pose of **DKFZ-711** to HDAC6 in a hydrophobic surface representation (**Figure 32A**), we see that the ammonium ion is located in a mostly hydrophobic tunnel flanked by F620, L749 and F680, the latter replacing HDAC10's W205. SAHA docked to HDAC6 on the other hand (**Figure 32B**), appears much better suited for the hydrophobic binding tunnel of HDAC6 due to its also hydrophobic unfunctionalized alkyl linker chain. In contrast stands the crystal structure of **DKFZ-711** bound to HDAC10 (**Figure 32C**), with a binding tunnel much better suited to accommodate basic ligands, as it is surrounded by E24 and gatekeeper E274, the latter residing in the approximate location of L749 in HDAC6. These two glutamic acid residues provide a matching electrostatic environment for the cationic ligand **DKFZ-711** which is also benefitting from the surface water network. On the contrary, the HDAC10–SAHA complex (**Figure 32D)** shows that SAHA with its unfunctionalized linker cannot benefit from the glutamic acids 24 and 274 to the same extent. SAHA is also not connected to a larger surface water H-bond network, like in the case of **DKFZ-711**; the only polar interaction is a water-mediated hydrogen bond with E274.

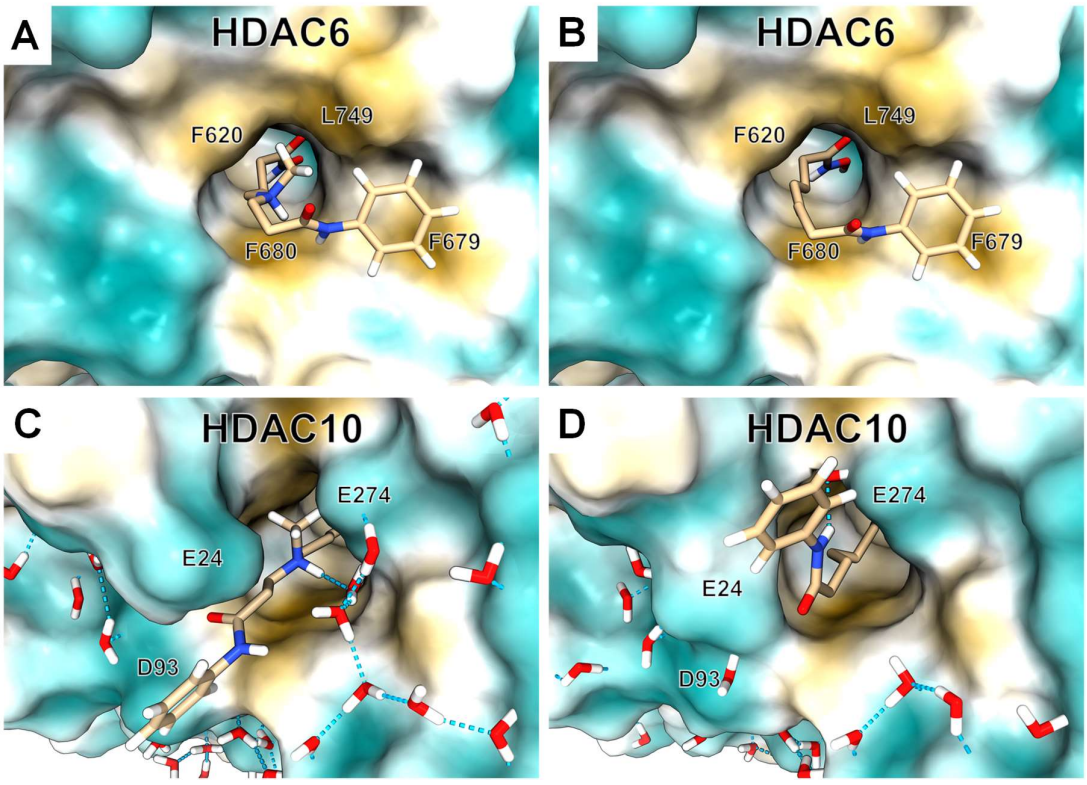


**Figure 32.** Comparison of HDAC6 docking models of **DKFZ-711** (A) or SAHA (B) calculated by Dr. Ulrike Uhrig based on PDB 5EDU, with crystal structures of HDAC10–DKFZ-711 (C) and HDAC10–SAHA (D) revealing selectivity-driving interactions. Hydrogen atoms were modeled into crystal structures to emphasize surface water networks. Surface colors: ocher: hydrophobic; turquois: hydrophilic. Methylene hydrogens are omitted for clarity. Hydrogen bonds are depicted as dashed blue lines. Figure is own work taken from Steimbach et al.[1]; see publication for method descriptions.

Comparing the HDAC10–**DKFZ-711** complex with the SAHA complex (**Figure 32C** and **D)** and the HDAC6 models (**Figure 32A** and **B)** in hydrophobic surface representation reveals another important feature of HDAC10: the constriction at the binding tunnel entrance formed by E24 is the most obvious difference between the binding tunnels of HDAC10 and 6. E24 is part of the $P^{23}ECE^{26}$ motif ($P^{23}ACE^{26}$ in zHDAC10), which is unique to HDAC10 orthologues, as it differs by a two-residue insertion, combined with a two-residue mutation in the L1 loop relative to HDAC6.[27,41] The $P^{23}ECE^{26}$ motif is structured in a flexible one-turn $3_{10}$ helix, which allows E24 to move depending on the bound ligand. This flexibility of the $P^{23}ECE^{26}$ $3_{10}$ helix has already been observed with the bulky Tubastatin A derivatives[48] and is also evident here. The $P^{23}ECE^{26}$ helix appears to be "pushed out" in the SAHA complex, instead of "pulled in" like in the **DKFZ-711** structure due to electrostatic attraction.

From these data, I conclude that the poor HDAC6 activity of γ-amino hydroxamic acids appears to be rooted in unfavorable electrostatics of a cation close to the hydroxamic acid and therefore too deep in the hydrophobic binding tunnel. Perhaps there is even electrostatic repulsion with catalytic histidine residues that are protonated to act as general acids. The same explanation can be applied to Class I enzymes. Only HDAC10 with its binding site having evolved to

accommodate polycations, provides a complementary electrostatic environment for γ-amino ligands. This allows a positive charge to be brought closer to the catalytic center, at least until a certain proximity. A limit is revealed by β-amine **DKFZ-848**. With its positive charge even closer to the $Zn^{2+}$ ion, it is a poor fit for all tested isozymes.

### 3.2.4 Chemical proteomics selectivity profiling including non-HDAC off-targets

For a high-quality chemical probe, target specificity is essential. I wanted to exclude potential for any off-target activity, ideally on a proteome-wide scale. Therefore, we collaborated with the Médard Lab at Technische Universität München, where Severin Lechner developed a powerful chemical proteomic profiling approach[128] that uses an affinity matrix of beads functionalized with three different hydroxamic acid-based HDAC binders. Combined, they can pull down and enrich nine out of the eleven HDAC isozymes from native cell lysates and furthermore identified novel off-targets of common HDAC inhibitors, including SAHA and Tubastatin A. Their approach allows for the determination of apparent p$K_D$ values by dose-dependent competition of inhibitors against the HDAC affinity matrix followed by mass spectrometric quantification of captured proteins. This enabled the proteome-wide selectivity profiling of novel inhibitors within the HDACi target landscape.

**Table 4. Apparent p$K_D$ values[a] of DKFZ-748 and reference compounds by chemical proteomic profiling**

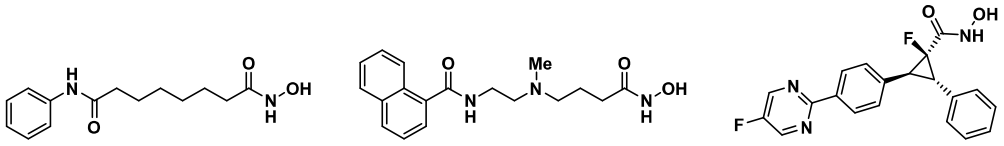


| p$K_D^{app}$ | HDAC1 | HDAC2 | HDAC5 | HDAC6 | HDAC8 | HDAC10 | ISOC1 | ISOC2 | ALDH1B1 | ALDH2 | GAT3DA | MBLAC2 |
|---|---|---|---|---|---|---|---|---|---|---|---|---|
| SAHA | 6.1 | 5.9 | <4 | 6.4 | <4 | 5.7 | 6.6 | 7.1 | 5.8 | 6.0 | 5.5 | 4.7 |
| DKFZ-748 | <4 | <4 | <4 | <4 | <4 | 6.8 | 4.4 | 4.9 | <4 | <4 | <4 | <4 |
| CHDI00465983[b] | <4 | <4 | 6.2 | <4 | 4.8 | <4 | <4 | <4 | <4 | <4 | <4 | 6.8 |

[a] Determined by Severin Lechner (Technische Universität München) using LC-MS/MS-based dose-dependent competition pulldown assay[128] in native BE(2)-C lysates from three or two[b] separate experiments, each performed with eleven dose levels. CHDI00465983[131] is reported as Class IIA selective inhibitor, pan-inhibitor SAHA serves as HDAC Class I/IIB control. Figure taken from Steimbach et al.[1]; for full method description and dose-response curves see publication.

Severin profiled my selective HDAC10i **DKFZ-748**, together with SAHA as Class I/IIB control and **CHDI00465983**[131] as Class IIA control in native BE(2)-C lysates that I prepared according to their protocol. The Class IIA control was particularly important since so far, I did not obtain

any data regarding HDAC Class IIA activity of my probes. Pleasingly, the chemical proteomic profiling confirmed the excellent HDAC10 selectivity of **DKFZ-748** across the entire HDACi target landscape. Not only is the previously established selectivity over Class I and HDAC6 independently confirmed, but the data also show no measurable affinity for the Class IIA representative HDAC5. Additionally, despite being a close structural relative of SAHA, **DKFZ-748** does not bind the SAHA off-targets to any comparable extent. The only detectable off-target affinity is for isochorismatase domain-containing proteins (ISOC) 1 and 2, but with two orders of magnitude lower affinity than SAHA.

Another class of enzymes that could be potential off-targets of hydroxamic acid compounds are matrix metalloproteinases (MMPs). They are also zinc-dependent hydrolases, but are often excreted and require extracellular activation.[189] Therefore, these enzymes may be missed by the Médard Group's chemical proteomic profiling approach. To also cover this enzyme class that can be bound by hydroxamic acids[190] as well, we collaborated with the Nuti Lab (University of Pisa). They tested amino hydroxamic acid **DKFZ-711** against MMP-9 and 13, which at 100 µM showed only 6.9% and 6.5% inhibition, respectively.[1]

Taken together, these data confirm selectivity for HDAC10 of my γ-amino hydroxamic acids not only within the zinc-dependent HDAC family, but also within broad coverage of the human proteome, especially regarding potential metal-dependent off-target enzymes.

## 3.3 Functional pharmacology and phenotype of selective HDAC10 inhibitors

### 3.3.1 Cytotoxicity of HDAC10 inhibitors

HDACis acting on Class I are cytotoxic agents.[7,191] Due to the lack of well characterized selective HDAC10is prior to this work, the effects of pharmacological HDAC10 inhibition on cell proliferation were not well documented. One may expect that selective HDAC10 inhibition should not be generally cytotoxic, since HDAC10 knockout mice, systemically lacking the HDAC10 gene, are healthy and develop normally.[57] To investigate the effect of selective HDAC10 inhibition on cell viability, I treated three representative cell lines with SAHA, Tubastatin A, and four selective HDAC10is with different potencies for 72 h. The cell lines were chosen to represent human cells not derived from cancer (HEK293T), a classical cancer cell line (HeLa) and an additional human cancer entity (BE(2)-C). While SAHA, and at higher dose-levels also Tubastatin A, led to reduced cell viability (CellTiter-Blue readout) in all three cell lines, no growth inhibition or cytotoxic effect linked to HDAC10 binding was observed with my selective HDAC10is (**Figure 33**). This is remarkable, as **DKFZ-711** differs from SAHA only by an amino group in the linker region and cellular target engagement was demonstrated for the tested HDAC10is as well (see **Figure 29**, page 62).

Moreover, I conducted a colony formation assay on BE(2)-C cells using the selective HDAC10i **DKFZ-728** and pan-inhibitor SAHA. This assay determines the ability of cell lines to develop colonies from single, isolated cells during drug treatment over a period of days. Generally,

tumor cells with high proliferation rates are more sensitive in the colony formation assay, and it is an effective way to evaluate anti-proliferative properties even when direct cytotoxicity of the drug is absent. Indeed, the full-effect dose for SAHA is lower in the colony formation assay (**Figure 34**, black curve), compared to the CellTiter-Blue cytotoxicity assay on the same cell line (**Figure 33**, right graph, black diamond curve), but **DKFZ-728** (**Figure 34**, red curve) does not inhibit colony formation in doses below 100 µM. The cellular target engagement of **DKFZ-728** for HDAC10 (BRET assay $IC_{50}$ = 118 nM) is much lower than needed to affect colony formation, meaning no growth inhibition can be attributed to HDAC10 binding, not even in this sensitive colony formation assay.

Additionally, **DKFZ-711** was also screened in the one-dose NCI-60 screening at 10 µM.[1] However, no cancer entity with susceptibility towards **DKFZ-711** was revealed. The average viability was 99 ± 8% with the lowest 10th percentile covering 72–91%. This further demonstrates the lack of HDAC10 inhibition-related cytotoxicity in cancer cells. Parallel to my investigations, others also worked on the development of HDAC10is, which also barely showed cytotoxicity on HEK293 cells,[138] confirming my data on this cell line and my overall conclusion using a different inhibitor scaffold.

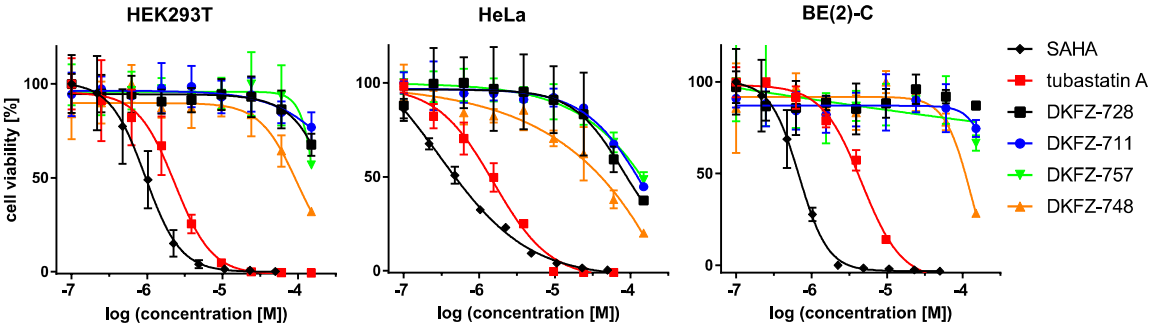


**Figure 33.** No cytotoxicity (CellTiter-Blue) associated with HDAC10 inhibition in three representative cell lines is observed after 72 h treatment, in contrast to SAHA (pan-inhibitor) and Tubastatin A (HDAC6/10 selective). Taken from Steimbach et al.[1]

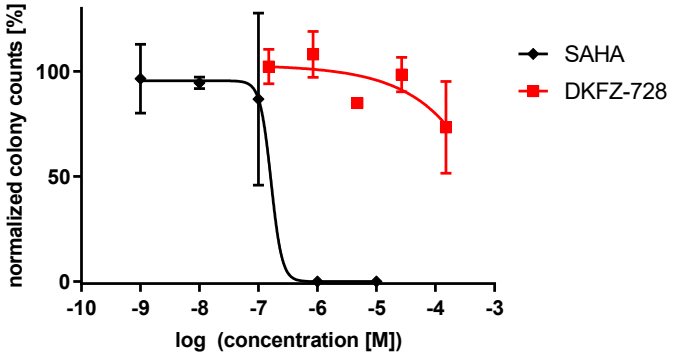


**Figure 34.** Dose-dependent colony formation of BE(2)-C cells treated with pan-inhibitor SAHA or selective HDAC10i **DKFZ-728** for seven days, normalized to DMSO controls. SAHA fully suppresses colony formation at the 1 µM dose-level, but no anti-proliferative effects can be attributed to HDAC10 inhibition with **DKFZ-728**.

#### 3.3.1.1 Co-treatment with the Helmholtz Drug Repurposing Library

Since monotherapy with selective HDAC10is does not elicit cytotoxic effects in a wide range of cancer cell lines, I pursued a combination treatment approach. Previous work on the therapeutic potential of HDAC10 inhibition suggests that it may be involved in autophagy-mediated chemotherapy resistance of neuroblastoma. Treatment with doxorubicin in combination with (unselective) HDAC10 inhibition or HDAC10 knock-down decreased neuroblastoma cell survival more than doxorubicin alone.[50] Therefore, I wanted to explore the potential of selective HDAC10 inhibition as part of a combination treatment against neuroblastoma at scale.

We performed a large-scale co-treatment screening on BE(2)-C neuroblastoma cells in collaboration with the Chemical Biology Core Facility at EMBL Heidelberg using the Helmholtz Drug Repurposing Library (HDRL), a collection of over 5,600 pharmaceuticals and bioactive compounds. Kerstin Putzker conducted the high-throughput screening by pretreating BE(2)-C cells with 5 µM selective HDAC10i **DKFZ-757** for 20 h, which ensures complete inhibition of HDAC10 without reducing cell proliferation. The HDRL drugs were then dosed at 0.1 µM or 5 µM and cell viability was measured after 48 h and compared with HDRL treatment alone. Cytotoxicity was normalized for each plate using vehicle control samples as negative controls and 5 µM mitoxantrone treated wells as positive controls, which resulted in z'-values[181] in the range of 0.69–0.85, indicating overall excellent assay data quality.

**Figure 35** depicts scatter plots of normalized cytotoxicity on BE(2)-C cells treated with the drug library alone vs. combination treatment of 5 µM **DKFZ-757** with the drug library. Since the treatment with **DKFZ-757** alone does not reduce cell viability, library members are expected to cluster along the diagonals of the scatter plots if no cooperative cytotoxic effect is induced. If, on the other hand, BE(2)-C cells are more sensitive to the combination of a library compound and HDAC10 inhibition, the compound will locate above the diagonal. Conversely, compounds that become less toxic when combined with **DKFZ-757** will locate below the diagonal. It was required to screen the HDRL in a high and a low concentration since cooperative effects depend on the absolute toxicity of the test compound. No sensitization is to be expected at doses causing maximum toxicity in mono-treatment or at doses far below minimum effects. Compounds that do not impact cell viability in mono- or combination treatment cluster around the axis origin.

I analyzed the dataset and categorized compounds as hits if an increase in cytotoxicity of >20% was observed with the HDAC10i combination treatment, compared to mono-treatment. If cytotoxic effects were higher in the 0.1 µM treatment than at 5 µM with the same compound, I defined these compounds as false hits (colored blue) in the low dose screening plot (**Figure 35A**). I conducted hit validation dose-response viability assays for all remaining "true hits" (red dots in **Figure 35**) with and without 5 µM **DKFZ-757** to reproduce the screening conditions and extend the dosing window of the library drug. Unfortunately, none of the hits could be validated and I obtained identical dose-response data for the HDRL hits with and without **DKFZ-757** combination treatment. To this end, compounds that became less toxic with **DKFZ-**

**757** co-treatment (dots below the diagonal) were not investigated, since they are likely to be caused by chemical incompatibility of the library drug with **DKFZ-757**.

Notably, α-difluoromethylornithine (DFMO) is also part of the HDRL, but did not produce a hit under the screening conditions. However, collaboration partners in the Casero Lab (Johns Hopkins, Baltimore) demonstrated that DFMO-induced growth inhibition can be rescued by an exogenous supply of $N^8$-acetylspermidine, but only when HDAC10 is active. Co-treatment of DFMO with a selective HDAC10i prevented the growth inhibition rescue by $N^8$-acetylspermidine. For details see section 3.3.4, page 81.

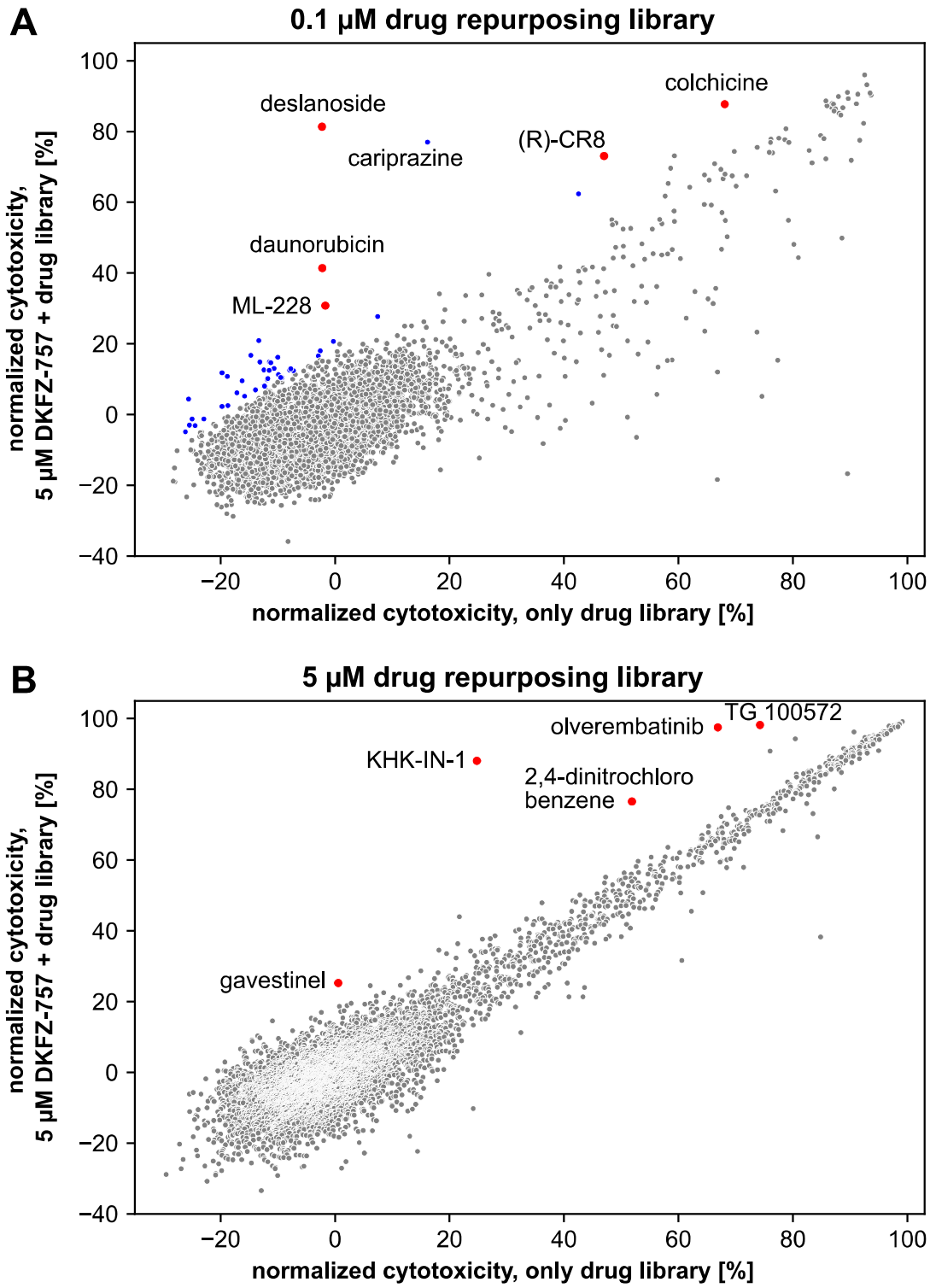


**Figure 35.** Co-treatment screen of HDAC10i **DKFZ-757** with the Helmholtz Drug Repurposing Library. Scatter plots show normalized cytotoxicity on BE(2)-C cells treated with drug library alone vs. combination treatment of 5 µM **DKFZ-757** and 0.1 µM (A) or 5 µM (B) library drugs. Compounds selected for hit validation are highlighted in red, false hits (not reproduced in 5 µM screen) are highlighted in blue. Screening was performed by Kerstin Putzker (Chemical Biology Core Facility, EMBL Heidelberg), data was analyzed by me. For the method description of the screening, see Steimbach et al.[1]

### 3.3.2 Off-target histone and tubulin acetylation

In addition to demonstrating selectivity over HDAC6 and Class I in the biochemical HDAC-Glo assay using an artificial peptide substrate, we wanted to prove cellular selectivity on the physiological substrates of HDAC6, which is tubulin, and Class I enzymes, which act on histones. Therefore, Johanna Hummel-Eisenbeiß performed Western blot analysis of inhibitor-treated BE(2)-C cells with my assistance. I selected antibodies against histone H3 and against acetylation of H3 at position K9 to determine histone hyperacetylation, a drug effect marker for HDAC Class I inhibition. To evaluate native HDAC6 activity, I chose antibodies against α-tubulin and against its K40 acetylation site to detect tubulin hyperacetylation associated with HDAC6 inhibition.

Johanna prepared acetylation Western blots (**Figure 36**) using whole cell lysates from treated BE(2)-C cells to quantify α-tubulin acetylation, and following a reported procedure,[192] she isolated histones to accurately determine H3 acetylation after inhibitor treatment. Satisfactorily, my selective HDAC10 probes did not induce histone acetylation at concentrations required for full HDAC10 engagement. Even at 100 µM, **DKFZ-728** did not cause hyperacetylation of histone H3, while at 1 µM and, more pronounced, at 10 µM SAHA did. The higher-affinity HDAC10 probes **DKFZ-748** and **DKFZ-757** did lead to increased H3 acetylation, but only at 100 µM, which is over three orders of magnitude beyond the cellular $IC_{50}$ of those probes. Similarly convincing results were provided by the tubulin acetylation Western blots: Tubastatin A and SAHA induced α-tubulin acetylation in accordance with their respective HDAC6 affinities. Aza-SAHA derivatives did not cause α-tubulin acetylation in doses sufficient for full target occupancy in cells. Only at the excessive dose-level of 100 µM, did **DKFZ-748** induce a still comparatively weak accumulation of K40 acetylated α-tubulin. This important experiment clearly demonstrates the selectivity of my HDAC10 probes over HDAC6 and Class I enzymes in a functional cellular environment.

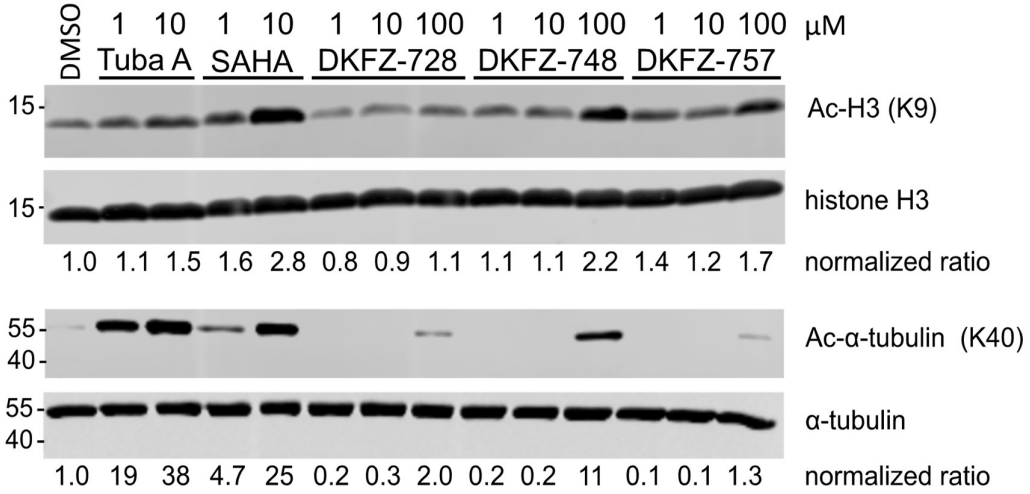


**Figure 36.** Acetylation Western blots of histone H3 and α-tubulin from BE(2)-C cells treated with inhibitors or vehicle for 4 h. No off-target hyperacetylation occurs at concentrations required for full inhibition of HDAC10. SDS-PAGE and Western blot analysis was performed by Johanna Hummel-Eisenbeiß. Figure taken from Steimbach et al.[1]

### 3.3.3 Metabolomics quantification of acetylspermidines

Hai et al.[41] identified HDAC10 as the $N^8$-acetylspermidine deacetylase, responsible for the selective polyamine deacetylation[44,46] by cytoplasmatic enzymes mainly found in rat liver decades ago. However, Hai et al. investigated the substrate specificity of HDAC10 only biochemically by steady-state kinetics using an LC/MS-based approach with purified enzyme. There were no literature reports on HDAC10 activity/inhibition in cells. Therefore, our lab collaborated with the Centre of Organismal Studies (COS) Heidelberg and established a method to detect native HDAC10 activity in cells to demonstrate enzymatic inhibition by my chemical probes. Dr. Glynis Klinke, with my assistance, developed a targeted metabolomics LC-MS/MS approach based on a method by the Globisch Lab.[89] I provided cell pellets and synthesized acetylspermidine reference samples for calibration using phenyl acetate as a selective acetylation reagent,[193] and purified the acetylation isomers as previously reported.[89] Dr. Klinke extracted polyamines and achieved simultaneous quantification of $N^1$-, $N^8$- and $N^{1,8}$-diacetylspermidine based on reported procedures[89,194] with fragmentation patterns and relative retention times of the acetylation isomers in accordance with literature.[89]

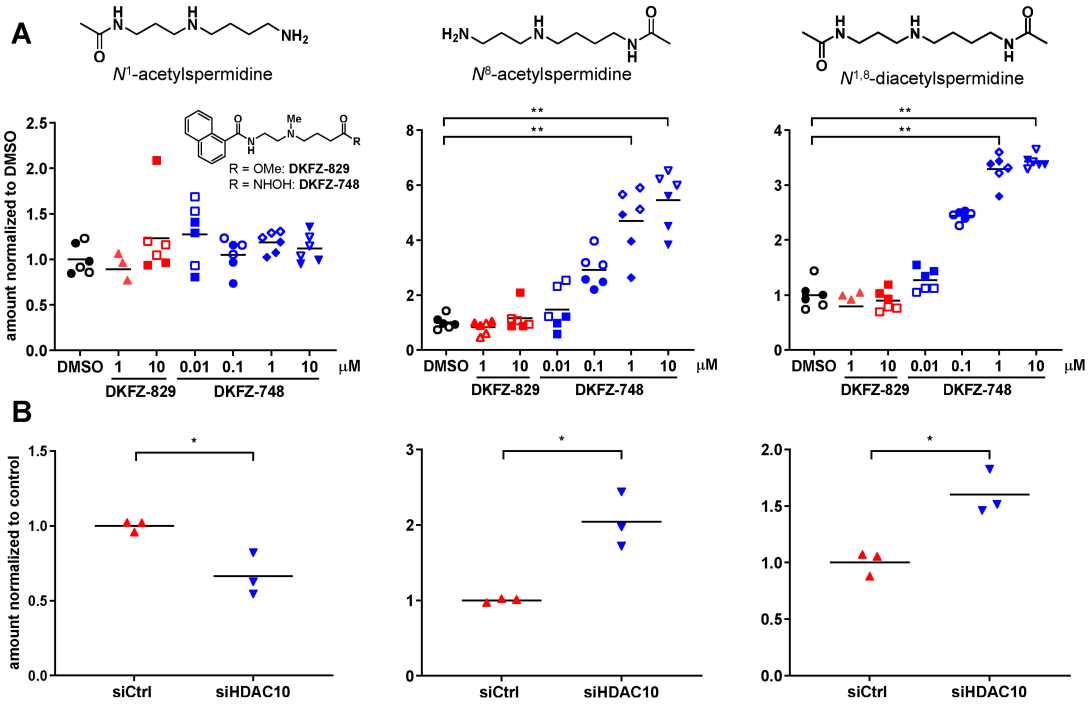


**Figure 37.** HDAC10 inhibition and knockdown affect polyamine acetylation. Targeted metabolomics quantification by LC-MS/MS of $N^1$-, $N^8$- and $N^{1,8}$-diacetylspermidine in BE(2)-C cells after 24 h treatment with DKFZ-748 or inactive ester DKFZ-829 (A) and after knockdown (B). Data in (A) is pooled from two separate experiments, indicated by solid or hollow symbols. Significance of inhibitor treatment was calculated between DMSO controls and samples by Kruskal-Wallis test (one-way ANOVA on ranks), following Dunn's multiple comparison test. Significance of knockdown vs. control was determined by unpaired t-test with Welch's correction. *: p-value < 0.05, **: <0.01. Metabolomics was performed by Dr. Glynis Klinke (COS Heidelberg), HDAC10

knockdown by Dr. Johannes Ridinger (Oehme Lab, DKFZ Heidelberg). Based on Steimbach et al.[1]

With a targeted metabolomics method established, I prepared cell pellets (min. $10^7$ cells each) from BE(2)-C cells treated with selective HDAC10i **DKFZ-748**, the corresponding but inactive ester **DKFZ-829**, or vehicle control for 24 h. This experiment was performed multiple times to validate and optimize the metabolomics method. **Figure 37A** shows pooled data of two identical biological replicates (indicated by solid or hollow symbols), each performed in triplicates. The two biological replicates are not fully independent, as evident from the data point distribution, but rather biased due to biological and technical variances of the metabolomics workflow. In Steimbach et al., the two datasets are presented and analyzed separately by one-way ANOVA. For the statistical analysis of the pooled data in **Figure 37A** I performed the non-parametric Kruskal-Wallis test, followed by Dunn's multiple comparison test, due to the non-normal distribution of the pooled data. Nevertheless, the conclusions are independent of the statistical method: treatment with HDAC10 selective **DKFZ-748,** but not **DKFZ-829**, leads to a dose-dependent significant accumulation of the putative HDAC10 substrates $N^8$- and $N^{1,8}$-diacetylspermidine. The effect onset dose is aligned with the cellular target engagement (BRET $IC_{50}$ of **DKFZ-748** = 22 nM). $N^1$-acetylspermidine levels, on the other hand, are not affected by the inhibitor treatment. This is the first time that the reported polyamine substrate specificity of HDAC10 is confirmed in live cells.

Further evidence validating HDAC10 as the inhibitor target responsible for the accumulation of only certain acetylspermidine isomers is presented in **Figure 37B**: HDAC10 knockdown in BE(2)-C cells performed by Dr. Johannes Ridinger (Oehme Lab, DKFZ Heidelberg) also shows a significant accumulation of $N^8$- and $N^{1,8}$-diacetylspermidine, as with pharmacological inhibition, but differs by a significant decrease in $N^1$-acetylspermidine. This might be due to regulation of the polyamine metabolism mediated by the HDAC10 protein. We later confirmed the metabolomics data of the knockdown with CRISPR/Cas9-mediated *HDAC10* knockout in HeLa S3 and HTC116 cells generated by Dr. Tracy M. Stewart (Casero Lab, Johns Hopkins, Baltimore).[65] The HeLa $HDAC10^{KO}$ cells also exhibited a significant reduction in $N^1$-acetylspermidine levels, supporting the regulation hypothesis.

### 3.3.4 Suppression of tumor cell growth under polyamine-limiting conditions

For a long time, the project was lacking functional pharmacology and potential for therapeutic applications of my inhibitors. Although cellular target engagement and later even cellular enzymatic inhibition of HDAC10 by **DKFZ-748** was demonstrated, I could not demonstrate any cellular phenotype associated with HDAC10 inhibition, other than hyperacetylation of certain polyamines. Especially applications in oncology, which initially sparked this project, were unattainable. This changed when we started a collaboration with the Casero Lab Johns Hopkins, Baltimore, who are experts on the oncology related biology of polyamines.

Dr. Tracy M. Stewart (Casero Lab, Johns Hopkins, Baltimore) designed and performed an experiment that utilizes my HDAC10 selective inhibitors based on the lab's expertise in

polyamine-targeting anti-cancer strategies.[66] Those treatment strategies are often impeded by redundant metabolic pathways and compensatory mechanisms, as polyamines are essential to all life[70] and also cancer progression. The Casero Lab hypothesized that HDAC10 may allow cancer cells to generate essential spermidine from extracellular sources of $N^8$-acetylspermidine when regular polyamine synthesis is inhibited, e.g. in the case of polyamine blocking cancer therapy.

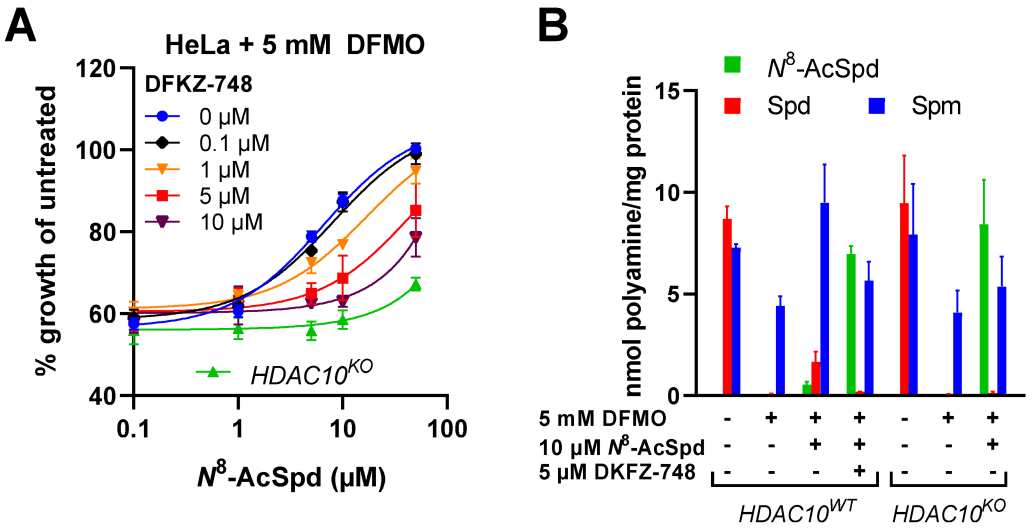


**Figure 38.** HDAC10 can replenish the polyamine pool, required for cancer cell growth under polyamine-limiting conditions, from extracellular $N^8$-AcSpd. A: DKFZ-748 prevents growth rescue by $N^8$-AcSpd in DFMO-treated HeLa S3 cells by inhibition of HDAC10. B: HPLC quantification of polyamines in treated HeLa S3 cells. Data is pooled from at least two biological replicates, each performed in technical triplicates, and represented as mean with standard error. Experiments were performed by Dr. Tracy M. Stewart and Jackson R. Foley (Casero Lab, Johns Hopkins Baltimore). Figure is taken from Steimbach et al.[1] and was prepared by Dr. Stewart; for method description see publication.

Treating HeLa cells with α-difluoromethylornithine (DFMO), an irreversible inhibitor of the enzyme ornithine decarboxylase, which is critical for polyamine biosynthesis, results in growth reduction. In wild-type HeLa cells, which express HDAC10, this growth reduction can be rescued by a large (multi micromolar) extracellular supply of $N^8$-acetylspermidine ($N^8$-AcSpd), as shown in **Figure 38A** (blue curve). Identically treated CRISPR/Cas9-mediated HeLa *HDAC10*$^{KO}$ cells on the other hand are resistant against growth reduction rescue by $N^8$-AcSpd (green curve). Corresponding to the case of genetic knockout, growth rescue could also be prevented in wild-type cells by treatment with HDAC10 inhibitor **DKFZ-748** in a dose-dependent manner (**Figure 38A,** other curves). **DKFZ-748** treatment effectively phenocopies genetic HDAC10 knockout.

Additionally, Dr. Stewart quantified intracellular polyamines by HPLC (**Figure 38B**) together with Jackson R. Foley. DFMO-treatment of HeLa cells universally depleted them of spermidine (Spd) and reduced spermine (Spm) levels. $N^8$-AcSpd levels are below the detection limit of the

HPLC assay unless supplied endogenously. With a 10 µM extracellular supply of $N^8$-AcSpd, Spd levels are partially, and Spm levels are fully restored despite DFMO treatment. Only little $N^8$-AcSpd was detected intracellularly, which is consistent with the enzymatic deacetylation of $N^8$-AcSpd to Spd by HDAC10 and the alkylation of Spd to Spm by spermine synthase. Co-treatment of HeLa cells with 5 mM DFMO and 5 µM **DKFZ-748** with an extracellular supply of $N^8$-AcSpd reduces polyamine pools back to pure DFMO treatment, but with greatly increased levels of intracellular $N^8$-AcSpd. This strongly suggests uptake of extracellular $N^8$-AcSpd, likely by active transporters, and intracellular assimilation of $N^8$-AcSpd as a polyamine source requiring HDAC10. The same observations as with pharmacological HDAC10 inhibition can be made when HeLa cells with genetic *HDAC10* knockout are treated with DFMO alone, or with DFMO and extracellular $N^8$-AcSpd. HDAC10 inhibition by **DKFZ-748** and cells lacking HDAC10 show the same polyamine profile under polyamine-limiting conditions with extracellular supply of $N^8$-AcSpd. Again, treatment with my selective HDAC10i phenocopies genetic *HDAC10* knockout, similar to the metabolomics data with HDAC10 knockdown cells (**Figure 37**, page 80).

Taken together, these data highlight a new cancer-relevant physiological role of HDAC10. While intracellular levels of $N^8$-AcSpd are very low, especially compared to spermidine levels, polyamines occur in the gut lumen in acetylated forms (incl. $N^8$-AcSpd) from bacterial sources.[195,196] We demonstrated that these acetylated polyamines can serve as an alternative source for essential polyamines when normal polyamine biosynthesis is limited or insufficient as with rapidly growing tumors and under polyamine-limiting cancer therapy using DFMO. Pharmacological inhibition of HDAC10 can therefore be beneficial in such clinical applications since HDAC10 inhibition itself does not show cytotoxicity and HDAC10 activity is not required for normal physiology[57] as demonstrated with HDAC10$^{-/-}$ mice.

## 3.4 Alternatives to hydroxamic acid HDAC10 inhibitors

Hydroxamic acids are often seen as undesirable, but necessary zinc binding groups (ZBGs) for potent HDACis. They are infamous for their poor ADMET properties, which limits their clinical use, especially for applications beyond cancer therapy. Alternatives for hydroxamic acids are therefore desirable. Furthermore, isozyme selectivity could potentially be modulated by using less promiscuous ZBGs. Therefore, I investigated non-hydroxamate zinc binders with a focus on HDAC10 selectivity.

The best described and most utilized hydroxamic acid alternatives for HDAC inhibition are *ortho*-aminoanilides and thiols, especially mercaptoacetamides. Further details regarding previous work on alternative ZBGs are summarized in section 1.3.1.1, page 29. Testing of commercially available SAHA-like *ortho*-aminoanilides PAOA and BML-210 revealed no Class IIB binding, only activity on HDAC1-3 (see Table S4). This confirmed the conjecture that o*rtho*-aminoanilide zinc binders are too bulky for the narrow active site of Class IIB HDACs. This was later confirmed by a large scale chemical proteomics approach that tested the target landscape of 53 HDACi drugs. Therefore, I describe in section 3.4.1 an approach where the hydroxamic acid zinc binder of aza-SAHA derivative **DKFZ-728** is replaced with the Class IIB selective α-mercaptoacetamide ZBG.

Furthermore, in a second approach, detailed in section 3.4.2, I investigated new ZBGs for selective HDAC10 inhibition based on a compound library screen. This approach aimed to develop non-hydroxamate selective HDAC10is without the use of amino linkers. The SAR study points towards the 4-(2-mercaptoacetamido)benzamide scaffold, on which further variations of the α-mercaptoacetamide ZBG were investigated (see section 3.4.3).

### 3.4.1 (Aza)-SAHA-based mercaptoacetamide inhibitors

Prompted by the successful development of selective HDAC10i **DKFZ-728** based on the SAHA-scaffold, I designed a non-hydroxamate HDACi guided by the same principle of C→N replacement in the linear linker region of a non-selective inhibitor (**Scheme 12**). Based on the present literature of alternative zinc-binding moieties, I decided to investigate α-mercaptoacetamides for selective HDAC10 inhibition. Linear α-mercaptoacetamides are well-documented HDAC6 inhibitors,[145,148,153,154] with reported selectivity over Class I. However, literature data for selectivity within Class IIB are typically hard to interpret due to the challenge of correctly assessing HDAC10 activity.

Therefore, I synthesized the previously reported inhibitor **DKFZ-812** (**154**)[152], as it is a close derivative of SAHA, with the zinc-binding hydroxamic acid replaced by a α-mercaptoacetamide and the cap group amide in the benzamide configuration, which is preferable for HDAC10 inhibition. Testing of **DKFZ-812** revealed a strong Class IIB selectivity and good potency (see section 3.4.1.1), which made it a suitable structural candidate to confirm that an appropriately placed amine, as in **DKFZ-825 (155)** could also abolish HDAC6 activity and provide selective HDAC10 inhibition beyond hydroxamic acid inhibitors (section 3.2).

**Scheme 12. Design of selective HDAC10is by C→N replacement in SAHA-based mercaptoacetamide inhibitor DKFZ-812**

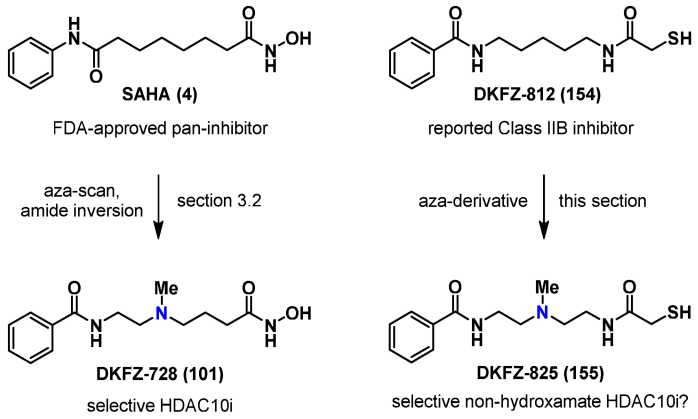


### 3.4.1.1 Inhibitor evaluation

Selectivity profiles of linear α-mercaptoacetamide inhibitor **DKFZ-812** (**154**) and its aza-derivative **DKFZ-825** (**155**) are depicted in **Figure 39** together with their hydroxamic acid parents SAHA (**4**) and **DKFZ-728** (**101**), respectively. As described in section 3.2, an appropriately placed amino functionality transforms the pan-inhibitor SAHA into an HDAC10 selective inhibitor. Inversion of the cap amide further increased HDAC10 potency to about 10-fold above the HDAC10 activity of SAHA. Mercaptoacetamide SAHA derivative **DKFZ-812** without an amino functionality exhibits a clear HDAC Class IIB preferences, since compared to SAHA, inhibition of all Class I enzymes is reduced from the two/three-digit nanomolar regime down to one/two-digit micromolar $IC_{50}$s. Only Class IIB binding is maintained with the mercaptoacetamide zinc binder, showing $pIC_{50}$s above 7 only for HDAC6 and 10. Compared to SAHA, HDAC6 inhibition is slightly reduced and HDAC10 binding is slightly increased. The same effect was observed to a similar extent when the amide in aza-SAHA derivative **DKFZ-711** was inverted resulting in **DKFZ-728**. Therefore I suspect that the mercaptoacetamide zinc-binding moiety is responsible for the pronounced loss of Class I activity without much effect on Class IIB compared to the parent hydroxamic acid, while inversion of the amide from the anilide to the benzamide configuration favors HDAC10 over HDAC6.

The promising HDAC10 activity of **DKFZ-812** validates the α-mercaptoacetamide zinc-binding moiety for the development of HDAC10 selective non-hydroxamate inhibitors. Furthermore, this result raises questions about the HDAC6 selectivity of reported HDAC6is using the same linker and zinc-binder scaffold as **DKFZ-812**. I suggest that the HDAC10 activity of mercaptoacetamides is neglected in the literature[145] similarly to the HDAC10 activity of Tubastatin A, which could implicate HDAC10 as a target responsible for observed drug effects of mercaptoacetamides.

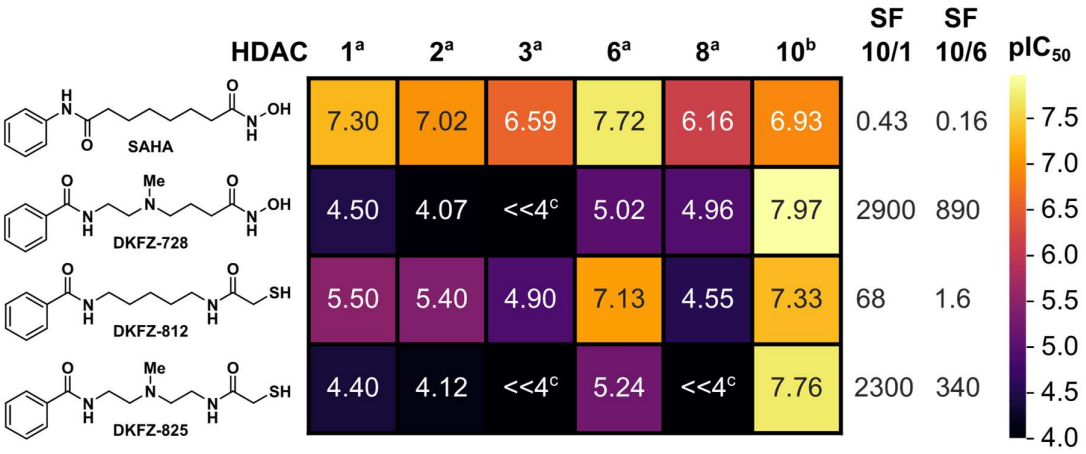


**Figure 39.** HDAC isozyme selectivity heatmap and $pIC_{50}$ values of (aza)-SAHA-based mercaptoacetamide and hydroxamic acid inhibitors. $pIC_{50}$ values are determined by four-parameter non-linear regression analysis with eight dose levels in triplicate with HDAC Glo assay[a] or FRET assay[b]. [c] Curve fit was not convergent at 100 µM. SF (selectivity factor) = $10^{(pIC50(HDAC10) - pIC50(HDAC6 \text{ or } HDAC1))}$ rounded to two significant figures. For 95% confidence intervals, see Table S4.

With the SAR progression of SAHA, **DKFZ-728**, and **DKFZ-812** at hand, the next step was the conceptual transfer of the HDAC10 selectivity provided by polyamine substrate mimicry through introducing a basic amine into the alkyl linker region. The authors that reported an HDAC6 crystal structure complexed with a linear α-mercaptoacetamide inhibitor[154] similar to **DKFZ-812** concluded that this ZBG is an apt functional mimic for hydroxamic acids with an identical zinc-binding constellation. Therefore, I synthesized and tested **DKFZ-825** with the same three-atom distance between the amine and the zinc-binder carbonyl. Pleasingly, I could successfully repeat the transformation into a selective HDAC10i by C→N replacement in the alkyl linker region. The weak Class I activity of **DKFZ-812** is fully abolished in its aza-derivative **DKFZ-825**, but more importantly, the initially good HDAC6 activity is also greatly reduced by introducing the amine, while HDAC10 binding could be further enhanced. Selectivity of **DKFZ-825** over HDAC8 is even higher than with hydroxamate **DKFZ-728**. HDAC10/6 selectivity of amine-containing α-mercaptoacetamide **DKFZ-825** is very good (340-fold), but lower than with the corresponding amino hydroxamic acid **DKFZ-728** (890-fold). Therefore, according to this biochemical assay data, mercaptoacetamide **DKFZ-825** is a non-hydroxamic acid alternative for selective HDAC10 inhibition with a comparable potency and a selectivity profile similar to that of **DKFZ-728**.

### 3.4.1.2 Synthesis strategy

**Scheme 13. Synthesis of linear α-mercaptoacetamides DKFZ-812 and DKFZ-825**[a]

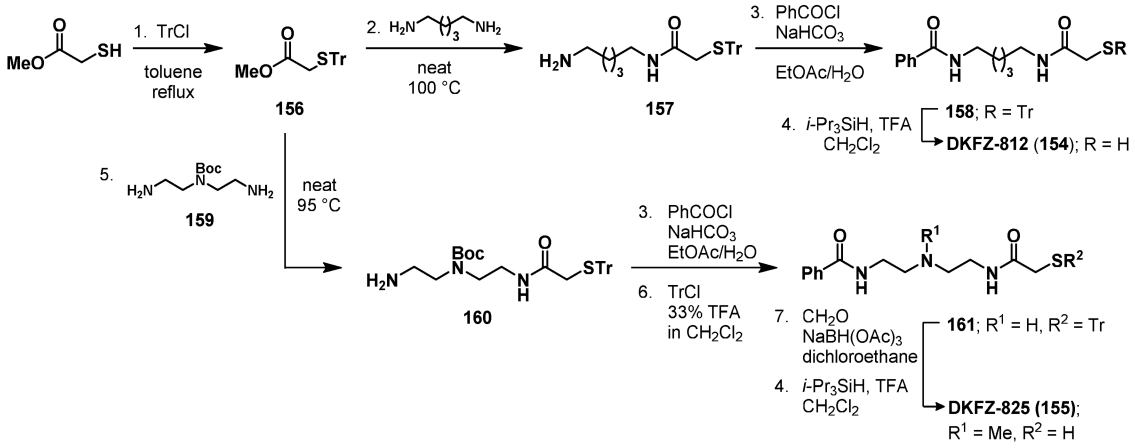


[a] Reagents and conditions 1. trityl chloride, PhMe, reflux, 2 h, 90%; 2. 1,5-diaminopentane, neat, 100 °C, 2 h, 73%; 3. PhCOCl, $NaHCO_3$, EtOAc/$H_2O$, rt, 15 min, 86% for **158**; 4. *i*-$Pr_3SiH$, TFA, $CH_2Cl_2$, rt, 90% for **DKFZ-812**, 91% for **DKFZ-825** (2 steps); 5. **156**, neat, 95 °C, 5 h, 68%; 6. trityl chloride, 33% TFA in $CH_2Cl_2$, rt, 2 h, 66% (2 steps); 7. $CH_2O$, $NaBH(OAc)_3$, $(CH_2Cl)_2$, rt, 45 min.

My synthesis of inhibitor **DKFZ-812** (**154**) (**Scheme 13,** top), following a previously reported route,[152] started with trityl protection of methyl thioglycolate to afford **156**[197], which I used to desymmetrize cadaverine by solvent-free amidation to provide amine intermediate **157**[148] in good yield. Schotten–Baumann amidation with benzoyl chloride provided **158**, which was deprotected to mercaptoacetamide inhibitor **DKFZ-812** (**154**).

For the synthesis of **DKFZ-825** (**Scheme 13,** bottom), I envisaged a route similar to the preparation of its conceptual parent **DKFZ-812**, where the key step would also be the desymmetrization of a diamine precursor. I chose **159** as the diamine precursor for **DKFZ-825** as it was unclear whether it would be necessary to prepare this aza-derivative as tertiary methylamine or if the secondary amine would be stable. Diamine **159** provides the flexibility to methylate the central amine, if required, later in the synthesis route and also avoids issues with chemoselectivity between the central secondary and terminal primary amines. Furthermore, polar diamine intermediates are avoided after the desymmetrization reaction and a reliable gram-scale preparation of **159** in three steps from diethylenetriamine is reported.[198]

I prepared $N^3$-Boc-protected diethylenetriamine **159** according to the reported procedure[198] and successfully desymmetrized it with **156** under the same solvent-free conditions as previously cadaverine to provide monoamine **160**, which was further amidated with benzoyl chloride. Complete – Boc and trityl – deprotection of **161** did not afford the desired secondary amino α-mercaptoacetamide. Reaction controls by LC/MS did confirm complete deprotection and clean formation of a polar product that conforms to the product mass, but upon basic work-up and extraction with a polar solvent system like 20% MeOH in $CH_2Cl_2$, only little material was isolated, indicating that desmethyl-**DKFZ-825** may be instable, perhaps due to migration of the

mercaptoacetamide to the secondary amine. Therefore, **161** was prepared by trityl-orthogonal Boc deprotection using trityl chloride in TFA/$CH_2Cl_2$, following reductive amination with formaldehyde and $NaBH(OAc)_3$. Trityl deprotection of the trityl sulfide allowed isolation of α-mercaptoacetamide **DKFZ-825** (**155**) in good yield.

### 3.4.2 SAR study of new zinc-binding groups based on library screening hits

The starting point for the development of HDAC10 inhibitors based on new ZBGs was a compound library screen performed at the EMBL Chemical Biology Core Facility using the HDAC10 FRET assay developed by Dr. Peter Sehr in collaboration with our group. Starting in 2014, a total of 97 000 compounds were screened, 90 of which were retested because they were potential hits. When I joined the project, the screening campaign was completed and no interesting lead compound was identified and validated. Of the 90 promising candidates, I reviewed a reproduced top hit list of 17 compounds and grouped them by manual visual inspection. HDAC10 $pIC_{50}$ data of the resulting four groups is plotted in **Figure 40**. Group 1 consists of α-mercaptocarbonyls, *S*-substituted to the 2-position of a five-membered heterocycle (thiazole, thiazoline, or imidazoline). Notably, hit compound **773981** has remarkable similarity with hydroxamic acid **40** (**Figure 11**, page 29), which was developed as a selective HDAC10i by Daniel Herp (Jung Group, University of Freiburg) independently. Group 2 compounds are all 2,4-substituted thiazoles with a (hetero)aromatic substituent at the 4-position and alkyl, (hetero)aryl or a 1,2-substituted hydrazine at the 2-position of the thiazole. Although the structural motif of group 2 is most abundant in this top hit list, this group does not show a consistent ZBG at either end of the molecules, therefore group 2 compounds do not conform to the HDACi pharmacophore. Instead, group 2 compounds all share an extended heteroaromatic system, which could interfere with the TR-FRET readout of the assay system. Group 3 compounds do not share a common structural motif and are not structurally related to any of the other groups, except for compound **700509**, which is an α-mercaptoacetamide, like most of the group 1 compounds, but is lacking the heterocyclic *S*-substituent. Instead, the thiol is esterified with benzoic acid. Group 4 consists of two triazolo-thiadiazoles, which are also lacking a common zinc-binding motif, but may interfere with the fluorescence assay readout.

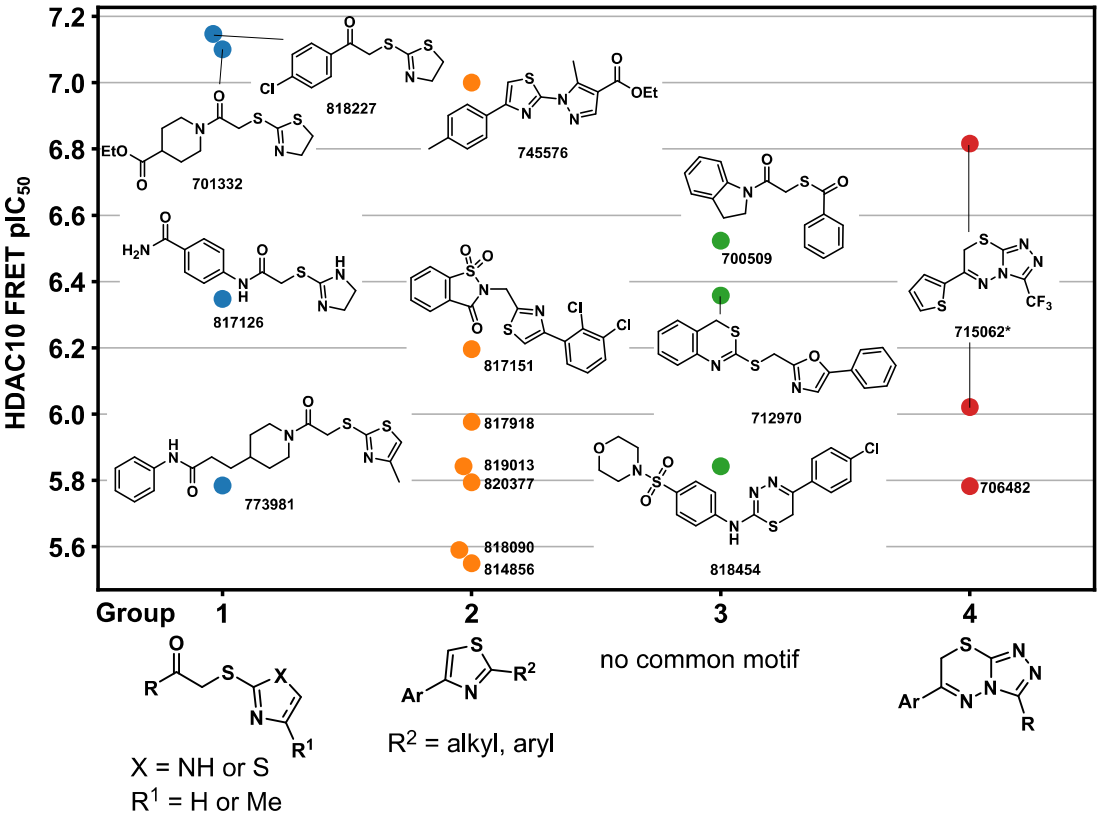


**Figure 40.** Grouped summary of selected hits from compound library screening using the HDAC10 FRET assay. The screening campaign was started in 2014 at the EMBL Chemical Biology Core Facility and led by Dr. Peter Sehr. *: two different batches of the same target compound.

Based on the grouping and activity data in **Figure 40**, I concluded that group 1 contains promising hits since it is the only group with a consistent zinc-binding topology located at one end of molecules with overall elongated shapes that fit the HDACi pharmacophore. It is also noteworthy that all group 1 compounds have a six-membered ring next to the assumed ZBG, either as a para-substituted phenyl ring or as a 1,4-subsituted piperidine. Furthermore, compounds in group 1 seem to be the only ones that achieve double digit nanomolar HDAC10 binding without extended π-systems. Unsubstituted α-mercaptoacetamides with slender alkyl linker regions, as in SAHA, had already been demonstrated as HDACis,[199] especially for HDAC6 inhibition.[145] This made compounds in group 1 good candidates for potent HDAC10 binders as well. However, free thiol impurities either from the synthesis or caused by hydrolysis were a major concern. Initially, there was no literature precedence for mercaptoacetamides with a cyclic linker as in group 1, but at a later stage of the project, mercaptoacetamides of tubathians were reported as HDAC6is.[155] These inhibitors are free thiol-derivatives of the group 1 scaffold, especially with respect to compound **817126**.

Liberation of a free α-mercaptoacetamide by hydrolysis could also be the reason for screening hit **712970** in group 3 and is reasonable as well for most group 1 compounds. Therefore, I tested aliquots of the library stock solutions for purity by LC/MS. The target mass could not be confirmed for the top hit **818227**, but the other promising group 1 hits **701332** and **817126**

did show the target mass and UV-, as well as ELS-detection indicated 95% purity without signs of decomposition in the DMSO stock solution. Still, free thiol derivatives were included in the SAR campaign around the new ZBG of group 1. Resulting SAR data suggested that HDAC10 activity may at least partially originate from the corresponding free thiols due to their high potency (vide infra). Therefore, hydrolytic stability of **DKFZ-832** was revisited in the assay buffer at a later stage (see section 3.4.2.2).

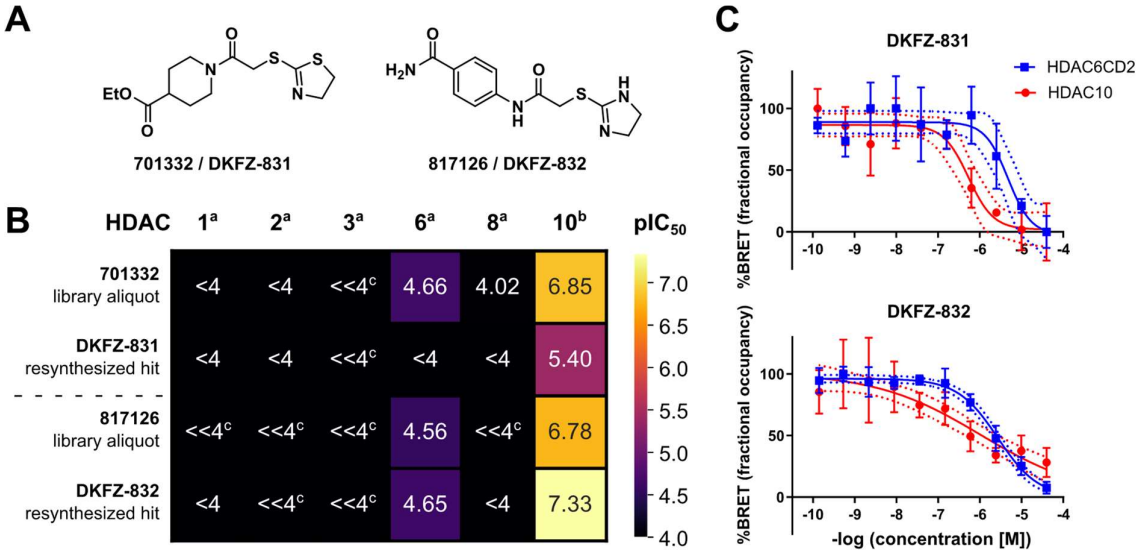


**Figure 41.** Screening hit validation data. A: Validated screening hit structures. B: HDAC isozyme selectivity heatmap and $pIC_{50}$ values of original screening hits and resynthesized compounds. $pIC_{50}$ values are determined by four-parameter non-linear regression analysis with eight dose levels in triplicate with HDAC Glo assay[a] or FRET assay[b]. [c] Curve fit was not convergent at 100 µM. For 95% confidence intervals, see Table S4. C: Cellular target engagement (BRET assay) on HDAC10 and HDAC6.

I decided to validate the two top hits in group 1 for which the compound identity and purity could be confirmed: library compounds **701332** and **817126**. These compounds were also resynthesized by Taddäus Strunden, a Bachelor student under my supervision, as **DKFZ-831** and **DKFZ-832**, respectively (**Figure 41A**). I then tested both, the resynthesized compounds and aliquots of the originally screened library components, in the HDAC10 FRET and the Glo assay to confirm HDAC10 binding and to evaluate the HDAC selectivity profile (**Figure 41B**). Indeed, HDAC10 activity in the FRET assay could be confirmed with an HDAC10 $pIC_{50}$ of ~6.8 for both library compounds. HDAC10 affinities for resynthesized compounds **DKFZ-831** and **DKFZ-832** diverge substantially, especially for **701332** and **DKFZ-831** with a 28-fold difference between the library hit and the resynthesized compound. For **817126** and **DKFZ-832**, I did also measure a notable, but much smaller difference of 3.5-fold. Pleasingly, the hit compounds do not show any HDAC Class I activity and very poor HDAC6 inhibition. Nevertheless, the observation of weak HDAC6 inhibition is promising for hit validation, since it renders pure assay interference in the HDAC10 FRET assay unlikely due to the fluorescence-independent luminescence readout used in the Glo assay for HDAC6. Furthermore, I could show cellular target engagement of the two screening hits in the BRET assay for HDAC6 and

HDAC10, with a clear HDAC10-preference (**Figure 41C**). Non-hydroxamic acid ZBGs tend to give flat curve slopes for HDAC10, but interestingly not for HDAC6 in the BRET assay. The mechanistic reason for this behavior is still elusive. Therefore, another independent method to confirm HDAC10 binding of **DKFZ-831** and **DKFZ-832** was employed. Dr. Kathryn Perez (EMBL Protein Expression and Purification Core Facility) performed a differential scanning fluorimetry thermal shift assay with recombinant HDAC10, which confirmed HDAC10 binding of **DKFZ-831** and **DKFZ-832** by a thermal shift of 5.82 °C and 4.53 °C, respectively. This thermal shift is consistent with a sub-micromolar HDAC10 binder, as control compound SAHA gave a thermal shift of 4.98 °C in the same experiment.

Overall, these hit validation data suggest that group 1 compounds **DKFZ-831** and **DKFZ-832** are indeed non-hydroxamate HDAC10 binders with excellent selectivity over Class I, as well as good selectivity over HDAC6. The group 1 scaffold appears to provide an inherent HDAC10-selectivity, therefore I initiated an SAR study around the validated hits in order to explore this scaffold's potential for selective HDAC10 binding and to further validate *S*-substituted α-mercaptoacetamides. Compounds prepared for this SAR study are shown in **Figure 42**. Taddäus Strunden prepared most *S*-substitution derivatives (**Figure 42A**) in order to evaluate the influence of the heteroatoms in the 5-membered ring that defines the group 1 screening hits. Methyl thioethers **DKFZ-880** and **DKFZ-877** and free thiols **DKFZ-889** and **DKFZ-877** served as controls for the involvement of the heterocycle in zinc binding. Thioesters **DKFZ-855** and **DKFZ-887** were prepared as potential pro-drugs but also due to literature reports indicating that HDACs may bind to thioesters without requiring ester hydrolysis.[199] A new ZBG should be generally applicable to different inhibitor scaffolds, therefore I decided for "scaffold hopping" with compound **DKFZ-872** and three SAHA-derivatives (**Figure 42B**). Furthermore, I prepared three additional derivatives of **DKFZ-887** (**Figure 42C**) to determine whether HDAC10 selectivity is at least partially governed by the 4-acetamidobenzamide linker structure and to investigate if the selectivity can be applied to more conventional ZBGs such as hydroxamic acids. Despite their simple structure, compounds in **Figure 42C** have never been tested against HDACs and only few related compounds are reported.

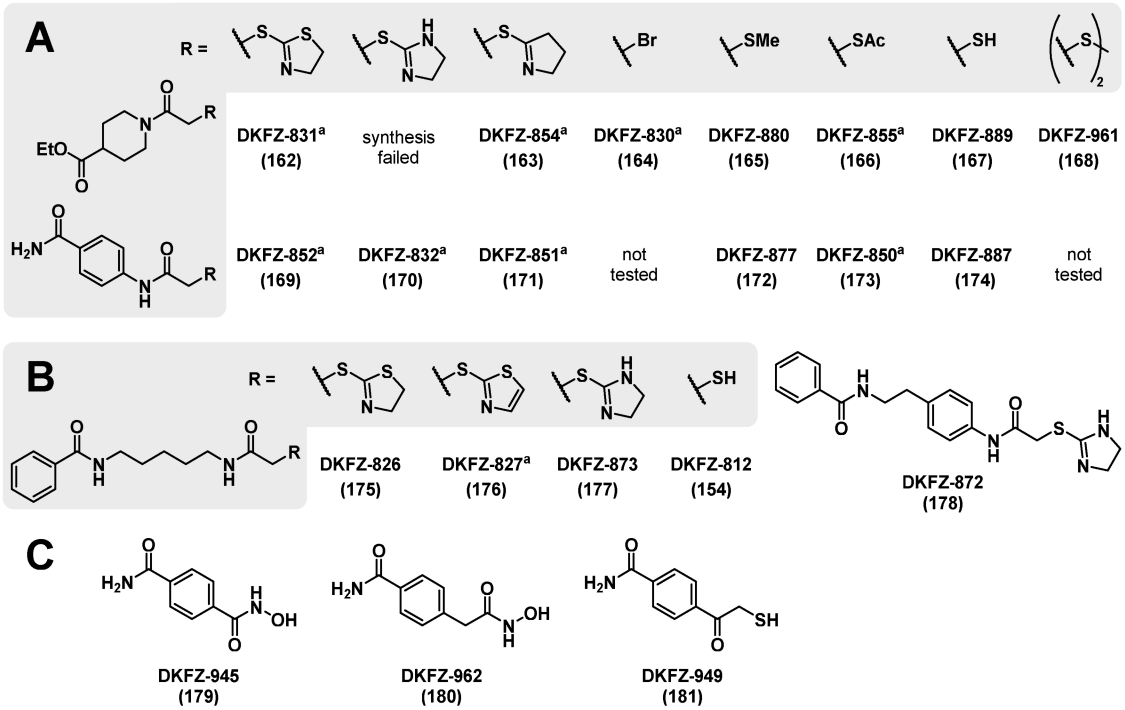


**Figure 42**. SAR campaign compounds surrounding validated screening hits **DKFZ-831** and **DKFZ-832**. A: Zinc-binder SAR compounds. B: "Scaffold hopping" with selected ZBGs. C: Additional derivatives of **DKFZ-887** with conventional ZBGs [a] Compound prepared by Taddäus Strunden for his Bachelor thesis[200] under my supervision.

### 3.4.2.1 Evaluation of inhibitors **162–178**

SAR results of screening hit **701332** (resynthesized as **DKFZ-831**) and screening hit **817126** (resynthesized as **DKFZ-832**) are shown as heatmaps in **Figure 43A** and **B**, respectively. Overall, the SAR study reveals a nearly exclusive activity on Class IIB and a pronounced HDAC10 selectivity for both scaffolds. The best HDAC10 binders are the free α-mercaptoacetamides **DKFZ-889** and **DKFZ-887**, both with $IC_{50}$s below 20 nM. Interestingly, disulfide **DKFZ-961** also shows high HDAC10 activity with excellent 850-fold selectivity. Zinc-binding via the ethyl ester moiety in the scaffold of **DKFZ-831** (**Figure 43A)** can be excluded, since thioether **DKFZ-880** and bromide **DKFZ-830** are inactive. Therefore, activity of disulfide **DKFZ-961** is most likely a result of partial reduction in the assay buffer, although the HDAC10 FRET assay was not performed under controlled reducing conditions, since the assay dilution buffer does not contain a reducing agent. However, the recombinant HDAC10 enzyme storage buffer contains 1.8 M DTT, which results in a final concentration of 11.5 µM DTT for each assay well. Considering the high activity of the free thiol, in situ reduction of disulfides is a likely explanation for their activity. The Glo assay buffer and the enzyme storage buffer for HDAC6 do not contain any reducing agents, but **DKFZ-961** still shows some HDAC6 activity, likely by formation of small amounts of **DKFZ-889** by protein-mediated redox chemistry. This difference in reduction capacity between the HDAC10 and HDAC6 assay is expected to greatly overestimate the 10/6 selectivity factor, especially for **DKFZ-961**.

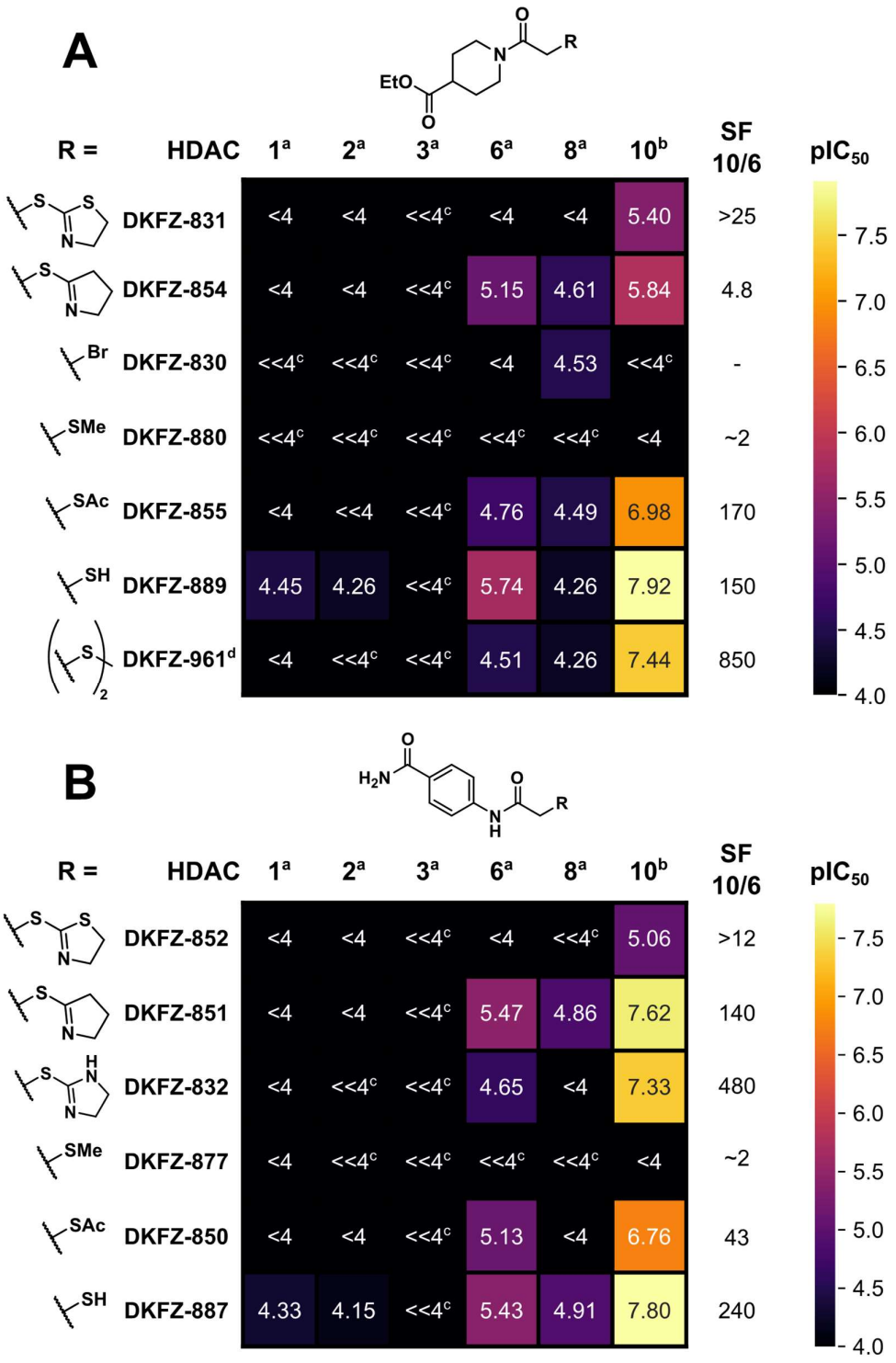


**Figure 43.** HDAC isozyme selectivity heatmap and $pIC_{50}$ values of ZBG SAR study around DKFZ-831 (A) and DKFZ-832 (B). $pIC_{50}$ values are determined by four-parameter non-linear regression analysis with eight dose levels in triplicate with HDAC Glo assay[a] or FRET assay[b]. [c] Curve fit was not convergent at 100 µM. [d] Activity per sulfide unit, disulfide dosed in ½ molar concentration. SF (selectivity factor) = $10^{(pIC50(HDAC10) - pIC50(HDAC6))}$ rounded to two significant figures. For 95% confidence intervals, see Table S4.

Thioester **DKFZ-855** shows one order of magnitude lower HDAC10 activity but HDAC10/6 selectivity similar to the corresponding thiol. For **DKFZ-831** and **DKFZ-854**, the HDAC10 activity is more than 10-fold lower compared to thioester **DKFZ-855**. Furthermore, **DKFZ-854** also shows greatly reduced HDAC10/6 selectivity. This makes the 2-thio-2-thiazoline and 3,4-dihydro-*2H*-pyrrole zinc-binder unattractive in this scaffold when compared to the free thiol.

The SAR study around screening hit **DKFZ-832** (**Figure 43B**) confirms that the 2-thio-substituted thiazoline ZBG (as in **DKFZ-852**) is inferior to the corresponding free thiol regarding potency and selectivity. Although the 3,4-dihydro-*2H*-pyrrole zinc-binder in **DKFZ-851** performs better than **DKFZ-854** in the other scaffold, it does still not surpass thiol **DKFZ-887**. The original screening hit **DKFZ-832** shows reduced HDAC10 binding compared to **DKFZ-851** and thiol **DKFZ-887**, yet provides the best selectivity (480-fold) in this series. Methyl thioether **DKFZ-877** is entirely inactive like **DKFZ-880**. Thioester **DKFZ-850** shows the same 10-fold reduction in HDAC10 activity as **DKFZ-855**, compared to the corresponding free thiols, but for **DKFZ-850** a sharp drop in selectivity can be observed as well.

Intrigued by the remarkable HDAC10 selectivity of **DKFZ-832**, I wanted to confirm that 2-thio-substituted imidazolines are indeed a generally applicable HDAC10 binding motif. Therefore, I attempted "scaffold hopping" and applied the 2-thio-2-imidazoline of **DKFZ-832** to the SAHA-scaffold (**Figure 44**, scaffold A) in **DKFZ-873** and to scaffold B with an anilide linker core and benzamide cap group in **DKFZ-872**. Both inhibitors show sub-micromolar HDAC10 binding in the FRET assay and an HDAC10 selectivity of 10 and 60-fold, respectively. No Class I activity was observed. Applying the 2-thio-2-thiazoline zinc binder of screening hit **DKFZ-831** to the SAHA scaffold in **DKFZ-826** yielded an even poorer HDAC10 binder than **DKFZ-831** without HDAC10 preference. The aromatized thiazole derivative **DKFZ-827** is completely inactive.

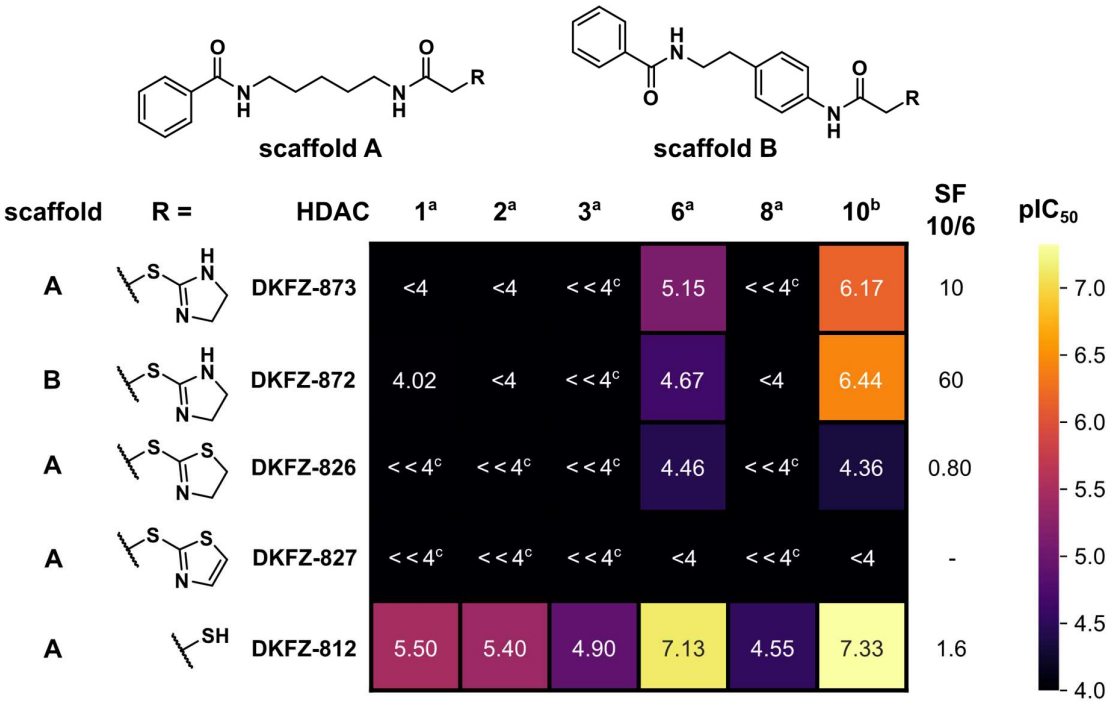


**Figure 44.** HDAC isozyme selectivity heatmap and $pIC_{50}$ values of selected new ZBG on two different scaffolds with **DKFZ-812** as reference for scaffold A. $pIC_{50}$ values are determined by four-parameter non-linear regression analysis with eight dose levels in triplicate with HDAC Glo assay[a] or FRET assay[b]. [c] Curve fit was not convergent at 100 µM. SF (selectivity factor) = $10^{(pIC50(HDAC10) - pIC50(HDAC6))}$ rounded to two significant figures. For 95% confidence intervals, see Table S4.

Aiming for a generally applicable new ZBG with inherent HDAC10 selectivity and good potency, I excluded 2-thio-subsituted 2-thiazolines and thiazoles, due to poor activity and comparably low selectivity across four tested scaffolds. The 3,4-dihydro-*2H*-pyrrole zinc-binder in **DKFZ-851** and **DKFZ-854** does not consistently provide high HDAC10 selectivity. This leaves me with 2-thio-substituted 2-imidazolines as in **DKFZ-832**, **DKFZ-873** and **DKFZ-872**, which consistently show good HDAC10 binding ($pIC_{50}$ = 6.17–7.33) and at least 10-fold HDAC10/6 selectivity, even in a pan-inhibitor scaffold.

### 3.4.2.2 Hydrolytic stability of **DKFZ-832**

Hydrolytic instability was a concern from the start, especially with the library compounds, therefore I confirmed purity and identity of screening hits first. The large difference in activity between the free mercaptoacetamides **DKFZ-889**, **DKFZ-887** and **DKFZ-812** and their heterocyclic substituted derivatives presents the possibility that even partial hydrolysis of 2-thio-substituted heterocycles to stable 2-pyrrolidone, 2-thiazolidinone or 2-imidazolidinone liberating the free thiol would suggest false activity of the ZBG. In that case, the synthesized compounds act only as prodrugs, but since activation in the assay is not monitored and only poorly controlled, SAR-data is less reliable.

Except for the synthesis of the imidazoline derivative of **DKFZ-889**, no stability issues occurred during synthesis and purification of the 2-thio-substituted heterocyclic compounds. **DKFZ-832** also did not show decomposition in DMSO solution, as confirmed by LC/MS of a library aliquot of the initial screening hit. Still, I performed an LC/MS-based stability determination of **DKFZ-832** under FRET assay conditions as well, since the 2-thio-2-imidazoline ZBG provides good HDAC10 binding across scaffolds and, especially in **DKFZ-832**, excellent selectivity. **DKFZ-832** was dissolved in FRET assay buffer containing HDAC10 enzyme, and subjection to LC/MS analysis after different incubation times at rt. Thiol **DKFZ-887** and the corresponding disulfide were formed in a time-dependent manner, and significant amounts of hydrolysis product were present shortly after dissolving **DKFZ-832** in FRET assay buffer. Hydrolysis occurred also in absence of recombinant HDAC10, but with protein, more free thiol **DKFZ-887** was observed. This is likely due to the introduction of DTT together with the HDAC10 enzyme. These data suggest that the tested heterocyclic substitutions of mercaptoacetamides do not offer a significant benefit over the free thiol in terms of selectivity and potency for HDAC10. This is likely due to the hydrolysis of the compounds to the free thiols under assay conditions. The thiol appears to be the major contributor to HDAC10 activity. The stability issues of **DKFZ-832** under the assay conditions make it likely to act as a prodrug, mainly hydrolyzed independently of HDAC10 enzymatic activity.

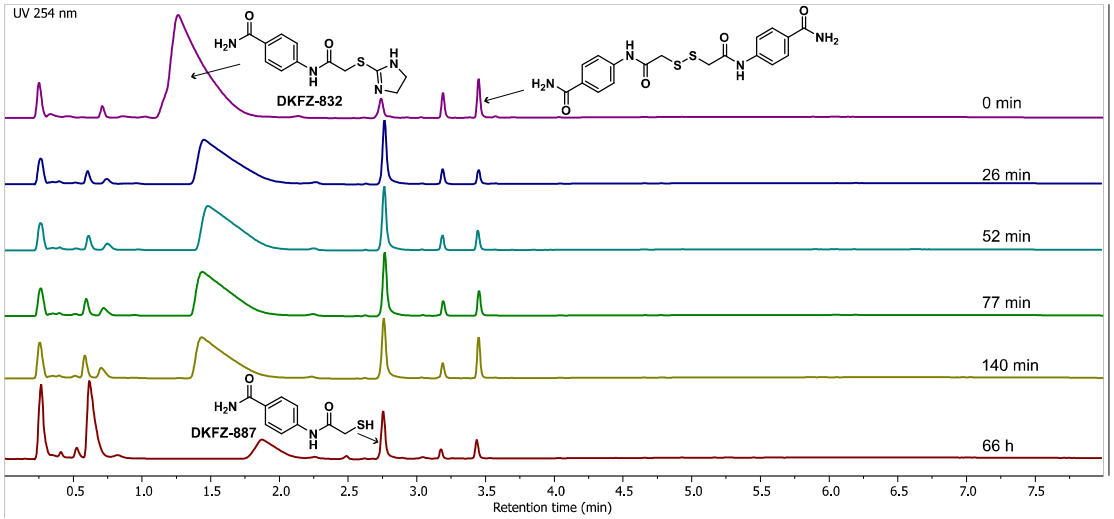


**Figure 45.** LC/MS chromatograms at 254 nm of pure DKFZ-832 dissolved to 1 mM in FRET assay buffer with 50 nM TS-GST-HDAC10, injected after incubation at rt for indicated incubation time.

However, prodrug strategies using hydrolysis-sensitive thiol substitutions like 2-thio-2-imidazoline or thioesters could prove useful for in vivo applications, especially if the hydrolysis reaction to liberate the active thiol was catalyzed by the HDAC target enzyme and therefore depending on remaining HDAC activity. This would provide a Type 1A prodrug[201] if no other pathways for hydrolysis are available.

### 3.4.2.3 Evaluation of inhibitors **179–181**

Free α-mercaptoacetamides emerged as the most active ZBG with nearly exclusive activity on Class IIB and over 100-fold selectivity for HDAC10 over 6, when combined with a cyclic linker that contains a carbonyl group in 1,4-position to the ZBG, as in **DKFZ-889** and **DKFZ-887**. When the same mercaptoacetamide zinc-binder is applied to a linear SAHA-like scaffold as in **DKFZ-812**, the HDAC10 selectivity is lost because additional Class I activity is gained, but a preference for Class IIB is maintained. Subsequently, HDAC10 selectivity is not solely driven by the ZBG in this compound set, but the cap-less cyclic linker seems to play an important role as well. Therefore, I prepared three more derivatives of **DKFZ-887** in order to investigate the relationship between the benzamide linker and the zinc-binder. Selectivity profiles are presented in **Figure 46**.

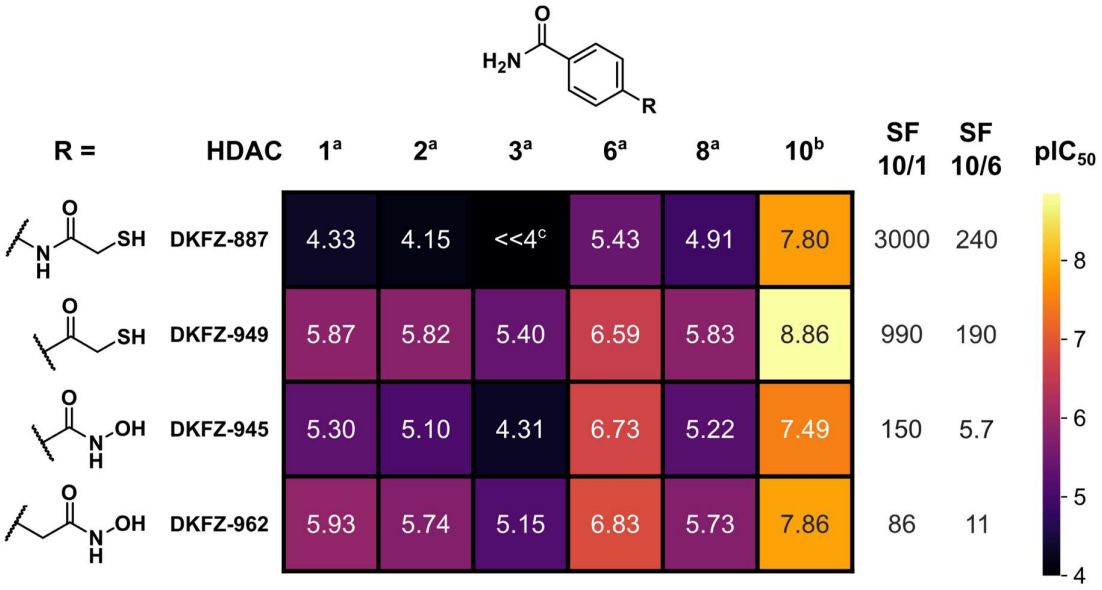


**Figure 46.** HDAC isozyme selectivity heatmap and $pIC_{50}$ values of zinc-binder analogues of DKFZ-887. $pIC_{50}$ values are determined by four-parameter non-linear regression analysis with eight dose levels in triplicate with HDAC Glo assay[a] or FRET assay[b]. [c] Curve fit was not convergent at 100 µM. SF (selectivity factor) = $10^{(pIC50(HDAC10) - pIC50(HDAC6\ or\ HDAC1))}$ rounded to two significant figures. For 95% confidence intervals, Table S4.

The α-thio acetophenone **DKFZ-949** (**181**), conceptually derived from **DKFZ-887** (**174**) by removal of the anilide nitrogen, shows an 11-fold increase in potency against HDAC10 with an outstanding $IC_{50}$ of 1.37 nM. Selectivity over HDAC6 is slightly reduced compared to mercaptoacetamide **DKFZ-887**, but is still in the same range of two orders of magnitude. A substantial gain in Class I activity can be observed as well, but selectivity over HDAC1 is still 990-fold. This makes **DKFZ-949** by far the most potent non-hydroxamate HDAC10i I prepared. Despite Gu et al.[199] reporting in 2006 a SAHA-based α-mercaptoketone inhibitor that exhibits higher Class I/II inhibition than the parent hydroxamic acid, the α-mercaptoketone ZBG remains mostly underexplored. No studies concerning the HDAC selectivity profile of such compounds are available and α-thio acetophenones appear only in few examples in the patent

space[202,203] but also without data on the selectivity profile or Class II-specific activity. Therefore, α-thio acetophenones should be further investigated as selective HDAC10is due to the high potency and promising selectivity profile of **DKFZ-949**. Another advantage of α-thio acetophenone **DKFZ-949** compared to α-mercaptoacetamide **DKFZ-887** is the oxidation resistance of the thio acetophenone in solution. While mercaptoacetamides tend to form disulfides in solution when exposed to air, no disulfide formation was observed during the synthesis and purification of **DKFZ-949**. This oxidation resistance could potentially also contribute to the higher activity in the HDAC assays.

Benzhydroxamic acid **DKFZ-945** (**179**), a close structural analogue of **DKFZ-949,** and phenyl acetohydroxamic acid **DKFZ-962** (**180**), related to **DKFZ-887**, both expose the necessity for non-hydroxamic acid ZBGs for selective HDAC10 inhibition, even within the benzamide scaffold depicted in **Figure 46**. While both hydroxamic acids provide excellent HDAC10 binding with $pIC_{50}$s of 7.49 and 7.86, selectivity over HDAC6 and Class I is roughly one order magnitude lower compared to thiol-based zinc binders on the same scaffold. This SAR data concludes that α-thio acetanilide and α-thio acetophenone inhibitors are good candidates for the further development of selective HDAC10is beyond amino-linkers with hydroxamic acids warheads.

#### 3.4.2.4 Synthesis strategy

Screening hit compound **DKFZ-831** and derivatives were synthesized (**Table 5**) from the common α-bromoacetamide precursor **DKFZ-830**, which was prepared by Taddäus Strunden from isonipecotic acid (**182**) via esterification followed by amidation with bromoacetyl bromide. **DKFZ-831** and **DKFZ-854** were prepared in one step from bromoacetamide **DKFZ-830** by $S_N2$ reaction in DMF at 40–60 °C with *i*-$Pr_2NEt$ as a base. When 2-imidazolidinethione was used as a nucleophile, no product could be isolated under these reaction conditions. Using different solvents ($CH_3CN$, $CH_2Cl_2$, EtOAc and EtOH) and a reduced temperature (0 °C) and varying the base ($K_2CO_3$ instead of *i*-$Pr_2NEt$) did not lead to the desired product. Instead, traces of **DKFZ-889** and its thioether dimer were observed. These observations point towards instability of the *S*-substituted 2-thioimidazoline moiety in this scaffold.

For the synthesis of methyl thioether **DKFZ-880**, I had to employ EtOH instead of DMF as a solvent to mitigate transesterification to the methyl thioester. **DKFZ-855** was obtained in quantitative yield with KSAc as nucleophile in DMF at rt without the need of an additional base. Thiol **DKFZ-889** and the respective disulfide **DKFZ-961** were prepared by transesterification of thioacetate **DKFZ-855** in EtOH. Free thiol **DKFZ-889** was observed to readily oxidize to the disulfide when exposed to air during work-up. Therefore, I used dithiothreitol (DTT) as a nucleophile for transesterification with the thioester, which allowed for a reductive environment during work-up and facilitated the isolation of **DKFZ-889** in sufficient purity. For the preparation of pure disulfide **DKFZ-961**, I employed acid-catalysed transesterification using 2M HCl in EtOH without excluding air from the reaction. Oxidation to the disulfide by air was either incomplete or led to overoxidation when additional oxygen was supplied by

hydrogen peroxide or bubbling air through the reaction mixture. Therefore, I employed a mild thiol oxidation procedure using catalytic amounts of iodine and DMSO as the oxidizing agent.[204]

**Table 5. Synthesis of inhibitors 162–168**[a]

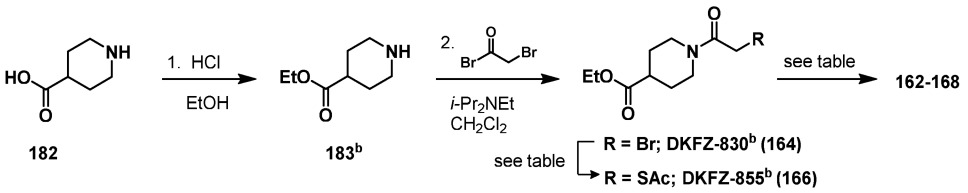


| starting material | reactant/reagent | conditions | yield | product |
|---|---|---|---|---|
| DKFZ-830[b] (164) |  | *i*-$Pr_2$NEt, DMF 60°C, 1 h | 48% | 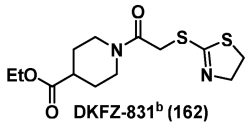 DKFZ-831[b] (162) |
| DKFZ-830[b] (164) |  | *i*-$Pr_2$NEt or $K_2CO_3$, DMF or MeCN or $CH_2Cl_2$ or EtOAc or EtOH 0 or 40 or 60°C | no product | synthesis failed |
| DKFZ-830[b] (164) |  | *i*-$Pr_2$NEt, DMF 40°C, 2 h | 24% | 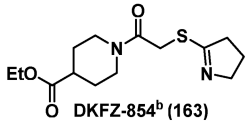 DKFZ-854[b] (163) |
| DKFZ-830[b] (164) | NaSMe | EtOH, rt, 3.5 h | 48% | 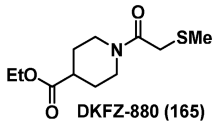 DKFZ-880 (165) |
| DKFZ-830[b] (164) | KSAc | DMF, rt, 45 min | quant | 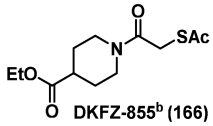 DKFZ-855[b] (166) |
| DKFZ-855[b] (166) | DTT | $NaHCO_3$, EtOH, rt, 24 h | 21% |  DKFZ-889 (167) |
| DKFZ-855[b] (166) | EtOH/HCl, then oxidation | 2 M HCl in EtOH, rt, 18 h, then cat. $I_2$, DMSO, $CH_2Cl_2$, rt, 2 h | 61% | 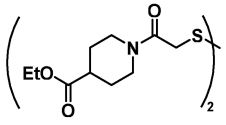 DKFZ-961 (168) |

[a] Reagents and conditions 1. 2 M HCl in EtOH, reflux, 1.5 h; 2. bromoacetyl bromide, *i*-$Pr_2$NEt, $CH_2Cl_2$, –40 °C, 2 h. [b] Compound prepared by Taddäus Strunden for his Bachelor thesis[200] under my supervision.

Screening hit compound **DKFZ-832** and derivatives were synthesized (**Table 6**) from the common α-bromoacetanilide precursor **184**, which was prepared by Taddäus Strunden from 4-aminobenzamide by amidation with bromoacetyl bromide. Compounds **169–171** were prepared similar to their respective counterparts **DKFZ-831** and **DKFZ-854** in one step from α-bromoacetanilide **184** by $S_N2$ reaction in DMF at 40–60 °C with *i*-$Pr_2$NEt as a base. No stability issues of *S*-substituted 2-imidazolidinethione **DKFZ-832** were observed during the

synthesis. **DKFZ-850** and **DKFZ-877** were prepared in good yields in DMF at rt without an additional base. Free thiol **DKFZ-887** was accessed using the same transesterification protocol as with thiol **DKFZ-889**. The corresponding disulfide was not isolated in this scaffold due to the low water solubility of this compound, which would cause assay artifacts and prevent evaluation of activity.

**Table 6. Synthesis of inhibitors 169–174**[a]

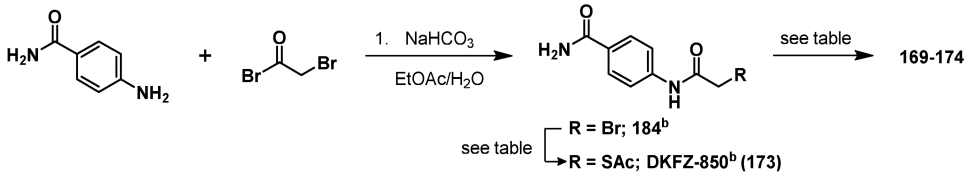


| starting material | reactant/reagent | conditions | yield | product |
|---|---|---|---|---|
| **184**[b] |  | *i*-$Pr_2$NEt, DMF 60°C, 2 h | 88% | 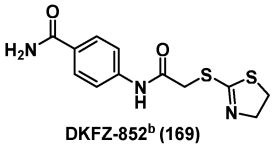 **DKFZ-852**[b] **(169)** |
| **184**[b] |  | *i*-$Pr_2$NEt, DMF 60°C, 1.5 h | 26% | 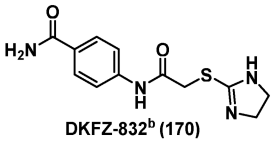 **DKFZ-832**[b] **(170)** |
| **184**[b] |  | *i*-$Pr_2$NEt, DMF 60°C, 1 h | 56% | 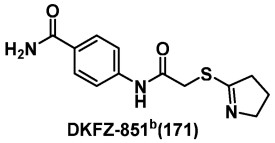 **DKFZ-851**[b] **(171)** |
| **184**[b] | **NaSMe** | DMF, rt, 2 h | 62% | 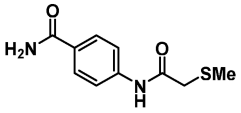 **DKFZ-877 (172)** |
| **184**[b] | **KSAc** | *i*-$Pr_2$NEt, DMF rt, 45 min | 71% | 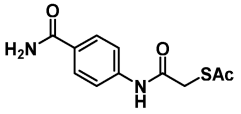 **DKFZ-850**[b] **(173)** |
| **DKFZ-850**[b] | **DTT** | cat. $NaHCO_3$ DMA, 50 °C | 15% | 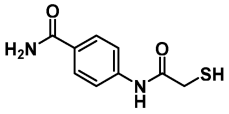 **DKFZ-887 (174)** |

[a] Reagents and conditions 1. $NaHCO_3$, EtOAc/$H_2O$, rt, 45 min, 91%. [b] Compound prepared by Taddäus Strunden for his Bachelor thesis[200] under my supervision.

SAHA-like compounds **175–177** were synthesized (**Scheme 14**) from the common α-bromoacetamide precursor **186**, derived from mono-*N*-Boc-1,5-diaminopentane by sequential amidation in THF with benzoyl chloride, then with bromoacetyl bromide after Boc

deprotection. This synthetic strategy is different from the synthesis of SAHA-like thiol **DKFZ-812** (**Scheme 13**, page 87), which employed a trityl protecting group strategy for the thiol that facilitated desymmetrization of 1,5-diaminopentane. The late divergent route via α-bromoacetamide **186** is advantageous as it facilitates diversification of the ZBG in the same scaffold. In this scaffold, the $S_N2$ reaction with 2-imidazolidinethione in DMF was successful, although with reduced yield compared to the reaction with 2-mercaptothiazoline, leading to **DKFZ-826,** and 2-mercaptothiazole, leading to **DKFZ-827**.

**Scheme 14. Synthesis of 175–177**[a]

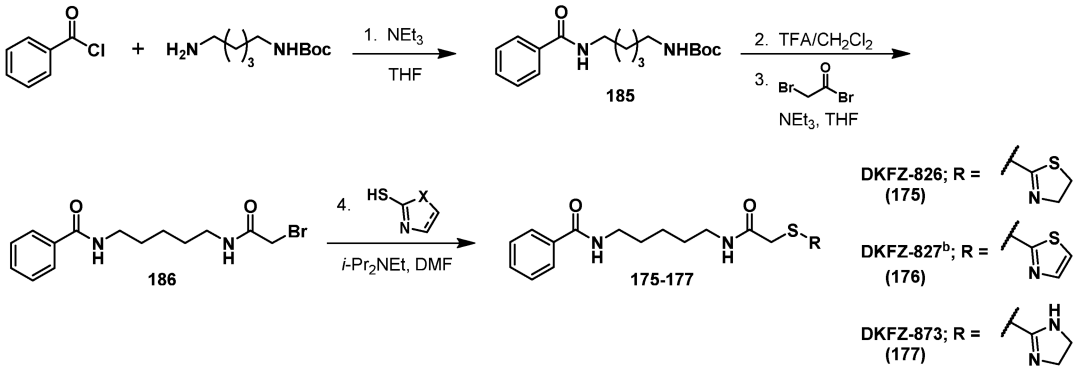


[a] Reagents and conditions 1. $NEt_3$, THF, rt, 30 min, 88%; 2. TFA/$CH_2Cl_2$, rt, 30 min; 3. bromoacetyl bromide, $NEt_3$, THF, 0 °C, 1 h, 51% (2 steps); 4. 2-thio-heterocycle, *i*-$Pr_2NEt$, DMF, 60 °C, 1h, 48% for **176**, 83% for **175**, 25% for **177**. [b] Compound prepared by Taddäus Strunden for his Bachelor thesis[200] under my supervision.

Hydroxamic acids **DKFZ-945** and **DKFZ-962** were prepared (**Scheme 15**) from their respective methyl esters **188** and **189**. While **189** was commercially available, I synthesized **188** from commercial acyl chloride **187** by amidation of with ammonia. α-Mercaptoketone **DKFZ-949** (**181**) was prepared (**Scheme 15**) in four steps starting with the potassium carbonate catalyzed hydrolysis of 4-acetylbenzonitrile (**190**) in DMSO/water to benzamide **191**. α-Bromination of the ketone in **191** using NBS/pTSA provided bromide **192** in good yield, which was converted to α-mercaptoketone **DKFZ-949** (**181**) in two sequential steps by treating with potassium thioacetate in DMF, followed by sodium thiomethoxide in methanol.

**Scheme 15. Synthesis of inhibitors 179–181**[a]

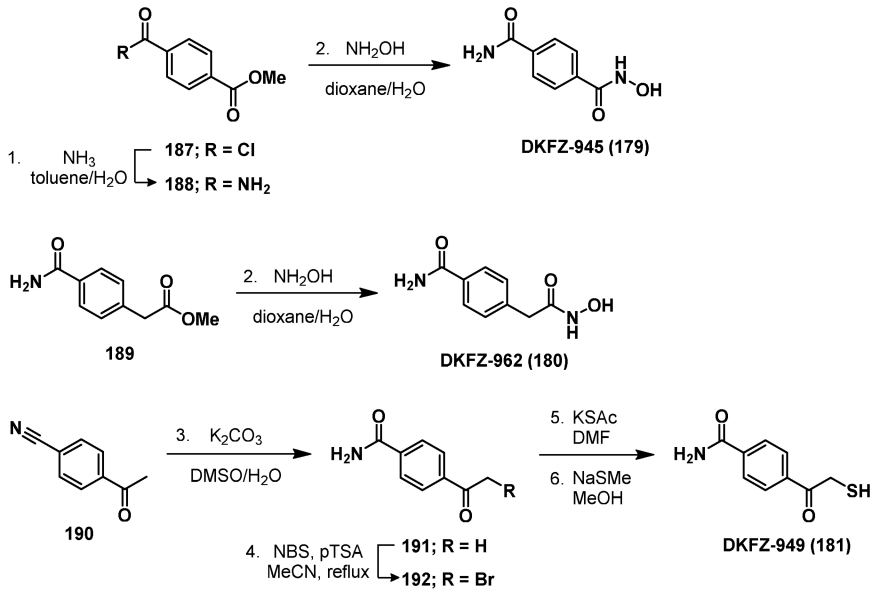


[a] Reagents and conditions 1. 25% aqueous ammonia, PhMe, 0 °C, 5 min, 21%; 2. KCN, dioxane, rt, 1 h, then $NH_2OH$ (50 wt% in $H_2O$), rt, 65 h, 58% for **179**, 24 h, 23% for **180**; 3. $K_2CO_3$, 25% water in DMSO, reflux, 4 h, 80%; 4. NBS, pTSA, MeCN, reflux, 4 h, 72%; 5. KSAc, DMF, rt, 30 min; 6. NaSMe, MeOH, rt, 5 min, 25% (2 steps).

### 3.4.3 SAR of the 4-(2-mercaptoacetamido)benzamide scaffold

Benzamide containing α-mercaptoacetamide inhibitor **DKFZ-887** emerged as a promising lead with 16 nM $IC_{50}$ in the HDAC10 FRET assay, 239-fold selectivity over HDAC6 and more than 3000-fold over HDAC1. This potency and selectivity profile is remarkable considering the simple, cap-less and fragment-like structure of **DKFZ-887**. The influence of the ZBG in this scaffold is evaluated in section 3.4.2.3, page 97. A distinctive feature of **DKFZ-887** is the para-benzamide functionality that provides a hydrogen bond donor-acceptor system, which may be crucial for the HDAC inhibitory profile of this compound.

Due to the fragment-like nature of **DKFZ-887**, I anticipated that the addition of a hydrophobic cap group could further increase the already high potency, while the linker and ZBG would ensure HDAC10 selectivity. Therefore, I synthesized mercaptoacetamide **DKFZ-942,** the corresponding disulfide **DKFZ-965** for comparison and thioester **DKFZ-958**, a precursor of the latter two compounds. In order to determine the role of the benzamide hydrogen bond donor/acceptor, 3-phenylpropyl capped compounds **DKFZ-963**, **DKFZ-960** and **DKFZ-964** were made as a direct benzamide-free comparison.

**Scheme 16. Structure-activity relationship study design of the 4-(2-mercaptoacetamide) benzamide scaffold**

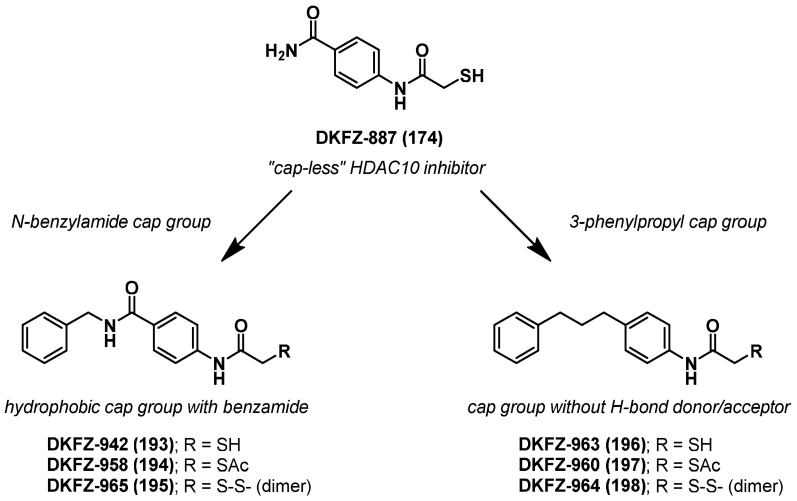


### 3.4.3.1 Evaluation of inhibitors **193–198**

Selectivity profiles of capped derivatives of **DKFZ-887** are shown in **Figure 47**. Comparing *N*-benzyl mercaptoacetamide inhibitor **DKFZ-942** with **DKFZ-963**, where the benzamide cap linkage is replaced with an alkyl chain, reveals a clear shift of the selectivity profile. **DKFZ-942** has slightly better HDAC10 activity and an HDAC10/6 selectivity factor of 160, while for **DKFZ-963** SF 10/6 is only 48. Besides the reduced HDAC10 activity, **DKFZ-963** shows slightly increased activity on HDAC1, 2, 3 and 6. The trend continues with thioacetates **DKFZ-958** and **DKFZ-960** as well as disulfides **DKFZ-965** and **DKFZ-964**: inhibitors without a benzamide in the linker region are less active on HDAC10 and less selective. This SAR indicates that the amide group is beneficial for HDAC10 activity, but does not influence HDAC6 affinity. Class I activity even increases when the amide is replaced by an alkyl chain.

Equally informative is the loss of HDAC10 activity by 0.51 log units in **DKFZ-942** compared to **DKFZ-887,** when the amide is *N*-benzylated. Since large, hydrophobic capping groups typically increase binding nonspecifically (see **Figure 28**, page 60), the activity drop in this case further indicates that the benzamide protons are involved in a strong binding interaction with HDAC10. This could likely be hydrogen bonding to the glutamate gatekeeper residue. A steric factor from the *N*-benzylation that restricts the inhibitor orientation upon zinc binding should also be considered. Still, even without further polar interactions, **DKFZ-963** achieves an HDAC10 activity similar to SAHA and a clear HDAC10 preference only with the mercaptoacetanilide ZBG/linker combination. This is further evidence for the suitability of mercaptoacetanilides as selective HDAC10is and confirms the suspected role of the benzamide functionality as an additional driver of HDAC10 selectivity.

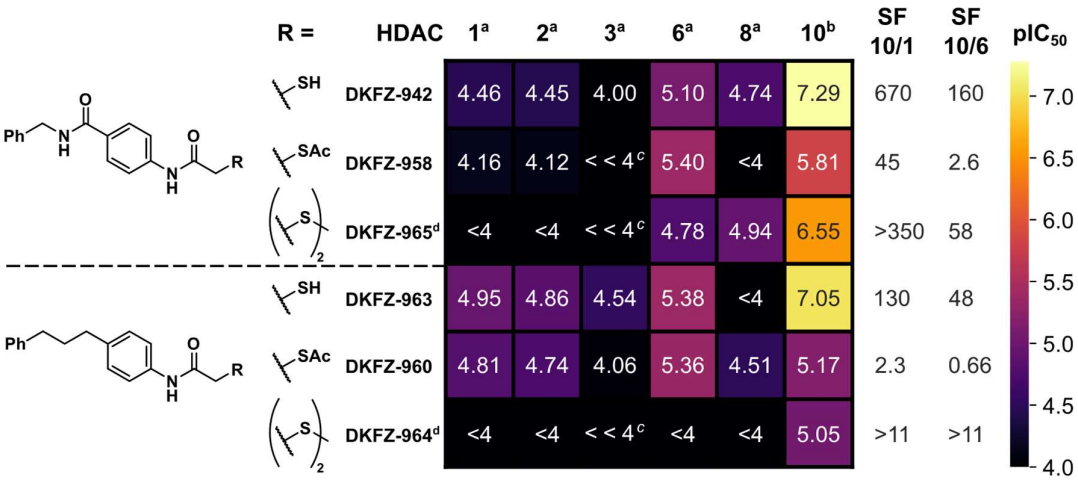


**Figure 47.** HDAC isozyme selectivity heatmap and $pIC_{50}$ values of DKFZ-942–964. $pIC_{50}$ values are determined by four-parameter non-linear regression analysis with eight dose levels in triplicate with HDAC Glo assay[a] or FRET assay[b]. [c] Curve fit was not convergent at 100 µM. [d] Activity per sulfide unit, disulfide dosed in ½ molar concentration. SF (selectivity factor) = $10^{(pIC50(HDAC10) - pIC50(HDAC6\ or\ HDAC1))}$ rounded to two significant figures. For 95% confidence intervals, see Table S4.

### 3.4.3.2 Synthesis strategy

Aniline **199** was prepared as previously described[205] to access thioacetate **DKFZ-958** via bromide **200** by amidation with bromoacetyl bromide under Schotten–Baumann conditions. Substitution of the bromide with potassium thioacetate in DMF provided me with **DKFZ-958**, which I in turn converted to thiol **DKFZ-942** by transesterification with sodium thiomethoxide in methanol. Inhibitor **DKFZ-942** was cleanly oxidized to disulfide **DKFZ-965** using catalytic amounts of iodine and DMSO as the oxidizing agent.[204] The same synthetic route starting from commercial aniline **201** allowed me, via bromide **202**, access to thioester **DKFZ-960**, thiol **DKFZ-963** and disulfide **DKFZ-964** in excellent yields.

**Scheme 17. Synthesis[a] of DKFZ-942–964**

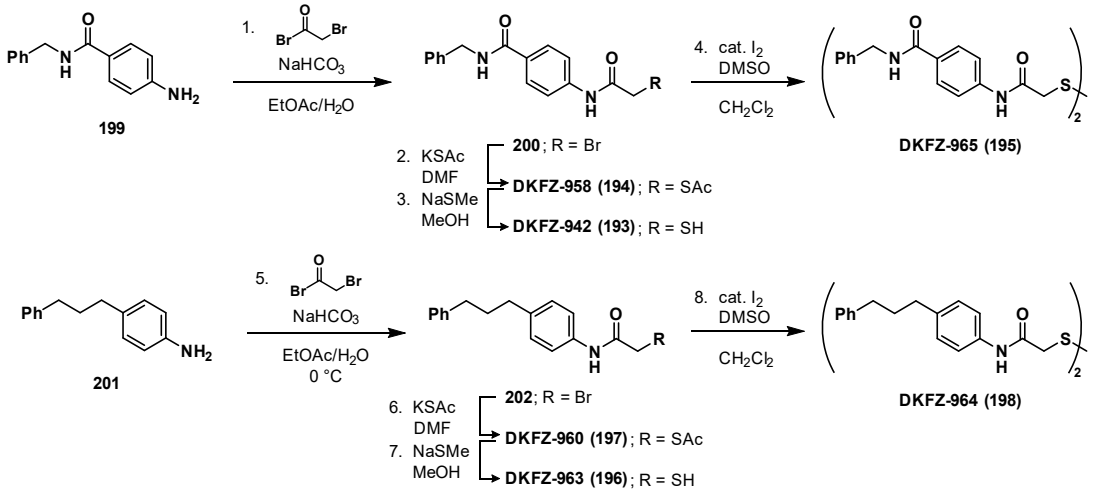


[a] Reagents and conditions 1. bromoacetyl bromide, $NaHCO_3$, $EtOAc/H_2O$, rt, 2 h, 93%; 2. KSAc, DMF, rt, 30 min, 76%; 3. NaSMe, MeOH, rt, 10 min, 81% (2 steps); 4. cat. $I_2$, DMSO, $CH_2Cl_2$, rt, 2 h, 76% (2 steps);

5. bromoacetyl bromide, $NaHCO_3$, EtOAc/$H_2O$, 0 °C, 10 min, quant; 6. KSAc, DMF, rt, 1 h, 87%; 7. NaSMe, MeOH, rt, 20 min, 56%; 8. cat. $I_2$, DMSO, $CH_2Cl_2$, rt, 15 min, 99%.

### 3.4.4 Comparison and overview of non-hydroxamic acid HDAC10 inhibitors

To this end, I have tested a total of 28 compounds within the new ZBG project, consisting of nine different ZBGs, distributed among nine structural scaffolds. An overview of all compounds discussed in chapter 3.2.4 is depicted in **Figure 48** as an HDAC10 potency (FRET $pIC_{50}$) versus selectivity (HDAC10/6) plot with ZBGs color coded and the structural scaffolds indicated by symbols. Comparing the ZBGs across scaffolds reveals that free thiols (red dots) in the form of α-mercaptoacetamides and α-mercaptoacetophenone **DKFZ-949** exhibit the highest HDAC10 potency, comparable and sometimes exceeding the activity of hydroxamic acid inhibitors. α-Mercaptoacetamides in all tested scaffolds show an HDAC10 $pIC_{50}$ between 7 and 8 just like hydroxamic acids (pink dots) on similar inhibitor scaffolds. For comparison, SAHA only shows an HDAC10 $pIC_{50}$ of 6.93. This indicates that α-mercaptoacetamides are strong HDAC10 binders on multiple inhibitor scaffolds. α-Mercaptoacetophenone **DKFZ-949** stands out as the most potent compound in this series, outperforming related hydroxamic acids **DKFZ-962** and **DKFZ-945** regarding HDAC10 potency as well as selectivity over HDAC6.

However, the HDAC6 activity seems not so much dependent on the zinc binder, but more so on the inhibitor scaffold, and HDAC6 activity can be modulated by small changes in the linker structure. The largest difference in HDAC10/6 selectivity could be achieved between SAHA-like inhibitors **DKFZ-812** and **DKFZ-825**. Similar to hydroxamate bearing aza-SAHA derivative **DKFZ-711** (section 3.2.1, page 46), the non-selective α-mercaptoacetamide **DKFZ-812** (selectivity factor HDAC10/6 = 1.6) was developed into HDAC10 selective **DKFZ-825** (selectivity factor HDAC10/6 = 340) by one C → N replacement in the alkyl linker region. Another example is the loss of HDAC10 selectivity from **DKFZ-942** to **DKFZ-963**, when the linker benzamide is removed. Many SAR trends of the linker structures are repeated with the other ZBGs, but unsubstituted α-mercaptoacetamides or the mercaptoacetophenone are typically superior regarding potency and, except for the outliers **DKFZ-961** and **DKFZ-832**, also regarding selectivity.

In conclusion, the given SAR study results in the discovery of non-hydroxamate amine-free selective HDAC10is. The appropriate combination of a 4-acetamidobenzamide or a 1-acetylpiperidine-4-carboxylate linker with an α-mercaptoacetamide or α-mercaptoacetophenone ZBG provides inhibitors with excellent biochemical potency and HDAC10 selectivity.

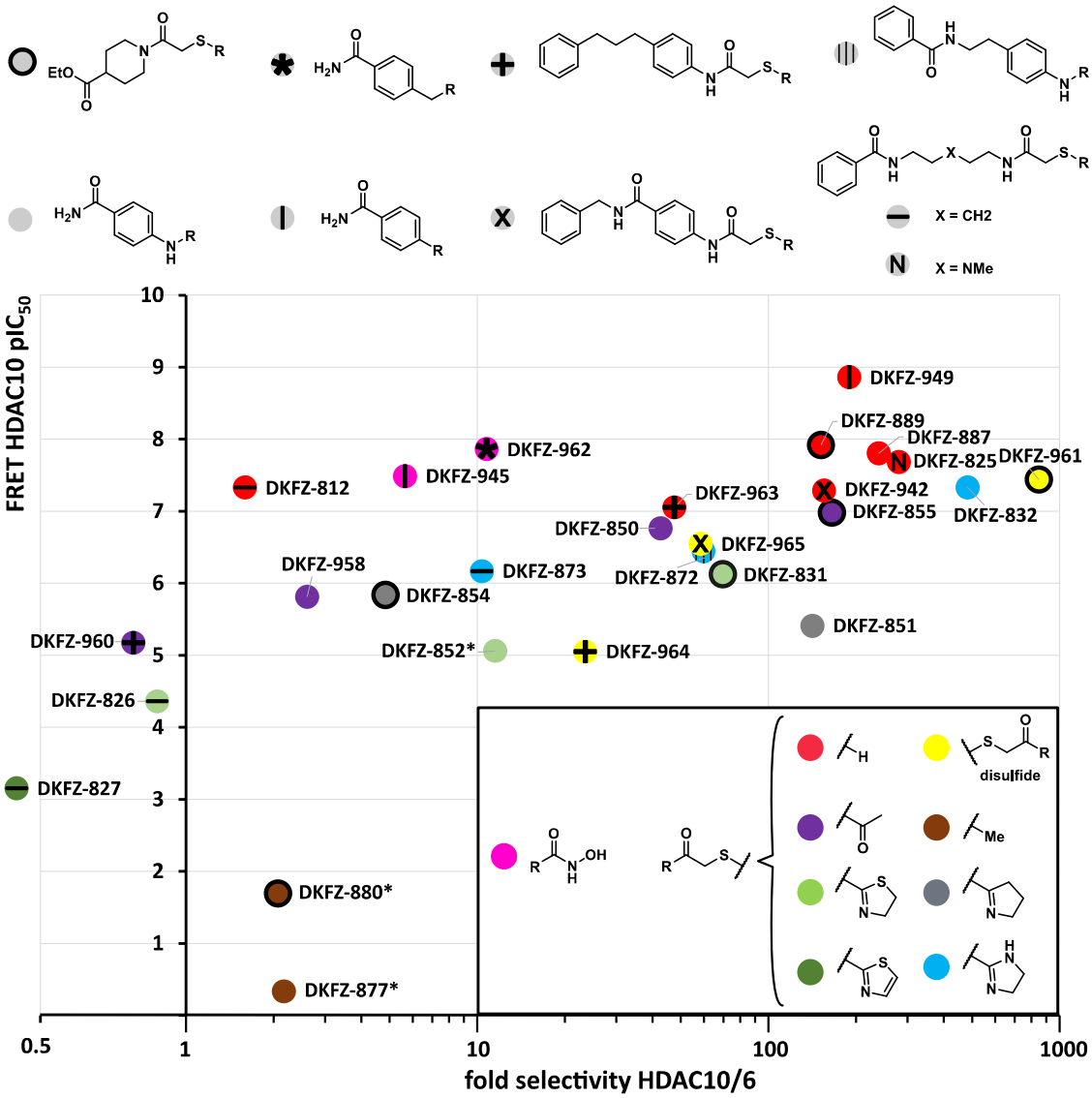


**Figure 48.** HDAC10 potency versus selectivity plot of non-hydroxamate inhibitors and reference compounds. Symbols represent structural scaffold, colors represent ZBG. For a tabulated and extended version of this plot with 95% confidence intervals, see Table S4. *: HDAC6 $pIC_{50}$ could not be accurately determined due to lack of activity. Selectivity was calculated using the HDAC6 assay limit ($pIC_{50}$ of 4.0); actual selectivity may be higher.

## 3.5 Targeted HDAC10 degraders

With potent and selective compounds that inhibit the enzymatic function of HDAC10 at hand, I took the next step and transitioned from the occupancy-driven pharmacology of inhibitors to the event-driven pharmacology of targeted degraders (PROTACs) that allow the removal of HDAC10 including potential scaffolding functions of the HDAC10 protein. When I initiated the project, no HDAC10 degraders were reported, but multiple pan-inhibitor based degraders were reported as HDAC6 selective (see section 1.5). With this information, I hypothesized that HDAC10 might be readily degradable together with its closest relative HDAC6 using a thalidomide based CRBN recruiter and the SAHA pan-inhibitor scaffold.

Therefore, I started the development of selective HDAC10 degraders with the synthesis of a reported HDAC6 degrader, which uses a SAHA warhead, and performed a linker exploration study. The goal was to identify a linkage for a SAHA–thalidomide chimera that leads to the degradation of HDAC10, perhaps even exclusively, just due to a ternary complex geometry that allows ubiquitination of HDAC10 but no other isozymes. This selectivity in degraders from non-selective warheads is often observed, e.g. with PROTACs that bind Class I HDACs through the SAHA warhead but do not lead to their degradation, even when proximity with an E3 ligase is induced.[179] I supposed that only if a SAHA-based (unselective) HDAC10 degrader were possible, a degrader with a selective aza-SAHA warhead could work as well. However, preparing and purifying a potentially large amount of PROTACs for a linker exploration study would be much easier using the non-basic SAHA scaffold and established synthesis procedures to access them. If the first exploration yielded an HDAC10 degrader that is unselective due to the SAHA warhead, transforming it into a truly selective HDAC10 degrader would then only be a matter of changing the warhead from SAHA to an aza-SAHA inhibitor as described in section 3.2, likely without the need of a broad linker exploration study.

### 3.5.1 Design and synthesis strategy

For the linker exploration study towards selective HDAC10 degraders, I decided to follow the method for solid phase synthesis (SPS) of PROTACs with hydroxamic acid based warheads and a thalidomide based CRBN recruiter by Sinatra et al.[178] As a proof of principle, they prepared a targeted degrader of HDAC6, which also showed some activity on HDAC1. This compound could also potentially be an HDAC10 degrader but was not tested for this capability. Therefore, I found their PROTAC – resynthesized as **DKFZ-899** – a good starting point for my study towards selective HDAC10 degraders.

The SPS method of HDAC PROTACs by Sinatra et al.[178] also has a number of distinct advantages: it is a divergent synthesis approach that allows efficient preparation of PROTACs with different linkers, but with a shared hydroxamic acid SAHA warhead. Once the ideal linker length for HDAC10 degradation is identified, the same synthetic route can be employed to make HDAC10 selective aza-SAHA derivatives. Since the entire degrader compound is assembled on solid phase, no purification of polar intermediates is required. Especially aliphatic (amino) hydroxamic acids are quite polar and can be challenging to purify by chromatography. The

nucleophilicity of hydroxamic acids and their propensity for hydrolysis limits further transformations on the molecule without protecting the hydroxamic acid. For these reasons, I typically form the hydroxamic acid in the last step of the synthetic sequence. To access PROTACs with a thalidomide CRBN recruiter, the hydroxamic acid cannot be made from the corresponding ester with hydroxylamine in the last step since the thalidomide imide is susceptible to nucleophilic attacks. Milder conditions like amide coupling of the free carboxylic acid would be required. The SPS approach solves all of these problems by utilizing "hydroxamic acids immobilized on resins (HAIRs)",[178] essentially a solid support 2-chlorotrityl protecting group for hydroxamic acids.

SPS of PROTACs is detailed in **Scheme 18A** and was mainly carried out by Hannah Steffke during her Fulbright internship under my supervision. The SPS strategy dictated that the CRBN recruiter (**Scheme 18A,** blue box) is connected via a linker (grey) to the HDAC-binding warhead (red box) by four amide bonds (in red) in the final product. These bonds are all formed on solid support in a total of 10 steps, including initial resin loading and the final cleavage step. Designing peptide-like PROTACs enables the usage of high-yielding amide coupling reactions to assemble the complex products effectively.

The methodology starts with the *N*-hydroxyphtalimide loading of 2-chlorotrityl chloride resin, followed by capping unreacted 2-chlorotrityl chloride groups on the resin with methanol to prevent later immobilization of carboxylic acids or acylhydrazines, which would be hard to separate from the desired hydroxamic acid. Loading of the resulting resin **203** was quantified and served as the basis for yield calculations of the final products. Hannah prepared multiple grams of resin **203**, as it is shelf stable and the starting material for all HDAC PROTACs. She deprotected the resin-bound hydroxylamine by treatment with 5% hydrazine in MeOH and then coupled the warhead linkers as Fmoc-protected amino acids to the resin using HATU peptide coupling conditions. The Fmoc-protected amine was then liberated by treatment with 20% piperidine in DMF to allow for the next coupling step. That way, the individual PROTACs were built in a linear sequence starting from the hydroxamic acid as part of the warhead linker that can be SAHA-like (warhead linker A) or HDAC10 selective (warhead linker B). Then, the warhead cap group was attached to provide resins **204** and **205**. At this stage, the resin loading was determined by Fmoc quantification after deprotection and the equivalents of the subsequent coupling partners were adjusted to save Fmoc carboxylic acid building blocks. Amide coupling reactions were typically carried out using 2–3 equiv of carboxylic acid to ensure complete conversion of resin-bound primary amines. Starting from resin **204**, Hannah used a variety of different Fmoc-protected amino acid linkers to explore the linker SAR. I decided to limit the linker exploration to flexible non-polar alkyl and polar PEG linkers ranging from four to 16 atoms length. Flexible linkers provide more conformational freedom to form the correct ternary complex, and optimization with rigidified linkers can be a focus of second-generation degraders, once a suitable linker length has been established. The last coupling step was the attachment of CRBN recruiter acid **206**, following cleavage of the product from the resin using 5% TFA in $CH_2Cl_2$. Overall yields based off the determined loading of resin **203** were typically around 30%. Lower yields occurred sometimes due to incomplete couplings and losses during preparative HPLC purification.

**Scheme 18. Synthesis of HDAC PROTACs 207–217 by solid phase synthesis (SPS)[a]**

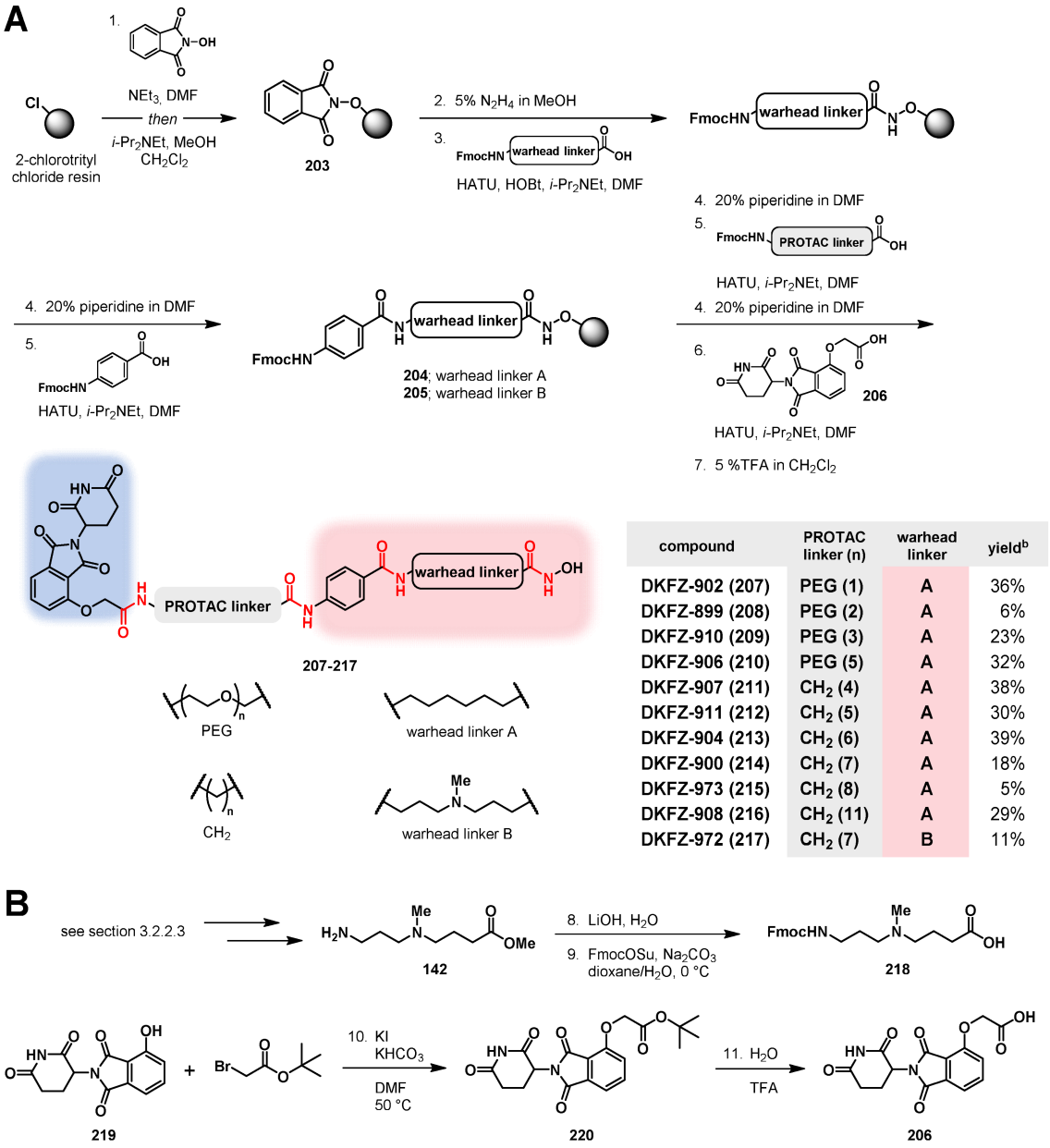


| compound | PROTAC linker (n) | warhead linker | yield[b] |
|---|---|---|---|
| DKFZ-902 (207) | PEG (1) | A | 36% |
| DKFZ-899 (208) | PEG (2) | A | 6% |
| DKFZ-910 (209) | PEG (3) | A | 23% |
| DKFZ-906 (210) | PEG (5) | A | 32% |
| DKFZ-907 (211) | $CH_2$ (4) | A | 38% |
| DKFZ-911 (212) | $CH_2$ (5) | A | 30% |
| DKFZ-904 (213) | $CH_2$ (6) | A | 39% |
| DKFZ-900 (214) | $CH_2$ (7) | A | 18% |
| DKFZ-973 (215) | $CH_2$ (8) | A | 5% |
| DKFZ-908 (216) | $CH_2$ (11) | A | 29% |
| DKFZ-972 (217) | $CH_2$ (7) | B | 11% |

[a] Reagents and conditions 1. *N*-hydroxyphtalimide, $NEt_3$, DMF, 24–48 h, then *i*-$Pr_2NEt$/MeOH/$CH_2Cl_2$ (5%/15%/80%), 2 × 15 min; 2. 5% $NH_2H_4$ in MeOH, 2 × 15 min; 3. Fmoc-amino acid (2.0 equiv), HATU, HOBt, *i*-$Pr_2Net$, DMF, 16 h; 4. 20% piperidine in DMF, 2 × 7 min; 5. Fmoc-amino acid (3.0 equiv), HATU, *i*-$Pr_2Net$, DMF, 16 h; 6. acid **206** (2.0 equiv), HATU, *i*-$Pr_2Net$, DMF, 6–16 h; 7. 5% TFA in $CH_2Cl_2$, 1 h, 8. 3 M LiOH in $H_2O$, rt, 1.5 h; 9. FmocOSu, FmocCl, 10% aqueous $Na_2CO_3$, dioxane, 0 °C, 4 h 76% (2 steps); 10. cat. KI, $KHCO_3$, DMF, 50 °C, 3 h, quant; 11. $H_2O$/TFA (5:95), rt, 7 h, quant. All compounds, except for **DKFZ-972** and **DKFZ-973,** were prepared by Hannah Steffke under my supervision. [b] yield calculated based on loading capacity determined for resin **203**. Blue box: CRBN ligand, red box: HDAC binder (warhead). Amide bonds formed by SPS are highlighted red in the structure of the final degrader molecule.

The required Fmoc-protected amino acid building blocks are straightforward to access and mostly available from commercial sources, as they are also used in the modification of synthetic peptides made with Fmoc SPS. Aza-SAHA warhead building block **218** (**Scheme 18B**)

was synthesized by Hannah in a one-pot two step process starting from diamino ester **142**, which I prepared for the SAR study of γ-amino hydroxamic acids (see section 3.2.2.3, **Scheme 10**, page 66) with excellent yield.

Acid **206** was originally developed in our lab by Lohbeck and Miller[206] as a PROTAC building block and also employed as CRBN recruiter by Sinatra et al.[178] Therefore, we used **206** as well and Hannah and I further optimized the synthesis (**Scheme 18B**) of **206** starting from **219**, which was prepared by Jasmin Lohbeck in multi gram-scale as described previously.[206] The improved synthesis of **206** proceeds through *tert*-butyl ester **220**, which was prepared using $KHCO_3$ as a mild base and activation of *tert*-butyl 2-bromoacetate by in situ Finkelstein reaction. This allowed the selective alkylation of the phenol in quantitative yield without alkylation of the imide. The *tert*-butyl ester could be cleaved conveniently in quantitative yield using 5% $H_2O$ in TFA at rt without the need for purification.

## 3.5.2 Degrader evaluation

To evaluate the potency and selectivity of our targeted HDAC degraders, I decided to start with a classical immunoblotting approach focusing on HDAC10, its closest relative HDAC6 and Class I representative HDAC1. The overall goal was to establish an HDAC family-wide and ideally proteome-wide degradation selectivity profile. This, however, is slow and labor intensive using traditional Western blots and limited by the availability of good antibodies. Therefore, we used immunoblotting only as a proof-of-principle for the most important HDAC targets. Once an active HDAC10 degrader was identified, I employed a proteomics approach with collaboration partners in order to establish a broader degrader selectivity profile. Such a large-scale proteomics approach towards HDAC degraders was in the meantime reported by the group of Eric Fischer.[179]

### 3.5.2.1 Immunoblotting against HDAC10, 6 and 1

Hannah Steffke treated human leukemia HL-60 cells and neuroblastoma BE(2)-C cells in five dose levels ranging from 16 nM to 10 µM for 6 h and prepared cell lysates evaluate the SAHA-based chimeras **207**–**214** and **216**. I selected the dose-levels based on the SAHA binding affinity for HDACs ($pIC_{50}$ = 20–700 nM) and with the aim to cover a broad concentration range. This is important when testing PROTACS, since effective degrader concentrations do not only depend on the affinity of the warhead and higher treatment concentrations can lead to reduction or even absence of degradation due to the Hook-Effect.[207] I based the six-hour treatment time and choice of the HL-60 leukemia cell line on the available literature.[178] Johanna Hummel-Eisenbeiß used the lysates from treated cells to perform Western blots against my protein of interest – HDAC10 – using a hybridoma cell supernatant provided by Dr. Johannes Ridinger (Oehme Lab, DKFZ Heidelberg). To evaluate degrader selectivity, Johanna also tested for degradation of HDAC1, as an HDAC Class I representative, and for the other Class IIB member HDAC6. As a loading control, tubulin was detected together with the respective HDAC protein on the same blot simultaneously using a second fluorescence channel.

Degradation Western blots of chimeras **207**–**208** and **213**–**214** with SAHA as a control are shown in **Figure 49**, and for chimeras **209**–**212** and **216** in **Figure 51**. To convey the Western blot quality and antibody specificity, the blots are cut to include all observed bands for the respective antibody. The unpurified HDAC10 antibodies in the hybridoma supernatant gave surprisingly clean Western blots with only one band at the expected height of 75 kDa. In our hands, HDAC6 immunoblotting was more challenging than with HDAC10 and required trials with different commercial antibodies. The HDAC6 band is expected at 130 kDa, but due to cell line-dependent modifications, bands at 150–160 kDa are observed by us and others as well.[178,208] Additionally, we observed two bands around 110 kDa with the HDAC6 antibody in BE(2)-C cells. The HDAC6 bands are also comparatively weak in the DMSO controls, therefore the degradation blots do not always provide a definite result. HDAC1, on the other hand, gave clean Western blots with only one band at the expected molecular weight of 60 kDa using a commercial antibody.

In our six-hour treatment condition, Sinatra et al.'s PEG-linked degrader **DKFZ-899** did not degrade HDAC10 in HL-60 cells (**Figure 49A**). However, at a higher dose (10 µM), it was able to degrade HDAC6 but not HDAC1. This contrasts partially with their evaluation of the degrader, also performed in HL-60 cells, but with a longer 48-hour treatment time. They observed degradation of both HDAC6 and HDAC1, at 1 µM and 10 µM **DKFZ-899**, respectively.[178] My octanoic acid-linked compound **DKFZ-900,** on the other hand, is an effective degrader of both HDAC10 and HDAC6 in submicromolar concentrations, with protein depletion starting at the 80 nM dose-level. However, it does not show any activity towards HDAC1. **DKFZ-902**, with one PEG unit less than **DKFZ-899**, demonstrated an ability to degrade HDAC6 in the micromolar range, better than **DKFZ-899**, but less efficacious than alkyl-linked **DKFZ-900.** Surprisingly, **DKFZ-902** does not show any effect on HDAC10 or HDAC1 protein levels. **DKFZ-904** shows degradation of HDAC10 starting at 0.4 µM, with efficient removal of HDAC10 observed at 2 µM and higher. The potential for degradation of HDAC6 by **DKFZ-904** is less clear from the available Western blot, but some capability to degrade HDAC6 is suggested. Again, no degradation of HDAC1 can be observed.

In addition to the DMSO vehicle control as a baseline comparison for HDAC expression, I also included SAHA as a warhead target-occupancy control. No effect on protein levels relative to the vehicle control was observed for HDAC10 and 1 with the well-performing antibodies at any of the treatment concentrations. For HDAC6, on the other hand, reduced HDAC6 degradation or reduced expression is suggested by the Western blot, especially at 2 µM. The effect does not appear to be strictly dose-dependent and further replicates are required to draw a definite conclusion. Due to the comparatively poor performance of the HDAC6 antibody, I cannot disregard technical reasons for this outcome.

To further characterize the HDAC degraders, I decided to test the compounds in **Figure 49A** under the same conditions again, but with the human neuroblastoma BE(2)-C cell line (see **Figure 49B)** due to its clinical relevance associated with HDAC10's role in chemotherapy-resistant neuroblastoma.[50,52] To our surprise, none of the active (or inactive) compounds in HL-60 cells induced targeted protein degradation of HDAC10, 6 or 1 in BE(2)-C cells. These results were particularly clear with HDAC10 and 1, while the Western blots against HDAC6 are again

harder to interpret due to the poor performance of the HDAC6 antibody. It is also noteworthy that the band pattern resulting from this antibody differs between the cell lines and also within the BE(2)-C samples. Further investigations are required to rationalize this observation, but I hypothesize that BE(2)C cells differ from HL-60 in the makeup of their ubiquitination machinery. This is supported by data in The Human Protein Atlas, showing that leukemia cell lines like HL-60 have the highest CRBN expression levels of all cancer cell lines and neuroblastoma, especially BE(2) cells, transcribe 2.3-fold less CRBN encoding RNA than HL-60.[209] This makes HL-60 cells particularly suitable for the development of CRBN recruiting PROTACs independent of the target protein of interest and can explain why all degradation capabilities are lost when the same degraders were used in BE(2)-C cells.

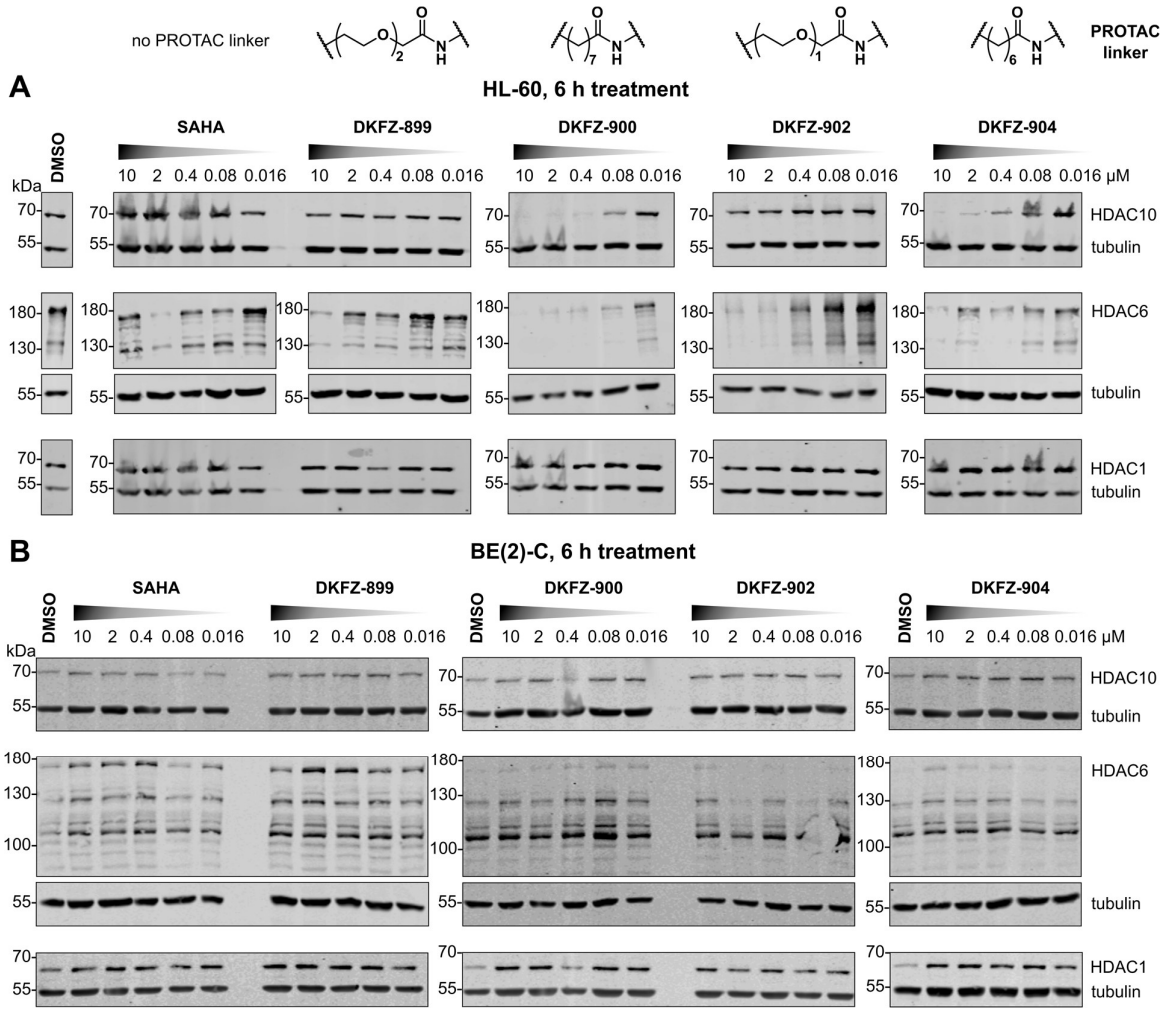


**Figure 49.** Degradation Western blots against HDAC10, 6 and 1 of HL-60 (A) or BE(2)-C (B) cells treated for 6 h with CRBN recruiting SAHA chimeras, SAHA or vehicle control at the indicated concentrations. Tubulin was detected on the same blot as loading control together with the respective HDAC protein. Cell treatment was performed by Hannah Steffke under my supervision, SDS-PAGE and Western blot analysis was performed by Johanna Hummel-Eisenbeiß.

The observed cell line-dependent PROTAC efficacy prompted me to also investigate HDAC10 expression levels at the protein level, enabled by the availability of a hybridoma supernatant containing an excellent HDAC10 antibody. Dr. Jana Samarin performed Western blot analysis and quantified the HDAC10 protein content relative to GAPDH (**Figure 50**) of nine untreated cell lines, including the HL-60 and BE(2)-C, which were used to evaluate my HDAC degraders. The seven other cell lines she tested were lung adenocarcinomas. None of the tested cell lines showed additional, unspecific bands in the Western blot and the HDAC10 content ranged across two orders of magnitude. Interestingly, it was three times higher in HL-60 cells than in BE(2)-C. Amongst the lung cancer cell lines, H2122 showed the highest HDAC10 content, followed by H441 and H2023, while A549 had the least. This comparison is particularly informative since it highlights that HDAC10 can be efficiently degraded in a cell line with a higher target protein expression (HL-60), but not necessarily in one with comparatively lower expression (BE(2)-C). It also indicates differential expression of HDAC10 in different cancer cell types and within adenocarcinomas in particular.

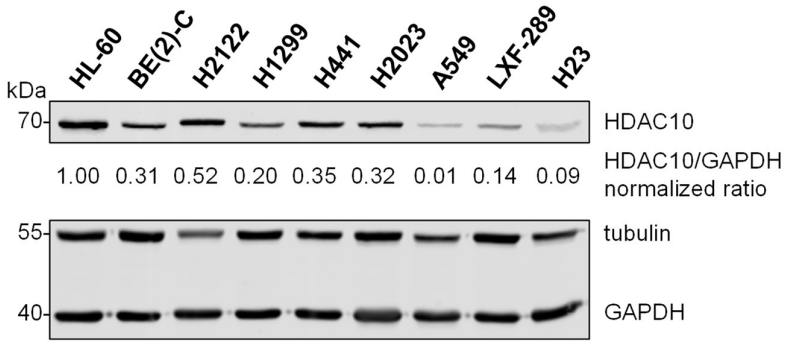


**Figure 50.** Western blot against HDAC10, tubulin and GAPDH as loading controls of untreated cell lines reveals cell line-dependent HDAC10 expression. HDAC10 band intensity was quantified and normalized to GAPDH. Cell lysis, SDS-PAGE and Western blot analysis was performed by Dr. Jana Samarin.

Since BE(2)-C cells appear to be incapable of targeted degradation by CRBN recruitment, at least for HDAC10 and 6, the next set of degrader candidates was only tested in HL-60 cells under the same conditions as previously discussed compounds. Degradation Western blots of compounds **DKFZ-906**–**DKFZ-911** against HDAC10, 6 and 1 (**Figure 51**) revealed that again, none of the tested compounds induced HDAC1 degradation. However, a linker SAR trend for HDAC10 and HDAC6 could be established. **DKFZ-906** with the longest employed PEG linker was found to be a degrader of HDAC10 and HDAC6 in the micromolar concentration range, exhibiting better efficacy than shorter PEG-linked chimeras, such as **DKFZ-899** and **DKFZ-910**. Additionally, pentanoic acid-linked **DKFZ-907** was also found to be a potent degrader of HDAC10 and 6 with an efficacy only slightly lower than octanoic acid-linked **DKFZ-900**. Dodecanoic acid-linked **DKFZ-908** with the longest employed alkyl linker appears to be slightly better than shorter **DKFZ-900**, as even the lowest tested dose-level of 16 nM showed reduced HDAC10 levels compared to the vehicle control. HDAC6 appears to be affected by **DKFZ-908** similarly to HDAC10, although the Western blot does not clearly show dose-

dependent degradation, possibly due to the fact that even the lowest dose-level is sufficient to deplete HDAC6 substantially compared to the vehicle control. **DKFZ-910,** with one PEG unit more than previously reported PROTAC **DKFZ-899**, appears to be a better HDAC6 degrader than its analogue and is potentially also a weak HDAC10 degrader. Hexanoic acid-linked **DKFZ-911** degrades HDAC10 and HDAC6 in the micromolar range and was found to be similar in potency to **DKFZ-904** with a one carbon longer linker.

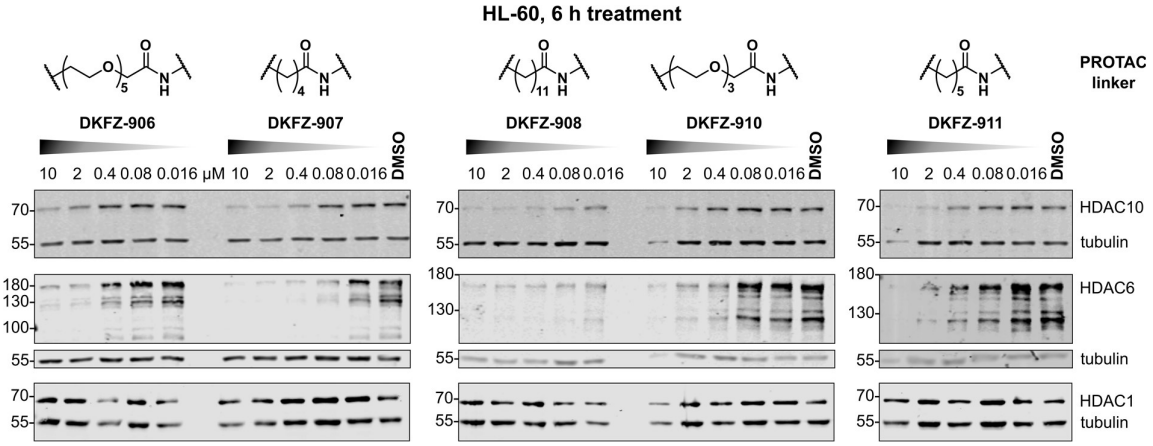


**Figure 51.** Degradation Western blots against HDAC10, 6 and 1 of HL-60 cells treated for 6 h with CRBN recruiting SAHA chimeras or vehicle control at the indicated concentrations. Tubulin was detected on the same blot as loading control together with the respective HDAC protein. Cell treatment was performed by Hannah Steffke under my supervision, SDS-PAGE and Western blot analysis was performed by Johanna Hummel-Eisenbeiß.

In summary, I established a SAR between the linker length/composition and degrader efficacy in HL-60 cells. Alkyl linkers provided generally superior degraders, especially for targeting HDAC10, as all alkyl-linked chimeras degraded HDAC10 effectively. However, I also found a strong linker length dependency for the degrader efficacy. Only the two longest PEG-linked compounds **DKFZ-906** and **DKFZ-910** induced some HDAC10 degradation at high concentration. This PEG linker length trend was less pronounced in the case of HDAC6, where short (**DKFZ-902**) and long (**DKFZ-906**) linker compounds both induced HDAC6 degradation in the micromolar concentration range. Looking at alkyl-linked chimeras, the data suggests a good correlation of HDAC10 degrader potency and linker length, with long linkers like in **DKFZ-900** and **DKFZ-908** providing the best HDAC10 degraders. The trend is again less pronounced when evaluating the HDAC6 degradation by alkyl-linked chimeras, since short linker compounds such as **DKFZ-907** and **DKFZ-911** are able to degrade HDAC6 in as low as sub-micromolar treatments, while the longest alkyl-linked compound **DKFZ-908** provided good HDAC6 depletion already at low treatment concentrations. Based on these promising results, I later prepared an even longer alkyl-linked SAHA chimera (**DKFZ-973**), but it has yet to be tested for its HDAC degradation profile.

None of the pan-HDAC binding SAHA-based chimeras were found to be selective degraders of only HDAC10, as HDAC6 was always co-degraded. However, selectivity over HDAC1 could be demonstrated with all tested compounds, and one PEG-linked chimera (**DKFZ-902**) was found

to be a degrader of only HDAC6, but not HDAC10, under the tested conditions. Subsequently, I began to prepare PROTACs with an HDAC10 selective aza-SAHA warhead, and thus far have prepared one example (**DKFZ-972**) which verifies the applicability of the solid-phase synthesis method also for amino hydroxamic acids. In the near future, more examples will be prepared using the validated synthesis strategy described in section 3.5.1. Then, the aza-SAHA chimeras will be tested together with **DKFZ-972** for their HDAC degradation profile by immunoblotting to confirm their suspected potential as HDAC10 selective degraders.

Hannah further investigated the first HDAC10 degrader (**DKFZ-900**) we identified in a time course experiment with HL-60 cells. The cells were treated at 1 µM and harvested after different incubation times, and Johanna performed Western blot analysis to provide insights into the degradation kinetics, degrader stability, and resynthesis rate of the degrader targets. The Western blot (**Figure 52**) demonstrates that >30 min are required to initiate the targeted degradation of HDAC10 and maximal depletion is reached after 3 h. Protein resynthesis surpassed the degradation rate after 16 h, and HDAC10 returned to basal levels similar to those of vehicle control samples. A similar time course was observed for HDAC6 with a 30 min long degradation lag phase, followed by near full depletion for up to 16 h. Base levels of HDAC6 were probably reestablished around the 30 h mark, but due to the poor performance of the HDAC6 antibody and partly unequal protein loading, this could not be accurately determined so far. For HDAC1, on the other hand, the data confirmed a lack of degradation during the entire treatment time period; protein levels remained unchanged from vehicle control samples when accounting for differences in loading, as indicated by the tubulin loading control.

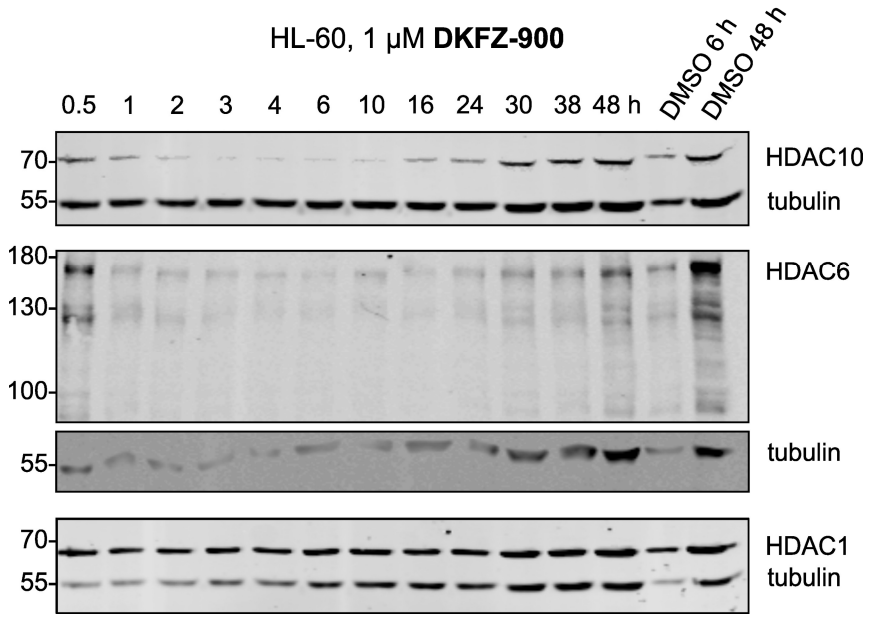


**Figure 52.** Degradation time course Western blots against HDAC10, 6 and 1 of HL-60 cells treated for 6 h with targeted HDAC degrader DKFZ-900, vehicle control at the indicated time points. Tubulin was detected on the same blot as loading control together with the respective HDAC protein. Cell treatment was performed by Hannah Steffke under my supervision, SDS-PAGE and Western blot analysis was performed by Johanna Hummel-Eisenbeiß.

#### 3.5.2.2 Proteomics

My goal was to establish a comprehensive selectivity profile for my selective HDAC10 degraders across the HDAC family and, ideally, the entire proteome. Therefore, we employed label-free quantification (LFQ) proteomics to evaluate the relative abundance of proteins upon treatment with a previously confirmed HDAC10 degrader. Hannah treated HL-60 cells in triplicates with her HDAC10 degrader **DKFZ-900** or SAHA as a warhead occupancy control at 1 µM for 6 h, then prepared cell lysates for quantitative proteomics in collaboration with Dr. Dominic Helm at the in-house Genomics and Proteomics Core Facility.

Proteomics results are depicted in **Figure 53** as a Volcano plot of HDAC10 degrader **DKFZ-900**- vs. SAHA-treated samples, with identified members of the HDAC family highlighted. Unfortunately, only HDAC1, 2 and 3 could be robustly quantified in treatment and control samples. HDAC6 could only be identified confidently in the control samples. All other HDACs, including HDAC10, could not be robustly quantified in both treatment groups using the core facility's routine LFQ quantification method. Therefore, I cannot draw any conclusion about depletion by degradation or potential increase of relative protein levels. The data for HDACs 1, 2, and 3 suggests that these enzymes are among the most depleted proteins in **DKFZ-900** treated samples, compared to the SAHA control group; however they are only reduced by 0.34–0.47 $\log_2$-fold at a significance of -$\log_{10}$(p-value) 2.26–2.47 (see labels in **Figure 53**). Additionally, many other proteins are enriched to at least the same degree, with some even having higher significance than the identified HDACs. This may indicate that HDACs 1, 2 and 3 with low fold changes and low significances should be categorized as proteomics noise and cannot be regarded as significantly depleted from the proteome. I must draw the same conclusion for HDAC6, which does not show significant differences in abundance between the two treatment groups.

To conclude, degradation of HDAC10 and most other HDAC isozymes could not be evaluated by routine label-free quantitative proteomics due to the low native protein levels for these enzymes. Even HL-60 cells, which are classified as highly HDAC10 expressing by transcriptomics analysis,[210] which we could confirm on the HDAC10 protein expression level (**Figure 50**), do not provide sufficient HDAC10 levels for robust quantification by LFQ proteomics. Therefore, I have been unable to establish a proteome- or HDAC family-wide degrader selectivity profile thus far. However, while this study was still ongoing, Eric Fischer and colleagues succeeded in quantifying HDAC1 to 10 in the myeloma MM1.S cell line using a tandem mass tag (TMT) LC-MS3-based global quantitative chemo-proteomics approach.[179] Interestingly, in the neuroblastoma Kelly cell line they were only able to quantify HDAC1 to 9; HDAC10 levels were too low, even for the superior TMT approach.

Therefore, my next steps in this project require better quantitative proteomics methods. For example, the chemical proteomics approach by Lechner et al.[128] involving an affinity matrix of beads functionalized with HDAC binders could be used to selectively enrich HDAC family members for more accurate quantification of low-abundance HDACs and evaluation of their targeted degradation. Another additional option would be a TMT-based quantification, potentially in collaboration with the Fischer Group.


**Figure 53.** Label-free quantitative proteomics of HL-60 cells treated in triplicates with HDAC degrader DKFZ-900 or SAHA (warhead occupancy control) at 1 µM for 6 h. Relative protein abundance of treatment vs. control groups is represented as –log(p-value) over $\log_2$ fold change. All identified HDAC family members are highlighted. Proteomics analysis was performed at the Genomics and Proteomics Core Facility (DKFZ Heidelberg) in collaboration with Dr. Dominic Helm, and statistical analysis was conducted by Martin Schneider.

# 4 Conclusions and outlook

In summary, the aim of developing chemical probes for HDAC10 was achieved with aza-SAHA derivatives (section 3.2). A rational design approach based on HDAC10's substrate specificity led to γ-amino hydroxamic acids as HDAC10 selective inhibitors. The scaffold was further optimized in a medicinal chemistry campaign and the resulting compounds are exceptionally potent HDAC10 binders with single-digit nanomolar $IC_{50}$s in the cell-free FRET assay, and low double-digit $IC_{50}$s in the cellular target engagement BRET assay. At the same time, these compounds show excellent and unprecedented selectivity for HDAC10 over its closest relative HDAC6 and Class I enzymes. This was independently confirmed in the Médard Group using chemo-proteomics profiling against the entire target landscape of HDAC10is, including non-HDAC off-targets. Moreover, my chemical probes do not lead to hyperacetylation of tubulin nor histones in cells, which is a functional confirmation of selectivity. A structural rationale for the potent HDAC10 binding and low HDAC6 affinity was provided by HDAC10 co-crystal structures and HDAC6 docking models.

**DKFZ-748** (**Figure 54**) with a 22 nM $IC_{50}$ against HDAC10 and >500-fold selectivity in cells was shown to be a valuable chemical tool to decipher the enigmatic HDAC10 biology. Treatment of neuroblastoma cells with **DKFZ-748**, followed by quantification of acetylated polyamines, confirmed for the first time in cells the HDAC10 polyamine substrate specificity and its physiological role as polyamine deacetylase. The Casero Group leveraged this to a new approach in cancer therapy, where **DKFZ-748** prevented the growth rescue of HeLa cells by exogenously supplied $N^8$-acetylspermidine under polyamine limiting conditions. This demonstrated that acetylated polyamines (e.g. produced by bacteria in the gut) can serve as an alternative source for essential polyamines when normal polyamine biosynthesis is limited or insufficient, as with rapidly growing tumors and under polyamine-limiting cancer therapy. Notably, selective HDAC10is were found to be non-cytotoxic in human cell lines under normal circumstances. This shows that selective HDAC10is like **DKFZ-748** are valuable chemical probes that will enable further research on HDAC10 and acetylated polyamines, as well as target validation studies to find new therapeutic approaches surrounding HDAC10.

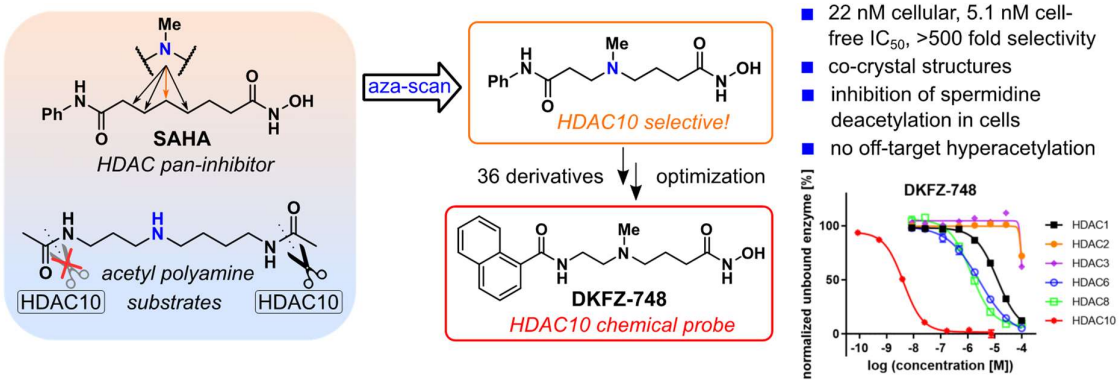


**Figure 54.** Summary of the development of HDAC10 chemical probes. Dose-response curves are from the cell-free FRET assay for HDAC10 and the Glo assay for the other isozymes.

In a separate approach, I investigated alternative zinc binding groups (ZBG) for selective HDAC10 inhibition without hydroxamic acids (section 3.4). An SAR study based on screening hits of a high-throughput compound library screen identified α-mercaptoacetamides **DKFZ-889** and **DKFZ-887** (**Figure 55**) as interesting candidates for the further development of selective HDAC10is with alternative ZBGs. Both scaffolds can provide >100-fold selectivity for HDAC10 over 6 without the need for a basic linker and still show $pIC_{50}$s between 7 and 8. Thiols can be potent zinc binders for HDACs and are used clinically, but they are oxidation-sensitive, which limits their bioavailability and effective concentration in vitro. A possible remedy could be the use of prodrugs to protect the active thiol, such as in thioacetate **DKFZ-855** or with disulfide **DKFZ-961**. However, the ideal prodrug strategy still needs to be determined.

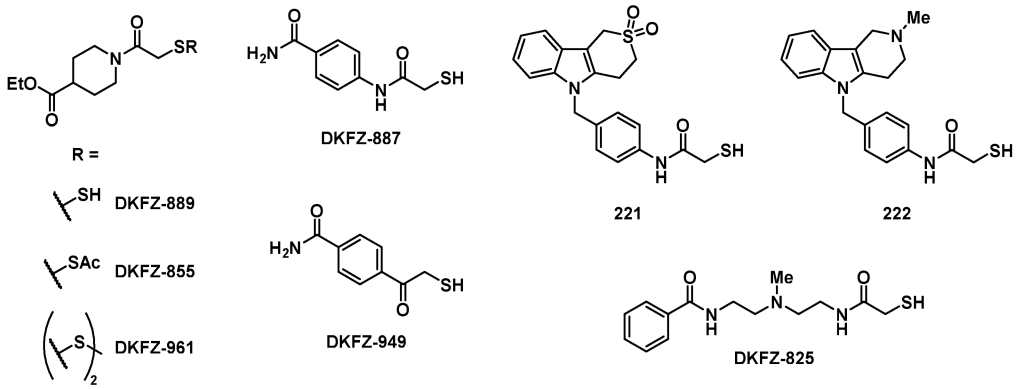


**Figure 55**. Potential starting points for the further development of non-hydroxamate selective HDAC10 chemical probes.

α-Mercaptoacetophenone **DKFZ-949** (**Figure 55**) is also an interesting candidate for further development, as it does not readily oxidize in solution and showed a $pIC_{50}$ of 8.86 in the FRET assay with 190-fold selectivity over HDAC6. While I was unable to improve **DKFZ-887** by substitution at the benzamide, derivatives of **DKFZ-949** or replacement of the ester in **DKFZ-889** with an amide could yield better inhibitors. Mercaptoacetamide derivatives of Tubathian like **221** were recently reported as selective HDAC6 inhibitors.[155] The mercaptoacetamide Tubastatin A derivative **222** with the basic amine responsible for HDAC10 activity of this scaffold, could be interesting for targeting HDAC10. Especially since I already demonstrated with **DKFZ-825** that non-selective mercaptoacetamides can be transformed into selective HDAC10is using the same strategy as with hydroxamic acid based aza-SAHA-derivatives.

Selective HDAC10is without a hydroxamic acid, or even without a basic functionality, open up an entirely different chemical space to target HDAC10, but I think a systematic evaluation of thiol-prodrug strategies in cells is required to judge the potential and drawbacks of thiol-based HDAC10is. Still, selective non-hydroxamate HDAC10is could be beneficial as immunomodulators to prevent transplant rejection or treat autoimmune disorders. Hydroxamic acids are due to their potential mutagenicity[139] unfeasible for such applications. The therapeutic potential for HDAC10 inhibition outside of cancer therapy was highlighted by a study that showed long-term allograft survival of $HDAC10^{-/-}$ mice receiving fully MHC-mismatched cardiac transplants.[57] Therefore, mouse studies using a well-tolerated HDAC10i

could pave the way to new therapeutic applications beyond oncology. Even aminohydroxamic acid HDAC10is are not cytotoxic in vitro and phenocopy HDAC10 knock-out. These are good prerequisites for the application of comparably potent non-hydroxamate HDAC10is in immunology. However, more work, especially cellular testing of thiol-based HDAC10is, and potentially more medicinal chemistry towards a suitable prodrug candidate is required.

Using my HDAC10 selective aza-SAHA derivatives, I developed targeted degraders (PROTACs) of HDAC10 (section 3.5) to not only inhibit its enzymatic function, but to remove the entire HDAC10 protein including functions that are independent of its active site. As a proof of principle and to explore the linkerology around HDAC PROTACs, I started with SAHA as the PROTAC warhead, since SAHA-based HDAC6 degraders were already reported at that time and I hypothesized that these compounds may also degrade HDAC10. Indeed SAHA–Thalidomide chimeras like **DKFZ-900** are able to effectively degrade HDAC10 in HL-60 cells, however HDAC6 and potentially other isozymes were also targeted for degradation. Therefore, I synthesized HDAC10 selective degrader **DKFZ-972**, which has not yet been tested. I established a solid-phase PROTAC synthesis[178] of aza-SAHA based degraders which does not require the purification of polar intermediates during the degrader synthesis. Using this solid-phase approach, more derivatives of **DKFZ-972** can be readily prepared. To establish a proteome-wide degrader selectivity profile of my selective PROTACs, I utilized a global proteomics approach. However, in-house LFQ proteomics methods could not quantify HDAC10, even in control samples. A better alternative could be the chemical proteomics approach by Lechner et al.,[128] involving an affinity matrix of beads functionalized with HDAC binders which could be used to selectively enrich HDAC family members for more accurate quantification of low-abundance HDACs and evaluation of their targeted degradation.

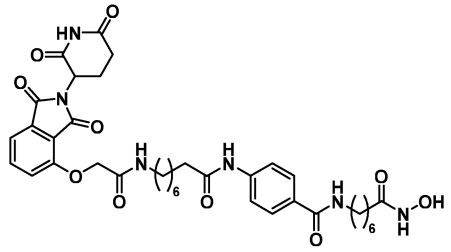


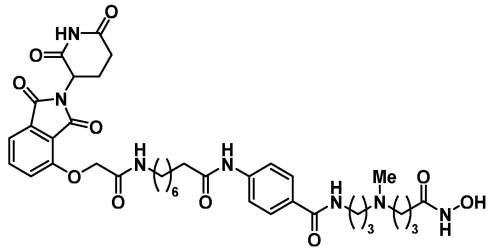


**Figure 56.** Confirmed, unselective SAHA-based HDAC10 degrader (**DKFZ-900**) and potentially HDAC10 selective aza-SAHA-based degrader (**DKFZ-972**).

During my investigations, after I confirmed the degradability of HDAC10 with **DKFZ-900**, Eric Fischer and co-workers reported a large scale chemo-proteomics exploration of the HDAC degradability using a library of 48 pan-inhibitor-based PROTACs.[179] They also found that HDAC10 can be degraded using CRBN-recruiting SAHA-chimeras or Class IIB selective VHL-recruiting chimeras. While they reported multiple HDAC10 degraders, they did not identify a selective HDAC10 degrader, since HDAC6 (and for some compounds also other isozymes) were always co-degraded. Therefore, selective HDAC10 degradation is still an open challenge and compounds like **DKFZ-972** are likely to succeed in it. Another potentially interesting approach could be the utilization of non-hydroxamate scaffolds in targeted HDAC10 degraders.

# 5 Materials and methods

Parts of the materials and methods section were previously published in Steimbach et al.[1] and are reproduced here if necessary in the context of this work. Adopted passages were originally written by me.

## 5.1 Biological methods

### 5.1.1 Cell culture

All cell lines were cultivated under sterile conditions in polystyrene cell culture flasks (Greiner 658170 for adherent cells, Greiner 690195 for suspension cells) at 37 °C and 5% $CO_2$ in a humidified atmosphere using D-MEM growth medium (Sigma D5796), supplemented with 10% FCS (Capricorn Scientific FBS-12A) and 1% penicillin–streptomycin (Sigma P4333) unless stated otherwise. Medium for BE(2)-C cells (full name: "SK-N-BE(2)-C", RRID: CVCL_0529) was additionally supplemented with 1% non-essential amino acids (Sigma M7145). Medium for HL-60 cells was RPMI 1640 (Gibco A1049101), supplemented with 10% FCS and 1% penicillin–streptomycin. Adherent cells were passaged near confluency by removing old medium, washing with DPBS (Gibco 14190-094), trypsinization (Sigma T4049) and seeding in fresh growth medium. HL-60 cells were passaged when the medium became acidic (typically around 1 mio cells/mL) by 1:5 dilution with fresh medium. Cell lines were routinely screened for mycoplasma in-house and verified using DNA fingerprinting authentication by Multiplexion (Heidelberg, Germany).

### 5.1.2 HDAC-Glo assay for HDAC 1, 2, 3, 6 and 8

HDAC6 and Class I HDAC inhibition was tested as previously described[1,182] in using the HDAC-Glo™ I/II Assay and Screening System (G6421, Promega) with recombinant human HDACs (BPS Bioscience; HDAC1 cat. #50051; HDAC2 cat. #50002; HDAC3/NcoR2 complex cat. #50003; HDAC6 cat. #50006; HDAC8 cat. #50008). The assay was carried out in a 384-well plate (Corning 4512) format according to the manufacturer's description. Inhibitors were tested at eight serial dilutions in triplicates ranging from 50 µM – 86.7 pM or 100 µM – 8.67 nM. Drug dosing was performed from 10 mM and 0.1 mM DMSO stock solutions with a D300e Digital Dispenser (Tecan). HDACs (7 ng/mL for HDAC1, 25 ng/mL for HDAC2, 200 ng/mL for HDAC3/Ncor2 complex, 100 ng/mL for HDAC6, 200 ng/mL for HDAC8) and inhibitors were incubated together at rt for 30 min. After addition of the HDAC-Glo™ I/II reagent, plates were shaken (800 rpm orbital shaker, 30 s), centrifuged (300 g, 1 min) and incubated at rt for 30 min. Luminescence was detected with a CLARIOstar (BMG Labtech) plate reader. Luminescence signal was normalized with 100 µM SAHA treated negative controls and uninhibited positive controls. $pIC_{50}$-values were calculated from log(inhibitor) vs normalized luminescence by nonlinear regression four parameters least squares fit of Y=Bottom + (Top-

Bottom)/(1+10^((LogIC$_{50}$-X)*HillSlope)) in GraphPad Prism version 7.05 for Windows, GraphPad Software, La Jolla California USA, www.graphpad.com.

### 5.1.3 HDAC10 TR-FRET assay

TR-FRET assays were performed as previously described[1,182] in white 384-well plates (Corning 4512) using 50 mM HEPES pH 8.0, 150 mM NaCl, 10 mM $MgCl_2$, 1 mM EGTA and 0.01% Brij-35 as buffer. The concentrations of reagent in 15 µL final assay volume were 5 nM TwinStrep-GST-HDAC10 (preparation described previously[182]), 25 nM "Tubastatin-AF647-Tracer" (synthesis described previously[182]) and 0.1 nM DTBTA-$Eu^{3+}$-labelled Streptactin (synthesis described previously[182]). Inhibitors were tested at eight serial dilutions in triplicates ranging from 50 µM – 86.7 pM or 100 µM – 8.67 nM and dosed from 10 mM and 0.1 mM DMSO stock solutions with a D300e Digital Dispenser (Tecan). After drug dosing to the premixed assay reagents in buffer, plates were shaken (800 rpm orbital shaker, 30 s), centrifuged (300 g, 1 min) and incubated at rt in the dark for 90 min. TR-FRET was measured with a CLARIOstar (BMG Labtech) plate reader, equipped with TR-FRET filters. Sample wells were excited with 100 flashes and fluorescence emission detected at 665 nm and 620 nm. FRET ratios were calculated from 665 nm/620 nm ratio and normalized for each plate using 50 µM SAHA treated negative controls and uninhibited positive controls. $pIC_{50}$-values were calculated as described in the HDAC-Glo assay.

### 5.1.4 BRET assay for HDAC6 and HDAC10

Production and cultivation of transfected HeLa mono-clones stably expressing HDAC-nanoBRET fusion proteins for HDAC10 and HDAC6-catalytic domain 2 (HDAC6CD2) was described previously.[1,182] The intracellular target engagement assay on HDAC10 and HDAC6CD2 was performed using the NanoBRET™ Target Engagement Intracellular HDAC Assay[164] (Promega N2081 and N2090) as described by the kit manufacturer in a 96-well plate (Corning 3600) format with $2\times10^4$ cells per well and a tracer concentration of 0.3 µM. Inhibitors were tested at ten serial dilutions in triplicates ranging from 10 µM – 12.9 pM or 40 µM – 139 pM and dosed from 10 mM and 0.1 mM DMSO stock solutions with a D300e Digital Dispenser (Tecan). DMSO concentrations were normalized to 0.5 % for all wells. For the cellular compound stability experiment, **DKFZ-728** was diluted to 10 µM and Tubastatin A to 1 µM in OPTI-MEM (Gibco #11058021), which was used to cultivate BE(2)-C cells for 72 h. After 0, 24, 48 and 72 h, some cell culture medium was removed from the live culture and used to perform the NanoBRET assay with HeLa HDAC10 cells as described above, but by manual serial dilution to eight dose levels in triplicates ranging from 10 µM – 61 nM or 1 µM – 6.1 nM. After dosing, assay plates were shaken at 800 rpm and incubated at 37 °C for 2 h followed by measurement of 450 nm and 650 nm luminescence (80 nm bandwidth) at room temperature with a CLARIOstar (BMG Labtech) plate reader 2 min after NanoLuc substrate addition.

BRET ratios were calculated from 650 nm/450 nm luminescence and normalized for each plate using 50 µM SAHA treated negative controls and uninhibited positive controls. $pIC_{50}$-values were calculated as described in the HDAC-Glo assay.

### 5.1.5 Chemoproteomic profiling

**Preparation of cell lysates for affinity pulldown assays.** BE(2)-C cell lysates were prepared from 30–50 confluent T175 flasks, harvested by trypsination, following three PBS washes and flash freezing of the combined pellets in liquid nitrogen. Lysis was performed by re-suspending the cell pellets in 0.35 mL freshly prepared lysis buffer per harvested confluent T175 flask, incubation for 5 min on ice, then lysates were cleared by ultracentrifugation. Lysis buffer composition: 0.8% IGEPAL, 50 mM Tris-HCl pH 7.5, 5% glycerol, 1.5 mM $MgCl_2$, 150 mM NaCl, 1 mM $Na_3VO_4$, 25 mM NaF, 1 mM DTT, supplemented with protease inhibitors (Sigma S8820-20TAB).

For a description of the competition pulldown assays by LC-MS/MS measurement and proteomics data analysis, see Steimbach et al.[1] For details on the development of the chemoproteomic profiling method, see Lechner et al.[128]

### 5.1.6 SDS-PAGE and Western blot analysis

**Acetylation Western blots** were performed by Johanna Hummel-Eisenbeiß. BE(2)-C cells were seeded in full medium at a density of 5 x $10^6$ cells per 15 cm dish the night before treatment, then treated by replacing the seeding medium with treatment medium containing the indicated drug concentration and 0.2% DMSO for all treatment conditions. Cells were incubated for 4 h, then harvested by PBS wash, trypsinization at 37 °C for 5 min, diluted with full medium at 4 °C and washed by centrifugation and subsequent re-suspending in fresh PBS at 4 °C. Then the cell suspension for each treatment was split into two aliquots for preparation of a whole cell lysate and an aliquot for histone isolation. The supernatant was removed and cell pellets were flash frozen. Whole cell lysates were prepared by adding 1x lysis buffer (Cell Signaling #9803) containing 1x protease inhibitor (Serva #39101.01) to cell pellets, then sonication 2x for 30 s and removal of cell debris by centrifugation with 17000 g at 4 °C for 10 min. Histones were isolated by cell lysis with hypotonic lysis buffer and precipitation with trichloroacetic acid as described previously.[192] Protein concentrations were determined by Bradford assay (Bio-Rad #5000006), then 15 µg protein from histone preparation or whole cell lysate were diluted 5:1 with 5x Lämmli buffer (30% (v/v) glycerin, 3% (wt/v) SDS), 62.5 mM Tris, 4.3 mM bromophenol blue, adjusted to pH 6.8, 0.15 M DTT added freshly) and denatured at 95 °C for 10 min. Samples were loaded onto a freshly prepared 15% polyacrylamide gel. SDS-PAGE and blotting was performed with a Mini PROTEAN Tetra Cell (Bio-Rad, Germany) electrophoresis system and a PowerPac Basic (Bio-Rad, Germany) power supply. SDS-PAGE was run at 80–120 V with running buffer containing 25 mM Tris, 0.19 M glycine and 0.1 % (wt/v) SDS. Proteins were blotted onto a 0.2 µm Amersham Protran nitrocellulose membrane (Cytiva 1060001) for 70 min at 90 V (blotting buffer: 20 mM boric acid, 1 mM EDTA, adjusted to pH 8.8 with NaOH). The membrane was blocked for 1 h at rt with 5% skimmed milk powder (Gerbu #1602) in TBST buffer (20 mM Tris, 136 mM NaCl, 0.1% Tween-20), then incubated with the respective primary antibody, diluted in 5% skimmed milk powder in TBST, overnight at 4 °C. The blot was washed 3 x 10 min with TBST buffer, then incubated with the respective secondary antibody at rt for 1 h, and washed 3 x 10 min prior to

fluorescence readout using an Odyssey Sa Near-Infrared Imaging System. Quantification was performed using Image Studio Lite Version 5.2. Protein Ladder: PageRuler Prestained (Thermo Scientific #26616), primary antibodies: α-tubulin (mouse monoclonal, diluted 1:2000, abcam ab7291), α-tubulin acetyl K40 (rabbit monoclonal, diluted 1:2000, abcam ab179484), histone H3 (rabbit polyclonal, diluted 1:1000, Cell Signaling #9715) and histone H3 acetyl K9 (rabbit monoclonal, diluted 1:1000, Cell Signaling #9649), secondary antibodies: IRDye 680RD donkey anti-mouse IgG (diluted 1:10000, LI-COR Biosciences #926-68072), IRDye 800CW donkey anti-rabbit IgG (diluted 1:10000, LI-COR Biosciences #926-32213).

**HDAC degradation Western blots against HDAC10, 6 and 1** were performed by Hannah Steffke and Johanna Hummel-Eisenbeiß. Cells were treated in 6-well plates (HL-60: 1.5 mio cells per well, BE(2)-C: 0.75 mio cells per well) in a final volume of 4 mL full medium per well by adding 1 mL of 4x drug treatment solution to reach the desired drug concentration, DMSO content was normalized to 0.1 %. Cell were incubated for the indicated treatment time at 37 °C and 5% $CO_2$ in a humidified atmosphere. HL-60 cells were harvested by centrifugation followed by PBS wash. BE(2)-C were harvested by, trypsinization, diluted with full medium at 4 °C and washed with PBS. Supernatants were removed and cell pellets were flash frozen. Whole cell lysates were prepared using 50 µL lysis buffer as described for the acetylation Western blots. SDS-PAGE and Western blotting was performed as described for the acetylation Western blots. Primary antibodies: HDAC1 (mouse monoclonal, diluted 1:1000, Cell Signaling #5356 clone 10E2), HDAC6 (rabbit monoclonal, diluted 1:1000, Cell Signaling #7558 clone D2E5), HDAC10 (mouse hybridoma supernatant supplemented with 0.03% $NaN_3$, used without dilution, supplied by Dr. Johannes Ridinger (Oehme Lab, DKFZ Heidelberg)).

### 5.1.7 Label-free quantification proteomics for evaluation of targeted degraders

Proteomics analysis was performed at the Genomics and Proteomics Core Facility (DKFZ Heidelberg) in collaboration with Dr. Dominic Helm, and statistical analysis was conducted by Martin Schneider. They provided the method description for sample preparation, LC/MS analysis of the full proteome and data analysis.

**Cell treatment and lysis** was performed by Hannah Steffke as described for the HDAC degradation Western blots.

**Sample Preparation.** Proteins were run for 0.5 cm into an SDS-PAGE. After Coomassie staining the whole band was cut out and used for subsequent tryptic digestion according to Shevchenko et al.[211] adapted to on a DigestPro MSi robotic system (INTAVIS Bioanalytical Instruments AG).

**LC/MS analysis of full proteome (150 min method)** was carried out for a total of 150 mins on an Ultimate 3000 UPLC system directly connected to an Orbitrap Exploris 480 mass spectrometer (both Thermo Fisher Scientific). Peptides were online desalted on a trapping cartridge (Acclaim PepMap300 C18, 5 µm, 300Å wide pore; Thermo Fisher Scientific) for 3 min using 30 µL/min flow of 0.05% TFA in water. The analytical multistep gradient was carried out on a nanoEase MZ Peptide analytical column (300 Å, 1.7 µm, 75 µm x 200 mm, Waters) using

solvent A (0.1% formic acid in water) and solvent B (0.1% formic acid in acetonitrile). For 134 min the concentration of B was linearly ramped from 4% to 30%, followed by a quick ramp to 78%, after two minutes the concentration of B was lowered to 2% and a 10 min equilibration step appended. Eluting peptides were analyzed in the mass spectrometer using data depend acquisition (DDA) mode. A full scan at 120k resolution (380-1400 m/z, 300% AGC target, 45 ms maxIT) was followed by up to 2 seconds of MS/MS scans. Peptide features were isolated with a window of 1.4 m/z, fragmented using 26% NCE. Fragment spectra were recorded at 15k resolution (100% AGC target, 22 ms maxIT). Unassigned and singly charged eluting features were excluded from fragmentation and dynamic exclusion was set to 35 s.

**Data analysis** was carried out by MaxQuant (version 1.6.14.0),[212] using databases extracted from Uniprot.org under default settings (human containing 74811 entries from 27.02.2020). Identification FDR cutoffs were 0.01 on peptide level and 0.01 on protein level. The match between runs (MBR) option was enabled to transfer peptide identifications across RAW files based on accurate retention time and m/z. LFQ quantification was done using a label free quantification approach based on the MaxLFQ algorithm.[213] A minimum of 2 quantified peptides per protein was required for protein quantification.

**Statistics** was adapted from the Perseus recommendations[214] protein groups with valid LFQ values in 70% of the samples of at least one condition were used for statistics. For the LFQ values, no further normalization was performed. Adapted from the Perseus recommendations,[214] missing LFQ values being completely absent in one condition were imputed with random values drawn from a downshifted (2.2 standard deviation) and narrowed (0.3 standard deviations) intensity distribution of the individual samples. For missing values with no complete absence in one condition, the R package missForest was used for imputation.[215] The statistical analysis was performed with the R-package limma.[216] The p-values were adjusted with the Benjamini–Hochberg method for multiple testing.[217]

### 5.1.8 Cytotoxicity assay

Cells were seeded the previous day in 96-well plates (Greiner 655 180) in full medium. Initial seeding densities were for BE(2)-C 5.5k, for HEK293T 2.5k and for HeLa 1.25k cells per well. Drugs were dosed in triplicates for each dose level from DMSO stock solutions with a D300e Digital Dispenser (Tecan) once and all wells were normalized to 0.5% DMSO. Cells were cultivated for 72 h after dosing, then per well 50 µL CellTiter-Blue (Promega G8081) solution, diluted 1:5 in medium, was added and plates were incubated at 37 °C for at least 90 min. Fluorescence was recorded at 560/590 nm in a CLARIOstar (BMG Labtech) plate reader. Full viability was defined by vehicle controls, 0% viability was defined by only medium containing wells. $pIC_{50}$-values were calculated using log(inhibitor) vs normalized fluorescence by nonlinear regression four parameters least squares fit in GraphPad Prism version 7.05 for Windows, GraphPad Software, La Jolla California USA, www.graphpad.com.

### 5.1.9 Targeted metabolomics of acetylated spermidines

**Preparation of inhibitor-treated cell samples.** BE(2)-C cells were seeded in a volume of 19 mL full medium at a density of 2.9 x $10^6$ cells per 15 cm dish the night before treatment, then 1 mL of 20x drug treatment solution in full medium was added to reach the indicated drug concentration and 0.4% DMSO for all treatment conditions. Cells were cultivated for 24 h and checked for equal confluency (70–100%) in all treatment conditions before harvest. Then, the medium was removed, cells were washed with 0.9% NaCl (Braun #08609249), detached by trypsinization at 37 °C for 5 min, diluted with full medium at 4 °C and washed two times at 4 °C by centrifugation at 300 g and 4 °C for 5 min and subsequent re-suspending in fresh 0.9% NaCl. Then, 10 x $10^6$ cells from each replicate were taken, as confirmed by cell counting of small aliquots, and pelleted by centrifugation at 1000 g and 4 °C for 5 min. Supernatant was aspirated and cell pellets were snap-frozen in liquid nitrogen before storage at –80 °C.

**Preparation of HDAC10 knockdown cell samples** was performed by Dr. Johannes Ridinger. BE(2)-C cells were seeded at a density of 0.4 x $10^6$ cells per 10 cm dish on 17 dishes per replicate, allowing for three technical replicates per condition. Transfection with siRNAs against HDAC10 or with control siRNAs was performed as described previously.[218] A pool of two siRNAs was used against HDAC10 (Ambion/ThermoFisher Scientific siRNA IDs 33581, 120681) and for negative control transfection, respectively (Silencer Negative Control #1 and Silencer Negative Control #5, Ambion/ThermoFisher Scientific AM4611, AM4642). Medium was changed on the morning following transfection. For harvesting, cells were washed in ice-cold sterile 0.9% NaCl, then trypsinized and transferred to 50 mL Falcon tubes. A fraction of the cell suspension (750 µL) was used for cell counting (Vi-Cell XR automated cell counter, Beckmann Coulter). Cells were centrifuged at 300 g and 4 °C for 5 min and washed with 0.9% NaCl, then resuspended in 0.9% NaCl at a cell number of 10 x $10^6$ cells per mL. Of this cell suspension, 15 x $10^6$ cells for quantification of acetyled spermidines were transferred to pre-cooled 1.5 mL Eppendorf tubes. Cells were centrifuged in a table-top centrifuge at 2700 g for 3 min at 4 °C. Supernatant was aspirated and cell pellets were snap-frozen in liquid nitrogen before storage at –80°C.

**Extraction and quantification of acetylated spermidines**[89,194] was performed by Dr. Glynis Klinke, the method was developed in collaboration with me. For quantification of acetylated spermidines, pellets of at least 10 x $10^6$ cells were extracted two times on ice with 300 µL MeOH/MeCN (50:50) by vortexing, followed by 5 min centrifugation. The resulting supernatants were transferred to a new Eppendorf tube, dried without heat using the Eppendorf Concentrator Plus (Eppendorf, Hamburg), then re-suspended in 75 µL water. LC-MS/MS analysis was performed on a Waters Acquity I-class Plus UPLC system (Binary Solvent Manager, thermostatic Column Manager and FTN Sample Manager) (Waters, USA) coupled to an QTRAP 6500+ (Sciex, USA) mass spectrometer with electrospray ionization (ESI) source using the following settings: curtain gas: 30 psi; collision gas: low; ion spray: 4500 V; source temperature: 500 °C; ion source gas 1:40 (GS1) and ion source gas 2:50 (GS2).

Acetylated spermidines were separated by chromatography on an Acquity HSS T3 column (150 mm x 2.1 mm, 1.7 µm, Waters) kept at 20 °C and a flow rate of 0.3 mL/min. Eluent A: water +

0.1% formic acid, eluent B: MeCN + 0.1% formic acid. Gradient: 0% B for 1 min, 0 → 20% B over 4 min, 20 → 100% B in 0.5 min, then 100% B for 1 min.

Identification and quantification of acetylation isomers was based on unique transitions extracted from the MS/MS fragmentation patterns of commercially available standards of $N^1$-acetylspermidine (Cayman Chemical #9001535), $N^8$-acetylspermidine (MedChemExpress #HY-113253A) and $N^{1,8}$-diacetylspermidine (Cayman Chemical #21588). Fragmentation patterns and relative retention times shown below are in accordance with previously reported data.[89]

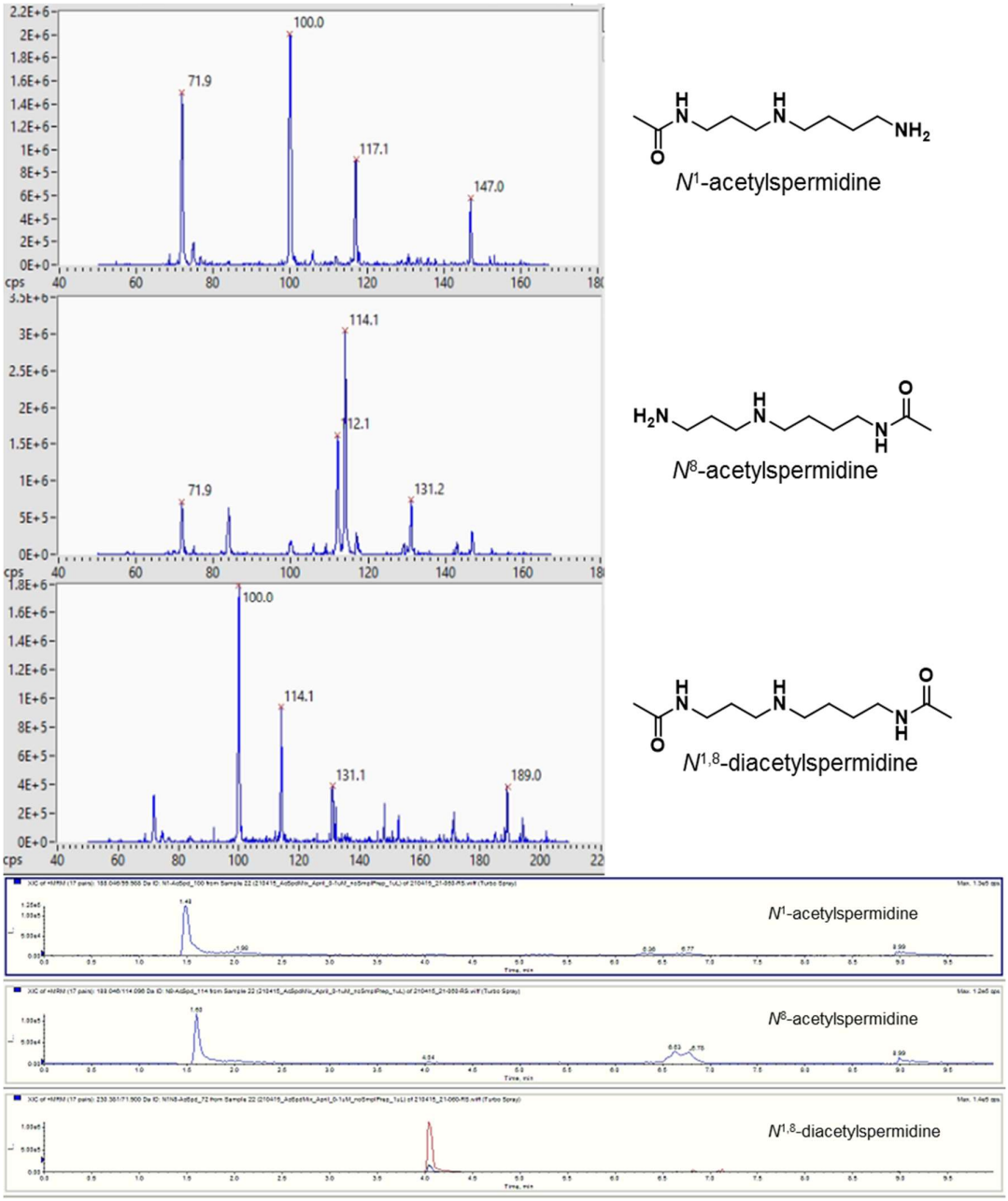


Fragmentation patterns of acetylated spermidines (top) and chromatographic traces (bottom) of acetylation isomer specific transitions. $N^1$-acetylspermidine: 188.046/99.998; $N^8$-acetylspermidine: 188.046/114.096; $N^{1,8}$-diacetylspermidine: 230.381/99.990 (red), 230.381/71.900 (blue).

Acetylated spermidines were quantified in positive electrospray ion mode with the settings and specific transitions described in the following table:

| Compound | Quantifier/ Qualifier transition | Q1 mass (Da) | Q3 mass (Da) | Dwell time (msec) | DP (volt) | EP (volt) | CE (volt) | CXP (volt) |
|---|---|---|---|---|---|---|---|---|
| ***N*$^{1}$-acetylspermidine** | Quantifier | 188.046 | 99.988 | 60 | 25 | 10 | 23 | 11 |
| | Qualifier 1 | 188.046 | 117.118 | 60 | 25 | 10 | 16 | 13 |
| ***N*$^{1,8}$-diacetylspermidine** | Quantifier | 230.381 | 99.99 | 60 | 71 | 10 | 29 | 54 |
| | Qualifier 1 | 230.381 | 114.065 | 60 | 71 | 10 | 27 | 52 |
| | Qualifier 2 | 230.381 | 71.9 | 60 | 71 | 10 | 39 | 4 |
| ***N*$^{8}$-acetylspermidine** | Quantifier | 188.046 | 114.096 | 60 | 25 | 10 | 23 | 12 |
| | Qualifier 1 | 188.046 | 112.149 | 60 | 25 | 10 | 27 | 7 |
| | Qualifier 2 | 188.046 | 131.192 | 60 | 25 | 10 | 20 | 8 |

Q1 mass: precursor ion (m/z), Q3 mass: product ion (m/z). EP: entrance potential, CE: collision energy, CXP: cell exist potential.

Calibration curves were generated from standard solutions prepared in 0.1 M HCl and are depicted below. Data acquisition was performed with Analyst (Sciex, USA), while data quantification was performed with the SciexOS software suite (Sciex, USA).

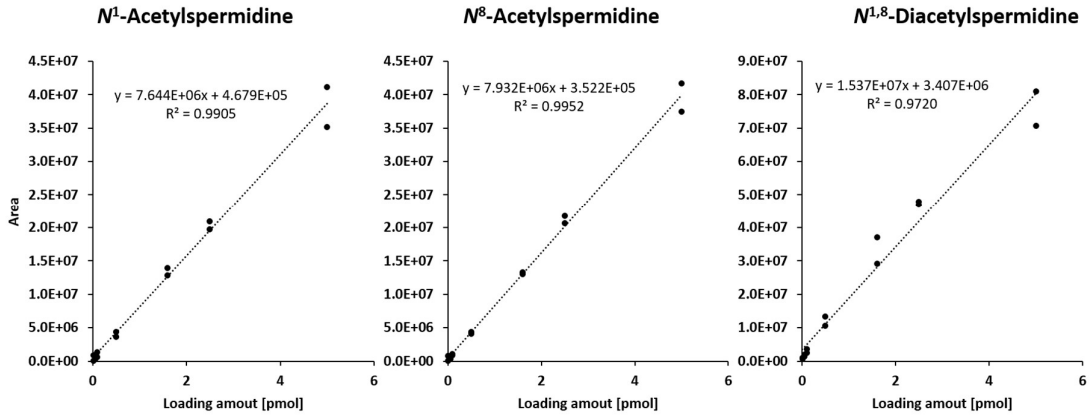


Calibration curves generated for *N*$^{1}$-acetylspermidine ($R_t$ = 1.49 min), *N*$^{8}$-acetylspermidine ($R_t$ = 1.62 min) and *N*$^{1,8}$-diacetylspermidine ($R_t$ = 4.05 min) from external standards using seven calibration points in duplicates.

## 5.2 Organic synthesis

Chemicals and solvents were purchased from commercial sources (Sigma-Aldrich, Merck, Acros Organics, VWR, Roth, Alfa Aesar, Th. Geyer, Fisher Chemical and abcr) at the highest level of purity and were used without purification unless stated otherwise. Anhydrous tetrahydrofuran and $CH_2Cl_2$ were dispensed with an MBraun SPS800 Solvent Purification System. All reactions were stirred magnetically and external bath temperatures are reported for heating.

**Solid phase synthesis (SPS)** was performed in 5 mL fritted syringes with Luer stop caps using 2-chlorotrityl chloride resin either from Novabiochem (100–200 mesh, 1% DVB, 1.06 mmol/g loading capacity, #8.55017.0005) or from Bachem (200–400 mesh, 1% DVB, 1.90 mmol/g loading capacity, #4025425). Washes were performed by removing the previous solution and replacing it with the largest possible amount of washing solvent (4–5 mL) and an air bubble (~0.5 mL), which was used to agitate the suspended resin by end over end rotation (~1.5 $s^{-1}$) at rt for at least 5 min per wash. Reactions were performed at rt with the minimal amount of solvent required to suspend the resin and to allow for effective mixing with an air bubble in the syringe by end over end rotation (~1.5 $s^{-1}$). Complete removal of reagents from the resin, especially after piperidine Fmoc deprotection, was routinely tested by TLC of the eluting wash solution. Reactions were monitored by ninhydrin testing of a small amount of beads, if applicable, or by test cleavage (2 × 0.1 mL, 5% TFA in $CH_2Cl_2$, 5 min each) of a small amount of beads and LC/MS analysis of the cleavage solution diluted with MeOH. The ninhydrin test was performed by suspending beads in a 1.5 mL Eppendorf tube in 0.25 mL ninhydrin TLC stain solution and heating to 85°C with 300 rpm shaking for 5 min. Yellow beads in a yellow solution indicated that no free amines are present. A blue to purple solution and blue to brown beads indicated presence of unprotected primary amines. Tertiary amine containing resins typically gave a yellow solution and green beads.

**Thin layer chromatography (TLC)** was carried out on glass silica plates (TLC Silica gel 60 $F_{254}$; Merck). TLC visualization was accomplished using 254 and 366 nm UV light, iodine saturated silica gel, ninhydrin stain (3 g ninhydrin, 200 mL n-butanol, 6 mL AcOH) or permanganate stain (6 g $KMnO_4$, 40 g $K_2CO_3$, 6.2 mL 2 M NaOH, 800 mL $H_2O$).

**High resolution mass spectrometry** was recorded on a Bruker ApexQe FT-ICR instrument, (Institute of Organic Chemistry, Heidelberg University).

**NMR** spectra were recorded on Bruker Avance 14.1 T and Avance III 9.4 T (German Cancer Research Center Heidelberg) or Bruker Avance III 14.1 T (Institute of Inorganic Chemistry, Heidelberg University) NMR spectrometers operating at 600 or 400 MHz for $^{1}H$ nuclei and 150 or 100 MHz for $^{13}C$ nuclei. Spectra were recorded at 298.1 K. Spectra were analyzed in MestReNova 14.3.0 and referenced to the residual solvent signal.

**Analytical HPLC/MS** was performed on an Agilent 1260 Infinity system equipped with a 6120 Quadrupole mass detector and evaporative light scattering detector (ELSD).

| method name | column | solvent system | gradient |
|---|---|---|---|
| Acidic Method | Kinetex 2.6 µm C18 100 Å, LC column 50 x 2.1 mm; 40 °C; flow rate: 0.06 mL/min | A: $H_2O$, 0.01% HCOOH<br>B: MeCN | 1% B → 90% B over 6 min, then 90% B to 99% B over 2 min |
| Basic Method | Gemini 5 µm C18 110 Å, LC column 50 x 2 mm; 40 °C; flow rate: 0.06 mL/min | A: $H_2O$, 0.1% $NH_4OH$ (25% aqueous solution);<br>B: MeCN | 1% B → 90% B over 6 min, then 90% B to 99% B over 2 min |

UV-detection at 210 to 500 nm in 4 nm steps.

**Medium pressure column chromatography (MPLC)** was performed in normal or reverse phase (RP) with a RediSep Rf system (Teledyne Isco) and RediSep Rf columns (Teledyne Isco). For RP purification, solvent A was $H_2O$ and B was MeCN unless stated otherwise. Normal phase separations used eluents as described.

**Preparative HPLC** was performed on an Agilent 1260 Infinity system.

| method name | column | solvent system |
|---|---|---|
| Acidic Method | Kinetex 5 µm C18 100 Å, AXIA packed column 250 x 21.2 mm; 20 °C; flow rate: 15.0 mL/min | A: $H_2O$, 0.05% TFA; B: MeCN |
| Basic Method | Gemini 5 µm C18 110 Å, AXIA packed column 250 x 21.2 mm; 20 °C; flow rate: 15.0 mL/min | A: $H_2O$, 0.1% $NH_3$; B: MeCN |

Fractions were collected by UV-signal at 254 and 230 nm.

Water was removed by lyophilization with a Christ alpha 2-4 LD plus freeze-dryer.

## 5.2.1 General procedures

**General Procedure A: preparation of hydroxamic acids with hydroxylamine[1]**

To a stirred solution of "methyl ester" (typically 50–200 mg, 1.0 equiv) in 1,4-dioxane (0.5–2 mL), was added KCN (0.6 equiv) and the resulting mixture was stirred at rt for 1 h. Then an aqueous solution of hydroxylamine (50%, 0.5–2 mL, minimum of 30 equiv) was added. The solution was stirred at rt for usually up to 24 hours, until TLC indicated complete conversion. The reaction mixture was concentrated in vacuo, re-concentrated from MeOH to dryness, and then dissolved in a minimal volume of water/MeOH. Purification was usually carried out by preparative RP-HPLC or RP-MPLC as described in the respective procedures.

**General Procedure B: amide coupling with EDC[1]**

To a suspension of diamine **S17**·2HCl (typically 80–200 mg, 1.0 equiv), "carboxylic acid" (1.1 equiv), HOBt (catalytic amounts; only for sterically hindered acids) and EDC (1.3 equiv) in $CH_2Cl_2$ (5–10 mL) was added *i*-$Pr_2NEt$ (3.5 equiv). The reaction mixture was stirred at rt for 12–48 h, until TLC indicated complete consumption of the amine, then concentrated in vacuo, redissolved in EtOAc (50 mL) and washed with saturated aqueous $NaHCO_3$ (2 × 40 mL), brine (40 mL), then dried ($MgSO_4$) and concentrated. The residue was used without further purification unless stated otherwise.

**General Procedure C: reductive amination and esterification of gamma-amino acids[1]**

To a suspension of amino acid **123**·HCl (100–150 mg, 1.0 equiv) and $Na(OAc)_3BH$ (1.5 equiv) in anhydrous THF (2.0 mL) was added "aldehyde" or "ketone" (10 equiv) and $Et_3N$ (2.0 equiv) at 0 °C under nitrogen. After addition, the cooling bath was removed and the reaction mixture

was stirred at rt for 2–3 h, then diluted with water (10 mL), basified with saturated aqueous $NaHCO_3$ to pH 12.0, then concentrated to dryness. The residue was re-dissolved in water (10 mL) and acidified with HCl (25%) to pH 1.0, then the solvent was removed in vacuo. MeOH (25 mL) was added to the residue, stirred for 12–18 h, and then concentrated. The residue was partitioned between saturated aqueous $NaHCO_3$ (30 mL) and $CH_2Cl_2$ (20 mL) and the layers were separated. The aqueous layer was then extracted with $CH_2Cl_2$ (2 × 20 mL). The combined organic layers were dried ($MgSO_4$) and concentrated in vacuo.

**General Procedure D: Coupling of HDACi linker and cap group to *N*-hydroxyphthalimide-loaded resin[178]**

Resin **203** (0.25–0.70 g, 0.2–0.9 mmol resin capacity, 1.0 equiv) was swelled in a 5 mL fritted syringe in DMF for at least 30 min, then washed with MeOH (3 × 5 mL). The phthaloyl group was removed by treatment with 5% hydrazine monohydrate in MeOH (2 × 5 mL, 15 min each), then washed with DMF, MeOH, $CH_2Cl_2$, then again DMF (min 5 × 5 mL each) until no more phthalic acid derivative eluted as observed by TLC (UV and permanganate stain). The desired carboxylic acid (2.0 equiv), HATU (2 equiv), HOBt·$H_2O$ (2 equiv), and *i*-$Pr_2NEt$ (3 equiv, or 5 equiv in the case of linkers with a protonated amine) were dissolved in a minimal amount of DMF (<2.5 mL/mmol acid) required to obtain a clear solution after vortex mixing. The resin was soaked in the coupling solution and agitated by an end over end sample rotator at rt for 16 h, or until negative ninhydrin test, then washed with DMF and $CH_2Cl_2$ (min. 10 × 5 mL each) until no further reactants eluted, as observed by TLC, followed by additional DMF washes (3 × 5 mL).

Fmoc deprotection was performed by soaking the resin in 20% piperidine in DMF (2 × 5 mL, at least 7 min each), followed by washes with DMF and $CH_2Cl_2$ (min. 10 × 5 mL each) until no further reactants eluted as observed by TLC (UV and ninhydrin stain), followed by additional DMF washes (3 × 5 mL).

4-(Fmoc-amino)benzoic acid (3.0 equiv), HATU (3 equiv), and *i*-$Pr_2NEt$ (5 equiv) were dissolved in a minimal amount of DMF (<2.0 mL/mmol acid) required to obtain a clear solution after vortex mixing. The resin was soaked in the coupling solution and agitated by an end over end sample rotator at rt for 16 h, or until negative ninhydrin test, then washed with DMF and $CH_2Cl_2$ (min. 10 × 5 mL each) until no further reactans eluted, as observed by TLC. The resin was washed with DMF (3 × 5 mL) before the next deprotection step, or dried by nitrogen flow followed by vacuum for storage.

Resin loading was determined at this stage by suspending a precisely known amount (10–20 mg) of dry resin in a fresh, fritted syringe and cleaving the Fmoc group with 20% piperidine in DMF (2 mL, at least 20 min), followed by washes with 20% piperidine in DMF (3 × 1 mL). All cleavage and washing solutions were combined quantitatively and adjusted with 20% piperidine in DMF to an exact volume of 5.00 mL. The fulvene-piperidine adduct concentration was determined from a 1:20 dilution in EtOH of the cleavage solution with the same dilution of 20% piperidine in DMF as a blank reference using UV-VIS spectroscopy and $\varepsilon_{300\ nm} = 7800\ M^{-1}cm^{-1}$. The resin loading was calculated from the fulvene-piperidine adduct concentration in the

cleavage solution adjusted to 5.00 mL and the amount of resin cleaved. Typical loadings, depending on the resin used, were in the range of 0.46–0.89 mmol/g.

**General Procedure E: Coupling of PROTAC linker and CRBN ligand to HDACi loaded Fmoc protected resin[178]**

HDACi loaded Fmoc protected resin (0.20–0.25 g, 0.12–0.28 mmol resin capacity, 1.0 equiv) was swelled in a 5 mL fritted syringe in DMF for at least 30 min and Fmoc deprotection was performed as described in General Procedure D. The desired linker carboxylic acid (2.5–3.0 equiv), HATU (2.5–3.0 equiv), and *i*-$Pr_2$NEt (4 equiv) were dissolved in a minimal amount of DMF (<2.0 mL/mmol acid) required to obtain a clear solution after vortex mixing. The resin was soaked in the coupling solution and agitated by an end over end sample rotator at rt for 16 h, or until negative ninhydrin test, then washed with DMF and $CH_2Cl_2$ (min. 10 × 5 mL each) until no further reactants eluted, as observed by TLC, followed by additional DMF washes (3 × 5 mL). Then, Fmoc deprotection was performed as described in General Procedure D.

Acid **206** (2.0 equiv), HATU (2.2 equiv), and *i*-$Pr_2$NEt (4 equiv) were dissolved in a minimal amount of DMF (<3.5 mL/mmol acid) required to obtain a clear solution after vortex mixing. The resin was soaked in the coupling solution and agitated by an end over end sample rotator at rt for 6–16 h, then washed with DMF and $CH_2Cl_2$ (min. 10 × 5 mL each) until no further reactants eluted, as observed by TLC.

The resin was cleaved with 5% TFA in $CH_2Cl_2$ (1 mL) by mixing at rt for 1 h, followed by washes with 5% TFA in $CH_2Cl_2$ (at least 5 × 5 mL). Longer and repeated incubation with the cleaving solution can provide higher yields, but also resulted in increased hydrolysis of the hydroxamic acid and difficult separations. Combined cleavage solutions were concentrated under reduced pressure and the residue was purified by preparative RP-HPLC or RP-MPLC as described in the respective procedures.

## 5.2.2 Synthesis procedures

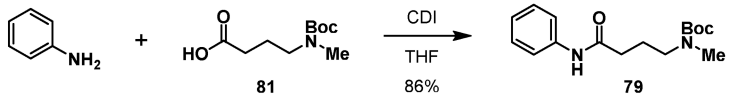


***tert*-Butyl methyl(4-oxo-4-(phenylamino)butyl)carbamate (79)**: To a suspension of carbonyldiimidazole (0.616 g, 3.80 mmol, 1.1 equiv) in THF (5 mL) was added **81**[219] (0.750 g, 3.45 mmol, 1.0 equiv). After 3 h of stirring at rt, aniline (0.299 mL, 3.28 mmol, 0.95 equiv) was added and the reaction mixture was stirred for 5 h at rt, then diluted with EtOAc (50 mL) and water (200 mL). The phases were separated and the aqueous layer was extracted with EtOAc (2 × 50 mL). The combined organic layers were washed with ice cold 0.1 M HCl (2 × 100 mL), saturated aqueous $Na_2CO_3$ (100 mL), then dried ($MgSO_4$), filtered, and concentrated in vacuo to provide **79** as a yellow oil, which solidified into an off-white solid (0.821 g, 2.81 mmol, 86% yield).

**TLC** $R_f$ 0.47 (10% MeOH in $CH_2Cl_2$)

**$^1$H NMR** (600 MHz, $CDCl_3$) δ 9.37 (br s, 1H), 7.64 (br s, 2H), 7.31 (t, *J* = 7.8 Hz, 2H), 7.07 (t, *J* = 7.5 Hz, 1H), 3.36 (br s, 2H), 2.86 (s, 3H), 2.31 (t, *J* = 6.3 Hz, 2H), 1.91 (app p, *J* = 6.5 Hz, 2H), 1.49 (s, 9H) ppm; $^1$H NMR-signals appeared very broad, likely caused by hindered bond rotation.

**$^{13}$C NMR** (151 MHz, $CDCl_3$) δ 171.5, 157.4, 138.9, 129.0, 123.8, 119.7, 80.3, 47.0, 34.6, 34.3, 28.6, 24.4 ppm

**LC/MS** (*m/z*): $[M+Na]^+$ calcd for $C_{16}H_{24}N_2NaO_3^+$: 315.2; found: 315.2

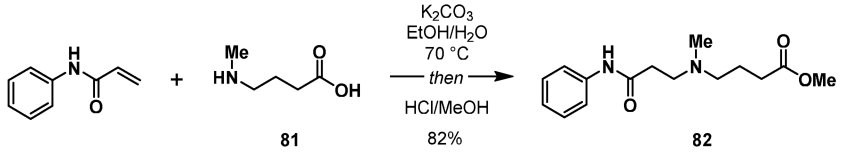


**Methyl 4-(methyl(3-oxo-3-(phenylamino)propyl)amino)butanoate** (**82**): *N*-phenylacrylamide (2.00 g, 13.59 mmol, 1.0 equiv), **81**·HCl (2.30 g, 14.95 mmol, 1.1 equiv) and $K_2CO_3$ (3.76 g, 27.18 mmol, 2.0 equiv) were suspended in water/EtOH (1:1, 40 mL) and heated to 70 °C. After 7 h, the reaction mixture was cooled to rt, acidified to pH ~1 with 3 M HCl, and evaporated to dryness. The residue was suspended in MeOH (25 mL) and stirred at rt for 3 days, then concentrated in vacuo and purified by MPLC (80 g silica, gradient: 0 → 10% MeOH in $CH_2Cl_2$) to provide the HCl salt of **82** as a yellow amorphous solid, which crystallized over time into a yellow/green solid (3.49 g, 11.09 mmol, 82% yield).

**TLC** $R_f$ 0.4 (10% MeOH in $CH_2Cl_2$)

**$^1$H NMR** (400 MHz, MeOD-$d_4$) δ 7.64 – 7.54 (m, 2H), 7.34 – 7.28 (m, 2H), 7.13 – 7.07 (m, 1H), 3.69 (s, 3H), 3.60 (br s, 1H), 3.45 (br s, 1H), 3.26 (br s, 2H), 2.96 (t, *J* = 6.6 Hz, 2H), 2.93 (s, 3H), 2.52 (t, *J* = 7.0 Hz, 2H), 2.13 – 2.02 (m, 2H) ppm

**$^{13}$C NMR** (101 MHz, MeOD-$d_4$) δ 172.3, 167.9, 137.4, 127.7, 123.3, 119.0, 54.8, 51.2, 50.2, 38.9, 29.1 ($2CH_2$), 18.3 ppm

**LC/MS** (*m/z*): $[M+H]^+$ calcd for $C_{15}H_{23}N_2O_3^+$: 279.2; found: 279.2


**5-(Methylamino)pentanoic acid** (**84**)[220]: A mixture of 1-methylpiperidin-2-one (1.95 g, 17.2 mmol), HCl (8 M, 16 mL) and water (4 mL) was heated to reflux for 18 h, then cooled to rt, diluted with $H_2O$ (20 mL), and concentrated in vacuo. The residue was then re-concentrated from water (20 mL) and then acetone (2 × 20 mL) to provide the HCl salt of **84** as an off-white solid (3.02 g, quant. yield).

**TLC** $R_f$ 0.57 (20% MeOH and 0.5% $NH_4OH$ in $CH_2Cl_2$)

**$^1$H NMR** (400 MHz, DMSO-$d_6$) δ 9.26 – 8.80 (m, 2H), 2.87 – 2.75 (m, 2H), 2.46 (t, *J* = 5.5 Hz, 3H), 2.24 (t, *J* = 7.1 Hz, 2H), 1.68 – 1.56 (m, 2H), 1.56 – 1.46 (m, 2H) ppm

**$^{13}$C NMR** (101 MHz, DMSO-$d_6$) δ 174.1, 47.8, 33.1, 32.2, 24.8, 21.5 ppm

**LC/MS** (*m/z*): $[M+H]^+$ calcd for $C_6H_{14}NO_2^+$: 132.1; found: 132.2

Analytical data is in agreement with literature.[220]

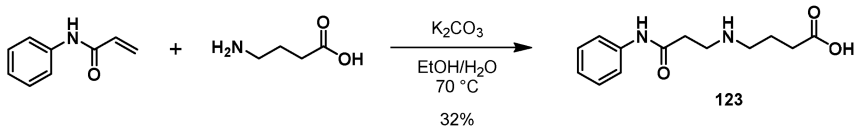


**4-((3-Oxo-3-(phenylamino)propyl)amino)butanoic acid** (**123**): To a stirred solution of gamma-aminobutyric acid (GABA) (3.14 g, 29.90 mmol, 2.2 equiv) and $K_2CO_3$ (2.68 g, 19.40 mmol, 1.4 equiv) in water (27 mL)/EtOH (17 mL), was added dropwise a solution of *N*-phenylacrylamide (2.00 g, 13.59 mmol, 1.0 equiv) in EtOH (10 mL) at 70 °C. The reaction was stirred at 70 °C for 3.5 h, partially concentrated to remove EtOH and the remaining aqueous mixture was extracted with $CH_2Cl_2$ (5 × 20 mL). The organic layers were discarded and the aqueous phase was acidified with HCl, then evaporated to dryness to yield a white solid, which was recrystallized by dissolving in a minimal amount of water/MeOH at 50 °C and then concentrating under reduced pressure at 50 °C until precipitation was visible, followed by cooling to –20 °C overnight in a freezer. After melting the mixture at rt, crystals were filtered and washed once with ice cold water, then with acetone, to provide the HCl salt of **123** as white crystals (1.239 g, 4.32 mmol, 32% yield).

**TLC** $R_f$ 0.05 (10% water in MeCN)

**$^1$H NMR** (400 MHz, MeOD-$d_4$) δ 7.61 – 7.55 (m, 2H), 7.34 – 7.27 (m, 2H), 7.15 – 7.05 (m, 1H), 3.36 (t, *J* = 6.4 Hz, 2H), 3.18 – 3.09 (m, 2H), 2.87 (t, *J* = 6.4 Hz, 2H), 2.49 (t, *J* = 7.1 Hz, 2H), 2.00 (app p, *J* = 7.1 Hz, 2H) ppm

**$^{13}$C NMR** (101 MHz, MeOD-$d_4$) δ 176.0, 170.1, 139.6, 129.8, 125.3, 121.1, 48.4, 44.8, 32.8, 31.6, 22.4 ppm

**LC/MS** (*m/z*): $[M+H]^+$ calcd for $C_{13}H_{19}N_2O_3^+$: 251.1; found: 251.2, $[M–H]^-$ calcd for $C_{13}H_{17}N_2O_3^-$: 249.1; found: 249.2

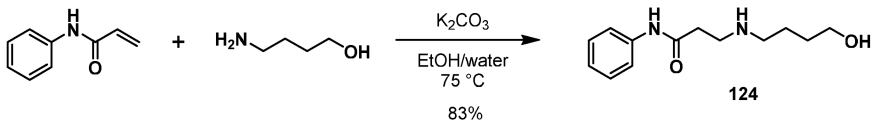


**3-((4-Hydroxybutyl)amino)-*N*-phenylpropanamide** (**124**): To a stirred solution of 1,4-aminobutanol (1.576 g, 17.68 mmol, 2.2 equiv) and $K_2CO_3$ (1.666 g, 12.05 mmol, 1.5 equiv) in water (15 mL), was added dropwise a solution of *N*-phenylacrylamide (1.183 g, 8.036 mmol, 1.0 equiv) in EtOH (15 mL) at 75 °C. After 2 h, the reaction mixture was concentrated in vacuo

until the clear solution became opaque. Saturated aqueous $Na_2CO_3$ (20 mL) was added and the mixture was extracted with EtOAc (2 × 25 mL). The combined organic layers were washed with saturated aqueous $Na_2CO_3$ (1 × 50 mL) then dried ($MgSO_4$), filtered, and concentrated. The product was purified by MPLC (40 g silica, gradient: 5 → 10% MeOH and 0.5% $NH_4OH$ in $CH_2Cl_2$ over 5 CV, 10 → 15% over 14 CV, then 15% → 30% over 8 CV) to provide **124** as a slightly yellow oil (1.576 g, 6.67 mmol, 83% yield).

**TLC** $R_f$ 0.19 (20% MeOH and 0.5% $NH_4OH$ in $CH_2Cl_2$)

**$^1$H NMR** (400 MHz, $CDCl_3$) δ 9.66 (br s, 1H), 7.56 – 7.48 (m, 2H), 7.33 – 7.24 (m, 2H), 7.11 – 7.02 (m, 1H), 3.65 – 3.56 (m, 2H), 3.47 – 3.44 (m, 1H), 2.99 – 2.90 (m, 3H), 2.72 – 2.62 (m, 2H), 2.55 – 2.47 (m, 2H), 1.72 – 1.57 (m, 4H) ppm

**$^{13}$C NMR** (151 MHz, $CDCl_3$) δ 170.8, 138.5, 129.0, 124.0, 119.9, 62.5, 49.5, 45.2, 36.4, 31.7, 27.9 ppm

**LC/MS** (*m/z*): $[M+H]^+$ calcd for $C_{13}H_{21}N_2O_2^+$: 237.2; found: 237.2

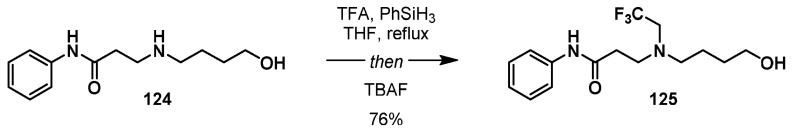


**3-((4-Hydroxybutyl)(2,2,2-trifluoroethyl)amino)-*N*-phenylpropanamide** (**125**): To a solution of **124** (0.613 g, 2.594 mmol, 1.0 equiv) in dry THF (3 mL) was added $PhSiH_3$ (0.640 mL, 5.188 mmol, 2.0 equiv), then TFA (0.397 mL, 5.188 mmol, 2.0 equiv) at 70 °C under an argon atmosphere.[187] Vigorous bubbling ($H_2$ evolution) was immediately observed. The reaction mixture was heated to reflux for 4 h, then concentrated in vacuo, redissolved in $CH_2Cl_2$ (50 mL), then quenched with 1 M NaOH (50 mL) and TBAF (2.60 mL, 1 M solution in THF, 1.0 equiv). The phases were separated and the organic layer was washed with 1 M NaOH (2 × 50 mL), dried ($MgSO_4$), filtered, and concentrated. The product was purified by FCC (160 g silica, eluent: 5% MeOH in $CH_2Cl_2$) to provide **125** as a pale yellow oil (0.701 g, 1.982 mmol based on 90% purity, 76% yield).

**TLC** $R_f$ 0.28 (5% MeOH in $CH_2Cl_2$)

**$^1$H NMR** (400 MHz, $CDCl_3$) δ 9.17 (s, 1H), 7.56 – 7.47 (m, 2H), 7.36 – 7.27 (m, 2H), 7.15 – 7.03 (m, 1H), 3.62 (t, *J* = 5.9 Hz, 2H), 3.16 (app q, *J* = 9.4 Hz, 2H), 3.01 (t, *J* = 6.1 Hz, 2H), 2.76 (t, *J* = 7.2 Hz, 2H), 2.54 (t, *J* = 6.1 Hz, 2H), 2.16 (s, 1H), 1.68 – 1.50 (m, 4H) ppm

**$^{13}$C NMR** (151 MHz, $CDCl_3$) δ 170.0, 138.3, 129.1, 125.5 (q, *J* = 280 Hz), 124.2, 119.9, 62.4, 55.1 (q, *J* = 31 Hz), 54.9, 51.6, 34.9, 30.1, 23.2 ppm

**$^{19}$F NMR** (376 MHz, $CDCl_3$) δ –72.08 ppm

**LC/MS** (*m/z*): $[M+H]^+$ calcd for $C_{15}H_{22}F_3N_2O_2^+$: 319.2; found: 319.2

Note: The compound was obtained with 90% purity, but was sufficiently pure for the next reaction and was used without further purification.

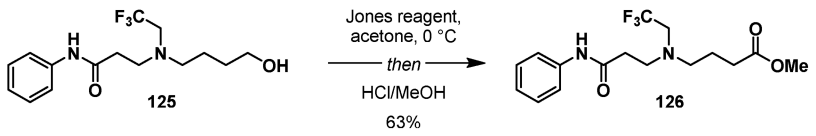


**Methyl 4-((3-oxo-3-(phenylamino)propyl)(2,2,2-trifluoroethyl)amino)butanoate (126)**: To a stirred solution of **125** (0.403 g, 1.138 mmol based on 90% purity, 1.0 equiv) in acetone (7 mL), cooled in an ice bath, was added Jones reagent (2.00 M $CrO_3$ and 3.16 M $H_2SO_4$ in water, 1.26 mL, 2.0 equiv) dropwise until conversion to the carboxylic acid was complete as indicated by TLC (~2.5 h). The reaction was carefully quenched by addition of MeOH (10 mL), then concentrated in vacuo, and re-dissolved in 1 M HCl in MeOH (50 mL). To this solution was added $MgSO_4$ (approx. 1 g) and the mixture stirred for 16 h. Upon complete esterification, solid $NaHCO_3$ was added until the reaction became neutral then the suspension was concentrated to dryness and redissolved in saturated aqueous $NaHCO_3$ (150 mL), then extracted with EtOAc (2 × 60 mL). The combined organic layers were washed with saturated aqueous $NaHCO_3$ (100 mL), dried ($MgSO_4$), filtered, and concentrated. The crude product was purified by MPLC (12 g silica, gradient: 20 → 60% EtOAc in hexane) to provide **126** as a clear, brown oil (246.4 mg, 0.711 mmol, 63% yield).

**TLC** $R_f$ 0.51 (60% EtOAc in hexane)

**$^1$H NMR** (400 MHz, $CDCl_3$) δ 9.03 (s, 1H), 7.56 – 7.47 (m, 2H), 7.33 – 7.27 (m, 2H), 7.11 – 7.05 (m, 1H), 3.65 (s, 3H), 3.13 (q, *J* = 9.4 Hz, 2H), 3.00 (t, *J* = 6.1 Hz, 2H), 2.73 (dd, *J* = 8.5, 6.3 Hz, 2H), 2.50 (t, *J* = 6.1 Hz, 2H), 2.35 (t, *J* = 7.0 Hz, 2H), 1.83 (app p, *J* = 7.0 Hz, 2H) ppm

**$^{13}$C NMR** (151 MHz, $CDCl_3$) δ 173.8, 170.1, 138.2, 129.1, 124.7 (q, *J* = 280.7 Hz), 124.2, 119.9, 55.2 (q, *J* = 30.9 Hz), 53.7, 51.9, 51.8, 35.3, 31.1, 21.9

**$^{19}$F NMR** (376 MHz, $CDCl_3$) δ –72.5 ppm

**LC/MS** (*m/z*): $[M+H]^+$ calcd for $C_{16}H_{22}F_3N_2O_3^+$: 347.2; found: 347.2, $[M+Na]^+$ calcd for $C_{16}H_{21}F_3N_2NaO_3^+$: 369.1; found: 369.2

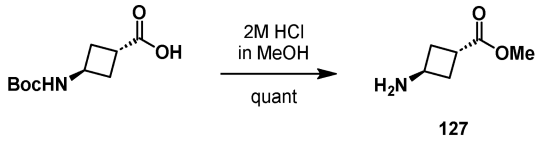


***trans*-Methyl 3-aminocyclobutanecarboxylate (127)**: *N*-Boc-*trans*-3-aminocyclobutane-1-carboxylic acid (0.600 g, 2.79 mmol, 1.0 equiv) was dissolved in 2 M HCl in MeOH (20 mL, 40 mmol, 14.4 equiv) and stirred at rt overnight, then concentrated to dryness and concentrated from MeOH to provide the HCl salt of **127** as slightly yellow solid (0.483 g, quant yield).

**TLC** $R_f$ 0.18 (20% MeOH in $CH_2Cl_2$)

**$^1$H NMR** (400 MHz, MeOD-$d_4$) δ 3.99 – 3.87 (m, 1H), 3.72 (s, 3H), 3.30 – 3.22 (m, 1H), 2.67 – 2.58 (m, 2H), 2.52 – 2.42 (m, 2H) ppm

**$^{13}$C NMR** (151 MHz, MeOD-$d_4$) δ 176.5, 52.6, 45.2, 33.8, 30.9 ppm

**LC/MS** (*m/z*): $[M+H]^+$ calcd for $C_6H_{12}NO_2^+$: 130.1; found: 130.2

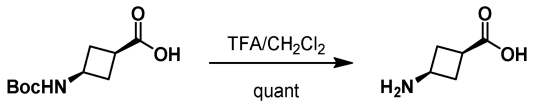


**128**

***cis*-3-Aminocyclobutanecarboxylic acid** (**128**): To a stirred suspension of *N*-Boc-*cis*-3-aminocyclobutane-1-carboxylic acid (0.402 g, 1.87 mmol, 1.0 equiv) in $CH_2Cl_2$ (12 mL) was added TFA (3.0 mL, 39.17 mmol, 21 equiv) at 0 °C. After addition, the ice-bath was removed and the reaction mixture was allowed to warm to rt. After 3.5 h, the reaction mixture was concentrated, dissolved in $CH_2Cl_2$/MeOH, and concentrated provide the TFA salt of **128** as colorless crystals (0.434 g, quant yield).

**TLC** $R_f$ 0.18 (20% MeOH in $CH_2Cl_2$)

**$^1$H NMR** (600 MHz, $D_2O$) δ 3.79 (app p, *J* = 8.3 Hz, 1H), 3.07 (tt, *J* = 9.8, 8.3 Hz, 1H), 2.67 – 2.58 (m, 2H), 2.40 – 2.31 (m, 2H) ppm

**$^{13}$C NMR** (151 MHz, $D_2O$) δ 178.0, 163.0 (q, *J* = 34 Hz), 116.3 (q, *J* = 292 Hz), 41.0, 31.1, 30.1 ppm

**$^{19}$F NMR** (376 MHz, $D_2O$) δ –75.65

**LC/MS** (*m/z*): $[M+H]^+$ calcd for $C_5H_{10}NO_2^+$: 116.1; found: 116.2

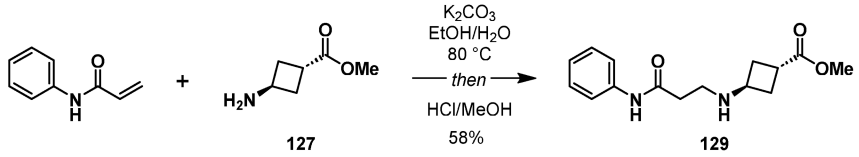


***trans*-Methyl 3-((3-oxo-3-(phenylamino)propyl)amino)cyclobutanecarboxylate** (**129**): A mixture of amino ester **127**·HCl (0.165 g, 1.00 mmol, 1.0 equiv), *N*-phenylacrylamide (0.155 g, 1.05 mmol, 1.05 equiv) and $K_2CO_3$ (0.276 g, 2.00 mmol, 2.0 equiv) in water/EtOH (1:1, 10 mL) was heated to 80 °C. After 38 h, the reaction mixture was cooled to rt, diluted with 1 M HCl (40 mL), washed with EtOAc (2 × 30 mL), and the aqueous layer was then evaporated to dryness. The residue was suspended in MeOH (25 mL), treated with 2 M HCl in MeOH (5 mL), stirred at rt for 3 h, and then concentrated. The residue was partitioned between half saturated aqueous $K_2CO_3$ (40 mL) and $CH_2Cl_2$ and the two layers were separated. The aqueous layer was extracted with $CH_2Cl_2$ (2 × 25 mL), dried ($MgSO_4$), filtered, and concentrated in vacuo. The

product was purified by MPLC (24 g silica, gradient: $CH_2Cl_2$ for 1 CV, then 0 → 10% MeOH in $CH_2Cl_2$ over 10 CV) to provide **129** as a slightly yellow oil (0.160 g, 0.578 mmol, 58% yield).

**TLC** $R_f$ 0.68 (20% MeOH in $CH_2Cl_2$)

**$^1$H NMR** (600 MHz, $CDCl_3$) δ 10.07 (s, 1H), 7.51 – 7.47 (m, 2H), 7.31 – 7.26 (m, 2H), 7.05 (tt, *J* = 7.3, 1.1 Hz, 1H), 3.69 (s, 3H), 3.61 – 3.50 (m, 1H), 3.11 – 3.03 (m, 1H), 2.87 – 2.83 (m, 2H), 2.59 – 2.49 (m, 2H), 2.49 – 2.43 (m, 2H), 2.13 – 2.01 (m, 2H), 1.80 (br s, 1H) ppm

**$^{13}$C NMR** (151 MHz, $CDCl_3$) δ 176.3, 170.9, 138.5, 129.0, 123.9, 119.8, 52.0, 51.3, 42.5, 36.3, 33.0, 32.8 ppm

**LC/MS** (*m/z*): $[M+H]^+$ calcd for $C_{15}H_{21}N_2O_3^+$: 277.2; found: 277.2

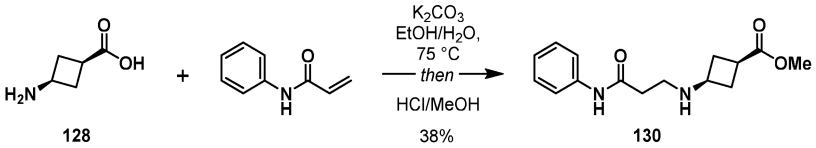


128 38% 130

***cis*-Methyl 3-((3-oxo-3-(phenylamino)propyl)amino)cyclobutanecarboxylate (130)**: Amino acid **128**·TFA (0.243 g, 1.06 mmol, 1.0 equiv), *N*-phenylacrylamide (0.172 g, 1.17 mmol, 1.1 equiv) and $K_2CO_3$ (0.330 g, 2.39 mmol, 2.25 equiv) were dissolved in water/EtOH (1:1, 8 mL) and stirred at 75 °C for 24 h, then cooled to rt, diluted with 1 M HCl (30 mL), extracted with EtOAc (2 × 25 mL) and the aqueous layer evaporated to dryness. The residue was suspended in MeOH (25 mL), acidified with HCl (2 M in MeOH, 1 mL), stirred at rt for 4 h, then concentrated to dryness. The residue was dissolved in half saturated aqueous $K_2CO_3$ (30 mL) and extracted with $CH_2Cl_2$ (4 × 20 mL), dried ($MgSO_4$), filtered, and concentrated in vacuo. The product was purified by MPLC (24 g silica, gradient: 0 → 5% MeOH in $CH_2Cl_2$ over 9 CV, then 5% MeOH over 8 CV) to provide **130** as a slightly colorless oil (0.111 g, 0.402 mmol, 38% yield).

**TLC** $R_f$ 0.40 (20% MeOH in $CH_2Cl_2$)

**$^1$H NMR** (600 MHz, $CDCl_3$) δ 10.15 (br s, 1H), 7.54 – 7.49 (m, 2H), 7.33 – 7.26 (m, 2H), 7.06 (tt, *J* = 7.4, 1.2 Hz, 1H), 3.68 (s, 3H), 3.29 (tt, *J* = 8.5, 7.2 Hz, 1H), 2.89 (br t, *J* = 5.7 Hz, 2H), 2.83 (tt, *J* = 9.2, 8.0 Hz, 1H), 2.59 – 2.53 (m, 2H), 2.46 (br t, *J* = 5.7 Hz, 2H), 2.10 – 2.01 (m, 2H), 1.67 (br s, 1H) ppm

**$^{13}$C NMR** (151 MHz, $CDCl_3$) δ 175.3, 170.9, 138.6, 129.0, 123.9, 119.8, 52.0, 49.3, 42.4, 36.3, 34.0, 31.2 ppm

**LC/MS** (*m/z*): $[M+H]^+$ calcd for $C_{15}H_{21}N_2O_3^+$: 277.2; found: 277.2

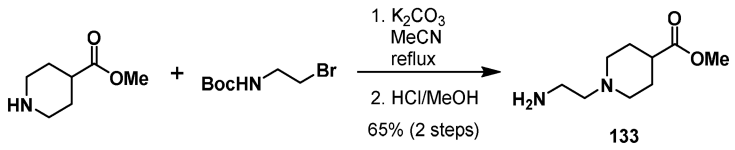


**Methyl 1-(2-aminoethyl)piperidine-4-carboxylate** (**133**): A suspension of methyl piperidine-4-carboxylate hydrochloride (2.50 g, 13.92 mmol, 1.0 equiv), *tert*-butyl (2-bromoethyl)carbamate (3.28 g, 14.61 mmol, 1.05 equiv) and $K_2CO_3$ (5.77 g, 41.75 mmol, 3.0 equiv) in acetonitrile (60 mL) was stirred for 20 h at rt, and then heated to reflux for 3 h, until TLC indicated complete consumption of starting material. The white suspension was filtered, the filter cake washed with $CH_2Cl_2$ (2 × 30 mL) and the filtrate concentrated. The residue was purified by FCC (300 g silica, eluent: 10% MeOH and 0.5% $NH_4OH$ in $CH_2Cl_2$) to provide Boc-protected **133** as a yellow oil that solidified into off-white crystals (2.594 g, 9.059 mmol, 65% yield, *m/z*: $[M+H]^+$: 287.2, TLC $R_f$ 0.65 in 10% MeOH and 0.5% $NH_4OH$ in $CH_2Cl_2$), which were dissolved in 2M HCl in MeOH (113 mL) and stirred at rt for 1.5 h, then concentrated to dryness and further concentrated from MeOH (3 x 100 mL) to provide **133**·2HCl as an off-white solid (2.350 g, 9.059 mmol, quant yield).

**TLC** $R_f$ 0.11 (50% MeOH and 0.5% $NH_4OH$ in $CH_2Cl_2$)

**$^1$H NMR** (400 MHz, DMSO) δ 11.16 (br s, 1H), 8.60 (br s, 3H), 3.63 (s, 3H), 3.60 – 3.48 (m, 2H), 3.37 – 3.25 (m, 4H), 3.05 (br t, *J* = 12.7 Hz, 2H), 2.68 (br t, *J* = 12.5 Hz, 1H), 2.19 – 1.81 (m, 4H) ppm

**$^{13}$C NMR** (151 MHz, MeOD-$d_4$) δ 174.7, 54.7, 53.7, 52.6, 39.3, 35.2, 26.8 ppm

**LC/MS** (*m/z*): $[M+H]^+$ calcd for $C_9H_{19}N_2O_2^+$: 187.1; found: 187.2

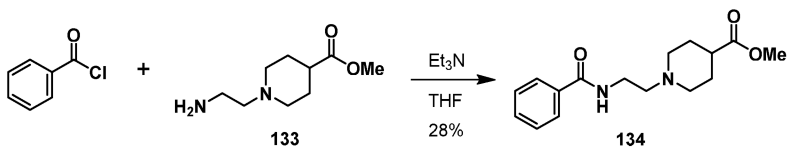


**Methyl 1-(2-benzamidoethyl)piperidine-4-carboxylate** (**134**): To a solution of **133**·2HCl (1.00 g, 3.858 mmol, 1.0 equiv) and $Et_3N$ (2.69 mL, 19.29 mmol, 5.0 equiv) in anhydrous THF (30 mL) was added benzoyl chloride (0.493 mL, 4.244 mmol, 1.1 equiv) at rt under argon. After 2.5 h, the reaction mixture was concentrated under reduced pressure, and partitioned between saturated aqueous $NaHCO_3$ (20 mL) and EtOAc (15 mL). The layers were separated and the aqueous layer was extracted with EtOAc (15 mL). The combined organic layers were dried ($MgSO_4$), filtered, concentrated and purified by FCC (125 g silica, eluent: 4% MeOH and 0.5% $NH_4OH$ in $CH_2Cl_2$) to provide **134** as an off-white solid (343 mg, 1.181 mmol, 28% yield).

**TLC** $R_f$ 0.23 (5% MeOH and 0.5% $NH_4OH$ in $CH_2Cl_2$)

**$^1$H NMR** (400 MHz, DMSO-$d_6$) δ 8.36 (t, *J* = 5.6 Hz, 1H), 7.85 – 7.78 (m, 2H), 7.55 – 7.49 (m, 1H), 7.48 – 7.41 (m, 2H), 3.59 (s, 3H), 3.39 – 3.34 (m, 2H), 2.83 (dt, *J* = 11.6, 3.5 Hz, 2H), 2.44 (t, *J* =

7.0 Hz, 2H), 2.34 – 2.24 (m, 1H), 2.03 (td, *J* = 11.4, 2.6 Hz, 2H), 1.82 – 1.75 (m, 2H), 1.62 – 1.48 (m, 2H) ppm

**$^{13}$C NMR** (151 MHz, DMSO-$d_6$) δ 174.9, 166.1, 134.6, 131.1, 128.3, 127.1, 57.1, 52.4, 51.4, 40.2, 37.0, 28.0 ppm

**LC/MS** (*m/z*): $[M+H]^+$ calcd for $C_{16}H_{23}N_2O_3^+$: 291.2; found: 291.2

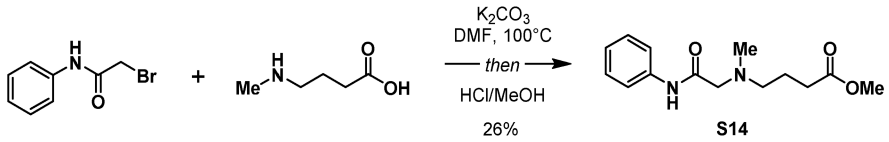


**Methyl 4-(methyl(2-oxo-2-(phenylamino)ethyl)amino)butanoate** (**135**): A suspension of 2-bromo-*N*-phenylacetamide (0.600 g, 2.80 mmol, 1.0 equiv), **81**·HCl (0.450 g, 2.94 mmol, 1.05 equiv) and $K_2CO_3$ (0.775 g, 5.61 mmol, 2.0 equiv) in DMF (10 mL) was stirred at 100 °C for 1 h, then acidified with 2 M HCl (10 mL), and evaporated to dryness. The residue was suspended in MeOH (15 mL), acidified with HCl (2 M in MeOH, 0.5 mL), stirred at rt for 18 h, then concentrated. The residue was partitioned between half saturated aqueous $K_2CO_3$ (25 mL) and $CH_2Cl_2$ (20 mL) and the two layers were separated. The aqueous layer was extracted with $CH_2Cl_2$ (2 × 20 mL). The combined organic layers were dried ($MgSO_4$), filtered, and concentrated in vacuo. The product was purified by MPLC (24 g silica, gradient: 0 → 10% MeOH in $CH_2Cl_2$ over 20 CV) to provide **135** as a colorless oil (0.192 g, 0.726 mmol, 26% yield).

**TLC** $R_f$ 0.69 (10% MeOH in $CH_2Cl_2$)

**$^1$H NMR** (600 MHz, $CDCl_3$) δ 9.06 (br s, 1H), 7.66 – 7.61 (m, 2H), 7.35 – 7.29 (m, 2H), 7.09 (tt, *J* = 7.5, 1.2 Hz, 1H), 3.65 (s, 3H), 3.12 (s, 2H), 2.51 (t, *J* = 7.0 Hz, 2H), 2.39 (t, *J* = 7.0 Hz, 2H), 2.32 (s, 3H), 1.87 (app p, *J* = 7.0 Hz, 2H) ppm

**$^{13}$C NMR** (151 MHz, $CDCl_3$) δ 174.0, 169.1, 137.9, 129.1, 124.2, 119.5, 62.6, 57.5, 51.8, 42.8, 32.2, 22.9 ppm

**LC/MS** (*m/z*): $[M+H]^+$ calcd for $C_{14}H_{21}N_2O_3^+$: 265.2; found: 265.2

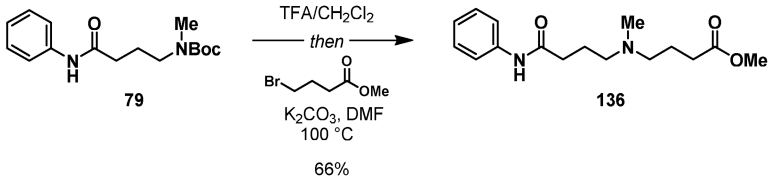


**Methyl 4-(methyl(4-oxo-4-(phenylamino)butyl)amino)butanoate** (**136**): To a solution of **79** (0.810 g, 2.77 mmol, 1.0 equiv) in $CH_2Cl_2$ (8 mL) was added TFA (2.1 mL, 27.7 mmol, 10 equiv). After 1 h, the reaction mixture was concentrated to dryness. The residue was dissolved in DMF (5 mL), and $K_2CO_3$ (1.15 g, 8.31 mmol, 3.0 equiv) and methyl 4-bromobutyrate (0.37 mL, 2.91 mmol, 1.05 equiv) were added. This suspension was heated to 100 °C for 4.5 h, then concentrated and partitioned between half saturated aqueous $K_2CO_3$

(100 mL) and $CH_2Cl_2$ (60 mL). The two layers were separated and the aqueous layer was extracted with $CH_2Cl_2$ (3 × 60 mL). The combined organic layers were washed with saturated aqueous $NaHCO_3$ (100 mL), dried ($MgSO_4$), filtered, and concentrated in vacuo. The crude product was purified by FCC (78 g silica, eluent: 5% then 10% MeOH and 0.5% $NH_4OH$ in $CH_2Cl_2$) to provide **136** as a yellow oil (0.537 g, 1.84 mmol, 66% yield).

**TLC** $R_f$ 0.17 (10% MeOH and 0.5% $NH_4OH$ in $CH_2Cl_2$)

**$^1$H NMR** (600 MHz, $CDCl_3$) δ 9.08 (br s, 1H), 7.56 (d, *J* = 8.0 Hz, 2H), 7.29 (t, *J* = 7.3 Hz, 2H), 7.06 (t, *J* = 7.3 Hz, 1H), 3.66 (s, 3H), 2.48 – 2.40 (m, 6H), 2.35 (t, *J* = 7.0 Hz, 2H), 2.24 (s, 3H), 1.90 – 1.80 (m, 4H) ppm

**$^{13}$C NMR** (151 MHz, $CDCl_3$) δ 174.3, 171.8, 138.8, 129.0, 123.8, 119.6, 57.0, 56.9, 51.8, 41.6, 36.0, 32.3, 23.0, 22.4 ppm

**LC/MS** (*m/z*): $[M+H]^+$ calcd for $C_{16}H_{25}N_2O_3^+$: 293.2; found: 293.2

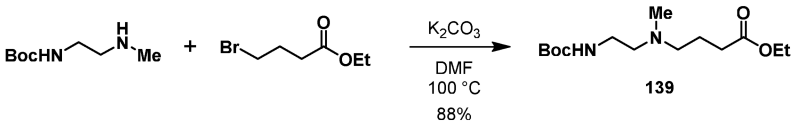


**Ethyl 4-((2-((*tert*-butoxycarbonyl)amino)ethyl)(methyl)amino)butanoate** (**139**): To a suspension of *tert*-butyl (2-(methylamino)ethyl)carbamate (1.52 g, 8.74 mmol, 1.0 equiv) and $K_2CO_3$ (2.42 g, 17.49 mmol, 2.0 equiv) in DMF (9 mL) was added ethyl 4-bromobutyrate (1.38 mL, 9.62 mmol, 1.1 equiv). The reaction mixture was stirred at 100 °C for 16 h, then cooled to rt, poured into water (100 mL) and extracted with EtOAc (3 × 100 mL). The combined organic layers were dried ($MgSO_4$), filtered, and concentrated in vacuo. The product was purified by FCC (280 g silica, eluent: 8% then 20% MeOH in $CH_2Cl_2$) to provide **139** as brown oil (2.21 g, 7.67 mmol, 88% yield).

**TLC** $R_f$ 0.41 (10% MeOH in $CH_2Cl_2$)

**$^1$H NMR** (600 MHz, $CDCl_3$) δ 5.06 (br s, 1H), 4.12 (q, *J* = 7.1 Hz, 2H), 3.18 (app q, *J* = 5.9 Hz, 2H), 2.44 (t, *J* = 5.9 Hz, 2H), 2.37 (t, *J* = 7.2 Hz, 2H), 2.31 (t, *J* = 7.2 Hz, 2H), 2.18 (s, 3H), 1.78 (p, *J* = 7.2 Hz, 2H), 1.43 (s, 9H), 1.24 (t, *J* = 7.1 Hz, 3H) ppm

**$^{13}$C NMR** (151 MHz, $CDCl_3$) δ 173.8, 156.2, 79.1, 60.4, 56.8, 56.7, 41.6, 37.9, 32.2, 28.5, 22.6, 14.4 ppm

**LC/MS** (*m/z*): $[M+H]^+$ calcd for $C_{14}H_{29}N_2O_4^+$: 289.2; found: 289.2

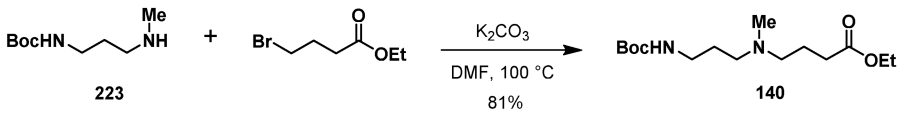


**Ethyl 4-((3-((*tert*-butoxycarbonyl)amino)propyl)(methyl)amino)butanoate (140):** To a stirred suspension of **223** (2.50 g, 13.28 mmol, 1.0 equiv) and $K_2CO_3$ (3.67 g, 26.56 mmol, 2.0

equiv) in DMF (10 mL) was added ethyl 4-bromobutyrate (2.09 mL, 14.61 mmol, 1.1 equiv). The reaction mixture was stirred at 100 °C for 16 h, then cooled to rt and poured into water (180 mL) and extracted with EtOAc (3 × 75 mL). Combined organic layers were dried ($MgSO_4$), filtered and concentrated in vacuo. The crude product was purified by FCC (500 g silica, eluent: 8%, then 12%, then 20% MeOH in $CH_2Cl_2$) and combined product fractions were filtered through a pad of celite to provide **140** as a clear, yellow oil (3.27 g, 10.82 mmol, 81% yield).

**TLC** $R_f$ 0.23 (10% MeOH in $CH_2Cl_2$)

**$^1$H NMR** (400 MHz, $CDCl_3$) δ 5.33 (br s, 1H), 4.12 (q, *J* = 7.1 Hz, 2H), 3.19 (app q, *J* = 6.3 Hz, 2H), 2.50 (br s, 4H), 2.35 (t, *J* = 7.3 Hz, 2H), 2.30 (br s, 3H), 1.91 – 1.79 (m, 2H), 1.78 – 1.66 (m, 2H), 1.43 (s, 9H), 1.25 (t, *J* = 7.1 Hz, 3H) ppm

**LC/MS** (*m/z*): $[M+H]^+$ 303.0

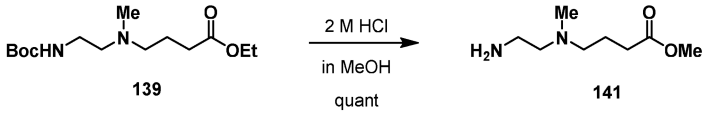


139 141

**Methyl 4-((2-aminoethyl)(methyl)amino)butanoate** (**141**): Ethyl ester **139** (1.80 g, 6.27 mmol, 1 equiv) was dissolved in 2 M HCl in MeOH (8 mL, 156.74 mmol, 25 equiv) and stirred at rt for 26 h. The solvent was removed in vacuo and residual acid was removed by co-evaporation with MeOH (3 × 10 mL) to provide the 2·HCl salt of **141** as a yellow amorphous solid (1.54 g, 6.24 mmol, quant yield). The product was stored as a stock solution in MeOH and used without further purification.

**TLC** $R_f$ 0.08 (20% MeOH in $CH_2Cl_2$), 0.21 (20% MeOH and 0.5% $NH_4OH$ in $CH_2Cl_2$)

**$^1$H NMR** (400 MHz, MeOD-$d_4$) δ 3.70 (s, 3H), 3.62 – 3.43 (m, 4H, $2CH_2$), 3.39 – 3.23 (m, 2H, $CH_2$), 2.98 (s, 3H), 2.53 (t, *J* = 7.0 Hz, 2H), 2.17 – 2.04 (m, 2H) ppm

**$^{13}$C NMR** (101 MHz, MeOD-$d_4$) δ 174.3, 57.1, 53.7, 52.4, 41.0, 35.3, 31.1, 20.4 ppm

**LC/MS** (*m/z*): $[M+H]^+$ calcd for $C_8H_{19}N_2O_2^+$: 175.1; found: 175.2

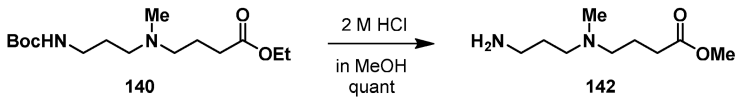


140 142

**Methyl 4-((3-aminopropyl)(methyl)amino)butanoate (142):** Ethyl ester **140** (3.27 g, 10.82 mmol, 1.0 equiv) was dissolved in 2 M HCl in MeOH (135 mL, 270.4 mmol, 25 equiv) and stirred at rt for 26 h. The solvent was removed in vacuo and residual acid was removed by co-evaporation with MeOH (3 × 50 mL) and high vacuum to provide the 2·HCl salt of **142** as a brown-orange amorphous solid (2.924 g, 11.20 mmol, quant yield). The product was stored as a stock solution in MeOH and used without further purification.

**$^1$H NMR** (400 MHz, MeOD-$d_4$) δ 3.70 (s, 3H), 3.44 – 3.14 (m, 4H, partly overlapped with MeOD signal), 3.08 (t, *J* = 7.6 Hz, 2H), 2.93 (s, 3H), 2.52 (t, *J* = 7.0 Hz, 2H), 2.18 (app p, *J* = 7.7 Hz, 2H), 2.13 – 2.02 (m, 2H) ppm

**LC/MS** (*m/z*): $[M+H]^+$ 189.1

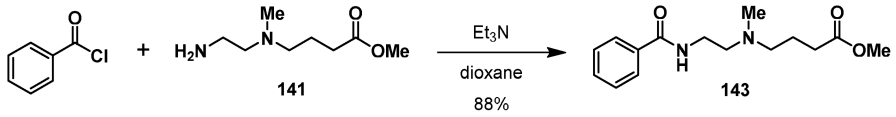


**Methyl 4-((2-benzamidoethyl)(methyl)amino)butanoate** (**143**): To a stirred suspension of **141**·2HCl (375 mg, 1.519 mmol, 1.0 equiv) and $Et_3N$ (0.85 mL, 6.07 mmol, 4.0 equiv) in dioxane (10 mL) was slowly added benzoyl chloride (0.22 mL, 1.898 mmol, 1.25 equiv) at rt. After 2 h, TLC indicated complete conversion. The resulting suspension was filtered, the filter cake washed with dioxane (100 mL) and the filtrate concentrated in vacuo. The residue was dissolved in $CH_2Cl_2$ (40 mL) and washed with saturated aqueous $NaHCO_3$ (2 × 40 mL), dried ($MgSO_4$), filtered, and concentrated. The product was purified by MPLC (12 g silica, gradient: 0 → 2.1% MeOH and 0.5% $NH_4OH$ in $CH_2Cl_2$ over 11.5 CV, then 2.1 → 3% MeOH over 10 CV) to provide **143** as a yellow oil (373 mg, 1.338 mmol, 88% yield).

**TLC** $R_f$ 0.40 (5% MeOH and 0.5% $NH_4OH$ in $CH_2Cl_2$)

**$^1$H NMR** (400 MHz, $CDCl_3$) δ 7.88 – 7.77 (m, 2H), 7.52 – 7.37 (m, 3H), 6.95 (br s, 1H), 3.59 (s, 3H), 3.54 – 3.46 (m, 2H), 2.60 – 2.52 (m, 2H), 2.42 (t, *J* = 6.8 Hz, 2H), 2.36 (t, *J* = 7.1 Hz, 2H), 2.21 (s, 3H), 1.82 (app p, *J* = 6.8 Hz, 2H) ppm

**$^{13}$C NMR** (101 MHz, $CDCl_3$) δ 174.3, 167.5, 134.8, 131.4, 128.6, 127.2, 56.8, 56.5, 51.7, 41.6, 37.3, 32.2, 22.8 ppm

**LC/MS** (*m/z*): $[M+H]^+$ calcd for $C_{15}H_{23}N_2O_3^+$: 279.2; found: 279.2

**HR-MS** (*m/z*): $[2M+Na]^+$ calcd for $C_{30}H_{44}N_4NaO_6^+$: 579.3153; found: 579.3152

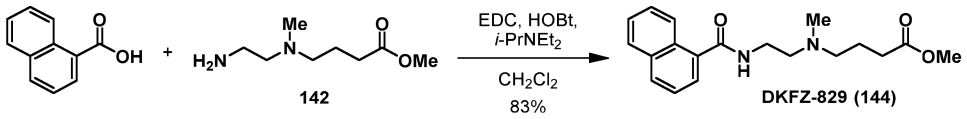


**Methyl 4-((2-(1-naphthamido)ethyl)(methyl)amino)butanoate** (**DKFZ-829, 144**): The title compound was prepared from ester **141**·2HCl (418 mg, 1.692 mmol, 1.0 equiv) and recrystallized 1-naphthoic acid (321 mg, 1.861 mmol, 1.1 equiv) according to General Procedure B. The product was purified by MPLC (12 g silica, gradient: 0 → 7% MeOH with 0.5% NH4OH in $CH_2Cl_2$ over 10 CV) to provide **144** as a pale yellow oil (459 mg, 1.398 mmol, 83% yield).

**TLC** $R_f$ 0.58 (10% MeOH and 0.5% $NH_4OH$ in $CH_2Cl_2$)

**$^1$H NMR** (400 MHz, $CDCl_3$) δ 8.38 – 8.30 (m, 1H), 7.93 – 7.82 (m, 2H), 7.63 (dd, *J* = 7.0, 1.3 Hz, 1H), 7.58 – 7.41 (m, 3H), 6.71 (br s, 1H), 3.64 – 3.55 (m, 2H), 3.48 (s, 3H), 2.64 – 2.57 (m, 2H), 2.41 (t, *J* = 6.9 Hz, 2H), 2.28 (t, *J* = 7.1 Hz, 2H), 2.22 (s, 3H), 1.78 (app p, *J* = 7.0 Hz, 2H) ppm

**$^{13}$C NMR** δ (101 MHz, $CDCl_3$) δ 174.2, 169.7, 134.8, 133.8, 130.5, 130.3, 128.4, 127.1, 126.4, 125.6, 125.2, 124.9, 56.8, 56.4, 51.5, 41.6, 37.4, 32.0, 22.7 ppm

**HR-MS** (*m/z*): $[M+H]^+$ calcd for $C_{19}H_{25}N_2O_3^+$: 329.1860; found: 329.1861

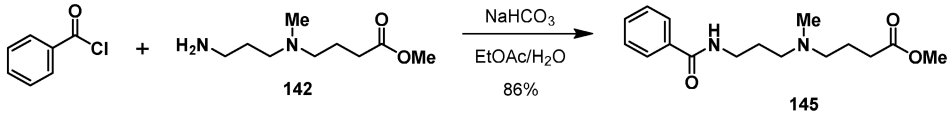


**Methyl 4-((3-benzamidopropyl)(methyl)amino)butanoate (145):** To **142** 2·HCl (182.8 mg, 0.700 mmol, 1.0 equiv) vigorously stirred in sat. $NaHCO_3$ solution (4 mL) and EtOAc (4 mL) was added benzoyl chloride (0.177 mL, 1.54 mmol, 2.2 equiv). After stirring for 90 min, the reaction mixture was diluted with EtOAc (15 mL) and sat. $NaHCO_3$ solution (15 mL), phases were separated, and the aqueous layer was extracted with EtOAc (2 × 20 mL), combined organic layers were dried ($MgSO_4$) and concentrated. The crude product was purified by MPLC (12 g silica, gradient: 0 → 8% for 12 CV, then 8% MeOH in $CH_2Cl_2$ for 12 CV) to provide sufficiently pure **145** as a yellow oil (175.2 mg, approx. 0.599 mmol, approx. 86% yield).

**TLC** $R_f$ 0.20 (10% MeOH in $CH_2Cl_2$)

**$^1$H NMR** (400 MHz, CDCl3) δ 8.10 – 8.01 (m, 1H), 7.87 – 7.80 (m, 2H), 7.51 – 7.33 (m, 4H, impurities), 6.67 (s, 1H), 3.63 (s, 3H), 3.58 – 3.52 (m, 2H), 2.66 (t, *J* = 6.3 Hz, 2H), 2.58 – 2.50 (m, 2H), 2.36 (s, 3H), 2.32 (t, *J* = 7.2 Hz, 2H), 1.92 – 1.80 (m, 4H) ppm

**LC/MS** (*m/z*): $[M+H]^+$ 292.9

Note: The compound was obtained with less than 95% purity. Benzoyl chloride was the main impurity, but the material was sufficiently pure for the next reaction and was used without further purification.

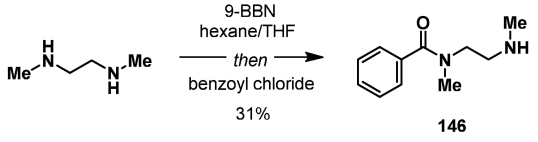


***N*-methyl-*N*-(2-(methylamino)ethyl)benzamide (146)**[188]: To a stirred solution of 9-BBN in hexanes (0.40 M, 15.95 mL, 6.379 mmol, 1.05 equiv) was added a solution of 1,2-dimethylethylenediamine (0.69 mL, 6.379 mmol, 1.05 equiv) in anhydrous THF (25 mL) at rt. After 1 h, benzoyl chloride (0.70 mL, 6.075 mmol, 1.0 equiv) was added. After 2.5 h, the reaction mixture was quenched with saturated aqueous $NaHCO_3$ (300 mL) and extracted with EtOAc (3 × 120 mL). The combined organic layers were dried ($MgSO_4$), filtered, and concentrated. The crude product was purified by MPLC (24 g silica, gradient: 0 → 9% MeOH and 0.5% $NH_4OH$ in

$CH_2Cl_2$ over 5 CV, 9% for 2 CV, 9 → 15% over 2.5 CV, then 15% for 3 CV) to provide **146** as a yellow oil (357 mg, 1.857 mmol, 31% yield).

**TLC** $R_f$ 0.27 (20% MeOH and 0.5% $NH_4OH$ in $CH_2Cl_2$)

**$^1$H NMR** (400 MHz, $CDCl_3$) δ 7.55 – 7.28 (m, 5H), 3.66 (br s, 2H, rotamer A), 3.37 (br s, 2H, rotamer B), 3.09 (br s, 3H. rotamer B), 2.99 (s, 3H, rotamer A), 2.88 (s, 2H, rotamer A), 2.72 (s, 2H, rotamer B), 2.49 (s, 3H, rotamer A), 2.29 (s, 3H, rotamer B) ppm

**LC/MS** *m/z*: $[M+H]^+$: calcd for $C_{11}H_{17}N_2O^+$: 193.1; found: 193.2

Analytical data is in agreement with literature.[188]

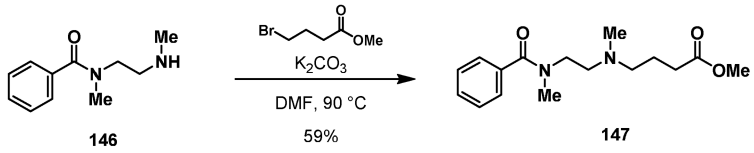


146 147

**Methyl 4-(methyl(2-(*N*-methylbenzamido)ethyl)amino)butanoate** (**147**): To a solution of amine **146** (357 mg, 1.857 mmol) in DMF (4.5 mL) was added $K_2CO_3$ (0.763 g, 5.521 mmol, 3.0 equiv) and methyl 4-bromobutyrate (0.37 mL, 2.899 mmol, 1.56 equiv). The suspension was stirred at 90 °C for 4 h, then poured into saturated aqueous $NaHCO_3$ (150 mL) and extracted with $CH_2Cl_2$ (3 × 60 mL). The combined organic layers were dried ($MgSO_4$), filtered, and concentrated. The product was purified by MPLC (12 g silica, gradient: 1 → 4.5% MeOH and 0.5% $NH_4OH$ in $CH_2Cl_2$ over 7 CV, then 4.5 → 5% over 9 CV) to provide **147** as a yellow oil (320 mg, 1.093 mmol, 59%).

**TLC** $R_f$ 0.49 (10% MeOH and 0.5% $NH_4OH$ in $CH_2Cl_2$).

**$^1$H NMR** (400 MHz, $CDCl_3$) δ 7.38 (s, 5H, Ar H), 3.65 (s, 4H, –$COOCH_3$ and $CH_2$ rotamer A), 3.30 (t, *J* = 5.9 Hz, 1H, $CH_2$ rotamer B), 3.17 – 2.89 (m, 3H, –$CONCH_3$– both rotamers), 2.67 (br s, 1H, $CH_2$ rotamer A), 2.57 – 2.14 (m, 6.5H, $CH_2$ rotamer B, $2CH_2$ both rotamers and –$NCH_3$ rotamer A), 1.98 (s, 1.5H, –$NCH_3$ rotamer B), 1.90 – 1.73 (m, 1H, $CH_2$ rotamer A), 1.73 – 1.57 (m, 1H, $CH_2$ rotamer B) ppm.

**$^{13}$C NMR** (151 MHz, $CDCl_3$) δ 174.2 (*C*OOMe rotamer A), 174.1 (*C*OOMe rotamer B), 172.3(Ar–*C*ONMe rotamer A), 171.4 (Ar–*C*ONMe rotamer B), 136.8 (Ar*C*–CO), 129.5 (ArCH rotamer A), 129.4 (ArCH rotamer B), 128.5 (ArCH), 127.1 (ArCH rotamer A), 126.8 (ArCH rotamer B), 57.2 (N–*C*$H_2$–$CH_2$–$CH_2$– rotamer A), 57.1 (N–*C*$H_2$–$CH_2$–$CH_2$– rotamer B), 55.6 (CON–$CH_2$–*C*$H_2$–N rotamer A), 54.9 (CON–$CH_2$–*C*$H_2$–N rotamer B), 51.7 (COO*C*$H_3$), 49.5 (CON–*C*$H_2$–$CH_2$–N rotamer A), 45.5 (CON–*C*$H_2$–$CH_2$–N rotamer B), 42.2 (–N*C*$H_3$), 38.4 (–CON*C*$H_3$– rotamer A), 33.5(–CON*C*$H_3$– rotamer B), 31.8 (–*C*$H_2$COOMe rotamer A), 31.7 (–*C*$H_2$COOMe rotamer B), 22.8 (–$CH_2$–*C*$H_2$–$CH_2$– rotamer A), 22.6 (–$CH_2$–*C*$H_2$–$CH_2$– rotamer B) ppm; The NMR spectra show two rotamers with overlapping signals in $^1$H NMR. The EXSY experiment confirmed that each set of two signals originates from the same nucleus. Overlapping rotamer signals were differentiated by an HSQC edit experiment and are listed separately, if they could be distinguished. The

approximate ratio of rotamer A to B is 1.2:1, but they are treated as if they are in a 1:1 ratio for the signals reported above.

**LC/MS** (*m/z*): $[M+H]^+$ calcd for $C_{16}H_{25}N_2O_3^+$: 293.2; found: 293.2

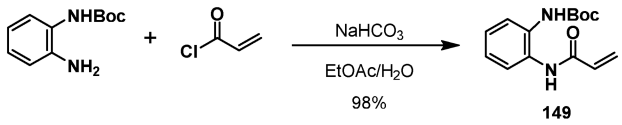


***tert*-Butyl (2-acrylamidophenyl)carbamate** (**149**): To a vigorously stirred mixture of *N*-Boc-1,2-phenylenediamine (500 mg, 2.40 mmol, 1.0 equiv) in saturated aqueous $NaHCO_3$ (10 mL) and EtOAc (10 mL) was added acryloyl chloride (0.217 mL, 2.64 mmol, 1.1 equiv). After stirring for 5 min, the reaction mixture was diluted with EtOAc (20 mL), the phases were separated, and the organic layer was washed with saturated aqueous $NaHCO_3$ (2 × 20 mL) and water (20 mL), then dried ($MgSO_4$), filtered, and concentrated to provide **149** as an off–white solid (619 mg, 2.36 mmol, 98% yield).

**TLC** $R_f$ 0.24 (30% EtOAc in hexane)

**$^1$H NMR** (600 MHz, $CDCl_3$) δ 8.45 (s, 1H), 7.55 (t, *J* = 4.9 Hz, 1H), 7.31 (dd, *J* = 6.1, 3.5 Hz, 1H), 7.19 – 7.09 (m, 2H), 6.92 (s, 1H), 6.40 (d, *J* = 17.0 Hz, 1H), 6.24 (dd, *J* = 17.0, 10.3 Hz, 1H), 5.76 (d, *J* = 10.3 Hz, 1H), 1.51 (s, 9H) ppm

**$^{13}$C NMR** (151 MHz, $CDCl_3$) δ 164.3, 154.5, 131.3, 130.5, 130.1, 127.7, 126.3, 125.7, 125.6, 124.6, 81.3, 28.4 ppm

**LC/MS** (*m/z*): $[M+Na]^+$ calcd for $C_{14}H_{18}N_2NaO_3^+$: 285.1; found: 285.1

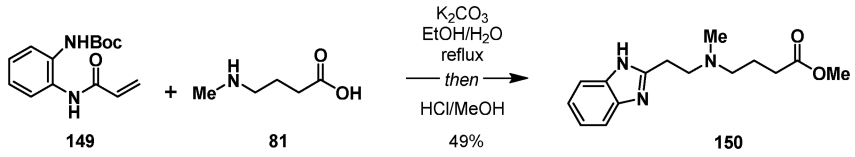


**Methyl 4-((2-(benzimidazol-2-yl)ethyl)(methyl)amino)butanoate** (**150**): A mixture of acrylamide **149** (0.609 g, 2.32 mmol, 1.0 equiv), **81**·HCl (0.373 g, 2.44 mmol, 1.05 equiv) and $K_2CO_3$ (0.642 g, 4.64 mmol, 2.0 equiv) in water/EtOH (1:1, 10 mL) was heated to reflux. After 16 h, the reaction mixture was cooled to rt, diluted with 2 M HCl (10 mL) and evaporated to dryness. Residual water was removed by successive concentration from MeOH and toluene (2 × 20 mL each). The residue was dissolved in anhydrous methanolic HCl (0.5 M, 30 mL) and heated to reflux. After 18 h, the reaction mixture was concentrated, and partitioned between half saturated aqueous $K_2CO_3$ (30 mL) and $CH_2Cl_2$ (30 mL). The layers were separated and the aqueous layer was extracted with $CH_2Cl_2$ (2 × 25 mL). The combined organics were dried ($MgSO_4$), filtered, and concentrated in vacuo. The product was purified by MPLC (24 g silica, gradient: 0 → 8% MeOH in $CH_2Cl_2$ over 8 CV, then 8% MeOH over 10 CV) to provide **150** as a brown oil (0.312 g, 1.133 mmol, 49% yield).

**TLC** $R_f$ 0.28 (20% MeOH in $CH_2Cl_2$)

**$^1$H NMR** (600 MHz, $CDCl_3$) δ 7.59 – 7.51 (m, 2H), 7.21 – 7.15 (m, 2H), 3.65 (s, 3H), 3.08 (t, *J* = 6.2 Hz, 2H), 2.78 (t, *J* = 6.2 Hz, 2H), 2.47 (t, *J* = 7.1 Hz, 2H), 2.37 (t, *J* = 7.1 Hz, 2H), 2.29 (s, 3H), 1.87 (app p, *J* = 7.1 Hz, 2H) ppm

**$^{13}$C NMR** (151 MHz, $CDCl_3$) δ 174.1, 154.7, 122.0, 56.9, 55.7, 51.8, 41.0, 32.0, 26.1, 22.5 ppm; Due to tautomerism of the benzimidazole NH, two benzimidazole carbon signals are too broad to be identified in $^{13}$C spectra.

**LC/MS** (*m/z*): $[M+H]^+$ calcd for $C_{15}H_{22}N_3O_2^+$: 276.2; found: 276.2

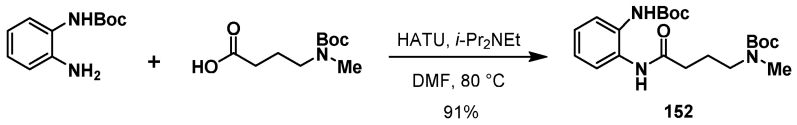


***tert*-Butyl (4-((2-((*tert*-butoxycarbonyl)amino)phenyl)amino)-4-oxobutyl)(methyl) carbamate (152)**: A solution of *N*-Boc-1,2-phenylenediamine (0.200 g, 0.960 mmol, 1.0 equiv), *N*-Boc,*N*-MeGABA[219] (0.209 g, 0.960 mmol, 1.0 equiv) HATU (0.438 g, 1.15 mmol, 1.2 equiv) , and *i*-$Pr_2$NEt (0.384 mL, 2.88 mmol, 3.0 equiv) in DMF (2.5 mL) was heated by microwave irradiation to 80 °C for 20 min. The reaction mixture was diluted with EtOAc (50 mL), washed with half saturated aqueous $K_2CO_3$ (30 mL) and brine (2 × 30 mL), dried ($MgSO_4$), filtered, and concentrated in vacuo. The product was purified by MPLC (10 g silica, gradient: 20 → 60% EtOAc in hexane) to provide **152** as a white foam (355 mg, 0.870 mmol, 91% yield)

**TLC** $R_f$ 0.57 (60% EtOAc in hexane)

**$^1$H NMR** (600 MHz, MeOD) δ 7.63 – 7.50 (m, 1H), 7.40 (br s, 1H), 7.20 (td, *J* = 7.7, 1.6 Hz, 1H), 7.13 (t, *J* = 7.7 Hz, 1H), 3.33 (t, *J* = 7.1 Hz, 2H), 2.89 (br s, 3H), 2.42 (t, *J* = 7.4 Hz, 2H), 1.93 (app p, *J* = 7.2 Hz, 2H), 1.52 (s, 9H), 1.47 (s, 9H) ppm

**$^{13}$C NMR** (151 MHz, MeOD) δ 172.2 and 172.1 (–$CH_2$–<u>C</u>ONHAr), 155.6 and 155.4 (MeN<u>C</u>OO$^t$Bu), 153.6 (ArN<u>C</u>OO$^t$Bu), 131.1 and 130.9 (ArCN), 128.9 and 128.8 (ArCN), 125.2 (ArCH), 124.5 (ArCH, broad), 123.7 and 123.6 (ArCH), 123.2 (ArCH, very broad), 79.3 (–O<u>C</u>$Me_3$, broad), 78.9 and 78.8 (–O<u>C</u>$Me_3$), 47.4 (–<u>C</u>$H_2$NMe, overlapped with solvent signal), 32.7 and 32.5 (–$NCH_3$), 32.4 (–$CH_2$N–), 26.7 (–OC<u>C</u>$H_3$), 26.6 (–OC<u>C</u>$H_3$), 22.9 and 22.5 (–$CH_2$–<u>C</u>$H_2$–$CH_2$–) ppm; The NMR spectra show rotamers due to hindered rotation around amide and carbamate C–N bonds, resulting in two signals per nucleus or very broad signals. Rotamers were confirmed by the EXSY experiment.

**LC/MS** (*m/z*): $[M+Na]^+$ calcd for $C_{21}H_{33}N_3NaO_5^+$: 430.2; found: 430.2

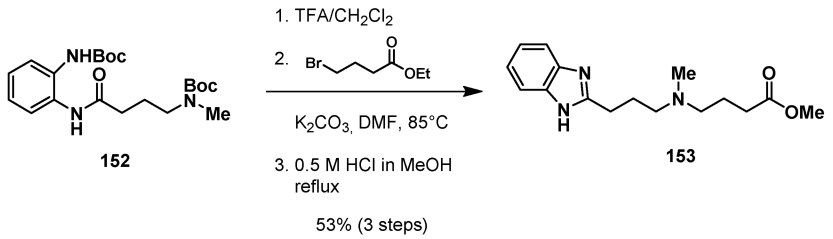


**Methyl 4-((3-(benzimidazol-2-yl)propyl)(methyl)amino)butanoate** (**153**): To a solution of Boc-protected amine **152** (355 mg, 0.870 mmol, 1.0 equiv) in $CH_2Cl_2$ (7.5 mL) was added TFA (2.5 mL) at rt. After 90 min, the reaction mixture was concentrated to dryness. The residue was dissolved in DMF (2.0 mL), ethyl 4-bromobyturate (0.131 mL, 0.914 mmol, 1.05 equiv) and $K_2CO_3$ (0.481 g, 3.48 mmol, 4.0 equiv) were added, and the mixture stirred at 85 °C for 18 h, then acidified with 1 M aqueous HCl (10 mL), and the solution concentrated to dryness. The residue was then heated to reflux in methanolic HCl (0.5 M, 30 mL). After 21 h the reaction mixture was concentrated in vacuo, and partitioned between aqueous $K_2CO_3$ (30 mL) and $CH_2Cl_2$ (30 mL). The two layers were separated and the aqueous layer was extracted with $CH_2Cl_2$ (3 × 30 mL). The combined organic layers were dried ($MgSO_4$), filtered, and concentrated in vacuo. The product was purified by MPLC (12 g silica, gradient: 0 → 20% MeOH in $CH_2Cl_2$) to provide **153** as a brown oil, which solidified upon standing (0.133 g, 0.460 mmol, 53% yield over three steps).

**TLC** $R_f$ 0.19 (20% MeOH in $CH_2Cl_2$)

**$^1$H NMR** (600 MHz, $CDCl_3$) δ 9.99 (br s, 1H), 7.56 – 7.50 (m, 2H), 7.20 – 7.15 (m, 2H), 3.65 (s, 3H), 3.02 (t, *J* = 6.7 Hz, 2H), 2.48 (t, *J* = 6.2 Hz, 2H), 2.43 (t, *J* = 7.3 Hz, 2H), 2.35 (t, *J* = 7.2 Hz, 2H), 2.24 (s, 3H), 1.98 (p, *J* = 6.4 Hz, 2H), 1.85 (app p, *J* = 7.2 Hz, 2H) ppm

**$^{13}$C NMR** (151 MHz, $CDCl_3$) δ 174.1, 155.5, 138.9, 121.9, 114.7, 57.6, 56.8, 51.8, 41.4, 31.9, 27.9, 24.8, 22.3 ppm
**LC/MS** (*m/z*): $[M+H]^+$ calcd for $C_{16}H_{24}N_3O_2^+$: 290.2; found: 290.2

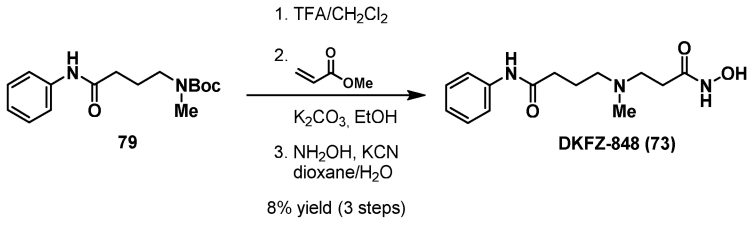


**4-((3-(Hydroxyamino)-3-oxopropyl)(methyl)amino)-*N*-phenylbutanamide** (**DKFZ-848**, **73**): To a solution of Boc-amine **79** (0.359 g, 1.229 mmol, 1.0 equiv) in $CH_2Cl_2$ (5 mL), was added TFA (2.15 mL, 27.04 mmol, 22 equiv) at rt. After 1 h, the reaction mixture was concentrated to dryness and re-concentrated from MeOH (3 × 10 mL) to remove excess acid. To a solution of the resulting residue in EtOH (5 mL) was added $K_2CO_3$ (0.340 g, 2.459 mmol, 2.0 equiv) and methyl acrylate (0.123 mL, 1.352 mmol, 1.1 equiv) at rt. After stirring for 66 h, the mixture was diluted with water (20 mL) and saturated aqueous $NaHCO_3$ (50 mL) and

extracted with $CH_2Cl_2$ (3 × 30 mL). The combined organic layers were dried ($MgSO_4$), filtered, and concentrated in vacuo. The residue was then stirred in 1 M HCl in MeOH (10 mL) at rt for 16 h (significant transesterification to the ethyl ester had occurred during the Michael addition) and concentrated. The product was purified by MPLC (4 g silica, gradient: 0 → 10% MeOH and 0.5% $NH_4OH$ in $CH_2Cl_2$ over 32 CV, 10 → 14% MeOH over 2.5 CV, then 14% for 3 CV) to provide the corresponding ester to the title compound as a yellow oil (121 mg, *m/z*: $[M+H]^+$: 279.2), which was directly converted to hydroxamic acid **73** according to General Procedure A. The product was purified by RP-MPLC (15.5 g C18Aq Teledyne Isco #69-2203-559, gradient: 0 → 21% B over 24 CV) to provide **73** as a colorless amorphous solid (27.0 mg, 0.097 mmol, 8% yield (3 steps)).

**TLC** $R_f$ 0.12 (10% MeOH and 0.5% $NH_4OH$ in $CH_2Cl_2$)

**$^1$H NMR** (400 MHz, DMSO-$d_6$) δ 10.38 (br s, 1H*), 9.85 (s, 1H), 8.74 (br s, 1H*), 7.64 – 7.54 (m, 2H), 7.33 – 7.21 (m, 2H), 7.06 – 6.95 (m, 1H), 2.54 (t, *J* = 7.1 Hz, 2H), 2.36 – 2.23 (m, 4H), 2.13 (s, 3H), 2.12 – 2.02 (m, 2H), 1.70 (app p, *J* = 7.2 Hz, 2H) ppm; *partially exchanged with adventitious water.

**$^{13}$C NMR** (151 MHz, DMSO-$d_6$) δ 171.3, 168.1, 139.4, 128.6, 122.9, 119.0, 56.1, 53.1, 41.5, 34.3, 30.5, 22.9 ppm

**HR-MS** (*m/z*): $[2M+Na]^+$ calcd for $C_{28}H_{42}N_6NaO_6^+$: 581.3058; found: 581.3058

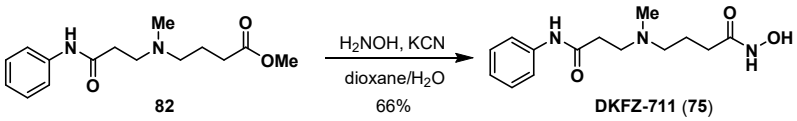


82 DKFZ-711 (75)

***N*-(2-((4-(Hydroxyamino)-4-oxobutyl)(methyl)amino)ethyl)benzamide (DKFZ-711, 75)**: Ester **82** (187.3 mg, 0.673 mmol, 1.0 equiv) was converted to hydroxamic acid **75** according to General Procedure A. The product was purified by HPLC Acidic Method (gradient: 1 → 10% B in 3 min, then 10 → 45% B in 11 min) to provide the TFA salt of **DKFZ-711** as an orange, hygroscopic, amorphous solid (174.2 mg, 0.443 mmol, 66% yield).

**TLC** $R_f$ 0.21 (10% MeOH and 0.5% $NH_4OH$ in $CH_2Cl_2$)

**$^1$H NMR** (400 MHz, $D_2O$) δ 7.49 – 7.40 (m, 4H), 7.33 – 7.22 (m, 1H), 3.70 – 3.58 (m, 1H), 3.51 – 3.37 (m, 1H), 3.33 – 3.18 (m, 2H), 2.97 (t, *J* = 6.7 Hz, 2H), 2.93 (s, 3H), 2.32 (t, *J* = 7.2 Hz, 2H), 2.14 – 2.03 (m, 2H) ppm

**$^{13}$C NMR** (101 MHz, $D_2O$) δ 171.1, 170.1, 162.9 (q, *J* = 34 Hz), 136.5, 129.2, 125.7, 121.8, 116.3 (q, *J* = 292 Hz), 55.5, 51.8, 40.0, 30.0, 29.0, 19.6 ppm

**$^{19}$F NMR** (376 MHz, $D_2O$) δ –78.4 ppm

**HR-MS** (*m/z*): $[M+H]^+$ calcd for $C_{14}H_{22}N_3O_3^+$: 280.1656; found: 280.1656

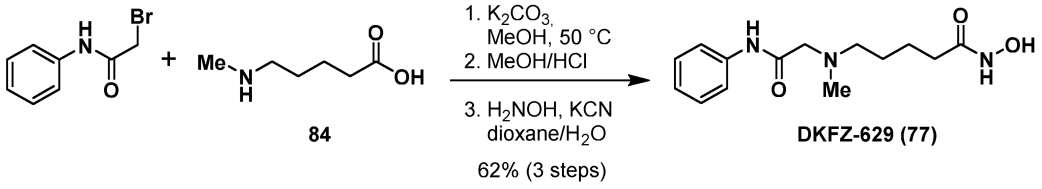


***N*-hydroxy-5-(methyl(2-oxo-2-(phenylamino)ethyl)amino)pentanamide** (**DKFZ-629**, **77**): A suspension of 2-bromo-*N*-phenylacetamide (0.184 g, 0.859 mmol, 1.2 equiv), **84**·HCl (0.120 g, 0.716 mmol, 1.00 equiv) and $K_2CO_3$ (0.317 g, 2.291 mmol, 3.2 equiv) in MeOH (9 mL) was stirred at 50 °C for 45 h. It was then acidified with 2 M HCl (50 mL), washed with $Et_2O$ (4 × 20 mL), and the aqueous layer was evaporated to dryness. The residue was re-suspended in MeOH (40 mL), acidified with HCl (2 M in MeOH, 0.5 mL), stirred at rt for 18 h, and then concentrated. The residue was dissolved in half saturated aqueous $K_2CO_3$ (25 mL) and extracted with $CH_2Cl_2$ (4 × 20 mL), dried ($MgSO_4$) and concentrated in vacuo. The crude methyl ester was converted to hydroxamic acid **77** according to General Procedure A. The product was purified by HPLC Acidic Method (gradient: 1 → 25% B in 3 min, then 25 → 45% B in 11 min) to provide the TFA salt of **77** as an off-white solid (0.175 g, 0.445 mmol, 62% yield (3 steps)).

**TLC** $R_f$ 0.24 (10% MeOH and 0.5% $NH_4OH$ in $CH_2Cl_2$)

**$^1$H NMR** (400 MHz, DMSO-$d_6$) δ 10.63 (s, 1H), 10.42 (s, 1H*), 9.83 (br s, 1H*), 8.72 (br s, 1H*), 7.63 – 7.54 (m, 2H), 7.40 – 7.32 (m, 2H), 7.12 (tt, *J* = 7.4, 1.1 Hz, 1H), 4.11 (s, 2H), 3.21 – 3.08 (m, 2H), 2.85 (s, 3H), 2.00 (t, *J* = 7.2 Hz, 2H), 1.72 – 1.60 (m, 2H), 1.52 (app p, *J* = 7.4 Hz, 2H) ppm; *partially exchanged with adventitious water

**$^{13}$C NMR** (101 MHz, DMSO-$d_6$) δ 168.6, 163.2, 158.0 (q, *J* = 31 Hz), 137.9, 129.0, 124.2, 119.5, 117.3 (q, *J* = 301 Hz), 56.7, 55.9, 41.0, 31.6, 23.1, 22.1 ppm

**$^{19}$F NMR** (376 MHz, DMSO-$d_6$) δ –76.3
**HR-MS** (*m/z*): $[M+H]^+$ calcd for $C_{14}H_{22}N_3O_3^+$: 280.1656; found: 280.1655

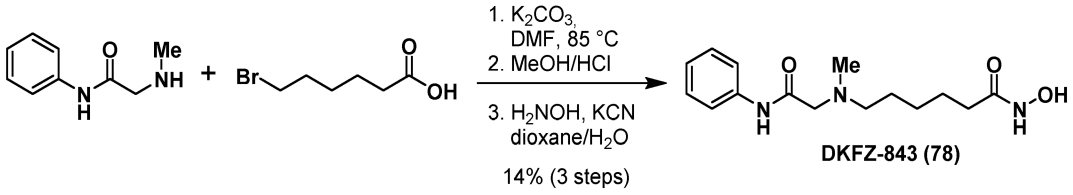


***N*-Hydroxy-6-(methyl(2-oxo-2-(phenylamino)ethyl)amino)hexanamide** (**DKFZ-843**, **78**): To a suspension of 2-methylamino)-*N*-phenylacetamide[221] (0.288 g, 1.755 mmol, 1.0 equiv) and $K_2CO_3$ (0.606 g, 4.388 mmol, 2.5 equiv) in DMF (5 mL) at 85 °C was added 6-bromohexanoic acid (0.787 g, 4.037 mmol, 2.30 equiv) in two portions, stirring at 85 °C for 20 h after each addition. After consumption of the amine, the reaction mixture was acidified with 20 mL 1 M HCl, and evaporated to dryness. The residue was re-suspended in 1 M HCl in MeOH (20 mL), stirred at rt for 16 h, then concentrated, re-dissolved in water (pH < 2) and extracted with EtOAc (2 × 40 mL). The aqueous phase was basified with $K_2CO_3$ until pH > 12, then extracted with $CH_2Cl_2$ (3 × 50 mL). The combined organic phases were dried ($MgSO_4$),

filtered, and concentrated in vacuo. The product was purified by MPLC (12 g silica, gradient: 0% MeOH and 0.5% $NH_4OH$ in $CH_2Cl_2$ for 3 CV, then 0 → 1% MeOH and 0.5% $NH_4OH$ in $CH_2Cl_2$ over 10 CV, then 1 → 3% over 8 CV) to provide the methyl ester of **78** as a yellow oil (97 mg, *m/z*: $[M+H]^+$: 293.2, $[M-H]^-$: 291.2), which was directly converted to **78** according to General Procedure A. The product was purified by RP-MPLC (15.5 g C18Aq Teledyne Isco #69-2203-559, gradient: 0% B for 2 CV, 0 → 28% B over 19 CV, then 28% B over 6 CV) to provide **78** as a white solid (72.5 mg, 0.247 mmol, 14% yield (3 steps)).

**TLC** $R_f$ 0.36 (10% MeOH in $CH_2Cl_2$)

**$^1$H NMR** (400 MHz, DMSO-$d_6$) δ 9.62 (br s, 3H*), 7.68 – 7.59 (m, 2H), 7.34 – 7.25 (m, 2H), 7.04 (tt, *J* = 7.3, 1.2 Hz, 1H), 3.10 (s, 2H), 2.41 (t, *J* = 7.3 Hz, 2H), 2.27 (s, 3H), 1.93 (t, *J* = 7.3 Hz, 2H), 1.56 – 1.38 (m, 4H), 1.32 – 1.19 (m, 2H) ppm; *partially exchanged with adventitious water

**$^{13}$C NMR** (101 MHz, DMSO-$d_6$) δ 169.0, 168.8, 138.6, 128.7, 123.3, 119.3, 61.4, 57.0, 42.4, 32.3, 26.4 ($2CH_2$ overlapped), 25.1 ppm

**HR-MS** (*m/z*): $[2M+Na]^+$ calcd for $C_{30}H_{46}N_6NaO_6^+$: 609.3371; found: 609.3371

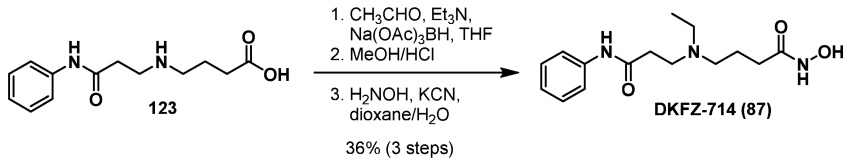


**4-(Ethyl(3-oxo-3-(phenylamino)propyl)amino)-*N*-hydroxybutanamide** (**DKFZ-714**, **87**): The corresponding methyl ester of the title compound was prepared from **123**·HCl (100 mg, 0.349 mmol, 1.0 equiv) and acetaldehyde (192 µL, 3.49 mmol, 10 equiv) according to General Procedure C. The crude product was converted to hydroxamic acid **87** according to General Procedure A. The product was purified by HPLC Acidic Method (gradient: 1 → 10% B in 3 min, then 10 → 45% B in 11 min) to provide the TFA salt of **87** as a yellow, hygroscopic, amorphous solid (51.8 mg, 0.127 mmol, 36% yield (3 steps)).

**TLC** $R_f$ 0.08 (10% MeOH in $CH_2Cl_2$)

**$^1$H NMR** (400 MHz, $D_2O$) δ 7.48 – 7.41 (m, 4H), 7.32 – 7.22 (m, 1H), 3.59 – 3.50 (m, 2H), 3.31 (q, *J* = 7.3 Hz, 2H), 3.28 – 3.18 (m, 2H), 2.95 (t, *J* = 6.8 Hz, 2H), 2.36 – 2.28 (m, 2H), 2.12 – 2.01 (m, 2H), 1.34 (t, *J* = 7.3 Hz, 3H) ppm

**$^{13}$C NMR** (101 MHz, $D_2O$) δ 174.0, 173.0, 139.3, 132.1, 128.6, 124.7, 165.8 (q, *J* = 36 Hz), 119.2 (q, *J* = 292 Hz), 54.7, 51.3, 51.1, 32.9, 31.9, 22.1, 11.0 ppm

**$^{19}$F NMR** (376 MHz, $D_2O$) δ –75.6 ppm

**HR-MS** (*m/z*): $[M+H]^+$ calcd for $C_{15}H_{24}N_3O_3^+$: 294.1812; found: 294.1816

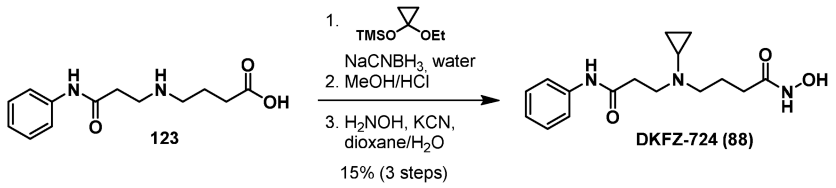


**4-(Cyclopropyl(3-oxo-3-(phenylamino)propyl)amino)-*N*-hydroxybutanamide** (**DKFZ-724**, **88**): To a Schlenk tube charged with **123**·HCl (150 mg, 0.523 mmol, 1.0 equiv) and $NaCNBH_3$ (49.3 mg, 0.785 mmol, 1.5 equiv) was added degassed water (1.5 mL), (1-ethoxycyclopropoxy)trimethylsilane (1.05 mL, 5.23 mmol, 10 equiv) and HCl (37%, 51.5 µL, 0.523 mmol, 1.0 equiv) under argon. After 1 d, additional $NaCNBH_3$ (as a freshly prepared 1 mmol solution in degassed $H_2O$) was added daily for 6 d (total 1.15 mL, 2.2 equiv) until complete consumption of the amine starting material. The reaction was evaporated to dryness. The residue was re-dissolved in water (10 mL) and acidified with HCl (25%) to pH 1.0, then the solvent was removed in vacuo. MeOH (25 mL) was added to the residue, stirred for 18 h, and then concentrated. The residue was partitioned between saturated aqueous $NaHCO_3$ (30 mL) and $CH_2Cl_2$ (20 mL) and the layers were separated. The aqueous layer was then extracted with $CH_2Cl_2$ (2 × 20 mL). The combined organic layers were dried ($MgSO_4$) and concentrated in vacuo. The crude product was converted to hydroxamic acid **88** according to General Procedure A. The product was purified by HPLC Acidic Method (gradient: 1 → 10% B in 3 min, then 10 → 45% B in 11 min) to provide the TFA salt of **88** as a white solid (32.8 mg, 0.078 mmol, 15% yield (3 steps)).

**TLC** $R_f$ 0.17 (10% MeOH in $CH_2Cl_2$)

**$^1$H NMR** (400 MHz, $D_2O$) δ 7.50 – 7.40 (m, 4H), 7.29 (qt, *J* = 5.5, 2.9 Hz, 1H), 3.71 (t, *J* = 6.7 Hz, 2H), 3.42 – 3.31 (m, 2H), 3.04 (t, *J* = 6.7 Hz, 2H), 2.86 (ddd, *J* = 11.2, 7.2, 4.6 Hz, 1H), 2.33 (t, *J* = 7.1 Hz, 2H), 2.15 (dq, *J* = 14.6, 7.2 Hz, 2H), 1.06 (dd, *J* = 13.8, 3.2 Hz, 2H), 1.05 (s, 2H) ppm

**$^{13}$C NMR** (101 MHz, $D_2O$) δ 174.1, 173.1, 165.9 (q, *J* = 36 Hz), 139.3, 132.1, 128.6, 124.7, 119.2 (q, *J* = 292 Hz), 58.1, 54.0, 40.4, 33.3, 32.0, 22.3, 7.3 (2 $CH_2$)* ppm; *broadened due to relatively slow nitrogen inversion.[222]

**$^{19}$F NMR** (376 MHz, $D_2O$) δ –78.4 ppm

**HR-MS** (*m/z*): $[M+H]^+$ calcd for $C_{16}H_{24}N_3O_3^+$: 306.1812; found: 306.1817

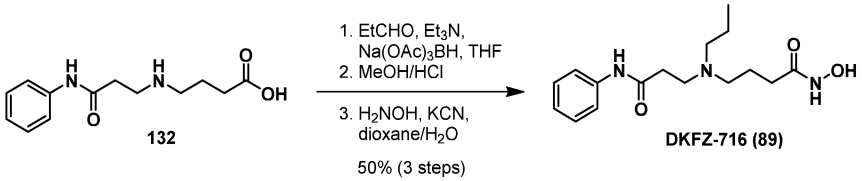


**4-(Propyl(3-oxo-3-(phenylamino)propyl)amino)-*N*-hydroxybutanamide** (**DKFZ-716**, **89**): The corresponding methyl ester of the title compound was prepared from **123**·HCl (150 mg, 0.523 mmol, 1.0 equiv) and propanal (375 µl, 5.23 mmol, 10 equiv) according to General Procedure C. The crude product was converted to hydroxamic acid **89** according to

General Procedure A. The product was purified by HPLC Acidic Method (gradient: 1 → 10% B in 3 min, then 10 → 45% B in 11 min) to provide the TFA salt of **89** as a yellow, hygroscopic, amorphous solid (110 mg, 0.260 mmol, 50% yield (3 steps)).

**TLC** $R_f$ 0.17 (10% MeOH in $CH_2Cl_2$).

**$^1$H NMR** (600 MHz, $D_2O$) δ 7.44 – 7.37 (m, 4H), 7.24 (tt, *J* = 5.8, 2.6 Hz, 1H), 3.51 (q, *J* = 6.5 Hz, 2H), 3.25 – 3.17 (m, 2H), 3.17 – 3.09 (m, 2H), 2.90 (t, *J* = 6.8 Hz, 2H), 2.28 (t, *J* = 7.1 Hz, 2H), 2.06 – 1.97 (m, 2H), 1.78 – 1.68 (m, 2H), 0.95 (t, *J* = 7.4 Hz, 3H) ppm

**$^{13}$C-NMR** (151 MHz, $D_2O$) δ 171.1, 170.1, 162.9 (q, *J* = 36 Hz), 136.4, 129.2, 125.7, 121.7, 116.3 (q, *J* = 292 Hz), 54.8, 52.3, 48.7, 29.9, 28.9, 19.1, 16.8, 10.0 ppm

**$^{19}$F NMR** (376 MHz, $D_2O$) δ –75.6 ppm

**HR-MS** (*m/z*): $[M+H]^+$ calcd for $C_{16}H_{26}N_3O_3^+$: 308.1969; found: 308.1974

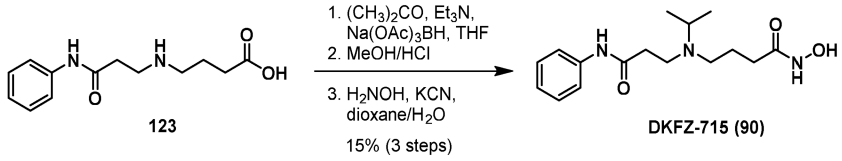


**4-(Isopropyl(3-oxo-3-(phenylamino)propyl)amino)-*N*-hydroxybutanamide** (**DKFZ-715**, **90**): The corresponding methyl ester of the title compound was prepared from **123**·HCl (150 mg, 0.523 mmol, 1.0 equiv) and acetone (390 µL, 5.23 mmol, 10 equiv) according to General Procedure C. The crude product was converted to hydroxamic acid **90** according to General Procedure A. The product was purified by HPLC Acidic Method (gradient: 1 → 10% B in 3 min, then 10 → 45% B in 11 min) to provide the TFA salt of **90** as a yellow, hygroscopic, amorphous solid (33.0 mg, 0.078 mmol, 15% yield (3 steps)).

**TLC** $R_f$ 0.04 (10% MeOH in $CH_2Cl_2$)

**$^1$H NMR** (400 MHz, $D_2O$) δ 7.48 – 7.39 (m, 4H), 7.28 (dtd, *J* = 8.4, 5.0, 3.1 Hz, 1H), 3.78 (hept, *J* = 6.6 Hz, 1H), 3.59 (dt, *J* = 13.9, 7.0 Hz, 1H), 3.39 (dt, *J* = 13.4, 6.5 Hz, 1H), 3.25 (ddd, *J* = 13.3, 9.0, 6.8 Hz, 1H), 3.14 (ddd, *J* = 13.4, 9.0, 6.5 Hz, 1H), 2.94 (t, *J* = 6.8 Hz, 2H), 2.33 (t, *J* = 7.0 Hz, 2H), 2.14 – 1.96 (m, 2H), 1.35 (t, *J* = 7.1 Hz, 6H) ppm

**$^{13}$C NMR** (101 MHz, $D_2O$) δ 174.0, 173.1, 165.8 (q, *J* = 35 Hz), 139.3, 132.1, 128.6, 124.7, 119.2 (q, *J* = 292 Hz), 58.6, 52.7, 48.9, 33.5, 32.1, 23.2, 18.7, 18.3 ppm

**$^{19}$F NMR** (376 MHz, $D_2O$) δ –78.4 ppm

**HR-MS** (*m/z*): $[M+H]^+$ calcd for $C_{16}H_{26}N_3O_3^+$: 308.1969; found: 308.1974

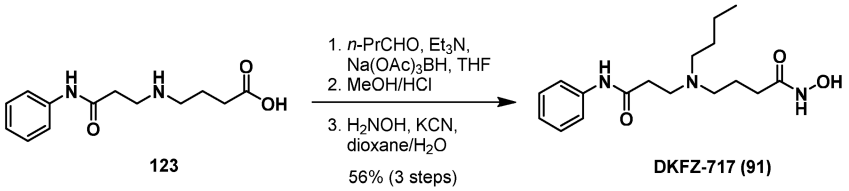


**4-(Butyl(3-oxo-3-(phenylamino)propyl)amino)-*N*-hydroxybutanamide** (**DKFZ-717, 91**): The corresponding methyl ester of the title compound was prepared from **123**·HCl (150 mg, 0.523 mmol, 1.0 equiv) and *n*-butanal (472 µL, 5.23 mmol, 10 equiv) according to General Procedure C. The crude product was converted to hydroxamic acid **91** according to General Procedure A. The product was purified by HPLC Acidic Method (gradient: 1 → 10% B in 3 min, then 10 → 45% B in 11 min) to provide the TFA salt of **91** as a yellow, hygroscopic, amorphous solid (127 mg, 0.292 mmol, 56% yield (3 steps)).

**TLC** $R_f$ 0.08 (10% MeOH in $CH_2Cl_2$).

**$^1$H NMR** (400 MHz, $D_2O$) δ 7.46 – 7.40 (m, 4H), 7.30 – 7.22 (m, 1H), 3.59 – 3.48 (m, 2H), 3.27 – 3.14 (m, 4H), 2.98 – 2.88 (m, 2H), 2.35 – 2.25 (m, 2H), 2.10 – 1.98 (m, 2H), 1.77 – 1.65 (m, 2H), 1.38 (app p, *J* = 7.5 Hz, 2H), 0.97 – 0.89 (m, 3H) ppm

**$^{13}$C NMR** (101 MHz, $D_2O$) δ 171.2, 170.2, 163.5 (q, *J* = 39 Hz), 136.5, 129.3, 125.8, 121.9, 116.4 (q, *J* = 291 Hz), 53.3, 52.4, 48.9, 30.0, 29.0, 25.2, 19.3 (2 $CH_2$), 12.8 ppm

**$^{19}$F NMR** (376 MHz, $D_2O$) δ –75.6 ppm

**HR-MS** (*m/z*): $[M+H]^+$ calcd for $C_{17}H_{28}N_3O_3^+$: 322.2125; found: 322.2127

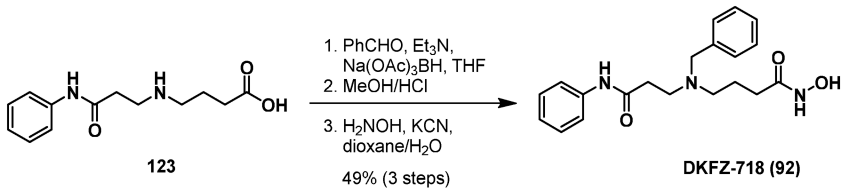


**4-(Benzyl(3-oxo-3-(phenylamino)propyl)amino)-*N*-hydroxybutanamide** (**DKFZ-718, 92**): The corresponding methyl ester of the title compound was prepared from **123**·HCl (150 mg, 0.523 mmol, 1.0 equiv) and benzaldehyde (539 µL, 5.23 mmol, 10 equiv) according to General Procedure C. The crude product was converted to hydroxamic acid **92** according to General Procedure A. The produce was purified by HPLC Acidic Method (gradient: 1 → 10% B in 3 min, then 10 → 45% B in 11 min) to provide the TFA salt of **92** as an off-white solid (119 mg, 0.254 mmol, 49% yield (3 steps)).

**TLC** $R_f$ 0.17 (10% MeOH in $CH_2Cl_2$)

**$^1$H NMR** (400 MHz, MeOD-$d_4$) δ 7.62 – 7.48 (m, 7H), 7.35 – 7.29 (m, 2H), 7.11 (tt, *J* = 7.4, 1.2 Hz, 1H), 4.45 (s, 2H), 3.54 (t, *J* = 6.8 Hz, 2H), 3.28 (t, *J* = 7.4 Hz, 2H), 2.91 (t, *J* = 6.8 Hz, 2H), 2.27 (t, *J* = 6.3 Hz, 2H), 2.09 (p, *J* = 6.7 Hz, 2H) ppm

**$^{13}$C NMR** (101 MHz, MeOD-$d_4$) δ 171.4, 170.1, 163.0 (q, *J* = 34 Hz), 139.4, 132.1, 131.3, 130.8, 130.6, 129.9, 125.5, 121.3, 118.2 (q, *J* = 293 Hz), 58.9, 54.6, 50.3, 31.1, 30.6, 20.7 ppm

**$^{19}$F NMR** (376 MHz, MeOD-$d_4$) δ –79.7 ppm

**HR-MS** (*m/z*): $[M+H]^+$ calcd for $C_{20}H_{26}N_3O_3^+$: 356.1969; found: 356.1972

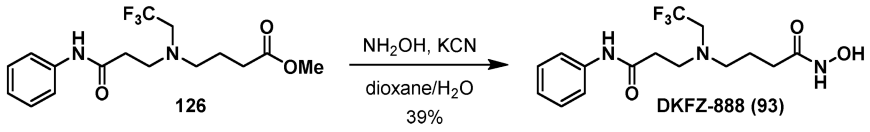


***N*-Hydroxy-4-((3-oxo-3-(phenylamino)propyl)(2,2,2-trifluoroethyl)amino)butanamide (DKFZ-888, 93)**: Ester **126** (164 mg, 0.473 mmol, 1.0 equiv) was converted to hydroxamic acid **93** according to General Procedure A. The product was purified by RP-MPLC (15.5 g C18Aq Teledyne Isco #69-2203-559, gradient: 15 → 23% B over 11 CV, then 23% B for 16.5 CV) to provide **93** as a white solid (63.3 mg, 0.182 mmol, 39% yield).

**TLC** $R_f$ 0.16 (5% MeOH in $CH_2Cl_2$)

**$^1$H NMR** (400 MHz, DMSO-$d_6$) δ 10.32 (br s, 1H*), 9.44 (br s, 2H*), 7.59 (app d, *J* = 7.4 Hz, 2H), 7.27 (app t, *J* = 7.8 Hz, 2H), 7.01 (app t, *J* = 7.4 Hz, 1H), 3.22 (q, *J* = 10.1 Hz, 2H), 2.91 (t, *J* = 7.1 Hz, 2H), 2.56 (t, *J* = 7.3 Hz, 2H), 2.46 (t, *J* = 7.1 Hz, 2H), 1.95 (t, *J* = 7.2 Hz, 2H), 1.62 (app p, *J* = 7.3 Hz, 2H) ppm; *partially exchanged with adventitious water.

**$^{13}$C NMR** (101 MHz, DMSO-$d_6$) δ 170.0, 168.6, 139.4, 128.6, 126.1 (q, *J* = 281 Hz), 122.9, 119.1, 53.98 (q, *J* = 29 Hz), 53.4, 51.0, 34.7, 29.6, 23.2 ppm

**$^{19}$F NMR** (376 MHz, DMSO-$d_6$) δ –71.9 ppm

**HR-MS** (*m/z*): $[2M+Na]^+$ calcd for $C_{30}H_{40}F_6N_6NaO_6^+$: 717.2806; found: 717.2807

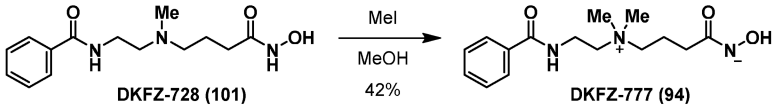


**(4-((2-benzamidoethyl)dimethylammonio)butanoyl)(hydroxy)amide (DKFZ-777, 94):** To a stirred solution of **DKFZ-728**[1] (40.0 mg, 0.143 mmol, 1.0 equiv) in MeOH (1 mL) was added MeI (90.7 µL, 1.457 mmol, 10.2 equiv) in small portions over 7 h and stirred at rt until LC/MS indicated complete conversion. The reaction mixture was concentrated in vacuo, dissolved in 0.1% aqueous ammonia (0.5 mL) and purified by cation exchange chromatography (500 mg Isolute SCX-2 (Biotage), elution: 2 CV MeOH, then 8 CV 0.2 M aqueous HBr). Aqueous fractions were diluted with water and lyophilized. The product was further purified by HPLC Basic Method A (gradient: 1 → 25% B in 11 min, then 25% B for 7 min) to provide the internal salt of **DKFZ-777** as off-white solid (19.8 mg, 0.068 mmol, 42% yield).

Note: HPLC purification was required due to the formation of the carboxylic acid after elution with 0.2 M aqueous HBr. **DKFZ-777** and the corresponding carboxylic acid are poorly soluble in water.

**$^1$H NMR** (600 MHz, DMSO-$d_6$) δ 9.36 (br s, 1H), 7.91 (d, $J$ = 7.7 Hz, 2H), 7.54 (t, $J$ = 7.2 Hz, 1H), 7.48 (t, $J$ = 7.2 Hz, 2H), 3.67 (t, $J$ = 6.5 Hz, 2H), 3.47 (t, $J$ = 6.5 Hz, 2H*), 3.43 – 3.30 (br s, 1×$CH_2$*) 3.08 (s, 6H), 2.01 – 1.73 (m, 4H) ppm; *overlapped with water signal.

**$^{13}$C NMR** (151 MHz, DMSO-$d_6$) δ 166.6, 165.6, 133.7, 131.5, 128.3, 127.3, 63.0, 61.3, 50.8, 33.3, 29.8, 18.9 ppm

**LC/MS** (*m/z*): $[M+H]^+$ calcd for $C_{15}H_{24}N_3O_3^+$: 294.2; found: 294.2

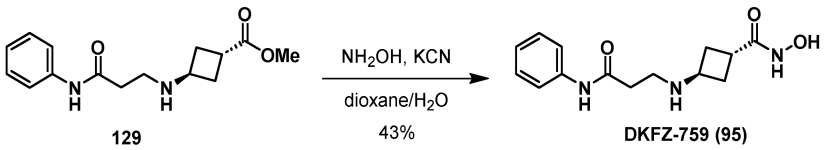


**(1*r*,3*r*)-*N*-Hydroxy-3-((3-oxo-3-(phenylamino)propyl)amino)cyclobutanecarboxamide** (**DKFZ-759, 95**): Ester **129** (131.2 mg, 0.475 mmol, 1.0 equiv) was converted to hydroxamic acid **95** according to General Procedure A. The product was purified by RP-MPLC (15.5 g C18 Teledyne Isco #69-2203-334, gradient: 0% B for 3 CV, then 0 → 20% over 20 CV). The resulting solid was triturated with EtOAc (twice) and $Et_2O$ (once) to provide **95** as a white solid (56.3 mg, 0.203 mmol, 43% yield).

**TLC** $R_f$ 0.25 (20% MeOH in $CH_2Cl_2$)

**$^1$H NMR** (400 MHz, DMSO-$d_6$) δ 10.29 (br s, 1H*), 10.02 (s, 1H), 8.66 (br s, 1H*), 7.62 – 7.53 (m, 2H), 7.33 – 7.23 (m, 2H), 7.01 (tt, $J$ = 7.4, 1.2, 1.2 Hz, 1H), 3.43 – 3.24 (m, overlapped with water peak), 2.79 – 2.66 (m, 3H), 2.40 (t, $J$ = 6.7 Hz, 2H), 2.29 – 2.18 (m, 2H), 1.91 – 1.79 (m, 2H) ppm; *partially exchanged with adventitious water.

**$^{13}$C NMR** (101 MHz, DMSO-$d_6$) δ 172.0, 170.5, 139.3, 128.7, 123.0, 119.1, 51.2, 42.6, 37.1, 32.5, 30.7 ppm

**HR-MS** (*m/z*): $[M+H]^+$ calcd for $C_{14}H_{20}N_3O_3^+$: 278.1499; found: 278.1500

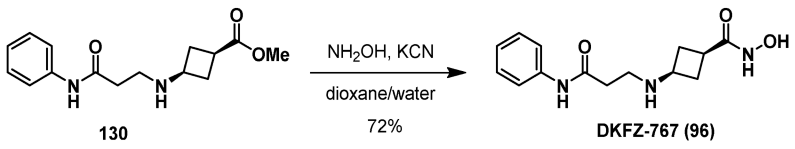


**(1*s*,3*s*)-*N*-Hydroxy-3-((3-oxo-3-(phenylamino)propyl)amino)cyclobutanecarboxamide** (**DKFZ-767, 96**): Ester **130** (138.6 mg, 0.502 mmol, 1.0 equiv) was converted to hydroxamic acid **96** according to General Procedure A. The product was purified by RP-MPLC (15.5 g C18Aq #69-2203-559, gradient: 0% B for 3 CV, 0 → 20% over 20 CV, then 20% over 10 CV) to provide **96** as a white solid (100.2 mg, 0.361 mmol, 72% yield).

**TLC** $R_f$ 0.07 (20% MeOH in $CH_2Cl_2$)

**$^1$H NMR** (600 MHz, DMSO-$d_6$) δ 10.34 (br s, 1H*), 10.03 (s, 1H), 9.12 – 8.28 (br, 1H*), 7.60 – 7.55 (m, 2H), 7.31 – 7.24 (m, 2H), 7.01 (tt, *J* = 7.4, 1.2 Hz, 1H), 3.36 (br s, 1H*), 3.12 – 2.98 (m, 1H), 2.71 (t, *J* = 6.8 Hz, 2H), 2.46 – 2.41 (m, 1H), 2.41 – 2.37 (m, 2H), 2.25 – 2.17 (m, 2H), 1.88 – 1.76 (m, 2H) ppm; *partially exchanged with adventitious water.

**$^{13}$C NMR** (151 MHz, DMSO-$d_6$) δ 170.5, 170.5, 139.3, 128.7, 122.9, 119.0, 49.5, 42.5, 37.1, 33.6, 29.1 ppm

**HR-MS** (*m/z*): $[M+H]^+$ calcd for $C_{14}H_{20}N_3O_3^+$: 278.1499; found: 278.1499

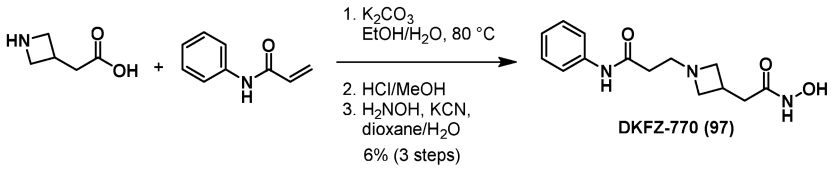


**3-(3-(2-(Hydroxyamino)-2-oxoethyl)azetidin-1-yl)-*N*-phenylpropanamide (DKFZ-770, 97)**: To a stirred solution of 2-(azetidin-3-yl)acetic acid (1.102 g, 4.809 mmol, 1.0 equiv) and *N*-phenylacrylamide (0.743 g, 5.05 mmol, 1.05 equiv) in $H_2O$/EtOH (1:1, 15 mL), was added $K_2CO_3$ (1.994 g, 14.43 mmol, 3.0 equiv) and the reaction mixture was stirred at 80 °C. After 5 h, the reaction mixture was cooled to rt, diluted with 1 M HCl (40 mL), washed with EtOAc (2 × 30 mL) and the aqueous layer was evaporated to dryness. The residue was suspended in MeOH (25 mL), acidified with 2M HCl in MeOH (5 mL), stirred at rt for 3 h, then concentrated to dryness. The residue was dissolved in half saturated aqueous $K_2CO_3$ (40 mL) and extracted with $CH_2Cl_2$ (3 × 25 mL), dried ($MgSO_4$), filtered, and concentrated in vacuo. The product was purified by MPLC (40 g silica, gradient: pure $CH_2Cl_2$ for 2 CV, 0 → 7% MeOH in $CH_2Cl_2$ over 8 CV, then 7% MeOH in $CH_2Cl_2$ over 7 CV) to provide the corresponding methyl ester of the title compound as a yellow oil (0.173 g, TLC $R_f$ 0.50 (20% MeOH in $CH_2Cl_2$), LC/MS (*m/z*): $[M+H]^+$ 277.2). The material was directly converted to hydroxamic acid **97** according to General Procedure A. The product was purified by RP-MPLC (15.5 g C18Aq Teledyne Isco #69-2203-559, gradient: 0% B for 3 CV, then 0 → 15% over 25 CV) to provide **25** as a white solid (76.0 mg, 0.274 mmol, 6% yield (3 steps)).

**$^1$H NMR** (600 MHz, DMSO-$d_6$) δ 9.98 (s, 1H), 9.90 (br s, 1H*), 9.14 (br s, 1H*), 7.58 (d, *J* = 8.1 Hz, 2H), 7.28 (t, *J* = 7.8 Hz, 2H), 7.01 (t, *J* = 7.4 Hz, 1H), 3.28 (t, *J* = 7.0 Hz, 2H), 2.75 (t, *J* = 6.6 Hz, 2H), 2.61 (t, *J* = 7.0 Hz, 2H), 2.59 – 2.52 (m, 1H), 2.27 (t, *J* = 6.9 Hz, 2H), 2.19 (d, *J* = 7.7 Hz, 2H) ppm; *partially exchanged with adventitious water.

**$^{13}$C NMR** (151 MHz, DMSO-$d_6$) δ 170.0, 167.7, 139.3, 128.7, 123.0, 119.0, 59.5, 55.0, 36.9, 35.1, 27.4 ppm

**HR-MS** (*m/z*): $[M+H]^+$ calcd for $C_{14}H_{20}N_3O_3^+$: 278.1499; found: 278.1503

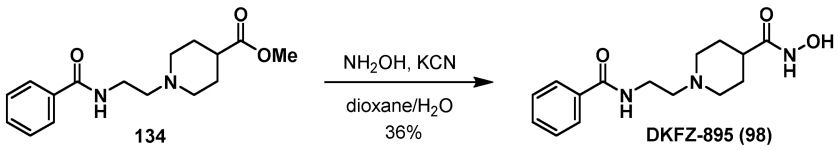


**1-(2-Benzamidoethyl)-*N*-hydroxypiperidine-4-carboxamide** (**DKFZ-895, 98**): Ester **134** (183 mg, 0.629 mmol, 1.0 equiv) was converted to hydroxamic acid **98** according to General Procedure A. The product was purified by RP-MPLC (15.5 g C18Aq Teledyne Isco #69-2203-559, gradient: 0 → 9% B over 4 CV, 9% B for 4 CV, 9 → 21% B over 6 CV, then 21% B for 4 CV) to provide **98** as a white solid (65.5 mg, 0.225 mmol, 36% yield).

**TLC** $R_f$ 0.08 (10% MeOH and 0.5% $NH_4OH$ in $CH_2Cl_2$)

**$^1$H NMR** (400 MHz, DMSO-$d_6$) δ 9.51 (br s, 2H*), 8.37 (t, $J$ = 5.6 Hz, 1H), 7.89 – 7.76 (m, 2H), 7.56 – 7.49 (m, 1H), 7.48 – 7.40 (m, 2H), 3.36 (app q, $J$ = 6.6 Hz, 2H), 2.91 (dt, $J$ = 11.4, 3.5 Hz, 2H), 2.44 (t, $J$ = 7.0 Hz, 2H), 2.05 – 1.82 (m, 3H), 1.67 – 1.46 (m, 4H) ppm; *partially exchanged with adventitious water.

**$^{13}$C NMR** (101 MHz, DMSO-$d_6$) δ 171.5, 166.1, 134.6, 131.0, 128.3, 127.1, 57.2, 52.8, 39.4, 37.0, 28.5 ppm

**LC/MS** ($m/z$): $[M+H]^+$ 292.2

**HR-MS** ($m/z$): $[2M+Na]^+$ calcd for $C_{30}H_{42}N_6NaO_6^+$: 605.3064; found: 605.3062

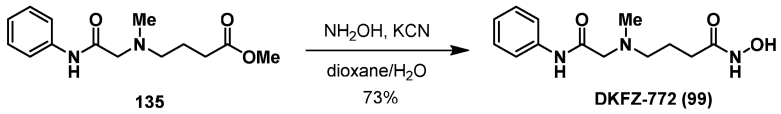


***N*-Hydroxy-4-(methyl(2-oxo-2-(phenylamino)ethyl)amino)butanamide** (**DKFZ-772, 99**): Ester **135** (165 mg, 0.625 mmol, 1.0 equiv) was converted to hydroxamic acid **99** according to General Procedure A. The product was purified by RP-MPLC (15.5 g C18Aq Teledyne Isco #69-2203-559, gradient: 0 → 20% B over 25 CV, then 20% B for 10 CV) to provide **99** as an off-white solid (121 mg, 0.457 mmol, 73% yield).

**TLC** $R_f$ 0.29 (20% MeOH in $CH_2Cl_2$)

**$^1$H NMR** (600 MHz, DMSO-$d_6$) δ 10.11 – 8.98 (br, 3H*), 7.69 – 7.63 (m, 2H), 7.32 – 7.27 (m, 2H), 7.05 (tt, $J$ = 7.4, 1.2 Hz, 1H), 3.09 (s, 2H), 2.41 (t, $J$ = 7.1 Hz, 2H), 2.25 (s, 3H), 2.01 (t, $J$ = 7.3 Hz, 2H), 1.69 (app p, $J$ = 7.0 Hz, 2H) ppm; *partially exchanged with adventitious water.

**$^{13}$C NMR** (151 MHz, DMSO-$d_6$) δ 169.3, 169.0, 138.6, 128.6, 123.3, 119.4, 61.5, 56.7, 42.4, 30.4, 23.0 ppm

**HR-MS** ($m/z$): $[M+H]^+$ calcd for $C_{13}H_{20}N_3O_3^+$: 266.1499; found: 266.1504

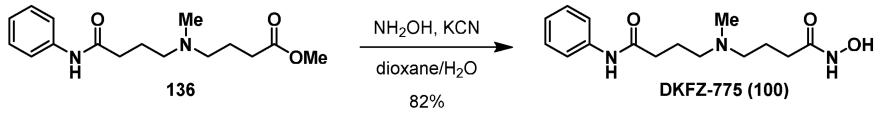


***N*-Hydroxy-4-(methyl(4-oxo-4-(phenylamino)butyl)amino)butanamide (DKFZ-775, 100)**: Ester **136** (156 mg, 0.535 mmol, 1.0 equiv) was converted to hydroxamic acid **100** according to General Procedure A. The product was purified by RP-MPLC (15.5 g C18Aq Teledyne Isco #69-2203-559, gradient: 0% B for 4 CV, 0 → 20% B over 23 CV, then 20% B for 10 CV) to provide **100** as a white solid (129 mg, 0.440 mmol, 82% yield).

**TLC** $R_f$ 0.11 (10% MeOH and 0.5% $NH_4OH$ in $CH_2Cl_2$)

**$^1$H NMR** (600 MHz, DMSO-$d_6$) δ 11.13 – 8.04 (br, 2H*), 9.87 (s, 1H), 7.62 – 7.56 (m, 2H), 7.30 – 7.23 (m, 2H), 7.01 (tt, *J* = 7.3, 1.2 Hz, 1H), 2.36 – 2.26 (m, 4H), 2.24 (t, *J* = 7.3 Hz, 2H), 2.11 (s, 3H), 1.96 (t, *J* = 7.5 Hz, 2H), 1.70 (app p, *J* = 7.3 Hz, 2H), 1.61 (app p, *J* = 7.4 Hz, 2H) ppm; *partially exchanged with adventitious water.

**$^{13}$C NMR** (151 MHz, DMSO-$d_6$) δ 171.2, 169.2, 139.4, 128.6, 122.9, 119.0, 56.5 ($2CH_2$ overlapped), 41.7, 34.3, 30.2, 22.9, 22.8 ppm

**HR-MS** (*m/z*): $[M+H]^+$ calcd for $C_{15}H_{24}N_3O_3^+$: 294.1812; found: 294.1814

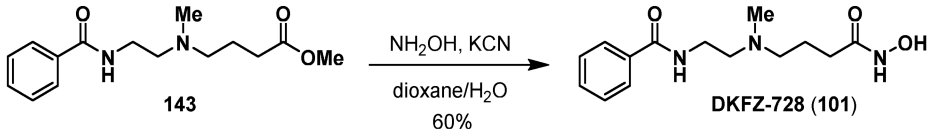


***N*-(2-((4-(Hydroxyamino)-4-oxobutyl)(methyl)amino)ethyl)benzamide (DKFZ-728, 101)**: Ester **143** (259 mg, 0.931 mmol, 1.0 equiv) was converted to hydroxamic acid **101** according to General Procedure A. The product was purified by RP-MPLC (15.5 g C18Aq Teledyne Isco #69-2203-559, gradient: 0 → 17% B over 17 CV) to provide **101** as a white solid (155 mg, 0.55 mmol, 60% yield).

**TLC** $R_f$ 0.26 (20% MeOH in $CH_2Cl_2$)

**$^1$H NMR** (400 MHz, DMSO-$d_6$) δ 9.49 (br s, 2H*), 8.38 (t, *J* = 5.7 Hz, 1H), 7.89 – 7.77 (m, 2H), 7.54 – 7.41 (m, 3H), 3.34 (app q, *J* = 6.4 Hz, 2H), 2.46 (t, *J* = 7.0 Hz, 2H), 2.31 (t, *J* = 7.2 Hz, 2H), 2.18 (s, 3H), 1.96 (t, *J* = 7.4 Hz, 2H), 1.62 (app p, *J* = 7.2 Hz, 2H) ppm; *partially exchanged with adventitious water.

**$^{13}$C NMR** (101 MHz, DMSO-$d_6$) δ 169.1, 166.1, 134.6, 131.0, 128.3, 127.1, 56.5, 56.1, 42.0, 37.3, 30.1, 22.9 ppm

**LC/MS** (*m/z*): $[M+H]^+$ 280.2, $[M-H]^-$ 278.2

**HR-MS** (*m/z*): $[M+H]^+$ calcd for $C_{14}H_{22}N_3O_3^+$: 280.1656; found: 280.1657

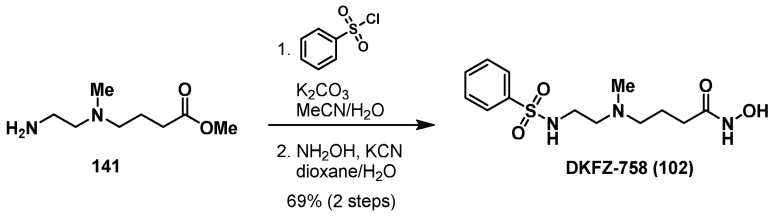


***N*-Hydroxy-4-(methyl(2-(phenylsulfonamido)ethyl)amino)butanamide (DKFZ-758, 102)**: To a stirred solution of **141**·2HCl (121.9 mg, 0.493 mmol, 1.0 equiv) and $K_2CO_3$ (239 mg, 1.726 mmol, 3.5 equiv) in MeCN/water (5:1, 12 mL) was added benzenesulfonyl chloride (82 µL, 0.641 mmol, 1.3 equiv) at rt. After 16 h, TLC indicated complete consumption of **141**, and the reaction mixture was concentrated in vacuo. The residue was partitioned between EtOAc (25 mL) and half saturated aqueous $K_2CO_3$ (30 mL). The phases were separated and the aqueous phase was extracted with EtOAc (2 × 25 mL). The combined organic layers were washed with half saturated aqueous $K_2CO_3$ (2 × 25 mL) and brine (25 mL), dried ($MgSO_4$), filtered, and concentrated. The crude product was directly converted to hydroxamic acid **102** according to General Procedure A. The product was purified by HPLC Basic Method (gradient: 1 → 40% B in 13 min) to provide **102** as white solid (112.3 mg, 0.341 mmol, 69% yield (2 steps)).

**TLC** $R_f$ 0.33 (20% MeOH in $CH_2Cl_2$)

**$^1$H NMR** (400 MHz, DMSO-$d_6$) δ 8.83 (br s, 3H*), 7.81 (d, *J* = 7.2 Hz, 2H), 7.71 – 7.52 (m, 3H), 2.81 (t, *J* = 7.0 Hz, 2H), 2.28 (t, *J* = 7.0 Hz, 2H), 2.17 (t, *J* = 7.2 Hz, 2H), 2.02 (s, 3H), 1.90 (t, *J* = 7.4 Hz, 2H), 1.52 (app p, *J* = 7.3 Hz, 2H) ppm; *partially exchanged with adventitious water.

**$^{13}$C NMR** (101 MHz, DMSO-$d_6$) δ 169.0, 140.6, 132.3, 129.2, 126.5, 56.4, 56.2, 41.6, 40.6, 30.1, 22.8 ppm

**HR-MS** (*m/z*): $[M+H]^+$ calcd for $C_{13}H_{22}N_3O_4S^+$: 316.1326; found: 316.1328

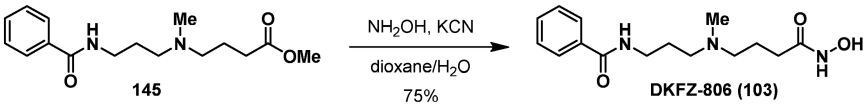


***N*-(3-((4-(hydroxyamino)-4-oxobutyl)(methyl)amino)propyl)benzamide (DKFZ-806, 103): 145** (162 mg, 0.552 mmol, 1.0 equiv) was converted to the hydroxamic acid according to General Procedure A, and purified by RP-MPLC (15.5 g C18Aq #69-2203-559, gradient: 0% B over 5 CV, 0 → 11% B over 15 CV, then 11% B over 20 CV) to provide **DKFZ-806** as a white solid (120 mg, 0.412 mmol, 75% yield).

**TLC** $R_f$ 0.26 (20% MeOH in $CH_2Cl_2$)

**$^1$H NMR** (400 MHz, DMSO-$d_6$) δ 10.34 (br s, 1H*), 8.70 (br s, 1H*), 8.48 (t, *J* = 5.6 Hz, 1H), 7.91 – 7.76 (m, 2H), 7.54 – 7.41 (m, 3H), 3.27 (td, *J* = 7.1, 5.6 Hz, 2H), 2.32 (t, *J* = 7.1 Hz, 2H), 2.25 (t, *J* = 7.2 Hz, 2H), 2.12 (s, 3H), 1.96 (t, *J* = 7.3 Hz, 2H), 1.73 – 1.54 (m, 4H) ppm; *: partially exchanged with adventitious water.

**$^{13}$C NMR** (101 MHz, DMSO-$d_6$) δ 169.1, 166.1, 134.7, 131.0, 128.2, 127.1, 56.6, 55.0, 41.7, 37.8, 30.2, 26.8, 22.9 ppm

**HR-MS** (*m/z*): $[M+H]^+$ calcd for $C_{15}H_{24}N_3O_3^+$: 294.1812; found: 294.1814

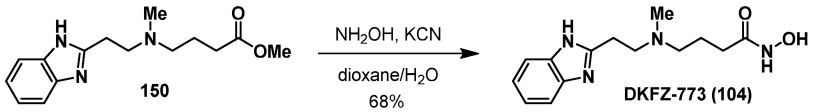


**4-((2-(Benzimidazol-2-yl)ethyl)(methyl)amino)-*N*-hydroxybutanamide (DKFZ-773, 104):** Ester **150** (178 mg, 0.646 mmol, 1.0 equiv) was converted to hydroxamic acid **104** according to General Procedure A. The product was purified by RP-MPLC (15.5 g C18Aq Teledyne Isco #69-2203-559, gradient: 0% B for 6 CV, 0 → 18% B over 25 CV, then 18% B over 4 CV) to provide **104** as white solid (122 mg, 0.442 mmol, 68% yield).

**TLC** $R_f$ 0.10 (20% MeOH in $CH_2Cl_2$)

**$^1$H NMR** (600 MHz, DMSO-$d_6$) δ 13.37 – 9.78 (br, 2H*), 9.71 – 7.75 (br, 1H*), 7.50 – 7.41 (m, 2H, Ar H), 7.13 – 7.07 (m, 2H, Ar H), 2.93 (t, $J$ = 7.5 Hz, 2H, $NCH_2$), 2.76 (t, $J$ = 7.5 Hz, 2H, Ar–$CH_2$), 2.33 (t, $J$ = 7.1 Hz, 2H, $NCH_2$), 2.18 (s, 3H, Me), 1.95 (t, $J$ = 7.4 Hz, 2H, $COCH_2$), 1.63 (app p, $J$ = 7.3 Hz, 2H, $CH_2$–C$H_2$–$CH_2$) ppm; *partially exchanged with adventitious water.

**$^{13}$C NMR** (151 MHz, DMSO-$d_6$) δ 169.2 (CONHOH), 153.9 (N=CNH), 121.1 (Ar CH), 55.9 ($CH_2$), 55.3 (Ar–$CH_2$), 41.6 (Me), 30.1 ($CH_2$), 26.6 ($CH_2$), 22.8 ($CH_2$) ppm; Due to tautomerism of the benzimidazole NH, two benzimidazole carbon signals were too broad to be identified in $^{13}$C spectra. See the spectrum for **33**, where very broad signals could be observed.

**HR-MS** (*m/z*): $[M+H]^+$ calcd for $C_{14}H_{21}N_4O_2^+$: 277.1659; found: 277.1661

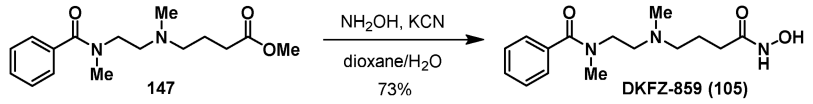


***N*-(2-((4-(Hydroxyamino)-4-oxobutyl)(methyl)amino)ethyl)-*N*-methylbenzamide (DKFZ-859, 105)**: Ester **147** (179 mg, 0.613 mmol, 1.0 equiv) was converted to hydroxamic acid **105** according to General Procedure A. The product was purified by RP-MPLC (15.5 g C18Aq Teledyne Isco #69-2203-559, gradient: 0% B for 2 CV, 0 → 14% B over 14 CV, then 14% B for 10 CV) to provide **105** as an amorphous, colorless solid (131 mg, 0.447 mmol, 73% yield).

**TLC** $R_f$ 0.26 (10% MeOH and 0.5% $NH_4OH$ in $CH_2Cl_2$)

**$^1$H NMR** (400 MHz, DMSO-$d_6$) δ 9.49 (br s, 2H*, –NH–OH), 7.52 – 7.39 (m, 3H, Ar H), 7.39 – 7.25 (m, 2H, Ar H), 3.52 (t, $J$ = 6.8 Hz, 1H, –CONMeC$\underline{H_2}$– rotamer A), 3.24 (t, $J$ = 6.8 Hz, 1H, CONMeC$\underline{H_2}$ rotamer B), 2.96 (s, 1.5H, –CONC$\underline{H_3}$ rotamer A), 2.89 (s, 1.5H, –CONC$\underline{H_3}$ rotamer B), 2.59 – 2.51 (m, 1H, N–$CH_2$–C$\underline{H_2}$–N rotamer A), 2.43 – 2.27 (m, 2H, N–$CH_2$–C$\underline{H_2}$–N rotamer B and N–C$\underline{H_2}$–$CH_2$–$CH_2$– rotamer A), 2.26 – 2.05 (m, 2.5H, –$CH_2$–NC$\underline{H_3}$–$CH_2$– rotamer A and N–C$\underline{H_2}$–$CH_2$–$CH_2$– rotamer B), 2.05 – 1.74 (m, 3.5H, –C$\underline{H_2}$CONHOH and –$CH_2$–NC$\underline{H_3}$–$CH_2$– rotamer B), 1.73 – 1.58

(m, 1H, –$CH_2$–C$\underline{H_2}$–$CH_2$– rotamer A), 1.58 – 1.40 (m, 1H, –$CH_2$–C$\underline{H_2}$–$CH_2$– rotamer B) ppm; *partially exchanged with adventitious water.

**$^{13}$C NMR** (101 MHz, DMSO-$d_6$) δ 170.9 (Ar–CO rotamer A), 169.9 (Ar–CO rotamer B), 169.0 (CONHOH), 136.8 (Ar$\underline{C}$–CO), 129.1 (ArCH rotamer A), 129.1 (ArCH rotamer B), 128.3 (ArCH), 126.6 (ArCH), 56.8 (N–$\underline{C}$$H_2$–$CH_2$–$CH_2$–), 54.8 (N–$CH_2$–$\underline{C}$$H_2$–N rotamer A), 54.2 (N–$CH_2$–$\underline{C}$$H_2$–N rotamer B), 48.4 (N–$\underline{C}$$H_2$–$CH_2$–N rotamer A), 44.6 (N–$\underline{C}$$H_2$–$CH_2$–N rotamer B), 41.9 (–$CH_2$–N$\underline{C}$$H_3$–$CH_2$– rotamer A), 41.7 (–$CH_2$–N$\underline{C}$$H_3$–$CH_2$– rotamer B), 37.6 (–CON$\underline{C}$$H_3$ rotamer A), 32.7 (–CON$\underline{C}$$H_3$ rotamer B), 30.1 (–$\underline{C}$$H_2$CONHOH rotamer A), 30.0 (–$\underline{C}$$H_2$CONHOH rotamer B), 23.1 (–$CH_2$–$\underline{C}$$H_2$–$CH_2$– rotamer A), 22.9 (–$CH_2$–$\underline{C}$$H_2$–$CH_2$– rotamer B) ppm

Note: The $^1$H and $^{13}$C NMR spectra each show two rotamers with overlapping signals. An EXSY experiment confirmed that each set of two signals originates from the same nucleus**.** Overlapping rotamer signals were differentiated by the attached HSQC edit experiment. The ratio of rotamer A to B is 1:1.

**HR-MS** (*m/z*): $[2M+Na]^+$ calcd for $C_{30}H_{46}N_6NaO_6^+$: 609.3371; found: 609.3371

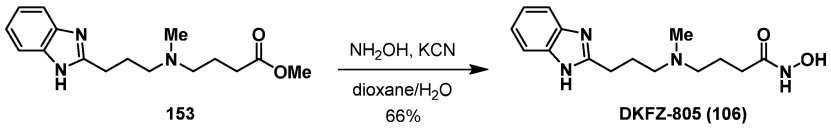


**153** **DKFZ-805 (106)**

**4-((3-(Benzimidazol-2-yl)propyl)(methyl)amino)-*N*-hydroxybutanamide** (**DKFZ-805, 106**): Ester **153** (118 mg, 0.408 mmol, 1.0 equiv) was converted to hydroxamic acid **106** according to General Procedure A. The product was purified by RP-MPLC (15.5 g C18Aq Teledyne Isco #69-2203-559, gradient: 0% B for 8 CV, 0 → 19% B over 22 CV, then 19% B over 5 CV) to provide **106** as a colorless solid (78.6 mg, 0.271 mmol, 66% yield).

**TLC** $R_f$ 0.07 (20% MeOH in $CH_2Cl_2$)

**$^1$H NMR** (600 MHz, DMSO-$d_6$) δ 12.17 (br s, 1H*), 10.47 (br s, 1H*), 9.43 – 8.42 (br, 1H*), 7.50 – 7.41 (m, 2H), 7.12 – 7.08 (m, 2H), 2.81 (t, *J* = 7.7 Hz, 2H), 2.33 (t, *J* = 7.0 Hz, 2H), 2.25 (t, *J* = 7.1 Hz, 2H), 2.12 (s, 3H), 1.98 (t, *J* = 7.4 Hz, 2H), 1.87 (app p, *J* = 7.3 Hz, 2H), 1.62 (app p, *J* = 7.3 Hz, 2H) ppm; *partially exchanged with adventitious water.

**$^{13}$C NMR** (101 MHz, DMSO-$d_6$) δ 169.2, 155.2, 142.2 (br), 134.9 (br), 121.1, 117.3 (br), 111.7 (br), 56.6, 56.4, 41.7, 30.2, 26.4, 25.4, 22.9 ppm; the broad signals are due to tautomerism of the benzimidazole NH.

**HR-MS** (*m/z*): $[M+H]^+$ calcd for $C_{15}H_{23}N_4O_2^+$: 291.1816; found: 291.1816

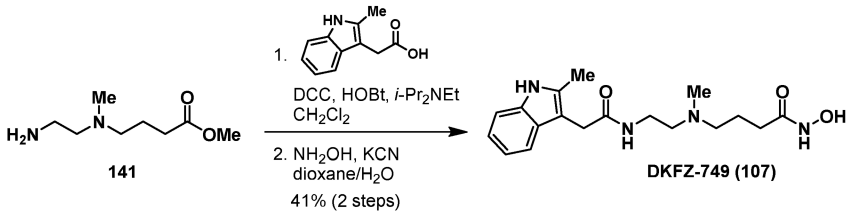


***N*-Hydroxy-4-(methyl(2-(2-(2-methyl-1*H*-indol-3-yl)acetamido)ethyl)amino) butanamide** (**DKFZ-749, 107**): To a suspension of diamine **141**·2HCl (84.6 mg, 0.342 mmol, 1.0 equiv), DCC (106 mg, 0.513 mmol, 1.5 equiv), HOBt (5 mg, 0.034 mmol, 0.1 equiv) and 2-methyl-3-indoleacetic acid (71.2 mg, 0.377 mmol, 1.1 equiv) in $CH_2Cl_2$ (8 mL) was added *i*-$Pr_2NEt$ (0.146 mL, 0.856 mmol, 2.5 equiv). The reaction mixture was stirred at rt for 16 h, then cooled to –20 °C and filtered through a fritted syringe into EtOAc (50 mL). The solution was washed with saturated aqueous $NaHCO_3$ (3 × 40 mL), then dried ($MgSO_4$), filtered, and concentrated. The residue still contained DCU crystals and was therefore suspended in $Et_2O$/MeCN (1:1, 3 mL) and filtered through a cotton plug. The concentrated filtrate was directly converted to hydroxamic acid **107** according to General Procedure A. The product was purified by HPLC Basic Method (gradient: 1 → 50% B in 12 min) to provide **107** as an off-white solid (48.1 mg, 0.139 mmol, 41% yield (2 steps)).

**TLC** $R_f$ 0.33 (20% MeOH in $CH_2Cl_2$)

**$^1$H NMR** (400 MHz, DMSO-$d_6$) δ 10.78 (br s, 1H*), 9.45 (br s, 2H*), 7.60 (t, *J* = 5.6 Hz, 1H), 7.43 (dt, *J* = 7.6, 1.0 Hz, 1H), 7.22 (dt, *J* = 8.0, 1.0 Hz, 1H), 6.96 (ddd, *J* = 8.0, 7.0, 1.3 Hz, 1H), 6.90 (ddd, *J* = 8.0, 7.0, 1.2 Hz, 1H), 3.43 (s, 2H), 3.09 (app q, *J* = 6.4 Hz, 2H), 2.33 (s, 3H), 2.29 (t, *J* = 6.8 Hz, 2H), 2.22 (t, *J* = 7.2 Hz, 2H), 2.08 (s, 3H), 1.91 (t, *J* = 7.4 Hz, 2H), 1.55 (app p, *J* = 7.3 Hz, 2H) ppm; *partially exchanged with adventitious water.

**$^{13}$C NMR** (101 MHz, DMSO-$d_6$) δ 170.6, 169.0, 135.1, 133.0, 128.4, 119.9, 118.1, 117.8, 110.2, 104.9, 56.5, 56.3, 41.7, 36.7, 31.6, 30.2, 22.9, 11.4 ppm

**HR-MS** (*m/z*): $[M+H]^+$ calcd for $C_{18}H_{27}N_4O_3^+$: 347.2078; found: 347.2077

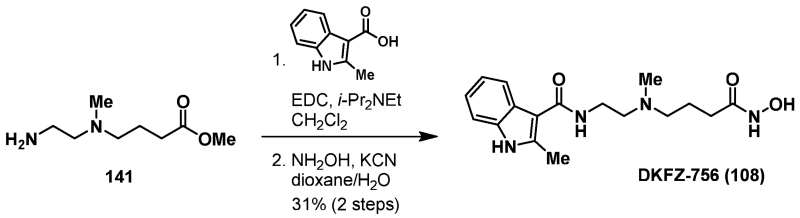


***N*-(2-((4-(Hydroxyamino)-4-oxobutyl)(methyl)amino)ethyl)-2-methyl-1*H*-indole-3-carboxamide** (**DKFZ-756, 108**): The corresponding methyl ester of the title compound was prepared from ester **141**·2HCl (70.4 mg, 0.285 mmol, 1.0 equiv) and 2-methyl-1*H*-indole-3-carboxylic acid (54.9 mg, 0.313 mmol, 1.1 equiv) according to General Procedure B. The crude product was directly converted to hydroxamic acid **108** according to General Procedure A. The product was purified by RP-MPLC (15.5 g C18 Teledyne Isco #69-2203-334, gradient: 0% B for

3 CV, then 0 → 15% over 12 CV) to provide **108** as white, fluffy solid (29.7 mg, 0.089 mmol, 31% yield (2 steps)).

**TLC** $R_f$ 0.17 (20% MeOH in $CH_2Cl_2$)

**$^1$H NMR** (400 MHz, DMSO-$d_6$) δ 11.44 (s, 1H*), 10.80 – 8.18 (br, 2H*), 7.78 – 7.71 (m, 1H), 7.35 – 7.28 (m, 1H), 7.20 (t, *J* = 5.5 Hz, 1H), 7.11 – 7.01 (m, 2H), 3.41 – 3.33 (m, overlapped with water peak), 2.57 (s, 3H), 2.54 – 2.46 (m, overlapped with DMSO signal), 2.34 (t, *J* = 7.2 Hz, 2H), 2.20 (s, 3H), 1.98 (t, *J* = 7.5 Hz, 2H), 1.66 (app p, *J* = 7.3 Hz, 2H) ppm; *partially exchanged with adventitious water.

**$^{13}$C NMR** (101 MHz, DMSO-$d_6$) δ 169.0, 165.2, 139.3, 134.6, 125.9, 120.9, 119.9, 119.2, 110.9, 107.7, 56.7, 56.5, 41.7, 36.6, 30.2, 23.1, 13.2 ppm

**HR-MS** (*m/z*): $[M+H]^+$ calcd for $C_{17}H_{25}N_4O_3^+$: 333.1921; found: 333.1921

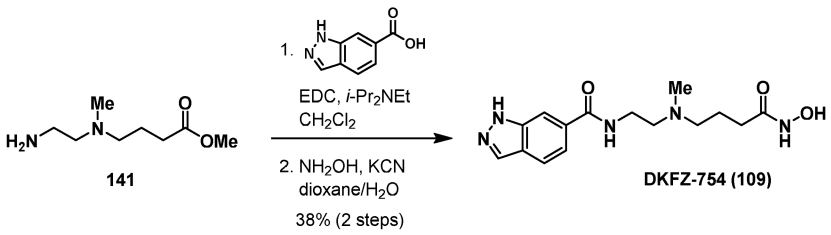


***N*-(2-((4-(Hydroxyamino)-4-oxobutyl)(methyl)amino)ethyl)-1H-indazole-6-carboxamide** (**DKFZ-754, 109**): The corresponding methyl ester of the title compound was prepared from ester **141**·2HCl (65.1 mg, 0.263 mmol, 1.0 equiv) and 1*H*-indazole-6-carboxylic acid (44.8 mg, 0.277 mmol, 1.05 equiv) according to General Procedure B. The crude product was directly converted to hydroxamic acid **109** according to General Procedure A. The product was purified by HPLC Basic Method (gradient: 1 → 25% B in 12 min) to provide **109** as a pale yellow solid (32.3 mg, 0.101 mmol, 38% yield (2 steps)).

**$^1$H NMR** (400 MHz, DMSO-$d_6$) δ 12.54 – 9.09 (br, 3H*), 8.50 (t, *J* = 5.7 Hz, 1H), 8.13 (d, *J* = 0.9 Hz, 1H), 8.04 (s, 1H), 7.80 (dd, *J* = 8.5, 0.9 Hz, 1H), 7.57 (dd, *J* = 8.5, 1.4 Hz, 1H), 3.38 (app q, *J* = 6.5 Hz, 2H), 2.56 – 2.45 (m, overlapped with DMSO signal), 2.33 (t, *J* = 7.3 Hz, 2H), 2.20 (s, 3H), 1.97 (t, *J* = 7.3 Hz, 2H), 1.64 (app p, *J* = 7.3 Hz, 2H) ppm; *partially exchanged with adventitious water.

**$^{13}$C NMR** (101 MHz, DMSO-$d_6$) δ 169.1, 166.5, 139.5, 133.4, 132.4, 124.2, 120.2, 119.2, 109.6, 56.5, 56.2, 42.0, 37.4, 30.2, 22.9 ppm

**HR-MS** (*m/z*): $[M+Na]^+$ calcd for $C_{15}H_{21}N_5NaO_3^+$: 342.1537; found: 342.1541

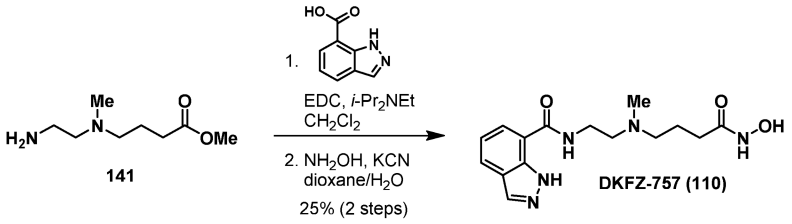


***N*-(2-((4-(Hydroxyamino)-4-oxobutyl)(methyl)amino)ethyl)-1*H*-indazole-7-carboxamide (DKFZ-757, 110)**: The corresponding methyl ester of the title compound was prepared from ester **141**·2HCl (196.0 mg, 0.793 mmol, 1.0 equiv) and 1*H*-indazole-6-carboxylic acid (141 mg, 0.872 mmol, 1.1 equiv) according to General Procedure B. The crude product was directly converted to hydroxamic acid **110** according to General Procedure A. The product was purified by HPLC Basic Method (gradient: 1 → 40% B in 12 min) to provide **110** as white solid (67.0 mg, 0.202 mmol, 25% yield (2 steps)).

**TLC** $R_f$ 0.08 (20% MeOH in $CH_2Cl_2$)

**$^1$H NMR** (400 MHz, DMSO-$d_6$) δ 8.73 (br s, 1H*), 8.15 (s, 1H), 7.96 – 7.90 (m, 1H), 7.90 – 7.81 (m, 1H), 7.20 – 7.12 (m, 1H), 3.44 (app q, *J* = 6.5 Hz, 2H), 2.52 (t, *J* = 7.3 Hz, 2H), 2.34 (t, *J* = 7.1 Hz, 2H), 2.21 (s, 3H), 2.00 (t, *J* = 7.4 Hz, 2H), 1.65 (app p, *J* = 7.4 Hz, 2H) ppm; *partially exchanged with adventitious water.

**$^{13}$C NMR** (101 MHz, DMSO-$d_6$) δ 169.2, 165.7, 138.5, 133.0, 124.5, 124.2, 124.1, 119.4, 117.5, 56.6, 56.2, 41.9, 37.1, 30.1, 22.9 ppm

**HR-MS** (*m/z*): $[M+H]^+$ calcd for $C_{15}H_{22}N_5O_3^+$: 320.1717; found: 320.1719

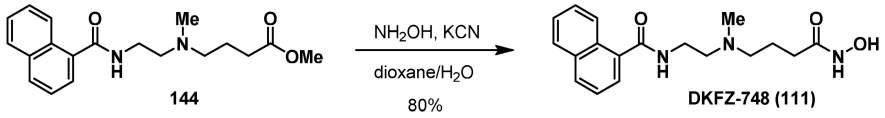


***N*-(2-((4-(Hydroxyamino)-4-oxobutyl)(methyl)amino)ethyl)-1-naphthamide (DKFZ-748, 111)**: Ester **144** (206 mg, 0.628 mmol, 1.0 equiv) was converted to hydroxamic acid **111** according to General Procedure A. The product was purified by RP-MPLC (15.5 g C18Aq Teledyne Isco #69-2203-559, gradient: 0% B for 3.5 CV, 0 → 25% over 22.5 CV, then 25% B for 9 CV) to provide **DKFZ-748** (**111**) as a white solid (166 mg, 0.504 mmol, 80% yield).

**TLC** $R_f$ 0.28 (20% MeOH in $CH_2Cl_2$)

**$^1$H NMR** (400 MHz, DMSO-$d_6$) δ 10.37 (br s, 1H), 8.81 (br s, 1H*), 8.43 (t, *J* = 5.7 Hz, 1H), 8.27 – 8.20 (m, 1H*), 8.05 – 7.92 (m, 2H), 7.62 – 7.49 (m, 4H), 3.42 (app q, *J* = 6.5 Hz, 2H), 2.54 (t, *J* = 6.8 Hz, 2H), 2.35 (t, *J* = 7.2 Hz, 2H), 2.23 (s, 3H), 1.99 (t, *J* = 7.4 Hz, 2H), 1.67 (app p, *J* = 7.3 Hz, 2H) ppm; *partially exchanged with adventitious water.

**$^{13}$C NMR** (101 MHz, DMSO-$d_6$) δ 169.1, 168.5, 135.2, 133.1, 129.7, 129.6, 128.2, 126.6, 126.2, 125.5, 125.0, 125.0, 56.6, 56.3, 41.9, 37.2, 30.2, 23.1 ppm

**HR-MS** (*m/z*): $[M+H]^+$ calcd for $C_{18}H_{24}N_3O_3^+$: 330.1812; found: 330.1814

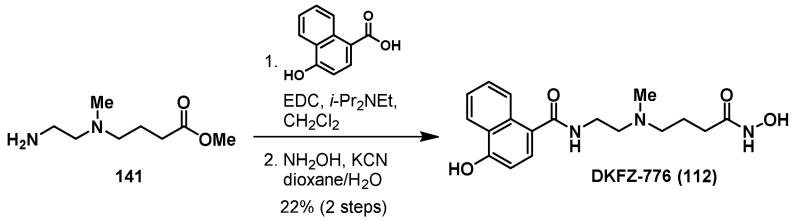


**4-Hydroxy-*N*-(2-((4-(hydroxyamino)-4-oxobutyl)(methyl)amino)ethyl)-1-naphthamide** (**DKFZ-776, 112**): The corresponding methyl ester of the title compound was prepared from ester **141**·2HCl (71.3 mg, 0.288 mmol, 1.0 equiv) and 4-hydroxy-1-naphthoic acid[223] (100 mg, 0.531 mmol, 1.0 equiv) according to General Procedure B. The product was purified by MPLC (4 g silica, gradient: 0 → 5% MeOH in $CH_2Cl_2$ over 20 CV, 5% MeOH for 30 CV, then 5 → 20% MeOH over 20 CV) to provide the corresponding methyl ester of **112** (78.4 mg, *m/z*: $[M+H]^+$: 345.2, $[M-H]^-$: 343.2), which was directly converted to hydroxamic acid **112** according to General Procedure A. The product was purified by RP-MPLC (15.5 g C18Aq Teledyne Isco #69-2203-559, gradient: 0% B for 6 CV, 0 → 14% over 20 CV, 14 → 17% B over 10 CV, then 17% B over 4 CV) to provide **112** as off-white solid (22.4 mg, 0.065 mmol, 22% yield (2 steps)).

**TLC** $R_f$ 0.03 (20% MeOH in $CH_2Cl_2$)

**$^1$H NMR** (600 MHz, DMSO-$d_6$) δ 10.98 – 9.72 (br, 2H*), 8.31 (d, *J* = 8.5 Hz, 1H), 8.21 – 8.14 (m, 2H), 7.55 – 7.49 (m, 1H), 7.49 – 7.43 (m, 2H), 6.84 (d, *J* = 7.8 Hz, 1H), 3.37 (app q, *J* = 6.5 Hz, 2H), 2.54 – 2.48 (m, overlapped with DMSO signal), 2.34 (t, *J* = 7.2 Hz, 2H), 2.21 (s, 3H), 1.99 (t, *J* = 7.4 Hz, 2H), 1.66 (app p, *J* = 7.4 Hz, 2H) ppm; *partially exchanged with adventitious water.

**$^{13}$C NMR** (151 MHz, DMSO-$d_6$) δ 169.2, 168.6, 155.0, 131.6, 126.7, 126.7, 125.5, 125.2, 124.7, 124.5, 122.2, 106.6, 56.6, 56.3, 41.9, 37.2, 30.2, 23.0 ppm

**HR-MS** (*m/z*): $[M+H]^+$ calcd for $C_{18}H_{24}N_3O_4^+$: 346.1761; found: 346.1762

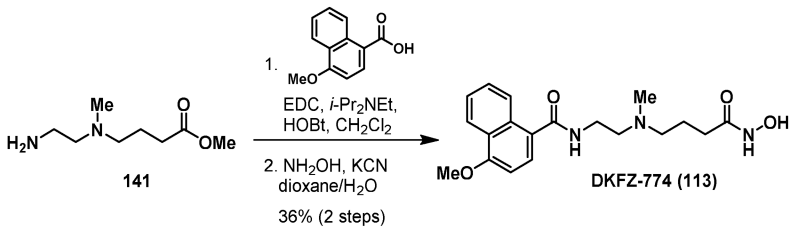


***N*-(2-((4-(Hydroxyamino)-4-oxobutyl)(methyl)amino)ethyl)-4-methoxy-1-naphthamide** (**DKFZ-774, 113**): The corresponding methyl ester of the title compound was prepared from ester **141**·2HCl (113.7 mg, 0.460 mmol, 1.0 equiv) and 4-methoxy-1-naphthoic acid (102 mg, 0.506 mmol, 1.1 equiv) according to General Procedure B. The crude product was directly converted to hydroxamic acid **113** according to General Procedure A. The product was purified by RP-MPLC (15.5 g C18Aq Teledyne Isco #69-2203-559, gradient: 0 → 4% B over 12 CV, 4 → 20% B over 16 CV, then 20% B for 2 CV) to provide **113** as white fluffy powder (59.7 mg, 0.166 mmol, 36% yield (2 steps)).

**TLC** $R_f$ 0.11 (20% MeOH in $CH_2Cl_2$)

**$^1$H NMR** (600 MHz, DMSO-$d_6$) δ 10.26 – 8.91 (br, 2H*), 8.32 (d, *J* = 8.4 Hz, 1H), 8.29 (t, *J* = 5.7 Hz, 1H), 8.20 (d, *J* = 8.4 Hz, 1H), 7.59 – 7.55 (m, 2H), 7.55 – 7.50 (m, 1H), 6.98 (d, *J* = 8.0 Hz, 1H), 4.00 (s, 3H), 3.39 (app q, *J* = 6.5 Hz, 2H), 2.52 (t, *J* = 6.9 Hz, 2H), 2.34 (t, *J* = 7.2 Hz, 2H), 2.22 (s, 3H), 1.98 (t, *J* = 7.4 Hz, 2H), 1.66 (app p, *J* = 7.3 Hz, 2H) ppm; *partially exchanged with adventitious water.

**$^{13}$C NMR** (151 MHz, DMSO-$d_6$) δ 169.1, 168.4, 155.9, 131.1, 127.1, 127.0, 126.3, 125.6, 125.5, 124.7, 121.6, 103.1, 56.6, 56.3, 55.8, 41.9, 37.2, 30.2, 23.1 ppm

**HR-MS** (*m/z*): $[M+H]^+$ calcd for $C_{19}H_{26}N_3O_4^+$: 360.1918; found: 360.1919

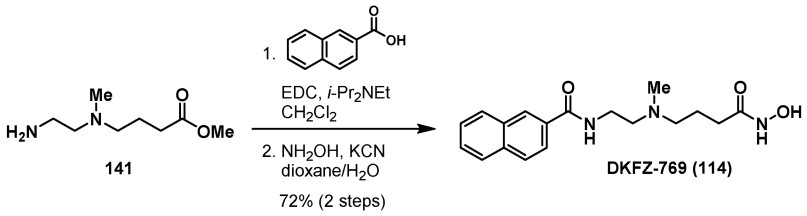


***N*-(2-((4-(Hydroxyamino)-4-oxobutyl)(methyl)amino)ethyl)-2-naphthamide (DKFZ-769, 114)**: The corresponding methyl ester of the title compound was prepared from ester **141**·2HCl (86.1 mg, 0.348 mmol, 1.0 equiv) and 2-naphthoic acid (66.0 mg, 0.383 mmol, 1.1 equiv) according to General Procedure B. The crude product was directly converted to hydroxamic acid **114** according to General Procedure A. The product was purified by RP-MPLC (15.5 g C18Aq Teledyne Isco #69-2203-559, gradient: 0% B for 3 CV, then 0 → 20% over 22 CV, then 50% B for 4 CV) to provide **114** as white solid (82.8 mg, 0.251 mmol, 72% yield (2 steps)).

**TLC** $R_f$ 0.13 (20% MeOH in $CH_2Cl_2$)

**$^1$H NMR** (600 MHz, DMSO-$d_6$) δ 9.53 (br s, 2H*), 8.58 (t, *J* = 5.7 Hz, 1H), 8.44 (s, 1H), 8.05 – 7.89 (m, 4H), 7.64 – 7.56 (m, 2H), 3.41 (app q, *J* = 6.6 Hz, 2H), 2.52 (t, *J* = 7.1 Hz, 2H), 2.34 (t, *J* = 7.2 Hz, 2H), 2.21 (s, 3H), 1.99 (t, *J* = 7.4 Hz, 2H), 1.65 (app p, *J* = 7.3 Hz, 2H) ppm; *partially exchanged with adventitious water.

**$^{13}$C NMR** (151 MHz, DMSO-$d_6$) δ 169.1, 166.2, 134.1, 132.2, 132.0, 128.8, 127.8, 127.6, 127.5, 127.3, 126.7, 124.1, 56.5, 56.2, 42.0, 37.4, 30.2, 22.9 ppm

**HR-MS** (*m/z*): $[M+H]^+$ calcd for $C_{18}H_{24}N_3O_3^+$: 330.1812; found: 330.1814

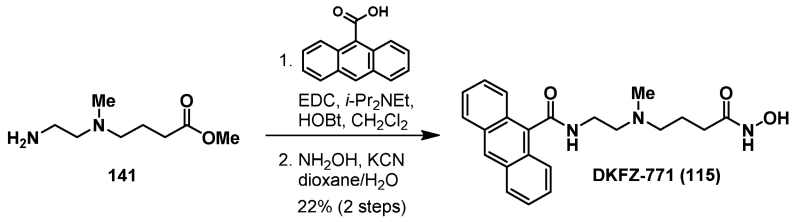


***N*-(2-((4-(Hydroxyamino)-4-oxobutyl)(methyl)amino)ethyl)anthracene-9-carboxamide (DKFZ-771, 115)**: The corresponding methyl ester of the title compound was prepared from ester **141**·2HCl (92.7 mg, 0.375 mmol, 1.0 equiv) and anthracene-9-carboxylic acid (91.7 mg, 0.413 mmol, 1.1 equiv) according to General Procedure B. The crude product was purified by MPLC (12 g silica, gradient: 0 → 4% MeOH in $CH_2Cl_2$ over 13 CV, then 4% MeOH for 20 CV, then 4 → 8% MeOH over 10 CV) to provide the corresponding methyl ester of **115** (62.3 mg, TLC $R_f$ 0.46 (20% MeOH in $CH_2Cl_2$), *m/z*: $[M+H]^+$: 379.2), which was directly converted to hydroxamic acid **115** according to General Procedure A. The product was purified by RP-MPLC (15.5 g C18Aq Teledyne Isco #69-2203-559, gradient: 0% B for 2 CV, 0 → 22% B over 12 CV, 22% B for 9 CV, 22 → 36% B over 5 CV, then 36% B over 5 CV) to provide **115** as off-white fluffy powder (31.2 mg, 0.082 mmol, 22% yield (2 steps)).

**TLC** $R_f$ 0.16 (20% MeOH in $CH_2Cl_2$)

**$^1$H NMR** (600 MHz, DMSO-$d_6$) δ 8.74 (t, *J* = 5.8 Hz, 1H), 8.64 (s, 1H), 8.14 – 8.10 (m, 2H), 8.09 – 8.04 (m, 2H), 7.60 – 7.51 (m, 4H), 3.58 (app q, *J* = 6.3 Hz, 2H), 2.62 (t, *J* = 6.6 Hz, 2H), 2.40 (t, *J* = 7.2 Hz, 2H), 2.29 (s, 3H), 2.01 (t, *J* = 7.5 Hz, 2H), 1.73 (app p, *J* = 7.5 Hz, 2H) ppm; *partially exchanged with adventitious water.

**$^{13}$C NMR** (151 MHz, DMSO-$d_6$) δ 169.1, 168.1, 133.5, 130.7, 128.3, 127.3, 127.0, 126.3, 125.5 (2 Ar CH), 56.8, 56.6, 41.7, 37.2, 30.3, 23.2 ppm

**HR-MS** (*m/z*): $[M+H]^+$ calcd for $C_{22}H_{26}N_3O_3^+$: 380.1969; found: 380.1974

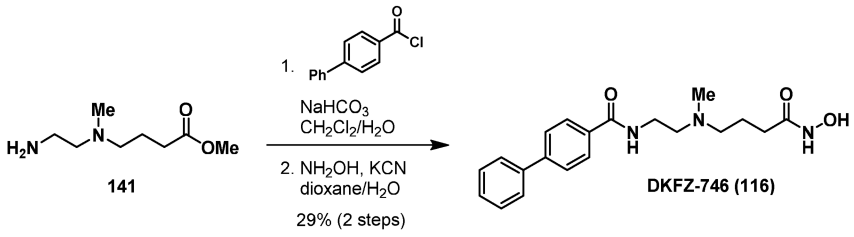


***N*-(2-((4-(Hydroxyamino)-4-oxobutyl)(methyl)amino)ethyl)-[1,1'-biphenyl]-4-carboxamide (DKFZ-746, 116)**: To a vigorously stirred solution of **141**·2HCl (82 mg, 0.330 mmol, 1.0 equiv) in saturated aqueous $NaHCO_3$ (6 mL) and $CH_2Cl_2$ (10 mL) was added 4-phenylbenzoyl chloride (125 mg, 0.577 mmol, 1.8 equiv). After 135 min, the reaction mixture was diluted with water (100 mL) and extracted with $CH_2Cl_2$ (3 × 30 mL). The combined organic layers were washed with half saturated aqueous $K_2CO_3$ (twice) and brine (50 mL), dried ($MgSO_4$), filtered, and concentrated. The residue was directly converted to hydroxamic acid **116** according to General Procedure A. The product was purified by HPLC Basic Method

(gradient: 1 → 75% B in 12 min) to provide **116** as a white fluffy solid (34.3 mg, 0.097 mmol, 29% yield (2 steps)).

**$^1$H NMR** (400 MHz, MeOD-$d_4$) δ 7.94 – 7.87 (m, 2H), 7.73 – 7.68 (m, 2H), 7.68 – 7.62 (m, 2H), 7.49 – 7.42 (m, 2H), 7.40 – 7.33 (m, 1H), 3.53 (t, *J* = 6.8 Hz, 2H), 2.63 (t, *J* = 6.8 Hz, 2H), 2.50 – 2.43 (m, 2H), 2.32 (s, 3H), 2.12 (t, *J* = 7.3 Hz, 2H), 1.81 (app p, *J* = 7.3 Hz, 2H) ppm

**$^{13}$C NMR** (101 MHz, MeOD-$d_4$) δ 172.1, 169.9, 145.7, 141.3, 134.3, 130.0, 129.1, 128.9, 128.1, 128.0, 57.9, 57.3, 42.4, 38.5, 31.6, 24.1 ppm

**HR-MS** (*m/z*): $[M+H]^+$ calcd for $C_{20}H_{26}N_3O_3^+$: 356.1969; found: 356.1972

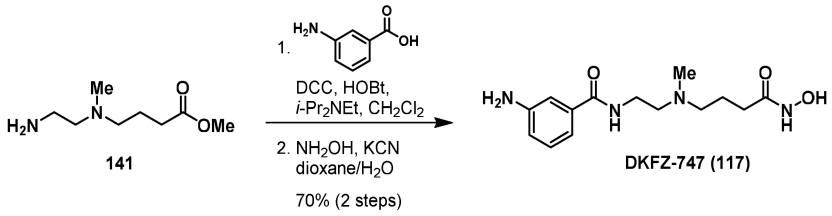


**3-Amino-*N*-(2-((4-(hydroxyamino)-4-oxobutyl)(methyl)amino)ethyl)benzamide (DKFZ-747, 117)**: To a suspension of diamine **141**·2HCl (80.0 mg, 0.324 mmol, 1.0 equiv), DCC (100 mg, 0.486 mmol, 1.5 equiv), HOBt (5 mg, 0.032 mmol, 0.1 equiv) and 3-aminobenzoic acid (48.8 mg, 0.356 mmol, 1.1 equiv) in $CH_2Cl_2$ (8 mL) was added *i*-$Pr_2NEt$ (0.138 mL, 0.809 mmol, 2.5 equiv). The reaction mixture was stirred at rt for 16 h, then cooled to –20 °C and filtered through a fritted syringe. The filter cake was washed with ice-cold $CH_2Cl_2$ (4 mL), and the combined filtrates were concentrated in vacuo. The crude product was directly converted to hydroxamic acid **117** according to General Procedure A. The product was purified by HPLC Basic Method (gradient: 1 → 30% B in 12 min) to provide **117** as an off-white powder (66.8 mg, 0.227 mmol, 70% yield (2 steps)).

**$^1$H NMR** (400 MHz, DMSO-$d_6$) δ 10.82 – 8.38 (br, 2H), 8.08 (t, *J* = 5.7 Hz, 1H), 7.05 (t, *J* = 7.8 Hz, 1H), 7.00 (t, *J* = 2.0 Hz, 1H), 6.91 (dt, *J* = 7.6, 1.4 Hz, 1H), 6.70 – 6.63 (m, 1H), 5.20 (s, 2H*), 3.32 – 3.24 (m, overlapped with water peak), 2.43 (t, *J* = 7.0 Hz, 2H), 2.30 (t, *J* = 7.2 Hz, 2H), 2.17 (s, 3H), 1.96 (t, *J* = 7.4 Hz, 2H), 1.61 (app p, *J* = 7.4 Hz, 2H) ppm; *partially exchanged with adventitious water.

**$^{13}$C NMR** (101 MHz, DMSO-$d_6$) δ 169.1, 166.9, 148.6, 135.6, 128.6, 116.3, 114.2, 112.7, 56.5, 56.2, 41.9, 37.1, 30.1, 22.9 ppm

**HR-MS** (*m/z*): $[M+H]^+$ calcd for $C_{14}H_{23}N_4O_3^+$: 295.1765; found: 295.1768

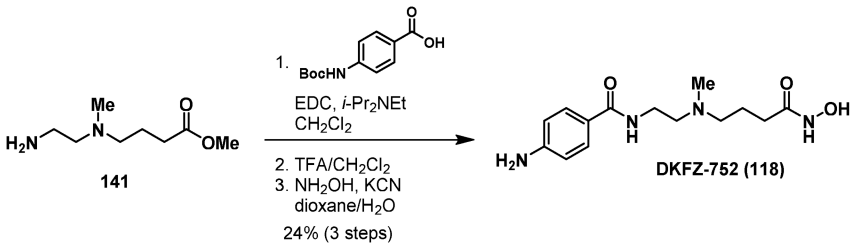


**4-Amino-*N*-(2-((4-(hydroxyamino)-4-oxobutyl)(methyl)amino)ethyl)benzamide (DKFZ-752, 118)**: The corresponding methyl ester of the title compound was prepared from ester **141**·2HCl (103.8 mg, 0.420 mmol, 1.0 equiv) and Boc-protected 4-aminobenzoic acid (107 mg, 0.462 mmol, 1.1 equiv) according to General Procedure B. The crude product was dissolved in TFA/$CH_2Cl_2$ (5 mL, 20% TFA in $CH_2Cl_2$), stirred at rt for 1 h, then concentrated and residual TFA co-evaporated with MeOH (2 x 20 mL). The crude TFA salt was directly converted to hydroxamic acid **118** according to General Procedure A. The product was purified by HPLC Basic Method (gradient: 1 → 30% B in 12 min) to provide **118** as off-white solid (30.2 mg, 0.103 mmol, 24% yield (3 steps)).

**$^1$H NMR** (400 MHz, DMSO-$d_6$) δ 8.42 (s, 1H), 10.66 – 8.26 (m, 2H), 7.87 (t, *J* = 5.6 Hz, 1H), 7.58 – 7.49 (m, 2H), 6.56 – 6.48 (m, 2H), 5.57 (s, 2H), 3.27 (app q, *J* = 6.4 Hz, 2H), 2.41 (t, *J* = 7.1 Hz, 2H), 2.29 (t, *J* = 7.2 Hz, 2H), 2.16 (s, 3H), 1.95 (t, *J* = 7.4 Hz, 2H), 1.61 (app p, *J* = 7.2 Hz, 2H) ppm

**$^{13}$C NMR** (101 MHz, DMSO-$d_6$) δ 169.1, 166.1, 151.5, 128.6, 121.3, 112.5, 56.5, 56.4, 42.0, 37.0, 30.1, 22.9 ppm

**HR-MS** (*m/z*): $[M+H]^+$ calcd for $C_{14}H_{23}N_4O_3^+$: 295.1765; found: 295.1768

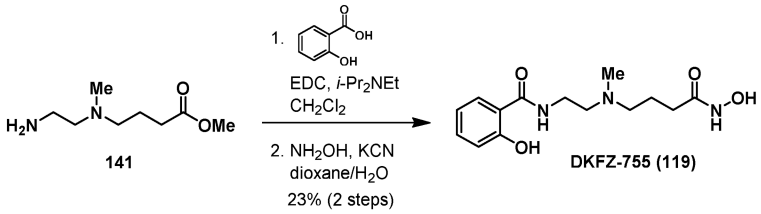


**2-Hydroxy-*N*-(2-((4-(hydroxyamino)-4-oxobutyl)(methyl)amino)ethyl)benzamide (DKFZ-755, 119)**: The corresponding methyl ester of the title compound was prepared from ester **141**·2HCl (88.7 mg, 0.359 mmol, 1.0 equiv) and salicylic acid (54.5 mg, 0.395 mmol, 1.1 equiv) according to General Procedure B. The crude product was directly converted to hydroxamic acid **119** according to General Procedure A. The product was purified by HPLC Basic Method (gradient: 1 → 5% B in 9 min) to provide **119** as an off-white solid (24.9 mg, 0.084 mmol, 23% yield (2 steps)).

**TLC** $R_f$ 0.24 (20% MeOH in $CH_2Cl_2$)

**$^1$H NMR** (400 MHz, DMSO-$d_6$) δ 10.34 (s, 1H*), 8.97 – 8.42 (m, 2H*), 8.77 (t, *J* = 5.5 Hz, 1H), 7.82 (dd, *J* = 7.9, 1.7 Hz, 1H), 7.43 – 7.34 (m, 1H), 6.93 – 6.83 (m, 2H), 3.42 – 3.36 (m, overlapped with water peak), 2.57 – 2.51 (m, 2H), 2.36 (t, *J* = 7.3 Hz, 2H), 2.23 (s, 3H), 1.96 (t, *J* = 7.4 Hz,

2H), 1.70 – 1.58 (m, 2H) ppm; The four Ar H show rotamer signals with a ratio of 1:0.16. Only the major rotamer is reported. *partially exchanged with adventitious water.

**$^{13}$C NMR** (151 MHz, DMSO-$d_6$) δ 169.1, 168.5, 159.7, 133.5, 127.9, 118.6, 117.3, 115.8, 56.4, 55.6, 41.7, 36.8, 30.0, 22.7 ppm; Only signals of the major rotamer are reported.

**HR-MS** (*m/z*): $[M+H]^+$ calcd for $C_{14}H_{22}N_3O_4^+$: 296.1605; found: 296.1609

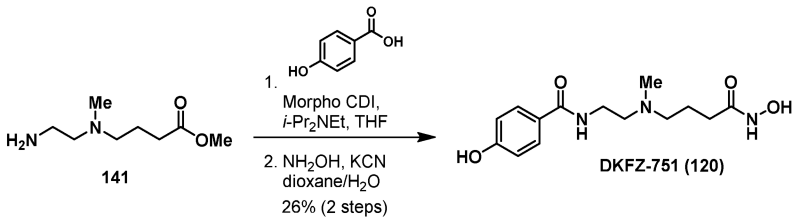


**4-Hydroxy-*N*-(2-((4-(hydroxyamino)-4-oxobutyl)(methyl)amino)ethyl)benzamide (DKFZ-751, 120)**: The corresponding methyl ester of the title compound was prepared from ester **141**·2HCl (103.8 mg, 0.420 mmol, 1.0 equiv) and 4-hydroxybenzoic acid (63.8 mg, 0.462 mmol, 1.1 equiv) according to General Procedure B, but in THF with Morpho CDI (N-Cyclohexyl-N′-(2-morpholinoethyl)carbodiimide methyl-p-toluenesulfonate) as coupling reagent. The crude product was directly converted to hydroxamic acid **120** according to General Procedure A. The product was purified by HPLC Acidic Method but with 0.05% formic acid as pH modifier (gradient: 1 → 8% B in 12 min) to provide the formate salt of **120** as an orange-red amorphous solid (37.1 mg, 0.109 mmol, 26% yield (2 steps)).

**$^{1}$H NMR** (400 MHz, $D_2O$) δ 8.42 (s, 1H), 7.66 (d, *J* = 7.5 Hz, 2H), 6.91 (d, *J* = 7.5 Hz, 2H), 3.72 (t, *J* = 5.6 Hz, 2H), 3.37 (t, *J* = 5.6 Hz, 2H), 3.29 – 3.14 (m, 2H), 2.91 (s, 3H), 2.26 (t, *J* = 6.9 Hz, 2H), 2.01 (app p, *J* = 7.5 Hz, 2H) ppm

**$^{13}$C NMR** (101 MHz, $D_2O$) δ 173.9, 173.8 (br, $HCO_2^-$), 173.6, 162.5, 132.3, 127.2, 118.3, 58.2, 58.1, 43.1, 37.7, 31.9, 22.4 ppm

**HR-MS** (*m/z*): $[M+H]^+$ calcd for $C_{14}H_{22}N_3O_4^+$: 296.1605; found: 296.1607

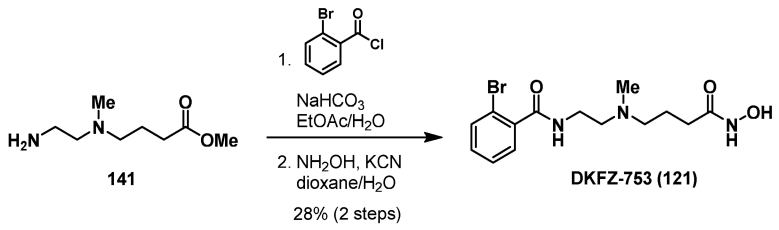


**2-Bromo-*N*-(2-((4-(hydroxyamino)-4-oxobutyl)(methyl)amino)ethyl)benzamide (DKFZ-753, 121)**: To a solution of **141**·2HCl (103.8 mg, 0.420 mmol, 1.0 equiv) partitioned in saturated aqueous $NaHCO_3$ (25 mL) and EtOAc (25 mL) in a separatory funnel was added 2-bromo benzoyl chloride (120 µL, 0.924 mmol, 2.2 equiv) in two portions, followed by vigorous shaking. The phases were separated and the organic layer was washed with half saturated

aqueous $K_2CO_3$ (2 × 25 mL) and brine (25 mL), then dried ($MgSO_4$), filtered, and concentrated. The residue was directly converted to hydroxamic acid **121** according to General Procedure A. The product was purified by HPLC Basic Method (gradient: 1 → 30% B in 15 min) to provide **121** as an off-white solid (41.5 mg, 0.116 mmol, 28% yield (2 steps)).

**TLC** $R_f$ 0.13 (10% MeOH in $CH_2Cl_2$)

**$^1$H NMR** (400 MHz, DMSO-$d_6$) δ 10.64 – 8.57 (br, 2H) 8.31 (t, $J$ = 5.7 Hz, 1H), 7.68 – 7.60 (m, 1H), 7.45 – 7.39 (m, 1H), 7.39 – 7.30 (m, 2H), 3.32 – 3.24 (m, overlapped with water peak), 2.46 (t, $J$ = 7.0 Hz, 2H), 2.30 (t, $J$ = 7.2 Hz, 2H), 2.18 (s, 3H), 1.97 (t, $J$ = 7.4 Hz, 2H), 1.62 (app p, $J$ = 7.3 Hz, 2H) ppm

**$^{13}$C NMR** (101 MHz, DMSO-$d_6$) δ 169.1, 167.1, 139.3, 132.7, 130.7, 128.7, 127.5, 118.9, 56.5, 56.0, 41.9, 37.2, 30.1, 23.0 ppm

**HR-MS** (*m/z*): $[M+H]^+$ calcd for $C_{14}H_{21}BrN_3O_3^+$: 358.0761; found: 358.0764

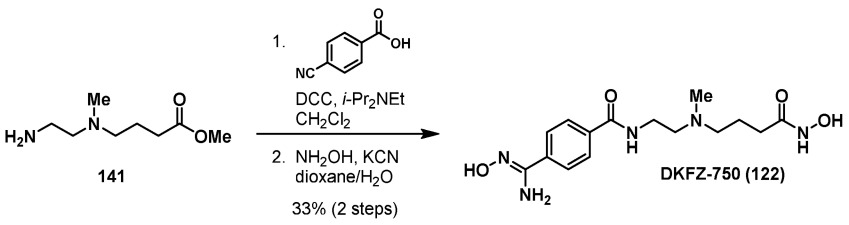


***N*-(2-((4-(hydroxyamino)-4-oxobutyl)(methyl)amino)ethyl)-4-(*N*'-hydroxycarbamimidoyl)benzamide (DKFZ-750, 122):** To a suspension of diamine **141** 2·HCl (95.8 mg, 0.388 mmol, 1.0 equiv), 4-cyanobenzoic acid (62.7 mg, 0.426 mmol, 1.1 equiv) and DCC (120 mg, 0.581 mmol, 1.5 equiv) in $CH_2Cl_2$ (8 mL) was added *i*-$Pr_2NEt$ (0.165 mL, 0.969 mmol, 2.5 equiv). The reaction mixture was stirred at rt for 16 h, until TLC indicated complete consumption of the amine. Precipitating DCU was removed by cooling the reaction mixture to –20 °C following filtration. The filtrate was diluted with EtOAc (50 mL), washed with saturated aqueous NaHCO3 (2 ×50 mL) and brine (50 mL), dried (MgSO4), and concentrated, then dissolved in 3 mL $Et_2O$/MeCN (1:1). Precipitation was filtered again and the concentrated filtrate was directly converted to the hydroxamic acid according to General Procedure A, and purified by HPLC Basic Method A (gradient: 1 → 20% B in 12 min) to provide **DKFZ-750** as an off-white solid (42.6 mg, 0.126 mmol, 33% yield over two steps).

**TLC** $R_f$ 0.27 (20% MeOH in $CH_2Cl_2$)

**$^1$H NMR** (400 MHz, DMSO-$d_6$) δ 9.58 (br s, 3H*, –NH–OH and =NOH), 8.48 (t, $J$ = 5.6 Hz, 1H, CONH), 7.86 – 7.79 (m, 2H, Ar H), 7.77 – 7.71 (m, 2H, Ar H), 5.88 (s, 2H, $NH_2$), 3.34 (app q, $J$ = 6.4 Hz, 2H (overlapped with water signal), NHC$H_2$), 2.46 (t, $J$ = 6.9 Hz, 2H, $NCH_2$), 2.30 (t, $J$ = 7.1 Hz, 2H, $NCH_2$), 2.18 (s, 3H, Me), 1.95 (t, $J$ = 7.4 Hz, 2H, $COCH_2$), 1.61 (app p, $J$ = 7.3 Hz, 2H, $CH_2$–C$H_2$–$CH_2$); ppm *: partially exchanged with adventitious water.

**$^{13}$C NMR** (101 MHz, DMSO-$d_6$) δ 168.9 (CONHOH), 165.7 (CONH), 150.2 (HON=$CNH_2$), 135.7 (Ar C), 134.7 (Ar C), 127.0 (2Ar CH), 125.1 (2Ar CH), 56.4 ($CH_2$), 56.1 ($CH_2$), 42.0 (Me), 37.3 ($CH_2$), 30.2 ($CH_2$), 23.0 ($CH_2$) ppm

**HR-MS** (*m/z*): $[M+Na]^+$ calcd for $C_{15}H_{23}N_5NaO_4^+$: 360.1642; found: 360.1646

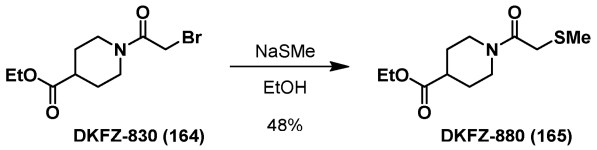


**Ethyl 1-(2-(methylthio)acetyl)piperidine-4-carboxylate (DKFZ-880, 165):** To a stirred solution of **DKFZ-830** (**164**)[200] (250 mg, 0.945 mmol, 1.0 equiv) in EtOH (10 mL) was added sodium methanethiolate (66.2 mg, 0.945 mmol, 1.0 equiv). The reaction mixture was stirred at rt for 3.5 h, then concentrated in vacuo and redissolved in EtOAc (50 mL), washed with saturated aqueous $NaHCO_3$ (2 × 50 mL), dried ($MgSO_4$) and concentrated. The product was purified by MPLC (12 g silica, gradient: 20 → 27% EtOAc in hexane over 3.5 CV, 27 → 50% EtOAc over 8 CV, then 50 → 100% EtOAc over 8 CV) to provide **DKFZ-880** as a pale yellow oil (111.5 mg, 0.454 mmol, 48% yield).

**TLC** $R_f$ 0.41 (75% EtOAc in hexane)

**$^1$H NMR** (400 MHz, $CDCl_3$) δ 4.41 – 4.30 (m, 1H), 4.13 (q, *J* = 7.1 Hz, 2H), 3.80 (dtd, *J* = 13.6, 4.1, 1.6 Hz, 1H), 3.27 (s, 2H), 3.14 (ddd, *J* = 13.9, 11.1, 3.1 Hz, 1H), 2.83 (td, *J* = 11.1, 3.2 Hz, 1H), 2.52 (tt, *J* = 10.7, 4.1 Hz, 1H), 2.17 (s, 3H), 1.99 – 1.88 (m, 2H), 1.80 – 1.70 (m, 1H), 1.69 – 1.56 (m, 1H), 1.24 (t, *J* = 7.1 Hz, 3H) ppm

**$^{13}$C NMR** (101 MHz, $CDCl_3$) δ 174.3, 167.5, 60.8, 45.9, 41.3, 40.9, 35.4, 28.5, 28.0, 15.8, 14.3 ppm

**HR-MS** (*m/z*): major: $[2M-SMe]^+$ calcd for $C_{21}H_{35}N_2O_6S^+$: 443.2210; found: 443.2211, minor: $[M+Na]^+$ calcd for $C_{11}H_{19}NNaO_3S^+$: 268.0978; found: 268.0979

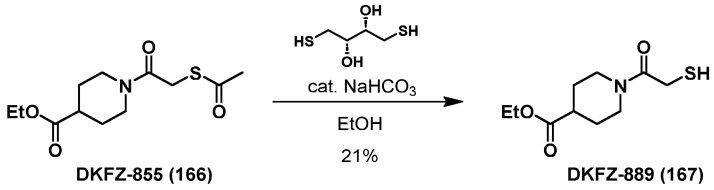


**Ethyl 1-(2-mercaptoacetyl)piperidine-4-carboxylate (DKFZ-889, 167):** To a stirred solution of **DKFZ-855**[200] (**166**) (142 mg, 0.518 mmol, 1.0 equiv) and $NaHCO_3$ (8.7 mg, 0.104 mmol, 0.2 equiv) in degassed EtOH under argon, was added dithiothreitol (120 mg, 0.778 mmol, 1.5 equiv) and stirred at rt for 24 h. The reaction mixture was diluted with degassed EtOAc (40 mL), washed with degassed water (1 × 40 mL) and degassed brine (1 × 40 mL). The organic layer was dried ($MgSO_4$), concentrated and the product was purified by MPLC (4 g silica, gradient: 25 → 65% EtOAc in hexane over 15 CV, then 65% EtOAc for 8 CV) to provide **DKFZ-889** as a colorless oil (25.7 mg, 0.111 mmol, 21% yield).

**TLC** $R_f$ 0.45 (75% EtOAc in hexane)

**$^1$H NMR** (400 MHz, DMSO-$d_6$) δ 4.23 – 4.13 (m, 1H), 4.07 (q, *J* = 7.1 Hz, 2H), 3.83 – 3.73 (m, 1H), 3.40 (d, *J* = 7.3 Hz, 2H), 3.11 (ddd, *J* = 13.9, 11.5, 2.9 Hz, 1H), 2.81 (t, *J* = 7.3 Hz, 1H), 2.75 (ddd, *J* = 13.2, 11.5, 2.9 Hz, 1H), 2.59 (tt, *J* = 11.0, 4.0 Hz, 1H), 1.90 – 1.76 (m, 2H), 1.63 – 1.49 (m, 1H), 1.44 – 1.31 (m, 1H), 1.18 (t, *J* = 7.1 Hz, 3H) ppm

**$^{13}$C NMR** (101 MHz, DMSO-$d_6$) δ 173.8, 167.8, 60.0, 44.7, 40.7, 39.9*, 28.2, 27.5, 25.5, 14.1 ppm; *overlapping with DMSO signal, confirmed by HSQC.

**HR-MS** (*m/z*): $[2M-2H+Na]^+$ calcd for $C_{20}H_{32}N_2NaO_6S_2^+$: 483.1594; found: 483.1596

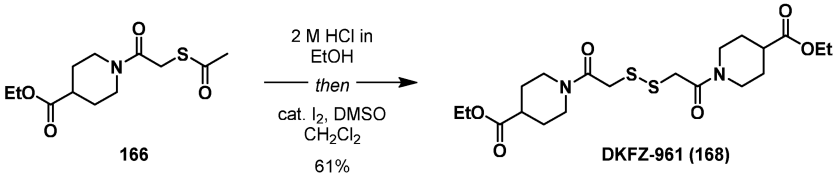


**Diethyl 1,1'-(2,2'-disulfanediylbis(acetyl))bis(piperidine-4-carboxylate) (DKFZ-961, 168):** Ester **166**[200] (134 mg, 0.490 mmol, 1.0 equiv) was dissolved in 2 M HCl in EtOH (5 mL, 10.00 mmol, 20.4 equiv) and stirred at rt for 18 h, then the solvent was removed in vacuo and residual acid was removed by co-evaporation with EtOH (2 × 10 mL). The residue was dissolved in $CH_2Cl_2$ (2 mL), DMSO (0.070 mL, 0.980 mmol, 2.0 equiv) and iodine (62.2 mg, 0.245 mmol, 0.5 equiv) were added and the solution was stirred at rt for 2 h, then diluted with 10% aqueous $Na_2S_2O_3$ solution (60 mL) and extracted with $CH_2Cl_2$ (3 × 20 mL). Combined organic layers were dried ($MgSO_4$), concentrated and the product was purified by MPLC (4 g silica, gradient: 0 → 10% MeOH in $CH_2Cl_2$ over 26 CV) to provide **DKFZ-961** (68.7 mg, 0.149 mmol, 61% yield) as a brown oil.

**TLC** $R_f$ 0.36 (5% MeOH in $CH_2Cl_2$)

**$^1$H NMR** (600 MHz, $CDCl_3$) δ 4.34 (s, 1H), 4.31 (s, 1H), 4.12 (q, *J* = 7.1 Hz, 4H), 3.83 (s, 1H), 3.80 (s, 1H), 3.69 (s, 4H), 3.17 (tt, *J* = 13.5, 2.7 Hz, 2H), 2.85 (tt, *J* = 14.0, 3.3 Hz, 2H), 2.51 (tt, *J* = 10.4, 4.0 Hz, 2H), 1.98 – 1.88 (m, 4H), 1.75 – 1.67 (m, 2H), 1.67 – 1.57 (m, 2H), 1.23 (t, *J* = 7.1 Hz, 6H) ppm

**$^{13}$C NMR** (151 MHz, $CDCl_3$) δ 174.08, 166.48, 166.47, 60.73, 45.83, 45.82, 41.43, 41.01, 40.98, 40.78, 40.76, 28.53, 27.79, 14.26 ppm; Note: disulfide symmetry appears to be broken due to slow bond rotation.

**HR-MS** (*m/z*): $[M+Na]^+$ calcd for $C_{20}H_{32}N_2NaO_6S_2^+$: 483.1594; found: 483.1597

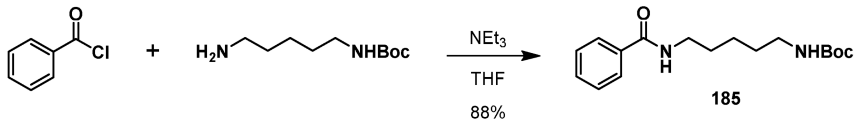


***tert*-butyl (5-benzamidopentyl)carbamate (185):** To a stirred solution of *N*-Boc-cadaverine (0.730 mL, 3.51 mmol, 1.0 equiv) and $NEt_3$ (587 mL, 4.21 mmol, 1.2 equiv) in dry THF (25 mL) was added benzoyl chloride (0.469 mL, 4.04 mmol, 1.0 equiv). After stirring at rt for 30 min, the resulting suspension was filtered, washed with THF (2 × 15 mL) and the filtrate concentrated in vacuo. The residue was re-dissolved in EtOAc (50 mL), washed with 0.1 M aqueous HCl (1 × 40 mL) and saturated aqueous $NaHCO_3$ (2 × 40 mL), then the organic layer was dried ($MgSO_4$) and concentrated to provide **185** (1.088 g, 3.551 mmol, 88% yield) as off-white crystals.

**TLC** $R_f$ 0.63 (10% MeOH and 0.5% $NH_4OH$ in $CH_2Cl_2$)

**$^1$H NMR** (400 MHz, $CDCl_3$) δ 7.80 – 7.73 (m, 2H), 7.52 – 7.45 (m, 1H), 7.45 – 7.37 (m, 2H), 6.30 (br s, 1H), 4.57 (br s, 1H), 3.45 (app q, *J* = 6.6 Hz, 2H), 3.12 (t, *J* = 6.9 Hz, 2H), 1.72 – 1.56 (m, 2H), 1.57 – 1.47 (m, 2H), 1.45 – 1.36 (s, 9H overlapped with m, 2H) ppm

**LC/MS** (*m/z*): $[M+Na]^+$ 329.2

Analytical data is in agreement with literature.[224]

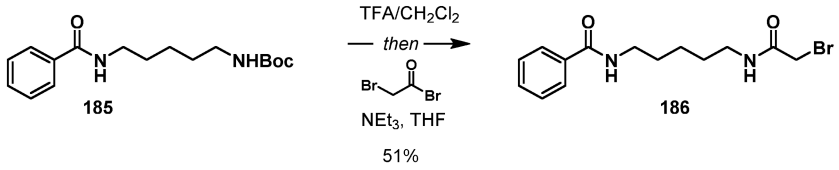


***N*-(5-(2-bromoacetamido)pentyl)benzamide (186):** To a stirred solution of **185** (620 mg, 2.02 mmol, 1.0 equiv) in $CH_2Cl_2$ (10 mL) was added TFA (2.46 mL, 32.67 mmol, 16.0 equiv) and stirred at rt for 30 min, then the solvent was removed in vacuo and residual acid was removed by co-evaporation with $CH_2Cl_2$ (3 × 15 mL). The residue was dissolved in dry THF (15 mL) and cooled to 0 °C, then $NEt_3$ (1.41 mL, 10.11 mmol, 5.0 equiv) and bromoacetyl bromide (0.282 mL, 3.24 mmol, 1.6 equiv) were added in three portions to the stirred solution over the course of 45 min. After stirring a total of 60 min, TLC indicated complete conversion and the reaction was quenched by addition of MeOH (5 mL), then dissolved in EtOAc (50 mL) and washed with 1 M aqueous HCl (1 × 50 mL) and saturated aqueous $NaHCO_3$ (1 × 50 mL). The organic layer was dried ($MgSO_4$), concentrated and the product was purified by MPLC (4 g silica, gradient: 40 → 85% EtOAc in hexane over 16 CV, 85 → 100% EtOAc over 12.5 CV, then 100% EtOAc for 10 CV) to provide **186** (335.8 mg, 1.026 mmol, 51% yield) as an off-white solid.

**TLC** $R_f$ 0.36 (100% EtOAc)

**$^1$H NMR** (400 MHz, $CDCl_3$) δ 7.84 – 7.70 (m, 2H), 7.53 – 7.47 (m, 1H), 7.46 – 7.35 (m, 2H), 6.61 (br s, 1H), 6.29 (br s, 1H), 3.84 (s, 2H), 3.47 (td, *J* = 6.9, 5.8 Hz, 2H), 3.31 (td, *J* = 6.9, 5.8 Hz, 2H), 1.68 – 1.56 (m, 4H), 1.49 – 1.36 (m, 2H) ppm

**LC/MS** (*m/z*): $[M+H]^+$ 327.1

Analytical data is in agreement with literature.[225]

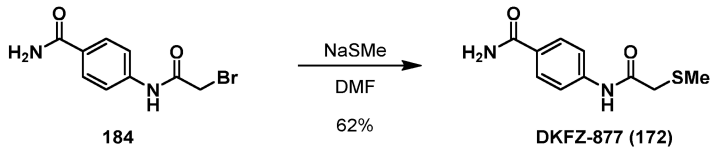


**4-(2-(Methylthio)acetamido)benzamide (DKFZ-877, 172):** Sodium methanethiolate (90.0 mg, 1.284 mmol, 1.1 equiv) and **184**[200] (300 mg, 1.167 mmol, 1.0 equiv) were dissolved in DMF (5 mL) and stirred at rt for 2 h, then water (40 mL) was added and the solution was frozen at –20 °C, then kept at 4 °C for 17 h. The fine precipitate was filtered and washed with water (2 × 10 mL) to provide **DKFZ-877** as tan crystals (161.9 mg, 0.722 mmol, 62 % yield).

**TLC** $R_f$ 0.41 (10% MeOH in $CH_2Cl_2$)

**$^1$H NMR** (400 MHz, DMSO-$d_6$) δ 10.26 (s, 1H), 7.86 (br s, 1H), 7.85 – 7.80 (m, 2H), 7.68 – 7.61 (m, 2H), 7.25 (s, 1H), 2.16 (s, 3H), 3.29 (s, 2H) ppm

**$^{13}$C NMR** (101 MHz, DMSO-$d_6$) δ 168.2, 167.4, 141.6, 128.9, 128.4, 118.2, 37.5, 15.5 ppm

**HR-MS** (*m/z*): $[2M+Na]^+$ calcd for $C_{20}H_{24}N_4NaO_4S_2^+$: 471.1131; found: 471.1133

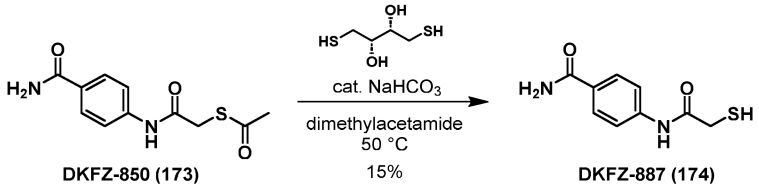


**4-(2-Mercaptoacetamido)benzamide (DKFZ-887, 174):** To a stirred solution of **DKFZ-850**[200] (**173**) (96.5 mg, 0.382 mmol, 1.0 equiv) and $NaHCO_3$ (6.4 mg, 0.076 mmol, 0.2 equiv) in dry dimethylacetamide, heated to 50 °C under argon, was added dithiothreitol (207 mg, 1.339 mmol, 3.5 equiv) in three portions over the course of 24 h. The reaction mixture was diluted with degassed water (80 mL), lyophillized and the product was purified by MPLC (4 g silica, gradient: 2 → 4% MeOH in $CH_2Cl_2$ over 7.5 CV, 4% MeOH for 8.5 CV, 4 → 10% MeOH over 14 CV, then 10% MeOH for 10 CV). Product fractions were cooled to –20 °C for 16 h and **DKFZ-887** (12.0 mg, 0.057 mmol, 15% yield) was collected by filtration as a white precipitate.

**TLC** $R_f$ 0.24 (10% MeOH in $CH_2Cl_2$)

**$^1$H NMR** (400 MHz, DMSO-$d_6$) δ 10.29 (s, 1H), 7.91 – 7.78 (m, 3H), 7.68 – 7.59 (m, 2H), 7.24 (s, 1H), 3.32 (s, 2H), 2.98 (s, 1H) ppm

**$^{13}$C NMR** (101 MHz, DMSO-$d_6$) δ 169.0, 167.3, 141.6, 129.0, 128.4, 118.2, 28.4 ppm

**HR-MS** (*m/z*): [2M-2H+Na]$^+$ calcd for $C_{18}H_{18}N_4NaO_4S_2^+$: 441.0662; found: 441.0662

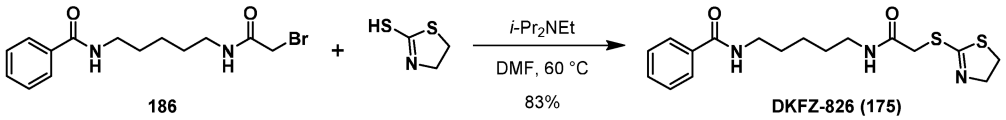


186 DKFZ-826 (175)

***N*-(5-(2-((4,5-dihydrothiazol-2-yl)thio)acetamido)pentyl)benzamide (DKFZ-826, 175):** To a solution of **186** (121 mg, 0.371 mmol, 1.0 equiv) in DMF (2 mL) were added 2-thiazoline-2-thiol (44.2 mg, 0.371 mmol, 1.0 equiv) and *i*-$Pr_2NEt$ (0.129 mL, 0.742 mmol, 2.0 equiv). The reaction mixture was stirred at 60 °C for 1 h, cooled to rt, then dissolved in EtOAc (30 mL) and washed with water (1 × 50 mL) and brine (2 × 50 mL). The organic layer was dried ($MgSO_4$), concentrated and the product was purified by MPLC (4 g silica, gradient: 0 → 5% MeOH in $CH_2Cl_2$ over 19 CV, 5 → 14% MeOH over 10 CV, then 14% MeOH for 4 CV) to provide **DKFZ-826** as a yellow viscous oil (112 mg, 0.306 mmol, 83% yield).

**TLC** $R_f$ 0.29 (5% MeOH in $CH_2Cl_2$)

**$^1$H NMR** (400 MHz, $CDCl_3$) δ 7.80 – 7.75 (m, 2H), 7.49 – 7.43 (m, 1H), 7.42 – 7.36 (m, 2H), 7.34 (t, *J* = 6.7 Hz, 1H), 6.57 (t, *J* = 5.8 Hz, 1H), 4.15 (t, *J* = 8.0 Hz, 2H), 3.61 (s, 2H), 3.46 – 3.36 (m, 4H), 3.21 (td, *J* = 6.7, 5.8 Hz, 2H), 1.66 – 1.58 (m, 2H), 1.54 – 1.43 (m, 2H), 1.41 – 1.30 (m, 2H) ppm

**$^{13}$C NMR** (101 MHz, $CDCl_3$) δ 168.9, 167.7, 166.9, 134.8, 131.4, 128.5, 127.0, 63.7, 39.9, 39.2, 36.4, 35.8, 29.2, 29.1, 24.0 ppm

**HR-MS** (*m/z*): [M+Na]$^+$ calcd for $C_{17}H_{23}N_3NaO_2S_2^+$: 388.1124; found: 388.1124

Note: HPLC and NMR analyses indicate a purity of 90-95%.

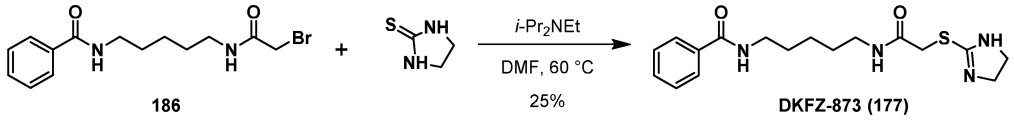


186 DKFZ-873 (177)

***N*-(5-(2-((4,5-dihydro-1*H*-imidazol-2-yl)thio)acetamido)pentyl)benzamide (DKFZ-873, 177):** To a solution of **186** (153 mg, 0.467 mmol, 1.0 equiv) in DMF (2 mL) were added 2-imidazolidinethione (47.7 mg, 0.467 mmol, 1.0 equiv) and *i*-$Pr_2NEt$ (0.163 mL, 0.933 mmol, 2.0 equiv). The reaction mixture was stirred at 60 °C for 1 h, cooled to rt, then poured into brine (60 mL) and extracted with $CH_2Cl_2$ (3 × 25 mL). Combined organic layers were dried ($MgSO_4$), concentrated and the product was purified by MPLC (4 g silica, gradient: 5 → 8% MeOH and 0.5% $NH_4OH$ in $CH_2Cl_2$ over 20 CV, 8 → 10% MeOH over 8 CV, then 10 → 20% MeOH over 8 CV). Combined product fractions were concentrated and further purified by trituration to provide **DKFZ-873** as a white solid (40.9 mg, 0.117 mmol, 25% yield).

**TLC** $R_f$ 0.21 (10% MeOH and 0.5% $NH_4OH$ in $CH_2Cl_2$)

**$^1$H NMR** (400 MHz, DMSO-$d_6$) δ 8.43 (t, *J* = 5.6 Hz, 1H), 8.27 (t, *J* = 5.6 Hz, 1H*), 7.88 – 7.78 (m, 2H), 7.55 – 7.40 (m, 3H), 6.76 (br s, 1H*), 3.62 (br s, 4H*, 2 × $CH_2$), 3.34 (br s, 2H), 3.27 – 3.21 (m, 2H), 3.11 – 2.99 (m, 2H), 1.52 (p, *J* = 7.4 Hz, 2H), 1.47 – 1.36 (m, 2H), 1.35 – 1.23 (m, 2H) ppm; *: partially exchanged with adventitious water.

**$^{13}$C NMR** (101 MHz, DMSO-$d_6$) δ 167.8, 166.1, 163.3, 134.7, 131.0, 128.2, 127.1, 54.4 (br), 45.5 (br), 39.1, 38.7, 34.0, 28.8, 28.6, 23.8 ppm

**HR-MS** (*m/z*): $[M+H]^+$ calcd for $C_{17}H_{25}N_4O_2S^+$: 349.1693; found: 349.1693

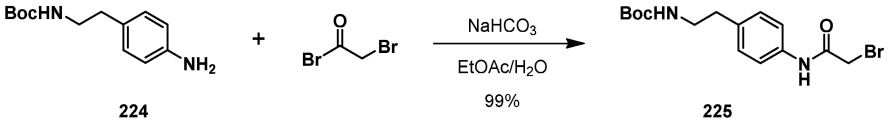


224 225

***tert*-butyl (4-(2-bromoacetamido)phenethyl)carbamate (225):** To a vigorously stirred solution of aniline **224** (500 mg, 2.12 mmol, 1.0 equiv) in EtOAc (10 mL) and saturated aqueous $NaHCO_3$ (10 mL) was added bromoacetyl bromide (0.221 mL, 2.54 mmol, 1.2 equiv) in two portions with 1 h of stirring in between and 15 min stirring after the second addition. Then, the reaction mixture was diluted with EtOAc (50 mL) and saturated aqueous $NaHCO_3$ (50 mL). Phases were separated and the organic layer was washed with 0.1 M aqueous HCl (2 × 50 mL) and saturated aqueous $NaHCO_3$ (1 × 50 mL). The organic layer was dried ($MgSO_4$) and concentrated to provide the product as a pale yellow solid (751.0 mg, 2.102 mmol, 99% yield).

**TLC** $R_f$ 0.56 (60% EtOAc in hexane)

**$^1$H NMR** (400 MHz, $CDCl_3$) δ 8.11 (br s, 1H), 7.52 – 7.42 (m, 2H), 7.22 – 7.14 (m, 2H), 4.52 (br s, 1H), 4.02 (s, 2H), 3.35 (app q, *J* = 7.7 Hz, 2H), 2.78 (t, *J* = 7.0 Hz, 2H), 1.43 (s, 9H) ppm

**LC/MS** (*m/z*): $[M+Na]^+$ 379.0 and 308.1

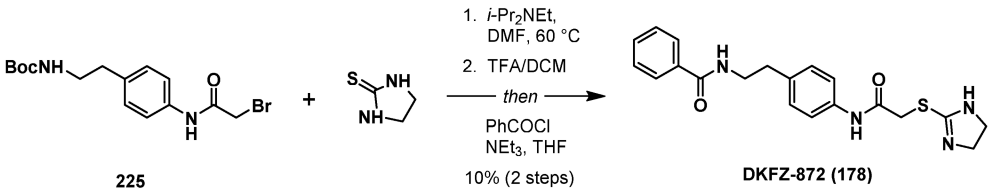


225 DKFZ-872 (178)

***N*-(4-(2-((4,5-dihydro-1*H*-imidazol-2-yl)thio)acetamido)phenethyl)benzamide (DKFZ-872, 178):** To a solution of **225** (250 mg, 0.700 mmol, 1.0 equiv) in DMF (2 mL) were added 2-imidazolidinethione (71.5 mg, 0.700 mmol, 1.0 equiv) and *i*-$Pr_2NEt$ (0.181 mL, 1.40 mmol, 2.0 equiv). The reaction mixture was stirred at 60 °C for 80 min, cooled to rt, then diluted with EtOAc (50 mL) and washed with saturated aqueous $Na_2CO_3$ (2 × 50 mL). Combined aqueous layers were extracted with $CH_2Cl_2$ (2 × 30 mL). Combined organic layers were dried ($MgSO_4$), concentrated and the product was purified by MPLC (4 g silica, gradient: 0 → 3.6% MeOH and 0.5% $NH_4OH$ in $CH_2Cl_2$ over 8 CV, 3.6 → 6% over 11 CV, then 6 → 10% over 4 CV) to provide the

Boc-precursor of **DKFZ-872** as a colorless amorphous solid (TLC $R_f$ 0.37 (10% MeOH and 0.5% $NH_4OH$ in $CH_2Cl_2$, LC/MS (*m/z*): $[M+H]^+$ 379.2).
To a stirred solution of this intermediate (150 mg, 0.396 mmol, 1.0 equiv) in $CH_2Cl_2$ (2.5 mL) was added TFA (0.482 mL, 6.34 mmol, 16.0 equiv) and stirred at rt for 60 min, then the solvent was removed in vacuo and residual acid was removed by co-evaporation with $CH_2Cl_2$ (3 × 10 mL). The residue was dissolved in dry THF (2.5 mL) and $NEt_3$ (0.276 mL, 1.98 mmol, 5.0 equiv), then benzoyl chloride (0.053 mL, 0.456 mmol, 1.15 equiv) was added slowly and the reaction mixture was stirred for 15 min. Precipitation was filtered and washed with THF (2 × 5 mL). The filtrate was concentrated to dryness and the product was purified by MPLC (4 g silica, gradient: 2.5 → 3.8% MeOH and 0.5% $NH_4OH$ over 14.5 CV, 3.8% → 5% MeOH over 11 CV, then 5% → 10% MeOH over 12.5 CV). The product was further purified by crystallization from DMSO/water at 4 °C to provide **DKFZ-872** (27.2 mg, 0.071 mmol, 10% yield over two steps) as an off-white solid.

**TLC** $R_f$ 0.31 (10% MeOH and 0.5% $NH_4OH$ in $CH_2Cl_2$)

**$^1$H NMR** (400 MHz, DMSO-$d_6$) δ 10.62 (s, 1H*), 8.52 (t, *J* = 5.6 Hz, 1H), 7.85 – 7.77 (m, 2H), 7.55 – 7.40 (m, 5H), 7.22 – 7.14 (m, 2H), 6.92 (br s, 1H*), 3.84 (s, 2H*), 3.53 (br s, 4H*), 3.48 – 3.42 (m, 2H), 2.79 (t, *J* = 7.4 Hz, 2H) ppm; *: partially exchanged with adventitious water.

**$^{13}$C NMR** (101 MHz, DMSO-$d_6$) δ 166.7, 166.1, 163.6, 137.0, 134.6, 134.5, 131.0, 129.0, 128.2, 127.1, 118.9, 40.9, 35.1, 34.5 ppm. Note: Due to tautomerism of the 2-thioimidazoline, the two methylenes in the imidazoline moiety are too broad to be identified in $^{13}$C spectra.

**HR-MS** (*m/z*): $[M+H]^+$ calcd for $C_{20}H_{23}N_4O_2S^+$: 383.1536; found: 383.1539

Note: HPLC and NMR analyses indicate a purity of 90-95%.

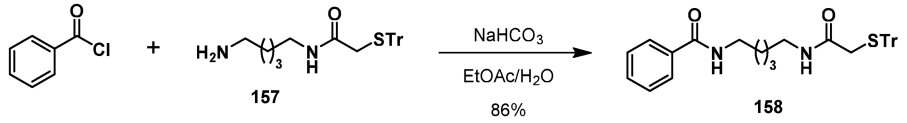


***N*-(5-(2-(tritylthio)acetamido)pentyl)benzamide (158):** To a vigorously stirred solution of **157**[148] (489 mg, 1.405 mmol, 1.0 equiv) in EtOAc (15 mL) and saturated aqueous $NaHCO_3$ (15 mL) was added benzoyl chloride (0.202 mL, 1.756 mmol, 1.25 equiv). After 15 min, the phases were separated, and the aqueous layer was extracted with $CH_2Cl_2$ (3 × 15 mL). Combined organic layers were dried ($MgSO_4$) and concentrated to provide **158** as a white solid (628 mg, 1.201 mmol, 86% yield).

**$^1$H NMR** (400 MHz, $CDCl_3$) δ 7.80 – 7.73 (m, 2H), 7.50 – 7.43 (m, 1H), 7.42 – 7.35 (m, 8H), 7.34 – 7.26 (m, 6H), 7.25 – 7.20 (m, 3H), 6.28 (t, *J* = 5.9 Hz, 1H), 6.03 (t, *J* = 5.6 Hz, 1H), 3.42 (app q, *J* = 6.9 Hz, 2H), 3.09 (s, 2H), 2.97 (app q, *J* = 6.7 Hz, 2H), 1.60 (p, *J* = 7.1 Hz, 2H), 1.44 – 1.32 (m, 2H), 1.32 – 1.20 (m, 2H) ppm

**TLC** $R_f$ 0.36 (10% MeOH in $CH_2Cl_2$).

**LC/MS** (*m/z*): $[M+Na]^+$ 545.2

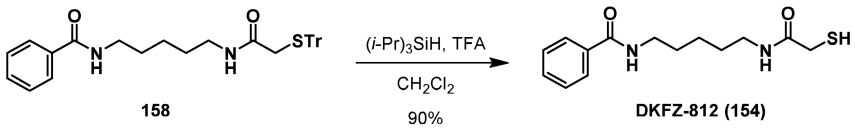


***N*-(5-(2-Mercaptoacetamido)pentyl)benzamide**[226] **(DKFZ-812, 154):** To a stirred solution of **158** (0.276 g, 0.528 mmol, 1.0 equiv) in $CH_2Cl_2$ (10 mL) was added TFA (1.02 mL, 13.20 mmol, 25 equiv), then (*i*-Pr)$_3$SiH (0.228 mL, 1.114 mmol, 2.1 equiv). The mixture was stirred at rt for 30 min until it became colorless, then saturated aqueous $NaHCO_3$ (70 mL) was added and stirred for 10 min until no more bubbling occurred, then the solution was extracted with $CH_2Cl_2$ (3 × 30 mL) and the combined organic layers were dried ($MgSO_4$) and concentrated. The product was purified by FCC (80 g silica, eluent: 10% MeOH in $CH_2Cl_2$) to provide **DKFZ-812** as an off-white solid (133 mg, 0.476 mmol, 90% yield).

**TLC** $R_f$ 0.46 (10% MeOH in $CH_2Cl_2$).

**$^1$H NMR** (400 MHz, $CDCl_3$) δ 7.81 – 7.74 (m, 2H), 7.51 – 7.44 (m, 1H), 7.44 – 7.37 (m, 2H), 6.89 (br, 1H), 6.62 – 6.49 (br, 1H), 3.43 (td, *J* = 6.7, 6.4 Hz, 2H), 3.26 (app q, *J* = 6.5 Hz, 2H), 3.16 (d, *J* = 9.0 Hz, 2H), 1.88 (t, *J* = 9.0 Hz, 1H), 1.64 (app q, *J* = 7.2 Hz, 2H), 1.60 – 1.50 (m, 2H), 1.44 – 1.33 (m, 2H) ppm

**$^{13}$C NMR** (101 MHz, $CDCl_3$) δ 169.7, 167.9, 134.7, 131.5, 128.6, 127.0, 39.7, 39.6, 29.1, 29.0, 28.3, 23.9 ppm

**HR-MS** (*m/z*): $[M+H]^+$ calcd for $C_{14}H_{21}N_2O_2S^+$: 281.1318; found: 281.1322

Analytical data is in agreement with literature.[226]

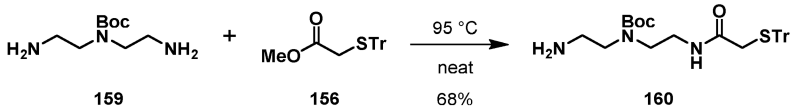


***tert*-butyl (2-aminoethyl)(2-(2-(tritylthio)acetamido)ethyl)carbamate (160):** Methyl 2-(tritylthio)acetate[197] (**156**, 0.628 g, 1.804 mmol, 1.0 equiv) was added in small portions to neat diamine **159**[198] (0.734 g, 3.608 mmol, 2.0 equiv) heated to 95 °C in an open flask and stirred for 3.5 h, then cooled to rt, dissolved in EtOAc (100 mL) and washed with saturated aqueous $NaHCO_3$ (2 × 80 mL), dried ($MgSO_4$) and concentrated. The crude product was purified by MPLC (12 g silica, gradient: 0 → 20% MeOH and 0.5% $NH_4OH$ in $CH_2Cl_2$ over 20 CV) to provide **160** as a white foam (638 mg, 1.228 mmol, 68% yield).

**TLC** $R_f$ 0.61 (20% MeOH and 0.5% $NH_4OH$ in $CH_2Cl_2$)

**$^1$H NMR** (400 MHz, $CDCl_3$) δ 7.44 – 7.39 (m, 6H), 7.32 – 7.26 (m, 6H), 7.25 – 7.18 (m, 3H), 6.88 (br s, 1H), 3.28 – 3.11 (m, 6H), 3.02 (s, 2H), 2.79 (t, *J* = 6.3 Hz, 2H), 1.46 (br s, 2H), 1.42 (s, 9H) ppm

**LC/MS** (*m/z*): $[M+H]^+$ 520.3

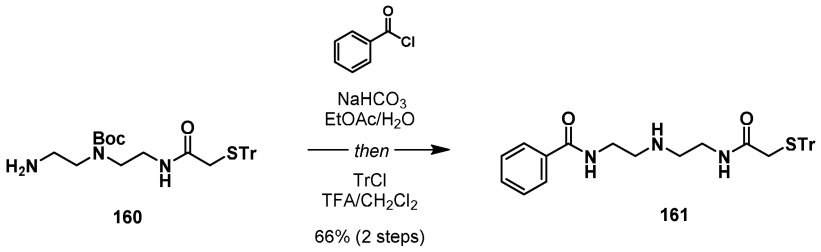


***N*-(2-((2-(2-(Tritylthio)acetamido)ethyl)amino)ethyl)benzamide (161):** To a vigorously stirred solution of **160** (638 mg, 1.228 mmol, 1.0 equiv) in EtOAc (10 mL) and saturated aqueous $NaHCO_3$ (10 mL) was added benzoyl chloride (0.163 mL, 1.412 mmol, 1.15 equiv). After 10 min, the reaction mixture was diluted with saturated aqueous $NaHCO_3$ (40 mL) and EtOAc (40 mL), phases were separated, and the organic layer was washed with saturated aqueous $NaHCO_3$ (40 mL), then dried ($MgSO_4$) and concentrated. The obtained white foam (787 mg) was dissolved in $CH_2Cl_2$ (10 mL), trityl chloride (0.103 mg, 0.368 mmol, 0.3 equiv), then TFA (5.0 mL, 65.1 mmol, 53 equiv) was added and the orange solution was stirred at rt for 2 h. Then, the reaction was diluted with $CH_2Cl_2$ (80 mL), cooled to 0 °C and quenched with 1 M NaOH (100 mL). Phases were separated and the aqueous phase extracted with $CH_2Cl_2$ (4 × 50 mL). The combined organic layers were dried ($MgSO_4$) and concentrated. The product was purified by MPLC (12 g silica, gradient: 0 → 10% MeOH and 0.5% $NH_4OH$ in $CH_2Cl_2$ over 10 CV, then 10% MeOH for 10 CV) to provide sufficiently pure (approx. 80%) **161** as a white foam (528 mg, approx. 0.807 mmol, approx. 66% yield over two steps).

**TLC** $R_f$ 0.41 (10% MeOH and 0.5% $NH_4OH$ in $CH_2Cl_2$)

**$^1$H NMR** (400 MHz, $CDCl_3$) δ 7.41 – 7.35 (m, 8H), 7.31 – 7.18 (m, overlapped with $CDCl_3$ peak), 6.84 – 6.72 (br, 1H), 6.32 (t, *J* = 5.5 Hz, 1H), 3.50 (app q, *J* = 5.4 Hz, 2H), 3.10 (s, 2H), 3.06 (app q, *J* = 5.9 Hz, 2H), 2.86 – 2.79 (m, 2H), 2.65 – 2.58 (m, 2H), 1.77 (s, 3H) ppm. Impurity signals are not listed.

**LC/MS** (*m/z*): $[M+H]^+$ 524.2. Purity by evaporative light scattering: approx. 80% by weight.

Note: The compound was obtained with approx. 80% purity, but the material was sufficiently pure for the next reaction and was therefore used without further purification. The impurity gave an (*m/z*) of 243.2 ($Tr^+$) and was removed in the subsequent steps. Reported yield is corrected for purity.

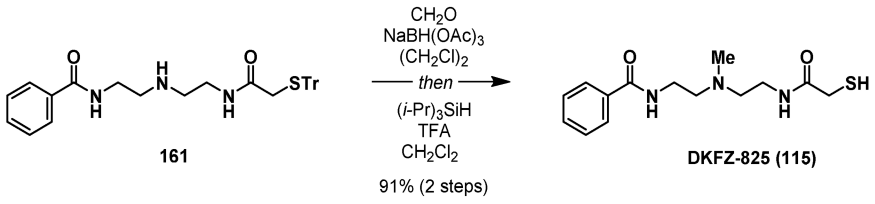


***N*-(2-((2-(2-Mercaptoacetamido)ethyl)(methyl)amino)ethyl)benzamide (DKFZ-825, 115)**: To a stirred solution of **161** (342 mg with approx. 80% purity, approx. 0.522 mmol, 1.0 equiv) in $(CH_2Cl)_2$ (8 mL) was added formaldehyde (37–41% aqueous solution, 0.101 mL,

1.312 mmol, 2.5 equiv), then $NaBH(OAc)_3$ (0.305 mg, 1.437 mmol, 2.7 equiv). After stirring at rt for 45 min, the reaction was quenched by addition of 1 M NaOH (50 mL) and extracted with $CH_2Cl_2$ (3 × 30 mL). The combined organic layers were dried ($MgSO_4$) and concentrated. The trityl-protected product (*m/z*: $[M+H]^+$ 538.2, TLC $R_f$ 0.47 10% MeOH and 0.5% $NH_4OH$ in $CH_2Cl_2$) was dissolved in $CH_2Cl_2$ (12 mL), TFA (1.26 mL, 16.31 mmol, 31 equiv), then $(i\text{-Pr})_3SiH$ (0.241 mL, 1.176 mmol, 2.25 equiv) was added and the mixture was stirred for 30 min at rt until it became colorless. Then, the reaction mixture was diluted with $CH_2Cl_2$ (50 mL) and saturated aqueous $NaHCO_3$ (75 mL) and stirred for 10 min until no more bubbling occurred, then extracted with $CH_2Cl_2$ (4 × 50 mL) and the combined organic layers were dried ($MgSO_4$) and concentrated. The product was purified by MPLC (4 g silica, gradient: 0% for 5 CV, 0 → 20% 20% MeOH and 0.5% $NH_4OH$ in $CH_2Cl_2$ over 12 CV, then 20% MeOH and 0.5% $NH_4OH$ in $CH_2Cl_2$ for 15 CV) to provide **DKFZ-825** as a colorless amorphous solid (140 mg, 0.474 mmol, approx. 91% yield over two steps).

**TLC** $R_f$ 0.14 (10% MeOH and 0.5% $NH_4OH$ in $CH_2Cl_2$)

**$^1$H NMR** (400 MHz, $CDCl_3$) δ 7.83 – 7.76 (m, 2H), 7.53 – 7.46 (m, 1H), 7.46 – 7.38 (m, 2H), 7.30 (br s, 1H), 6.98 (br s, 1H), 3.59 (app q, *J* = 5.6 Hz, 2H), 3.40 (app q, *J* = 5.6 Hz, 2H), 3.10 (s, 2H), 2.74 (t, *J* = 5.5 Hz, 2H), 2.67 (t, *J* = 5.6 Hz, 2H), 2.38 (s, 3H), 1.79 (s, 1H) ppm

**$^{13}$C NMR** (101 MHz, $CDCl_3$) δ 171.1, 168.2, 133.3, 132.2, 128.8, 127.3, 57.4, 56.9, 41.8, 35.7, 35.4, 28.1 ppm

**HR-MS** (*m/z*): $[M+H]^+$ calcd for $C_{14}H_{22}N_3O_2S^+$: 296.1427; found: 296.1430

Note: The material was found to readily form the disulfide when exposed to air, especially in solution.

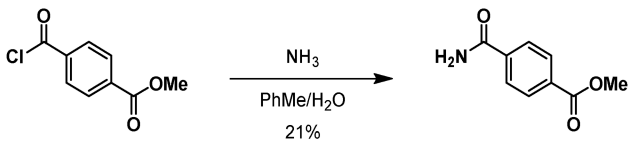


187 188

**Methyl 4-carbamoylbenzoate (188):** To a stirred aqueous solution of ammonia (25%, 0.942 mL, 12.59 mmol, 10 equiv), cooled by ice-bath was added a suspension of methyl 4-(chlorocarbonyl)benzoate (**187**, 250 mg, 1.259 mmol, 1.0 equiv) in toluene (3 mL) and stirred for 5 min. The reaction mixture was diluted with MeOH (5 mL), concentrated to dryness, suspended in EtOAc (20 mL), filtered and concentrated. The product was further purified by recrystallization from boiling MeOH and cooling to 4°C, then –20°C. Crystals were filtered and washed with ice-cold hexane (3 × 5 mL) to provide the product in sufficient purity for the next step as colorless needles (59.9 mg, 80% purity, 0.267 mmol*, 21% yield*). *: yield corrected for 80% purity.

**TLC** $R_f$ 0.65 (10% MeOH in $CH_2Cl_2$)

**$^1$H NMR** (600 MHz, MeOD-$d_4$) δ 8.12 – 8.06 (m, 2H), 7.98 – 7.92 (m, 2H), 3.93 (s, 3H) ppm

**LC/MS** (*m/z*): $[M+H]^+$ 180.1

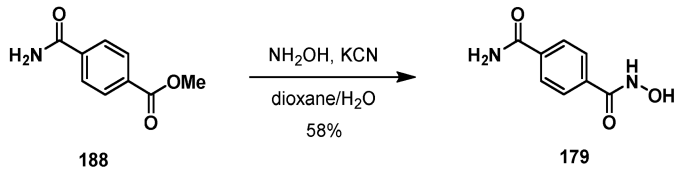


188 179

***N*-hydroxyterephthalamide (DKFZ-945, 179):** Ester **188** (58.4 mg, 80% purity, 0.261 mmol, 1.0 equiv) was converted to hydroxamic acid **DKFZ-945** according to General Procedure A, but with 65 h reaction time. The cloudy reaction mixture was diluted with water (5 mL), then washed with $CH_2Cl_2$ (4 × 10 mL) and the aqueous phase was concentrated to dryness. The product was purified from the residue by crystallization from boiling water (2 mL) and slowly freezing to –20 °C. After melting the ice, the obtained yellow crystals were washed with ice-cold water (2 × 3 mL) and dried to provide **DKFZ-945** (27.4 mg, 152 mmol, 58% yield).

Note: The material has poor solubility in most common solvents. Solubility in DMSO at rt is about 50 mM.

**TLC** $R_f$ 0.55 (30% MeOH in $CH_2Cl_2$)

**$^1$H NMR** (600 MHz, DMSO-$d_6$) δ 9.70 (br s, 2H*), 7.97 (s, 1H), 7.82 (d, *J* = 8.3 Hz, 2H), 7.77 (d, *J* = 8.3 Hz, 2H), 7.36 (s, 1H) ppm; *partially exchanged with adventitious water.

**$^{13}$C NMR** (151 MHz, DMSO-$d_6$) δ 167.7, 163.2, 138.4, 134.5, 127.0, 125.9 ppm

**LC/MS** (*m/z*): $[M+H]^+$ 181.1

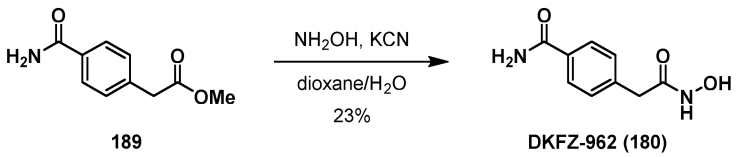


189 DKFZ-962 (180)

**4-(2-(hydroxyamino)-2-oxoethyl)benzamide (DKFZ-962, 180):** Ester **189** (150 mg, 0.776 mmol, 1.0 equiv) was converted to hydroxamic acid **DKFZ-962** according to General Procedure A. The cloudy reaction mixture was concentrated in vacuo, re-concentrated from MeOH to dryness, dissolved in warm water (20 mL) and extracted with $CH_2Cl_2$ (3 × 10 mL) to remove remaining starting material. The aqueous phase was concentrated to dryness and the residue was recrystallized from boiling water (15 mL) by slowly cooling to rt. Crystals were filtered and washed with ice-cold water, MeOH, and $CH_2Cl_2$ (10 mL each) to provide **DKFZ-962** as colorless crystals (35.1 mg, 0.181 mmol, 23% yield).

**TLC** $R_f$ 0.37 (30% MeOH/AcOH (9:1) in $CH_2Cl_2$)

**$^1$H NMR** (600 MHz, DMSO-$d_6$) δ 11.09 (br s, 1H), 10.87 (br s, 1H), 9.00 (s, 1H), 8.93 (s, 1H), 7.74 – 7.69 (m, 2H), 7.05 – 6.93 (m, 2H), 4.52 (s, 2H) ppm

**$^{13}$C NMR** (151 MHz, DMSO-$d_6$) δ $^{13}$C NMR (151 MHz, DMSO) δ 164.0, 163.9, 160.0, 128.6, 125.6, 114.3, 65.8 ppm

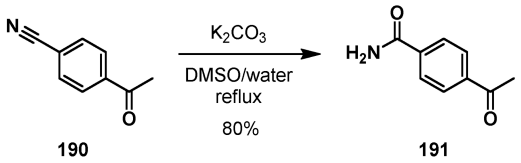


190 191

**4-acetylbenzamide (191):** A stirred solution of 4-acetylbenzonitrile (0.500 g, 3.44 mmol, 1.0 equiv) in DMSO (10 mL) and water (3.5 mL) was heated to reflux for 4 h, allowed to cool, then the reaction mixture was poured into brine (150 mL) and extracted with EtOAc (6 × 50 mL). Combined organic layers were dried ($MgSO_4$) and concentrated to provide the product as a brown solid (450.0 mg, 2.748 mmol, 80% yield).

**TLC** $R_f$ 0.30 (5% MeOH in $CH_2Cl_2$)

**$^1$H NMR** (600 MHz, DMSO-$d_6$) δ 8.14 (s, 1H), 8.03 – 8.00 (m, 2H), 8.00 – 7.96 (m, 2H), 7.57 (s, 1H), 2.61 (s, 3H) ppm

**LC/MS** (*m/z*): $[M+H]^+$ 162.2

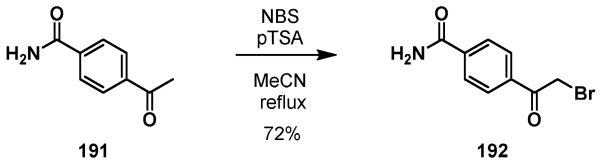


191 192

**4-(2-bromoacetyl)benzamide (192):** A stirred solution of **191** (0.337 g, 2.06 mmol, 1.0 equiv), pTSA (0.393 g, 2.06 mmol, 1.0 equiv) and NBS (0.477 g, 2.68 mmol, 1.3 equiv) in MeCN (15 mL) was heated to reflux for 4 h, then concentrated in vacuo. The residue was partitioned between in EtOAc (100 mL) and saturated aqueous $NaHCO_3$ (100 mL) and the aqueous phase was extracted with EtOAc (2 × 100 mL). Combined organic layers were dried ($MgSO_4$) and concentrated. The product was purified by trituration with $CH_2Cl_2$ (3 × 5 mL) to provide **192** as a light ochre solid (360.0 mg, 1.487 mmol, 72% yield).

**TLC** $R_f$ 0.26 (7.5% MeOH in $CH_2Cl_2$)

**$^1$H NMR** (600 MHz, DMSO-$d_6$) δ 8.17 (s, 1H), 8.08 – 8.05 (m, 2H), 8.02 – 7.98 (m, 2H), 7.61 (s, 1H), 4.98 (s, 2H) ppm

**LC/MS** (*m/z*): $[M+H]^+$ 242.0 and 244.0

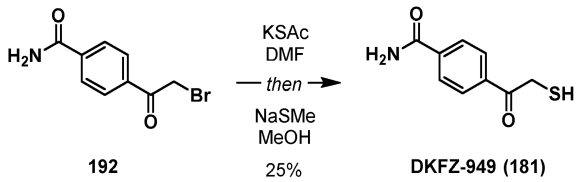


**4-(2-mercaptoacetyl)benzamide (DKFZ-949, 181):** A Schlenk tube was charged with **192** (161.7 mg, 0.668 mmol, 1.0 equiv) and potassium thioacetate (99.2 mg, 0.868 mmol, 1.3 equiv), then dry DMF (2 mL) was added under an argon atmosphere and the reaction mixture was stirred at rt for 30 min. Then, sodium thiomethoxide (117 mg, 1.67 mmol, 2.5 equiv) was added as a solution in dry MeOH (2 mL) under argon. After stirring for 5 min, the reaction mixture was diluted with saturated aqueous $NH_4Cl$ (40 mL) and extracted with EtOAc (4 × 15 mL). The combined organic layers were dried ($MgSO_4$) and concentrated. The product was purified by MPLC (4 g silica, gradient: 0 → 4% MeOH in $CH_2Cl_2$ over 15 CV, 4 → 18% over 13 CV, then 18 → 20% over 10 CV) and then by HPLC Acidic Method (gradient: 1 → 15% B in 1 min, then 15 → 45% B in 9 min) to provide **DKFZ-949** as a white solid (33.0 mg, 0.169 mmol, 25% yield).

**TLC** $R_f$ 0.33 (7.5% MeOH in $CH_2Cl_2$)

**$^1$H NMR** (600 MHz, DMSO-$d_6$) δ 8.16 (s, 1H), 8.08 – 8.02 (m, 2H), 8.01 – 7.96 (m, 2H), 7.59 (s, 1H), 4.13 (d, $J$ = 6.4 Hz, 2H), 2.91 (t, $J$ = 6.4 Hz, 1H*) ppm; *: partially exchanged with adventitious water.

**$^{13}$C NMR** (151 MHz, DMSO-$d_6$) δ 195.4, 167.0, 138.3, 136.9, 128.5, 127.8, 30.8 ppm

**LC/MS** ($m/z$): $[M+H]^+$ 196.1

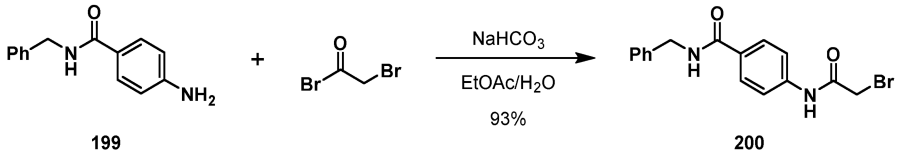


***N*-benzyl-4-(2-bromoacetamido)benzamide (200):** To a vigorously stirred solution of **199**[205] (300 mg, 1.326 mmol, 1.0 equiv) in EtOAc (20 mL) and saturated aqueous $NaHCO_3$ (15 mL) was added bromoacetyl bromide (0.346 mL, 3.977 mmol, 3.0 equiv) at rt in small portions over 2 h until TLC indicated complete conversion. Then, precipitation was removed from the reaction mixture by filtration and the filter cake was washed with EtOAc (5 mL) and water (2 × 15 mL), then dried to provide pure **200** as an off-white solid (204.0 mg). The layers of the filtrate were separated and the organic layer was washed with saturated aqueous $NaHCO_3$ (30 mL) and 1 M HCl, (30 mL), then dried ($MgSO_4$) and concentrated to provide **200** as an ochre solid (total amount: 427 mg, 1.230 mmol, 93% yield).

**TLC** $R_f$ 0.44 (10% MeOH and 0.5% AcOH in $CH_2Cl_2$)

**$^1$H NMR** (600 MHz, DMSO-$d_6$) δ 10.61 (s, 1H), 8.96 (t, $J$ = 6.0 Hz, 1H), 7.98 – 7.80 (m, 2H), 7.72 – 7.62 (m, 2H), 7.35 – 7.28 (m, 4H), 7.27 – 7.20 (m, 1H), 4.47 (d, $J$ = 6.0 Hz, 2H), 4.06 (s, 2H) ppm

**LC/MS** (*m/z*): $[M+H]^+$ 347.0 and 349.0

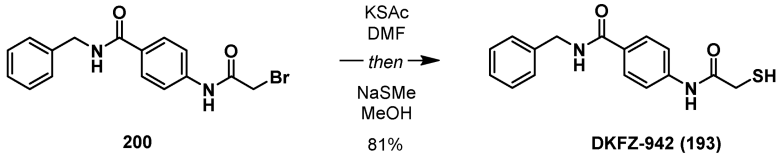


***N*-benzyl-4-(2-mercaptoacetamido)benzamide (DKFZ-942, 193):** A Schlenk tube was charged with **200** (219 mg, 0.629 mmol, 1.0 equiv) and potassium thioacetate (93.4 mg, 0.818 mmol, 1.3 equiv), then dry DMF (2 mL) was added under an argon atmosphere and the reaction mixture was stirred at rt for 15 min. Then, sodium thiomethoxide (110 mg, 1.573 mmol, 2.5 equiv) was added as a solution in dry MeOH (2 mL) under argon. After stirring for 10 min, the reaction mixture was diluted with saturated aqueous $NH_4Cl$ (30 mL) and extracted with EtOAc (4 × 15 mL). The combined organic layers were dried ($MgSO_4$) and concentrated. The product was purified by MPLC (12 g silica, gradient: 0 → 3% MeOH in $CH_2Cl_2$ over 13 CV) to provide **DKFZ-942** as a pale yellow solid (152.9 mg, 0.509 mmol, 81% yield).

**TLC** $R_f$ 0.52 (10% MeOH in $CH_2Cl_2$)

**$^1$H NMR** (600 MHz, DMSO-$d_6$) δ 10.33 (s, 1H), 8.95 (t, *J* = 6.0 Hz, 1H), 7.92 – 7.84 (m, 2H), 7.71 – 7.62 (m, 2H), 7.34 – 7.28 (m, 4H), 7.27 – 7.20 (m, 1H), 4.47 (d, *J* = 6.0 Hz, 2H), 3.33 (s, 2H, overlapping with HDO signal, confirmed by HSQC), 3.01 (br s, 1H*) ppm; *: partially exchanged with adventitious water.

**$^{13}$C NMR** (151 MHz, DMSO-$d_6$) δ 169.0, 165.7, 141.6, 139.8, 129.0, 128.3, 128.2, 127.2, 126.7, 118.3, 42.6, 28.4 ppm

**HR-MS** (*m/z*): $[2M-2H+H]^+$ calcd for $C_{32}H_{31}N_4O_4S_2^+$: 599.1781; found: 599.1788

Note: The material was found to readily form the disulfide when exposed to air, especially in solution. The tested sample contains 10–15% disulfide as estimated by NMR and HPLC.

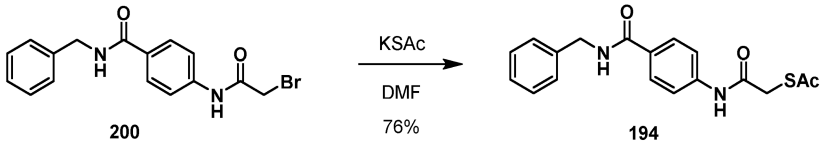


***S*-(2-((4-(benzylcarbamoyl)phenyl)amino)-2-oxoethyl) ethanethioate (DKFZ-958, 194):** A Schlenk tube was charged with **200** (196 mg, 0.564 mmol, 1.0 equiv) and potassium thioacetate (83.8 mg, 0.734 mmol, 1.3 equiv), then dry DMF (2 mL) was added under an argon atmosphere and the reaction mixture was stirred at rt for 30 min. Then, the reaction mixture was diluted with brine (25 mL) and water (25 mL) and extracted with EtOAc (4 × 20 mL). The combined organic layers were washed with brine (2 × 30 mL), then dried ($MgSO_4$) and concentrated. The product was purified by crystallization from a saturated solution in EtOAc,

which was carefully covered with a layer of hexane and cooled to –20 °C for 4 h. The precipitate was filtered and washed with ice-cold hexane (2 × 10 mL) to provide **DKFZ-958** as a tan solid (147.7 mg, 0.431 mmol, 76% yield).

**TLC** $R_f$ 0.41 (75% EtOAc in hexane)

**$^1$H NMR** (600 MHz, DMSO-$d_6$) δ 10.48 (s, 1H), 8.95 (t, $J$ = 6.0 Hz, 1H), 7.91 – 7.84 (m, 2H), 7.69 – 7.61 (m, 2H), 7.35 – 7.29 (m, 4H), 7.26 – 7.20 (m, 1H), 4.47 (d, $J$ = 6.0 Hz, 2H), 3.86 (s, 2H), 2.39 (s, 3H) ppm

**$^{13}$C NMR** (151 MHz, DMSO-$d_6$) δ 194.6, 166.1, 165.6, 141.5, 139.8, 129.1, 128.3, 128.2, 127.2, 126.7, 118.3, 42.6, 33.9, 30.1 ppm

**LC/MS** (*m/z*): $[M+H]^+$ 343.1

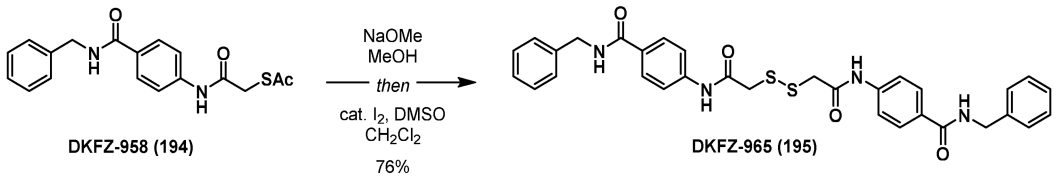


**4,4'-((2,2'-Disulfanediylbis(acetyl))bis(azanediyl))bis(*N*-benzylbenzamide) (DKFZ-965, 195):** To a suspension of thioester **DKFZ-958** (**194**) (74.3 mg, 0.217 mmol, 1.0 equiv) in MeOH (2 mL) was added sodium methoxide (35.2 mg, 0.651 mmol, 3.0 equiv) and the mixture was stirred at rt for 2 h. Then, the reaction mixture was diluted with MeOH (3 mL) and acidified (0.35 mL 2 M HCl in MeOH), then the solvent was removed in vacuo and residual acid was removed by co-evaporation with MeOH (10 mL). The residue was dissolved in a mixture of $CH_2Cl_2$ (3 mL) and MeOH (1.5 mL), then DMSO (0.031 mL, 0.434 mmol, 2.0 equiv) and iodine (11.0 mg, 0.043 mmol, 0.2 equiv) were added and the solution was stirred at rt for 30 min. Upon complete conversion, the reaction mixture was diluted with EtOAc (50 mL) and washed with 10% aqueous $Na_2S_2O_3$ solution (2 × 30 mL) and brine (2 × 30 mL). A white precipitate formed in the organic phase, which was filtered and washed with water (3 × 20 mL), MeOH (2 × 10 mL) and EtOAc (20 mL) to provide **DKFZ-965** as an off-white solid (49.5 mg, 0.083 mmol, 76% yield).

**TLC** $R_f$ 0.38 (100% EtOAc)

**$^1$H NMR** (600 MHz, DMSO-$d_6$) δ 10.41 (s, 2H*), 8.94 (t, $J$ = 6.0 Hz, 2H), 7.87 (d, $J$ = 8.4 Hz, 4H), 7.67 (d, $J$ = 8.4 Hz, 4H), 7.42 – 7.27 (m, 8H), 7.26 – 7.19 (m, 2H), 4.47 (d, $J$ = 5.9 Hz, 4H), 3.77 (s, 4H*) ppm; *: partially exchanged with adventitious water.

**$^{13}$C NMR** (151 MHz, DMSO-$d_6$) δ 167.1, 165.6, 141.4, 139.8, 129.2, 128.3, 128.2, 127.2, 126.7, 118.5, 43.2, 42.6 ppm

**HR-MS** (*m/z*): $[M+H]^+$ calcd for $C_{32}H_{31}N_4O_4S_2^+$: 599.1781; found: 599.1789

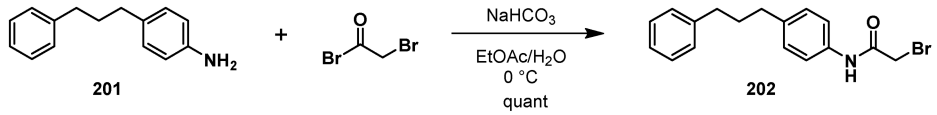


**2-Bromo-*N*-(4-(3-phenylpropyl)phenyl)acetamide (202):** To a vigorously stirred solution of 4-(3-phenylpropyl)aniline (**201**, 250 mg, 1.183 mmol, 1.0 equiv) in EtOAc (10 mL) and saturated aqueous $NaHCO_3$ (10 mL), cooled by ice-bath, was added bromoacetyl bromide (0.134 mL, 1.538 mmol, 1.3 equiv) in one portion and stirred for 10 min. The reaction mixture was diluted with EtOAc (20 mL) and water (10 mL), phases were separated and the organic phase was washed with saturated aqueous $NaHCO_3$ (3 × 50 mL) and 1 M HCl, (50 mL), then dried ($MgSO_4$) and concentrated to provide sufficiently pure **202** as a brown solid (382 mg, 1.183 mmol, quant yield).

**TLC** $R_f$ 0.59 (40% EtOAc in hexane)

**$^1$H NMR** (400 MHz, $CDCl_3$) δ 8.12 (br s, 1H), 7.47 – 7.41 (m, 2H), 7.32 – 7.27 (m, 2H), 7.22 – 7.14 (m, 5H), 4.02 (s, 2H), 2.68 – 2.60 (m, 4H), 1.99 – 1.90 (m, 2H) ppm

**LC/MS** (*m/z*): $[M+H]^+$ 332.0 and 334.1

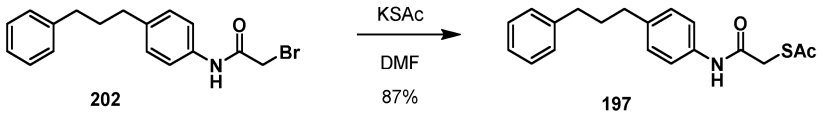


***S*-(2-oxo-2-((4-(3-phenylpropyl)phenyl)amino)ethyl) ethanethioate (DKFZ-960, 197):** Bromide **202** (178.5 mg, 0.537 mmol, 1.0 equiv) and potassium thioacetate (73.6 mg, 0.645 mmol, 1.2 equiv) were dissolved in DMF (2 mL) and stirred at rt for 1 h, then the reaction mixture was diluted with EtOAc (30 mL) and washed with saturated aqueous $NaHCO_3$ (2 × 50 mL) and brine (50 mL). The organic layer was dried ($MgSO_4$) and concentrated. The product was purified by MPLC (4 g silica, gradient: 10% EtOAc in hexane for 2 CV, 10 → 35% over 10 CV, 35 → 45% over 7 CV, then 45% for 8 CV) to provide **DKFZ-960** as a brown solid (152.6 mg, 0.466 mmol, 87% yield).

**TLC** $R_f$ 0.41 (40% EtOAc in hexane)

**$^1$H NMR** (600 MHz, $CDCl_3$) δ 8.11 (s, 1H), 7.46 – 7.37 (m, 2H), 7.32 – 7.27 (m, 2H), 7.22 – 7.16 (m, 3H), 7.15 – 7.09 (m, 2H), 3.66 (s, 2H), 2.63 (t, *J* = 7.6 Hz, 2H), 2.61 (t, *J* = 7.6 Hz, 2H), 2.44 (s, 3H), 1.98 – 1.88 (m, 2H) ppm

**$^{13}$C NMR** (151 MHz, $CDCl_3$) δ 197.2, 166.4, 142.3, 138.8, 135.5, 129.0, 128.5, 128.4, 125.9, 120.0, 35.4, 34.9, 34.3, 33.1, 30.4 ppm

**LC/MS** (*m/z*): $[M+H]^+$ 328.1

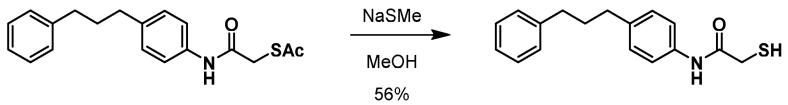


DKFZ-960 (197) DKFZ-963 (196)

**2-Mercapto-*N*-(4-(3-phenylpropyl)phenyl)acetamide (DKFZ-963, 196):** A Schlenk tube was charged with **DKFZ-960** (**197**, 108 mg, 0.330 mmol, 1.0 equiv) and potassium thioacetate (57.8 mg, 0.825 mmol, 2.5 equiv), then dry MeOH (3 mL) was added under an argon atmosphere and the reaction mixture was stirred at rt for 20 min. Then, the reaction mixture was diluted with EtOAc (20 mL) and washed with saturated aqueous $NH_4Cl$ (2 × 30 mL) and brine (30 mL). The organic layer was dried ($MgSO_4$) and concentrated. The product was purified by MPLC (4 g silica, gradient: 10% EtOAc in hexane for 3 CV, 10 → 30% over 8 CV, 30% for 5 CV, then 30 → 60% over 9 CV) to provide **DKFZ-963** as a tan solid (52.6 mg, 0.184 mmol, 56% yield).

**TLC** $R_f$ 0.26 (40% EtOAc in hexane)

**$^1$H NMR** (600 MHz, $CDCl_3$) δ 8.49 (s, 1H*), 7.50 – 7.42 (m, 2H), 7.33 – 7.26 (m, 2H), 7.23 – 7.10 (m, 5H), 3.39 (d, *J* = 9.2 Hz, 2H*), 2.64 (app q, *J* = 7.5 Hz, 4H), 2.02 (t, *J* = 9.2 Hz, 1H), 1.98 – 1.90 (m, 2H) ppm; *: partially exchanged with adventitious water.

**$^{13}$C NMR** (151 MHz, $CDCl_3$) δ 167.2, 142.3, 139.1, 135.2, 129.1, 128.6, 128.4, 125.9, 120.1, 35.4, 34.9, 33.1, 29.2 ppm

**HR-MS** (*m/z*): $[M-2H+Na]^+$ calcd for $C_{34}H_{36}N_2NaO_2S_2^+$: 591.2110; found: 591.2115

Note: The material was found to readily form the disulfide when exposed to air, especially in solution. The tested sample contains ~10% disulfide as estimated by NMR and HPLC.

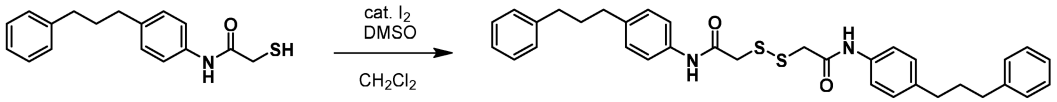


DKFZ-963 (196) DKFZ-964 (198)

**2,2'-Disulfanediylbis(N-(4-(3-phenylpropyl)phenyl)acetamide) (DKFZ-964, 198):** Thiol **DKFZ-963** (**196**, 30.7 mg, 0.108 mmol, 1.0 equiv) was dissolved in $CH_2Cl_2$ (1 mL), DMSO (0.015 mL, 0.215 mmol, 2.0 equiv) and iodine (5.5 mg, 0.022 mmol, 0.2 equiv) were added. The solution was stirred at rt for 15 min, then diluted with EtOAc (25 mL) and washed with 10% aqueous $Na_2S_2O_3$ solution (2 × 30 mL) and brine (30 mL). The organic phase, was dried ($MgSO_4$) and concentrated to provide **DKFZ-964** as a brown solid (30.3 mg, 0.053 mmol, 99% yield).

**TLC** $R_f$ 0.51 (40% EtOAc in hexane)

**$^1$H NMR** (600 MHz, $CDCl_3$) δ 8.89 (s, 2H*), 7.61 – 7.44 (m, 4H), 7.32 – 7.26 (m, 4H), 7.23 – 7.16 (m, 6H), 7.16 – 7.08 (m, 4H), 3.60 (s, 4H*), 2.64 (t, *J* = 7.6 Hz, 4H), 2.61 (t, *J* = 7.6 Hz, 4H), 1.98 – 1.87 (m, 4H) ppm; *: partially exchanged with adventitious water.

**$^{13}$C NMR** (151 MHz, $CDCl_3$) δ 167.4, 142.3, 139.0, 135.5, 129.1, 128.6, 128.4, 125.9, 120.4, 43.9, 35.5, 35.0, 33.1 ppm

**HR-MS** (*m/z*): $[M+Na]^+$ calcd for $C_{34}H_{36}N_2NaO_2S_2^+$: 591.2110; found: 591.2118

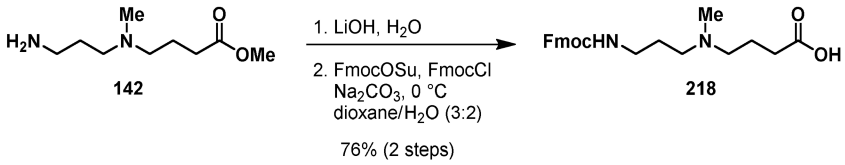


**4-((3-((((9*H*-fluoren-9-yl)methoxy)carbonyl)amino)propyl)(methyl)amino)butanoic acid (218):** A solution of **142** 2·HCl (1.081 g, 4.139 mmol, 1.0 equiv) in 3 M aqueous lithium hydroxide solution (20.7 mL, 62.0 mmol, 15.0 equiv) was stirred at rt for 1.5 h, then neutralized with 3 M aqueous HCl and concentrated in vacuo. The residue was dissolved in a 3:2 mixture of 10% aqueous $Na_2CO_3$ and 1,4-dioxane (83 mL), cooled by an ice-bath and then FmocOSu (1.535 g, 4.552 mmol, 1.1 equiv) and FmocCl (1.178 g, 4.552 mmol, 1.1 equiv) were added in 5 portions over a period of 20 min. Note: Only adding FmocOSu (1.2 equiv) was later found to be sufficient for similar amine substrates. The reaction mixture was stirred at 0 °C for 4 h until TLC and LC/MS indicated complete conversion of the amine starting material. Then, the reaction mixture was diluted with water (200 mL) and extracted with $Et_2O$ (3 × 50 mL). The aqueous phase was acidified to pH 1 with 3 M HCl and concentrated to dryness. The residue was suspended in 30% MeOH in $CH_2Cl_2$ (200 mL), filtered, concentrated and purified by RP-MPLC (43 g C18 Teledyne Isco #69-2203-413, gradient: 0.5% TFA in $H_2O$ (A) for 2 CV, 0 → 15% MeCN (B) in 2 CV, 15 → 21% B in 6 CV, 21% B for 13 CV, then 21 → 25% B in 2 CV) in two batches to provide the HCl salt of **218** as a sticky, beige amorphous solid (1.3549 g, 3.130 mmol, 76% over two steps). Note: The product is susceptible to Fmoc cleavage under neutral and basic conditions, especially in water and was therefore kept in the protonated state throughout the purification.

**TLC** $R_f$ 0.41 (30% MeOH and 0.5% TFA in $CH_2Cl_2$).

**$^1$H NMR** (400 MHz, DMSO-$d_6$) δ 12.37 (br s, 1H*), 9.48 (br s, 1H*), 7.89 (d, *J* = 7.5 Hz, 2H), 7.68 (d, *J* = 7.5 Hz, 2H), 7.49 – 7.37 (m, 3H), 7.34 (t, *J* = 1.2 Hz, 2H), 4.34 (d, *J* = 6.7 Hz, 2H), 4.22 (t, *J* = 6.7 Hz, 1H), 3.18 – 2.94 (m, 6H), 2.74 (s, 3H), 2.32 (t, *J* = 7.2 Hz, 2H), 1.93 – 1.70 (m, 4H) ppm; *: partially exchanged with adventitious water.

**$^{13}$C NMR** (101 MHz, DMSO-$d_6$) δ 173.47, 156.22, 143.88, 140.77, 127.62, 127.06, 125.06, 120.15, 65.27, 54.37, 52.86, 46.75, 39.40, 37.48, 30.38, 24.12, 18.97 ppm. Note: No TFA signals were observed in $^{13}$C NMR, which suggests the amine was isolated as the HCl salt.

**LC/MS** (*m/z*): $[M+H]^+$ 397.2

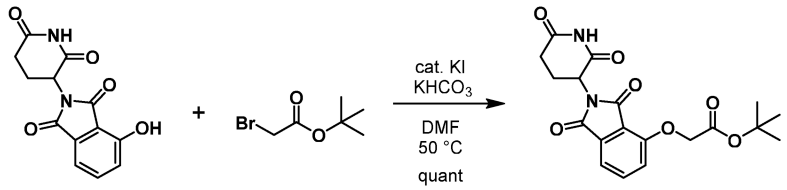


219 220

***Tert*-butyl 2-((2-(2,6-dioxopiperidin-3-yl)-1,3-dioxoisoindolin-4-yl)oxy)acetate (220):** To a stirred solution of **219**[206] (1.000 g, 3.647 mmol, 1.0 equiv) in DMF (11.5 mL) were added $KHCO_3$ (0.548 g, 5.47 mmol, 1.5 equiv) and KI (60.0 mg, 365 nmol, 0.1 equiv), then *tert*-butyl 2-bromoacetate (0.646 mL, 4.38 mmol, 1.2 equiv) was added slowly. The olive green suspension was heated in a 50 °C metal block for 3 h, then diluted with water (175 mL) and extracted with EtOAc (3 × 100 mL). The combined organic layers were washed with water (1 × 200 mL) and brine (2 × 200 mL), then dried ($MgSO_4$) and concentrated under reduced pressure. The product was purified by FCC (125 g silica, eluent: 65% EtOAc in hexane) to provide **220** (1.4378 g, quant yield) as a lime green solid.

**TLC** $R_f$ 0.68 (60% EtOAc in hexane)

**$^1$H NMR** (600 MHz, DMSO-$d_6$) δ 11.12 (s, 1H), 7.80 (dd, *J* = 8.5, 7.3 Hz, 1H), 7.48 (d, *J* = 7.2 Hz, 1H), 7.38 (d, *J* = 8.6 Hz, 1H), 5.11 (dd, *J* = 12.9, 5.4 Hz, 1H), 4.97 (s, 2H), 2.89 (ddd, *J* = 17.0, 13.9, 5.4 Hz, 1H), 2.64 – 2.51 (m, 2H), 2.07 – 2.01 (m, 1H), 1.43 (s, 9H) ppm

**LC/MS** (*m/z*): $[M+NH_4]^+$ 406.2

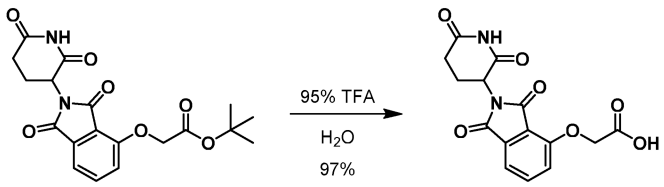


220 206

**2-((2-(2,6-Dioxopiperidin-3-yl)-1,3-dioxoisoindolin-4-yl)oxy)acetic acid (206)[206]:** A solution of **220** (1.217 g, 3.13 mmol, 1.0 equiv) in 95% TFA/$H_2O$ (12.2 mL) was stirred for 7 h and then concentrated under reduced pressure to provide pure **206** (1.0104 g, 3.041 mmol, 97%) as a light yellow/green solid, which was used without further purification.

**$^1$H NMR** (600 MHz, DMSO-$d_6$) δ 13.26 (br s, 1H), 11.12 (s, 1H), 7.79 (dd, *J* = 8.5, 7.3 Hz, 1H), 7.48 (d, *J* = 7.2 Hz, 1H), 7.39 (d, *J* = 8.6 Hz, 1H), 5.10 (dd, *J* = 12.9, 5.4 Hz, 1H), 4.99 (s, 2H), 2.94 – 2.84 (m, 1H), 2.64 – 2.51 (m, 2H), 2.08 – 2.00 (m, 1H) ppm

**TLC** $R_f$ 0.30 (0.5% AcOH and 20% MeOH in $CH_2Cl_2$)

**LC/MS** (*m/z*): $[M+H]^+$ 333.1

Analytical data is in agreement with literature.[206]

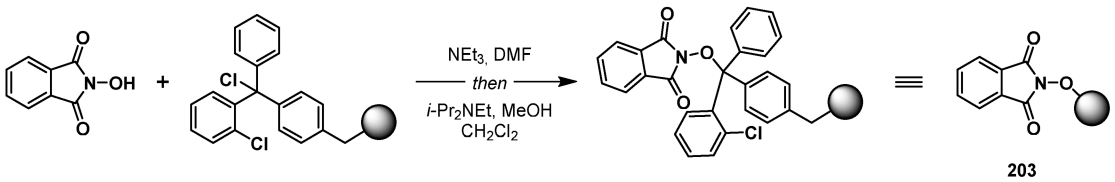


**2-(λ¹-Oxidaneyl)isoindoline-1,3-dione2-chlorotrityl resin (203)[178]:** 2-Chlorotrityl chloride resin (1.000 g, loading capacity: ~1.06 mmol/g, 1.0 equiv) was swelled in a 5 mL fritted syringe in DMF for at least 30 min, then the solvent was replaced with a solution of *N*-hydroxyphthalimide (0.605 g, 3.71 mmol, 3.5 equiv) and $NEt_3$ (0.514 mL, 3.71 mmol, 3.5 equiv) in DMF (1.5 mL) and the suspension was agitated by an end over end sample rotator at rt for 24–48 h. The resin was washed with DMF (10 × 5 mL) and $CH_2Cl_2$ (10 × 5 mL), and then capped with a mixture of then *i*-$Pr_2$Net/MeOH/$CH_2Cl_2$ (5%/15%/80%, 2 × 5 mL, 15 min each). Then, the resin was washed with DMF (2 × 5 mL) and $CH_2Cl_2$ (10 × 5 mL), and then dried by nitrogen flow followed by vacuum.

Resin loading was determined by suspending a precisely known amount (10–40 mg) of dry resin in a fresh, fritted syringe and cleaving the resin in 5% TFA in $CH_2Cl_2$ (1 mL) by mixing for 1 h, followed by washes with 5% TFA in $CH_2Cl_2$ (5 × 4 mL). All cleavage and washing solutions were combined quantitatively and concentrated in vacuo. The residue was dissolved in EtOH to an exact volume of 5.00 mL and the concentration was determined by analytical HPLC (Acidic Method) using a 5-point calibration curve of *N*-hydroxyphthalimide in EtOH ranging from 1 mM to 20 mM. Resin loading was calculated based on the concentration of the *N*-hydroxyphthalimide in the cleavage solution adjusted to 5.00 mL and the amount of resin cleaved. Typical loadings, depending on the resin used, were in the range of 1.0–1.3 mmol/g.

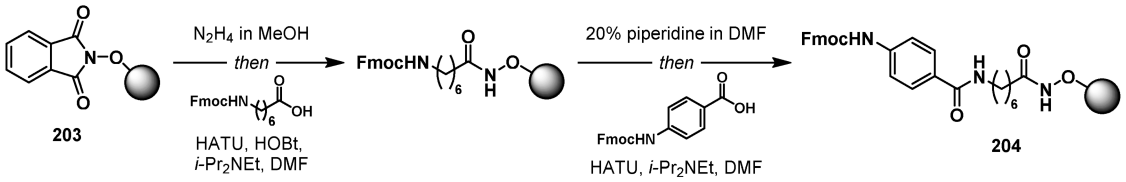


**(9*H*-fluoren-9-yl)methyl (4-((7-((λ¹-oxidaneyl)amino)-7-oxoheptyl)carbamoyl)phenyl)carbamate 2-chlorotrityl resin (204)[178]:** The title resin was prepared from *N*-hydroxyphthalimide loaded resin **203** (0.250 g, 0.278 mmol loading, 1.0 equiv), 7-(Fmoc-amino)heptanoic acid (0.204 g, 0.556 mmol, 2.0 equiv) and 4-(Fmoc-amino)benzoic acid (0.300 g, 0.834 mmol, 3.0 equiv) according to General Procedure D.

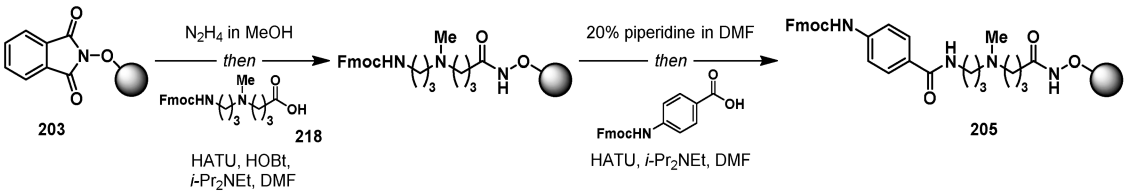


**(9*H*-fluoren-9-yl)methyl (4-((3-((4-((λ¹-oxidaneyl)amino)-4-oxobutyl)(methyl)amino) propyl)carbamoyl)phenyl)carbamate 2-chlorotrityl resin (205):** The title resin was prepared from *N*-hydroxyphthalimide loaded resin **203** (0.278 g, 0.355 mmol loading, 1.0 equiv), **218**·HCl (0.362 g, 0.836 mmol, 2.4 equiv) and 4-(Fmoc-amino)benzoic acid (0.132 g, 0.368 mmol, 1.04 equiv relative to **203**, 3.0 equiv based on Fmoc quantification of previous step) according to General Procedure D.

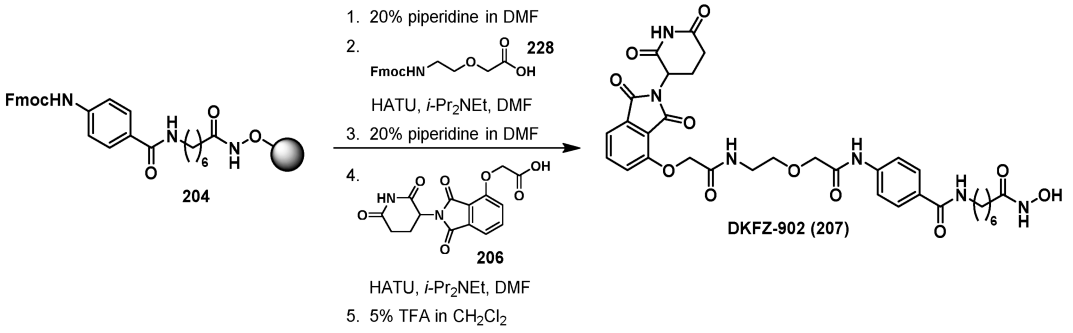


**4-(2-(2-(2-((2-(2,6-Dioxopiperidin-3-yl)-1,3-dioxoisoindolin-4-yl)oxy)acetamido)ethoxy)acetamido)-*N*-(7-(hydroxyamino)-7-oxoheptyl)benzamide (DFKZ-902, 207):** The title compound was prepared from resin **204** (0.235 g, 0.185 mmol loading, 1.0 equiv), acid **228** (0.187 g, 0.548 mmol, 3.0 equiv) and CRBN ligand **206** (0.109 g, 0.328 mmol, 1.8 equiv) according to General Procedure E, and purified twice by HPLC Acidic Method (first gradient: 1 → 31% B in 5 min, then 31 → 45.5% B in 8 min, second gradient: 1 → 26% B in 5 min, then 26 → 40% B in 8 min) to provide **DKFZ-902** as a white fluffy solid (46.1 mg, 66.4 nmol, 36% based on PhtNOH resin **203**).

**TLC** $R_f$ 0.69 (20% MeOH in $CH_2Cl_2$)

**$^1$H NMR** (600 MHz, DMSO-$d_6$) δ 11.12 (s, 1H), 10.34 (s, 1H), 9.78 (s, 1H), 8.66 (br s, 1H*), 8.31 (t, *J* = 5.6 Hz, 1H), 8.22 (t, *J* = 5.8 Hz, 1H), 7.80 – 7.75 (m, 3H), 7.70 – 7.66 (m, 2H), 7.45 (d, *J* = 7.2 Hz, 1H), 7.38 (d, *J* = 8.6 Hz, 1H), 5.09 (dd, *J* = 12.9, 5.4 Hz, 1H), 4.82 (s, 2H), 4.08 (s, 2H), 3.59 (t, *J* = 5.5 Hz, 3H), 3.41 (app q, *J* = 5.6 Hz, 2H), 3.22 (app q, *J* = 6.6 Hz, 2H), 2.87 (ddd, *J* = 17.1, 13.9, 5.4 Hz, 1H), 2.63 – 2.51 (m, 2H), 2.02 – 1.96 (m, 1H), 1.94 (t, *J* = 7.4 Hz, 2H), 1.52 – 1.45 (m, 4H), 1.33 – 1.21 (m, 4H) ppm; *: partially exchanged with adventitious water.

**$^{13}$C NMR** (151 MHz, DMSO-$d_6$) δ 172.80, 169.93, 169.14, 168.40, 167.27, 166.72, 165.50, 165.44, 155.10, 140.73, 136.90, 133.05, 129.55, 127.88, 120.31, 118.75, 116.79, 116.04, 69.96, 69.65, 67.61, 48.81, 39.15, 38.34, 32.27, 30.97, 29.12, 28.40, 26.28, 25.13, 21.99 ppm

Note: HPLC and NMR analyses indicate a purity of 90-95%.

**HR-MS** (*m/z*): $[M+Na]^+$ calcd for $C_{33}H_{38}N_6NaO_{11}^+$: 717.2491; found: 717.2491

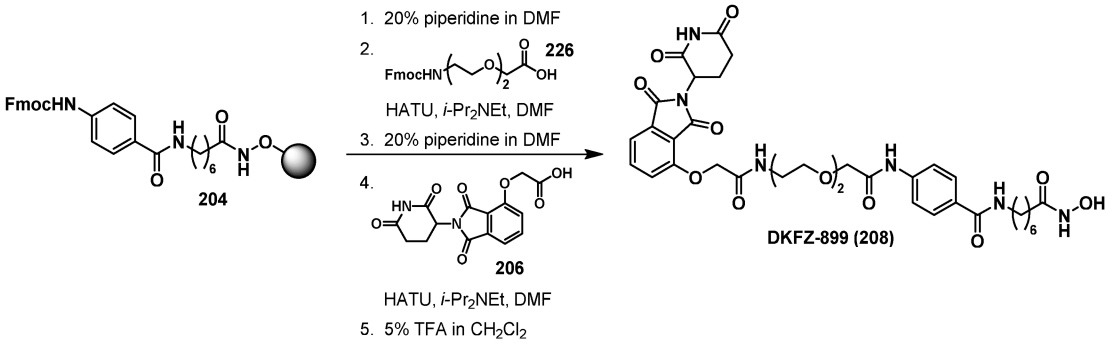


**4-(2-(2-(2-(2-((2-(2,6-Dioxopiperidin-3-yl)-1,3-dioxoisoindolin-4-yl)oxy)acetamido)ethoxy)ethoxy)acetamido)-*N*-(7-(hydroxyamino)-7-oxoheptyl)benzamide (DFKZ-899, 208)[178]:** The title compound was prepared from resin **204** (0.250 g, 0.278 mmol, 1.0 equiv), acid **226** (0.321 g, 0.834 mmol, 3.0 equiv) and CRBN ligand **206** (0.185 g, 0.556 mmol, 2.0 equiv) according to General Procedure E, and purified by HPLC Acidic Method (gradient: 1 → 30% B in 5 min, then 30 → 42% B in 8 min) to provide **DKFZ-899** as a white fluffy solid (12.6 mg, 17.1 nmol, 6% based on PhtNOH resin **203**).

**TLC** $R_f$ 0.66 (20% MeOH in $CH_2Cl_2$)

**$^1$H NMR** (600 MHz, DMSO-$d_6$) δ 11.13 (s, 1H), 10.34 (s, 1H), 9.82 (s, 1H), 8.31 (t, *J* = 5.6 Hz, 1H), 8.02 (t, *J* = 5.7 Hz, 1H), 7.83 – 7.75 (m, 3H), 7.70 – 7.66 (m, 2H), 7.47 (d, *J* = 7.3 Hz, 1H), 7.38 (d, *J* = 8.5 Hz, 1H), 5.11 (dd, *J* = 12.9, 5.4 Hz, 1H), 4.77 (s, 2H), 4.10 (s, 2H), 3.71 – 3.64 (m, 2H), 3.66 – 3.58 (m, 2H), 3.51 (t, *J* = 5.7 Hz, 2H), 3.35 (app q, *J* = 5.7 Hz, 2H), 3.21 (app q, *J* = 6.7 Hz, 2H), 2.89 (ddd, *J* = 17.0, 13.9, 5.5 Hz, 1H), 2.64 – 2.50 (m, 2H), 2.08 – 2.00 (m, 1H), 1.93 (t, *J* = 7.4 Hz, 2H), 1.54 – 1.44 (m, 4H), 1.32 – 1.22 (m, 4H) ppm

**$^{13}$C NMR** (151 MHz, DMSO-$d_6$) δ 172.83, 169.93, 169.12, 168.68, 166.96, 166.75, 165.47 (2 × C=O overlapped), 154.93, 140.74, 136.94, 133.03, 129.53, 127.90, 120.31, 118.69, 116.75, 116.05, 70.35, 70.23, 69.45, 68.87, 67.47, 48.81, 39.17*, 38.35, 32.26, 30.97, 29.11, 28.39, 26.27, 25.12, 22.01 ppm; *: overlapped with DMSO peak, chemical shift obtained from HSQC edit.

**HR-MS** (*m/z*): $[M+Na]^+$ calcd for $C_{35}H_{42}N_6NaO_{12}^+$: 761.2753; found: 761.2756

Analytical data is in agreement with literature.[178]

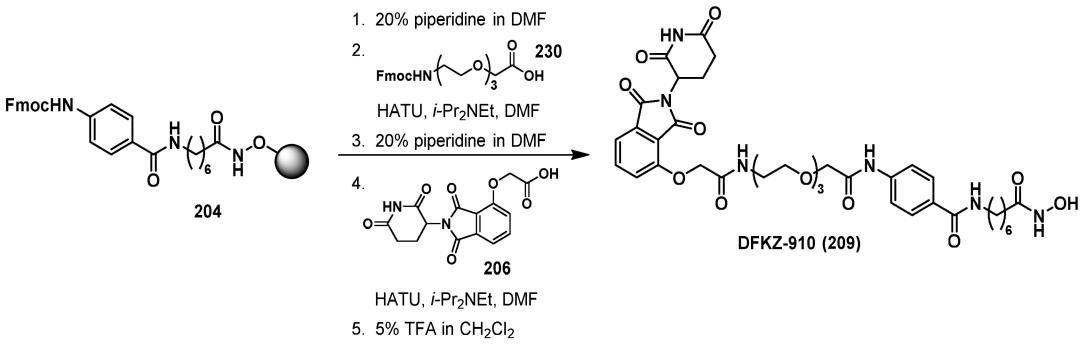


**4-(1-((2-(2,6-Dioxopiperidin-3-yl)-1,3-dioxoisoindolin-4-yl)oxy)-2-oxo-6,9,12-trioxa-3-azatetradecan-14-amido)-*N*-(7-(hydroxyamino)-7-oxoheptyl)benzamide (DFKZ-910, 209):** The title compound was prepared from resin **204** (0.200 g, 0.178 mmol loading, 1.0 equiv), acid **230** (0.230 g, 0.535 mmol, 3.0 equiv) and CRBN ligand **206** (0.118 g, 0.356 mmol, 2.0 equiv) according to General Procedure E, and purified twice by HPLC Acidic Method (gradient: 1 → 25% B in 5 min, then 25 → 39% B in 8 min) to provide **DKFZ-910** as a white fluffy solid (32.7 mg, 41.8 nmol, 23% based on PhtNOH resin **203**).

**TLC** $R_f$ 0.43 (15% MeOH in $CH_2Cl_2$).

**$^1$H NMR** (600 MHz, DMSO-$d_6$) δ 11.13 (s, 1H), 10.35 (s, 1H), 9.81 (s, 1H), 8.32 (t, *J* = 5.6 Hz, 1H), 8.01 (t, *J* = 5.7 Hz, 1H), 7.86 – 7.74 (m, 3H), 7.70 (d, *J* = 8.4 Hz, 2H), 7.49 (d, *J* = 7.2 Hz, 1H), 7.39 (d, *J* = 8.5 Hz, 1H), 5.12 (dd, *J* = 12.9, 5.4 Hz, 1H), 4.78 (s, 2H), 4.09 (s, 2H), 3.68 – 3.50 (m, 8H), 3.47 (t, *J* = 5.7 Hz, 2H), 3.31 (app q, *J* = 5.7 Hz, 2H), 3.21 (app q, *J* = 6.7 Hz, 2H), 2.89 (ddd, *J* = 17.1, 13.9, 5.5 Hz, 1H), 2.64 – 2.51 (m, 2H), 2.08 – 1.99 (m, 1H), 1.94 (t, *J* = 7.4 Hz, 2H), 1.48 (p, *J* = 4.6 Hz, 4H), 1.32 – 1.24 (m, 4H) ppm

**$^{13}$C NMR** (151 MHz, DMSO-$d_6$) δ 172.85, 169.95, 169.15, 168.72, 166.96, 166.78, 165.53, 165.50, 154.98, 140.77, 136.98, 133.06, 129.58, 127.95, 120.34, 118.74, 116.78, 116.09, 70.41, 70.20, 69.80, 69.67, 69.62, 68.87, 67.50, 48.84, 39.16, 38.43, 32.27, 30.99, 29.13, 28.40, 26.29, 25.14, 22.04 ppm

**HR-MS** (*m/z*): $[M+Na]^+$ calcd for $C_{37}H_{46}N_6NaO_{13}^+$: 805.3015; found: 805.3017

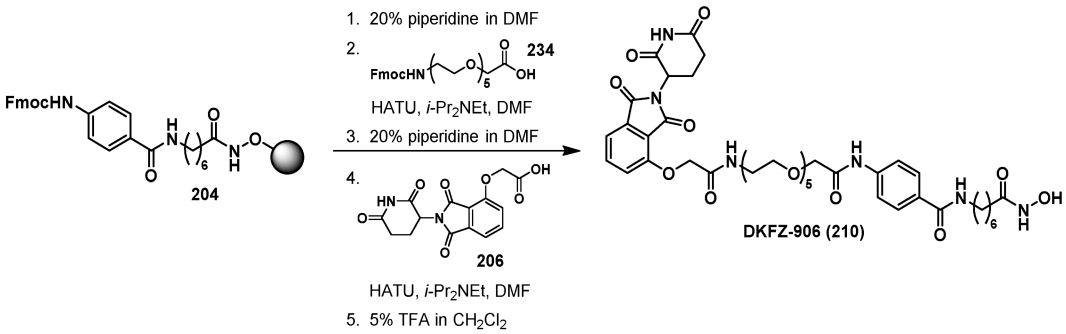


**4-(1-((2-(2,6-Dioxopiperidin-3-yl)-1,3-dioxoisoindolin-4-yl)oxy)-2-oxo-6,9,12,15,18-pentaoxa-3-azaicosan-20-amido)-*N*-(7-(hydroxyamino)-7-oxoheptyl)benzamide (DFKZ-906, 210):** The title compound was prepared from resin **204** (0.200 g, 0.115 mmol loading, 1.0 equiv), acid **234** (0.179 g, 0.346 mmol, 3.0 equiv) and CRBN ligand **206** (0.077 g, 0.230 mmol, 2.0 equiv) according to General Procedure E, and purified twice by HPLC Acidic Method (gradient: 1 → 33 % B in 5 min, then 33 → 47% B in 8 min) to provide **DKFZ-906** as a white fluffy solid (49.8 mg, 57.2 nmol, 32% based on PhtNOH resin **203**).

**TLC** $R_f$ 0.45 (15% MeOH in $CH_2Cl_2$)

**$^1$H NMR** (600 MHz, DMSO-$d_6$) δ 11.13 (s, 1H), 10.35 (br s, 1H), 9.82 (s, 1H), 8.33 (t, *J* = 5.7 Hz, 1H), 8.02 (t, *J* = 5.6 Hz, 1H), 7.83 – 7.77 (m, 3H), 7.70 (d, *J* = 8.6 Hz, 2H), 7.49 (d, *J* = 7.3 Hz, 1H), 7.39 (d, *J* = 8.5 Hz, 1H), 5.12 (dd, *J* = 12.9, 5.4 Hz, 1H), 4.79 (s, 2H), 4.10 (s, 2H), 3.69 – 3.64 (m, 2H), 3.60 (m, 2H), 3.56 – 3.53 (m, 2H), 3.53 – 3.51 (m, 2H), 3.51 – 3.46 (m, 8H), 3.45 (t, *J* = 5.7 Hz, 2H), 3.31 (app q, *J* = 5.7 Hz, 2H), 3.22 (app q, *J* = 6.7 Hz, 2H), 2.90 (ddd, *J* = 17.1, 13.9, 5.5 Hz, 1H), 2.67 – 2.51 (m, 2H), 2.07 – 2.01 (m, 1H), 1.94 (t, *J* = 7.4 Hz, 2H), 1.52 – 1.45 (m, 4H), 1.31 – 1.23 (m, 4H) ppm

**$^{13}$C NMR** (151 MHz, DMSO-$d_6$) δ 172.83, 169.93, 169.15, 168.71, 166.94, 166.78, 165.53, 165.48, 155.01, 140.77, 136.98, 133.07, 129.57, 127.94, 120.35, 118.74, 116.77, 116.07, 70.41, 70.19, 69.83, 69.81 (2 × $CH_2$ overlapped), 69.75, 69.73, 69.64, 69.61, 68.84, 67.50, 48.84, 39.15, 38.44, 32.27, 30.98, 29.13, 28.40, 26.28, 25.14, 22.03 ppm

**HR-MS** (*m/z*): $[M+Na]^+$ calcd for $C_{41}H_{54}N_6NaO_{15}^+$: 893.3539; found: 893.3546

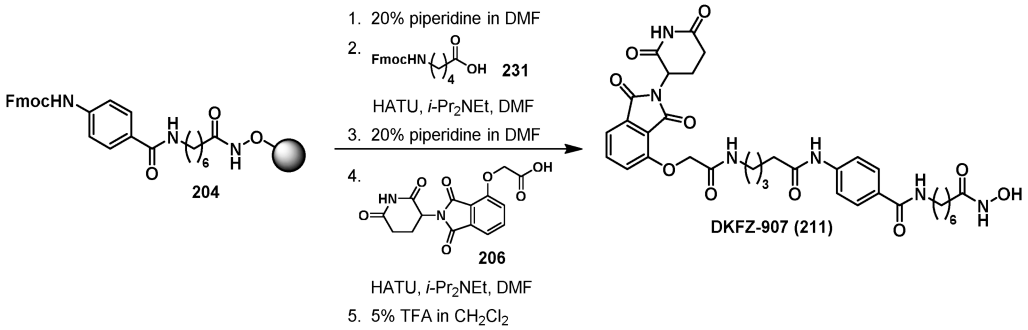


**4-(5-(2-((2-(2,6-Dioxopiperidin-3-yl)-1,3-dioxoisoindolin-4-yl)oxy)acetamido)pentanamido)-*N*-(7-(hydroxyamino)-7-oxoheptyl)benzamide**

**(DFKZ-907, 211):** The title compound was prepared from resin **204** (0.200 g, 0.178 mmol loading, 1.0 equiv), acid **231** (0.181 g, 0.535 mmol, 3.0 equiv) and CRBN ligand **206** (0.118 g, 0.356 mmol, 2.0 equiv) according to General Procedure E, and purified by HPLC Acidic Method (gradient: 10 → 31% B in 5 min, then 31 → 43% B in 8 min) to provide **DKFZ-907** as a white fluffy solid (46.6 mg, 67.3 nmol, 38% based on PhtNOH resin **203**).

**TLC** $R_f$ 0.24 (15% MeOH in $CH_2Cl_2$)

**$^1$H NMR** (600 MHz, DMSO-$d_6$) δ 11.13 (s, 1H), 10.35 (s, 1H), 10.09 (s, 1H), 8.63 (br s, 1H*), 8.30 (t, *J* = 5.7 Hz, 1H), 8.02 (t, *J* = 5.8 Hz, 1H), 7.79 (m, 3H), 7.64 (d, *J* = 8.3 Hz, 2H), 7.48 (d, *J* = 7.3 Hz, 1H), 7.38 (d, *J* = 8.5 Hz, 1H), 5.12 (dd, *J* = 12.9, 5.4 Hz, 1H), 4.78 (s, 2H), 3.21 (app q, *J* = 6.8 Hz, 2H), 3.17 (app q, *J* = 6.6 Hz, 2H), 2.89 (ddd, *J* = 16.9, 13.8, 5.5 Hz, 1H), 2.65 – 2.51 (m, 2H), 2.34 (t, *J* = 7.3 Hz, 2H), 2.08 – 1.98 (m, 1H), 1.94 (t, *J* = 7.4 Hz, 2H), 1.60 (p, *J* = 7.5 Hz, 2H), 1.52 – 1.44 (m, 6H), 1.31 – 1.22 (m, 4H) ppm; *: partially exchanged with adventitious water.

**$^{13}$C NMR** (151 MHz, DMSO-$d_6$) δ 172.84, 171.46, 169.95, 169.15, 166.78, 166.76, 165.58, 165.53, 155.12, 141.73, 136.96, 133.07, 128.98, 127.97, 120.39, 118.11, 116.83, 116.05, 67.64, 48.83, 39.13, 38.14, 36.01, 32.27, 30.98, 29.14, 28.69, 28.40, 26.28, 25.14, 22.39, 22.02 ppm

**HR-MS** (*m/z*): $[M+Na]^+$ calcd for $C_{34}H_{40}N_6NaO_{10}^+$: 715.2698; found: 715.2699

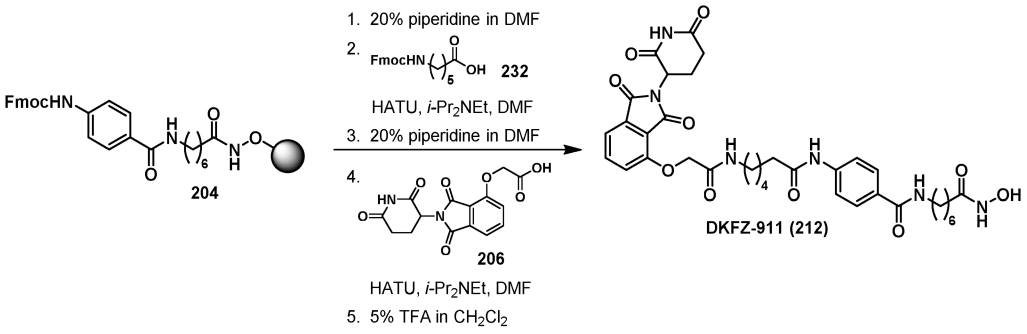


**4-(6-(2-((2-(2,6-Dioxopiperidin-3-yl)-1,3-dioxoisoindolin-4-yl)oxy)acetamido)hexanamido)-*N*-(7-(hydroxyamino)-7-oxoheptyl)benzamide (DFKZ-911, 212):** The title compound was prepared from resin **204** (0.200 g, 0.178 mmol loading, 1.0 equiv), acid **232** (0.189 g, 0.535 mmol, 3.0 equiv) and CRBN ligand **206** (0.118 g, 0.356 mmol, 2.0 equiv) according to General Procedure E, and purified by HPLC Acidic Method (gradient: 10 → 38% B in 5 min, then 38 → 50% B in 8 min) to provide **DKFZ-911** as a white fluffy solid (38.2 mg, 54.1 nmol, 30% based on PhtNOH resin **203**).

**TLC** $R_f$ 0.24 (15% MeOH in $CH_2Cl_2$)

**$^1$H NMR** (600 MHz, DMSO-$d_6$) δ 11.13 (s, 1H), 10.34 (s, 1H), 10.07 (s, 1H), 8.67 (br s, 1H*), 8.30 (t, *J* = 5.9 Hz, 1H), 7.98 (t, *J* = 5.9 Hz, 1H), 7.80 (app t, *J* = 7.9 Hz, 1H), 7.77 (d, *J* = 8.4 Hz, 2H), 7.64 (d, *J* = 8.2 Hz, 2H), 7.48 (d, *J* = 7.3 Hz, 1H), 7.38 (d, *J* = 8.5 Hz, 1H), 5.12 (dd, *J* = 13.0, 5.5 Hz, 1H), 4.77 (s, 2H), 3.21 (app q, *J* = 6.6 Hz, 2H), 3.15 (app q, *J* = 6.7 Hz, 2H), 2.98 – 2.82 (m, 1H), 2.66 – 2.51 (m, 2H), 2.32 (t, *J* = 7.4 Hz, 2H), 2.09 – 1.99 (m, 1H), 1.93 (t, *J* = 7.5 Hz, 2H), 1.59 (p, *J* = 7.5

Hz, 2H), 1.52 – 1.39 (m, 6H), 1.35 – 1.22 (m, 6H) ppm; *: partially exchanged with adventitious water.

**$^{13}$C NMR** (151 MHz, DMSO-$d_6$) δ 172.84, 171.56, 169.95, 169.15, 166.77, 166.69, 165.57, 165.55, 155.09, 141.75, 136.96, 133.06, 128.95, 127.96, 120.39, 118.11, 116.83, 116.07, 67.64, 48.83, 39.13*, 38.28, 36.37, 32.27, 30.98, 29.13, 28.87, 28.40, 26.28, 26.02, 25.14, 24.72, 22.02 ppm; *: overlapped with DMSO peak, chemical shift obtained from HSQC edit.

**HR-MS** (*m/z*): $[M+Na]^+$ calcd for $C_{35}H_{42}N_6NaO_{10}^+$: 729.2855; found: 729.2856

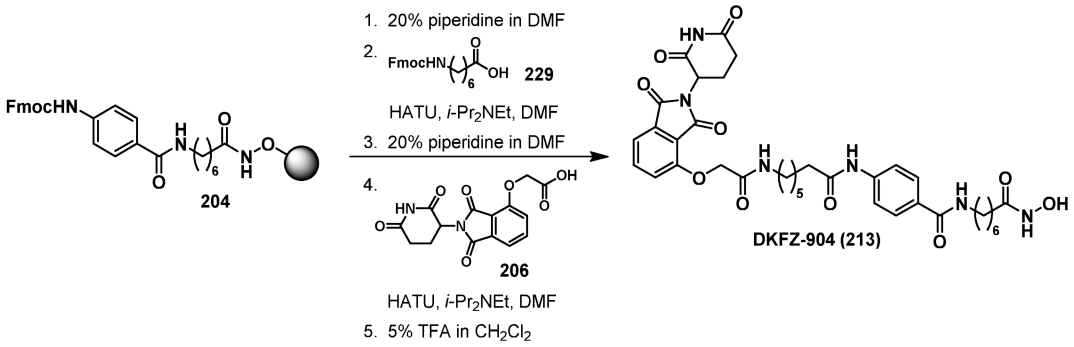


**4-(7-(2-((2-(2,6-Dioxopiperidin-3-yl)-1,3-dioxoisoindolin-4-yl)oxy)acetamido) heptanamido)-*N*-(7-(hydroxyamino)-7-oxoheptyl)benzamide (DFKZ-904, 213):** The title compound was prepared from resin **204** (0.232 g, 0.182 mmol loading, 1.0 equiv), acid **229** (0.178 g, 0.484 mmol, 2.7 equiv) and CRBN ligand **206** (0.107 g, 0.322 mmol, 1.8 equiv) according to General Procedure E, and purified by HPLC Acidic Method (gradient: 10 → 40% B in 5 min, then 40 → 52% B in 8 min) to provide **DKFZ-904** as a white fluffy solid (50.9 mg, 70.6 nmol, 39% based on PhtNOH resin **203**).

**TLC** $R_f$ 0.74 (20% MeOH in $CH_2Cl_2$)

**$^1$H NMR** (600 MHz, DMSO-$d_6$) δ 11.14 (s, 1H), 10.36 (s, 1H), 10.10 (s, 1H), 8.67 (br s, 1H*), 8.32 (t, *J* = 5.7 Hz, 1H), 7.96 (t, *J* = 5.8 Hz, 1H), 7.81 (dd, *J* = 8.5, 7.3 Hz, 1H), 7.77 (d, *J* = 8.6 Hz, 2H), 7.64 (d, *J* = 8.4 Hz, 2H), 7.49 (d, *J* = 7.3 Hz, 1H), 7.38 (d, *J* = 8.5 Hz, 1H), 5.13 (dd, *J* = 12.9, 5.5 Hz, 1H), 4.77 (s, 2H), 3.21 (app q, *J* = 6.6 Hz, 2H), 3.14 (app q, *J* = 6.7 Hz, 2H), 2.89 (ddd, *J* = 17.0, 13.8, 5.4 Hz, 1H), 2.64 – 2.51 (m, 2H), 2.31 (t, *J* = 7.4 Hz, 2H), 2.07 – 2.01 (m, 1H), 1.93 (t, *J* = 7.4 Hz, 2H), 1.57 (p, *J* = 7.2 Hz, 2H), 1.49 (app q, *J* = 7.1 Hz, 4H), 1.46 – 1.41 (m, 2H), 1.33 – 1.24 (m, 8H) ppm; *: partially exchanged with adventitious water.

**$^{13}$C NMR** (151 MHz, DMSO-$d_6$) δ 172.88, 171.69, 169.99, 169.18, 166.81, 166.70, 165.61, 165.58, 155.09, 141.79, 136.99, 133.08, 128.95, 127.99, 120.38, 118.13, 116.84, 116.09, 67.63, 48.84, 39.16, 38.34, 36.45, 32.29, 31.00, 29.16, 28.93, 28.42 (2 × $CH_2$ overlapped), 26.31, 26.16, 25.17, 25.02, 22.05 ppm

**HR-MS** (*m/z*): $[M+Na]^+$ calcd for $C_{36}H_{44}N_6NaO_{10}^+$: 743.3011; found: 743.3012

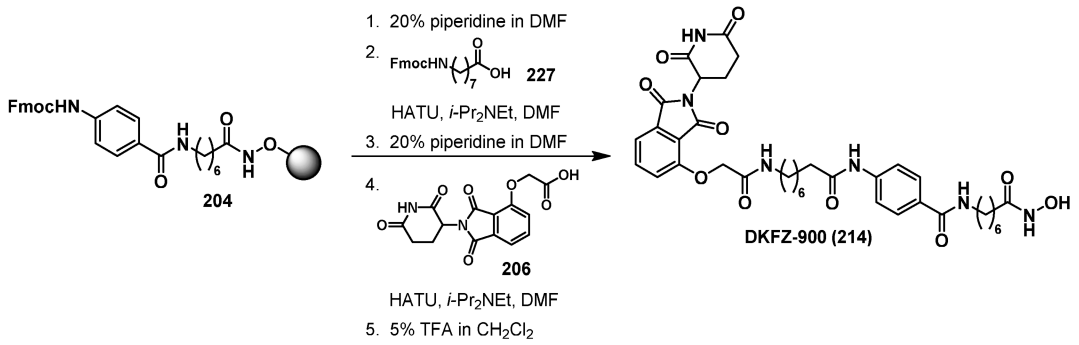


**4-(8-(2-((2-(2,6-Dioxopiperidin-3-yl)-1,3-dioxoisoindolin-4-yl)oxy)acetamido)octanamido)-*N*-(7-(hydroxyamino)-7-oxoheptyl)benzamide (DFKZ-900, 214):** The title compound was prepared from resin **204** (0.235 g, 0.185 mmol loading, 1.0 equiv), acid **227** (0.187 g, 0.490 mmol, 2.7 equiv) and CRBN ligand **206** (0.109 g, 0.328 mmol, 1.8 equiv) according to General Procedure E, and purified by HPLC Acidic Method (gradient: 10 → 40% B in 5 min, then 40 → 52% B in 8 min) to provide **DKFZ-900** as a white fluffy solid (24.3 mg, 33.1 nmol, 18% based on PhtNOH resin **203**).

**TLC** $R_f$ 0.56 (20% MeOH in $CH_2Cl_2$)

**$^1$H NMR** (600 MHz, DMSO-$d_6$) δ 11.13 (s, 1H), 10.34 (s, 1H), 10.07 (s, 1H), 8.66 (br s, 1H*), 8.30 (t, *J* = 5.6 Hz, 1H), 7.95 (t, *J* = 5.7 Hz, 1H), 7.80 (app t, 1H), 7.77 (d, *J* = 8.5 Hz, 2H), 7.64 (d, *J* = 8.5 Hz, 2H), 7.48 (d, *J* = 7.2 Hz, 1H), 7.38 (d, *J* = 8.5 Hz, 1H), 5.12 (dd, *J* = 12.9, 5.4 Hz, 1H), 4.77 (s, 2H), 3.21 (app q, *J* = 6.7 Hz, 2H), 3.14 (app q, *J* = 6.8 Hz, 2H), 2.90 (ddd, *J* = 17.0, 13.9, 5.5 Hz, 1H), 2.62 – 2.51 (m, 2H), 2.31 (t, *J* = 7.4 Hz, 2H), 2.08 – 2.00 (m, 1H), 1.93 (t, *J* = 7.4 Hz, 2H), 1.57 (p, *J* = 7.2 Hz, 2H), 1.49 (p, *J* = 7.1 Hz, 4H), 1.42 (p, *J* = 6.9 Hz, 2H), 1.32 – 1.23 (m, 10H) ppm; *: partially exchanged with adventitious water.

**$^{13}$C NMR** (151 MHz, DMSO-$d_6$) δ 172.83, 171.65, 169.93, 169.13, 166.77, 166.66, 165.57, 165.54, 155.08, 141.76, 136.94, 133.06, 128.94, 127.95, 120.37, 118.09, 116.83, 116.06, 67.63, 48.82, 39.15*, 38.33, 36.45, 32.26, 30.97, 29.13, 29.01, 28.65, 28.51, 28.39, 26.27, 26.21, 25.13, 24.98, 22.02 ppm; *: overlapped with DMSO peak, chemical shift obtained from HSQC edit.

**HR-MS** (*m/z*): $[M+Na]^+$ calcd for $C_{37}H_{46}N_6NaO_{10}^+$: 757.3168; found: 757.3169

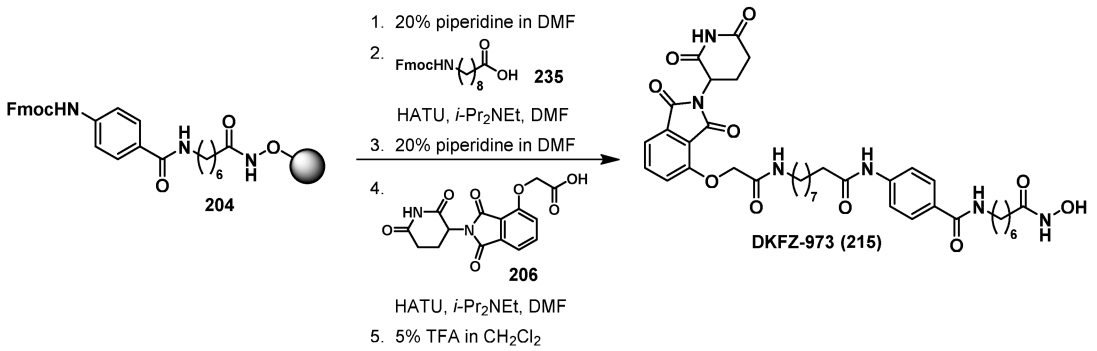


**4-(9-(2-((2-(2,6-Dioxopiperidin-3-yl)-1,3-dioxoisoindolin-4-yl)oxy)acetamido) nonanamido)-*N*-(7-(hydroxyamino)-7-oxoheptyl)benzamide (DFKZ-973, 215):** The title compound was prepared from resin **204** (0.200 g, 0.178 mmol loading, 1.0 equiv), acid **235** (0.211 g, 0.535 mmol, 3.0 equiv) and CRBN ligand **206** (0.077 g, 0.230 mmol, 2.0 equiv) according to General Procedure E, and purified by HPLC Acidic Method (gradient: 10 → 35 % B in 3 min, then 35 → 43% B in 8 min) to provide **DKFZ-973** as a white fluffy solid (6.6 mg, 8.8 nmol, 5% based on PhtNOH resin **203**).

**$^1$H NMR** (600 MHz, DMSO-$d_6$) δ 11.13 (s, 1H*), 10.34 (s, 1H*), 10.07 (s, 1H), 8.67 (s, 1H*), 8.30 (t, *J* = 5.6 Hz, 1H), 7.94 (t, *J* = 5.8 Hz, 1H), 7.81 (dd, *J* = 8.5, 7.3 Hz, 1H), 7.79 – 7.73 (m, 2H), 7.64 (d, *J* = 8.6 Hz, 2H), 7.49 (d, *J* = 7.3 Hz, 1H), 7.38 (d, *J* = 8.6 Hz, 1H), 5.12 (dd, *J* = 12.9, 5.4 Hz, 1H), 4.77 (s, 2H), 3.21 (app q, *J* = 6.7 Hz, 2H), 3.13 (app q, *J* = 6.5 Hz, 2H), 2.94 – 2.86 (m, 1H), 2.64 – 2.57 (m, 1H), 2.57 – 2.52 (m, 1H), 2.31 (t, *J* = 7.4 Hz, 2H), 2.07 – 2.01 (m, 1H), 1.93 (t, *J* = 7.4 Hz, 2H), 1.57 (p, *J* = 7.2 Hz, 2H), 1.48 (p, *J* = 7.0 Hz, 4H), 1.43 (p, *J* = 7.0 Hz, 2H), 1.32 – 1.21 (m, 12H) ppm; *: partially exchanged with adventitious water.

**$^{13}$C NMR** (151 MHz, DMSO-$d_6$) δ 172.82, 171.65, 169.93, 169.11, 166.77, 166.64, 165.55, 165.54, 155.07, 141.75, 136.95, 133.05, 128.92, 127.95, 120.37, 118.08, 116.82, 116.06, 67.62, 48.81, 40.06, 38.33, 36.46, 32.25, 30.97, 29.13, 29.01, 28.80, 28.65, 28.62, 28.39, 26.30, 26.27, 25.12, 25.02, 22.01 ppm

**HR-MS** (*m/z*): $[M+Na]^+$ calcd for $C_{38}H_{48}N_6NaO_{10}^+$: 771.3324; found: 771.3332

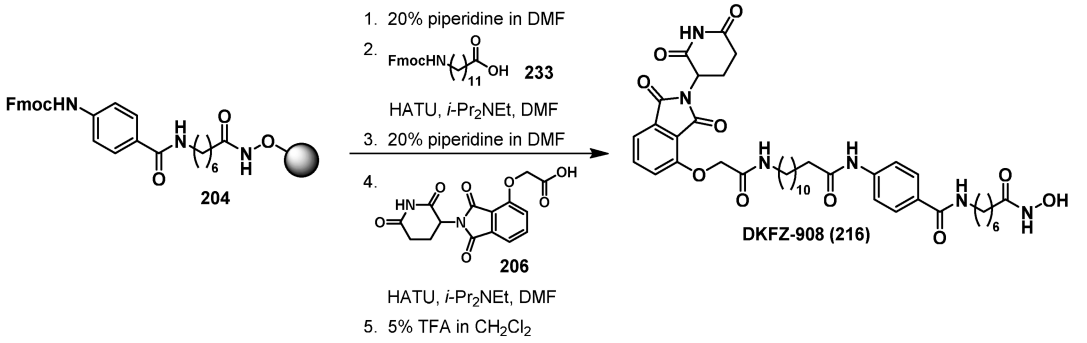


**4-(12-(2-((2-(2,6-Dioxopiperidin-3-yl)-1,3-dioxoisoindolin-4-yl)oxy)acetamido)dodecanamido)-*N*-(7-(hydroxyamino)-7-oxoheptyl)benzamide (DFKZ-908, 216):** The title compound was prepared from resin **204** (0.232 g, 0.134 mmol

loading, 1.0 equiv), acid **233** (0.175 g, 0.401 mmol, 3.0 equiv) and CRBN ligand **206** (0.118 g, 0.356 mmol, 2.0 equiv) according to General Procedure E, and purified by HPLC Acidic Method (gradient: 10 → 48 % B in 5 min, then 48 → 56% B in 8 min) to provide **DKFZ-908** as a white fluffy solid (40.2 mg, 50.8 nmol, 29% based on PhtNOH resin **203**).

**TLC** $R_f$ 0.36 (15% MeOH in $CH_2Cl_2$)

**$^1$H NMR** (600 MHz, DMSO-$d_6$) δ 11.13 (s, 1H), 10.34 (s, 1H), 10.06 (s, 1H), 8.67 (br s, 1H*), 8.30 (t, *J* = 5.6 Hz, 1H), 7.93 (t, *J* = 5.8 Hz, 1H), 7.80 (app t, *J* = 7.9 Hz, 1H), 7.77 (d, *J* = 8.3 Hz, 2H), 7.64 (d, *J* = 8.3 Hz, 2H), 7.49 (d, *J* = 7.2 Hz, 1H), 7.39 (d, *J* = 8.5 Hz, 1H), 5.12 (dd, *J* = 12.9, 5.4 Hz, 1H), 4.77 (s, 2H), 3.21 (app q, *J* = 6.7 Hz, 2H), 3.13 (app q, *J* = 7.1 Hz, 2H), 2.90 (ddd, *J* = 16.8, 13.9, 5.5 Hz, 1H), 2.66 – 2.51 (m, 2H), 2.31 (t, *J* = 7.4 Hz, 2H), 2.08 – 1.99 (m, 1H), 1.94 (t, *J* = 7.4 Hz, 2H), 1.57 (p, *J* = 7.1 Hz, 2H), 1.48 (p, *J* = 7.2 Hz, 4H), 1.42 (p, *J* = 6.9 Hz, 2H), 1.31 – 1.19 (m, 18H) ppm; *: partially exchanged with adventitious water.

**$^{13}$C NMR** (151 MHz, DMSO-$d_6$) δ 172.81, 171.66, 169.91, 169.15, 166.77, 166.65, 165.58, 165.55, 155.07, 141.77, 136.94, 133.06, 128.93, 127.95, 120.39, 118.09, 116.84, 116.08, 67.66, 48.84, 39.13, 38.36, 36.49, 32.27, 30.99, 29.14, 29.02 (3 × $CH_2$ overlapped), 28.97, 28.86, 28.76, 28.71, 28.40, 26.34, 26.28, 25.14, 25.05, 22.03 ppm

**HR-MS** (*m/z*): $[M+Na]^+$ calcd for $C_{41}H_{54}N_6NaO_{10}^+$: 813.3794; found: 813.3794

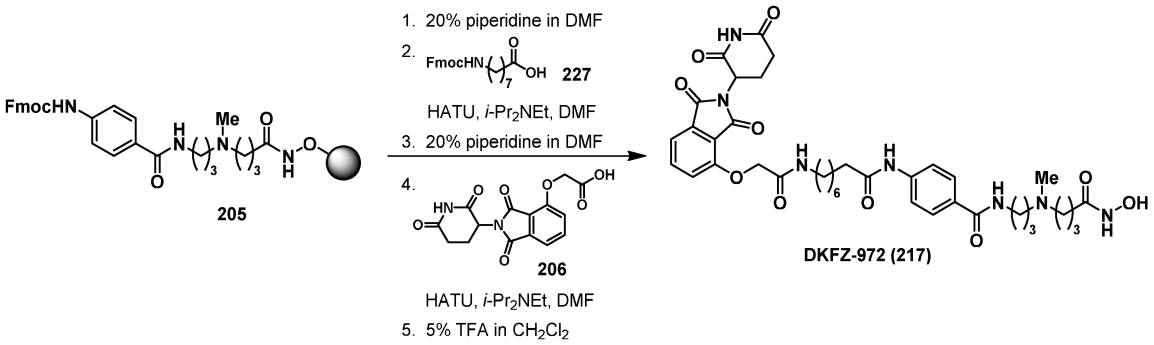


**4-(8-(2-((2-(2,6-Dioxopiperidin-3-yl)-1,3-dioxoisoindolin-4-yl)oxy)acetamido) octanamido)-*N*-(3-((4-(hydroxyamino)-4-oxobutyl)(methyl)amino)propyl)benzamide (DFKZ-972, 217):** The title compound was prepared from resin **205** (0.268 g, 0.123 mmol loading, 1.0 equiv), acid **227** (0.140 g, 0.368 mmol, 3.0 equiv) and CRBN ligand **206** (0.081 g, 0.245 mmol, 2.0 equiv) according to General Procedure E, and purified by RP-MPLC (43 g C18 Teledyne Isco #69-2203-413, gradient: 5% MeCN (B) in $H_2O$ (A) for 3 CV, 5 → 22% B in 4 CV, 22% B for CV, then 22 → 55% B in 8 CV) and HPLC Acidic Method (gradient: 10 → 20% B in 5 min, then 20 → 55% B in 8 min) to provide the TFA salt of **DKFZ-972** as an orange amorphous solid (35.8 mg, 40.8 nmol, 11% based on PhtNOH resin **203**).

**TLC** $R_f$ 0.18 (40% MeOH and 0.5% $NH_4OH$ in $CH_2Cl_2$)

**$^1$H NMR** (600 MHz, DMSO-$d_6$) δ 11.13 (s, 1H), 10.53* (s, 1H), 10.12 (s, 1H), 9.52 (br s, 1H*), 8.82 (s, 1H*), 8.50 (t, *J* = 5.8 Hz, 1H), 7.95 (t, *J* = 5.8 Hz, 1H), 7.83 – 7.77 (m, 3H), 7.69 – 7.64 (m, 2H),

7.48 (d, *J* = 7.3 Hz, 1H), 7.38 (d, *J* = 8.5 Hz, 1H), 5.12 (dd, *J* = 12.9, 5.5 Hz, 1H), 4.77 (s, 2H), 3.31 (app q, *J* = 6.4 Hz, 2H), 3.14 (app q, *J* = 6.5 Hz, 2H), 3.13 – 2.98 (m, 4H), 2.90 (ddd, *J* = 17.0, 13.9, 5.4 Hz, 1H), 2.75 (s, 3H), 2.63 – 2.52 (m, 2H), 2.32 (t, *J* = 7.4 Hz, 2H), 2.13 – 1.97 (m, 3H), 1.91 – 1.80 (m, 4H), 1.57 (p, *J* = 7.2 Hz, 2H), 1.43 (p, *J* = 7.0 Hz, 2H), 1.31 – 1.22 (m, 6H) ppm; *: partially exchanged with adventitious water.

**$^{19}$F NMR** (376 MHz, DMSO-$d_6$) δ -73.49 ppm

**$^{13}$C NMR** (151 MHz, DMSO-$d_6$) δ 172.83, 171.72, 169.92, 168.01, 166.76, 166.65, 166.08, 165.54, 158.03 (q, *J* = 30.9 Hz), 155.08, 142.03, 136.94, 133.05, 128.44, 128.05, 120.37, 118.13, 116.82, 116.33 (q, *J* = 300.7 Hz), 116.05, 67.63, 54.78, 53.23, 48.82, 40.06, 38.32, 36.44, 36.36, 30.97, 29.04, 29.01, 28.64, 28.51, 26.21, 24.96, 24.26, 22.01, 19.63 ppm

**HR-MS** (*m/z*): $[M+H]^+$ calcd for $C_{38}H_{50}N_7O_{10}^+$: 764.3614; found: 764.3621

# 6 References


(1) Steimbach, R. R.; Herbst-Gervasoni, C. J.; Lechner, S.; Stewart, T. M.; Klinke, G.; Ridinger, J.; Géraldy, M. N. E.; Tihanyi, G.; Foley, J. R.; Uhrig, U.*; et al.* Aza-SAHA Derivatives Are Selective Histone Deacetylase 10 Chemical Probes That Inhibit Polyamine Deacetylation and Phenocopy HDAC10 Knockout. *J. Am. Chem. Soc.* **2022**, *144*, 18861–18875.

(2) Taunton, J.; Hassig, C. A.; Schreiber, S. L. A mammalian histone deacetylase related to the yeast transcriptional regulator Rpd3p. *Science* **1996**, *272*, 408–411.

(3) Gregoretti, I. V.; Lee, Y.-M.; Goodson, H. V. Molecular evolution of the histone deacetylase family: functional implications of phylogenetic analysis. *J. Mol. Biol.* **2004**, *338*, 17–31.

(4) Smith, B. C.; Hallows, W. C.; Denu, J. M. Mechanisms and molecular probes of sirtuins. *Chem. Biol.* **2008**, *15*, 1002–1013.

(5) Nakagawa, T.; Guarente, L. Sirtuins at a glance. *J. Cell Sci.* **2011**, *124*, 833–838.

(6) Bolden, J. E.; Peart, M. J.; Johnstone, R. W. Anticancer activities of histone deacetylase inhibitors. *Nature reviews. Drug discovery* **2006**, *5*, 769–784.

(7) Ho, T. C. S.; Chan, A. H. Y.; Ganesan, A. Thirty Years of HDAC Inhibitors: 2020 Insight and Hindsight. *J. Med. Chem.* **2020**, *63*, 12460–12484.

(8) Kelly, R. D. W.; Cowley, S. M. The physiological roles of histone deacetylase (HDAC) 1 and 2: complex co-stars with multiple leading parts. *Biochem. Soc. Trans.* **2013**, *41*, 741–749.

(9) Emmett, M. J.; Lazar, M. A. Integrative regulation of physiology by histone deacetylase 3. *Nat. Rev. Mol. Cell Biol.* **2019**, *20*, 102–115.

(10) Haberland, M.; Montgomery, R. L.; Olson, E. N. The many roles of histone deacetylases in development and physiology: implications for disease and therapy. *Nat. Rev. Genet.* **2009**, *10*, 32–42.

(11) Chakrabarti, A.; Oehme, I.; Witt, O.; Oliveira, G.; Sippl, W.; Romier, C.; Pierce, R. J.; Jung, M. HDAC8: a multifaceted target for therapeutic interventions. *Trends Pharmacol. Sci.* **2015**, *36*, 481–492.

(12) Aramsangtienchai, P.; Spiegelman, N. A.; He, B.; Miller, S. P.; Dai, L.; Zhao, Y.; Lin, H. HDAC8 Catalyzes the Hydrolysis of Long Chain Fatty Acyl Lysine. *ACS Chem. Biol.* **2016**, *11*, 2685–2692.

(13) Kutil, Z.; Novakova, Z.; Meleshin, M.; Mikesova, J.; Schutkowski, M.; Barinka, C. Histone Deacetylase 11 Is a Fatty-Acid Deacylase. *ACS Chem. Biol.* **2018**, *13*, 685–693.

(14) Moreno-Yruela, C.; Galleano, I.; Madsen, A. S.; Olsen, C. A. Histone Deacetylase 11 Is an ε-N-Myristoyllysine Hydrolase. *Cell chemical biology* **2018**, *25*, 849-856.e8.

(15) Lahm, A.; Paolini, C.; Pallaoro, M.; Nardi, M. C.; Jones, P.; Neddermann, P.; Sambucini, S.; Bottomley, M. J.; Lo Surdo, P.; Carfí, A.*; et al.* Unraveling the hidden catalytic activity of vertebrate class IIa histone deacetylases. *Proc. Natl. Acad. Sci. U.S.A.* **2007**, *104*, 17335–17340.

(16) Luo, L.; Martin, S. C.; Parkington, J.; Cadena, S. M.; Zhu, J.; Ibebunjo, C.; Summermatter, S.; Londraville, N.; Patora-Komisarska, K.; Widler, L.*; et al.* HDAC4 Controls Muscle Homeostasis through Deacetylation of Myosin Heavy Chain, PGC-1α, and Hsc70. *Cell Rep.* **2019**, *29*, 749-763.e12.

(17) Hubbert, C.; Guardiola, A.; Shao, R.; Kawaguchi, Y.; Ito, A.; Nixon, A.; Yoshida, M.; Wang, X.-F.; Yao, T.-P. HDAC6 is a microtubule-associated deacetylase. *Nature* **2002**, *417*, 455–458.

(18) Hai, Y.; Christianson, D. W. Histone deacetylase 6 structure and molecular basis of catalysis and inhibition. *Nat. Chem. Biol.* **2016**, *12*, 741–747.
(19) Seto, E.; Yoshida, M. Erasers of histone acetylation: the histone deacetylase enzymes. *Cold Spring Harb. Perspect. Biol.* **2014**, *6*, a018713.
(20) Kornberg, R. D.; Lorch, Y. Twenty-five years of the nucleosome, fundamental particle of the eukaryote chromosome. *Cell* **1999**, *98*, 285–294.
(21) Mariño-Ramírez, L.; Kann, M. G.; Shoemaker, B. A.; Landsman, D. Histone structure and nucleosome stability. *Expert Rev. Proteomics* **2005**, *2*, 719–729.
(22) Kelly, W. K.; O'Connor, O. A.; Marks, P. A. Histone deacetylase inhibitors: from target to clinical trials. *Expert opinion on investigational drugs* **2002**, *11*, 1695–1713.
(23) Guha, M. HDAC inhibitors still need a home run, despite recent approval. *Nature reviews. Drug discovery* **2015**, *14*, 225–226.
(24) Witt, O.; Deubzer, H. E.; Milde, T.; Oehme, I. HDAC family: What are the cancer relevant targets? *Cancer letters* **2009**, *277*, 8–21.
(25) Roche, J.; Bertrand, P. Inside HDACs with more selective HDAC inhibitors. *Eur. J. Med. Chem.* **2016**, *121*, 451–483.
(26) Varga, J. K.; Diffley, K.; Welker Leng, K. R.; Fierke, C. A.; Schueler-Furman, O. Structure-based prediction of HDAC6 substrates validated by enzymatic assay reveals determinants of promiscuity and detects new potential substrates. *Sci Rep* **2022**, *12*, 1788.
(27) Herbst-Gervasoni, C. J.; Christianson, D. W. X-ray Crystallographic Snapshots of Substrate Binding in the Active Site of Histone Deacetylase 10. *Biochemistry* **2021**, *60*, 303–313.
(28) Osko, J. D.; Christianson, D. W. Structural Basis of Catalysis and Inhibition of HDAC6 CD1, the Enigmatic Catalytic Domain of Histone Deacetylase 6. *Biochemistry* **2019**, *58*, 4912–4924.
(29) Kaluza, D.; Kroll, J.; Gesierich, S.; Yao, T.-P.; Boon, R. A.; Hergenreider, E.; Tjwa, M.; Rössig, L.; Seto, E.; Augustin, H. G.*; et al.* Class IIb HDAC6 regulates endothelial cell migration and angiogenesis by deacetylation of cortactin. *EMBO J.* **2011**, *30*, 4142–4156.
(30) Yan, J. Interplay between HDAC6 and its interacting partners: essential roles in the aggresome-autophagy pathway and neurodegenerative diseases. *DNA Cell Biol.* **2014**, *33*, 567–580.
(31) Li, T.; Zhang, C.; Hassan, S.; Liu, X.; Song, F.; Chen, K.; Zhang, W.; Yang, J. Histone deacetylase 6 in cancer. *J. Hematol. Oncol.* **2018**, *11*, 111.
(32) Bali, P.; Pranpat, M.; Bradner, J.; Balasis, M.; Fiskus, W.; Guo, F.; Rocha, K.; Kumaraswamy, S.; Boyapalle, S.; Atadja, P.*; et al.* Inhibition of histone deacetylase 6 acetylates and disrupts the chaperone function of heat shock protein 90: a novel basis for antileukemia activity of histone deacetylase inhibitors. *J. Biol. Chem.* **2005**, *280*, 26729–26734.
(33) Kovacs, J. J.; Murphy, P. J. M.; Gaillard, S.; Zhao, X.; Wu, J.-T.; Nicchitta, C. V.; Yoshida, M.; Toft, D. O.; Pratt, W. B.; Yao, T.-P. HDAC6 regulates Hsp90 acetylation and chaperone-dependent activation of glucocorticoid receptor. *Mol. Cell* **2005**, *18*, 601–607.
(34) Cohen, T. J.; Guo, J. L.; Hurtado, D. E.; Kwong, L. K.; Mills, I. P.; Trojanowski, J. Q.; Lee, V. M. Y. The acetylation of tau inhibits its function and promotes pathological tau aggregation. *Nat. Commun.* **2011**, *2*, 252.
(35) Noack, M.; Leyk, J.; Richter-Landsberg, C. HDAC6 inhibition results in tau acetylation and modulates tau phosphorylation and degradation in oligodendrocytes. *Glia* **2014**, *62*, 535–547.

(36) Zhang, Y.; Kwon, S.; Yamaguchi, T.; Cubizolles, F.; Rousseaux, S.; Kneissel, M.; Cao, C.; Li, N.; Cheng, H.-L.; Chua, K.*; et al.* Mice lacking histone deacetylase 6 have hyperacetylated tubulin but are viable and develop normally. *Mol. Cell. Biol.* **2008**, *28*, 1688–1701.

(37) Fischer, D. D.; Cai, R.; Bhatia, U.; Asselbergs, F. A.; Song, C. Z.; Terry, R.; Trogani, N.; Widmer, R.; Atadja, P.; Cohen, D. Isolation and characterization of a novel class II histone deacetylase, HDAC10. *J. Biol. Chem.* **2002**, *277*, 6656–6666.

(38) Guardiola, A. R.; Yao, T. P. Molecular cloning and characterization of a novel histone deacetylase HDAC10. *J. Biol. Chem.* **2002**, *277*, 3350–3356.

(39) Kao, H. Y.; Lee, C. H.; Komarov, A.; Han, C. C.; Evans, R. M. Isolation and characterization of mammalian HDAC10, a novel histone deacetylase. *J. Biol. Chem.* **2002**, *277*, 187–193.

(40) Tong, J. J.; Liu, J. H.; Bertos, N. R.; Yang, X. J. Identification of HDAC10, a novel class II human histone deacetylase containing a leucine-rich domain. *Nucleic Acids Res.* **2002**, *30*, 1114–1123.

(41) Hai, Y.; Shinsky, S. A.; Porter, N. J.; Christianson, D. W. Histone deacetylase 10 structure and molecular function as a polyamine deacetylase. *Nat. Commun.* **2017**, *8*, 15368.

(42) Bradner, J. E.; West, N.; Grachan, M. L.; Greenberg, E. F.; Haggarty, S. J.; Warnow, T.; Mazitschek, R. Chemical phylogenetics of histone deacetylases. *Nat. Chem. Biol.* **2010**, *6*, 238–243.

(43) Géraldy, M.; Morgen, M.; Sehr, P.; Steimbach, R. R.; Moi, D.; Ridinger, J.; Oehme, I.; Witt, O.; Malz, M.; Nogueira, M. S.*; et al.* Selective Inhibition of Histone Deacetylase 10: Hydrogen Bonding to the Gatekeeper Residue is Implicated. *J. Med. Chem.* **2019**, *62*, 4426–4443.

(44) Blankenship, J. Deacetylation of N8-acetylspermidine by subcellular fractions of rat tissue. *Archives of Biochemistry and Biophysics* **1978**, *189*, 20–27.

(45) Libby, P. R. Properties of an acetylspermidine deacetylase from rat liver. *Archives of Biochemistry and Biophysics* **1978**, *188*, 360–363.

(46) Marchant, P.; Manneh, V. A.; Blankenship, J. N1-Acetylspermidine is not a substrate for N-acetylspermidine deacetylase. *Biochim. Biophys. Acta Gen. Subj.* **1986**, *881*, 297–299.

(47) Marchant, P.; Dredar, S.; Manneh, V.; Alshabanah, O.; Matthews, H.; Fries, D.; Blankenship, J. A selective inhibitor of N8-acetylspermidine deacetylation in mice and hela cells without effects on histone deacetylation. *Arch. Biochem. Biophys.* **1989**, *273*, 128–136.

(48) Herbst-Gervasoni, C. J.; Steimbach, R. R.; Morgen, M.; Miller, A. K.; Christianson, D. W. Structural Basis for the Selective Inhibition of HDAC10, the Cytosolic Polyamine Deacetylase. *ACS Chem. Biol.* **2020**, *15*, 2154–2163.

(49) PAULING, L. Nature of forces between large molecules of biological interest. *Nature* **1948**, *161*, 707–709.

(50) Oehme, I.; Linke, J.-P.; Böck, B. C.; Milde, T.; Lodrini, M.; Hartenstein, B.; Wiegand, I.; Eckert, C.; Roth, W.; Kool, M.*; et al.* Histone deacetylase 10 promotes autophagy-mediated cell survival. *Proc. Nat. Acad. Sci.* **2013**, *110*, E2592-2601.

(51) Shinsky, S. A.; Christianson, D. W. Polyamine Deacetylase Structure and Catalysis: Prokaryotic Acetylpolyamine Amidohydrolase and Eukaryotic HDAC10. *Biochemistry* **2018**, *57*, 3105–3114.

(52) Ridinger, J.; Koeneke, E.; Kolbinger, F. R.; Koerholz, K.; Mahboobi, S.; Hellweg, L.; Gunkel, N.; Miller, A. K.; Peterziel, H.; Schmezer, P.*; et al.* Dual role of HDAC10 in lysosomal exocytosis and DNA repair promotes neuroblastoma chemoresistance. *Sci. Rep.* **2018**, *8*, 10039.

(53) Wang, Z.; Fries, D.; Blankenship, J. Effect of N8-acetylspermidine deacetylase inhibition on the growth of L1210 cells. *Biochem. Pharmacol.* **1999**, *57*, 1095–1103.
(54) Kotian, S.; Liyanarachchi, S.; Zelent, A.; Parvin, J. D. Histone Deacetylases 9 and 10 Are Required for Homologous Recombination. *J. Biol. Chem.* **2011**, *286*, 7722–7726.
(55) Radhakrishnan, R.; Li, Y.; Xiang, S.; Yuan, F.; Yuan, Z.; Telles, E.; Fang, J.; Coppola, D.; Shibata, D.; Lane, W. S.*; et al.* Histone Deacetylase 10 Regulates DNA Mismatch Repair and May Involve the Deacetylation of MutS Homolog 2. *J. Biol. Chem.* **2015**, *290*, 22795–22804.
(56) Duan, B.; Ye, D.; Zhu, S.; Jia, W.; Lu, C.; Wang, G.; Guo, X.; Yu, Y.; Wu, C.; Kang, J. HDAC10 promotes angiogenesis in endothelial cells through the PTPN22/ERK axis. *Oncotarget* **2017**, *8*, 61338–61349.
(57) Dahiya, S.; Beier, U. H.; Wang, L.; Han, R.; Jiao, J.; Akimova, T.; Angelin, A.; Wallace, D. C.; Hancock, W. W. HDAC10 deletion promotes Foxp3+ T-regulatory cell function. *Sci. Rep.* **2020**, *10*, 424.
(58) Islam, M. M.; Banerjee, T.; Packard, C. Z.; Kotian, S.; Selvendiran, K.; Cohn, D. E.; Parvin, J. D. HDAC10 as a potential therapeutic target in ovarian cancer. *Gynecol. Oncol.* **2017**, *144*, 613–620.
(59) Cheng, F.; Zheng, B.; Wang, J.; Zhao, G.; Yao, Z.; Niu, Z.; He, W. Histone deacetylase 10, a potential epigenetic target for therapy. *Biosci. Rep.* [Online early access]. DOI: 10.1042/BSR20210462. Published Online: May. 17, 2021.
(60) Tao, X.; Yan, Y.; Lu, L.; Chen, B. HDAC10 expression is associated with DNA mismatch repair gene and is a predictor of good prognosis in colon carcinoma. *Oncol. Lett.* **2017**, *14*, 4923–4929.
(61) Fan, W.; Huang, J.; Xiao, H. Histone deacetylase 10 suppresses proliferation and invasion by inhibiting the phosphorylation of β-catenin and serves as an independent prognostic factor for human clear cell renal cell carcinoma. *Int. J. Clin. Exp. Med.* **2015**, *8*, 3734–3742.
(62) Jin, Z.; Jiang, W.; Jiao, F.; Guo, Z.; Hu, H.; Wang, L.; Wang, L. Decreased expression of histone deacetylase 10 predicts poor prognosis of gastric cancer patients. *Int. J. Clin. Exp. Pathol.* **2014**, *7*, 5872–5879.
(63) Osada, H.; Tatematsu, Y.; Saito, H.; Yatabe, Y.; Mitsudomi, T.; Takahashi, T. Reduced expression of class II histone deacetylase genes is associated with poor prognosis in lung cancer patients. *Int. J. Cancer* **2004**, *112*, 26–32.
(64) Liao, W.; Sun, J.; Liu, W.; Li, W.; Jia, J.; Ou, F.; Su, K.; Zheng, Y.; Zhang, Z.; Sun, Y. HDAC10 upregulation contributes to interleukin 1β-mediated inflammatory activation of synovium-derived mesenchymal stem cells in temporomandibular joint. *J. Cell. Physiol.* **2019**, *234*, 12646–12662.
(65) Stewart, T. M.; Foley, J. R.; Holbert, C. E.; Klinke, G.; Poschet, G.; Steimbach, R. R.; Miller, A. K.; Casero, R. A. Histone deacetylase-10 liberates spermidine to support polyamine homeostasis and tumor cell growth. *J. Biol. Chem.* **2022**, *298*, 102407.
(66) Casero, R. A.; Murray Stewart, T.; Pegg, A. E. Polyamine metabolism and cancer: treatments, challenges and opportunities. *Nat. Rev. Cancer* **2018**, *18*, 681–695.
(67) Tabor, C. W.; Tabor, H. Polyamines. *Annu. Rev. Biochem.* **1984**, *53*, 749–790.
(68) Casero, R. A.; Marton, L. J. Targeting polyamine metabolism and function in cancer and other hyperproliferative diseases. *Nature reviews. Drug discovery* **2007**, *6*, 373–390.

(69) Michael, A. J. Polyamines in Eukaryotes, Bacteria, and Archaea. *J. Biol. Chem.* **2016**, *291*, 14896–14903.

(70) Kusano, T.; Berberich, T.; Tateda, C.; Takahashi, Y. Polyamines: essential factors for growth and survival. *Planta* **2008**, *228*, 367–381.

(71) Wallace, H. M.; Fraser, A. V.; Hughes, A. A perspective of polyamine metabolism. *Biochem. J.* **2003**, *376*, 1–14.

(72) Childs, A. C.; Mehta, D. J.; Gerner, E. W. Polyamine-dependent gene expression. *Cell. Mol. Life Sci.* **2003**, *60*, 1394–1406.

(73) Thomas, T. J.; Thomas, T. Collapse of DNA in packaging and cellular transport. *Int. J. Biol. Macromol.* **2018**, *109*, 36–48.

(74) Iacomino, G.; Picariello, G.; D'Agostino, L. DNA and nuclear aggregates of polyamines. *Biochim. Biophys. Acta* **2012**, *1823*, 1745–1755.

(75) Oguro, A.; Yanagida, A.; Fujieda, Y.; Amano, R.; Otsu, M.; Sakamoto, T.; Kawai, G.; Matsufuji, S. Two stems with different characteristics and an internal loop in an RNA aptamer contribute to spermine-binding. *J. Biochem.* **2017**, *161*, 197–206.

(76) Igarashi, K.; Kashiwagi, K. Polyamines: mysterious modulators of cellular functions. *Biochem. Biophys. Res. Commun.* **2000**, *271*, 559–564.

(77) Seiler, N.; Raul, F. Polyamines and apoptosis. *J. Cell. Mol. Med.* **2005**, *9*, 623–642.

(78) Oredsson, S. M. Polyamine dependence of normal cell-cycle progression. *Biochem. Soc. Trans.* **2003**, *31*, 366–370.

(79) Thomas, T.; Thomas, T. J. Polyamines in cell growth and cell death: molecular mechanisms and therapeutic applications. *Cell. Mol. Life Sci.* **2001**, *58*, 244–258.

(80) Seiler, N. Catabolism of polyamines. *Amino Acids* **2004**, *26*, 217–233.

(81) Coffino, P. Regulation of cellular polyamines by antizyme. *Nat. Rev. Mol. Cell Biol.* **2001**, *2*, 188–194.

(82) Wang, X.; Ying, W.; Dunlap, K. A.; Lin, G.; Satterfield, M. C.; Burghardt, R. C.; Wu, G.; Bazer, F. W. Arginine decarboxylase and agmatinase: an alternative pathway for de novo biosynthesis of polyamines for development of mammalian conceptuses. *Biol. Reprod.* **2014**, *90*, 84.

(83) Horyn, O.; Luhovyy, B.; Lazarow, A.; Daikhin, Y.; Nissim, I.; Yudkoff, M.; Nissim, I. Biosynthesis of agmatine in isolated mitochondria and perfused rat liver: studies with 15N-labelled arginine. *Biochem. J.* **2005**, *388*, 419–425.

(84) Seiler, N. Functions of polyamine acetylation. *Can. J. Physiol. Pharmacol.* **1987**, *65*, 2024–2035.

(85) Pegg, A. E. Spermidine/spermine-N(1)-acetyltransferase: a key metabolic regulator. *Am. J. Physiol. Endocrinol. Metab.* **2008**, *294*, E995-1010.

(86) Casero, R. A.; Pegg, A. E. Spermidine/spermine N1-acetyltransferase--the turning point in polyamine metabolism. *FASEB J.* **1993**, *7*, 653–661.

(87) Casero, R. A.; Pegg, A. E. Polyamine catabolism and disease. *Biochem. J.* **2009**, *421*, 323–338.

(88) Della Ragione, F.; Erwin, B. G.; Pegg, A. E. Studies of the acetyl-CoA-binding site of rat liver spermidine/spermine N1-acetyltransferase. *Biochem. J.* **1983**, *213*, 707–712.

(89) Conway, L. P.; Rendo, V.; Correia, M. S. P.; Bergdahl, I. A.; Sjöblom, T.; Globisch, D. Unexpected Acetylation of Endogenous Aliphatic Amines by Arylamine N-Acetyltransferase NAT2. *Angew. Chem. Int. Ed. Engl.* **2020**, *59*, 14342–14346.

(90) Hiramatsu, K.; Sugimoto, M.; Kamei, S.; Hoshino, M.; Kinoshita, K.; Iwasaki, K.; Kawakita, M. Determination of amounts of polyamines excreted in urine: demonstration of N1,N8-diacetylspermidine and N1,N12-diacetylspermine as components commonly occurring in normal human urine. *J. Biochem.* **1995**, *117*, 107–112.

(91) Blankenship, J.; Walle, T. Acetylation of spermidine and spermine by rat liver and kidney chromatin. *Arch. Biochem. Biophys.* **1977**, *179*, 235–242.

(92) Ortiz, J. G.; Giacobini, E.; Schmidt-Glenewinkel, T. Acetylation of polyamines in mouse brain: subcellular and regional distribution. *J. Neurosci. Res.* **1983**, *9*, 193–201.

(93) Seiler, N.; Al-Therib, M. J. Acetyl-CoA: 1,4-diaminobutane N-acetyltransferase. Occurrence in vertebrate organs and subcellular localization. *Biochim. Biophys. Acta* **1974**, *354*, 206–212.

(94) Seiler, N.; Deckardt, K. Association of putrescine, spermidine, spermine, and GABA with structural elements of brain cells. *Neurochem. Res.* **1976**, *1*, 469–499.

(95) Seiler, N.; Schmidt-Glenewinkel, T.; Sarhan, S. On the Formation of γ-Aminobutyric Acid from Putrescine in Brain. *The Journal of Biochemistry* **1979**, *86*, 277–279.

(96) Seiler, N.; Al-Therib, M. J. Putrescine catabolism in mammalian brain. *Biochem. J.* **1974**, *144*, 29–35.

(97) Burgio, G.; Corona, D. F. V.; Nicotra, C. M. A.; Carruba, G.; Taibi, G. P/CAF-mediated spermidine acetylation regulates histone acetyltransferase activity. *J. Enzyme Inhib. Med. Chem.* **2016**, *31*, 75–82.

(98) Miller-Fleming, L.; Olin-Sandoval, V.; Campbell, K.; Ralser, M. Remaining Mysteries of Molecular Biology: The Role of Polyamines in the Cell. *J. Mol. Biol.* **2015**, *427*, 3389–3406.

(99) Thomas, T. J.; Bloomfield, V. A.; Canellakis, Z. N. Differential effects on the B-to-Z transition of poly(dG-me5dC).poly(dG-me5dC) produced by N1- and N8-acetyl spermidine. *Biopolymers* **1985**, *24*, 725–729.

(100) Morgan, J. E.; Blankenship, J. W.; Matthews, H. R. Association constants for the interaction of double-stranded and single-stranded DNA with spermine, spermidine, putrescine, diaminopropane, N1- and N8-acetylspermidine, and magnesium: determination from analysis of the broadening of thermal denaturation curves. *Arch. Biochem. Biophys.* **1986**, *246*, 225–232.

(101) Saiki, S.; Sasazawa, Y.; Fujimaki, M.; Kamagata, K.; Kaga, N.; Taka, H.; Li, Y.; Souma, S.; Hatano, T.; Imamichi, Y.*; et al.* A metabolic profile of polyamines in parkinson disease: A promising biomarker. *Ann. Neurol.* **2019**, *86*, 251–263.

(102) Nayak, A.; Liu, C.; Mehta, A.; Ko, Y.-A.; Tahhan, A. S.; Dhindsa, D. S.; Uppal, K.; Jones, D. P.; Butler, J.; Morris, A. A.*; et al.* N8-Acetylspermidine: A Polyamine Biomarker in Ischemic Cardiomyopathy With Reduced Ejection Fraction. *J. Am. Heart Assoc.* **2020**, *9*, e016055.

(103) Abela, L.; Simmons, L.; Steindl, K.; Schmitt, B.; Mastrangelo, M.; Joset, P.; Papuc, M.; Sticht, H.; Baumer, A.; Crowther, L. M.*; et al.* N(8)-acetylspermidine as a potential plasma biomarker for Snyder-Robinson syndrome identified by clinical metabolomics. *J. Inherit. Metab. Dis.* **2016**, *39*, 131–137.

(104) Holbert, C. E.; Cullen, M. T.; Casero, R. A.; Stewart, T. M. Polyamines in cancer: integrating organismal metabolism and antitumour immunity. *Nat. Rev. Cancer* **2022**, *22*, 467–480.
(105) Gerner, E. W.; Meyskens, F. L. Polyamines and cancer: old molecules, new understanding. *Nat. Rev. Cancer* **2004**, *4*, 781–792.
(106) McCann, P. P.; Pegg, A. E. Ornithine decarboxylase as an enzyme target for therapy. *Pharmacol. Ther.* **1992**, *54*, 195–215.
(107) Pinto, G.; Shtaif, B.; Phillip, M.; Gat-Yablonski, G. Growth attenuation is associated with histone deacetylase 10-induced autophagy in the liver. *J. Nutr. Biochem.* **2016**, *27*, 171–180.
(108) Eisenberg, T.; Knauer, H.; Schauer, A.; Büttner, S.; Ruckenstuhl, C.; Carmona-Gutierrez, D.; Ring, J.; Schroeder, S.; Magnes, C.; Antonacci, L.*; et al.* Induction of autophagy by spermidine promotes longevity. *Nat. Cell Biol.* **2009**, *11*, 1305–1314.
(109) Richon, V. M.; Emiliani, S.; Verdin, E.; Webb, Y.; Breslow, R.; Rifkind, R. A.; Marks, P. A. A class of hybrid polar inducers of transformed cell differentiation inhibits histone deacetylases. *Proc. Natl. Acad. Sci. U.S.A.* **1998**, *95*, 3003–3007.
(110) Friend, C.; Scher, W.; Holland, J. G.; Sato, T. Hemoglobin synthesis in murine virus-induced leukemic cells in vitro: stimulation of erythroid differentiation by dimethyl sulfoxide. *Proc. Natl. Acad. Sci. U.S.A.* **1971**, *68*, 378–382.
(111) Marks, P. A.; Breslow, R. Dimethyl sulfoxide to vorinostat: development of this histone deacetylase inhibitor as an anticancer drug. *Nat. Biotechnol.* **2007**, *25*, 84–90.
(112) Breslow, R.; Marks, P. A.; Rifkind, R. A.; Jursic, B. NOVEL POTENT INDUCERS OF TERMINAL DIFFERENTIATION AND METHODS OF USE THEREOF. WO1992US08454 19921005, Oct 5, 1992.
(113) Stowell, J. C.; Huot, R. I.; van Voast, L. The synthesis of N-hydroxy-N'-phenyloctanediamide and its inhibitory effect on proliferation of AXC rat prostate cancer cells. *J. Med. Chem.* **1995**, *38*, 1411–1413.
(114) Yoshida, M.; Nomura, S.; Beppu, T. Effects of trichostatins on differentiation of murine erythroleukemia cells. *Cancer Res* **1987**, *47*, 3688–3691.
(115) Yoshida, M.; Kijima, M.; Akita, M.; Beppu, T. Potent and specific inhibition of mammalian histone deacetylase both in vivo and in vitro by trichostatin A. *J. Biol. Chem.* **1990**, *265*, 17174–17179.
(116) Qiu, X.; Zhu, L.; Wang, H.; Tan, Y.; Yang, Z.; Yang, L.; Wan, L. From natural products to HDAC inhibitors: An overview of drug discovery and design strategy. *Bioorg. Med. Chem.* **2021**, *52*, 116510.
(117) Holte, P. ten; van Emelen, K.; Janicot, M.; Fong, P. C.; Bono, J. S. de; Arts, J. HDAC Inhibition in Cancer Therapy: An Increasingly Intriguing Tale of Chemistry, Biology and Clinical Benefit. In *Cancer*; Bradbury, R. H., Ed.; Topics in Medicinal Chemistry; Springer Berlin Heidelberg: Berlin, Heidelberg, 2007; pp 293–331.
(118) Jung, M.; Hoffmann, K.; Brosch, G.; Loidl, P. Analogues of trichosтatin a and trapoxin B as histone deacetylase inhibitors. *Bioorg. Med. Chem. Lett.* **1997**, *7*, 1655–1658.
(119) Web of Science search query: Topic: Histone deacetylase inhibitor? OR HDAC inhibitor? www.webofscience.com (accessed January 10, 2023).
(120) Duvic, M.; Vu, J. Vorinostat: a new oral histone deacetylase inhibitor approved for cutaneous T-cell lymphoma. *Expert opinion on investigational drugs* **2007**, *16*, 1111–1120.

(121) Furumai, R.; Matsuyama, A.; Kobashi, N.; Lee, K.-H.; Nishiyama, M.; Nakajima, H.; Tanaka, A.; Komatsu, Y.; Nishino, N.; Yoshida, M.*; et al.* FK228 (depsipeptide) as a natural prodrug that inhibits class I histone deacetylases. *Cancer Res* **2002**, *62*, 4916–4921.

(122) Finn, P. W.; Loza, E.; Carstensen, E. The Discovery and Development of Belinostat. In *Successful drug discovery*; Fischer, J., Rotella, D. P., Eds.; Wiley-VCH: Weinheim, Germany, 2017; pp 31–57.

(123) Atadja, P.; Perez, L. Discovery and Development of Farydak (NVP-LBH589, Panobinostat) as an Anticancer Drug. In *Successful drug discovery*; Fischer, J., Rotella, D. P., Eds.; Wiley-VCH: Weinheim, Germany, 2017; pp 59–88.

(124) Lu, X.; Ning, Z.; Li, Z.; Cao, H.; Wang, X. Development of chidamide for peripheral T-cell lymphoma, the first orphan drug approved in China. *Intractable Rare Dis. Res.* **2016**, *5*, 185–191.

(125) Shah, R. R. Safety and Tolerability of Histone Deacetylase (HDAC) Inhibitors in Oncology. *Drug Saf.* **2019**, *42*, 235–245.

(126) Melesina, J.; Simoben, C. V.; Praetorius, L.; Bülbül, E. F.; Robaa, D.; Sippl, W. Strategies To Design Selective Histone Deacetylase Inhibitors. *ChemMedChem* **2021**, *16*, 1336–1359.

(127) Jones, P.; Altamura, S.; Francesco, R. de; Gallinari, P.; Lahm, A.; Neddermann, P.; Rowley, M.; Serafini, S.; Steinkühler, C. Probing the elusive catalytic activity of vertebrate class IIa histone deacetylases. *Bioorg. Med. Chem. Lett.* **2008**, *18*, 1814–1819.

(128) Lechner, S.; Malgapo, M. I. P.; Grätz, C.; Steimbach, R. R.; Baron, A.; Rüther, P.; Nadal, S.; Stumpf, C.; Loos, C.; Ku, X.*; et al.* Target deconvolution of HDAC pharmacopoeia reveals MBLAC2 as common off-target. *Nat. Chem. Biol.* **2022**, *18*, 812–820.

(129) Butler, K. V.; Kalin, J.; Brochier, C.; Vistoli, G.; Langley, B.; Kozikowski, A. P. Rational design and simple chemistry yield a superior, neuroprotective HDAC6 inhibitor, tubastatin A. *J. Am. Chem. Soc.* **2010**, *132*, 10842–10846.

(130) Bantscheff, M.; Hopf, C.; Savitski, M. M.; Dittmann, A.; Grandi, P.; Michon, A.-M.; Schlegl, J.; Abraham, Y.; Becher, I.; Bergamini, G.*; et al.* Chemoproteomics profiling of HDAC inhibitors reveals selective targeting of HDAC complexes. *Nat. Biotechnol.* **2011**, *29*, 255–265.

(131) Luckhurst, C. A.; Breccia, P.; Stott, A. J.; Aziz, O.; Birch, H. L.; Bürli, R. W.; Hughes, S. J.; Jarvis, R. E.; Lamers, M.; Leonard, P. M.*; et al.* Potent, Selective, and CNS-Penetrant Tetrasubstituted Cyclopropane Class IIa Histone Deacetylase (HDAC) Inhibitors. *ACS Med. Chem. Lett.* **2016**, *7*, 34–39.

(132) Lobera, M.; Madauss, K. P.; Pohlhaus, D. T.; Wright, Q. G.; Trocha, M.; Schmidt, D. R.; Baloglu, E.; Trump, R. P.; Head, M. S.; Hofmann, G. A.*; et al.* Selective class IIa histone deacetylase inhibition via a nonchelating zinc-binding group. *Nat. Chem. Biol.* **2013**, *9*, 319–325.

(133) Herbst-Gervasoni, C. J.; Christianson, D. W. Binding of N8-Acetylspermidine Analogues to Histone Deacetylase 10 Reveals Molecular Strategies for Blocking Polyamine Deacetylation. *Biochemistry* **2019**, *58*, 4957–4969.

(134) Dredar, S. A.; Blankenship, J. W.; Marchant, P. E.; Manneh, V.; Fries, D. S. Design and synthesis of inhibitors of N8-acetylspermidine deacetylase. *J. Med. Chem.* **1989**, *32*, 984–989.

(135) Huang, T. L.; Dredar, S. A.; Manneh, V. A.; Blankenship, J. W.; Fries, D. S. Inhibition of N8-acetylspermidine deacetylase by active-site-directed metal coordinating inhibitors. *J. Med. Chem.* **1992**, *35*, 2414–2418.

(136) Decroos, C.; Bowman, C. M.; Christianson, D. W. Synthesis and evaluation of N8-acetylspermidine analogues as inhibitors of bacterial acetylpolyamine amidohydrolase. *Bioorg. Med. Chem.* **2013**, *21*, 4530–4540.

(137) Herp, D.; Ridinger, J.; Robaa, D.; Shinsky, S. A.; Schmidtkunz, K.; Yesiloglu, T. Z.; Bayer, T.; Steimbach, R. R.; Herbst-Gervasoni, C. J.; Merz, A.*; et al.* First Fluorescent Acetylspermidine Deacetylation Assay for HDAC10 Identifies Selective Inhibitors with Cellular Target Engagement. *ChemBioChem* **2022**, *23*, e202200180.

(138) Zeyen, P.; Zeyn, Y.; Herp, D.; Mahmoudi, F.; Yesiloglu, T. Z.; Erdmann, F.; Schmidt, M.; Robaa, D.; Romier, C.; Ridinger, J.*; et al.* Identification of histone deacetylase 10 (HDAC10) inhibitors that modulate autophagy in transformed cells. *Eur. J. Med. Chem.* **2022**, *234*, 114272.

(139) Shen, S.; Kozikowski, A. P. Why Hydroxamates May Not Be the Best Histone Deacetylase Inhibitors--What Some May Have Forgotten or Would Rather Forget? *ChemMedChem* **2016**, *11*, 15–21.

(140) Fischer, A.; Sananbenesi, F.; Mungenast, A.; Tsai, L.-H. Targeting the correct HDAC(s) to treat cognitive disorders. *Trends Pharmacol. Sci.* **2010**, *31*, 605–617.

(141) Selenica, M.-L.; Benner, L.; Housley, S. B.; Manchec, B.; Lee, D. C.; Nash, K. R.; Kalin, J.; Bergman, J. A.; Kozikowski, A.; Gordon, M. N.*; et al.* Histone deacetylase 6 inhibition improves memory and reduces total tau levels in a mouse model of tau deposition. *Alzheimers. Res. Ther.* **2014**, *6*, 12.

(142) Sung, Y. M.; Lee, T.; Yoon, H.; DiBattista, A. M.; Song, J. M.; Sohn, Y.; Moffat, E. I.; Turner, R. S.; Jung, M.; Kim, J.*; et al.* Mercaptoacetamide-based class II HDAC inhibitor lowers Aβ levels and improves learning and memory in a mouse model of Alzheimer's disease. *Exp. Neurol.* **2013**, *239*, 192–201.

(143) Wang, X.-X.; Xie, F.; Jia, C.-C.; Yan, N.; Zeng, Y.-L.; Wu, J.-D.; Liu, Z.-P. Synthesis and biological evaluation of selective histone deacetylase 6 inhibitors as multifunctional agents against Alzheimer's disease. *Eur. J. Med. Chem.* **2021**, *225*, 113821.

(144) d'Ydewalle, C.; Krishnan, J.; Chiheb, D. M.; van Damme, P.; Irobi, J.; Kozikowski, A. P.; Vanden Berghe, P.; Timmerman, V.; Robberecht, W.; van den Bosch, L. HDAC6 inhibitors reverse axonal loss in a mouse model of mutant HSPB1-induced Charcot-Marie-Tooth disease. *Nat. Med.* **2011**, *17*, 968–974.

(145) Segretti, M. C. F.; Vallerini, G. P.; Brochier, C.; Langley, B.; Wang, L.; Hancock, W. W.; Kozikowski, A. P. Thiol-Based Potent and Selective HDAC6 Inhibitors Promote Tubulin Acetylation and T-Regulatory Cell Suppressive Function. *ACS Med. Chem. Lett.* **2015**, *6*, 1156–1161.

(146) Kalin, J. H.; Butler, K. V.; Akimova, T.; Hancock, W. W.; Kozikowski, A. P. Second-generation histone deacetylase 6 inhibitors enhance the immunosuppressive effects of Foxp3+ T-regulatory cells. *J. Med. Chem.* **2012**, *55*, 639–651.

(147) Zoeten, E. F. de; Wang, L.; Butler, K.; Beier, U. H.; Akimova, T.; Sai, H.; Bradner, J. E.; Mazitschek, R.; Kozikowski, A. P.; Matthias, P.*; et al.* Histone deacetylase 6 and heat shock protein 90 control the functions of Foxp3(+) T-regulatory cells. *Mol. Cell. Biol.* **2011**, *31*, 2066–2078.

(148) Kozikowski, A. P.; Chen, Y.; Gaysin, A.; Chen, B.; D'Annibale, M. A.; Suto, C. M.; Langley, B. C. Functional differences in epigenetic modulators-superiority of mercaptoacetamide-based

histone deacetylase inhibitors relative to hydroxamates in cortical neuron neuroprotection studies. *J. Med. Chem.* **2007**, *50*, 3054–3061.

(149) Frey, R. R.; Wada, C. K.; Garland, R. B.; Curtin, M. L.; Michaelides, M. R.; Li, J.; Pease, L. J.; Glaser, K. B.; Marcotte, P. A.; Bouska, J. J.*; et al.* Trifluoromethyl ketones as inhibitors of histone deacetylase. *Bioorg. Med. Chem. Lett.* **2002**, *12*, 3443–3447.

(150) Scarpelli, R.; Di Marco, A.; Ferrigno, F.; Laufer, R.; Marcucci, I.; Muraglia, E.; Ontoria, J. M.; Rowley, M.; Serafini, S.; Steinkühler, C.*; et al.* Studies of the metabolic stability in cells of 5-(trifluoroacetyl)thiophene-2-carboxamides and identification of more stable class II histone deacetylase (HDAC) inhibitors. *Bioorg. Med. Chem. Lett.* **2008**, *18*, 6078–6082.

(151) Frühauf, A.; Meyer-Almes, F.-J. Non-Hydroxamate Zinc-Binding Groups as Warheads for Histone Deacetylases. *Molecules* **2021**, *26*.

(152) Chen, B.; Petukhov, P. A.; Jung, M.; Velena, A.; Eliseeva, E.; Dritschilo, A.; Kozikowski, A. P. Chemistry and biology of mercaptoacetamides as novel histone deacetylase inhibitors. *Bioorg. Med. Chem. Lett.* **2005**, *15*, 1389–1392.

(153) Tavares, M. T.; Kozikowski, A. P.; Shen, S. Mercaptoacetamide: A promising zinc-binding group for the discovery of selective histone deacetylase 6 inhibitors. *Eur. J. Med. Chem.* **2021**, *209*, 112887.

(154) Porter, N. J.; Shen, S.; Barinka, C.; Kozikowski, A. P.; Christianson, D. W. Molecular Basis for the Selective Inhibition of Histone Deacetylase 6 by a Mercaptoacetamide Inhibitor. *ACS Med. Chem. Lett.* **2018**, *9*, 1301–1305.

(155) Geurs, S.; Clarisse, D.; Baele, F.; Franceus, J.; Desmet, T.; Bosscher, K. de; D'hooghe, M. Identification of mercaptoacetamide-based HDAC6 inhibitors via a lean inhibitor strategy: screening, synthesis, and biological evaluation. *Chem. Commun.* **2022**, *58*, 6239–6242.

(156) Dehmel, F.; Weinbrenner, S.; Julius, H.; Ciossek, T.; Maier, T.; Stengel, T.; Fettis, K.; Burkhardt, C.; Wieland, H.; Beckers, T. Trithiocarbonates as a novel class of HDAC inhibitors: SAR studies, isoenzyme selectivity, and pharmacological profiles. *J. Med. Chem.* **2008**, *51*, 3985–4001.

(157) Lee, J.; Han, Y.; Kim, Y.; Min, J.; Bae, M.; Kim, D.; Jin, S.; Kyung, J. 1,3,4-OXADIAZOLE SULFAMIDE DERIVATIVE COMPOUNDS AS HISTONE DEACETYLASE 6 INHIBITOR, AND THE PHARMACEUTICAL COMPOSITION COMPRISING THE SAME. WO2016KR08218 20160727, Jul 27, 2016.

(158) Keuler, T.; König, B.; Bückreiß, N.; Kraft, F. B.; König, P.; Schäker-Hübner, L.; Steinebach, C.; Bendas, G.; Gütschow, M.; Hansen, F. K. Development of the first non-hydroxamate selective HDAC6 degraders. *Chem. Commun.* **2022**, *58*, 11087–11090.

(159) Janzen, W. P. Screening technologies for small molecule discovery: the state of the art. *Chem. Biol.* **2014**, *21*, 1162–1170.

(160) Gao, K.; Oerlemans, R.; Groves, M. R. Theory and applications of differential scanning fluorimetry in early-stage drug discovery. *Biophys. Rev.* **2020**, *12*, 85–104.

(161) Wegener, D.; Wirsching, F.; Riester, D.; Schwienhorst, A. A Fluorogenic Histone Deacetylase Assay Well Suited for High-Throughput Activity Screening. *Chemistry & Biology* **2003**, *10*, 61–68.

(162) Marks, B. D.; Fakhoury, S. A.; Frazee, W. J.; Eliason, H. C.; Riddle, S. M. A substrate-independent TR-FRET histone deacetylase inhibitor assay. *J. Biomol. Screen.* **2011**, *16*, 1247–1253.

(163) Halley, F.; Reinshagen, J.; Ellinger, B.; Wolf, M.; Niles, A. L.; Evans, N. J.; Kirkland, T. A.; Wagner, J. M.; Jung, M.; Gribbon, P.*; et al.* A bioluminogenic HDAC activity assay: validation and screening. *J. Biomol. Screen.* **2011**, *16*, 1227–1235.

(164) Robers, M. B.; Dart, M. L.; Woodroofe, C. C.; Zimprich, C. A.; Kirkland, T. A.; Machleidt, T.; Kupcho, K. R.; Levin, S.; Hartnett, J. R.; Zimmerman, K.*; et al.* Target engagement and drug residence time can be observed in living cells with BRET. *Nat. Commun.* **2015**, *6*, 10091.

(165) Riester, D.; Wegener, D.; Hildmann, C.; Schwienhorst, A. Members of the histone deacetylase superfamily differ in substrate specificity towards small synthetic substrates. *Biochem. Biophys. Res. Commun.* **2004**, *324*, 1116–1123.

(166) Promega Corporation. *Technical Manual of the HDAC-Glo™ I/II Assay and Screening System: Instructions for Use of Products G6420, G6421, G6422, G6430, G6431, G6560 and G6570*; Madison, WI, 2016.

(167) Sharma, K.; Kumar, A.; Chandna, S. Constitutive hyperactivity of histone deacetylases enhances radioresistance in Lepidopteran Sf9 insect cells. *Biochim. Biophys. Acta* **2016**, *1860*, 1237–1246.

(168) Algar, W. R.; Hildebrandt, N.; Vogel, S. S.; Medintz, I. L. FRET as a biomolecular research tool - understanding its potential while avoiding pitfalls. *Nat. Methods* **2019**, *16*, 815–829.

(169) Herp, D.; Ridinger, J.; Robaa, D.; Shinsky, S. A.; Schmidtkunz, K.; Yesiloglu, T. Z.; Bayer, T.; Sehr, P.; Gunkel, N.; Miller, A. K.*; et al.* First Fluorescent Acetylspermidine Deacetylation Assay for HDAC10 Identifies Inhibitors of Neuroblastoma Cell Colony Growth That Increase Lysosome Accumulation. *ChemRxiv* [Online early access]. DOI: 10.26434/chemrxiv.12440096.v3.

(170) Békés, M.; Langley, D. R.; Crews, C. M. PROTAC targeted protein degraders: the past is prologue. *Nature reviews. Drug discovery* **2022**, *21*, 181–200.

(171) Casement, R.; Bond, A.; Craigon, C.; Ciulli, A. Mechanistic and Structural Features of PROTAC Ternary Complexes. *Methods Mol. Biol.* **2021**, *2365*, 79–113.

(172) Scheepstra, M.; Hekking, K. F. W.; van Hijfte, L.; Folmer, R. H. A. Bivalent Ligands for Protein Degradation in Drug Discovery. *Comput. Struct. Biotechnol. J.* **2019**, *17*, 160–176.

(173) Lai, A. C.; Crews, C. M. Induced protein degradation: an emerging drug discovery paradigm. *Nature reviews. Drug discovery* **2017**, *16*, 101–114.

(174) Yang, K.; Song, Y.; Xie, H.; Wu, H.; Wu, Y.-T.; Leisten, E. D.; Tang, W. Development of the first small molecule histone deacetylase 6 (HDAC6) degraders. *Bioorg. Med. Chem. Lett.* **2018**, *28*, 2493–2497.

(175) Gopalsamy, A. Selectivity through Targeted Protein Degradation (TPD). *J. Med. Chem.* **2022**, *65*, 8113–8126.

(176) An, Z.; Lv, W.; Su, S.; Wu, W.; Rao, Y. Developing potent PROTACs tools for selective degradation of HDAC6 protein. *Protein Cell* **2019**, *10*, 606–609.

(177) Yang, K.; Wu, H.; Zhang, Z.; Leisten, E. D.; Nie, X.; Liu, B.; Wen, Z.; Zhang, J.; Cunningham, M. D.; Tang, W. Development of Selective Histone Deacetylase 6 (HDAC6) Degraders Recruiting Von Hippel-Lindau (VHL) E3 Ubiquitin Ligase. *ACS Med. Chem. Lett.* **2020**, *11*, 575–581.

(178) Sinatra, L.; Bandolik, J. J.; Roatsch, M.; Sönnichsen, M.; Schoeder, C. T.; Hamacher, A.; Schöler, A.; Borkhardt, A.; Meiler, J.; Bhatia, S.*; et al.* Hydroxamic Acids Immobilized on Resins (HAIRs): Synthesis of Dual-Targeting HDAC Inhibitors and HDAC Degraders (PROTACs). *Angew. Chem. Int. Ed. Engl.* **2020**, *59*, 22494–22499.

(179) Xiong, Y.; Donovan, K. A.; Eleuteri, N. A.; Kirmani, N.; Yue, H.; Razov, A.; Krupnick, N. M.; Nowak, R. P.; Fischer, E. S. Chemo-proteomics exploration of HDAC degradability by small molecule degraders. *Cell Chem. Biol.* **2021**, *28*, 1514-1527.

(180) Kolbinger, F. R.; Koeneke, E.; Ridinger, J.; Heimburg, T.; Müller, M.; Bayer, T.; Sippl, W.; Jung, M.; Gunkel, N.; Miller, A. K.*; et al.* The HDAC6/8/10 inhibitor TH34 induces DNA damage-mediated cell death in human high-grade neuroblastoma cell lines. *Archives of toxicology* **2018**, *92*, 2649–2664.

(181) Zhang; Chung; Oldenburg. A Simple Statistical Parameter for Use in Evaluation and Validation of High Throughput Screening Assays. *J. Biomol. Screen.* **1999**, *4*, 67–73.

(182) Morgen, M.; Steimbach, R. R.; Géraldy, M.; Hellweg, L.; Sehr, P.; Ridinger, J.; Witt, O.; Oehme, I.; Herbst-Gervasoni, C. J.; Osko, J. D.*; et al.* Design and Synthesis of Dihydroxamic Acids as HDAC6/8/10 Inhibitors. *ChemMedChem* **2020**, *15*, 1163–1174.

(183) Decroos, C.; Christianson, D. W. Design, Synthesis, and Evaluation of Polyamine Deacetylase Inhibitors, and High-Resolution Crystal Structures of Their Complexes with Acetylpolyamine Amidohydrolase. *Biochemistry* **2015**, *54*, 4692–4703.

(184) Zohuriaan-Mehr, M. J.; Pourjavadi, A.; Salehi-Rad, M. Modified CMC. 2. Novel carboxymethylcellulose-based poly(amidoxime) chelating resin with high metal sorption capacity. *React. Funct. Polym.* **2004**, *61*, 23–31.

(185) Jiao, P.; Jin, P.; Li, C.; Cui, L.; Dong, L.; Pan, B.; Song, W.; Ma, L.; Dong, J.; Song, L.*; et al.* Design, synthesis and in vitro evaluation of amidoximes as histone deacetylase inhibitors for cancer therapy. *Bioorg. Med. Chem. Lett.* **2016**, *26*, 4679–4683.

(186) Hopkins, A. L.; Keserü, G. M.; Leeson, P. D.; Rees, D. C.; Reynolds, C. H. The role of ligand efficiency metrics in drug discovery. *Nat. Rev. Drug Discovery* **2014**, *13*, 105–121.

(187) Andrews, K. G.; Faizova, R.; Denton, R. M. A practical and catalyst-free trifluoroethylation reaction of amines using trifluoroacetic acid. *Nat. Commun.* **2017**, *8*, 15913.

(188) Wang, T.; Zhang, Z.; Meanwell, N. A. Benzoylation of Dianions: Preparation of Monobenzoylated Derivatives of Symmetrical Secondary Diamines. *J. Org. Chem.* **1999**, *64*, 7661–7662.

(189) Tallant, C.; Marrero, A.; Gomis-Rüth, F. X. Matrix metalloproteinases: fold and function of their catalytic domains. *Biochim. Biophys. Acta* **2010**, *1803*, 20–28.

(190) Li, K.; Tay, F. R.; Yiu, C. K. Y. The past, present and future perspectives of matrix metalloproteinase inhibitors. *Pharmacol. Ther.* **2020**, *207*, 107465.

(191) Xu, W. S.; Parmigiani, R. B.; Marks, P. A. Histone deacetylase inhibitors: molecular mechanisms of action. *Oncogene* **2007**, *26*, 5541–5552.

(192) Shechter, D.; Dormann, H. L.; Allis, C. D.; Hake, S. B. Extraction, purification and analysis of histones. *Nat. Protoc.* **2007**, *2*, 1445–1457.

(193) Ucal, S.; Khomutov, A. R.; Häkkinen, M. R.; Turhanen, P. A.; Vepsäläinen, J. J.; Weisella, J. Selective acetylation of primary amino groups with phenyl acetate; simple synthesis of N,N´-diacetyl polyamines. *ARKIVOC* **2015**, *2015*, 42–49.

(194) DeFelice, B. C.; Fiehn, O. Rapid LC-MS/MS quantification of cancer related acetylated polyamines in human biofluids. *Talanta* **2019**, *196*, 415–419.

(195) Milovic, V. Polyamines in the gut lumen: bioavailability and biodistribution. *Eur. J. Gastroenterol. Hepatol.* **2001**, *13*, 1021–1025.

(196) Dubin, D. T.; Rosenthal, S. M. The Acetylation of Polyamines in Escherichia coli. *J. Biol. Chem.* **1960**, *235*, 776–782.

(197) Schill, G.; Schweickert, N.; Fritz, H.; Vetter, W. Synthese von [2]-Catenanen aus [2]-Rotaxanen. *Chem. Ber.* **1988**, *121*, 961–970.

(198) Kang, S. O.; Powell, D.; Day, V. W.; Bowman-James, K. Trapped bifluoride. *Angew. Chem. Int. Ed. Engl.* **2006**, *45*, 1921–1925.

(199) Gu, W.; Nusinzon, I.; Smith, R. D.; Horvath, C. M.; Silverman, R. B. Carbonyl- and sulfur-containing analogs of suberoylanilide hydroxamic acid: Potent inhibition of histone deacetylases. *Bioorganic & medicinal chemistry* **2006**, *14*, 3320–3329.

(200) Taddäus Emil Noel Strunden. Novel Zinc Binding Moieties for the Inhibition of Human Histone Deacetylases. Bachelor Thesis, German Cancer Research Center, Heidelberg, 2020.

(201) Wu, K.-M. A New Classification of Prodrugs: Regulatory Perspectives. *Pharmaceuticals (Basel)* **2009**, *2*, 77–81.

(202) Wash, P. L.; Wiley, B. M.; Hassig, C.; Malecha, J. W.; Noble, S. A. CARBONYL COMPOUNDS AS INHIBITORS OF HISTONE DEACETYLASE FOR THE TREATMENT OF DISEASE. WO2004US18502 20040610, Jun 10, 2004.

(203) Yamashita, K.; Takaya, H.; Yamashita, N.; Muragata, T.; Imai, Y.; Kurokawa, M. HISTONE DEACETYLASE INHIBITOR. JP20040210365 20040716, Jul 16, 2004.

(204) Bettanin, L.; Saba, S.; Galetto, F. Z.; Mike, G. A.; Rafique, J.; Braga, A. L. Solvent- and metal-free selective oxidation of thiols to disulfides using I2/DMSO catalytic system. *Tetrahedron Lett.* **2017**, *58*, 4713–4716.

(205) Mu, F.; Coffing, S. L.; Riese, D. J.; Geahlen, R. L.; Verdier-Pinard, P.; Hamel, T. E.; Johnson, J.; Cushman, M. Design, synthesis, and biological evaluation of a series of lavendustin A analogues that inhibit EGFR and Syk tyrosine kinases, as well as tubulin polymerization. *J. Med. Chem.* **2001**, *44*, 441–452.

(206) Lohbeck, J.; Miller, A. K. Practical synthesis of a phthalimide-based Cereblon ligand to enable PROTAC development. *Bioorg. Med. Chem. Lett.* **2016**, *26*, 5260–5262.

(207) Han, B. A suite of mathematical solutions to describe ternary complex formation and their application to targeted protein degradation by heterobifunctional ligands. *J. Biol. Chem.* **2020**, *295*, 15280–15291.

(208) Chuang, H.-H.; Hsu, J.-F.; Chang, H.-L.; Wang, P.-H.; Wei, P.-J.; Wu, D.-W.; Huang, M.-S.; Hsiao, M.; Yang, C.-J. Pin1 coordinates HDAC6 upregulation with cell migration in lung cancer cells. *Int. J. Med. Sci.* **2020**, *17*, 2635–2643.

(209) Uhlén, M.; Fagerberg, L.; Hallström, B. M.; Lindskog, C.; Oksvold, P.; Mardinoglu, A.; Sivertsson, Å.; Kampf, C.; Sjöstedt, E.; Asplund, A.*; et al.* Proteomics. Tissue-based map of the human proteome. *Science* **2015**, *347*, 1260419, https://www.proteinatlas.org/ENSG00000113851-CRBN/cell+line#neuroblastoma.

(210) Uhlén, M.; Fagerberg, L.; Hallström, B. M.; Lindskog, C.; Oksvold, P.; Mardinoglu, A.; Sivertsson, Å.; Kampf, C.; Sjöstedt, E.; Asplund, A.*; et al.* Proteomics. Tissue-based map of the

human proteome. *Science* **2015**, *347*, 1260419, https://www.proteinatlas.org/ENSG00000100429-HDAC10/cell+line#leukemia.

(211) Shevchenko, A.; Tomas, H.; Havlis, J.; Olsen, J. V.; Mann, M. In-gel digestion for mass spectrometric characterization of proteins and proteomes. *Nat. Protoc.* **2006**, *1*, 2856–2860.

(212) Tyanova, S.; Temu, T.; Cox, J. The MaxQuant computational platform for mass spectrometry-based shotgun proteomics. *Nat. Protoc.* **2016**, *11*, 2301–2319.

(213) Cox, J.; Hein, M. Y.; Luber, C. A.; Paron, I.; Nagaraj, N.; Mann, M. Accurate proteome-wide label-free quantification by delayed normalization and maximal peptide ratio extraction, termed MaxLFQ. *Mol. Cell. Proteomics* **2014**, *13*, 2513–2526.

(214) Tyanova, S.; Cox, J. Perseus: A Bioinformatics Platform for Integrative Analysis of Proteomics Data in Cancer Research. *Methods Mol. Biol.* **2018**, *1711*, 133–148.

(215) Stekhoven, D. J.; Bühlmann, P. MissForest--non-parametric missing value imputation for mixed-type data. *Bioinformatics* **2012**, *28*, 112–118.

(216) Ritchie, M. E.; Phipson, B.; Di Wu; Hu, Y.; Law, C. W.; Shi, W.; Smyth, G. K. limma powers differential expression analyses for RNA-sequencing and microarray studies. *Nucleic Acids Res.* **2015**, *43*, e47.

(217) Benjamini, Y.; Hochberg, Y. Controlling the False Discovery Rate: A Practical and Powerful Approach to Multiple Testing. *Journal of the Royal Statistical Society: Series B (Methodological)* **1995**, *57*, 289–300.

(218) Körholz, K.; Ridinger, J.; Krunic, D.; Najafi, S.; Gerloff, X. F.; Frese, K.; Meder, B.; Peterziel, H.; Vega-Rubin-de-Celis, S.; Witt, O.*; et al.* Broad-Spectrum HDAC Inhibitors Promote Autophagy through FOXO Transcription Factors in Neuroblastoma. *Cells* **2021**, *10*, 1001.

(219) Galakatos, N. G.; Kemp, D. S. New S-protection from known N-protection: thio esters of N-urethanyl-N-methyl-.gamma.-aminobutyric acid as a class of protective groups for thiols in peptide synthesis. *J. Org. Chem.* **1985**, *50*, 1302–1304.

(220) Sulzer-Mosse, S.; Lamberth, C.; Kubizna, P. Synthesis of Ring-Opened Analogues of Oxysterol-Binding Protein-Inhibiting Piperidinyl-thiazole Fungicides. *Synlett* **2017**, *28*, 2277–2280.

(221) Pilkington, L.; Haverkate, N.; van Rensburg, M.; Reynisson, J.; Leung, E.; Barker, D. Synthesis of 3-Amino-2-carboxamide Tetrahydropyrrolo[2,3-b]quinolines. *Synlett* **2016**, *27*, 2811–2814.

(222) Steimbach, R. R.; Tihanyi, G.; Géraldy, M. N. E.; Wzorek, A.; Miller, A. K.; Klika, K. D. Can an Intermediate Rate of Nitrogen Inversion Affect Drug Efficacy? *Symmetry* **2021**, *13*, 1753.

(223) O'Meara, J. A.; Yoakim, C.; Bonneau, P. R.; Bös, M.; Cordingley, M. G.; Déziel, R.; Doyon, L.; Duan, J.; Garneau, M.; Guse, I.*; et al.* Novel 8-substituted dipyridodiazepinone inhibitors with a broad-spectrum of activity against HIV-1 strains resistant to non-nucleoside reverse transcriptase inhibitors. *J. Med. Chem.* **2005**, *48*, 5580–5588.

(224) Nakajima, M.; Oda, Y.; Wada, T.; Minamikawa, R.; Shirokane, K.; Sato, T.; Chida, N. Chemoselective reductive nucleophilic addition to tertiary amides, secondary amides, and N-methoxyamides. *Chemistry* **2014**, *20*, 17565–17571.

(225) Kwie, F. H. A.; Briet, M.; Soupaya, D.; Hoffmann, P.; Maturano, M.; Rodriguez, F.; Blonski, C.; Lherbet, C.; Baudoin-Dehoux, C. New potent bisubstrate inhibitors of histone

acetyltransferase p300: design, synthesis and biological evaluation. *Chem. Biol. Drug Des.* **2011**, *77*, 86–92.

(226) Kozikowski, A. P.; Dritschilo, A.; Jung, M.; Petukhov, P.; Chen, B. HISTONE DEACETYLASE INHIBITORS AND METHODS OF USE THEREOF. WO2004US21663 20040707, Jul 7, 2004.

# 7 Abbreviations

| | |
|---|---|
| **9-BBN** | 9-Borabicyclo[3.3.1]nonane |
| **AcCad** | *N*-acetylcadaverine |
| **acetyl-CoA** | acetyl coenzyme A |
| **AcPut** | *N*-acetylputrescine |
| **ADC** | arginine decarboxylase |
| **ADME(T)** | absorption, distribution, metabolism, excretion, (toxicology) |
| **Agm** | agmatine |
| **AMC** | 7-amino-4-methylcoumarin |
| **ANOVA** | analysis of variance |
| **APAO** | $N^1$-acetylpolyamine oxidase |
| **app** | apparent (NMR spectra) |
| **Arg** | arginine |
| **ATP** | adenosine triphosphate |
| **BOP-Cl** | bis(2-oxo-3-oxazolidinyl)phosphinic chloride |
| **BRET** | bioluminescence resonance energy transfer |
| **BSA** | bovine serum albumine |
| **DTT** | dithiothreitol |
| **EDC** | 1-ethyl-3-(3-dimethylaminopropyl) carbodiimid·HCl |
| **Fmoc** | fluorenylmethoxycarbonyl protecting group |
| **FmocOSu** | N-(9H-Fluoren-9-ylmethoxycarbonyloxy)-succinimid |
| **FRET** | fluorescence resonance energy transfer |
| **GABA** | gamma amino butyric acid |
| **GAPDH** | glyceraldehyde 3-phosphate dehydrogenase |
| **GST tag** | glutathione s-transferase tag |
| **HAIRs** | "hydroxamic acids immobilized on resins" |
| **HAT** | histone acetyltransferase |
| **HATU** | O-(7-azabenzotriazol-1-yl)-*N,N,N′,N′*-tetramethyluronium-hexafluorphosphate |
| **HDAC** | histone deacetylase |
| **HDACi** | histone deacetylase inhibitor |
| **HDRL** | Helmholtz Drug Repurposing Library |
| **hHDAC10** | human HDAC10 |
| **HOBt** | 1-hydroxybenzotriazol |
| **HPCs** | "hybrid polar compounds" |
| **HPLC** | high-performance liquid chromatography |
| **Hsc70** | heat shock cognate 71 kDa protein |
| **IAP** | inhibitor of apoptosis proteins, an E3 ligase |
| **$IC_{50}$** | half maximal inhibitory concentration |
| **IMiDs** | immunomodulatory imide drugs |
| **ISOC** | isochorismatase domain-containing protein |
| **KDAC** | lysine deacetylase |
| **LC/MS** | liquid chromatography/mass spectrometry |
| **LFQ** | label-free quantification (mass spectrometry) |
| **MELC** | murine erythroleukemia cells |
| **Mesna** | 2-mercaptoethane sulfonate Na |
| **MHC** | major histocompatibility complex |
| **MMPs** | matrix metalloproteinases |
| **Morpho CDI** | N-cyclohexyl-*N′*-(2-morpholinoethyl)carbodiimide methyl-*p*-toluenesulfonate |
| ***N*¹-AcSpm** | $N^1$-acetylspermine |

| | |
|---|---|
| **$N^{1,8}$-$Ac_2$Spd** | $N^{1,8}$-diacetylspermidine |
| **$N^1$-AcSpd** | $N^1$-acetylspermidine |
| **$N^8$-AcSpd** | $N^8$-acetylspermidine |
| **NAT2** | arylamine *N*-acetyltransferase 2 |
| **NBS** | *N*-Bromosuccinimide |
| **NCoR** | nuclear receptor co-repressor |
| **NDA** | naphthalene-2, 3-dicarboxaldehyde |
| **nLuc** | nanoLuciferase |
| **ODC** | ornithine decarboxylase |
| **Orn** | L-ornithine |
| **p** | pentett (NMR spectra) |
| **PCAF** | p300/CBP-associated factor |
| **PDAC** | polyamine deacetylase |
| **PEG** | polyethylene glycol |
| **PGC-1α** | peroxisome proliferator-activated receptor gamma co-activator 1alpha |
| **POI** | protein of interest |
| **PROTAC** | proteolysis-targeting chimera |
| **pTSA** | *p*-toluenesulfonic acid |
| **Put** | putrescine |
| **q** | quartett (NMR spectra) |
| **QTc interval** | QT interval corrected for heart rate |
| **quant** | quantitative (yield) |
| **rt** | room temperature, 22±2 °C |
| **SAHA** | suberoylanilide hydroxamic acid |
| **SAR** | structure-activity relationship |
| **SDS-PAGE** | sodium dodecyl sulfate–polyacrylamide gel electrophoresis |
| **SF** | selectivity factor |
| **SIRTs** | sirtuins |
| **SMC3** | structural maintenance of chromosomes protein 3 |
| **SMO** | spermine oxidase |
| **SMRT** | silencing mediator of retinoic and thyroid receptors |
| **SMS** | spermine synthase |
| **Spd** | spermidine |
| **Spm** | spermine |
| **SPS** | solid phase synthesis |
| **SRM** | spermidine synthase |
| **SSAT** | spermidine/spermine $N^1$-acetyltransferase |
| **Tau** | tubulin associated unit, a protein |
| **TFA** | trifluoroacetic acid |
| **THF** | tetrahydrofuran |
| **TMT** | tandem mass tag |
| **TR-FRET** | time-resolved fluorescence resonance energy transfer |
| **TSA** | trichostatin A |
| **VHL** | Hippel-Lindau E3 ligase |
| **ZBG** | zinc-binding group |
| **zHDAC10** | zebrafish HDAC10 |
| **ΨDAC** | pseudo-deacetylase |

# 8 Appendix

## 8.1 NMR spectra and HPLC chromatograms

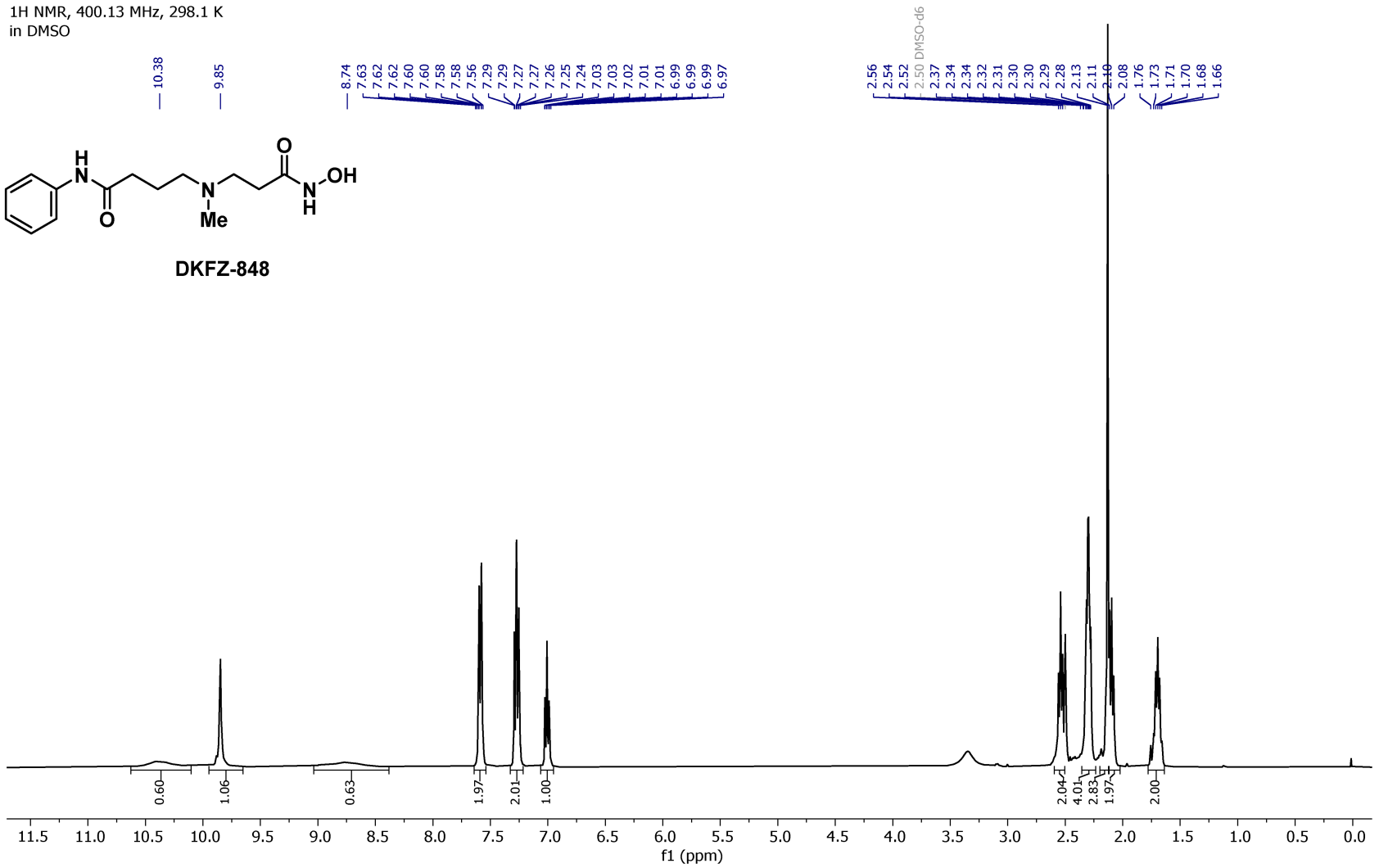
1H NMR, 400.13 MHz, 298.1 K
in DMSO
10.38
9.85
8.74
7.63
7.62
7.62
7.60
7.60
7.58
7.58
7.56
7.29
7.29
7.27
7.27
7.26
7.25
7.24
7.03
7.03
7.02
7.01
7.01
6.99
6.99
6.99
6.97
2.56
2.54
2.52
2.50 DMSO-d6
2.37
2.34
2.34
2.32
2.31
2.30
2.30
2.29
2.28
2.13
2.11
2.10
2.08
1.76
1.73
1.71
1.70
1.68
1.66
H
N
O
N
Me
O
N
H
OH
DKFZ-848
0.60
1.06
0.63
1.97
2.01
1.00
2.04
4.01
2.83
1.97
2.00
11.5
11.0
10.5
10.0
9.5
9.0
8.5
8.0
7.5
7.0
6.5
6.0
5.5
5.0
4.5
4.0
3.5
3.0
2.5
2.0
1.5
1.0
0.5
0.0
f1 (ppm)

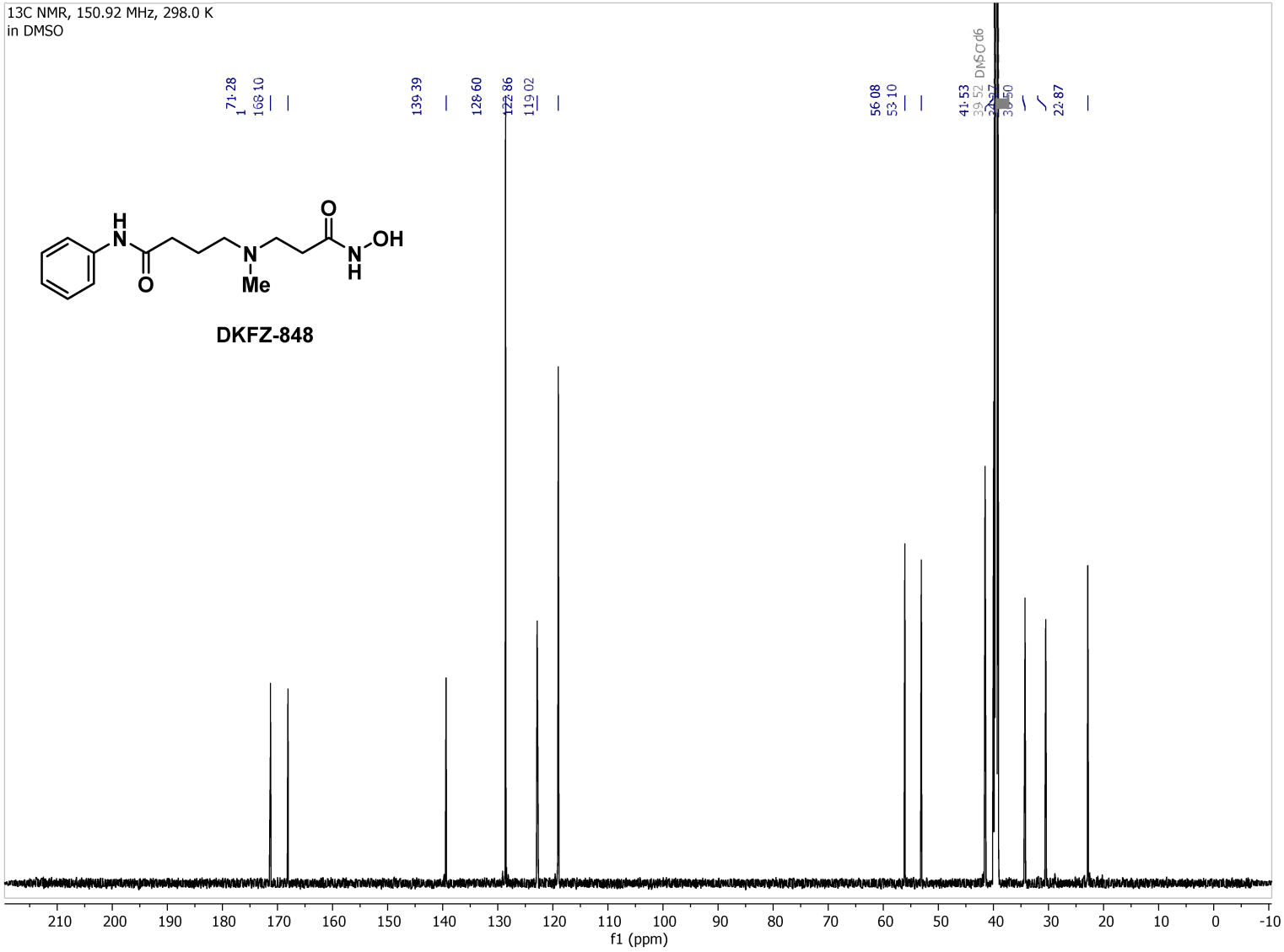
13C NMR, 150.92 MHz, 298.0 K
in DMSO
71.28
168.10
139.39
128.60
122.86
119.02
56.08
53.10
41.53
39.52
DMSO-d6
30.50
22.87
DKFZ-848
210 200 190 180 170 160 150 140 130 120 110 100 90 80 70 60 50 40 30 20 10 0 -10
f1 (ppm)

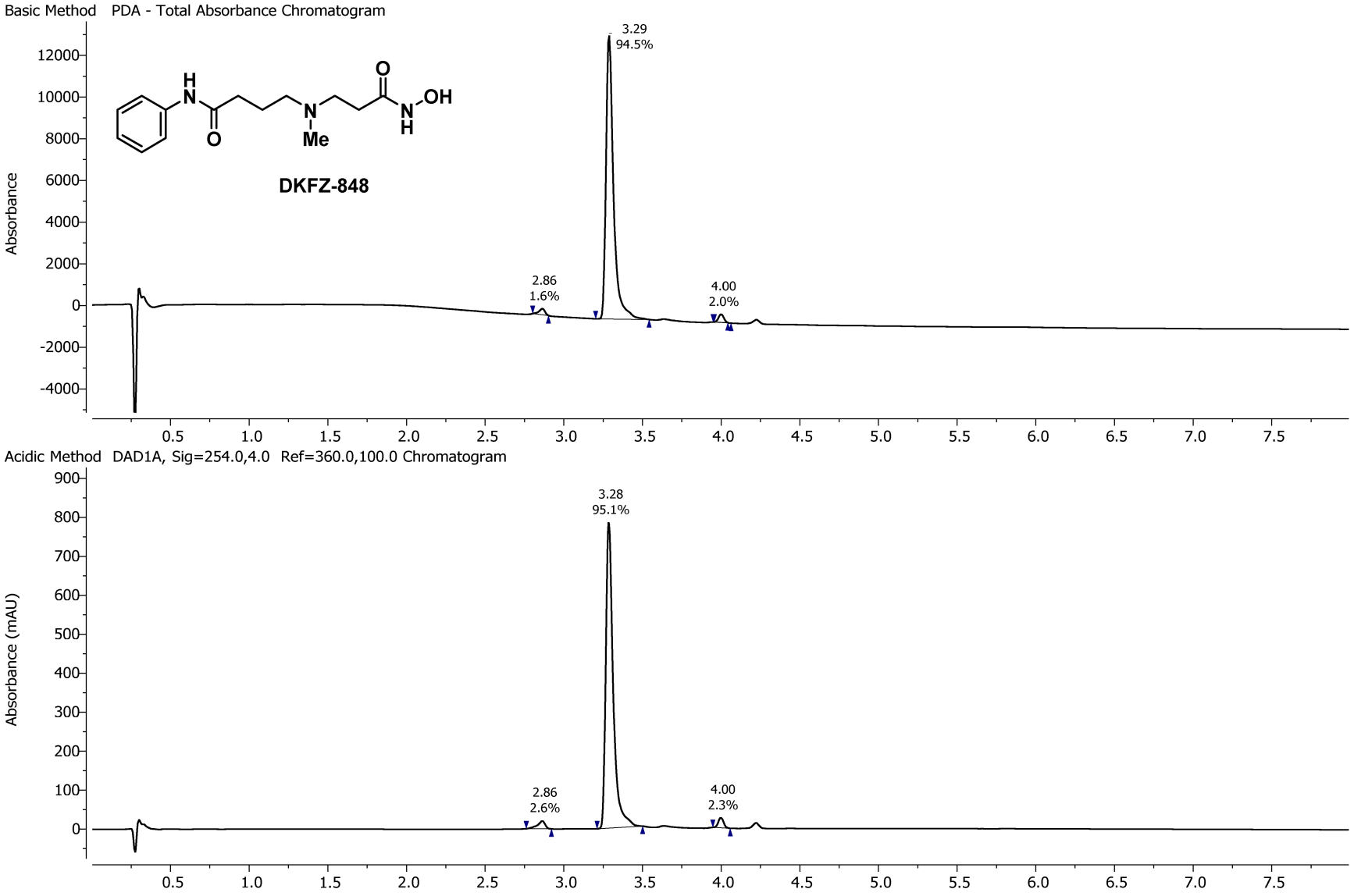
Basic Method PDA - Total Absorbance Chromatogram
Absorbance
12000
10000
8000
6000
4000
2000
0
-2000
-4000
3.29
94.5%
2.86
1.6%
4.00
2.0%
DKFZ-848
0.5
1.0
1.5
2.0
2.5
3.0
3.5
4.0
4.5
5.0
5.5
6.0
6.5
7.0
7.5
Acidic Method DAD1A, Sig=254.0,4.0 Ref=360.0,100.0 Chromatogram
Absorbance (mAU)
900
800
700
600
500
400
300
200
100
0
3.28
95.1%
2.86
2.6%
4.00
2.3%
0.5
1.0
1.5
2.0
2.5
3.0
3.5
4.0
4.5
5.0
5.5
6.0
6.5
7.0
7.5

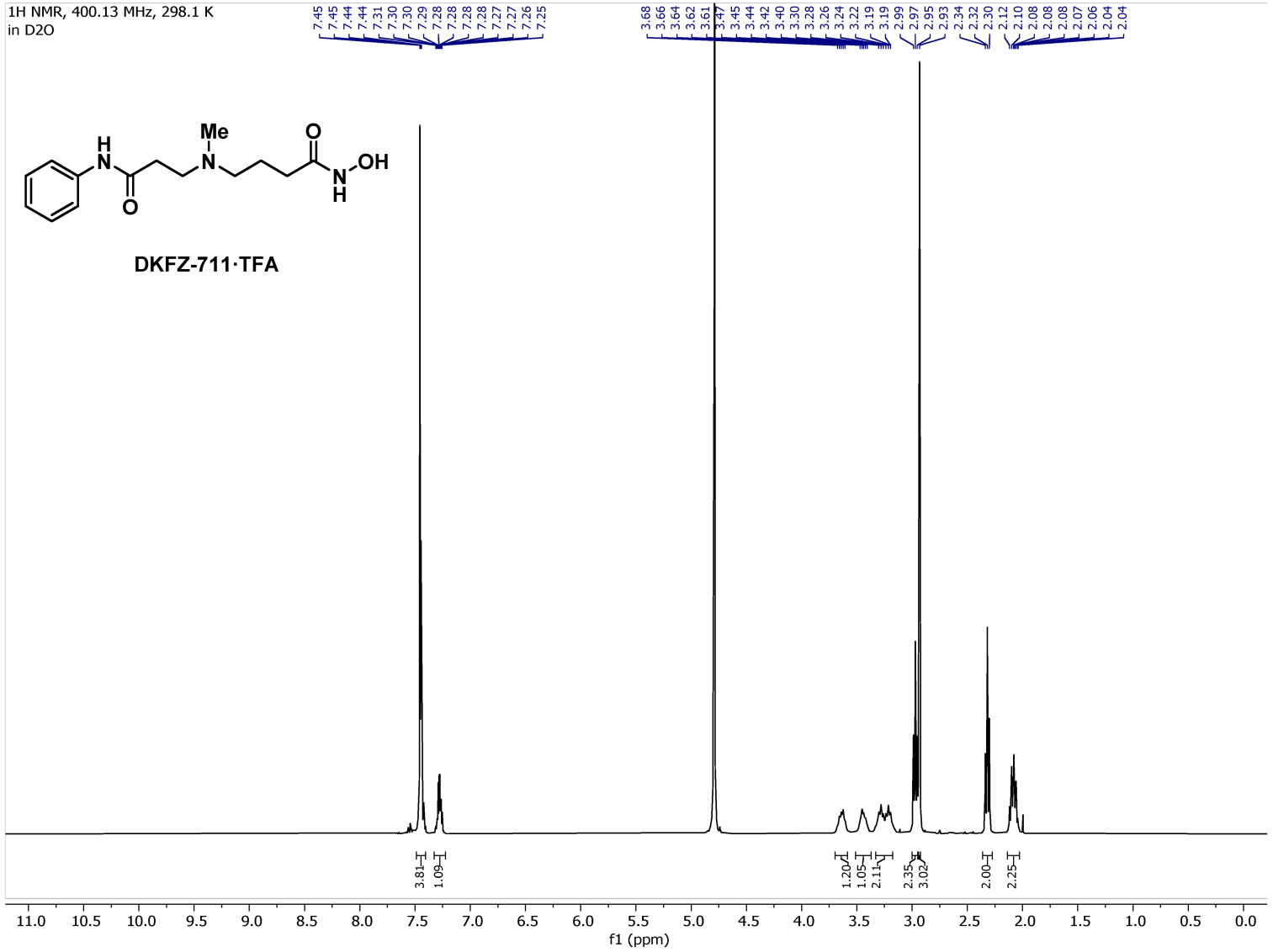
1H NMR, 400.13 MHz, 298.1 K
in D2O
DKFZ-711·TFA
f1 (ppm)

19F NMR, 376.46 MHz, 298.1 K
in D2O

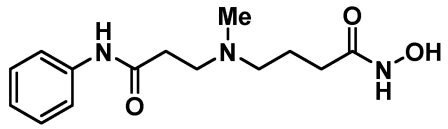


**DKFZ-711·TFA**

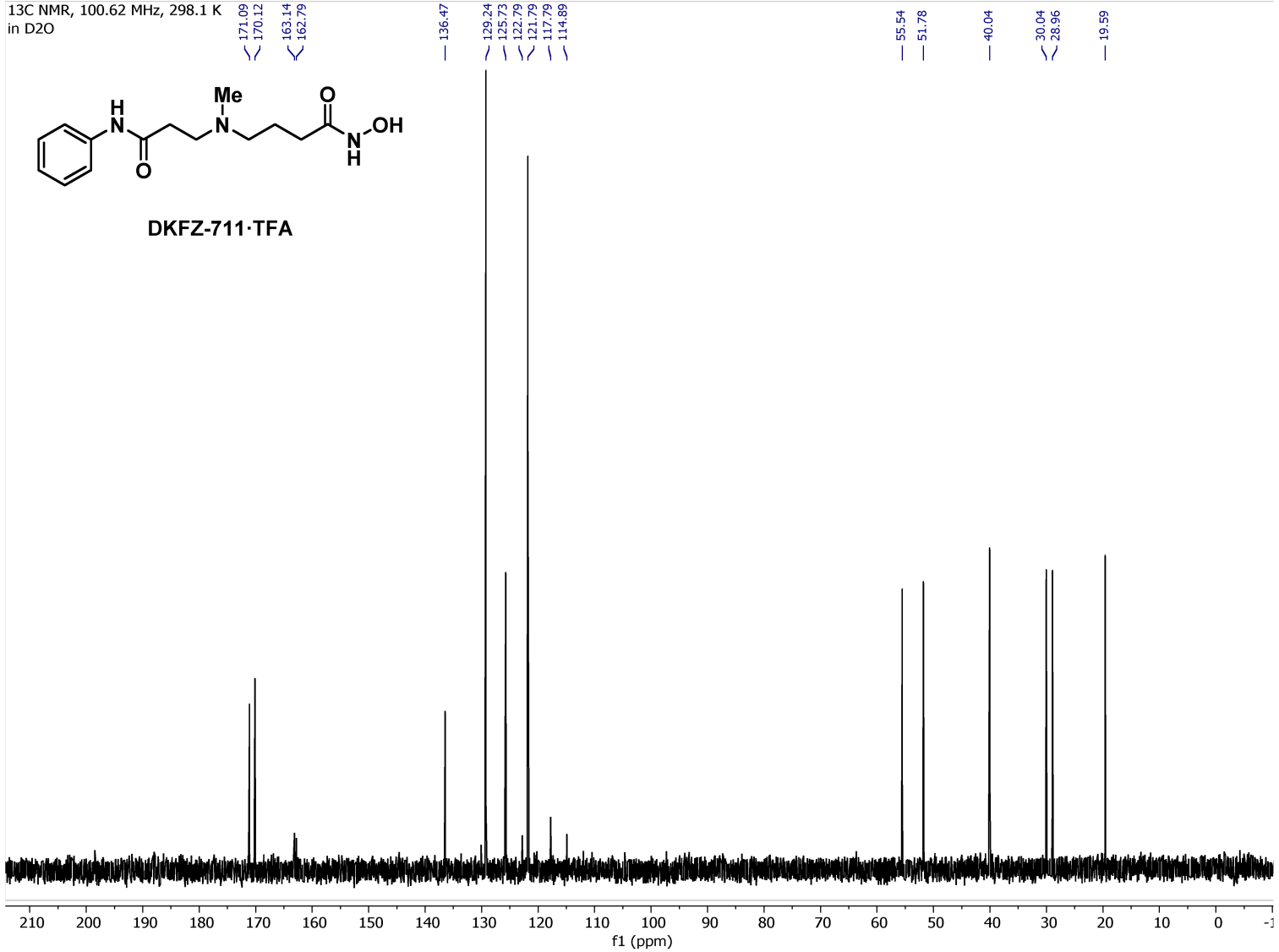
13C NMR, 100.62 MHz, 298.1 K
in D2O
171.09
170.12
163.14
162.79
136.47
129.24
125.73
122.79
121.79
117.79
114.89
55.54
51.78
40.04
30.04
28.96
19.59
Me
O
H
N
N
N
OH
H
O
DKFZ-711·TFA
210 200 190 180 170 160 150 140 130 120 110 100 90 80 70 60 50 40 30 20 10 0
f1 (ppm)

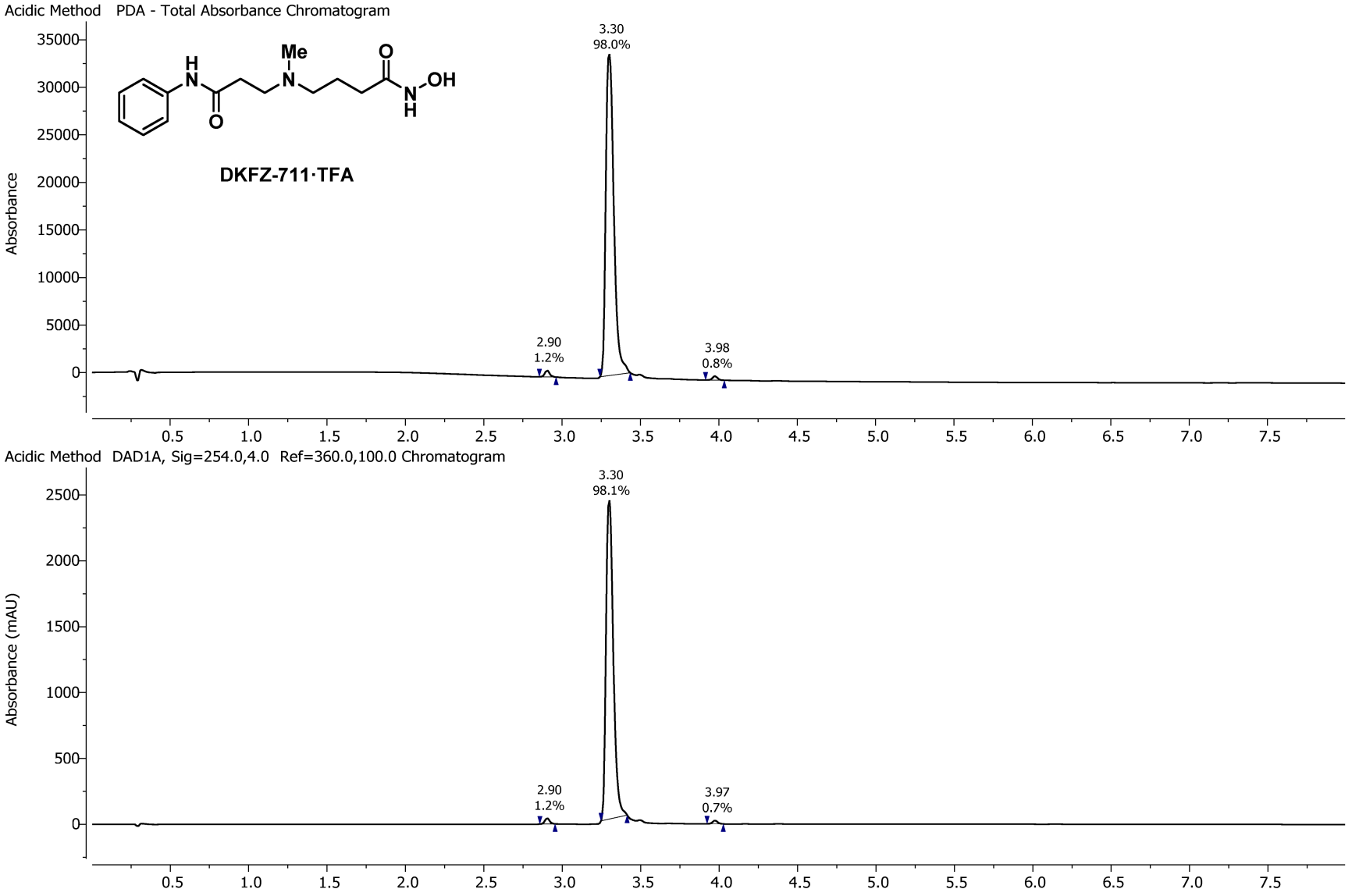
Acidic Method PDA - Total Absorbance Chromatogram
DKFZ-711·TFA
Absorbance
3.30
98.0%
2.90
1.2%
3.98
0.8%
Acidic Method DAD1A, Sig=254.0,4.0 Ref=360.0,100.0 Chromatogram
Absorbance (mAU)
3.30
98.1%
2.90
1.2%
3.97
0.7%

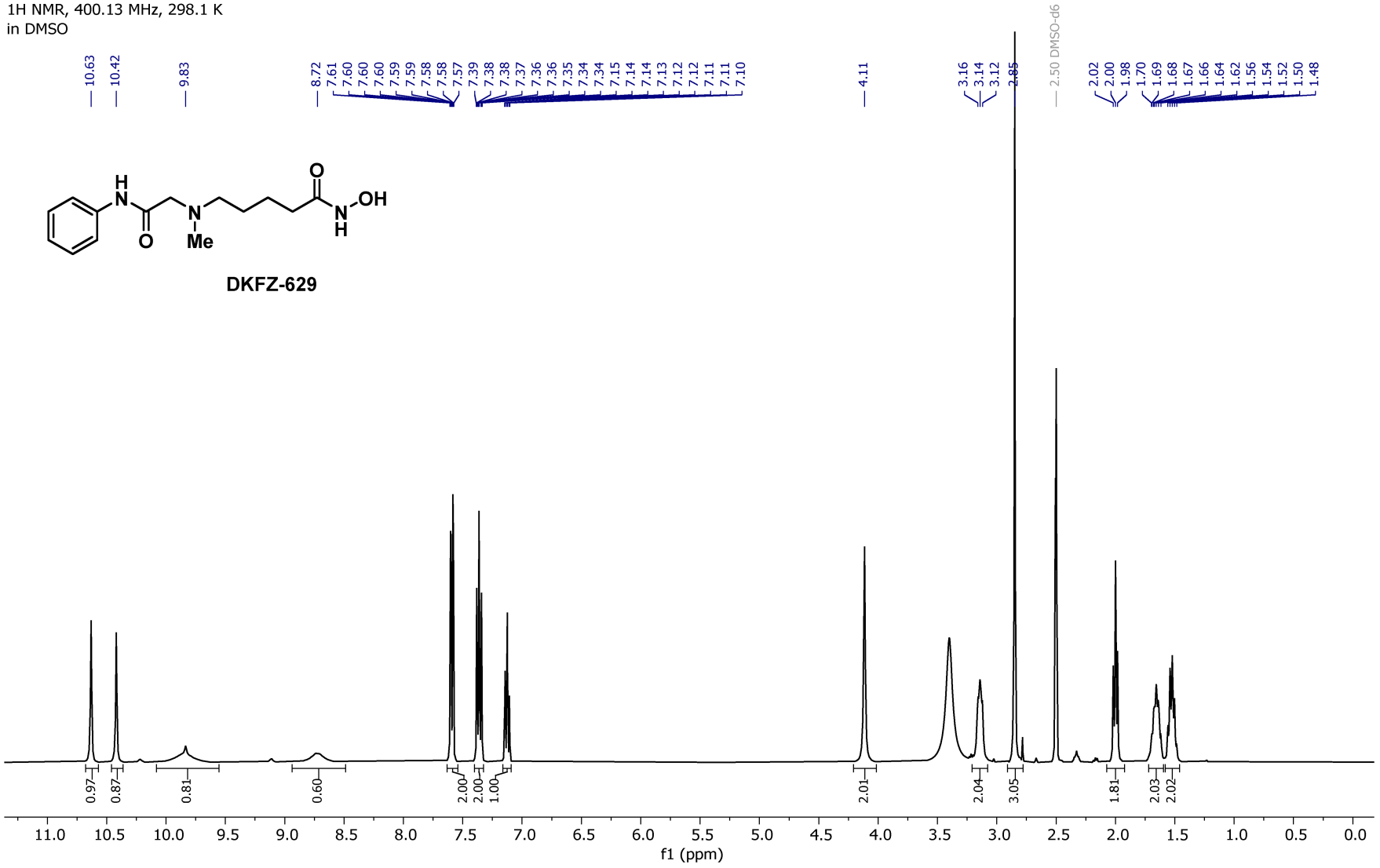
1H NMR, 400.13 MHz, 298.1 K
in DMSO
10.63
10.42
9.83
8.72
7.61
7.60
7.60
7.60
7.59
7.59
7.58
7.58
7.57
7.39
7.38
7.38
7.37
7.36
7.36
7.35
7.34
7.34
7.15
7.14
7.14
7.13
7.12
7.12
7.11
7.11
7.10
4.11
3.16
3.14
3.12
2.85
2.50 DMSO-d6
2.02
2.00
1.98
1.70
1.69
1.68
1.67
1.66
1.64
1.62
1.56
1.54
1.52
1.50
1.48
DKFZ-629
0.97
0.87
0.81
0.60
2.00
2.00
1.00
2.01
2.04
3.05
1.81
2.03
2.02
f1 (ppm)

19F NMR, 376.46 MHz, 298.1 K
in DMSO

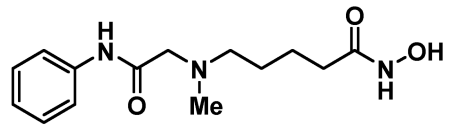


**DKFZ-629**

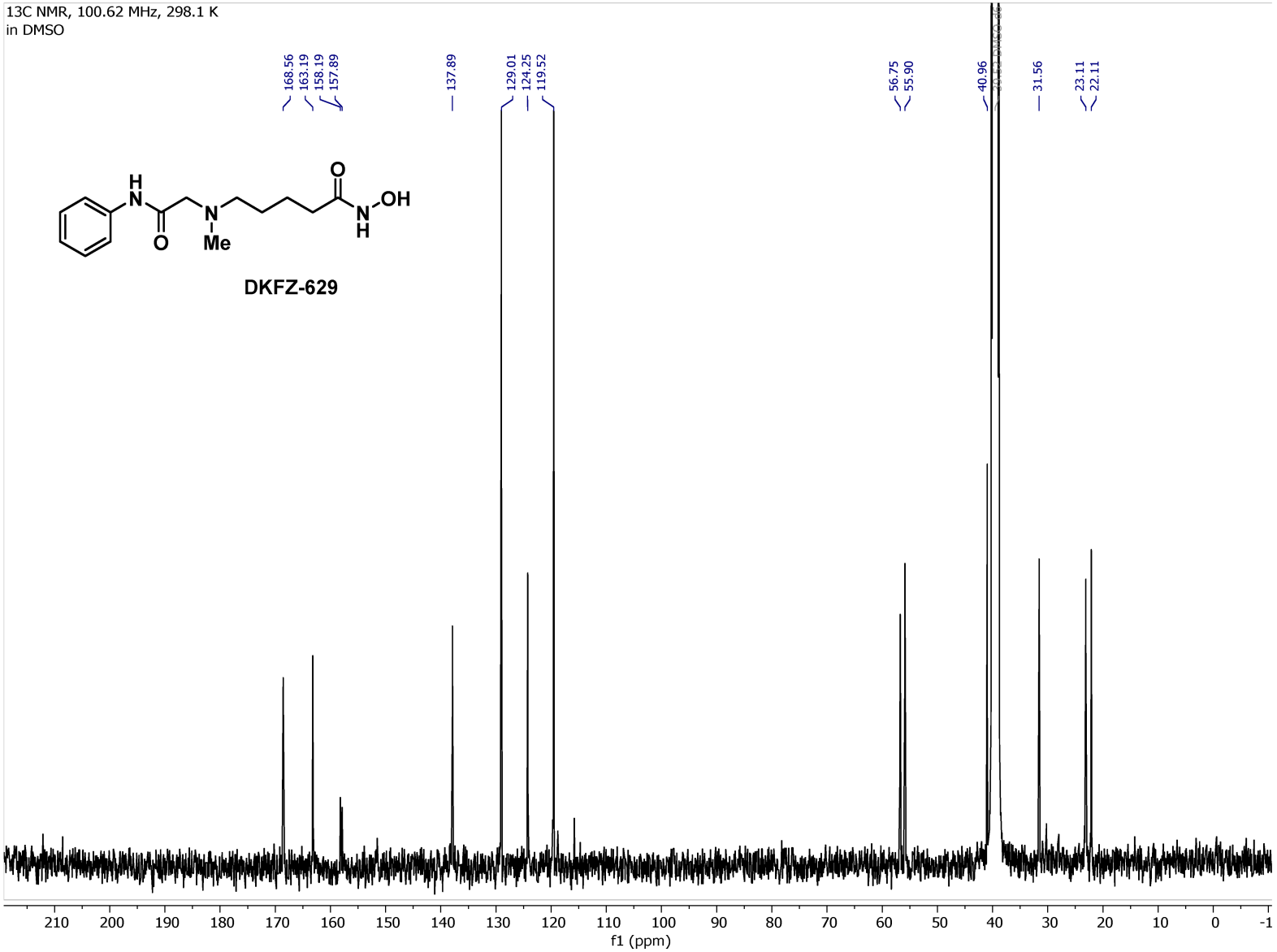
13C NMR, 100.62 MHz, 298.1 K
in DMSO
168.56
163.19
158.19
157.89
137.89
129.01
124.25
119.52
56.75
55.90
40.96
31.56
23.11
22.11
DKFZ-629
f1 (ppm)

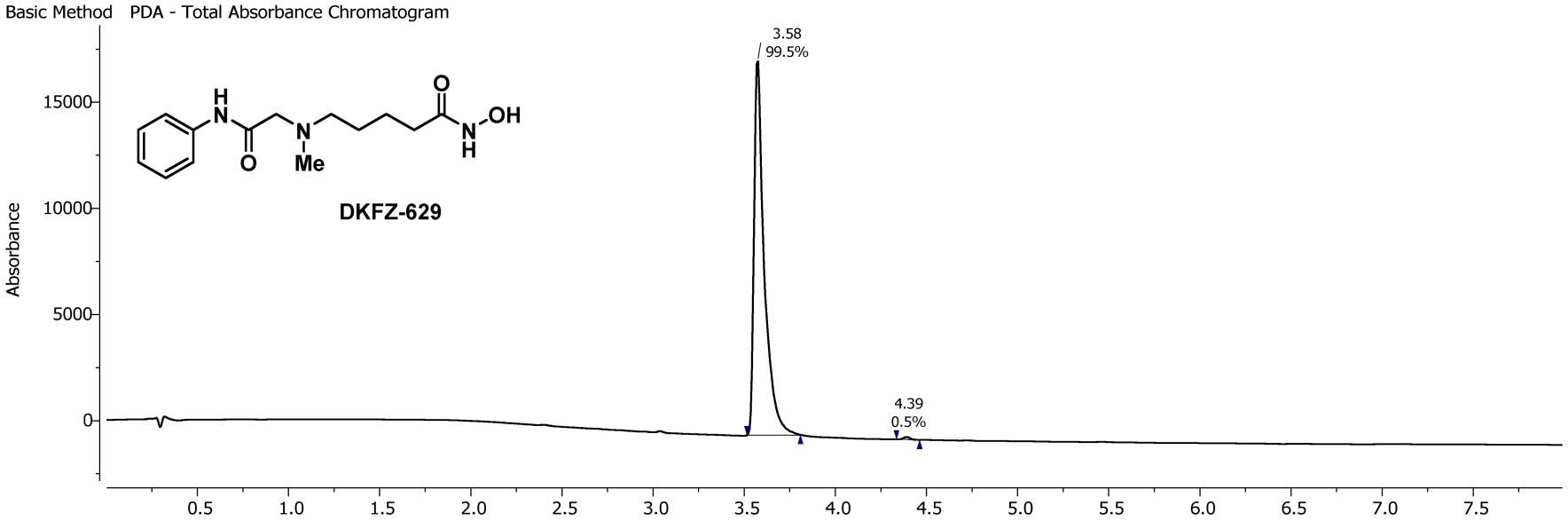
Basic Method PDA - Total Absorbance Chromatogram
3.58
99.5%
4.39
0.5%
Absorbance
15000
10000
5000
0
0.5
1.0
1.5
2.0
2.5
3.0
3.5
4.0
4.5
5.0
5.5
6.0
6.5
7.0
7.5
DKFZ-629

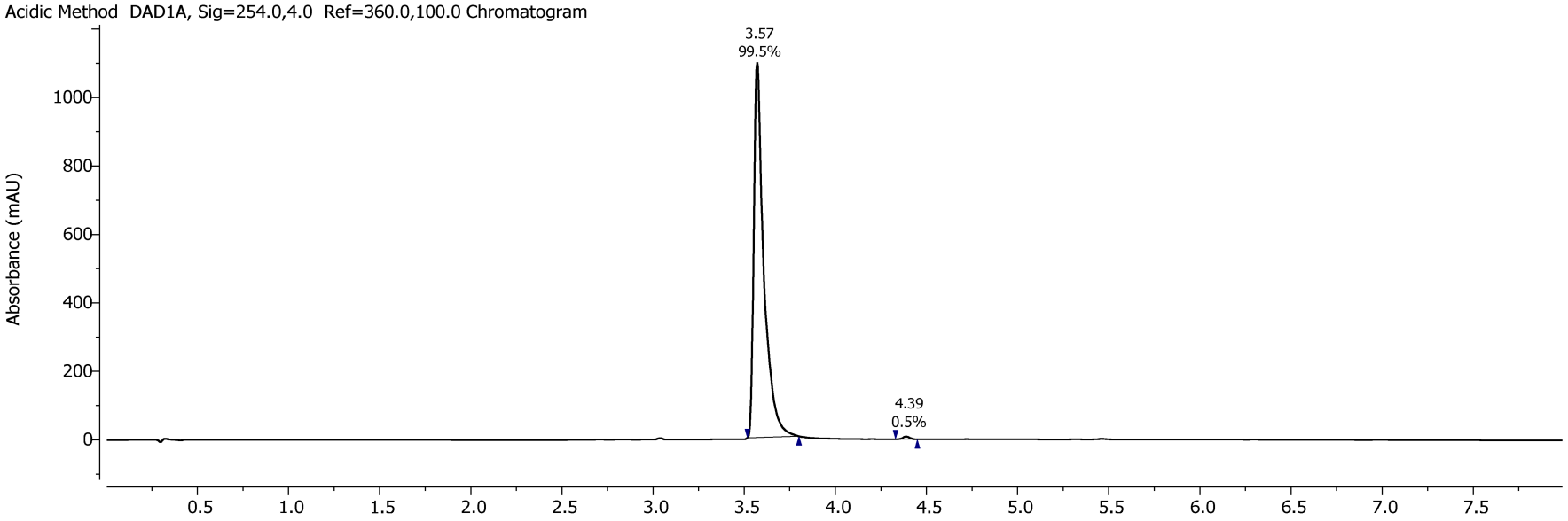
Acidic Method DAD1A, Sig=254.0,4.0 Ref=360.0,100.0 Chromatogram
3.57
99.5%
4.39
0.5%
Absorbance (mAU)
1000
800
600
400
200
0
0.5
1.0
1.5
2.0
2.5
3.0
3.5
4.0
4.5
5.0
5.5
6.0
6.5
7.0
7.5

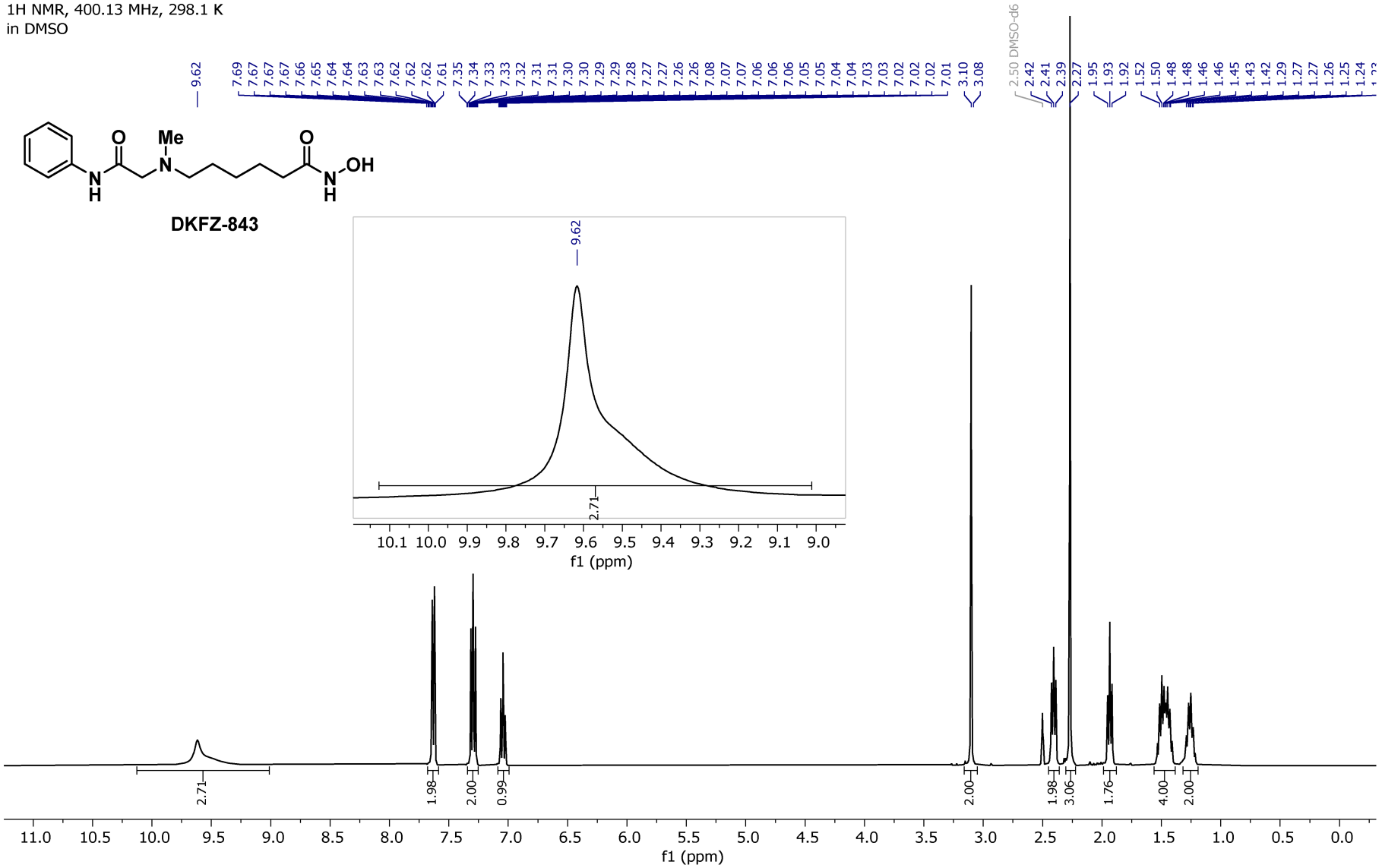
1H NMR, 400.13 MHz, 298.1 K
in DMSO
DKFZ-843
f1 (ppm)

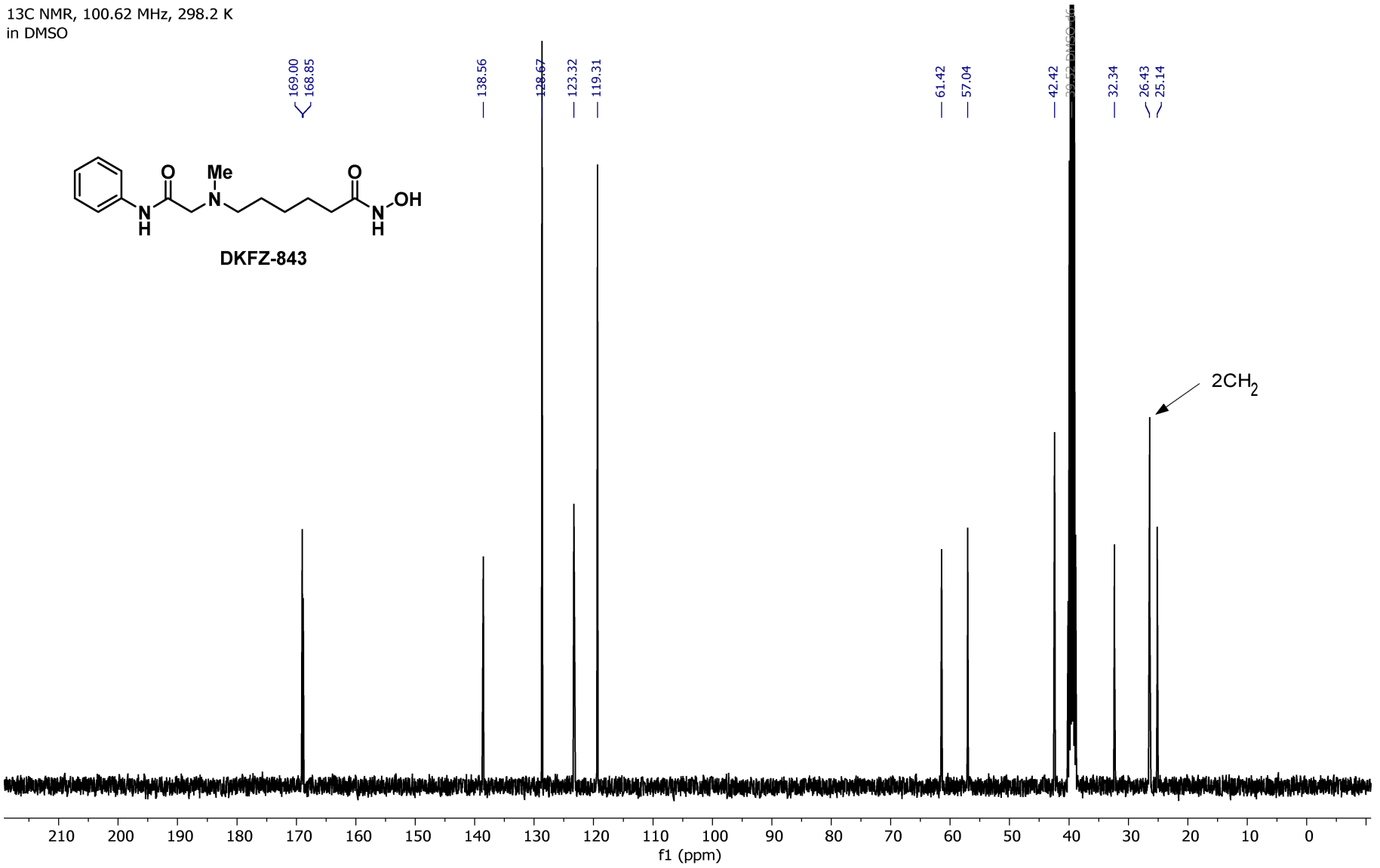
13C NMR, 100.62 MHz, 298.2 K
in DMSO
169.00
168.85
138.56
128.67
123.32
119.31
61.42
57.04
42.42
32.34
26.43
25.14
2CH2
DKFZ-843
f1 (ppm)

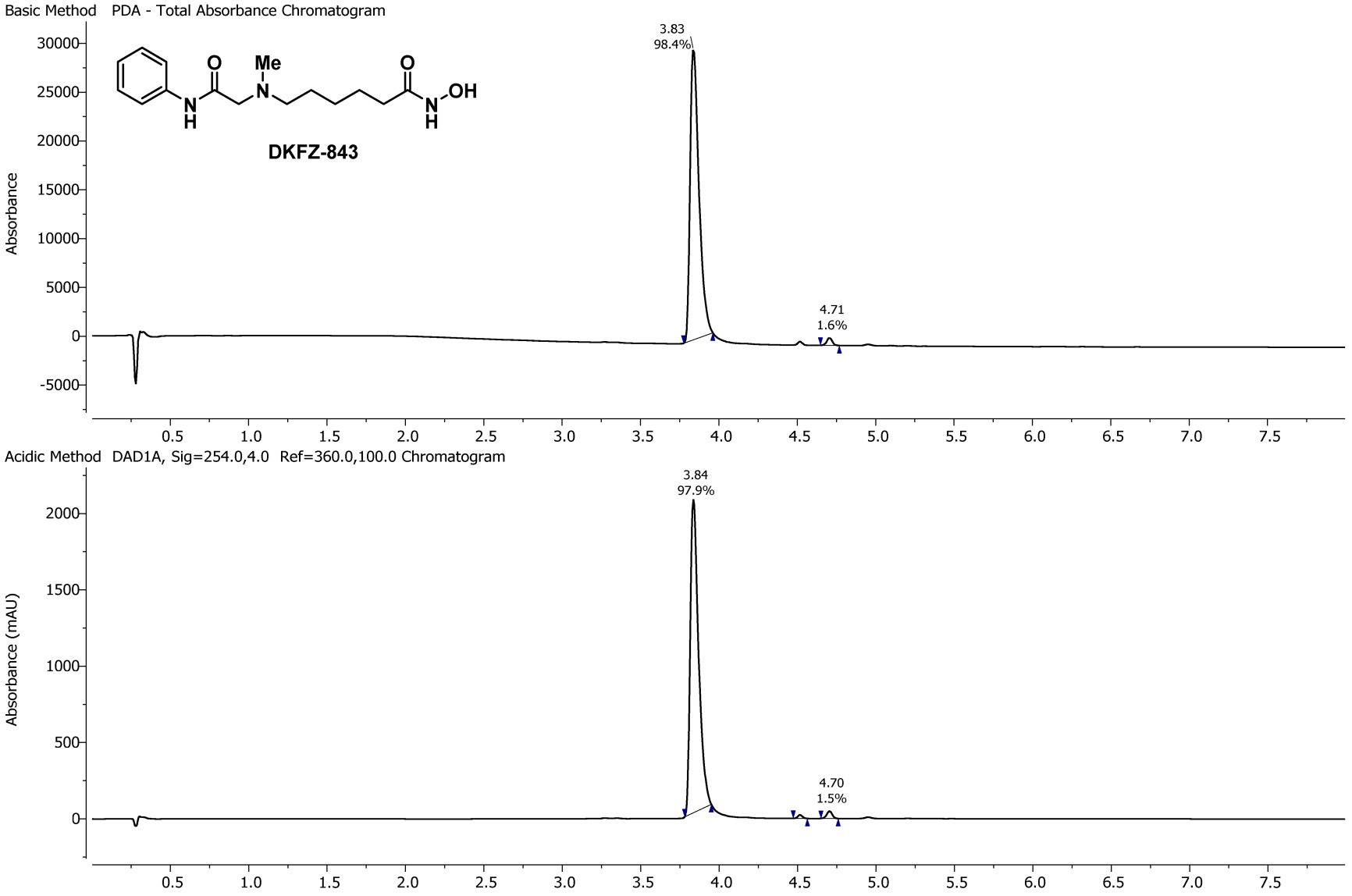
Basic Method PDA - Total Absorbance Chromatogram
Absorbance
3.83
98.4%
4.71
1.6%
DKFZ-843
Acidic Method DAD1A, Sig=254.0,4.0 Ref=360.0,100.0 Chromatogram
Absorbance (mAU)
3.84
97.9%
4.70
1.5%

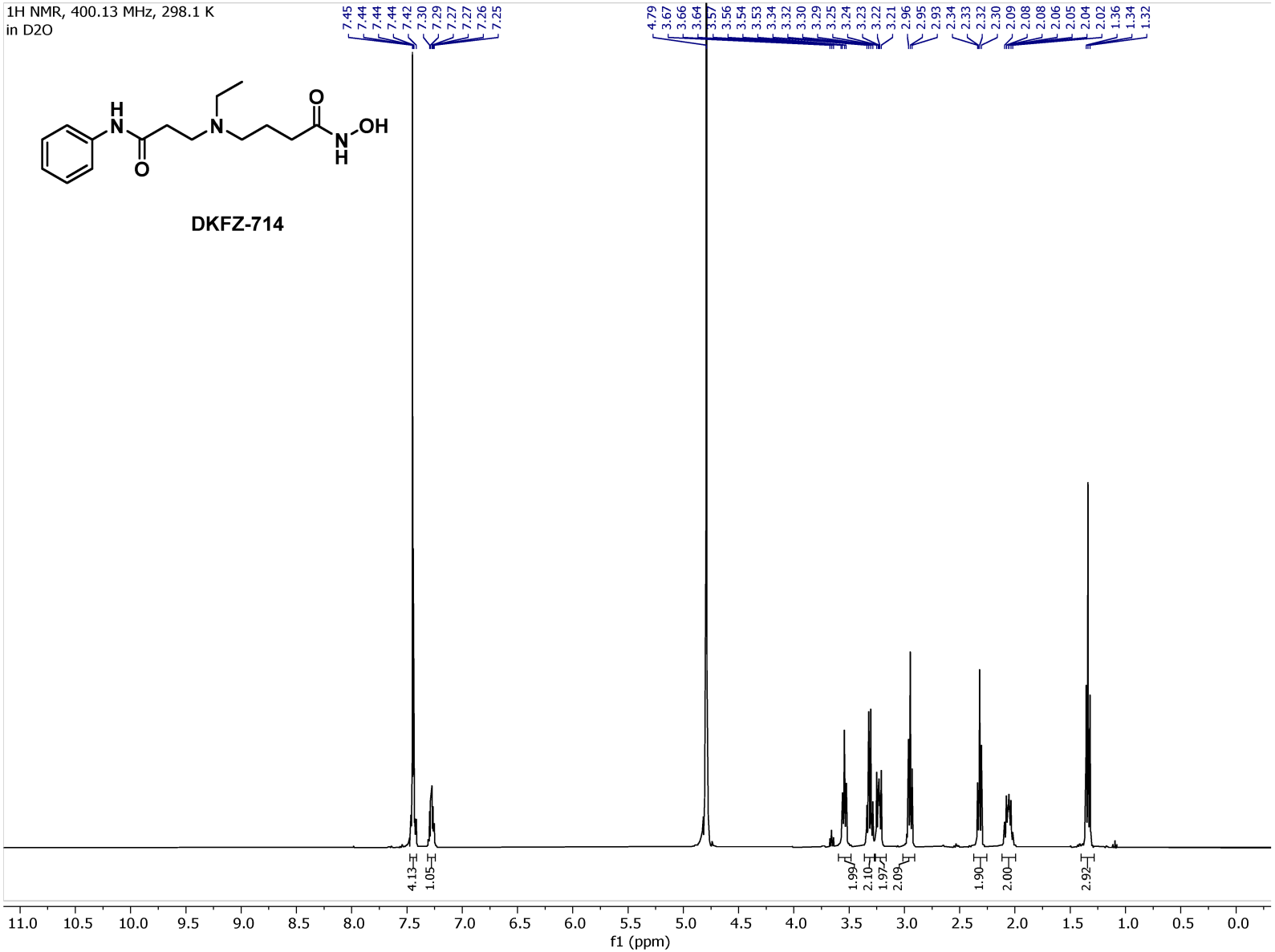
1H NMR, 400.13 MHz, 298.1 K
in D2O
DKFZ-714
7.45 7.44 7.44 7.44 7.42 7.30 7.29 7.27 7.27 7.26 7.25
4.79 3.67 3.66 3.64 3.57 3.56 3.54 3.53 3.34 3.32 3.30 3.29 3.25 3.24 3.23 3.22 3.21 2.96 2.95 2.93 2.34 2.33 2.32 2.30 2.09 2.08 2.08 2.06 2.05 2.04 2.02 1.36 1.34 1.32
4.13
1.05
1.99
2.10
1.97
2.09
1.90
2.00
2.92
11.0 10.5 10.0 9.5 9.0 8.5 8.0 7.5 7.0 6.5 6.0 5.5 5.0 4.5 4.0 3.5 3.0 2.5 2.0 1.5 1.0 0.5 0.0
f1 (ppm)

19F NMR, 376.23 MHz, 295.7 K
in D2O

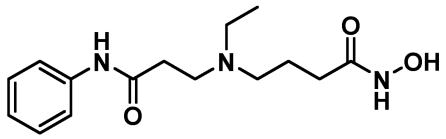


**DKFZ-714**

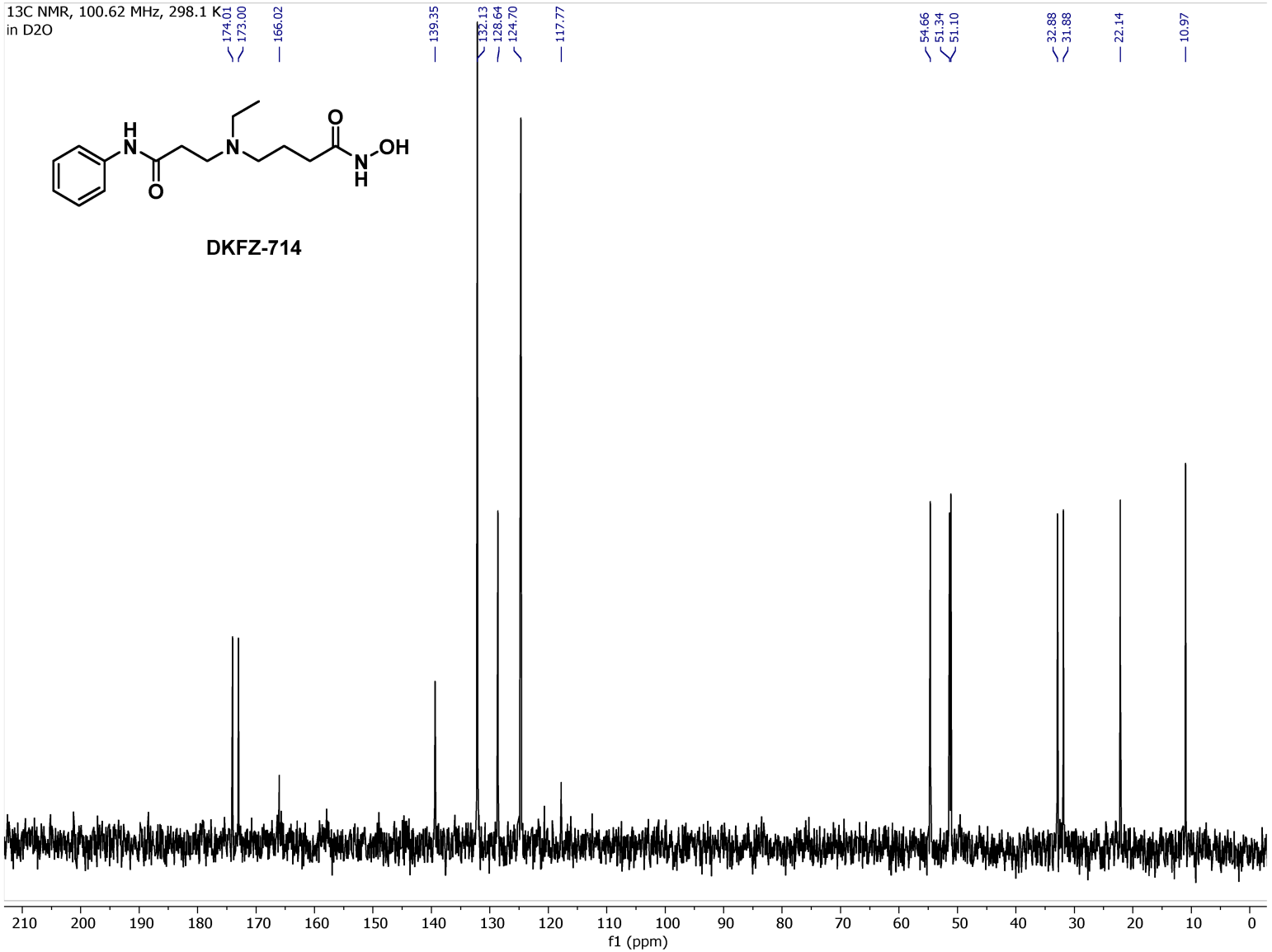
13C NMR, 100.62 MHz, 298.1 K
in D2O
174.01
173.00
166.02
139.35
132.13
128.64
124.70
117.77
54.66
51.34
51.10
32.88
31.88
22.14
10.97
DKFZ-714
f1 (ppm)

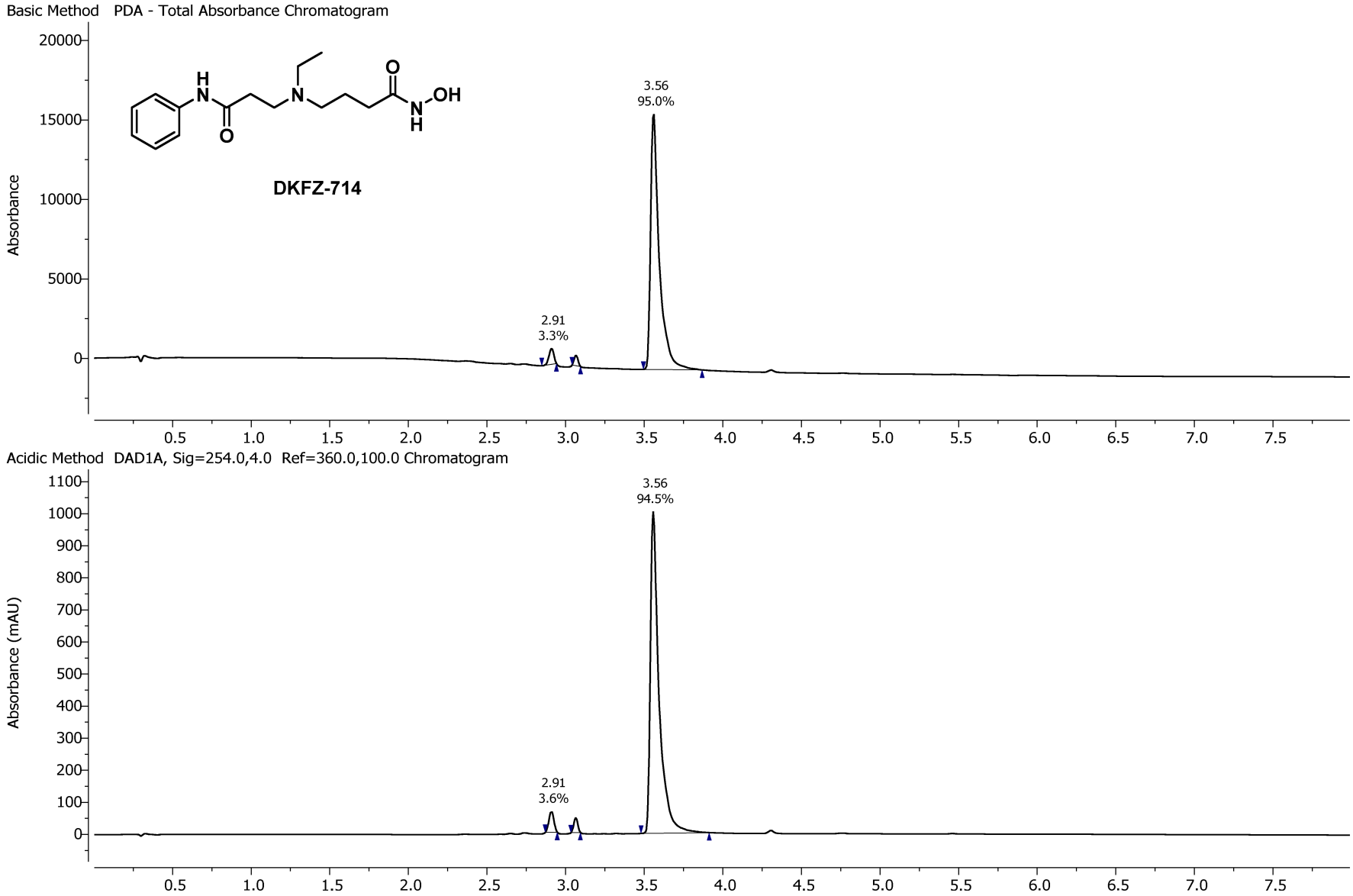
Basic Method PDA - Total Absorbance Chromatogram
Absorbance
20000
15000
10000
5000
0
DKFZ-714
3.56
95.0%
2.91
3.3%
0.5
1.0
1.5
2.0
2.5
3.0
3.5
4.0
4.5
5.0
5.5
6.0
6.5
7.0
7.5
Acidic Method DAD1A, Sig=254.0,4.0 Ref=360.0,100.0 Chromatogram
Absorbance (mAU)
1100
1000
900
800
700
600
500
400
300
200
100
0
3.56
94.5%
2.91
3.6%
0.5
1.0
1.5
2.0
2.5
3.0
3.5
4.0
4.5
5.0
5.5
6.0
6.5
7.0
7.5

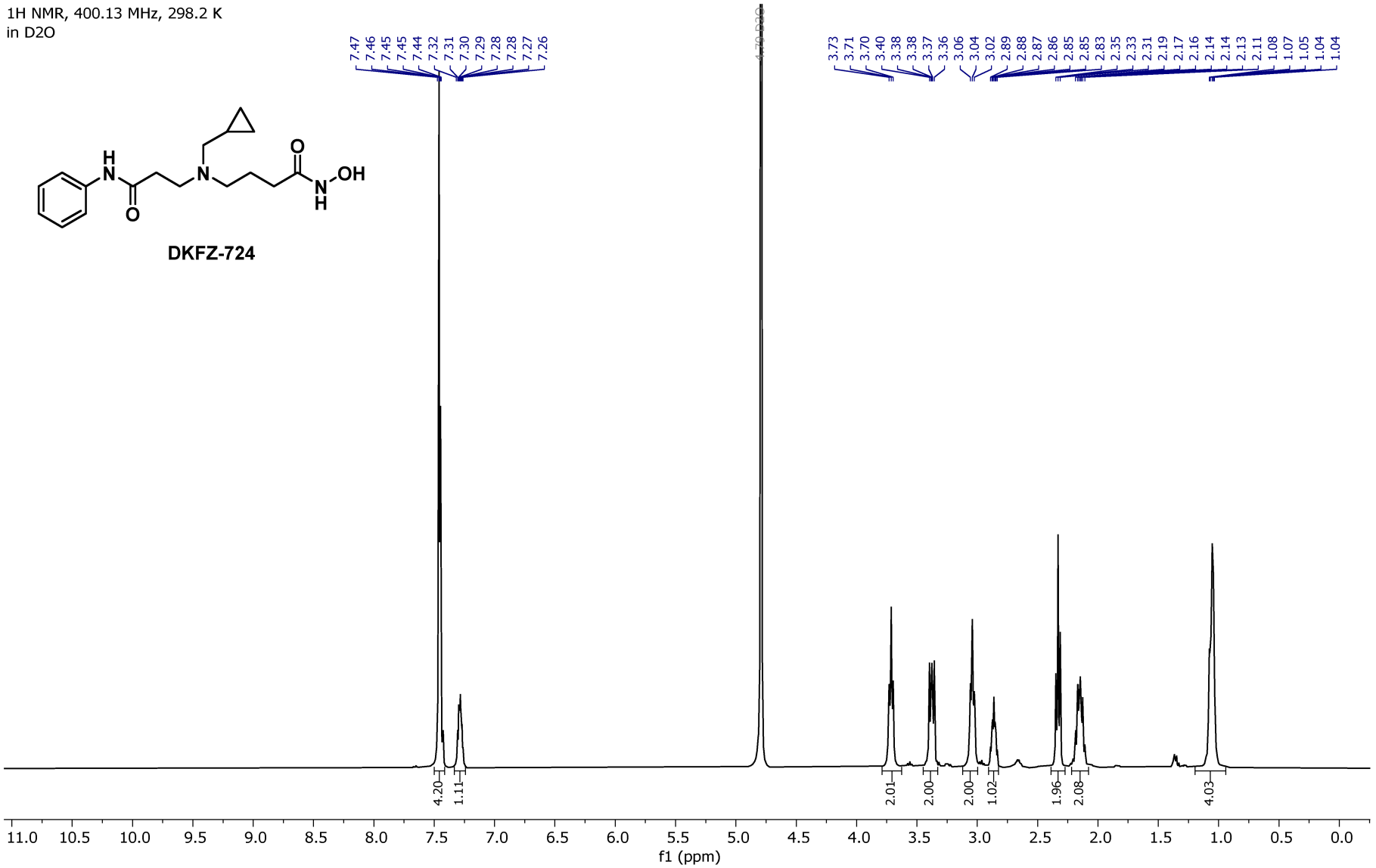
1H NMR, 400.13 MHz, 298.2 K
in D2O
DKFZ-724
7.47
7.46
7.45
7.45
7.44
7.32
7.31
7.30
7.29
7.28
7.28
7.27
7.26
4.70
3.73
3.71
3.70
3.40
3.38
3.38
3.37
3.36
3.06
3.04
3.02
2.89
2.88
2.87
2.86
2.85
2.85
2.83
2.35
2.33
2.31
2.19
2.17
2.16
2.14
2.14
2.13
2.11
1.08
1.07
1.05
1.04
1.04
4.20
1.11
2.01
2.00
2.00
1.02
1.96
2.08
4.03
11.0
10.5
10.0
9.5
9.0
8.5
8.0
7.5
7.0
6.5
6.0
5.5
5.0
4.5
4.0
3.5
3.0
2.5
2.0
1.5
1.0
0.5
0.0
f1 (ppm)

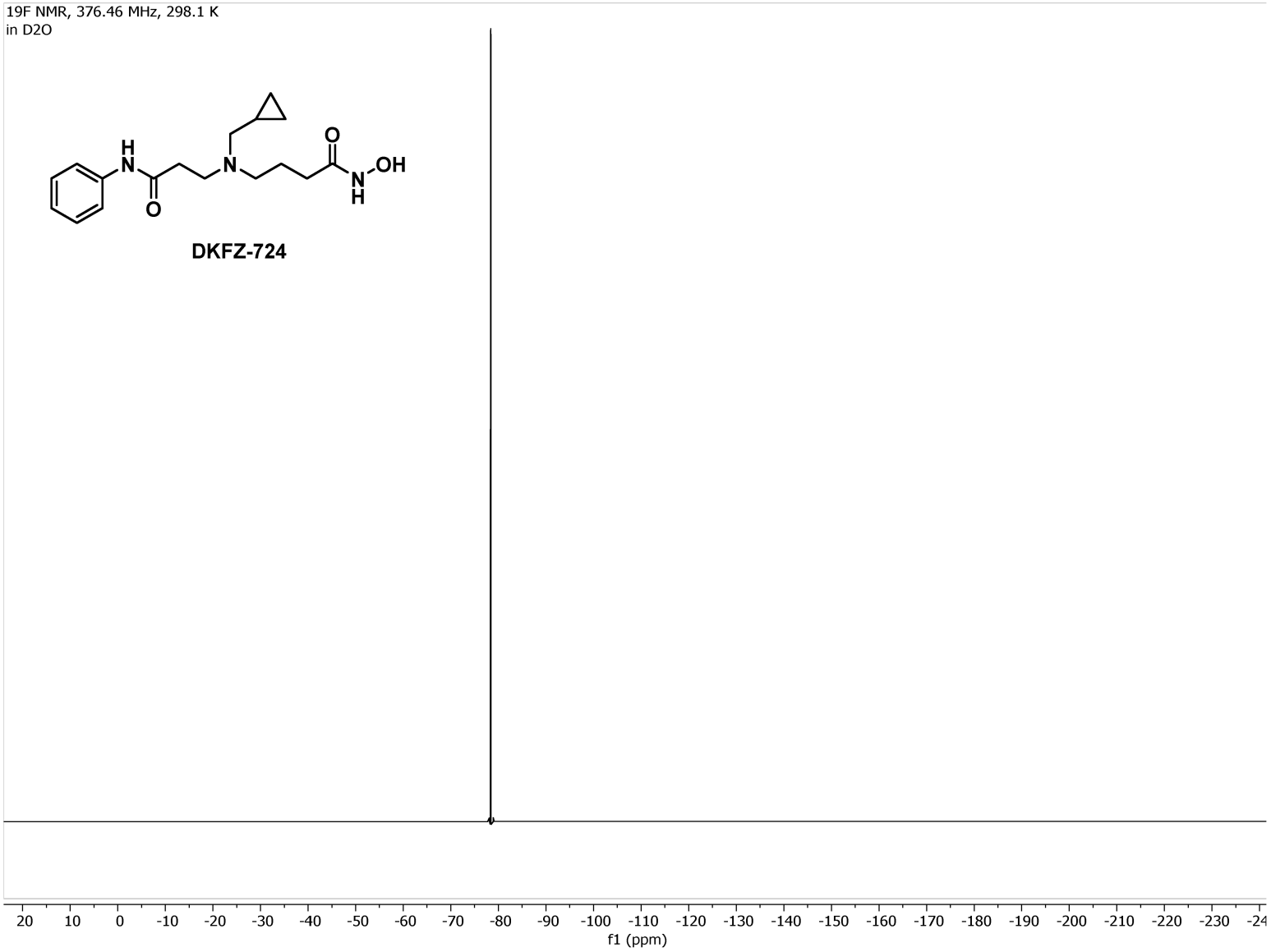
19F NMR, 376.46 MHz, 298.1 K
in D2O
H
N
O
N
O
N
H
OH
DKFZ-724
20 10 0 -10 -20 -30 -40 -50 -60 -70 -80 -90 -100 -110 -120 -130 -140 -150 -160 -170 -180 -190 -200 -210 -220 -230 -24
f1 (ppm)

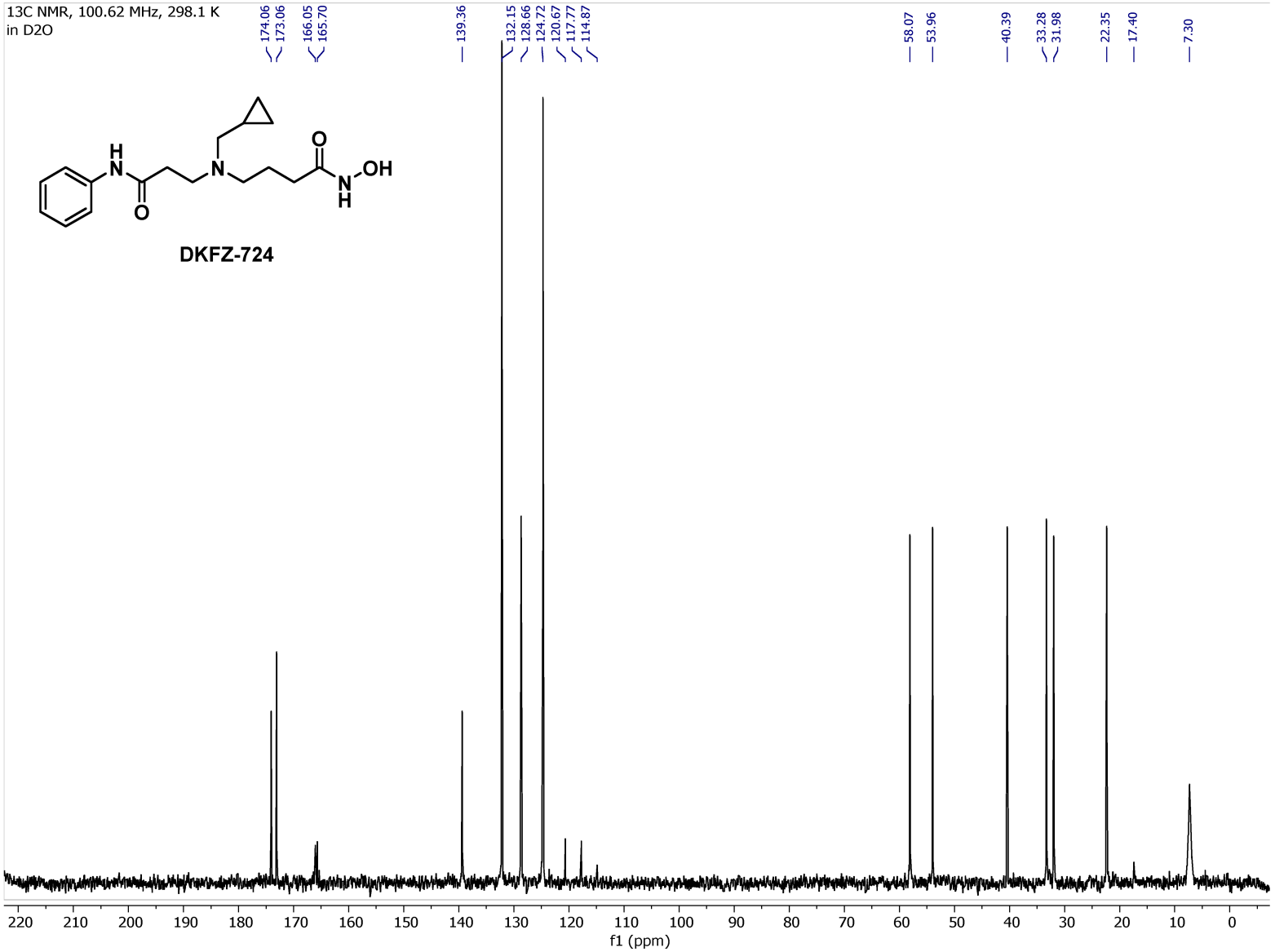
13C NMR, 100.62 MHz, 298.1 K
in D2O
174.06
173.06
166.05
165.70
139.36
132.15
128.66
124.72
120.67
117.77
114.87
58.07
53.96
40.39
33.28
31.98
22.35
17.40
7.30
DKFZ-724
f1 (ppm)

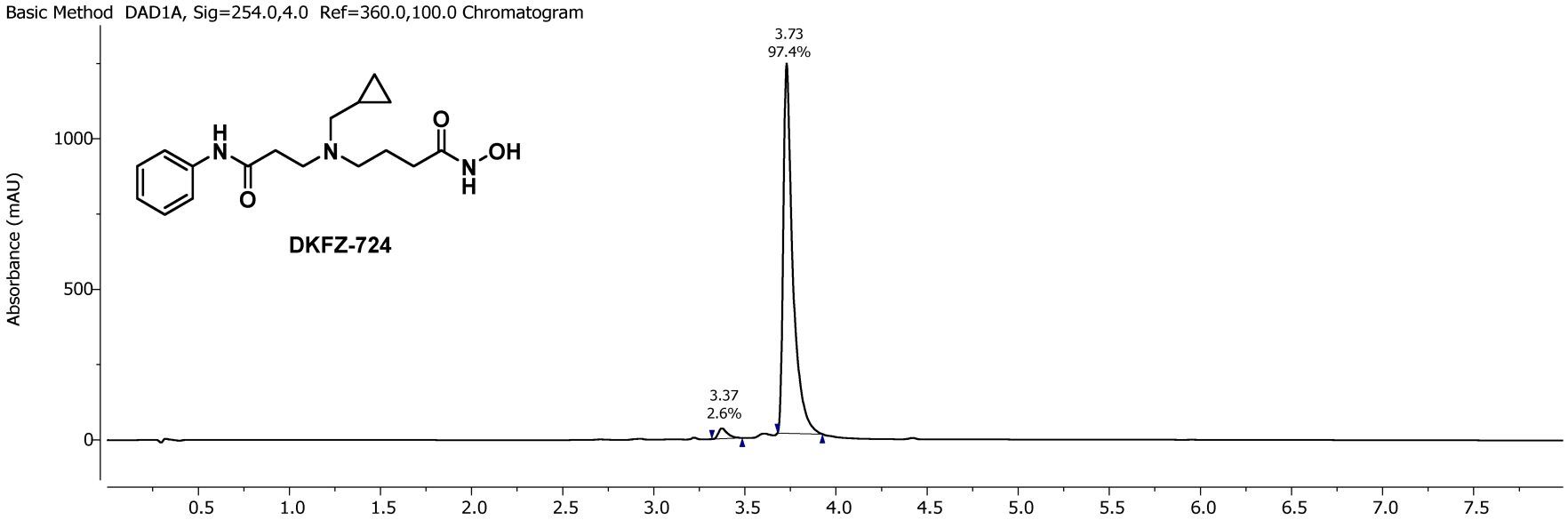
Basic Method DAD1A, Sig=254.0,4.0 Ref=360.0,100.0 Chromatogram
Absorbance (mAU)
1000
500
0
3.73
97.4%
3.37
2.6%
DKFZ-724
0.5
1.0
1.5
2.0
2.5
3.0
3.5
4.0
4.5
5.0
5.5
6.0
6.5
7.0
7.5

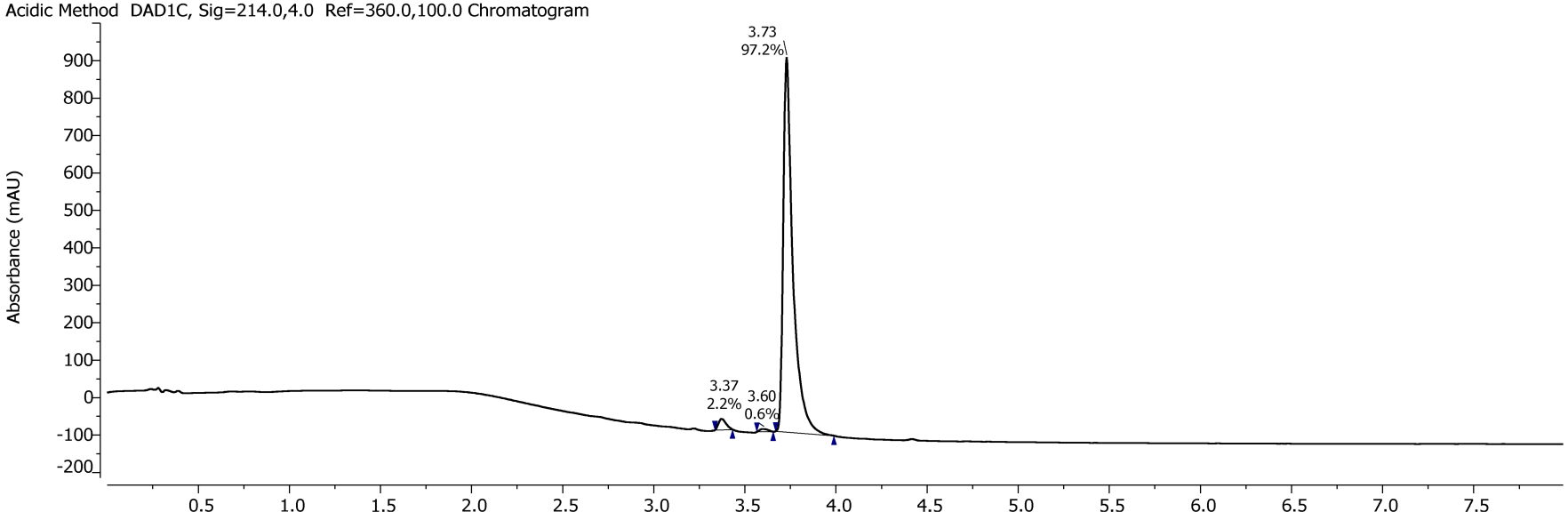
Acidic Method DAD1C, Sig=214.0,4.0 Ref=360.0,100.0 Chromatogram
Absorbance (mAU)
900
800
700
600
500
400
300
200
100
0
-100
-200
3.73
97.2%
3.37
2.2%
3.60
0.6%
0.5
1.0
1.5
2.0
2.5
3.0
3.5
4.0
4.5
5.0
5.5
6.0
6.5
7.0
7.5

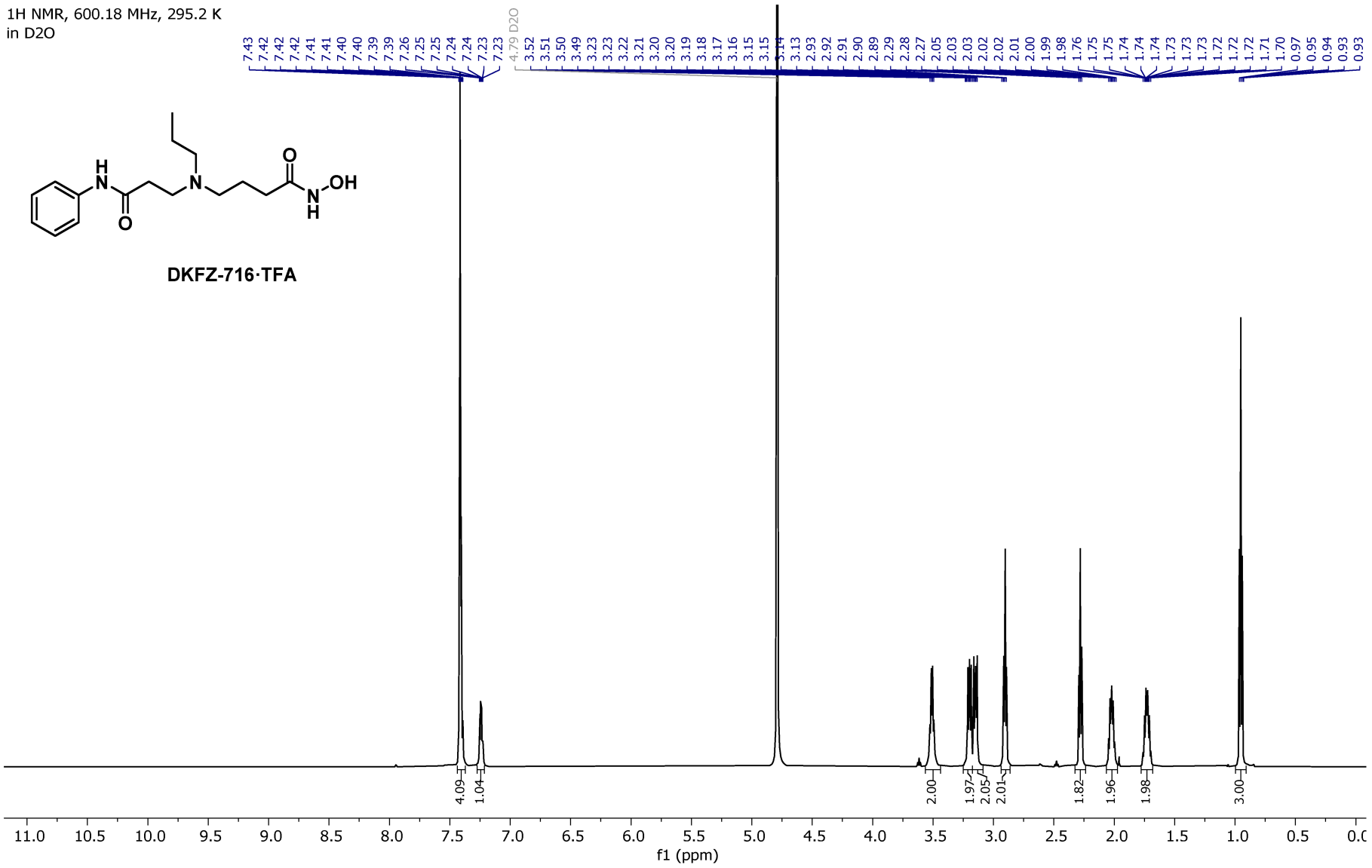
1H NMR, 600.18 MHz, 295.2 K
in D2O
DKFZ-716·TFA
f1 (ppm)

19F NMR, 376.23 MHz, 295.6 K
in D2O

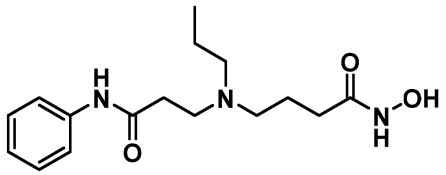


**DKFZ-716·TFA**

13C NMR, 150.93 MHz, 295.2 K
in D2O

171.05
170.09
163.28
163.05
162.81
162.58
136.41
129.20
125.70
121.75
119.19
117.26
115.32
113.39
54.85
52.25
48.72
29.86
28.93
19.12
16.81
9.97

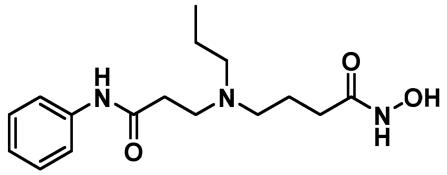


**DKFZ-716·TFA**

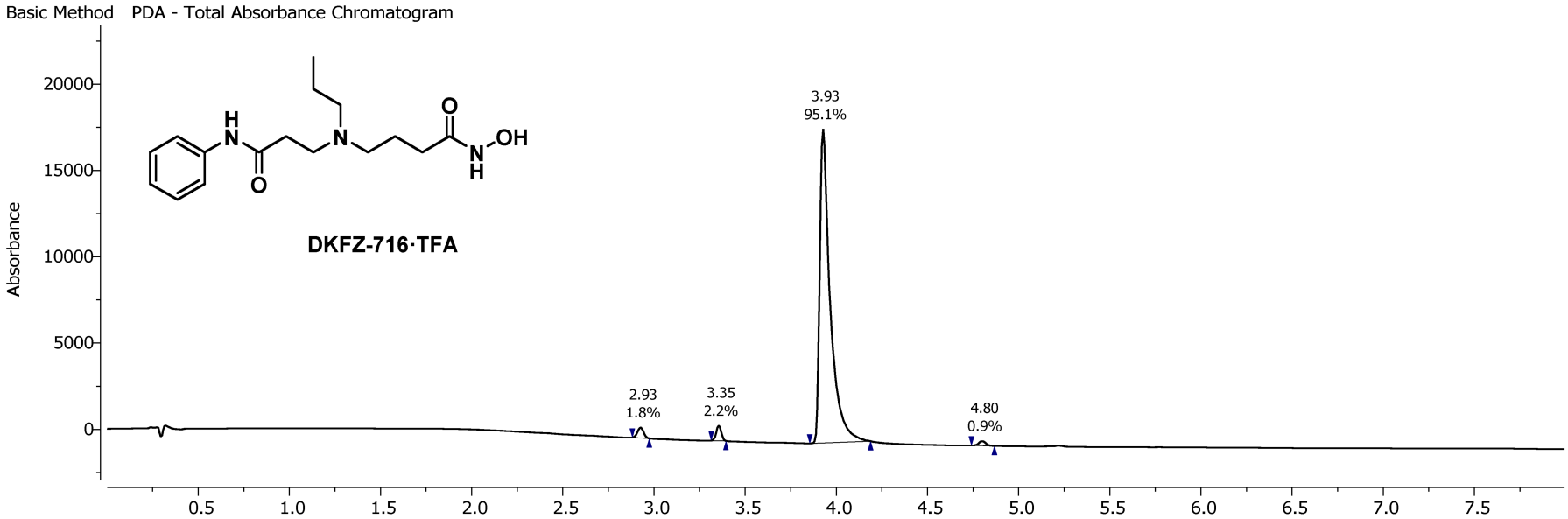
Basic Method PDA - Total Absorbance Chromatogram
Absorbance
20000
15000
10000
5000
0
DKFZ-716·TFA
3.93
95.1%
2.93
1.8%
3.35
2.2%
4.80
0.9%
0.5
1.0
1.5
2.0
2.5
3.0
3.5
4.0
4.5
5.0
5.5
6.0
6.5
7.0
7.5

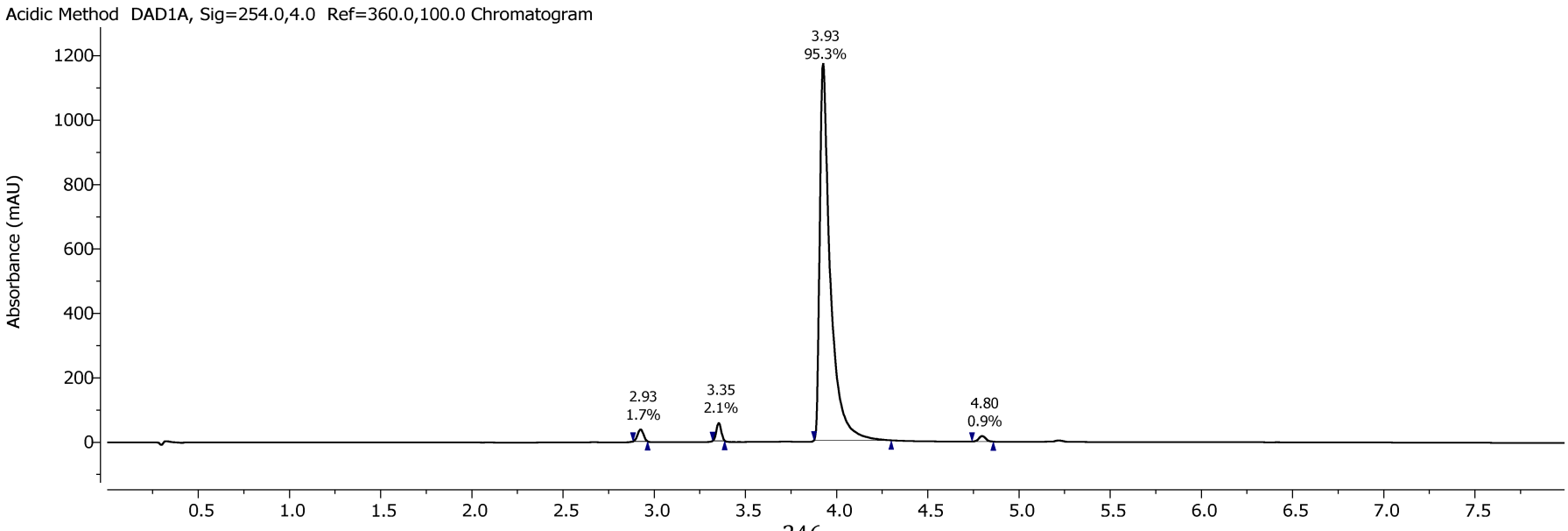
Acidic Method DAD1A, Sig=254.0,4.0 Ref=360.0,100.0 Chromatogram
Absorbance (mAU)
1200
1000
800
600
400
200
0
3.93
95.3%
2.93
1.7%
3.35
2.1%
4.80
0.9%
0.5
1.0
1.5
2.0
2.5
3.0
3.5
4.0
4.5
5.0
5.5
6.0
6.5
7.0
7.5

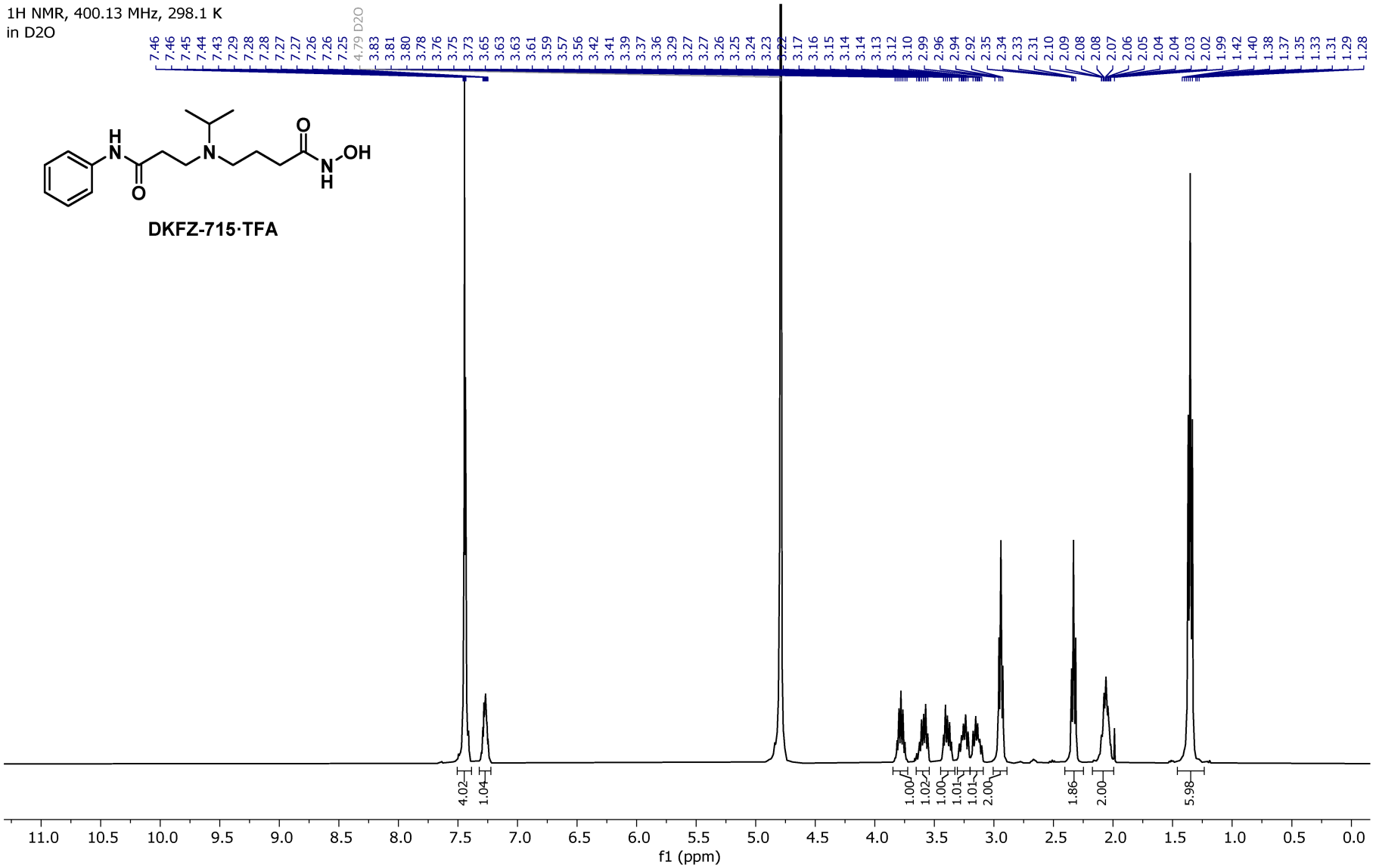
1H NMR, 400.13 MHz, 298.1 K
in D2O
DKFZ-715·TFA
f1 (ppm)

19F NMR, 376.46 MHz, 298.1 K
in D2O

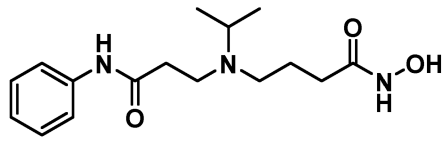


DKFZ-715·TFA

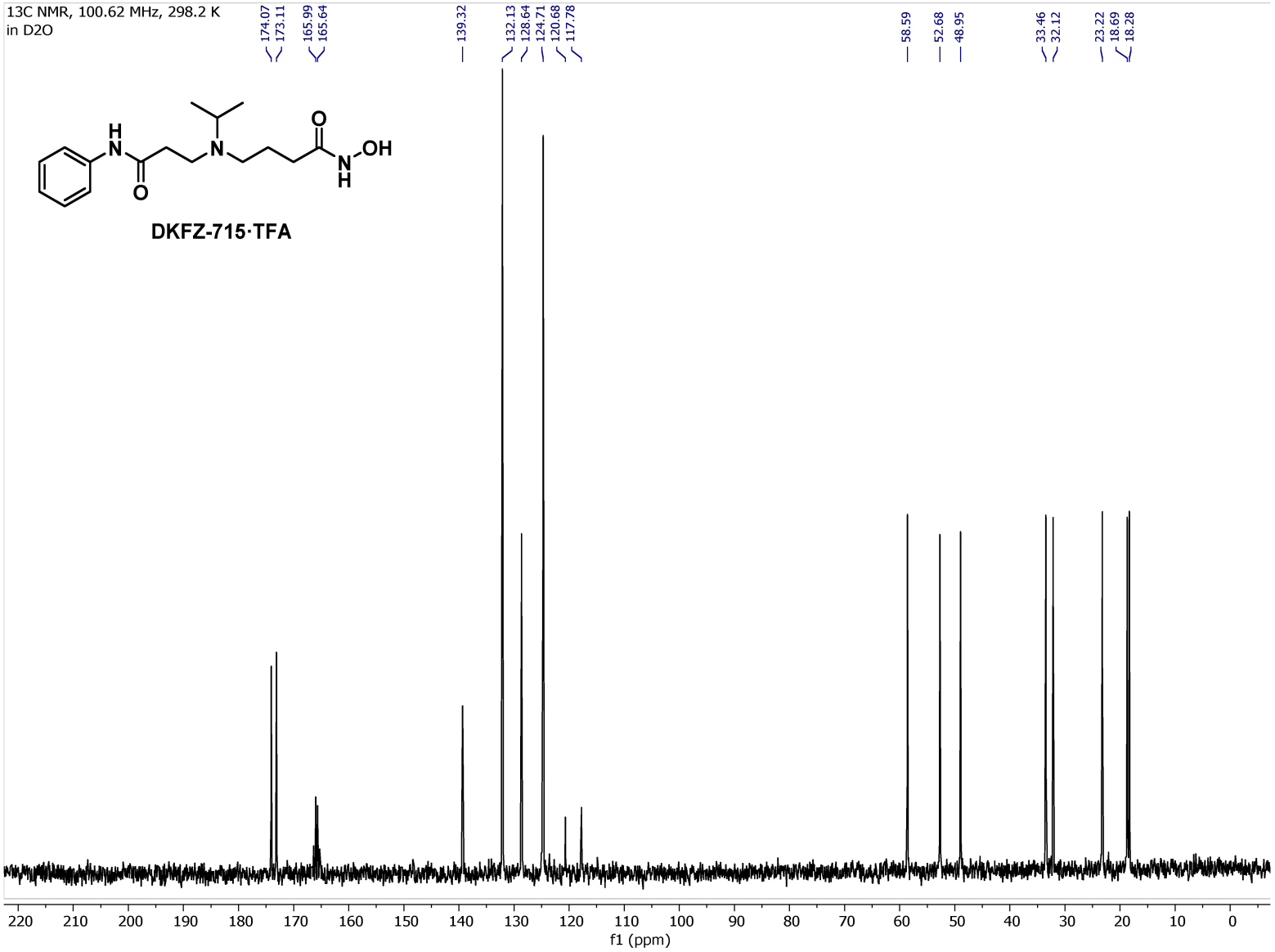
13C NMR, 100.62 MHz, 298.2 K
in D2O
174.07
173.11
165.99
165.64
139.32
132.13
128.64
124.71
120.68
117.78
58.59
52.68
48.95
33.46
32.12
23.22
18.69
18.28
DKFZ-715·TFA
220 210 200 190 180 170 160 150 140 130 120 110 100 90 80 70 60 50 40 30 20 10 0
f1 (ppm)

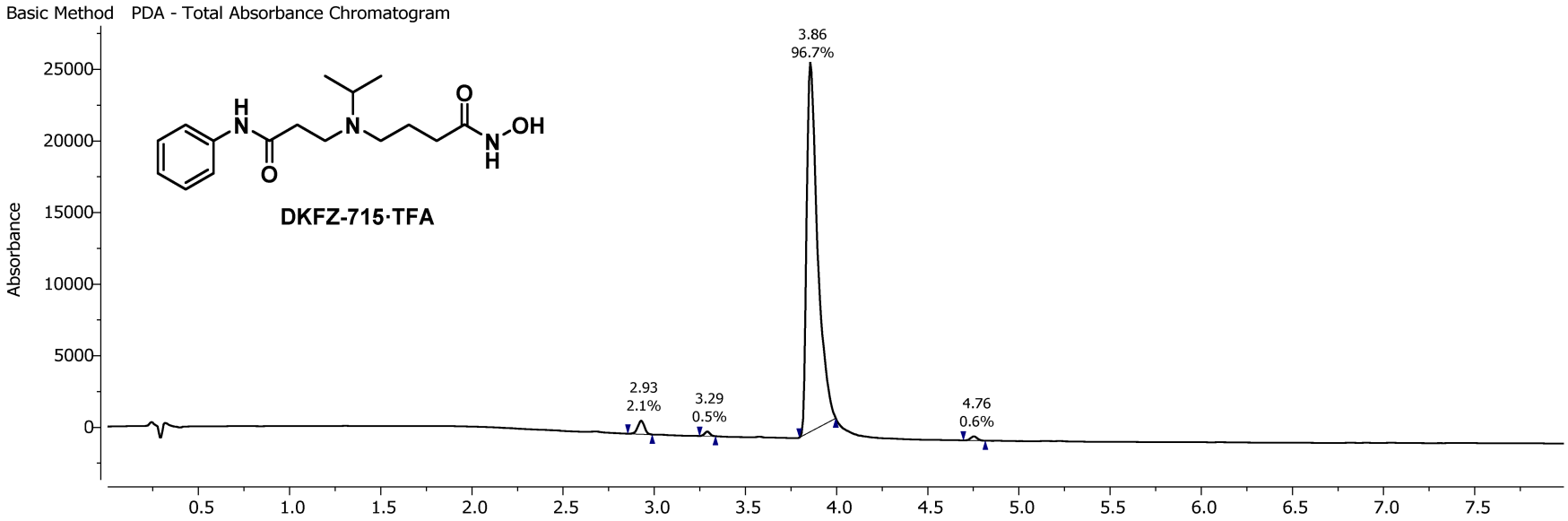
Basic Method PDA - Total Absorbance Chromatogram
Absorbance
25000
20000
15000
10000
5000
0
3.86
96.7%
2.93
2.1%
3.29
0.5%
4.76
0.6%
0.5
1.0
1.5
2.0
2.5
3.0
3.5
4.0
4.5
5.0
5.5
6.0
6.5
7.0
7.5
DKFZ-715·TFA

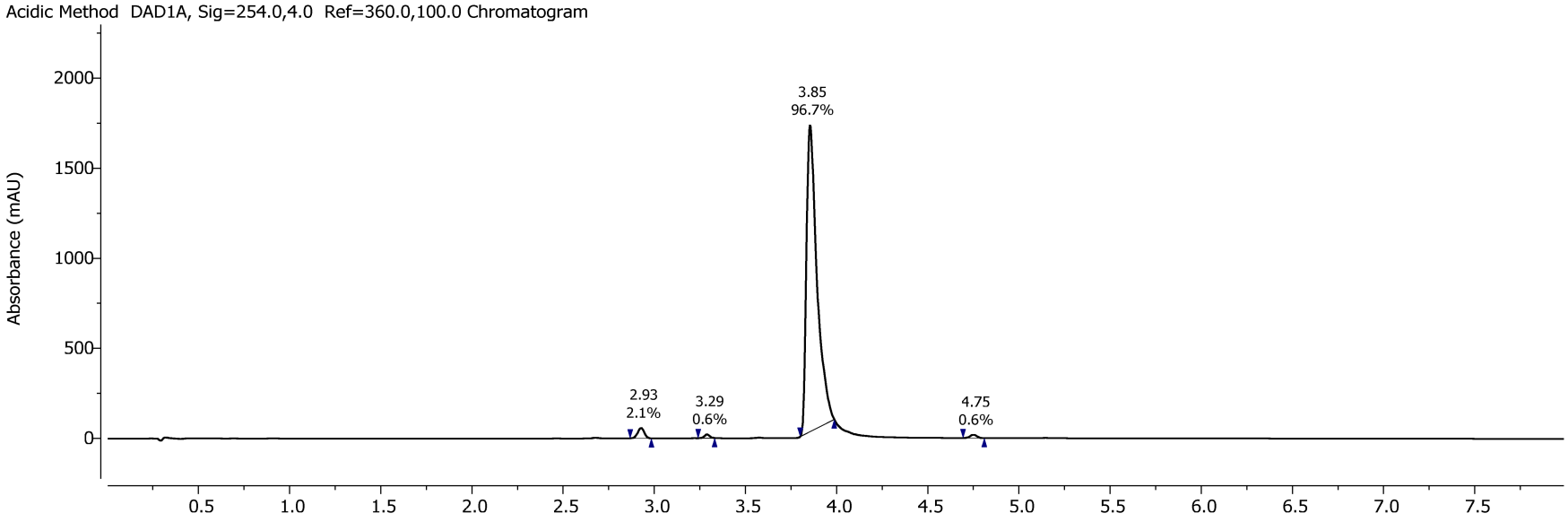
Acidic Method DAD1A, Sig=254.0,4.0 Ref=360.0,100.0 Chromatogram
Absorbance (mAU)
2000
1500
1000
500
0
3.85
96.7%
2.93
2.1%
3.29
0.6%
4.75
0.6%
0.5
1.0
1.5
2.0
2.5
3.0
3.5
4.0
4.5
5.0
5.5
6.0
6.5
7.0
7.5

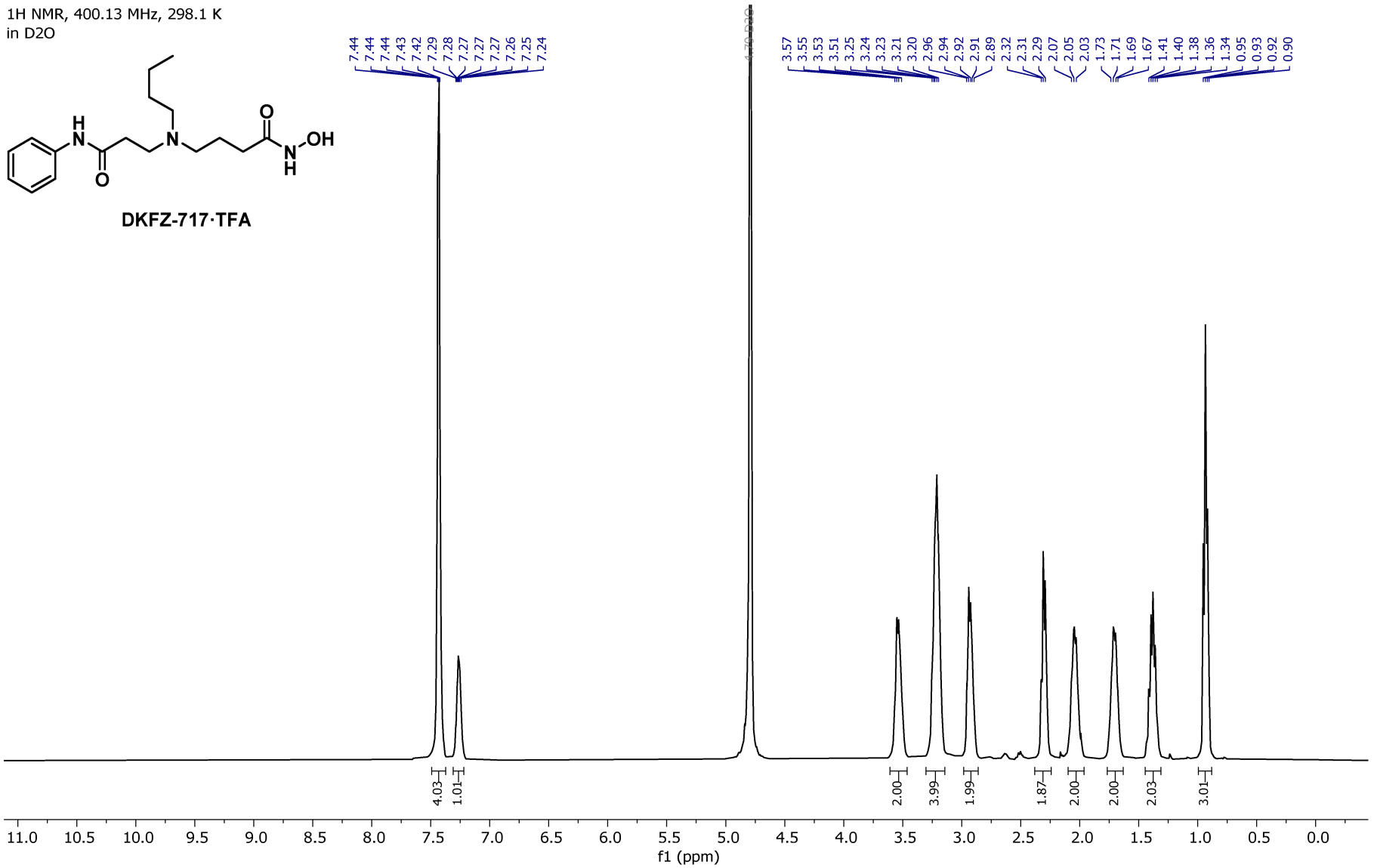
1H NMR, 400.13 MHz, 298.1 K
in D2O
DKFZ-717·TFA
7.44
7.44
7.44
7.43
7.42
7.29
7.28
7.27
7.27
7.27
7.26
7.25
7.24
4.70 D2O
3.57
3.55
3.53
3.51
3.25
3.24
3.23
3.21
3.20
2.96
2.94
2.92
2.91
2.89
2.32
2.31
2.29
2.07
2.05
2.03
1.73
1.71
1.69
1.67
1.41
1.40
1.38
1.36
1.34
0.95
0.93
0.92
0.90
4.03
1.01
2.00
3.99
1.99
1.87
2.00
2.00
2.03
3.01
11.0
10.5
10.0
9.5
9.0
8.5
8.0
7.5
7.0
6.5
6.0
5.5
5.0
4.5
4.0
3.5
3.0
2.5
2.0
1.5
1.0
0.5
0.0
f1 (ppm)

19F NMR, 376.23 MHz, 295.7 K
in D2O

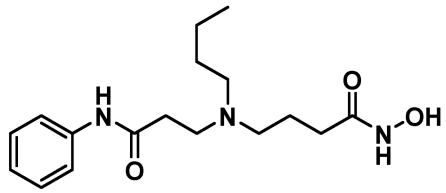


**DKFZ-717·TFA**

-75.59

30 20 10 0 -10 -20 -30 -40 -50 -60 -70 -80 -90 -100 -110 -120 -130 -140 -150 -160 -170 -180 -190 -200 -210 -220 -230 -240 -250 -260 -270
f1 (ppm)

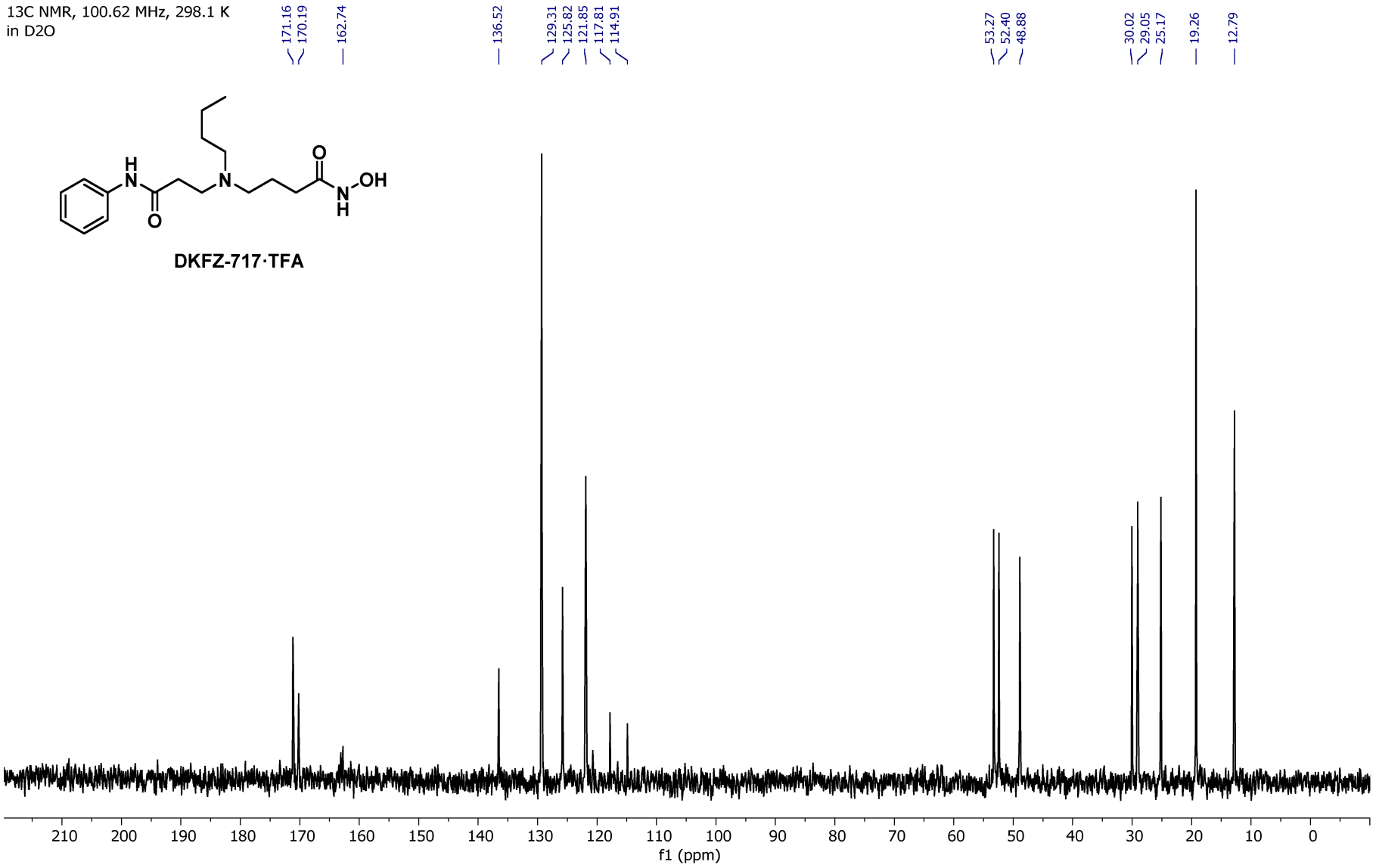
13C NMR, 100.62 MHz, 298.1 K
in D2O
171.16
170.19
162.74
136.52
129.31
125.82
121.85
117.81
114.91
53.27
52.40
48.88
30.02
29.05
25.17
19.26
12.79
DKFZ-717·TFA
f1 (ppm)

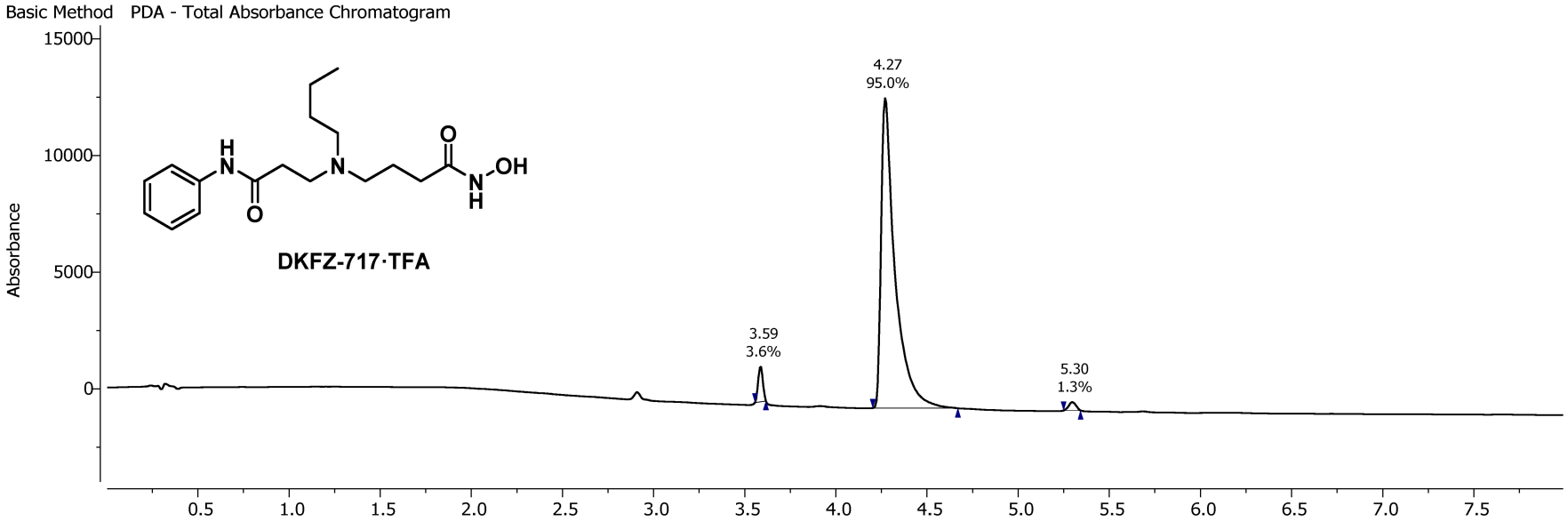
Basic Method PDA - Total Absorbance Chromatogram
Absorbance
15000
10000
5000
0
4.27
95.0%
3.59
3.6%
5.30
1.3%
DKFZ-717·TFA
0.5
1.0
1.5
2.0
2.5
3.0
3.5
4.0
4.5
5.0
5.5
6.0
6.5
7.0
7.5

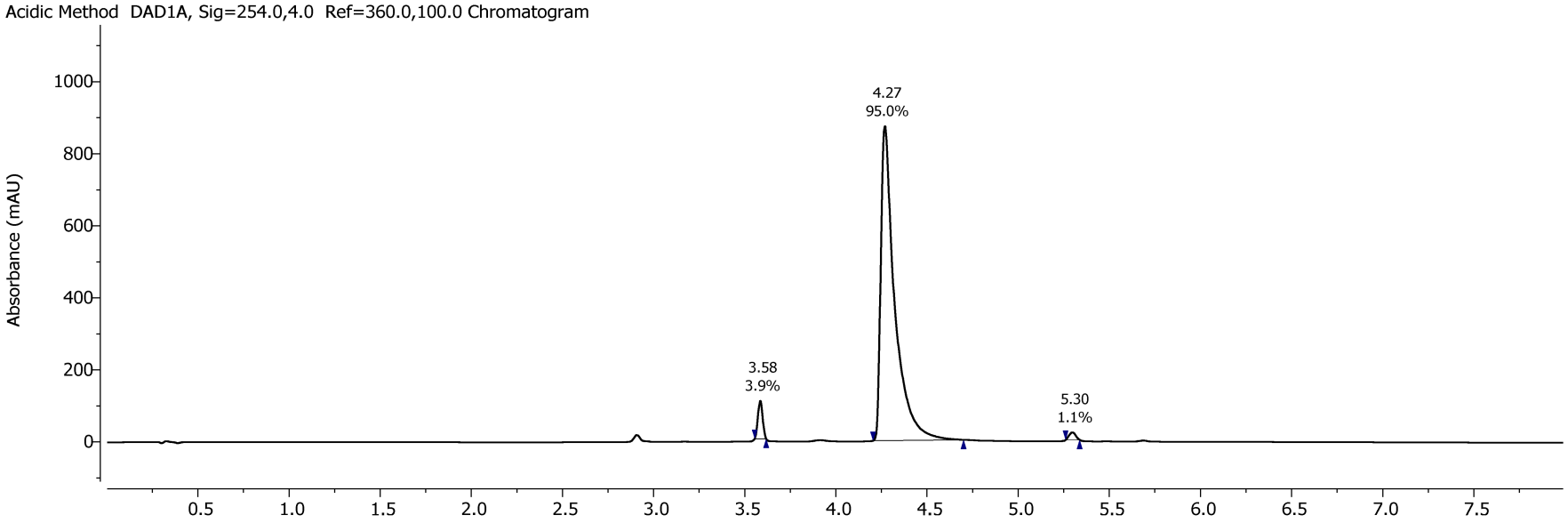
Acidic Method DAD1A, Sig=254.0,4.0 Ref=360.0,100.0 Chromatogram
Absorbance (mAU)
1000
800
600
400
200
0
4.27
95.0%
3.58
3.9%
5.30
1.1%
0.5
1.0
1.5
2.0
2.5
3.0
3.5
4.0
4.5
5.0
5.5
6.0
6.5
7.0
7.5

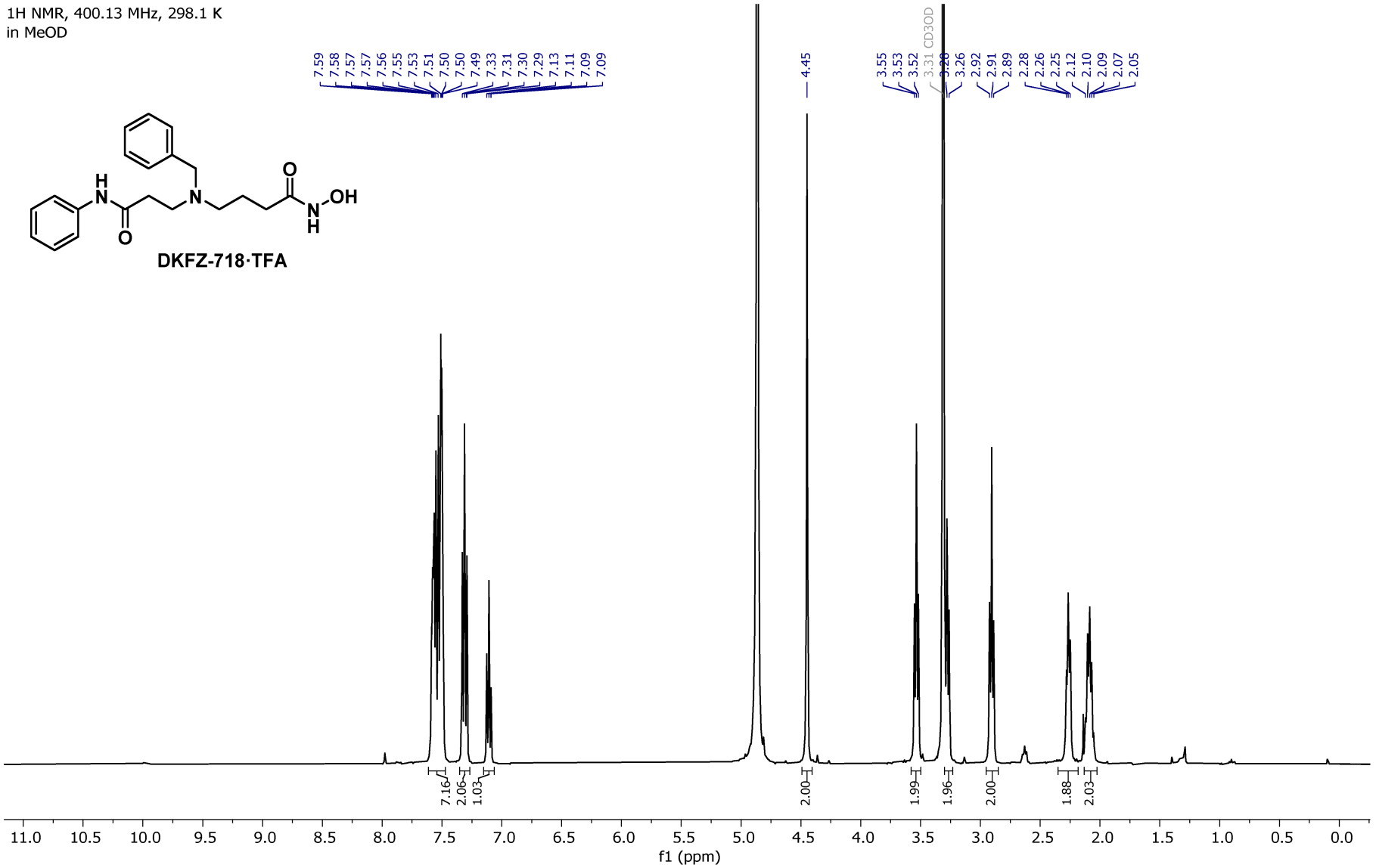
1H NMR, 400.13 MHz, 298.1 K
in MeOD
7.59
7.58
7.57
7.57
7.56
7.55
7.53
7.51
7.50
7.50
7.49
7.33
7.31
7.30
7.29
7.13
7.11
7.09
7.09
4.45
3.55
3.53
3.52
3.31 CD3OD
3.26
2.92
2.91
2.89
2.28
2.26
2.25
2.12
2.10
2.09
2.07
2.05
DKFZ-718·TFA
7.16
2.06
1.03
2.00
1.99
1.96
2.00
1.88
2.03
11.0
10.5
10.0
9.5
9.0
8.5
8.0
7.5
7.0
6.5
6.0
5.5
5.0
4.5
4.0
3.5
3.0
2.5
2.0
1.5
1.0
0.5
0.0
f1 (ppm)

19F NMR, 376.46 MHz, 298.1 K
in MeOD

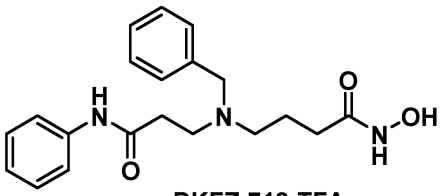


DKFZ-718·TFA

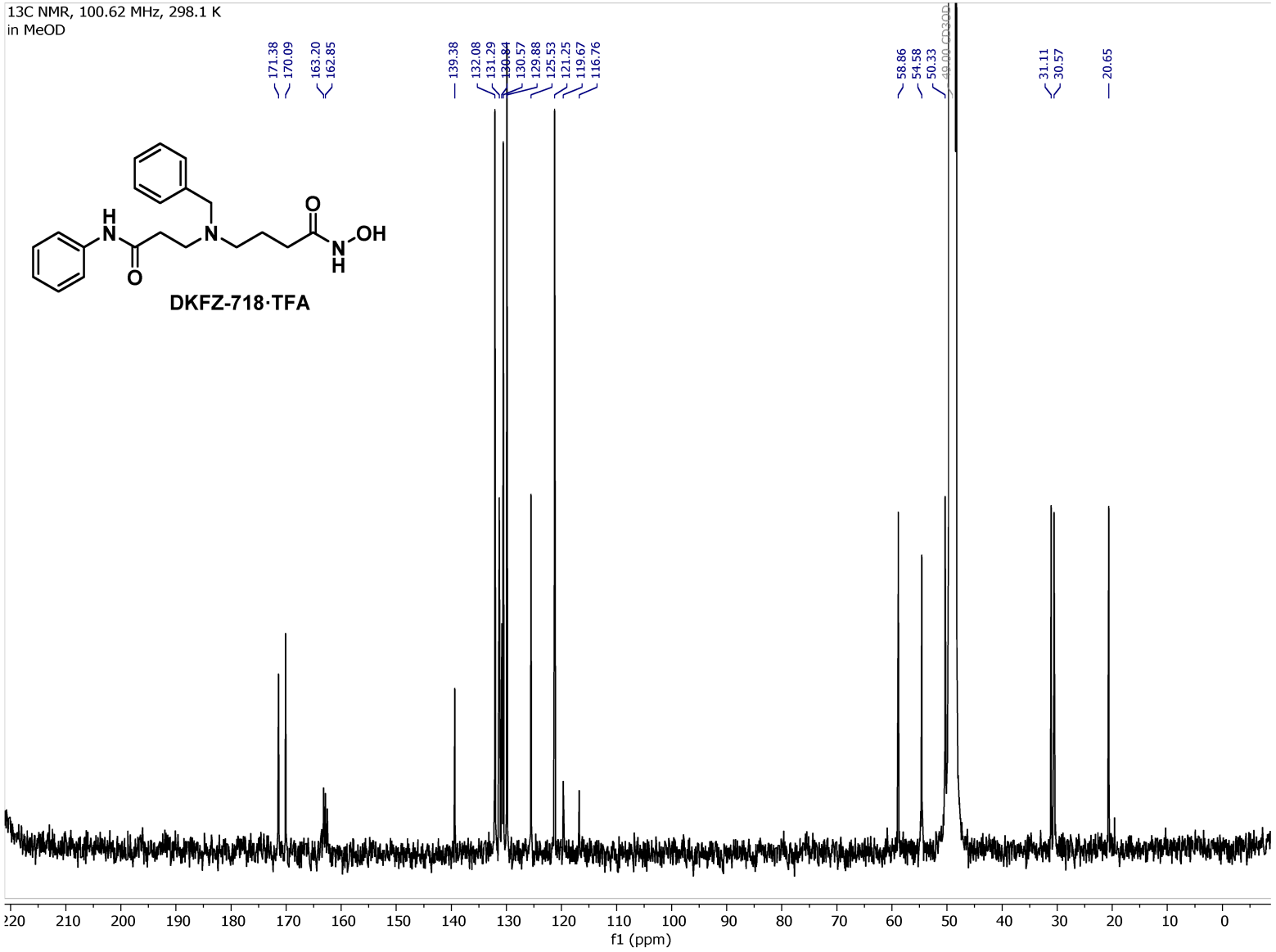
13C NMR, 100.62 MHz, 298.1 K
in MeOD
171.38
170.09
163.20
162.85
139.38
132.08
131.29
130.84
130.57
129.88
125.53
121.25
119.67
116.76
58.86
54.58
50.33
49.00 CD3OD
31.11
30.57
20.65
DKFZ-718·TFA
f1 (ppm)

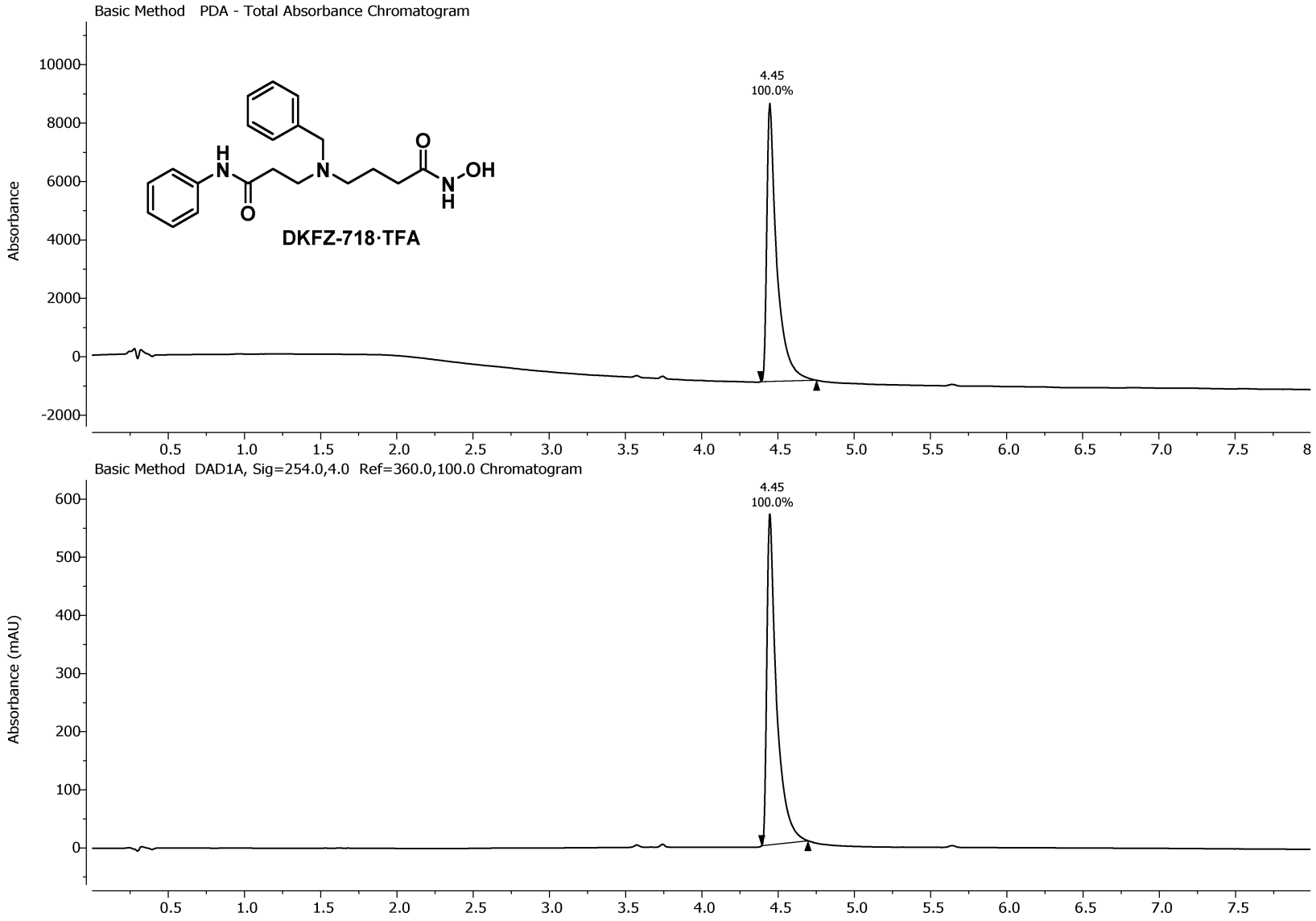
Basic Method PDA - Total Absorbance Chromatogram
Absorbance
10000
8000
6000
4000
2000
0
-2000
4.45
100.0%
DKFZ-718·TFA
0.5
1.0
1.5
2.0
2.5
3.0
3.5
4.0
4.5
5.0
5.5
6.0
6.5
7.0
7.5
8
Basic Method DAD1A, Sig=254.0,4.0 Ref=360.0,100.0 Chromatogram
Absorbance (mAU)
600
500
400
300
200
100
0
4.45
100.0%
0.5
1.0
1.5
2.0
2.5
3.0
3.5
4.0
4.5
5.0
5.5
6.0
6.5
7.0
7.5

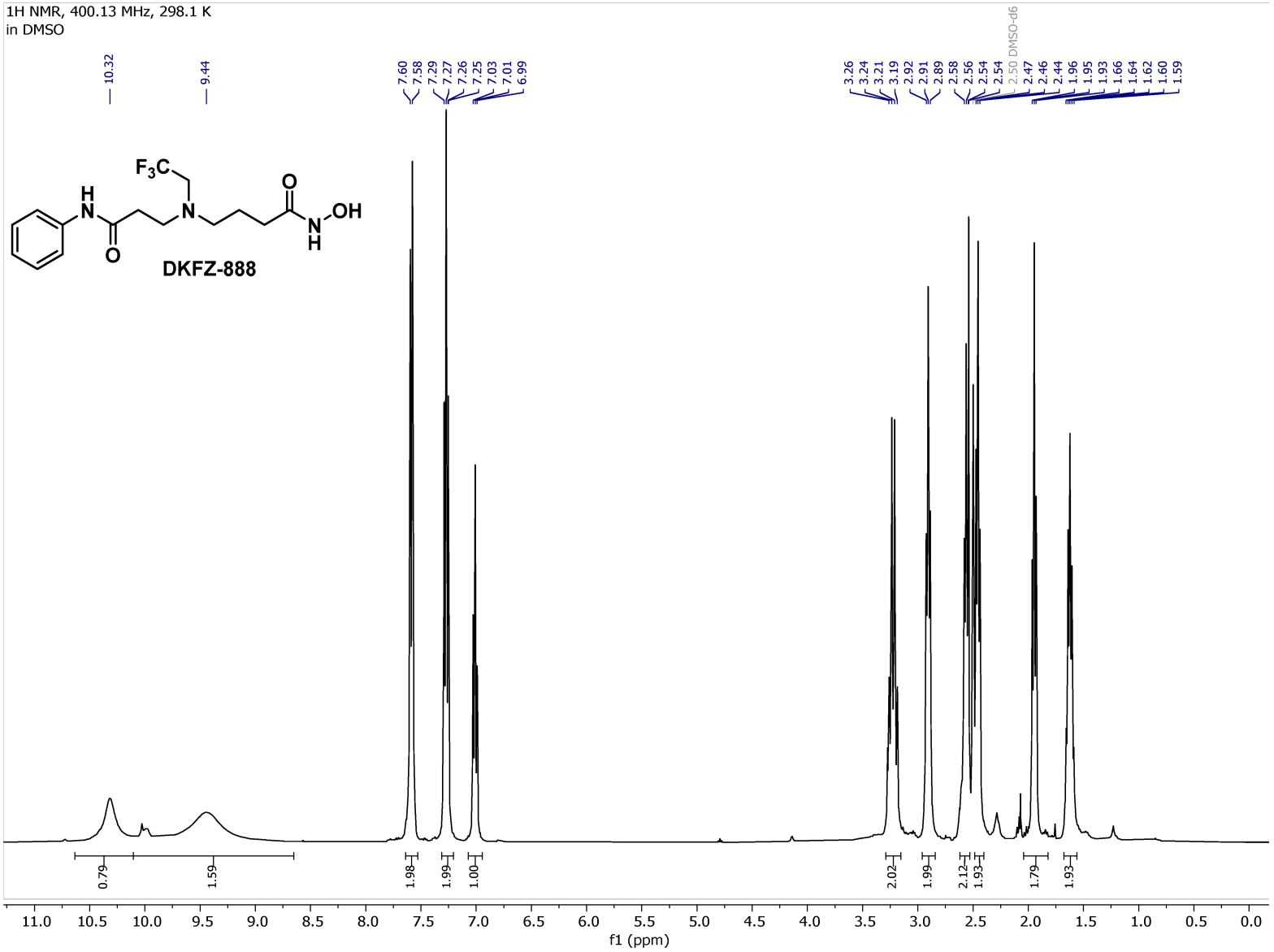
1H NMR, 400.13 MHz, 298.1 K
in DMSO
10.32
9.44
7.60
7.58
7.29
7.27
7.26
7.25
7.03
7.01
6.99
3.26
3.24
3.21
3.19
2.92
2.91
2.89
2.58
2.56
2.54
2.54
2.50 DMSO-d6
2.47
2.46
2.44
1.96
1.95
1.93
1.66
1.64
1.62
1.60
1.59
DKFZ-888
0.79
1.59
1.98
1.99
1.00
2.02
1.99
2.12
1.93
1.79
1.93
f1 (ppm)

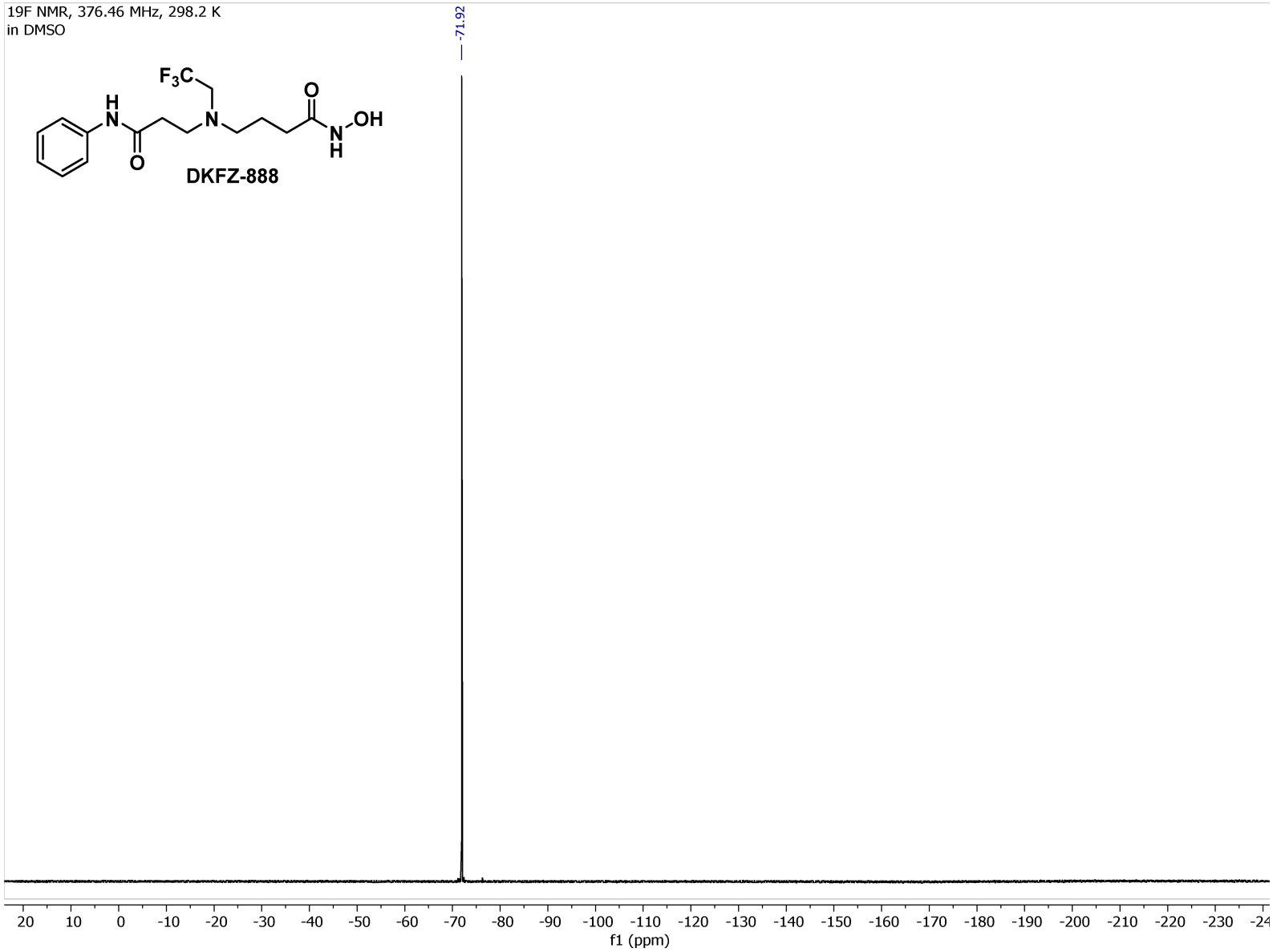
19F NMR, 376.46 MHz, 298.2 K
in DMSO
-71.92
DKFZ-888
20 10 0 -10 -20 -30 -40 -50 -60 -70 -80 -90 -100 -110 -120 -130 -140 -150 -160 -170 -180 -190 -200 -210 -220 -230
f1 (ppm)

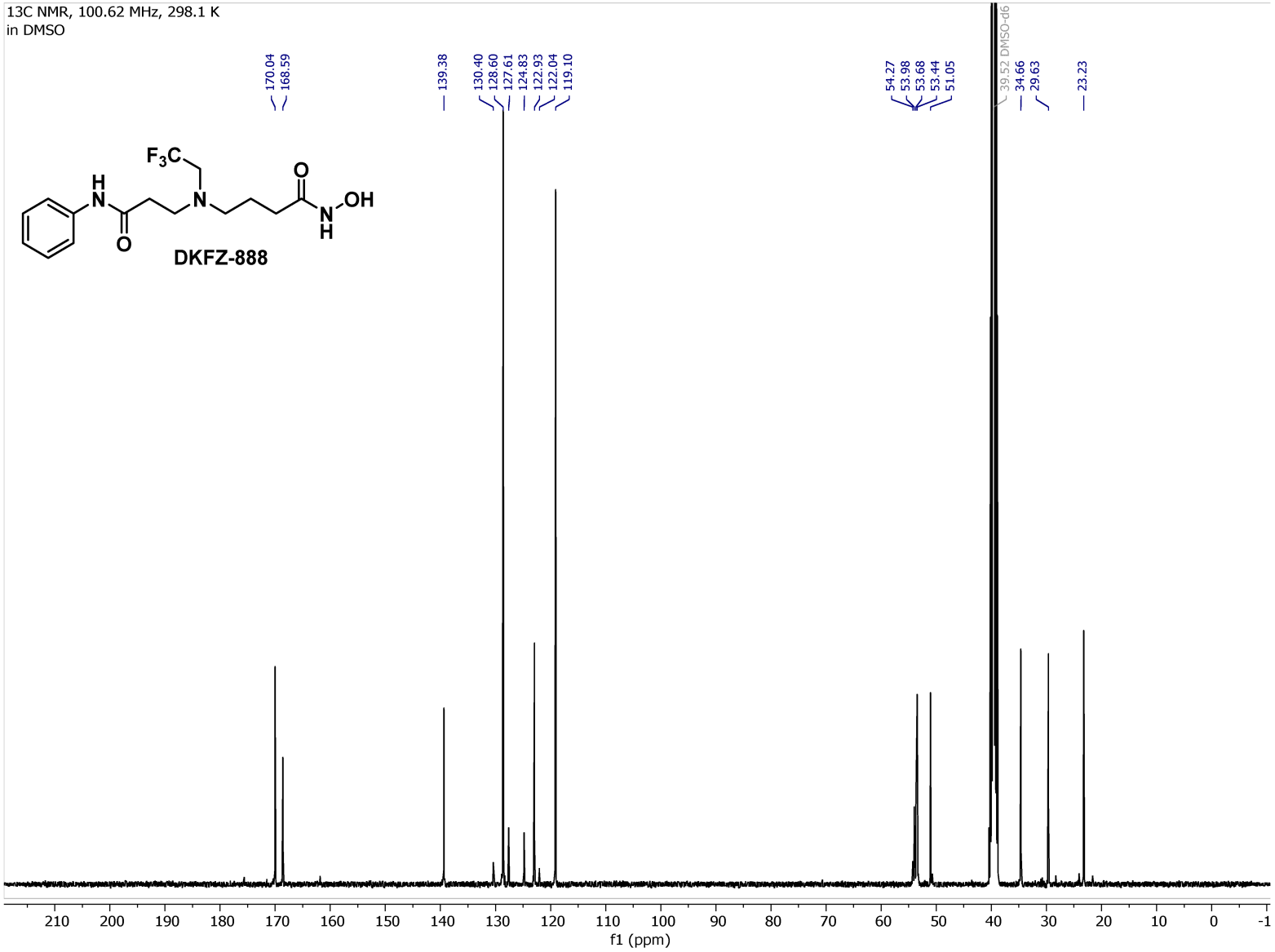
13C NMR, 100.62 MHz, 298.1 K
in DMSO
170.04
168.59
139.38
130.40
128.60
127.61
124.83
122.93
122.04
119.10
54.27
53.98
53.68
53.44
51.05
39.52 DMSO-d6
34.66
29.63
23.23
F3C
H
N
O
N
O
N
H
OH
DKFZ-888
210 200 190 180 170 160 150 140 130 120 110 100 90 80 70 60 50 40 30 20 10 0 -1
f1 (ppm)

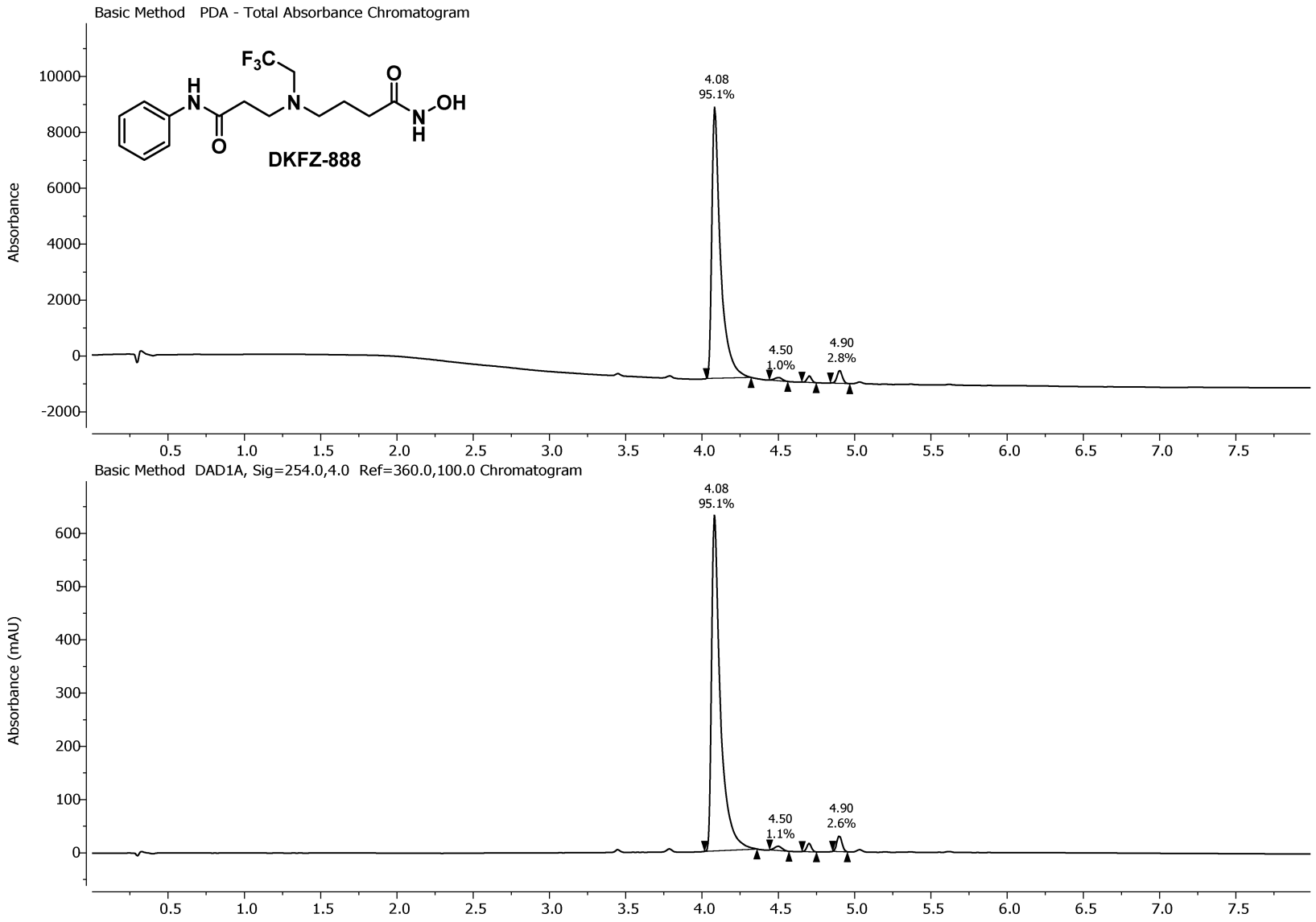
Basic Method PDA - Total Absorbance Chromatogram
DKFZ-888
Absorbance
4.08
95.1%
4.50
1.0%
4.90
2.8%
Basic Method DAD1A, Sig=254.0,4.0 Ref=360.0,100.0 Chromatogram
Absorbance (mAU)
4.08
95.1%
4.50
1.1%
4.90
2.6%

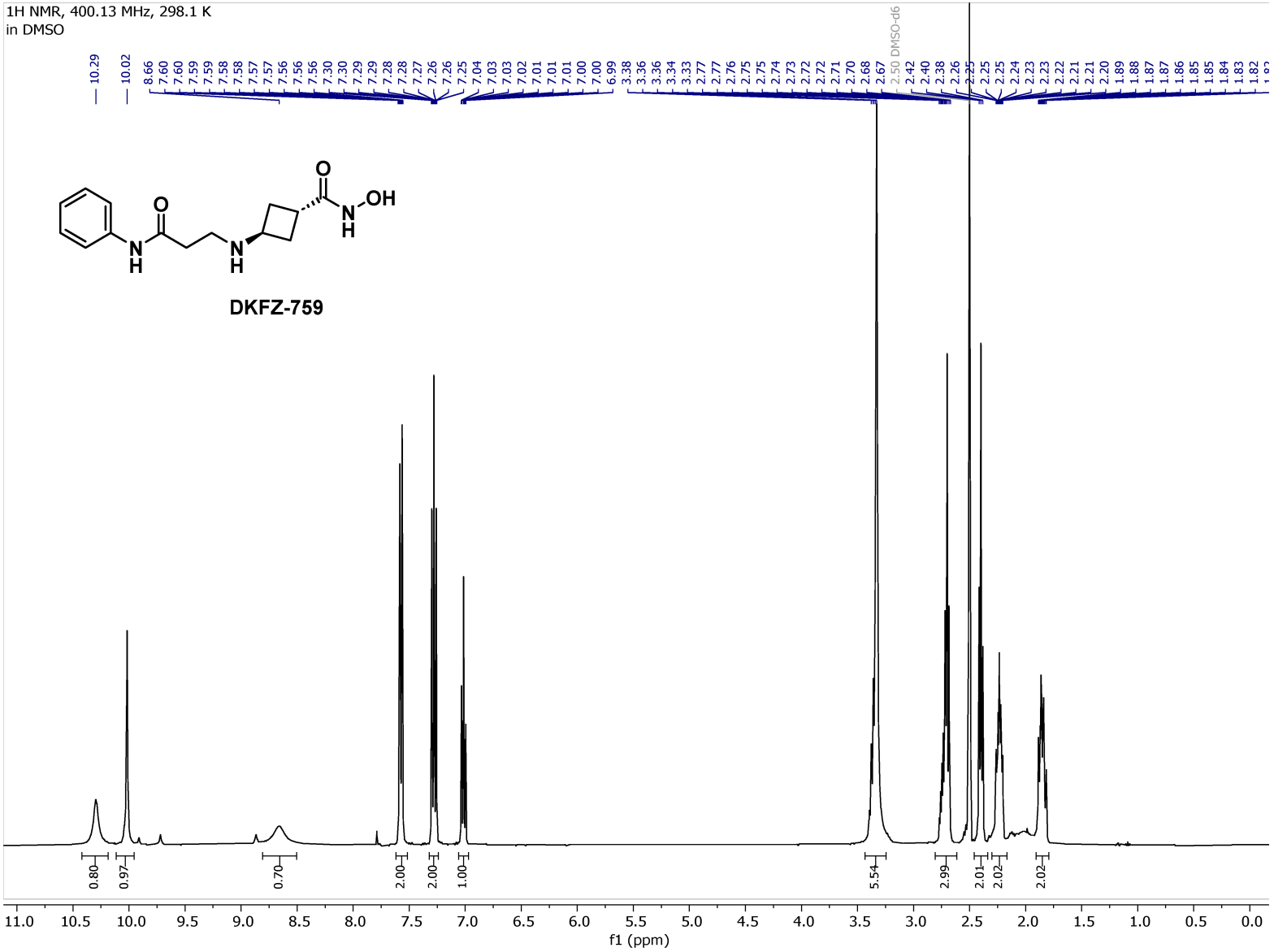
1H NMR, 400.13 MHz, 298.1 K
in DMSO
DKFZ-759
f1 (ppm)

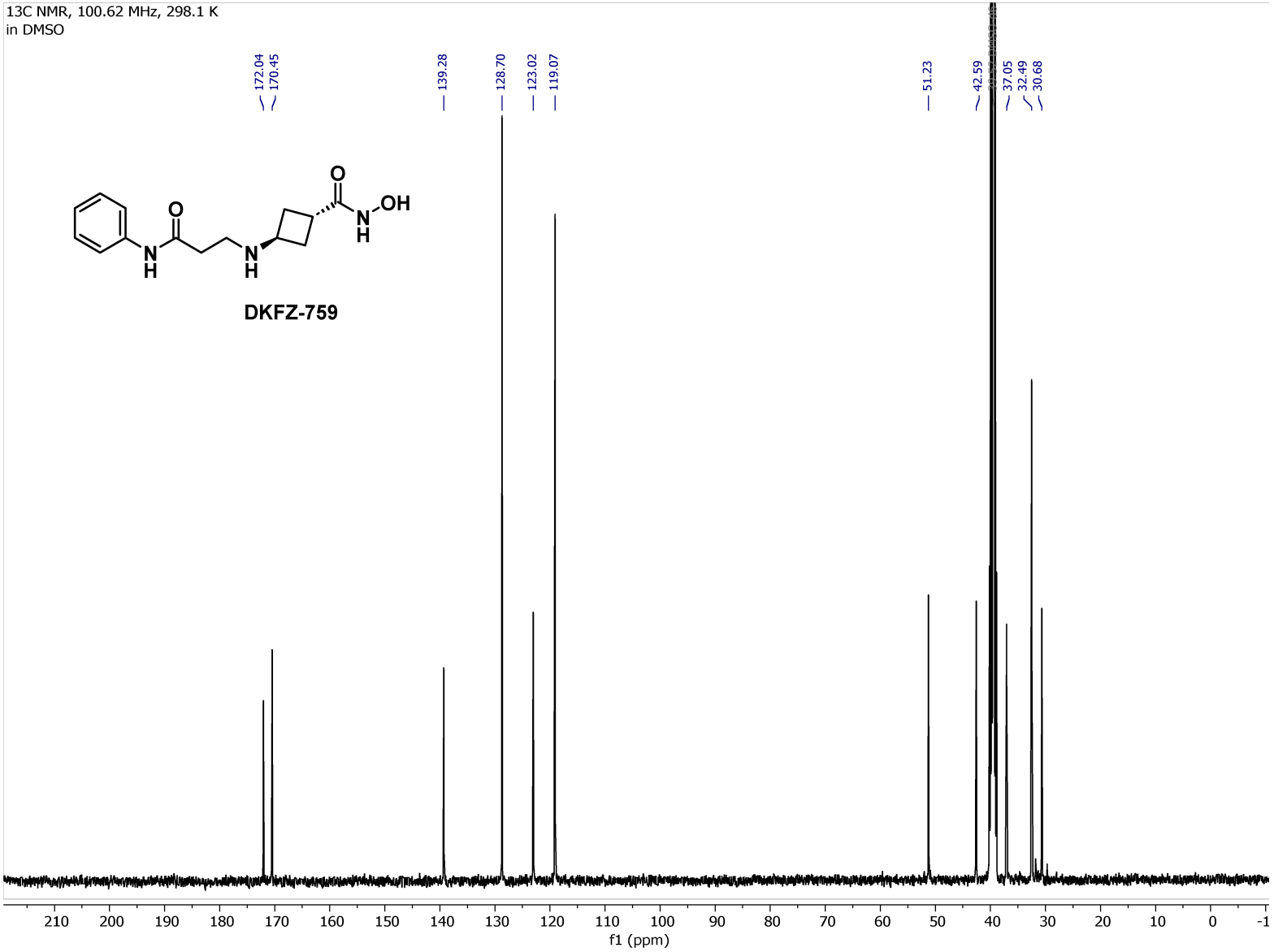
13C NMR, 100.62 MHz, 298.1 K
in DMSO
172.04
170.45
139.28
128.70
123.02
119.07
51.23
42.59
37.05
32.49
30.68
O
N
H
O
N
H
O
N
H
OH
DKFZ-759
210
200
190
180
170
160
150
140
130
120
110
100
90
80
70
60
50
40
30
20
10
0
-1
f1 (ppm)

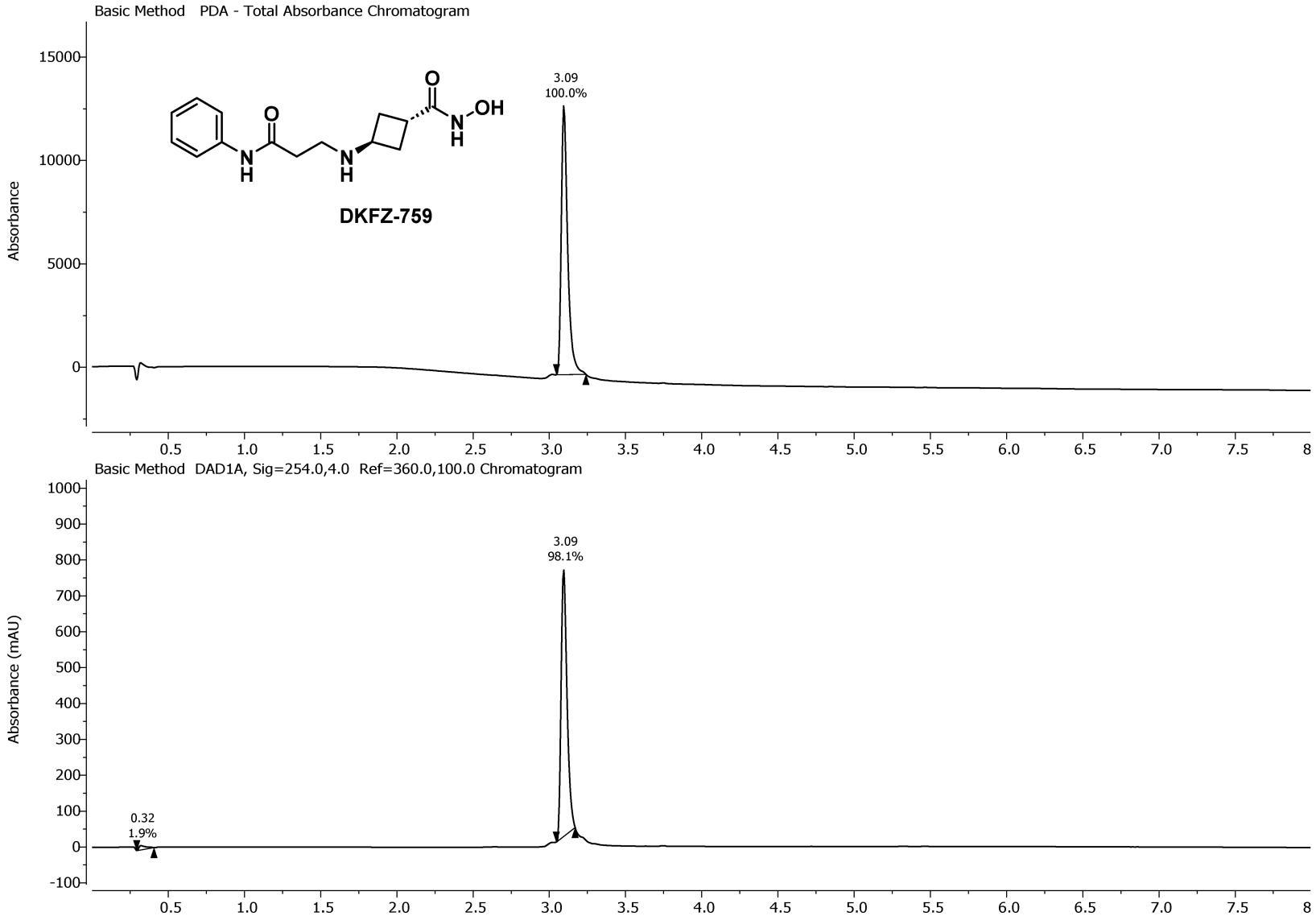
Basic Method PDA - Total Absorbance Chromatogram
Absorbance
15000
10000
5000
0
3.09
100.0%
DKFZ-759
0.5
1.0
1.5
2.0
2.5
3.0
3.5
4.0
4.5
5.0
5.5
6.0
6.5
7.0
7.5
8
Basic Method DAD1A, Sig=254.0,4.0 Ref=360.0,100.0 Chromatogram
Absorbance (mAU)
1000
900
800
700
600
500
400
300
200
100
0
-100
3.09
98.1%
0.32
1.9%

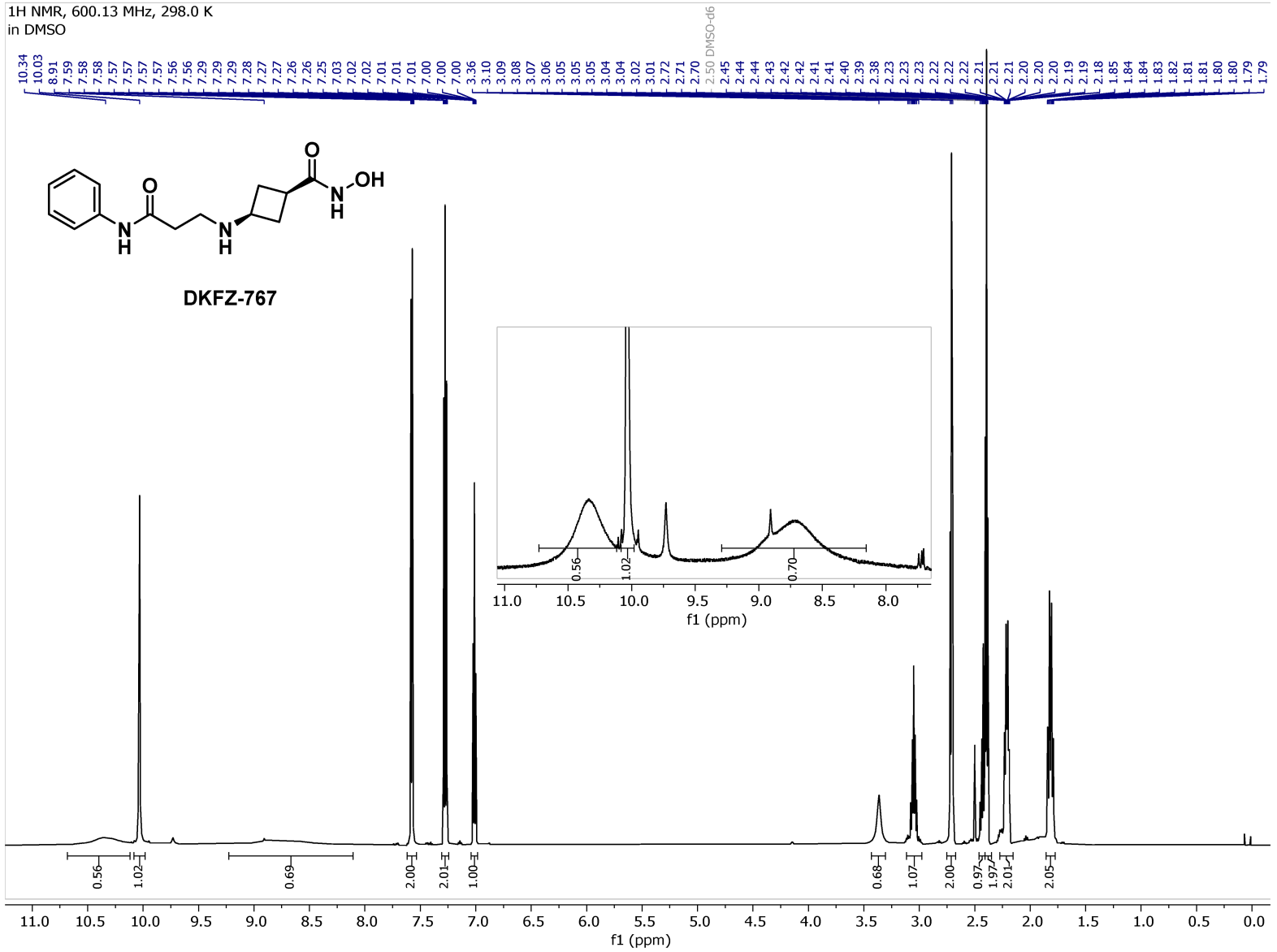
1H NMR, 600.13 MHz, 298.0 K
in DMSO
2.50 DMSO-d6
DKFZ-767
f1 (ppm)

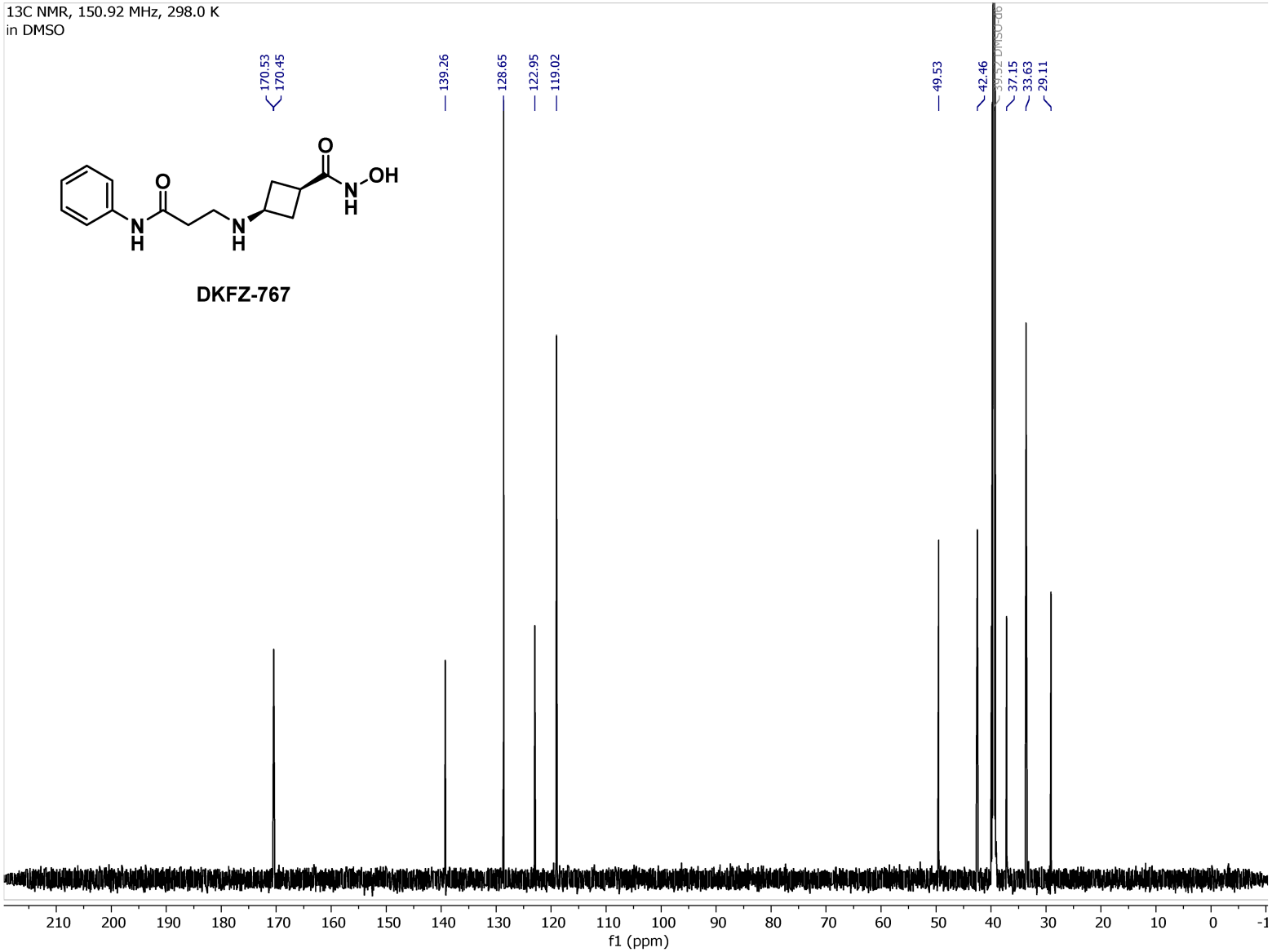
13C NMR, 150.92 MHz, 298.0 K
in DMSO
170.53
170.45
139.26
128.65
122.95
119.02
49.53
42.46
37.15
33.63
29.11
DKFZ-767
f1 (ppm)

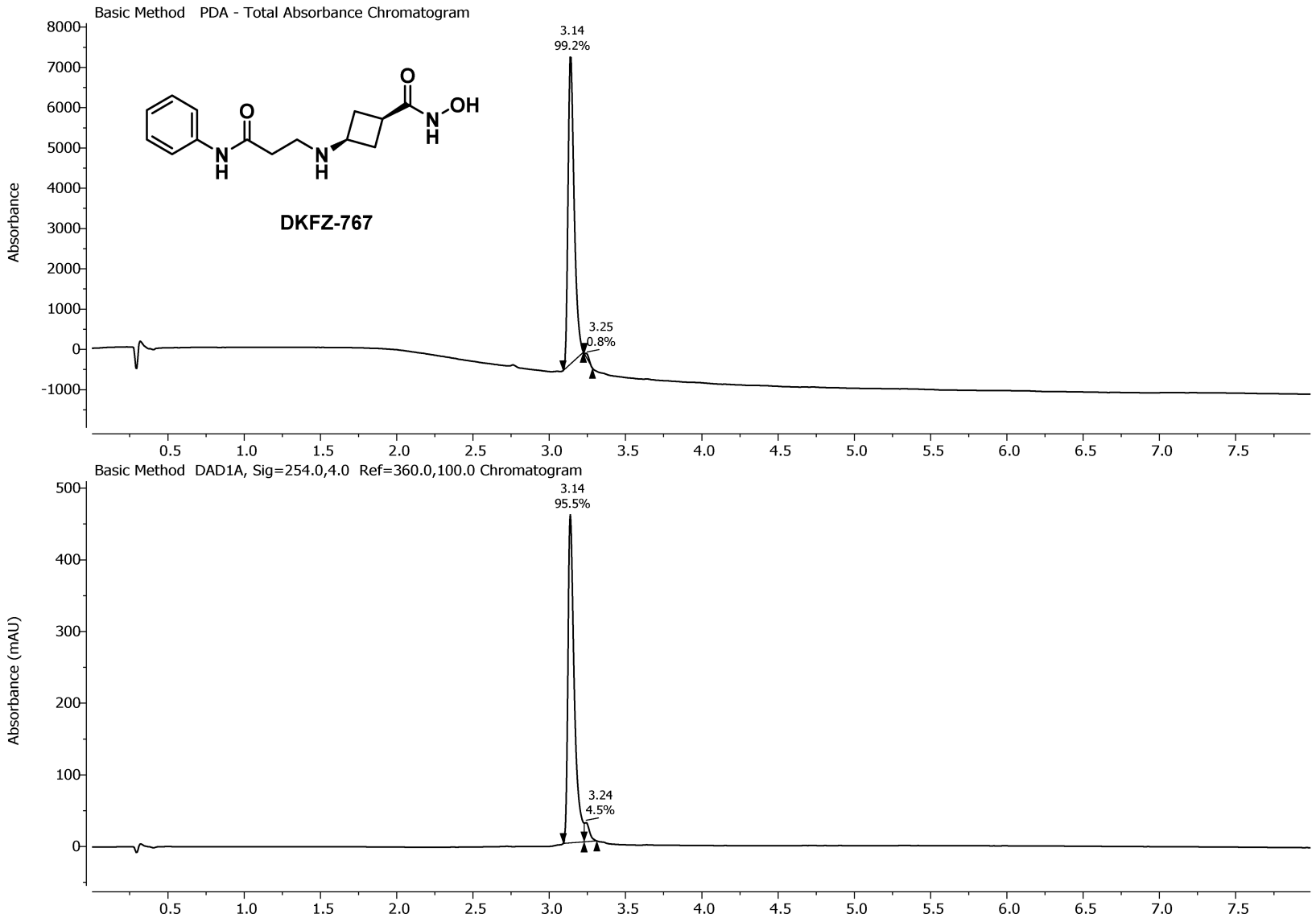
Basic Method PDA - Total Absorbance Chromatogram
Absorbance
3.14
99.2%
3.25
0.8%
DKFZ-767
Basic Method DAD1A, Sig=254.0,4.0 Ref=360.0,100.0 Chromatogram
Absorbance (mAU)
3.14
95.5%
3.24
4.5%

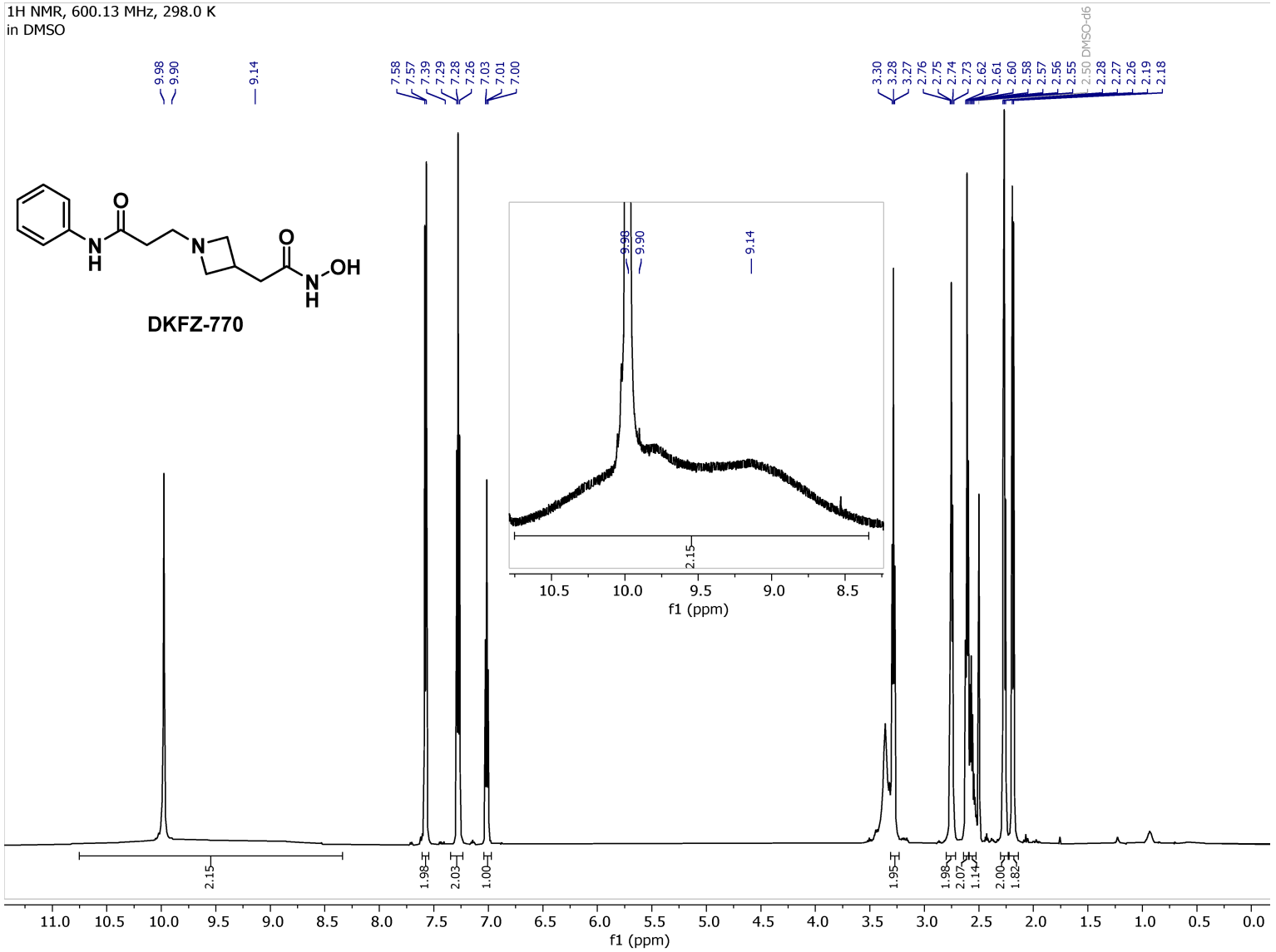
1H NMR, 600.13 MHz, 298.0 K
in DMSO
DKFZ-770
f1 (ppm)

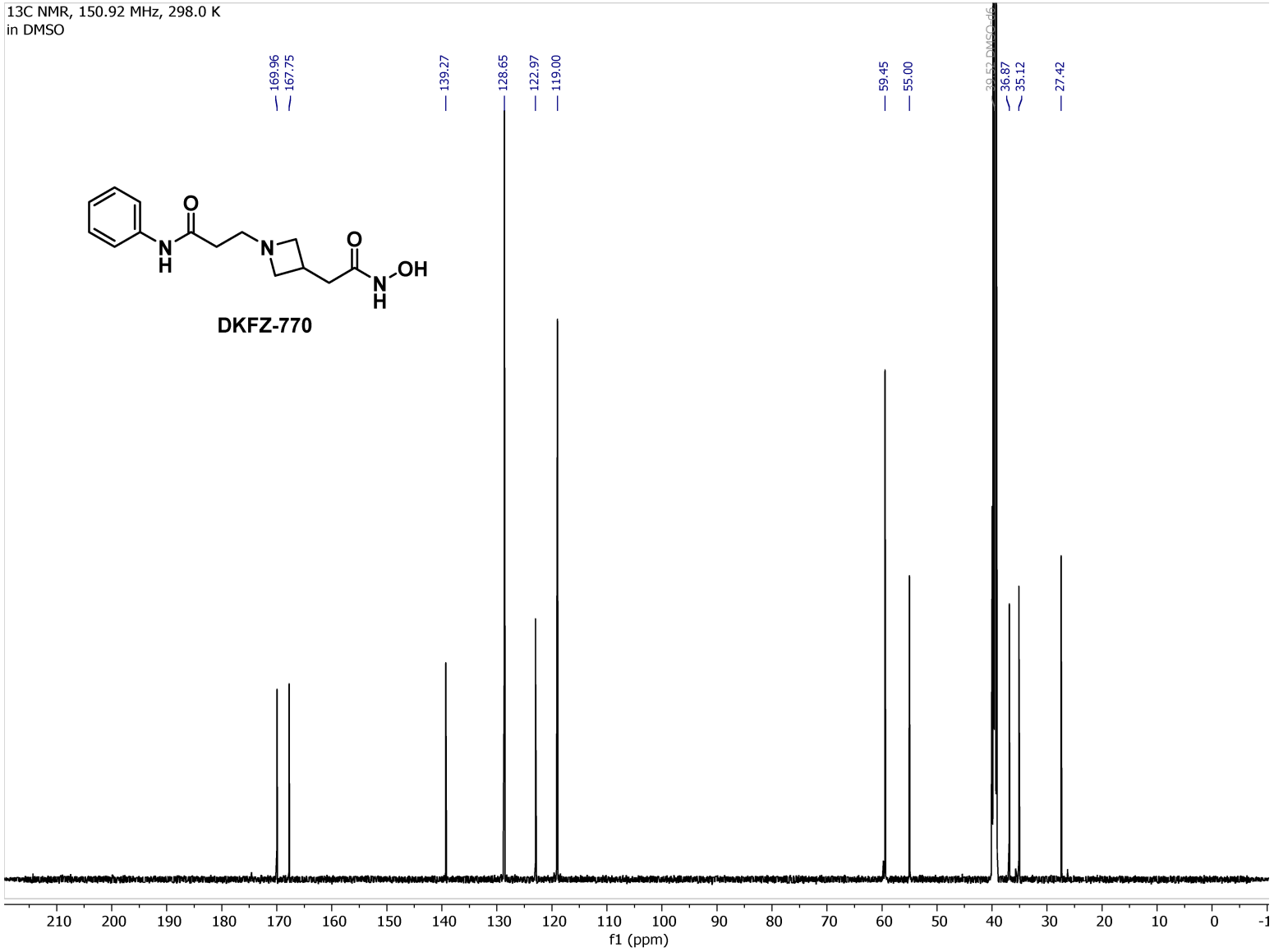
13C NMR, 150.92 MHz, 298.0 K
in DMSO
169.96
167.75
139.27
128.65
122.97
119.00
59.45
55.00
39.53 DMSO-d6
36.87
35.12
27.42
DKFZ-770
f1 (ppm)

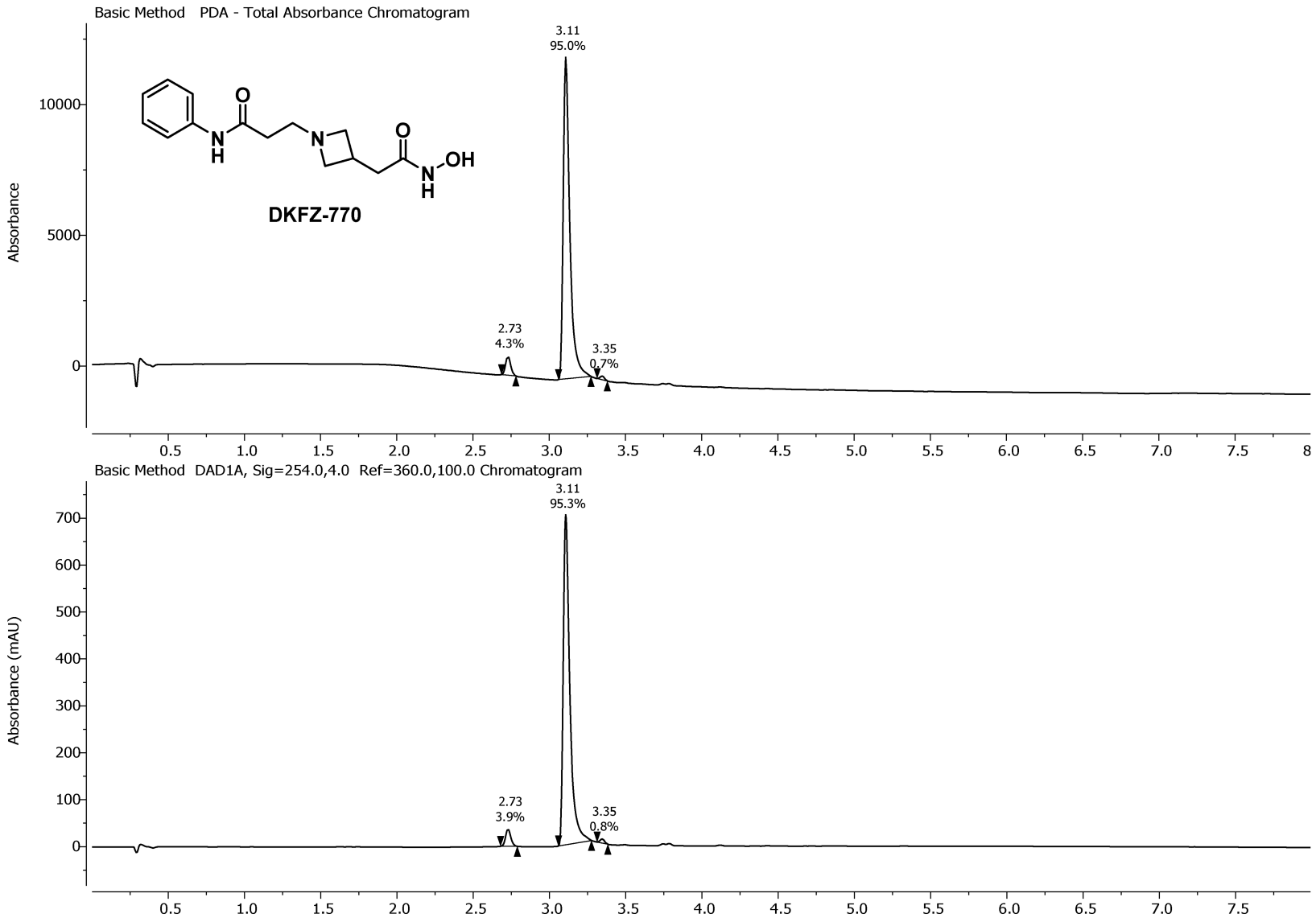
Basic Method PDA - Total Absorbance Chromatogram
3.11
95.0%
DKFZ-770
2.73
4.3%
3.35
0.7%
Absorbance
Basic Method DAD1A, Sig=254.0,4.0 Ref=360.0,100.0 Chromatogram
3.11
95.3%
2.73
3.9%
3.35
0.8%
Absorbance (mAU)

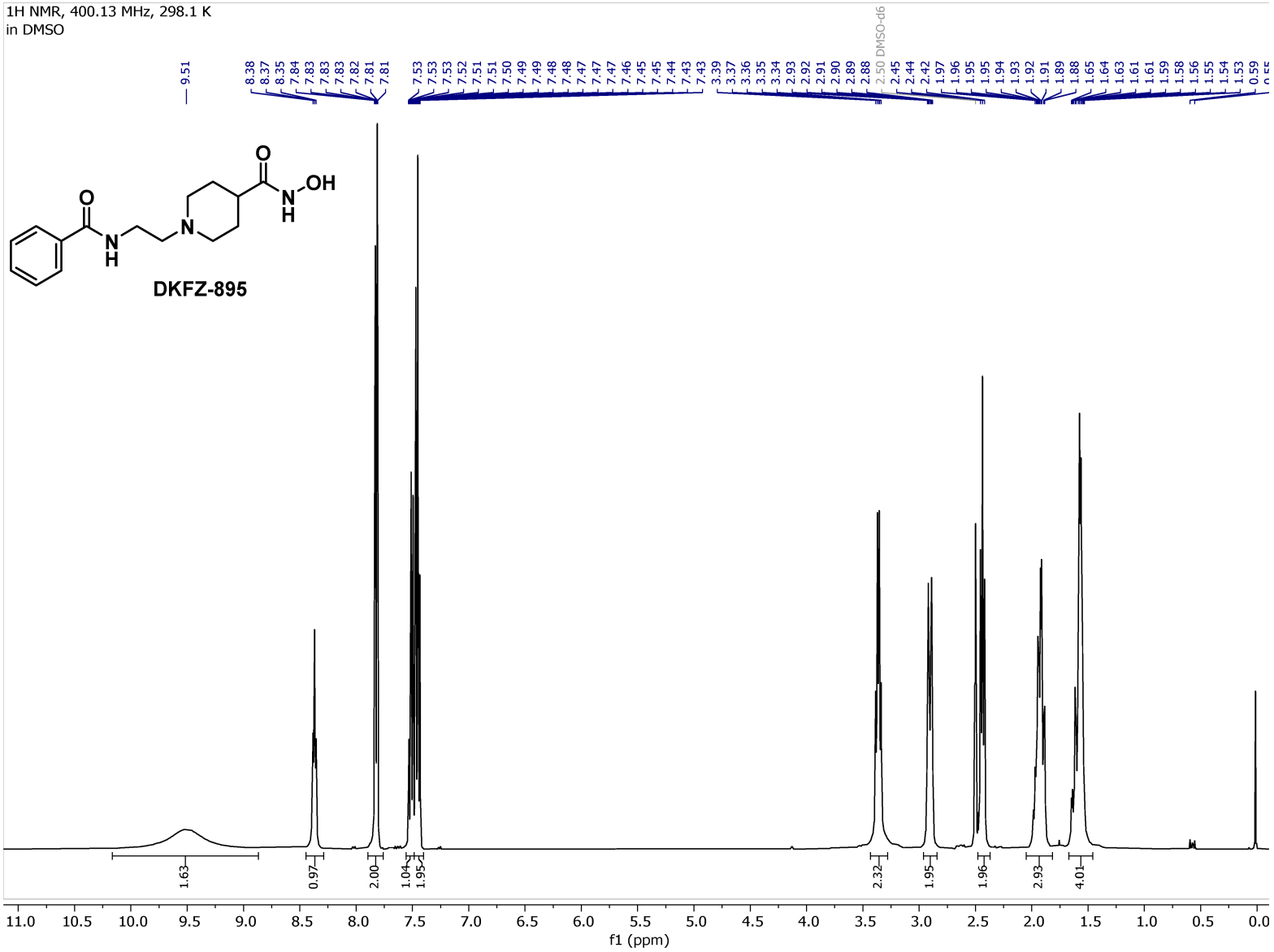
1H NMR, 400.13 MHz, 298.1 K
in DMSO
DKFZ-895
f1 (ppm)

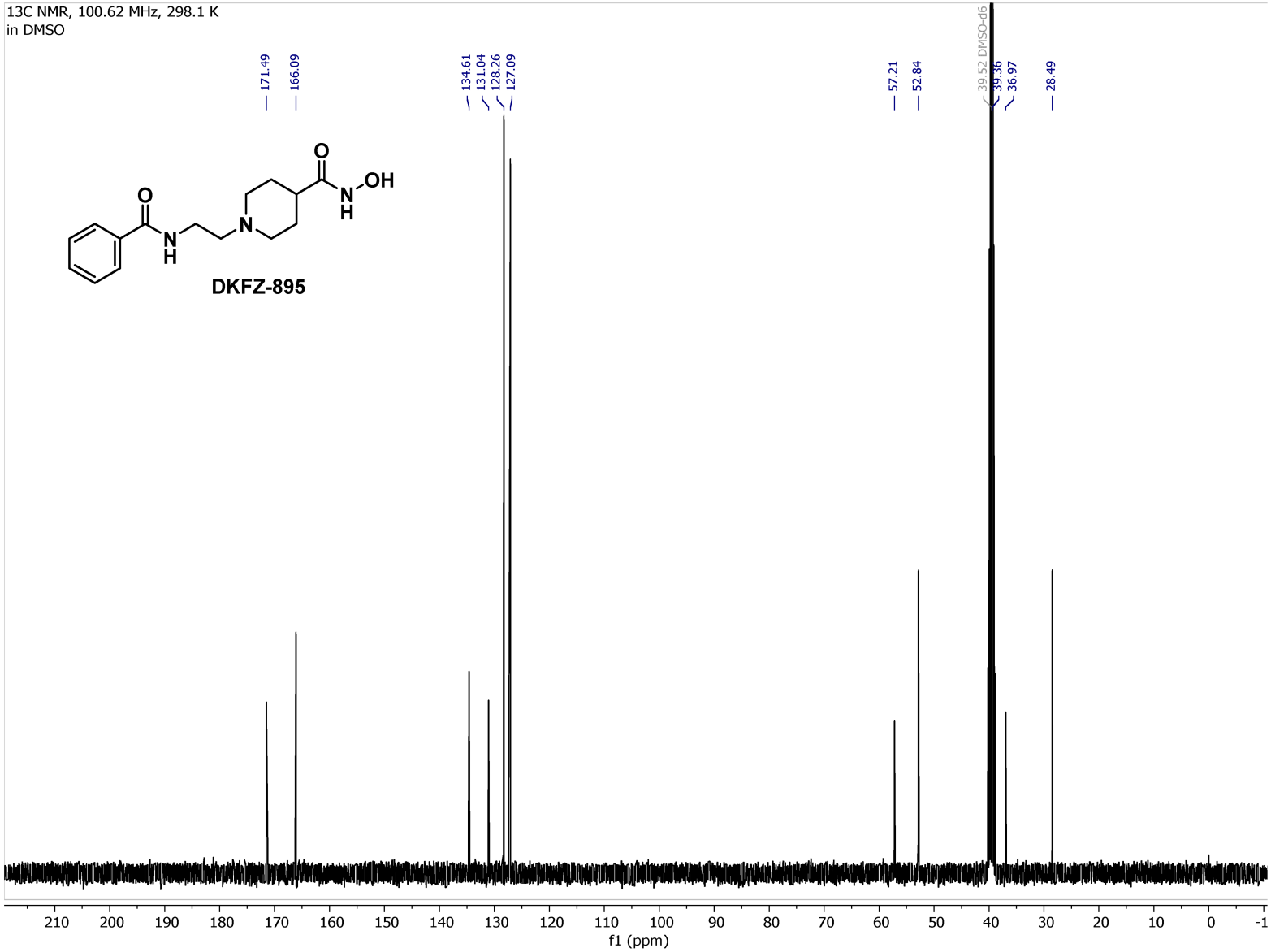
13C NMR, 100.62 MHz, 298.1 K
in DMSO
171.49
166.09
134.61
131.04
128.26
127.09
57.21
52.84
39.52 DMSO-d6
39.36
36.97
28.49
O
N
H
N
O
N
H
OH
DKFZ-895
210
200
190
180
170
160
150
140
130
120
110
100
90
80
70
60
50
40
30
20
10
0
-1
f1 (ppm)

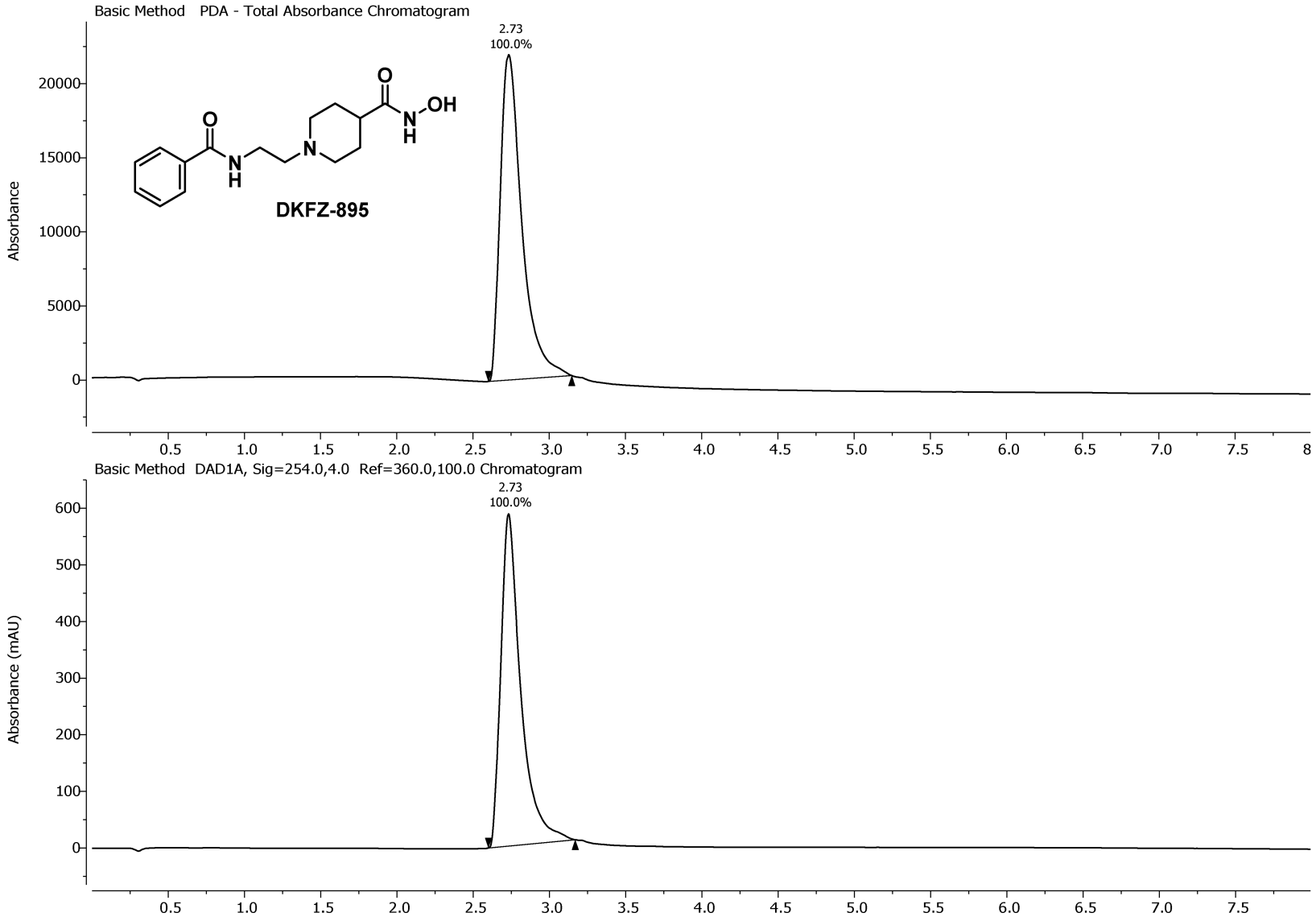
Basic Method PDA - Total Absorbance Chromatogram
2.73
100.0%
DKFZ-895
Absorbance
Basic Method DAD1A, Sig=254.0,4.0 Ref=360.0,100.0 Chromatogram
2.73
100.0%
Absorbance (mAU)

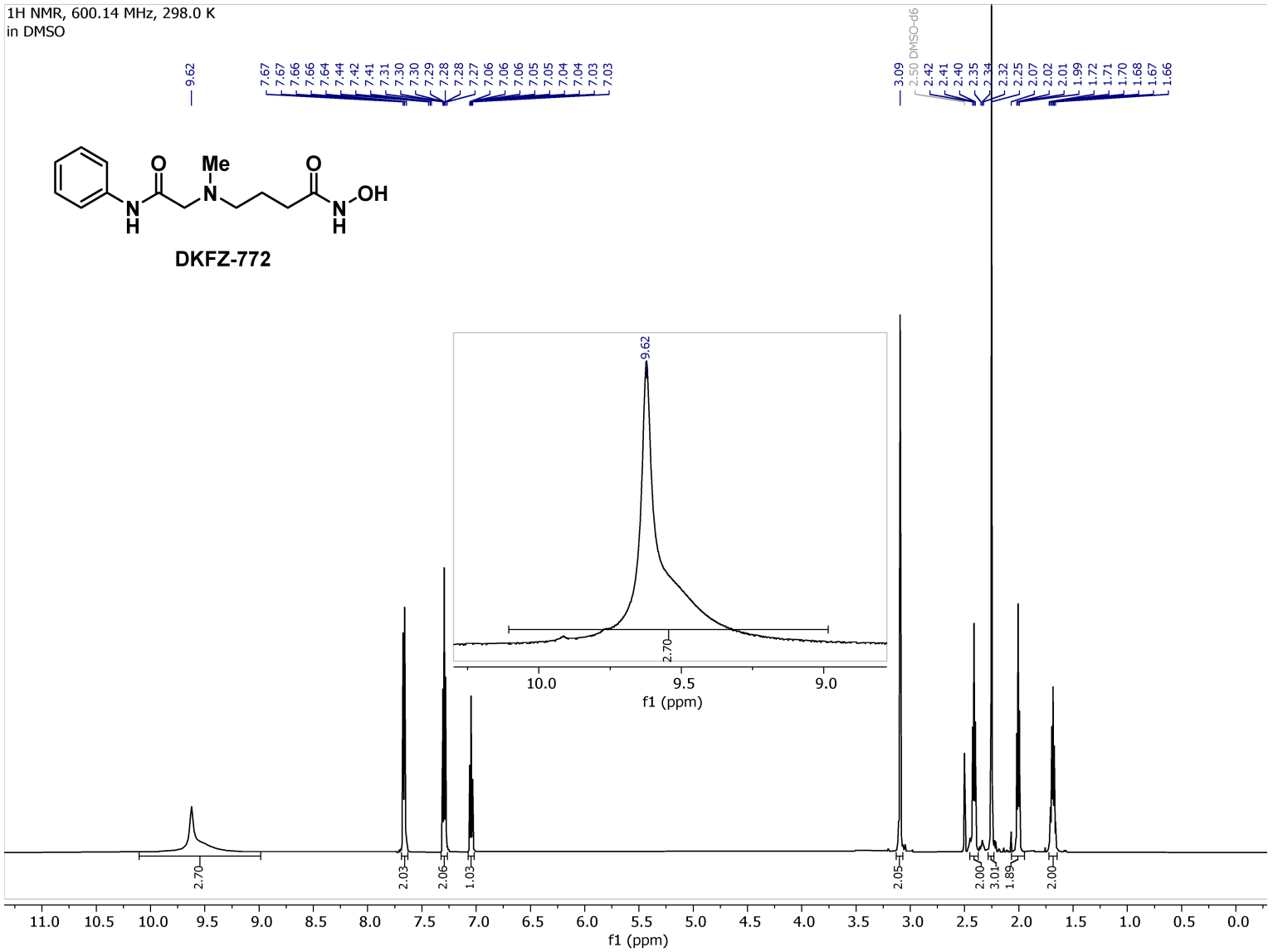
1H NMR, 600.14 MHz, 298.0 K
in DMSO
DKFZ-772
f1 (ppm)

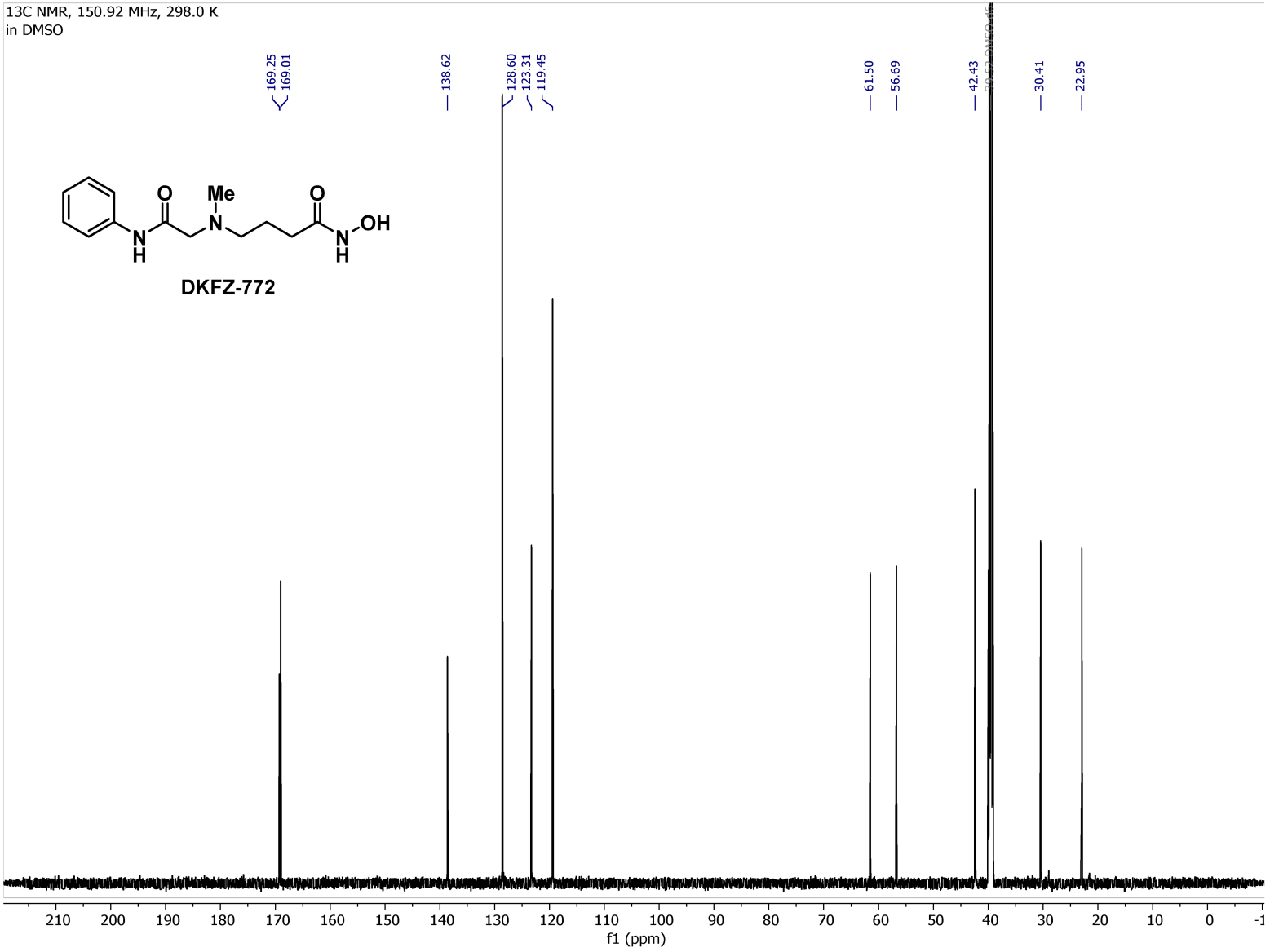
13C NMR, 150.92 MHz, 298.0 K
in DMSO
169.25
169.01
138.62
128.60
123.31
119.45
61.50
56.69
42.43
30.41
22.95
O
Me
O
N
N
H
N
OH
H
DKFZ-772
210
200
190
180
170
160
150
140
130
120
110
100
90
80
70
60
50
40
30
20
10
0
-1
f1 (ppm)

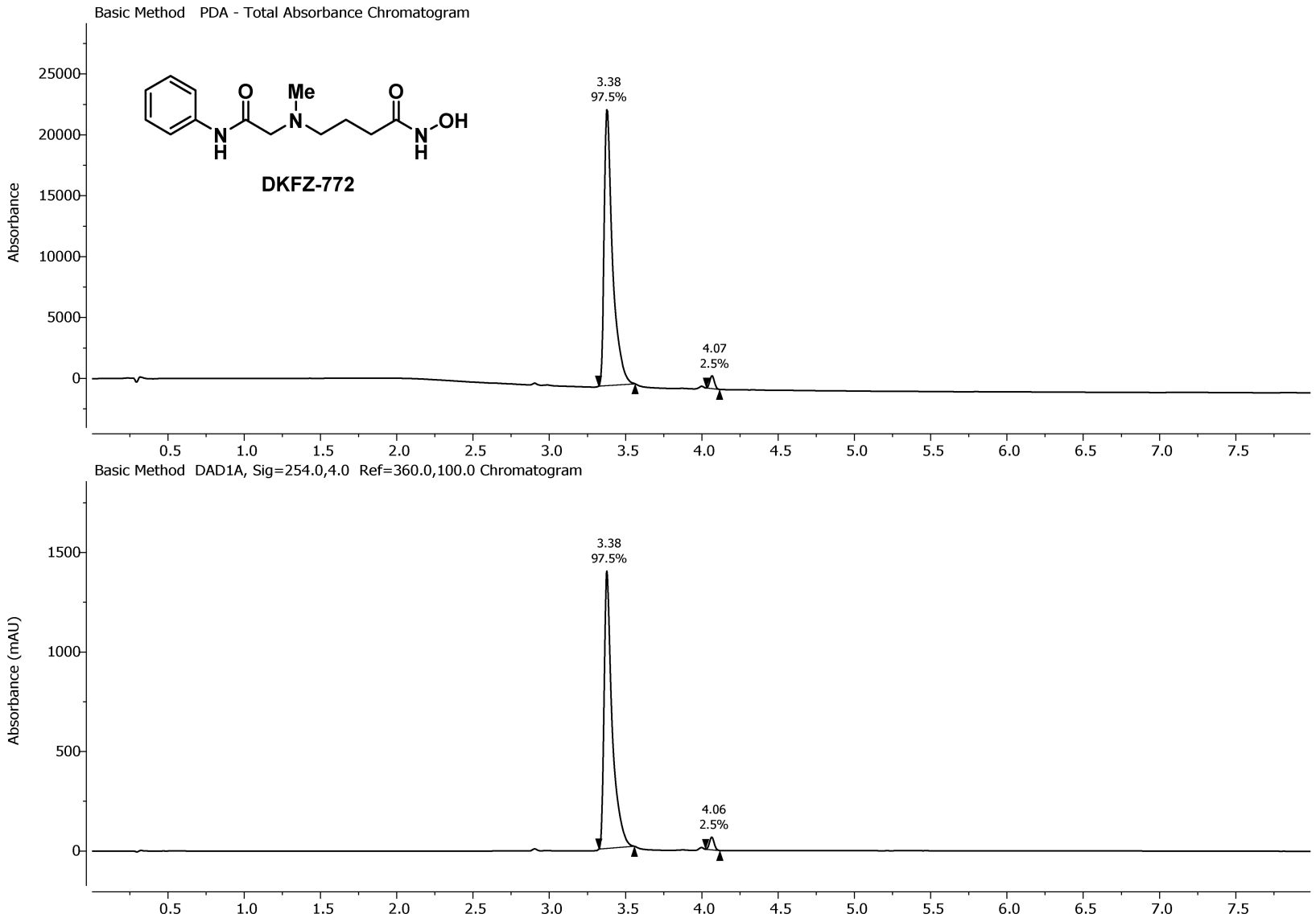
Basic Method PDA - Total Absorbance Chromatogram
Absorbance
25000
20000
15000
10000
5000
0
O
Me
O
N
H
N
N
H
OH
DKFZ-772
3.38
97.5%
4.07
2.5%
0.5
1.0
1.5
2.0
2.5
3.0
3.5
4.0
4.5
5.0
5.5
6.0
6.5
7.0
7.5
Basic Method DAD1A, Sig=254.0,4.0 Ref=360.0,100.0 Chromatogram
Absorbance (mAU)
1500
1000
500
0
3.38
97.5%
4.06
2.5%
0.5
1.0
1.5
2.0
2.5
3.0
3.5
4.0
4.5
5.0
5.5
6.0
6.5
7.0
7.5

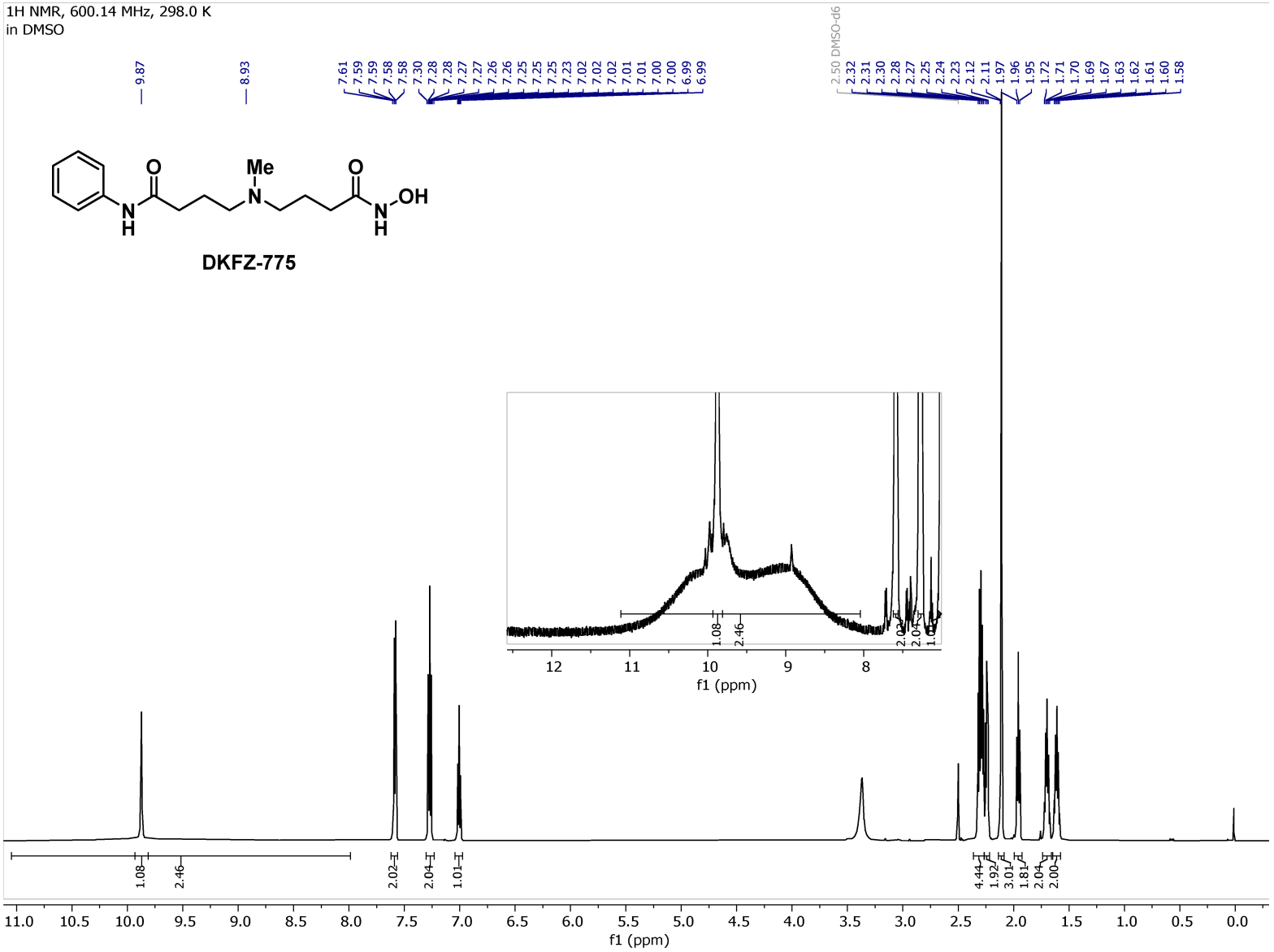
1H NMR, 600.14 MHz, 298.0 K
in DMSO
DKFZ-775
f1 (ppm)

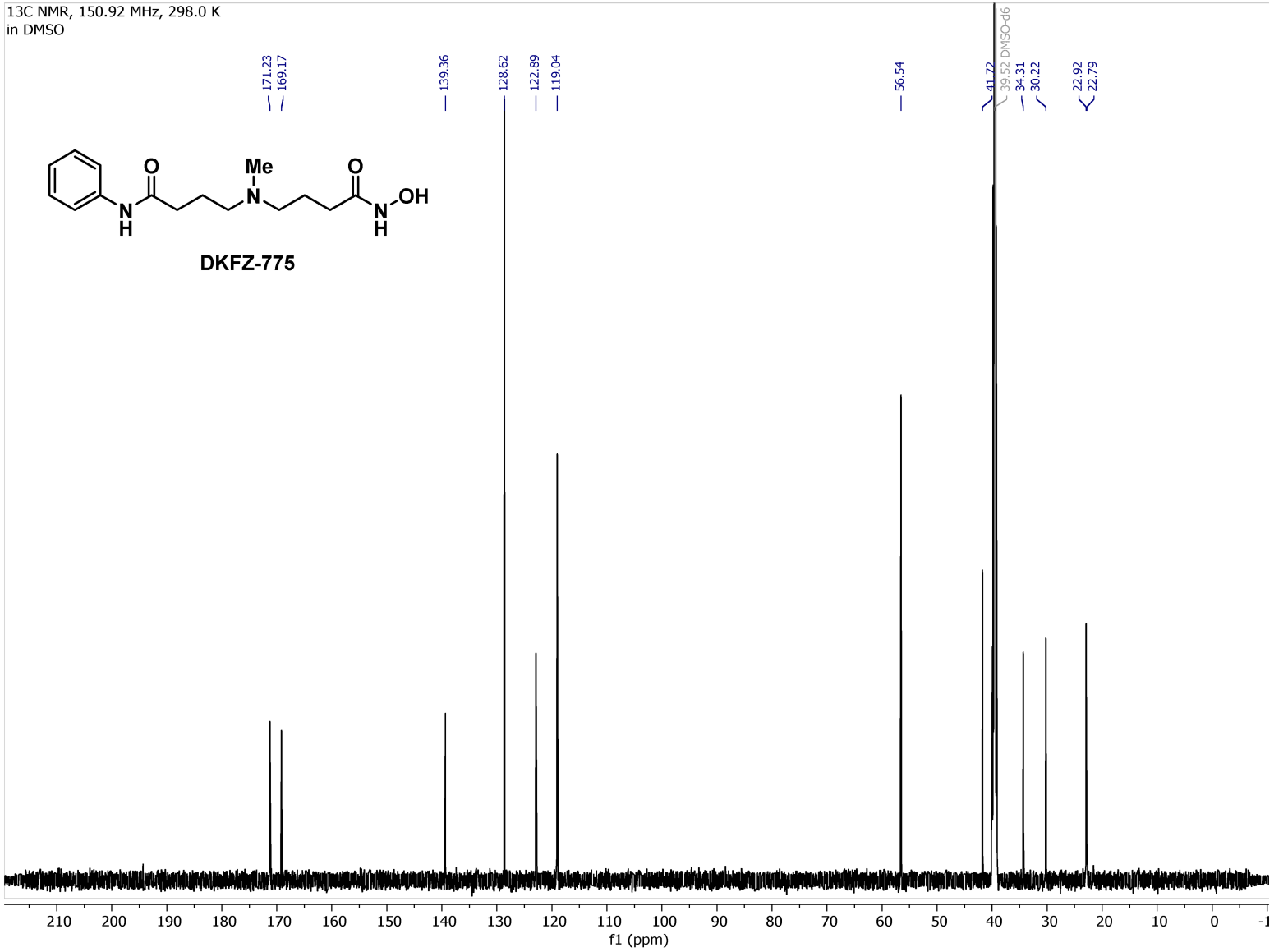
13C NMR, 150.92 MHz, 298.0 K
in DMSO
171.23
169.17
139.36
128.62
122.89
119.04
56.54
41.72
39.52 DMSO-d6
34.31
30.22
22.92
22.79
O
Me
O
N
H
N
N
H
OH
DKFZ-775
210 200 190 180 170 160 150 140 130 120 110 100 90 80 70 60 50 40 30 20 10 0 -1
f1 (ppm)

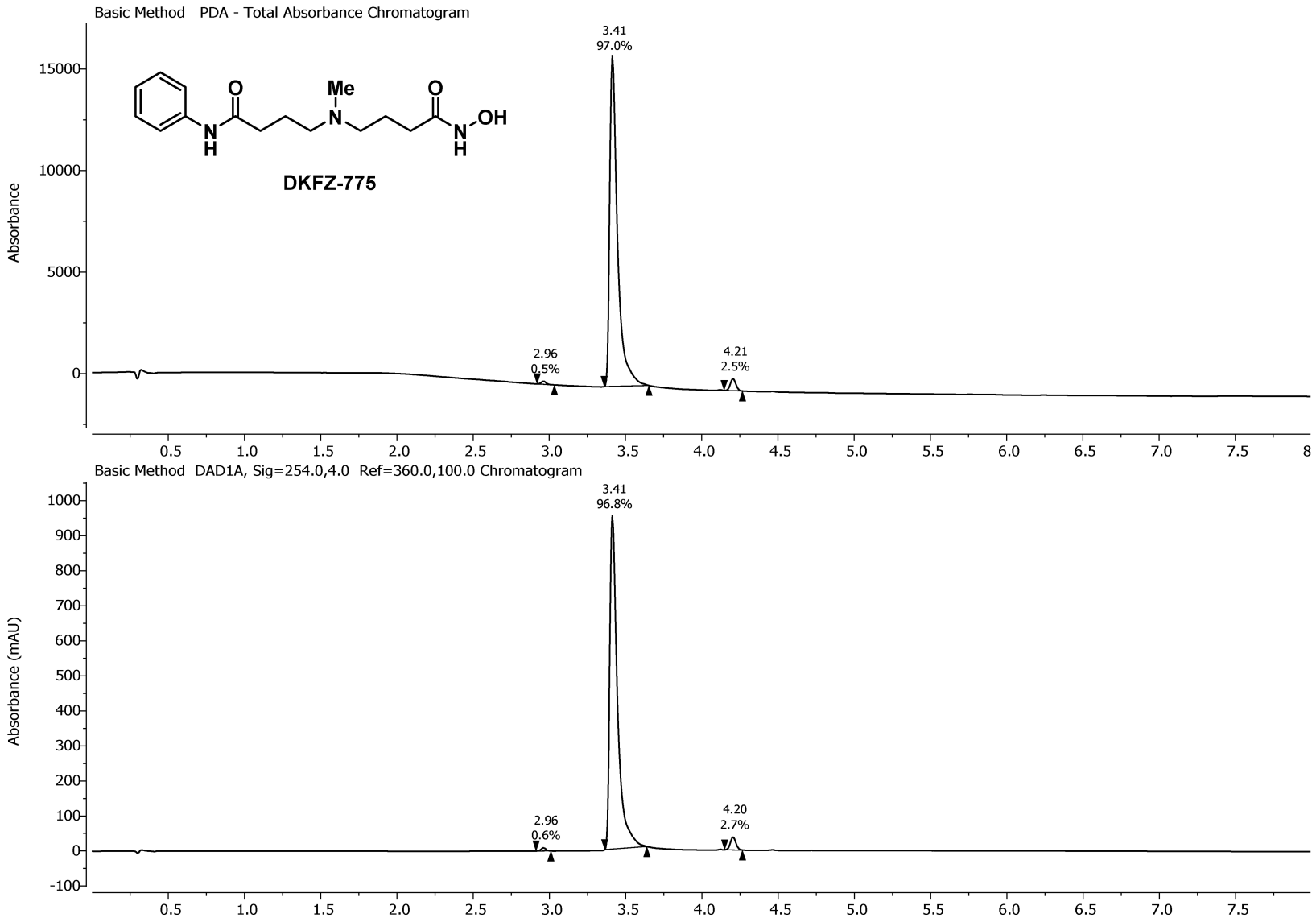
Basic Method PDA - Total Absorbance Chromatogram
3.41
97.0%
DKFZ-775
2.96
0.5%
4.21
2.5%
Absorbance
Basic Method DAD1A, Sig=254.0,4.0 Ref=360.0,100.0 Chromatogram
3.41
96.8%
2.96
0.6%
4.20
2.7%
Absorbance (mAU)

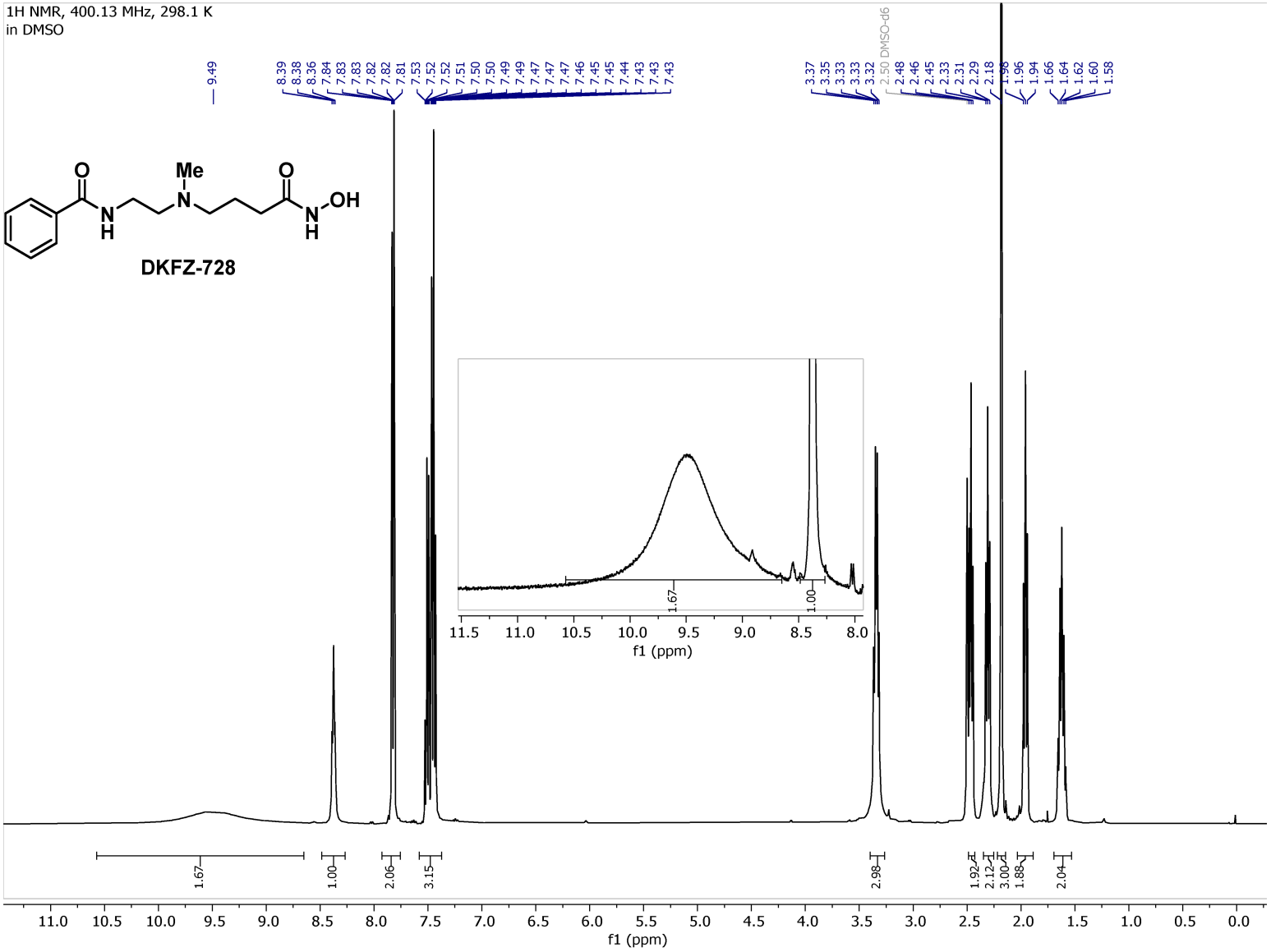
1H NMR, 400.13 MHz, 298.1 K
in DMSO
DKFZ-728
f1 (ppm)

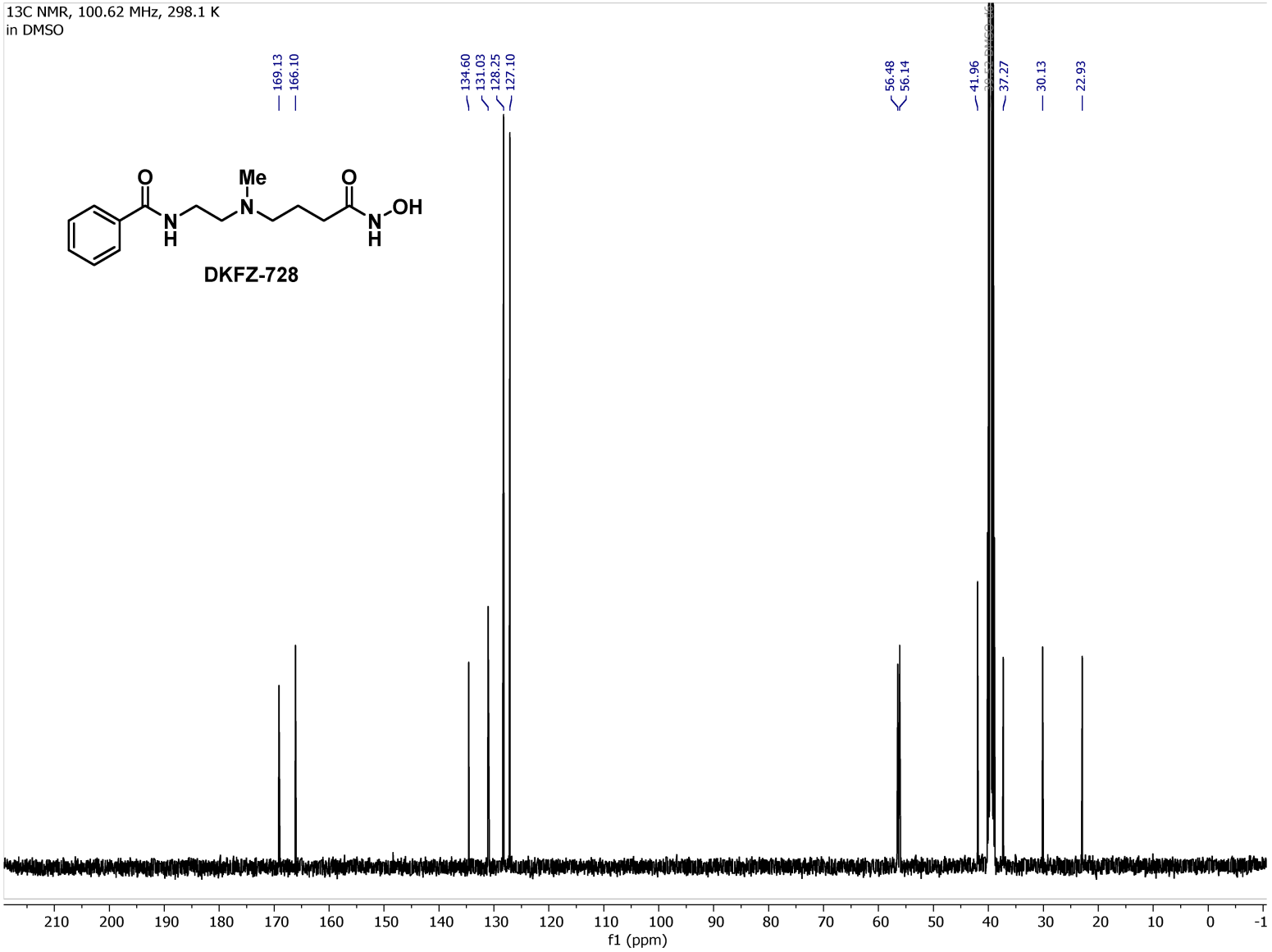
13C NMR, 100.62 MHz, 298.1 K
in DMSO
169.13
166.10
134.60
131.03
128.25
127.10
56.48
56.14
41.96
37.27
30.13
22.93
O
Me
O
N
N
N
OH
H
H
DKFZ-728
210 200 190 180 170 160 150 140 130 120 110 100 90 80 70 60 50 40 30 20 10 0 -1
f1 (ppm)

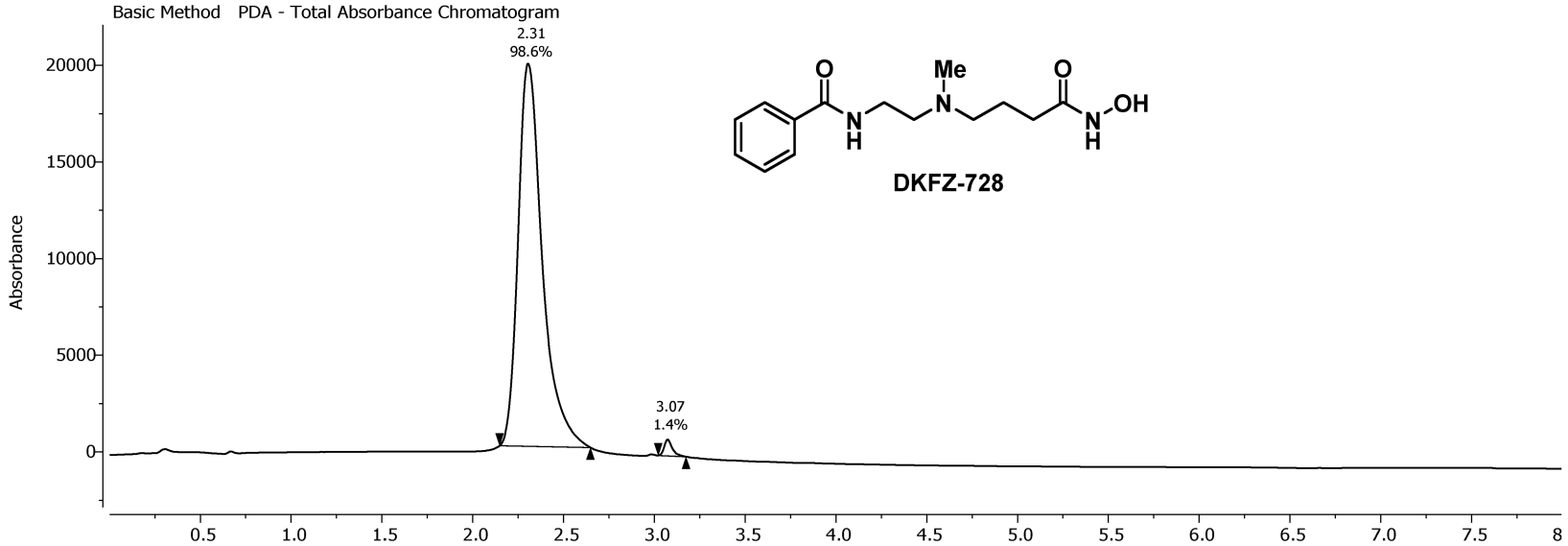
Basic Method PDA - Total Absorbance Chromatogram
2.31
98.6%
3.07
1.4%
Absorbance
20000
15000
10000
5000
0
0.5
1.0
1.5
2.0
2.5
3.0
3.5
4.0
4.5
5.0
5.5
6.0
6.5
7.0
7.5
8
O
Me
O
N
H
N
N
H
OH
DKFZ-728

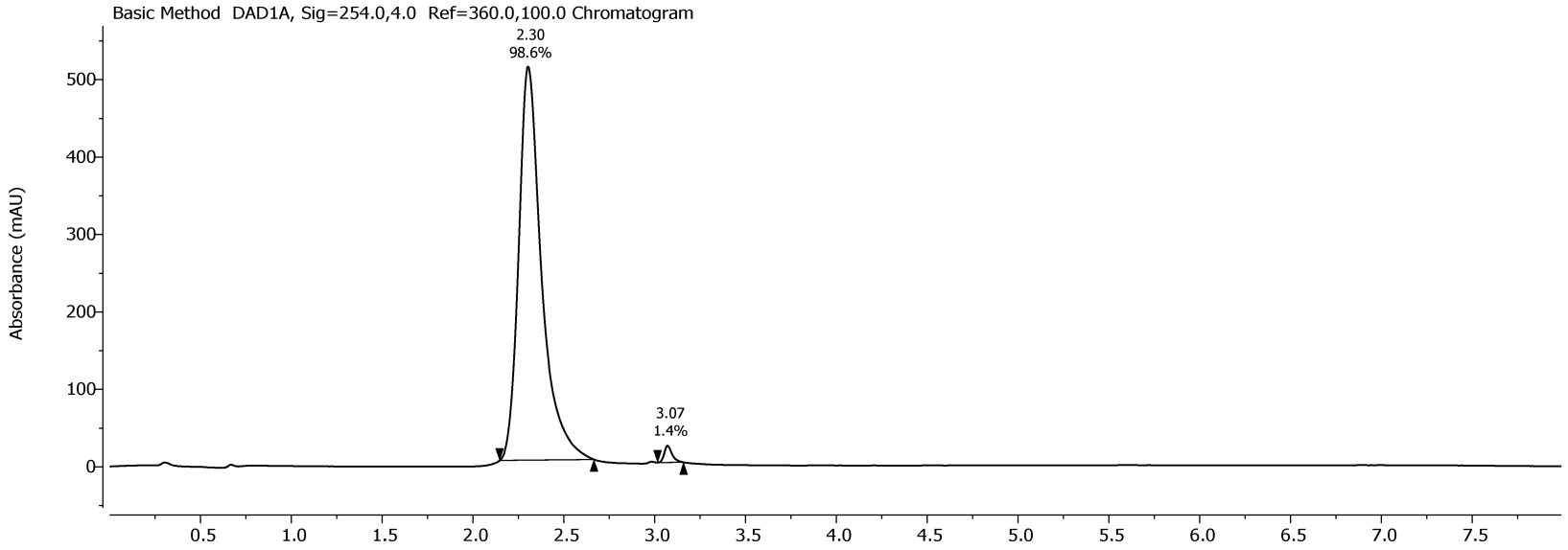
Basic Method DAD1A, Sig=254.0,4.0 Ref=360.0,100.0 Chromatogram
2.30
98.6%
3.07
1.4%
Absorbance (mAU)
500
400
300
200
100
0
0.5
1.0
1.5
2.0
2.5
3.0
3.5
4.0
4.5
5.0
5.5
6.0
6.5
7.0
7.5

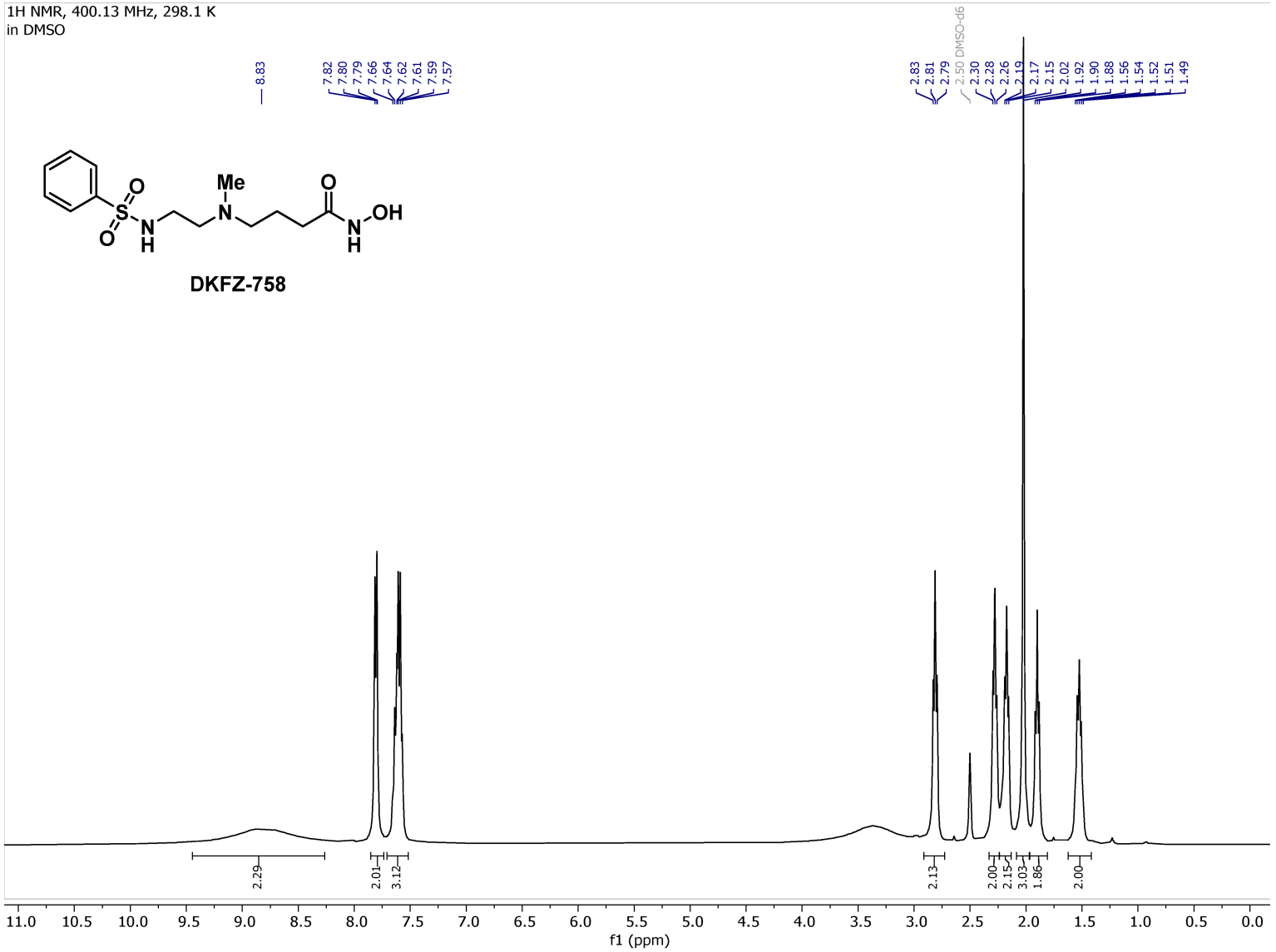
1H NMR, 400.13 MHz, 298.1 K
in DMSO
8.83
7.82
7.80
7.79
7.66
7.64
7.62
7.61
7.59
7.57
2.83
2.81
2.79
2.50 DMSO-d6
2.30
2.28
2.26
2.19
2.17
2.15
2.02
1.92
1.90
1.88
1.56
1.54
1.52
1.51
1.49
Me
O
S
O
N
H
N
O
N
H
OH
DKFZ-758
2.29
2.01
3.12
2.13
2.00
2.15
3.03
1.86
2.00
11.0
10.5
10.0
9.5
9.0
8.5
8.0
7.5
7.0
6.5
6.0
5.5
5.0
4.5
4.0
3.5
3.0
2.5
2.0
1.5
1.0
0.5
0.0
f1 (ppm)

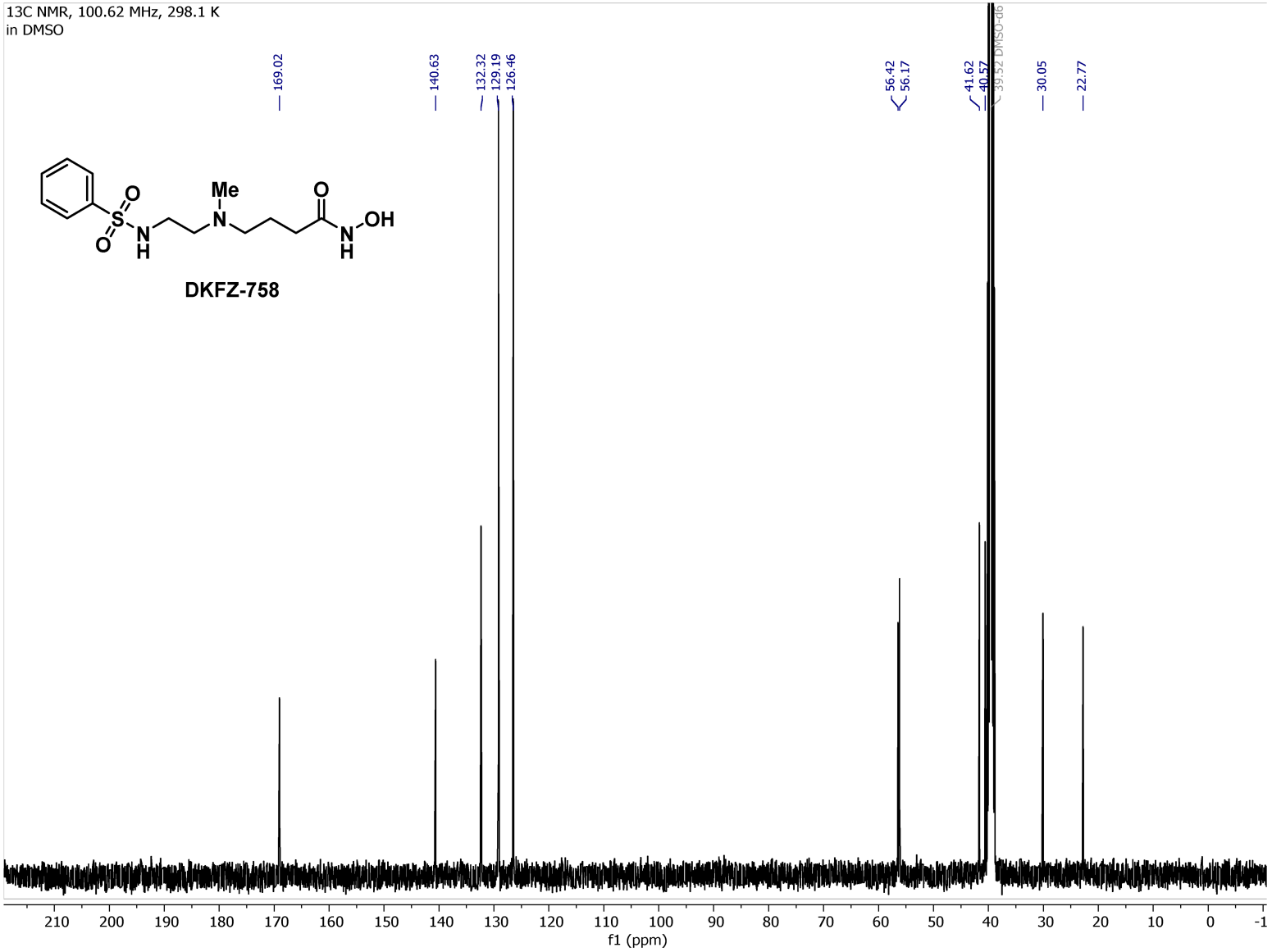
13C NMR, 100.62 MHz, 298.1 K
in DMSO
169.02
140.63
132.32
129.19
126.46
56.42
56.17
41.62
40.57
39.52 DMSO-d6
30.05
22.77
Me
O
S
O
O
N
H
N
N
H
OH
DKFZ-758
210 200 190 180 170 160 150 140 130 120 110 100 90 80 70 60 50 40 30 20 10 0 -1
f1 (ppm)

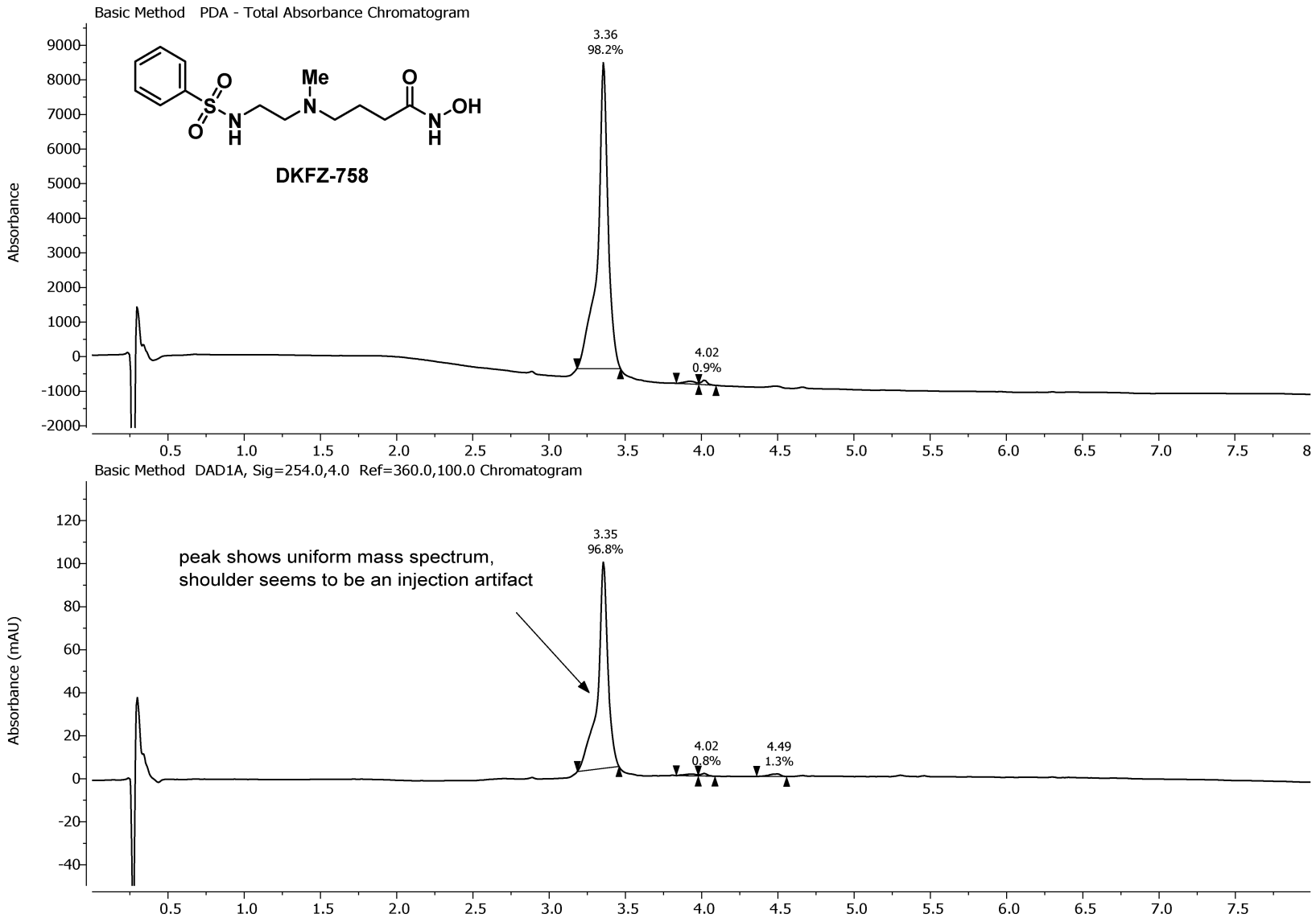
Basic Method PDA - Total Absorbance Chromatogram
Absorbance
3.36
98.2%
4.02
0.9%
DKFZ-758
Basic Method DAD1A, Sig=254.0,4.0 Ref=360.0,100.0 Chromatogram
Absorbance (mAU)
peak shows uniform mass spectrum,
shoulder seems to be an injection artifact
3.35
96.8%
4.02
0.8%
4.49
1.3%

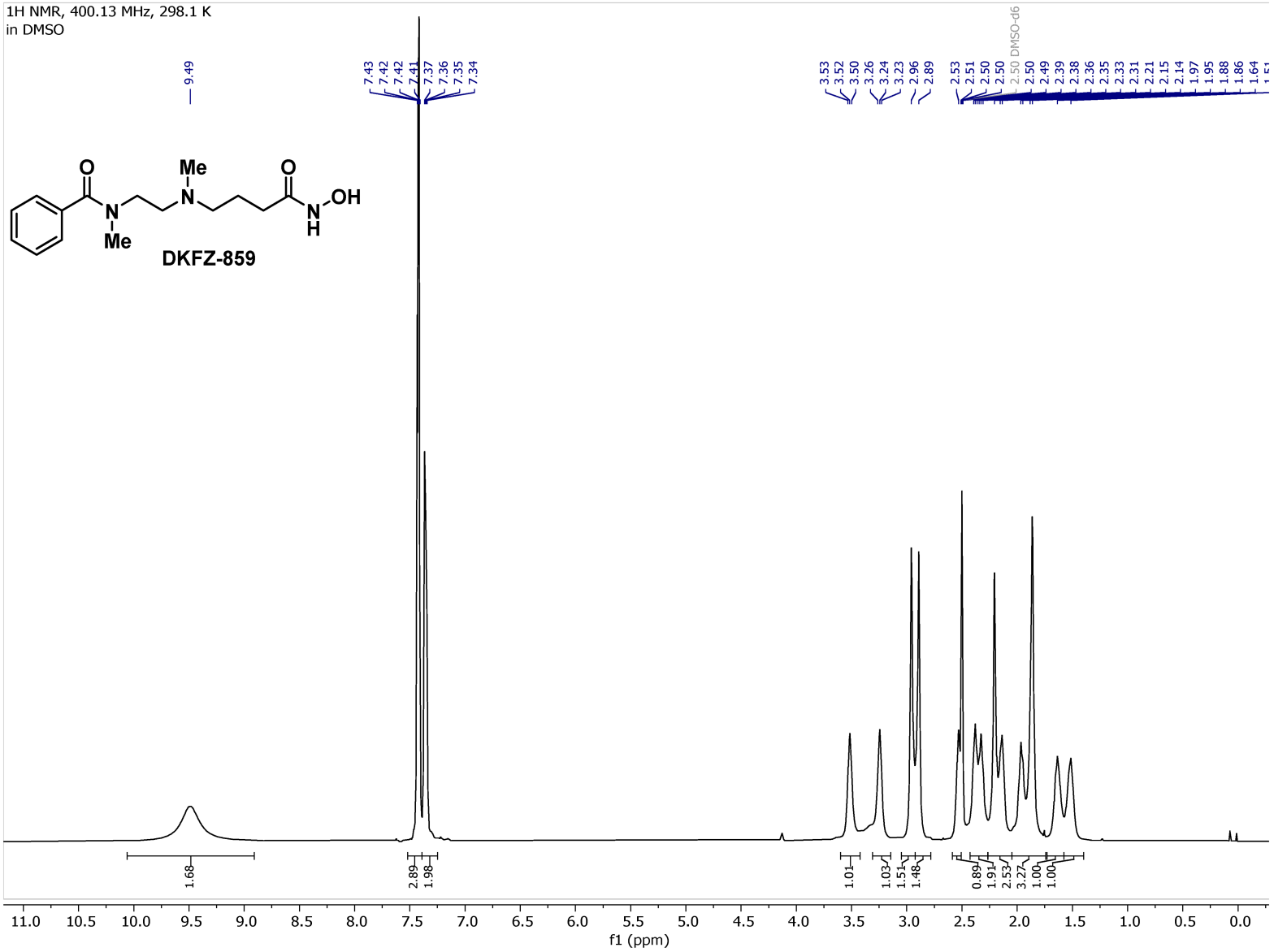
1H NMR, 400.13 MHz, 298.1 K
in DMSO
DKFZ-859
f1 (ppm)

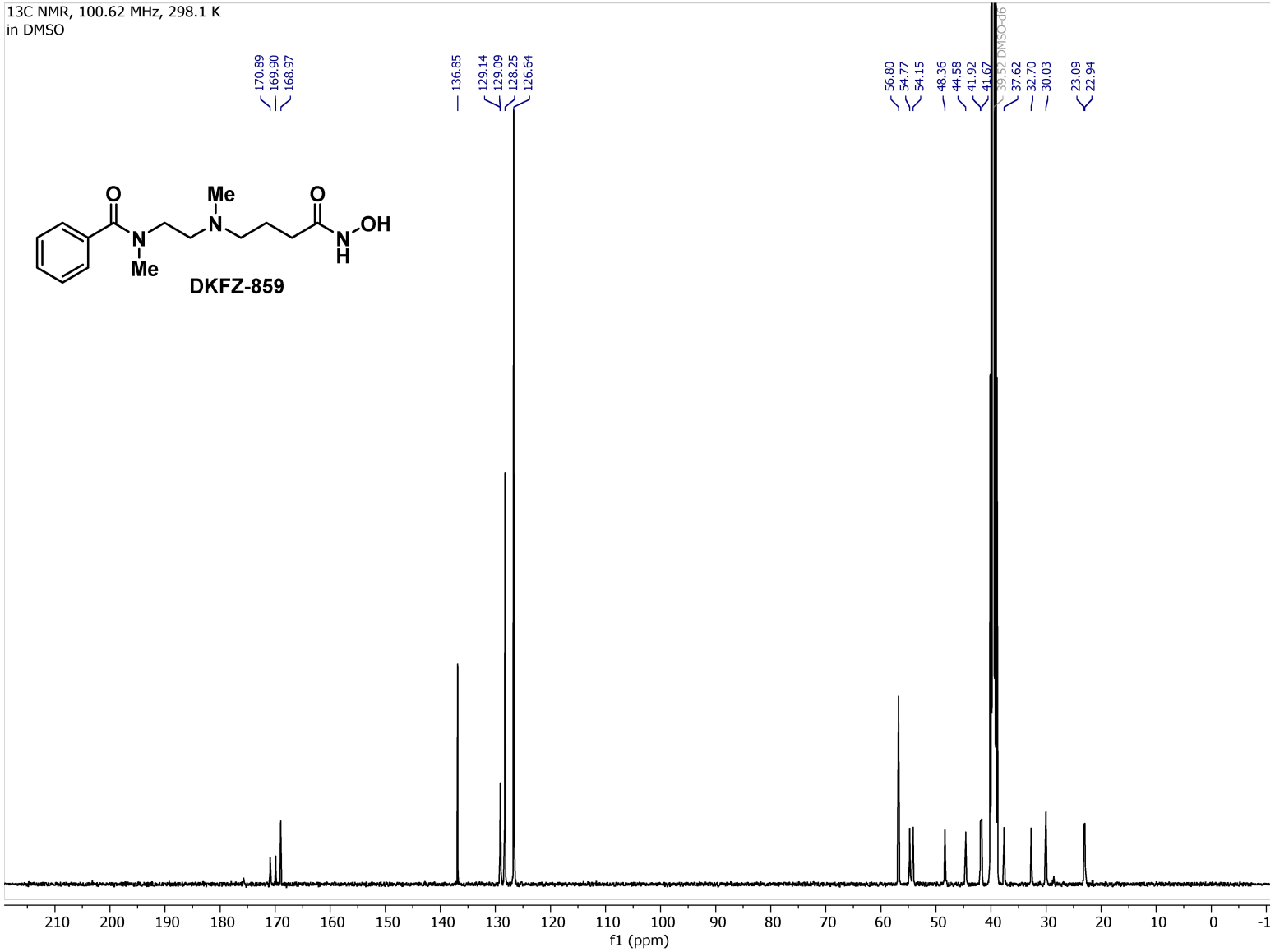
13C NMR, 100.62 MHz, 298.1 K
in DMSO
170.89
169.90
168.97
136.85
129.14
129.09
128.25
126.64
56.80
54.77
54.15
48.36
44.58
41.92
41.67
39.52 DMSO-d6
37.62
32.70
30.03
23.09
22.94
O
Me
O
N
N
OH
N
H
N
Me
DKFZ-859
210 200 190 180 170 160 150 140 130 120 110 100 90 80 70 60 50 40 30 20 10 0 -1
f1 (ppm)

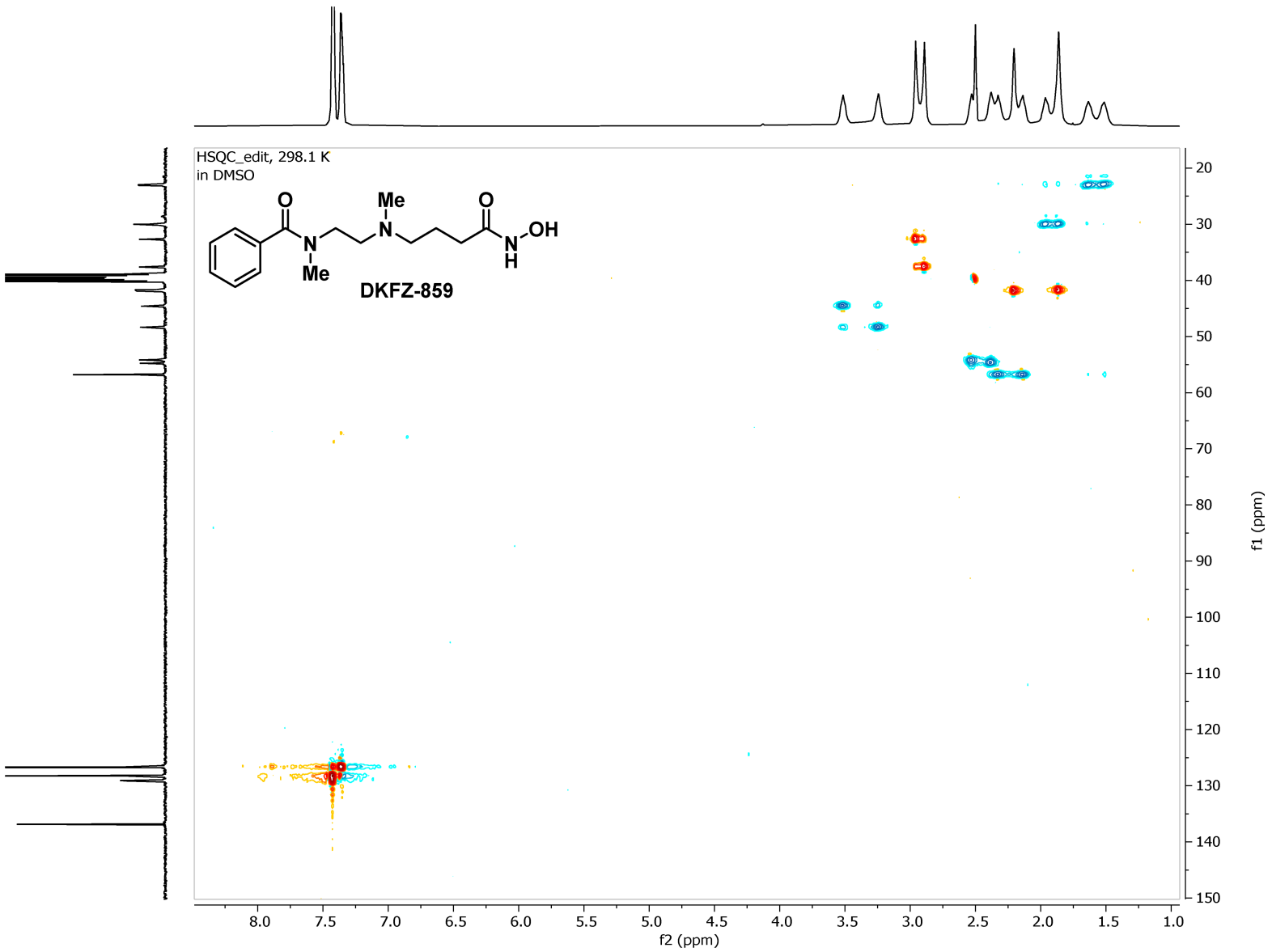
HSQC_edit, 298.1 K
in DMSO
O
Me
O
N
N
N
OH
Me
H
DKFZ-859
8.0
7.5
7.0
6.5
6.0
5.5
5.0
4.5
4.0
3.5
3.0
2.5
2.0
1.5
1.0
f2 (ppm)
20
30
40
50
60
70
80
90
100
110
120
130
140
150
f1 (ppm)

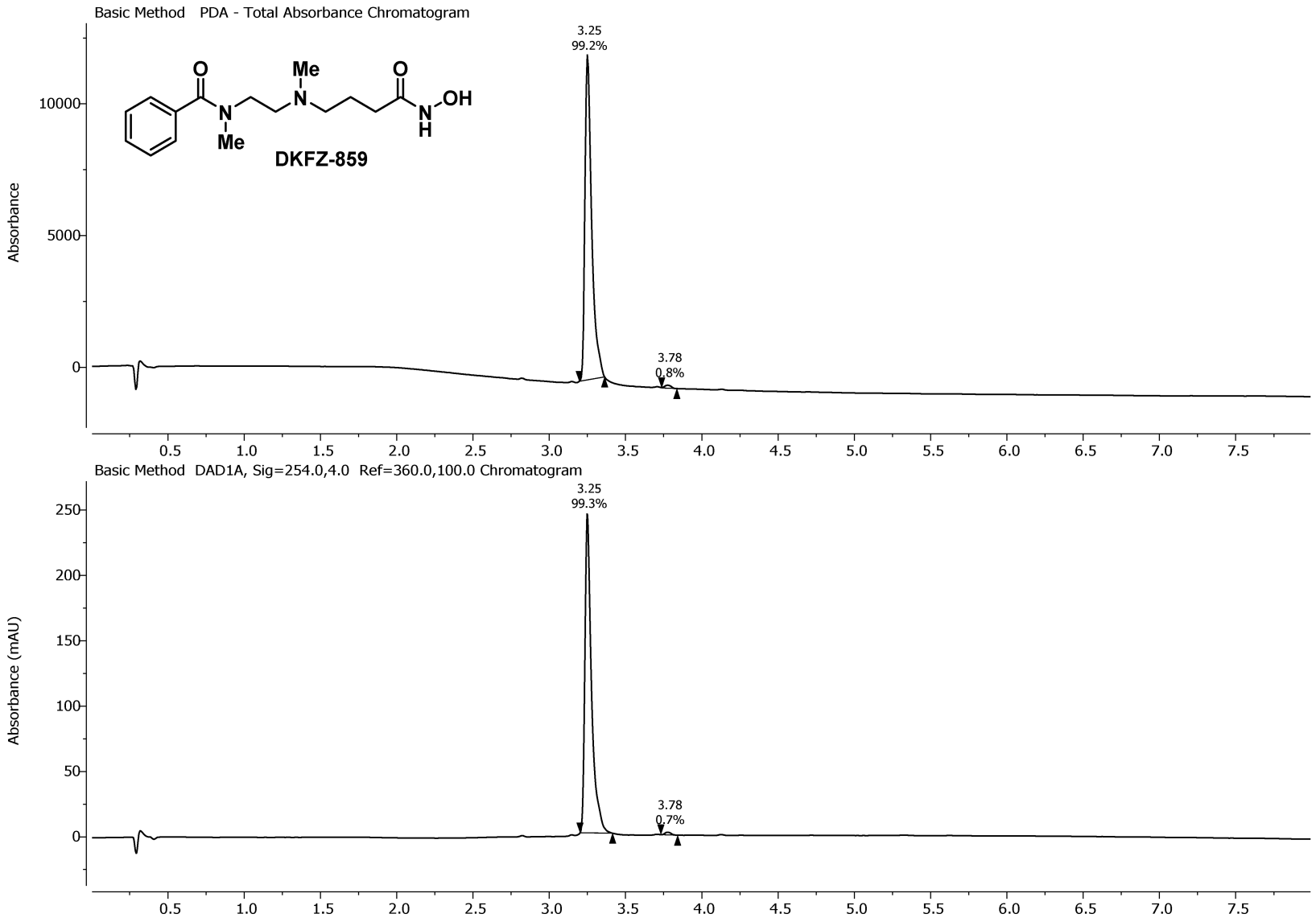
Basic Method PDA - Total Absorbance Chromatogram
3.25
99.2%
3.78
0.8%
DKFZ-859
Absorbance
Basic Method DAD1A, Sig=254.0,4.0 Ref=360.0,100.0 Chromatogram
3.25
99.3%
3.78
0.7%
Absorbance (mAU)

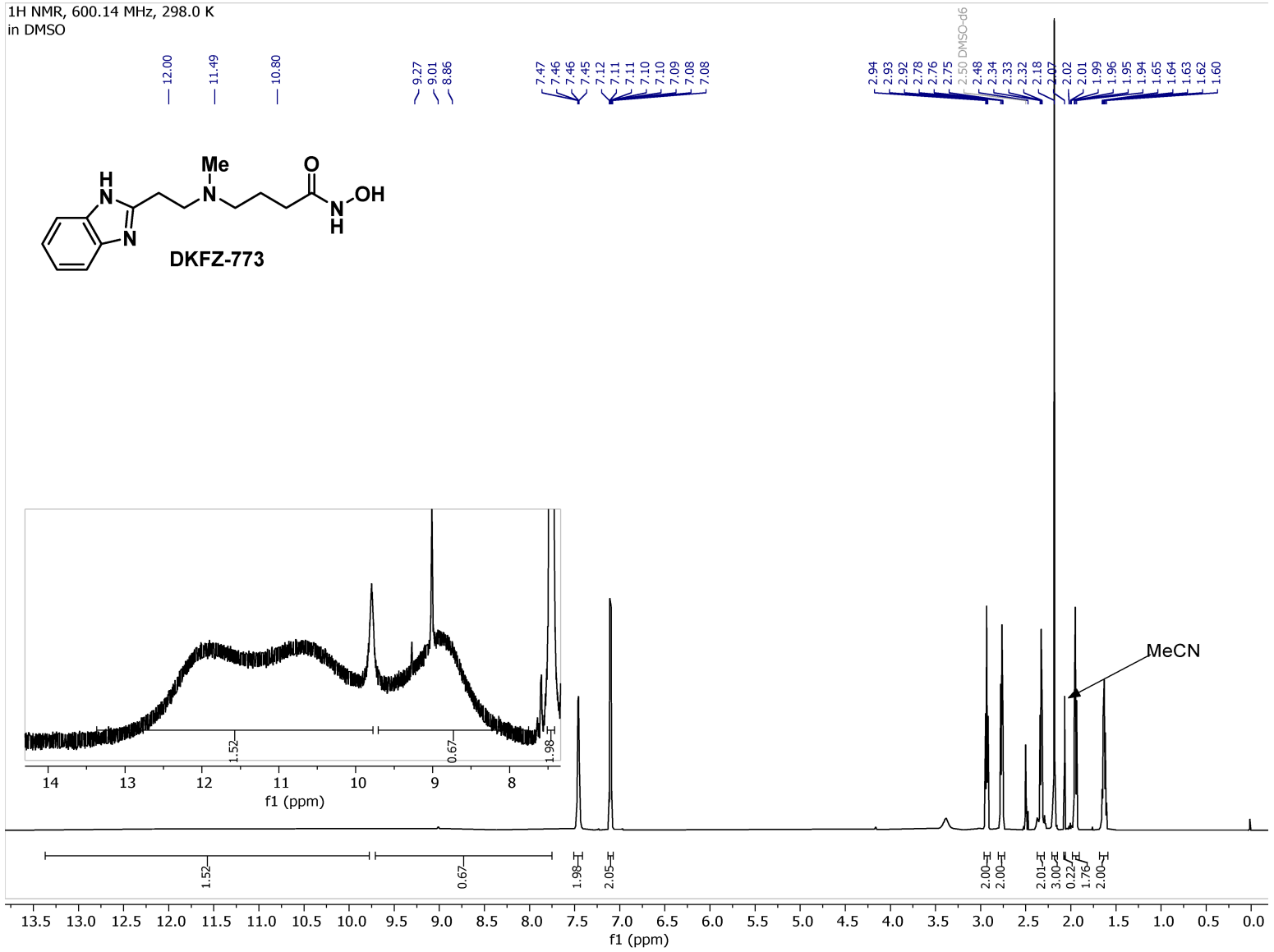
1H NMR, 600.14 MHz, 298.0 K
in DMSO
12.00
11.49
10.80
9.27
9.01
8.86
7.47
7.46
7.46
7.45
7.12
7.11
7.11
7.10
7.10
7.09
7.08
7.08
2.94
2.93
2.92
2.78
2.76
2.75
2.50 DMSO-d6
2.48
2.34
2.33
2.32
2.18
2.07
2.02
2.01
1.99
1.96
1.95
1.94
1.65
1.64
1.63
1.62
1.60
Me
O
H
N
N
N
N
OH
H
DKFZ-773
MeCN
1.52
0.67
1.98
f1 (ppm)
2.05
2.00
2.00
2.01
3.00
0.22
1.76
2.00

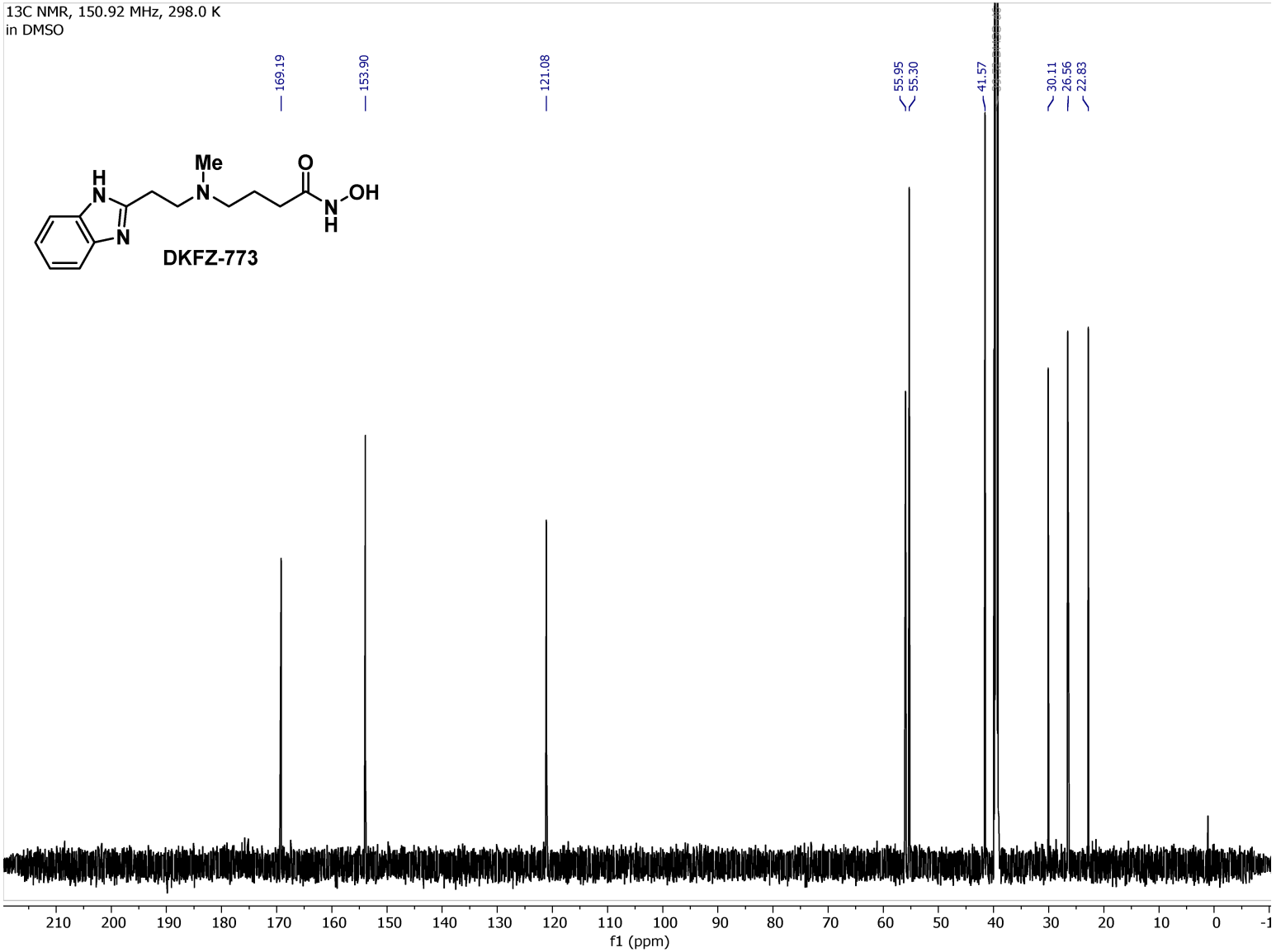
13C NMR, 150.92 MHz, 298.0 K
in DMSO
169.19
153.90
121.08
55.95
55.30
41.57
30.11
26.56
22.83
Me
O
H
N
N
N
N
H
OH
DKFZ-773
210 200 190 180 170 160 150 140 130 120 110 100 90 80 70 60 50 40 30 20 10 0 -1
f1 (ppm)

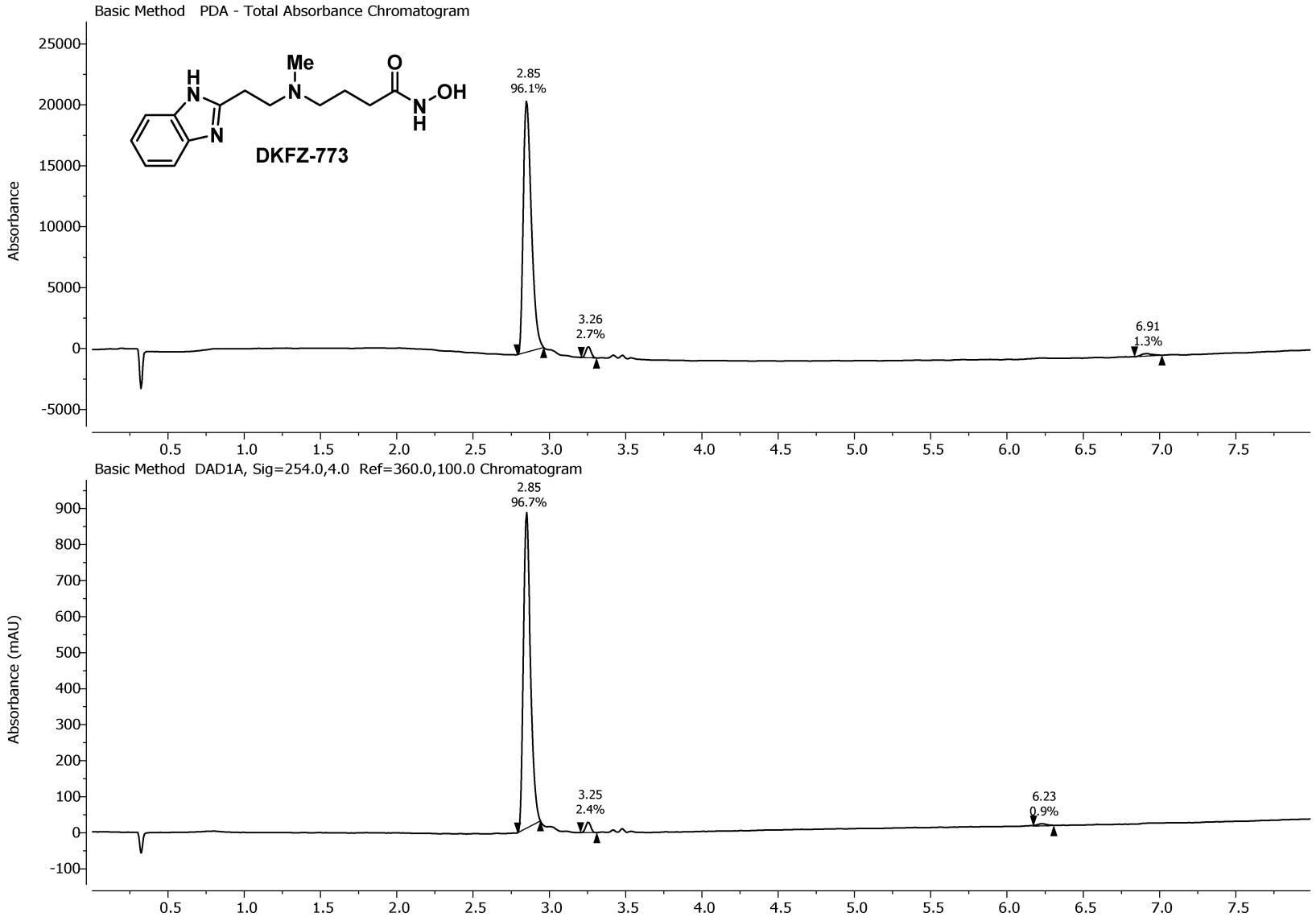
Basic Method PDA - Total Absorbance Chromatogram
Absorbance
25000
20000
15000
10000
5000
0
-5000
Me
O
H
N
N
N
OH
N
H
DKFZ-773
2.85
96.1%
3.26
2.7%
6.91
1.3%
0.5
1.0
1.5
2.0
2.5
3.0
3.5
4.0
4.5
5.0
5.5
6.0
6.5
7.0
7.5
Basic Method DAD1A, Sig=254.0,4.0 Ref=360.0,100.0 Chromatogram
Absorbance (mAU)
900
800
700
600
500
400
300
200
100
0
-100
2.85
96.7%
3.25
2.4%
6.23
0.9%
0.5
1.0
1.5
2.0
2.5
3.0
3.5
4.0
4.5
5.0
5.5
6.0
6.5
7.0
7.5

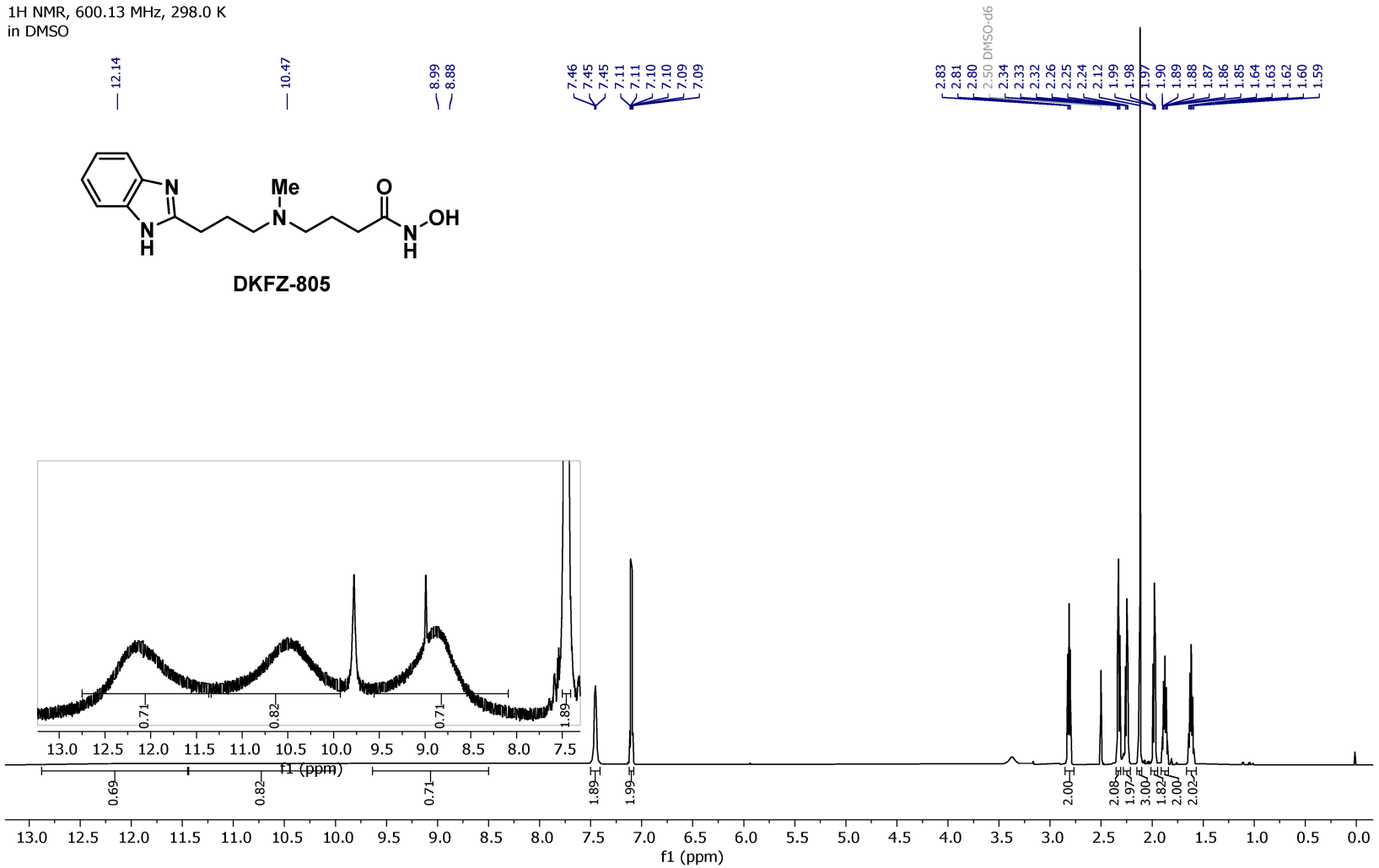
1H NMR, 600.13 MHz, 298.0 K
in DMSO
12.14
10.47
8.99
8.88
7.46
7.45
7.45
7.11
7.11
7.10
7.10
7.09
7.09
2.83
2.81
2.80
2.50 DMSO-d6
2.34
2.33
2.32
2.26
2.25
2.24
2.12
1.99
1.98
1.97
1.90
1.89
1.88
1.87
1.86
1.85
1.64
1.63
1.62
1.60
1.59
N
Me
O
N
N
H
N
OH
H
DKFZ-805
0.71
0.82
0.71
1.89
13.0 12.5 12.0 11.5 11.0 10.5 10.0 9.5 9.0 8.5 8.0 7.5
f1 (ppm)
0.69
0.82
0.71
1.89
1.99
2.00
2.08
1.97
3.00
1.82
2.00
2.02
13.0 12.5 12.0 11.5 11.0 10.5 10.0 9.5 9.0 8.5 8.0 7.5 7.0 6.5 6.0 5.5 5.0 4.5 4.0 3.5 3.0 2.5 2.0 1.5 1.0 0.5 0.0
f1 (ppm)

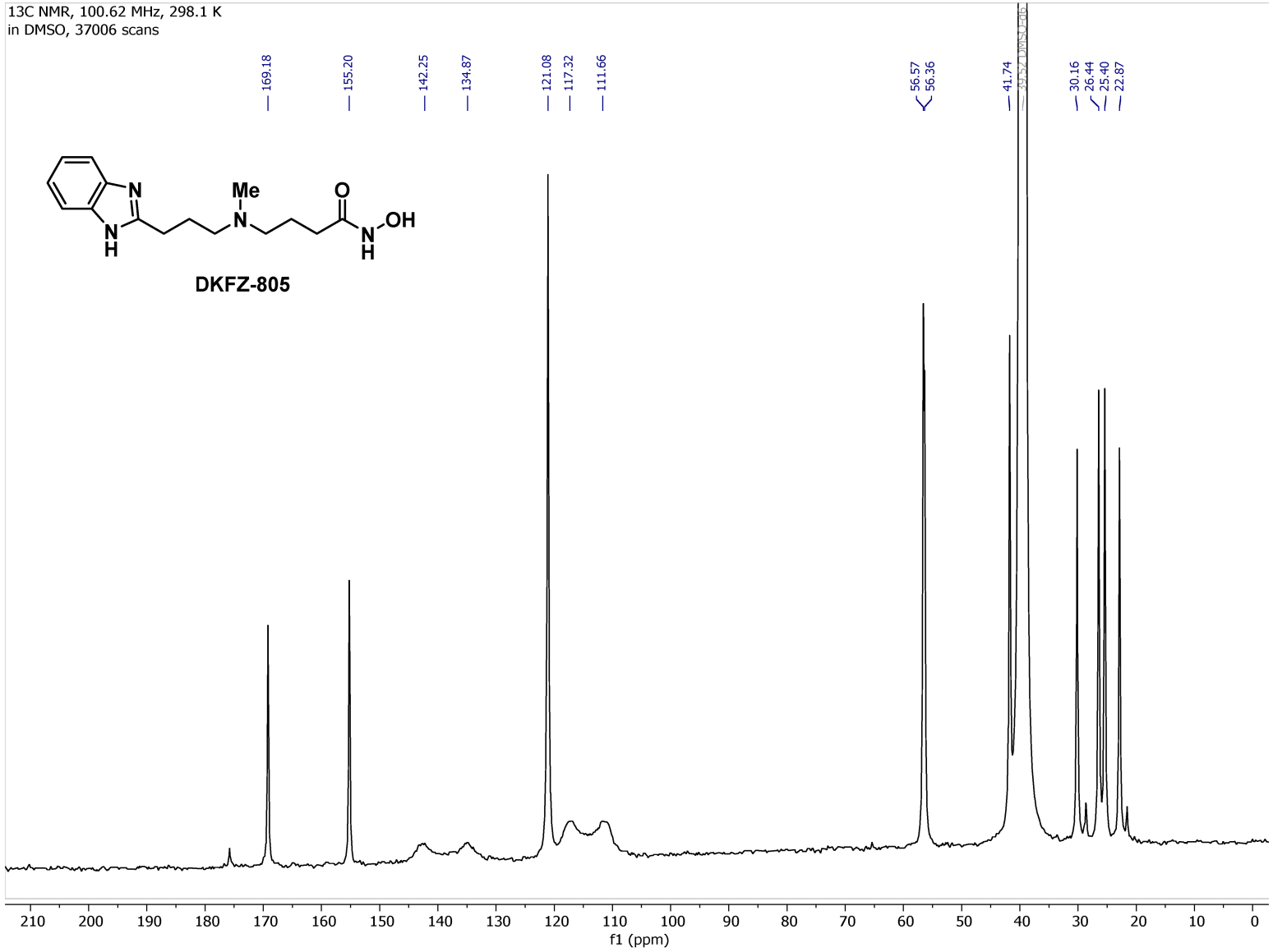
13C NMR, 100.62 MHz, 298.1 K
in DMSO, 37006 scans
169.18
155.20
142.25
134.87
121.08
117.32
111.66
56.57
56.36
41.74
30.16
26.44
25.40
22.87
Me
O
OH
DKFZ-805
f1 (ppm)

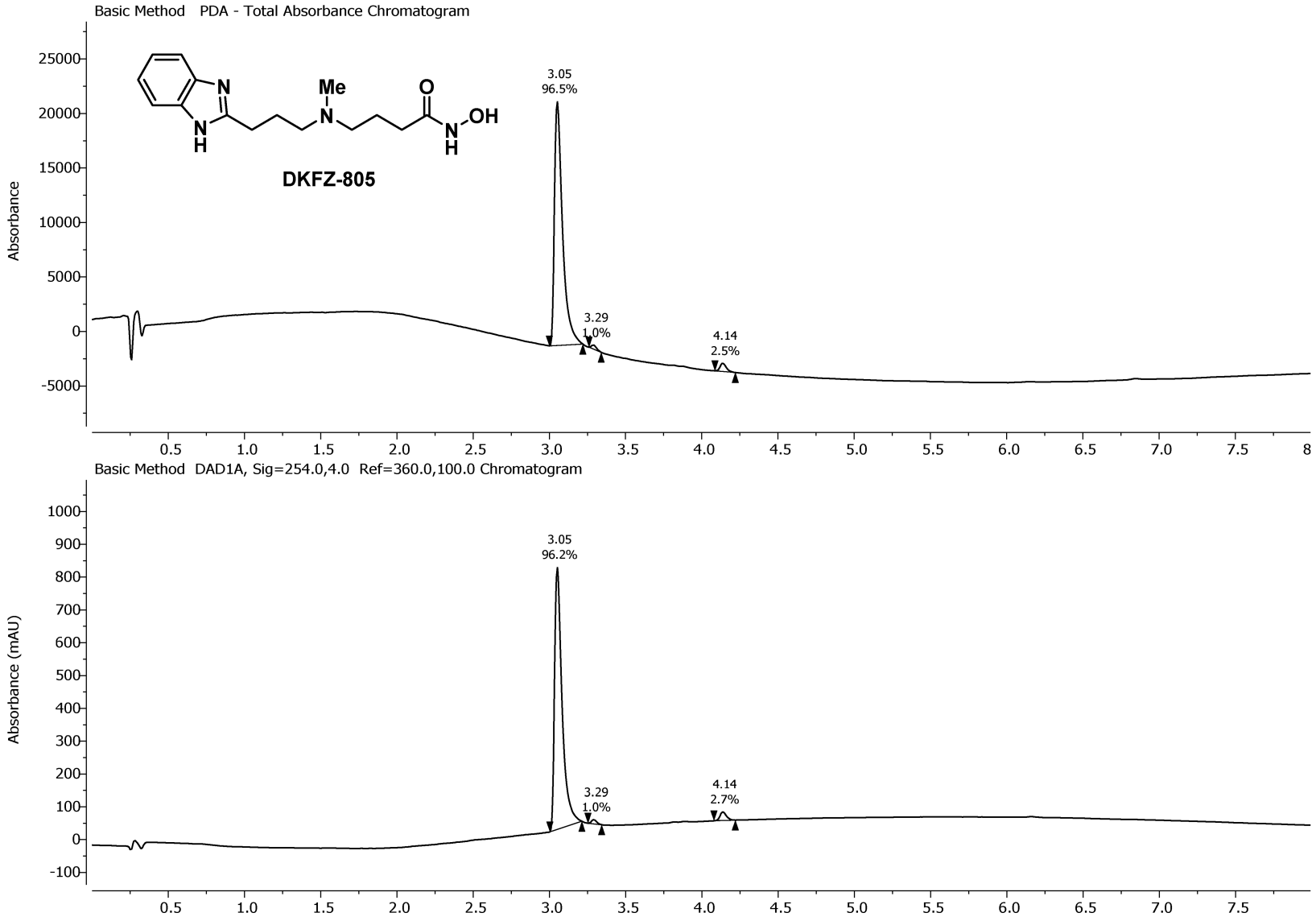
Basic Method PDA - Total Absorbance Chromatogram
Absorbance
25000
20000
15000
10000
5000
0
-5000
N
Me
O
N
N
H
N
OH
H
DKFZ-805
3.05
96.5%
3.29
1.0%
4.14
2.5%
0.5
1.0
1.5
2.0
2.5
3.0
3.5
4.0
4.5
5.0
5.5
6.0
6.5
7.0
7.5
8
Basic Method DAD1A, Sig=254.0,4.0 Ref=360.0,100.0 Chromatogram
Absorbance (mAU)
1000
900
800
700
600
500
400
300
200
100
0
-100
3.05
96.2%
3.29
1.0%
4.14
2.7%
0.5
1.0
1.5
2.0
2.5
3.0
3.5
4.0
4.5
5.0
5.5
6.0
6.5
7.0
7.5

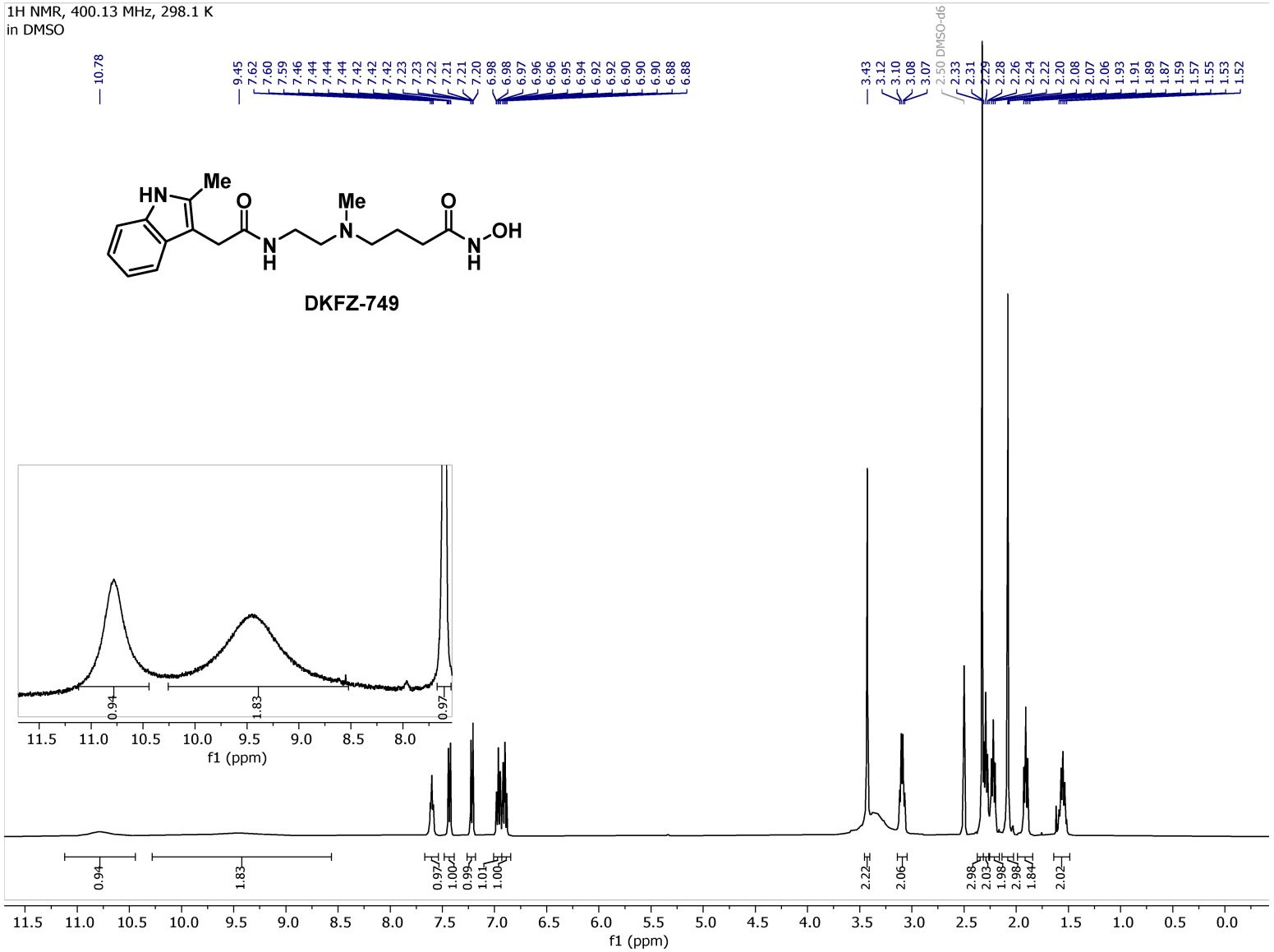
1H NMR, 400.13 MHz, 298.1 K
in DMSO
10.78
9.45
7.62
7.60
7.59
7.46
7.44
7.44
7.44
7.42
7.42
7.42
7.23
7.23
7.22
7.21
7.21
7.20
6.98
6.98
6.97
6.96
6.96
6.95
6.94
6.92
6.92
6.90
6.90
6.90
6.88
6.88
3.43
3.12
3.10
3.08
3.07
2.50 DMSO-d6
2.33
2.31
2.29
2.28
2.26
2.24
2.22
2.20
2.08
2.07
2.06
1.93
1.91
1.89
1.87
1.59
1.57
1.55
1.53
1.52
HN
Me
O
N
H
Me
N
O
N
H
OH
DKFZ-749
0.94
1.83
0.97
11.5 11.0 10.5 10.0 9.5 9.0 8.5 8.0
f1 (ppm)
0.94
1.83
0.97
1.00
0.99
1.01
1.00
2.22
2.06
2.98
2.03
1.98
2.98
1.84
2.02
11.5 11.0 10.5 10.0 9.5 9.0 8.5 8.0 7.5 7.0 6.5 6.0 5.5 5.0 4.5 4.0 3.5 3.0 2.5 2.0 1.5 1.0 0.5 0.0
f1 (ppm)

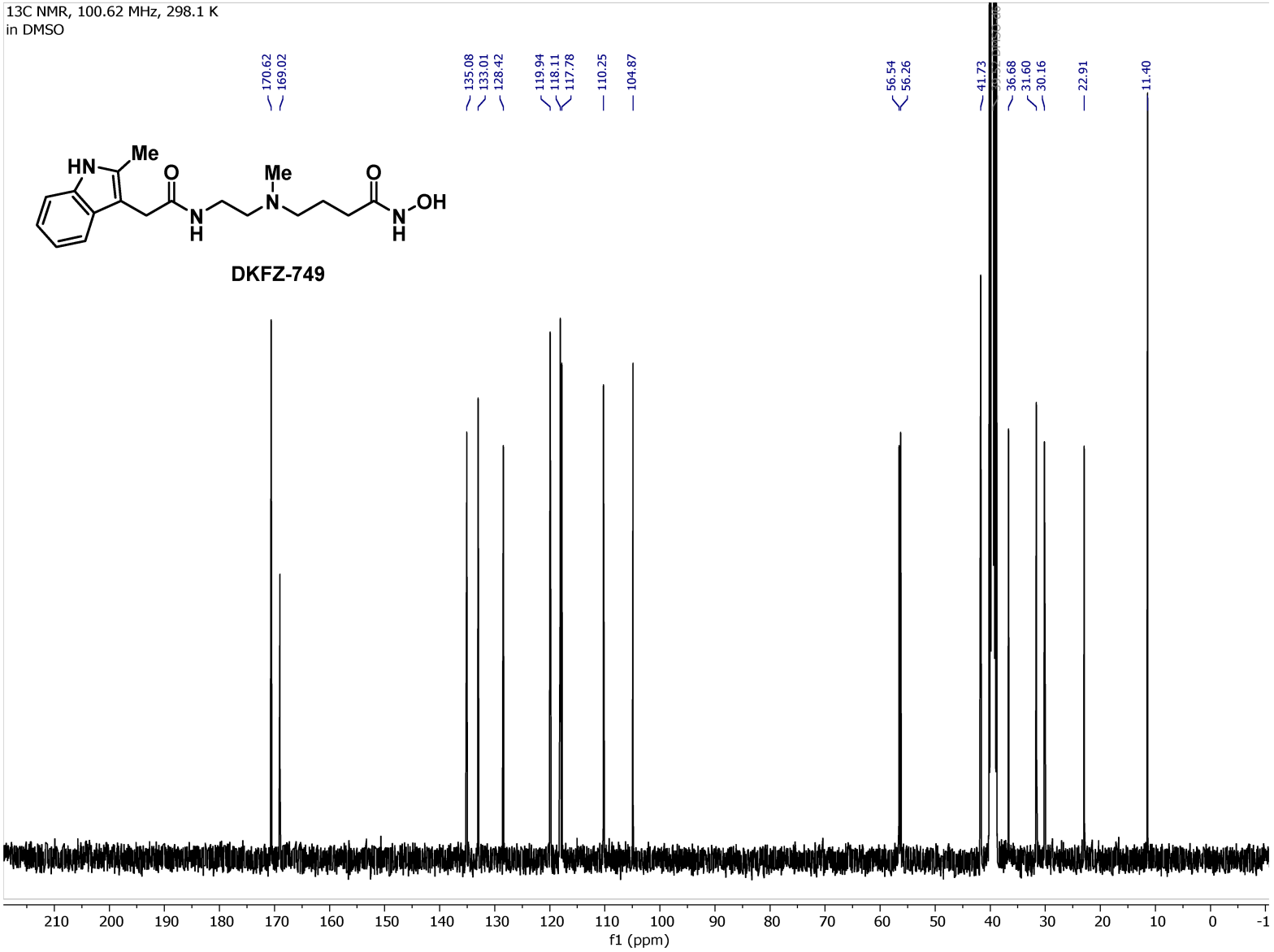
13C NMR, 100.62 MHz, 298.1 K
in DMSO
170.62
169.02
135.08
133.01
128.42
119.94
118.11
117.78
110.25
104.87
56.54
56.26
41.73
36.68
31.60
30.16
22.91
11.40
HN
Me
O
N
H
Me
N
O
N
H
OH
DKFZ-749
210
200
190
180
170
160
150
140
130
120
110
100
90
80
70
60
50
40
30
20
10
0
-1
f1 (ppm)

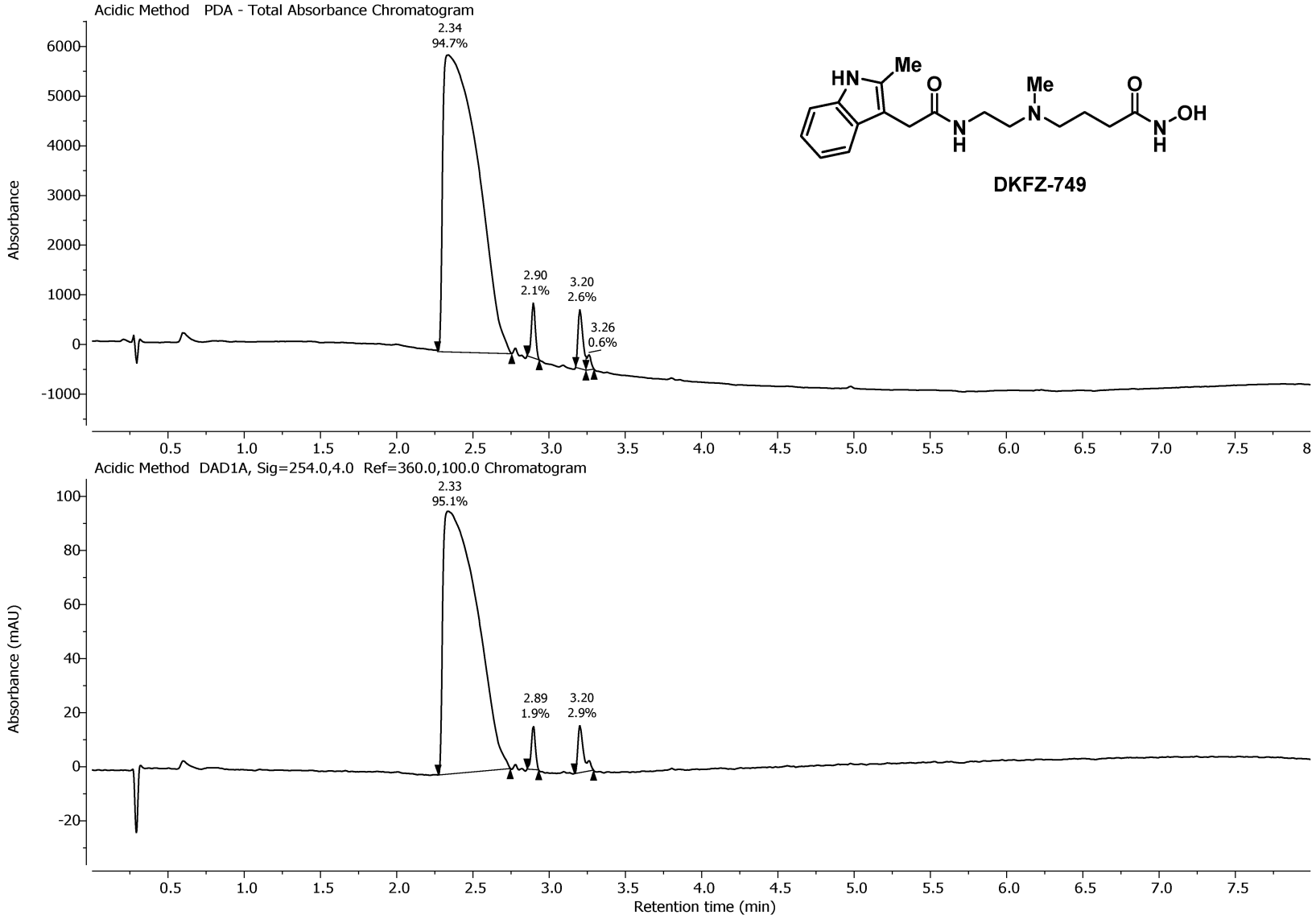
Acidic Method PDA - Total Absorbance Chromatogram
2.34
94.7%
2.90
2.1%
3.20
2.6%
3.26
0.6%
Absorbance
6000
5000
4000
3000
2000
1000
0
-1000
0.5
1.0
1.5
2.0
2.5
3.0
3.5
4.0
4.5
5.0
5.5
6.0
6.5
7.0
7.5
8
HN
Me
O
N
H
Me
N
O
N
H
OH
DKFZ-749
Acidic Method DAD1A, Sig=254.0,4.0 Ref=360.0,100.0 Chromatogram
2.33
95.1%
2.89
1.9%
3.20
2.9%
Absorbance (mAU)
100
80
60
40
20
0
-20
0.5
1.0
1.5
2.0
2.5
3.0
3.5
4.0
4.5
5.0
5.5
6.0
6.5
7.0
7.5
Retention time (min)

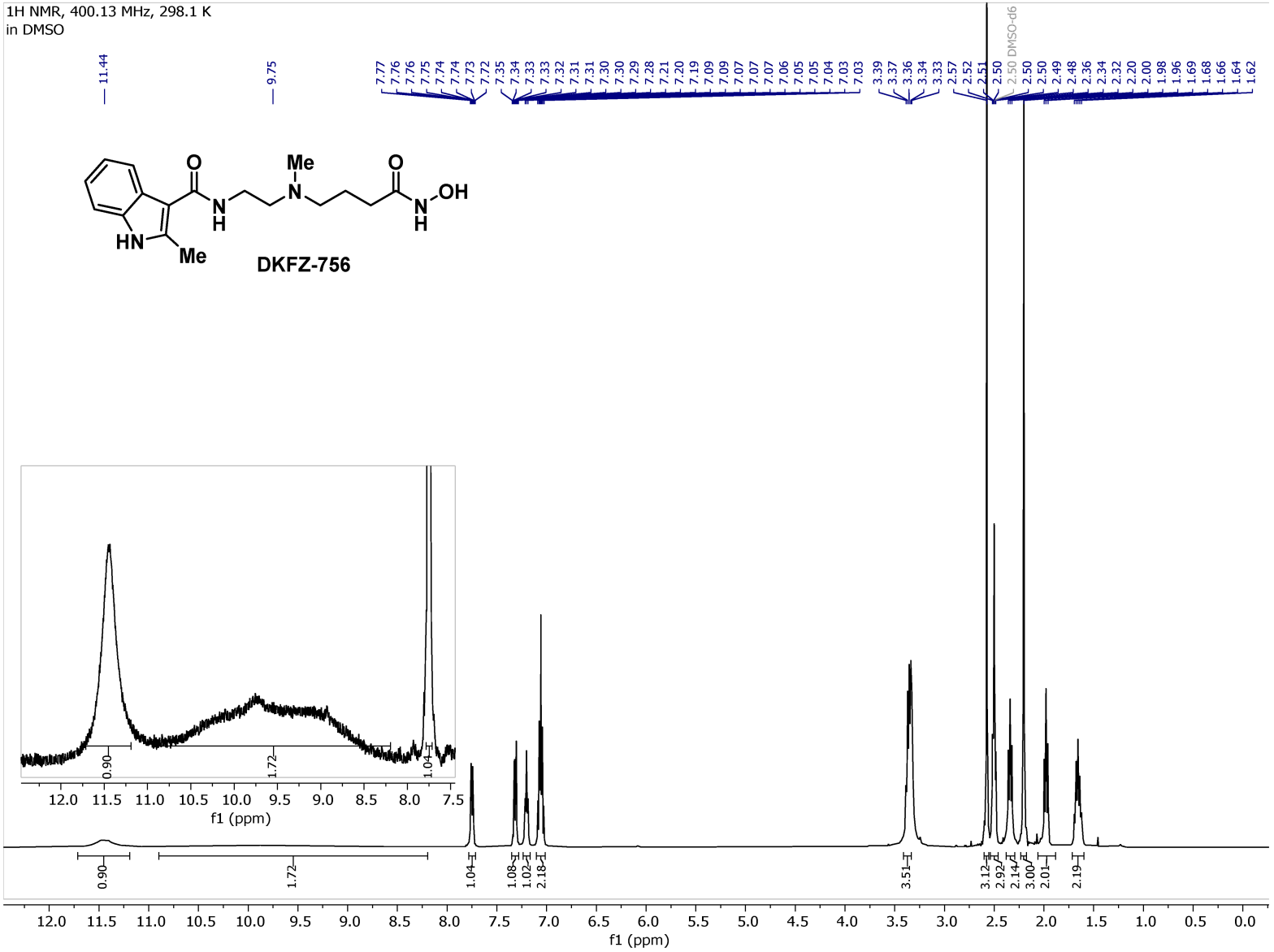
1H NMR, 400.13 MHz, 298.1 K
in DMSO
DKFZ-756
f1 (ppm)

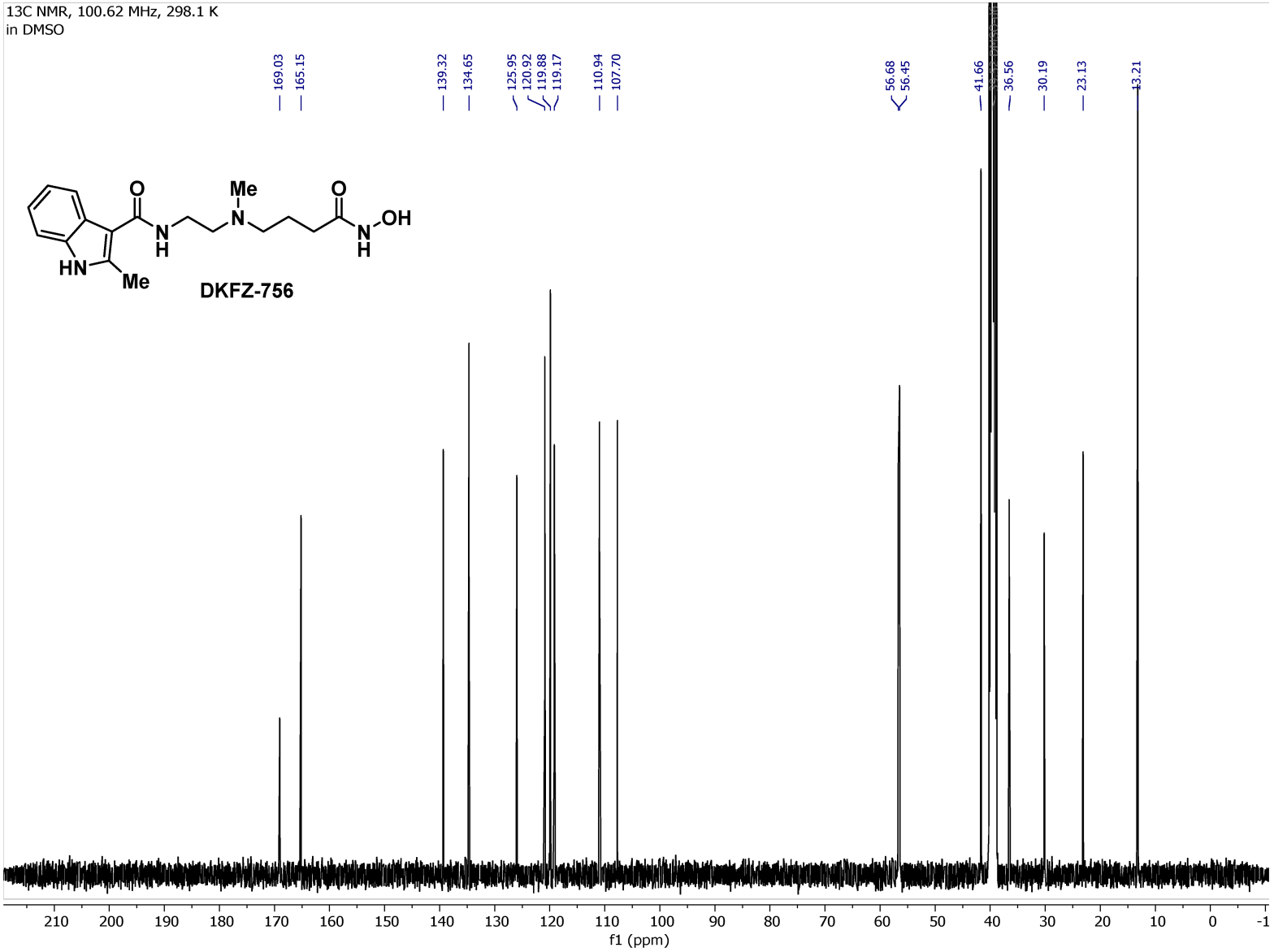
13C NMR, 100.62 MHz, 298.1 K
in DMSO
169.03
165.15
139.32
134.65
125.95
120.92
119.88
119.17
110.94
107.70
56.68
56.45
41.66
36.56
30.19
23.13
13.21
O
Me
O
N
N
N
OH
H
H
HN
Me
DKFZ-756
210
200
190
180
170
160
150
140
130
120
110
100
90
80
70
60
50
40
30
20
10
0
-1
f1 (ppm)

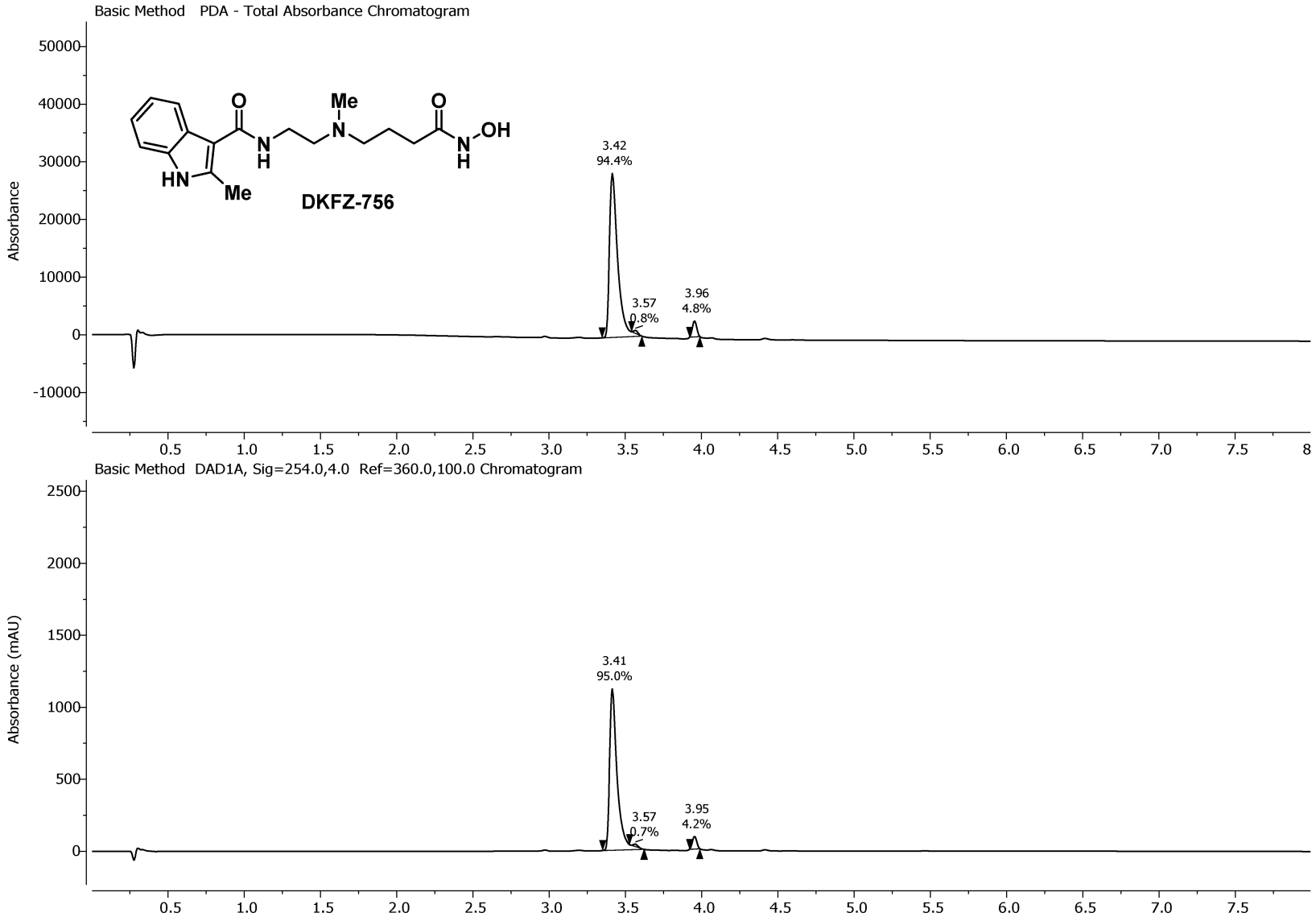
Basic Method PDA - Total Absorbance Chromatogram
Absorbance
50000
40000
30000
20000
10000
0
-10000
O
Me
O
N
N
OH
H
H
HN
Me
DKFZ-756
3.42
94.4%
3.57
0.8%
3.96
4.8%
0.5
1.0
1.5
2.0
2.5
3.0
3.5
4.0
4.5
5.0
5.5
6.0
6.5
7.0
7.5
8
Basic Method DAD1A, Sig=254.0,4.0 Ref=360.0,100.0 Chromatogram
Absorbance (mAU)
2500
2000
1500
1000
500
0
3.41
95.0%
3.57
0.7%
3.95
4.2%
0.5
1.0
1.5
2.0
2.5
3.0
3.5
4.0
4.5
5.0
5.5
6.0
6.5
7.0
7.5

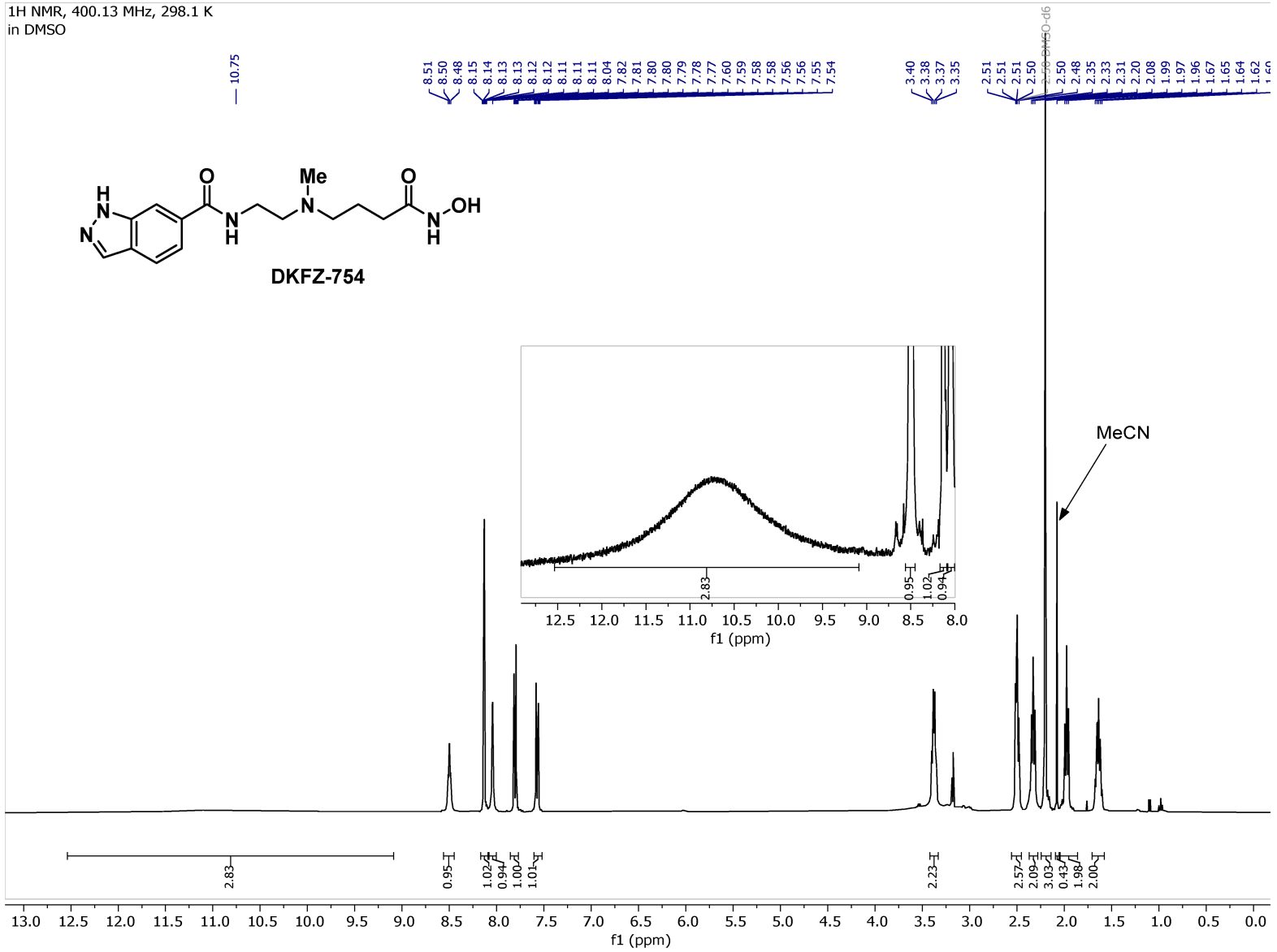
1H NMR, 400.13 MHz, 298.1 K
in DMSO
DKFZ-754
MeCN
f1 (ppm)

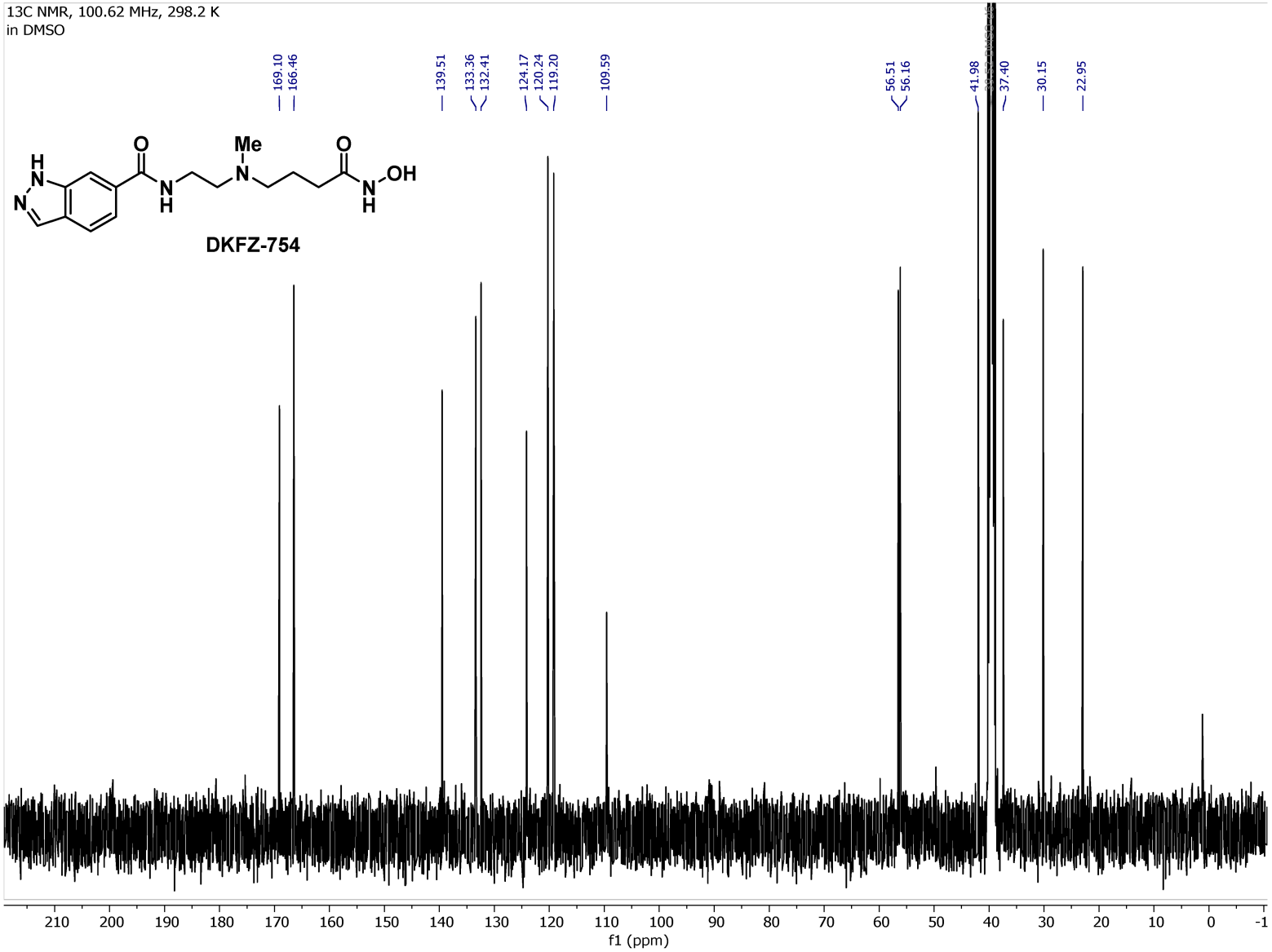
13C NMR, 100.62 MHz, 298.2 K
in DMSO
169.10
166.46
139.51
133.36
132.41
124.17
120.24
119.20
109.59
56.51
56.16
41.98
37.40
30.15
22.95
DKFZ-754
210 200 190 180 170 160 150 140 130 120 110 100 90 80 70 60 50 40 30 20 10 0 -1
f1 (ppm)

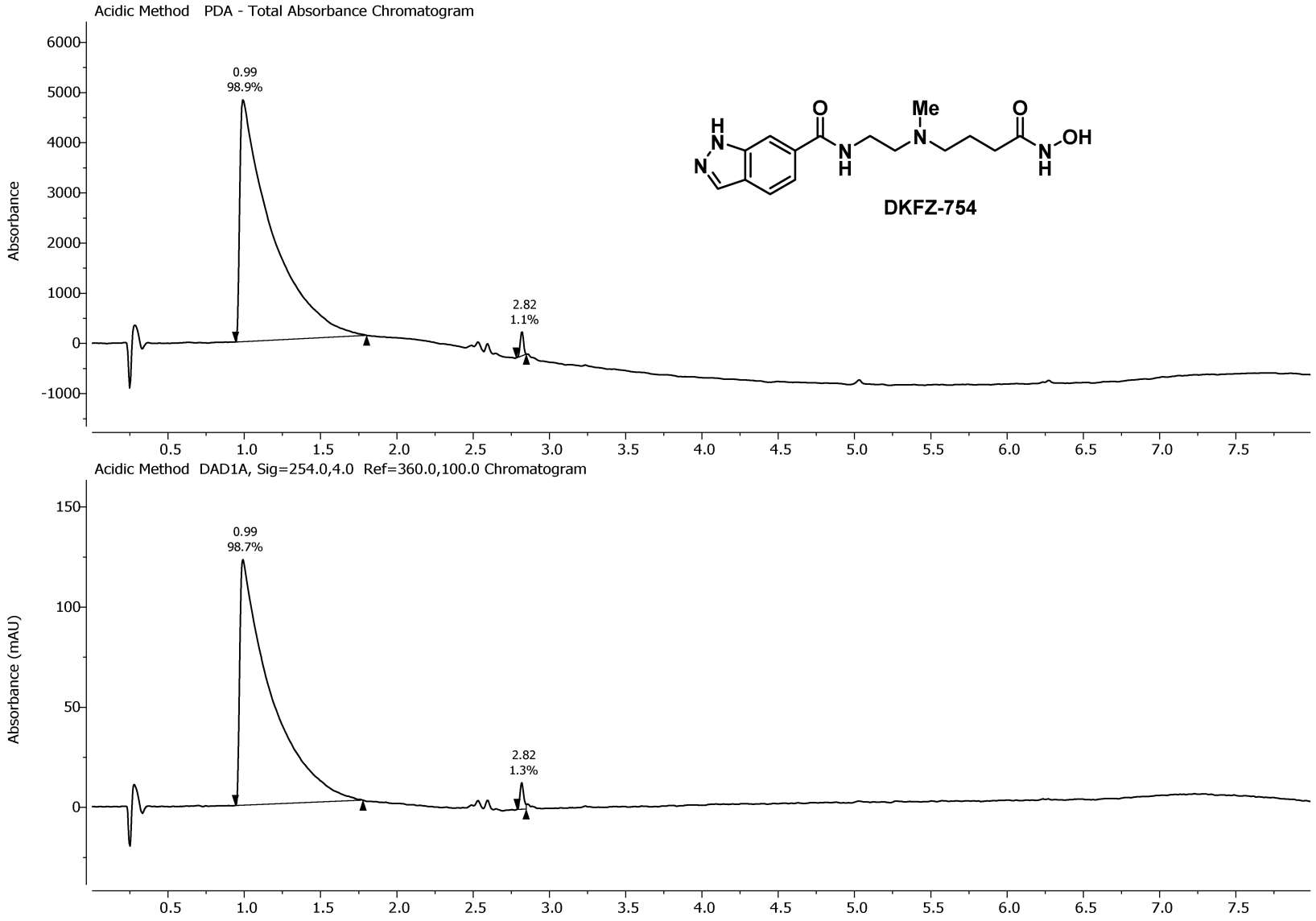
Acidic Method PDA - Total Absorbance Chromatogram
Absorbance
0.99
98.9%
2.82
1.1%
DKFZ-754
Acidic Method DAD1A, Sig=254.0,4.0 Ref=360.0,100.0 Chromatogram
Absorbance (mAU)
0.99
98.7%
2.82
1.3%

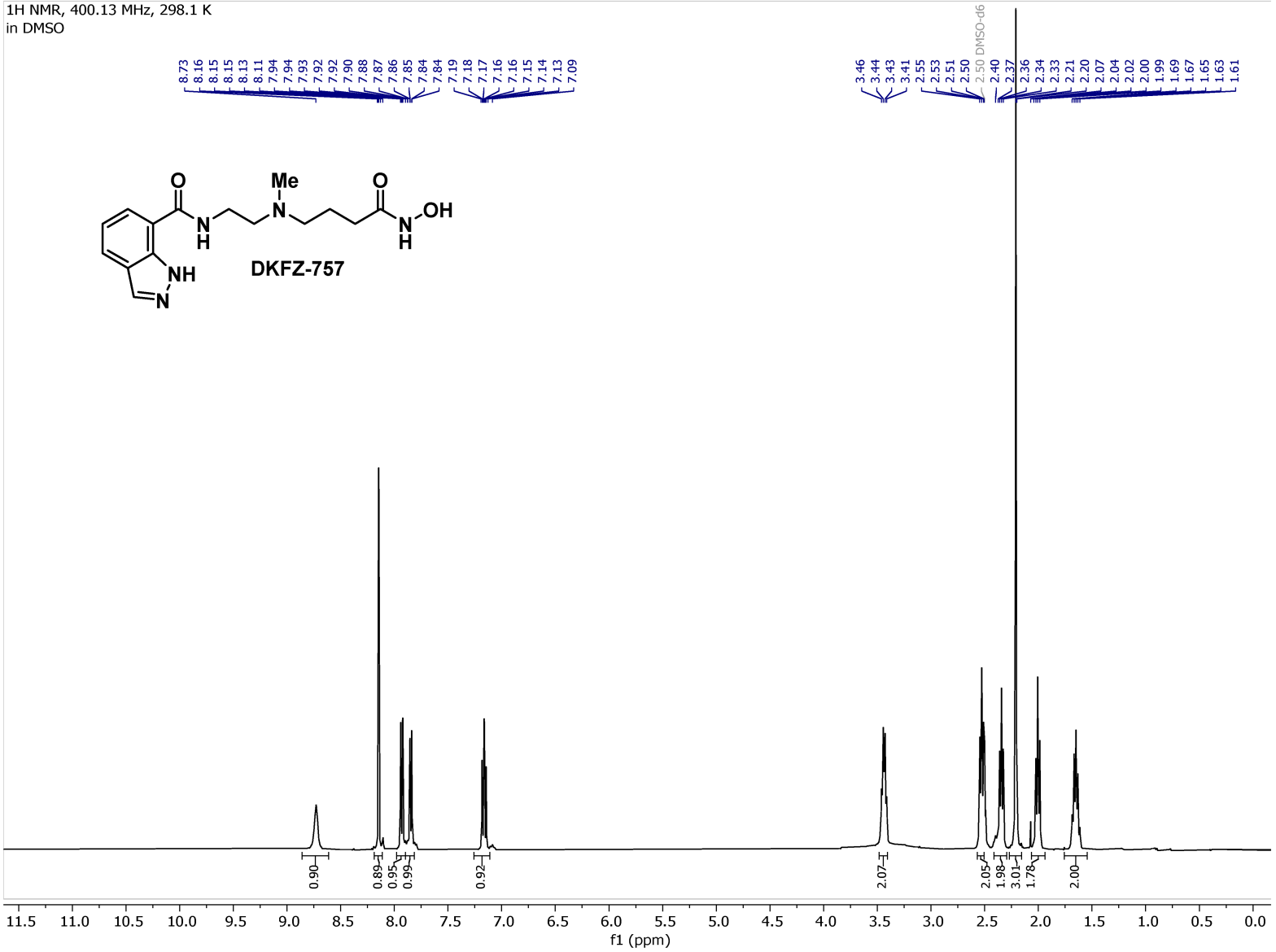
1H NMR, 400.13 MHz, 298.1 K
in DMSO
8.73
8.16
8.15
8.15
8.13
8.11
7.94
7.94
7.93
7.92
7.92
7.90
7.88
7.87
7.86
7.85
7.84
7.84
7.19
7.18
7.17
7.16
7.16
7.15
7.14
7.13
7.09
3.46
3.44
3.43
3.41
2.55
2.53
2.51
2.50
2.50 DMSO-d6
2.40
2.37
2.36
2.34
2.33
2.21
2.20
2.07
2.04
2.02
2.00
1.99
1.69
1.67
1.65
1.63
1.61
O
Me
O
N
N
N
OH
H
H
NH
N
DKFZ-757
0.90
0.89
0.95
0.99
0.92
2.07
2.05
1.98
3.01
1.78
2.00
11.5
11.0
10.5
10.0
9.5
9.0
8.5
8.0
7.5
7.0
6.5
6.0
5.5
5.0
4.5
4.0
3.5
3.0
2.5
2.0
1.5
1.0
0.5
0.0
f1 (ppm)

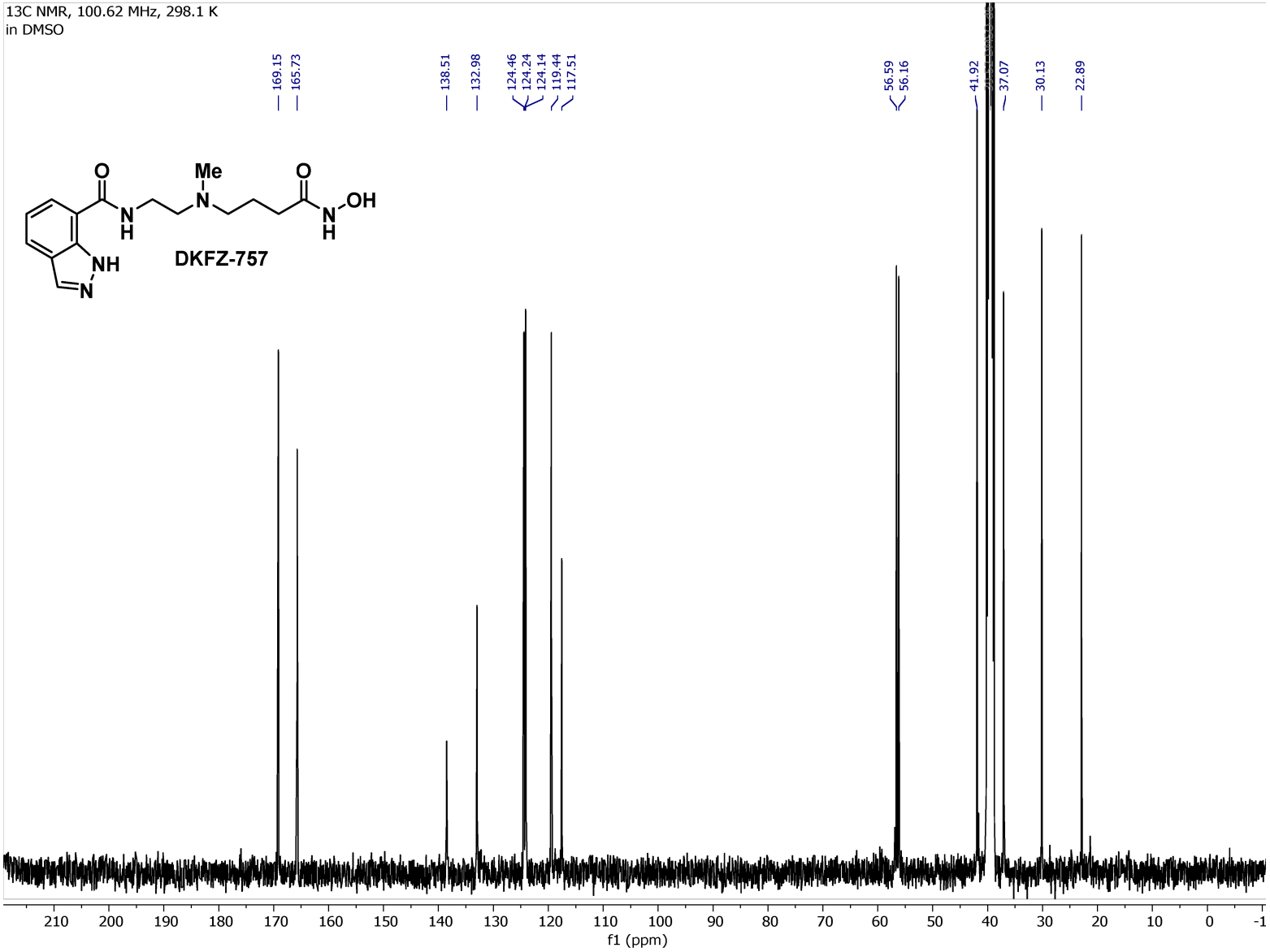
13C NMR, 100.62 MHz, 298.1 K
in DMSO
169.15
165.73
138.51
132.98
124.46
124.24
124.14
119.44
117.51
56.59
56.16
41.92
37.07
30.13
22.89
O
Me
O
N
H
N
N
H
OH
NH
N
DKFZ-757
210
200
190
180
170
160
150
140
130
120
110
100
90
80
70
60
50
40
30
20
10
0
-1
f1 (ppm)

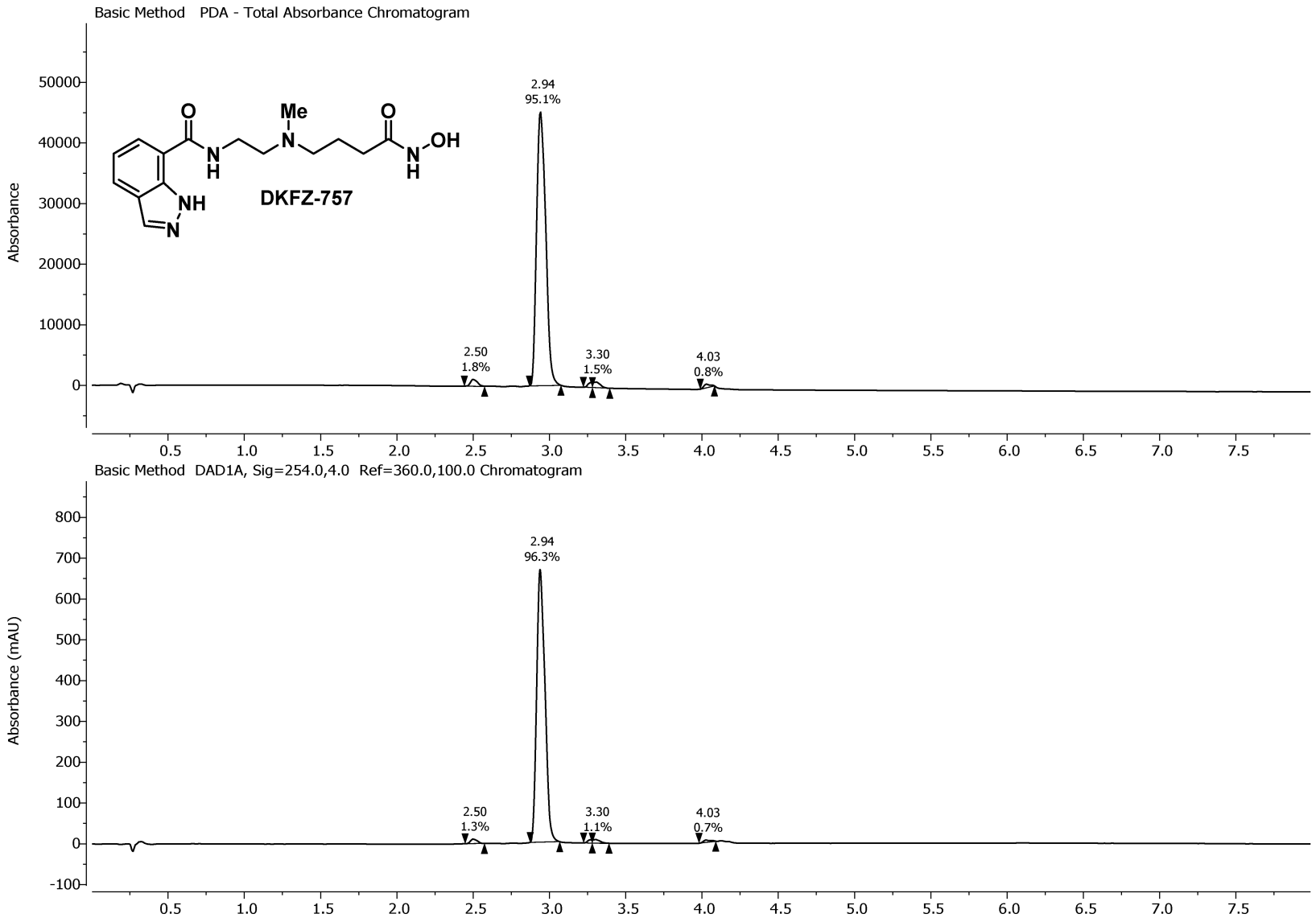
Basic Method PDA - Total Absorbance Chromatogram
Absorbance
DKFZ-757
2.94
95.1%
2.50
1.8%
3.30
1.5%
4.03
0.8%
Basic Method DAD1A, Sig=254.0,4.0 Ref=360.0,100.0 Chromatogram
Absorbance (mAU)
2.94
96.3%
2.50
1.3%
3.30
1.1%
4.03
0.7%

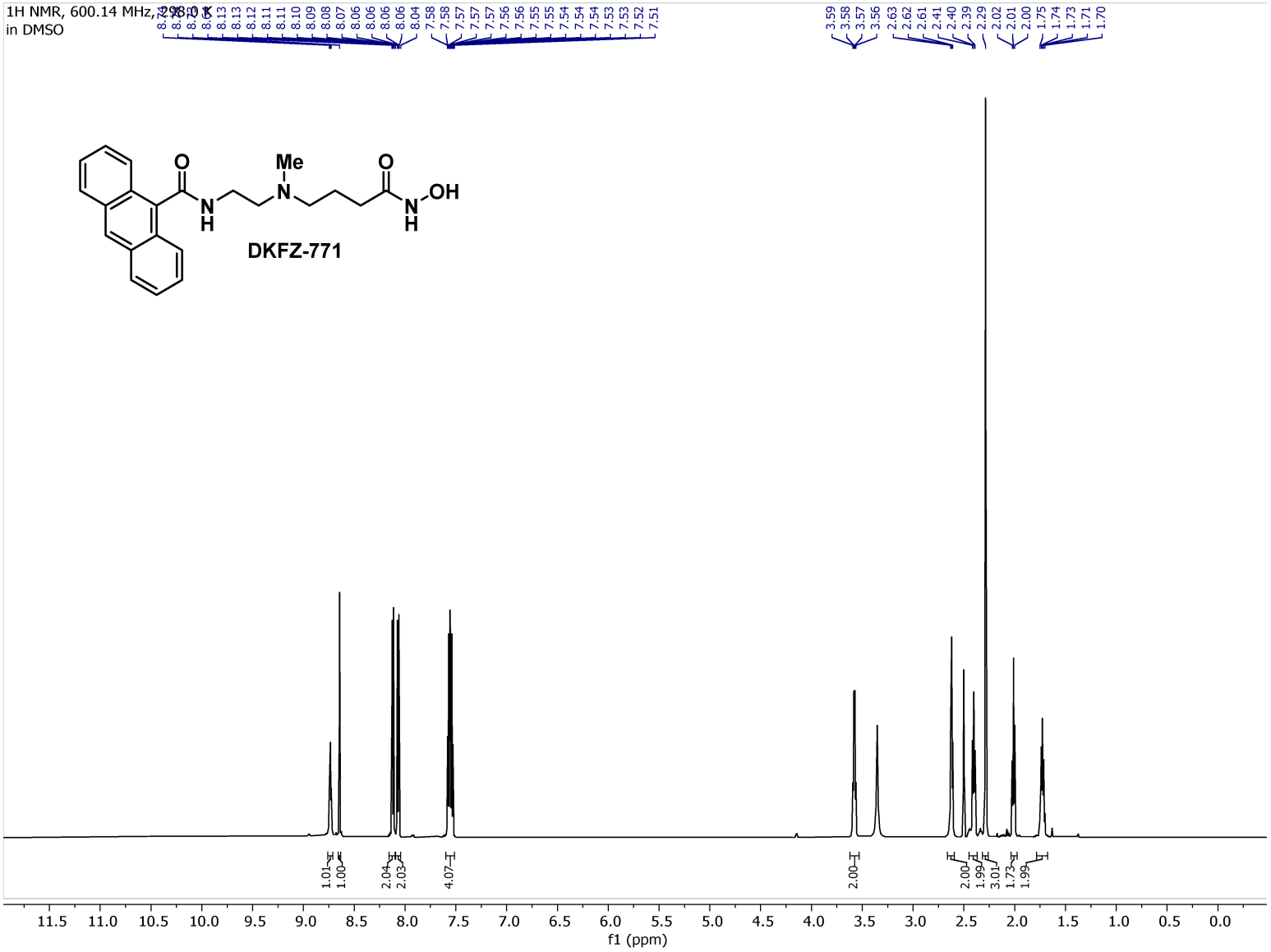
1H NMR, 600.14 MHz, 298.0 K
in DMSO
DKFZ-771
f1 (ppm)

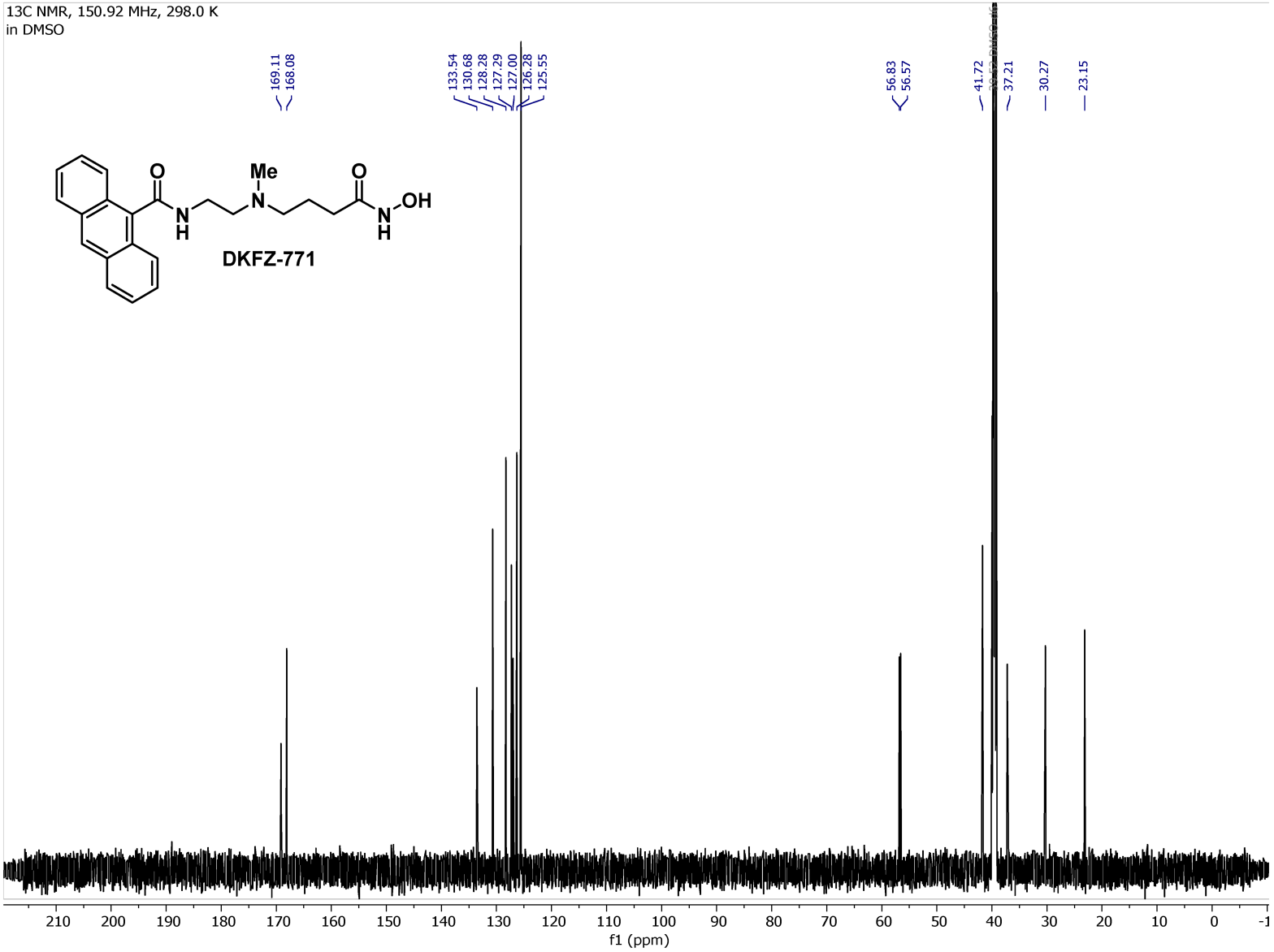
13C NMR, 150.92 MHz, 298.0 K
in DMSO
169.11
168.08
133.54
130.68
128.28
127.29
127.00
126.28
125.55
56.83
56.57
41.72
37.21
30.27
23.15
O
Me
O
N
N
N
OH
H
H
DKFZ-771
210
200
190
180
170
160
150
140
130
120
110
100
90
80
70
60
50
40
30
20
10
0
-1
f1 (ppm)

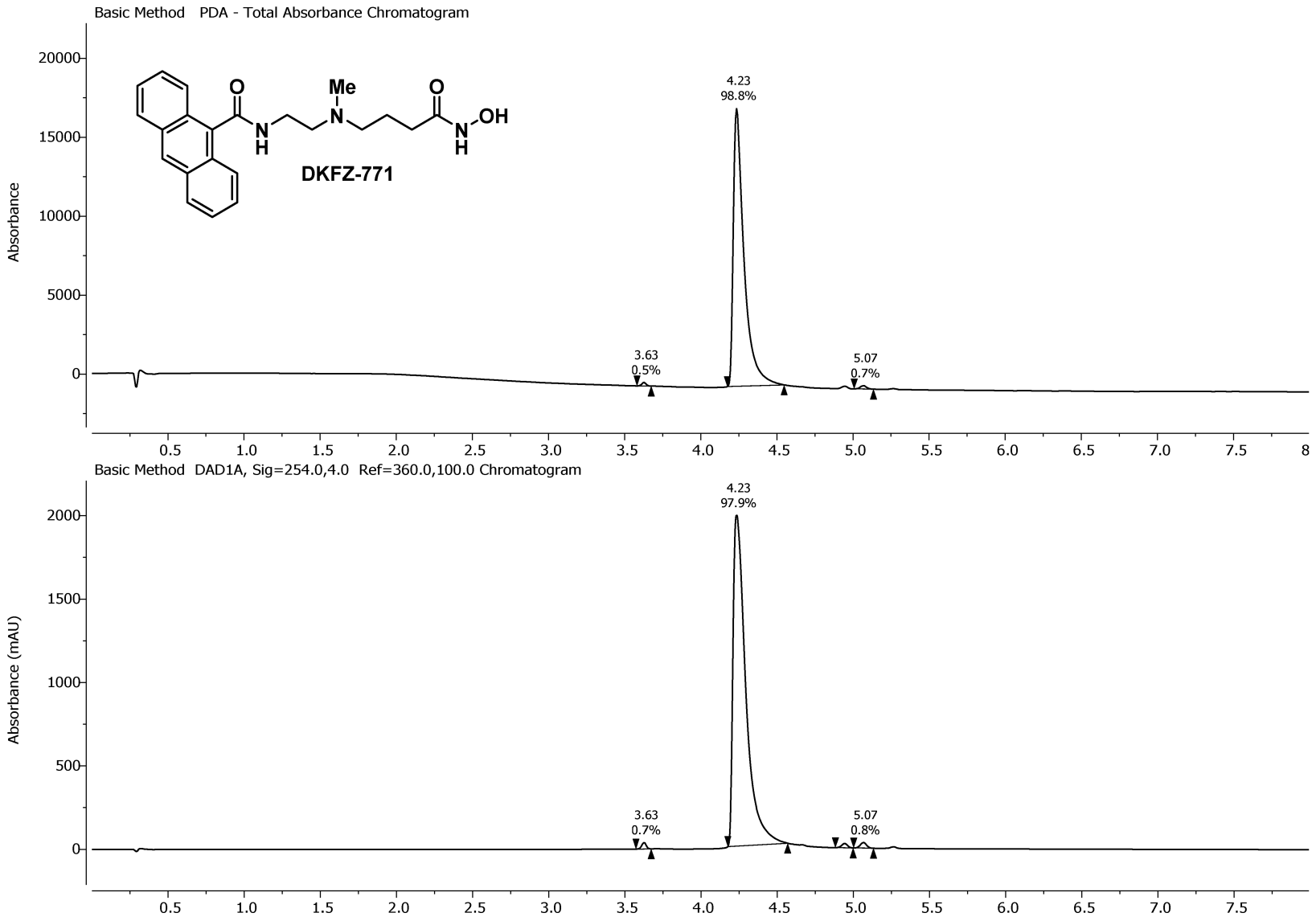
Basic Method PDA - Total Absorbance Chromatogram
Absorbance
20000
15000
10000
5000
0
O
Me
O
N
H
N
N
H
OH
DKFZ-771
4.23
98.8%
3.63
0.5%
5.07
0.7%
0.5
1.0
1.5
2.0
2.5
3.0
3.5
4.0
4.5
5.0
5.5
6.0
6.5
7.0
7.5
8
Basic Method DAD1A, Sig=254.0,4.0 Ref=360.0,100.0 Chromatogram
Absorbance (mAU)
2000
1500
1000
500
0
4.23
97.9%
3.63
0.7%
5.07
0.8%
0.5
1.0
1.5
2.0
2.5
3.0
3.5
4.0
4.5
5.0
5.5
6.0
6.5
7.0
7.5

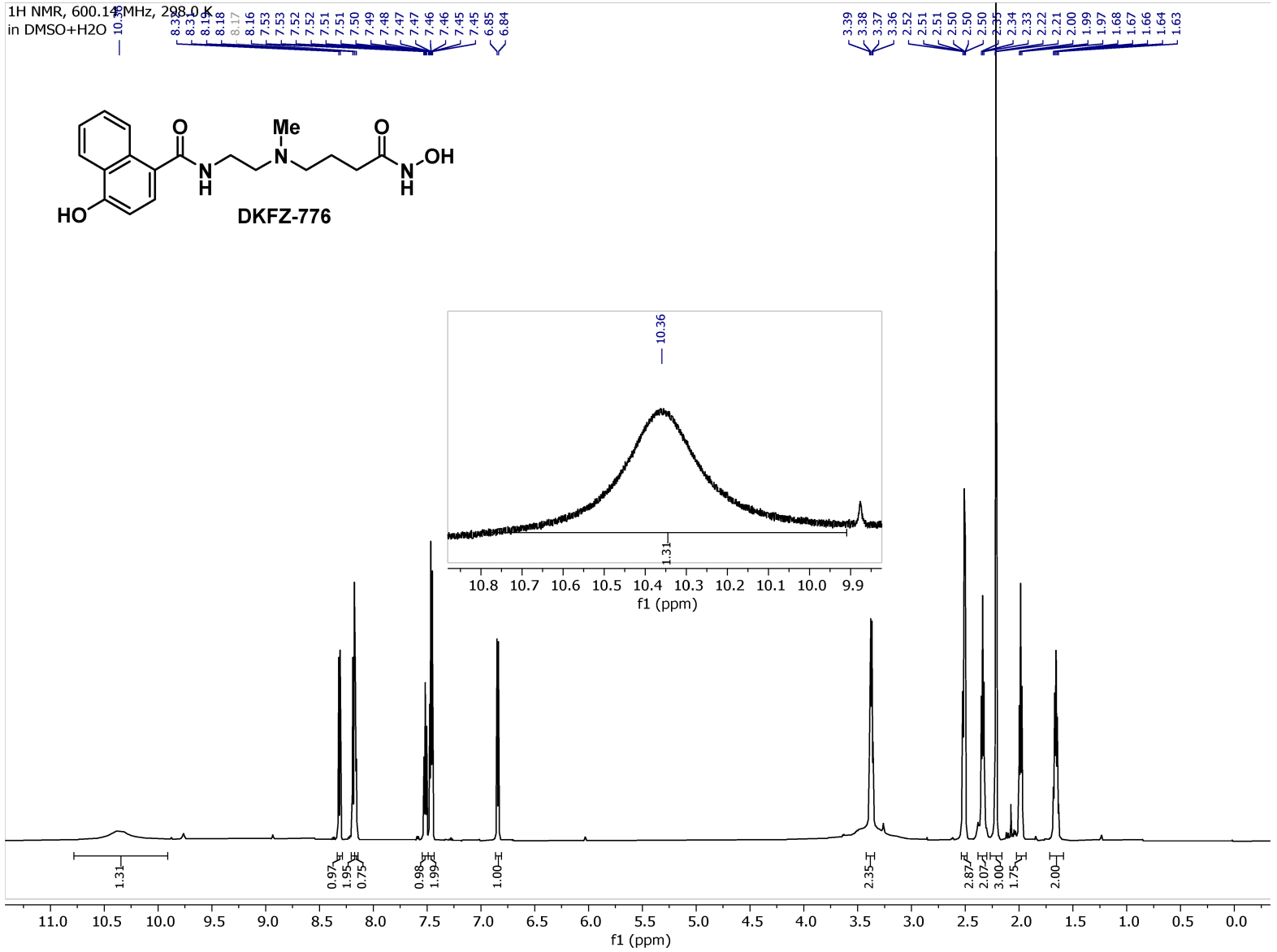
1H NMR, 600.13MHz, 298.0 K
in DMSO+H2O
DKFZ-776
f1 (ppm)

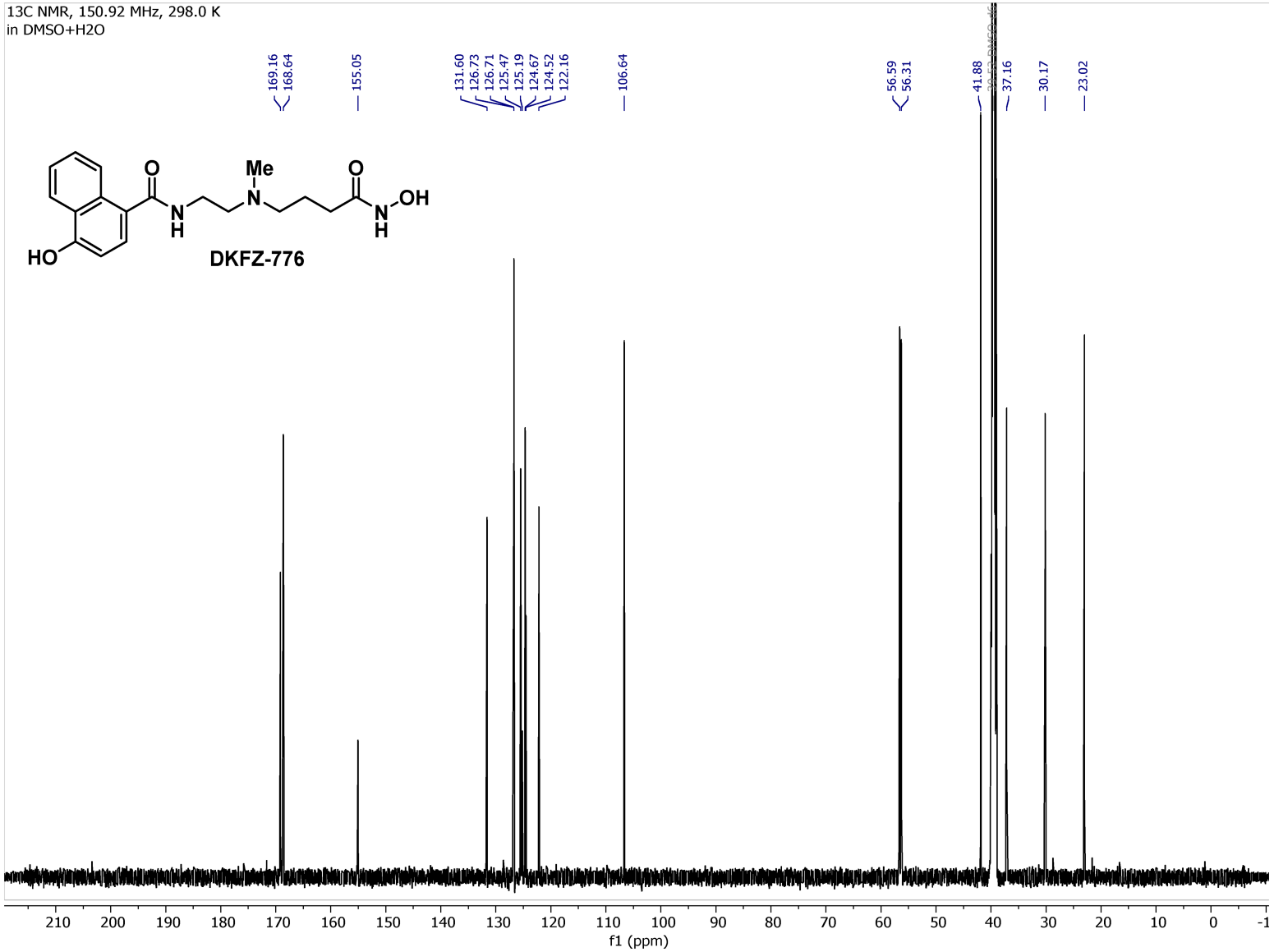
13C NMR, 150.92 MHz, 298.0 K
in DMSO+H2O
169.16
168.64
155.05
131.60
126.73
126.71
125.47
125.19
124.67
124.52
122.16
106.64
56.59
56.31
41.88
37.16
30.17
23.02
O
Me
O
N
N
N
OH
H
H
HO
DKFZ-776
210
200
190
180
170
160
150
140
130
120
110
100
90
80
70
60
50
40
30
20
10
0
-1
f1 (ppm)

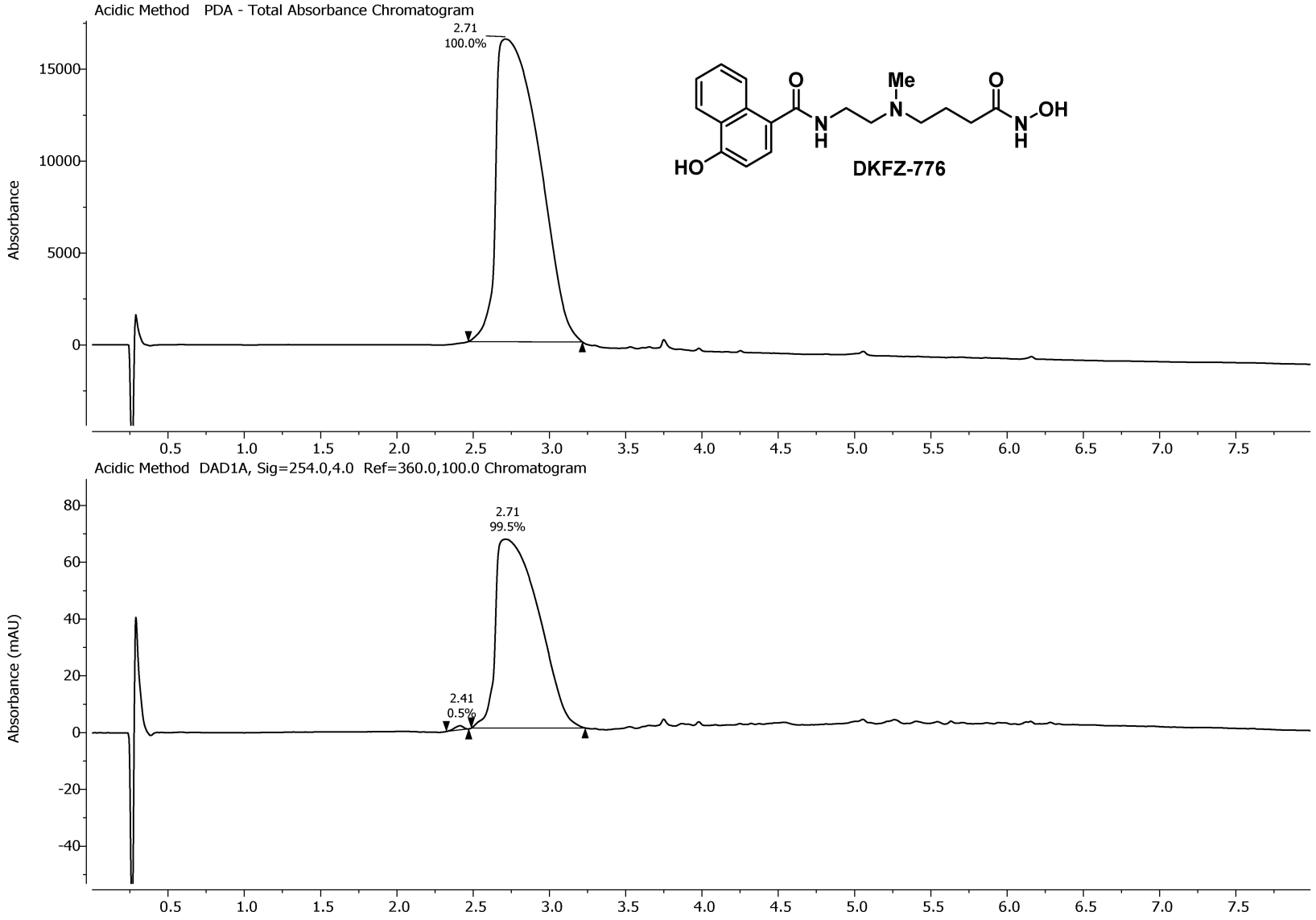
Acidic Method PDA - Total Absorbance Chromatogram
2.71
100.0%
Absorbance
15000
10000
5000
0
0.5
1.0
1.5
2.0
2.5
3.0
3.5
4.0
4.5
5.0
5.5
6.0
6.5
7.0
7.5
O
Me
O
N
N
OH
H
H
HO
DKFZ-776
Acidic Method DAD1A, Sig=254.0,4.0 Ref=360.0,100.0 Chromatogram
2.71
99.5%
2.41
0.5%
Absorbance (mAU)
80
60
40
20
0
-20
-40
0.5
1.0
1.5
2.0
2.5
3.0
3.5
4.0
4.5
5.0
5.5
6.0
6.5
7.0
7.5

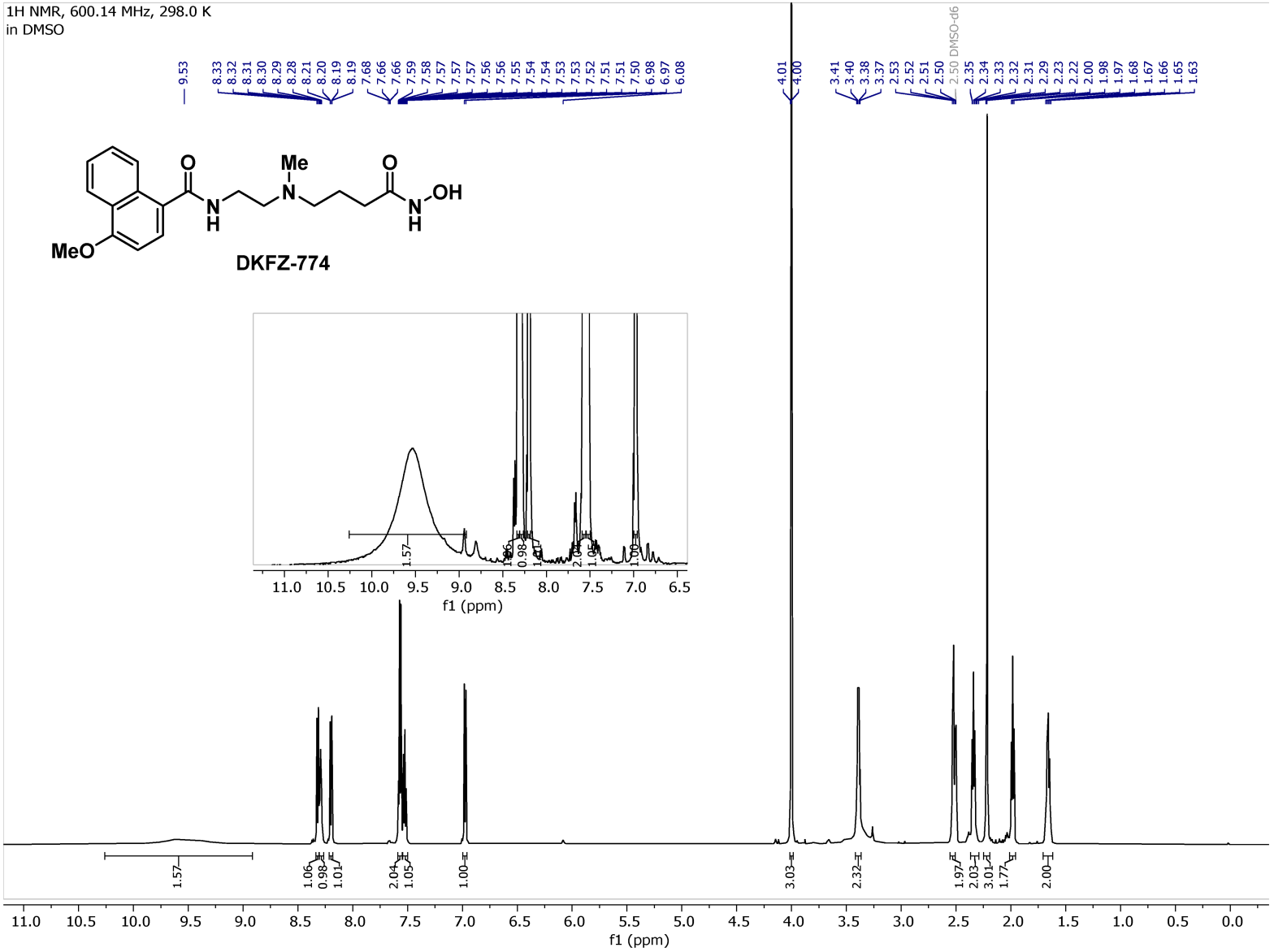
1H NMR, 600.14 MHz, 298.0 K
in DMSO
DKFZ-774
f1 (ppm)

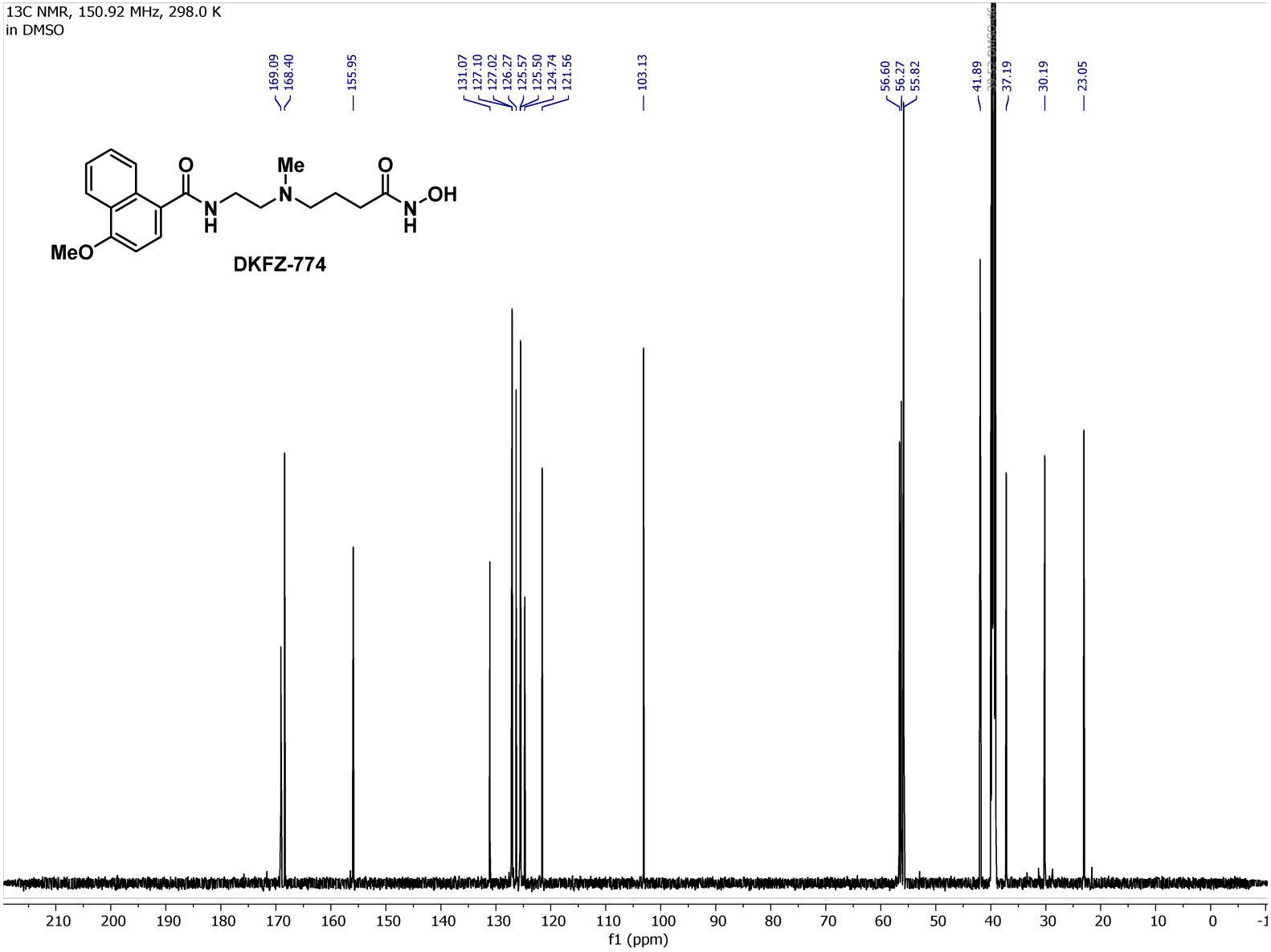
13C NMR, 150.92 MHz, 298.0 K
in DMSO
169.09
168.40
155.95
131.07
127.10
127.02
126.27
125.57
125.50
124.74
121.56
103.13
56.60
56.27
55.82
41.89
37.19
30.19
23.05
O
Me
O
N
H
N
N
H
OH
MeO
DKFZ-774
210
200
190
180
170
160
150
140
130
120
110
100
90
80
70
60
50
40
30
20
10
0
-1
f1 (ppm)

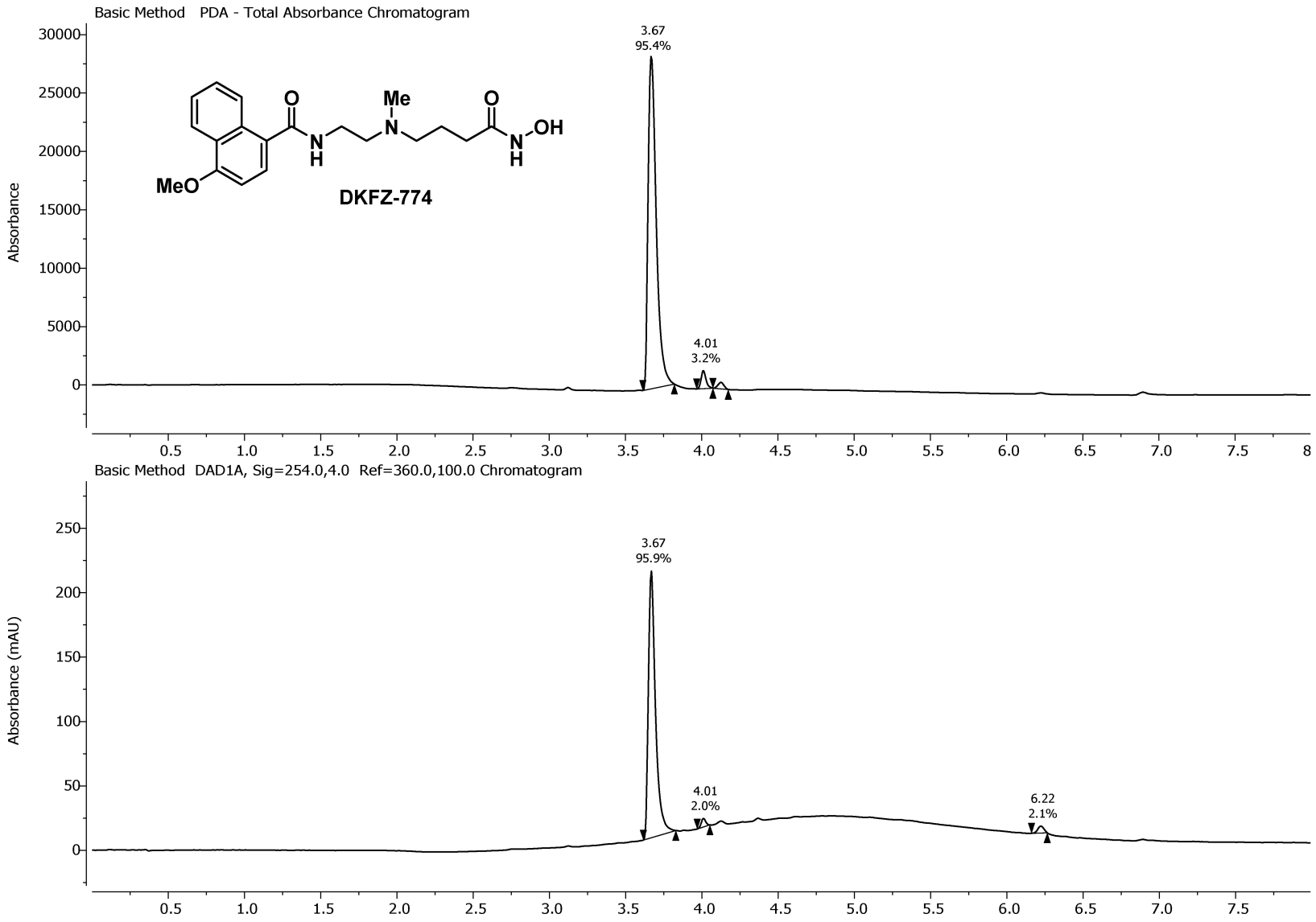
Basic Method PDA - Total Absorbance Chromatogram
Absorbance
30000
25000
20000
15000
10000
5000
0
3.67
95.4%
4.01
3.2%
MeO
O
N
H
Me
N
O
N
H
OH
DKFZ-774
0.5
1.0
1.5
2.0
2.5
3.0
3.5
4.0
4.5
5.0
5.5
6.0
6.5
7.0
7.5
8
Basic Method DAD1A, Sig=254.0,4.0 Ref=360.0,100.0 Chromatogram
Absorbance (mAU)
250
200
150
100
50
0
3.67
95.9%
4.01
2.0%
6.22
2.1%
0.5
1.0
1.5
2.0
2.5
3.0
3.5
4.0
4.5
5.0
5.5
6.0
6.5
7.0
7.5

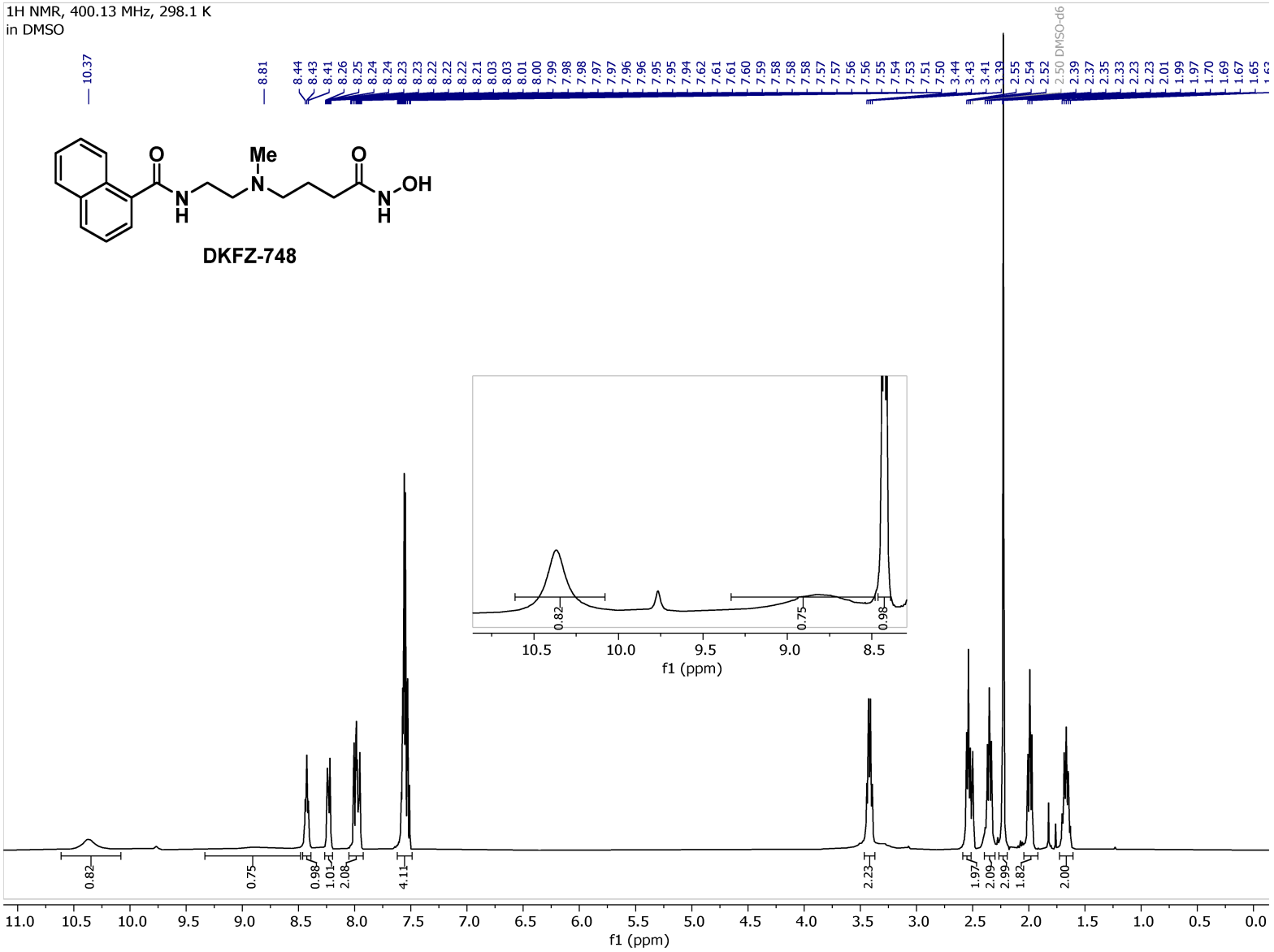
1H NMR, 400.13 MHz, 298.1 K
in DMSO
DKFZ-748
f1 (ppm)

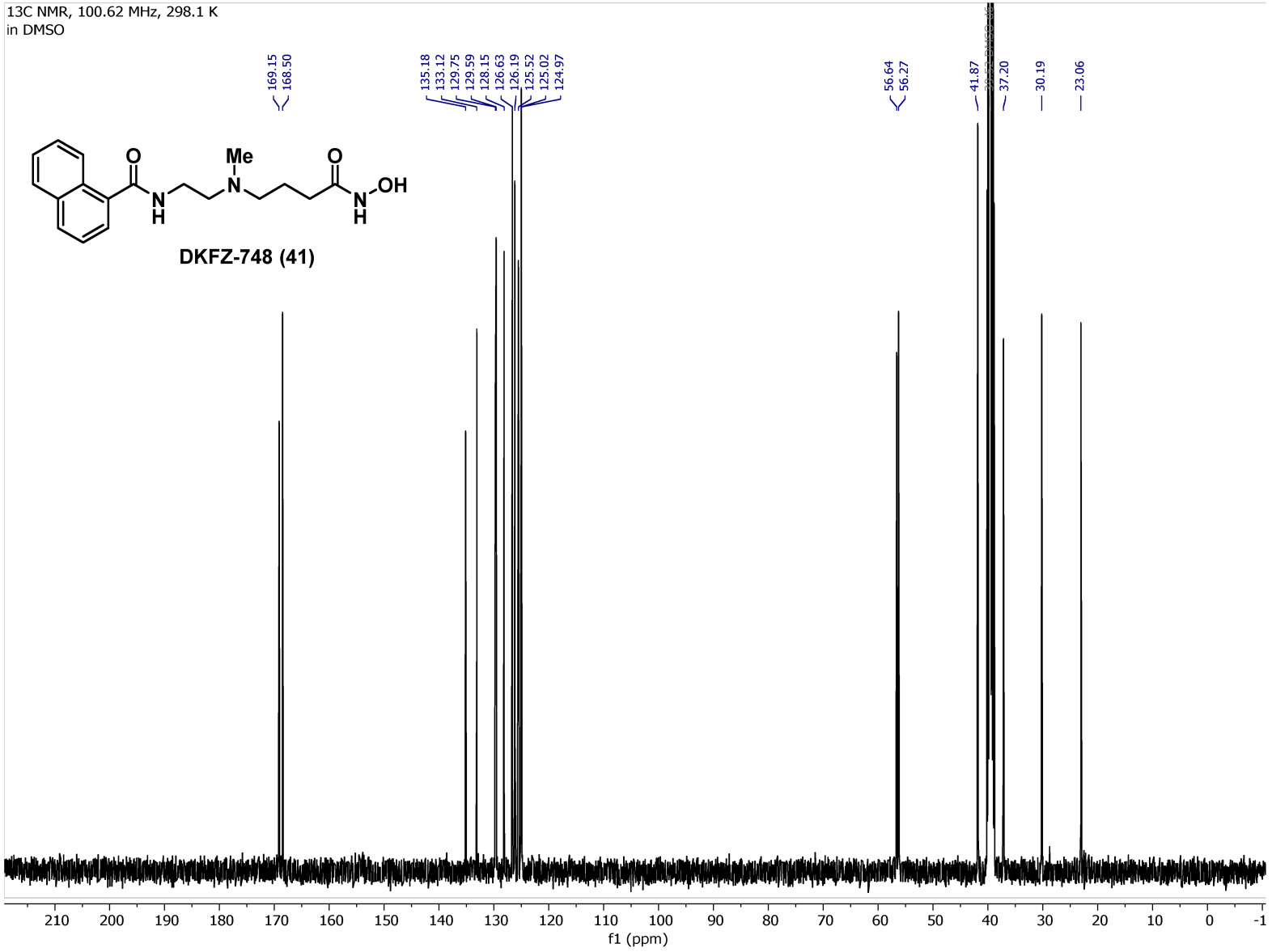
13C NMR, 100.62 MHz, 298.1 K
in DMSO
169.15
168.50
135.18
133.12
129.75
129.59
128.15
126.63
126.19
125.52
125.02
124.97
56.64
56.27
41.87
37.20
30.19
23.06
O
Me
O
N
N
N
OH
H
H
DKFZ-748 (41)
210 200 190 180 170 160 150 140 130 120 110 100 90 80 70 60 50 40 30 20 10 0 -1
f1 (ppm)

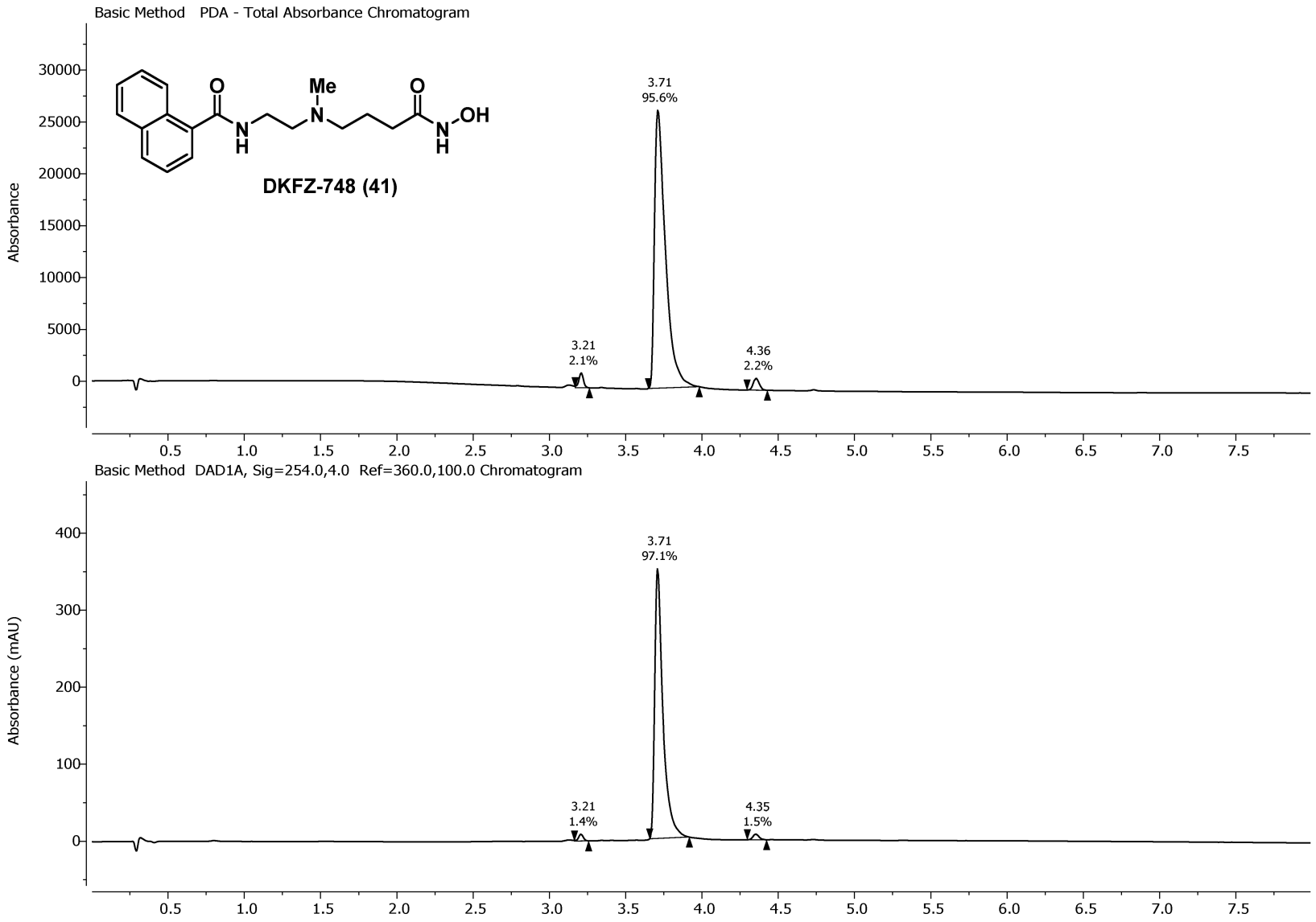
Basic Method PDA - Total Absorbance Chromatogram
Absorbance
30000
25000
20000
15000
10000
5000
0
O
Me
O
N
N
N
OH
H
H
DKFZ-748 (41)
3.71
95.6%
3.21
2.1%
4.36
2.2%
0.5
1.0
1.5
2.0
2.5
3.0
3.5
4.0
4.5
5.0
5.5
6.0
6.5
7.0
7.5
Basic Method DAD1A, Sig=254.0,4.0 Ref=360.0,100.0 Chromatogram
Absorbance (mAU)
400
300
200
100
0
3.71
97.1%
3.21
1.4%
4.35
1.5%
0.5
1.0
1.5
2.0
2.5
3.0
3.5
4.0
4.5
5.0
5.5
6.0
6.5
7.0
7.5

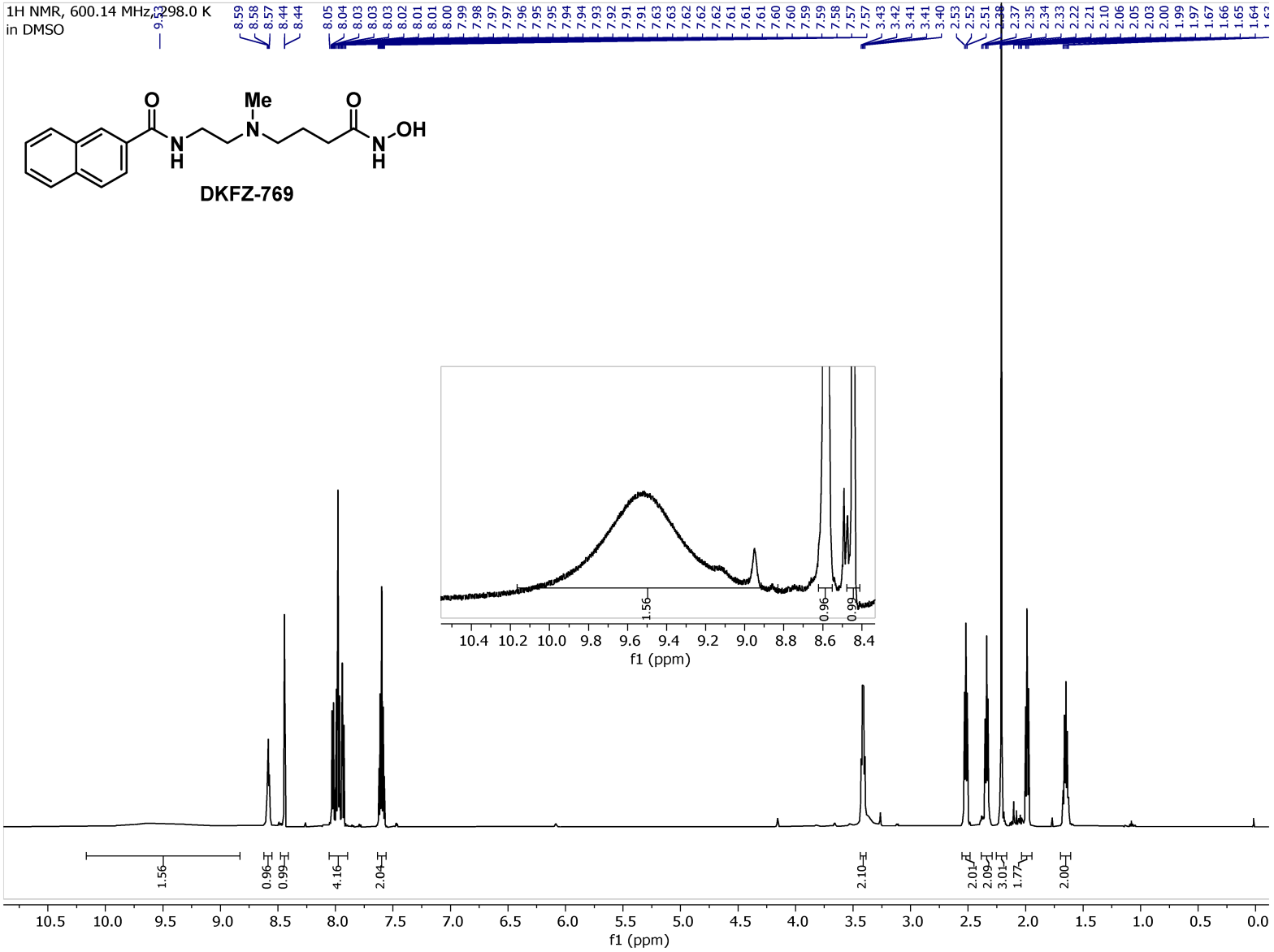
1H NMR, 600.14 MHz, 298.0 K
in DMSO
DKFZ-769
f1 (ppm)

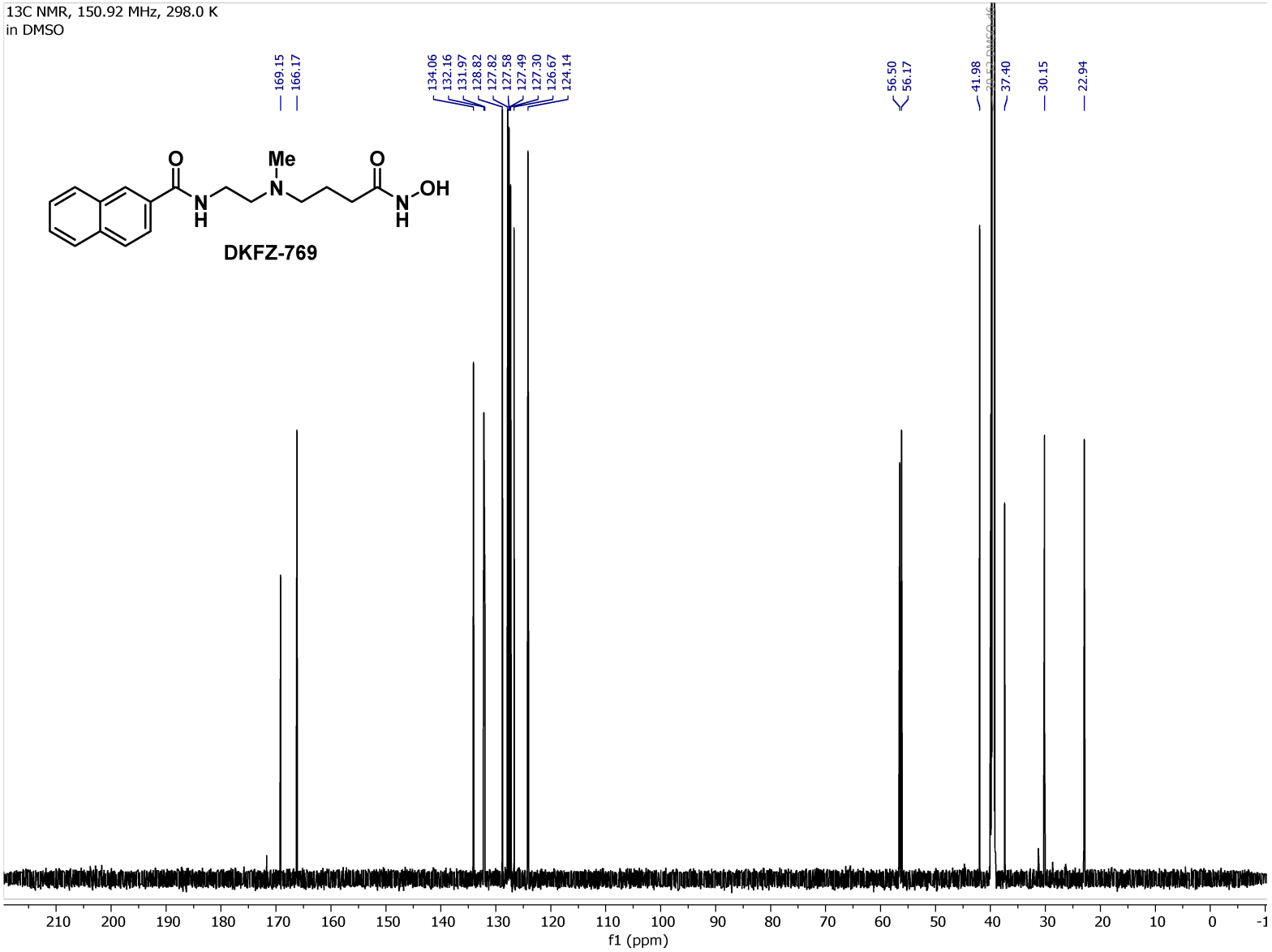
13C NMR, 150.92 MHz, 298.0 K
in DMSO
169.15
166.17
134.06
132.16
131.97
128.82
127.82
127.58
127.49
127.30
126.67
124.14
56.50
56.17
41.98
37.40
30.15
22.94
O
Me
O
N
N
N
OH
H
H
DKFZ-769
210
200
190
180
170
160
150
140
130
120
110
100
90
80
70
60
50
40
30
20
10
0
-1
f1 (ppm)

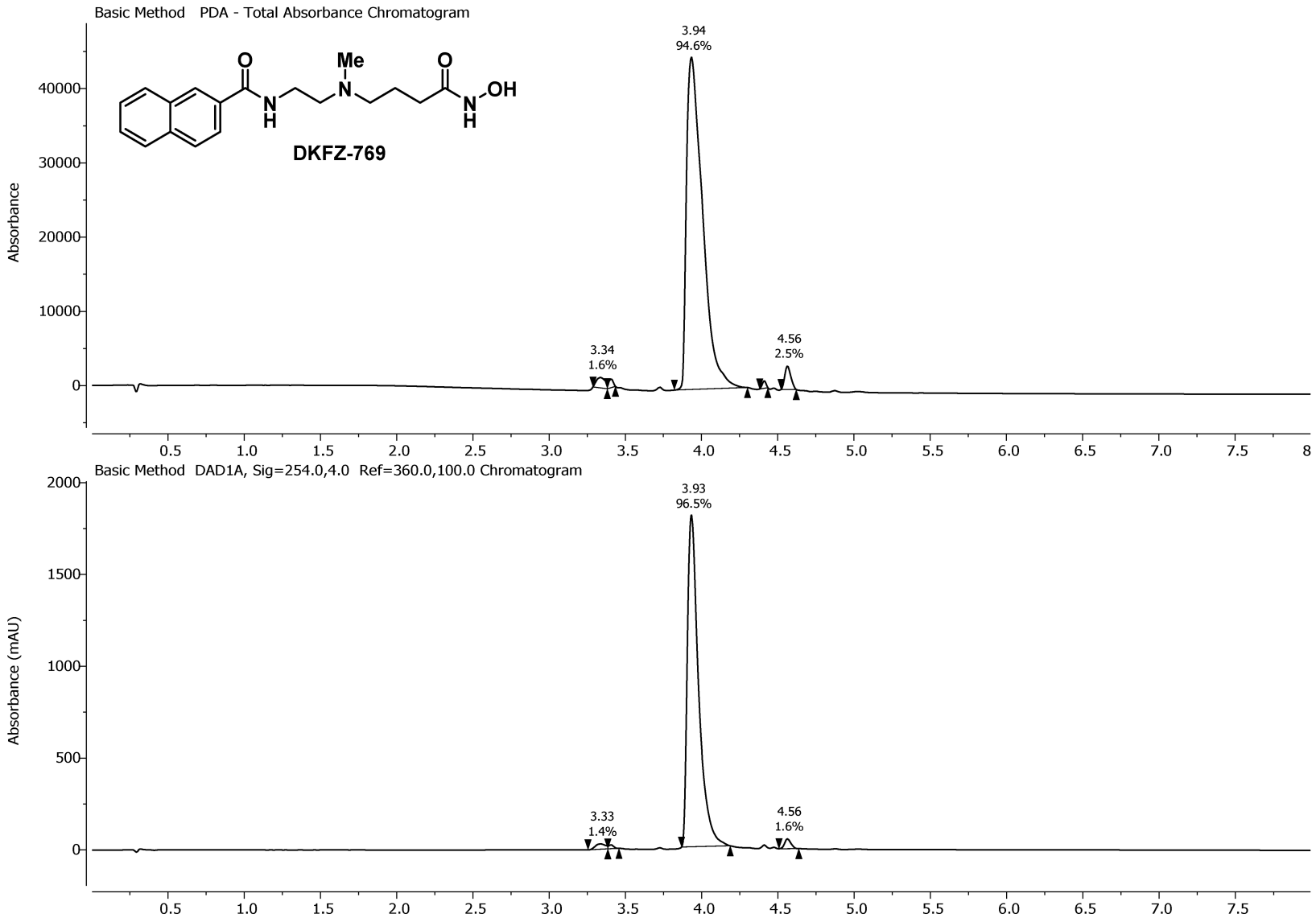
Basic Method PDA - Total Absorbance Chromatogram
DKFZ-769
3.94
94.6%
3.34
1.6%
4.56
2.5%
Absorbance
Basic Method DAD1A, Sig=254.0,4.0 Ref=360.0,100.0 Chromatogram
3.93
96.5%
3.33
1.4%
4.56
1.6%
Absorbance (mAU)

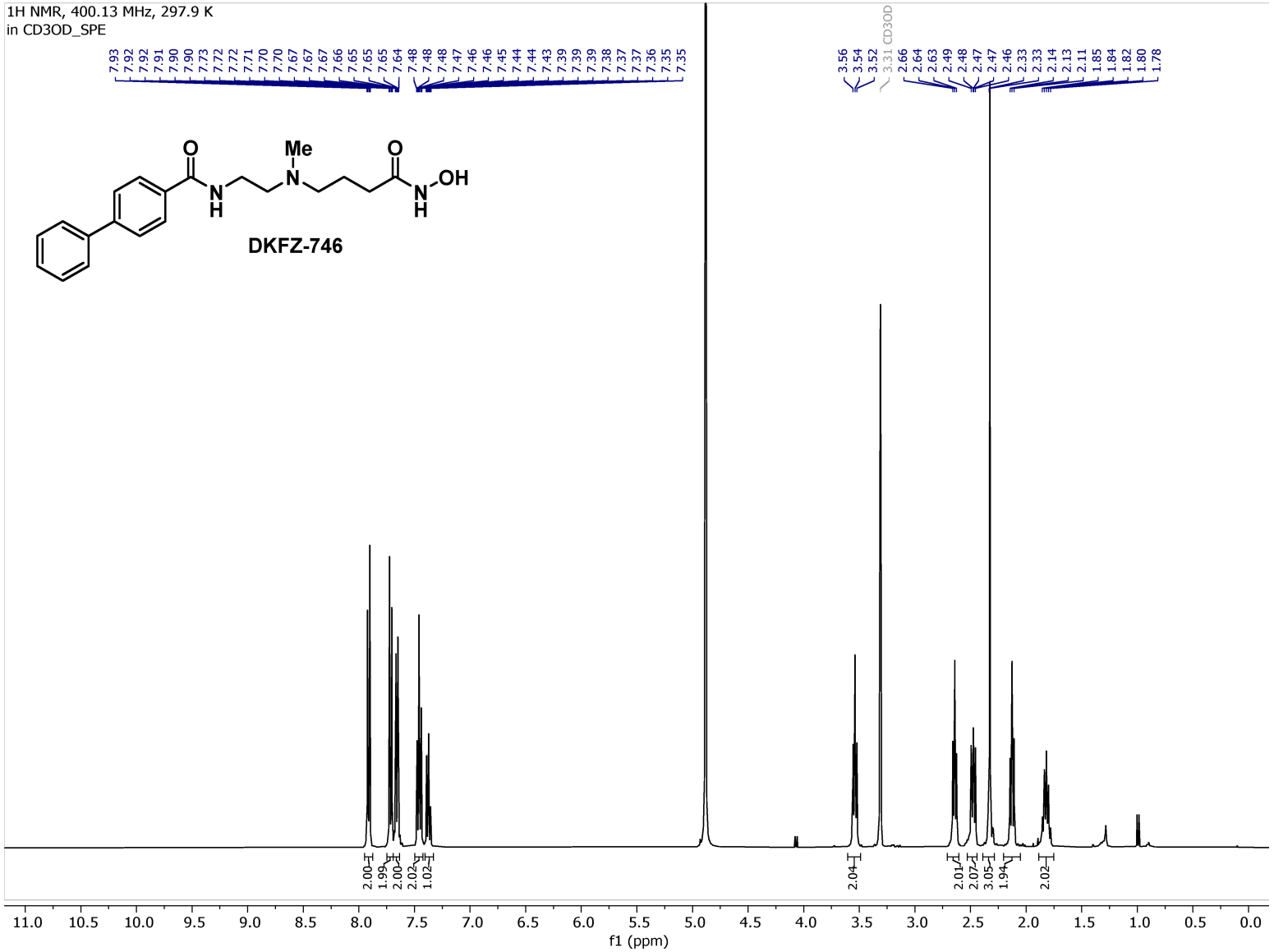
1H NMR, 400.13 MHz, 297.9 K
in CD3OD_SPE
DKFZ-746
f1 (ppm)

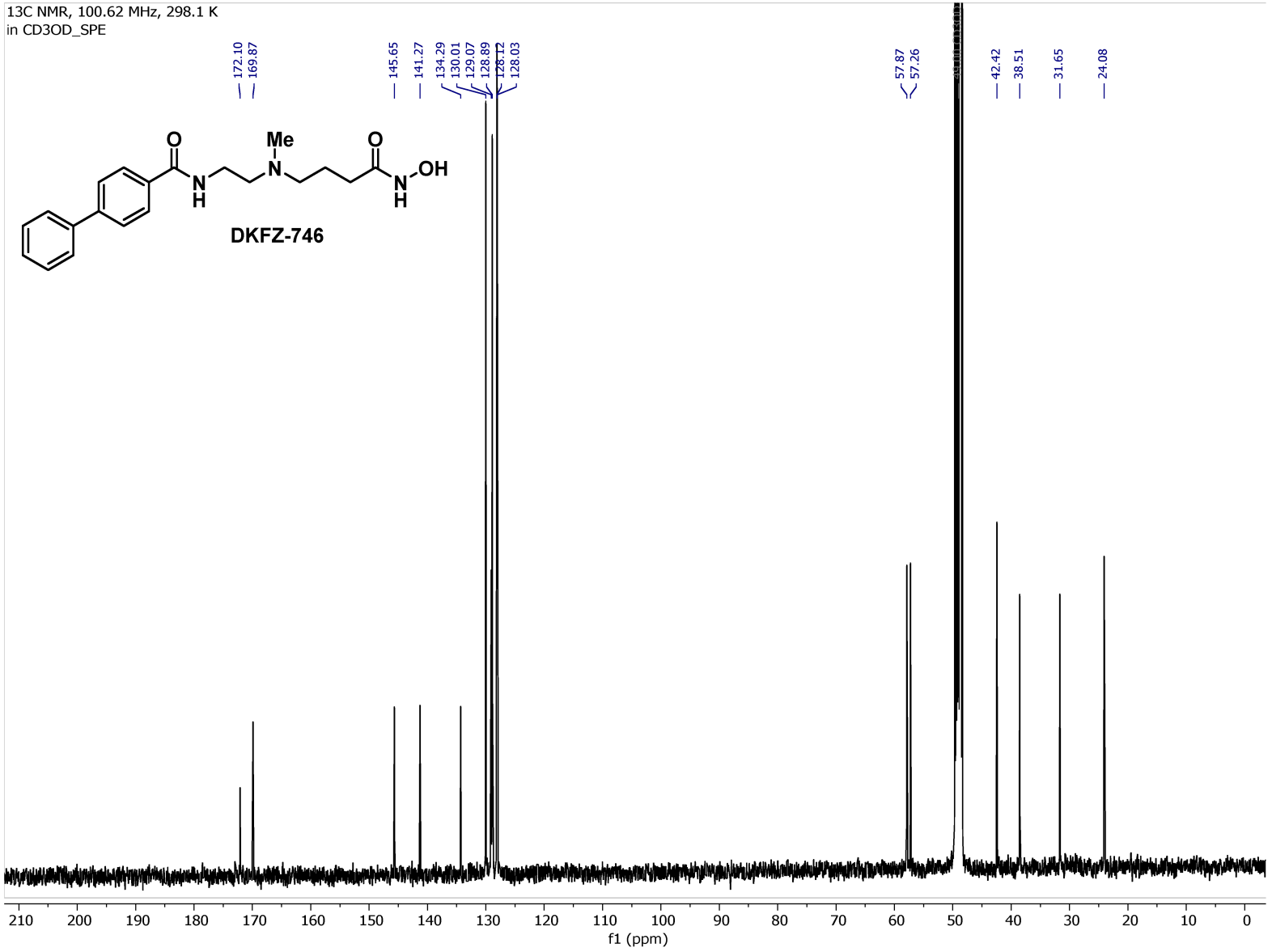
13C NMR, 100.62 MHz, 298.1 K
in CD3OD_SPE
172.10
169.87
145.65
141.27
134.29
130.01
129.07
128.89
128.12
128.03
57.87
57.26
42.42
38.51
31.65
24.08
O
Me
O
N
N
N
OH
H
H
DKFZ-746
210
200
190
180
170
160
150
140
130
120
110
100
90
80
70
60
50
40
30
20
10
0
f1 (ppm)

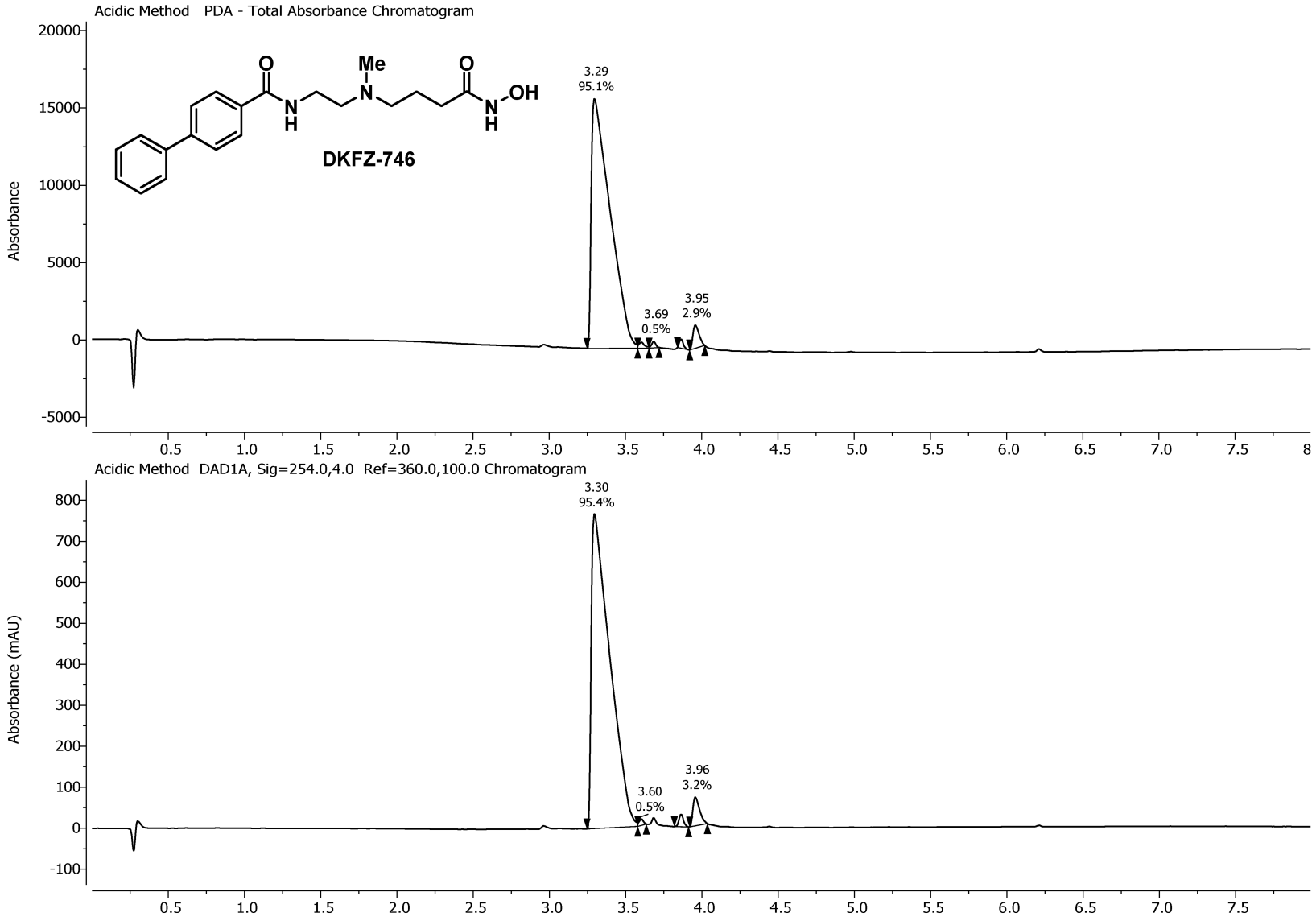
Acidic Method PDA - Total Absorbance Chromatogram
Absorbance
DKFZ-746
3.29
95.1%
3.69
0.5%
3.95
2.9%
Acidic Method DAD1A, Sig=254.0,4.0 Ref=360.0,100.0 Chromatogram
Absorbance (mAU)
3.30
95.4%
3.60
0.5%
3.96
3.2%

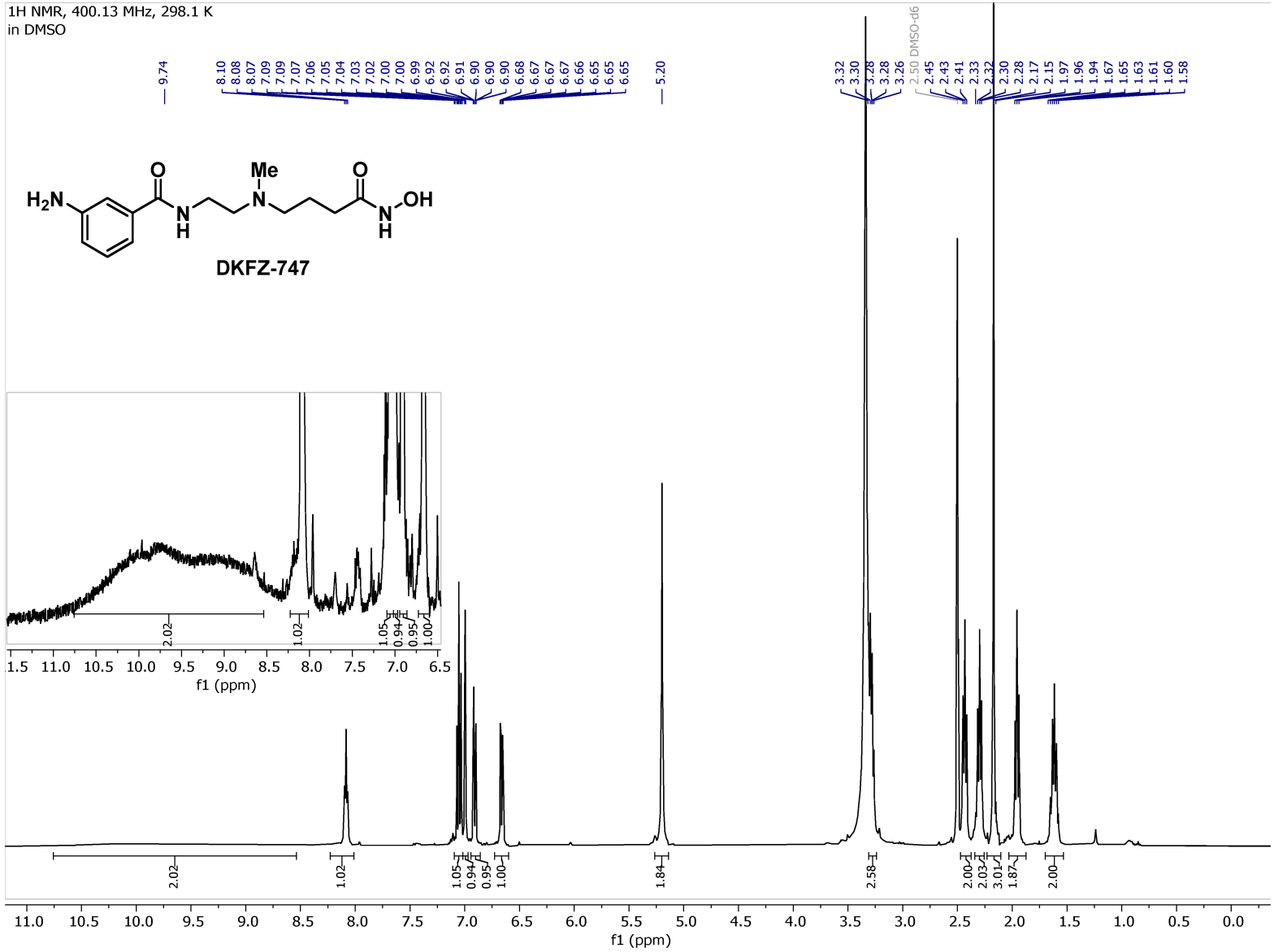
1H NMR, 400.13 MHz, 298.1 K
in DMSO
DKFZ-747
f1 (ppm)

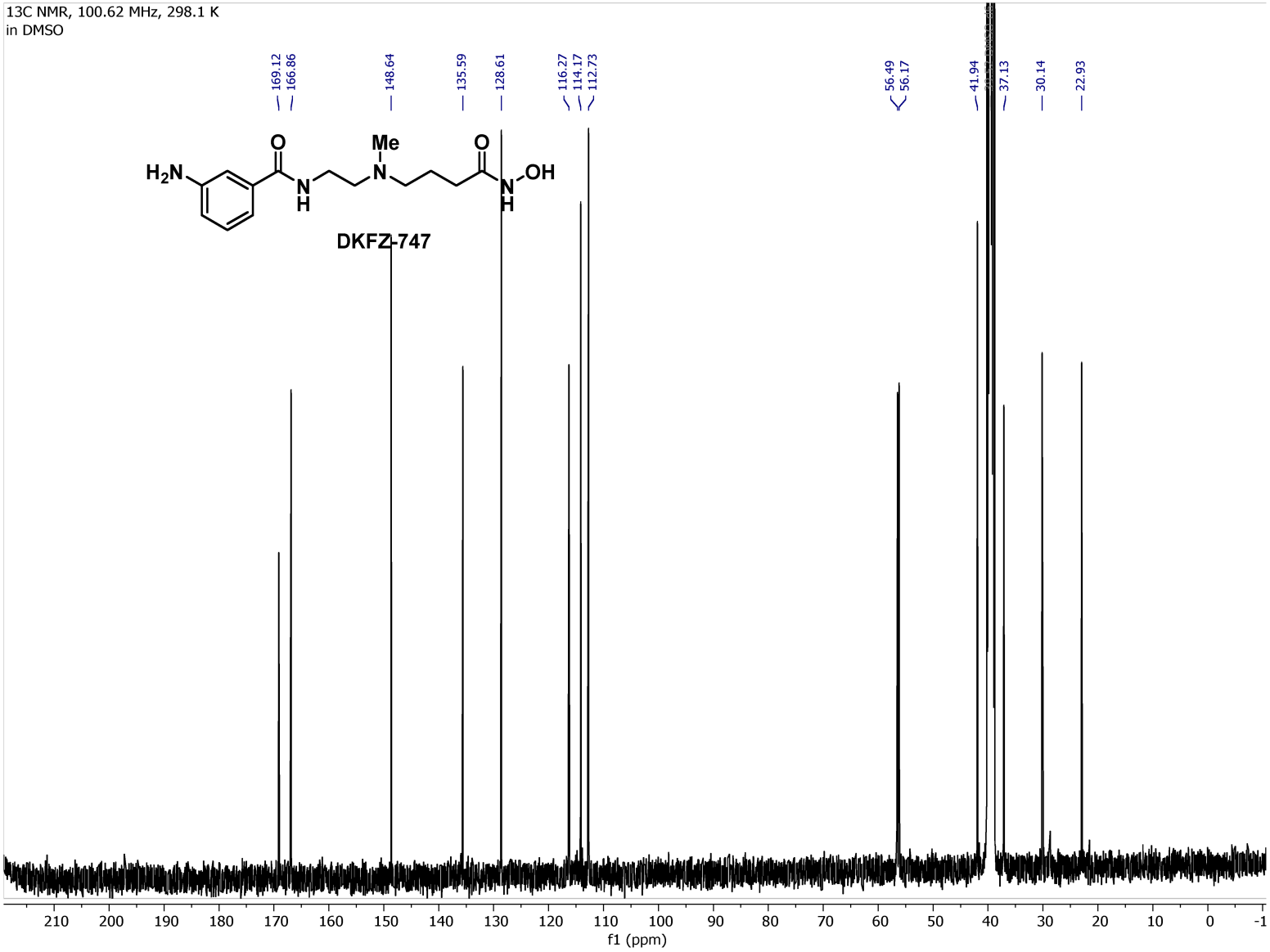
13C NMR, 100.62 MHz, 298.1 K
in DMSO
169.12
166.86
148.64
135.59
128.61
116.27
114.17
112.73
56.49
56.17
41.94
37.13
30.14
22.93
DKFZ-747
f1 (ppm)

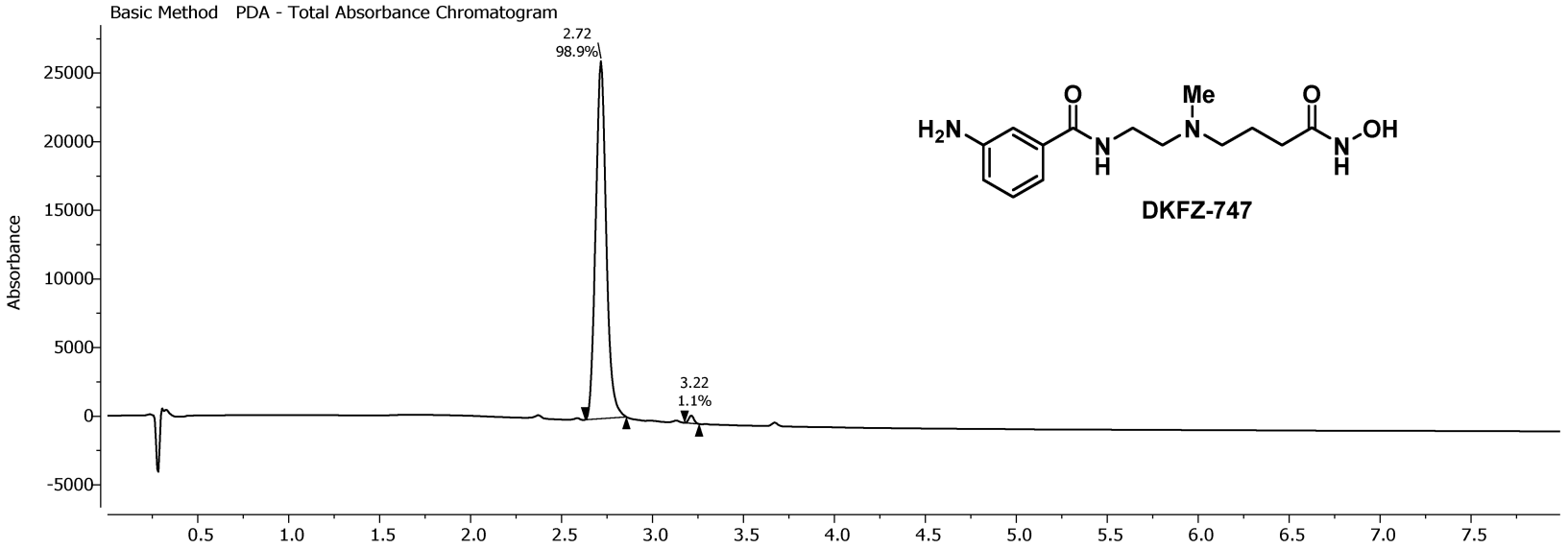
Basic Method PDA - Total Absorbance Chromatogram
Absorbance
2.72
98.9%
3.22
1.1%
DKFZ-747

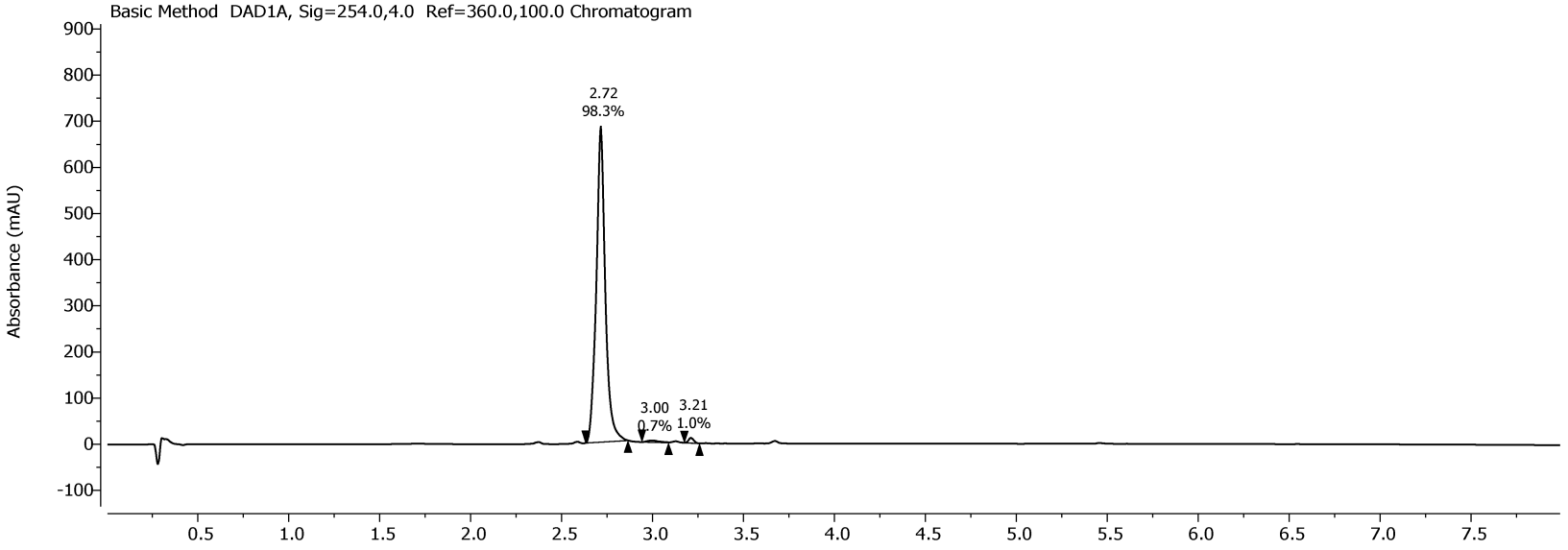
Basic Method DAD1A, Sig=254.0,4.0 Ref=360.0,100.0 Chromatogram
Absorbance (mAU)
2.72
98.3%
3.00
0.7%
3.21
1.0%

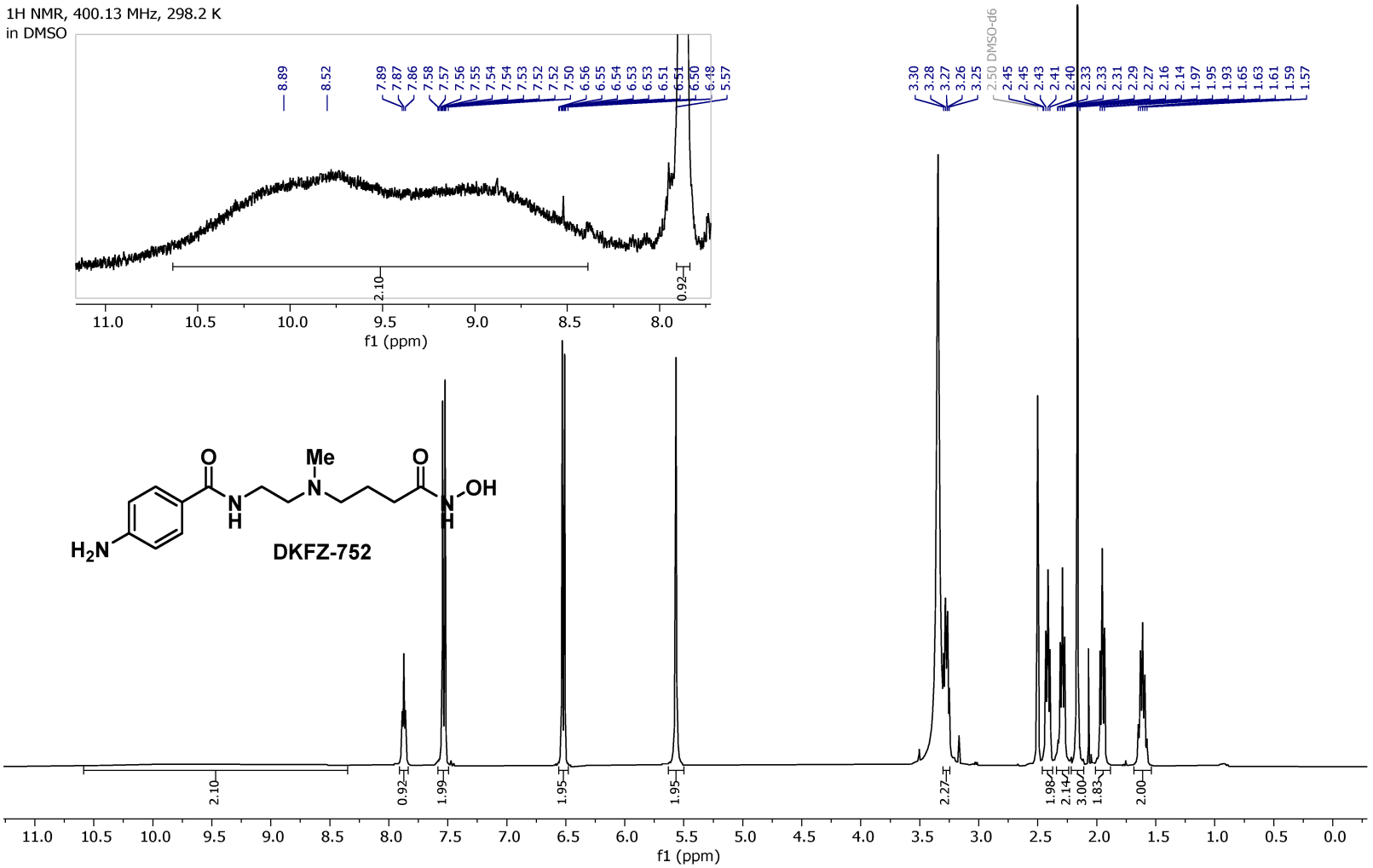
1H NMR, 400.13 MHz, 298.2 K
in DMSO
DKFZ-752
f1 (ppm)

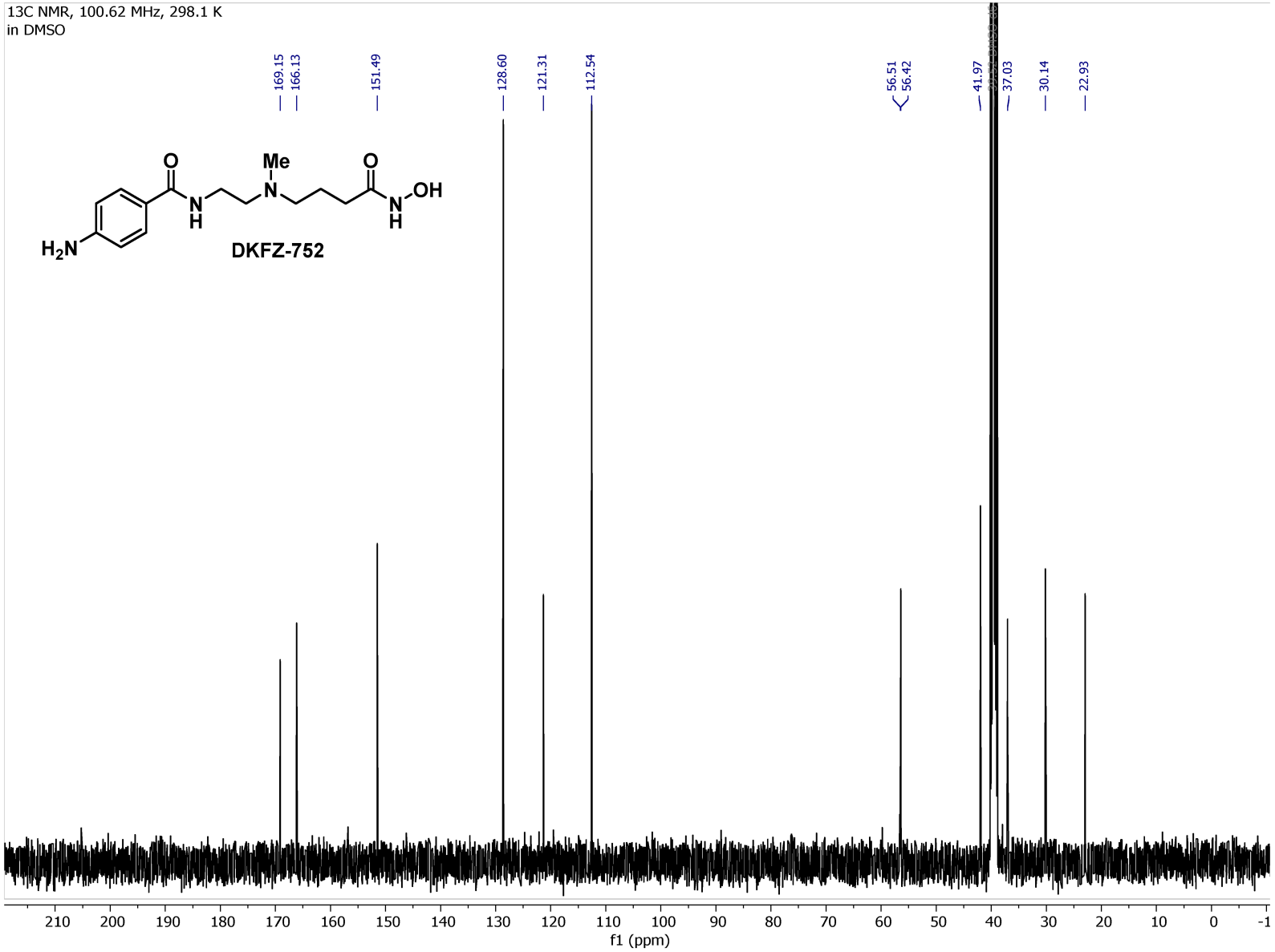
13C NMR, 100.62 MHz, 298.1 K
in DMSO
169.15
166.13
151.49
128.60
121.31
112.54
56.51
56.42
41.97
37.03
30.14
22.93
O
Me
O
N
H
N
N
H
OH
H2N
DKFZ-752
210 200 190 180 170 160 150 140 130 120 110 100 90 80 70 60 50 40 30 20 10 0 -1
f1 (ppm)

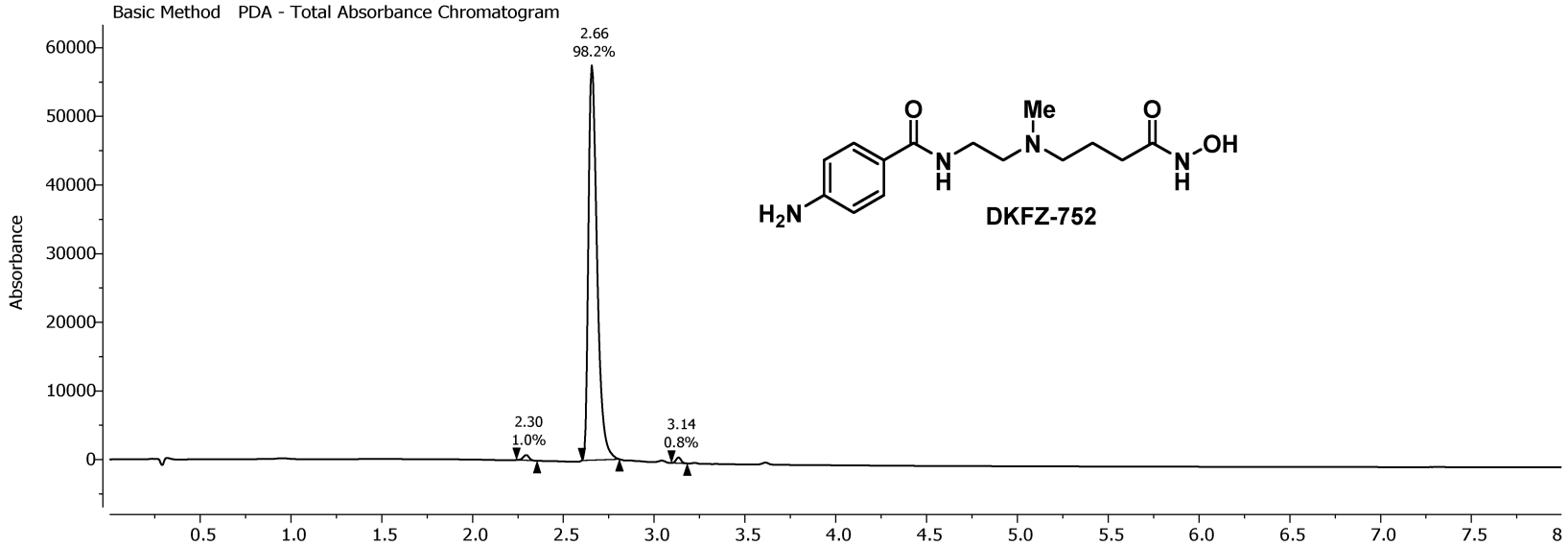
Basic Method PDA - Total Absorbance Chromatogram
Absorbance
2.66
98.2%
2.30
1.0%
3.14
0.8%
DKFZ-752

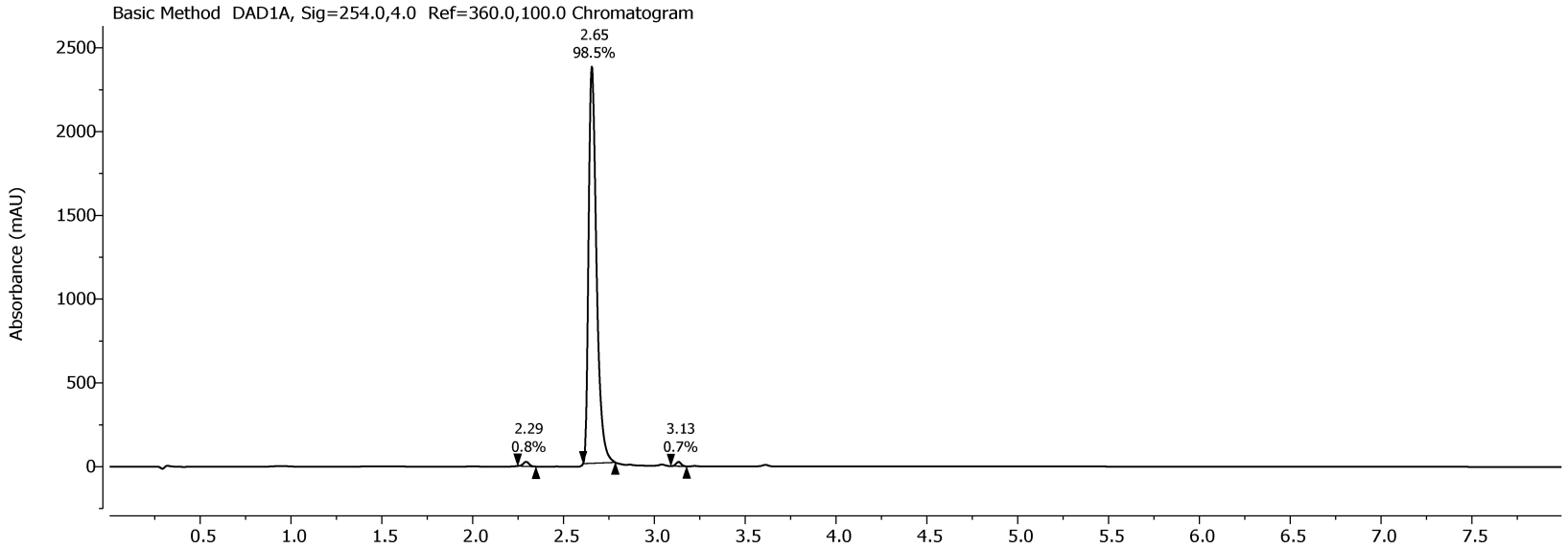
Basic Method DAD1A, Sig=254.0,4.0 Ref=360.0,100.0 Chromatogram
Absorbance (mAU)
2.65
98.5%
2.29
0.8%
3.13
0.7%

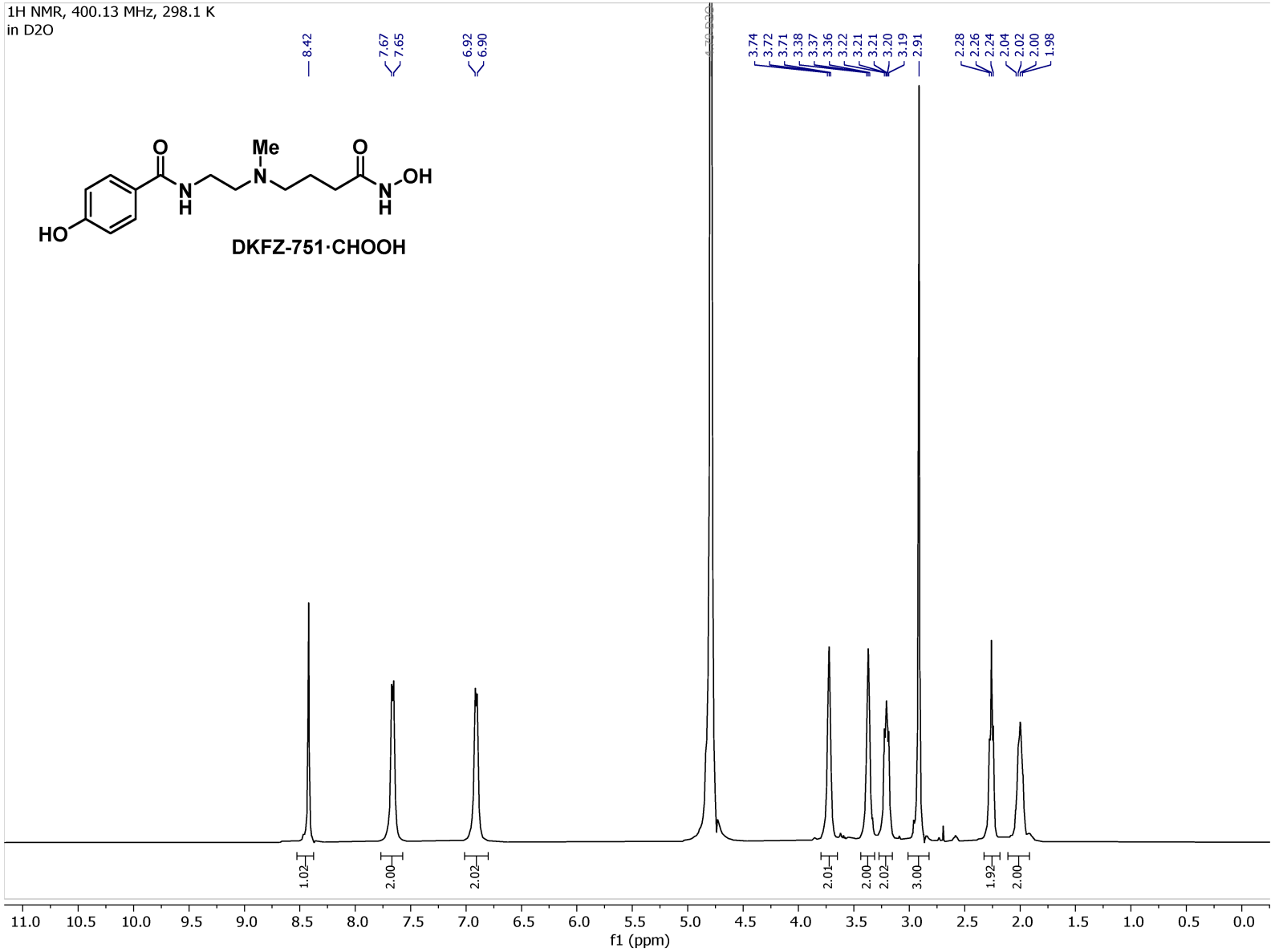
1H NMR, 400.13 MHz, 298.1 K
in D2O
8.42
7.67
7.65
6.92
6.90
4.70 D2O
3.74
3.72
3.71
3.38
3.37
3.36
3.22
3.21
3.21
3.20
3.19
2.91
2.28
2.26
2.24
2.04
2.02
2.00
1.98
O
Me
O
N
N
OH
H
H
HO
DKFZ-751·CHOOH
1.02
2.00
2.02
2.01
2.00
2.02
3.00
1.92
2.00
11.0
10.5
10.0
9.5
9.0
8.5
8.0
7.5
7.0
6.5
6.0
5.5
5.0
4.5
4.0
3.5
3.0
2.5
2.0
1.5
1.0
0.5
0.0
f1 (ppm)

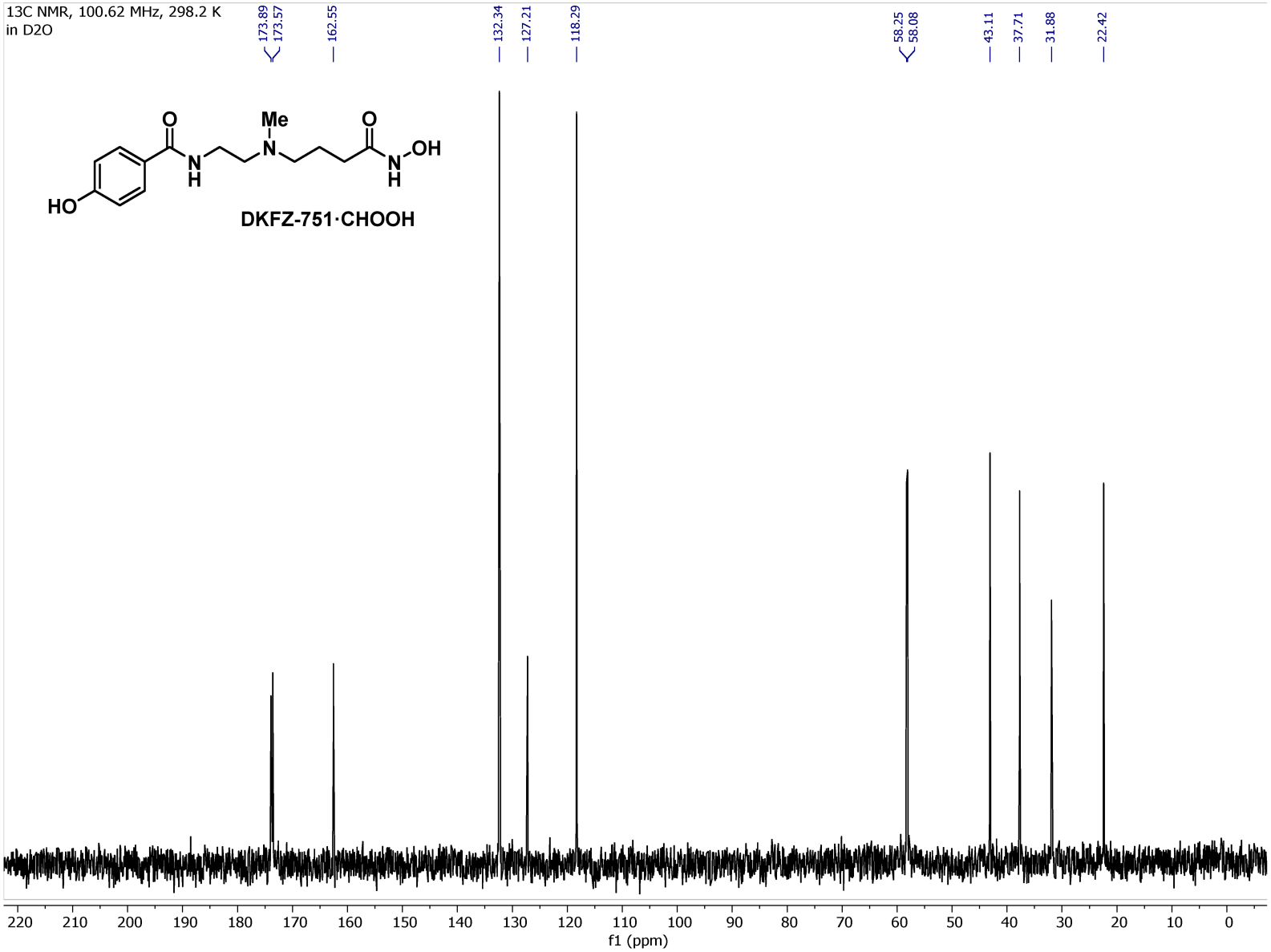
13C NMR, 100.62 MHz, 298.2 K
in D2O
173.89
173.57
162.55
132.34
127.21
118.29
58.25
58.08
43.11
37.71
31.88
22.42
Me
O
O
N
N
OH
H
H
HO
DKFZ-751·CHOOH
220 210 200 190 180 170 160 150 140 130 120 110 100 90 80 70 60 50 40 30 20 10 0
f1 (ppm)

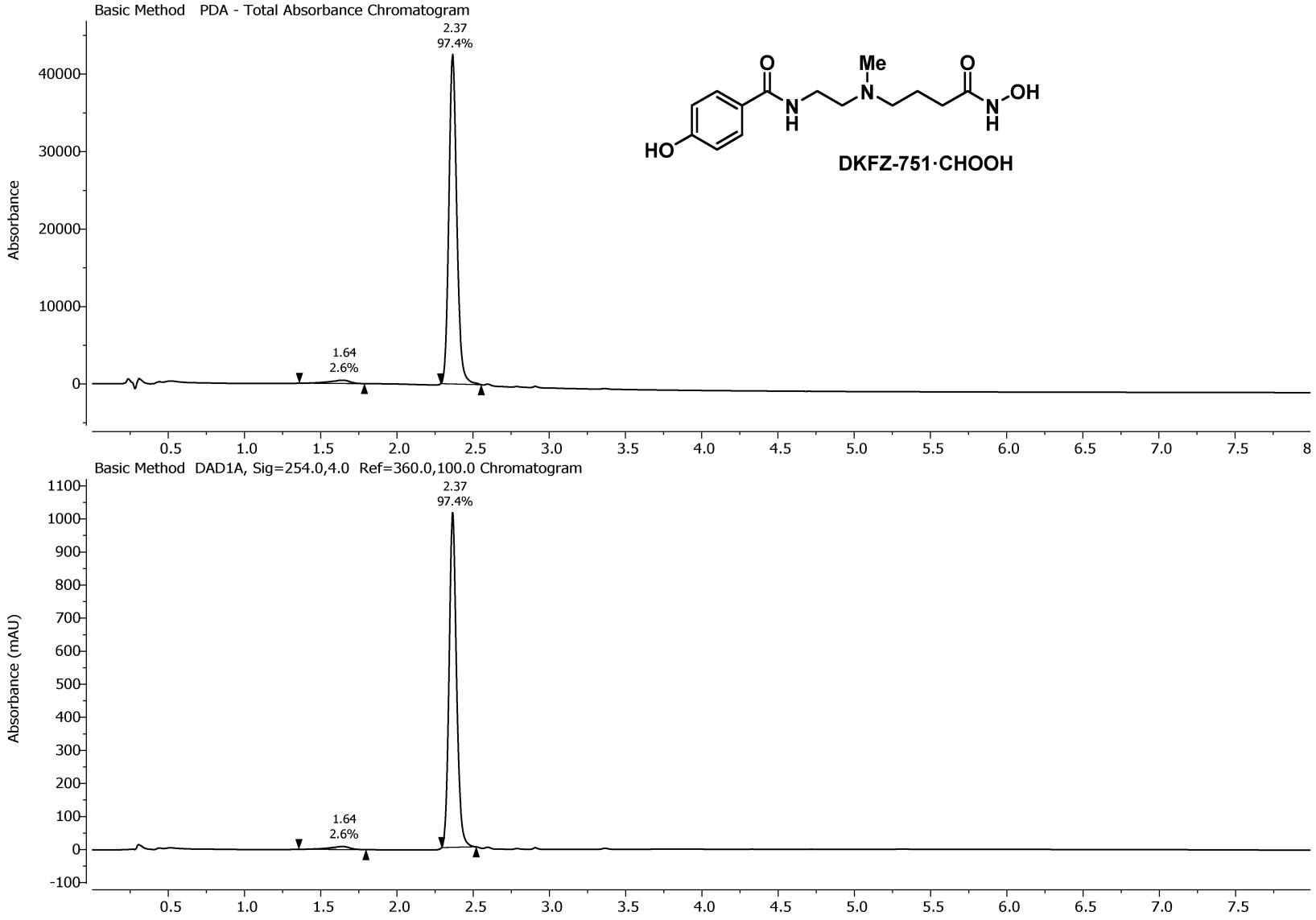
Basic Method PDA - Total Absorbance Chromatogram
2.37
97.4%
1.64
2.6%
Absorbance
40000
30000
20000
10000
0
0.5
1.0
1.5
2.0
2.5
3.0
3.5
4.0
4.5
5.0
5.5
6.0
6.5
7.0
7.5
8
O
Me
O
N
N
OH
H
H
HO
DKFZ-751·CHOOH
Basic Method DAD1A, Sig=254.0,4.0 Ref=360.0,100.0 Chromatogram
2.37
97.4%
1.64
2.6%
Absorbance (mAU)
1100
1000
900
800
700
600
500
400
300
200
100
0
-100
0.5
1.0
1.5
2.0
2.5
3.0
3.5
4.0
4.5
5.0
5.5
6.0
6.5
7.0
7.5

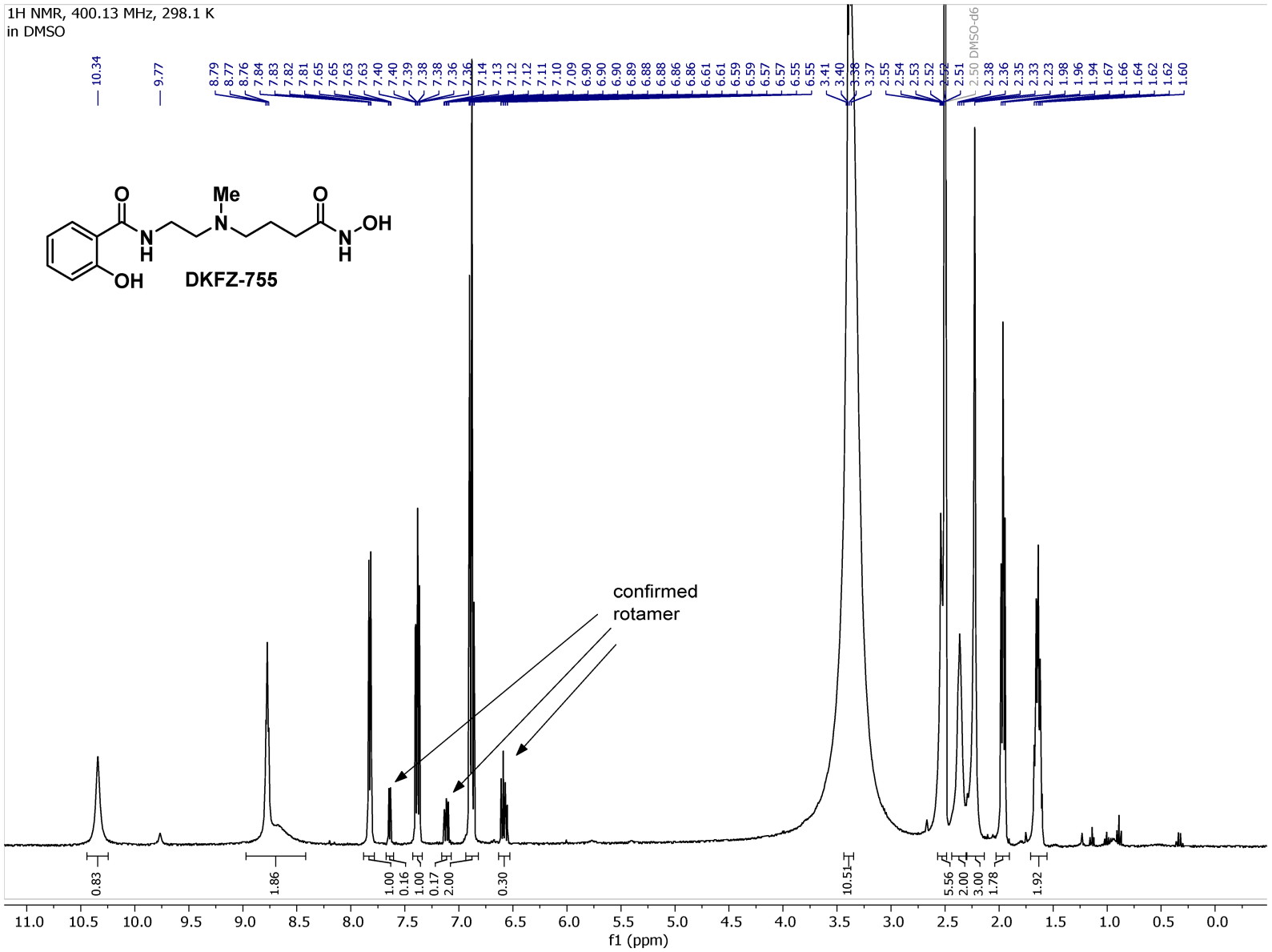
1H NMR, 400.13 MHz, 298.1 K
in DMSO
DKFZ-755
confirmed
rotamer
f1 (ppm)

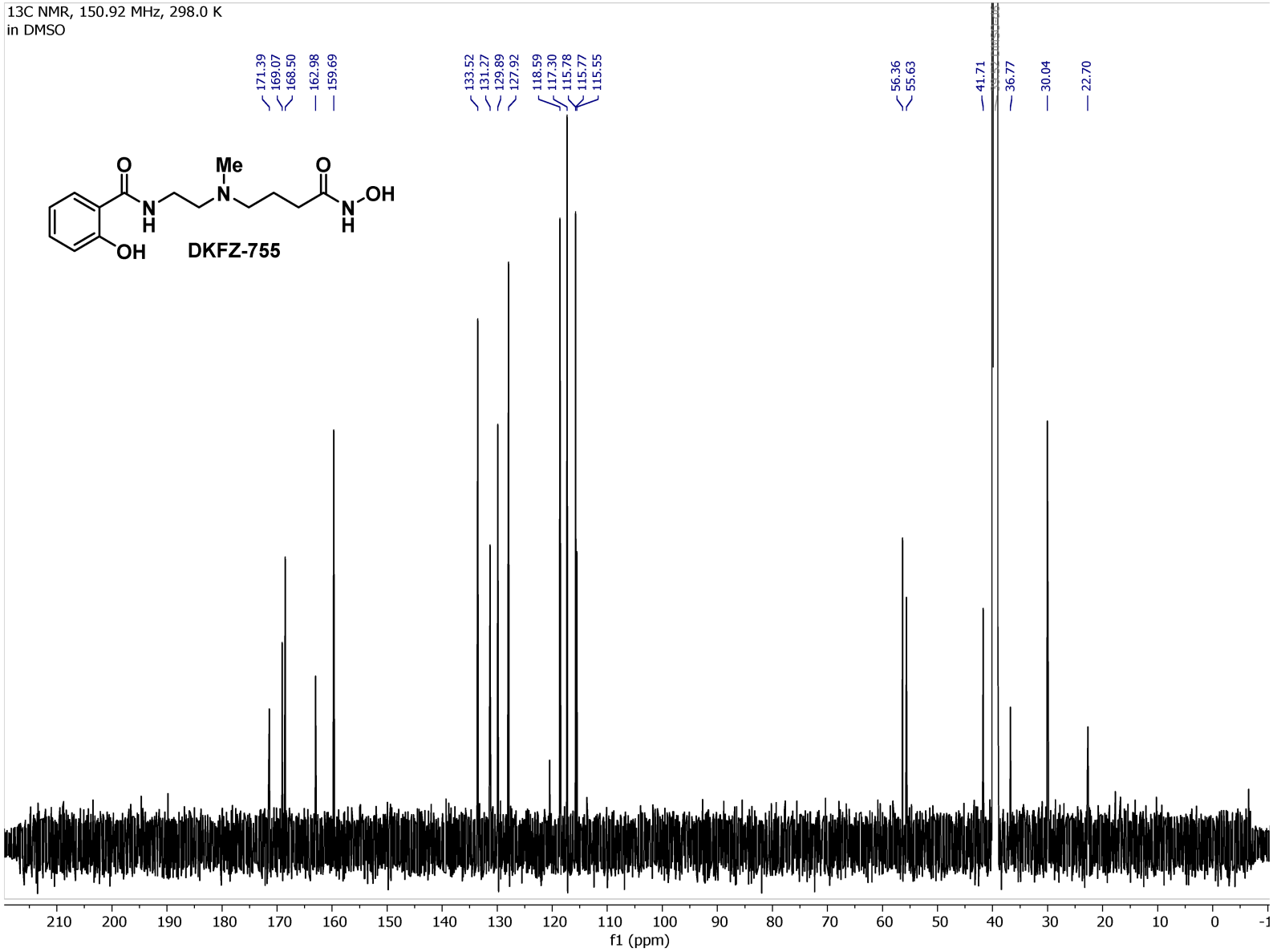
13C NMR, 150.92 MHz, 298.0 K
in DMSO
171.39
169.07
168.50
162.98
159.69
133.52
131.27
129.89
127.92
118.59
117.30
115.78
115.77
115.55
56.36
55.63
41.71
36.77
30.04
22.70
O
Me
O
N
N
OH
H
H
OH
DKFZ-755
210
200
190
180
170
160
150
140
130
120
110
100
90
80
70
60
50
40
30
20
10
0
f1 (ppm)

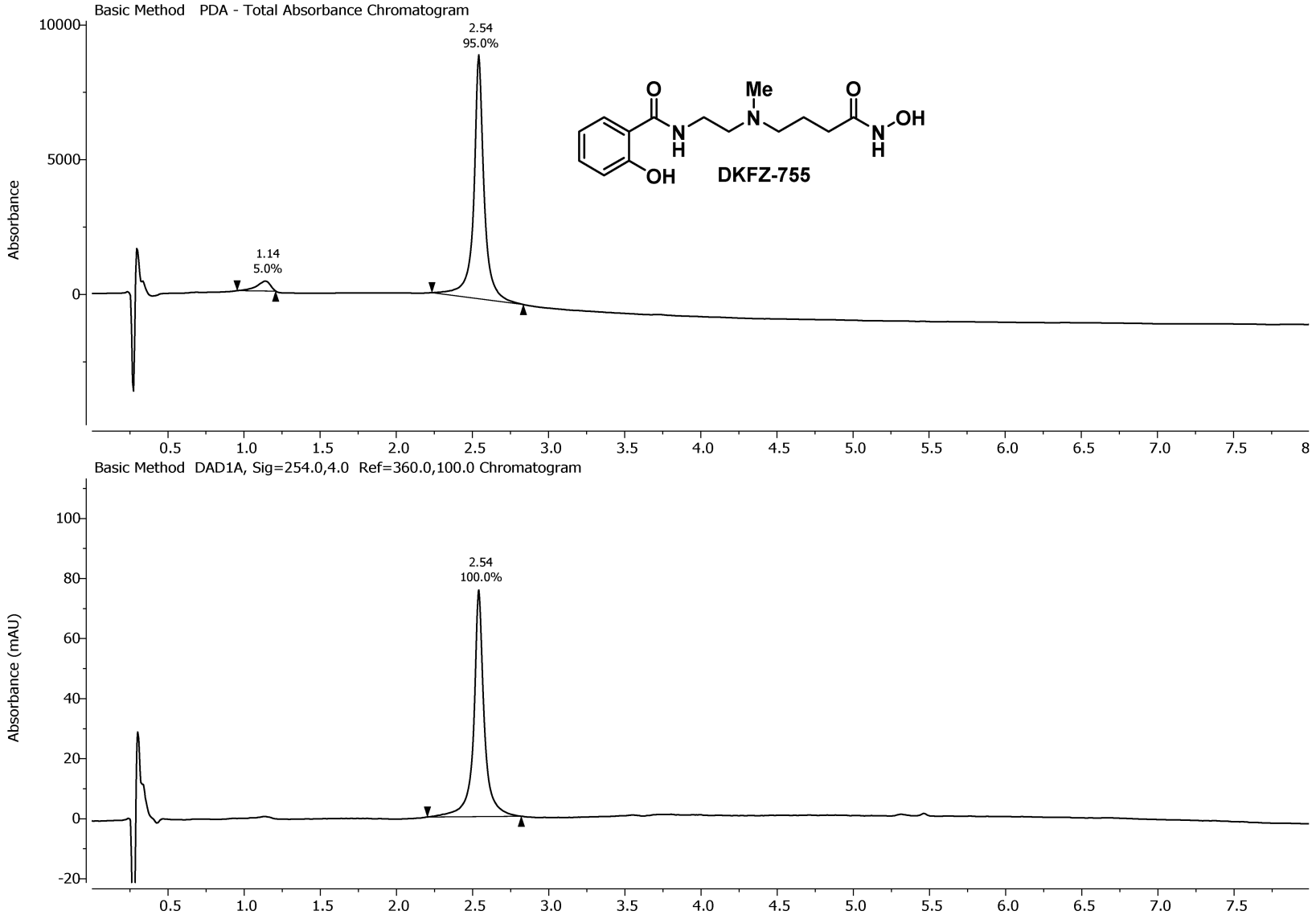
Basic Method PDA - Total Absorbance Chromatogram
Absorbance
2.54
95.0%
1.14
5.0%
DKFZ-755
Basic Method DAD1A, Sig=254.0,4.0 Ref=360.0,100.0 Chromatogram
Absorbance (mAU)
2.54
100.0%

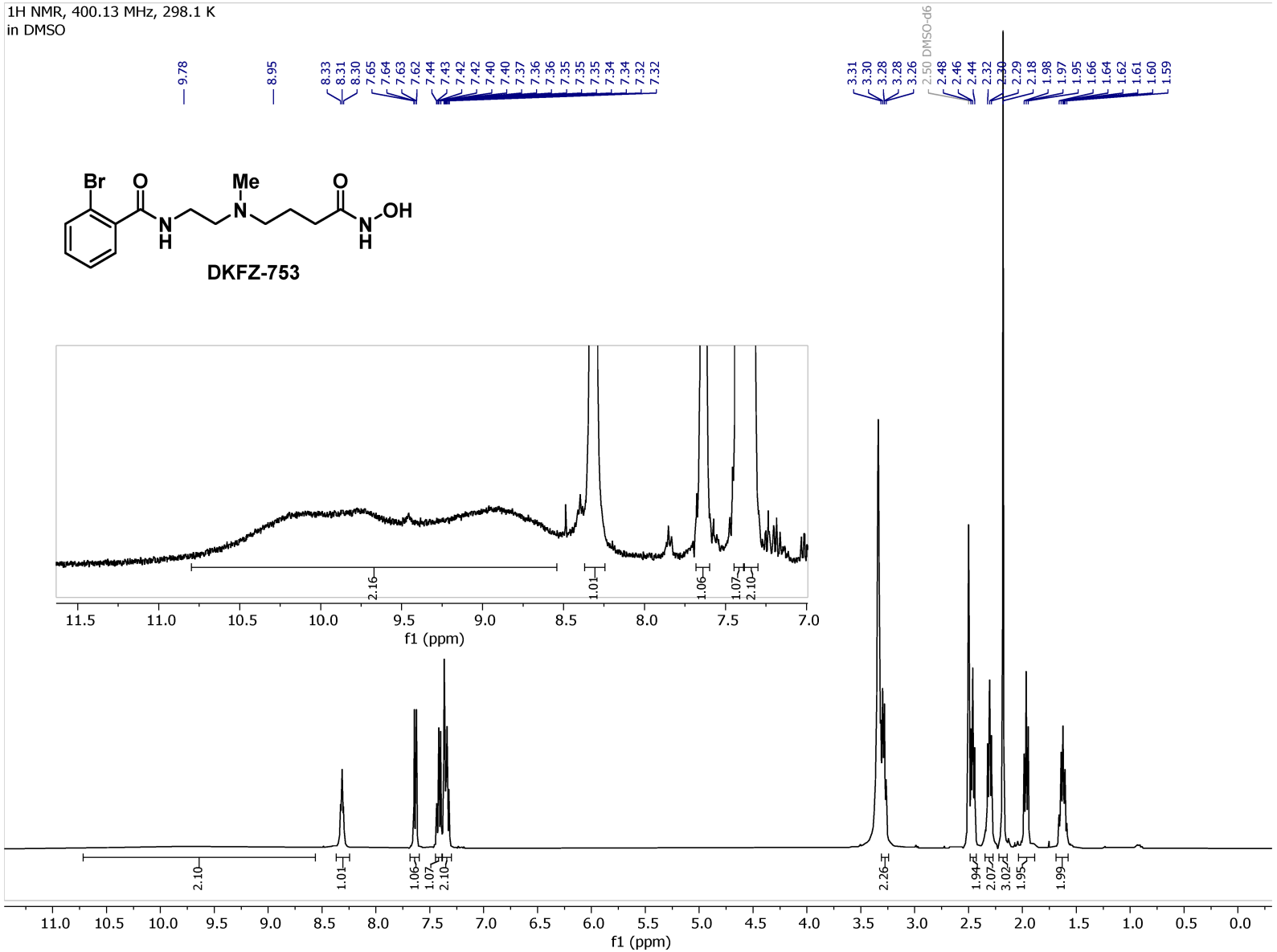
1H NMR, 400.13 MHz, 298.1 K
in DMSO
9.78
8.95
8.33
8.31
8.30
7.65
7.64
7.63
7.62
7.44
7.43
7.42
7.42
7.40
7.40
7.37
7.36
7.36
7.35
7.35
7.35
7.34
7.34
7.32
7.32
3.31
3.30
3.28
3.28
3.26
2.50 DMSO-d6
2.48
2.46
2.44
2.32
2.30
2.29
2.18
1.98
1.97
1.95
1.66
1.64
1.62
1.61
1.60
1.59
Br
O
N
H
Me
N
O
N
H
OH
DKFZ-753
2.16
1.01
1.06
1.07
2.10
11.5
11.0
10.5
10.0
9.5
9.0
8.5
8.0
7.5
7.0
f1 (ppm)
2.10
1.01
1.06
1.07
2.10
2.26
1.94
2.07
3.02
1.95
1.99
11.0
10.5
10.0
9.5
9.0
8.5
8.0
7.5
7.0
6.5
6.0
5.5
5.0
4.5
4.0
3.5
3.0
2.5
2.0
1.5
1.0
0.5
0.0
f1 (ppm)

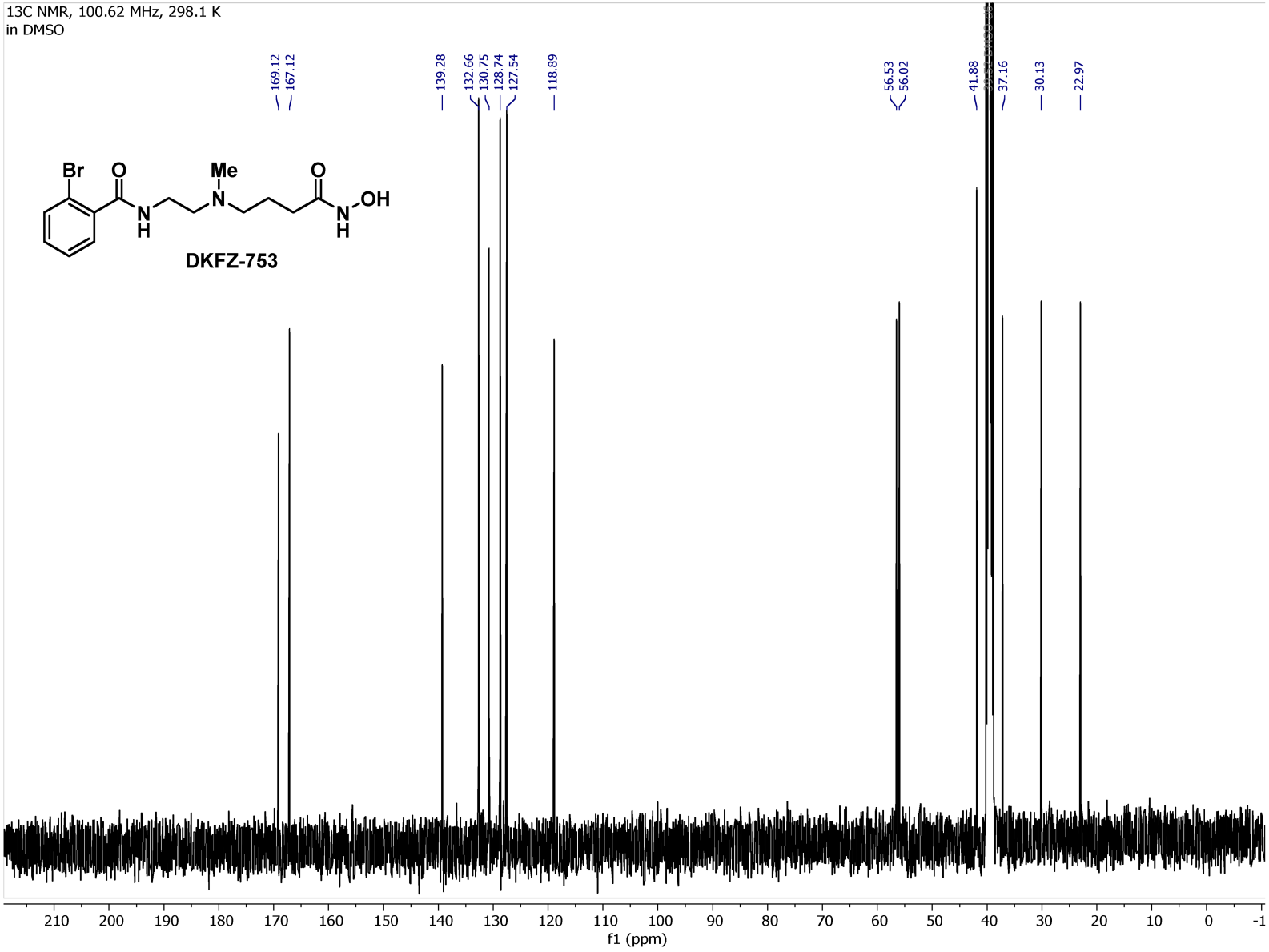
13C NMR, 100.62 MHz, 298.1 K
in DMSO
169.12
167.12
139.28
132.66
130.75
128.74
127.54
118.89
56.53
56.02
41.88
37.16
30.13
22.97
Br
O
Me
O
N
H
N
N
H
OH
DKFZ-753
210
200
190
180
170
160
150
140
130
120
110
100
90
80
70
60
50
40
30
20
10
0
-1
f1 (ppm)

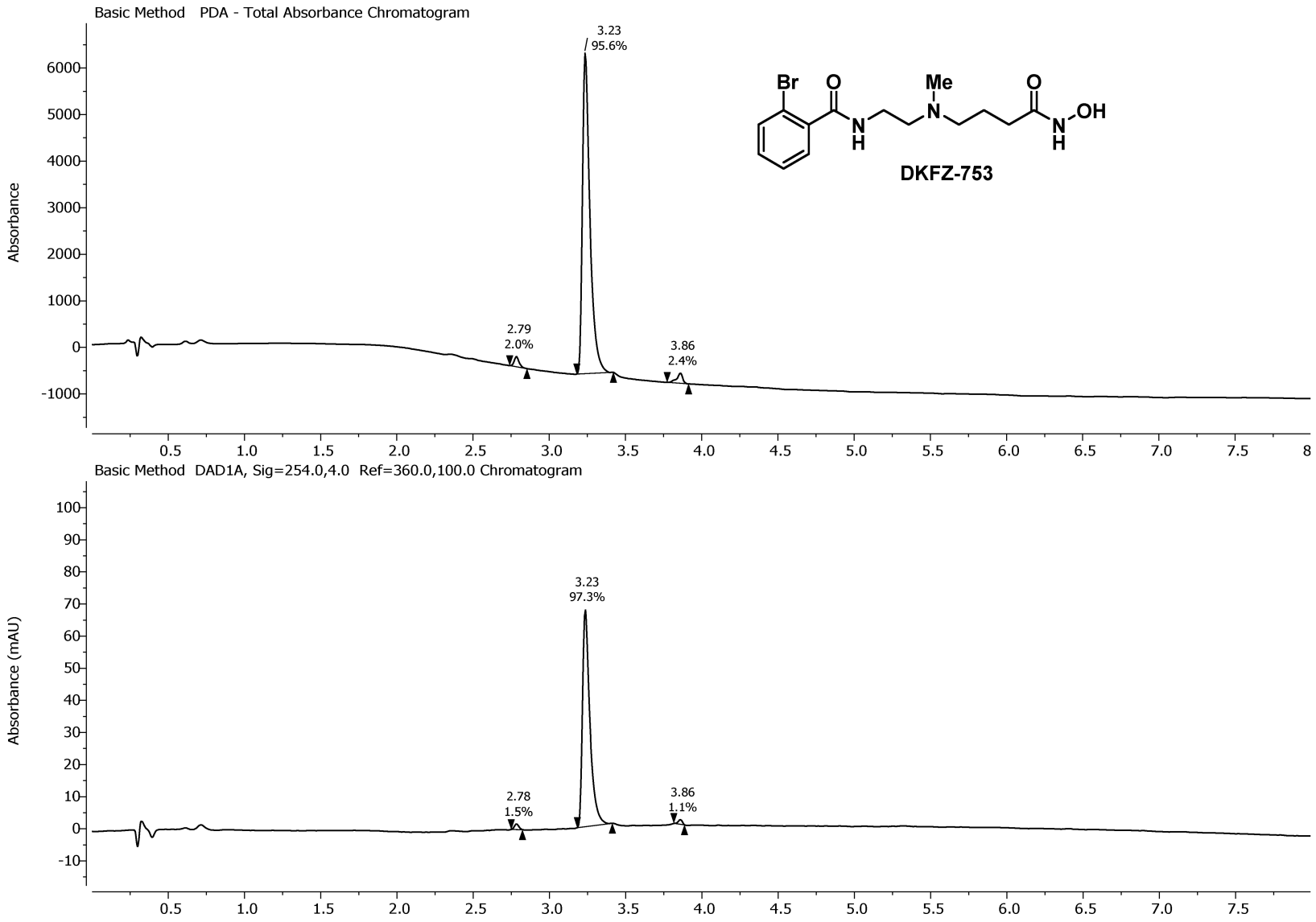
Basic Method PDA - Total Absorbance Chromatogram
Absorbance
3.23
95.6%
2.79
2.0%
3.86
2.4%
Br
O
Me
O
N
H
N
N
H
OH
DKFZ-753
Basic Method DAD1A, Sig=254.0,4.0 Ref=360.0,100.0 Chromatogram
Absorbance (mAU)
3.23
97.3%
2.78
1.5%
3.86
1.1%

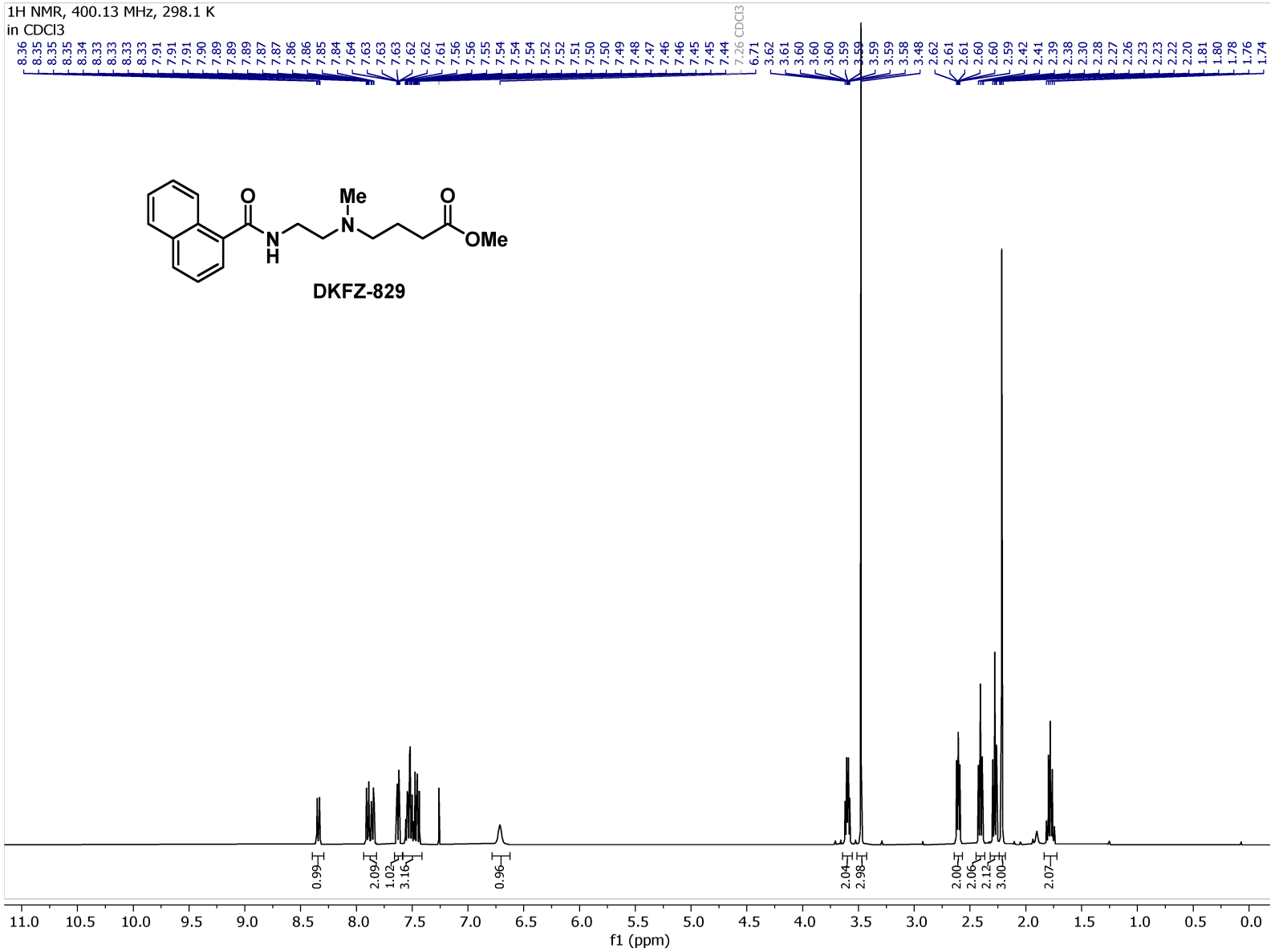
1H NMR, 400.13 MHz, 298.1 K
in CDCl3
CDCl3
Me
N
O
N
H
O
OMe
DKFZ-829
0.99
2.09
1.02
3.16
0.96
2.04
2.98
2.00
2.06
2.12
3.00
2.07
f1 (ppm)

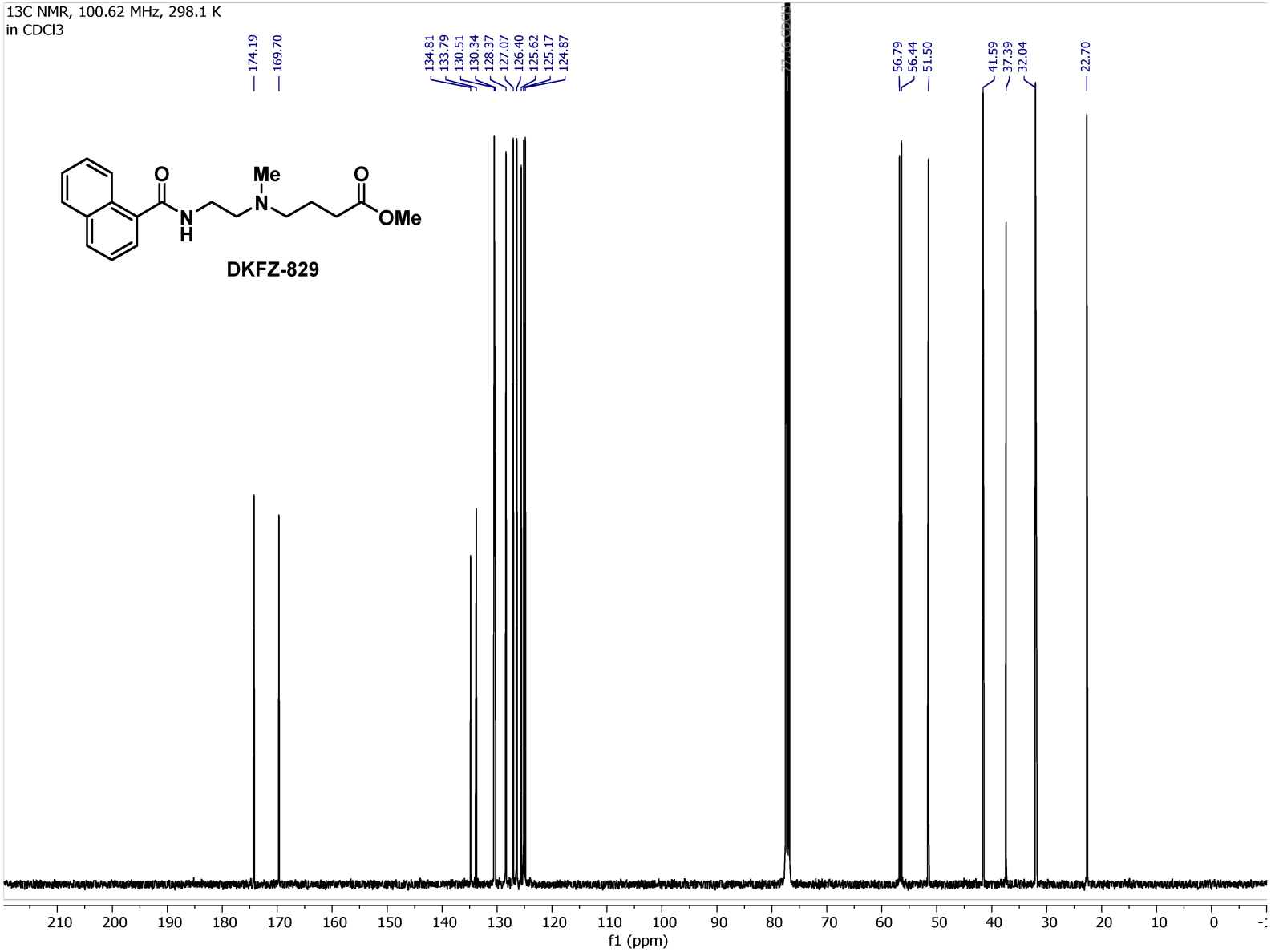
13C NMR, 100.62 MHz, 298.1 K
in CDCl3
174.19
169.70
134.81
133.79
130.51
130.34
128.37
127.07
126.40
125.62
125.17
124.87
77.16
56.79
56.44
51.50
41.59
37.39
32.04
22.70
O
Me
O
N
N
H
OMe
DKFZ-829
210
200
190
180
170
160
150
140
130
120
110
100
90
80
70
60
50
40
30
20
10
0
f1 (ppm)

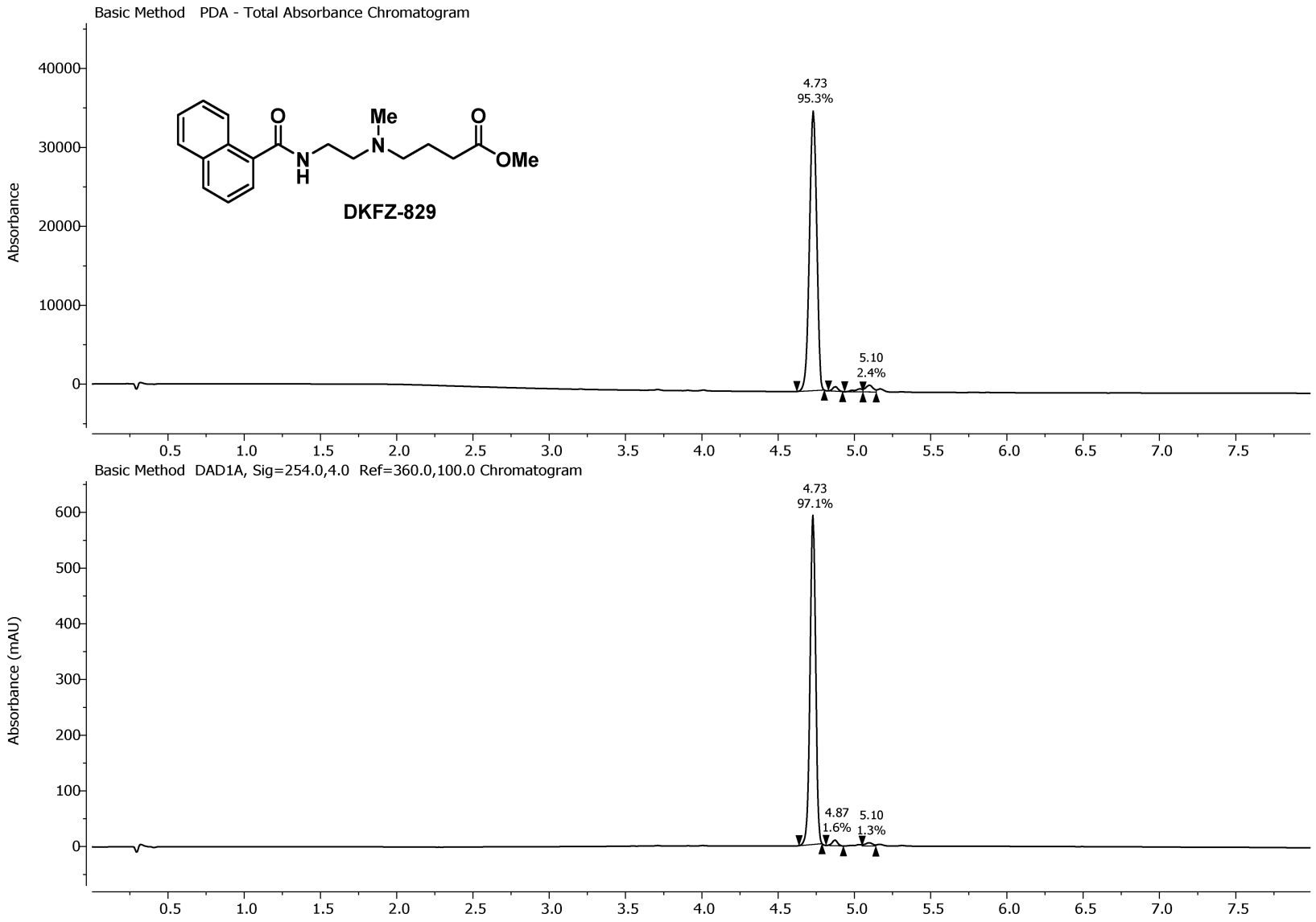
Basic Method PDA - Total Absorbance Chromatogram
Absorbance
40000
30000
20000
10000
0
O
Me
O
N
N
H
OMe
DKFZ-829
4.73
95.3%
5.10
2.4%
0.5
1.0
1.5
2.0
2.5
3.0
3.5
4.0
4.5
5.0
5.5
6.0
6.5
7.0
7.5
Basic Method DAD1A, Sig=254.0,4.0 Ref=360.0,100.0 Chromatogram
Absorbance (mAU)
600
500
400
300
200
100
0
4.73
97.1%
4.87
1.6%
5.10
1.3%
0.5
1.0
1.5
2.0
2.5
3.0
3.5
4.0
4.5
5.0
5.5
6.0
6.5
7.0
7.5

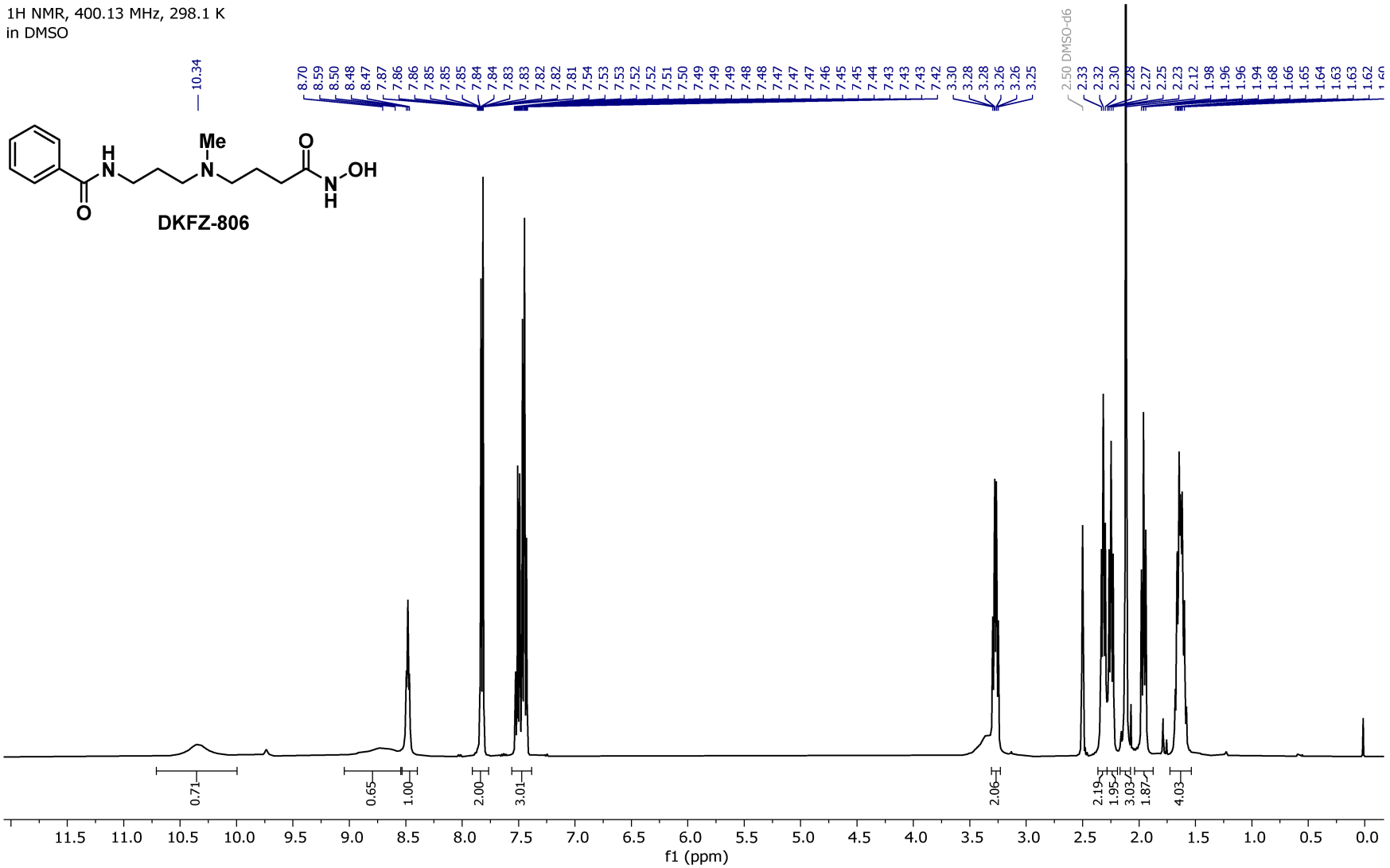
1H NMR, 400.13 MHz, 298.1 K
in DMSO
DKFZ-806
f1 (ppm)

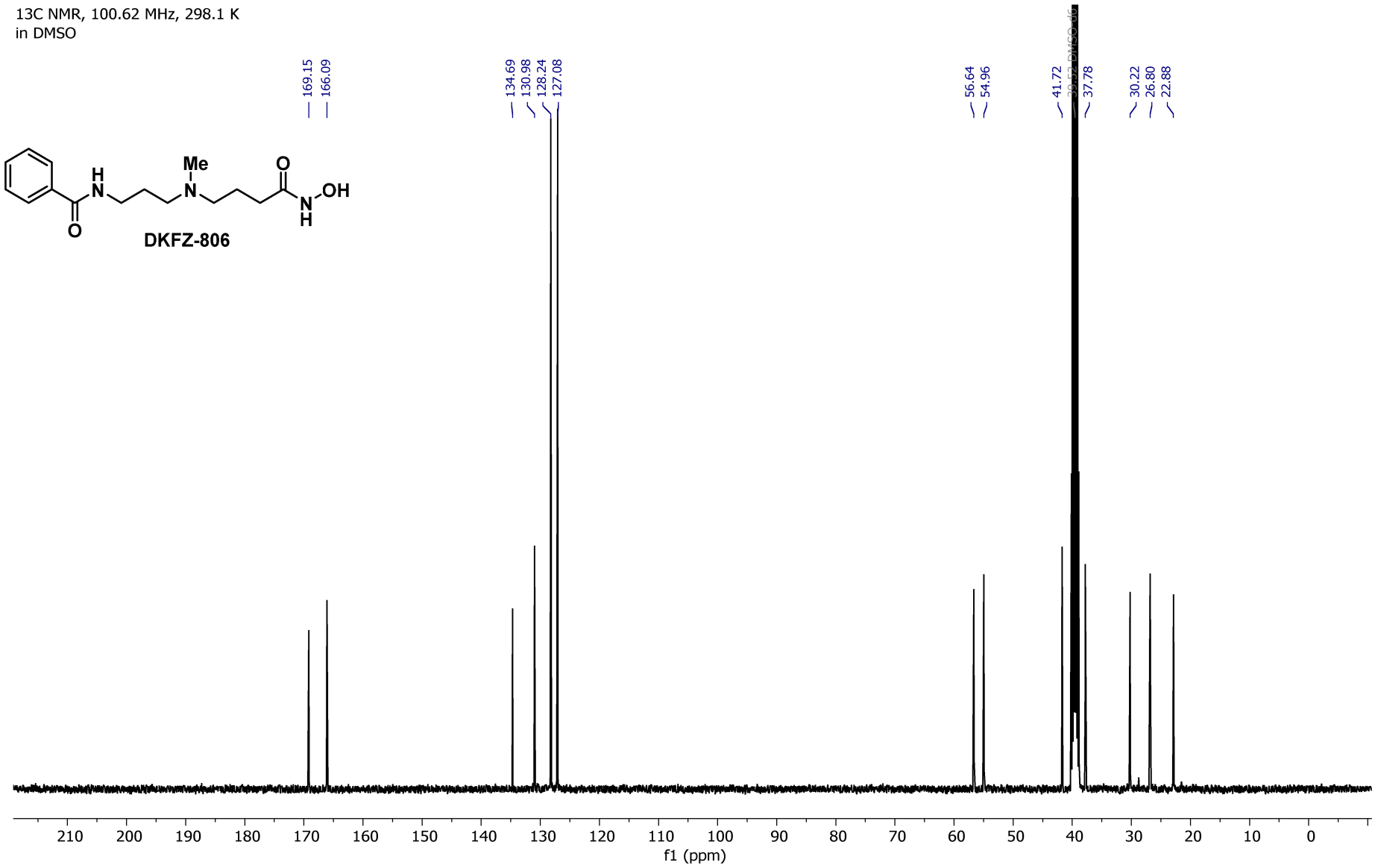
13C NMR, 100.62 MHz, 298.1 K
in DMSO
169.15
166.09
134.69
130.98
128.24
127.08
56.64
54.96
41.72
39.52 DMSO-d6
37.78
30.22
26.80
22.88
Me
H
N
N
O
N
H
OH
O
O
DKFZ-806
210
200
190
180
170
160
150
140
130
120
110
100
90
80
70
60
50
40
30
20
10
0
f1 (ppm)

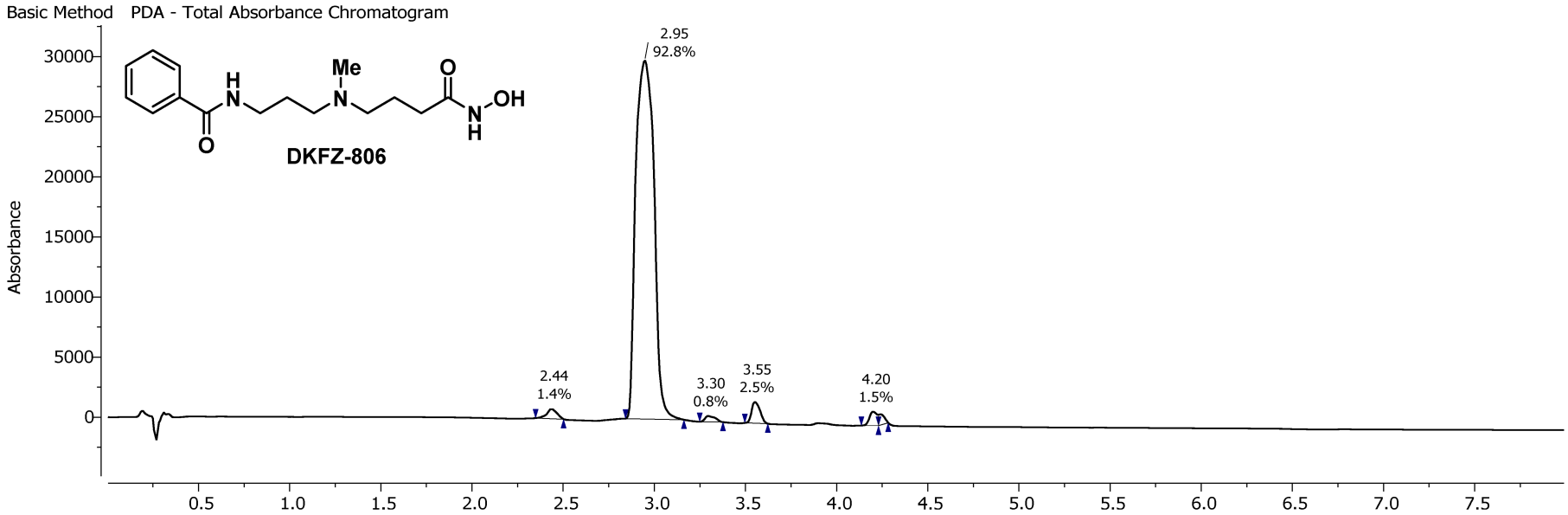
Basic Method PDA - Total Absorbance Chromatogram
Absorbance
DKFZ-806
2.95
92.8%
2.44
1.4%
3.30
0.8%
3.55
2.5%
4.20
1.5%

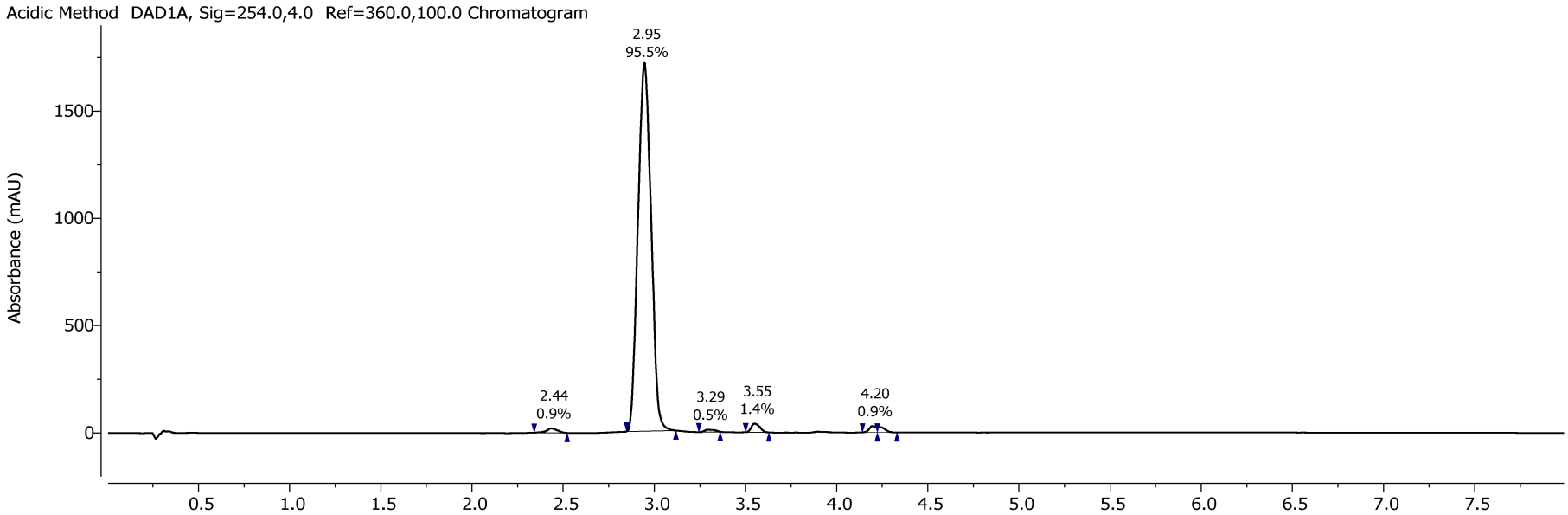
Acidic Method DAD1A, Sig=254.0,4.0 Ref=360.0,100.0 Chromatogram
Absorbance (mAU)
2.95
95.5%
2.44
0.9%
3.29
0.5%
3.55
1.4%
4.20
0.9%

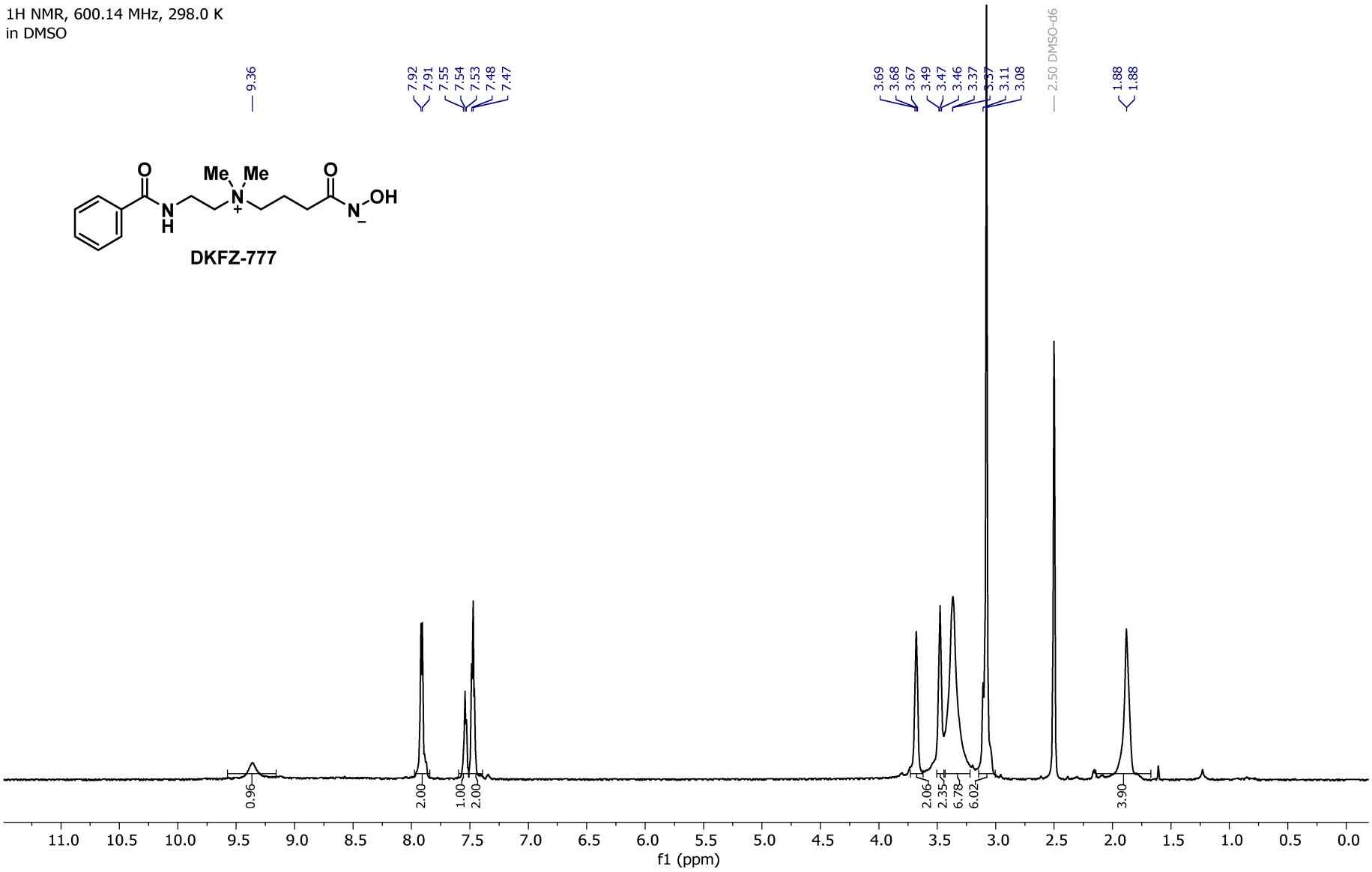
1H NMR, 600.14 MHz, 298.0 K
in DMSO
9.36
7.92
7.91
7.55
7.54
7.53
7.48
7.47
3.69
3.68
3.67
3.49
3.47
3.46
3.37
3.37
3.11
3.08
2.50 DMSO-d6
1.88
1.88
DKFZ-777
0.96
2.00
1.00
2.00
2.06
2.35
6.78
6.02
3.90
11.0
10.5
10.0
9.5
9.0
8.5
8.0
7.5
7.0
6.5
6.0
5.5
5.0
4.5
4.0
3.5
3.0
2.5
2.0
1.5
1.0
0.5
0.0
f1 (ppm)

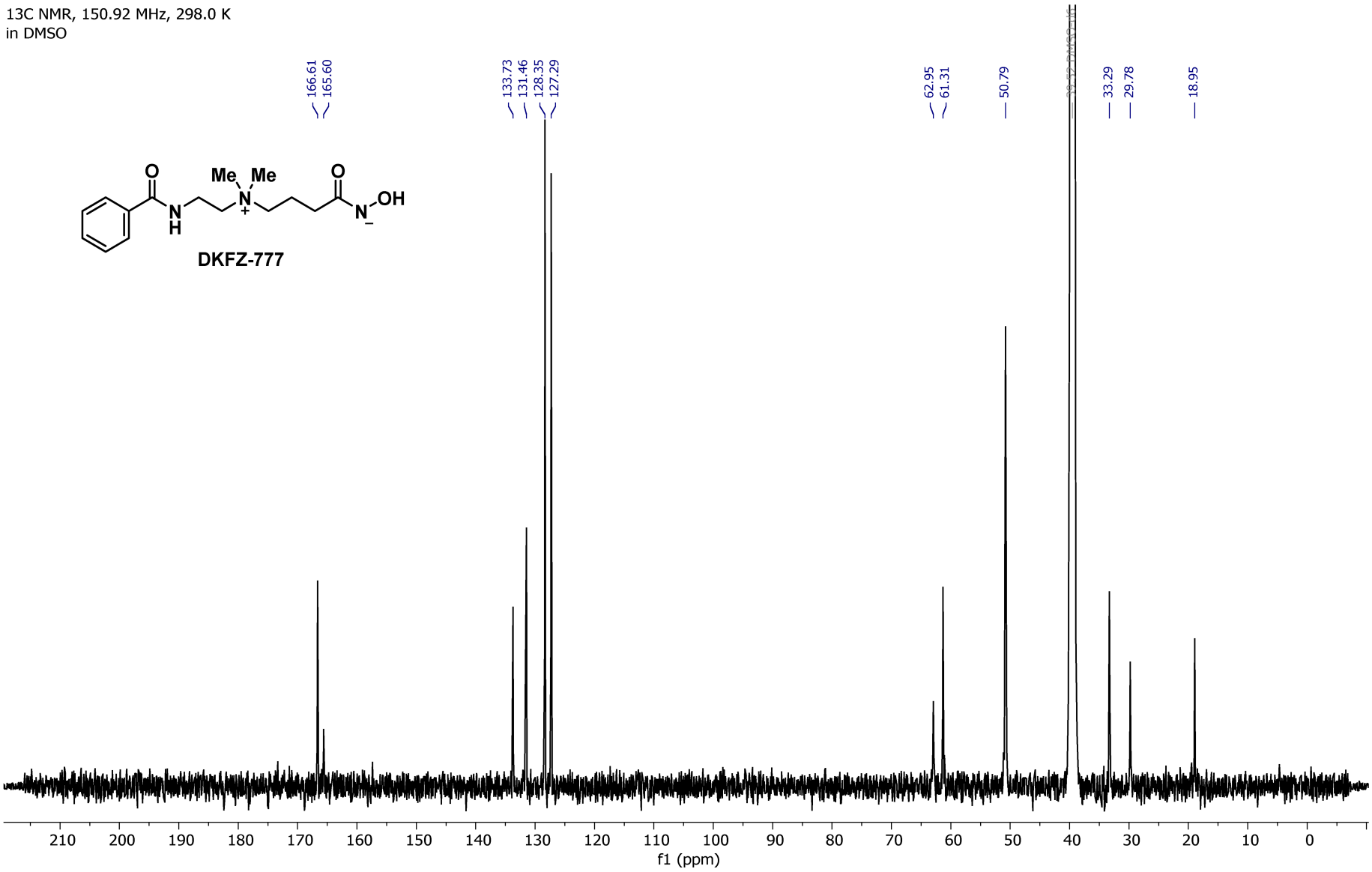
13C NMR, 150.92 MHz, 298.0 K
in DMSO
166.61
165.60
133.73
131.46
128.35
127.29
62.95
61.31
50.79
39.52 DMSO pent
33.29
29.78
18.95
Me
Me
O
N
H
N
+
O
N
−
OH
DKFZ-777
210
200
190
180
170
160
150
140
130
120
110
100
90
80
70
60
50
40
30
20
10
0
f1 (ppm)

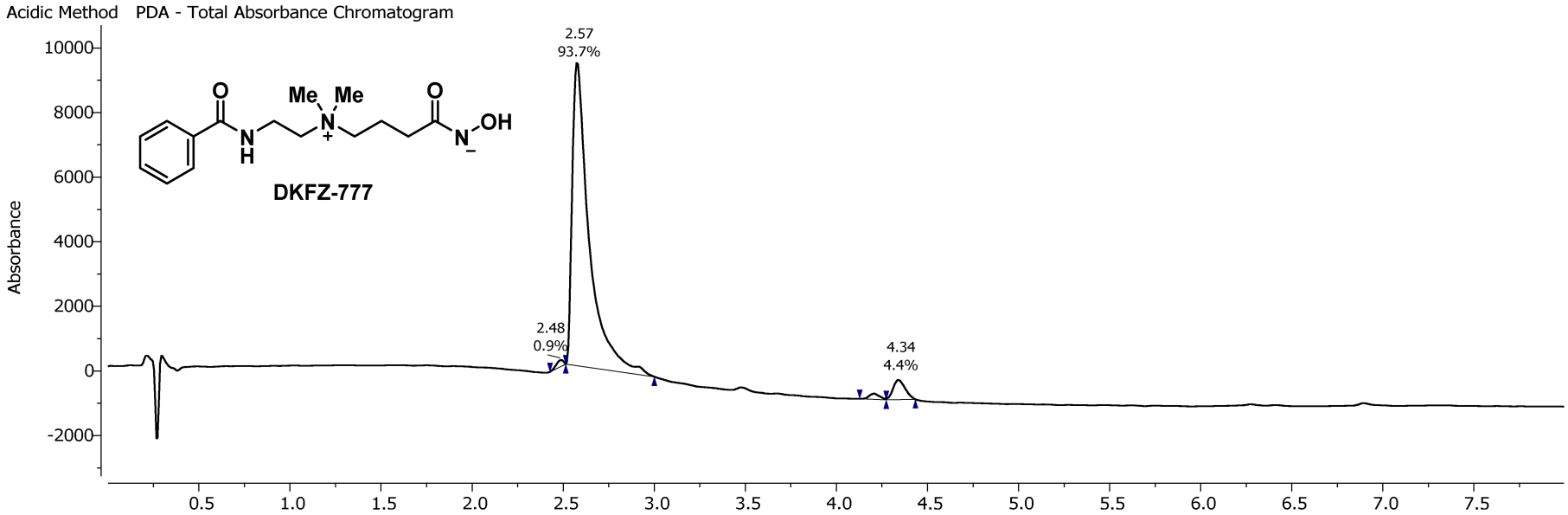
Acidic Method PDA - Total Absorbance Chromatogram
Absorbance
2.57
93.7%
2.48
0.9%
4.34
4.4%
DKFZ-777

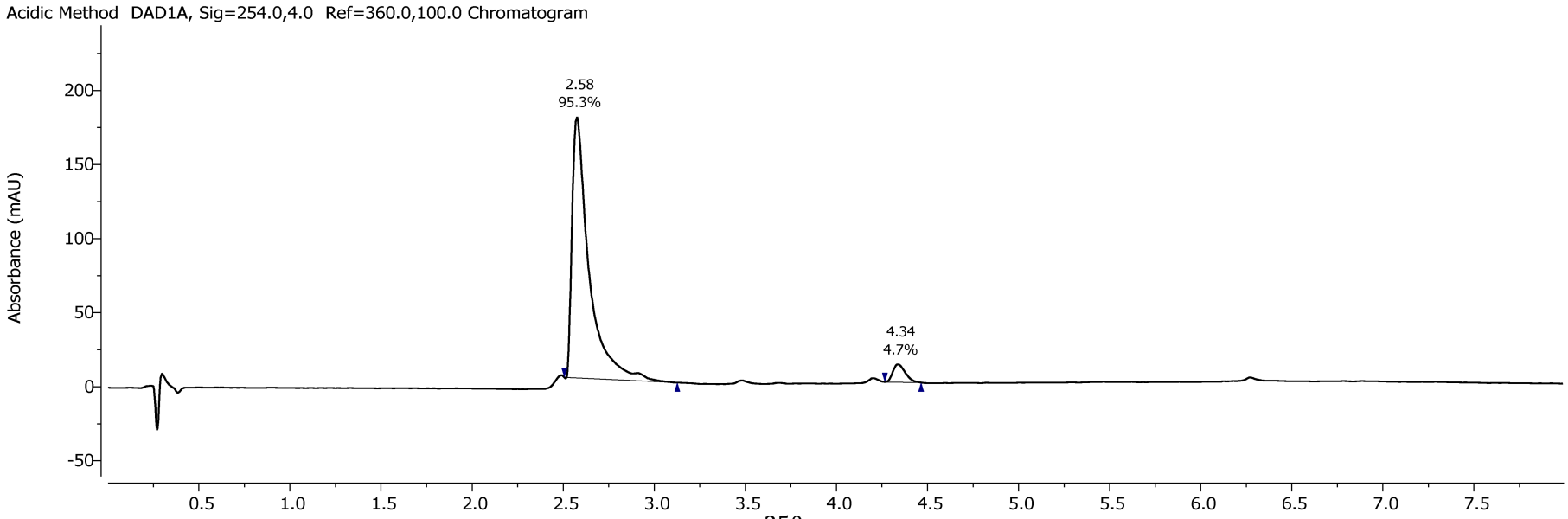
Acidic Method DAD1A, Sig=254.0,4.0 Ref=360.0,100.0 Chromatogram
Absorbance (mAU)
2.58
95.3%
4.34
4.7%

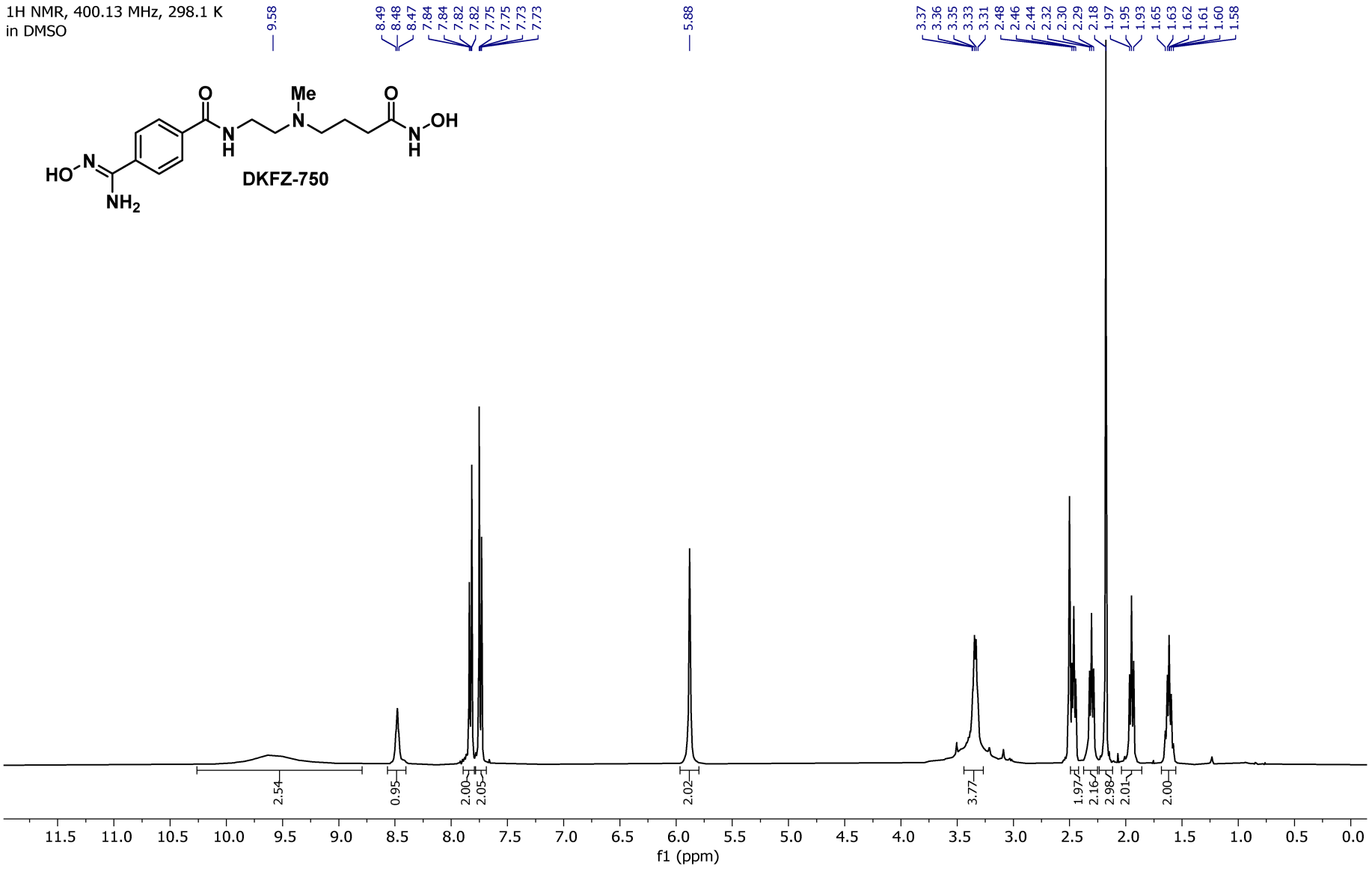
1H NMR, 400.13 MHz, 298.1 K
in DMSO
DKFZ-750
f1 (ppm)

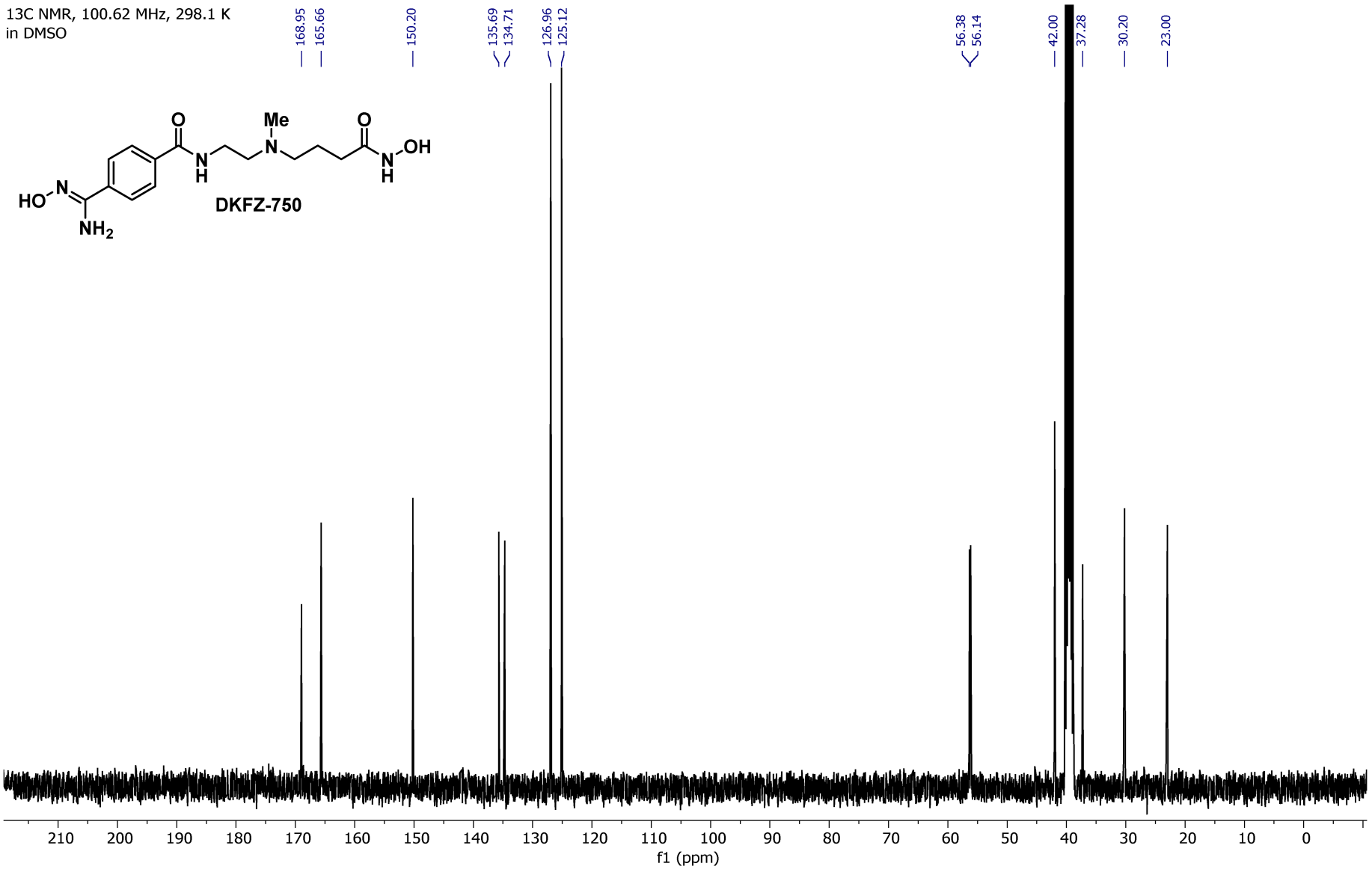
13C NMR, 100.62 MHz, 298.1 K
in DMSO
168.95
165.66
150.20
135.69
134.71
126.96
125.12
56.38
56.14
42.00
37.28
30.20
23.00
DKFZ-750
f1 (ppm)

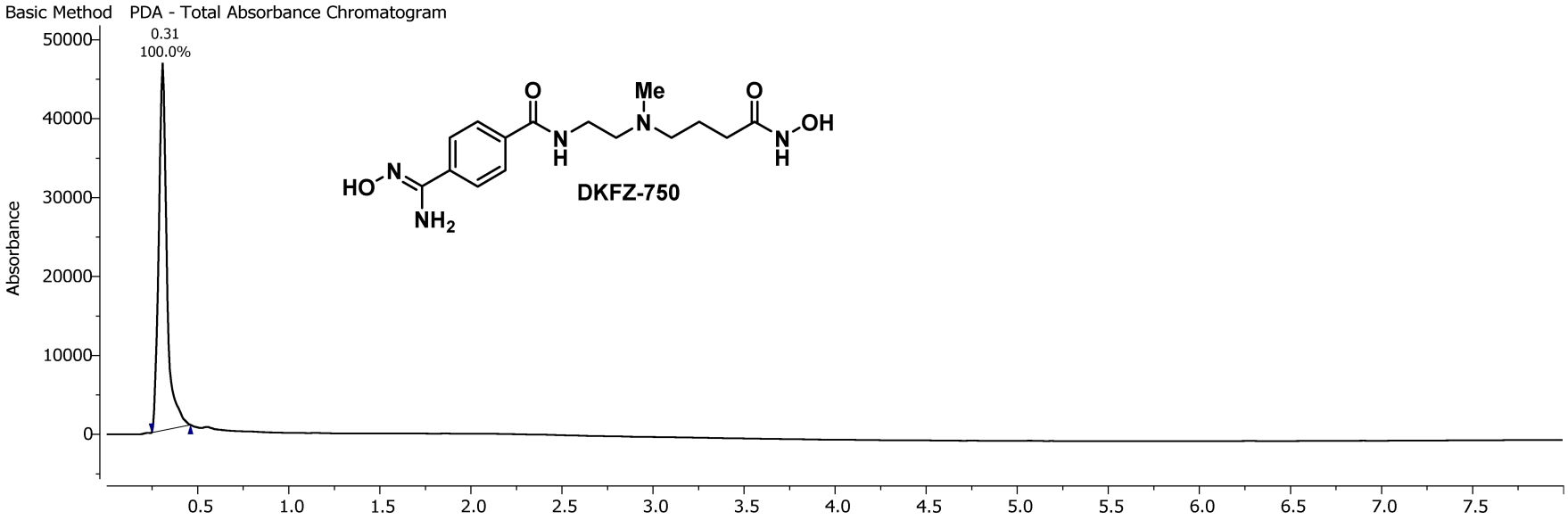
Basic Method PDA - Total Absorbance Chromatogram
0.31
100.0%
Absorbance
50000
40000
30000
20000
10000
0
0.5
1.0
1.5
2.0
2.5
3.0
3.5
4.0
4.5
5.0
5.5
6.0
6.5
7.0
7.5
HO
N
NH2
O
N
H
Me
N
O
N
H
OH
DKFZ-750

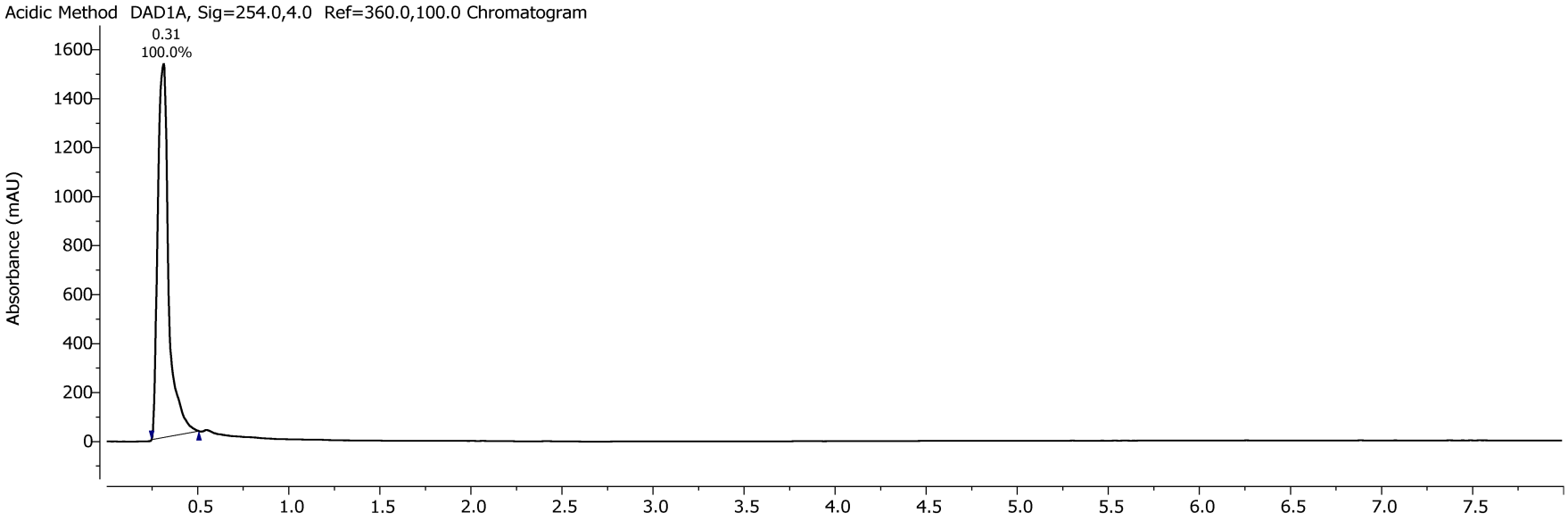
Acidic Method DAD1A, Sig=254.0,4.0 Ref=360.0,100.0 Chromatogram
0.31
100.0%
Absorbance (mAU)
1600
1400
1200
1000
800
600
400
200
0
0.5
1.0
1.5
2.0
2.5
3.0
3.5
4.0
4.5
5.0
5.5
6.0
6.5
7.0
7.5

1H NMR, 400.13 MHz, 298.1 K
in DMSO

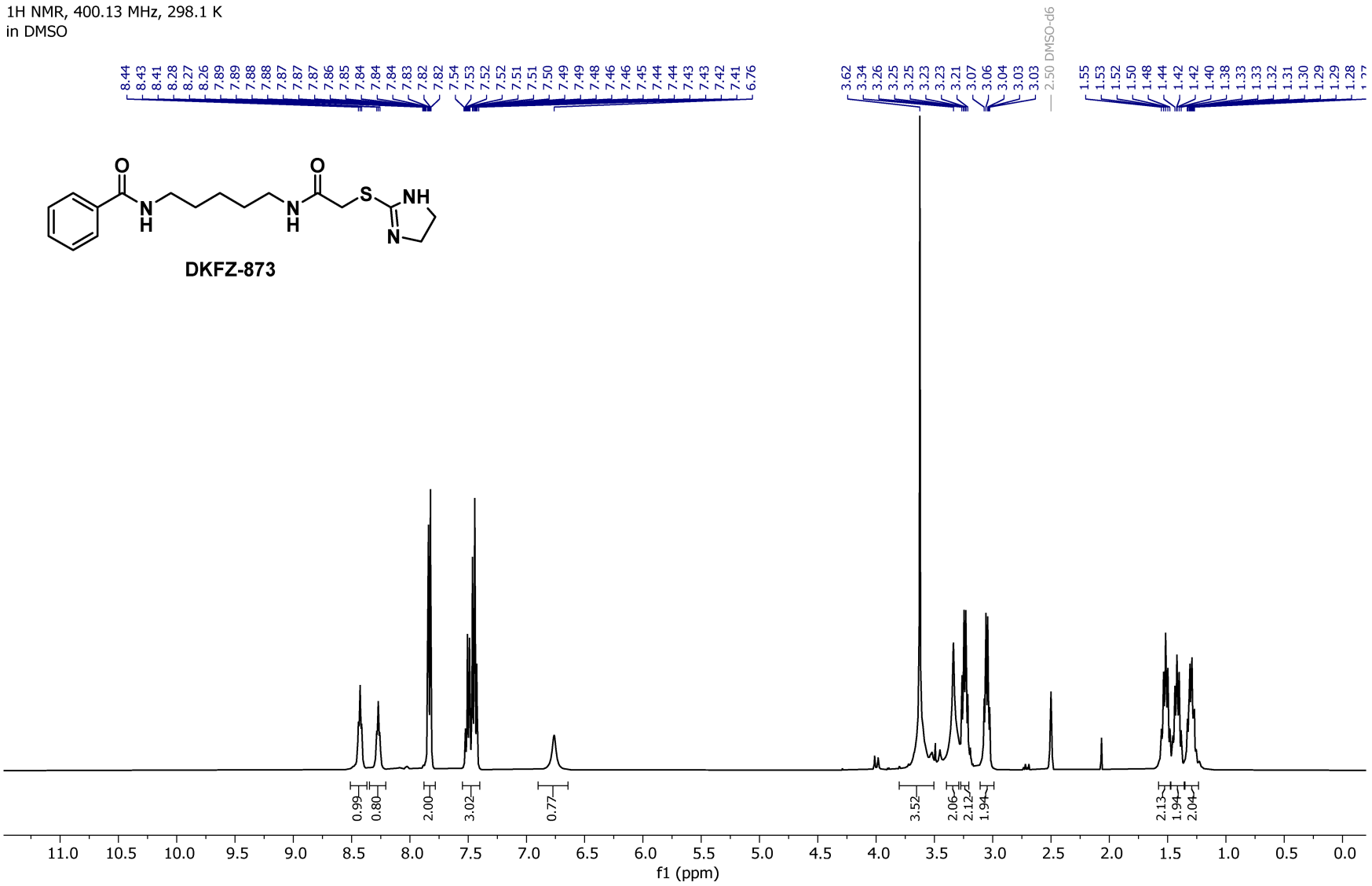

13C NMR, 100.62 MHz, 298.1 K
in DMSO

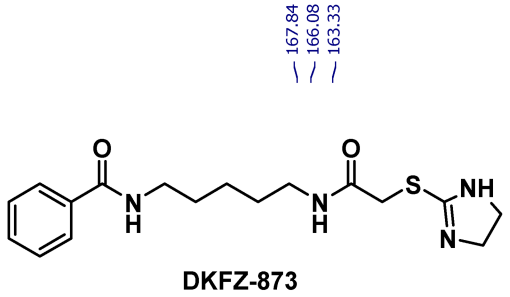


DKFZ-873

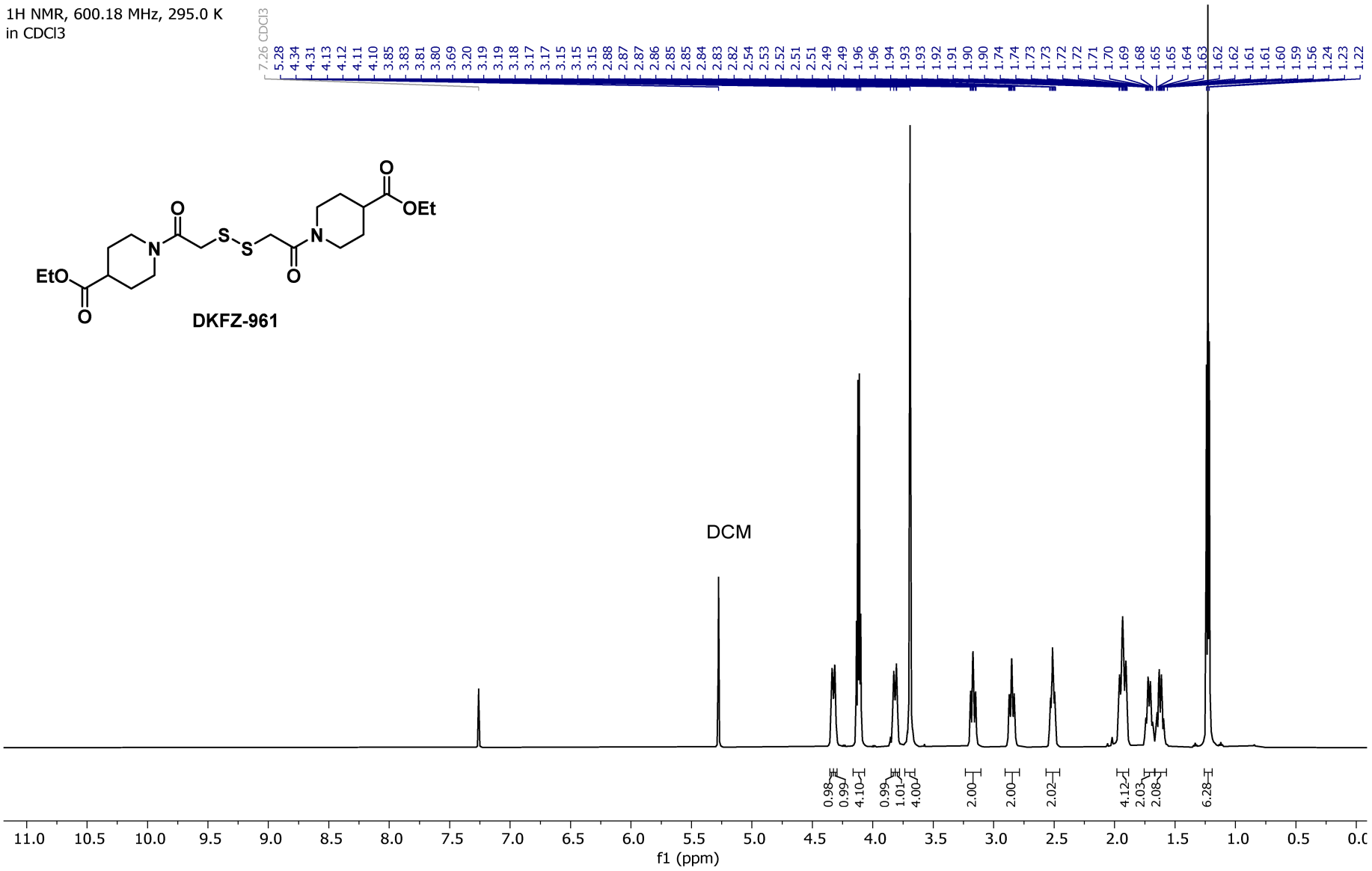
1H NMR, 600.18 MHz, 295.0 K
in CDCl3
DKFZ-961
DCM
f1 (ppm)

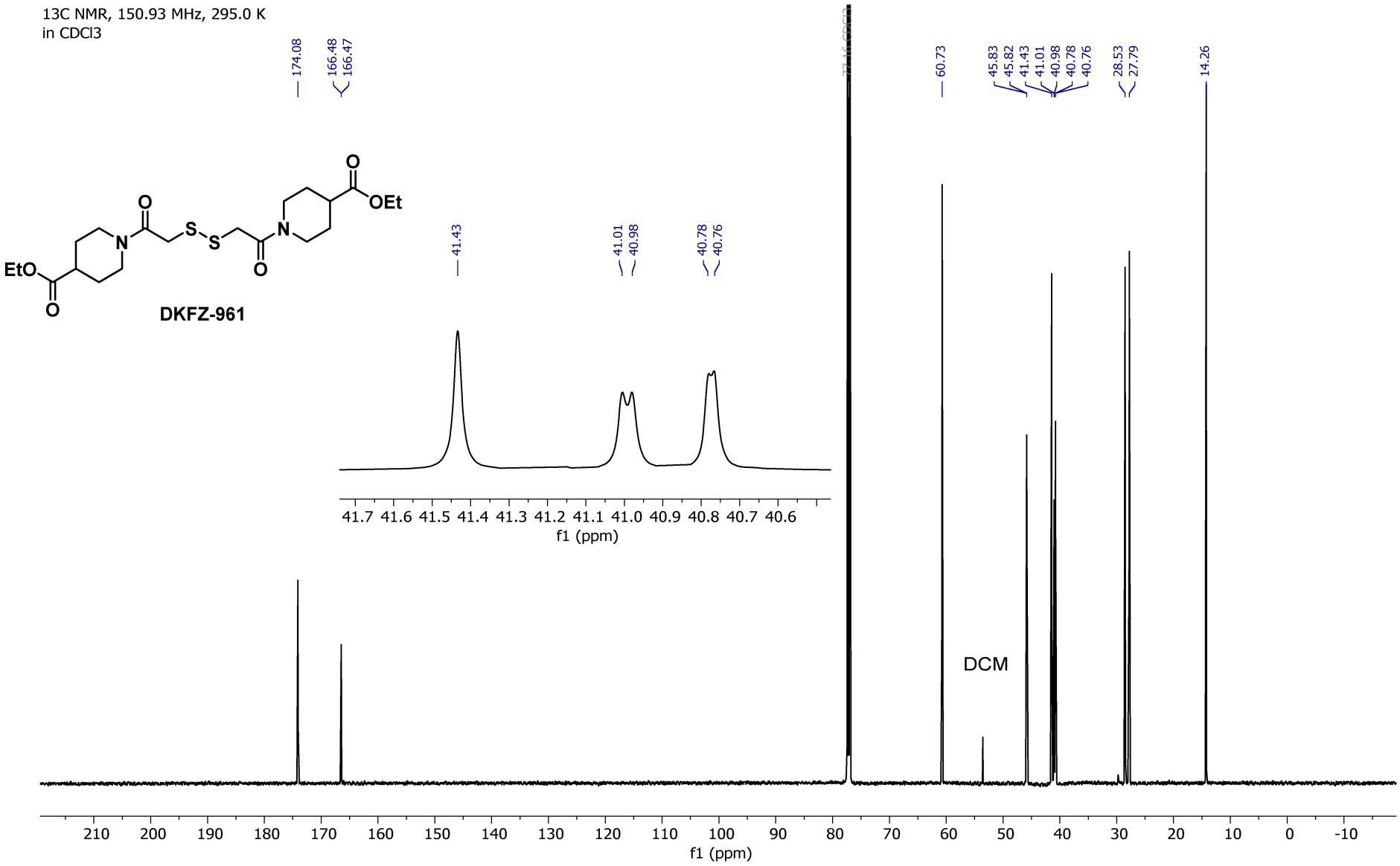
13C NMR, 150.93 MHz, 295.0 K
in CDCl3
174.08
166.48
166.47
77.16
60.73
45.83
45.82
41.43
41.01
40.98
40.78
40.76
28.53
27.79
14.26
DKFZ-961
EtO
OEt
41.43
41.01
40.98
40.78
40.76
41.7 41.6 41.5 41.4 41.3 41.2 41.1 41.0 40.9 40.8 40.7 40.6
f1 (ppm)
DCM
210 200 190 180 170 160 150 140 130 120 110 100 90 80 70 60 50 40 30 20 10 0 -10
f1 (ppm)

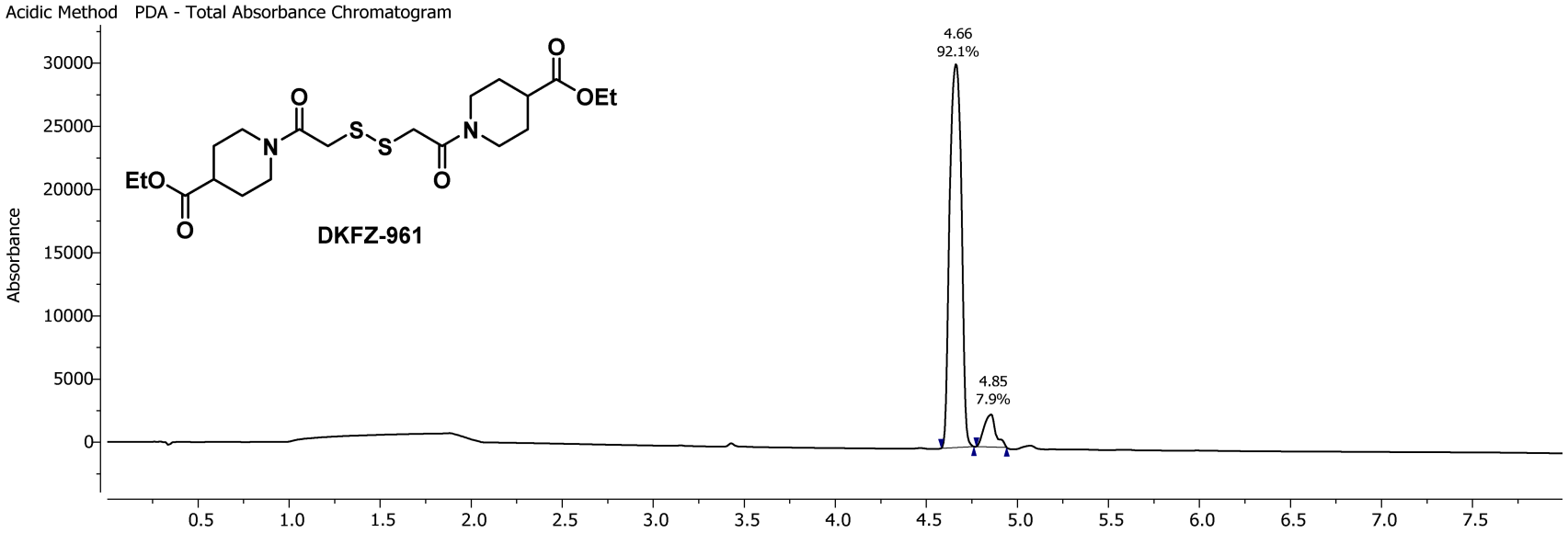
Acidic Method PDA - Total Absorbance Chromatogram
DKFZ-961
4.66
92.1%
4.85
7.9%
Absorbance
30000
25000
20000
15000
10000
5000
0
0.5
1.0
1.5
2.0
2.5
3.0
3.5
4.0
4.5
5.0
5.5
6.0
6.5
7.0
7.5

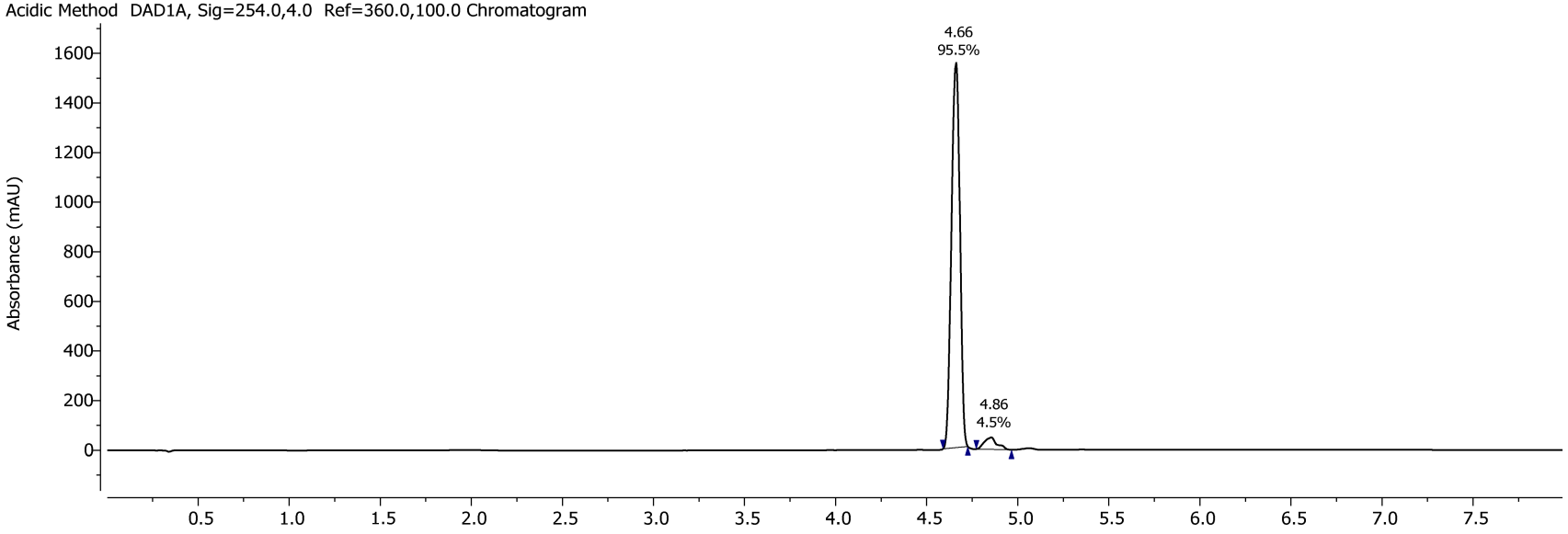
Acidic Method DAD1A, Sig=254.0,4.0 Ref=360.0,100.0 Chromatogram
4.66
95.5%
4.86
4.5%
Absorbance (mAU)
1600
1400
1200
1000
800
600
400
200
0
0.5
1.0
1.5
2.0
2.5
3.0
3.5
4.0
4.5
5.0
5.5
6.0
6.5
7.0
7.5

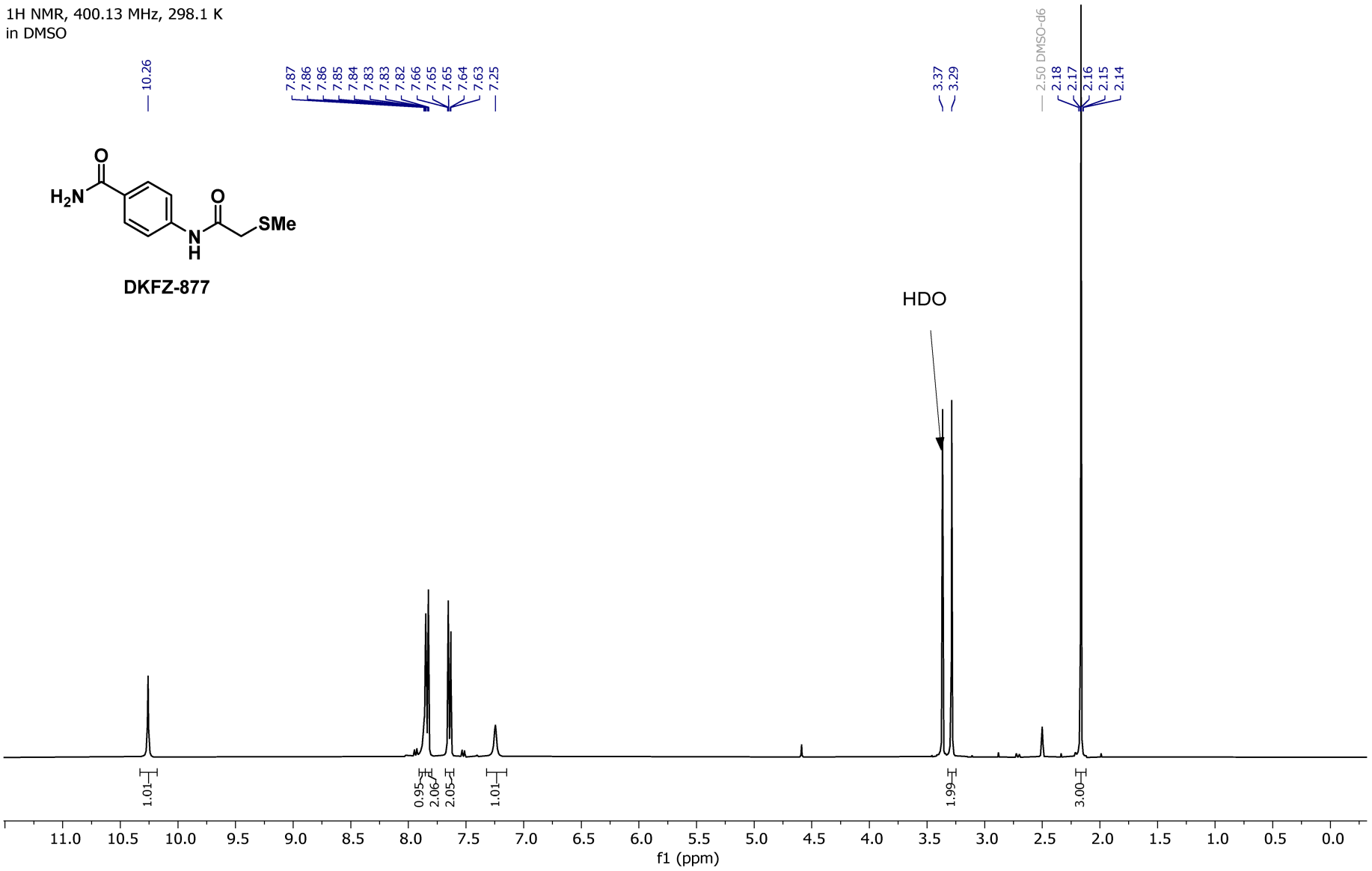
1H NMR, 400.13 MHz, 298.1 K
in DMSO
10.26
7.87
7.86
7.86
7.85
7.84
7.83
7.83
7.82
7.66
7.65
7.65
7.64
7.63
7.25
3.37
3.29
2.50 DMSO-d6
2.18
2.17
2.16
2.15
2.14
H2N
O
O
N
H
SMe
DKFZ-877
HDO
1.01
0.95
2.06
2.05
1.01
1.99
3.00
11.0
10.5
10.0
9.5
9.0
8.5
8.0
7.5
7.0
6.5
6.0
5.5
5.0
4.5
4.0
3.5
3.0
2.5
2.0
1.5
1.0
0.5
0.0
f1 (ppm)

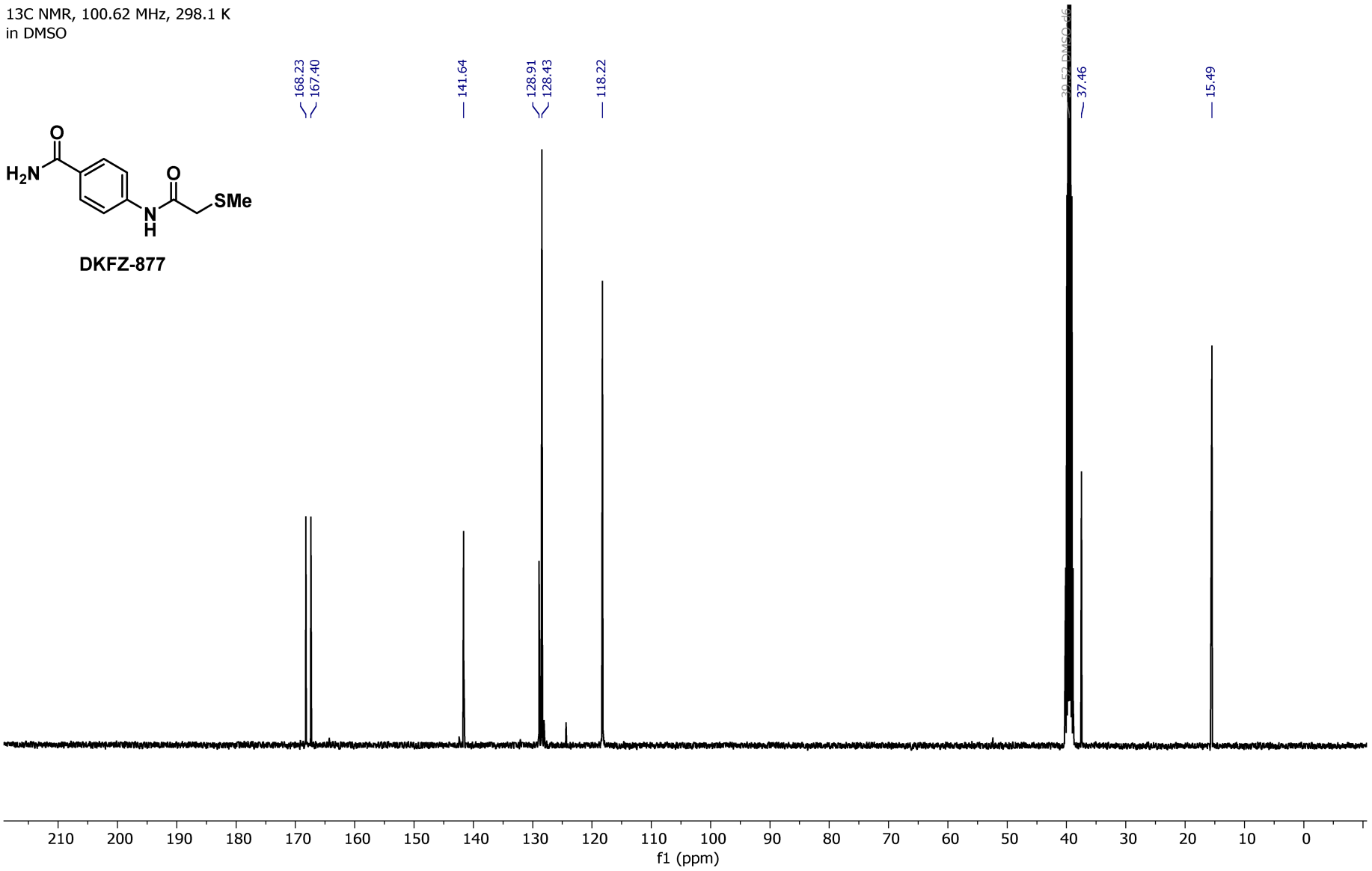
13C NMR, 100.62 MHz, 298.1 K
in DMSO
168.23
167.40
141.64
128.91
128.43
118.22
39.52 DMSO-d6
37.46
15.49
O
H2N
O
N
H
SMe
DKFZ-877
210
200
190
180
170
160
150
140
130
120
110
100
90
80
70
60
50
40
30
20
10
0
f1 (ppm)

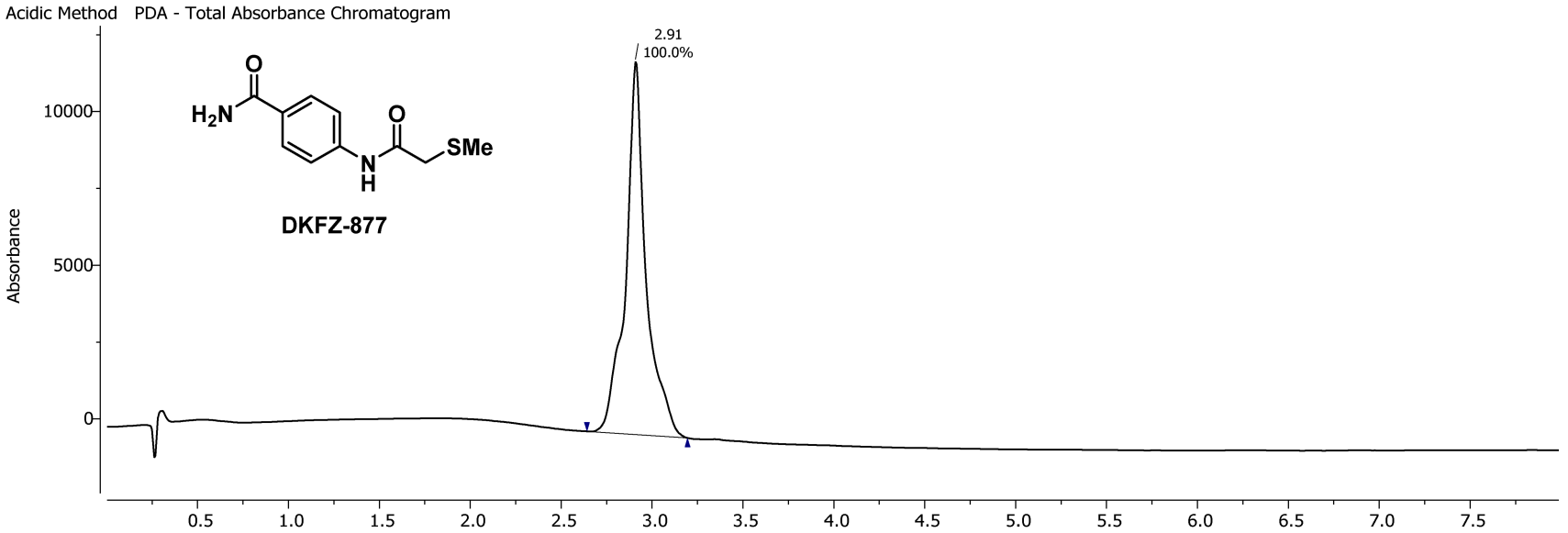
Acidic Method PDA - Total Absorbance Chromatogram
2.91
100.0%
10000
5000
0
Absorbance
DKFZ-877
0.5
1.0
1.5
2.0
2.5
3.0
3.5
4.0
4.5
5.0
5.5
6.0
6.5
7.0
7.5

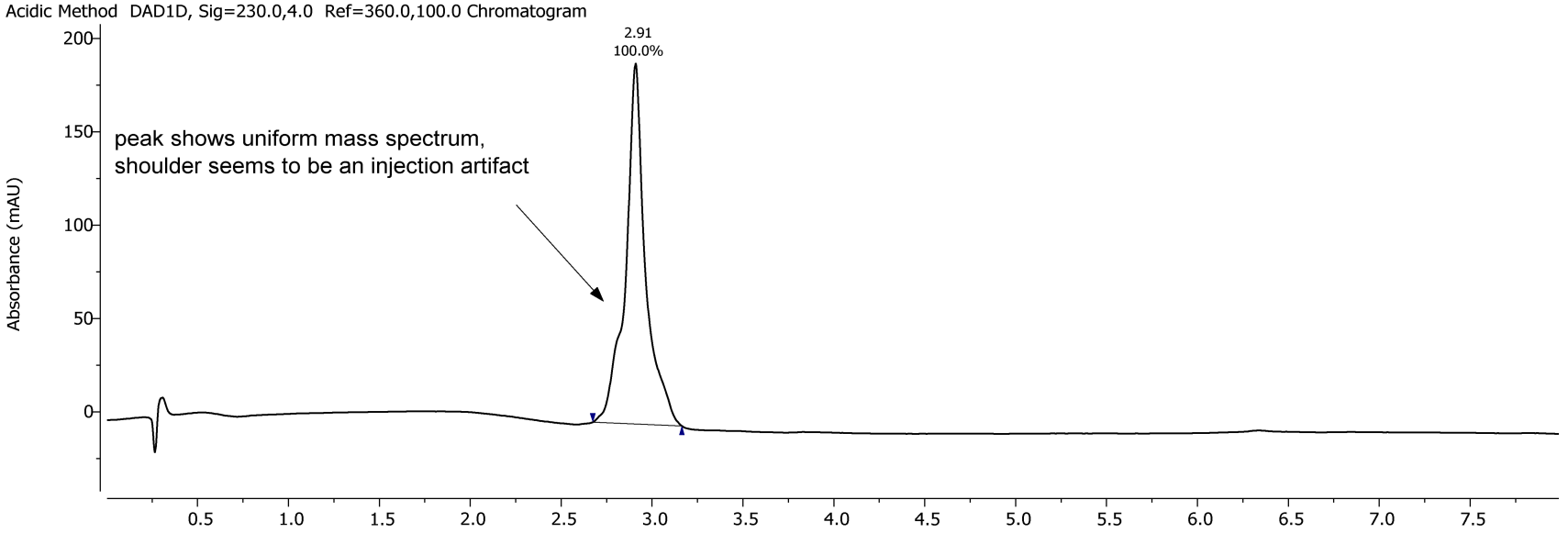
Acidic Method DAD1D, Sig=230.0,4.0 Ref=360.0,100.0 Chromatogram
2.91
100.0%
peak shows uniform mass spectrum,
shoulder seems to be an injection artifact
200
150
100
50
0
Absorbance (mAU)
0.5
1.0
1.5
2.0
2.5
3.0
3.5
4.0
4.5
5.0
5.5
6.0
6.5
7.0
7.5

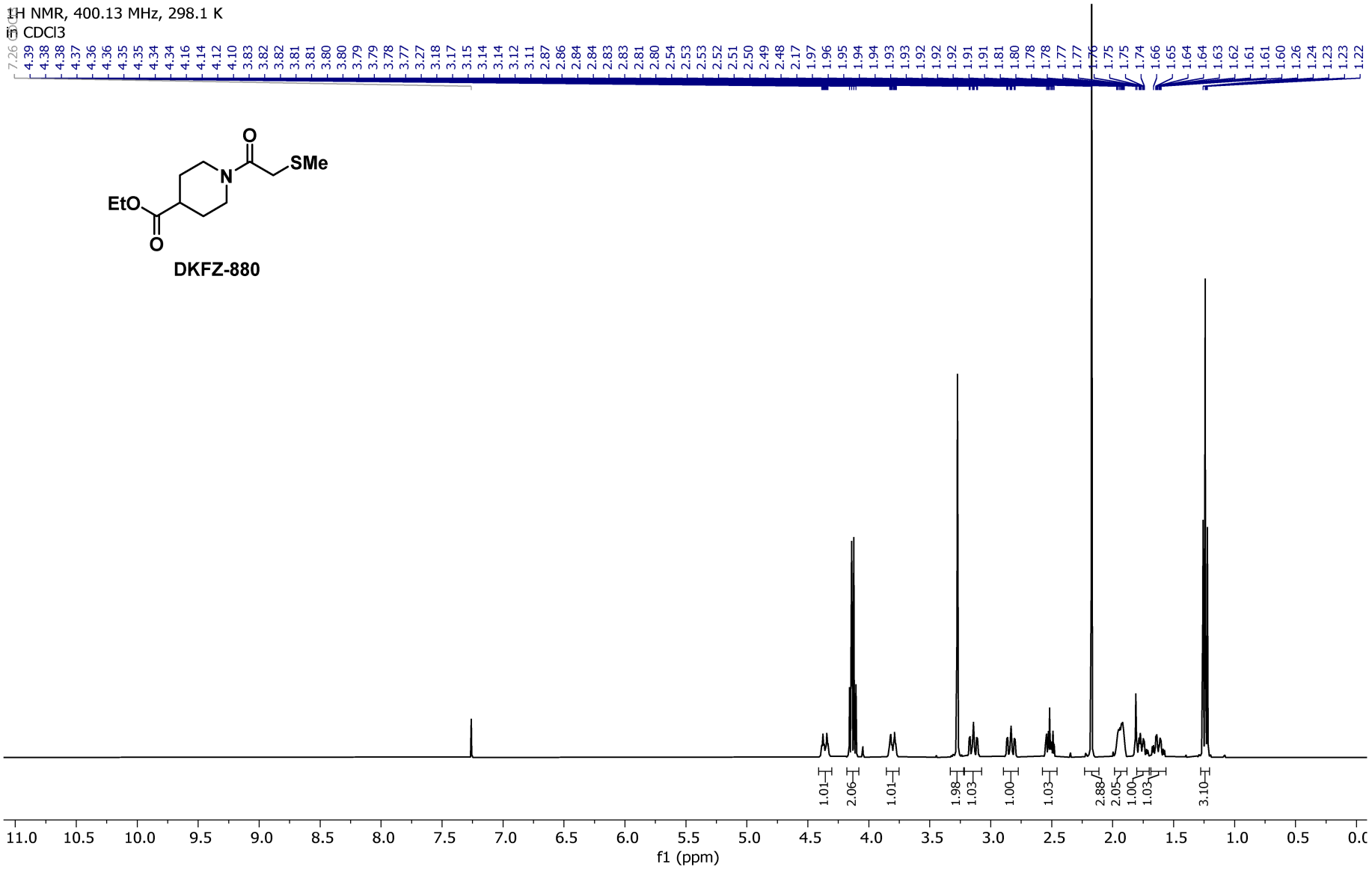
1H NMR, 400.13 MHz, 298.1 K
in CDCl3
DKFZ-880
f1 (ppm)

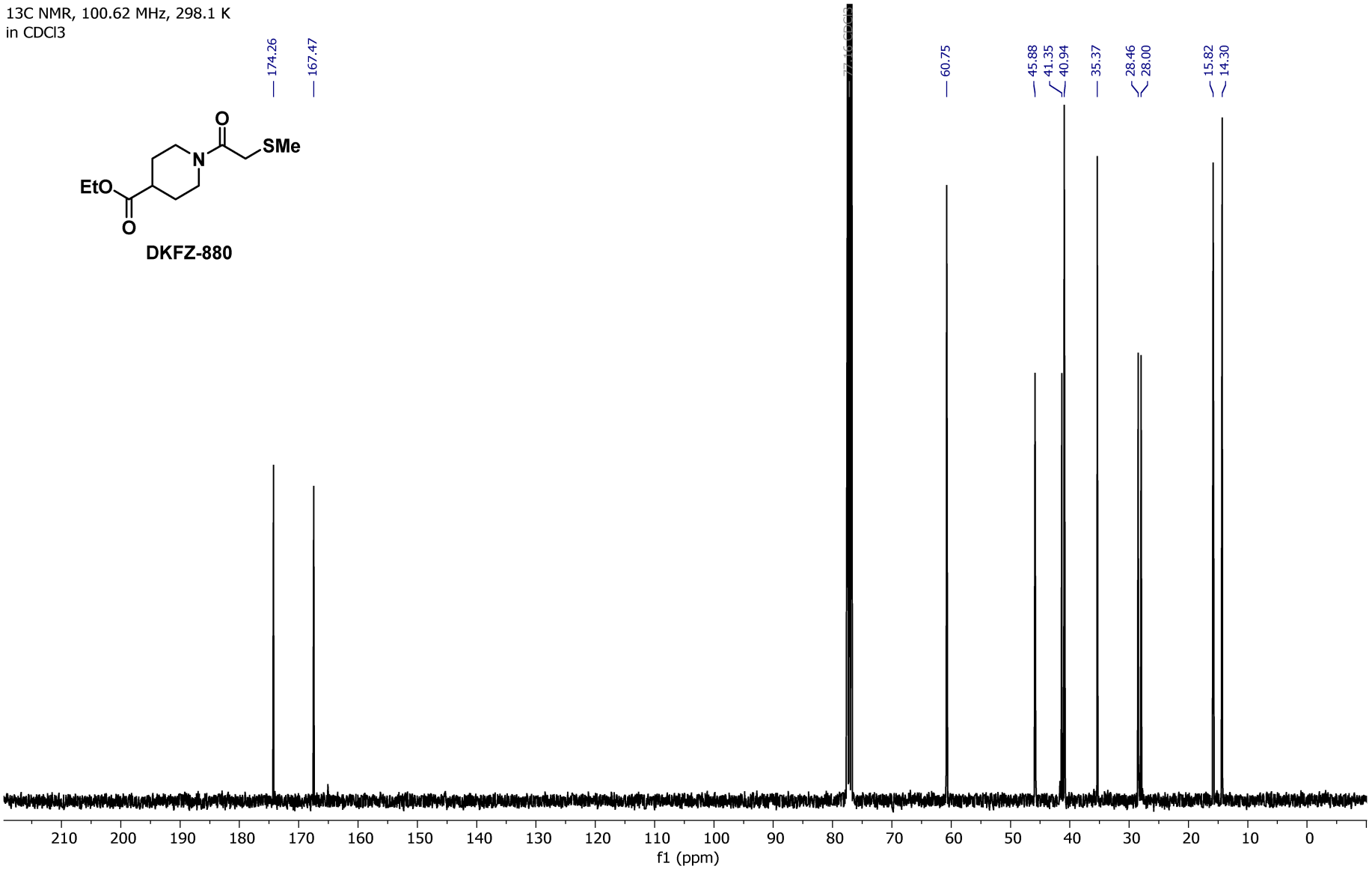
13C NMR, 100.62 MHz, 298.1 K
in CDCl3
174.26
167.47
77.16 CDCl3
60.75
45.88
41.35
40.94
35.37
28.46
28.00
15.82
14.30
O
N
SMe
EtO
O
DKFZ-880
210 200 190 180 170 160 150 140 130 120 110 100 90 80 70 60 50 40 30 20 10 0
f1 (ppm)

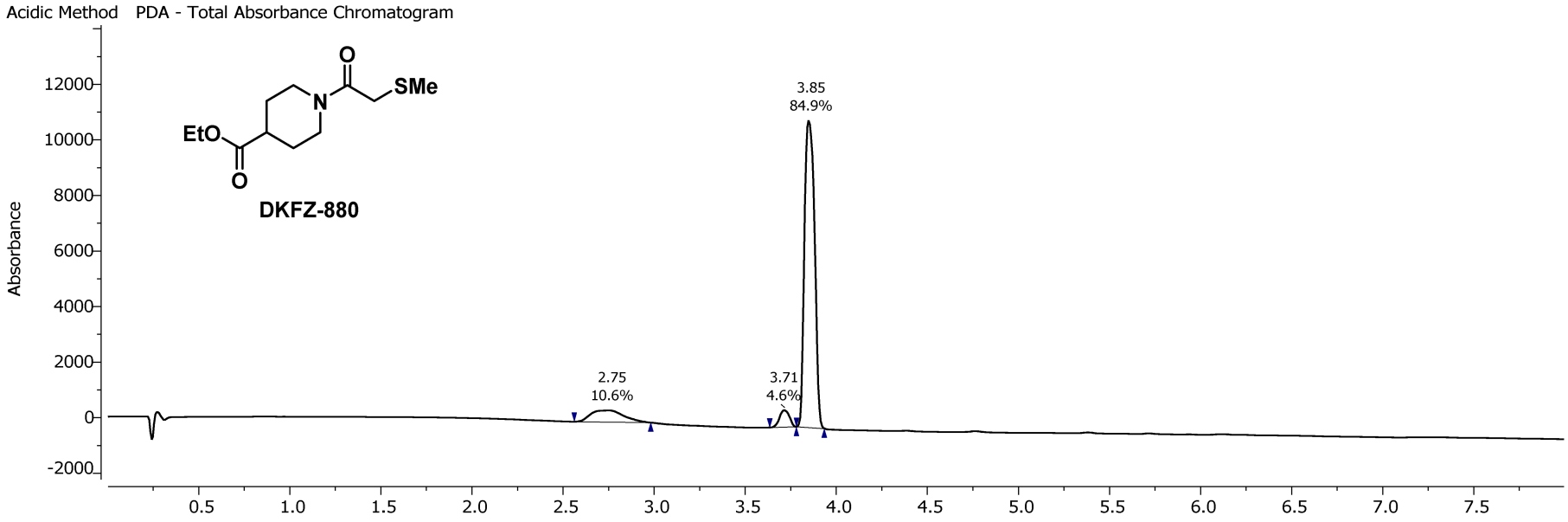
Acidic Method PDA - Total Absorbance Chromatogram
Absorbance
12000
10000
8000
6000
4000
2000
0
-2000
O
N
SMe
EtO
O
DKFZ-880
2.75
10.6%
3.71
4.6%
3.85
84.9%
0.5
1.0
1.5
2.0
2.5
3.0
3.5
4.0
4.5
5.0
5.5
6.0
6.5
7.0
7.5

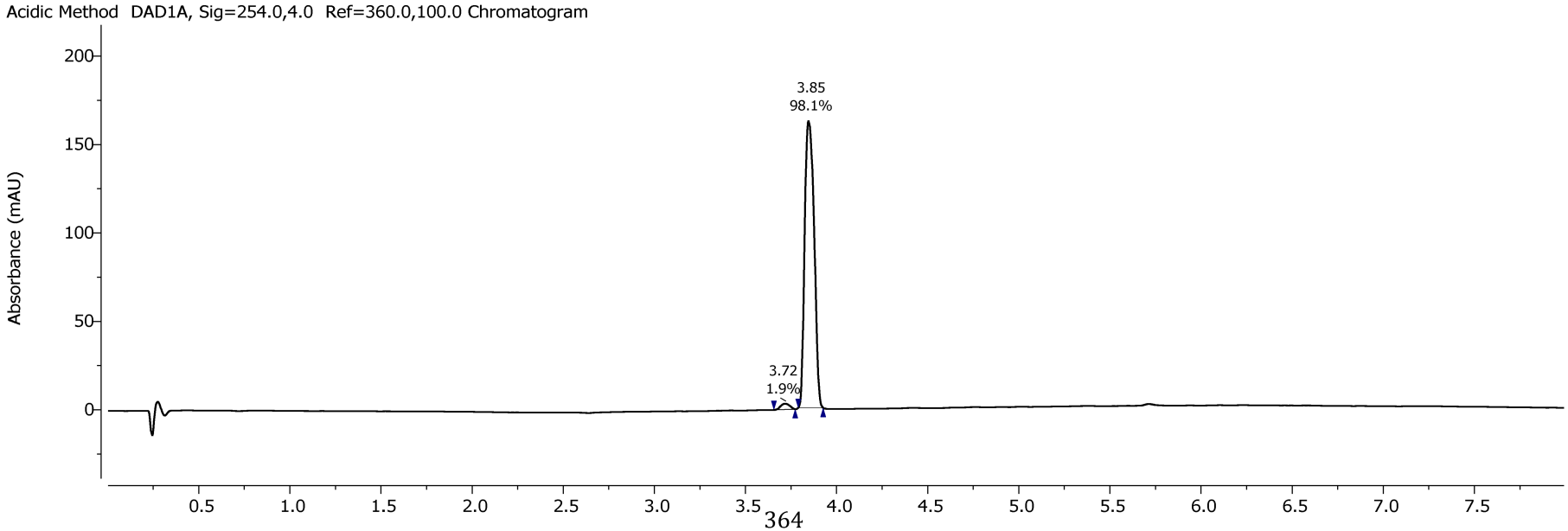
Acidic Method DAD1A, Sig=254.0,4.0 Ref=360.0,100.0 Chromatogram
Absorbance (mAU)
200
150
100
50
0
3.85
98.1%
3.72
1.9%
0.5
1.0
1.5
2.0
2.5
3.0
3.5
4.0
4.5
5.0
5.5
6.0
6.5
7.0
7.5

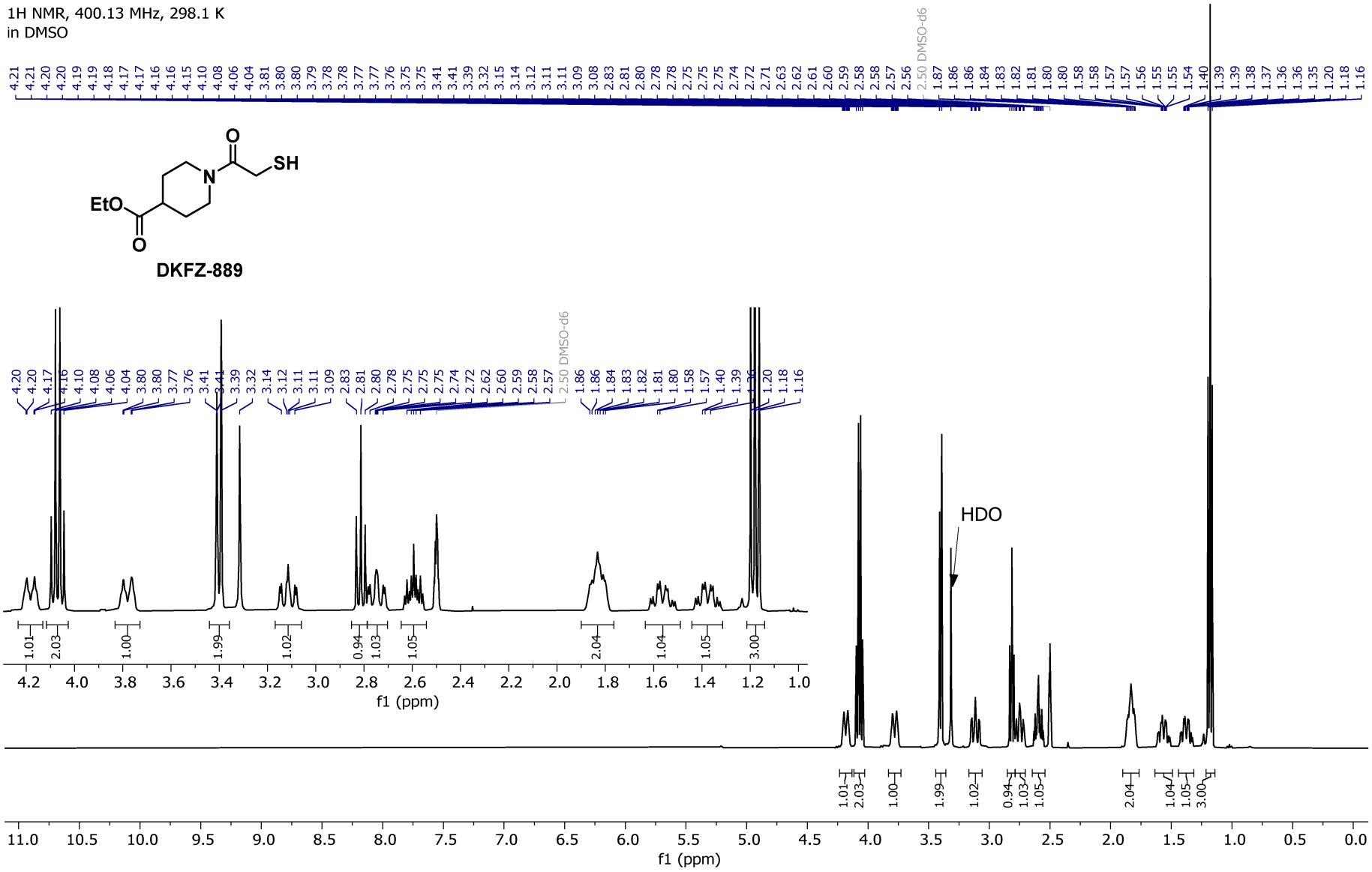
1H NMR, 400.13 MHz, 298.1 K
in DMSO
2.50 DMSO-d6
O
SH
N
EtO
O
DKFZ-889
HDO
f1 (ppm)

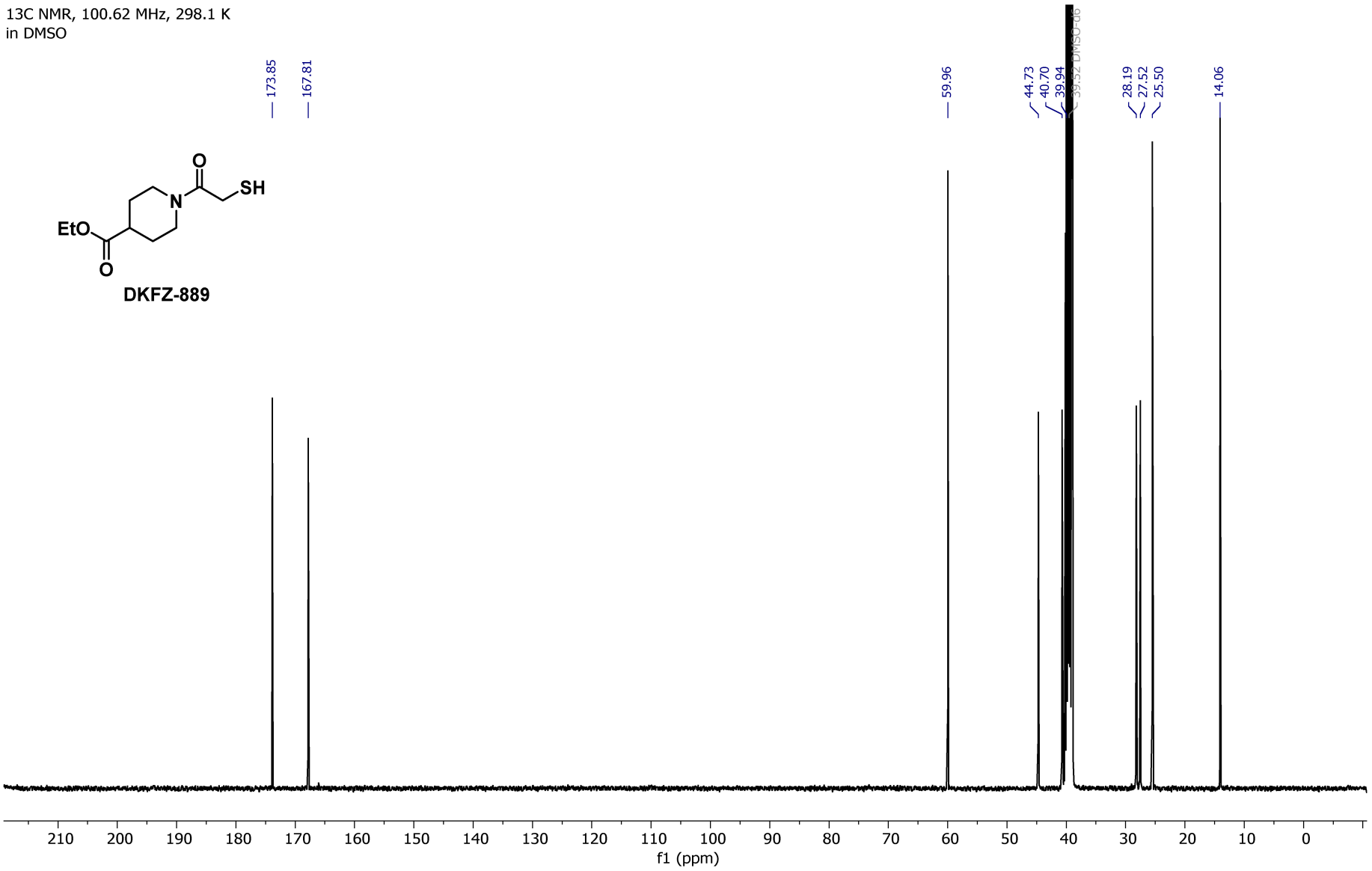
13C NMR, 100.62 MHz, 298.1 K
in DMSO
173.85
167.81
59.96
44.73
40.70
39.94
39.52 DMSO-d6
28.19
27.52
25.50
14.06
O
SH
N
EtO
O
DKFZ-889
210 200 190 180 170 160 150 140 130 120 110 100 90 80 70 60 50 40 30 20 10 0
f1 (ppm)

1H NMR, 400.13 MHz, 298.1 K
in DMSO

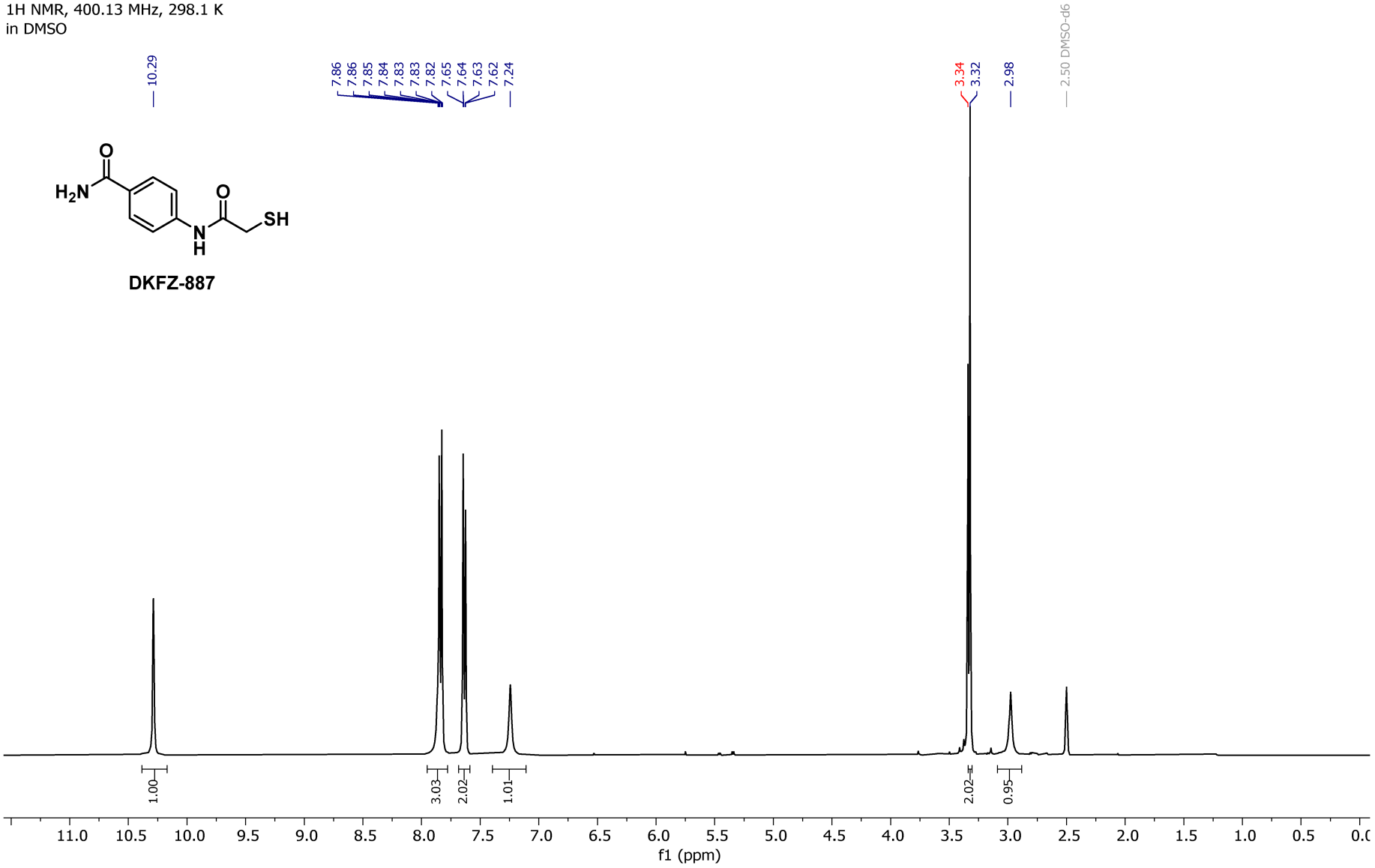

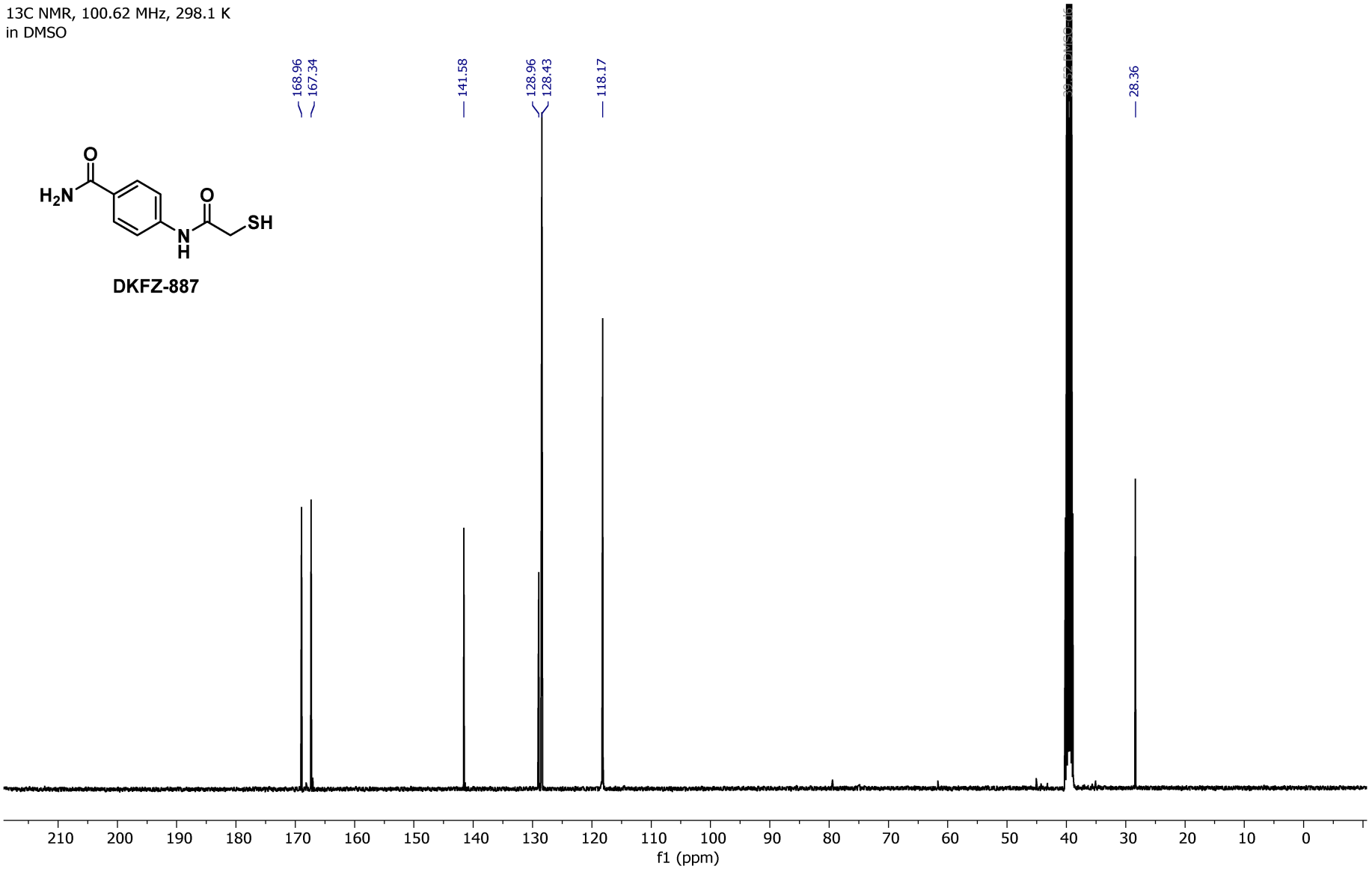
13C NMR, 100.62 MHz, 298.1 K
in DMSO
168.96
167.34
141.58
128.96
128.43
118.17
39.52
28.36
DKFZ-887
210
200
190
180
170
160
150
140
130
120
110
100
90
80
70
60
50
40
30
20
10
0
f1 (ppm)

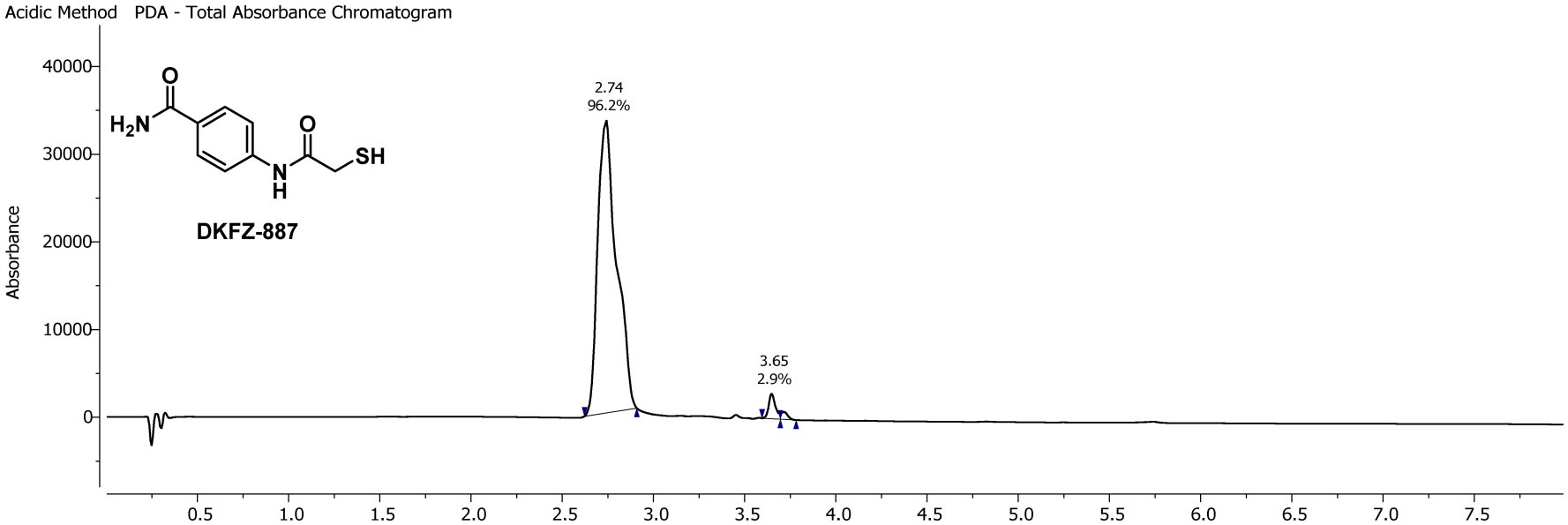
Acidic Method PDA - Total Absorbance Chromatogram
Absorbance
40000
30000
20000
10000
0
2.74
96.2%
3.65
2.9%
DKFZ-887
0.5
1.0
1.5
2.0
2.5
3.0
3.5
4.0
4.5
5.0
5.5
6.0
6.5
7.0
7.5

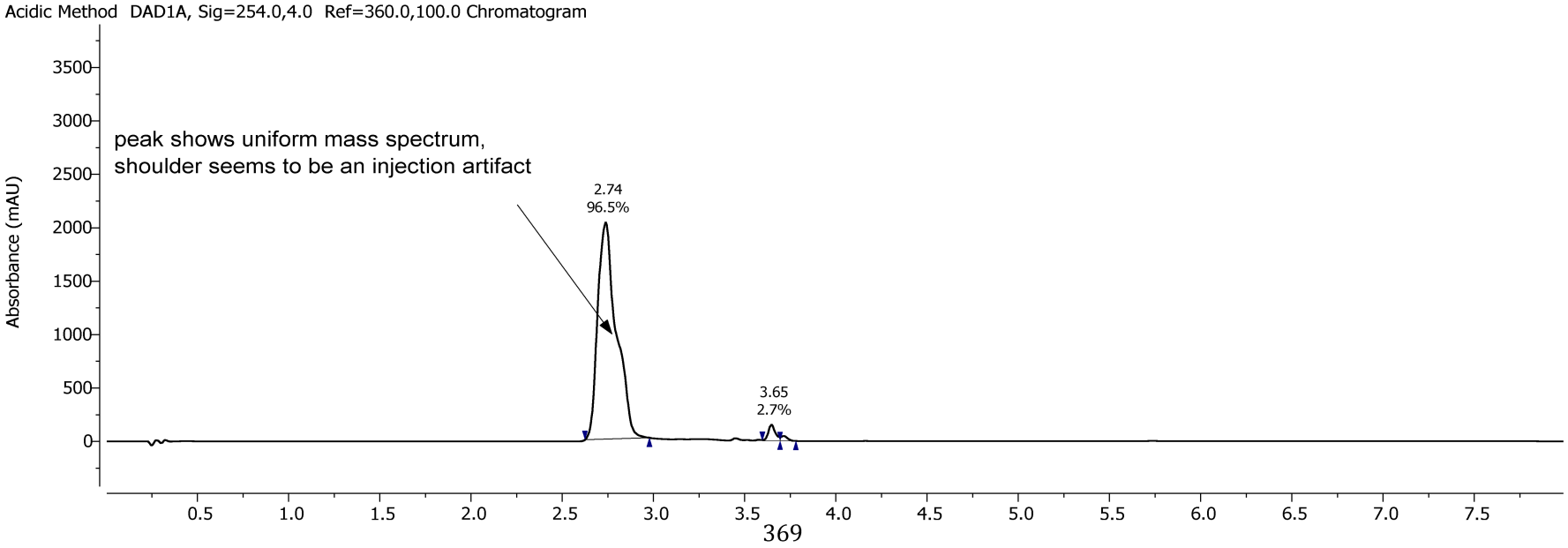
Acidic Method DAD1A, Sig=254.0,4.0 Ref=360.0,100.0 Chromatogram
Absorbance (mAU)
3500
3000
2500
2000
1500
1000
500
0
peak shows uniform mass spectrum,
shoulder seems to be an injection artifact
2.74
96.5%
3.65
2.7%
0.5
1.0
1.5
2.0
2.5
3.0
3.5
4.0
4.5
5.0
5.5
6.0
6.5
7.0
7.5

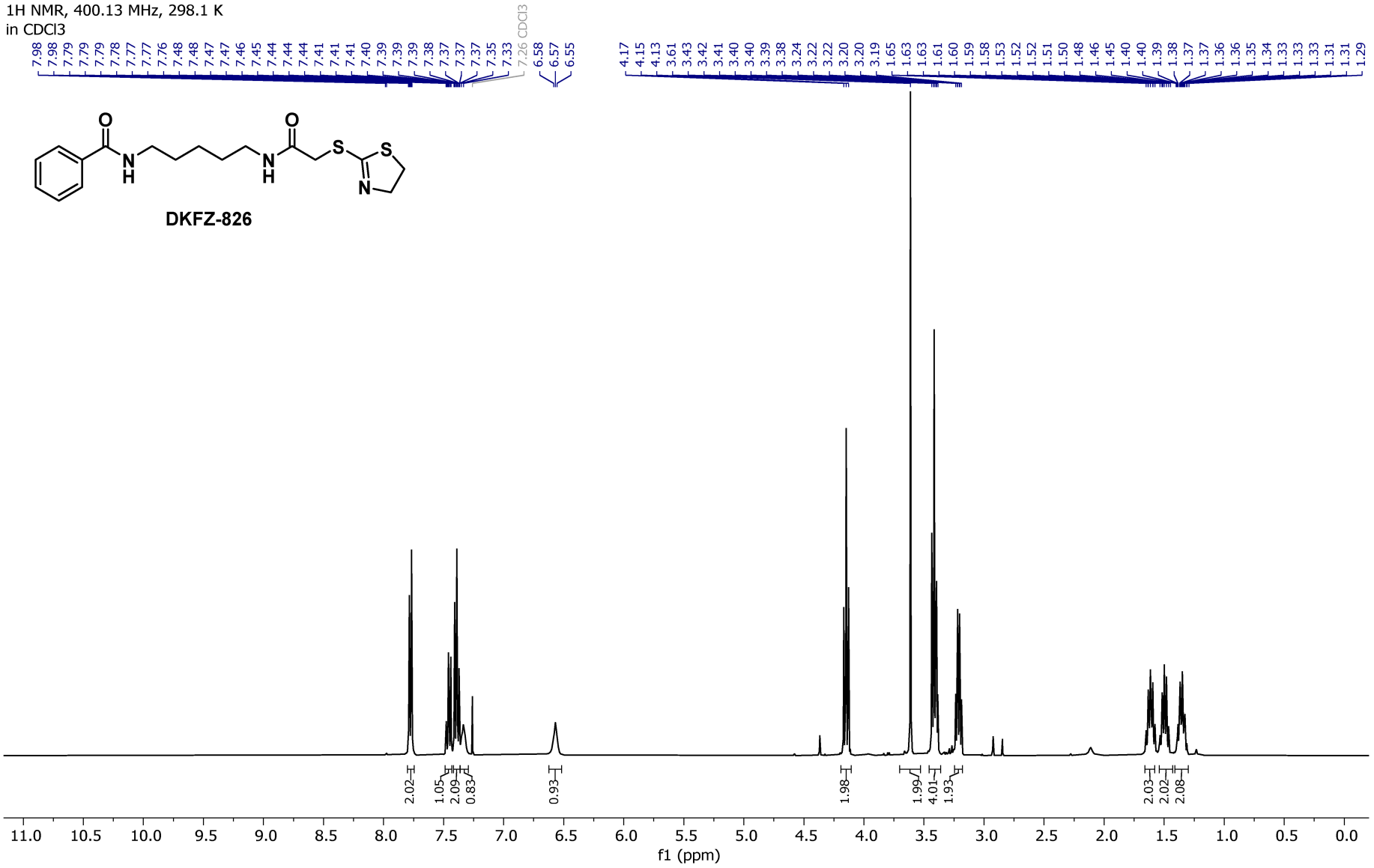
1H NMR, 400.13 MHz, 298.1 K
in CDCl3
DKFZ-826
f1 (ppm)

13C NMR, 100.62 MHz, 298.1 K
in CDCl3

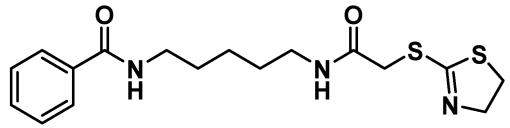

DKFZ-826

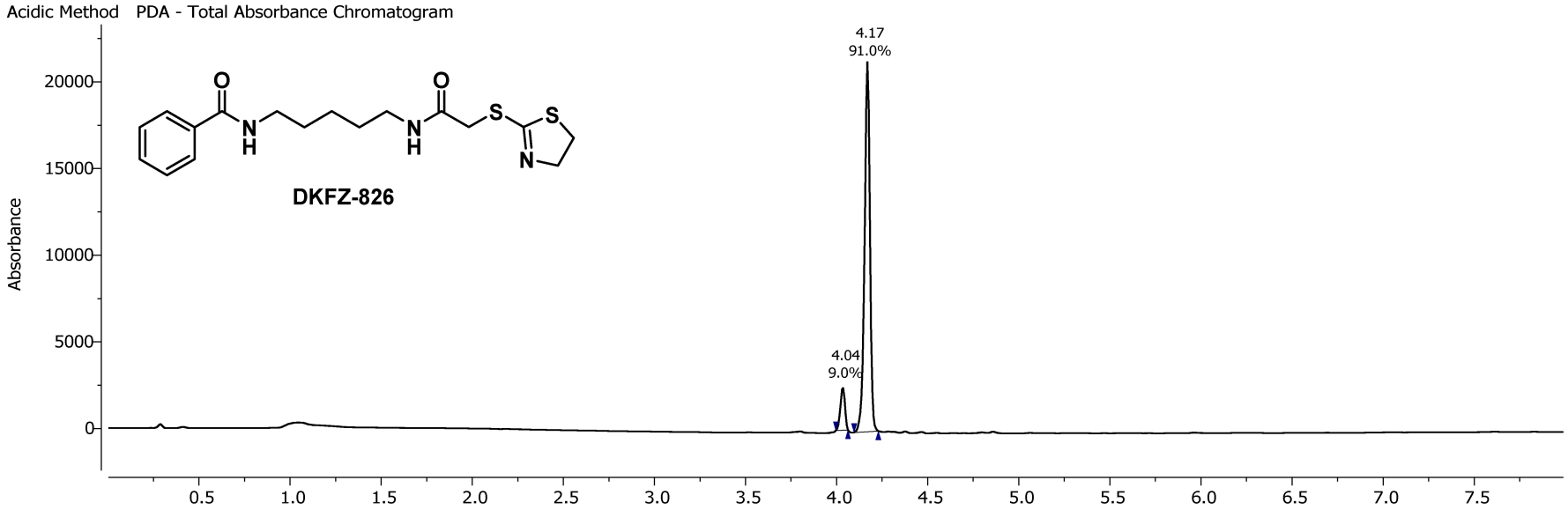
Acidic Method PDA - Total Absorbance Chromatogram
DKFZ-826
4.17
91.0%
4.04
9.0%
Absorbance
20000
15000
10000
5000
0
0.5
1.0
1.5
2.0
2.5
3.0
3.5
4.0
4.5
5.0
5.5
6.0
6.5
7.0
7.5

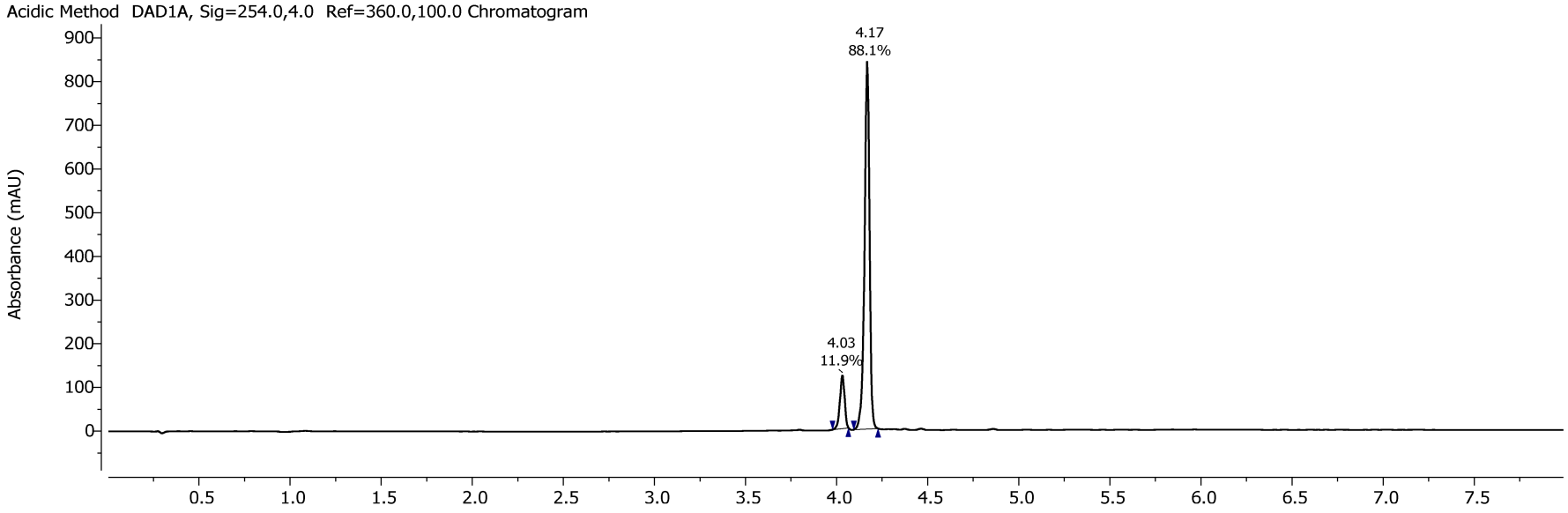
Acidic Method DAD1A, Sig=254.0,4.0 Ref=360.0,100.0 Chromatogram
4.17
88.1%
4.03
11.9%
Absorbance (mAU)
900
800
700
600
500
400
300
200
100
0
0.5
1.0
1.5
2.0
2.5
3.0
3.5
4.0
4.5
5.0
5.5
6.0
6.5
7.0
7.5

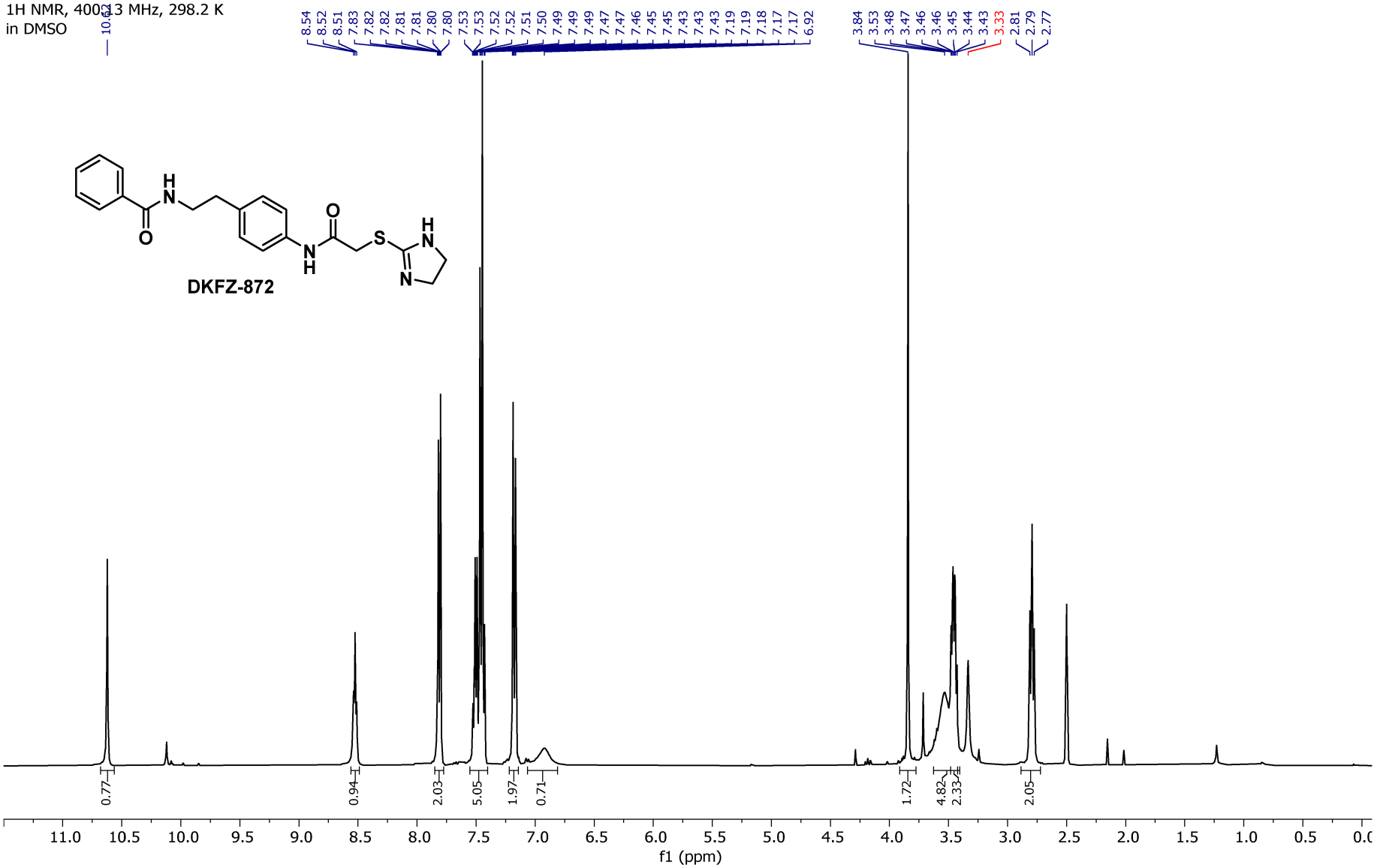
1H NMR, 400.13 MHz, 298.2 K
in DMSO
10.61
8.54
8.52
8.51
7.83
7.82
7.82
7.81
7.81
7.80
7.80
7.53
7.53
7.52
7.52
7.51
7.50
7.49
7.49
7.49
7.47
7.47
7.46
7.45
7.45
7.43
7.43
7.43
7.19
7.19
7.18
7.17
7.17
6.92
3.84
3.53
3.48
3.47
3.46
3.46
3.45
3.44
3.43
3.33
2.81
2.79
2.77
DKFZ-872
0.77
0.94
2.03
5.05
1.97
0.71
1.72
4.82
2.33
2.05
11.0
10.5
10.0
9.5
9.0
8.5
8.0
7.5
7.0
6.5
6.0
5.5
5.0
4.5
4.0
3.5
3.0
2.5
2.0
1.5
1.0
0.5
0.0
f1 (ppm)

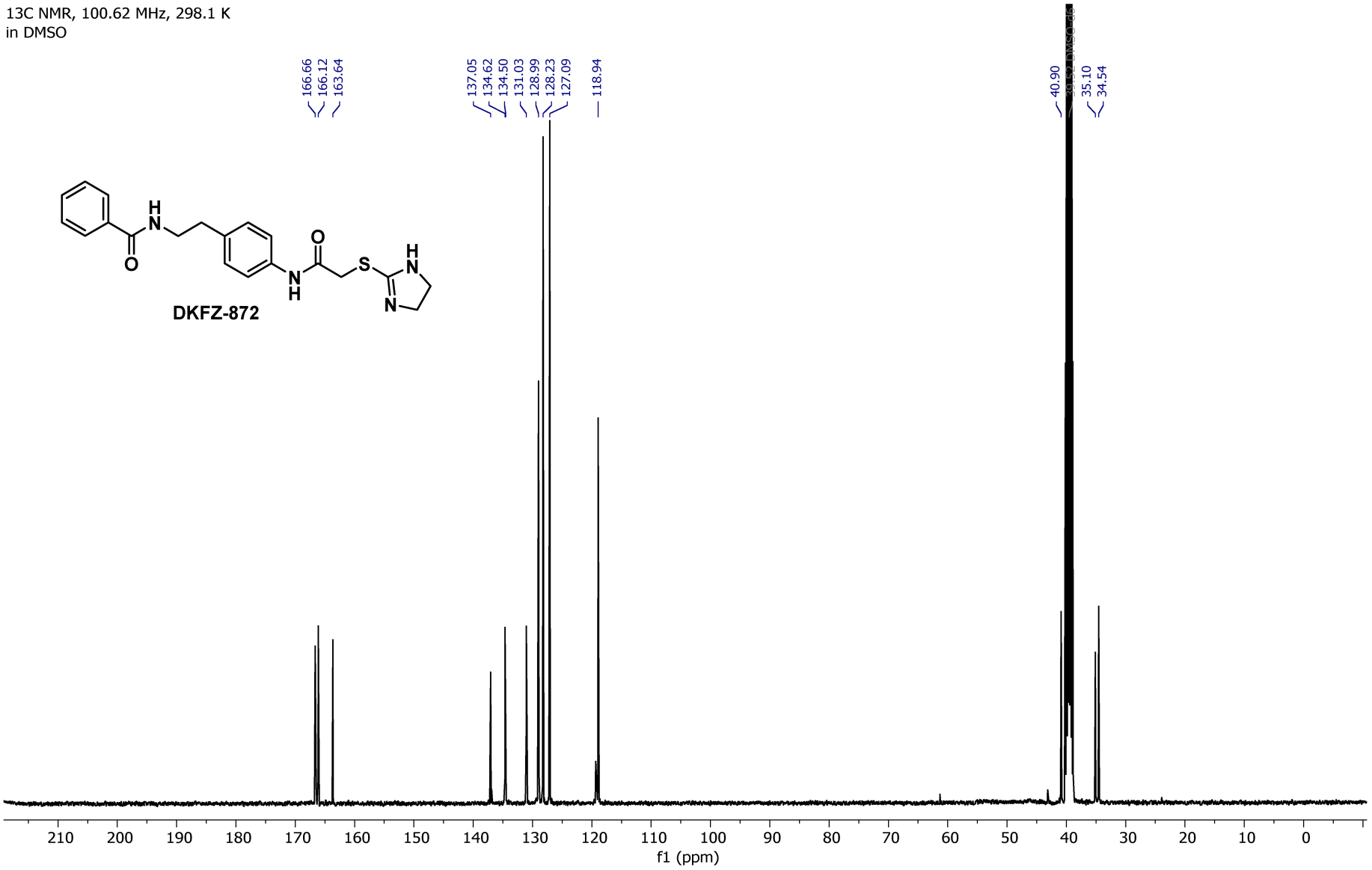
13C NMR, 100.62 MHz, 298.1 K
in DMSO
166.66
166.12
163.64
137.05
134.62
134.50
131.03
128.99
128.23
127.09
118.94
40.90
39.57 DMSO-d6
35.10
34.54
DKFZ-872
210
200
190
180
170
160
150
140
130
120
110
100
90
80
70
60
50
40
30
20
10
0
f1 (ppm)

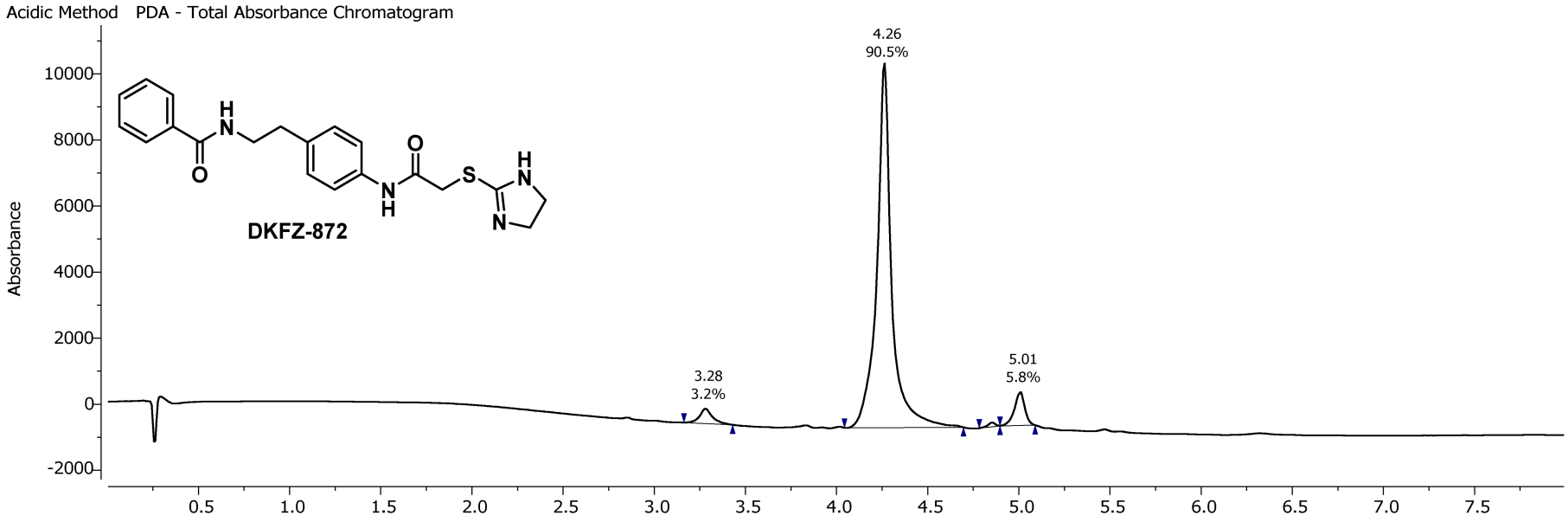
Acidic Method PDA - Total Absorbance Chromatogram
Absorbance
10000
8000
6000
4000
2000
0
-2000
DKFZ-872
4.26
90.5%
3.28
3.2%
5.01
5.8%
0.5
1.0
1.5
2.0
2.5
3.0
3.5
4.0
4.5
5.0
5.5
6.0
6.5
7.0
7.5

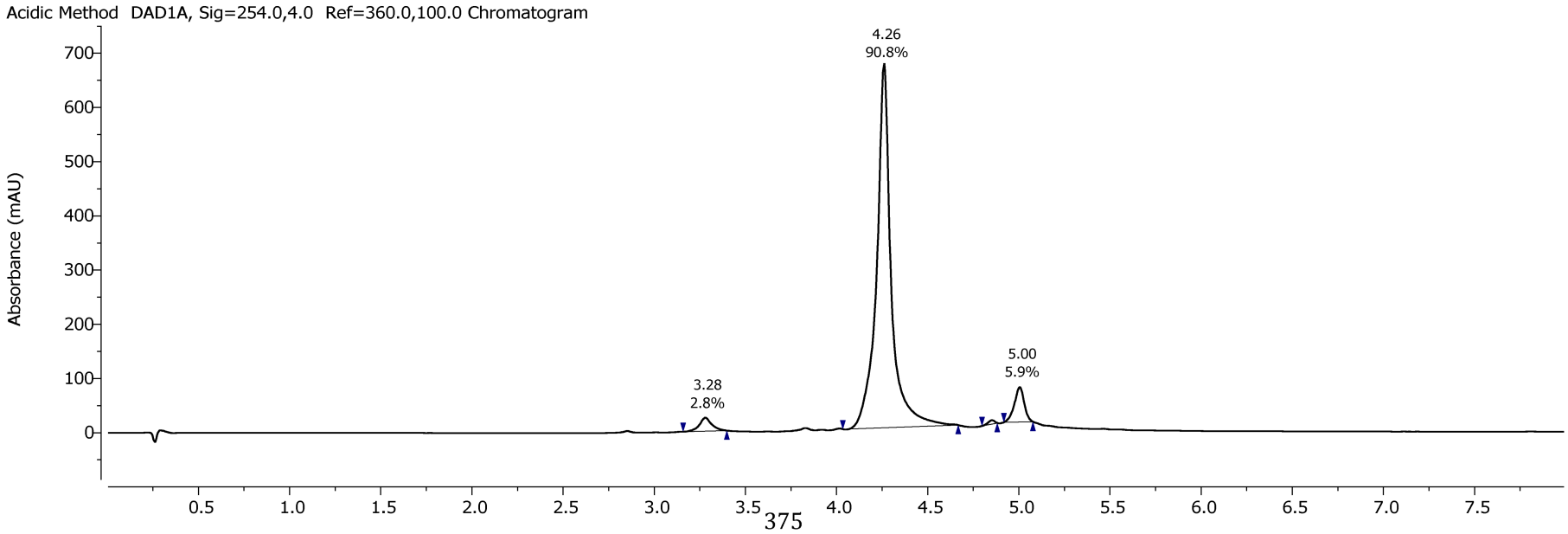
Acidic Method DAD1A, Sig=254.0,4.0 Ref=360.0,100.0 Chromatogram
Absorbance (mAU)
700
600
500
400
300
200
100
0
4.26
90.8%
3.28
2.8%
5.00
5.9%
0.5
1.0
1.5
2.0
2.5
3.0
3.5
4.0
4.5
5.0
5.5
6.0
6.5
7.0
7.5

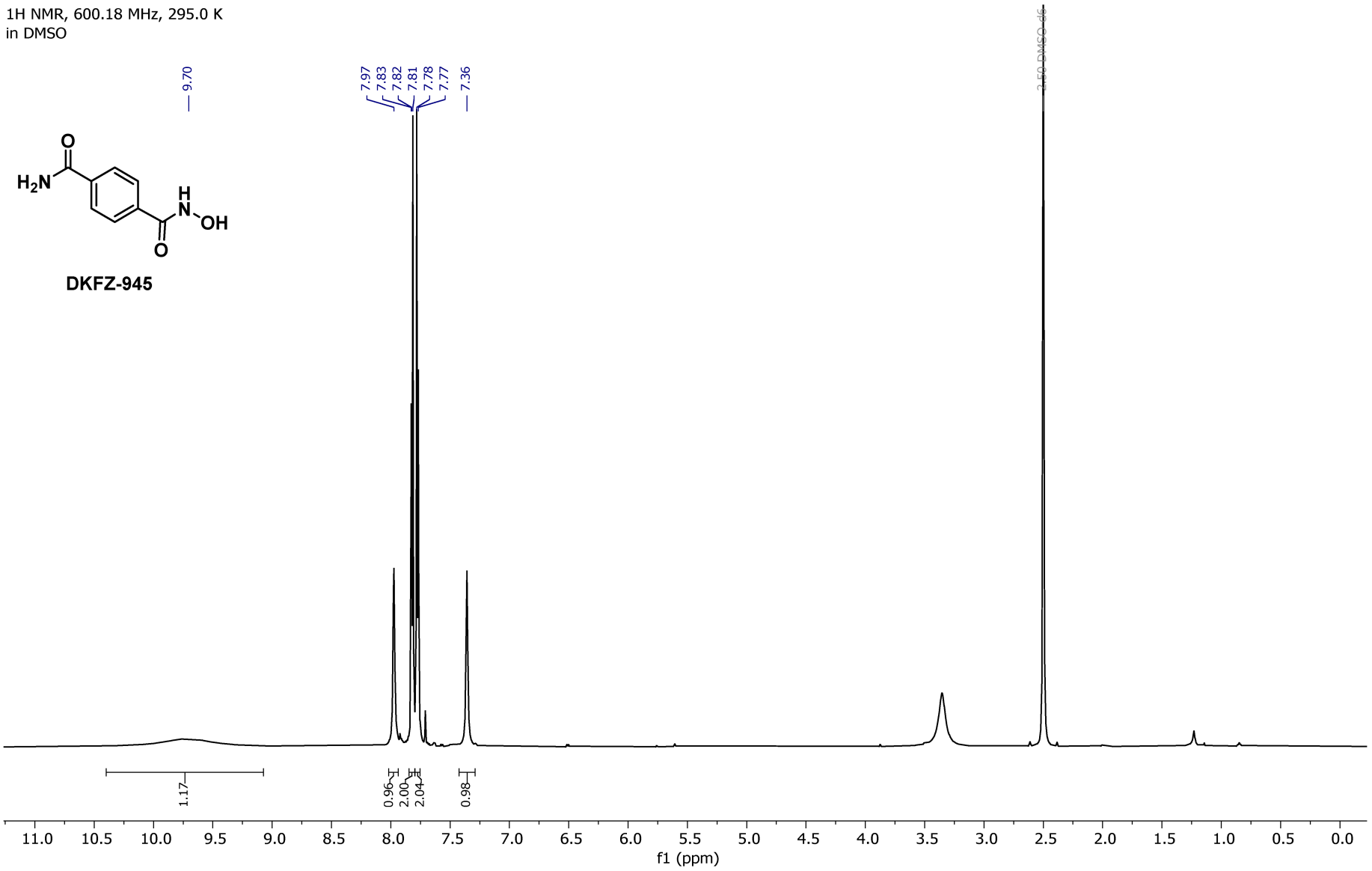
1H NMR, 600.18 MHz, 295.0 K
in DMSO
9.70
7.97
7.83
7.82
7.81
7.78
7.77
7.36
3.50 DMSO-d6
DKFZ-945
1.17
0.96
2.00
2.04
0.98
11.0 10.5 10.0 9.5 9.0 8.5 8.0 7.5 7.0 6.5 6.0 5.5 5.0 4.5 4.0 3.5 3.0 2.5 2.0 1.5 1.0 0.5 0.0
f1 (ppm)

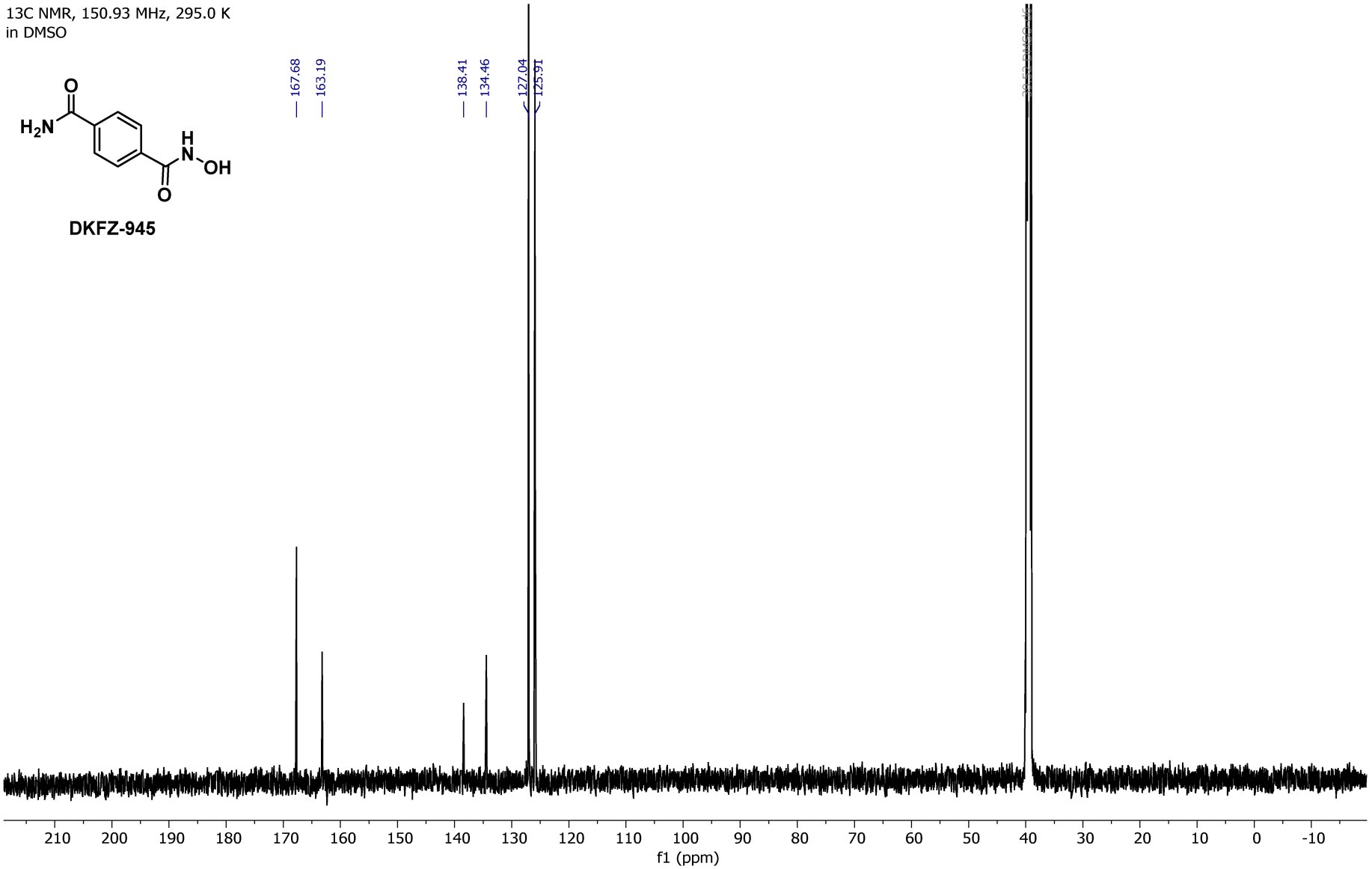
13C NMR, 150.93 MHz, 295.0 K
in DMSO
DKFZ-945
167.68
163.19
138.41
134.46
127.04
125.91
f1 (ppm)

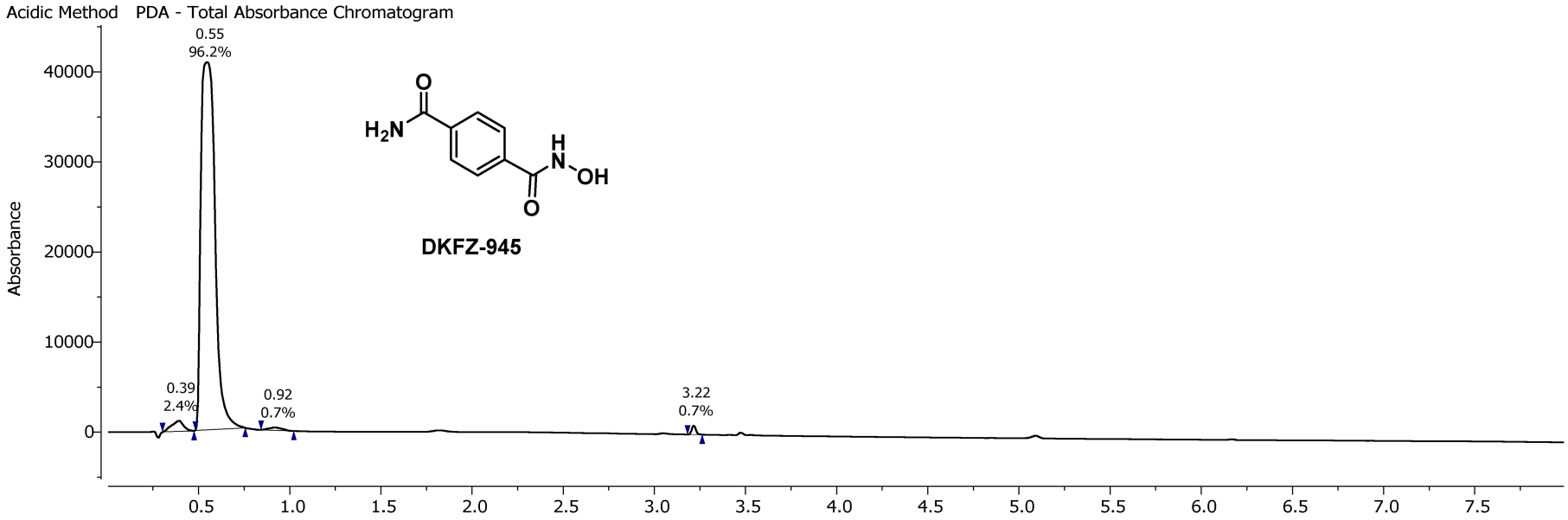
Acidic Method PDA - Total Absorbance Chromatogram
0.55
96.2%
0.39
2.4%
0.92
0.7%
3.22
0.7%
Absorbance
40000
30000
20000
10000
0
0.5
1.0
1.5
2.0
2.5
3.0
3.5
4.0
4.5
5.0
5.5
6.0
6.5
7.0
7.5
O
H2N
H
N
OH
O
DKFZ-945

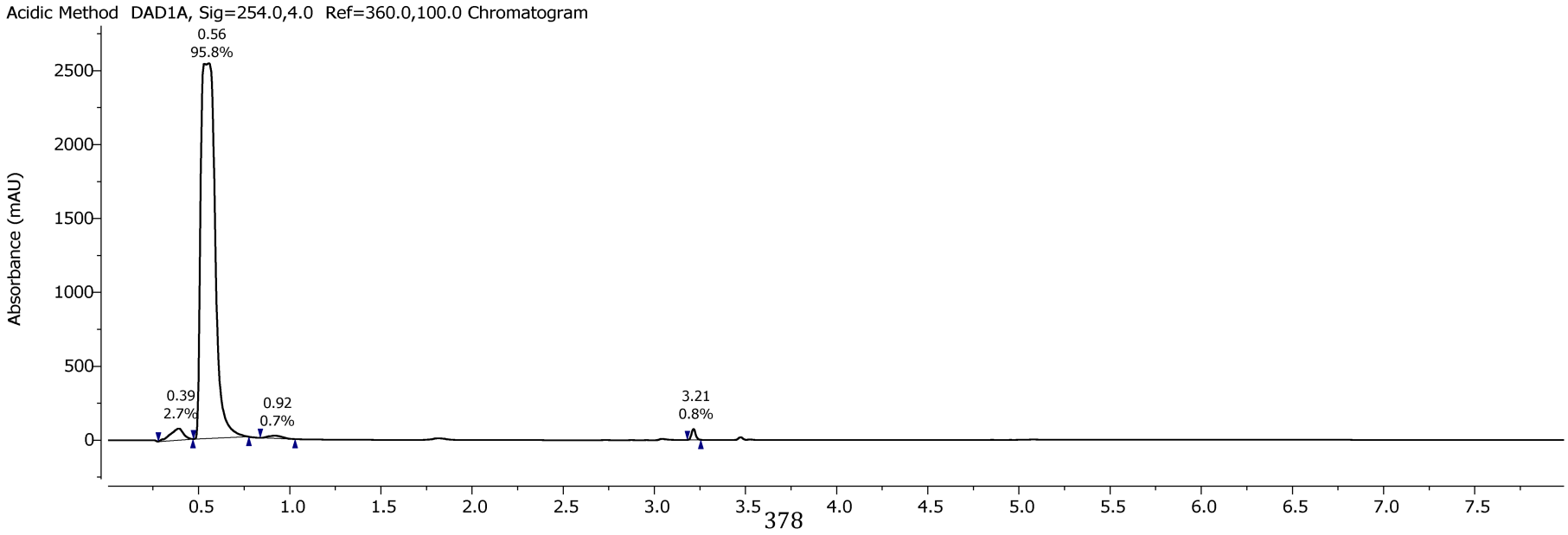
Acidic Method DAD1A, Sig=254.0,4.0 Ref=360.0,100.0 Chromatogram
0.56
95.8%
0.39
2.7%
0.92
0.7%
3.21
0.8%
Absorbance (mAU)
2500
2000
1500
1000
500
0
0.5
1.0
1.5
2.0
2.5
3.0
3.5
4.0
4.5
5.0
5.5
6.0
6.5
7.0
7.5

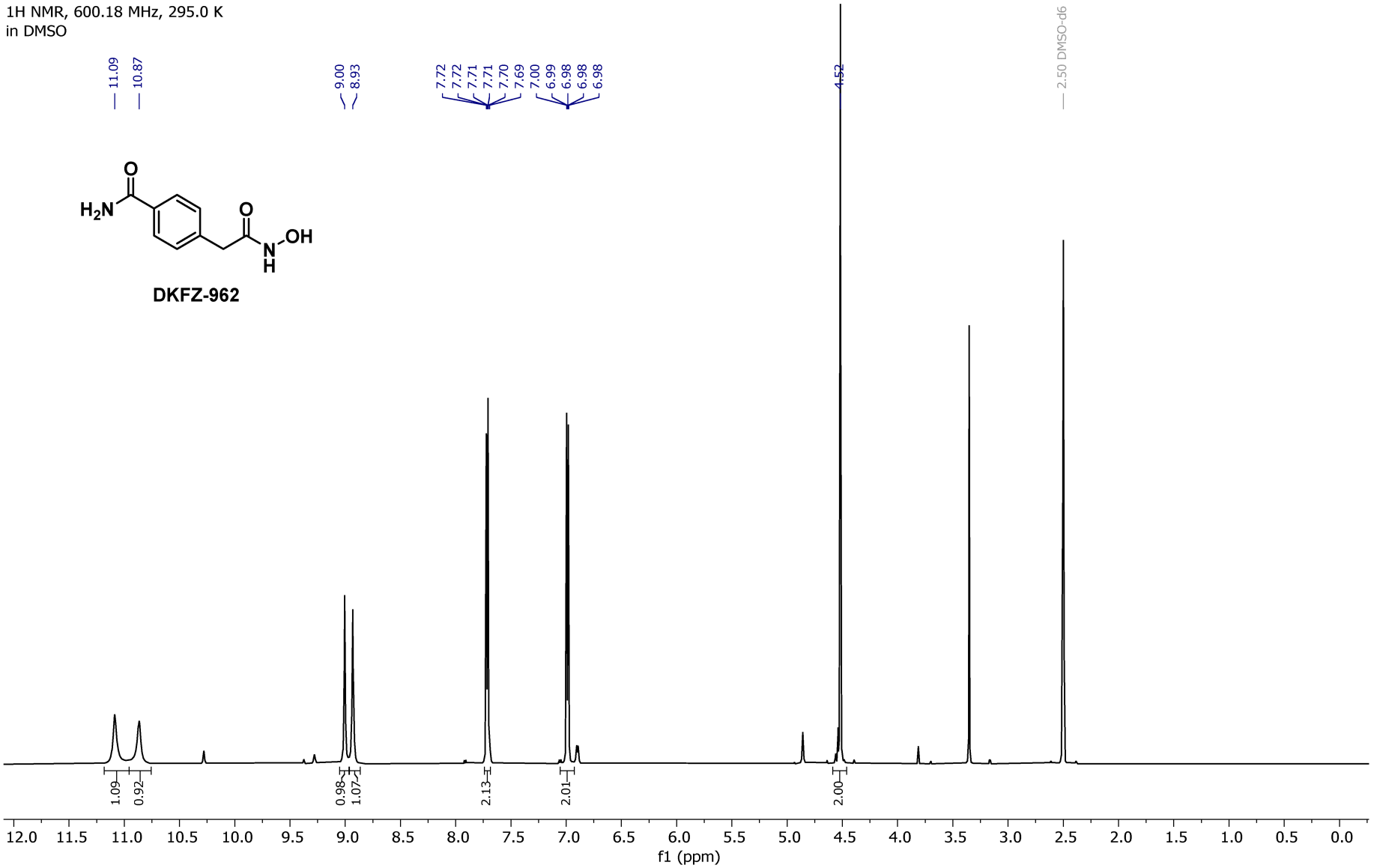
1H NMR, 600.18 MHz, 295.0 K
in DMSO
11.09
10.87
9.00
8.93
7.72
7.72
7.71
7.71
7.70
7.69
7.00
6.99
6.98
6.98
6.98
4.52
2.50 DMSO-d6
DKFZ-962
1.09
0.92
0.98
1.07
2.13
2.01
2.00
f1 (ppm)

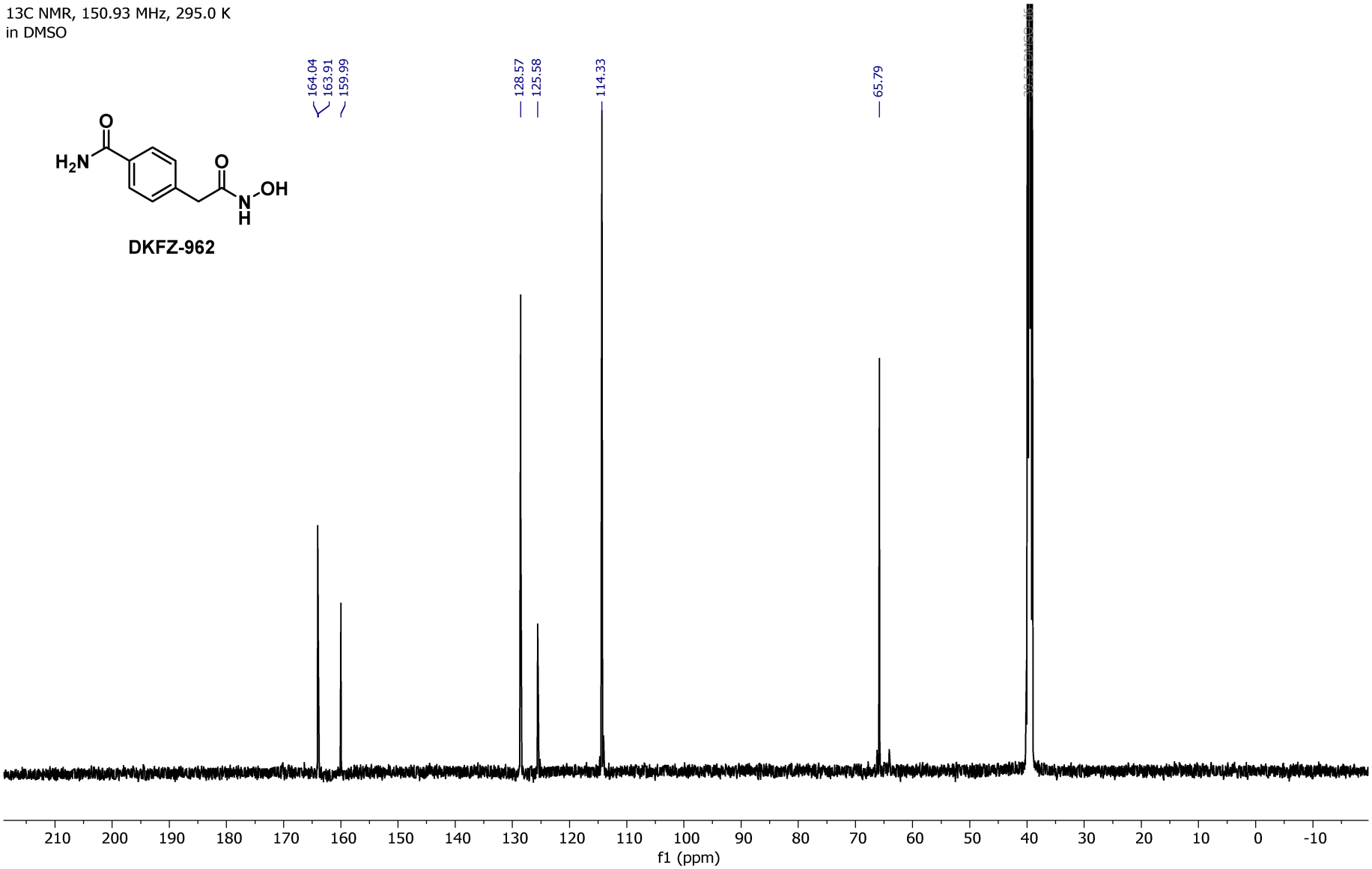
13C NMR, 150.93 MHz, 295.0 K
in DMSO
164.04
163.91
159.99
128.57
125.58
114.33
65.79
39.52
DKFZ-962
f1 (ppm)

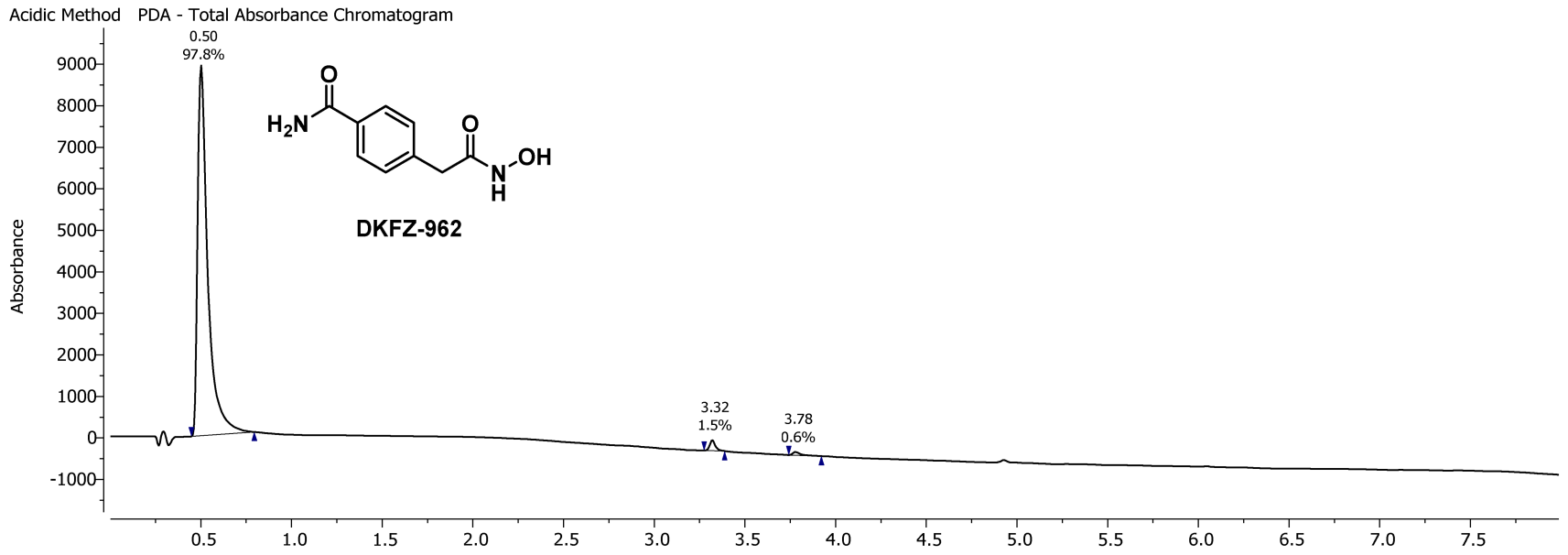
Acidic Method PDA - Total Absorbance Chromatogram
Absorbance
0.50
97.8%
3.32
1.5%
3.78
0.6%
DKFZ-962

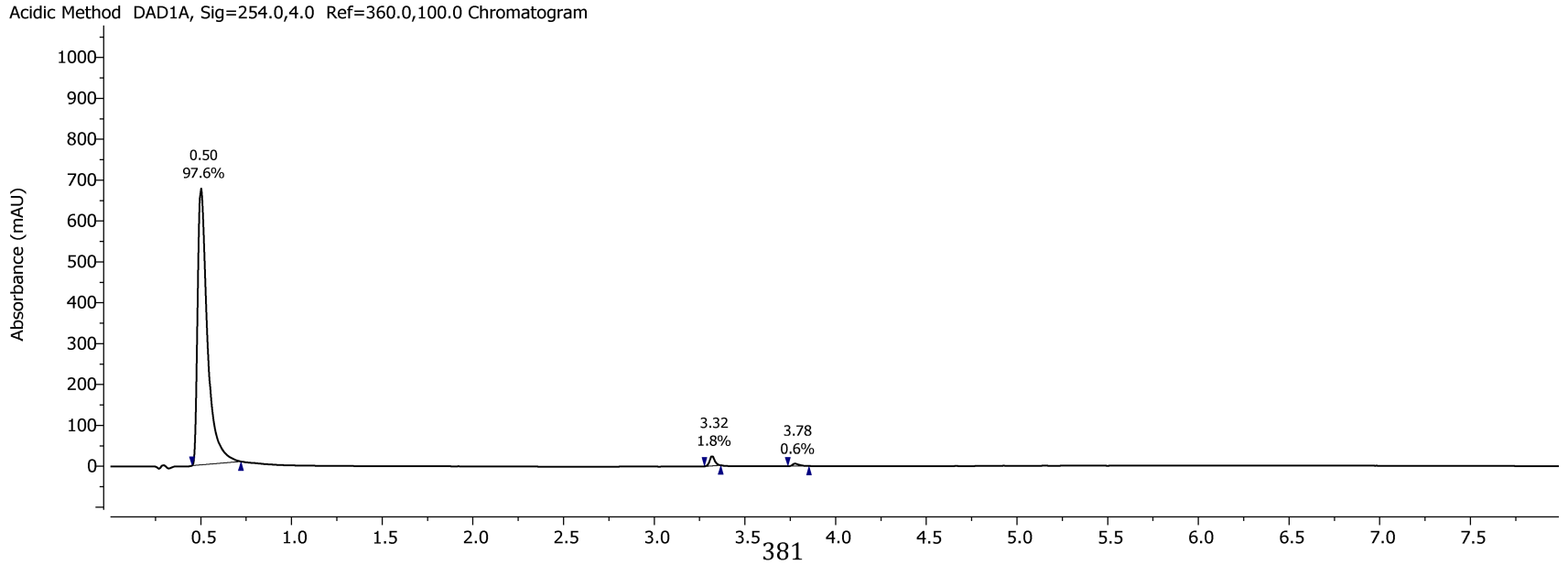
Acidic Method DAD1A, Sig=254.0,4.0 Ref=360.0,100.0 Chromatogram
Absorbance (mAU)
0.50
97.6%
3.32
1.8%
3.78
0.6%

1H NMR, 600.18 MHz, 295.0 K
in DMSO

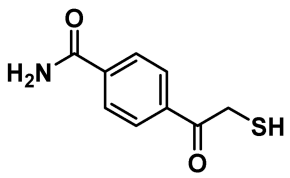


DKFZ-949

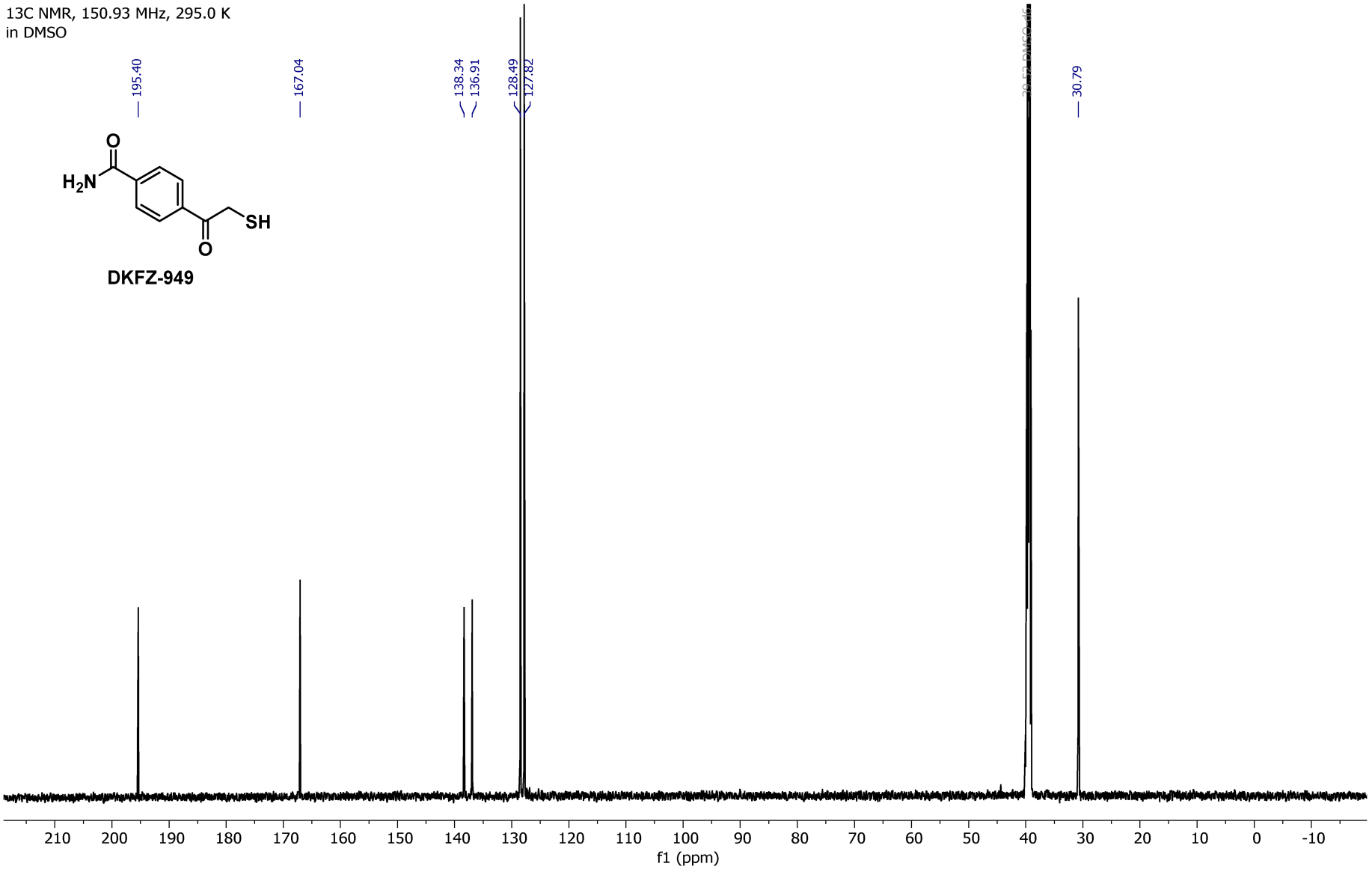
13C NMR, 150.93 MHz, 295.0 K
in DMSO
195.40
167.04
138.34
136.91
128.49
127.82
30.79
O
H2N
SH
O
DKFZ-949
210 200 190 180 170 160 150 140 130 120 110 100 90 80 70 60 50 40 30 20 10 0 -10
f1 (ppm)

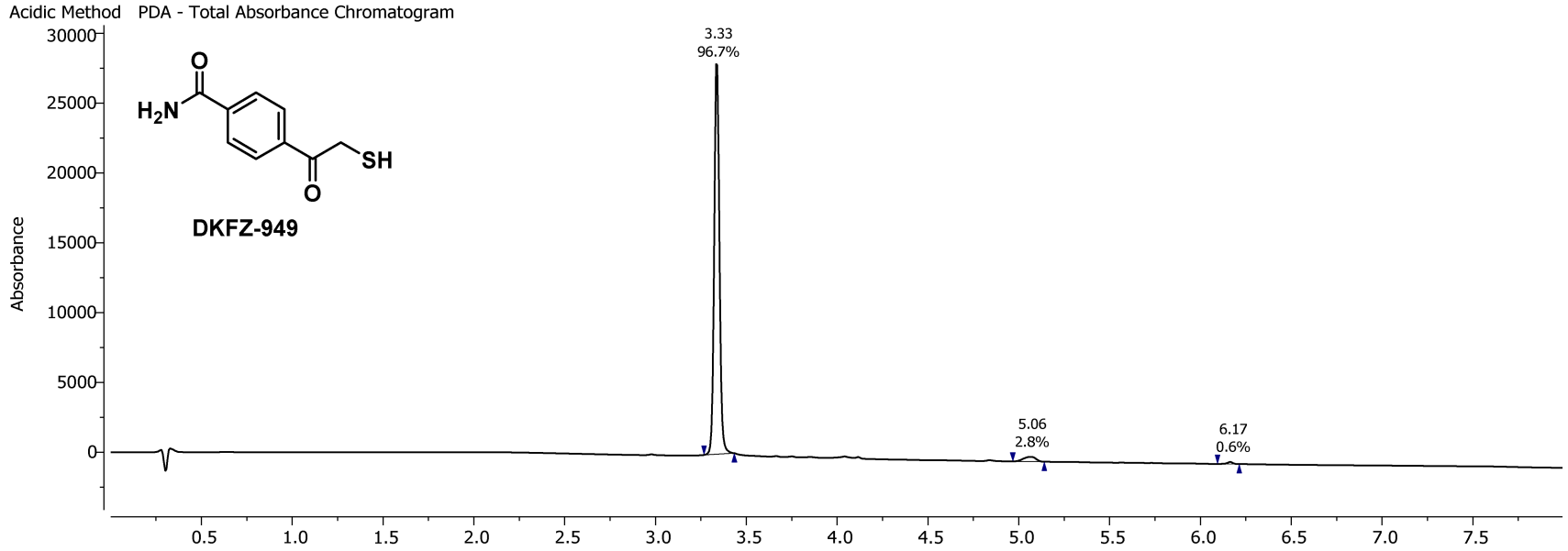
Acidic Method PDA - Total Absorbance Chromatogram
Absorbance
3.33
96.7%
5.06
2.8%
6.17
0.6%
DKFZ-949

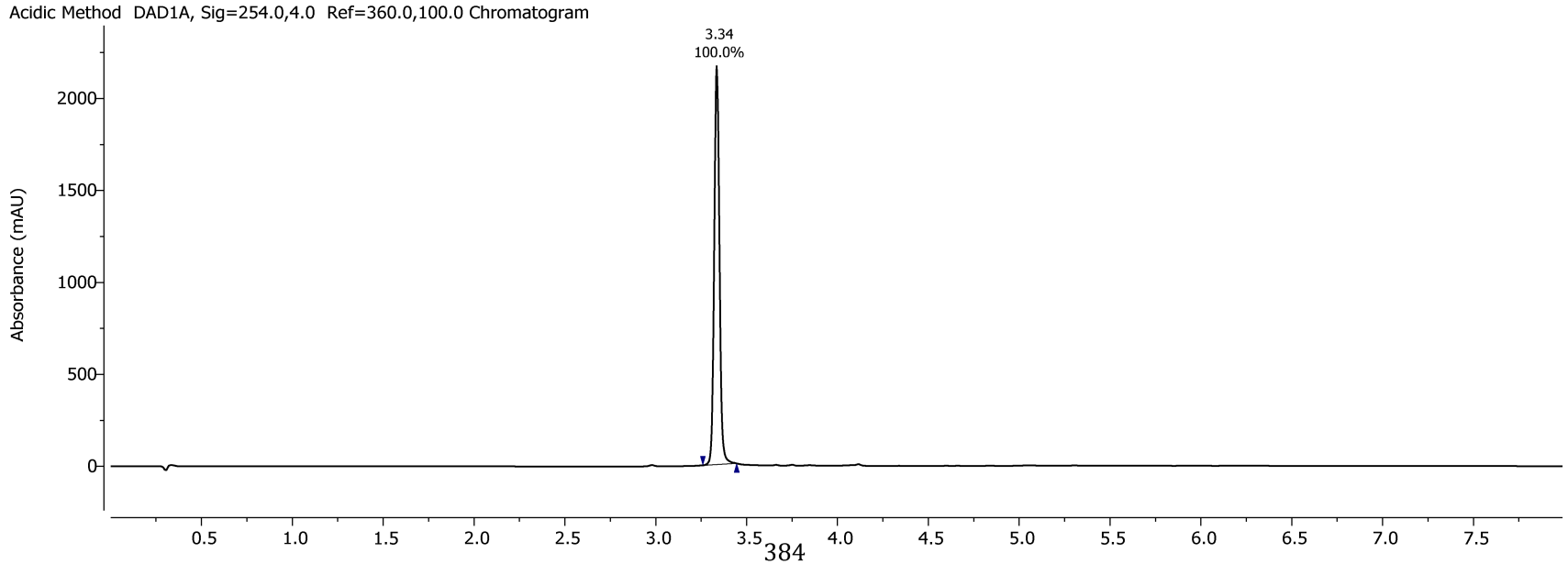
Acidic Method DAD1A, Sig=254.0,4.0 Ref=360.0,100.0 Chromatogram
Absorbance (mAU)
3.34
100.0%

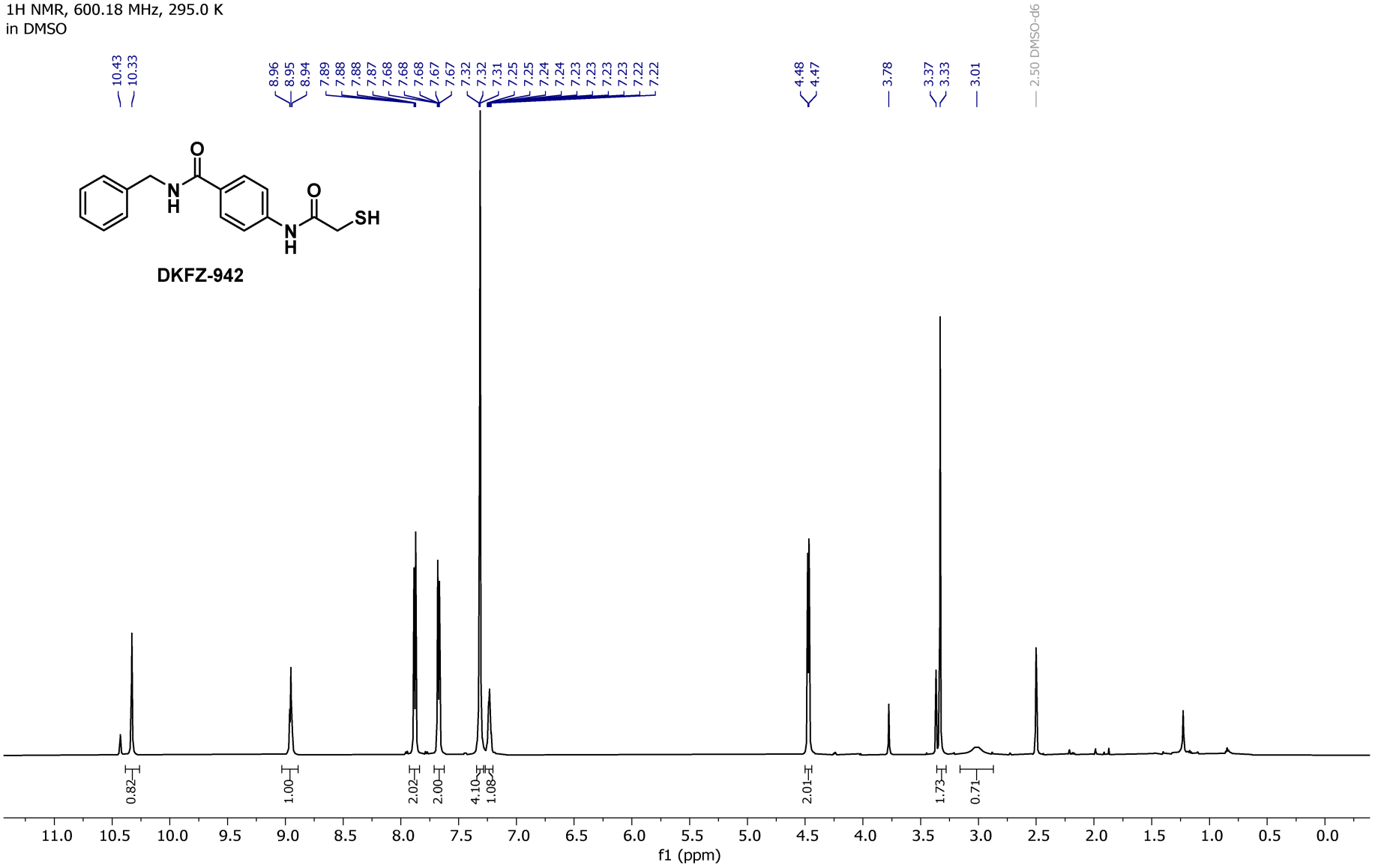
1H NMR, 600.18 MHz, 295.0 K
in DMSO
10.43
10.33
8.96
8.95
8.94
7.89
7.88
7.88
7.87
7.68
7.68
7.68
7.67
7.67
7.32
7.32
7.31
7.25
7.25
7.24
7.24
7.23
7.23
7.23
7.22
7.22
4.48
4.47
3.78
3.37
3.33
3.01
2.50 DMSO-d6
O
N
H
O
N
H
SH
DKFZ-942
0.82
1.00
2.02
2.00
4.10
1.08
2.01
1.73
0.71
11.0
10.5
10.0
9.5
9.0
8.5
8.0
7.5
7.0
6.5
6.0
5.5
5.0
4.5
4.0
3.5
3.0
2.5
2.0
1.5
1.0
0.5
0.0
f1 (ppm)

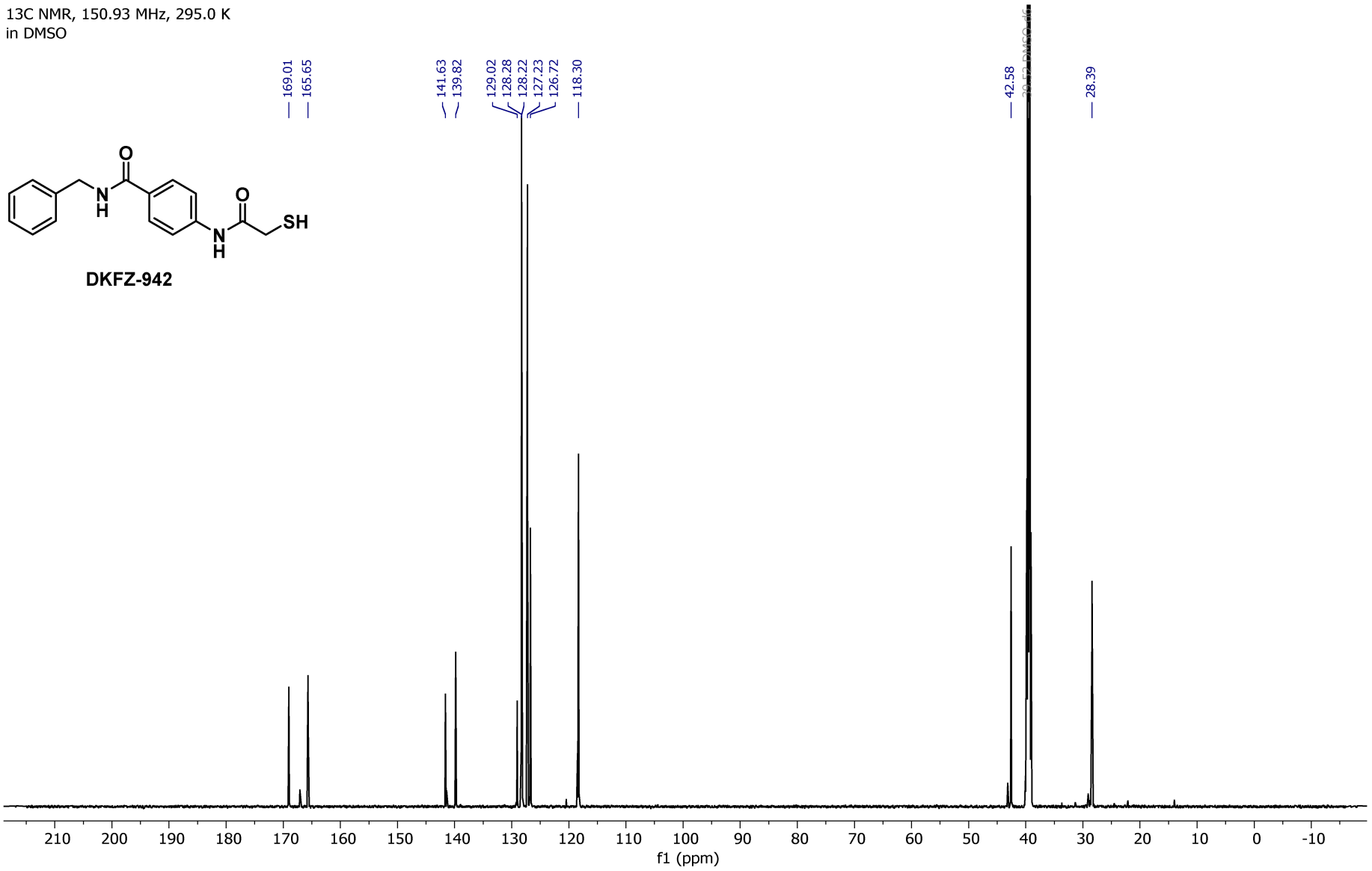
13C NMR, 150.93 MHz, 295.0 K
in DMSO
169.01
165.65
141.63
139.82
129.02
128.28
128.22
127.23
126.72
118.30
42.58
28.39
O
N
H
O
N
H
SH
DKFZ-942
210
200
190
180
170
160
150
140
130
120
110
100
90
80
70
60
50
40
30
20
10
0
-10
f1 (ppm)

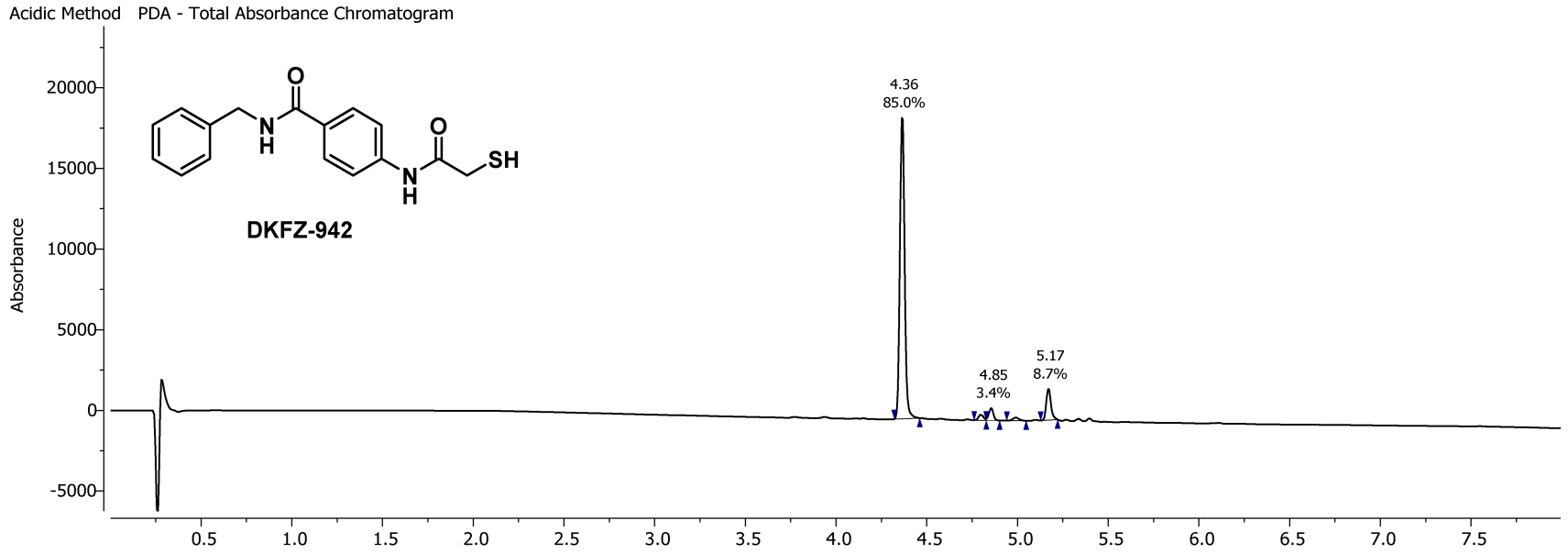
Acidic Method PDA - Total Absorbance Chromatogram
Absorbance
20000
15000
10000
5000
0
-5000
O
N
H
O
N
H
SH
DKFZ-942
4.36
85.0%
4.85
3.4%
5.17
8.7%
0.5
1.0
1.5
2.0
2.5
3.0
3.5
4.0
4.5
5.0
5.5
6.0
6.5
7.0
7.5

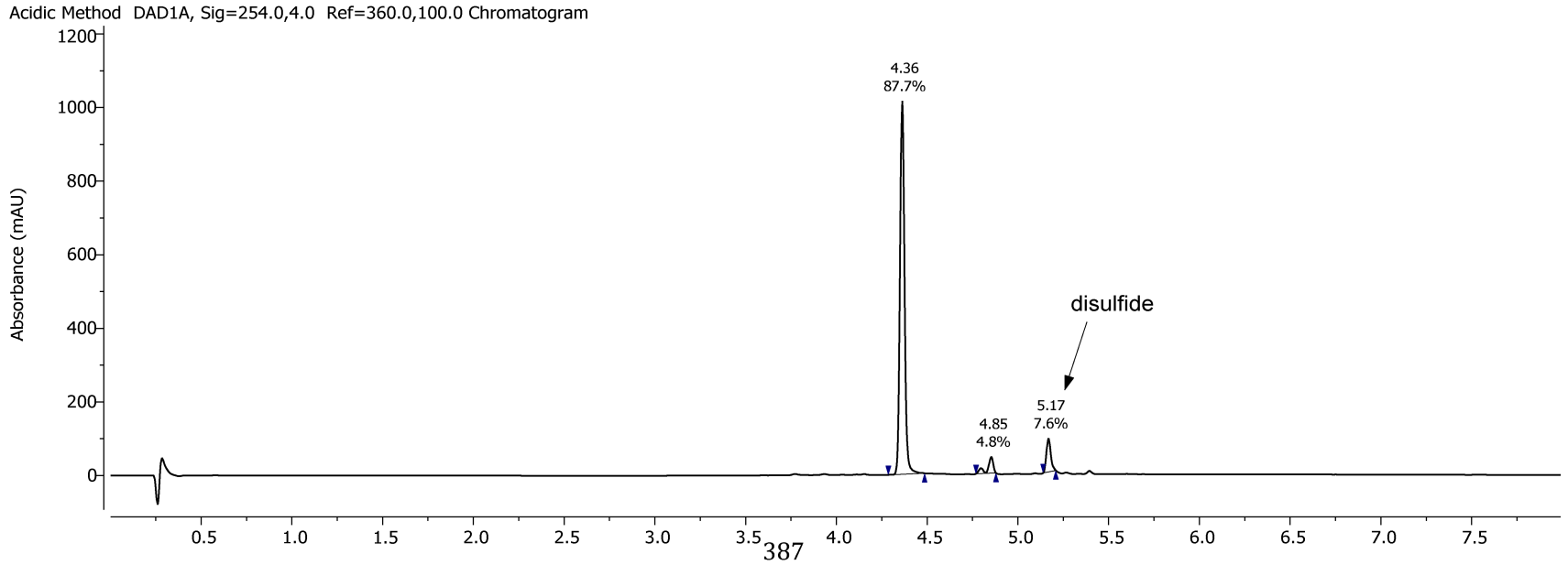
Acidic Method DAD1A, Sig=254.0,4.0 Ref=360.0,100.0 Chromatogram
Absorbance (mAU)
1200
1000
800
600
400
200
0
4.36
87.7%
disulfide
4.85
4.8%
5.17
7.6%
0.5
1.0
1.5
2.0
2.5
3.0
3.5
4.0
4.5
5.0
5.5
6.0
6.5
7.0
7.5

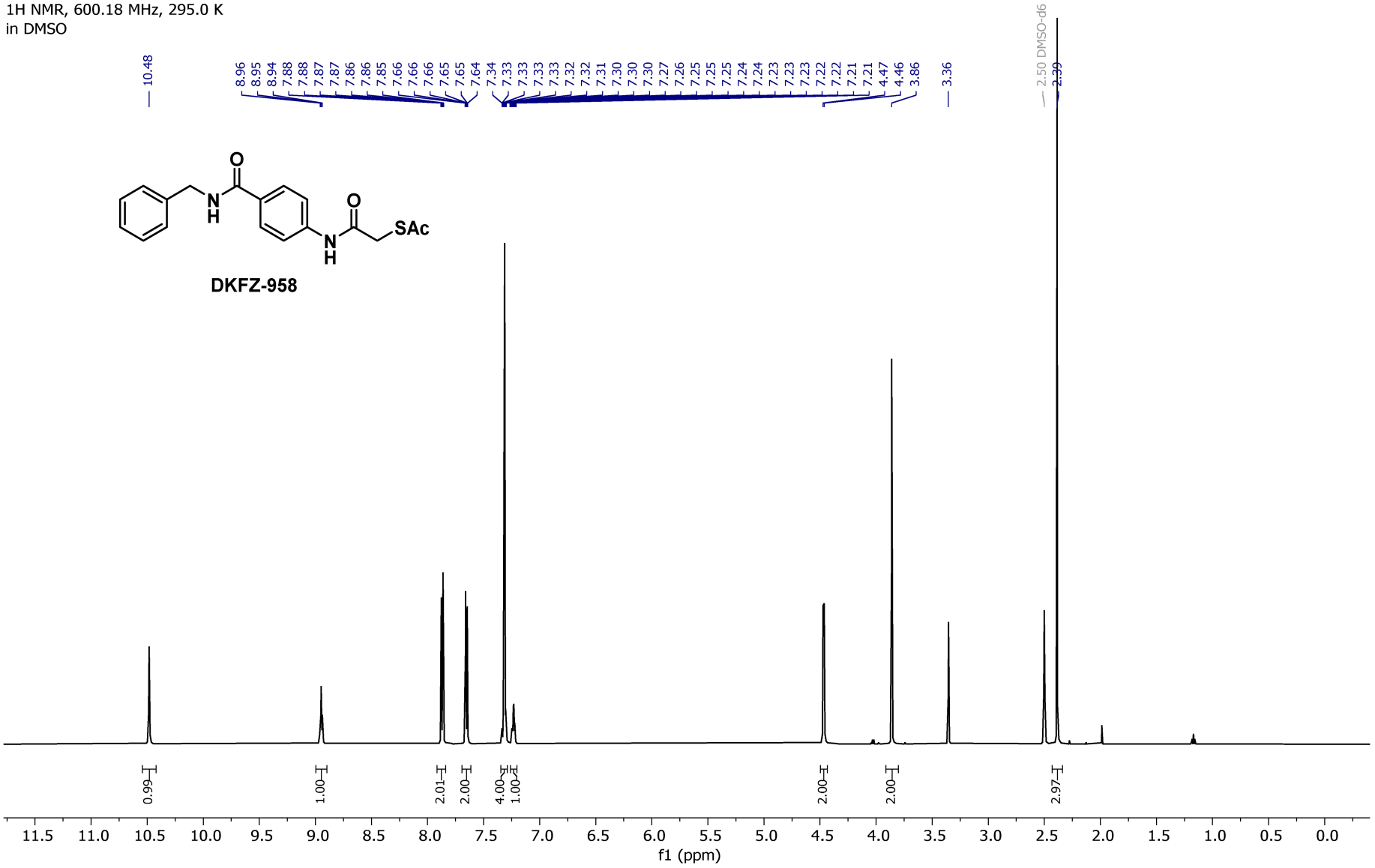
1H NMR, 600.18 MHz, 295.0 K
in DMSO
10.48
8.96
8.95
8.94
7.88
7.88
7.87
7.87
7.86
7.86
7.85
7.66
7.66
7.66
7.65
7.65
7.64
7.34
7.33
7.33
7.33
7.33
7.32
7.32
7.31
7.30
7.30
7.30
7.27
7.26
7.25
7.25
7.25
7.24
7.24
7.23
7.23
7.23
7.22
7.22
7.21
7.21
4.47
4.46
3.86
3.36
2.50 DMSO-d6
2.39
O
N
H
O
N
H
SAc
DKFZ-958
0.99
1.00
2.01
2.00
4.00
1.00
2.00
2.00
2.97
11.5
11.0
10.5
10.0
9.5
9.0
8.5
8.0
7.5
7.0
6.5
6.0
5.5
5.0
4.5
4.0
3.5
3.0
2.5
2.0
1.5
1.0
0.5
0.0
f1 (ppm)

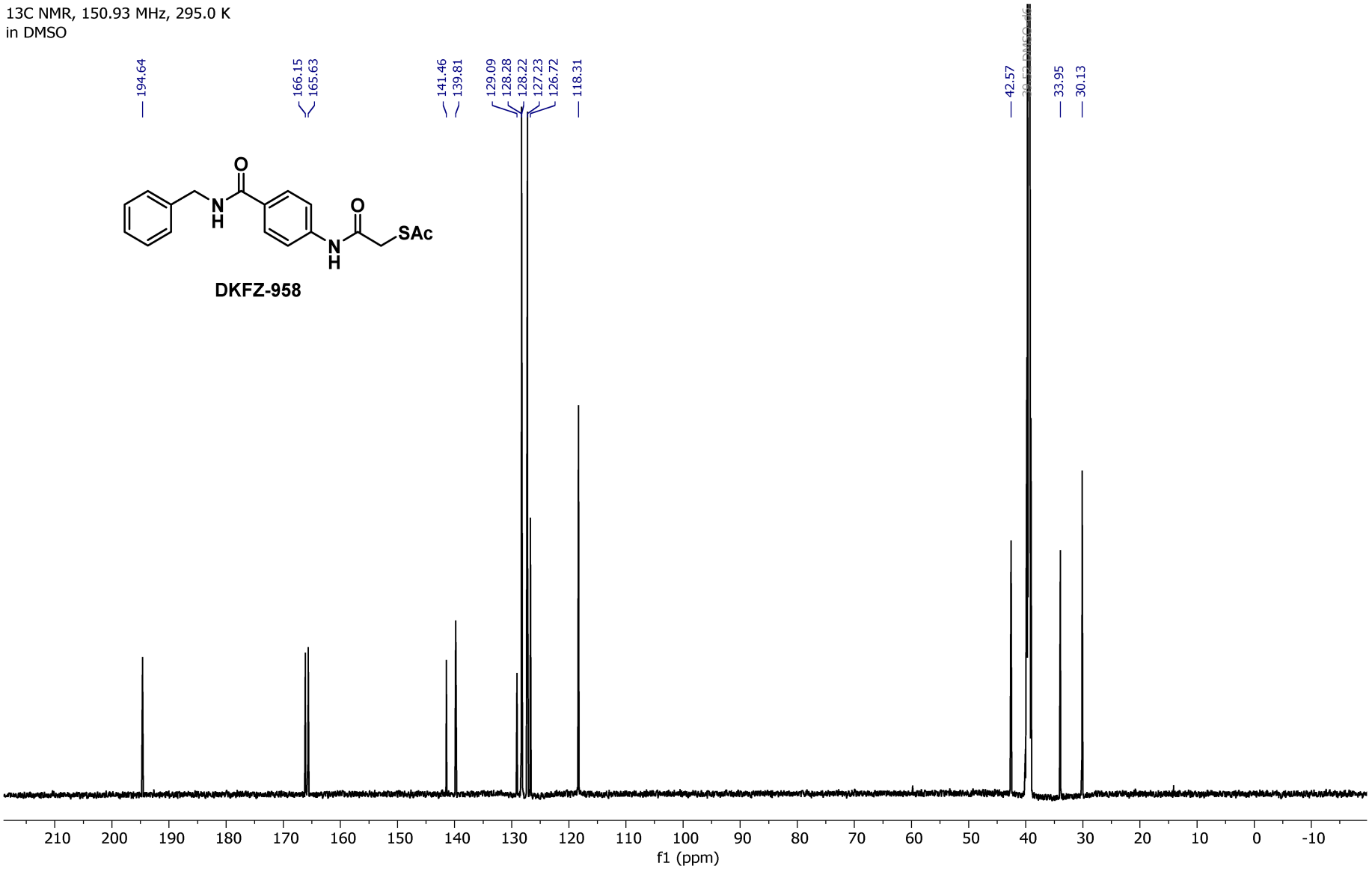
13C NMR, 150.93 MHz, 295.0 K
in DMSO
194.64
166.15
165.63
141.46
139.81
129.09
128.28
128.22
127.23
126.72
118.31
42.57
33.95
30.13
O
N
H
O
N
H
SAc
DKFZ-958
210 200 190 180 170 160 150 140 130 120 110 100 90 80 70 60 50 40 30 20 10 0 -10
f1 (ppm)

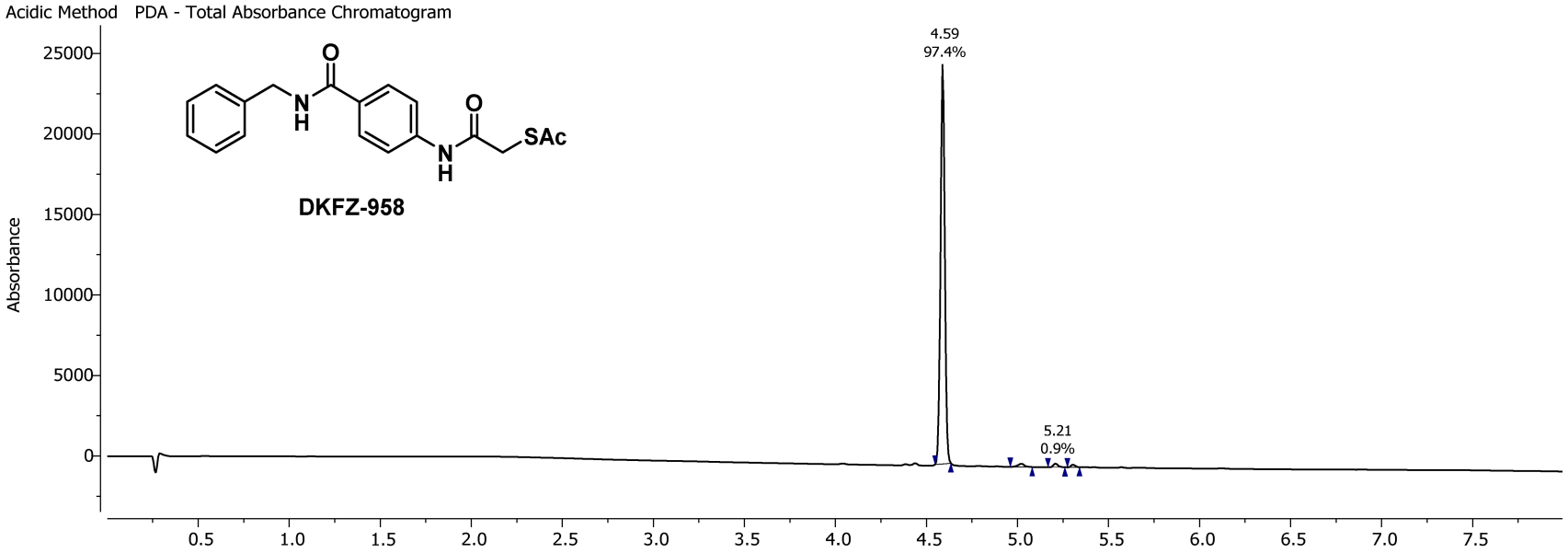
Acidic Method PDA - Total Absorbance Chromatogram
Absorbance
25000
20000
15000
10000
5000
0
4.59
97.4%
5.21
0.9%
0.5
1.0
1.5
2.0
2.5
3.0
3.5
4.0
4.5
5.0
5.5
6.0
6.5
7.0
7.5
O
N
H
O
N
H
SAc
DKFZ-958

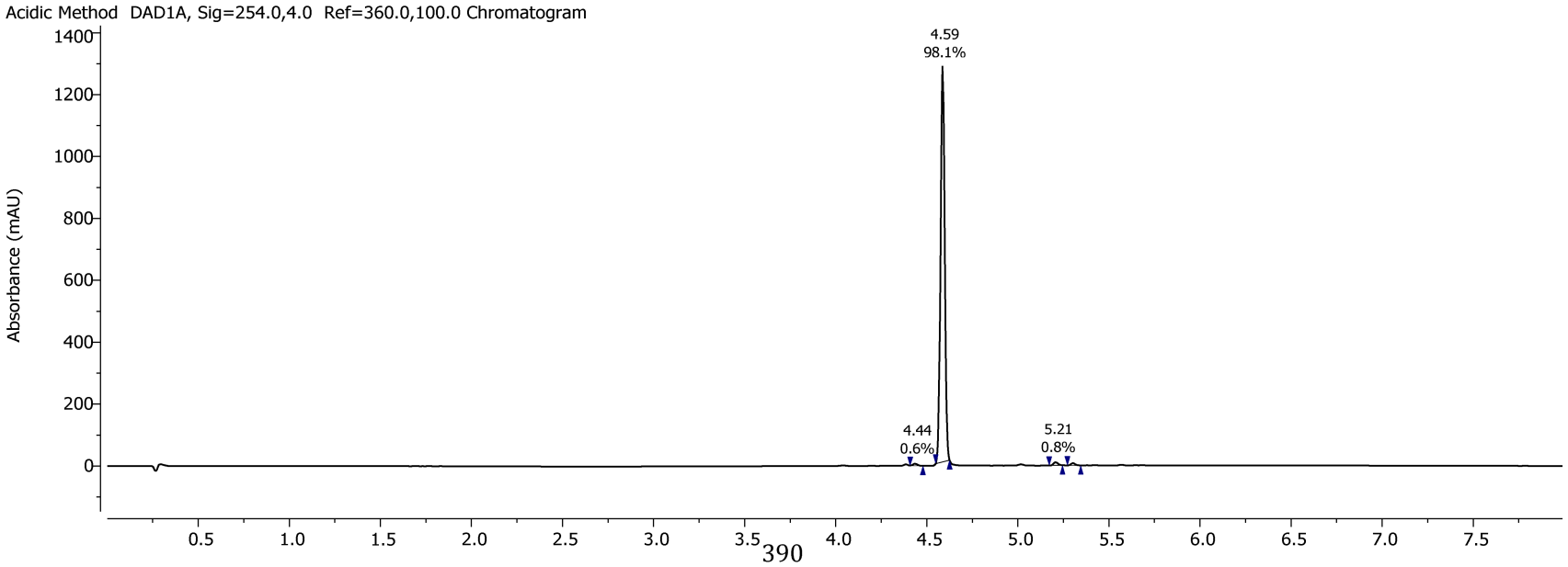
Acidic Method DAD1A, Sig=254.0,4.0 Ref=360.0,100.0 Chromatogram
Absorbance (mAU)
1400
1200
1000
800
600
400
200
0
4.59
98.1%
4.44
0.6%
5.21
0.8%
0.5
1.0
1.5
2.0
2.5
3.0
3.5
4.0
4.5
5.0
5.5
6.0
6.5
7.0
7.5

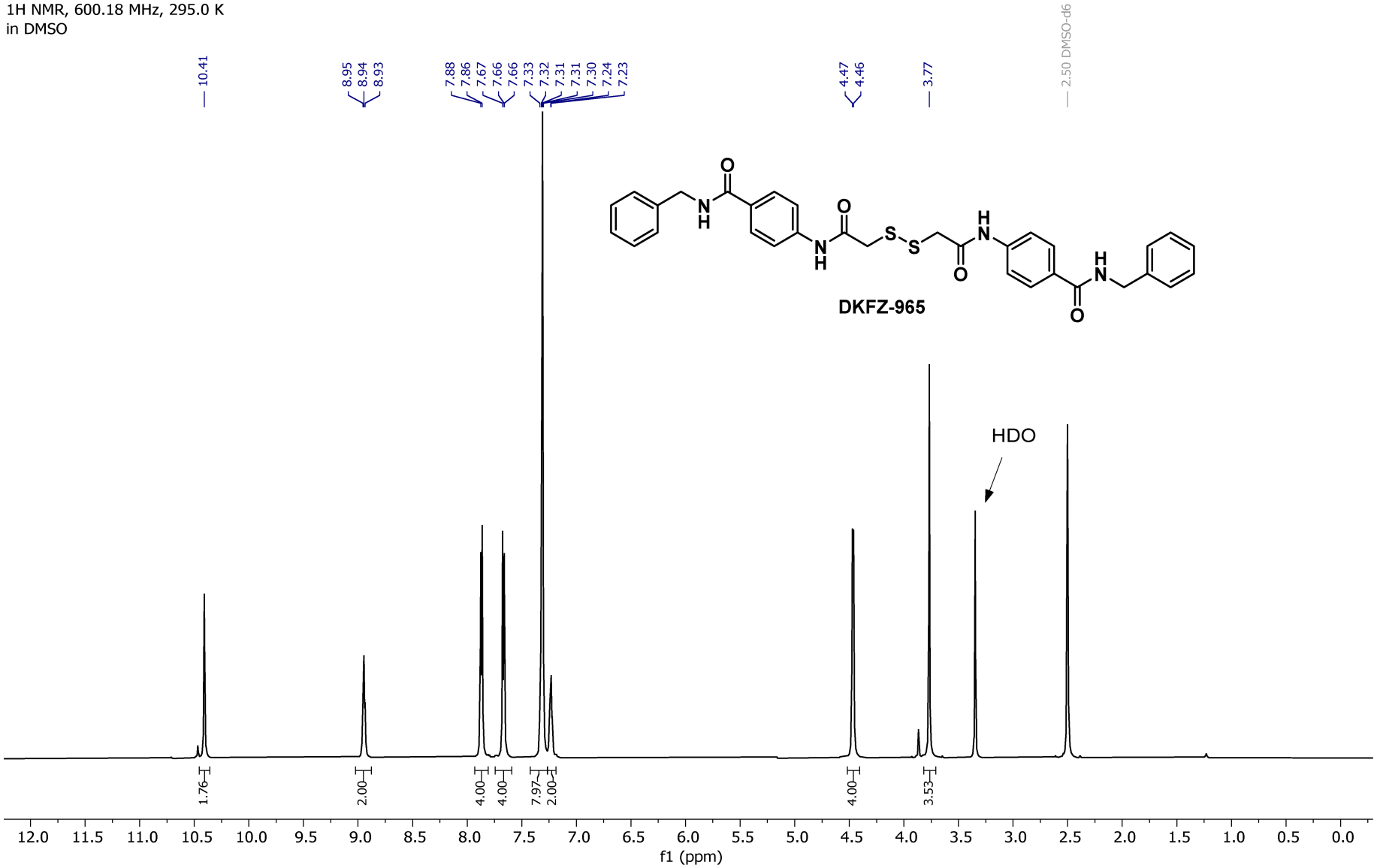
1H NMR, 600.18 MHz, 295.0 K
in DMSO
10.41
8.95
8.94
8.93
7.88
7.86
7.67
7.66
7.33
7.32
7.31
7.31
7.30
7.24
7.23
4.47
4.46
3.77
2.50 DMSO-d6
DKFZ-965
HDO
1.76
2.00
4.00
4.00
7.97
2.00
4.00
3.53
12.0 11.5 11.0 10.5 10.0 9.5 9.0 8.5 8.0 7.5 7.0 6.5 6.0 5.5 5.0 4.5 4.0 3.5 3.0 2.5 2.0 1.5 1.0 0.5 0.0
f1 (ppm)

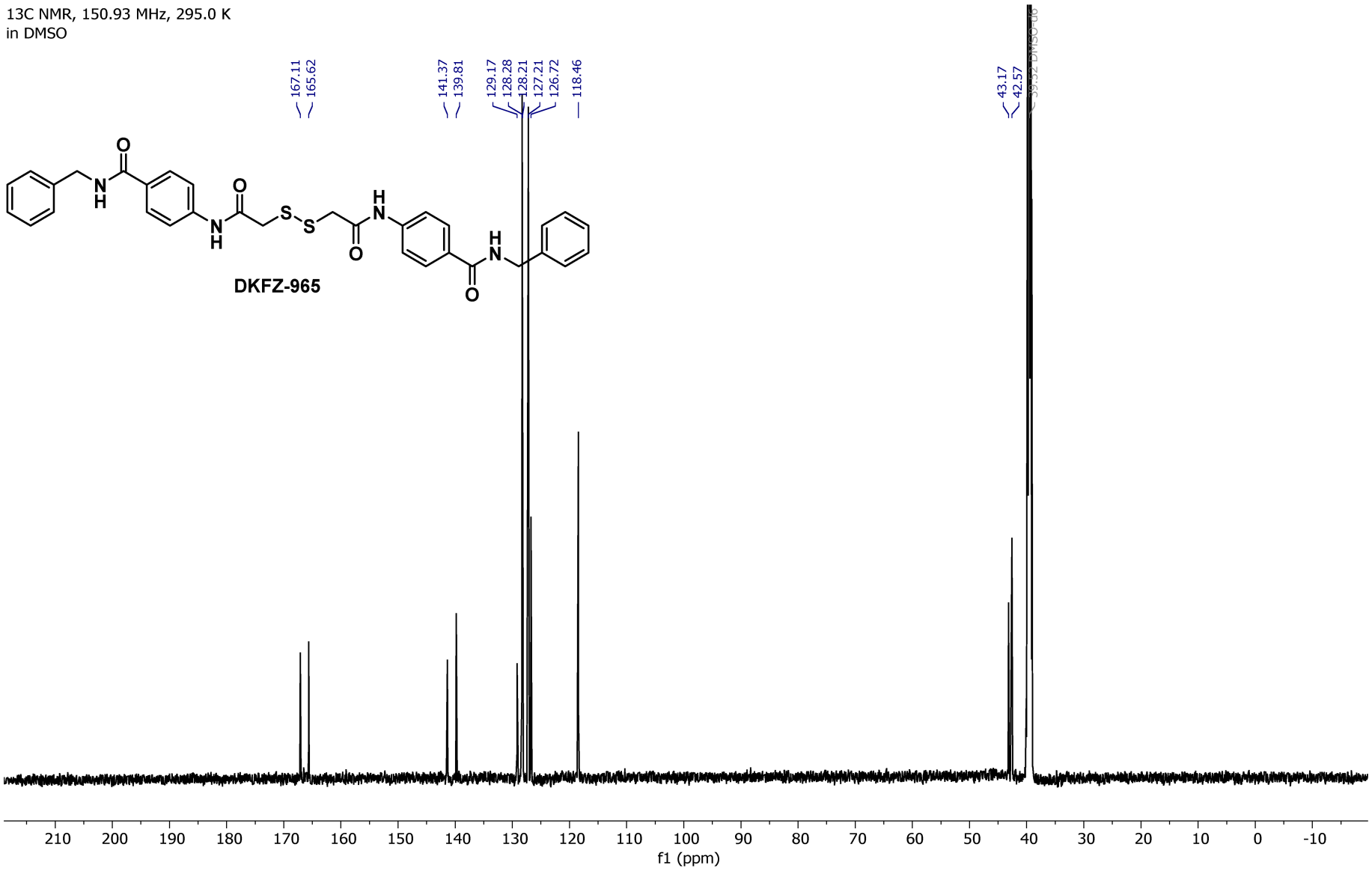
13C NMR, 150.93 MHz, 295.0 K
in DMSO
167.11
165.62
141.37
139.81
129.17
128.28
128.21
127.21
126.72
118.46
43.17
42.57
39.52 DMSO-d6
DKFZ-965
210
200
190
180
170
160
150
140
130
120
110
100
90
80
70
60
50
40
30
20
10
0
-10
f1 (ppm)

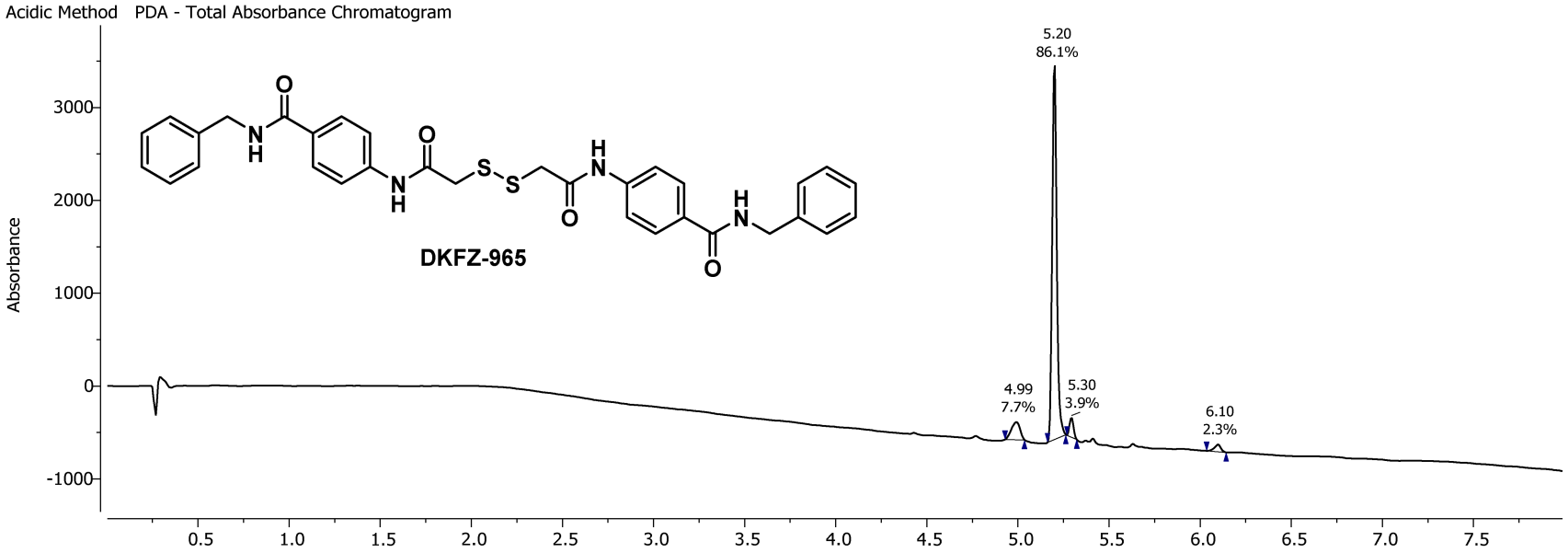
Acidic Method PDA - Total Absorbance Chromatogram
DKFZ-965
Absorbance
5.20
86.1%
4.99
7.7%
5.30
3.9%
6.10
2.3%

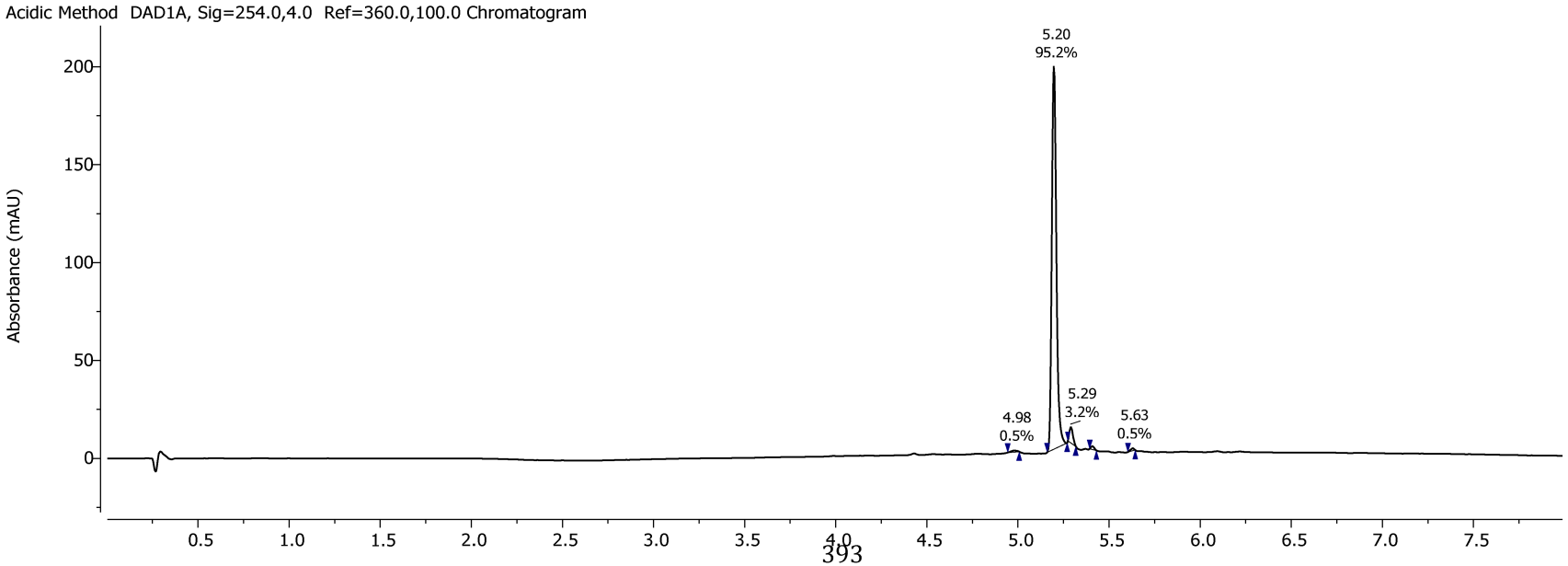
Acidic Method DAD1A, Sig=254.0,4.0 Ref=360.0,100.0 Chromatogram
Absorbance (mAU)
5.20
95.2%
4.98
0.5%
5.29
3.2%
5.63
0.5%

1H NMR, 600.18 MHz, 295.0 K
in CDCl3

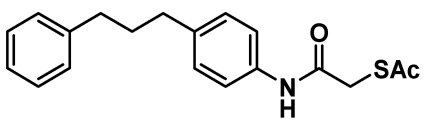


**DKFZ-960**

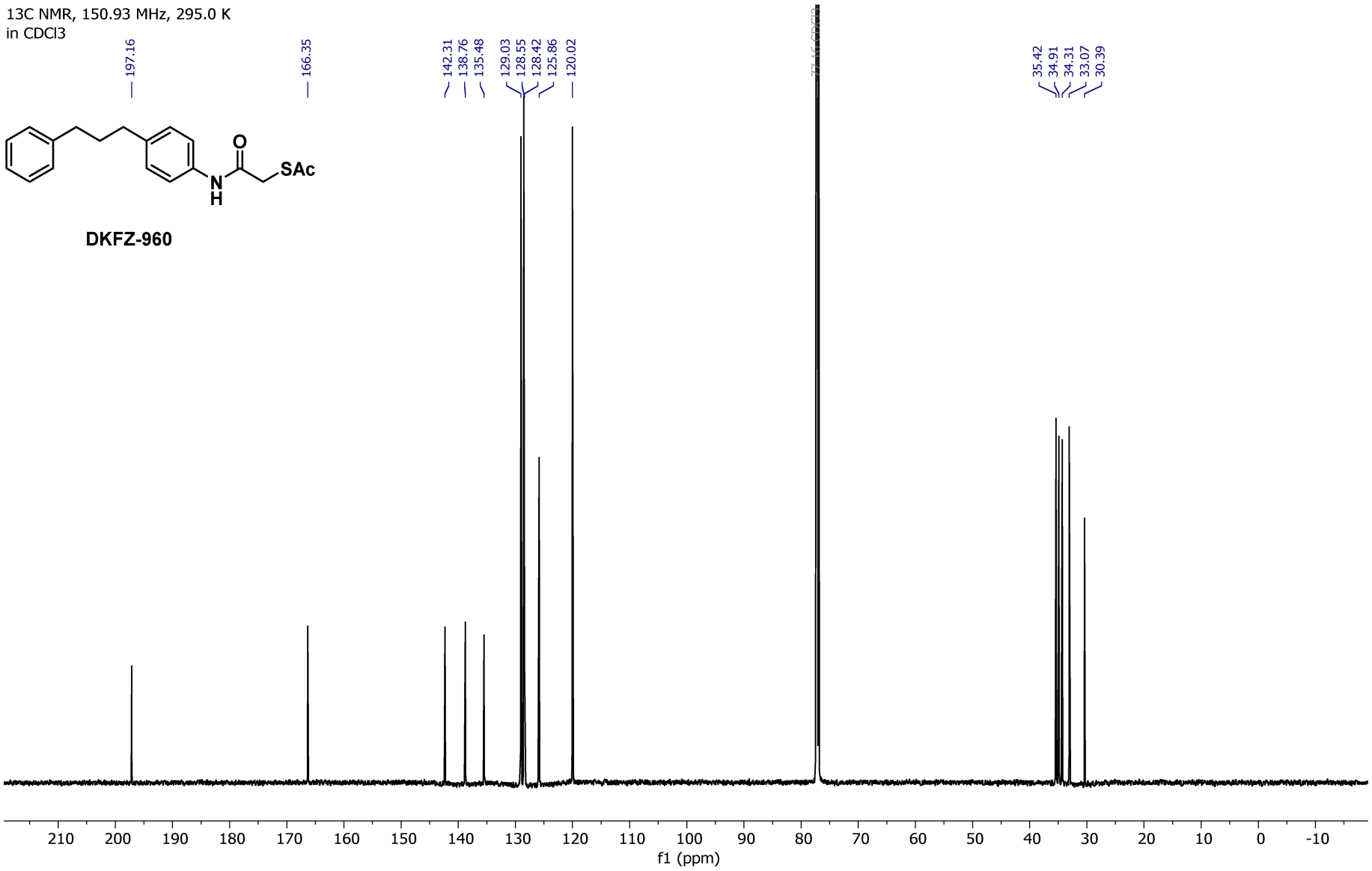
13C NMR, 150.93 MHz, 295.0 K
in CDCl3
197.16
166.35
142.31
138.76
135.48
129.03
128.55
128.42
125.86
120.02
35.42
34.91
34.31
33.07
30.39
O
N
H
SAc
DKFZ-960
210
200
190
180
170
160
150
140
130
120
110
100
90
80
70
60
50
40
30
20
10
0
-10
f1 (ppm)

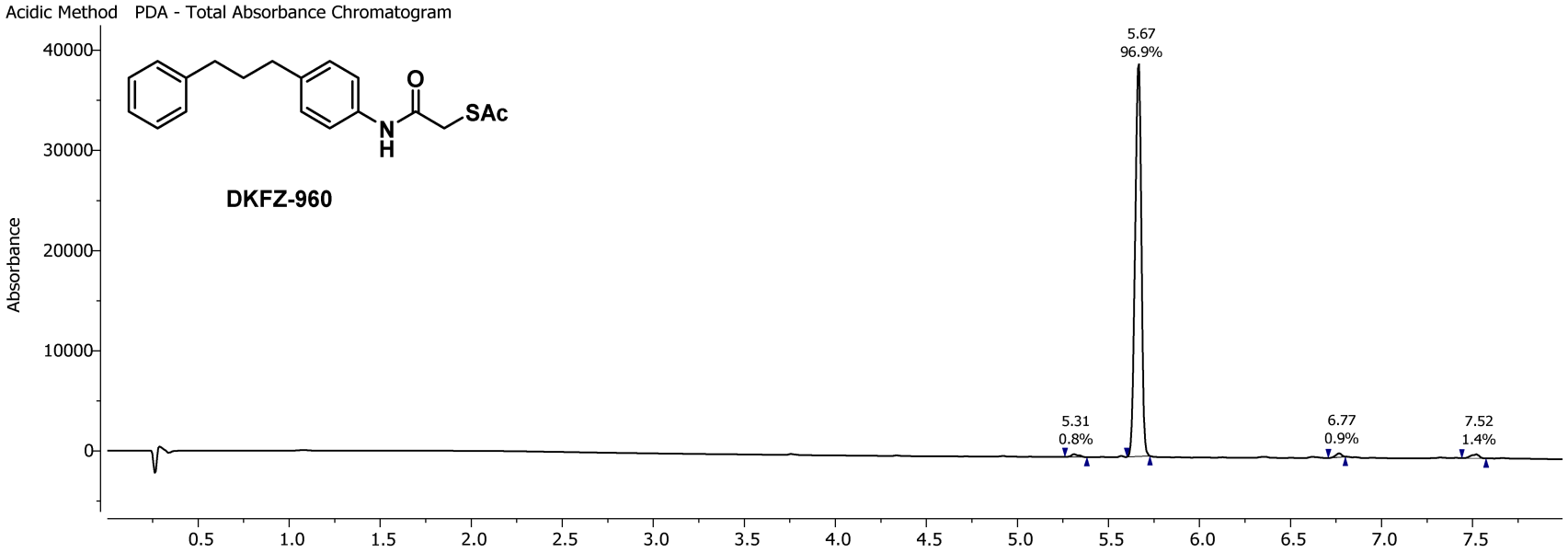
Acidic Method PDA - Total Absorbance Chromatogram
DKFZ-960
Absorbance
5.67
96.9%
5.31
0.8%
6.77
0.9%
7.52
1.4%

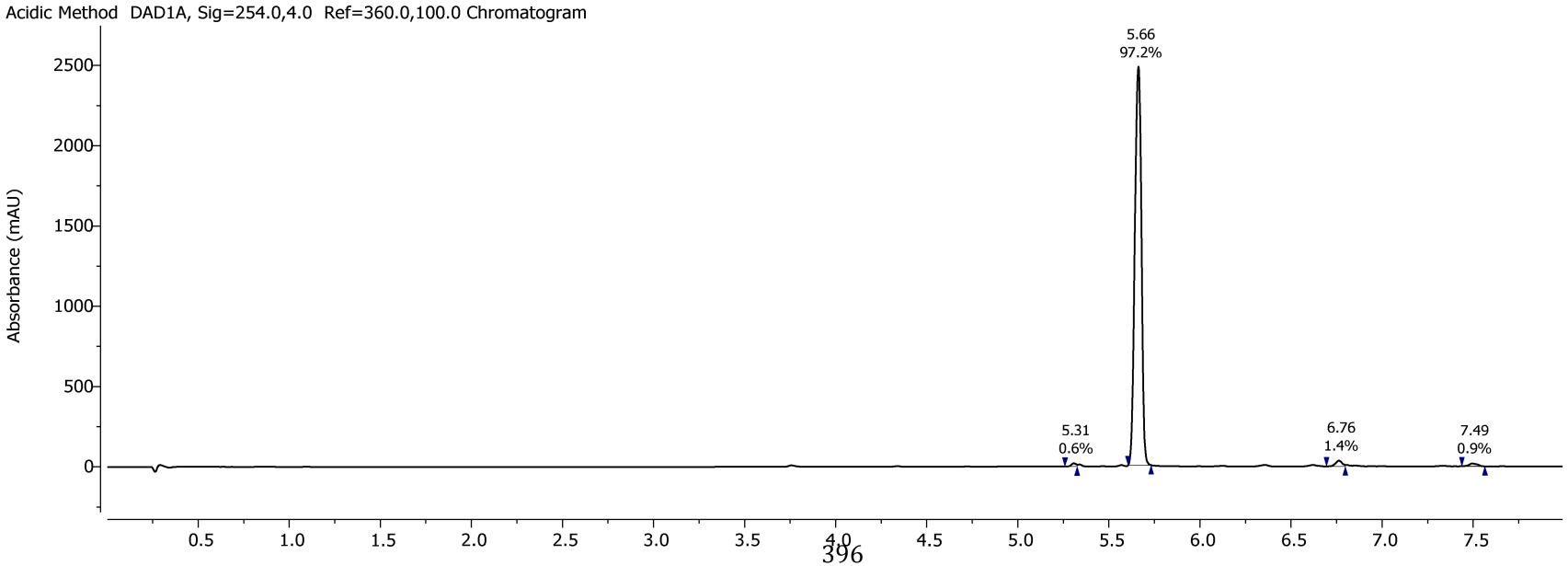
Acidic Method DAD1A, Sig=254.0,4.0 Ref=360.0,100.0 Chromatogram
Absorbance (mAU)
5.66
97.2%
5.31
0.6%
6.76
1.4%
7.49
0.9%

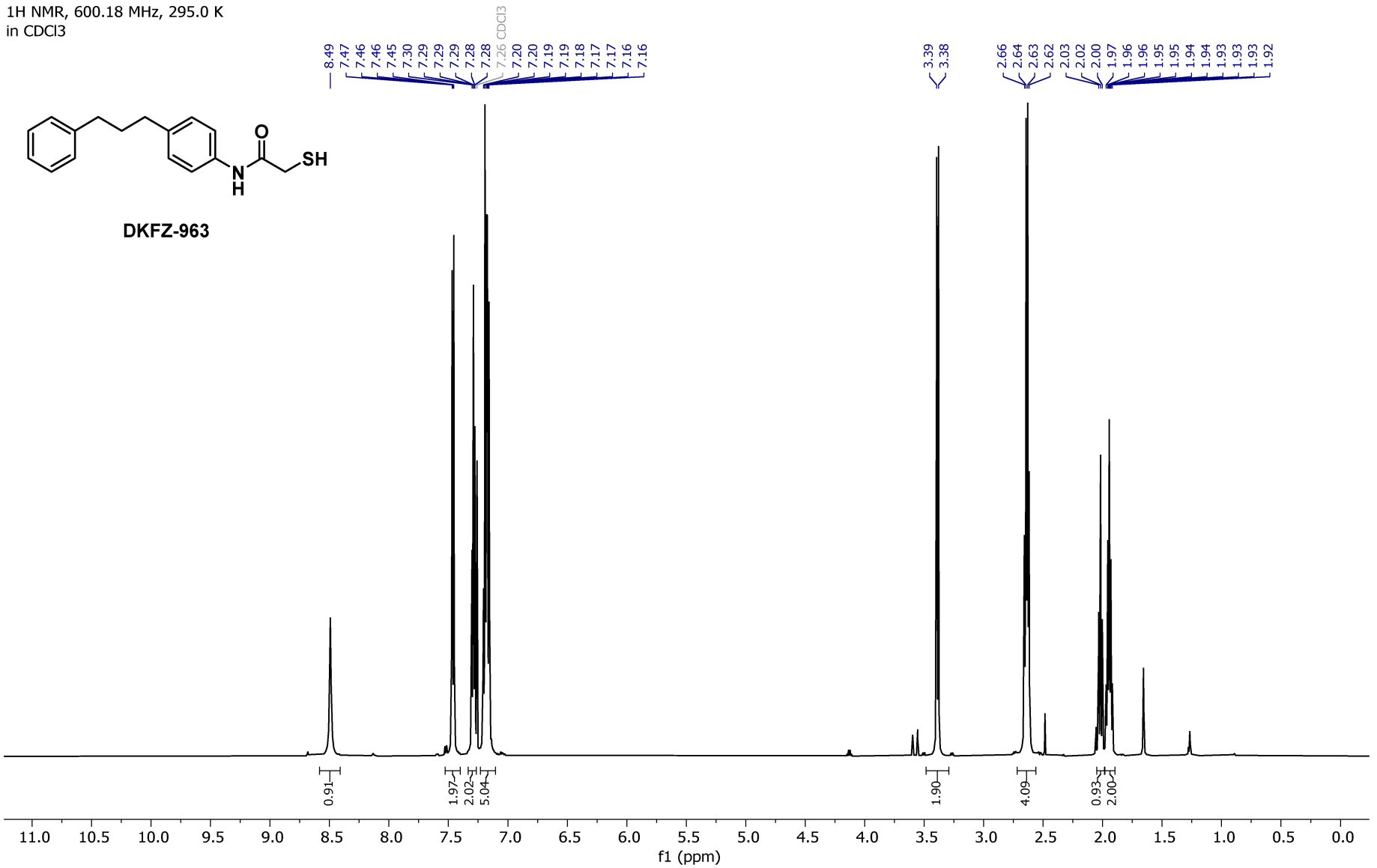
1H NMR, 600.18 MHz, 295.0 K
in CDCl3
DKFZ-963
O
N
H
SH
8.49
7.47
7.46
7.46
7.45
7.30
7.29
7.29
7.29
7.28
7.28
7.26 CDCl3
7.20
7.20
7.19
7.19
7.18
7.17
7.17
7.16
7.16
3.39
3.38
2.66
2.64
2.63
2.62
2.03
2.02
2.00
1.97
1.96
1.96
1.95
1.95
1.94
1.94
1.93
1.93
1.93
1.92
0.91
1.97
2.02
5.04
1.90
4.09
0.93
2.00
11.0
10.5
10.0
9.5
9.0
8.5
8.0
7.5
7.0
6.5
6.0
5.5
5.0
4.5
4.0
3.5
3.0
2.5
2.0
1.5
1.0
0.5
0.0
f1 (ppm)

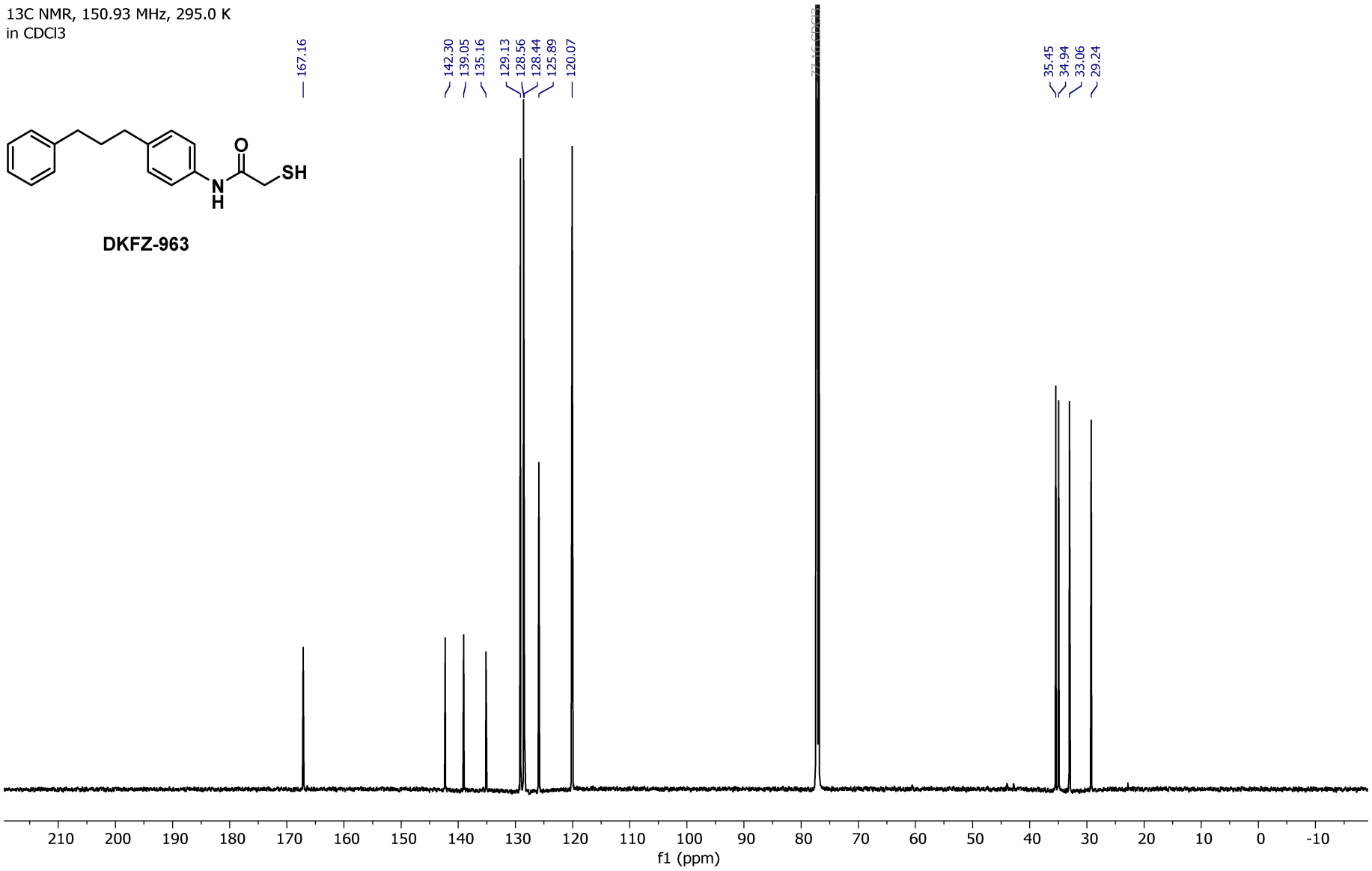
13C NMR, 150.93 MHz, 295.0 K
in CDCl3
167.16
142.30
139.05
135.16
129.13
128.56
128.44
125.89
120.07
77.16
35.45
34.94
33.06
29.24
O
N
H
SH
DKFZ-963
210 200 190 180 170 160 150 140 130 120 110 100 90 80 70 60 50 40 30 20 10 0 -10
f1 (ppm)

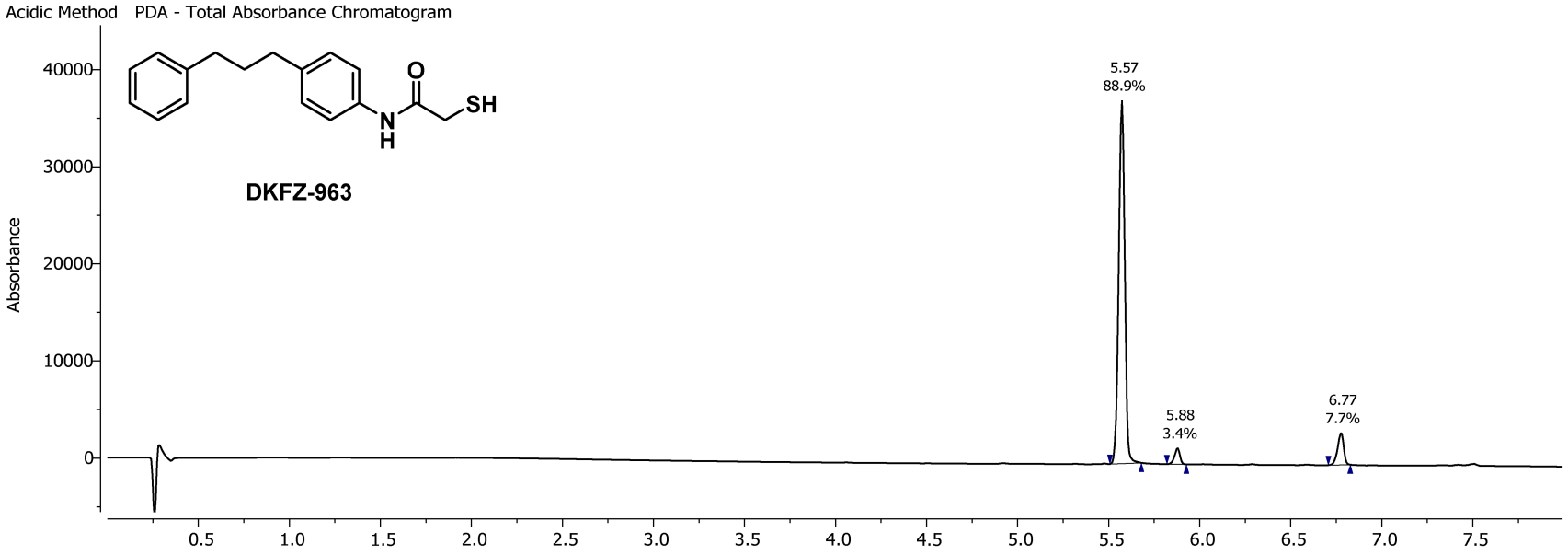
Acidic Method PDA - Total Absorbance Chromatogram
DKFZ-963
Absorbance
5.57
88.9%
5.88
3.4%
6.77
7.7%

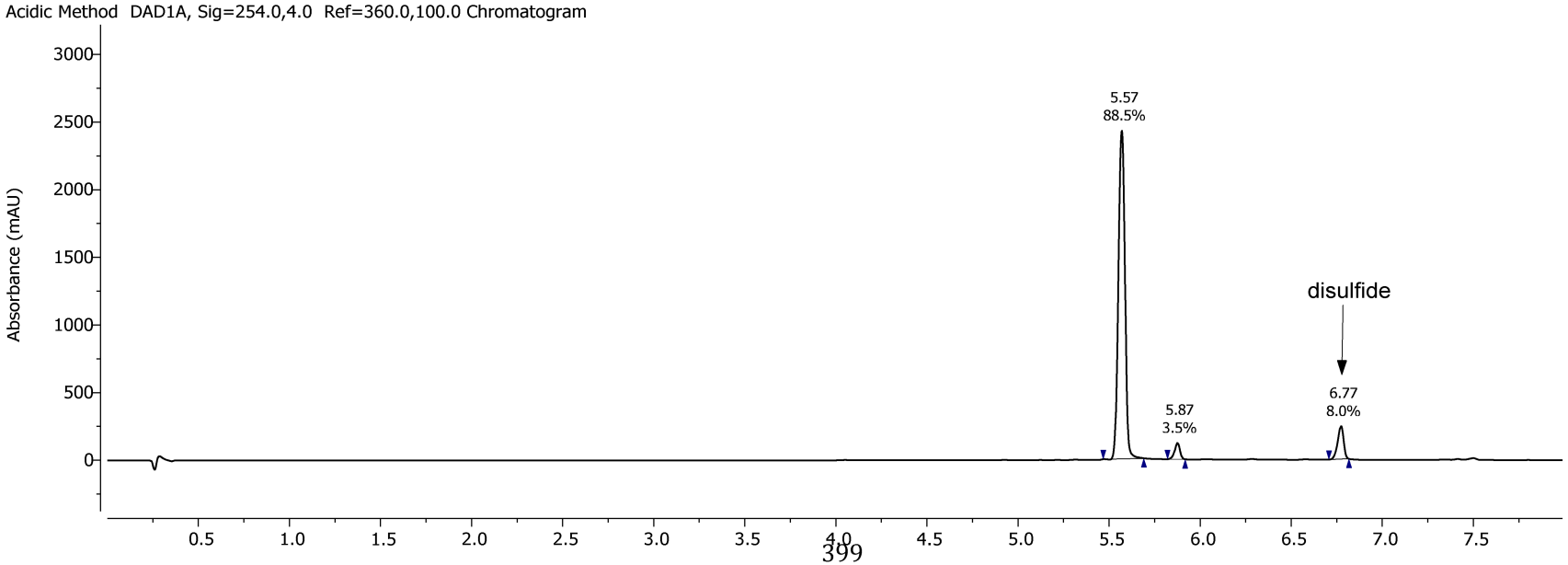
Acidic Method DAD1A, Sig=254.0,4.0 Ref=360.0,100.0 Chromatogram
Absorbance (mAU)
5.57
88.5%
disulfide
5.87
3.5%
6.77
8.0%

1H NMR, 600.18 MHz, 295.0 K
in CDCl3

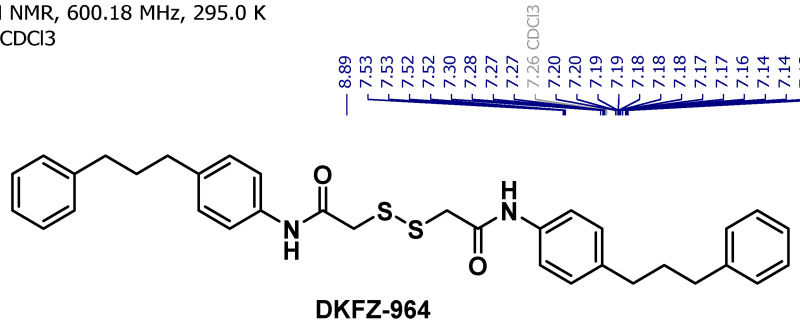


DKFZ-964

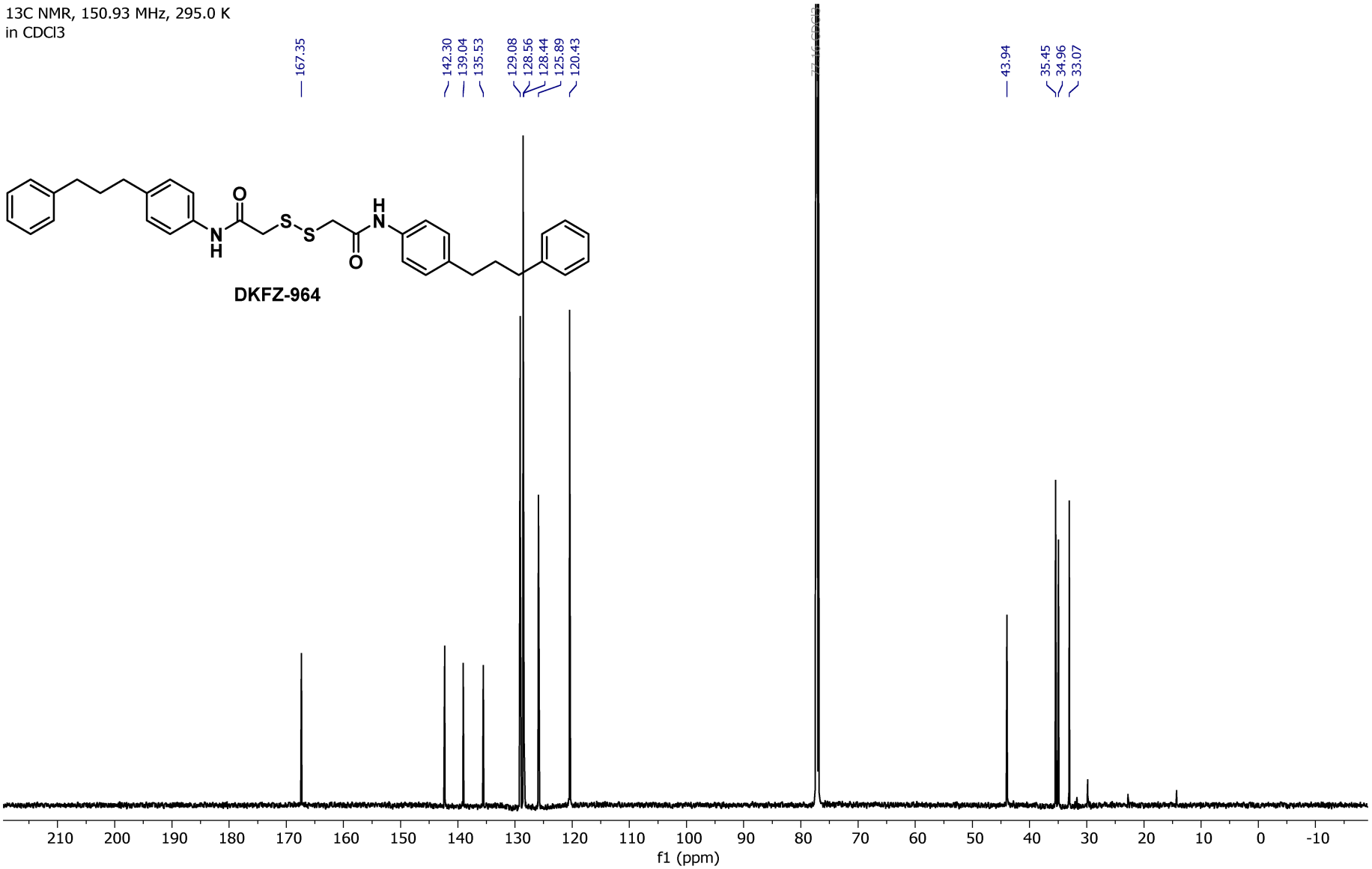
13C NMR, 150.93 MHz, 295.0 K
in CDCl3
167.35
142.30
139.04
135.53
129.08
128.56
128.44
125.89
120.43
77.16
43.94
35.45
34.96
33.07
DKFZ-964
210 200 190 180 170 160 150 140 130 120 110 100 90 80 70 60 50 40 30 20 10 0 -10
f1 (ppm)

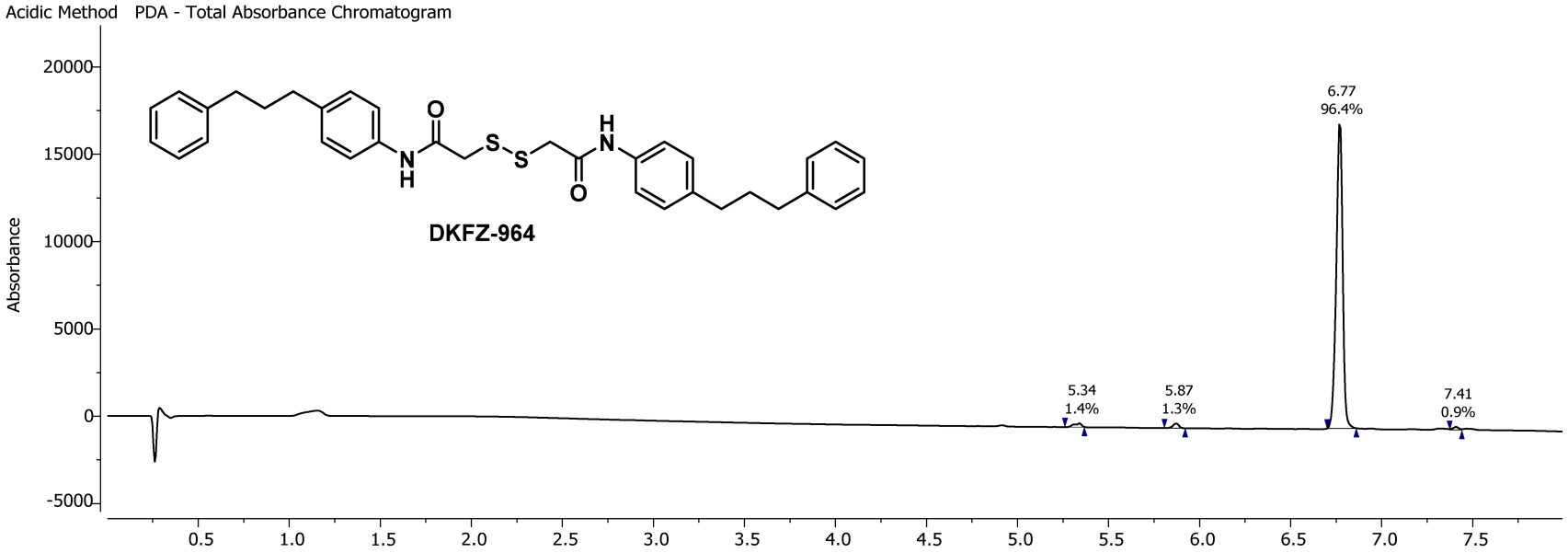
Acidic Method PDA - Total Absorbance Chromatogram
Absorbance
20000
15000
10000
5000
0
-5000
DKFZ-964
6.77
96.4%
5.34
1.4%
5.87
1.3%
7.41
0.9%
0.5
1.0
1.5
2.0
2.5
3.0
3.5
4.0
4.5
5.0
5.5
6.0
6.5
7.0
7.5

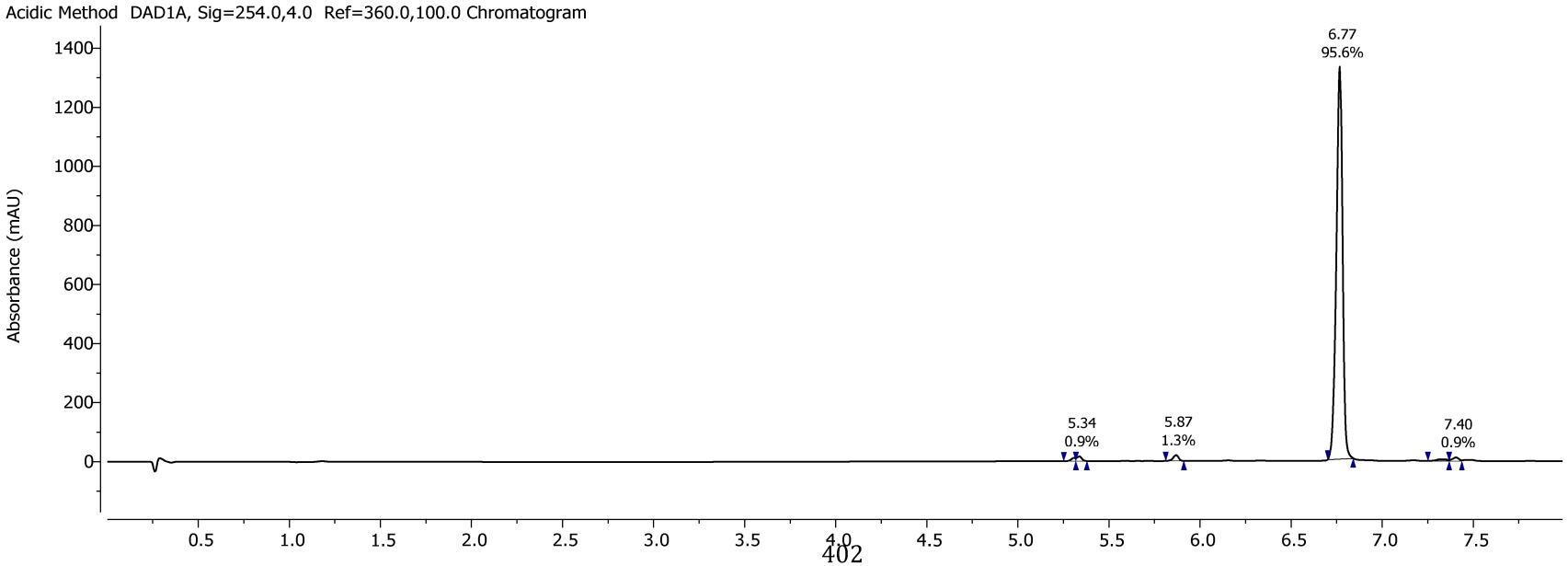
Acidic Method DAD1A, Sig=254.0,4.0 Ref=360.0,100.0 Chromatogram
Absorbance (mAU)
1400
1200
1000
800
600
400
200
0
6.77
95.6%
5.34
0.9%
5.87
1.3%
7.40
0.9%
0.5
1.0
1.5
2.0
2.5
3.0
3.5
4.0
4.5
5.0
5.5
6.0
6.5
7.0
7.5

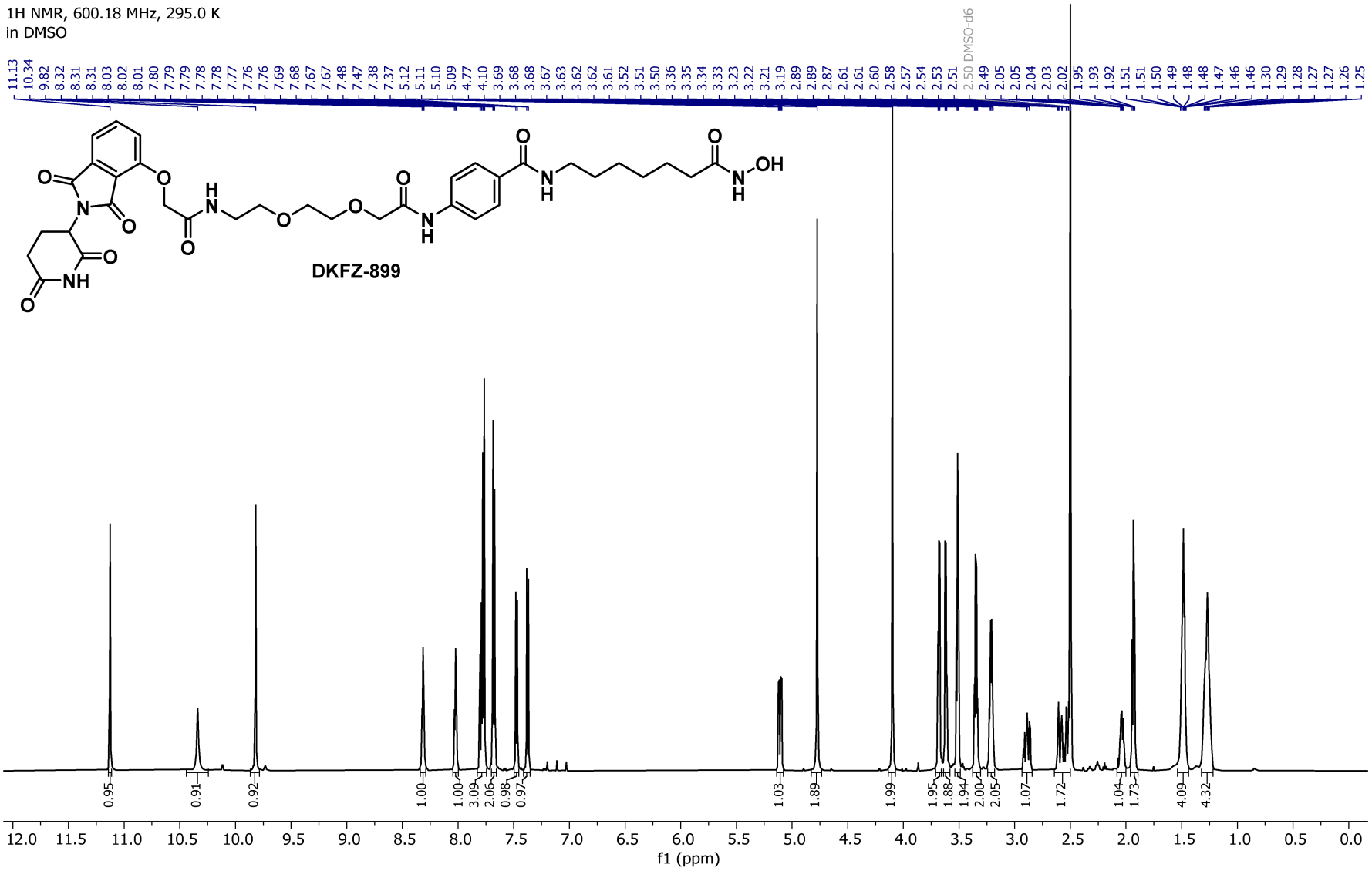
1H NMR, 600.18 MHz, 295.0 K
in DMSO
DKFZ-899
f1 (ppm)

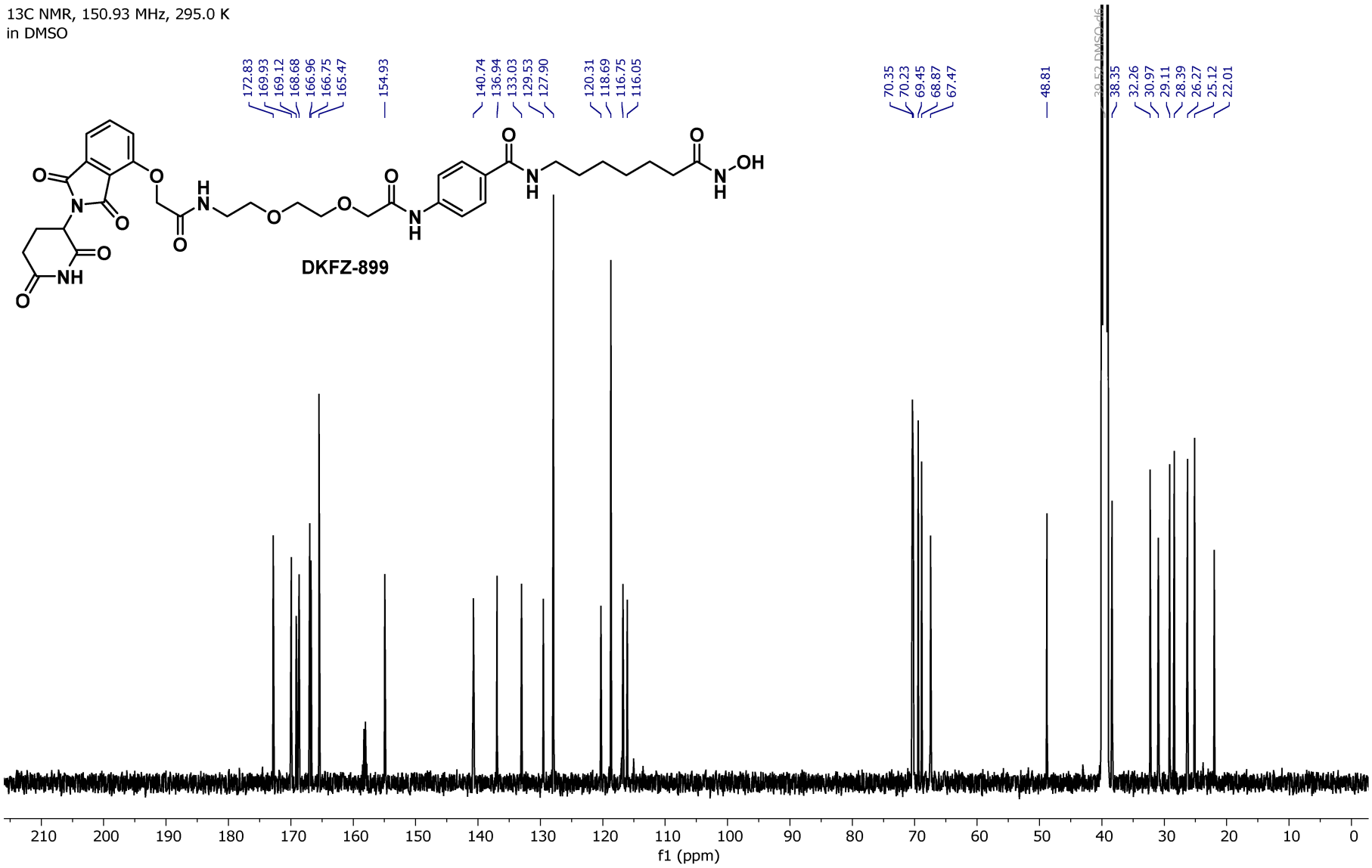
13C NMR, 150.93 MHz, 295.0 K
in DMSO
172.83
169.93
169.12
168.68
166.96
166.75
165.47
154.93
140.74
136.94
133.03
129.53
127.90
120.31
118.69
116.75
116.05
70.35
70.23
69.45
68.87
67.47
48.81
39.52 DMSO-d6
38.35
32.26
30.97
29.11
28.39
26.27
25.12
22.01
DKFZ-899
f1 (ppm)

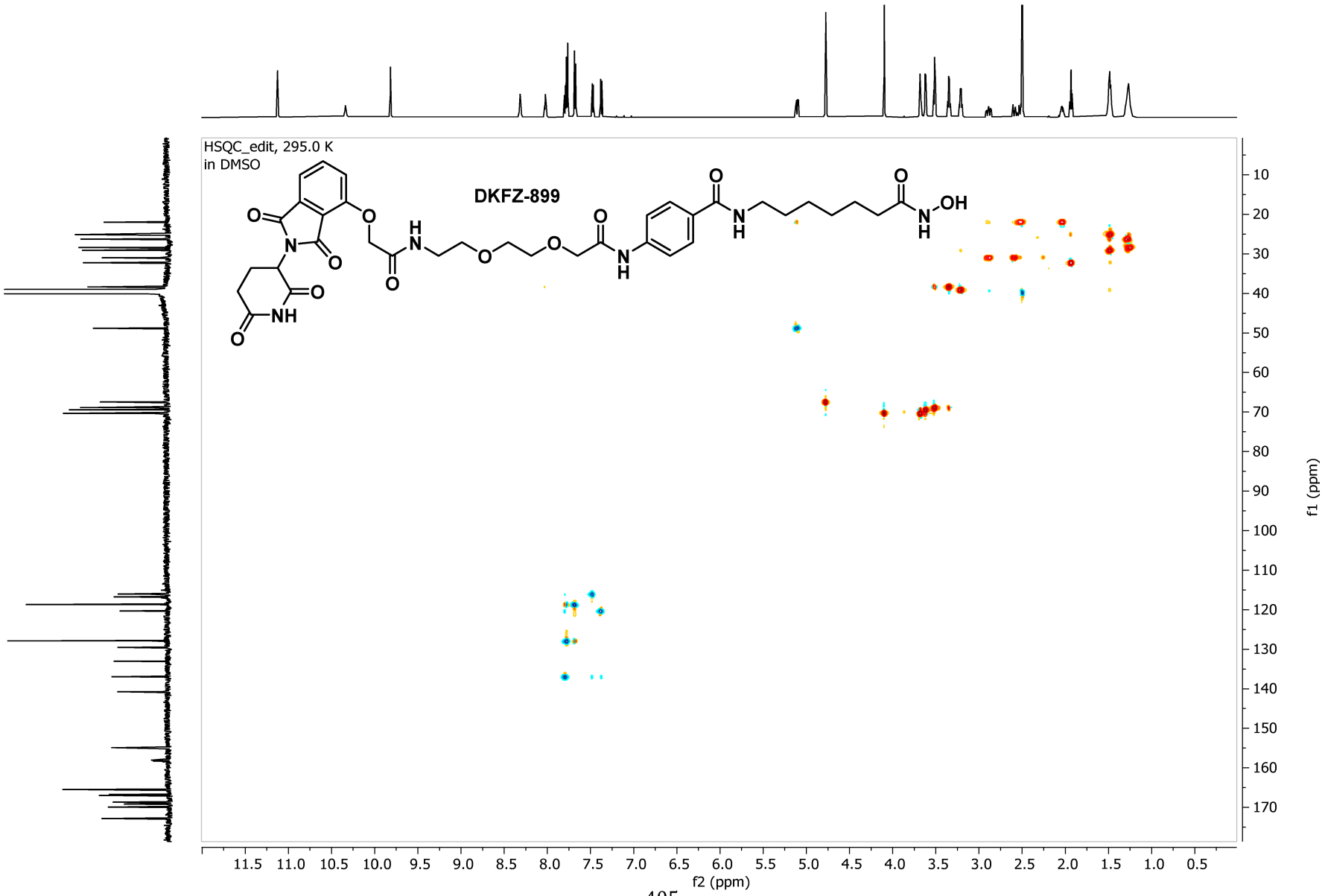
HSQC_edit, 295.0 K
in DMSO
DKFZ-899
f2 (ppm)
f1 (ppm)

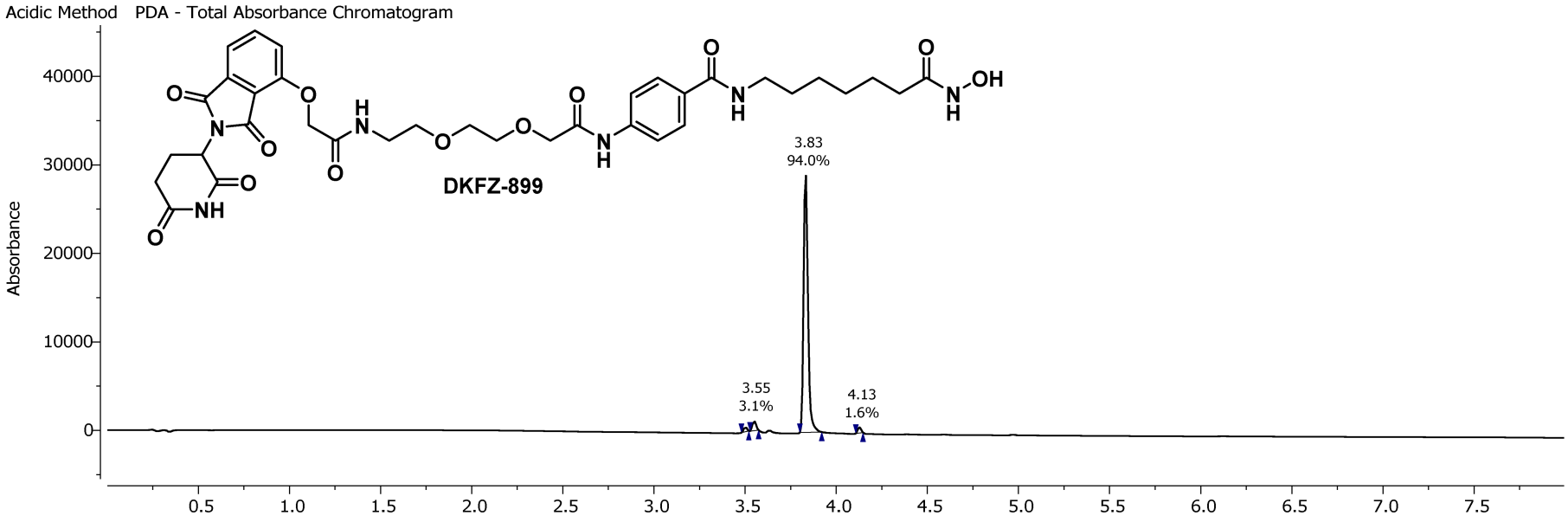
Acidic Method PDA - Total Absorbance Chromatogram
DKFZ-899
Absorbance
3.83
94.0%
3.55
3.1%
4.13
1.6%

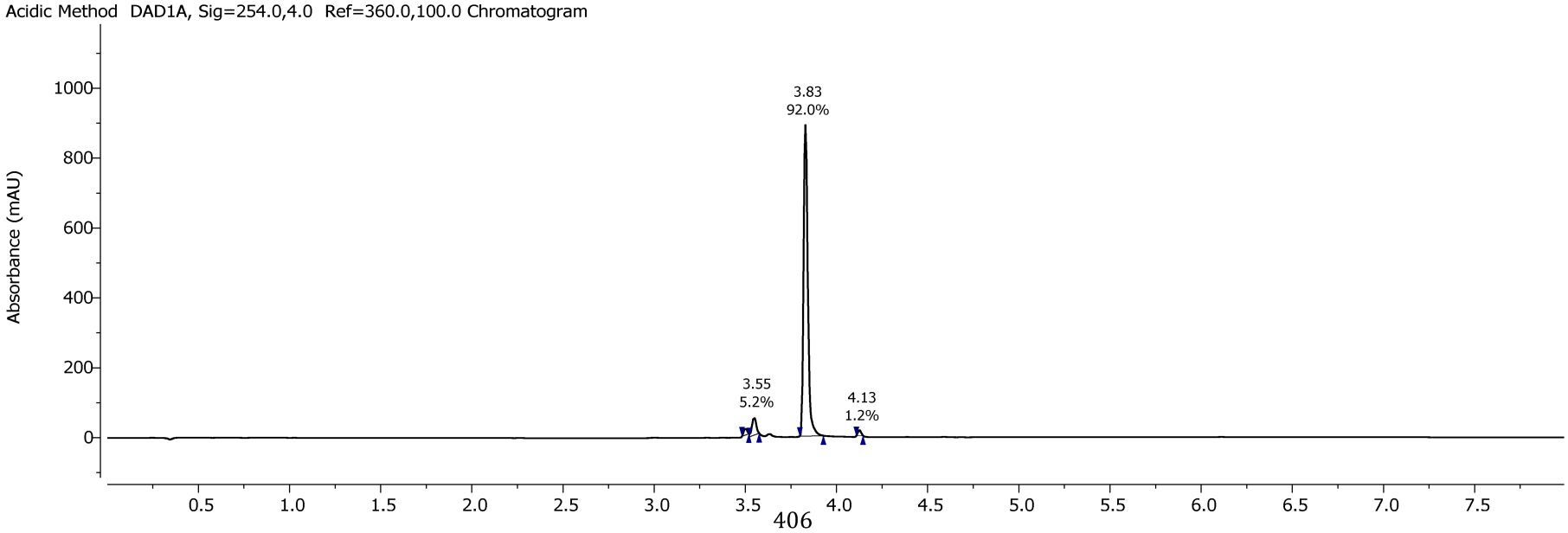
Acidic Method DAD1A, Sig=254.0,4.0 Ref=360.0,100.0 Chromatogram
Absorbance (mAU)
3.83
92.0%
3.55
5.2%
4.13
1.2%

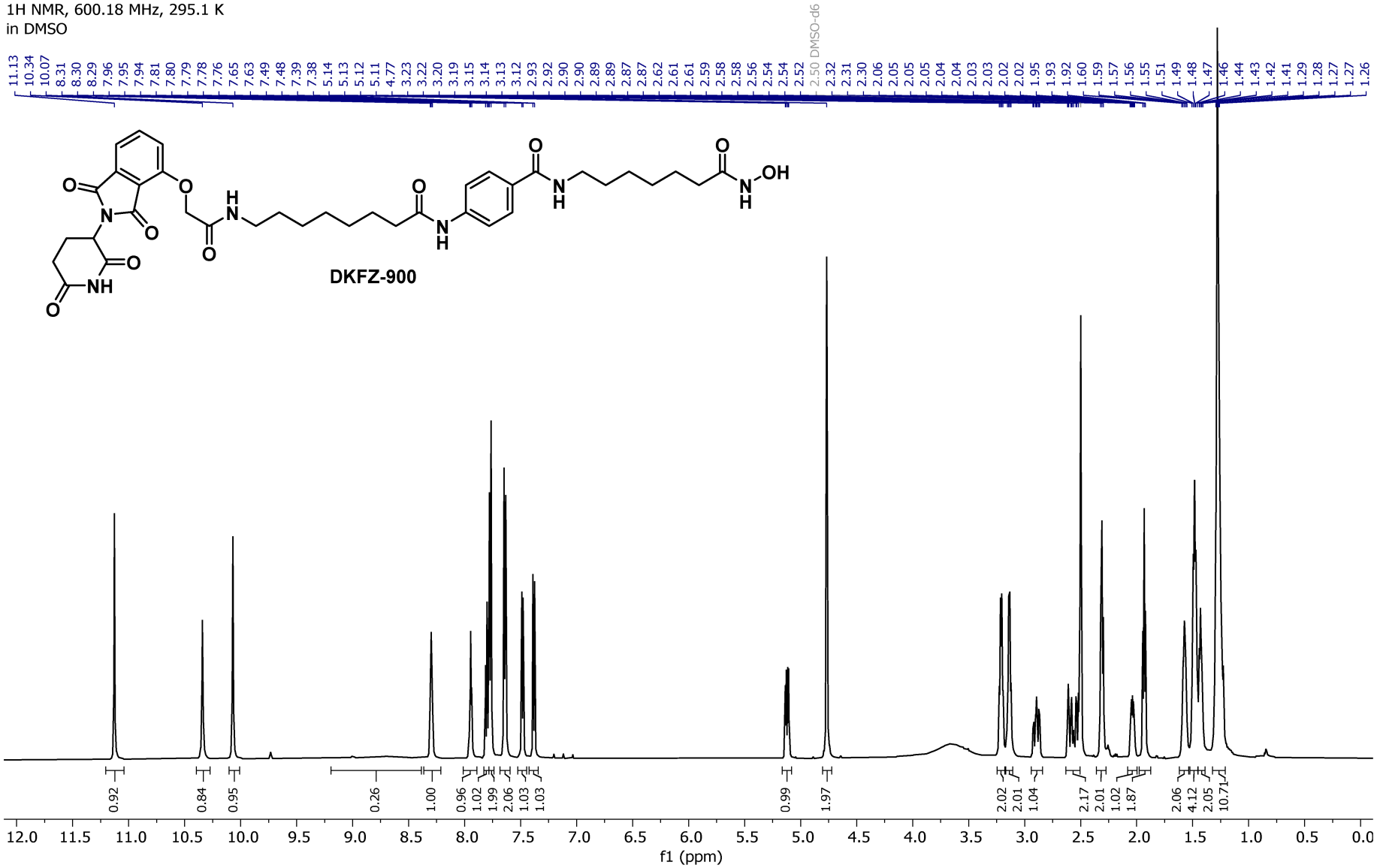
1H NMR, 600.18 MHz, 295.1 K
in DMSO
DKFZ-900
f1 (ppm)

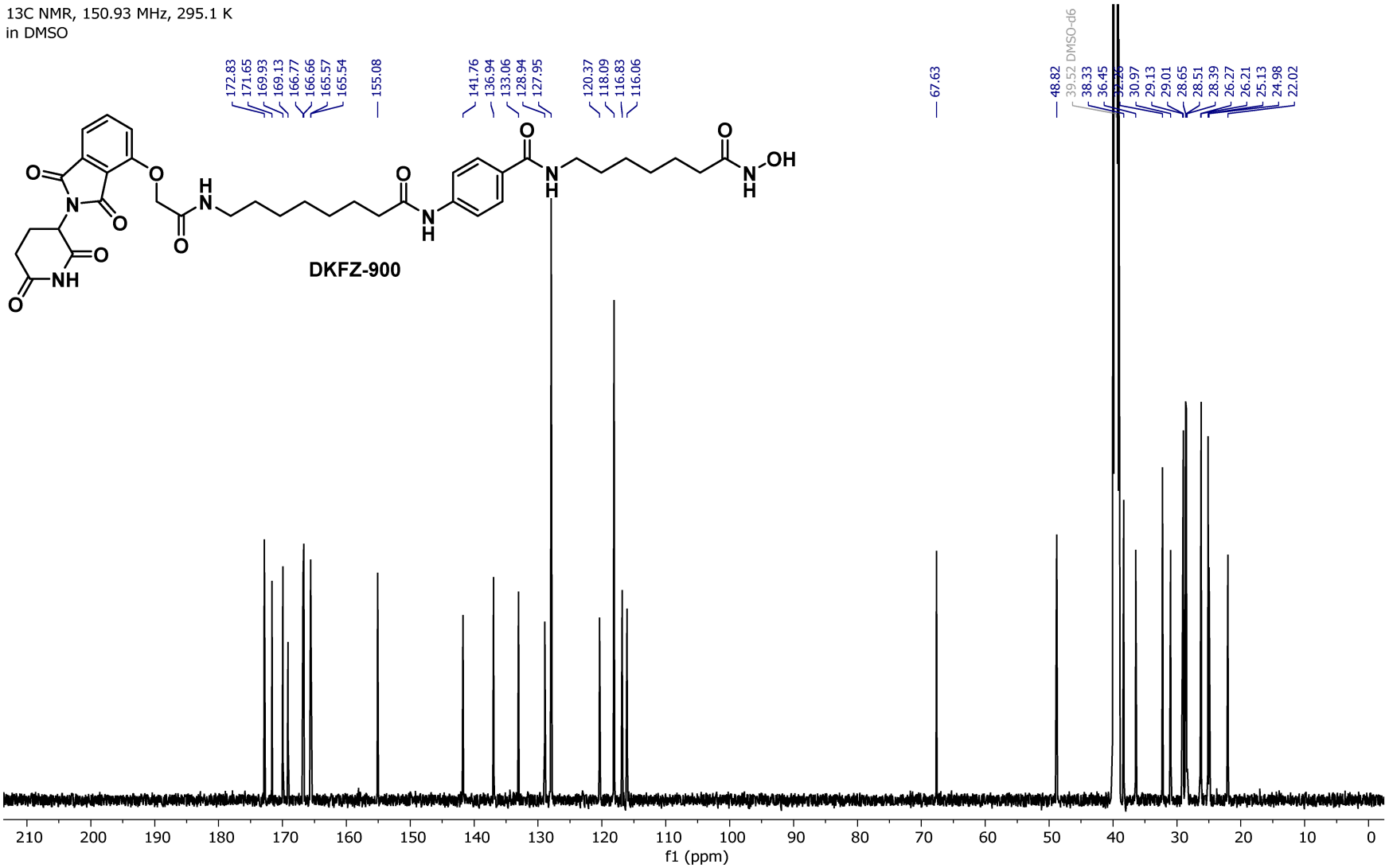
13C NMR, 150.93 MHz, 295.1 K
in DMSO
172.83
171.65
169.93
169.13
166.77
166.66
165.57
165.54
155.08
141.76
136.94
133.06
128.94
127.95
120.37
118.09
116.83
116.06
67.63
48.82
39.52 DMSO-d6
38.33
36.45
30.97
29.13
29.01
28.65
28.51
28.39
26.27
26.21
25.13
24.98
22.02
DKFZ-900
f1 (ppm)

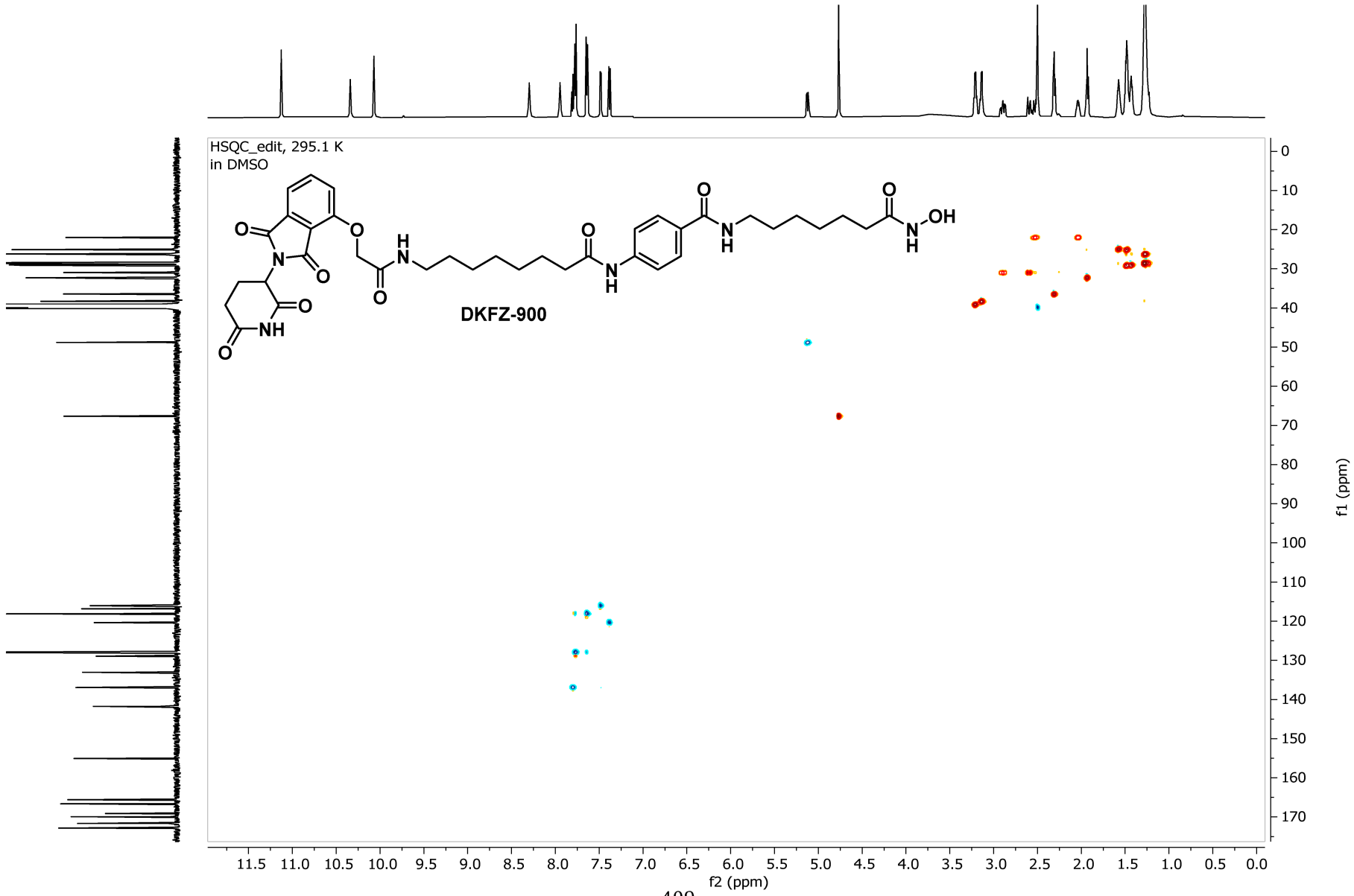
HSQC_edit, 295.1 K
in DMSO
DKFZ-900
f2 (ppm)
f1 (ppm)

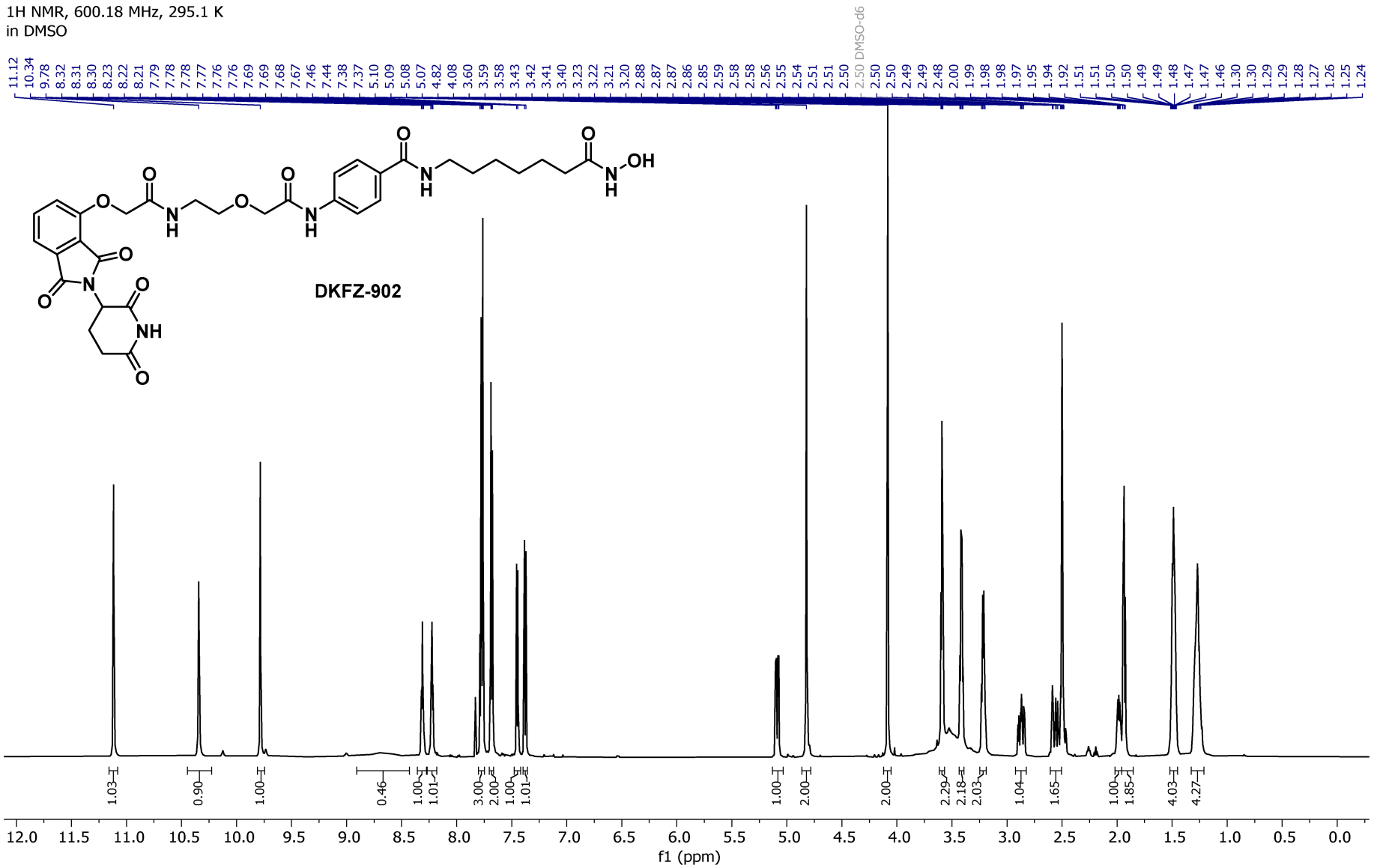
1H NMR, 600.18 MHz, 295.1 K
in DMSO
DKFZ-902
f1 (ppm)

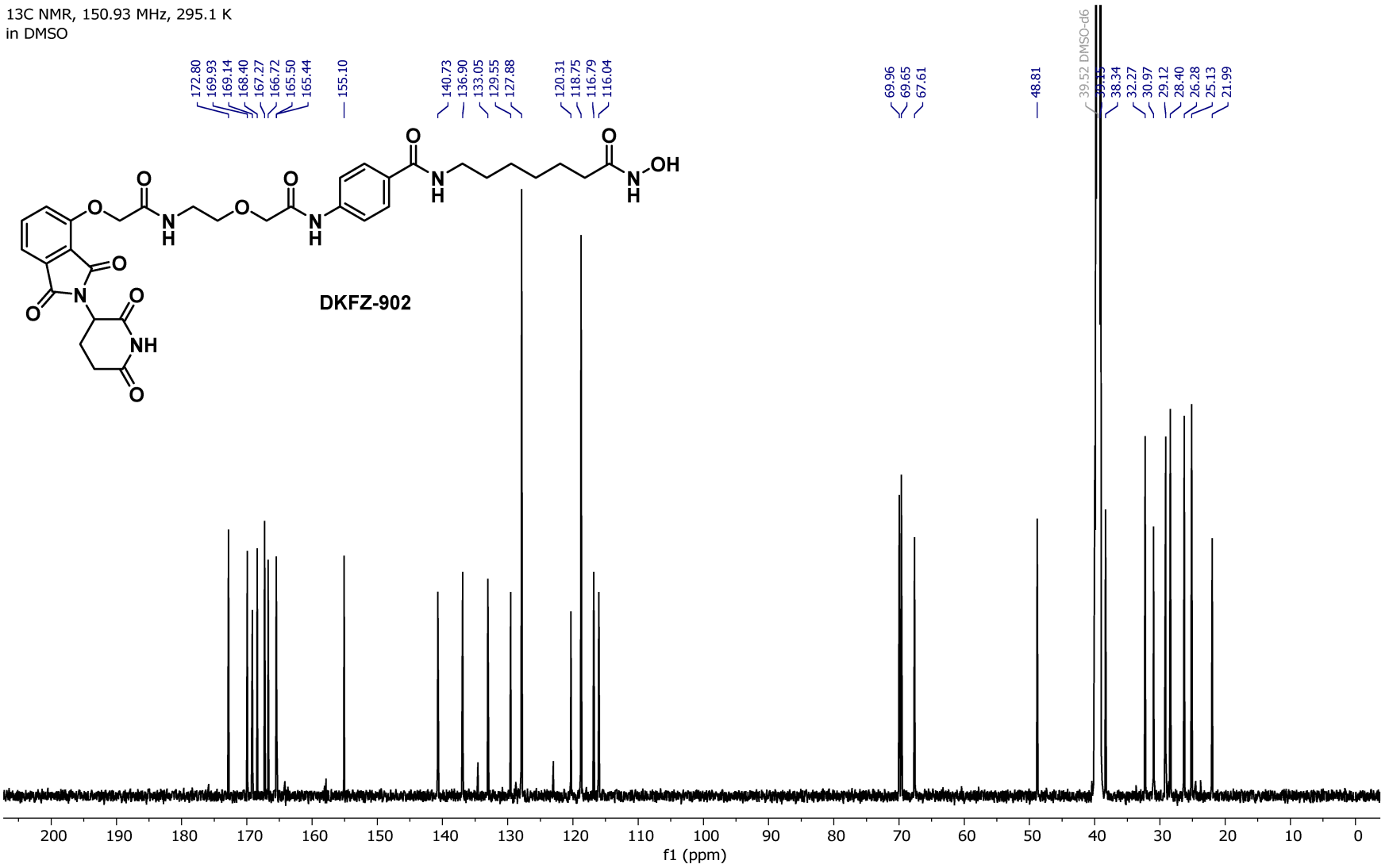
13C NMR, 150.93 MHz, 295.1 K
in DMSO
172.80
169.93
169.14
168.40
167.27
166.72
165.50
165.44
155.10
140.73
136.90
133.05
129.55
127.88
120.31
118.75
116.79
116.04
69.96
69.65
67.61
48.81
39.52 DMSO-d6
38.34
32.27
30.97
29.12
28.40
26.28
25.13
21.99
DKFZ-902
f1 (ppm)

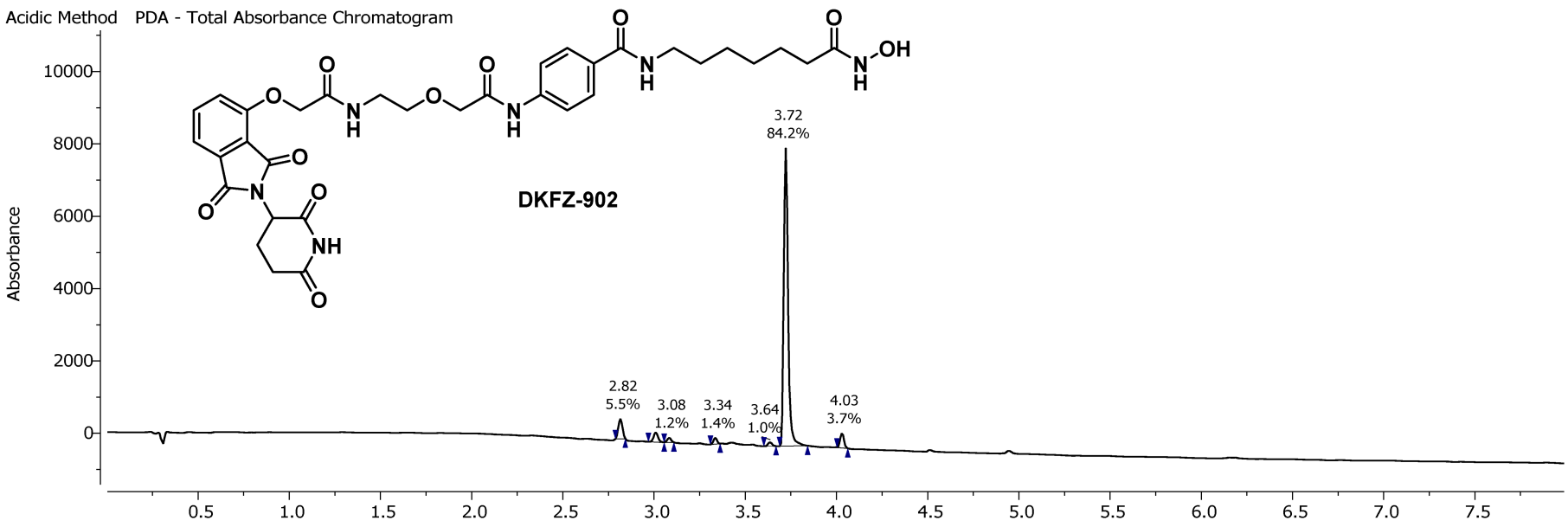
Acidic Method PDA - Total Absorbance Chromatogram
DKFZ-902
Absorbance
3.72
84.2%
2.82
5.5%
3.08
1.2%
3.34
1.4%
3.64
1.0%
4.03
3.7%

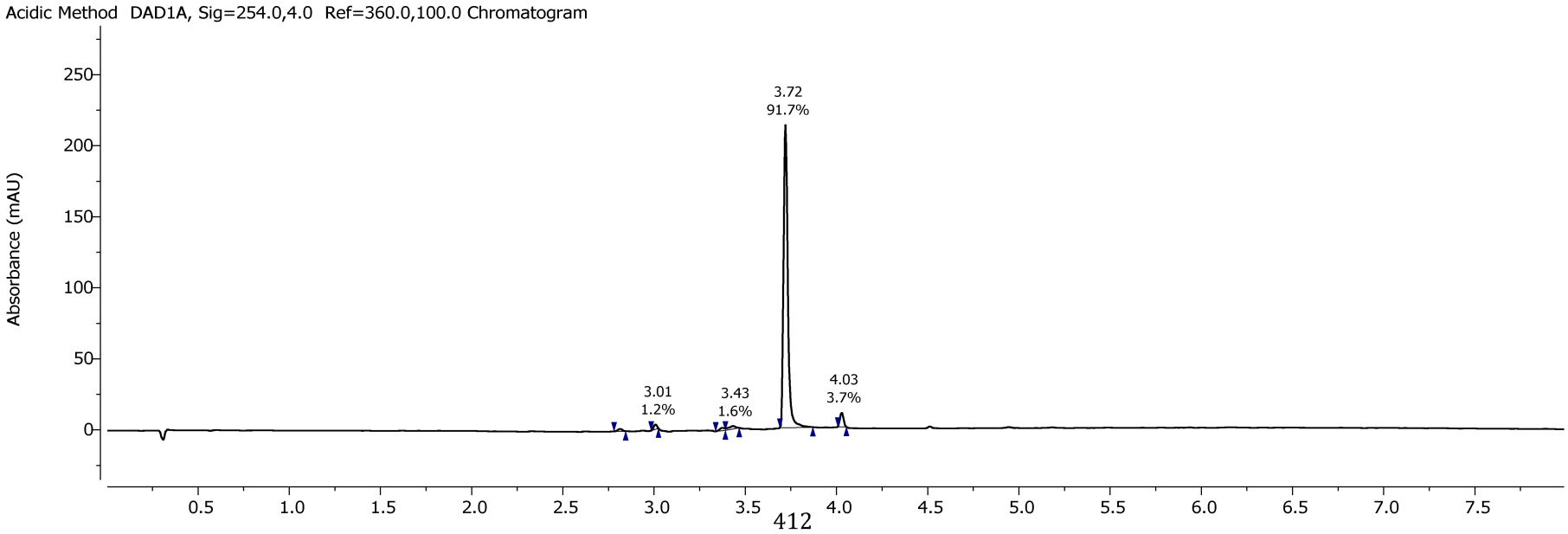
Acidic Method DAD1A, Sig=254.0,4.0 Ref=360.0,100.0 Chromatogram
Absorbance (mAU)
3.72
91.7%
3.01
1.2%
3.43
1.6%
4.03
3.7%

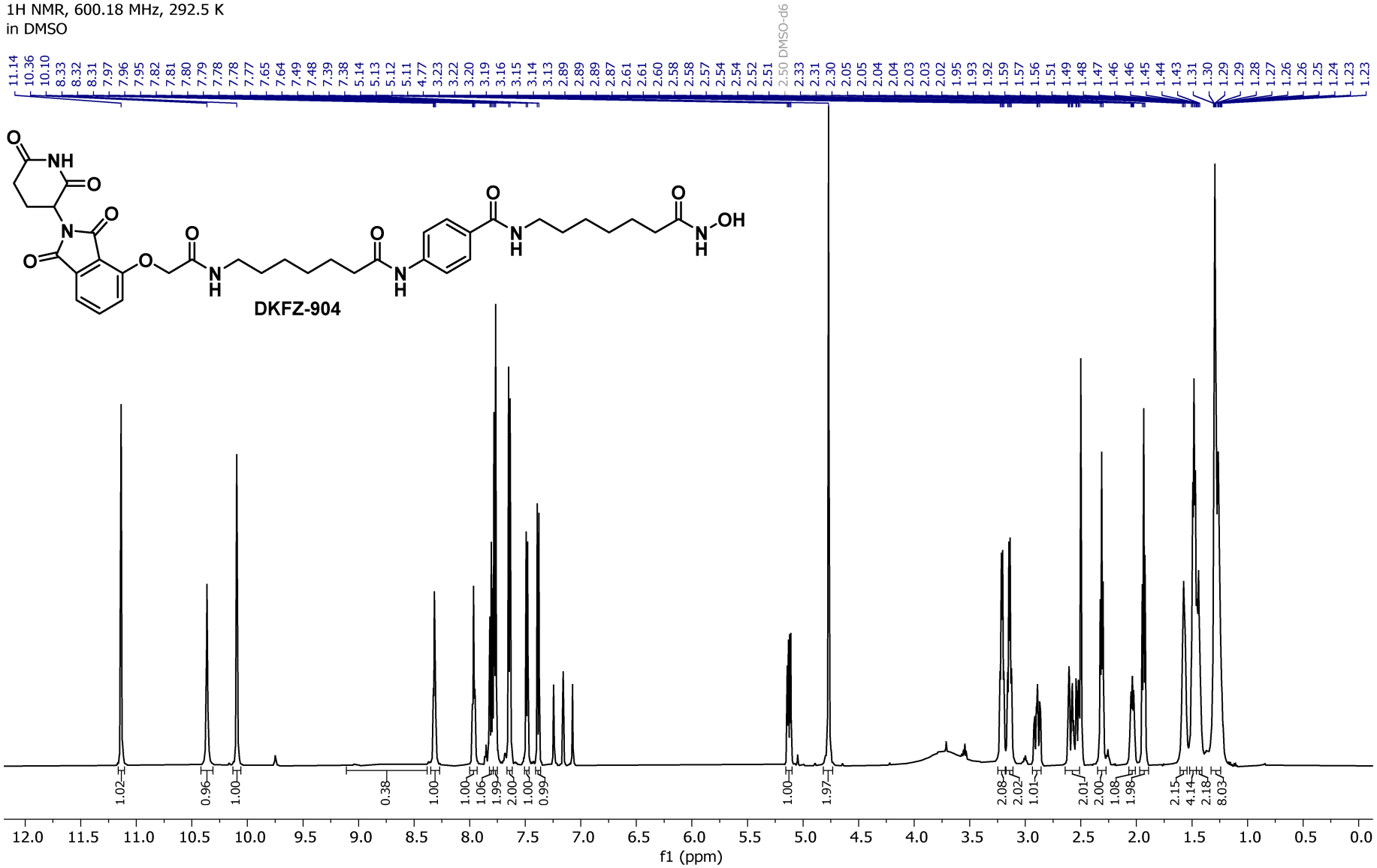
1H NMR, 600.18 MHz, 292.5 K
in DMSO
2.50 DMSO-d6
DKFZ-904
f1 (ppm)

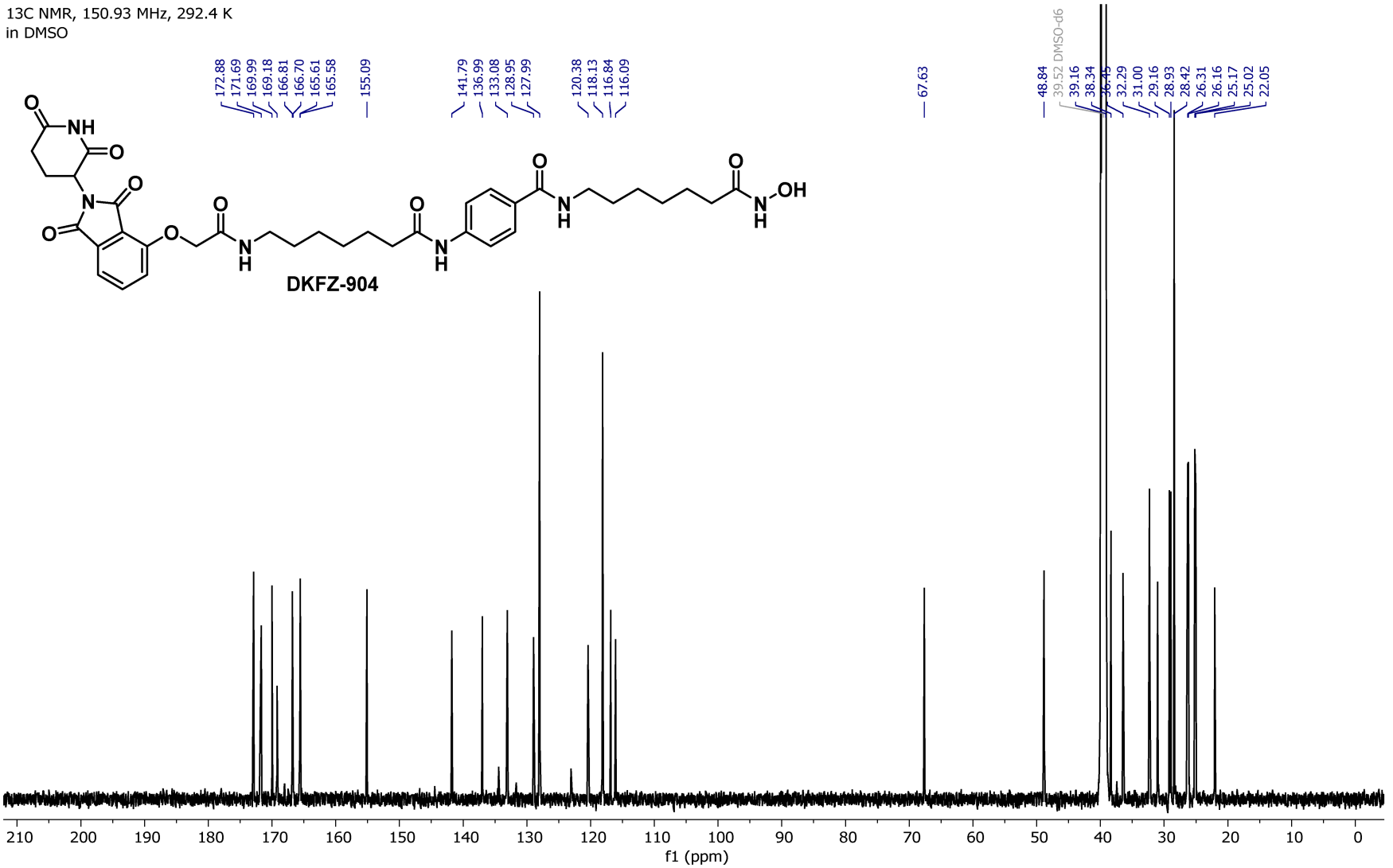
13C NMR, 150.93 MHz, 292.4 K
in DMSO
172.88
171.69
169.99
169.18
166.81
166.70
165.61
165.58
155.09
141.79
136.99
133.08
128.95
127.99
120.38
118.13
116.84
116.09
67.63
48.84
39.52 DMSO-d6
39.16
38.34
36.45
32.29
31.00
29.16
28.93
28.42
26.31
26.16
25.17
25.02
22.05
DKFZ-904
f1 (ppm)

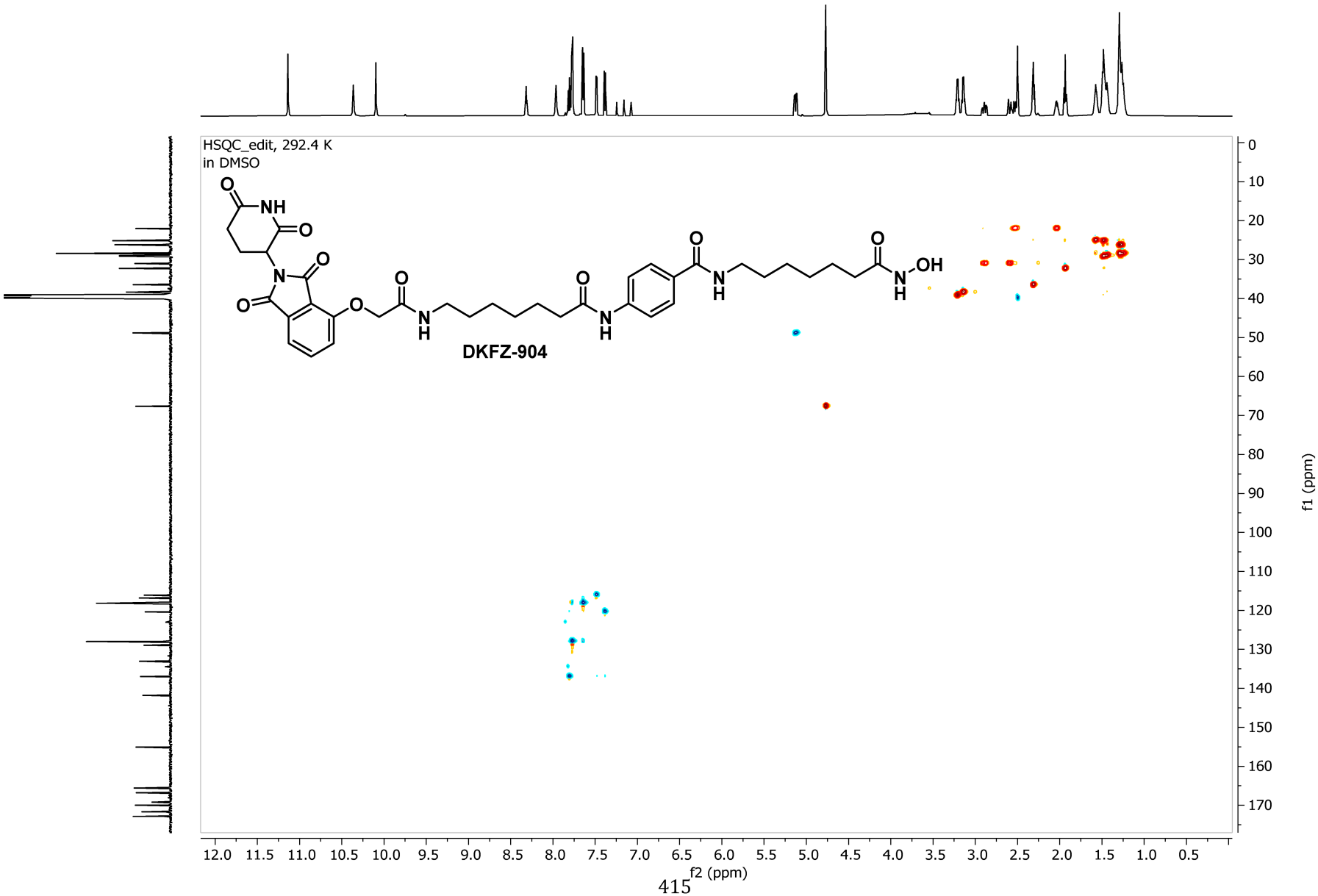
HSQC_edit, 292.4 K
in DMSO
DKFZ-904
f2 (ppm)
f1 (ppm)

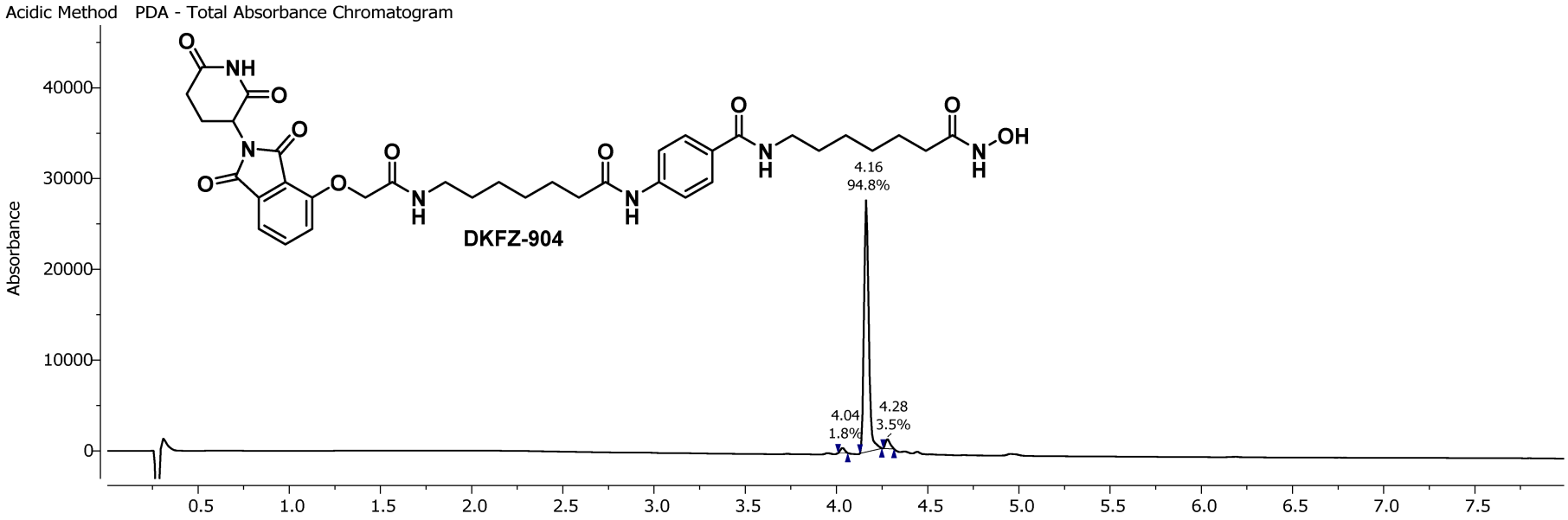
Acidic Method PDA - Total Absorbance Chromatogram
Absorbance
40000
30000
20000
10000
0
DKFZ-904
4.16
94.8%
4.04
1.8%
4.28
3.5%
0.5
1.0
1.5
2.0
2.5
3.0
3.5
4.0
4.5
5.0
5.5
6.0
6.5
7.0
7.5

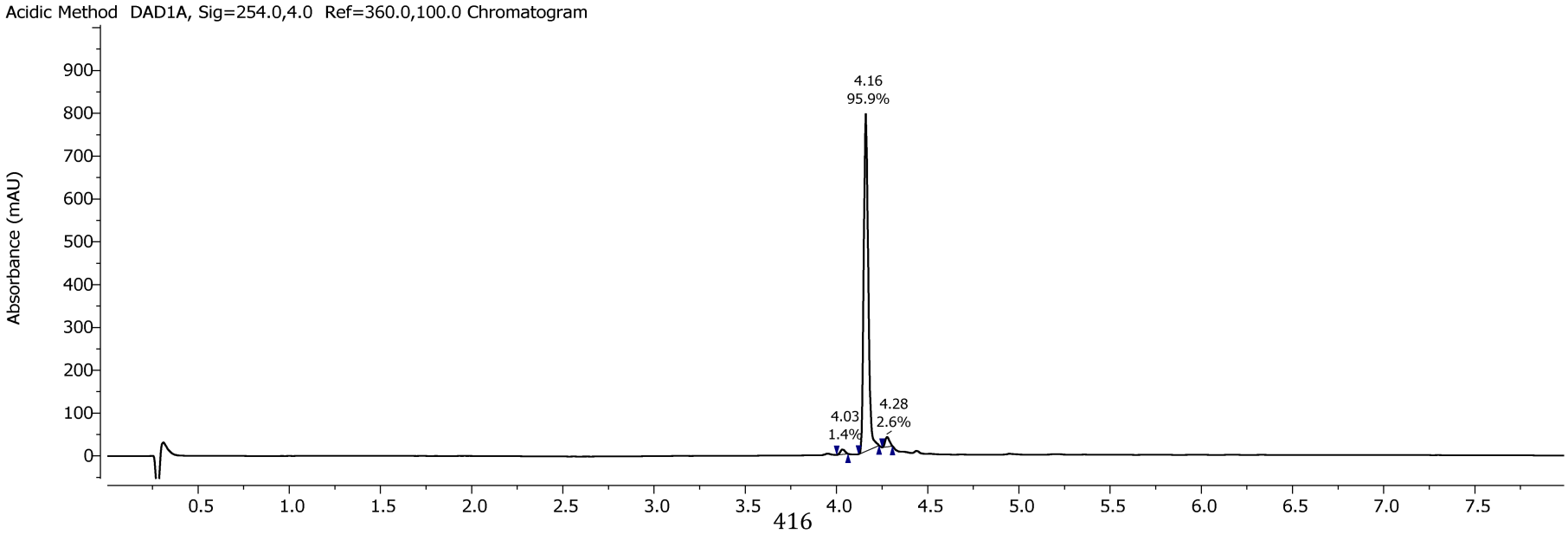
Acidic Method DAD1A, Sig=254.0,4.0 Ref=360.0,100.0 Chromatogram
Absorbance (mAU)
900
800
700
600
500
400
300
200
100
0
4.16
95.9%
4.03
1.4%
4.28
2.6%
0.5
1.0
1.5
2.0
2.5
3.0
3.5
4.0
4.5
5.0
5.5
6.0
6.5
7.0
7.5

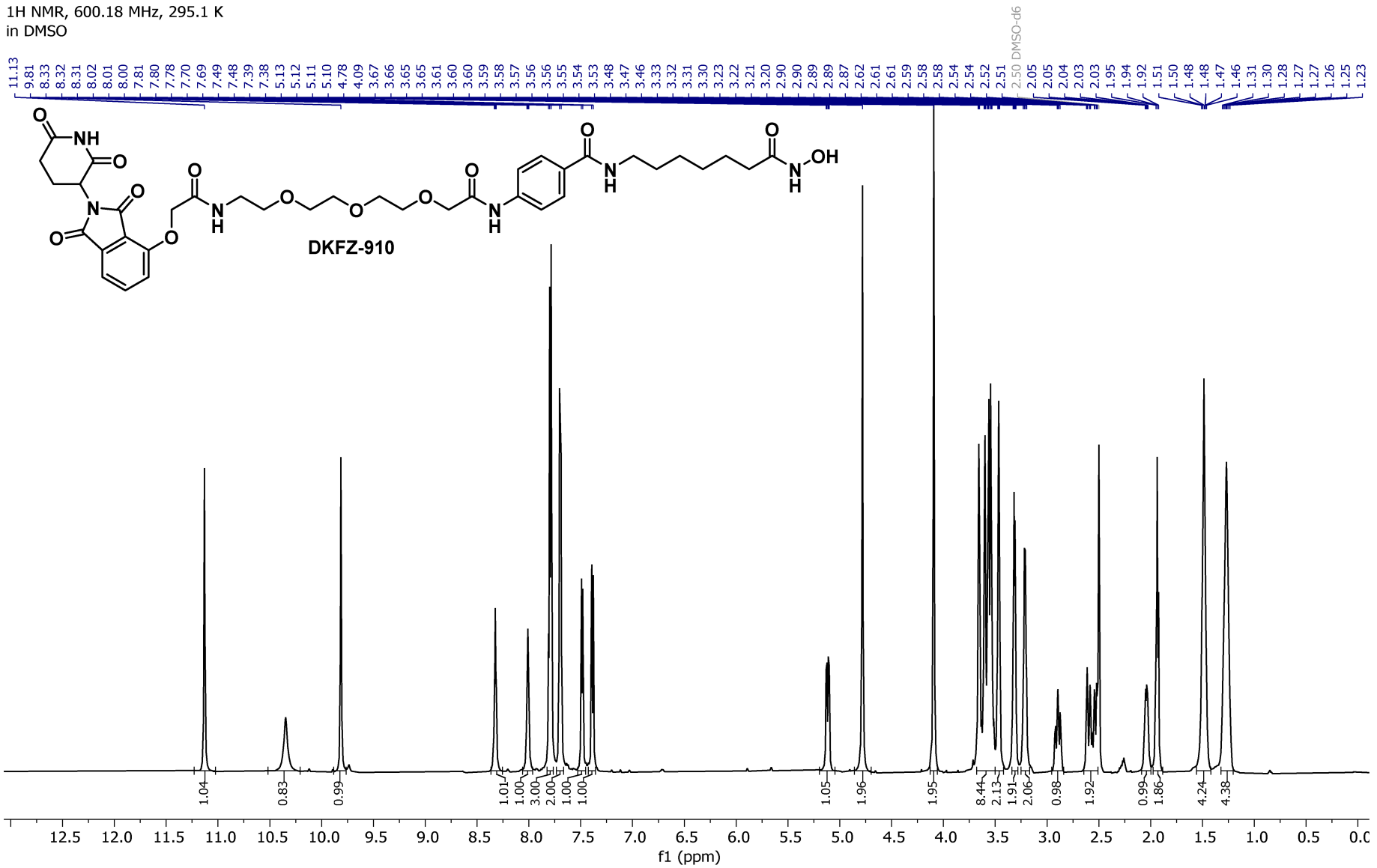
1H NMR, 600.18 MHz, 295.1 K
in DMSO
DKFZ-910
f1 (ppm)

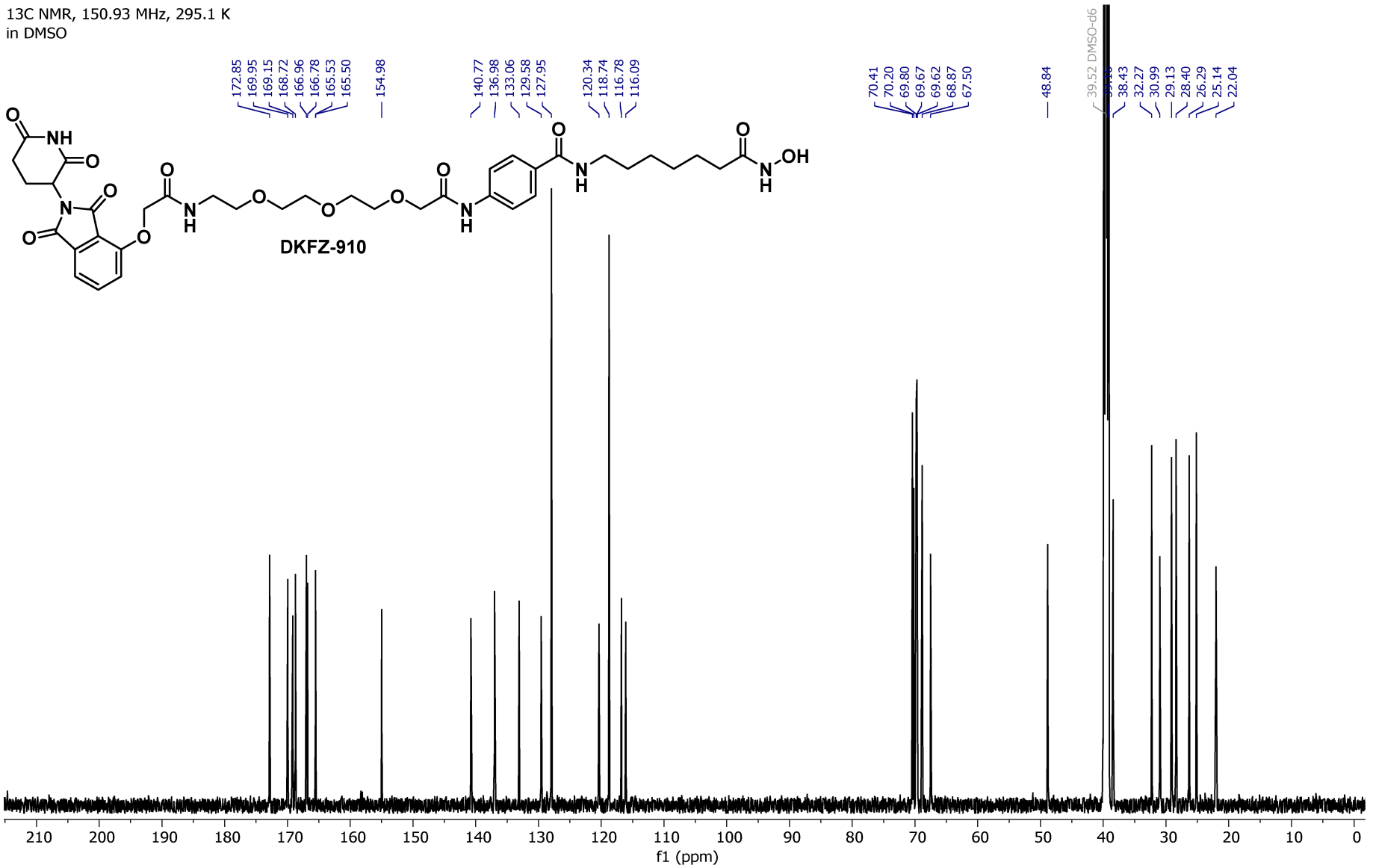
13C NMR, 150.93 MHz, 295.1 K
in DMSO
172.85
169.95
169.15
168.72
166.96
166.78
165.53
165.50
154.98
140.77
136.98
133.06
129.58
127.95
120.34
118.74
116.78
116.09
70.41
70.20
69.80
69.67
69.62
68.87
67.50
48.84
39.52 DMSO-d6
38.43
32.27
30.99
29.13
28.40
26.29
25.14
22.04
DKFZ-910
f1 (ppm)

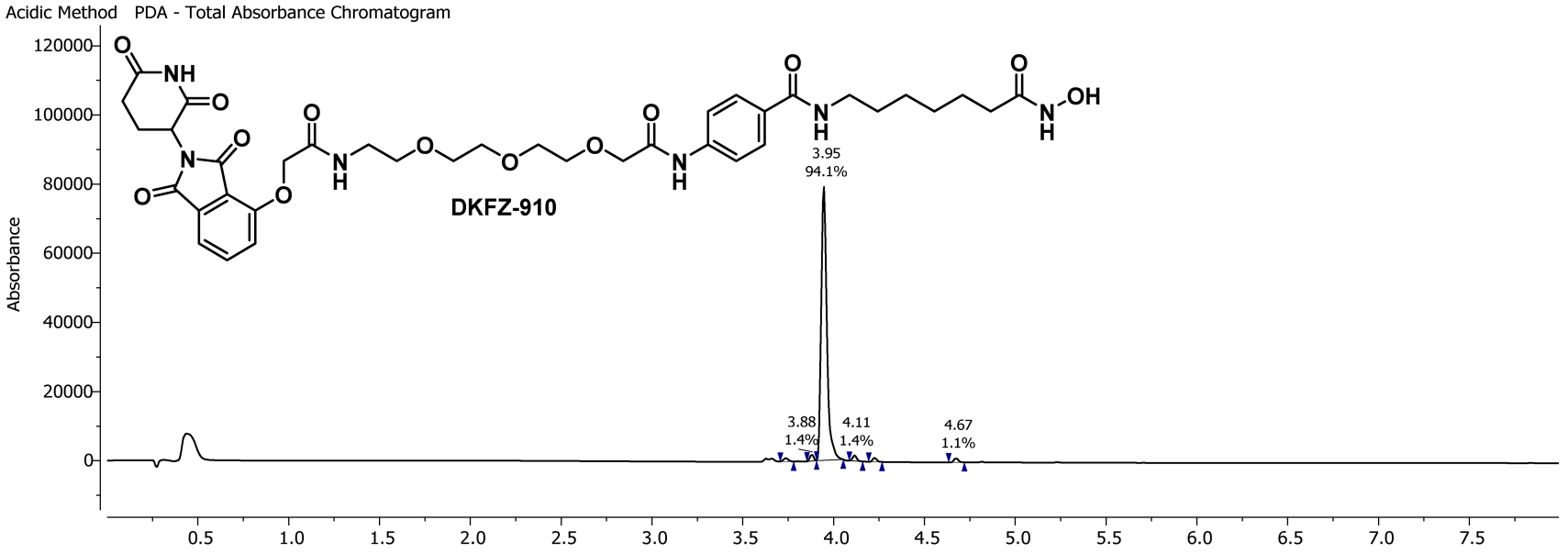
Acidic Method PDA - Total Absorbance Chromatogram
DKFZ-910
Absorbance
3.95
94.1%
3.88
1.4%
4.11
1.4%
4.67
1.1%

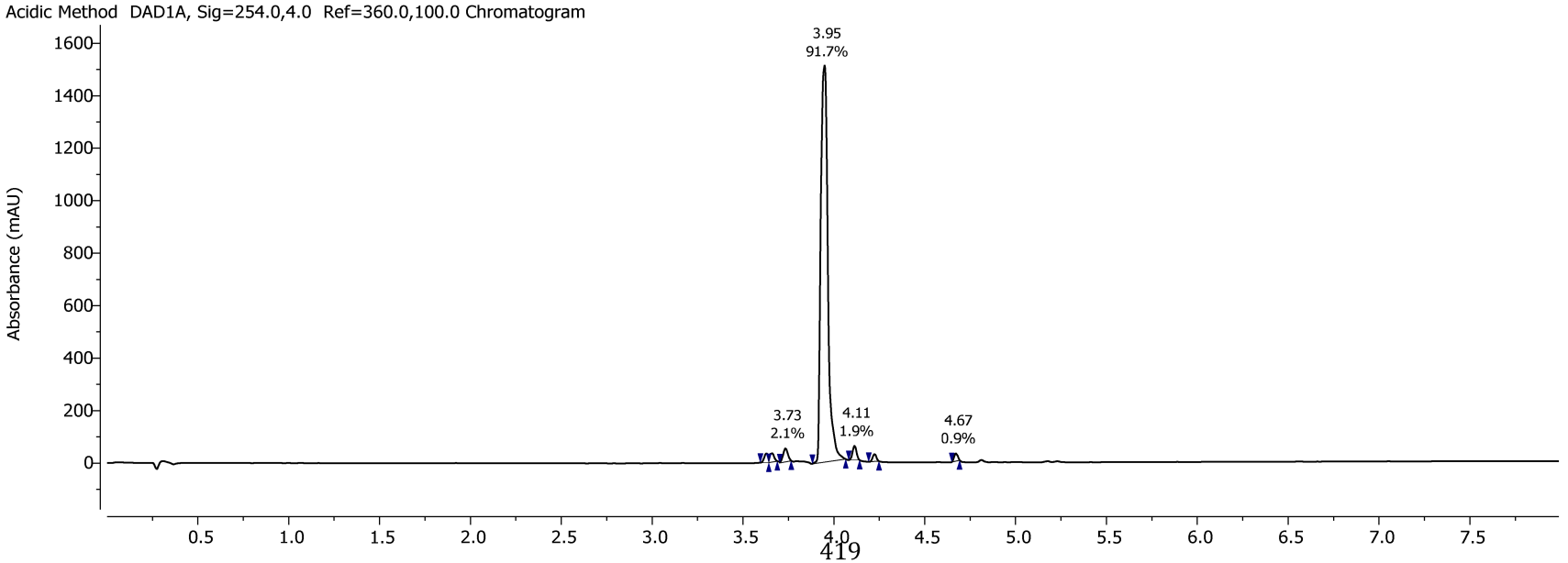
Acidic Method DAD1A, Sig=254.0,4.0 Ref=360.0,100.0 Chromatogram
Absorbance (mAU)
3.95
91.7%
3.73
2.1%
4.11
1.9%
4.67
0.9%

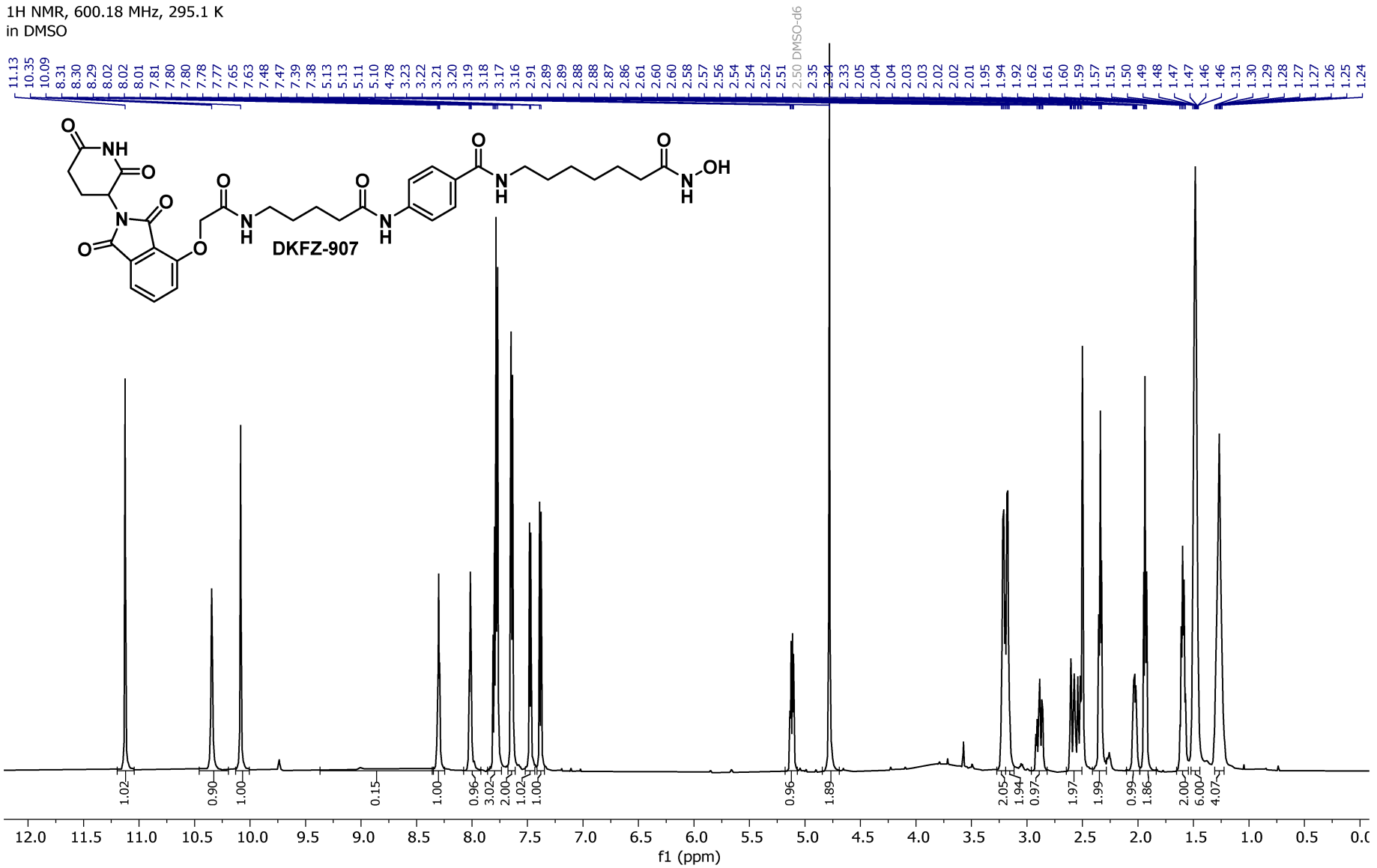
1H NMR, 600.18 MHz, 295.1 K
in DMSO
DKFZ-907
f1 (ppm)

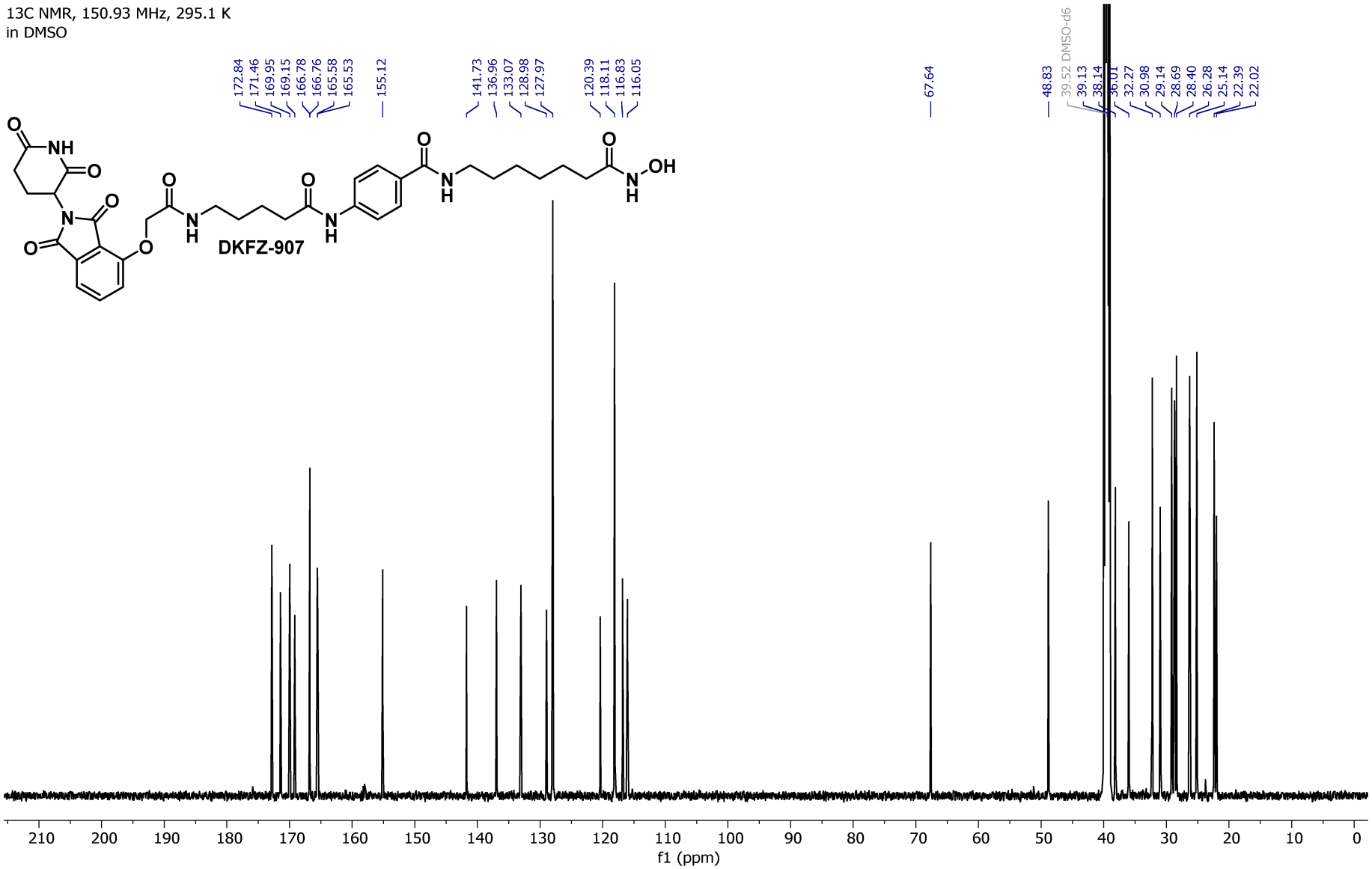
13C NMR, 150.93 MHz, 295.1 K
in DMSO
172.84
171.46
169.95
169.15
166.78
166.76
165.58
165.53
155.12
141.73
136.96
133.07
128.98
127.97
120.39
118.11
116.83
116.05
67.64
48.83
39.52 DMSO-d6
39.13
38.14
36.01
32.27
30.98
29.14
28.69
28.40
26.28
25.14
22.39
22.02
DKFZ-907
f1 (ppm)

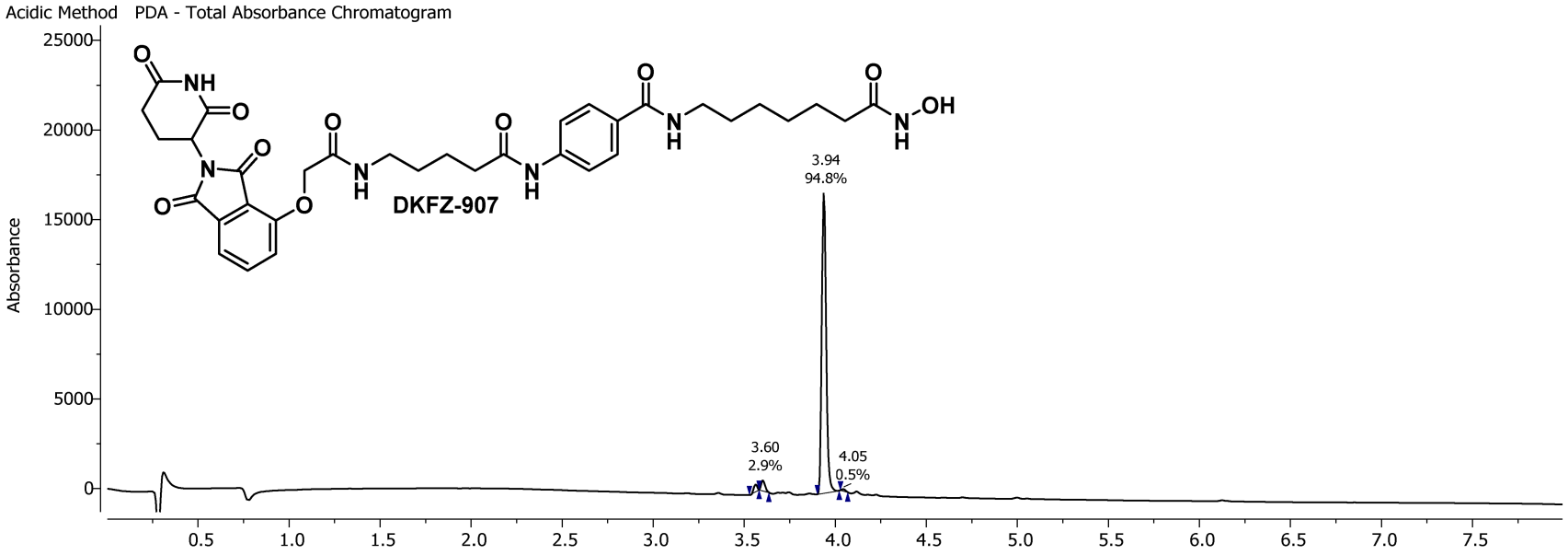
Acidic Method PDA - Total Absorbance Chromatogram
Absorbance
DKFZ-907
3.94
94.8%
3.60
2.9%
4.05
0.5%

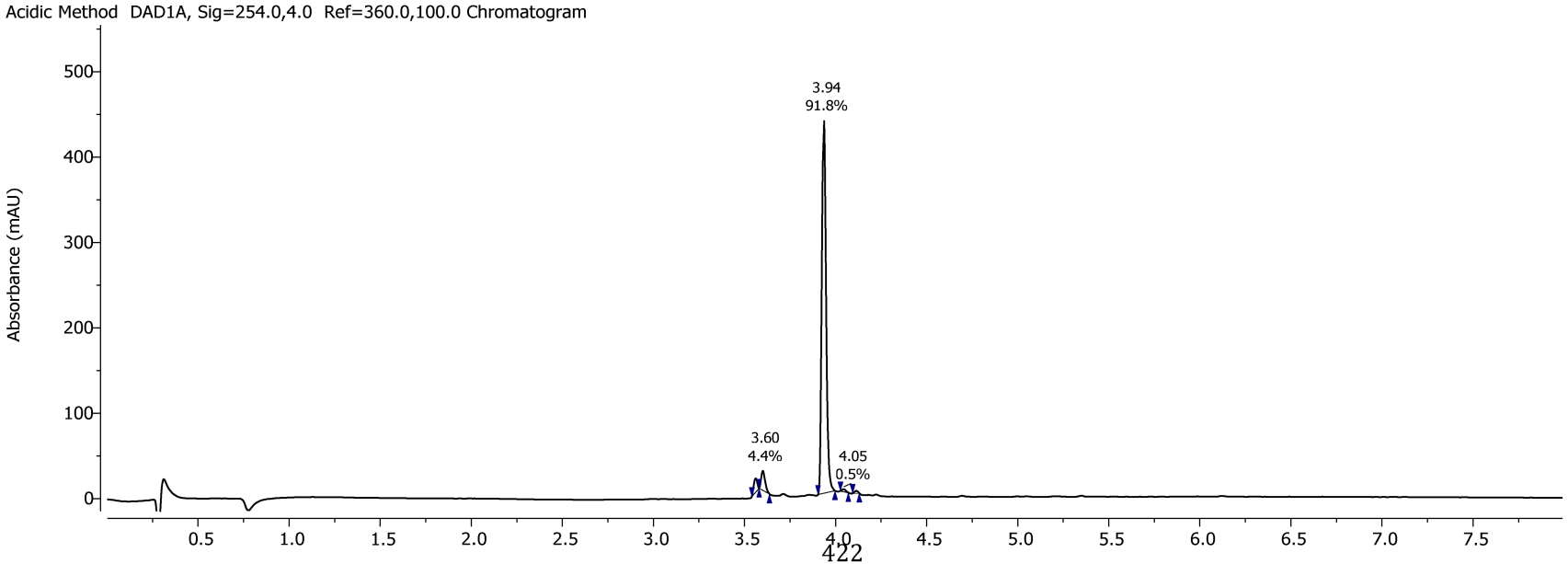
Acidic Method DAD1A, Sig=254.0,4.0 Ref=360.0,100.0 Chromatogram
Absorbance (mAU)
3.94
91.8%
3.60
4.4%
4.05
0.5%

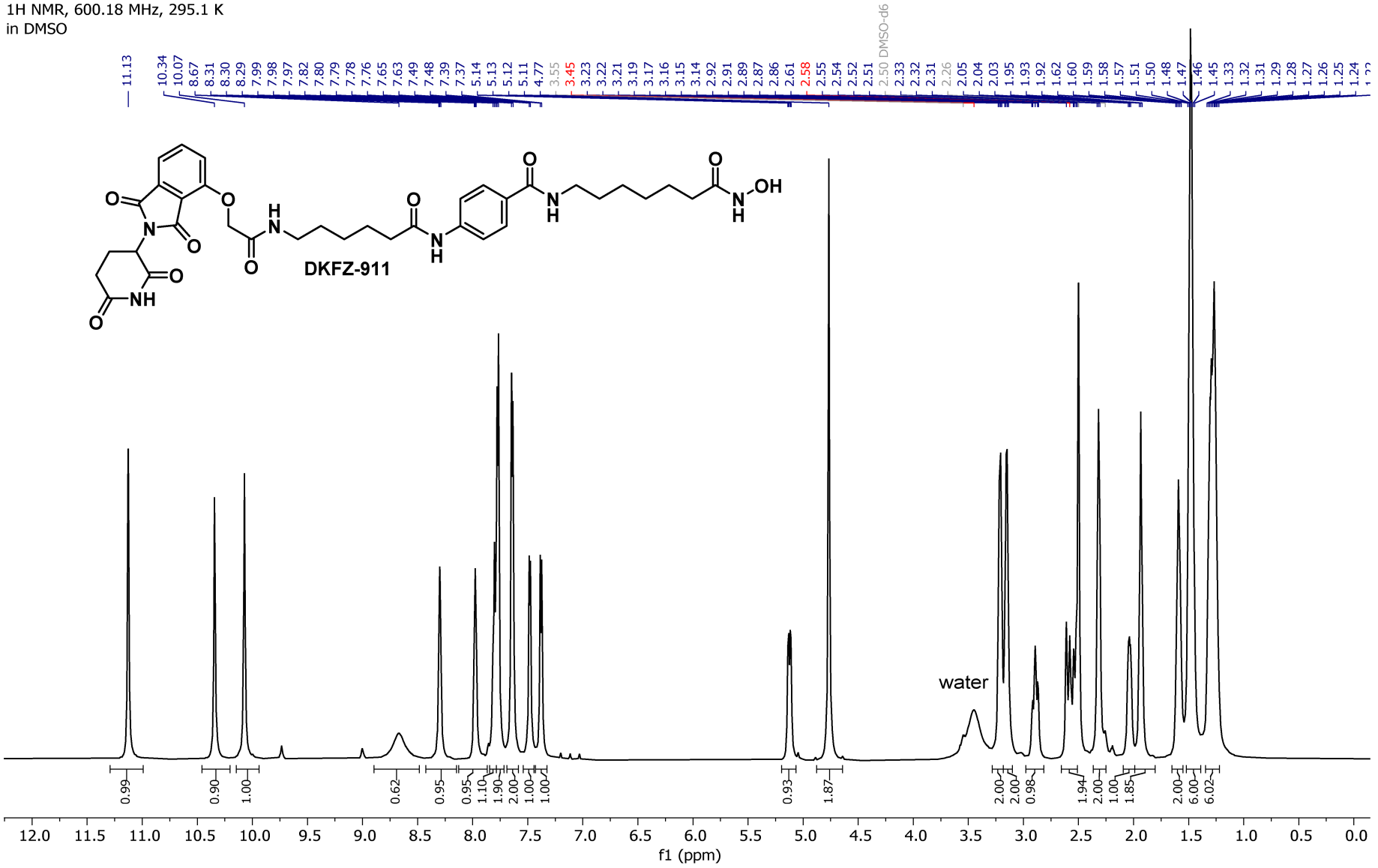
1H NMR, 600.18 MHz, 295.1 K
in DMSO
DKFZ-911
water
f1 (ppm)

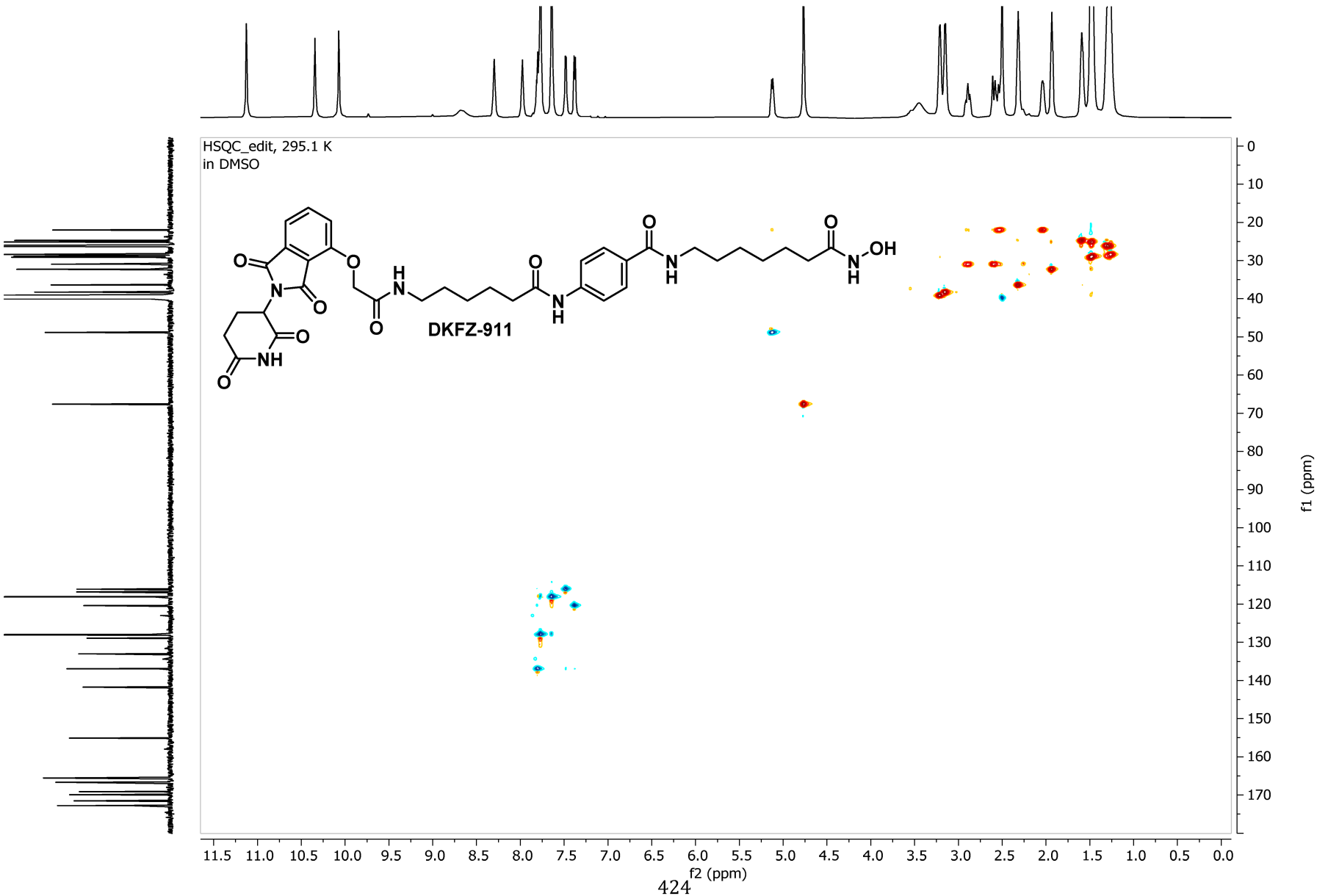
HSQC_edit, 295.1 K
in DMSO
DKFZ-911
f2 (ppm)
f1 (ppm)

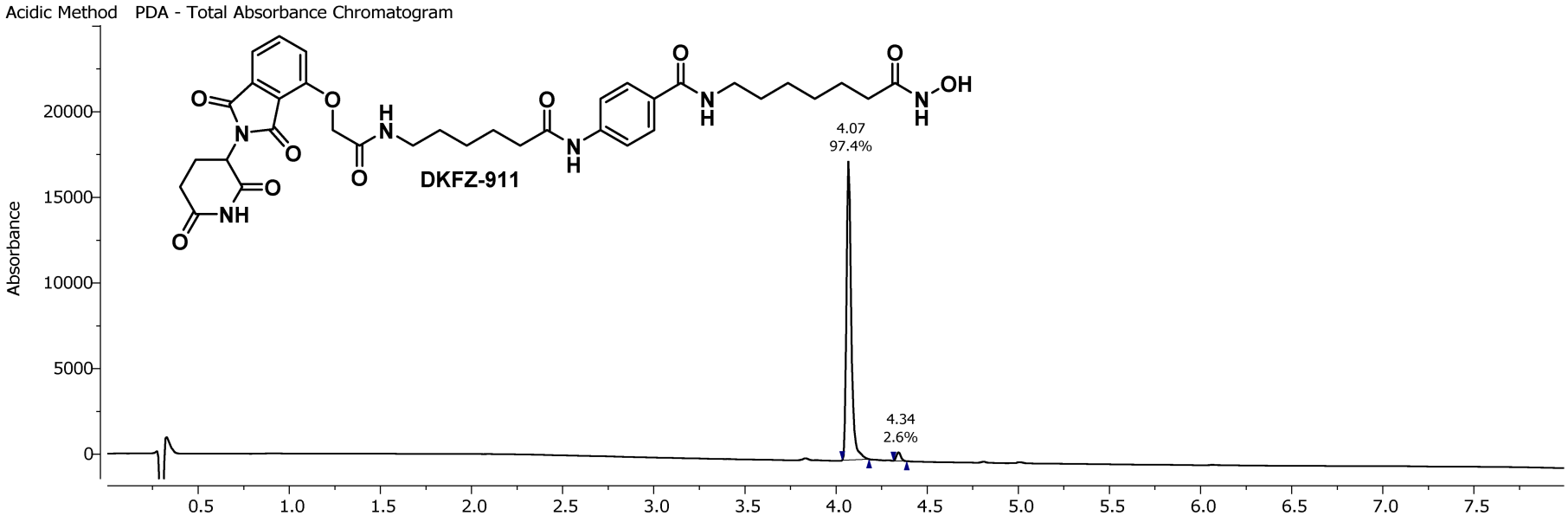
Acidic Method PDA - Total Absorbance Chromatogram
DKFZ-911
Absorbance
4.07
97.4%
4.34
2.6%

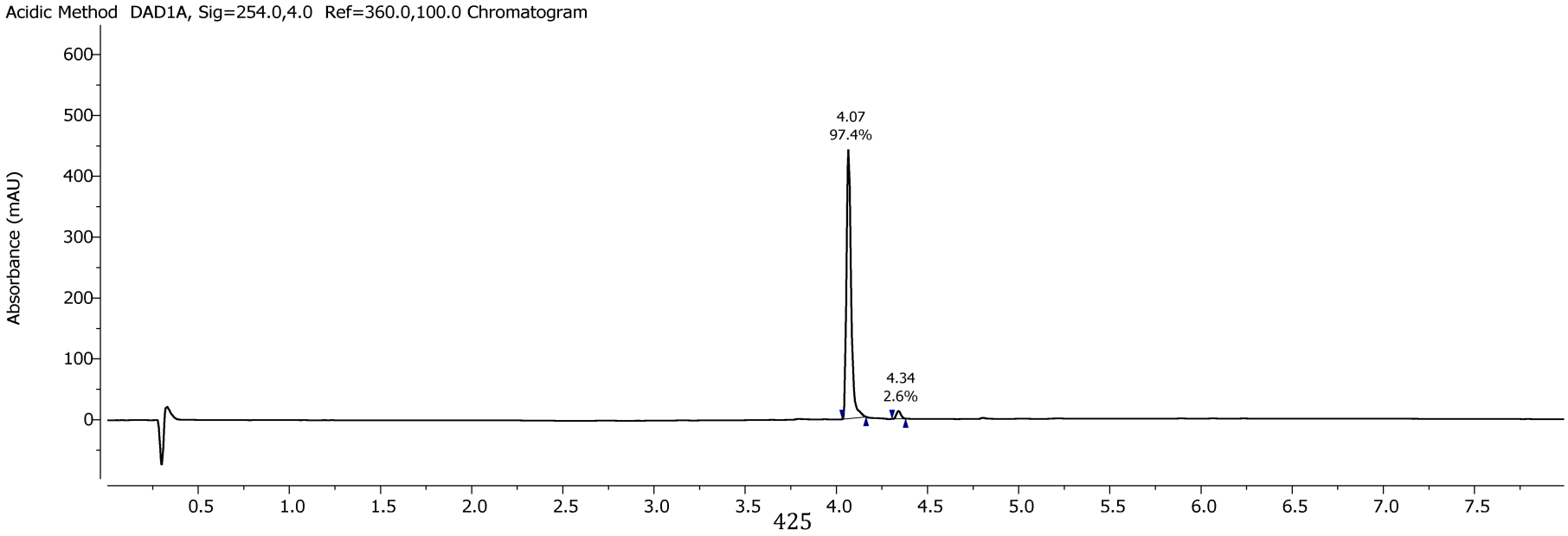
Acidic Method DAD1A, Sig=254.0,4.0 Ref=360.0,100.0 Chromatogram
Absorbance (mAU)
4.07
97.4%
4.34
2.6%

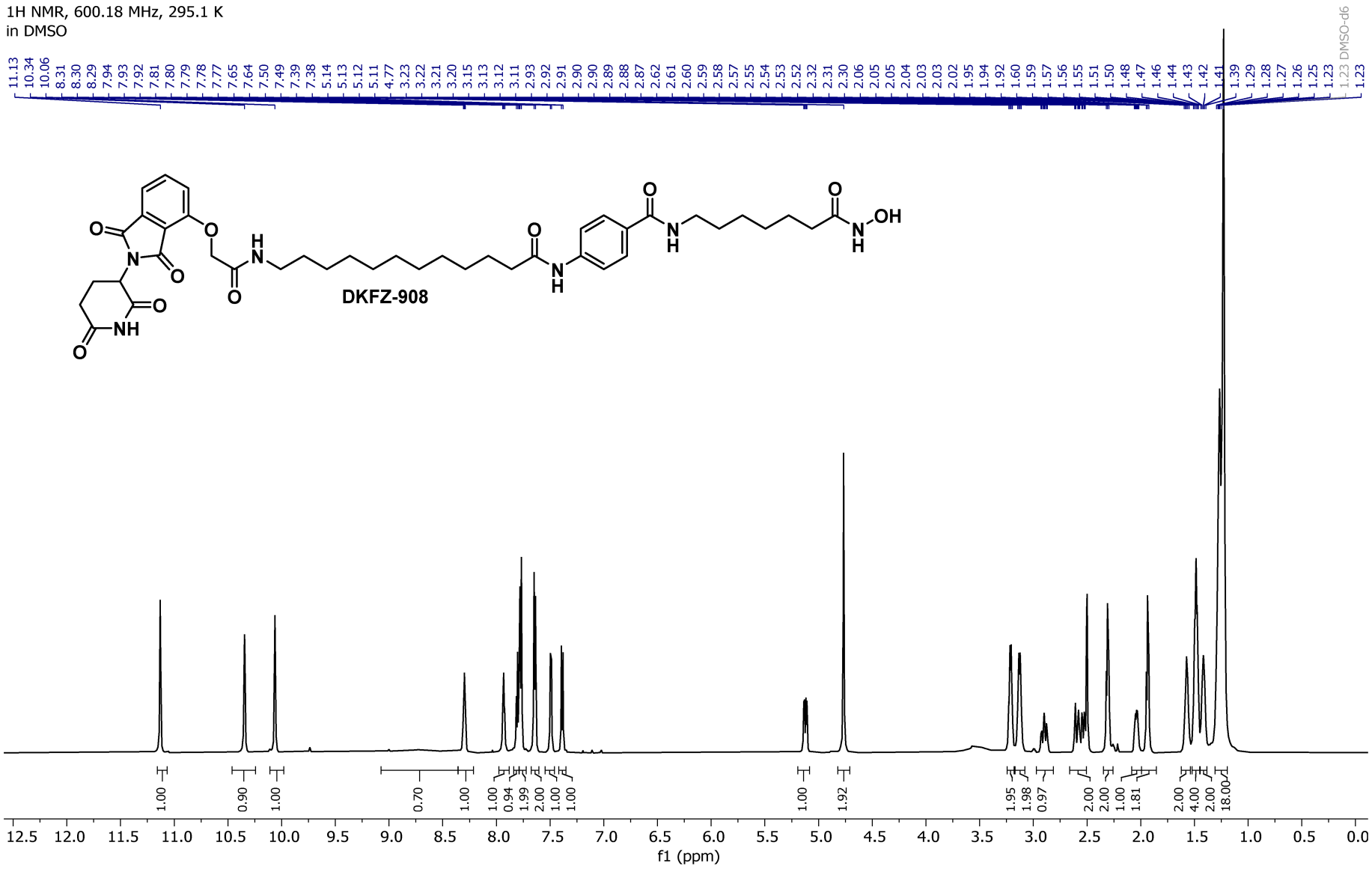
1H NMR, 600.18 MHz, 295.1 K
in DMSO
DKFZ-908
f1 (ppm)

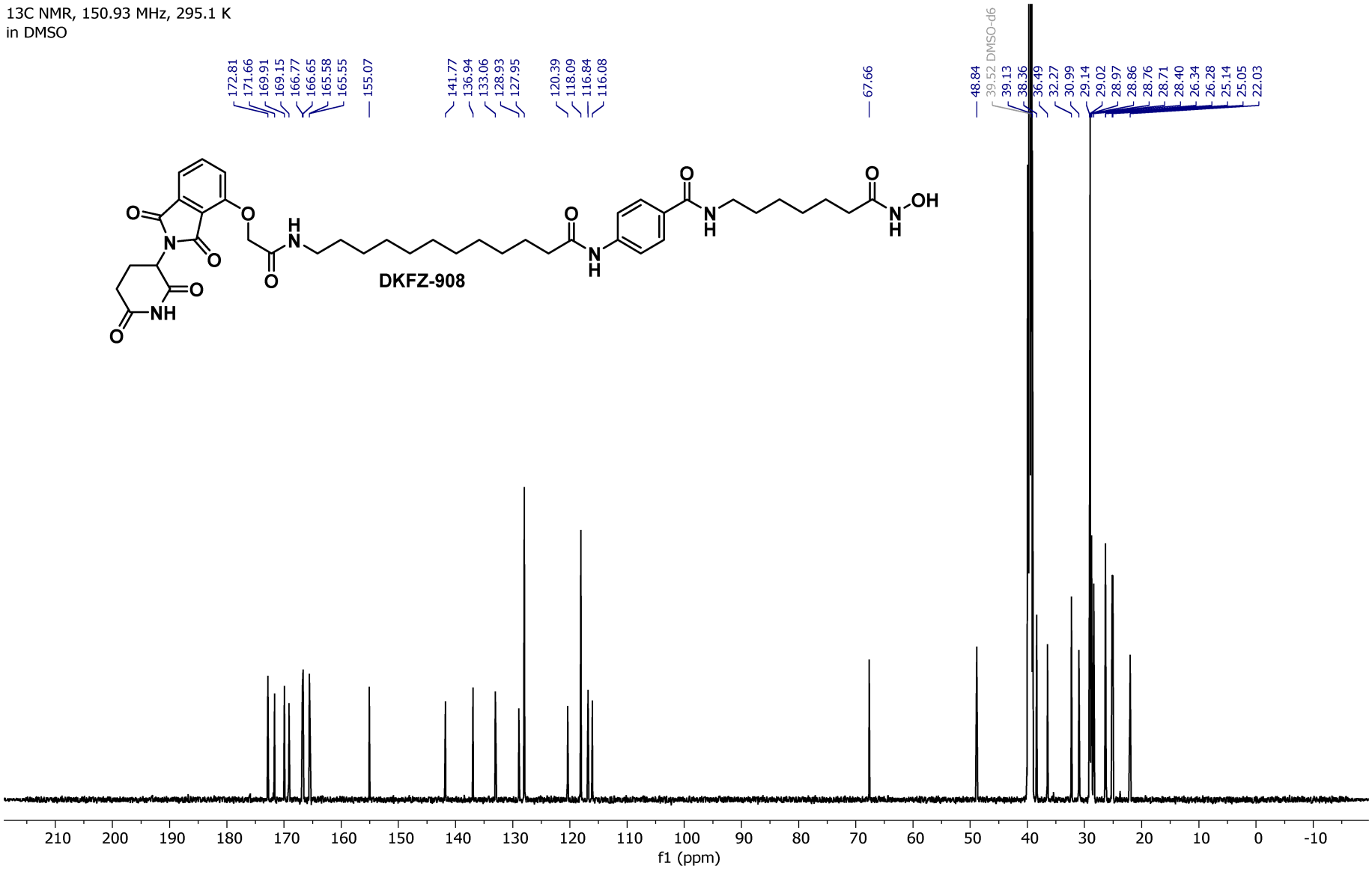
13C NMR, 150.93 MHz, 295.1 K
in DMSO
172.81
171.66
169.91
169.15
166.77
166.65
165.58
165.55
155.07
141.77
136.94
133.06
128.93
127.95
120.39
118.09
116.84
116.08
67.66
48.84
39.52 DMSO-d6
39.13
38.36
36.49
32.27
30.99
29.14
29.02
28.97
28.86
28.76
28.71
28.40
26.34
26.28
25.14
25.05
22.03
DKFZ-908
f1 (ppm)

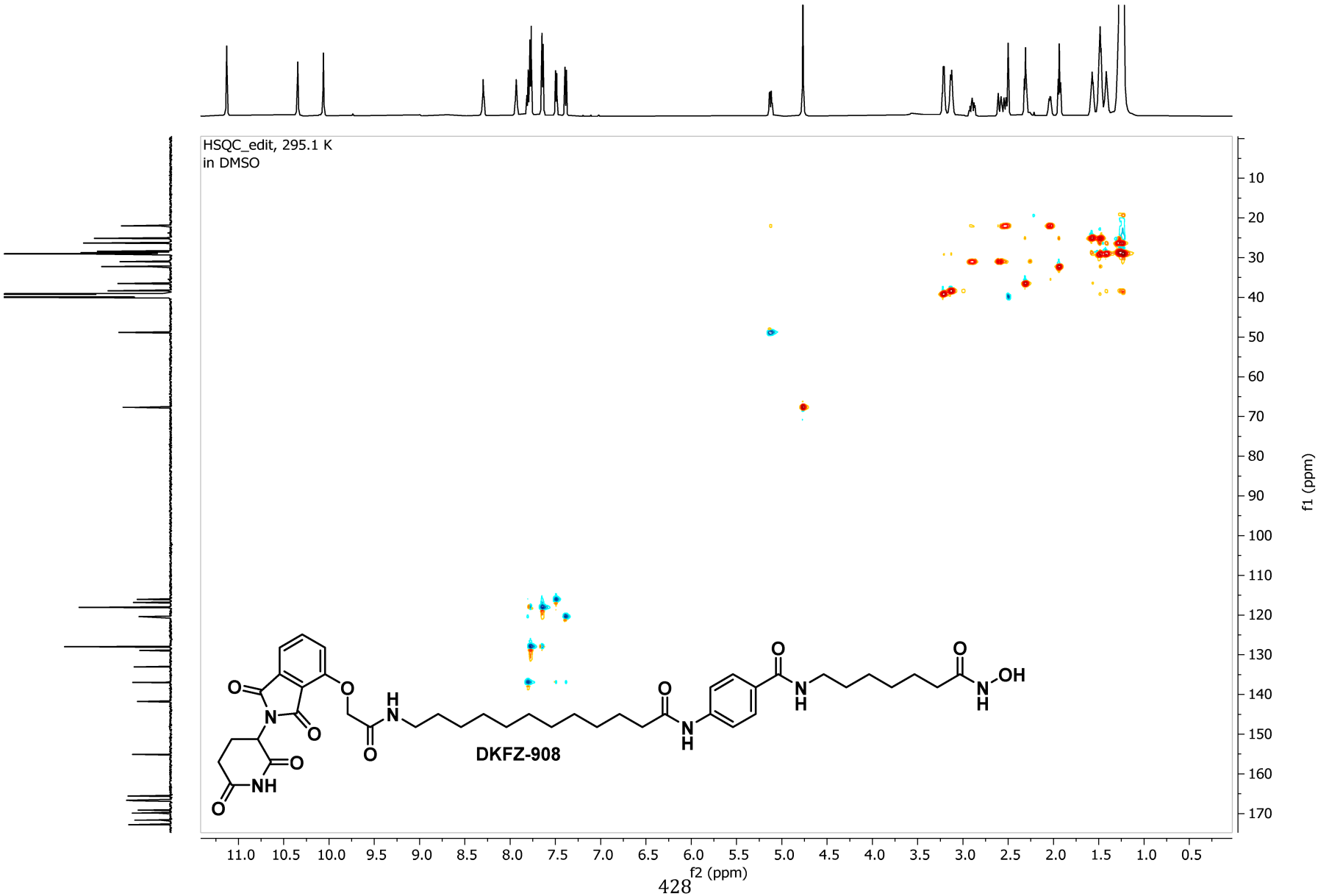
HSQC_edit, 295.1 K
in DMSO
DKFZ-908
f2 (ppm)
f1 (ppm)

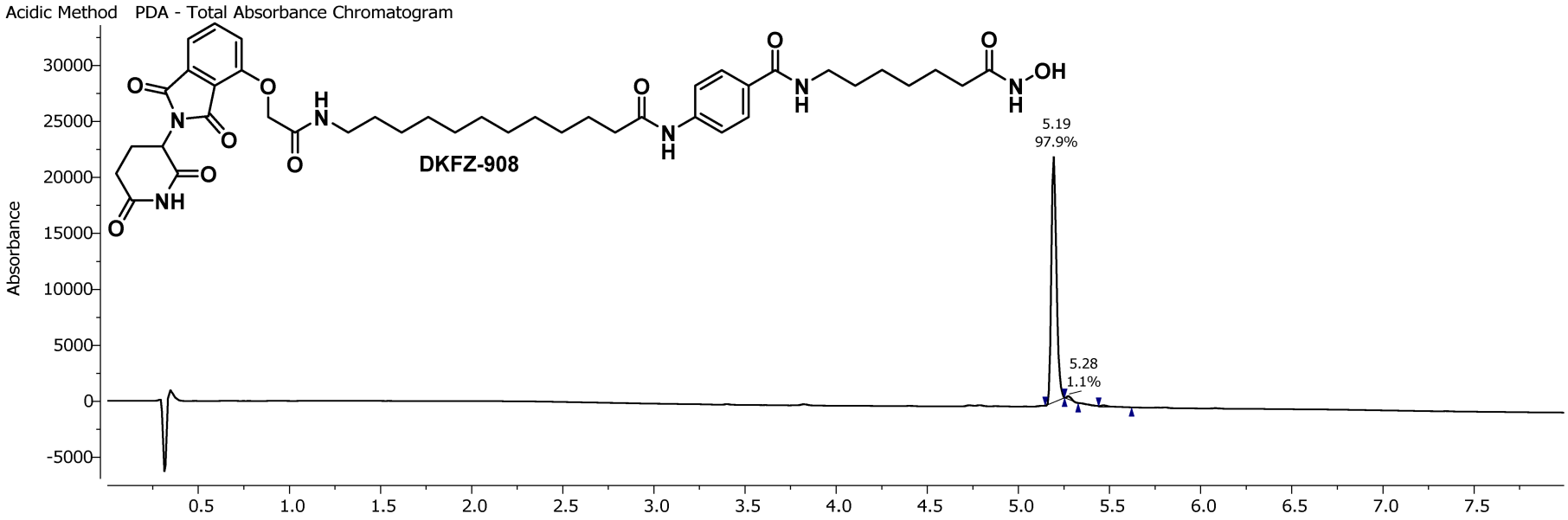
Acidic Method PDA - Total Absorbance Chromatogram
DKFZ-908
Absorbance
5.19
97.9%
5.28
1.1%

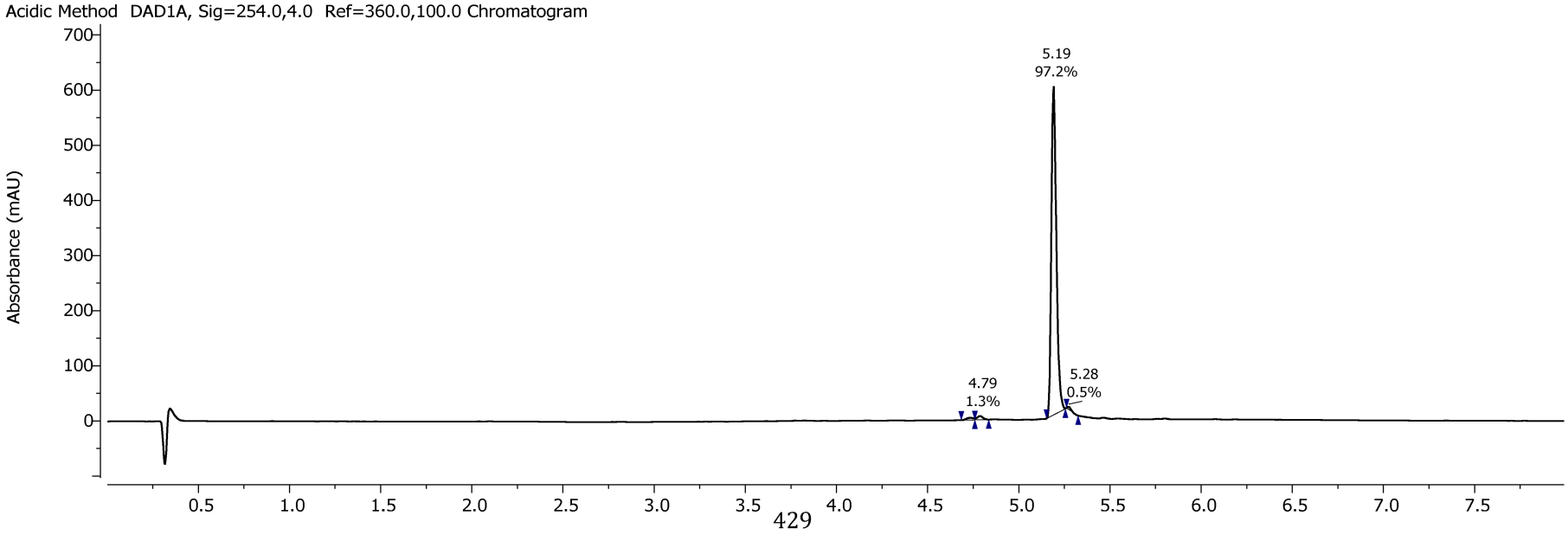
Acidic Method DAD1A, Sig=254.0,4.0 Ref=360.0,100.0 Chromatogram
Absorbance (mAU)
5.19
97.2%
4.79
1.3%
5.28
0.5%

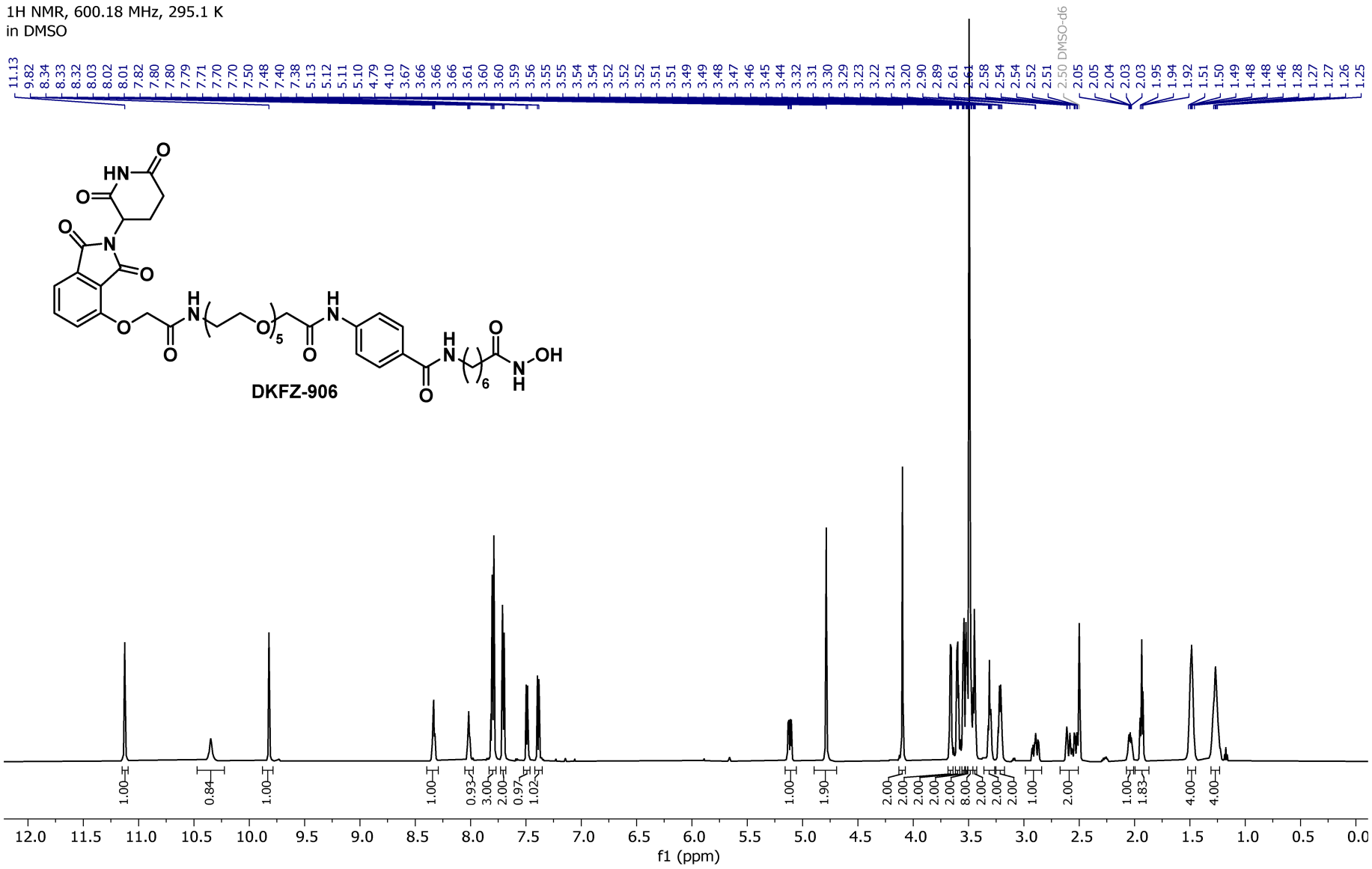
1H NMR, 600.18 MHz, 295.1 K
in DMSO
DKFZ-906
f1 (ppm)

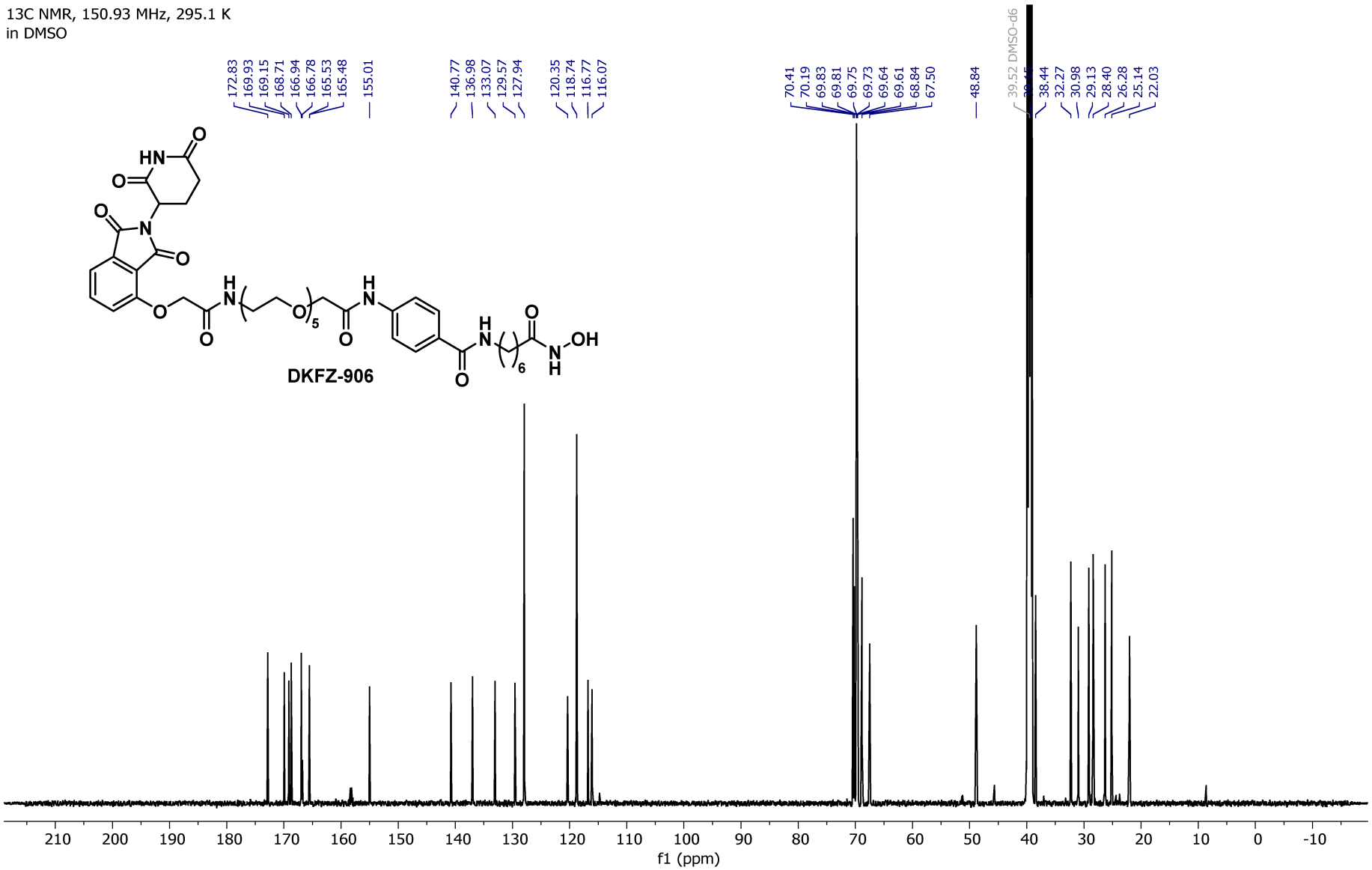
13C NMR, 150.93 MHz, 295.1 K
in DMSO
172.83
169.93
169.15
168.71
166.94
166.78
165.53
165.48
155.01
140.77
136.98
133.07
129.57
127.94
120.35
118.74
116.77
116.07
70.41
70.19
69.83
69.81
69.75
69.73
69.64
69.61
68.84
67.50
48.84
39.52 DMSO-d6
38.44
32.27
30.98
29.13
28.40
26.28
25.14
22.03
DKFZ-906
f1 (ppm)

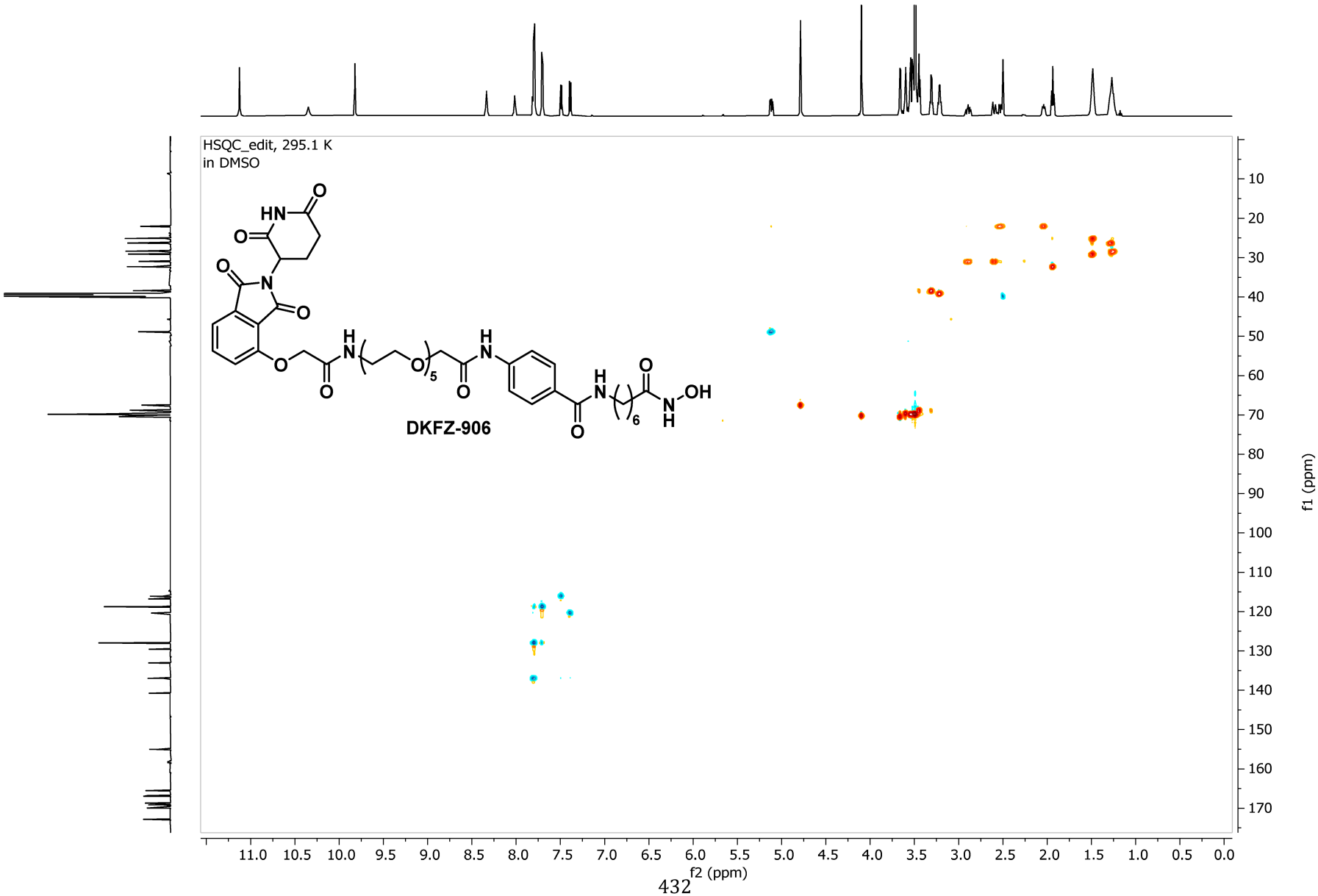
HSQC_edit, 295.1 K
in DMSO
DKFZ-906
f2 (ppm)
f1 (ppm)

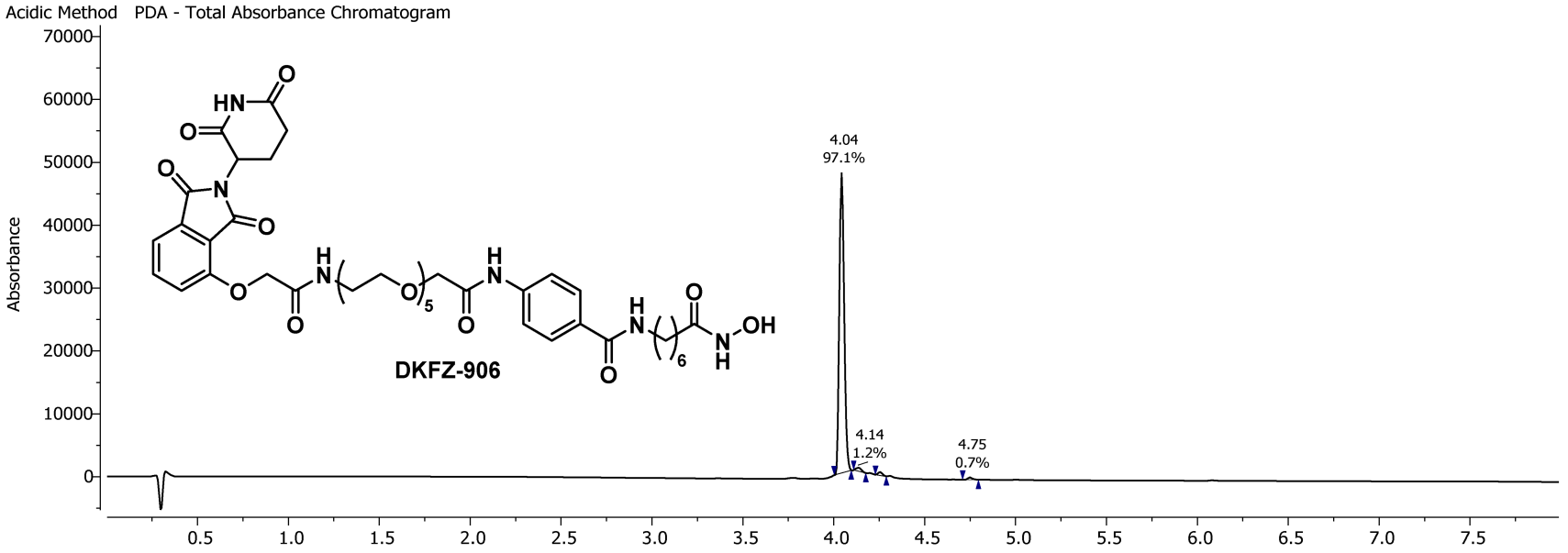
Acidic Method PDA - Total Absorbance Chromatogram
Absorbance
DKFZ-906
4.04
97.1%
4.14
1.2%
4.75
0.7%

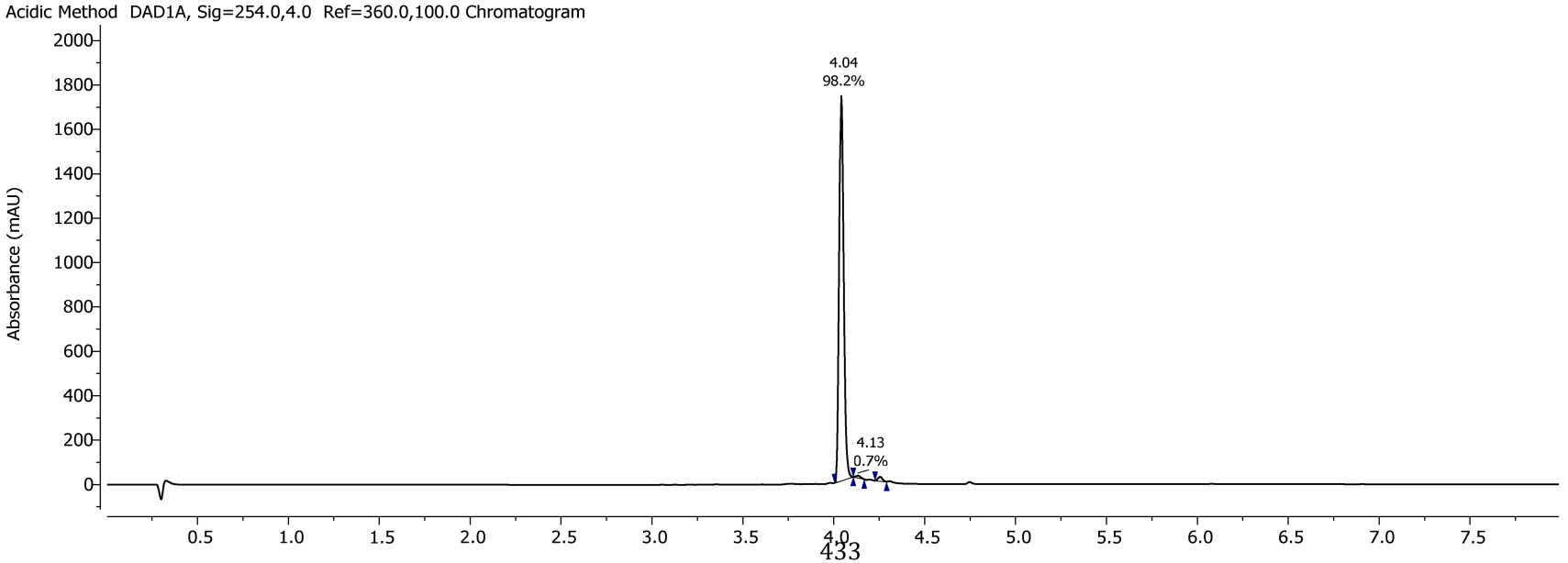
Acidic Method DAD1A, Sig=254.0,4.0 Ref=360.0,100.0 Chromatogram
Absorbance (mAU)
4.04
98.2%
4.13
0.7%

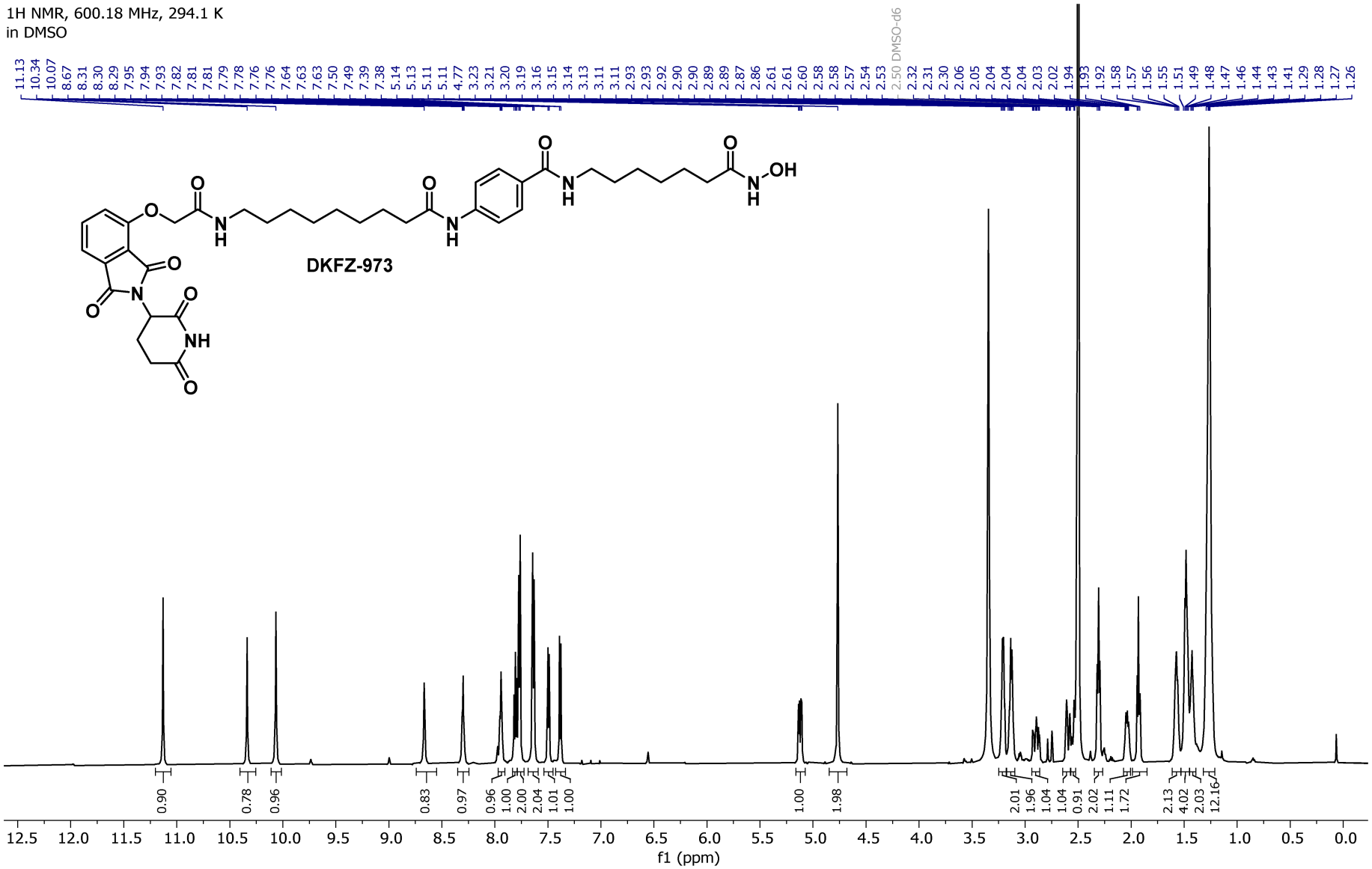
1H NMR, 600.18 MHz, 294.1 K
in DMSO
DKFZ-973
f1 (ppm)

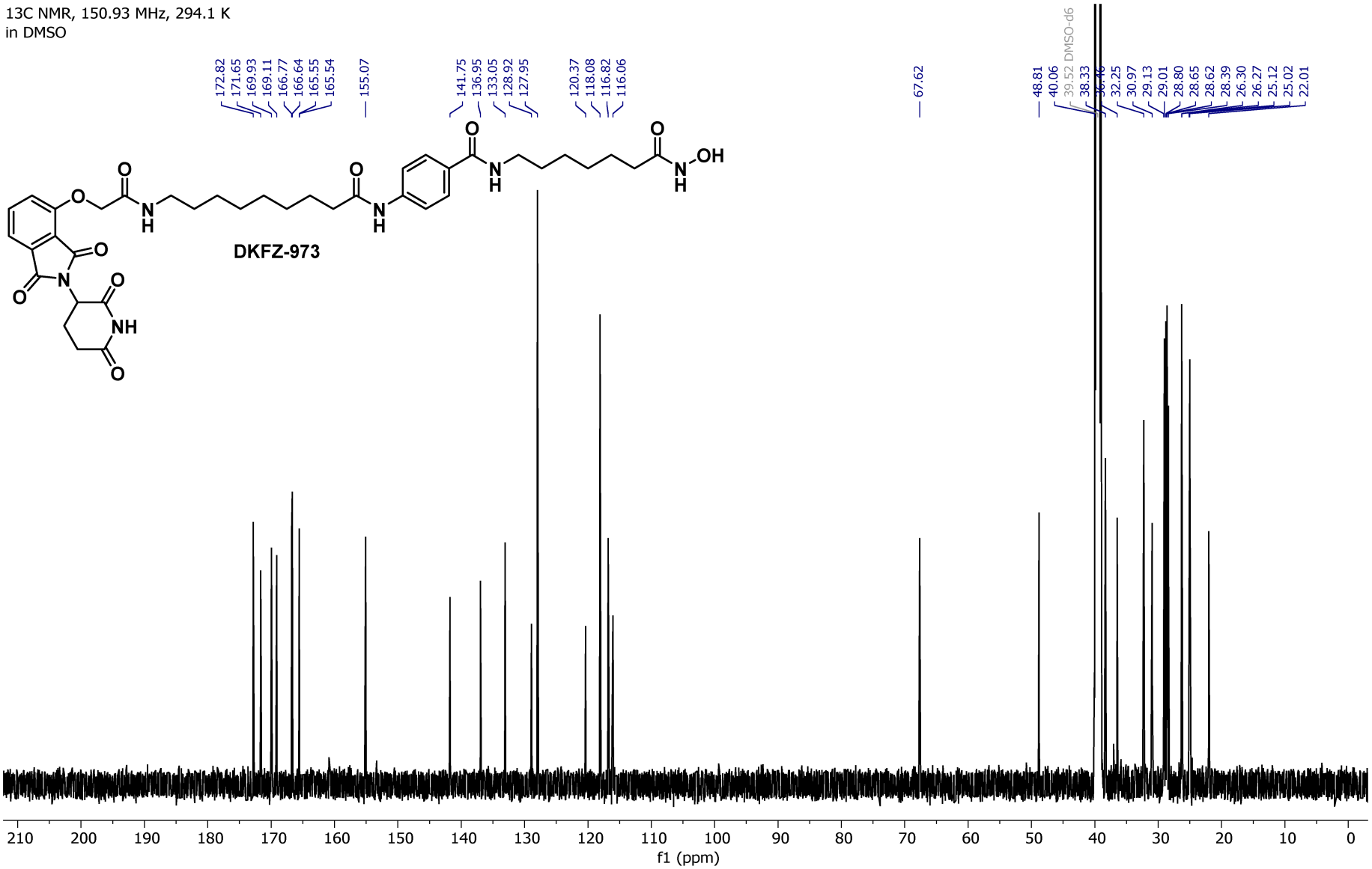
13C NMR, 150.93 MHz, 294.1 K
in DMSO
172.82
171.65
169.93
169.11
166.77
166.64
165.55
165.54
155.07
141.75
136.95
133.05
128.92
127.95
120.37
118.08
116.82
116.06
67.62
48.81
40.06
39.52 DMSO-d6
38.33
36.46
32.25
30.97
29.13
29.01
28.80
28.65
28.62
28.39
26.30
26.27
25.12
25.02
22.01
DKFZ-973
210
200
190
180
170
160
150
140
130
120
110
100
90
80
70
60
50
40
30
20
10
0
f1 (ppm)

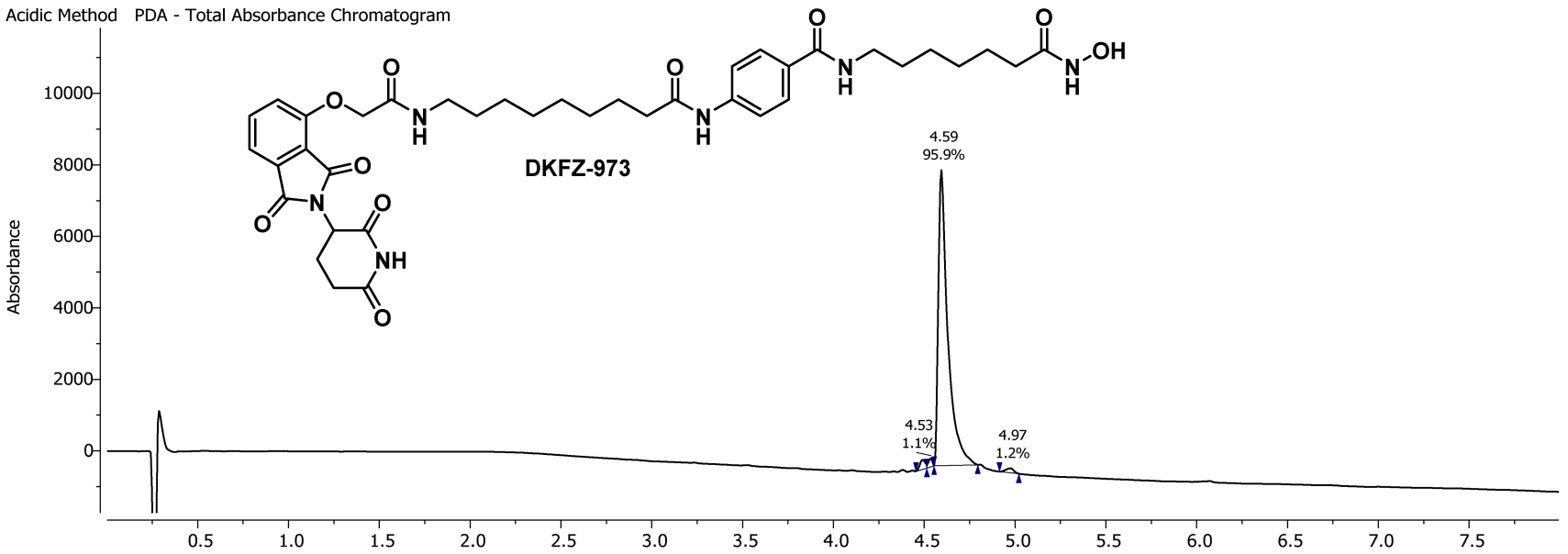
Acidic Method PDA - Total Absorbance Chromatogram
DKFZ-973
Absorbance
4.59
95.9%
4.53
1.1%
4.97
1.2%

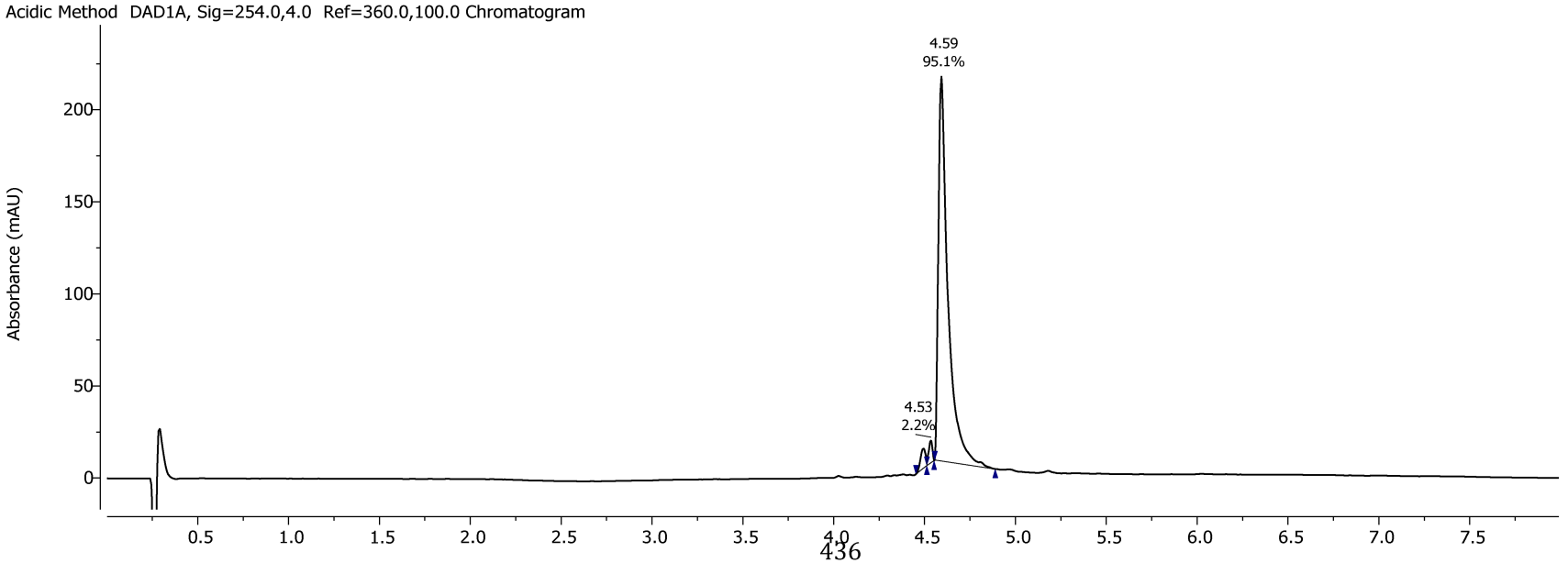
Acidic Method DAD1A, Sig=254.0,4.0 Ref=360.0,100.0 Chromatogram
Absorbance (mAU)
4.59
95.1%
4.53
2.2%

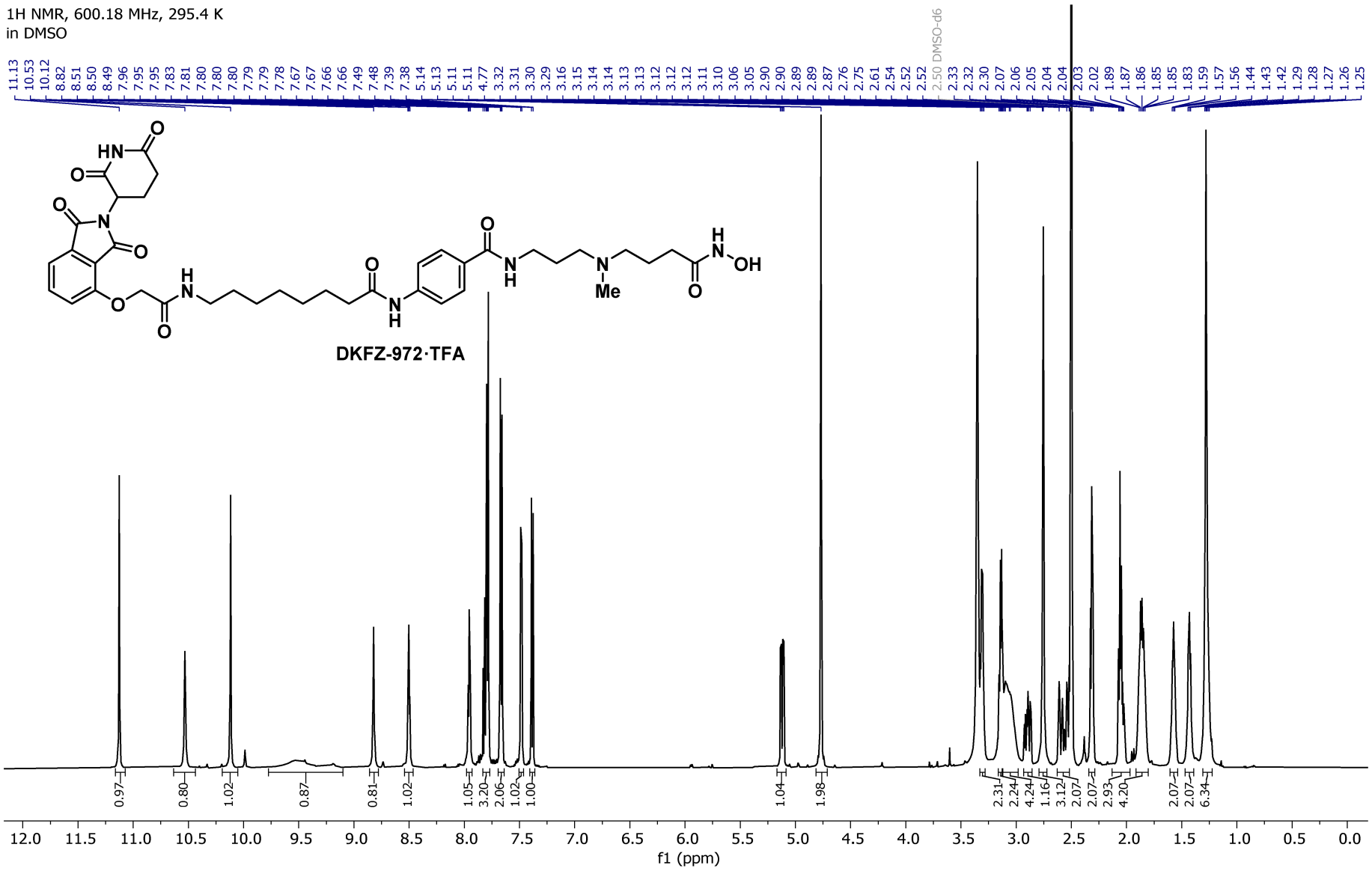
1H NMR, 600.18 MHz, 295.4 K
in DMSO
DKFZ-972·TFA
f1 (ppm)

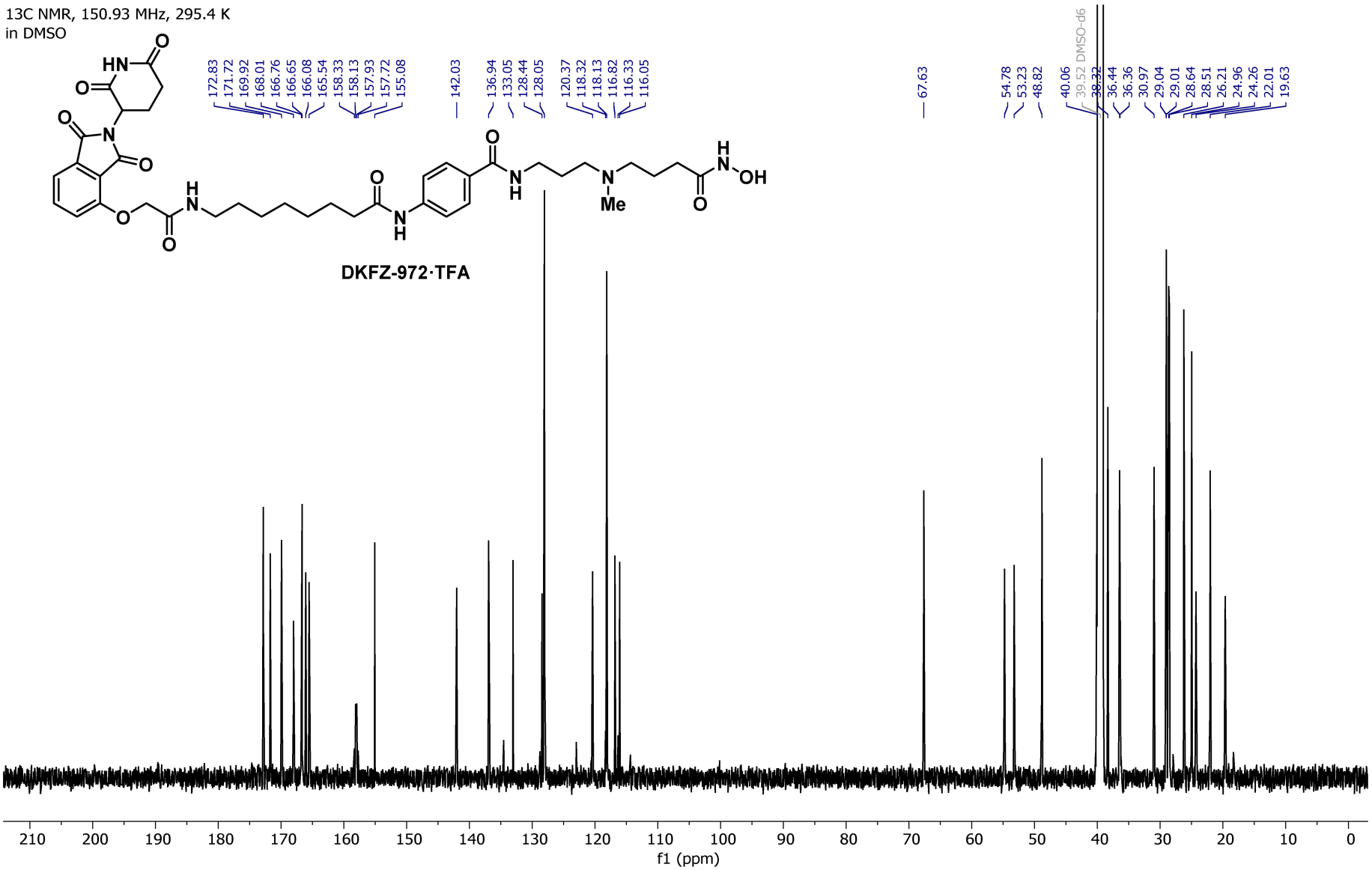
13C NMR, 150.93 MHz, 295.4 K
in DMSO
172.83
171.72
169.92
168.01
166.76
166.65
166.08
165.54
158.33
158.13
157.93
157.72
155.08
142.03
136.94
133.05
128.44
128.05
120.37
118.32
118.13
116.82
116.33
116.05
67.63
54.78
53.23
48.82
40.06
39.52 DMSO-d6
38.32
36.44
36.36
30.97
29.04
29.01
28.64
28.51
26.21
24.96
24.26
22.01
19.63
DKFZ-972·TFA
210
200
190
180
170
160
150
140
130
120
110
100
90
80
70
60
50
40
30
20
10
0
f1 (ppm)

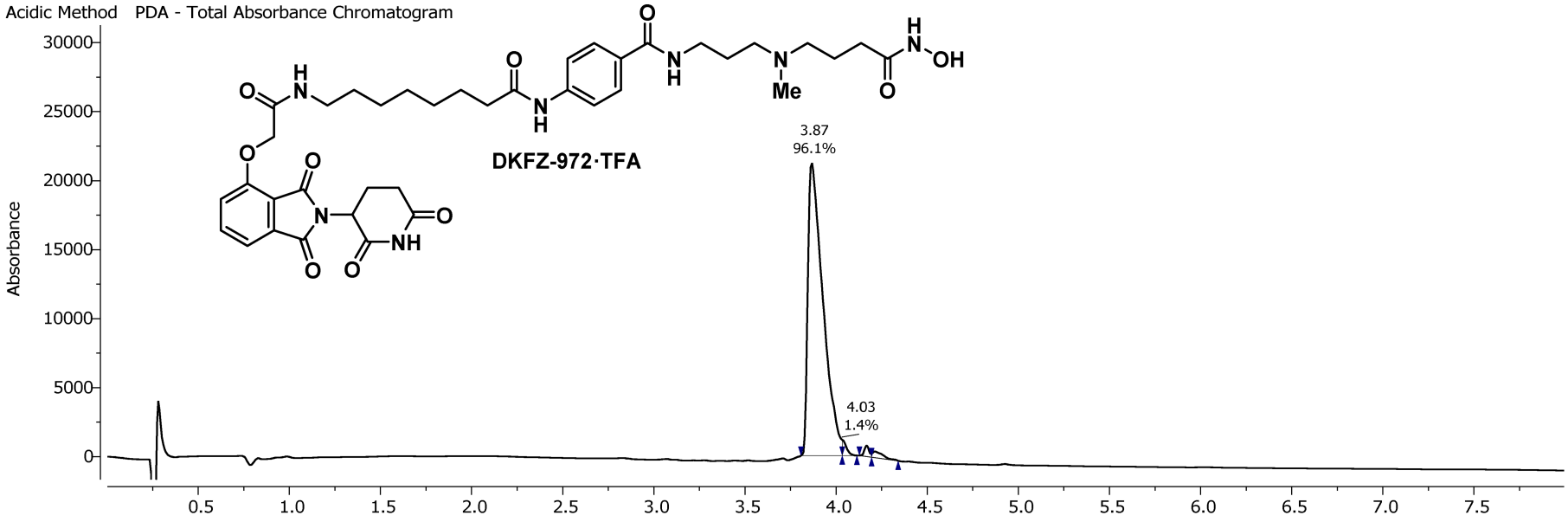
Acidic Method PDA - Total Absorbance Chromatogram
DKFZ-972·TFA
Absorbance
3.87
96.1%
4.03
1.4%

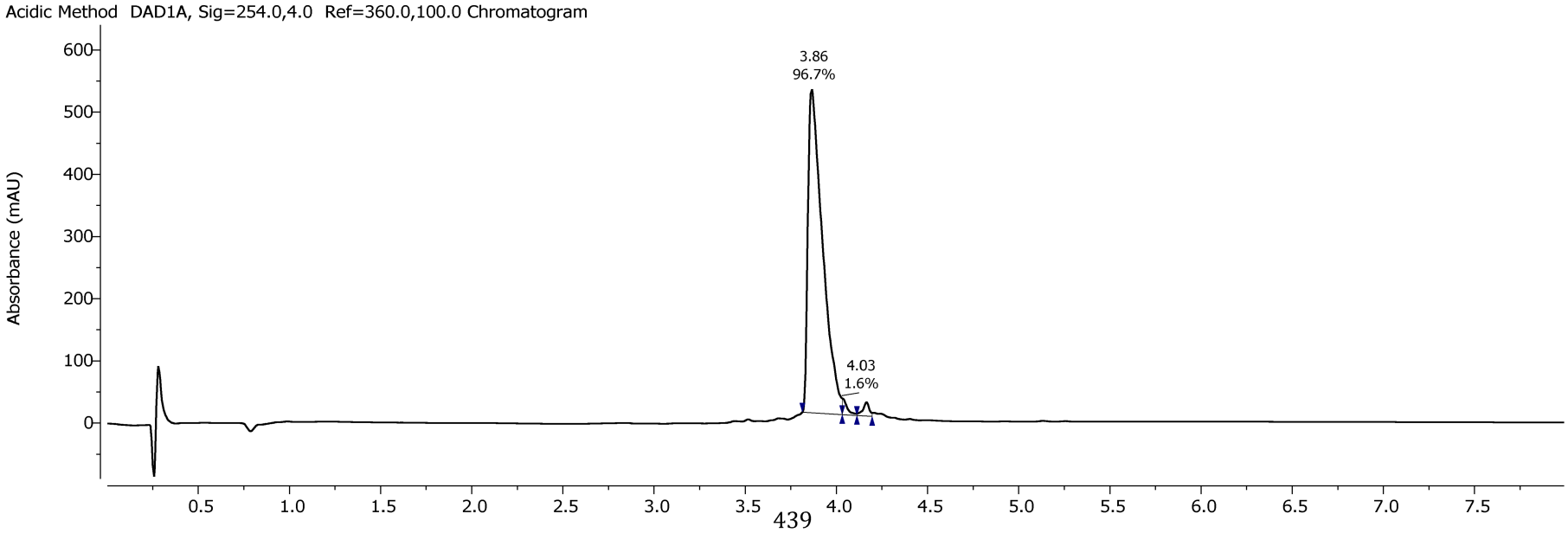
Acidic Method DAD1A, Sig=254.0,4.0 Ref=360.0,100.0 Chromatogram
Absorbance (mAU)
3.86
96.7%
4.03
1.6%

## 8.2 Tabulated assay data (Tables S1–S4)

**Table S1. Cell-free $pIC_{50}$ values[a] of aza-SAHA derivatives and SAHA**

| Compound | Structure | HDAC1 [b] | HDAC2 [b] | HDAC3 [b] | HDAC6 [b] | HDAC8 [b] | HDAC10 [c] | SF 10/1 | SF 10/6 | HDAC10 LE |
|---|---|---|---|---|---|---|---|---|---|---|
| **SAHA** | 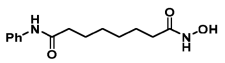 | 7.30[d] (7.25–7.36) | 7.02 (6.97–7.07) | 6.59[d] (6.55–6.63) | 7.72[d] (7.58–7.92) | 6.16[d] (6.11–6.21) | 6.93[d] (6.85–7.02) | 0.43 | 0.16 | 0.50 |
| **DKFZ-848** | 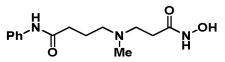 | <4.00 | <<4.00[e] | <<4.00[e] | 4.54 (4.46–4.65) | 4.74 (4.66–4.81) | 5.65 (5.44–5.83) | 117 | 13 | 0.39 |
| **DKFZ-711** | 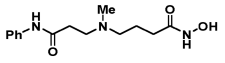 | 4.68 (4.59–4.75) | 4.13 (2.20–??) | 4.11 (1.99–??) | 5.44 (5.38–5.51) | 5.27 (5.19–5.34) | 7.48[d] (7.38–7.59) | 624 | 108 | 0.51 |
| **DKFZ-629** | 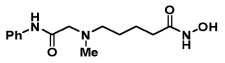 | 6.21 (6.18–6.24) | 5.74 (5.69–5.80) | 5.36 (5.30–5.42) | 6.50 (6.40–6.60) | 5.86 (5.78–5.94) | 7.05 (6.93–7.16) | 6.8 | 3.6 | 0.48 |
| **DKFZ-843** | 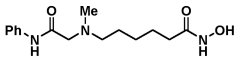 | 7.09 (7.06–7.12) | 6.88 (6.84–6.93) | 6.06 (6.04–6.26) | 7.32 (7.24–7.40) | 6.08 (6.00–6.16) | 8.73 (8.54–9.05) | 44 | 26 | 0.57 |

[a] Determined by four-parameter dose-response fit from two separate experiments each with eight dose levels in triplicates, reported as the mean, with 95% confidence intervals in parenthesis. [b] HDAC Glo assay. [c] FRET assay. [d] Mean of at least three separate experiments. [e] Curve fit analysis not convergent at 100 µM. SF (selectivity factor) = $10^{(pIC50(HDAC10) - pIC50(HDAC6\ or\ 1))}$. LE (ligand efficiency) = 1.37 x $pIC_{50}$(HDAC10) / number of heavy atoms.[186] 95% confidence intervals of dose-response fits are shown in parenthesis. "??" indicates that confidence intervals could not be calculated for low activity compounds. Taken from Steimbach et al.[1] and extended.

**Table S2. Cell-free $pIC_{50}$ values[a] of amino hydroxamic acids and reference compound**

| Compound | Structure | HDAC1 [b] | HDAC2 [b] | HDAC3 [b] | HDAC6 [b] | HDAC8 [b] | HDAC10 [c] | SF 10/1 | SF 10/6 | HDAC10 LE |
|---|---|---|---|---|---|---|---|---|---|---|
| **tubastatin A** | 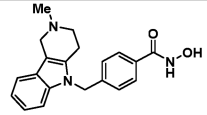 | 5.66 (5.61–5.71) | 4.78 (??–4.82) | 4.76 (0.00–??) | 7.88 (7.69–8.38) | 5.84 (5.75–5.93) | 8.28[d] (8.11–8.44) | 2.5 | 416 | 0.45 |
| **DKFZ-714** | 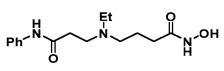 | 4.30 (4.27–4.36) | 4.13 (??–??) | <4 | 5.26 (5.14–5.36) | 5.07 (5.00–5.14) | 6.93 (6.81–7.05) | 47 | 425 | 0.45 |
| **DKFZ-724** | 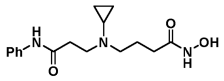 | 4.41 (4.35–4.53) | <4 (??–4.23) | <4 | 5.38 (5.26–5.50) | 5.58 (5.49–5.67) | 6.69 (6.61–6.77) | 20 | 188 | 0.42 |
| **DKFZ-716** | 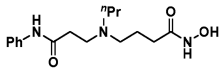 | 4.09 (4.05–4.22) | <4 (??–4.01) | <4 | 5.11 (4.94–5.25) | 5.00 (4.89–5.10) | 6.56 (6.50–6.63) | 29 | 294 | 0.41 |
| **DKFZ-715** | 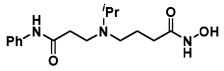 | <4 | <4 | <<4[e] | 4.68 (4.60–4.75) | 5.14 (5.05–5.22) | 6.44 (6.31–6.56) | 57 | 645 | 0.40 |
| **DKFZ-717** | 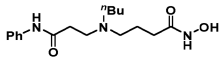 | 4.09 (??–4.22) | <4 (??–4.01) | <4 | 5.29 (5.23–5.34) | 5.05 (4.94–5.14) | 6.37 (6.28–6.44) | 12 | 188 | 0.38 |
| **DKFZ-718** | 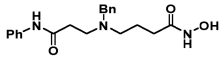 | 4.63 (4.56–4.69) | 4.21 (0.00–4.54) | <4 | 5.98 (5.90–6.06) | 5.65 (5.55–5.76) | 5.85 (5.54–5.94) | 0.74 | 16 | 0.31 |
| **DKFZ-888** | 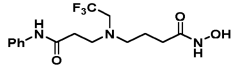 | 4.64 (4.61–4.67) | 4.46 (4.43–4.46) | <4 | 5.36 (5.30–5.42) | 5.20 (5.13–5.28) | 5.84 (5.75–5.92) | 3.0 | 16 | 0.33 |
| **DKFZ-759** | 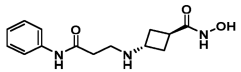 | 4.69 (4.51–4.73) | 4.25 (0.00–4.64) | <4 | 5.60 (5.37–5.76) | 4.84 (4.77–??) | 6.25 (6.08–6.38) | 4.4 | 36 | 0.43 |
| **DKFZ-767** | 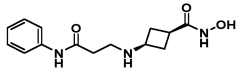 | 4.78 (4.73–4.82) | 4.57 (4.52–4.57) | <4 | 5.68 (5.55–5.82) | 5.05 (4.97–5.11) | 6.89 (6.79–6.99) | 16 | 129 | 0.47 |
| **DKFZ-770** | 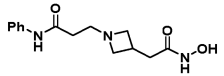 | 4.24 (4.07–4.34) | 4.05 (3.85–4.08) | <<4[e] | 5.05 (3.99–5.28) | 4.67 (??–4.83) | 6.87 (6.76–7.00) | 66 | 423 | 0.47 |

| Compound | Structure | HDAC1 [b] | HDAC2 [b] | HDAC3 [b] | HDAC6 [b] | HDAC8 [b] | HDAC10 [c] | SF 10/1 | SF 10/6 | HDAC10 LE |
|---|---|---|---|---|---|---|---|---|---|---|
| **DKFZ-895** | 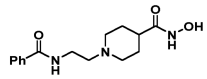 | <4 | <4 | <<4[e] | 5.04 (4.99–5.10) | 5.08 (4.96–5.19) | 7.06 (6.96–7.16) | 105 | 1998 | 0.46 |
| **DKFZ-772** | 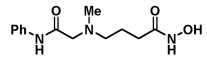 | 4.70 (4.57–4.79) | 4.55 (4.46–4.59) | <4 | 6.05 (5.95–6.17) | 5.48 (5.41–5.56) | 7.39 (7.28–7.49) | 21 | 483 | 0.53 |
| **DKFZ-775** | 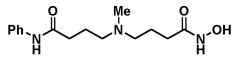 | 4.29 (4.21–4.33) | <4 | <<4[e] | 4.65 (4.59–4.71) | 4.61 (4.44–??) | 8.08 (7.96–8.21) | 2679 | 6173 | 0.53 |
| **DKFZ-728** | 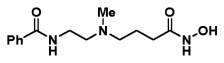 | 4.50[d] (4.46–4.59) | 4.07[d] (3.90–4.43) | ≪4[de] | 5.02[d] (4.74–5.22) | 4.96[d] (4.76–5.09) | 7.97[d] (7.90–8.10) | 889 | 2919 | 0.55 |
| **DKFZ-758** | 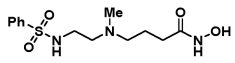 | 4.50 (4.40–4.55) | 4.06 (0.00–4.38) | <<4[e] | 5.30 (5.03–5.45) | 5.14 (4.99–5.28) | 7.44 (7.25–7.61) | 137 | 865 | 0.49 |
| **DKFZ-859** | 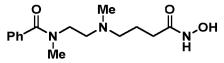 | 4.19 (4.11–4.20) | 4.00 (0.00–4.16) | <<4[e] | 5.03 (4.92–5.14) | 4.80 (4.74–4.86) | 6.86 (6.72–6.99) | 66 | 460 | 0.45 |
| **DKFZ-773** | 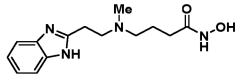 | 4.92 (4.87–4.96) | 4.67 (4.62–4.71) | <4 | 5.74 (5.56–5.91) | 5.23 (5.15–5.30) | 8.08 (7.98–8.18) | 219 | 1452 | 0.55 |
| **DKFZ-805** | 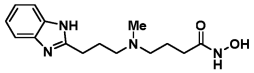 | 4.39 (4.32–4.37) | 4.26 (4.16–4.35) | <<4[e] | 4.79 (4.69–4.88) | 4.79 (4.74–4.84) | 8.09 (7.94–8.23) | 1970 | 4966 | 0.53 |
| **DKFZ-749** | 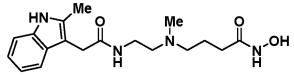 | 4.98 (4.94–5.02) | 4.35 (??–4.83) | <<4[e] | 5.43 (5.20–5.58) | 5.53 (5.43–5.62) | 7.22 (7.07–7.38) | 63 | 173 | 0.40 |
| **DKFZ-756** | 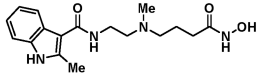 | 5.13 (5.07–5.19) | 4.52 (2.51–??) | 4.05 (1.93–??) | 5.82 (5.72–5.90) | 5.32 (5.22–5.42) | 7.68 (7.53–7.82) | 72 | 352 | 0.44 |
| **DKFZ-754** | 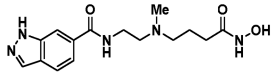 | 5.00 (4.94–5.05) | 4.43 (0.00–4.76) | <4 | 5.44 (5.24–5.72) | 4.95 (4.84–5.06) | 8.12 (7.98–8.26) | 481 | 1323 | 0.48 |

| Compound | Structure | HDAC1 [b] | HDAC2 [b] | HDAC3 [b] | HDAC6 [b] | HDAC8 [b] | HDAC10 [c] | SF 10/1 | SF 10/6 | HDAC10 LE |
|---|---|---|---|---|---|---|---|---|---|---|
| **DKFZ-757** | 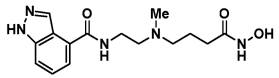 | 4.91 (4.88–4.94) | 4.34 (0.00–4.68) | <4 | 5.44 (5.28–5.60) | 5.08 (4.98–5.18) | 8.17 (7.98–8.38) | 531 | 1789 | 0.49 |
| **DKFZ-771** | 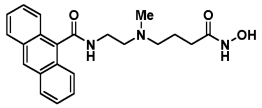 | 5.70 (5.67–5.74) | 5.58 (5.53–5.62) | 4.60 (4.49–4.67) | 6.05 (5.99–6.12) | 5.93 (5.79–6.06) | 8.47 (8.29–8.69) | 263 | 597 | 0.41 |
| **DKFZ-776** | 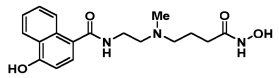 | 5.02 (4.99–5.07) | 4.82 (4.76–4.87) | <4 | 5.88 (5.80–5.97) | 5.98 (5.88–6.07) | 8.19 (8.03–8.34) | 201 | 1460 | 0.45 |
| **DKFZ-774** | 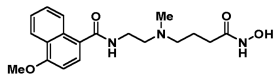 | 5.22 (5.16–5.27) | 5.01 (4.93–5.08) | <4 (??–4.10) | 5.71 (5.54–5.86) | 5.64 (5.54–5.74) | 8.34 (8.18–8.52) | 426 | 1324 | 0.44 |
| **DKFZ-748** | 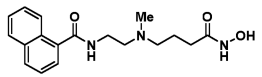 | 4.89 (4.86–4.93) | 4.29 (2.35–4.76) | <4 | 5.49 (5.28–5.65) | 5.87 (5.81–5.94) | 8.29[d] (8.12–8.56) | 636 | 2497 | 0.47 |
| **DKFZ-769** | 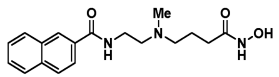 | 5.63 (??–5.66) | 5.39 (5.29–5.47) | 4.38 (4.12–4.42) | 5.81 (5.75–5.88) | 5.70 (5.60–5.79) | 8.22 (8.11–8.33) | 256 | 391 | 0.47 |
| **DKFZ-746** | 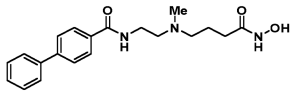 | 5.58 (5.55–5.61) | 4.95 (??–5.52) | 4.44 (4.36–4.49) | 5.52 (5.44–5.60) | 5.15 (5.06–5.21) | 7.90 (7.68–8.12) | 239 | 208 | 0.42 |
| **DKFZ-747** | 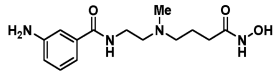 | 4.50 (4.42–4.56) | <4 | ≪4[e] | 5.23 (??–5.49) | 4.77 (3.70–4.94) | 7.62 (7.44–7.82) | 246 | 1315 | 0.50 |
| **DKFZ-752** | 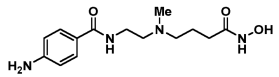 | 4.78 (4.75–4.81) | 4.26 (2.30–??) | <4 | 5.47 (5.39–5.54) | 4.63 (4.56–4.71) | 7.81 (7.68–7.94) | 219 | 1060 | 0.51 |
| **DKFZ-751** | 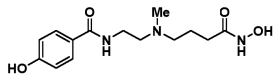 | 4.75 (4.71–4.78) | 4.23 (2.30–??) | <4 | 5.84 (5.79–5.90) | 4.65 (4.56–4.75) | 8.05 (7.92–8.19) | 161 | 1998 | 0.53 |

| Compound | Structure | HDAC1 [b] | HDAC2 [b] | HDAC3 [b] | HDAC6 [b] | HDAC8 [b] | HDAC10 [c] | SF 10/1 | SF 10/6 | HDAC10 LE |
|---|---|---|---|---|---|---|---|---|---|---|
| **DKFZ-755** | 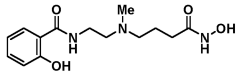 | 4.12 (3.88–4.16) | <4 (0.00–4.06) | ≪4 [e] | 4.92 (4.74–??) | 4.19 (4.10–4.31) | 7.41 (7.30–7.53) | 313 | 1986 | 0.48 |
| **DKFZ-753** | 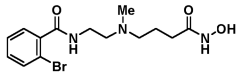 | 4.50 (4.30–4.61) | <4 (0.00–4.40) | ≪4 [e] | 5.26 (5.15–5.37) | 5.03 (4.92–5.13) | 7.76 (7.65–7.87) | 314 | 1822 | 0.51 |
| **DKFZ-829** | 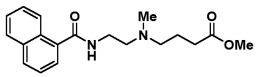 | ≪4 [e] | ≪4 [e] | ≪4 [e] | <4 | <4 | ≪4 [e] | – | – | – |
| **DKFZ-806** | 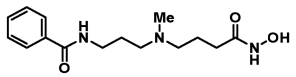 | 4.28 (4.21–??) | 4.10 (4.03–4.24) | <<4 [e] | 4.58 (4.36–4.71) | 4.58 (4.50–??) | 7.72 (7.60–7.84) | 1374 | 2754 | 0.50 |
| **DKFZ-750** | 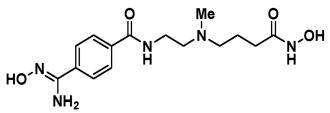 | 4.82 (4.72–4.89) | 3.85 (??–3.91) | <<4 [e] | 5.24 (4.81–5.51) | 4.60 (0.00–??) | 7.75 (7.35–8.23) | 327 | 859 | 0.44 |

[a] Determined by four-parameter dose-response fit from two separate experiments each with eight dose levels in triplicates, reported as the mean, with 95% confidence intervals in parenthesis. [b] HDAC Glo assay. [c] FRET assay. [d] Mean of at least three separate experiments. [e] Curve fit analysis not convergent at 100 µM. SF (selectivity factor) = $10^{(pIC50(HDAC10) - pIC50(HDAC6 \text{ or } 1))}$. LE (ligand efficiency) = 1.37 x $pIC_{50}$(HDAC10) / number of heavy atoms.[186] 95% confidence intervals of dose-response fits are shown in parenthesis. "??" indicates that confidence intervals could not be calculated for low activity compounds.

**Table S3. HDAC10 and 6 BRET $pIC_{50}$ values[a] of selected inhibitors and reference compounds**

| Compound | Structure | HDAC6[b] | HDAC10[b] | SF 10/6 | HDAC10 LE | HDAC10 BRET/FRET activity |
|---|---|---|---|---|---|---|
| **Tubastatin A** | 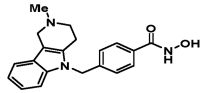 | 7.16 (6.89–7.41) | 8.04 (7.80–8.15) | 8 | 0.44 | 58% |
| **SAHA** | 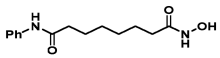 | 7.13[c] (6.96–7.31) | 6.41[c] (6.14–6.68) | 0.19 | 0.46 | 30% |
| **DKFZ-848** | 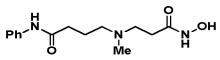 | 2.65 (1.13–??) | 4.63 (4.02–5.01) | 96 | 0.32 | 11% |
| **DKFZ-711** | 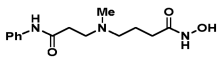 | 4.41[d] (??–4.79) | 6.73[d] (6.56–6.88) | 208 | 0.46 | 18% |
| **DKFZ-629** | 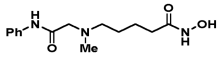 | 5.73 (5.18–6.00) | 6.53 (6.36–6.68) | 6.3 | 0.45 | 40% |
| **DKFZ-843** | 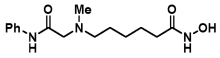 | 6.66 (6.53–6.79) | 8.30 (8.02–8.71) | 44 | 0.54 | 35% |
| **DKFZ-714** | 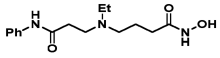 | <4.4 | 6.13 (5.85–6.35) | >54 | 0.40 | 24% |
| **DKFZ-724** | 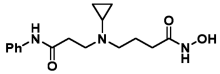 | <4.4 | 6.44 (6.26–6.60) | >109 | 0.40 | 66% |
| **DKFZ-716** | 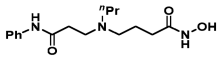 | ≪4.4[e] | 6.06 (5.87–6.21) | >45 | 0.38 | 48% |
| **DKFZ-715** | 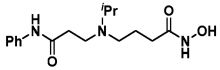 | ≪4.4[e] | 5.73 (5.08–6.04) | >21 | 0.36 | 37% |
| **DKFZ-717** | 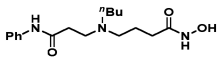 | 4.40 (3.46–5.39) | 5.80 (5.58–5.98) | 25 | 0.35 | 48% |
| **DKFZ-718** | 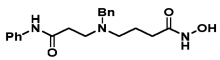 | 4.79 (??–5.41) | 6.34 (6.16–6.50) | 35 | 0.33 | 551% |

| Compound | Structure | HDAC6[b] | HDAC10[b] | SF 10/6 | HDAC10 LE | HDAC10 BRET/FRET activity |
|---|---|---|---|---|---|---|
| **DKFZ-770** | 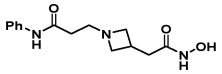 | <4.4 | 5.70 (4.99–6.03) | >20 | 0.39 | 7% |
| **DKFZ-895** | 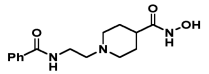 | <4.4 | 6.47 (6.22–6.73) | >117 | 0.42 | 27% |
| **DKFZ-772** | 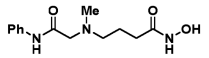 | 5.50 (4.02–5.84) | 6.53 (6.32–6.73) | 11 | 0.47 | 10% |
| **DKFZ-775** | 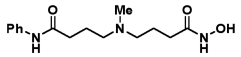 | <4.4 | 6.89 (6.52–7.23) | >305 | 0.45 | 5% |
| **DKFZ-728** | 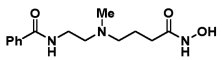 | <4.4[d] | 6.93[d] (6.79–7.06) | >338 | 0.47 | 9% |
| **DKFZ-859** | 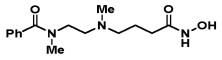 | 4.00 (3.34–4.37) | 6.31 (5.97–6.70) | 81 | 0.41 | 22% |
| **DKFZ-773** | 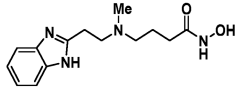 | 4.43 (4.18–5.12) | 6.93 (6.68–7.15) | 315 | 0.47 | 6% |
| **DKFZ-805** | 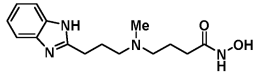 | <4.4 | 6.62 (6.53–6.72) | 167 | 0.43 | 4% |
| **DKFZ-757** | 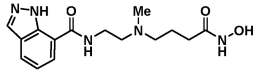 | 4.55 (??–4.76) | 7.18 (6.95–7.38) | 422 | 0.43 | 12% |
| **DKFZ-771** | 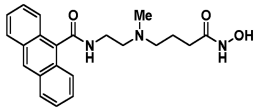 | 5.41 (5.26–5.57) | 7.91 (7.70–8.12) | 316 | 0.39 | 22% |
| **DKFZ-748** | 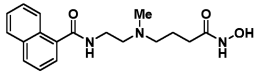 | 4.84 (??–5.02) | 7.66 (7.47–7.83) | 662 | 0.44 | 23% |

| Compound | Structure | HDAC6[b] | HDAC10[b] | SF 10/6 | HDAC10 LE | HDAC10 BRET/FRET activity |
|---|---|---|---|---|---|---|
| **DKFZ-774** | 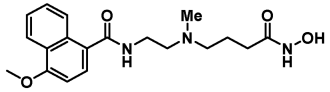 | 4.92 (0.00–??) | 7.52 (7.24–7.79) | 397 | 0.40 | 10% |
| **DKFZ-806** | 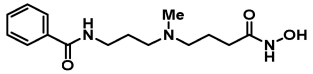 | 4.40 (3.77–5.51) | 6.65 (6.45–6.85) | 179 | 0.43 | 9% |
| **DKFZ-750** | 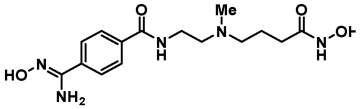 | <4.40 | 5.71 (5.27–5.96) | 21 | 0.33 | 1% |

[a] Determined from pooled data of two separate BRET assay[b] experiments by four-parameter dose-response fit, each with ten dose levels in triplicates. [c] Data pooled from six separate experiments. [d] Data pooled from four separate experiments. [e] Not convergent at 40 µM. SF (selectivity factor) = $10^{(pIC50(HDAC10) - pIC50(HDAC6))}$. LE (ligand efficiency) = 1.37 x $pIC_{50}$(HDAC10) / number of heavy atoms.[186] 95% confidence intervals of dose-response fits are shown in parenthesis. "??" indicates that confidence intervals could not be calculated for low activity compounds. Based on Steimbach et al.[1]

**Table S4. $pIC_{50}$ values[a] of non-hydroxamic acid inhibitors and reference compounds**

| Compound | Structure | HDAC1 [b] | HDAC2 [b] | HDAC3 [b] | HDAC6 [b] | HDAC8 [b] | HDAC10 [c] | SF 10/6 | SF 10/1 | HDAC10 LE |
|---|---|---|---|---|---|---|---|---|---|---|
| **SAHA** | 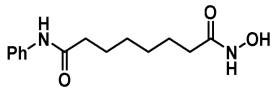 | 7.30 [d] (7.25–7.36) | 7.02 [e] (6.97–7.07) | 6.59 [d] (6.55–6.63) | 7.72 [d] (7.58–7.92) | 6.16 [d] (6.11–6.21) | 6.93 [d] (6.85–7.02) | 0.164 | 0.43 | 0.50 |
| **PAOA** | 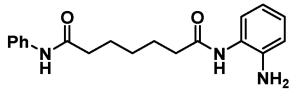 | 6.33 (6.25–6.42) | 5.47 (5.44–5.49) | 5.99 (5.93–6.06) | <<4 [f] | <<4 [f] | <<4 [f] | – | – | – |
| **BML-210** | 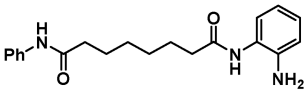 | 5.80 (5.71–5.88) | 5.48 (5.45–5.50) | 5.74 (5.64–5.82) | <<4 [f] | <<4 [f] | <<4 [f] | – | – | – |
| **DKFZ-728** | 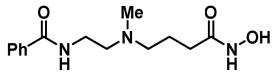 | 4.50 [d] (4.46–4.59) | 4.07 [d] (3.90–4.43) | <<4 [df] | 5.02 [d] (4.74–5.22) | 4.96 [d] (4.76–5.09) | 7.97 [d] (7.90–8.10) | 889 | 2920 | 0.55 |
| **DKFZ-812** | 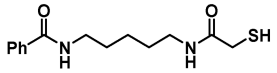 | 5.50 [e] (5.44–5.56) | 5.40 [e] (5.34–5.45) | 4.91 [e] (2.35–??) | 7.13 [e] (7.04–7.23) | ~4.55 [e] | 7.33 (7.20–7.46) | 1.59 | 68.5 | 0.53 |
| **DKFZ-825** | 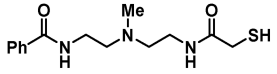 | 4.40 [e] (2.45–??) | 4.12 [e] (??–5.93) | <<4 [f] | 5.24 [e] (5.15–5.32) | <<4 [ef] | 7.76 [e] (7.61–7.93) | 338 | 2309 | 0.53 |
| **701332 (screening hit)** | 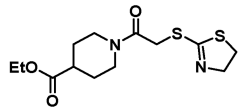 | 3.95 (3.88–3.99) | ~3.82 | <<4 [f] | 4.66 (??–4.80) | 4.02 (3.96–4.18) | 6.85 (6.62–??) | 157 | 800 | 0.47 |
| **DKFZ-831** | | ~3.83 | ~3.83 | <<4 [f] | ~3.91 | 3.31 (2.86–??) | 5.40 (5.26–5.53) | ~31 | ~37.3 | 0.37 |
| **817126 (screening hit)** | 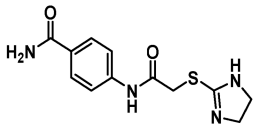 | <<4 [f] | <<4 [f] | <<4 [f] | 4.56 (4.46–??) | <<4 [f] | 6.78 (6.34–6.98) | 165 | >601 | 0.49 |
| **DKFZ-832** | | ~3.54 | <<4 | <<4 | 4.65 (4.58–4.70) | ~3.61 | 7.33 (7.01–??) | 483 | ~6150 | 0.53 |

| Compound | Structure | HDAC1 [b] | HDAC2 [b] | HDAC3 [b] | HDAC6 [b] | HDAC8 [b] | HDAC10 [c] | SF 10/6 | SF 10/1 | HDAC10 LE |
|---|---|---|---|---|---|---|---|---|---|---|
| **DKFZ-854** | 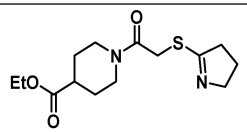 | 3.91 (3.76–3.96) | ~3.80 | <<4 [f] | 5.15 (5.06–??) | 4.61 (4.48–4.65) | ~5.84 | 4.84 | 85.5 | 0.40 |
| **DKFZ-830** | 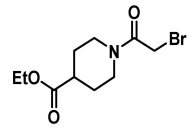 | <<4 [f] | <<4 [f] | <<4 [f] | ~2.95 | ~4.53 | <<4 [f] | – | – | – |
| **DKFZ-880** | 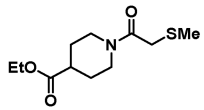 | <<4 [f] | <<4 [f] | <<4 [f] | <<4 [f] | <<4 [f] | <<4 [f] | – | – | – |
| **DKFZ-855** | 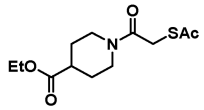 | ~3.54 | ~2.53 | <<4 [f] | 4.76 (4.57–4.84) | 4.49 (4.44–4.69) | 6.98 (0.00–??) | 165 | ~2750 | 0.53 |
| **DKFZ-889** | 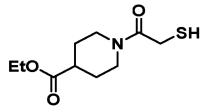 | 4.45 [e] (4.40–4.49) | 4.26 [e] (4.20–??) | <<4 [ef] | 5.74 [e] (??–5.80) | ~4.26 [e] | 7.92 [e] (7.78–8.09) | 152 | 2960 | 0.72 |
| **DKFZ-961** [g] | 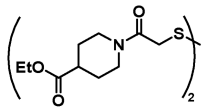 | 3.03 (2.16–3.50) | <<4 [f] | <<4 [f] | 4.51 (4.32–4.69) | ~4.26 | 7.44 (7.24–7.61) | 849 | 25500 | 0.68 |
| **DKFZ-852** | 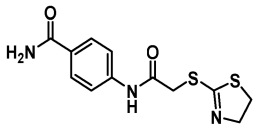 | ~3.60 | ~3.69 | <<4 [f] | ~4.00 | <<4 [f] | 5.06 (4.67–??) | ~11.5 | ~29.1 | 0.36 |
| **DKFZ-851** | 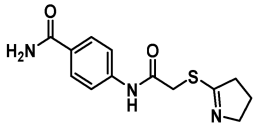 | ~3.95 | ~3.81 | <<4 [f] | 5.47 (5.41–5.52) | 4.86 (4.82–4.89) | 7.62 (7.54–8.19) | 142 | ~4680 | 0.55 |

| Compound | Structure | HDAC1 [b] | HDAC2 [b] | HDAC3 [b] | HDAC6 [b] | HDAC8 [b] | HDAC10 [c] | SF 10/6 | SF 10/1 | HDAC10 LE |
|---|---|---|---|---|---|---|---|---|---|---|
| **DKFZ-877** | 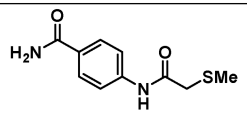 | ~2.88 | <<4 [f] | <<4 [f] | <<4 [f] | <<4 [f] | <<4 | – | – | – |
| **DKFZ-850** | 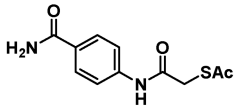 | ~3.78 | ~3.58 | <<4 [f] | 5.13 (5.09–5.17) | ~3.84 | 6.76 (6.33–??) | 42.7 | ~966 | 0.55 |
| **DKFZ-887** | 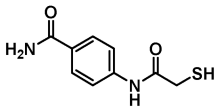 | 4.33 [e] (4.30–4.35) | 4.15 [e] (1.95–??) | ~2.01 [e] | 5.43 [e] (??–5.55) | 4.91 [e] (4.74–5.12) | 7.81 [e] (7.57–7.94) | 239 | 3010 | 0.76 |
| **DKFZ-873** | 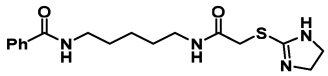 | 3.69 (0.00–??) | 3.58 (0.00–??) | <<4 [f] | 5.15 (5.05–5.32) | <<4 [f] | 6.17 (6.02–6.29) | 10.4 | 303 | 0.35 |
| **DKFZ-872** | 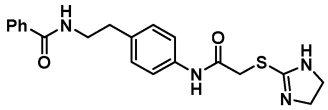 | 4.02 (0.00–??) | 3.74 (0.00–??) | <<4 [f] | 4.67 (4.59–??) | 3.99 (0.00–??) | 6.44 (0.00–??) | 59.8 | 267 | 0.33 |
| **DKFZ-826** | 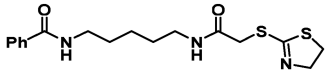 | <<4 [f] | <<4 [f] | <<4 [f] | 4.46 (4.31–??) | <<4 [f] | 4.36 (4.12–4.60) | 0.796 | 23000 | 0.25 |
| **DKFZ-827** | 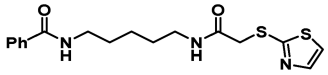 | <<4 [f] | <<4 [f] | <<4 [f] | 3.74 (??–4.44) | <<4 [f] | 3.15 (0.06–3.87) | 0.262 | 1430 | 0.18 |
| **DKFZ-949** | 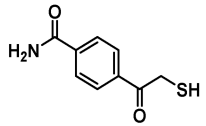 | 5.87 (5.84–5.90) | 5.82 (5.80–5.84) | 5.40 [e] (5.32–5.47) | 6.59 [e] (6.48–6.70) | 5.83 [e] (5.82–5.83) | 8.86 (8.78–8.94) | 189 | 989 | 0.93 |
| **DKFZ-945** | 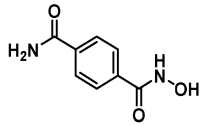 | 5.30 (5.28–5.32) | 5.10 (5.08–5.12) | 4.31 (4.17–4.45) | 6.73 [e] (6.65–6.84) | 5.22 (5.13–5.32) | 7.49 (7.40–7.57) | 5.66 | 154 | 0.79 |

| Compound | Structure | HDAC1 [b] | HDAC2 [b] | HDAC3 [b] | HDAC6 [b] | HDAC8 [b] | HDAC10 [c] | SF 10/6 | SF 10/1 | HDAC10 LE |
|---|---|---|---|---|---|---|---|---|---|---|
| **DKFZ-962** | 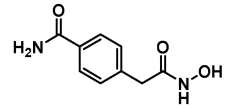 | 5.93 (5.91–5.95) | 5.74 (5.71–5.77) | 5.15 [e] (5.03–5.24) | 6.83 (6.67–7.00) | 5.73 [e] (5.80–5.66) | 7.86 [e] (7.77–7.96) | 10.8 | 85.5 | 0.77 |
| **DKFZ-942** | 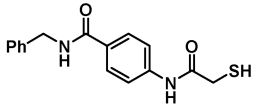 | 4.46 (4.42–4.50) | 4.45 (4.34–??) | ~4.00 | 5.10 (4.97–5.22) | 4.74 (4.64–4.83) | 7.29 (??–??) | 155 | 665 | 0.48 |
| **DKFZ-958** | 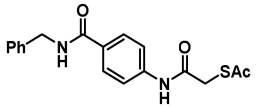 | 4.16 (4.10–4.21) | 4.12 (4.03–4.19) | <<4 [f] | 5.40 (5.28–5.52) | ~4.00 | 5.81 (5.70–6.52) | 2.61 | 45.5 | 0.33 |
| **DKFZ-965** [g] | 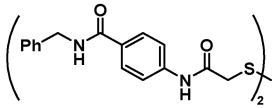 | 3.76 (3.66–3.83) | 3.51 (3.35–3.64) | 1.83 (1.22–3.05) | 4.78 (4.69–4.87) | 4.94 (4.78–5.11) | 6.55 (??–??) | 58.5 | 615 | 0.43 |
| **DKFZ-963** | 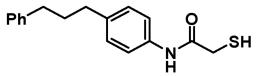 | 4.95 (4.93–4.98) | 4.86 (4.82–4.89) | ~4.54 | 5.38 (5.30–5.46) | ~3.73 | 7.05 (??–??) | 47.5 | 126 | 0.48 |
| **DKFZ-960** | 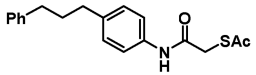 | 4.81 (4.78–4.84) | 4.74 (4.72–4.77) | ~4.06 | 5.36 (5.27–5.44) | ~4.51 | 5.18 (4.83–5.34) | 0.659 | 2.32 | 0.31 |
| **DKFZ-964** [g] | 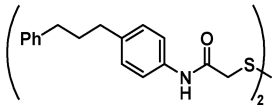 | 3.44 (3.06–3.70) | 3.78 (3.55–??) | <<4 [f] | 3.68 (2.91–3.93) | ~3.73 | 5.05 (??–??) | 23.5 | 40.5 | 0.35 |

[a] Determined by four-parameter dose-response fit from eight dose levels in triplicates, reported as the mean, with 95% confidence intervals in parenthesis. [b] HDAC Glo assay. [c] FRET assay. Mean of three [d]/two [e] separate experiments. [f] Curve fit analysis not convergent at 100 µM. [g] Activity per sulfide unit, disulfide dosed in ½ molar concentration. SF (selectivity factor) = $10^{(pIC50(HDAC10) - pIC50(HDAC6\ or\ 1))}$. LE (ligand efficiency) = 1.37 x $pIC_{50}$(HDAC10) / number of heavy atoms.[186] 95% confidence intervals of dose-response fits are shown in parenthesis. "??" indicates that confidence intervals could not be calculated.

## 8.3 List of compound numbers and batch codes

| number in dissertation | DKFZ-number | batch code | number in Steimbach et al.[1] | number in dissertation | DKFZ-number | batch code | number in Steimbach et al.[1] |
|---|---|---|---|---|---|---|---|
| **73** | **DKFZ-848** | RS-2-039-D | **12** | **96** | **DKFZ-767** | RS-1-093-A | **24** |
| **75** | **DKFZ-711** | RS-1-021-A | **13** | **97** | **DKFZ-770** | RS-1-098-C | **25** |
| **77** | **DKFZ-629** | GT-1-016<br>GT-1-030-A | **14** | **98** | **DKFZ-895** | HGS-1-009-A | **26** |
| **78** | **DKFZ-843** | RS-2-034-A | **15** | **99** | **DKFZ-772** | RS-1-111-B | **27** |
| **79** | | RS-1-119-crude<br>RS-2-132-A | **S1** | **100** | **DKFZ-775** | RS-1-122-A | **28** |
| **82** | | RS-1-008-D | **S2** | **101** | **DKFZ-728** | RS-2-066-A | **29** |
| **83** | | RS-1-104-crude | | **102** | **DKFZ-758** | RS-1-081-A | **30** |
| **84** | | EXP-17-AH1065-A | **S3** | **103** | **DKFZ-806** | RS-1-148-A | |
| **85** | | RS-2-029-A | | **104** | **DKFZ-773** | RS-1-114-A | **32** |
| **87** | **DKFZ-714** | GT-1-005-A | **16** | **105** | **DKFZ-859** | RS-2-047-A | **31** |
| **88** | **DKFZ-724** | GT-1-028-B | **17** | **106** | **DKFZ-805** | RS-1-131-A | **33** |
| **89** | **DKFZ-716** | GT-1-011-A | **18** | **107** | **DKFZ-749** | RS-1-050-A | **34** |
| **90** | **DKFZ-715** | GT-1-010-A | **19** | **108** | **DKFZ-756** | RS-1-063-A | **35** |
| **91** | **DKFZ-717** | GT-1-012-A | **20** | **109** | **DKFZ-754** | RS-1-059-B | **36** |
| **92** | **DKFZ-718** | GT-1-022-A | **21** | **110** | **DKFZ-757** | RS-1-075-D | **37** |
| **93** | **DKFZ-888** | RS-2-069-B | **22** | **111** | **DKFZ-748** | RS-1-076-C | **41** |
| **94** | **DKFZ-777** | RS-1-096-D | | **112** | **DKFZ-776** | RS-1-124-B | **39** |
| **95** | **DKFZ-759** | RS-1-084-C | **23** | **113** | **DKFZ-774** | RS-1-115-A | **40** |

| number in dissertation | DKFZ-number | batch code | number in Steimbach et al.[1] | number in dissertation | DKFZ-number | batch code | number in Steimbach et al.[1] |
|---|---|---|---|---|---|---|---|
| **114** | **DKFZ-769** | RS-1-094-A | **42** | **135** | | RS-1-106-A | **S14** |
| **115** | **DKFZ-771** | RS-1-105-D | **38** | **136** | | RS-1-120-A | **S15** |
| **116** | **DKFZ-746** | RS-1-044-A | **43** | **139** | | RS-1-058-A | **S16** |
| **117** | **DKFZ-747** | RS-1-045-A | **44** | **140** | | RS-1-138-A | |
| **118** | **DKFZ-752** | RS-1-056-D | **45** | **141** | | RS-1-064-crude | **S17** |
| **119** | **DKFZ-755** | RS-1-062-E | **47** | **142** | | RS-1-142-crude | |
| **120** | **DKFZ-751** | RS-1-053-A FA | **46** | **143** | **DKFZ-828** | RS-2-065-C | **S18** |
| **121** | **DKFZ-753** | RS-1-057-A | **48** | **144** | **DKFZ-829** | RS-2-027-A | **49** |
| **122** | **DKFZ-750** | RS-1-051-B | | **145** | | RS-1-150-A | |
| **123** | | RS-1-006-B HCl | **S4** | **146** | | RS-2-045-A | **S19** |
| **124** | | RS-2-059-A | **S5** | **147** | | RS-2-046-A | **S20** |
| **125** | | RS-2-060-A | **S6** | **149** | | RS-1-107-crude RS-2-131-crude | **S21** |
| **126** | | RS-2-068-A | **S7** | **150** | | RS-1-108-A | **S22** |
| **127** | | RS-1-073-crude | **S8** | **151** | | RS-1-117-A | |
| **128** | | RS-1-088-crude | **S9** | **152** | | RS-1-126-A | **S23** |
| **129** | | RS-1-078-B RS-2-133-B | **S10** | **153** | | RS-1-128-A | **S24** |
| **130** | | RS-1-089-B RS-2-134-A | **S11** | **154** | **DKFZ-812** | RS-2-002-A | |
| **133** | | HGS-1-003-crude 2HCl | **S12** | **156** | | RS-1-149-A | |
| **134** | | HGS-1-004-B | **S13** | **157** | | RS-1-154-AB | |

| number in dissertation | DKFZ-number | batch code | number in Steimbach et al.[1] | number in dissertation | DKFZ-number | batch code | number in Steimbach et al.[1] |
|---|---|---|---|---|---|---|---|
| **158** | | RS-1-155-cr | | **178** | **DKFZ-872** | RS-2-052-DE | |
| **159** | | RS-2-007-crude | | **179** | **DKFZ-945** | RS-2-120-A | |
| **160** | | RS-2-013-crude | | **180** | **DKFZ-962** | RS-2-140-D | |
| **161** | | RS-2-015-crude | | **181** | **DKFZ-949** | RS-2-124-D | |
| **162** | **DKFZ-831** | TS-1-094-B | | **184** | | TS-1-107-crude | |
| **163** | **DKFZ-854** | TS-1-110-B | | **185** | | RS-2-048-crude | |
| **164** | **DKFZ-830** | TS-1-092-A<br>TS-1-104-A | | **186** | | RS-2-050-A | |
| **165** | **DKFZ-880** | RS-2-055-A | | **188** | | RS-2-115-B | |
| **166** | **DKFZ-855** | TS-1-111-crude<br>TS-1-114-crude | | **191** | | RS-2-107-A | |
| **167** | **DKFZ-889** | RS-2-061-D | | **192** | | RS-2-118-A | |
| **168** | **DKFZ-961** | RS-2-141-A | | **193** | **DKFZ-942** | RS-2-116-B | |
| **169** | **DKFZ-852** | TS-1-103-A | | **194** | **DKFZ-958** | RS-2-138-A | |
| **170** | **DKFZ-832** | TS-1-095-A | | **195** | **DKFZ-965** | RS-2-146-A | |
| **171** | **DKFZ-851** | TS-1-108-A | | **196** | **DKFZ-963** | RS-2-144-A | |
| **172** | **DKFZ-877** | RS-2-056-A | | **197** | **DKFZ-960** | RS-2-142-A | |
| **173** | **DKFZ-850** | TS-1-114-A | | **198** | **DKFZ-964** | RS-2-145-crude | |
| **174** | **DKFZ-887** | RS-2-063-C | | **199** | | RS-2-100-crude2 XX | |
| **175** | **DKFZ-826** | RS-2-023-A | | **200** | | RS-2-109-crude | |
| **176** | **DKFZ-827** | TS-1-086-A | | **202** | | RS-2-139-crude | |
| **177** | **DKFZ-873** | RS-2-053-B | | **203** | | HGS-1-011 | |

| number in dissertation | DKFZ-number | batch code | number in Steimbach et al.[1] |
|---|---|---|---|
| **204** | | HGS-1-014 | |
| **205** | | RS-2-154 resin | |
| **206** | | HGS-1-036 | |
| **207** | **DKFZ-902** | HGS-1-028-A | |
| **208** | **DKFZ-899** | HGS-1-016-C | |
| **209** | **DKFZ-910** | HGS-1-048-B | |
| **210** | **DKFZ-906** | HGS-1-052-A | |
| **211** | **DKFZ-907** | HGS-1-049-A | |
| **212** | **DKFZ-911** | HGS-1-050-B | |
| **213** | **DKFZ-904** | HGS-1-032-A | |
| **214** | **DKFZ-900** | HGS-1-024-C | |
| **215** | **DKFZ-973** | HGS-1-065-C | |
| **216** | **DKFZ-908** | HGS-1-051-A | |
| **217** | **DKFZ-972** | RS-3-003-A TFA | |
| **218** | | HGS-1-070-A | |
| **219** | | JL-XV-004-B | |
| **220** | | HGS-1-066 | |